

AD-244038

Proceedings of the  
Fortieth

**IWCS**



# INTERNATIONAL WIRE AND CABLE SYMPOSIUM

November 18 thru 21, 1991

REPRODUCED FROM  
BEST AVAILABLE COPY

Sponsored by  
International Wire and Cable Symposium,  
Inc. (IWCS)  
Eatontown, New Jersey

With Participation by  
US Army Communications-Electronics Command  
(CECOM)  
Fort Monmouth, New Jersey

# REPORT DOCUMENTATION PAGE

Form Approved  
OPM No. 0704-0188

Public reporting burden for this collection of information is estimated to average 1 hour per response, including the time for reviewing instructions, searching existing data sources, gathering and maintaining the data needed, and reviewing the collection of information. Send comments regarding this burden estimate or any other aspect of this collection of information, including suggestions for reducing this burden, to Washington Headquarters Services, Directorate for Information Operations and Reports, 1215 Jefferson Davis Highway, Suite 1204, Arlington, VA 22202-4302, and to the Office of Information and Regulatory Affairs, Office of Management and Budget, Washington, DC 20503.

1. AGENCY USE ONLY (Leave Blank)		2. REPORT DATE Nov. 19-21, 1991	3. REPORT TYPE AND DATES COVERED Conference Proceedings Nov. 19-21, 1991	
4. TITLE AND SUBTITLE Proceedings of the Fortieth International Wire and Cable Symposium, Nov. 19-21, 1991			5. FUNDING NUMBERS	
6. AUTHOR(S)				
7. PERFORMING ORGANIZATION NAME(S) AND ADDRESS(ES)			8. PERFORMING ORGANIZATION REPORT NUMBER	
9. SPONSORING/MONITORING AGENCY NAME(S) AND ADDRESS(ES) US Army Communications-Electronics Command (CECOM) Fort Monmouth, NJ			10. SPONSORING/MONITORING AGENCY REPORT NUMBER	
11. SUPPLEMENTARY NOTES				
12a. DISTRIBUTION/AVAILABILITY STATEMENT  Approved for Public Release: Distribution is unlimited.  ..			12b. DISTRIBUTION CODE	
13. ABSTRACT (Maximum 200 words) Sessions: Intelligent Vehicle Highway Sys.; Fiber Optic Cable Design; Copper Cables: Design Materials and Performance; Optical Fiber Coatings; Fiber Optic Aerial Cables; Copper Cables: Design, Materials and Performance; Fiber Optic Splices, Connectors and Switches; Fiber Optic Cable Materials; Fire Hazard Considerations; Power and Industrial Cables; Intelligent Building Comm. Sys.; Poster Papers; Fiber Optic Submarine Cables; Environmental Effectson Optical Fibers and Cables; Fiber Optic Military Cables and Spec. Applications; Fiber Optic Cable Components, Installation and Practices; Manufacturing and Testing of Optical Fibers, Cables and Components; Implementation of "Fiber Distributed Data Interface"(FDDI).				
14. SUBJECT TERMS Fiber optics transmission lines; Fiber optics: Electric cables; electric wires, electric connectors; hazards; coatings; expert systems; symposia			15. NUMBER OF PAGES 594	
16. PRICE CODE			17. LIMITATION OF ABSTRACT	
18. SECURITY CLASSIFICATION OF REPORT	19. SECURITY CLASSIFICATION OF THIS PAGE	20. SECURITY CLASSIFICATION OF ABSTRACT	21. LIMITATION OF ABSTRACT	



# PROCEEDINGS OF 40TH INTERNATIONAL WIRE AND CABLE SYMPOSIUM

Sponsored by  
International Wire and Cable Symposium, Inc. (IWCS)  
Eatontown, New Jersey

With Participation by  
US Army Communications-Electronics Command (CECOM)  
Fort Monmouth, New Jersey

ADAM'S MARK HOTEL  
ST. LOUIS, MISSOURI  
NOVEMBER 18, 19, 20 and 21, 1991

Accession For	
NTIS	ORAS
DTIC	TAB
Unavail	Unavail
By	
Date	
Availability	
Dist	Availability
A-1	

APPROVED FOR PUBLIC RELEASE: DISTRIBUTION UNLIMITED



91-19183



91 1227 055

## MISSION

The International Wire and Cable Symposium provides a forum for the exchange of technical information amongst suppliers, manufacturers, and users on technological advancements in materials, processes, and products used for voice, data and video signal transmission systems.

## TECHNICAL PAPERS

### Tuesday, November 19, 1991

9:00 am	SESSION I	Intelligent Vehicle Highway Systems (IVHS)
1:00 pm	SESSION II	Fiber Optic Cable Design
1:00 pm	SESSION III	Copper Cables: Design, Materials and Performance I
1:00 pm	SESSION IV	Optical Fiber Coatings

### Wednesday, November 20, 1991

8:30 am	SESSION V	Fiber Optic Aerial Cables
8:30 am	SESSION VI	Copper Cables: Design, Materials & Performance II
8:30 am	SESSION VII	Fiber Optic Splices, Connectors and Switches
2:00 pm	SESSION VIII	Fiber Optic Cable Materials
2:00 pm	SESSION IX	Fire Hazard Considerations
2:00 pm	SESSION X	Power & Industrial Cables—Materials and Processing
2:00 pm	SESSION XI	Intelligent Building Communication Systems
3:30 pm	SESSION XII	Poster Papers

### Thursday, November 21, 1991

8:30 am	SESSION XIII	Fiber Optic Submarine Cables
8:30 am	SESSION XIV	Environmental Effects on Optical Fibers and Cables
8:30 am	SESSION XV	Fiber Optic Military Cables and Special Applications
1:00 pm	SESSION XVI	Fiber Optic Cable Components, Installation & Practices
1:00 pm	SESSION XVII	Manufacturing & Testing of Optical Fibers, Cables & Components
1:00 pm	SESSION XVIII	Implementation of "Fiber Distributed Data Interface" (FDDI)

## PAPERS

The papers in this volume were printed directly from unedited reproducible copies prepared by the authors. Responsibility for contents rests upon the authors and not the symposium committee or its members. All rights reserved by the International Wire and Cable Symposium, Inc., 174 Main Street, Eatontown, New Jersey 07724.

# PROCEEDINGS-INTERNATIONAL WIRE AND CABLE SYMPOSIUM (IWCS)

## *Bound—Available from IWCS*

30th International Wire & Cable Symposium Proceedings—1981—\$8.00  
31st International Wire & Cable Symposium Proceedings—1982—\$8.00  
32nd International Wire & Cable Symposium Proceedings—1983—\$8.00  
33rd International Wire & Cable Symposium Proceedings—1984—\$10.00  
34th International Wire & Cable Symposium Proceedings—1985—\$15.00  
35th International Wire & Cable Symposium Proceedings—1986—NOT AVAILABLE  
36th International Wire & Cable Symposium Proceedings—1987—NOT AVAILABLE  
37th International Wire & Cable Symposium Proceedings—1988—NOT AVAILABLE  
38th International Wire & Cable Symposium Proceedings—1989—\$20.00  
39th International Wire & Cable Symposium Proceedings—1990—\$25.00  
40th International Wire & Cable Symposium Proceedings—1991—\$50.00  
Index of IWCS Papers—1983-1990—\$15.00

Extra copies of the 1991 Proceedings: 1-3, \$50.00 per copy; 4-10, \$40.00 per copy; 11 and above \$30.00 per copy (plus an additional \$5.00 for shipping—U.S.A. only). Overseas shipping: **Surface Mail** is an additional \$10.00 per copy, however, delivery may take up to six weeks and cannot be traced in the event they are not received. **Overseas Air Mail** will be an additional \$35.00 per copy for Europe and \$40.00 per copy for Asia.

Make a check or bank draft payable in U.S. Dollars only to the INTERNATIONAL WIRE & CABLE SYMPOSIUM and forward request to:

International Wire and Cable Symposium, Inc.  
174 Main Street  
Eatontown, NJ 07724

Telephone inquiries may be directed to Pat Hudak (908) 389-0990.

Photocopies are available for complete sets of papers for 1964 thru 1990. Information on prices and shipping charges should be requested from the:

US Department of Commerce  
National Technical Information Service (NTIS)  
Springfield, Virginia 22151  
USA

Telephone: (703) 487-4650

Include Title, Year and "AD" Number

13th Annual Wire & Cable Symposium (1964)	—AD 787164
15th Annual Wire & Cable Symposium (1966)	—AD A006601
16th International Wire & Cable Symposium (1967)	—AD 787165
17th International Wire & Cable Symposium (1968)	—AD 787166
18th International Wire & Cable Symposium (1969)	—AD 787167
19th International Wire & Cable Symposium Proceedings 1970	—AD 714985
20th International Wire & Cable Symposium Proceedings 1971	—AD 733399
21st International Wire & Cable Symposium Proceedings 1972	—AD 752908
22nd International Wire & Cable Symposium Proceedings 1973	—AD 772914
23rd International Wire & Cable Symposium Proceedings 1974	—AD A003251
24th International Wire & Cable Symposium Proceedings 1975	—AD A017787
25th International Wire & Cable Symposium Proceedings 1976	—AD A032801
26th International Wire & Cable Symposium Proceedings 1977	—AD A047609
27th International Wire & Cable Symposium Proceedings 1978	—AD A062322
28th International Wire & Cable Symposium Proceedings 1979	—AD A081428
29th International Wire & Cable Symposium Proceedings 1980	—AD A096308
30th International Wire & Cable Symposium Proceedings 1981	—AD A110859
31st International Wire & Cable Symposium Proceedings 1982	—AD A125662
32nd International Wire & Cable Symposium Proceedings 1983	—AD A136749
33rd International Wire & Cable Symposium Proceedings 1984	—AD A152119
34th International Wire & Cable Symposium Proceedings 1985	—AD A164384
35th International Wire & Cable Symposium Proceedings 1986	—AD A180828
36th International Wire & Cable Symposium Proceedings 1987	—AD A189610
37th International Wire & Cable Symposium Proceedings 1988	—AD A200903
38th International Wire & Cable Symposium Proceedings 1989	—AD A216023
39th International Wire & Cable Symposium Proceedings 1990	—AD A233634
Kwic Index of Technical Papers, International Wire & Cable Symposium (1952-1975)	—AD A027588



### MESSAGE FROM THE PRESIDENT/DIRECTOR

Again, it is my pleasure on behalf of the International Wire and Cable Symposium (IWCS) Committee and CECOM, Fort Monmouth, New Jersey to welcome each one to the symposium, which should be an exciting and informative experience for all attendees. This year's symposium continues its traditional international reputation of excellence as demonstrated by the large number of speakers from fourteen different countries. The response to the committee's call-for-papers was outstanding, especially from our international supporters and attendees.

It is most gratifying each year to see and witness the enthusiasm and interest displayed by symposium attendees. It is the committee's aim and objective to continue this interest by presenting new features and the latest concepts in wire/cable development and usage. This year's program attempts to fulfill these objectives by offering a Suppliers Forum for the first time, in addition to the highly controversial and interesting concept of using wire technology in Vehicular Highway Systems. The popular poster session and six educational short courses that were so successful last year, will again be available.

The IWCS Committee continues to explore new ideas for improving the technical level of the symposium in order to increase the interest of its attendees. Many attendees have expressed a strong interest for information on new materials suitable for copper wire/cable developments and special applications. Therefore, in responding to the 1992 Call-for-Papers, all authors are urgently requested to submit abstracts related to these areas. The technical program is at all times a reflection of the responses received from the call-for-paper announcement.

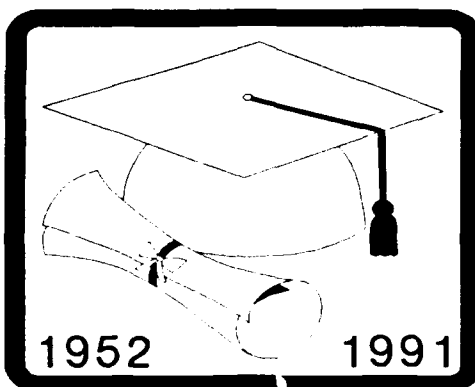
Committee members Dr. Ken-ichi Aihara of NTT America, Inc. and Mr. Hans A. Mayer of the Olex Cable Division of Pacific Dunlop Ltd. are retiring from the committee. Each committee member contributed significantly to the success of the symposium. On behalf of the IWCS Committee, I extend to each a very special thanks for their dedication, cooperation and support of the symposium objectives.

The ultimate credit for the continued success of the symposium belongs to a long list of dedicated and hard working committee members. In recognition of their service and on the occasion of the Fortieth Anniversary of the symposium, I am happy to salute them and inscribe their names on the accompanying honor roll.

The 1992 symposium will be in Reno, Nevada at the Bally's Reno Hotel. In 1993, the symposium will return to the Adam's Mark Hotel in St. Louis, Missouri.

ELMER F. GODWIN  
President/Director, IWCS

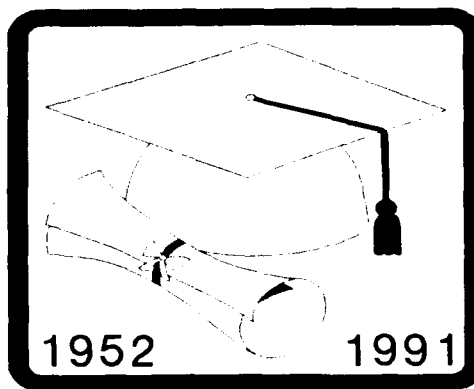
# Honor



# Roll

1952-63	Howard F.X. Kingsley -- U.S. Army Electronics Command
1952-52	Milton A. Lipton -- U.S. Army Electronics Command
1953-58	Howard L. Kitts -- U.S. Army Electronics Command
1953-61	Ray Blain -- U.S. Army Signal Engineering Agency
1953-61	C.T. Wyman -- Bell Telephone Laboratories
1953-54	R.C. Graham -- Rome Cable Corporation
1953-53	H. Weber -- U.S. Rubber Company
1953-53	A. Maibauer -- Bakelite Company
1953-53	G.E. Forsberg -- Suprenant Manufacturing Company
1954-54	W. Carter -- Naugatuck Chemical Company
1954-55	P.H. Grogan -- General Cable Corporation
1954-55	E.L. Love -- Whitney Blake Company
1955-56	E.J. Burrough -- E.I. DuPont de Nemours & Company, Inc.
1955-56	B.J. Jore -- Anaconda Wire and Cable Company
1956-57	G. Hamburger -- Copperweld Steel Company
1956-57	J.V. McBride -- Plastic Wire and Cable Corporation
1957-57	E.J. Merrell -- Phelps Dodge Copper Products Corporation
1957-58	M.G. Caine -- Monsanto Chemical Company
1958-58	A.L. McKean -- Phelps Dodge Copper Products Corporation
1958-59	J.L. Robb -- Superior Cable Corporation
1958-59	B. Levinson -- The Okonite Company
1959-60	I.T. Stoneback -- I.T.T. Laboratories
1959-63	Fred W. Wills -- U.S. Army Electronics Command
1959-60	H.L. Wuertn -- B.F. Goodrich Chemical Company
1960-61	R.P. Houlihan -- Gavitt Wire and Cable Company
1960-61	S. Montgomery, Jr. -- The Montgomery Company
1961-61	W.P. Acton -- Hercules Powder Company
1961-62	R.L. Spade -- The Belden Manufacturing Company
1962-62	W.O. Bracken -- Hercules Powder Company
1962-62	L.A. Kent -- Camden Wire Company
1962-64	A.N. Averill -- Phalo Plastics Corporation
1962-64	J.J. Roache -- Frankford Arsenal
1962-71	F.W. Horn -- Bell Telephone Laboratories
1963-64	F.E. Harden -- Camden Wire Company
1963-65	R.C. Mildner -- The Dow Chemical Company
1963-63	B.W. Tyrrell -- Northern Electric Company, Ltd.
1964-65	R.R. Watt -- Northern Electric Company, Ltd.
1964-78	Milton Tenzer -- U.S. Army Electronics Command
1964-73	Jack Spergel -- USA Electronics Command/General Cable Corp.
1965-65	L. Gumina -- Bureau of Ships, Department of Navy
1965-66	Maynard G. Noble -- General Electric Company

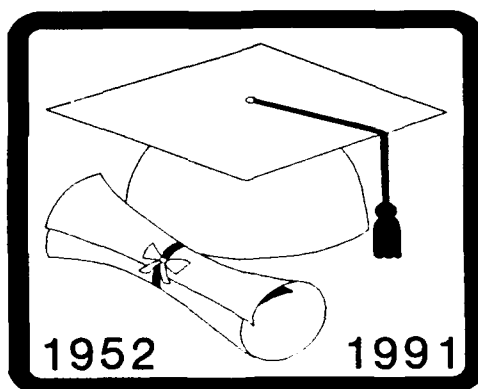
Honor



Roll

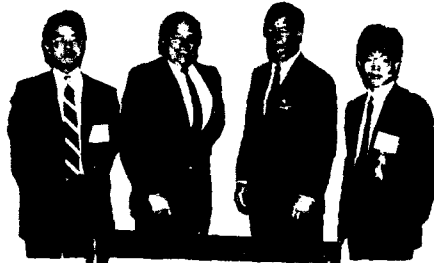
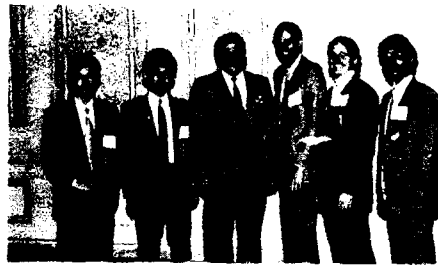
1965-66	Walter S. Rigling -- Martin Company
1966-67	Louis E. Marrin -- Canada Wire & Cable Company
1966-66	John W. Tamblyn -- Tennessee Eastman Company
1966-68	Richard G. Devany -- Tennessee Eastman Company
1967-68	Leo Adelson -- Picatinny Arsenal
1967-	Irving Kolodny -- General Cable Corp./Consultant
1967-69	Joseph R. Perkins -- I.E. DuPont de Nemours & Co., Inc.
1967-68	Linden L. Tomlinson -- T.R.W. Systems
1968-70	Jules Ruskin -- Phillips Cables, Ltd.
1969-69	J.T. Roark -- Phillips Petroleum Company
1969-70	Fred M. Oberlander -- RCA Corporation
1969-71	Gerald A. Lohsl -- REA, Department of Agriculture
1969-73	T. Ferris Scoville -- U.S. Army Electronics Command
1970-71	Dan F. Stewart -- Phillips Petroleum Company
1970-72	Michael M. Suba -- Union Carbide Corporation
1970-72	E. Mark Wolff -- Anaconda Wire and Cable Company
1971-73	Louis J. Frisco -- Raychem Corporation
1971-73	Jack D. Kirk -- Alberta Government Telephones
1972-89	George H. Webster -- Bell Laboratories
1972-72	John Toomey -- GTE Systems Engineering
1972-73	Stanley F. Luques -- Brand Rex Company
1973-	Elmer F. Godwin -- USA Elec Cmd/USA Comm R&D Cmd/GEF Assoc.
1972-74	W. Robert Smith -- Hercules Incorporated
1972-72	Clyde Hatch -- Naval Ship Engineering Center
1973-75	Jerome Hager -- Northern Petrochemical Company
1973-75	George W. Heller -- Tensolite Insulated Wire Company
1973-74	Les Dunlop -- GTE Service Corporation
1974-76	Joseph M. Flanigan -- REA, Washington, DC
1974-74	Warner T. Smith -- Superior Continental Corporation
1974-91	Marta Farago -- Northern Telecom Canada Ltd.
1974-75	Ronald Solomon -- McDonnell Aircraft Company
1975-76	James Kanely -- Superior Continental Corporation
1975-78	F.M. Farrell -- 3M Company
1975-86	Joe Neigh -- AMP, Incorporated
1976-77	Sherman Kottle, DOW Chemical USA
1976-93	Frank Short -- BICC Cables Limited (England)
1977-80	Adolf Asam -- ITT-Electro Optical Products Division
1977-77	Trish McGillen -- Icore International
1978-78	Paul Szulborski, Icore International
1978-80	Ken Bow -- Dow Chemical USA
1978-	Micheal DeLucia -- David W. Taylor R&D Center
1979-	Leo M. Chattler -- DQM Industries

# Honor



# Roll

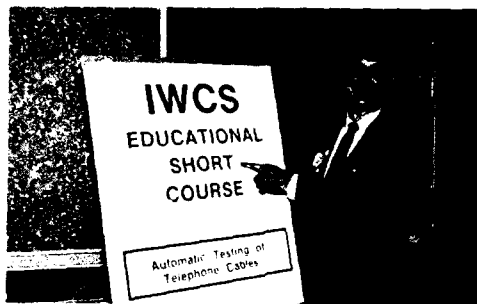
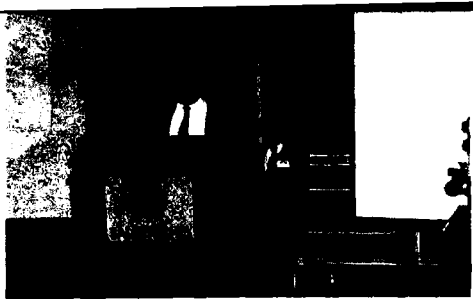
1979-79	John Lelivelt -- U.S. Army Communications R&D Command
1979-82	William Korcz -- Shell Development Company
1980-83	John Brazee -- Continental Telephone Service Corporation
1980-85	Joseph McCann -- U.S. Army Communications-Electronics Command
1981-86	William Chervenak -- Corning Glass Works
1981-84	Andrew Dunin -- DuPont Canada Incorporated
1981-83	John Santos -- Phelps Dodge Communications Company
1981-84	James Tyler -- Essex Group
1982-83	Paul Dobson -- Valtec Corporation
1982-85	Robert Depp -- Defense Electronic Supply Center
1982-85	Eugene Riley -- Ericsson, Incorporated
1982-85	Austin Wetherell -- Underwriters Laboratories
1983-86	Kazuo Nomura -- Sumitomo Electric USA, Incorporated
1983-86	John Thompson -- Nokia, Incorporated
1985-86	Allan G. Dwyer -- GTE Service Corporation
1987-88	Edward A. Gurney -- GTE Service Corporation
1985-	Raymond E. Jaeger -- SpecTran Corporation
1985-88	Tom Jones -- Wyrough & Loser, Incorporated
1985-88	Vieney Mascarenhas -- Canada Wire & Cable Limited
1986-86	Jean Harman -- Naval Sea Systems Command
1986-	Peter Bark -- Siecor Corporation
1986-	Reiner Gerdes -- Contel Lab/Consultant Telecommunications
1986-86	Anne Holt -- Celanese
1986-88	Les Hewitt -- Pacific Bell
1987-88	Keiji Tachikawa -- NIT America, Inc.
1987-89	Robert Streich -- AT&T Networks Systems
1987-90	C. Ronald Simpkins -- E.I. DuPont de Nemours & Co., Inc.
1988-91	Hans A. Mayer -- Olex Cables Melbourne (Australia)
1988-93	James J. Pickering -- Neste Chemicals, Inc.
1989-89	Patrick Hart -- Pacific Bell
1989-89	Richard Rossi -- General Cable Company
1989-89	Peter Stahl -- General Electric Company
1989-89	Bruce Gardner -- Brand Rex Telecommunications Systems
1989-91	Ken-ichi Aihara -- NIT America, Inc.
1990-92	Homer Vela -- AT&T Network Cable Systems
1989-92	David Fallowfield -- Telus Corporation (Canada)
1990-92	Manuel Santana -- AT&T Bell Laboratories
1990-93	Dave Fischer -- Superior Cable Corporation
1990-93	Robert Baboian -- Texas Instruments, Inc.
1990-94	Rene Freeman -- Union Carbide Chemicals & Plastics Co., Inc.
1991-94	Xavier Mann -- Fitel General Corporation
1991-94	Dieter Nordmann -- Kablemetlal Electro (Germany)

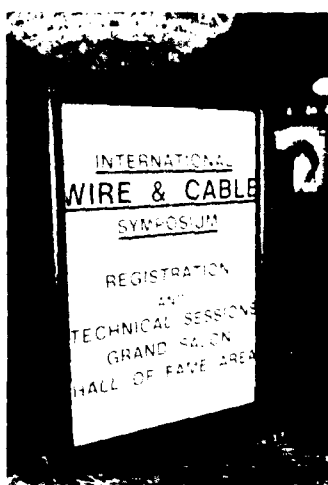
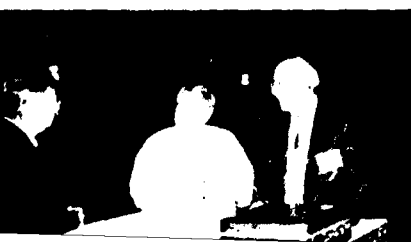
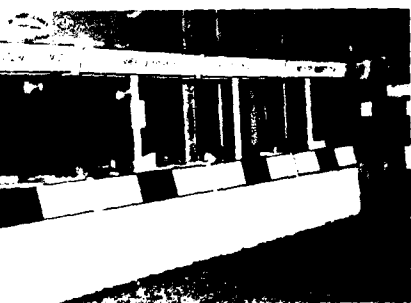


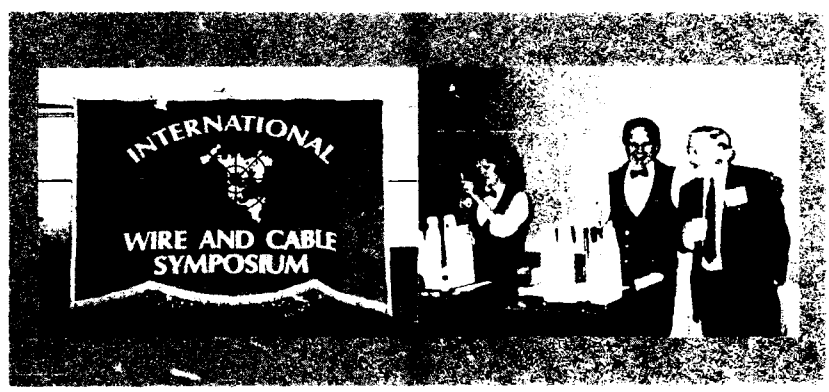
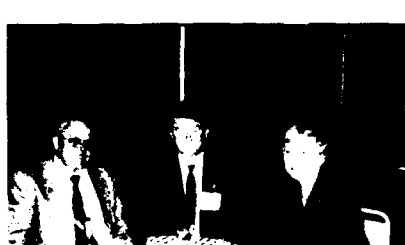
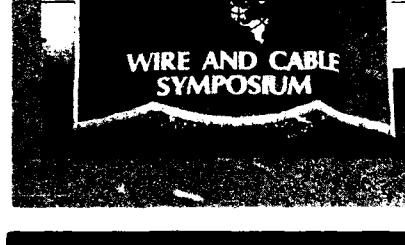
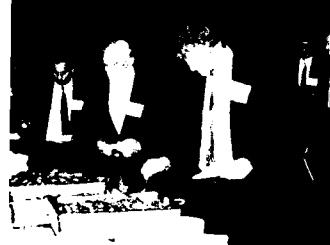
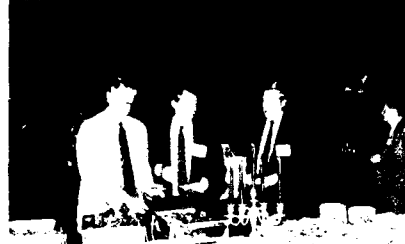
Breakfast

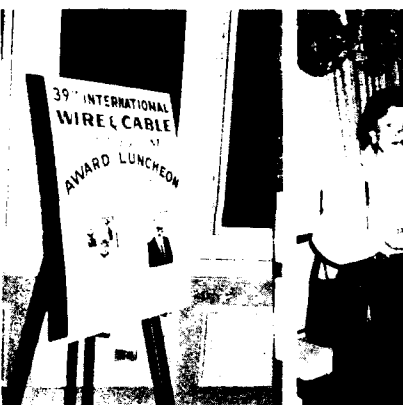












# AWARDS

## Outstanding Technical Paper

- H. Lubars and J. A. Olszewski, General Cable Corp. — 1968  
"Analysis of Structural Return loss in CATV Coaxial Cable"
- J. P. McCann, R. Sabia and B. Wargotz, Bell Laboratories — 1969  
"Characterization of Filler and Insulation in Waterproof Cable"
- D. E. Setzer and A. S. Windeler, Bell Laboratories — 1970  
"A Low Capacitance Cable for the T2 Digital Transmission line"
- R. Lyenger, R. McClean and T. McManus, Bell Northern Research — 1971  
"An Advanced Multi-Unit Coaxial Cable for Toll PCM Systems"
- J. B. Howard, Bell Laboratories — 1972  
"Stabilization Problems with Low Density Polyethylene Insulations"
- Dr. H. Margin, Kabelmetal — 1973  
"High Power Radio Frequency Coaxial Cables, Their Design and Rating"
- D. Doty, AMP Inc. — 1974  
"Mass Wire Insulation Displacing Termination of Flat Cable"
- T. S. Choo, Dow Chemical U.S.A. — 1975  
"Corrosion Studies on Shielding Materials for Underground Telephone Cables"
- N. J. Cogelia, Bell Telephone Laboratories and G. K. Lavoie and J. F. Glahn, US Department of Interior — 1976  
"Rodent Biting Pressure and Chemical Action and Their Effects on Wire and Cable Sheath"
- T. K. McManus, Northern Telecom Canada Ltd. and R. Beveridge, Saskatchewan Telecommunications, Canada — 1977  
"A New Generation of Filled Core Cable"
- F. Suzuki, S. Sato, A. Mori and Y. Suzuki, Sumitomo Electric Industries, Ltd. Japan — 1978  
"Microcoaxial Cables Insulated with Highly Expanded Polyethylene By Chemical Blowing Method"
- S. Masaki, Y. Yamazaki and T. Ideguchi, Nippon Telegraph and Telephone Public Corporation, Japan — 1979  
"New Aluminum Sheath Cable Used for Electromagnetic Shielding"
- P. Kish and Y. BeBorgne, Northern Telecom Canada Limited, Montreal, Canada — 1980  
"General Crosstalk Model For Paired Communication Cables"
- C. J. Arroyo, N. J. Cogelia, Bell Laboratories, and B. J. Darsey, Western Electric — 1981  
"Thermal Behavior of Experimental Plenum Cable Sheaths Determined in a Radiant Heat Chamber"
- R. H. Whiteley, Raychem Ltd. — 1982  
"A Comprehensive Small Scale Smoke Test"
- V. A. Fentress, Raychem Corp. and D. V. Nelson, Stanford University — 1983  
"Fracture Mechanics Evaluation of the Static Fatigue Life of Optical Fibers in Bending"
- M. Fujise and Y. Iwamoto, KDD Research & Development Laboratories, Tokyo, Japan — 1984  
"Self-Core-Alignment Arc-Fusion Splicer Based on a Simple Local Monitoring Method"
- James A. Krabec and John W. Kincaid, Jr., Belden Technical Research Center — 1985  
"Advances in the Optimization of Multi-Layer Shield Design"
- Simon D. Dadakarides and Bruce B. Lusignam, Stanford University — 1986  
"Magnetically Loaded Cables"

## Best Presentation

- N. Dean, B.I.C.C. — "The Development of Fully Filled Cables for Distribution Network"
- J. D. Kirk, Alberta Government Telephones — "Progress and pitfalls of Rural Buried Cable"
- Dr. O. Leuchs, Kable and Metalwerke — "A New Self-Extinguishing Hydrogen Chloride Binding PVC Jacketing Compound for Cables"
- S. Nordblad, Telefonaktiebolaget L. M. Ericsson — "Multi-Paired Cable of Nonlayer Design for Low Capacitance Unbalance Telecommunications Network"
- N. Kojima, Nippon Telegraph and Telephone — "New Type Paired Cable for High Speed PCM Transmission"
- S. Kaufman, Bell Laboratories — "Reclamation of Water-Logged Buried PIC Telephone Cable"
- R. J. Oakley, Northern Electric Co., Ltd. — "A Study Into Paired Cable Crosstalk"
- G. H. Webster, Bell Laboratories — "Material Savings by Design in Exchange and Trunk Telephone Cable"
- J. E. Wimsey, United States Air Force — "The Bare Base Electrical Systems"
- Michael DeLucia, Naval Ship Research and Development — "Highly Fire-Retardant Navy Shipboard Cable"
- William L. Schmacher, AMP Inc. — "Design Considerations for Single Fiber Connector"
- Richard C. Mondello, Bell Labs. — "Design and Manufacture of an Experimental Lightguide Cable For Undersea Transmission Systems"
- I. Wadehra, IBM Corporation — "Performance of Polyvinyl Chloride Communication Cables in Modified Steiner Tunnel Test"
- J. J. Refi, Bell Laboratories — "Mean Power Sum Far-End Crosstalk of PIC Cables as a Function of Average Twist Helix Angle"
- G. S. Anderson, Belden Corporation — "Installation of Fiber Optic Cable on 457 Meter Tower"
- A. Yoshizawa, The Furukawa Electric Co., Ltd. — "Structure and Characteristics of Cables for Robots"
- J. R. Bury, Standard Telecommunication Laboratories, Ltd., Hallow, England — "Development of Flame Retardant, Low Aggressivity Cables"
- William E. Dennis, Dow Corning Corporation, Midland, Michigan — "Hydrogen Evolving Tendencies of Cable Fillers and Optical Fiber Coatings"
- Stephen Hornung, British Telecom Research Laboratories — "Manufacture and Performance of Fibre Units for Installation by The Viscous Drag of Air"
- Dave Fischer, Superior Cable Corp. — "Progress Towards the Development of Lighting Test for Telecommunication Cables"
- John C. Chamberlain, Siecor Corp. — "Zero Halogen Fire Retardant Fiber Optic Shipboard Cable"

*Outstanding Technical Paper*

1987

Stephen B. Pierce—Conel Laboratories—"Digital Transmission on Customer Premises Wiring"

1988

Martin C. Light Jr., James A. Moses, Mark A. Sigmon and Christopher A. Story—Siecor Corp.—"Design and Performance of Telecommunication Cable Optimized for low Fiber Count"

1989

Michel Plasse, Lise Desroches and Paul-Andre Guilbert - Northern Telecom Canada Limited - "High Performance Twisted-Pair Cable for LAN Systems"

1990

Trevor N. Bowmer, Russell J. Miner, Irene M. Plitz, Joseph N. D'Amico and Lal M. Hore - Bellcore - "Thermal Stability Tests for Polyolefin Insulations"

*Outstanding Poster Paper*

William Wood—Bell Communication Research—"Performance Analysis of Optic Fiber Cleavers"

Dr. R. Raman - Contel Laboratories —"Loss at Dissimilar Fiber Splices"

Werner Bernard and Susan C. Grant - Siecor Corporation - "Fiber Optic Drop Cables in the Subscriber Loop"

Steve Lischynsky, Helmut Lukas, Robin McIntyre and Grant Pacey - Bell-Northern Research Ltd. - "New Technology for a Single Mode Mechanical Splice"

*Best Presentation*

Richard Rossi—General Cable Company—"Cable Sheathing Design and Performance Criteria"

Janice B. Haber - AT&T Laboratories—"Single-Mode Media and Apparatus for Fiber to the Home"

Michel de Vecchis - Les Cables de Lyon - "Results on a Large Scale Installation of a Fibre Optic Distribution Network"

Harold W. Friesen - AT&T Bell Laboratories - "An Improved Characteristic Impedance Measurement Technique"

# ***GOLD and SILVER CONTRIBUTORS***

## ***GOLD SUSTAINING CONTRIBUTORS***

**AFA Industries**  
20 Jewell Street  
Garfield, NJ 07026

**Akzo Fibers**  
801-F Blacklawn Road  
Conyers, GA 30207

**Atochem North America, Inc.**  
Three Parkway  
Philadelphia, PA 19102

**AT&T Bell Laboratories**  
2000 Northeast Expressway  
Norcross, GA 30071

**AT&T Network Cable Systems**  
505 N. 51st Avenue  
Phoenix, AZ 85043

**Ausimont U.S.A., Inc.**  
44 Whippany Road  
Morristown, NJ 07962-1838

**Belding Corticelli Thread Company**  
4421 Stuart Andrew Blvd.  
Charlotte, NC 28105

**BFGoodrich Company**  
6100 Oak Tree Boulevard  
Independence, OH 44131

**BICC Cables, Ltd.**  
Helsby, Warrington WA6 ODJ  
England

**Cary Chemicals, Inc.**  
10 Ruckle Avenue  
Farmingdale, NJ 07727

**Chromatics, Inc.**  
19 Francis J. Clarke Circle  
Bethel, CT 06801

**Communication Line Products  
Association of Japan**  
Toranomon Bldg, 1-1-12 Toranomon  
Minato-ku, Japan, 105 Japan

**Contel Laboratories**  
270 Scientific Drive, Suite 10  
Norcross, GA 30092

**Corning Incorporated**  
MP-RO-03-2  
Corning, NY 14831

**Daikin America, Inc.**  
375 Park Avenue, Suite 3308  
New York, NY 10152

**DCM International Corp.**  
2930 Faber St.  
Union City, CA 94587

**DSM Desotech, Inc.**  
1700 South Mount Prospect Road  
Box 5030  
Des Plaines, IL 60017

**Du Pont Company**  
Polymer Products  
Little Falls Center II  
Wilmington, DE 19880-0810

**Facile Holdings Inc.**  
185 6th Ave.  
Paterson, NJ 07509

**Fujikura, Ltd.**  
1-5-1 Kiba, Koto-ku  
Tokyo 135, Japan

**Fusion UV Curing Systems**  
7600 Standish Pl.  
Rockville, MD 20855-2798

**Gary Corporation**  
Pioneer Industrial Park  
Leominster, MA 01453

**GE Plastics**  
One Plastics Avenue  
Pittsfield, MA 01201

**Gem Gravure Co., Inc.**  
112 School Street  
W. Hanover, MA 02339

**GTE TestMark Labs**  
3050 Harrodsburg Road  
Lexington, KY 40503

**Hargro Industrial Packaging**  
20 Sand Park Rd.  
Cedar Grove, NJ 07009

**H. B. Fuller GmbH**  
An der Roten Bleiche 2-3  
D-2120 Lüneburg, FRG

**KT Industries Ltd.**  
1130 Wall St.  
Winnipeg, MB, Canada  
R3E 2R9

**Lantor, Inc.**  
125 Depot Street  
Bellingham, MA 02019



# TABLE OF CONTENTS

## TUESDAY MORNING—9:00 AM—12:00 PM (NOON) St. Louis Ballroom, Fourth Floor, Salons D & E

### Announcements/Greetings

Elmer F. Godwin, President/Director, IWCS, Inc., Eatontown, NJ  
James J. Pickering, Neste Chemicals, Inc., New Brunswick, NJ, Chairman IWCS  
Joseph J. Pucilowski, Jr., Director, CECOM Center for Command, Control and Communications Systems, U.S. Army CECOM, Fort Monmouth, NJ

### SESSION I: INTELLIGENT VEHICLE HIGHWAY SYSTEMS (IVHS)

*Chairperson:* Manuel R. Santana, AT&T Bell Laboratories, Norcross, GA

### Panelists (Invited Presentations):

Dr. Eckart Gleissner, ANT Backnang (Bosch Group), Backnang, Germany  
Mr. Brian Barcello, AT&T Bell Laboratory, Holmdel, NJ  
Mr. Richard J. Weiland, Vice President, SEI Information Technology, Chicago, IL  
Dr. James Constantino, Executive Director, IVHS America, Washington, DC

## TUESDAY AFTERNOON—1:00 PM—5:00 PM St. Louis Ballroom, Fourth Floor, Salon C

### SESSION II: FIBER OPTIC CABLE DESIGN

*Chairperson:* Dr. Peter R. Bark, Siecor Corporation, Hickory, NC

Preliminary Research into Ultra High Density and High Count Optical Fiber Cables—*S. Tomita, M. Matsumoto, T. Yabuta*, NTT Field Systems Research and Development Center, Tokai, Ibaraki, Japan; and *T. Uenoya*, NTT Network Systems Development Center, Uchisaiwaicho, Tokyo, Japan ..... 8

Design and Qualification of Gas Pressurized and Water Blocked Slotted Core Ribbon Cables—*H. Nassar*, Siecor Corporation, Hickory, NC; and *U. Oestreich*, Siemens AG, Neustadt/Coburg, Germany ..... 16

The Microsheath Cable: A Novel Design of Ultralightweight, Single Mode Optical Cable for Low Cost Subscriber Loop—*P. Trombert, P. Jamet, P. Cheron*, Societe Industrielle De Liaisons Electriques, Montereau, France; and *G. Le Noane, D. Boscher*, France Telecom, Lannion, France ..... 24

Specific Design of Optical Cables to be Used in Harsh Environment—*J.P. Bonicel, O. Tatat*, Alcatel Cable, Lyon, France; and *M. de Vecchis*, Alcatel Cable, Clichy, France ..... 31

Development of Non-Metallic Fiber Optic Cable for Indoor Use Applying Advanced FRP Forming Technology—*Y. Kuwata, H. Horima*, Sumitomo Electric Industries, Ltd., Yokohama, Japan; and *T. Ishii, S. Matsuno*, UBE-NITTO KASEI Co., Ltd., Gifu, Japan ..... 38

Evolution and Design of Fiber Optic Premise Cables—*A. C. Jenkins, D. Mathis, C. G. Wilson*, AT&T Bell Laboratories, Norcross, GA ..... 44

Design and Development of Steam Resistant Fiber Optic Cable—*M. K. R. Vyas, E. L. Buckland, P. Neveux, Jr.*, Sumitomo Electric Fiber Optics Corp., Research Triangle Park, NC ..... 55

## TUESDAY AFTERNOON—1:00 PM—5:00 PM St. Louis Ballroom, Fourth Floor, Salon D

### SESSION III: COPPER CABLES: DESIGN, MATERIALS AND PERFORMANCE I

*Chairperson:* Mr. Leo Chatter, DCM Industries, Inc., Union City, CA

Recent Advances in the Designs of Radiating (Leaky) Coaxial Cables—*S. Rampalli, H. R. Nudd*, Andrew Corporation, Orland Park, IL ..... 66

Advanced Pair Identification to Eliminate Interference in Data Services with Automatic Classification—*S. Asakawa, S. Matsushashi*, NTT Telecommunication Field Systems R&D Center, Ibaraki, Japan; and *T. Sakaguchi*, NTT Network Systems Development Center, Tokyo, Japan ..... 78

Template Testing at DS1 and DS3 Line Rates for Transmission Studies of Twisted Pair and Coaxial Cables—*W. Eng, Jr.*, Pacific Bell, San Ramon, CA ..... 86

An Evaluation of Measurement Techniques for Determining Copper Cable Structural Effects—*H. W. Friesen*, AT&T Bell Laboratories, Norcross, GA ..... 93

Development of Electronic Wire Harness for Mainframe (PTS-Cable)—*T. Yamamoto, S. Ashida, T. Hirahara, K. Ueda, H. Zako, Y. Nakagawa*, Fujikura Ltd., Chiba, Japan ..... 105

Prefabricated Cable Systems for the "Transrapid" Magnetic Levitation (MAGLEV) Train—*S. Richter*, Kabelmetal Electro GmbH, Nürnberg, Germany ..... 112

Characteristic Impedance Test Methods at Low Frequencies: UTP-STP Case—*R. D. Kenny, D. N. Koon*, Cooper Industries, Richmond, IN ..... 119

## TUESDAY AFTERNOON—1:00 PM—5:00 PM St. Louis Ballroom, Fourth Floor, Salon E

### SESSION IV: OPTICAL FIBER COATINGS

*Chairperson:* Dr. Raymond E. Jaeger, SpecTran Corporation, Sturbridge, MA

High-Speed Coating of Optical Fibers with UV Curable Resins—*K. Kobayashi, K. Tsurusaki, Y. Sato, S. Araki*, Fujikura Ltd., Sakura-Shi, Chiba, Japan ..... 126

Evaluation of Techniques for Determining the Extent of Cure of Optical Fiber Coatings—*R. A. Frantz*, Bellcore, Morristown, NJ; *I. M. Plitz*, Bellcore, Red Bank, NJ; and *S. R. Schmid*, DSM Desotech, Des Plaines, IL ..... 134

Effect of Chemical Environments on UV Curable Optical Fiber Coatings—*C. P. Chawla, D. M. Szum*, DSM Desotech Inc., Des Plaines, IL ..... 141

UV Resistance Property of UV-Cured Resin Coated Optical Fiber—*T. Hosoya, Y. Matsuda*, Sumitomo Electric Industries, Ltd., Sakae-ku, Yokohama, Japan ..... 149

Long-Term Reliability of a Carbon Coated Optical Fiber Cable— <i>T. Akiyama, Y. Kawada, H. Hiramatsu, K. Hirabayashi</i> , The Furukawa Electric Co., Ltd., Ichihara, Chiba, Japan.....	155
Carbon-Coated Polarization Maintaining Fibers for Compact Optical Gyro Module— <i>K. Hirabayashi, M. Nishimoto, Y. Matsuda</i> , The Furukawa Electric Co., Ltd., Ichihara, Chiba, Japan.....	161
Low Loss Metal-Coated Optical Fibers for Heat Resistant Cables— <i>M. Kuwabara, K. Kokura</i> , The Furukawa Electric Co., Ltd., Ichihara, Chiba, Japan; and <i>S. Ikegami</i> , The Kyowa Electric Wire Co., Ltd., Neyagawa, Osaka, Japan.....	167

**TUESDAY EVENING—6:30 PM—8:00 PM  
HOSPITALITY HOUR**

Promenade Ballroom, Second Floor

Admission by tickets issued to all registrants

**WEDNESDAY MORNING—8:30 AM—12:00 PM (NOON)  
St. Louis Ballroom, Fourth Floor, Salon C**

**SESSION V: FIBER OPTIC AERIAL CABLES**

*Chairperson:* Mr. Dieter Nordmann, Kabelmetal Electro, Hannover, Germany

Acrodynamic Force of Aerial Cables— <i>T. Kawanabe, S. Matsuhashi, I. Fujibayashi</i> , NTT Telecommunication Field Systems R&D Center, Ibaraki, Japan.....	172
Stress-Strain Characteristics of Self-Supporting Aerial Optical Fibre Cables— <i>S.-V. Chung, L. Ding</i> , MM Cables Communication Products, Clayton, Victoria, Australia.....	178
Short- and Long-Span, Self-Supporting, Non-Metallic Aerial Fiber Optic Cable— <i>S. Kloepper, B. Menze, J. Schulte, G. Maltz</i> , Kabelmetal Electro GmbH, Hannover, Germany; and <i>F. Teucher</i> , ABB Energiebau, Dresden, Germany.....	186
Portable Bypass Optical Cable System for Aerial Installation— <i>Y. Komaki</i> , Tohoku Electric Power Co., Inc., Aoba-ku, Sendai, Japan; <i>H. Tanji</i> , Sumitomo Electric Industries, Ltd., Yokohama, Japan; and <i>Y. Moriyo</i> , Kitanihon Electric Cable Co., Ltd., Taihaku-ku, Sendai, Japan.....	195
Self Supporting Optical Fibre Aerial Cable Constructions and Related Fibre Parameters for the Transmission at $\lambda = 1550$ nm— <i>H. G. Haag, G. F. Hög, M. Hoffart, R. G. Sommer, J. v. Wienskowski, P. E. Zamzow</i> , AEG Kabel AG, Mönchengladbach, Germany.....	206
Design and Operation of an Aerial Fiber-Optic Cable for Railroad Communications— <i>A. Bidingier</i> , German Federal Railroad, Frankfurt, Germany; and <i>W. Lynen, R. Ney</i> , Lynenwerk GmbH & Co. KG, Eschweiler, Germany.....	218
Development of Optical Composite Messenger Wire— <i>S. Shimizu, T. Akiyama, A. Otake</i> , The Furukawa Electric Co., Ltd., Ichihara, Chiba, Japan.....	227

**WEDNESDAY MORNING—8:30 AM—12:00 PM (NOON)  
St. Louis Ballroom, Fourth Floor, Salon D**

**SESSION VI: COPPER CABLES: DESIGN, MATERIALS & PERFORMANCE II**

*Chairperson:* Mr. Dave Fischer, Superior Cable Corporation, Atlanta, GA

New Expansion Technology of Insulated Core Without Chlorofluorocarbon (CFC)— <i>K. Sakamoto, M. Sugimura, I. Kobayashi, S. Hayashi</i> , The Furukawa Electric Co., Ltd., Ichihara, Chiba, Japan.....	234
Properties of Water Absorbent Gels Formulated for Use as Filling Compounds for Copper Telecommunications Cable and as Splice Case Encapsulants— <i>A. C. Levy, Alvin C. Levy &amp; Associates, Inc.</i> , Norcross, GA; <i>S. C. Welch</i> , California State University San Marcos, San Marcos, CA; and <i>P. V. Croft</i> , Waterguard Cable Products, Inc., Channelview, TX.....	242
Temperature Effect on High Frequency Data Transmission Through Plenum Wires— <i>L. M. Hore</i> , Bellcore, Morristown, NJ.....	251
New Extrusion Materials for Highly Expanded Insulations for Coaxial Cables— <i>Y. Morita, N. Matsuda, K. Suga, T. Takai</i> , Mitsubishi Cable Industries, Ltd., Itami-City, Japan.....	260
High Speed Transmission Coaxial Cable by a New Polyolefin Material— <i>T. Tanaka, S. Yamamoto</i> , The Furukawa Electric Co., Ltd., Ichihara, Chiba, Japan; and <i>M. Kado, R. Shimizu</i> , Ube Industries, Ltd., Ichihara, Chiba, Japan.....	270
Methods of Determining Thermal Stability of Polyolefin Insulations— <i>E. D. Nelson</i> , AT&T Bell Laboratories, Norcross, GA.....	277

**WEDNESDAY MORNING—8:30 AM—12:00 PM (NOON)  
St. Louis Ballroom, Fourth Floor, Salon E**

**SESSION VII: FIBER OPTIC SPLICES, CONNECTORS AND SWITCHES**

*Chairperson:* Mr. James J. Pickering, Neste Chemicals, Inc., New Brunswick, NJ

Nonblocking 100 x 100 Optomechanical Matrix Switch for Subscriber Networks— <i>T. Katagiri, Y. Koyamada, M. Tachikura, Y. Katsuyama</i> , NTT Telecommunication Field Systems R&D Center, Tokai, Ibaraki, Japan.....	285
A Low Loss Four-Fiber 1x2 Optical Switch— <i>Y. Nomura, K. Jimbo, H. Yokosuka</i> , Fujikura Ltd., Sakura-shi, Chiba, Japan.....	291
High-Speed, Low-Loss Connection Techniques for High-Count Pre-Connectorized Cables— <i>T. Haibara, S. Tomita, M. Matsumoto, T. Yabuta</i> , NTT Telecommunication Field Systems R&D Center, Tokai, Ibaraki, Japan.....	296
Automated Mounting of Connectors to Fiber Optic Cables— <i>J. Schulte</i> , Kabelmetal Electro GmbH, Hannover, Germany.....	303
Long-Term Reliability Assurance for Mass-Fusion Spliced Fiber Ribbon— <i>M. Hamada, I. Fujita, K. Osaka, Y. Asano</i> , Sumitomo Electric Industries, Ltd., Sakae-ku, Yokohama, Japan.....	309
New Compact, Easy to Operate Fiber Optic Connector Compatible with Existing Couplings— <i>J. C. Huber</i> , 3M Company, Austin, TX; and <i>N. H. Cubukciyan, A. Gennaro, J. T. Puchammer, M. T. Stender, T. Szostak</i> , 3M Company, Eatontown, NJ.....	316
High Performance and Low Cost Passive Optical Components for the Subscriber Loop— <i>G. Billet, H. B. Yin</i> , Radiall S.A., Viron, France; <i>J. Schulte</i> , Kabelmetal Electro GmbH, Stadthagen, Germany; <i>S. Crico</i> , SIRT SPA, Milano, Italy; <i>J. J. Crosnier, C. Lincot</i> , Souriau et Cie, Paray-Vieille-Poste, France; and <i>A. Fielding, J. Leach</i> , BNR Europe Ltd., Harlow-Essex, England.....	319

**AWARDS LUNCHEON  
12:00 NOON-2:00 PM  
Promenade Ballroom, Second Floor**

Admission by tickets issued to all registrants

**WEDNESDAY AFTERNOON—2:00 PM-3:45 PM  
St. Louis Ballroom, Fourth Floor, Salon C**

**SESSION VIII: FIBER OPTIC CABLE MATERIALS**

**Chairperson:** Mr. Rene G. Freeman, Union Carbide Chemicals & Plastic Company, Inc., Atlanta, GA

- The Use of Superabsorbent Materials in Optical Fiber Cable Design—*J. J. Sheu, C. J. Arroyo*, AT&T Bell Laboratories, Norcross, GA; and *W. J. Paucke*, AT&T Network Cable Systems, Norcross, GA..... 326
- The Reliability of Waterproof Optical Cable with a Plastic Sheath and Water Swellable Materials—*H. Sawano, Y. Sato, M. Miyamoto*, Fujikura Ltd., Sakura-shi, Chiba, Japan ..... 333
- Cable Polymer Reliability Testing—*P. E. Neveux, Jr., E. L. Buckland*, Sumitomo Electric Fiber Optics Corp., Research Triangle Park, NC ..... 341

**WEDNESDAY AFTERNOON—2:00 PM-3:45 PM  
St. Louis Ballroom, Fourth Floor, Salon D**

**SESSION IX: FIRE HAZARD CONSIDERATIONS**

**Chairperson:** Mr. David Fallowfield, Telus Corporation, Edmonton, Alberta, Canada

- Corrosivity Test Methods for Polymeric Materials—*S. L. Kessel*, Quantum Chemical Corporation, Cincinnati, OH; *J. G. Bennett, Jr.*, GE Plastics, Pittsfield, MA; and *C. E. Rogers*, Union Carbide Chemicals & Plastics Company, Inc., Weston Canal, NJ ..... 348
- Plenum Cable for the 90's—New Concerns for New Demands—*R. J. Rockosi*, Ausimont USA Inc., Morristown, NJ ..... 357
- Improved PVC Based Jacket Compound for Plenum Cable Applications—*P. W. Kroushi*, Cooper Industries, Belden Division, Richmond, IN ..... 361
- A Non-Metallic Water Proof Optical Fiber Cable with Halogen Free Fire Resistance—*H. Suzuki, Y. Sato, N. Sato*, Fujikura Ltd., Sakura-shi, Chiba, Japan ..... 365

**WEDNESDAY AFTERNOON—2:00 PM-3:45 PM  
St. Louis Ballroom, Fourth Floor, Salon E**

**SESSION X: POWER & INDUSTRIAL CABLES—MATERIALS AND PROCESSING**

**Chairperson:** Mr. Hans A. Mayer, Olex Cables Division of Pacific Dunlop Ltd., Melbourne, Australia

- Semi-Conductive and Halogen-Free Flame Retardant Cable Compounds Advanced Compounding Technologies—*P. Franz*, Buss AG, Basel, Switzerland; and *T. Kelly*, Buss (America) Inc., Bloomingdale, IL ..... 372
- Dry Cure Simulation with Shrinkback Minimizing for XLPE Insulation—*P. Huotari*, Nokia-Maillefer, Vantaa, Finland ..... 383

- Long-Term Service Degradation of Polyethylene and Rubber Insulated Power Cables—*J. H. Groeger, M. S. Mashikian*, University of Connecticut, Storrs, CT ..... 388
- Compounding New Specialty Linear Polymers for LV & MV Cables—*L. Spenadel*, Exxon Chemical Company, Baytown, TX; and *M. Hendewerk*, Exxon Chemical Company, Houston, TX ..... 397

**WEDNESDAY AFTERNOON—2:00 PM-3:45 PM  
St. Louis Ballroom, Fourth Floor, Salon F**

**SESSION XI: INTELLIGENT BUILDING COMMUNICATION SYSTEMS**

**Chairperson:** Mr. Manuel R. Santana, AT&T Bell Laboratories, Norcross, GA

**Moderator:** Mr. Jerry L. Hardiman, AT&T Bell Laboratories, Norcross, GA

**Invited Presentations**

- Meeting the Demands of Evolving Premises Networks—*D. R. Coover*, AT&T Network Cable Systems, Morristown, NJ ..... 404
- System Integrator's View of Intelligent Buildings—*R. Sumski*, Electronic Systems Associates, New York, NY ..... 410
- FDDI Technology and Implementation—*M. A. Botelho*, Corning Inc., Corning, NY ..... 413
- Cabling Systems for Industrial Applications—*T. K. Cahall*, AT&T Network Systems, Berkeley Heights, NJ ..... 417
- Overview of Wireless Building Systems for Voice and Data Communications—*J. Pryma*, Anixter Bros., Inc., Skokie, IL ..... 424

**WEDNESDAY AFTERNOON—3:30 PM-6:30 PM  
Promenade Ballroom, Second Floor, Salon E**

**SESSION XII: POSTER PAPERS**

**Chairpersons:** Mr. Reiner J. Gerdes, Consultant - Telecommunications, Atlanta, GA  
Dr. Ken-ichi Aihara, NTT America, Inc., Stamford, CT

- Wear Resistance of Optical Fiber Coatings Using a Modified Falling Sand Tester—*T. K. Vethanayagam, J. L. Smith, D. L. Taylor*, Corning Inc., Corning, NY .. 428
- Cost Effective Lightning Protection for Fiber Optic Based Communication Systems—*C. Davis*, Entergy Corporation, New Orleans, LA; and *R. B. Carpenter, Jr.*, Lightning Eliminators & Consultants, Inc., Boulder, CO ..... 433
- Dynamic Stress Analysis of Optical Fibers in Splice Closures in the Aerial Plant—*P. B. Grimado, R. A. Frantz*, Bellcore, Morristown, NJ ..... 438
- A New Fiber Optic Cable Assembly for HDTV Recording of Olympic Winter Games Ski Races—*P. Gaillard*, Alcatel Cable, Lyon, France; *J. Le Comte*, Alcatel Cable Systemes, Bezons, France; and *M. de Vecchis*, Alcatel Cable, Clichy, France ..... 444
- Design of Air Pressurized Optical Fiber Filled Tube Cable Minimizing the Pneumatic Resistance—*K. S. Ryoo, J. S. Lee, H. J. Kang*, Taihan Electric Wire Co., Ltd., Anyang City, Kyungki-Do, South Korea ..... 448

Chromatic Dispersion Dependence for Stress and Bending Loss by Phase Shift Methods—Y. T. Kim, K. I. Jun, Y. I. Lee, Taihan Electric Wire Co., Ltd., Anyang City, Kyungki-Do, South Korea.....	453	Evaluation of Antiballistic Sheathings for Aerial Fiber Cables—S. Camara, C. G. Cortines, Alcatel Standard Electrica, Maliaño, Cantabria, Spain.....	540
Long Length, High Speed Air Feeding of Optical Units by Pressurized Air—A. Sano, A. Mogi, M. Miyamoto, Fujikura Ltd., Sakura-shi, Chiba, Japan.....	457	Fiat Conductor Cable Systems for Transmission of Airbag Signals within the Steering Wheel of Cars—F. Schauer, Kabelmetal Electro GmbH, Nürnberg, Germany.....	545
Reducing Connecting Loss of Multiple Fiber Connectors by Expanding Mode Field Diameters—T. Ohmori, H. Hosoya, M. Akiyama, Fujikura Ltd., Sakura-shi, Chiba, Japan.....	463	A High Speed Coating Process for Optical Fibre Ribbon—J. Kohtala, J. Tanskanen, Nokia-Maillefer, Vantaa, Finland; and P. Fickling, M. Ericksson, Ericsson Cables, Hudiksvall, Sweden.....	550
An Evaluation of the Inter-Relationships Between Rheological Data of Filling Compounds and Fibre Optic Cable Performance—G. Morland, Pirelli Cables, Newport, Gwent, England; and D. Rees, G. White, The Polytechnic of Wales, Mid Glamorgan, England.....	469	Self-Supporting Optical Fibre Aerial Cable with Large Allowable Elongation—F. Krahn, N. Lenge, G. Weckerle, ANT Nachrichtentechnik GmbH, Backnang, Germany.....	556
Extending the Life of Polyethylene Wire Insulation—J. N. D'Amico, T. N. Bowmer, Bellcore, Red Bank, NJ.....	476	The Development and Testing of an Epoxiless Fiber Optic Connecting Systems—N. A. Lee, 3M Fiber Optics Laboratory, St. Paul, MN.....	561
Influence of the Quality of Plug-Jack Connect on the Transmission Characteristics—T-C. Chang, D-M. Fann, P-L. Yu, C-M. Hsiao, K-Y. Chen, Telecommunication Laboratories, Chung-Li, Taiwan, Republic of China.....	482	An Improved Measurement Technique for Determination of all Propagation Parameters in Balanced Cables—J-Y. Gobirot, K. Gautier, Acome, Mortain, France.....	565
Fiber Optic Copper Conductors Composite Cable for Submarine Sensors Systems—JP. Bonicel, P. F. Giraud, P. Gaillard, A. De Filippis, Alcatel Cable, Lynn, France.....	487	An Assessment of Measurement Error Associated with Clip-On Power Meters on Primary Coated Fibre—D. A. Ferguson, S. M. James, D. Drouet, S. M. Dennis, BT Labs, Ipswich, Suffolk, England.....	576
A Study on High Speed Telephone Wire Extrusion Line—Y. S. Kim, J. Y. Hah, Taihan Electric Wire Co., Ltd., Anyang City, Kyungki-Do, South Korea.....	492	The Effect of Proof Testing on the Minimum Strength of Optical Fiber—G. S. Glaesemann, Corning Incorporated, Corning, NY.....	582
Blown Fibre Junction Network Field Trial (13.6 km Spliceless Link)—N. J. Medlen, P. L. J. Frost, P. D. Jenkins, British Telecom Research Laboratories, Ipswich, England.....	499		
In Situ Characterization and Reliability Study of Coatings on Optical Fibers—Y-C. Lin, J-M. Hsiao, D-M. Fann, S-I. Wang, K-Y. Chen, Telecommunication Laboratories, Chung-Li, Taiwan, Republic of China.....	504		
Wear-Corrosion of Galvanized Steel and Stainless Steel Armor Wires in Submarine Cable—J. H. Wang, Y. T. Horng, D. M. Fann, K-Y. Chen, Telecommunication Laboratories, Chung-Li, Taiwan, Republic of China.....	511		
Analysis of Torsional Fiber Failures—L. A. Reith, J. P. Varachi, Jr., H. H. Yuce, Bellcore, Morristown, NJ.....	517		
Mobile Optical Cable Assembly on Transportable Rack—H. W. Brückner, G. Franken, D. S. Parmar, Kroschu-Kabelwerke, Kromberg & Schubert GmbH u. Co., Rhede, Germany.....	521		
How Improvement in Aramid Package Stability Can Lead to Higher Production Speed of Optical Fiber Cables—J. J. Bensink, A. L. van den Bos, AKZO Fibers, Arnhem, The Netherlands.....	526		
Design of an Articulated Repair Joint for a Light Weight, Open Fibre Optic Submarine Cable—E. Betten, M. Johansen, Alcatel Kabel Norge AS, Oslo, Norway.....	531		
Testing of Some Single Mode Fibre Cables and Ribbons by the $\alpha_{11}(\lambda)$ Method—T. Volatinen, A. Björk, Ericsson Cables, Hudiksvall, Sweden; and L. Stensland, Ericsson Cables and Networks, Sundbyberg, Sweden.....	535		
		<b>THURSDAY MORNING—8:30 AM—12:00 (NOON)</b> <b>St. Louis Ballroom, Fourth Floor, Salon C</b>	
		<b>SESSION XIII: FIBER OPTIC SUBMARINE CABLES</b>	
		<i>Chairperson:</i> Mr. Xavier Mann, Fitel General Corporation, Carrollton, GA	
		Deep Water Deployment of Armoured Optical Cable—D. I. Curtis, J. N. Russell, P. Worthington, STC Submarine Systems, Southampton, England.....	587
		The Impact of Submarine Networks on the Development of Fiber Optic Technologies—R. Jocteur, Alcatel Cable, Lyon, France; R. Boirat, Alcatel CIT, La Ville du Bois, France; and M. de Vecchis, Alcatel Cable, Clichy, France.....	596
		The First Commercial Introduction of Multi-fiber Optical Submarine Cable—M. Ohba, S. Ohshiro, T. Uenoya, NTT Network Systems Development Center, Tokyo, Japan; and O. Kawata, NTT General Planning Headquarters, Tokyo, Japan.....	602
		Optical Submarine Cables Without Submerged Repeaters for the Italian 565 Mbit/s Coastal Hopping Network ("Festoon Project")—A. Bolza, F. Magnani, E. Occhini, Pirelli Cavi SpA, Milan, Italy.....	612
		Design and Test Result of OS-560M Optical Submarine Cable, Repeater Housing and Coupling—Y. Noguchi, I. Marugome, N. Norimatsu, Y. Yamazaki, H. Yamamoto, Kokusai Denshin Denwa (KDD) Co., Ltd., Tokyo, Japan.....	620
		The World's First Commercial Submarine Cable with Hermetic Fibres—G. Berthelsen, J. S. Andreassen, T. Birkeland, G. Lang, K. Nyaas, Alcatel Kabel Norge AS, Oslo, Norway.....	628

Structure and High Voltage DC Behaviour of Submarine Cable Mouldings—*J. Bishop, I. Doble*, STC Submarine Systems, Southampton, England; *H. K. C. Chan, L. A. Dissado, S. V. Wolfe*, BNR Europe Ltd., Harlow, Essex, England; and *A. E. Davies*, University of Southampton, Southampton, England..... 634

**THURSDAY MORNING—8:30 AM–12:00 (NOON)**  
St. Louis Ballroom, Fourth Floor, Salon D

**SESSION XIV: ENVIRONMENTAL EFFECTS ON OPTICAL FIBERS AND CABLES**

*Chairperson:* Dr. Robert Baboian, Texas Instruments, Inc., Attleboro, MA

Hydrogen Sources for Signal Attenuation in Submarine Optical Fiber Cables and the Effect of Cable Design—*G. Schick, K. A. Tellefsen, A. J. Johnson, C. J. Wieczorek, R. M. Kanen*, Bellcore, Morristown, NJ..... 643

Hydrogen Effects in Optical Fiber Cables: A New Approach by Direct Pressure Measurement—*B. Missout*, Cables Pirelli, St. Maurice, France; and *A. Gouronnec*, France Telecom, CNET, Lannion, France..... 653

Examination of the Strength Characteristics, Hydrogen Permeation and Electrical Resistivity of the Carbon Coating of a Number of 'Hermetic' Optical Fibres—*E. S. R. Sikora, J. V. Wright, S. J. Pycock, M. J. Yates*, BT Laboratories, Ipswich, England..... 663

Stress-induced and Stress-free Ageing of Optical Fibres in Water—*W. Griffioen, W. Ahn, A. T. DeBoer, G. Segers*, PTT Research, Leidschendam, The Netherlands..... 673

Fatigue Behavior of Coated Optical Fibers in Water—*S. Okagawa, K. Maeda*, The Furukawa Electric Co., Ltd., Ichihara, Chiba, Japan..... 679

Mechanical Behavior of Hermetically Coated Optical Fiber—*H. H. Yuce, J. P. Varachi, Jr.*, Bellcore, Morristown, NJ; and *P. L. Key*, Bellcore, Red Bank, NJ..... 686

Long-Term Reliability of 900  $\mu$ m Buffered Fibers—*J. J. Farro, R. A. Frantz, J. P. Kilmer, C. J. Wieczorek, H. H. Yuce*, Bellcore, Morristown, NJ..... 693

**THURSDAY MORNING—8:30 AM–12:00 (NOON)**  
St. Louis Ballroom, Fourth Floor, Salon E

**SESSION XV: FIBER OPTIC MILITARY CABLES AND SPECIAL APPLICATIONS**

*Chairperson:* Mr. Michael A. DeLucia, David Taylor Research Center, Annapolis, MD

Effects of the Environment on an Unprotected Reel of Optical Fiber Cable—*H. H. Yuce, C. Wieczorek, A. DeVito, J. P. Varachi, Jr., J. P. Kilmer*, Bellcore, Morristown, NJ..... 700

Single-Fiber Cable Assemblies for Tactical Applications—*B. V. Darden, K. Katherisan, B. G. LeFevre*, AT&T Bell Laboratories, Norcross, GA; *J. B. Fluevog*, AT&T Network Cable Systems, Norcross, GA; and *V. E. Kalomiris*, U.S. Army CECOM, Ft. Monmouth, NJ..... 707

Single Fiber Tactical Cables with Multiple Fiber Designs—*J. B. Fluevog, W. H. Ficke*, AT&T Network Cable Systems, Norcross, GA; and *W. S. Liu, K. Kathiresan*, AT&T Bell Laboratories, Norcross, GA... 714

A Family of Non-Halogen Thermoplastic Fiber-Optic Cables for Shipboard Application—*K. Kathiresan, C. J. Arroyo, S. P. Gentry*, AT&T Bell Laboratories, Norcross, GA; and *J. B. Fluevog, L. R. Sherrets*, AT&T Network Cable Systems, Norcross, GA..... 723

Fiber Optics Assembly as Light Signal Concentrator in Indoor Diffuse Infrared Communications System—*C. J. Georgopoulos*, University of Patras, Greece; and *G. N. Bakalidis*, University of Thrace, Xanthi, Greece..... 733

External Photoelastic Polarization Modulation for Optical Fiber Data Transmission—*H. Nimura, A. Fujisaki*, The Furukawa Electric Co., Ltd., Ichihara, Chiba, Japan; and *H. Fudou*, Kansai Electric Power Co., Ltd., Kita Osaka, Japan..... 738

Measurements of Low Hydrogen Levels in Installed Open Fiberoptic Submarine Cables—*S. Hopland*, Norwegian Telecom, Oslo, Norway..... 742

**THURSDAY AFTERNOON—1:00 PM–5:00 PM**  
St. Louis Ballroom, Fourth Floor, Salon C

**SESSION XVI: FIBER OPTIC CABLE COMPONENTS, INSTALLATION & PRACTICES**

*Chairperson:* Mr. Frank Short, B.I.C.C. Cables Limited, Helsby, Warrington, Cheshire, England

O.F. Ribbon Cable System Technology: The Italian Experience—*F. Esposto, F. Montalti, F. Nanni*, SIP-DG, Rome, Italy..... 749

A Radically New, Ultra-High-Speed Method for the Installation of Cables in Ducts—*W. Griffioen, G. J. Prins*, PTT Research, AK Leidschendam, The Netherlands..... 758

Environmental Challenges Facing the Installation of the Second Perth to Adelaide Optical Fibre Cable Route—*G. Consiglio, J. Groom, E. Johansen, L. Kiss, P. Latoszynski*, Telecom Australia, Melbourne, Victoria, Australia..... 766

Optical Fiber Cable Transfer Splicing Machine—*Y. Tamaki, H. Katayose, H. Yokosuka*, Fujikura Ltd., Sakura-shi, Chiba, Japan..... 773

A New Series of Cable Accessories for Optical Fiber Subscriber Loop Networks and Premises Wiring Systems—*R. Biazzi, S. Crico*, SIRT SpA, Milano, Italy..... 779

Cable Transfer and Supervisory System for Trunk Optical Fiber Cables—*H. Matsumoto, K. Sato, T. Uenoya*, NTT Network Systems Development Center, Tokyo, Japan; and *Y. Yokoo*, NTT Telecommunications Software Headquarters, Kanagawa, Japan..... 787

A Real-Time Configuration Management System for Line Facilities in Optical Fiber Networks—*K. Yamashita, F. Ohtsuki, M. Tateda, Y. Koyamada*, NTT Telecommunication Field Systems R&D Center, Tokai, Ibaraki, Japan..... 793

**THURSDAY AFTERNOON—1:00 PM–5:00 PM**  
**St. Louis Ballroom, Fourth Floor, Salon D**

**SESSION XVII: MANUFACTURING & TESTING OF OPTICAL FIBERS, CABLES & COMPONENTS**

**Chairperson:** Mr. Manuel R. Santana, AT&T Bell Laboratories, Norcross, GA

High Potentialities in Fiber Preform Manufacturing Using Very Large and Precisely Bored Silica Ingots— <i>D. Pavy, M. Moisan, I. Hardy, P. Grosso</i> , Centre National d'Etudes des Telecommunications (CNET), Lannion, France; and <i>C. Le Sergent, D. Tregoeat</i> , Alcatel, Marcoussis, France .....	800
A Profiling System for Large Optical Fiber Preforms— <i>T. Abiru, M. Nakayama, R. Yamauchi</i> , Fujikura Ltd., Sakura-shi, Chiba, Japan .....	806
Relaxation of Internal Stress in Fully-Fluorine-Doped Single-Mode Fibers— <i>K. Maeda, S. Okagawa, H. Ohnuma</i> , The Furukawa Electric Co., Ltd., Ichihara, Chiba, Japan .....	810
Coating Stripping Force Measurement: A New and Quick Test Method for the Determination of the Degree of Curing for Optical Fibre Coating— <i>H. Marsman, R. Wauben, G. Kuyt</i> , Philips Optical Fibre B.V., Eindhoven, The Netherlands .....	815
Optical Fiber Failure Probability Predictions from Long-Length Strength Distributions— <i>G. S. Glaesemann</i> , Corning Incorporated, Corning, NY .....	819
Laboratory Testing and Failure Analysis of Fiber Interconnections— <i>T. Wei</i> , GTE Laboratories Inc., Waltham, MA; and <i>H. H. Yuce</i> , Bellcore, Morristown, NJ .....	826
Computerized Acceptance Test on Field-Installed Optical Fibre Cables: Applications and Results— <i>H. Middel, G. Schweiger</i> , Deutsche Bundespost TELEKOM, Darmstadt, Germany .....	830

**THURSDAY AFTERNOON—1:00 PM–5:00 PM**  
**St. Louis Ballroom, Fourth Floor, Salon E**

**SESSION XVIII: IMPLEMENTATION OF "FIBER DISTRIBUTED DATA INTERFACE" (FDDI)**

**Chairperson:** Mr. Homer Vela, AT&T Network Cable Systems, Phoenix, AZ

**Moderator:** Mr. Larry G. Romig, Building Industry Consulting Service International (BICSI), University of South Florida, Tampa, FL

**Invited Presentations**

Planning for the Future: The Importance of a Structured Fiber Cabling Strategy— <i>B. Hatfield, M. Coden, B. Ramsey</i> , Codenoll Technology Corp., Yonkers, NY .....	839
Installed Cost of Fiber Optic Connectors on Various Fiber Sizes— <i>J. C. Huber</i> , 3M Company, Austin, TX .....	848
FDDI Finds Fat Fiber— <i>R. A. Montgelas</i> , Ensign-Bickford Optics Co., Avon, CT .....	853
Comparison of Twisted Wire Pair and Optical Fibers for FDDI— <i>D. A. Krohn</i> , 3M Specialty Optical Fibers, West Haven, CT .....	861

## **GOLD SUSTAINING CONTRIBUTORS**

**LaserMike Inc.**  
6060 Executive Blvd.  
Dayton, OH 45424

**Lindsay & Williams, Ltd.**  
Ogden Lane Works  
Columbine Street  
Manchester M11 2LH England

**Mohawk Wire & Cable**  
9 Mohawk Drive  
Leominster, MA 01453

**NEPTCO, Inc.**  
Box 2323, 30 Hamlet St.  
Pawtucket, RI 02861-0323

**Nippon Telegraph and  
Telephone Corporation**  
Tokai, Ibaraki, 319-11, Japan

**Nokia-Mallefer, Inc.**  
749 New Ludlow Road  
South Hadley, MA 01075

**Northern Telecom**  
150 Montreal-Toronto Blvd.  
Lachine, Quebec H8S 1B6 Canada

**NTT America, Inc.**  
One Landmark Square, Rm 700  
Stamford, CT 06901

**Olex Cables**  
A Division of Pacific Dunlop  
207 Sunshine Road  
Tottenham, 3012  
Melbourne, Australia

**Optical Fibres**  
Second Avenue  
Deeside Industrial Park  
Deeside, Clwyd  
Great Britain, CH5 2NX

**Owens-Corning Fiberglas Corporation**  
Fiberglas Tower, T/8  
Toledo, OH 43659

**PENRECO**  
R.D. 2 - Box 1  
Karns City, PA 16041

**Quantum Chemical Corp.**  
11500 Northlake Drive  
Cincinnati, OH 45249

**Siecor Corporation**  
489 Siecor Park  
PO Box 489  
Hickory, NC 28603-0489

**SpecTran Corporation**  
50 Hall Road  
Sturbridge, MA 01566

**Sumitomo Electric U.S.A., Inc.**  
21221 S. Western Ave., Suite 200  
Torrance, CA 90501

**Teknor Apex Company**  
505 Central Avenue  
Pawtucket, RI 02861

**The Furukawa Electric Company, Ltd.**  
2-6-1 Marunouchi, Chiyoda-ku  
Tokyo 100, Japan

**The Stewart Group Ltd.**  
259 Steelcase Road West  
Markham, Ontario  
Canada L3R 2P6

**UBE Industries (America), Inc.**  
666 Fifth Ave., 14th Floor  
New York, NY 10103

**Union Carbide Chemical & Plastics Co.**  
39 Old Ridgebury Rd.  
Danbury, CT 06817

**VISTA Chemical Company**  
900 Threadneedle  
Houston, TX 77079

**WaterGuard Cable Products, Inc.**  
P.O. Box 1079  
16023 1-10 East, Suite 30  
Channelview, Texas 77530

**Weber & Scher Mfg. Co., Inc.**  
263 Sussex Avenue  
Newark, NJ 07017

**Witco Corporation**  
520 Madison Avenue  
New York, NY 10022-4236

## **SILVER SUSTAINING CONTRIBUTORS**

**ACOME**

50140 Mortain, France

**AEG KABEL Aktiengesellschaft**  
Monchengladbach, Germany

**Alcatel—Canada Wire**  
Winnipeg, Manitoba, Canada

**AT Plastics Inc.**  
Brampton, Ontario, Canada

**Breen Color Concentrates, Inc.**  
Lambertville, NJ 08530-3411

**Cooper Industries—Belden Division**  
Richmond, IN 47375

**Dow Chemical U.S.A.**  
Granville, OH 43023

**DuPont of Canada, Plastics Division**  
Mississauga, Ontario, Canada

**Dussek Campbell**  
Auburn, N.S.W., 2144 Australia

**Dussek Campbell, Ltd.**  
Belleville, Ontario, K8N 5A5 Canada

**Ericsson Cables AB**  
Hudiksvall, Sweden

**Essex Group, Inc.**  
Decatur, IL 62526

**FITEL General, Inc.**  
Carrollton, GA 30117

**General Cable**  
South Plainfield, NJ 07080

**Huls AG**  
Marl, Germany

**Kabelmetal Electro North America Inc.**  
Larchmont, NY 10538

**Kroschu-Kabelwerke**  
**Kromberg & Schubert GmbH u. Co**  
Wuppertal, Germany

**LONZA Inc.**  
Fair Lawn, NJ 07410

**MM Cables Communications Products**  
Clayton, Victoria, Australia 3168

**NKF Kabel B.V.**  
AB Waddinxveen, Netherlands

**RXS Schrumpftechnik-Garnituren GmbH**  
Hagen, Germany

**Siemens AG, NKE**  
Munich, Germany

**Solex Division/J.M. Huber Corp.**  
Norcross, GA 30071

**Sumitomo Electric Industries, Ltd.**  
Yokohama, Japan

**Superior Teletec**  
Atlanta, GA 30339

**Televerket, Nkk**  
S-123 86 Farsta, Sweden



## OPENING SPEAKERS



James J. Pickering  
Neste Chemicals, Inc.  
New Brunswick, New Jersey

Mr. Pickering is a native of New Jersey where he completed his studies at Rutgers University. Jim has worked in the Polyolefins Industry for thirty years in Research & Development, Sales and Marketing of Polyolefin Film Resin, Molding Products, and Wire & Cable materials. Presently he is Director of Sales and Marketing for Neste Chemicals, Inc. Mr. Pickering is a member of the New York Rubber Group, the Wire Association, ASTM, and the NFPA. He is chairman of Subcommittee 8 in the Insulated Conductors Committee of the Power Engineering Society of IEEE, and is Chairman of the International Wire & Cable Symposium Committee. Jim and his wife Lorraine live in Long Valley, New Jersey with their four children.



Joseph J. Pucilowski, Jr.  
Director, CECOM Center for C3 Systems  
U.S. Army Communications-Electronics  
Command and Fort Monmouth  
Fort Monmouth, NJ

Mr. Joseph J. Pucilowski, Jr. was appointed as Director of the Center for Command, Control and Communications (C3) Systems, U.S. Army CECOM, in August 1990.

He has command responsibility for formulating, coordinating, managing and implementing internal and external research, development and engineering programs to fill the Army's tactical C3 needs, while also providing full technical support to U.S. Army Program Executive Officers and Project Managers in C3.

He was awarded a Bachelor of Arts in Physics, with a minor in Mathematics from Rutgers University, and a Master of Science in Electrical Engineering from Fairleigh Dickinson University. He was appointed by the Secretary of the Army to the Senior Executive Service in November 1986.

Mr. Pucilowski was appointed Acting Deputy Chief of Staff for Concurrent Engineering at the U.S. Army Materiel Command Headquarters from February 1991 to September 1991. In that capacity he had command responsibility for Concurrent Engineering planning and implementation as well as test and evaluation, production base planning and product assurance for AMC.

Mr. Pucilowski began his government career in 1963 as a physicist for the U.S. Atomic Energy Commission. He transferred to Fort Monmouth in 1967 and has held various technical and managerial assignments at Fort Monmouth to include: Director of the CECOM Product Assurance and Test Directorate; Associate Director for Research & Technology, CECOM RD&E Center, Associate Director for Information Processing Technology, Center for COMM/ADP and Deputy Director and Acting Director of the Center for Tactical Computer Systems.

He has served as the NATO U.S. Dept. of Defense (DOD) Representative to SubGroup IX, Defense Equipment Reliability and Maintainability (R&M) Assurance and as a member of the American British Canadian Australian (ABCA) Committee on R&M.

Mr. Pucilowski served as President of the Armed Forces Communications-Electronics Association (AFCEA) Fort Monmouth Chapter and as the Chairman of the 14th and 17th Annual AFCEA Symposia. He also serves as an Honorary Advisor Member of the Board of AUSA. He has

been a member of the NJ Dept of Higher Education's Panel on Faculty Development in Telecommunications and Army Member of the Joint Directors of Laboratories Subcommittee on C3. He has published or presented thirty-five technical papers.

A native of New Jersey, Mr. Pucilowski currently resides in Howell with his wife Maryann. They have six children--Adam, Joseph, Linda Ann, Mary, Kristin and Francine.

## TUTORIAL SPEAKERS



Manuel R. Santana  
AT&T Bell Laboratories  
Norcross, Georgia

Manuel R. Santana is Supervisor of the Exploratory and Military Lightguide Cable Group with research and development responsibility for fiber-optic cables used in the outside plant and in military applications. He has been involved in research and product development in fiber-optic cable and he currently has been awarded eight patents has twenty-four publications to his credit.

Mr. Santana joined AT&T Bell Laboratories in 1970, having received his B.S.E.E. from the University of Hartford, and M.S.E.E. from Georgia Institute of Technology. He is a senior member of the IEEE.



Dr. Eckart Gleissner  
ANT Backnang (Bosch Group)  
Backnang, Germany

Dr. Eckart Gleissner was born in 1936 in Germany. He received his Dipl.-Ing. degree in 1961 and his Dr.-Ing. degree in 1971 from the Technische Universitat Munchen.

In 1961 he joined the former AEG Telefunken AG in Backnang and was engaged in the computer aided development of circuits and systems for telecommunication networks. Since 1975, in addition to his work in the company, he gives lectures on "Computer aided design of electrical networks" at the University of Stuttgart.

In 1983 he joined the telecommunication cable systems division of ANT Nachrichtentechnik in Backnang, a company belonging to the Bosch group, where at first he was responsible for the development. Since 1988 he is the head of the division, whose product scope includes the area of electronic traffic guide- and control-systems.

He is a member of the German Informationstechnische Gesellschaft (ITG).



Dr. Brian T. Barcelo  
Marketing Director  
AT&T Network Systems  
Holmdel, New Jersey

Brian T. Barcelo, a native of Louisiana, was graduated from Tulane University with a B.S. degree in Mechanical Engineering in 1965. He continued his education at the California Institute of Technology in Pasadena, California, receiving M.S. and Ph.D. degrees in Aeronautics in 1966 and 1971, respectively.

Dr. Barcelo has been a part of the AT&T family since 1971, when he joined the staff of Western Electric at the Engineering Research Center in Princeton. His career has included engineering research, editor of The Western Electric Engineer Magazine, switching product

management, and international market planning. At the present time, he is the Marketing Director for Network Systems, responsible for identifying network products and service opportunities in the telecommunications marketplace.

Dr. Barcelo has discussed AT&T Network Systems business opportunities in forums around the world. Currently, he is actively involved in investigating opportunities for bringing new technology to the customer.

Dr. Barcelo became involved in IVHS in 1990 while investigating opportunities for bringing new technologies to the customer. As part of this effort, he is responsible for AT&T Network System's study of automatic toll collection systems, video motion detectors, driver information systems, traffic management architectures and the IVHS network infrastructure.

Dr. Barcelo is a professional engineer in the state of Louisiana and is a member of the Louisiana Engineering Society and the ASME. He is on the Engineering Advisory Board of Tulane University and the Mechanical Engineering Advisory Board of Mercer County Community College and is the president of the South Brunswick Athletic Association.



Richard J. Weiland  
Vice President  
SEI Information Technology  
Chicago, IL

Mr. Richard J. Weiland is currently Corporate Vice President of SEI Information Technology. SEI is a leading national software consulting organization specializing in system planning and integration, and the development of complex application software products for clients nationwide.

Mr. Weiland is responsible for the support of new technology ventures and for internal coordination. In addition to these corporate management responsibilities, Mr. Weiland is a regular participant in major client studies, with emphasis on conceptual design, requirements analysis, and system planning.

In 1985, Mr. Weiland participated in the founding and planning of Navigation Technologies Corp., an SEI technology venture, and has served as a Director of NavTech since its formation. NavTech develops and markets navigable electronic street map databases to support vehicle route guidance systems and a variety of related products and services.

Mr. Weiland is an internationally recognized author and lecturer in Structured System Development, and has presented professional development seminars on this subject throughout the U.S. and in Australia, Brazil, Canada, and Great Britain. He is the Author of a book, "The Programmer's" Craft, published by Reston in 1983, and a number of papers.

Mr. Weiland is a member of the IEEE Computer Society, the Association for Computing Machinery, and the Society of Automotive Engineers. Mr. Weiland served as editor of IVHS Interchange, newsletter of the Task Force on Advanced Vehicle & Highway Technologies of the Transportation Research Board (National Research Council). He is SEI's representative to the Intelligent Vehicle-Highway Society of America (IVHS America), a utilized advisory body to the U.S. Dept. of Transportation. Mr. Weiland serves on IVHS America's Coordinating Council and is Chairman of its Committee on Standards & Protocols.

Prior to his association with SEI, Mr. Weiland was an Instructor of Computer Science at the Illinois Institute of Technology and a research and teaching assistant at the University of Chicago.

Mr. Weiland holds a BS in Mathematics from the University of Michigan, and an MS in Information Science and an MBA from the University of Chicago.



Dr. James Costantino  
Executive Director  
IVHS America  
Washington, DC

Dr. Costantino is a Director of the National Society of Professional Engineers, a Fellow of the American Association for the Advancement of Science, and other professional, technical, and community service organizations.

Dr. James Costantino is the first Executive Director of the Intelligent Vehicle Highway Society of America (IVHS America), an educational and scientific association established to coordinate the use of advanced computer and communications technology for so-called "smart" car and highways. Dr. Costantino has more than 20 years experience managing transportation research programs for government, industry and academia.

Before coming to IVHS America, Dr. Costantino was Professor of Transportation Systems in the School of Information Technology and Engineering at George Mason University. His teaching and research activities were related to multimodal transportation systems, systems integration, and strategic technology planning.

Previously, Dr. Costantino was Executive Vice President of the nonprofit Free Congress Research Foundation; Managing Partner of the Charles River Group; and Executive Vice President and Chief Operating Officer of JAYCOR, Inc.

In the Federal government, Dr. Costantino was with the Federal Aviation Administration, National Aeronautics and Space Administration and the Department of Transportation. In DOT, he worked as the U.S. Transportation Secretary's Representative to state and local governments. His most recent Federal position, from 1976 to 1984, was as the Director of the Transportation Systems Center in Cambridge, where DOT conducts a \$150 million multimodal transportation research program.



Julius Hunter  
News 4 St. Louis Veteran Anchorman  
4KMOV, St. Louis, MO

Award-winning Anchor Julius Hunter joined Channel 4 in May, 1974. He currently co-anchors "News 4 St. Louis" at 5 and 10PM weekdays with veteran Larry Connors. Mr. Hunter is a native of St. Louis, which gives him special expertise in gathering and delivering the latest news of the day.

Mr. Hunter's news assignments have taken him across the state, region, country, and world. He was the only St. Louis reporter dispatched to Rome twice in 1978, following the deaths of Popes Paul VI and John Paul I. From Rome, Mr. Hunter sent daily video tape reports via satellite back to St. Louis. In 1979, he accompanied Pope John Paul II on his historic six-city visit to America, and again in 1987 during the Pope's coast to coast American tour.

Mr. Hunter is the only reporter in St. Louis and one of the few journalists in the nation who has conducted exclusive television interviews with three U.S. Presidents. President Ford was a guest on Mr. Hunter's half-hour "Newsmakers" program on September 12, 1975. Mr. Hunter interviewed President Jimmy Carter on August 23, 1979 while the President cruised down the Mississippi River on the "Delta Queen." Mr. Hunter, thus, became the only reporter in the nation to interview President Carter on the President's entire cruise. When President Ronald Reagan came to St. Louis on July 22, 1982, Mr. Hunter was granted a twenty-minute exclusive television interview

with the President. It was from that interview that Mr. Hunter became the first reporter in the nation to learn of, and report, the resignation of Murray Wiedenbaum, who at that time was the Chairman of the Council of Economic Advisors.

In April, 1981, Mr. Hunter joined a small, but distinguished group of journalists, when he was named a recipient of the Missouri Medal of Honor from Missouri University's School of Journalism. Mr. Hunter was cited for "outstanding service to journalism and to the people of St. Louis as a reporter, television news anchor, author, and teacher."

In April, 1984, Mr. Hunter was selected as the recipient of the American Jewish Committee's "Micah Award" for his outstanding humanitarian service to the St. Louis community.

Mr. Hunter also holds five St. Louis Emmy Awards to attest to his professionalism. His five-part series, "Cults: Heaven or Hell?" won the national Religion In Media Award for 1980. And, in 1983, Mr. Hunter's in-depth

report on the insanity plea won an award from the American Bar Association. In 1990, Mr. Hunter's five-part series, "Dance or Deceit?" won the first place award for Investigative Reporting from the Missouri Broadcasters' Association.

Mr. Hunter was honored by The Saint Louis Ambassadors who presented him with their 1987 "Spirit of St. Louis Award" for his "...outstanding dedication and service to the community." He is also the recipient of the National Conference of Christians and Jews (NCCJ) Brotherhood/Sisterhood Award for his "...contributions to good human relations and to improving the quality of life in St. Louis."

Beginning his broadcast career in 1970, Mr. Hunter was a news reporter, weekend anchorman, and weekend news director for KSD-TV. From 1969 to 1970, he was an administrator at Washington University. From 1968 to 1969, he was a copywriter for Foote, Cone & Belding, an advertising agency in Chicago, and before that, he taught school in St. Louis. Mr. Hunter is a 1965 graduate of Harris-Stowe State College.

Mr. Hunter has served on the adjunct faculties of Maryville College, St. Louis University, Harris-Stowe State College, and Washington University, as an instructor in Communications and Broadcast Journalism. He has also conducted a number of seminars in the area dealing with television news and its impact on society. In his spare time, Hunter is a popular luncheon and dinner speaker who delivers about 60 addresses a year.

He is the author of the witty children's book Absurd Alphabettime Stories, Bethany Press, St. Louis, and is co-author of a college textbook called Broadcast News: The Inside Out, C.V. Mosby Company, St. Louis. Mr. Hunter is also author of Kingsbury Place: The First 200 Years, and the recently published Westmorland and Portland Places - 1888-1988. This book hit the bestseller list in St. Louis and remained number one for 11 weeks. Because of the overwhelming national response, the book went into a second printing after six months on the bookshelves.

Among his many avocations, Mr. Hunter was also a columnist for the St. Louis Post Dispatch for a year and a half. The column, titled "Past Times", featured interesting tidbits about St. Louis' rich and colorful history.

Mr. Hunter was a two-term member of the Board of Directors of the Missouri Historical Society. He currently serves on the Directors of the St. Louis Backstoppers. Backstoppers gives moral and financial support to the spouses and children of police officers and firefighters who are injured or killed in the line of duty.

St. Louis Magazine selected Julius Hunter as St. Louis' best Television News Anchorman in its July, 1982 edition. Mr. Hunter was chosen as the subject of the cover of the July issue of that magazine. A 1982 Post-Dispatch poll of its readers found Hunter to be the city's most popular television anchorperson. And an April, 1984 Globe Democrat article singled Mr. Hunter out as "The Real St. Louis Anchorman." Fitting honors for a "consummate pro."

# Preliminary Research into Ultra High Density and High Count Optical Fiber Cables

Shigeru TOMITA, Michito MATSUMOTO, Tetsuro YABUTA and Takuya UENOYA\*

NTT Field Systems Research and Development Center  
Tokai, Naka, Ibaraki, 319-11 JAPAN

\*NTT Network Systems Development Center  
Uchisaiwaicho, Chiyoda, Tokyo, 100 JAPAN

## Abstract

In order to construct optical subscriber cable networks for FTTH(Fiber To The Home), very high count optical fiber cables are required. However, if conventional cable design is used the cable is very large. We have designed a new cable called U-groove Unit Cable.

In this paper, first, we study subscriber cable network to determine the requirements that must be satisfied when the high count cable is installed. Second, we describe cable size requirements which are dependent on the size of outside plants and installation tools. Third, we study cable design method. Finally we clarify the requirements for optical fibers and ribbons.

## 1. Introduction

Currently, telephone companies are focusing their attention on ways to construct optical subscriber networks. Most telephone companies have selected FTTC(Fiber To The Curb) as a first step in the construction of FTTH networks, in order to minimize the initial financial outlay.

However, in Japan, NTT is discussing an FTTH construction program called OFL21[1]. This program will be completed in 2015. The reasons why the FTTH program will be started this early are, (1) project scale is very big, (2) development of new technologies including very high count optical fiber cable are required, (3) development and construction resources are limited.

Therefore, very high count optical fiber cable should be developed early, in order to construct subscriber networks that are all optical fiber. NTT has already developed a 1000-fiber cable which is 40mm in diameter. But, its fiber count is too small to provide a fiber to each subscriber, because 3600-pair cables are used in copper subscriber cable networks. Therefore, we designed a new cable, for application to future optical networks.

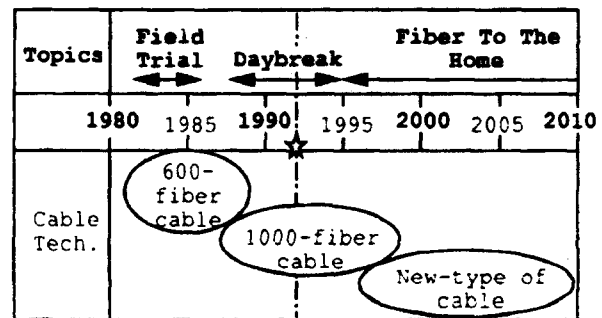


Figure 1 NTT Optical Subscriber Cables Past, Present and Future

## 2.1 Past Cable Design

NTT has been studying optical fiber cables for subscriber use since the middle of the 1980's. Figure 2 shows the first developed cable, which held 600 Graded-Index profile fibers[2]. This cable had a "ribbons in tubes" design. Each tube had four 5-fiber ribbons. Tubes were stranded around a central member in two layers. This type of cable was used in the first ISDN field trial in Tokyo. However, because of the following problems, this design is no longer used.

- (1) Loss increase at low-temperature
- (2) Difficulty in extracting fibers at points along the tubes
- (3) Low fiber density

## 2.2 Present cable design

To solve the above problems, we developed a new cable design called "slotted rod cable". In this cable design, ribbons are tightly inserted in rectangular slots helically shaped on a polyethylene rod.



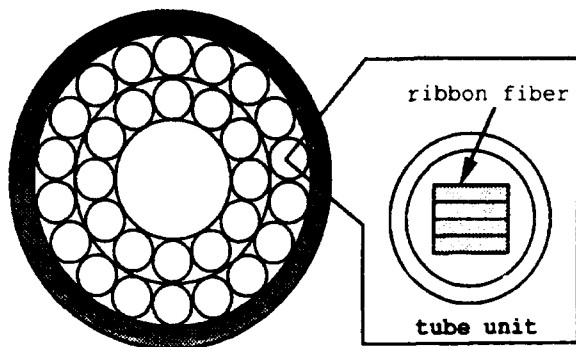


Figure 2 Loose tube cable structure

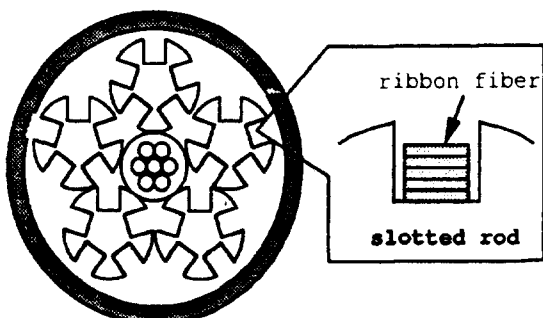


Figure 3 Slotted rod cable structure

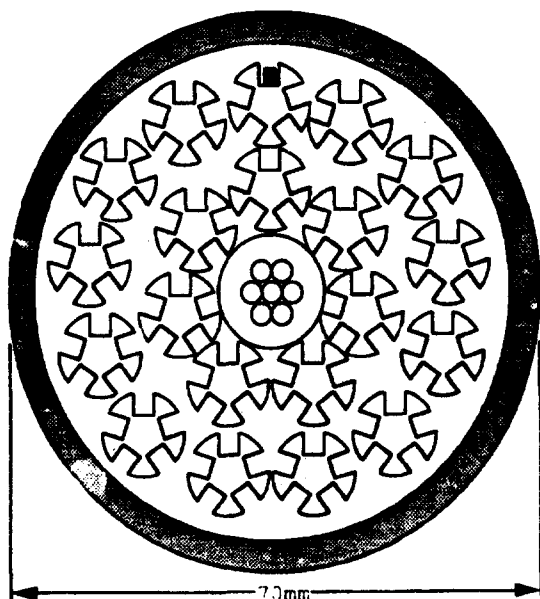


Figure 4 4000-fiber cable  
with 8-fiber ribbons  
(slotted rod type)

And five or six rods are stranded around a central member. The advantages of this design are as follows.

- (1) Compact (yet it protects fiber ribbons from lateral force)
- (2) Precise fiber strain control (to estimate the long term reliability of the fiber)

Figure 3 shows a cross-section of a 1000-Single-Mode fiber cable, using 8-fiber ribbons[3]. Each slot holds a five 8-fiber ribbons, and each rod has five slots. So, each rod holds 200 fibers.

NTT introduced this cable in 1988 for commercial optical subscriber services, in Tokyo and other metropolitan areas.

Its fiber count, however, is too small to provide a fiber to each subscriber in an future FTH network. If this structure is used with the same fiber ribbon to form a 4000-fiber cable, the cable diameter becomes very large as shown in figure 4. This causes installation work difficulties, fiber reliability problems and installation length limit in the short range.

Therefore, we began to study a new cable design and a new fiber ribbon.

### 3. Subscriber cable network for FTH

A long-term strategy is required to replace copper subscriber cable networks with optical subscriber networks. So, as a first step, we studied optical subscriber cable networks for FTH. Our future network plan is shown in figure 5. We will form this network in a Single-Star configuration, because the Passive Double Star configuration presents problems with regard to coupler transmission loss, fiber testing and network operation.

In our future network plan, an optical subscriber network consists of a loop configuration cable network and fixed distribution areas. A fixed number of cores are applied to each fixed distribution area. In a conventional copper subscriber network, the number of cores is 600. The number of cores for optical subscriber network, has not yet been determined. But, as the transmission loss of optical fiber cable is much lower than that of copper cable, the fixed distribution area will increase in size which will mean an increase the number of cores. Those cores are served, at a feeder point, from a loop cable installed from and back to the same telephone office through fixed distribution areas. In the fixed distribution area, each subscriber is wired to the nearest wiring box on a distribution cable.

High-count cables are essential in the loop configuration cable network. In order to make construction work easier, direct connection between two feeder points or between a telephone office and a feeder point is required. To install long cables

is needed to solve this problem. Below we discuss the conditions for long cable installation.

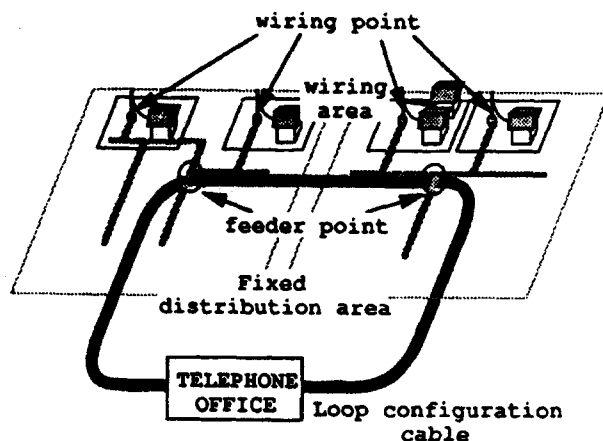


Figure 5 Optical Subscriber Cable Network

#### 4. Requirements

##### 4.1 Cable Dimensions

There are some cable diameter and weight requirements which are related to installation conditions. In NTT's subscriber loop, a cable should satisfy the following.

(1) Installation into a conventional conduit.

The inner diameter of a conventional conduit is 75mm. So, the cable diameter should be less than 75mm and the pulling head including connector protection should also be less than this value.

(2) Use of conventional installation tools.

Current installation tools were designed for conventional cables which have a maximum diameter of 40mm. If these tools are to be used, the cable diameter should be equal to or less than 40mm. The available installation force for these tools is 800kgf.

(3) Maximum length of 1500m.

The mean optical cable length in NTT's subscriber loops is about 700m. The maximum cable length depends on installation conditions. At present, optical cables are installed in metropolitan area. In rural area, distance between feeder points is longer than metropolitan area's. Considering increase of installation length, we think that double the present mean length is required.

There are two problems regarding 1500m installation. The first is cable reel size, and the second is installation force. The cable diameter should be equal to or less than 35mm in order to wind 1500m of cable on to the largest conventional cable reel.

The installation force should be less than 800kgf in accordance with (2) above. Where the friction coefficient between the cable and the inner wall of the conduit is 0.5, the cable weight should be less than 1.06kg/m. We also have to consider the friction increase due to reduced clearance between the cable and the inner wall of the conduit.

Figure 6 shows cable size and weight requirements based on above the conditions. 1... Conduit inner diameter, 2... Maximum diameter for conventional installation tools, 3... Maximum length for conventional cable reel use, 4... Installation force, 5... Friction increase between conduit and cable.

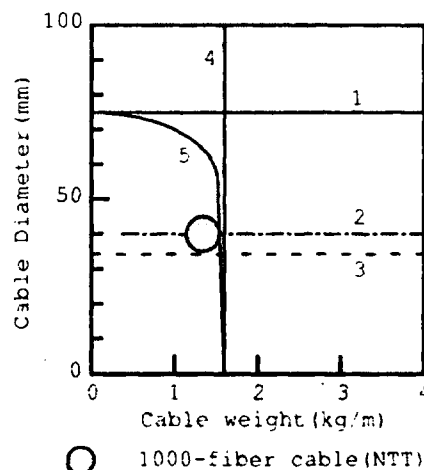


Figure 6 Cable dimension requirements

##### 4.2 Fiber Count

In order to replace copper wire subscriber networks with all optical fiber subscriber networks, the highest count optical fiber cable must include the same number of optical fibers as the number of copper pairs in the highest count conventional cable. The highest count cable in copper networks, has 3600 pairs. Similar fiber count cables are necessary, when the subscriber network has either a loop or star configuration. Therefore, we began to study high density and high count cable which can hold 4000 fibers, considering to the potential future increase in subscribers.

## 5. New cable design

### 5.1 Concept

When we consider the new cable structure, some conditions are required besides those described in section 4.

#### (1) Tight structure

To realize a high density cable, free space should be reduced. With a loose cable structure, where the clearance between the fiber or ribbon and the cable material is very small, attenuation loss may increase at low temperatures due to fiber buckling.

#### (2) Unit Branching

High count conventional copper pair cables consist of units which include 100 or 200 pairs. Cables are divided into units at cable splicing points. Therefore, high count optical fiber cables should consist of units with a fiber count in the 100 to 200 range.

### 5.2 Structure

To satisfy the above requirements, we propose a new cable structure called U-groove unit cable as shown in figure 7. Each unit consists of U-grooved material and stacked optical fiber ribbons. The U-groove units are stranded around a central member. With figure 8, we can calculate the cable size. The inscribed circle radius  $R_i$  of the stranded units is expressed as eq.1.

$$R_i = b/2(1/\sin(\pi/n)) \quad (1)$$

where  $a$  is unit height,  $b$  is unit width and  $n$  is the number of stranded units.

The circumscribed circle radius  $R_o$  is expressed as eq.2.

$$R_o = ((b/2)^2 + (a+R_i)^2)^{1/2} \quad (2)$$

### 5.3 Structure induced fiber stress

Where the distance between a fiber and the cable central axis is  $r_f$ , the distance between the center of the ribbon holding this fiber and the axis is  $r_r$ , and the unit stranding pitch is  $p$  as shown in figures 9 and 10, fiber strains due to structure are calculated as follows. [4]

Fiber elongation  $\epsilon_e$  due to local differences between the fiber and ribbon centers is expressed as eq.3.

$$\epsilon_e = ((2\pi r_f)^2 + p^2)^{1/2} / L_o - 1 \quad (3)$$

$$L_o = N \left( \sum_{i=1}^N (1 / ((2\pi r_{fi})^2 + p^2)^{1/2}) \right) - 1 \quad (4)$$

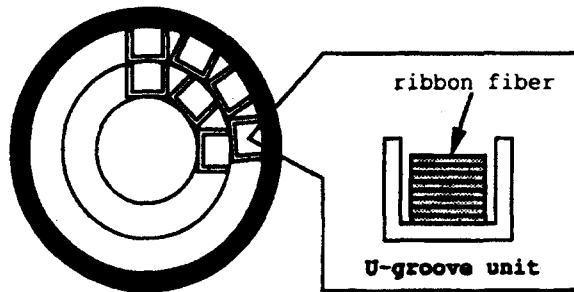


Figure 7 U-groove unit cable structure

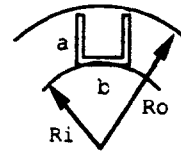


Figure 8 U-groove cable size calculation model

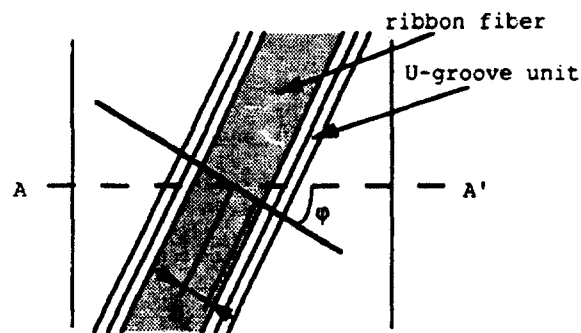


Figure 9 Top-view of Stranded U-groove

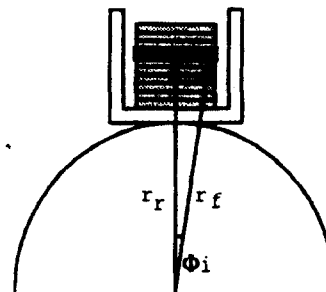


Figure 10 Cross-section of U-groove at A-A'

Bending strain  $\epsilon_b$  due to fiber diameter is expressed as eq.4.

$$\epsilon_b = d/2r_b \quad (5)$$

$$r_b = (r_f + (p/2\pi)^2) / r_f \quad (6)$$

where  $d$  is fiber diameter. Torsion strain  $\epsilon_t$  is expressed as eq.7.

$$\epsilon_t = d/2\tau_i \quad (7)$$

$$\tau_i = ((2\pi r_f)^2 + p^2)^{3/2} / (2\pi p L_0) \quad (8)$$

Total strain  $\epsilon$  of these 3-strains is expressed as eq.9.

$$\epsilon = 1/2 (\epsilon_e + \epsilon_b + ((\epsilon_e + \epsilon_b)^2 + (2G\epsilon_t/E)^2)^{1/2}) \quad (9)$$

where  $G$  is the modulus of elasticity in

shear and  $E$  is the Young's modulus of a fiber.

According to the requirements, the maximum cable diameter is 35mm. When cable sheath and core wrapping material thickness are taken into consideration, the maximum  $r_f$  is about 14mm. And when strength member for 800kgf installation force and its coating diameter are taken into consideration, the minimum  $r_f$  is about 7mm. Individual strain values and total strain are shown in figures 11 to figure 14, where  $r_f$  is 7 and 14mm. If strain reduction is required, the stranding pitch must be wide.

Another strain problem is caused by the tight insertion of the ribbon fiber. But this strain can be kept sufficiently small, because the backward tension on the ribbon can be precisely controlled. Residual strain due to the ribbon insertion process is less than 0.02%. [5]

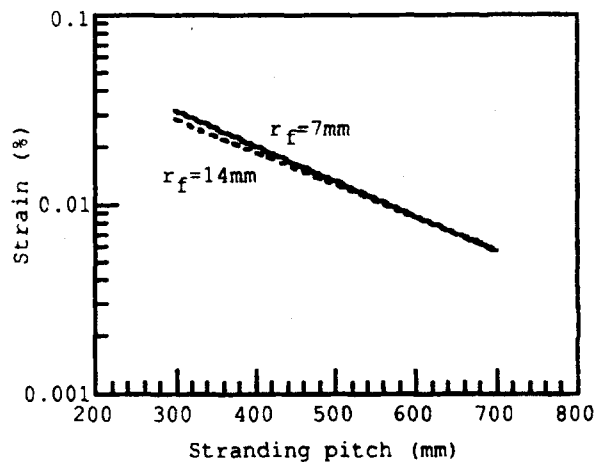


Figure 11 Elongation strain

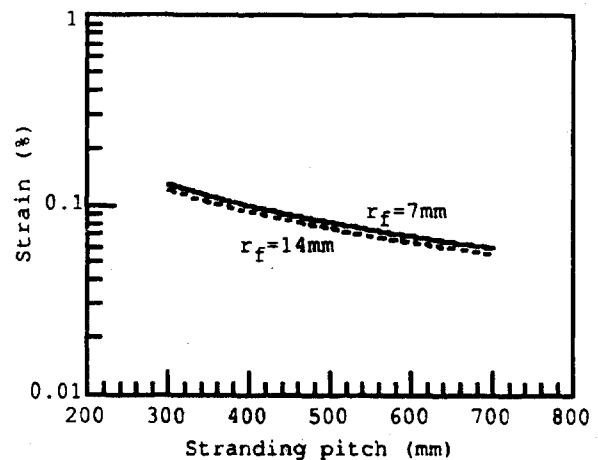


Figure 13 Torsion strain

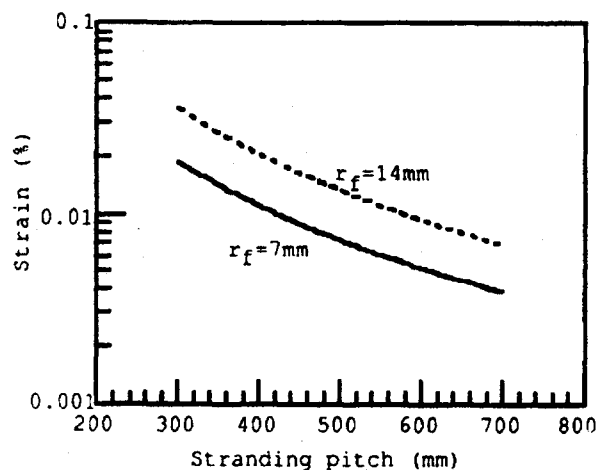


Figure 12 Bending strain

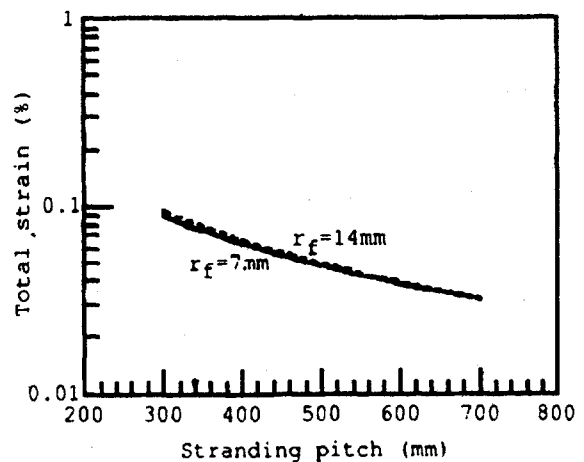


Figure 14 Total strain

#### 5.4 Bending strain due to ribbon width

As shown in figure 15, when a ribbon is bent along its horizontal plane, the outside of fibers in the ribbon are elongated. The maximum stress  $\epsilon_h$  is expressed as eq.10.

$$\epsilon_h = d_r / R \quad (10)$$

where  $d_r$  is the distance between the ribbon center and the center of the outermost fiber and  $R$  is the cable bending radius. This strain value is the worst case, because a fiber ribbon moves to reduce the strain. However, the reduction rate depends on cable structure and ribbon dimensions. So, we evaluate this strain with eq.10.

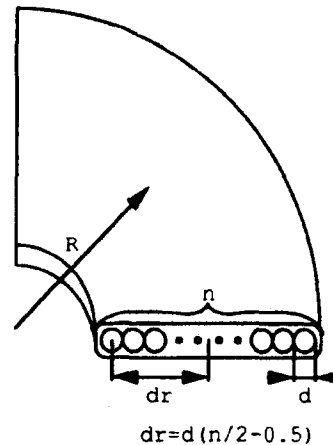


Figure 15 Strain due to ribbon bending

#### 6. Requirements for coated fiber

In this section, we clarify the requirements for a coated fiber and the fiber count in a ribbon.

##### 6.1 Requirements due to cable structure

Based on the above cable design, we studied the requirements for coated optical fiber.

Using figure 16, unit height  $a$  and unit width  $b$  are calculated with eq.11 and eq.12 respectively.

$$a = U_t + S_c(2T_t + F_d) + c \quad (11)$$

$$b = 2U_t + c + (F_d \times F_n) \quad (12)$$

Where unit wall thickness is  $U_t$ , the clearance to facilitate manufacture is  $c$ ,  $S_c$  is the number of stacked ribbons in a unit,  $T_t$  is ribbon coating thickness,  $F_d$  is coated fiber diameter and  $F_n$  is fiber count in a ribbon.

Using equations 1,2,11 and 12, we calculate the conditions required to make a cable with a diameter of less than 35mm including a sheath 2.5mm thick, with the same clearance value as with conventional cable. Figure 17 shows the relationship between fiber count in a ribbon and coated fiber diameter with the stacked ribbon count as a parameter. When the fiber count is high, the coated fiber diameter quickly approaches a given value. Those calculated lines have ripples, because fiber count is a discrete value. This indicates that increasing the fiber count in a ribbon is not very efficient for increasing fiber coating diameter. It is difficult to manufacture small diameter coated fiber. Therefore, increasing fiber diameter is of little advantage in cable manufacture. Increasing the stacked ribbon count is more effective.

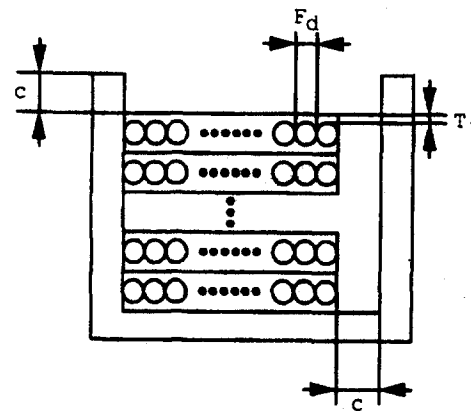


Figure 16 Ribbon fiber and unit size

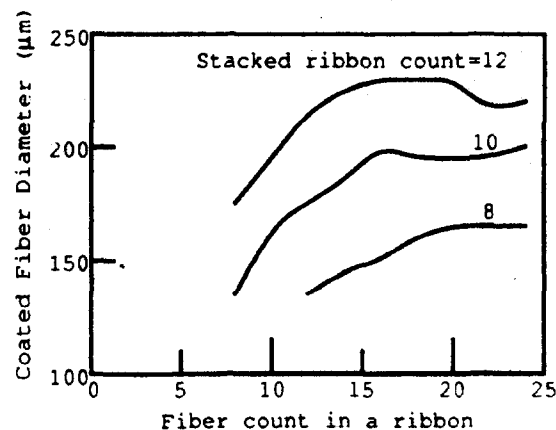


Figure 17 Relationship between fiber count in a ribbon and coated fiber diameter

## 6.2 Manufacturing requirements

It is difficult to make thin fiber coating without damaging effects to the fibers. We think that  $10\mu\text{m}$  is lower limit for the coating thickness of the soft layer. We also think that 2-layer coating (soft and hard layers) is required to avoid a loss increase due to microbending. With present manufacturing accuracy, the lower limit for the hard layer thickness is  $5\mu\text{m}$ . This gives a minimum coated fiber diameter of  $155\mu\text{m}$ .

## 6.3 Coated fiber diameter design

Based on the discussion in 6.1, 6.2 and 5.4, we are able to determine the coated fiber diameter. Figure 18 shows the conditions required to realize high count and high density cables. The hatched area in figure 18, shows appropriate design parameters for coated fiber diameter and fiber count in a ribbon.

We have been attempting to fabricate thin coated fibers and ribbons to satisfy these conditions.

Recently, we obtain some informations on a manufactured thin coated fiber.

(1) It is possible to manufacture thin coated fibers with an outer diameter of more than  $155\mu\text{m}$ .

(2) These fibers have no major problems apart from fiber strength. The fiber failure probability of these thin coated fibers is little higher than that of conventional fibers. The reasons for this are now being studied.

Our studies aimed at realizing high-count and high-density cables are continuing.

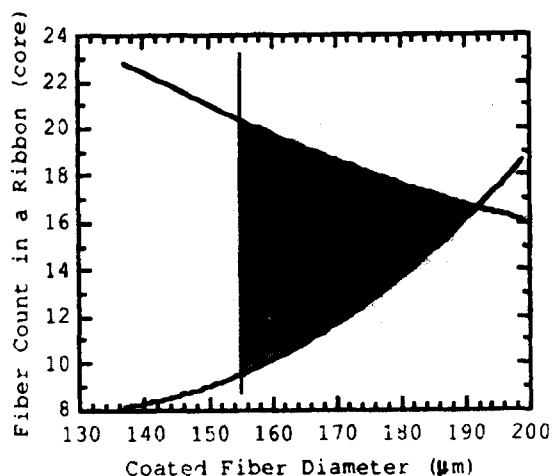


Figure 18 Optimization Of Optical Fiber and Ribbon

## 7. Conclusions

We began to study on high-count and high-density cables in order to construct optical subscriber cable networks for FTTH(OFL21).

We clarified the cable size requirements for this type of cable.

(1) Cable diameter is less than  $35\text{mm}$ .

(2) Cable weight is less than  $1.06\text{kg/m}$ .

We proposed a new cable design called U-groove unit cable. We calculated and studied the fiber strains caused by the cable structure. Through these investigation, it is clarified that the fiber strain is sufficiently low enough to ensure long-term reliability.

We also discussed the requirements for coated fiber diameter and fiber count in a ribbon, and have described appropriate optimization conditions.

Figure 19 shows a new cable structure, based on the above conclusions. The U-groove unit consists of ten fiber ribbons which include 16 coated fibers. The outer diameter of the coated fiber is  $160\mu\text{m}$ . The inner layer has 10 units, and the outer layer has 15 units.

We are continuing to study this cable in order to achieve on all optical fiber subscriber network.

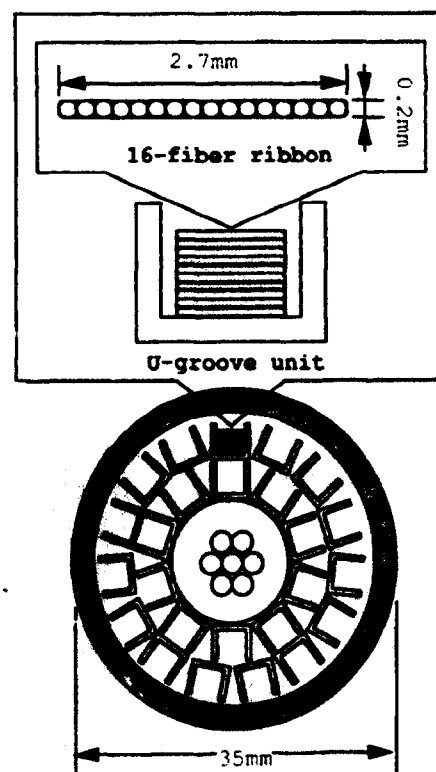


Figure 19 New 4000-Fiber Cable Structure

## **8. References**

- [1] T. Uenoya "The optical fiber loop 21 plan", OEC, 1990.
- [2] S. Hatano, Y. Katsuyama, T. Kokubun, and K. Hogari "Design and characteristics of Multi-Hundred-Core optical-fiber cable for use in subscriber line", J. of Lightwave Technology, Vol.4, No.8, August, 1986.
- [3] M. Kawase, T. Fuchigami, M. Matsumoto, S. Nagasawa, S. Tomita, and S. Takashima "Subscriber Single-Mode optical fiber ribbon cable technologies suitable for midspan access", J. of Lightwave Technology, Vol.7, No.11, November, 1989.
- [4] R. Yamauchi, K. Inada, and K. Ishihara "Residual stresses of fiber in tape type optical cable and their reduction", Trans. IECE Japan, Vol.J63-B, No.8, 1980. (in Japanese)
- [5] S. Hatano, Y. Katsuyama, T. Kokubun, and K. Hogari "Multi-Hundred-Fiber cable composed of optical fiber ribbons inserted tightly into slots", 35th IWCS, 1986.

### **Shigeru TOMITA**

NTT  
Telecommunication Field  
Systems Research &  
Development Center  
Tokai, Ibaraki,  
319-11, JAPAN



Shigeru Tomita is a Research Engineer.

He was born in 1960 and received a B.E. degree in electrical engineering from Nihon University in 1983.

He joined NTT in 1983. Since 1990 he has been engaged in research on High-density and Pre-connectorized optical fiber cable.

Mr. Tomita is a member of IEEE.

### **Michito MATSUMOTO**

NTT  
Telecommunication Field  
Systems Research &  
Development Center  
Tokai, Ibaraki,  
319-11, JAPAN



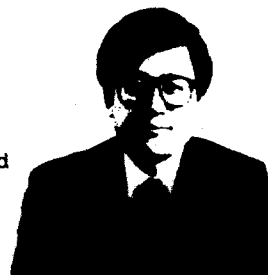
Michito Matsumoto is an Executive Research Engineer.

He was born in 1952 and received B.E. degree in electrical engineering from Kyushu Institute of Technology. He received M.E. and Ph.D. degrees in electronics engineering from Kyushu University in 1977 and 1987, respectively.

He joined NTT in 1977. Since 1990 he has been engaged in research on High-density and Pre-connectorized optical fiber cable.  
Dr. Matsumoto is a member of IEEE.

### **Tetsuro YABUTA**

NTT  
Telecommunication Field  
Systems Research &  
Development Center  
Tokai, Ibaraki,  
319-11, JAPAN



Tetsuro YABUTA is an Executive Research Engineer.

He was born in 1949 and received B.E. and M.E. degrees in electronics engineering from Tokyo University in 1972 and 1974, respectively. He received Ph.D. degrees in mechanical engineering from Tohoku University in 1984.

He joined NTT in 1974. Since 1990 he has been engaged in research on High-density and Pre-connectorized optical fiber cable.

Dr. Yabuta is a member of IEEE.

### **Takuya UENOYA**

NTT  
Network Systems  
Development Center  
Uchisaiwaicho, Tokyo,  
100, JAPAN



Takuya Ueno is an Executive Manager of Telecommunication Cable Systems & Outside plant systems Project Group.

He received B.E. and M.E. degrees in electronics engineering from Waseda University in 1971 and 1973, respectively.

He joined NTT in 1973. Since 1988 he has been engaged in Development on Transmission cable systems including both Metallic and optical.

Mr. Ueno is a member of IEICE of Japan.

## DESIGN AND QUALIFICATION OF GAS PRESSURIZED AND WATER BLOCKED SLOTTED CORE RIBBON CABLES

Hani Nassar

Siecor Corporation, 489 Siecor Park, Hickory, NC 28603

Ulrich Oestreich

Siemens AG, Austrasse 101, D-8632 Neustadt/Coburg, Germany

### ABSTRACT

A slotted core ribbon cable system is introduced which addresses both gas pressurized and water blocked cable designs.<sup>1</sup>

Designed to alert the user in the event of cable jacket damage, the former design employs the new "mini slots" approach allowing the free flow of air without sacrificing the cable size.

Both cable designs are based on a 0.05% maximum cabling construction strain enhancing the mechanical and environmental performance in the temperature range of -30 °C to +60 °C. The average attenuation increase in this range is 0.04 dB/km at 1550 nm.

### INTRODUCTION

The general need for compact high fiber count cables is leading to a widespread interest in optical fiber ribbon technology.<sup>2</sup> In slotted core ribbon cables, for example, four or eight fibers are encapsulated in a UV resin providing efficient positioning in the slots and a corresponding high packing density of fibers. However, it should be noted that, at room temperature, these ribbons are often under strain in contrast to loose tube cables and thus need to be handled accordingly.

Failure of cable sheaths caused by fatigue, rodents or other methods can cause damage to the cable components due to the penetration of water through the sheath. Avoiding this occurrence can be realized through gas pressurized and water blocked slotted core ribbon cables. Ribbon manufacturing, core extrusion processes, ribbon laying, stranding and jacketing all play their role in determining which design approach to consider.

The following theoretical calculations incorporate various assumptions to simplify the design approach and promote a general understanding of the slotted core ribbon cable design theory. Although, to a certain extent, theory has been backed up by actual testing, certain critical assumptions, such as negligible frictional coefficients between ribbons, linearity of thermal expansion coefficients and moduli within the operating temperature range need to be considered.

The current slotted core ribbon family of cables encompasses single and multi-element designs ranging from 8-fiber cables to 1000-fiber cables, both in the gas pressurized and water blocked cable versions. However, due to the amount of available information and the complexity (but similarity) of the designs, only the gas flow performance of the 80-fiber gas pressurized cable and the cable design of the 100-fiber water blocked cable are presented at this time.

### DESIGN CHARACTERISTICS

#### Mini slots

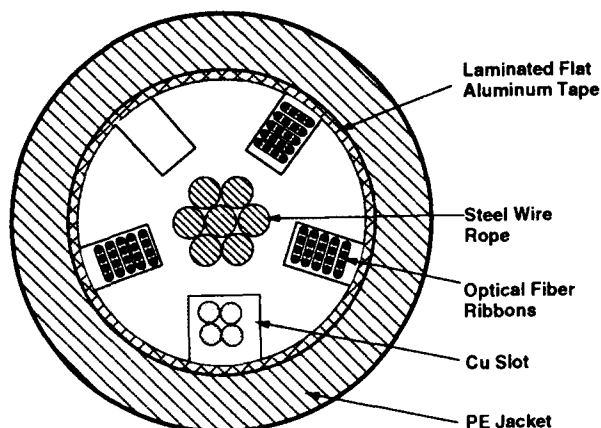
For the gas pressurized 80-fiber cable in Fig 1., five master slots and five "mini slots" constitute the core. The "mini slots" have a triple function: 1) They permit the flow of inert gas, thereby reducing the flow resistance, 2) they provide uniform cooling of the extrudate by reducing the volume of the crown material, and 3) they allow for a reduction in cable size.

For an additional master slot (e.g. 1.6 mm x 2.5 mm), the gained volume is roughly 4L mm<sup>3</sup> (L = length), whereas the introduction of five equilateral "mini slots" of 1.5 mm sides produces almost 5L mm<sup>3</sup> of free volume thereby either eliminating



the need of an empty master slot (resulting in a reduction of cable size) or maintaining the same cable size for a higher fiber count efficiency.

**60-Fiber Gas Pressurized  
Single Element Slotted Core  
Ribbon Cable**



**80-Fiber Gas Pressurized  
Single Element Slotted Core  
Ribbon Cable**

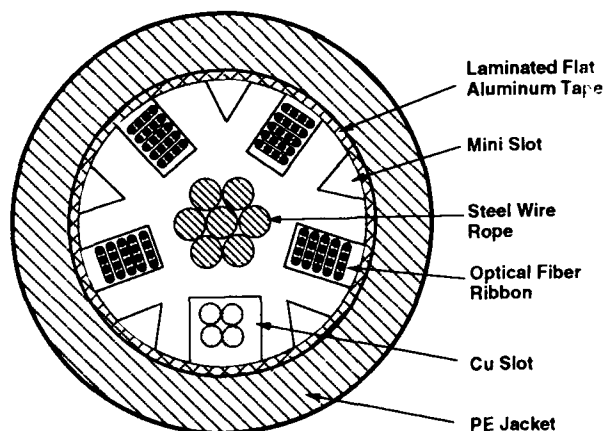


Fig. 1: Comparison of same diameter gas pressurized slotted core ribbon cable with and without mini slots

## Gas flow resistance

The gas flow resistance is strictly a function of the cable design and processing parameters. A cable with few small air channels and tight sheath will possess a much higher flow resistance than a cable with stranded elements, since stranded elements have inner and outer interstices facilitating the flow of air throughout the cable length (Fig. 2).

**600-Fiber Gas Pressurized  
Multi-Element Slotted Core  
Ribbon Cable**

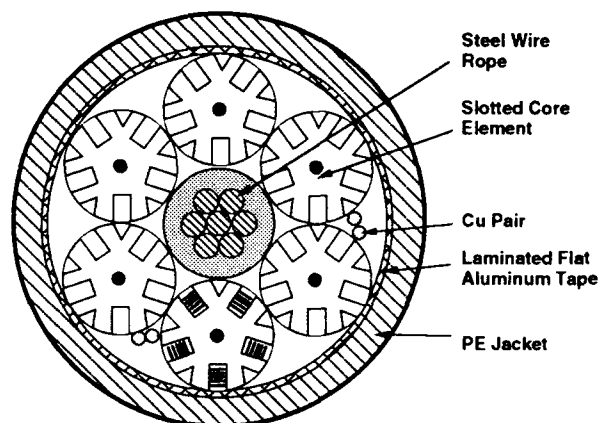


Fig. 2: 600 Fiber gas pressurized multi element slotted core ribbon cable

$$\text{The resistance of the air } R = \frac{P_1^2 - P_2^2}{2LS_0P_0} \quad (1)$$

where  $P_1$  = feed pressure (absolute)

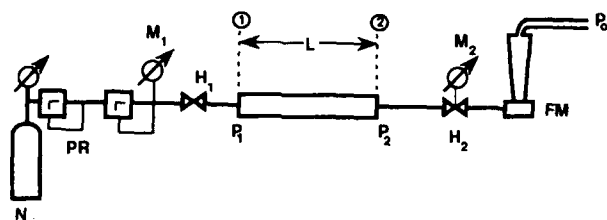
$P_2$  = outlet pressure (absolute) after a leak is detected and the output pressure is stabilized.

$L$  = cable length.

$S_0$  = flow rate of leak.

$P_0$  = atmospheric pressure

can be shown to vary from about 27 MPa.s.m<sup>-4</sup> for the 80-fiber single core design to about 7 MPa.s.m<sup>-4</sup> for the 600-fiber multi-core design using the setup in Fig. 3



where  $M_1, M_2$  = precision pressure gauges (absolute pressure)  
 $H_1, H_2$  = cutoff valves  
 FM = flow meter  
 PR = pressure reducer  
 $N_2$  = Nitrogen or dry air supply

Fig. 3: System for measurement of gas flow resistance

#### Constructional strains:

Fiber strains are very important to understand since they predict the cable's performance over its service life. For slotted core ribbon cable designs, the constructional strains of ribbons are defined as pure bending, pure torsion, fiber length differential within the ribbon and tensile strain effects during ribbon laying.

1. As for pure bending, this is related to the bending of the ribbons around the central member and is directly related to the bend radius  $\rho$  of each ribbon (Fig. 4).

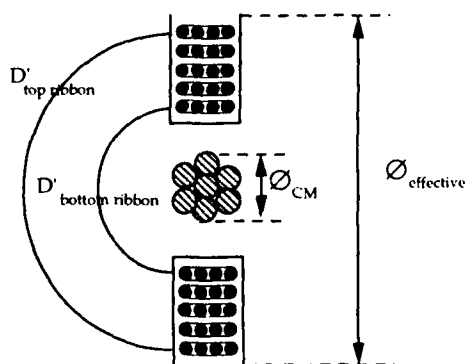


Fig. 4: Identifying pitch circle diameter for calculating ribbon bend radii

$$\rho_{\text{ribbon}} = \frac{D'}{2} + \frac{P^2}{2\pi^2 D'} \quad (2)$$

where  $D'$  = pitch circle diameter for each ribbon

$P$  = slot pitch, chosen for optimized mechanical and environmental performance

$$\text{The bending strain } \epsilon = \frac{d_f}{2\rho} \quad (3)$$

where  $d_f$  is the glass diameter, can then be calculated.

2. Pure torsion is not due to a tensile load but to the effect of fixing one ribbon end while twisting the other, such as in paying off into the slot. Accordingly, shearing takes place so that neither the tensile stress nor the tensile modulus plays a role, but the shear stress  $\tau$  and the shear modulus  $G$ . For a linearly elastic material, the shear stresses are related to the shear strains by Hooke's law<sup>3</sup> in shear, i.e.

$$\tau = G \cdot \frac{d_f}{2} \cdot \beta \quad (4)$$

where  $\beta$  = twisting angle  
 $\sim 2\pi/P$

and  $G$  for fiber is in the range of 29,700 MPa, equivalent to 4300 Kpsi.

3. The length differential in a ribbon is a function of twist. As the ribbon is twisted, the fibers in the center of the ribbon are compressed while those on the outside are in tension. For a 4-fiber ribbon, the distances are  $r_1$  and  $r_2$ , where  $r_1$  is the distance from the center of the ribbon to the center of the innermost (adjacent) fiber and  $r_2$  is the distance from the center of the ribbon to the center of the outermost fiber (Fig. 5)

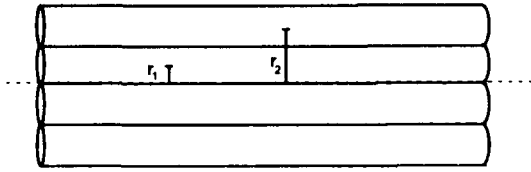


Fig. 5: Calculating length differential in a 4-fiber ribbon

The strain  $\epsilon = \frac{\Delta l}{l}$  can be represented by  $\frac{2\pi^2 r^2}{p^2}$ .

$$\text{Therefore } \Delta\epsilon = \frac{2\pi^2(r_2^2 - r_1^2)}{p^2}. \quad (5)$$

4. The tensile strain during ribbon laying is a function of several variables and depends entirely on the processing approach. At any rate, the slotted rod back tension, the varying tension of the ribbons (from top to bottom) and the final takeup tension dictate the amount of residual tensile strain in the ribbons (Fig. 6).

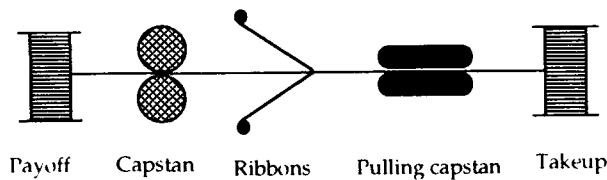


Fig. 6: Ribbon laying process<sup>4</sup>

Performing several simple but careful mathematical calculations, the theoretical tensile strain ( $\epsilon$ ) on each ribbon can be calculated:

$$\epsilon = F/EA \quad (6)$$

where  $F$  = tension  
 $E$  = modulus, and  
 $A$  = cross-sectional area.

According to principal stresses theories<sup>3</sup> (e.g. Mohr's circle), the total principal stress  $\sigma_{\text{total}}$  (tensile  $\sigma$  and shear  $\tau$ ) in such a system can be simplified to:

$$\sigma_{\text{total}} = \frac{\sigma}{2} + \left[ \left( \frac{\sigma}{2} \right)^2 + \tau^2 \right]^{\frac{1}{2}}. \quad (7)$$

Converting the bending strains (3), length differential strains (5) and back tension strains (6) into stresses  $\sigma$  using

$$\sigma = \epsilon E, \quad (8)$$

where  $E$  = glass modulus = 75000 MPa, equation (7) can be used to calculate the total constructional strains in the cable. It is important to note that the constructional strains differ for each ribbon depending on its position, necessitating a variation in payoff tensions between the top and bottom ribbons.

Another major consideration to the cable design is the contraction and expansion of the cable components between the specified lower and upper temperature ranges, i.e. the contraction of the cable at the lowest extreme is used to calculate the movement of the ribbons in the slots and thus is an effective method of determining the required slot depth.

Since the contraction of the cable due to temperature is much higher than that of the ribbon, the final effective strain  $\epsilon_{\text{eff}}$  is the difference between cable contraction and ribbon contraction, i.e.

$$\epsilon_{\text{final}} = (\alpha_{\text{eff}} \Delta T)_{\text{cable}} - (\alpha_{\text{eff}} \Delta T)_{\text{ribbons}} \quad (9)$$

where  $\alpha_{\text{eff}}$  = effective thermal expansion coefficient

$$= \frac{\sum_{i=1}^n A_i E_i \alpha_i}{\sum_{i=1}^n A_i E_i}$$

and  $\Delta T = T_{\text{extreme}} - T_{\text{ambient}}$

For example, for the 100F water blocked cable design in Fig. 7, it can be shown that an  $\epsilon_{\text{final}}$  of 0.06% (contraction) at -30 °C can be expected. Furthermore, subtracting the initial ribbon strain (6) actually gives us ~0.05% ribbon excess length at that temperature, i.e. free movement. Using this information, the upward movement of the ribbons in the slots at -30 °C can be determined ( $\epsilon_{\text{ribbon}} \times \rho$ ) providing the cable designer with a starting point to the required slot dimensions.

**100-Fiber Water Blocked  
Single Element Slotted Core  
Ribbon Cable**

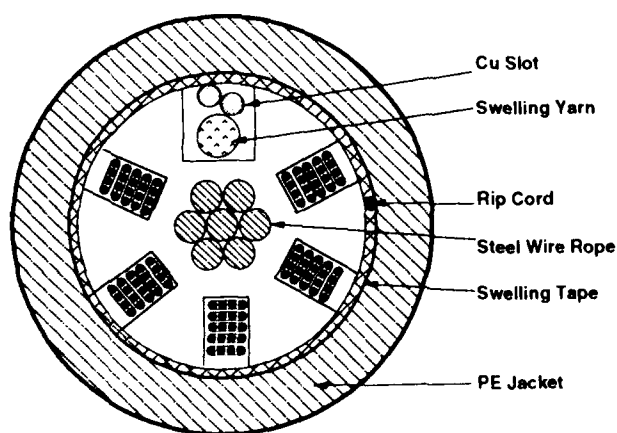
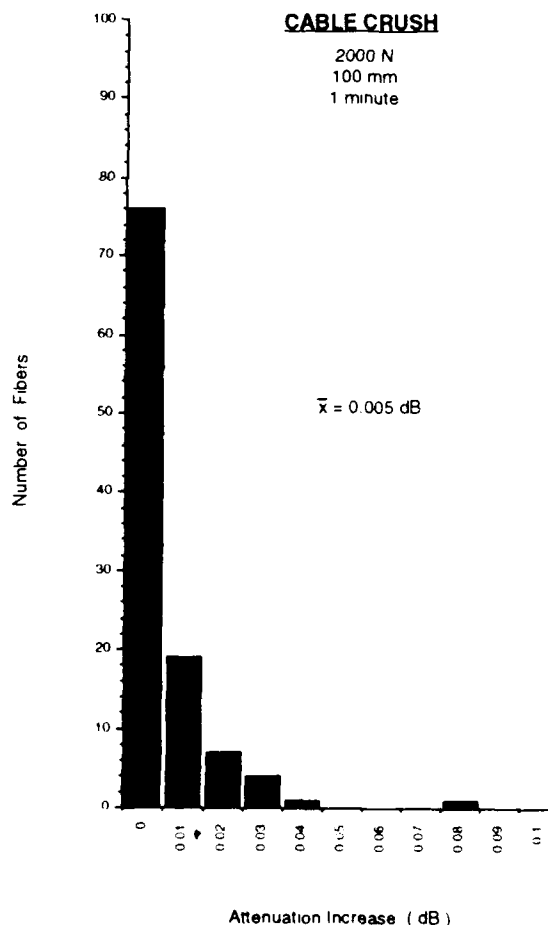
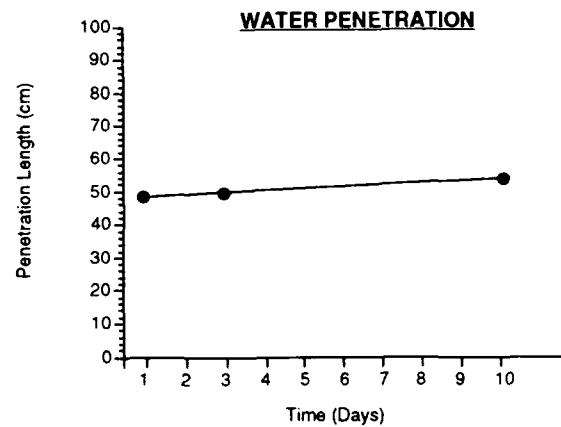
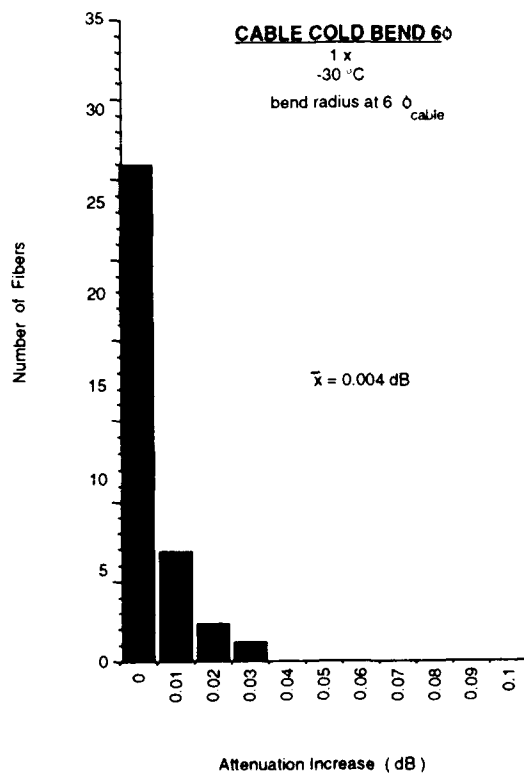
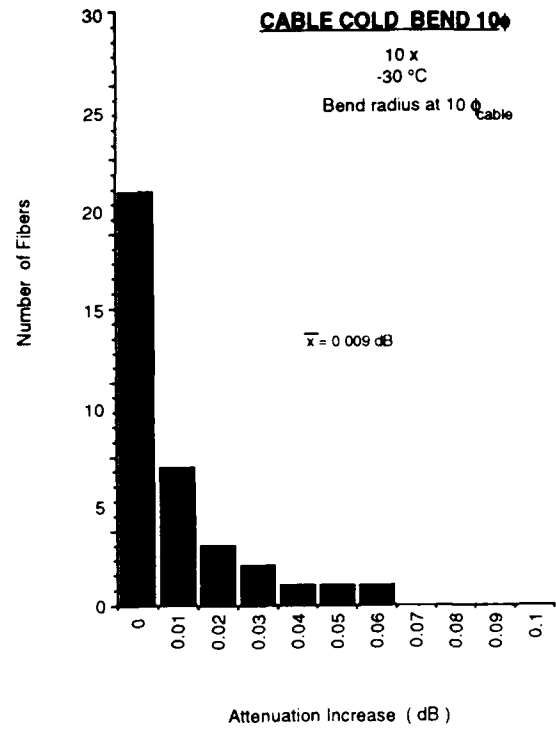
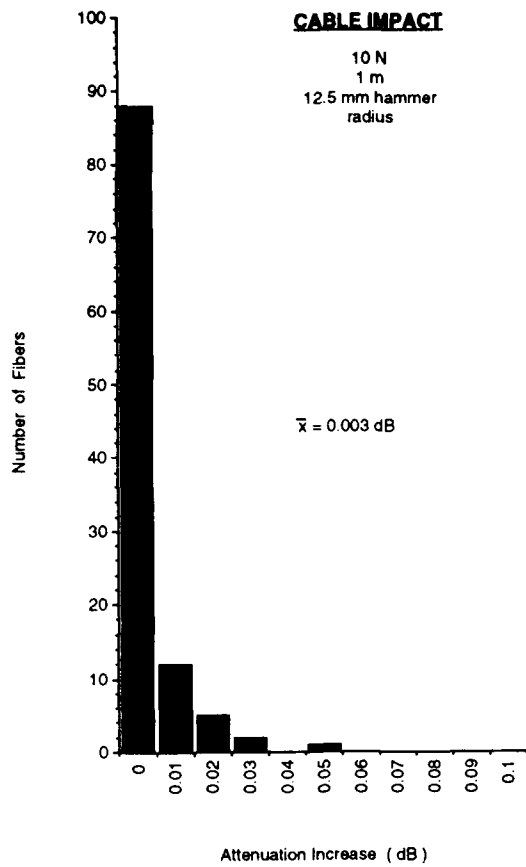


Fig. 7: 100-fiber water blocked single element slotted core ribbon cable

## Mechanical and Environmental Performance

Several mechanical and environmental requirements have to be met to insure the service life of such cables. These include crush, impact, bend, water penetration performance (or gas flow resistance) and temperature characterization tests. All test results are within 0.04 dB/km average attenuation change at the 1550 nm wavelength. The results of these tests are presented in Fig. 8.





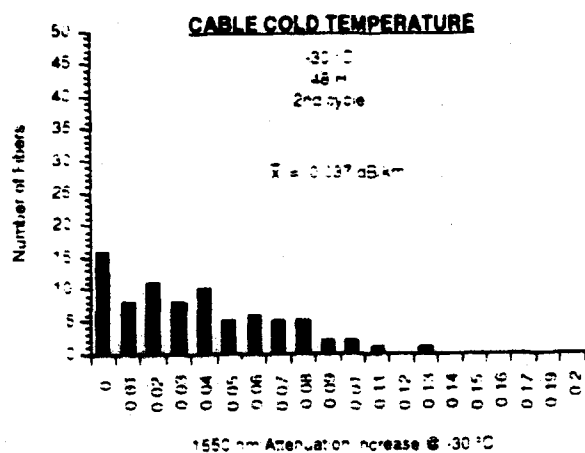


Fig. 8: Typical mechanical and environmental performance of 100-fiber single element water blocked slotted core ribbon cables

## CONCLUSION

The intention of this paper is to provide an understanding of the basics of slotted core ribbon cable design theory without emphasis on the history of these cables. It also assumes prior knowledge of the ribbon technology.

To simplify the design approach, certain practical assumptions have to be considered. Once a model has been established, actual trials are made to optimize the designs.

## ACKNOWLEDGEMENTS

The authors express their gratitude to Ernst Mayr and Reiner Schneider of Siemens AG, Germany and Steve Hassett of Siecor Corporation for their invaluable assistance and support in the preparation of this paper.

## REFERENCES

- 1 S. Hatano, Y. Katsuyama, T. Kokubon & K. Hogari, *Multi-Hundred-Fiber Cable Composed of Optical Fiber Ribbons Inserted Tightly into Slots*, Proceedings of the 35th International Wire & Cable Symposium, 1986, p.17.
- 2 B. Noethe, US Patent 4,176,910, 12/4/79J.
- 3 J. Gere & S. Timoshenko, *Mechanics of Materials*, 3rd ed., 1990
- 4 U. Oestreich, US Patent 4,199,224, 4/22/80.



Hani M. Nassar graduated from the Georgia Institute of Technology in 1981 with a Masters degree in Mechanical Engineering. He joined the RD&E department of Siecor Corporation in 1982 where he was initially involved with the development of products for both the copper and fiber optic cable industry. His major projects included the development of hybrid cables, feeder cable systems, design and qualification of Fiber Optic Ground Wires, submarine cables and is currently the project manager for the design and qualification of slotted core ribbon cables.



Dipl.-Ing. Ulrich Oestreich, has been active in the Siemens cable development and manufacture for 38 years; he has spent 16 years on power and high voltage cables and 22 years on communication cables. He started the fiber optic cable development in 1974 and is currently the head of this activity including all types of fiber optic cables.

**THE MICROSHEATH CABLE : A NOVEL DESIGN OF ULTRALIGHTWEIGHT SINGLE MODE  
OPTICAL CABLE FOR LOW COST SUBSCRIBER LOOP.**

P. TROMBERT<sup>1</sup> - P. JAMET<sup>1</sup> - P. CHERON<sup>1</sup>  
G. LE NOANE<sup>2</sup> - D. BOSCHER<sup>2</sup>

1 SILEC - MONTEREAU - FRANCE  
2 FRANCE TELECOM CNET - LANNION - FRANCE

### 1. ABSTRACT

This paper describes the successful development of a radically new design of ultralightweight optical cables offering novel performance and economical features in view of low cost implementation of subscriber loop networks.

Based on a global techno-economical analysis, this novel "microsheath" concept yields extremely compact medium fibre count cables, with, for example, an outer diameter and weight of only 6.2 mm and 34 kg/km in the case of a 35 fibre cable.

Testing results of prototypes are discussed, which show a performance level meeting the expected functional needs. Associated simple, space saving and low cost splices and closures are also presented.

### 2. INTRODUCTION

It is becoming more and more obvious that the introduction and full scale implementation of subscriber loop networks require the development of novel cable designs enabling a significant decrease in cable and installation costs, rather than mere evolutions of existing long haul dedicated cable structures and installation practices.

Indeed, prospective cost evaluations show that the building of the passive infrastructure (civil works, cables, laying, splicing and closures) has a major impact on the network global cost. This depends notably on assumptions made regarding network architecture and on the resulting cable family.

Recent works regarding network configurations met in Europe tend to suggest that the passive infrastructure will probably call for cables with low or medium (some tens) rather than high (several hundreds) single mode fibre counts<sup>1 2 3</sup>.

The main reasons are :

- . the relatively low density of business customers who will require interactive services justifying a full star topology,
- . the possibilities of sharing the fibre between several residential subscribers for providing mainly distributive services, at least during the introduction phase.

Even in the case of star networks, the range of cable fibre counts may be limited. As an example, the experience of a large scale installation of a fibre distribution network in FRANCE<sup>4</sup> indicates the following typical data :

- . average cable fibre count about 20 fibres
- . maximum cable fibre count : 150 fibres
- . average link length between distribution center and drop terminal : 400 m, with, usually 1 or 2 intermediary splices.

Considering the above framework, we have developed a radically new medium fibre count cable design philosophy, depicted as the "MICROSHEATH" concept, which will be described hereunder together with the main testing results obtained and associated jointing equipments.

### 3. TECHNO/ECONOMICAL OBJECTIVES

Present state of the art<sup>5</sup> of medium fibre count cables essentially stems from technological developments carried out in the framework of long haul or interoffice networks requiring "high grade" transmission medium, originally on multimode, then on singlemode fibres. To this end, special care was applied to cable designing in order to achieve high transmission, mechanical and environmental performance while keeping the fibres free from any strain.

This entailed using space consuming and costly design features such as large fibre excess length, clearance between fibres and surrounding layers and large size strength members.



Table 1 shows typical examples of present medium fibre count cable structures based on such principles<sup>4 6 7</sup>.

Fibre count and type of design	Diameter, mm	Weight, kg/km	Packing density*
30 OF slotted core (1 OF per slot)	18	230	0.12
36 OF loose tube or slotted core (several OF per slot)	14	130	0.23
40 OF 4 fibre ribbon/ slotted core	12	115	0.35
24 OF bundle/ single core tube	10	90	0.31

\* Packing density : number of fibres per sq.mm

Table 1

Now, local loop applications on single mode fibres present network planners and cable manufacturers with a totally new challenge, combining :

- . transmission requirements (power budget) less ambitious than for long haul networks,
- . specific topological and environmental constraints : relatively short and irregular link lengths, congested civil works in urban areas, etc...,
- . above all. low cost objectives.

To meet the cost objectives, it is necessary to reason on a global basis, in order to combine :

- . a low manufacturing cost, resulting from small volumes of low cost materials and from simple, efficient and reliable processes,
- . a low installation cost, including civil works and cable laying, handling and jointing.

To this end, it appears essential to achieve very high packing density and lightness features. This means reducing to a minimum the fibre excess length and clearance, which leads to a significant breakthrough in theoretical and practical cable design.

However, the performance of the cable must be kept at a level compatible with the requirements of local loop network applications. In particular, to avoid detrimental macro/microbending losses and strains on the fibres, it is then necessary that the cable structure offers :

- . negligible temperature elongation over the functional range,
- . high enough tensile modulus to ensure a limited strain on the fibres during installation,
- . high resistance to longitudinal and radial compression,
- . long term stability.

Furthermore, to enable easy fibre identification, organisation and splicing at the distribution points, it is necessary to group the fibres into modules of minimum dimensions.

#### 4. CABLE DESIGN

According to the above principles, the proposed cable design is based on the achievement of ultralightweight and extreme packing density features in a modular construction, in order to optimize the trade-off performance/cost.

It results in a fully dielectric cable containing for example as many as 35 singlemode fibres, having an outer diameter of only 6.2 mm, weighing only 34 kg/km while retaining transmission, mechanical and environmental performance meeting the functional requirements of subscriber loop applications : see figures 1 and 2.

Compared with some of the cables in table 1, this novel design concept yields cable size reduced by half and a fourfold packing density of about 1.2 fibre/sq.mm.

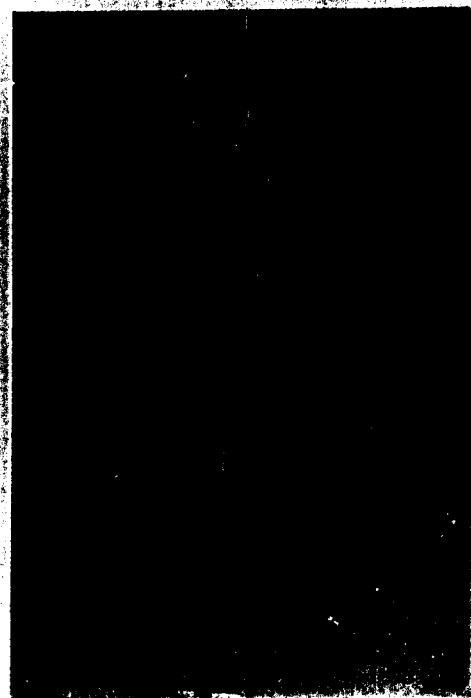
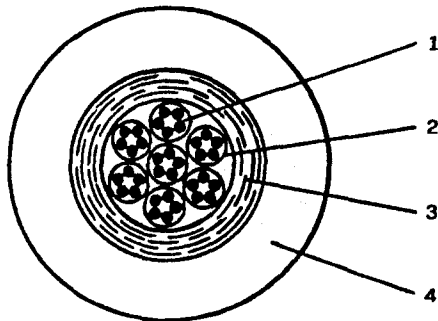


Fig. 1 : 35 OF microsheath cable

The cable construction is based on the combination of :

- fibre modules in which the fibre bundle (containing typically 4 to 8 SZ stranded fibres) is held without significant geometrical clearance by a very thin synthetic coloured "microsheath" which :
  - . enables easy module identification,
  - . ensures the proper cohesion of the module during cable manufacture and handling in the field,
  - . is easily removable for splice preparation.
- a protection "microsheath" surrounding without significant geometrical clearance the packing of fibre modules and associating :
  - . a thin specialty polymer reinforcing layer acting as a shell yielding high tensile modulus and crush resistance together with negligible temperature elongation and relaxation,
  - . a synthetic outer layer giving the flexibility and low friction characteristics required for installation in ducts.



- 1- Color coded optical fibre
- 2- Color coded microsheath
- 3- Self reinforcing resin
- 4- Black HDPE outer sheath

Diameter : 6.2 mm  
Weight : 34 kg/km

Fig. 2 : Cross-section of 35 OF microsheath cable

The choices regarding materials, dimensions and manufacturing processes ensure, in spite of the ultracompact design, a stress free state of the fibres over a wide range of mechanical and environmental conditions.

In particular, the material and thickness of the microsheath covering the fibre bundles are chosen so as its contribution to the combined product tensile moduli x cross sections of the various components of the fibre module (silica + primary coatings + microsheath) is only a few percent. As, in addition, its application prevents the possibility of fibre buckling, the microsheath thus does not present any risk of applying significant strain on the fibres.

In this respect, the microsheath concept fundamentally differs from the traditional loose tube buffer construction.

As regards the cable protection layer, use of emerging new families of polymer materials offering high tensile modulus, very low temperature elongation coefficient and negligible relaxation features, such as LCP, enables to achieve simply yet economically a protective microsheath yielding the desirable characteristics.

The small amounts of materials resulting from the compact design as well as the production conditions, combine towards low cable realization costs.

The manufacturing, based on well proven SZ cabling and extrusion processes, is characterized by the minimum number of operations and potentially high speeds and long cable lengths, owing to :

- . the small size and compactness of the microsheath fibre modules and cable,
- . the advantage of not having fibre excess length and clearance to be precisely controlled.

Furthermore the process lends itself to the integration of manufacturing operations, such as :

- . fibre drawing and microsheath module realization in a Multipulling and Cabling in Line process (MCL)<sup>8</sup>
- . on line transmission measurements (back-scattering) with the use of static take-up stands.

Equally decisive are the consequences implied by this new ultralightweight and miniaturized cable design on installation costs, especially regarding :

- . civil works : optimized use of existing congested ducting or of new underground facilities, or even aerial installation,
- . speeding up and simplification of cable laying operations.

## 5. CABLE TESTING

To assess the performance of this new cable design, a detailed testing programme has been carried out on several cable prototypes containing 35 fibres (see figures 1 and 2) or 50 fibres (outer diameter : 7 mm - weight : 40 kg/km). Various types of single mode fibres, having different index profiles (MC and DC) and mode field diameters (see Appendix 1), have been used in order to account for potentially different macro/micro bending sensitivities.

The main test results on 35 fibres count cable are described below :

### 5.1. Transmission performance

Appendix 2 shows the attenuation distribution at room temperature obtained on the completed cable. A comparison with the distribution measured on the fibres before cabling demonstrates that the cabling process does not significantly modify the fibre characteristics.

Appendix 3 shows typical results of temperature cycling test (according to IEC 794-1 method F1) over the range -30°C to +60°C at 1550 nm. According to theory, results depend notably on fibre design. The cable shows a satisfying behaviour down to -10°C with all fibre types, which is probably adequate to the functional needs of most local loop applications in temperate climates, and down to -30°C with some types of fibres.

### 5.2. Tensile performance

During tests according to IEC 794-1 method E1, no significant change in attenuation, both at 1300 and 1550 nm, was noted with all types of fibres up to a tensile strength of 100 daN. Furthermore, no residual cable elongation was measured after the test.

This result has to be assessed in relation with functional needs regarding the pulling force during cable laying, which, in the case of horizontal straight ducting, is given by :

$$T = kWL$$

where W is the cable weight per unit length, L is the laying length and k is the friction coefficient in the duct<sup>10</sup>.

The ratio T/W obtained, in the order of 3, fully compares with characteristics of more traditional cable designs, and indicates an equivalent laying ability.

In fact, real scale laying experiments in existing cable plants have demonstrated that, for example, 50 fibre cable lengths of more than 500 m can be pulled into contorted ducting routes with a pulling force not exceeding 20 daN.

### 5.3. Other mechanical tests

No change in attenuation, both at 1300 and 1550 nm, was measured during testing the cable :

- under compression strain up to 20 daN/cm,
- under repeated bending with radius under 100 mm.

These values comply with those generally considered for cables installed in ducts.

### 5.4. Long term stability

Long duration ageing tests, performed over 1 year in the following conditions :

- dry heat at 100°C,
- damp heat at 40°C - 93 % RH,
- immersion at 70°C in silicone based filling compound

have not resulted in any decrease of mechanical properties nor in relaxation effects, which proves the long term stability of the cable structure.

## 6. SPLICES AND CLOSURES

To enhance the global cost optimization, associated simple, space saving and low cost splices and closures have also been developed.

A preliminary techno-economical analysis has been carried out regarding the various manpower and equipment costs involved, on the basis of current experience of site installations with traditional cables and jointing techniques.

For instance, the typical breakdown of time spent on site for medium fibre count cable splicing in urban conditions indicates that only about a quarter of the manpower cost is devoted to actually splicing the fibres while the rest is shared between site organisation, cable and closure handling, measurements, supervision and transport.

This analysis and user's advice have led to focus the development work on the following main objectives :

- . simplicity and ease of operation, easy training,
- . simplicity, reliability and ease of maintenance of tool kits and splicing apparatus
- . reliability and stability of results (splice loss)
- . small dimensions, modularity and low cost of materials and equipments,
- . synergy with the novel cable design, which was confirmed to bring significant advantage regarding cable/modules handling and preparation as well as fibre identification.

Within this framework, the following equipments have been developed :

### 6.1. Splice

The well known ATI Placoptic System (based on bonding with UV curable adhesive) has been adapted to the splicing of microsheath single mode fibre modules, by combining :

- . mass operations for fibres preparation and prepositionning
- . individual alignment of the fibres on a common holder,
- . mass operations for adhesive curing and multifibre splice protection.

Splice overall dimensions (for 5 fibres) are 12.5 x 55 x 3.5 mm.

According to the measurement programme underway, the average splice loss is about 0.1 dB and maximum 0.4 dB.

### 6.2. Closure

Shown on fig. 3, this very compact and lightweight closure (overall dimensions for 50 fibre count : 170 x 170 x 360 mm) is based on a frame/organizer fulfilling the following purposes :

- clamping of the cables,
- management (distribution, guiding and identification) of the microsheath fibre modules,
- housing of simplified cassettes made of 2 plastic hinged parts, each accomodating a multifibre splice and the necessary reserve loops of microsheath modules and fibres,
- holding of the cassette during splicing operation and loops arrangement.

This organizer is then protected by a watertight metallic or plastic cover.

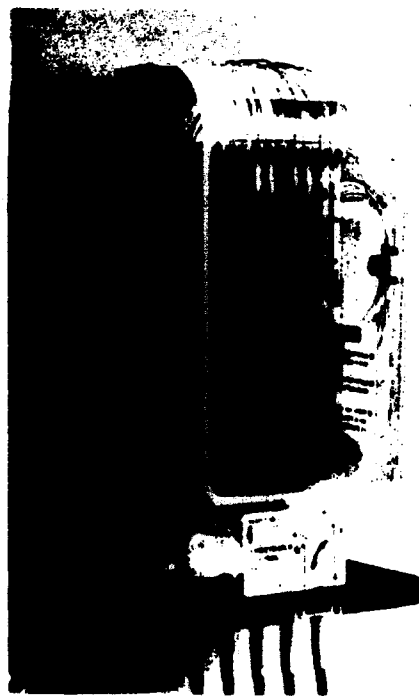


Fig. 3 : 50 fibres organizer

### 7. CONCLUSION

An in-depth analysis of modularity, compactness, lightness and cost objectives has led to the development of a new design of ultralightweight "microsheath" medium fibre count cables. The converging technological and economical progress brought by this novel cable technique constitute a significant step towards the low cost introduction, implementation and upgradability of subscriber optical networks.

### ACKNOWLEDGEMENTS

The authors would like to associate to this paper teams of ATI and SA Companies involved in the development of splices and closures techniques within this project supported by FRANCE TELECOM.

### REFERENCES

- 1- M.H. REEVE - "Optical fibre network architectures for the local loop"-EFOC/LAN 1989, p. 168.
- 2- J. ABIVEN - "La transmission de services à bas débit sur un bus passif". L'Echo des Recherches - n° 138 - 4ème trimestre 1989 - p. 13.
- 3- U.H.P. OESTREICH - "Design considerations for short haul cables" - 35th IWCS, 1986, p. 24.
- 4- J.P. BOINET, M. de VECCHIS, C. VERGEZ - "Results on a large scale installation of a fibre optic distribution network" 38th IWCS, 1989, p. 132.
- 5- H. MURATA - "Optical fibers, fiber cables and technologies concerned for local loops and local area networks" - EFOC/LAN 1990, p. 3.
- 6- T. MATSUO and al - "Development of single mode optical fiber cable for NTT" SUMITOMO Electric Technical Review, Number 29, January 1990, p.64
- 7- P.D. PATEL and A.J. PANUSKA - "Lightweight fiber optic cable" - 39th IWCS, 1990, p. 158.
- 8- G. LE NOANE and al - "A new process : Multipulling and Cabling in Line of optical fibers - Technical realization". 37th IWCS, 1988, p. 179.
- 9- P. GEITNER and al. - "Bend loss characteristics of single mode fibers" - ECOC 1987, p. 97.
- 10- H. MURATA - "Handbook of optical fibre and cable" - Marcel Dekker, New-York, 1988.



**Philippe TROMBERT**

Société Industrielle  
de Liaisons Electriques  
SILEC  
B P n° 6  
77871 MONTEREAU CEDEX  
FRANCE

Philippe TROMBERT, born in 1949, graduated from Institut National Polytechnique de GRENOBLE in 1970. He joined SILEC in 1973 where he first held positions in the field of power cables. He was appointed in 1984 responsible for development and manufacturing of optical fiber cables.



**Georges LE NOANE**

FRANCE TELECOM  
CNET LAB/OCM/FCO  
Route de Tregastel  
B P n° 40  
22301 LANNION CEDEX  
FRANCE

Georges LE NOANE, born in 1945, received his engineering degree from the Ecole Nationale Supérieure des Arts et Métiers and joined CNET in 1970. He began working on optical fiber connector techniques, then switched to cables. Since 1979, he has been responsible for the "Optical Fibers and Cables" Department at the CNET Lannion B Center.



**Patrick JAMET**

Société Industrielle  
de Liaisons Electriques  
SILEC  
B P n° 6  
77871 MONTEREAU CEDEX  
FRANCE

Patrick JAMET, born in 1950, received his Ph.D of Physical Chemistry from the DIJON University in 1976. He began working in 1978 in the cable industry, in the field of telecommunication and optical cables. He joined SILEC in 1989 and is presently responsible for Research and Development on optical cables.

**Daniel BOSCHER**

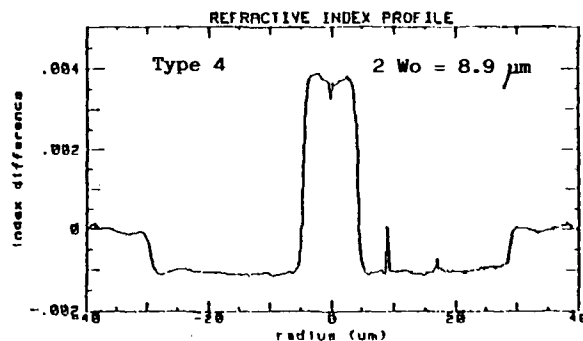
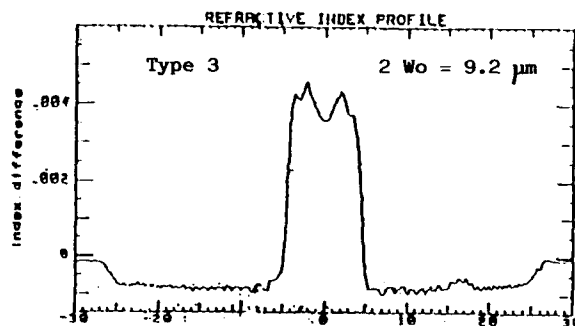
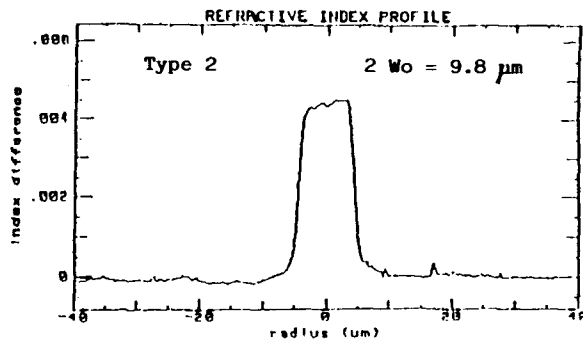
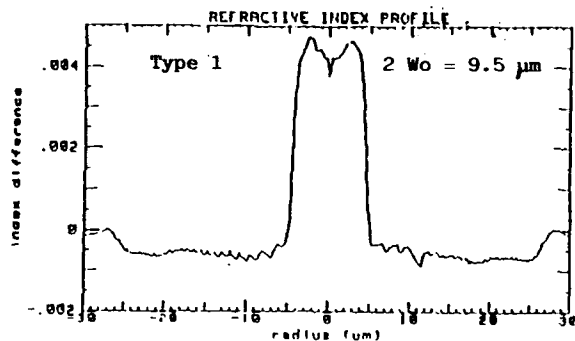
FRANCE TELECOM  
CNET LAB/OCM/FCO  
Route de Tregastel  
B P n° 40  
22301 LANNION CEDEX  
FRANCE

Daniel BOSCHER, born in 1951, began working at CNET in 1973 after earning his engineering degree from the Ecole Nationale Supérieure des Arts et Métiers. Placed in charge of studies on the mechanical characteristics of circular waveguides, he was appointed in 1979 head of studies on passive components, cables, and connector/coupler systems within the "Optical Fibers and Cables" Department.

**Philippe CHERON**

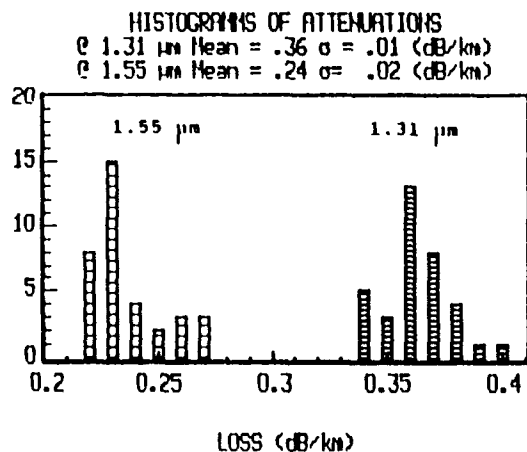
Société Industrielle  
de Liaisons Electriques  
SILEC  
B P n° 6  
77871 MONTEREAU CEDEX  
FRANCE

Philippe CHERON, born in 1948, graduated from the Institut National des Sciences Appliquées de LYON in 1973. He joined the telecommunication cables division of SILEC in 1974 and has been engaged since 1979 in the development and manufacture of optical fiber cables.

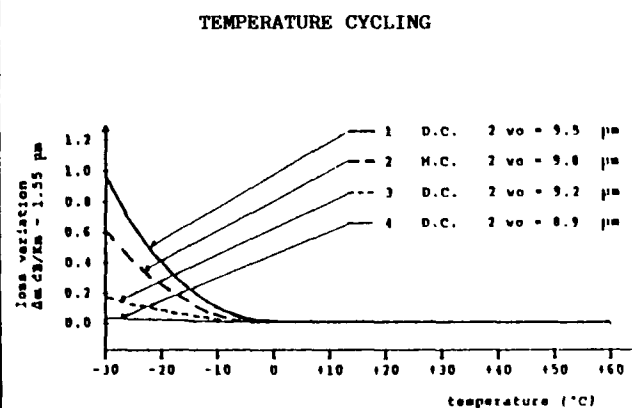


VARIOUS TYPICAL FIBRES USED IN CABLE PROTOTYPES

APPENDIX 1



APPENDIX 2



APPENDIX 3

## SPECIFIC DESIGN OF OPTICAL CABLES TO BE USED IN HARSH ENVIRONMENT

JP BONICEL \* - O. TATAT\* - M. de VECCHIS \*\*

\* Alcatel Cable - 148 Avenue Jean Jaurès - 69344 LYON - FRANCE

\*\* Alcatel Cable - 30 Rue des Chasses - 92111 CLICHY - FRANCE

### ABSTRACT

This paper presents several types of design for cable to be used in harsh environments. Different possibilities are reviewed and examples of practical realizations are given.

### INTRODUCTION

Environmental conditions for optical fiber cables used for Telecommunications may substantially differ depending on climatic and installation conditions. Optical cables can now be used in some areas where environmental conditions are especially difficult.

In particular, for very cold areas, cables must withstand harsh environments : for buried cables, installation must be done in permafrost and for aerial cables heavy ice and wind loading are often encountered.

In both cases a specific design is needed with improved tensile characteristics and reinforced protections. This paper presents design considerations for optical cables in harsh environments and, as an example, some specific designs of cables adapted to these conditions. Both aerial installation and burial are considered.

### AERIAL CABLES

Although they are known to present a reliability and a lifetime less attractive than duct or direct buried cables and therefore a higher maintenance cost they show a practical and an economical interest, specially for laying and jointing. These cables have an interest in some particular cases :

- mountain areas, having frequently rocky soils, where buried installation will be very expensive ; in these areas zigzags of the roads are also shunted. The distances between poles are generally large and with inclination (strong slopes) ;
- when crossing rivers without having the possibility of crossing a bridge, and where the laying of an underwater cable will be very expensive. In these cases also the distance between poles may be important.

The main constraints applied to aerial cables, in addition to laying conditions, are due to climatic conditions.

Concerning aerial cables the main parameters are :

For the cable :

- lineic weight,
- geometrical characteristics,
- elasticity modulus,
- dilatation coefficient,
- minimal breaking strength.

For the route :

- maximum distance between poles,
- possible unlevellings.

For environment :

- temperature range,
- ice loading per meter,
- maximum wind speed.

The specificity of aerial cables is that they contain one (or several) strength member which allows the cable to be installed on poles. This strength member may be made of steel wires, aluminium clad steel wires (ACS), aluminium alloy (ALDREY, ALMELEC,...), glass fibres, aramid yarns or fibre reinforced plastic (FRP) elements...

According to the position of the strength member in the cable, the main cable structures may be listed as follows :

a) eight-shaped cables : the outer sheath contains both the cable core and the strength member (the messenger). These cables cross section has then the shape of an "eight" (Figure 1 a).

b) cable with a supporting braid : the strength member is completely surrounding the cable core. It is realized with a metallic braid, generally made of steel (Figure 1 b) ; this structure is employed for reparation cable used temporarily when an aerial line is out of order.

c) cable with central strength member : in this case the strength member is located in the center of the cable (the cable core is stranded around the strength member)

d) cable with outer armouring : the strength members are helically stranded around the cable core (Figure 1 c). This kind of structure is mainly used when distances between poles are important (e.g. for overhead ground wires). The wires used may be of several kinds :

- high resistance galvanized steel wires ;
  - almelec wires, presenting a low electrical resistance, but also a poor mechanical strength ;
  - A.C.S. wires, with good mechanical characteristics.
- The armouring can be realized using two different kinds of wires.

e) cable with peripheral, non metallic strength members : fiber glass elements or aramid yarns are incorporated in the outer sheath (Figure 1 d). This kind of armouring is particularly convenient for optical fiber cables.

f) binded cable : the cable is binded to an independant messenger, generally made with a galvanized steel strand. In case of very harsh environment, these structures can be combined (i.e. reinforced central strength member plus armouring, reinforced cable core plus strong messenger,...) It is necessary to evaluate the effects of ice and wind loading and to determine the characteristics of strength members taking into account the distance between poles and sag limits.

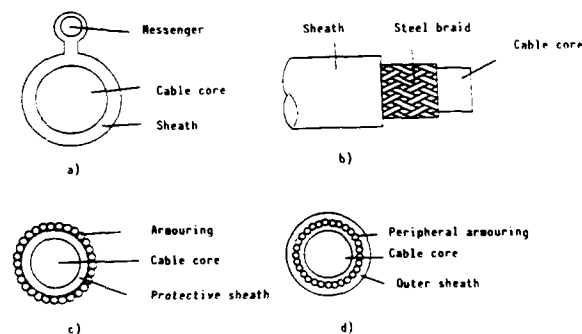


Figure 1

#### Static stability equation :

$$T = p.l^2/8. f, \quad \text{where}$$

T is the longitudinal tensile strength in the messenger;

l is the distance between poles ;

p is the load per unit length applied on the cable (including its proper weight) ;

f is the sag (within the plane defined by the resultant load).

#### Temperature conditions change equation

$$(T_2/s)^2(T_2/s-T_1/s+E\alpha(\theta_1-\theta_2)+Ep_1^2/24T_1^2)=Ep_2^2/24S^2,$$

where for the two conditions 1 and 2 :

Ti is the longitudinal tensile strength in the messenger ;

Pi is the load per unit length applied on the cable (including its proper weight) ;

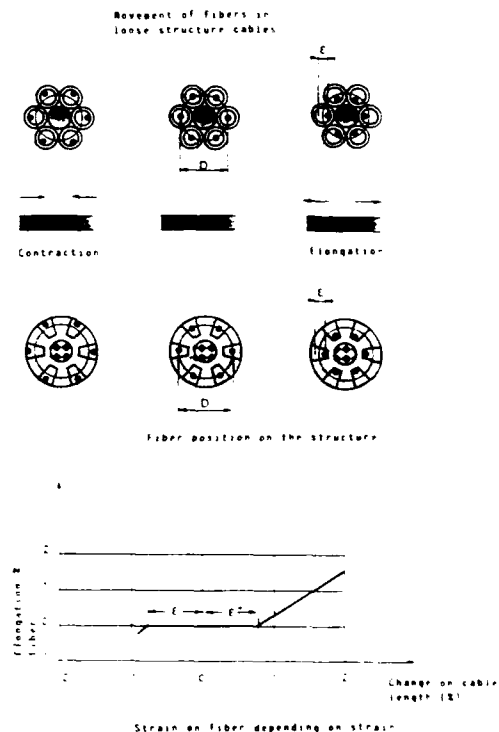
Θi is the temperature of the messenger ;

S is the total section of the messenger ;

E is the elastic modulus of the messenger ;

α is the linear dilatation coefficient of the messenger.

During the design of the cable the possibility for fibers to move inside a loose structure is taken into account (see Table I)



Movement of fibers in a loose structure  
Table I



### Examples of possible solutions

As example of possible solutions, three different types of cables are presented.

Figure 2 shows the cross section of a dielectric aerial cable for span up to 500 m. It can withstand ice loading of 2 cm thickness and the breaking load of the messenger is 15000 daN.

This type of cable is shown on figure 3 .

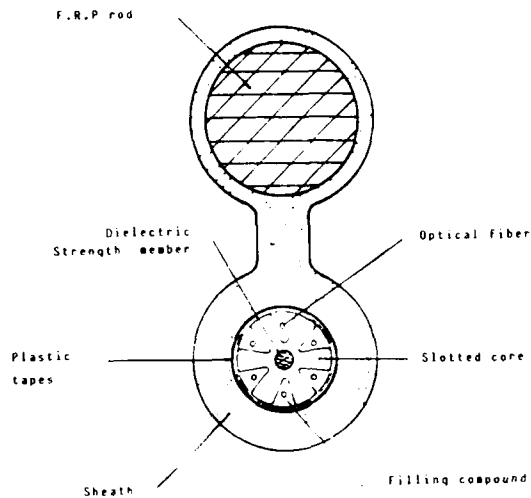


Figure 2

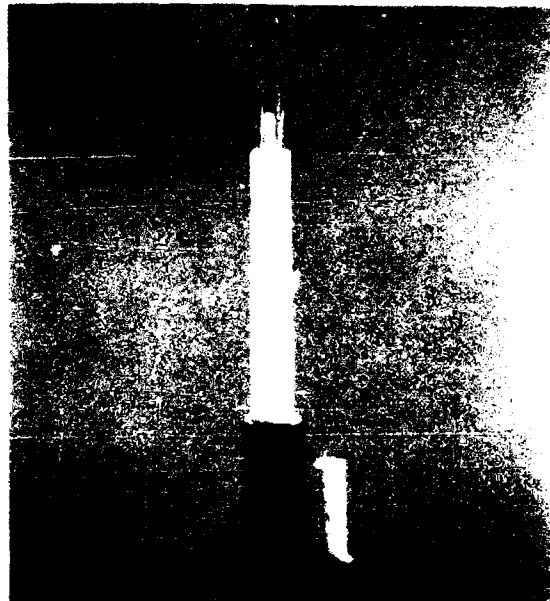


Figure 3

Figure 4 shows the cross section of a concentric structure reinforced by a steel braid. Tensile characteristics can be adjusted by selecting number and dimension of wires.

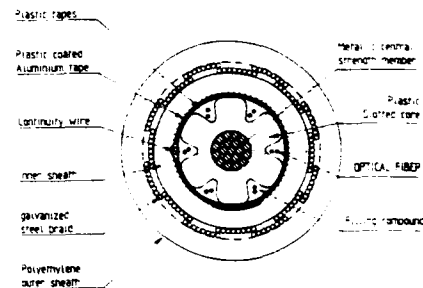


Figure 4

Figure 5 shows the cross section of an optical ground wire with a 2 layer design for armouring. The first layer is made of steel wires in order to adjust the mechanical characteristics.

As an example of a standard design the span can be 500 m and the breaking force 11 tons.

Figure 6 shows such a cable and Figure 7 shows a cable with a single layer of A.C.S. wires.

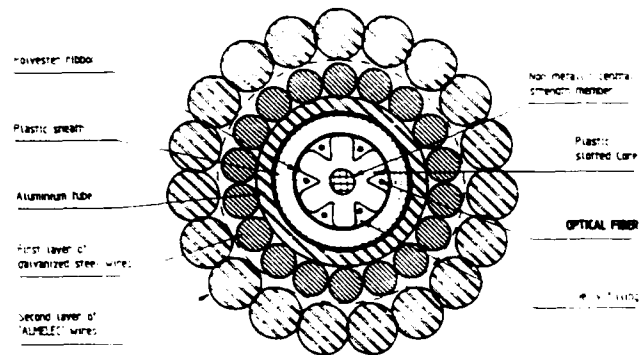


Figure 5

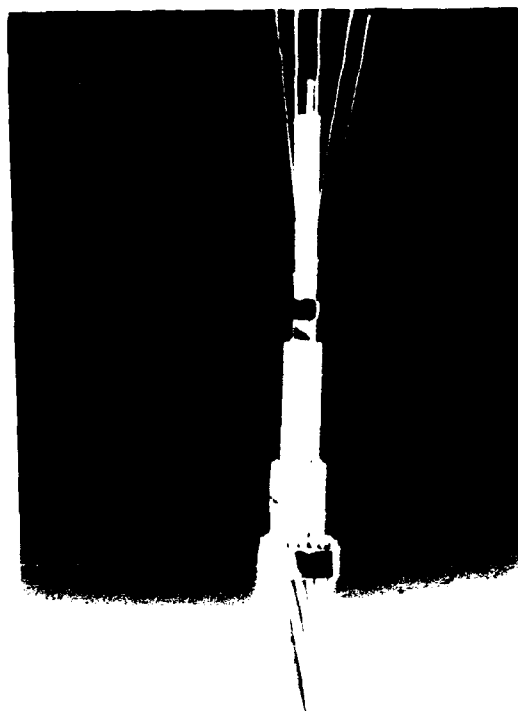


Figure 6

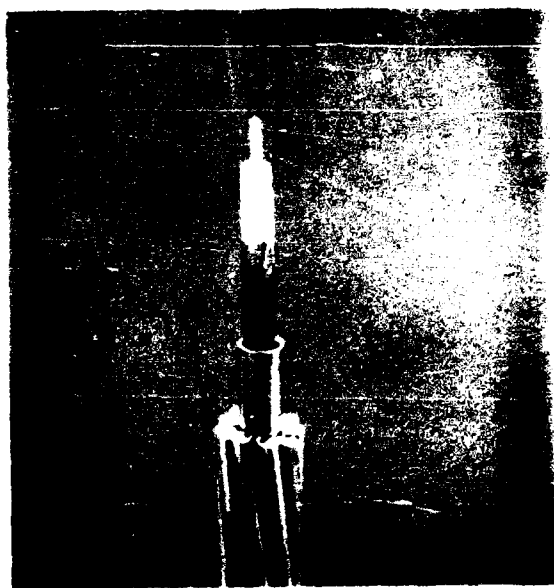
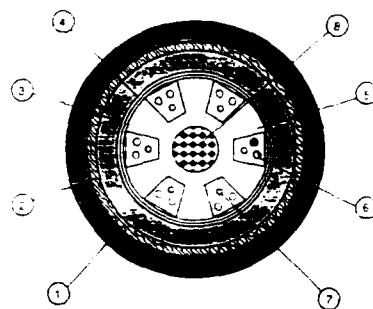


Figure 7

### BURIED CABLES

For buried cables, the conditions are different : cables are sometime buried in permafrost that can create compression strengths on cables and splice closures. Consequently cables must be reinforced by an external armouring . A basic design (cross section) is shown on figure 8 This type of cable can withstand a crush resistance of 450 daN for 10 cm. The cable is shown on figure 9



- 1. Central core
- 2. First layer
- 3. Second layer
- 4. Third layer
- 5. Fourth layer
- 6. Fifth layer
- 7. Sixth layer
- 8. Outermost layer

Figure 8

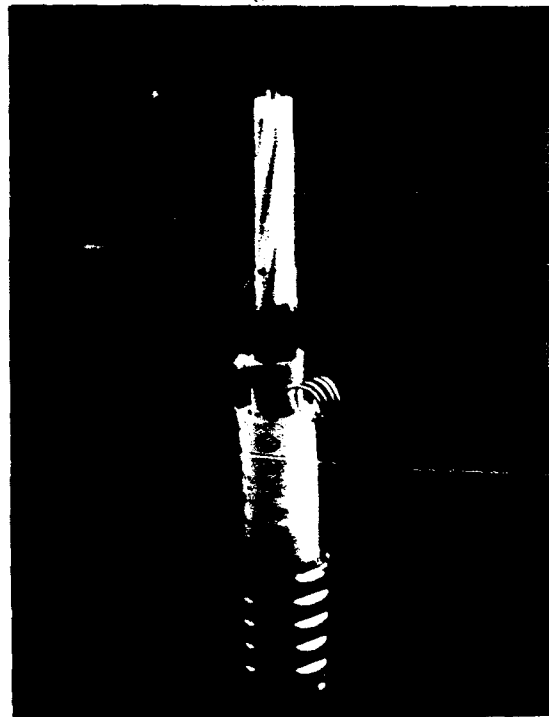


Figure 9

A greater level of protection can be obtained by using steel wire armouring.

A typical cross section is shown on figure 10 and figure 11 shows an example of cable with two layers of steel wires, which can withstand a tension of 3350 daN.

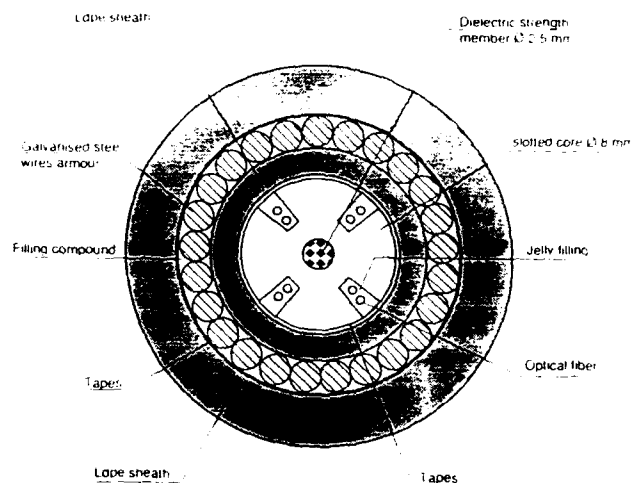


Figure 10

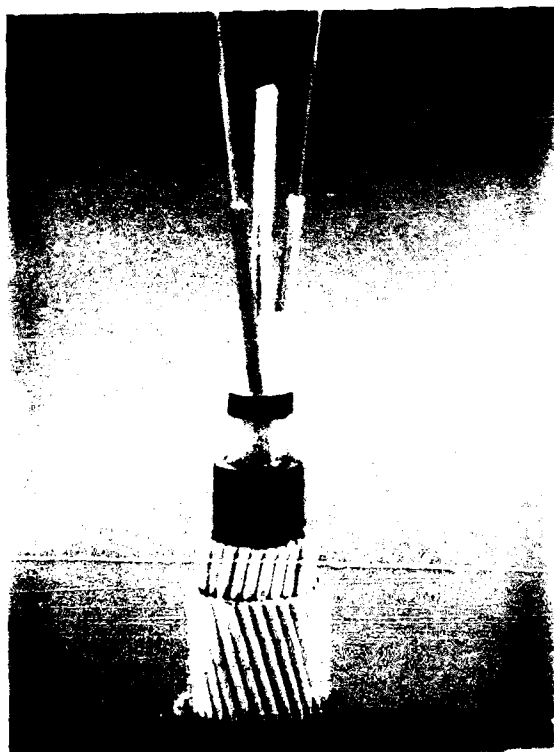


Figure 11

When dielectric cables are necessary it is possible to replace steel wires by Fibre Glass rods. The structure of such cables are given in Figure 12 and 13 for different tensile strengths (2 and 7 tons without stress on fibres), obtained by using one or two layers of armouring.

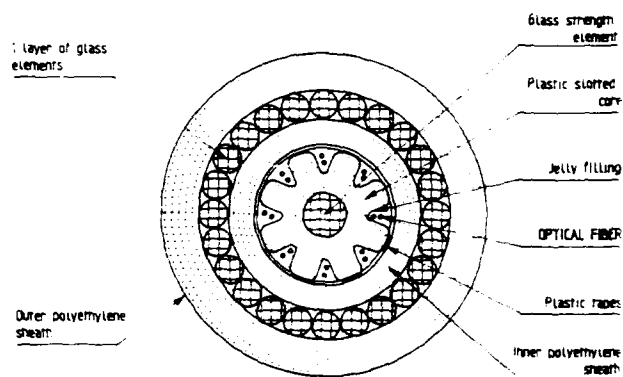


Figure 12

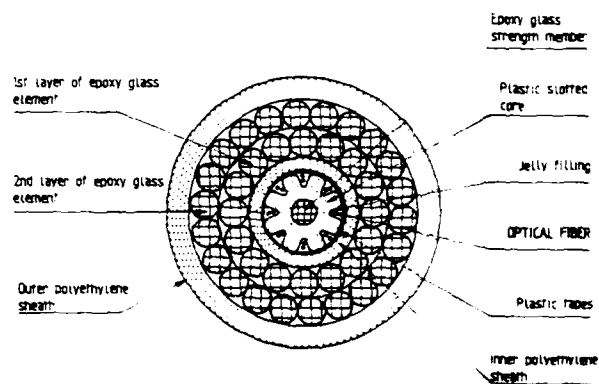


Figure 13

Examples of cables using this type of design are presented on figure 14 and 15 where Fibre glass rods (Figure 14 ) or a combination of aramid yarns and Fibre glass rods (Figure 15) are used.

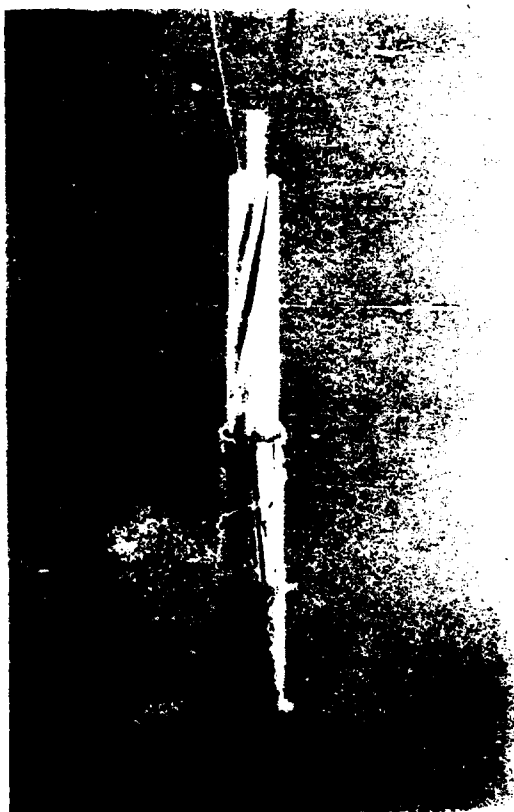


Figure 14

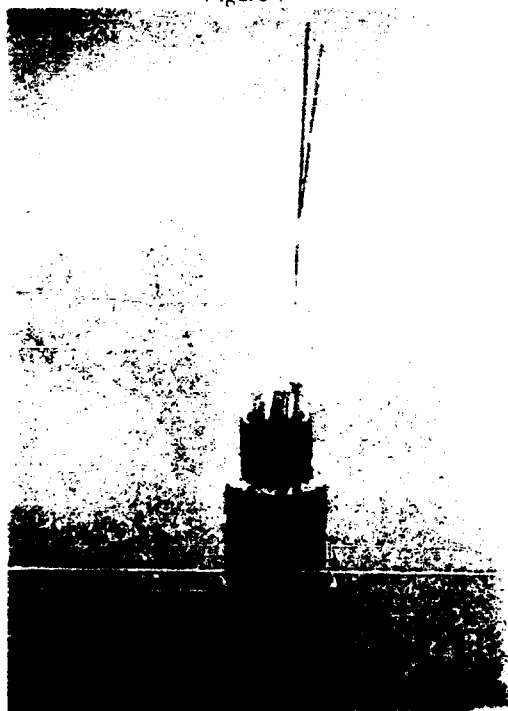


Figure 15

Specific protections are also needed for splice closures and for the connexion of cable to buried repeaters : As the same environmental conditions are applicable, these parts also need specific reinforcements to achieve similar characteristics. Furthermore, these reinforcements have to be connected to cable reinforcements to insure the continuity of mechanical resistance.

**CONCLUSION :** The design of optical cables for harsh environments must be done considering the specific requirements due to the environmental conditions. A reinforcement of strength members and sheath protection is, in general, the basic solution. Several types of technologies are available depending on other requirements (i.e. if the cable can have metallic parts or not).

Considering the different environmental conditions, a qualification is needed for each specification.

#### BIOGRAPHY

**JP. BONICEL - ALCATEL CABLE**  
148 Av Jean Jaurès - 69344 LYON - FRANCE



Jean Pierre BONICEL was born in 1952. He received his engineer degree from the Institut des Sciences de l'Ingénieur de Montpellier (ISIM) in 1976. He joined Les Câbles de Lyon now Alcatel Cable in 1977 where he was in charge of material and mechanical problems for telecommunication cables. Now he is the head of telecommunication cables laboratory.

**O. TATAT - ALCATEL CABLE**  
148 Av Jean Jaurès - 69344 LYON - FRANCE



Olivier TATAT was born in 1959. He received his engineer degree from the Institut des Sciences de l'Ingénieur de Montpellier (ISIM) in 1982. He joined Les Câbles de Lyon now Alcatel Cable in 1985 where he is in charge of material and mechanical problems for telecommunication cables.

M. de VECCHIS - ALCATEL CABLE  
30 Rue des Chasses - 92111 CLICHY - FRANCE



Michel de VECCHIS was born in 1946. He is graduated from Ecole Nationale Supérieure des Télécommunications (1969). He joined LTT in 1970 where he worked on microwave components. He started to work on fiber optics in 1974 and has been Technical Director of the cable Division until the merging in 1986 of LTT cable activities with Les Câbles de Lyon now Alcatel Cable. He is now Director of Technical International Marketing at Alcatel Cable Telecommunications Branch. He is involved in International Standardization of optical fibers and cables (Chairman of CECC WG 28 and Secretary of IEC SC 86 A).

# DEVELOPMENT OF NON-METALLIC FIBER OPTIC CABLE FOR INDOOR USE APPLYING ADVANCED FRP FORMING TECHNOLOGY

Y. Kuwata\*, H. Horima\*, T. Ishii\*\*, S. Matsuno\*\*

\* Sumitomo Electric Industries, Ltd. 1, Taya-cho, Sakae-ku, Yokohama 244, Japan

\*\* UBE-NITTO KASEI CO., Ltd.

579-1, Yabuta, Gifu 500, Japan

## Abstract

Non-metallic fiber optic cables have a remarkable structure which takes maximum advantage of the induction-free characteristic of optical fibers. The need for this structure seems to be increasing with expansion of the range of its application.

In this background, we manufactured fiber reinforced plastic (FRP) strength members of various shapes, such as square- and oval-shaped strength members, in which FRP rod forming technology is developed on the assumption of its application on the strength members of fiber optic cables for indoor use, especially, where flexibility is required. We also designed, manufactured, and evaluated various fiber optic cables for indoor use using them.

## 1. Introduction

The movement to introduce fiber optic cables in various fields is increasing. Especially, the need for non-metallic fiber optic cables, which take maximum advantage of their-induction free characteristics seems to be greatly increasing.

In general, Fiber Reinforced Plastic (FRP) rods are often used as strength members of non-metallic fiber optic cables. The FRP rod, however, has the following disadvantages: its Young's modulus is as small as one-fourth that of the steel wire which is used in metallic fiber optic cables. Therefore, this increases its diameter, resulting in lowering its flexibility. Consequently, there is a problem in using the conventional FRP strength members as the fiber optic cables for indoor use as is where flexibility is required.

Therefore, to improve this FRP rod, we developed FRP strength members of various shapes, such as square-and oval-shaped strength members, that are different from the general round-shaped FRP rod by utilizing the conventional FRP processing technology.

Furthermore, we designed and manufactured various non-metallic fiber optic cables having a small diameter and sufficient mechanical characteristics for indoor use by using these FRP rods.

This paper describes the structure of FRP rods of various shapes, the methods of manufacturing them, their characteristics, and further, the structure and characteristics of the non-metallic fiber optic cables for indoor use applying this FRP.

## 2. Structure and Characteristics of FRP Rods of Various Shapes

When the application of the indoor distribution fiber optic cable that has a small diameter to a strength member is taken into consideration, the use of the FRP rods having a cross section of various shapes, such as square- and oval-shaped strength members, has more advantages than that of the conventional FRP rod having a round cross section. Therefore, we designed and manufactured FRP rods of various shapes by developing the FRP-forming technology to various fiber materials and evaluated their characteristics.

### 2.1 Manufacturing Process of Square- and Oval-Shaped FRP Rods

Figure 1 shows the outline of the manufacturing process of FRP rods of various shapes. Glass fiber, Aramid fiber, poly-amid fiber, or polypropylene is used as a reinforced fiber. The surface is hardened by the UV-ray irradiation lamp after it is dipped in the ultraviolet curable resin containing a photoinitiator and organic peroxide and is shaped by the squeezing die. After that, it is passed through the dry heat duct for complete hardening and then taken out. The FRP rods of various shapes are manufactured by this process.

### 2-2 Characteristics of The Square- and Oval-Shaped FRP Rods

We evaluated various mechanical characteristics of the square- and oval-shaped FRP rods that were manufactured at this time and also evaluated that of round-shaped FRP rod for comparison. Table 1 shows their results. All the rods of different materials and shapes have sufficient flexibility and can be bent at a diameter of 20 mm or less though it depends slightly on the direction. Besides, they can easily stand comparison with the conventional round-shaped FRP rods in the tractive and compressive characteristics. It is expected that they can be applied sufficiently as the strength member of thin non-metallic fiber optic cables for indoor use.

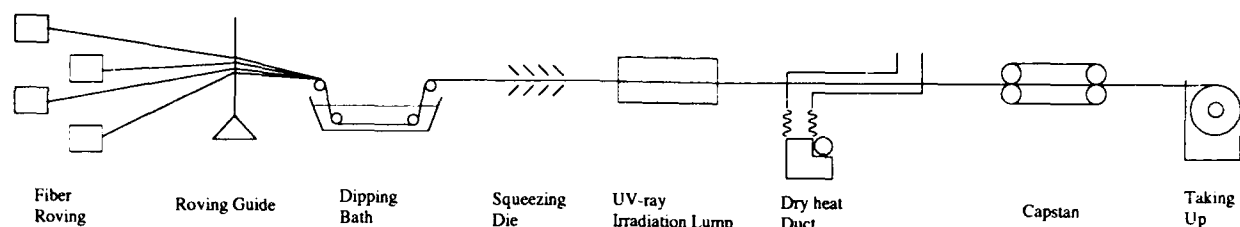


Fig.1 Outline of manufacturing process of square & oval FRP rod

Table 1 Mechanical characteristics of various-shaped FRP rod with various material

Reinforcement fiber material	E-glass	E-glass	E-glass	Polyvinyl-alcohol	Polyamide	Polypropylene
Shape	Round 0.4φ	Oval 1.3 x 0.6	Square 1.6 x 0.5	Square 1.6 x 0.5	Square 1.6 x 0.5	Square 1.6 x 0.5
Weight (g/m)	0.26	1.2	1.5	0.93	0.87	0.71
UV-acrylate resin material	* A	* A	* A	* A	* A	* B
Breaking strength (kg)	20	90	97	55	30	4.8
0.2% elongation strength(kg)	1.25	7.0	7.0	4.3	0.64	0.27
Elongation at breaking strength(kg)	3.0	3.0	3.0	3.1	11.2	25
Minimum bending diameter(mm)	10	20	15	5	5	5
Thermal resistive bending diameter at 80°C(mm)	24	35	30	18	10	10
Compressive strength(kg)	50	>500	>500	>500	>500	>500
Thermal expansion coefficient(%)	$5.9 \times 10^{-6}$	$6.0 \times 10^{-6}$	$6.0 \times 10^{-6}$	$8.9 \times 10^{-6}$	$2.1 \times 10^{-5}$	—
Flexural rigidity(g)	100φ 200φ	2 0.5	30 7	30 7	8 4	2 0.4

- \* A : Phenol novolak type epoxy acrylate
- B : Urethane acrylate

### 3. Application of Square- and Oval-Shaped FRP Rods

The square- and oval-shaped rods can be used in various ways by utilizing their special shapes. Figure 2-1 shows an example of the non-metallic ribbon-slot-type fiber optic cable. In this case, the square-shaped FRP rod is inserted in the square-shaped groove in which a fiber ribbon is inserted. It is used as a reinforcement to improve the tensile strength and resistance to crushing of the cables. Figures 2-2 and 2-3 show other examples of applying them to the non-metallic indoor distribution fiber optic cables by combining them with fiber ribbons and single-core tight buffered fibers.

We manufactured the latter products, 2-types of non-metallic flat type fiber optic cables, this time and evaluated their mechanical and transmission characteristics.

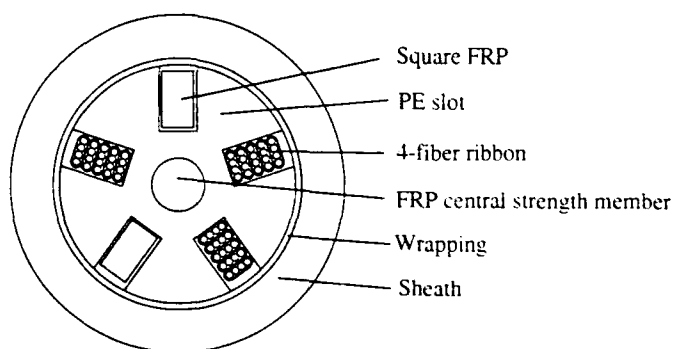


Fig.2-1 Cross section of non-metallic PE-slot type optical cable with square-shaped FRP rods

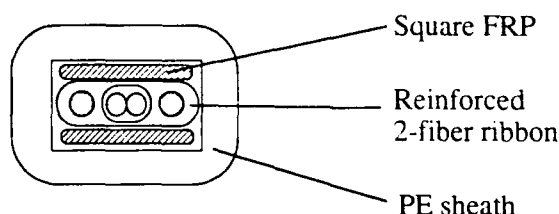


Fig.2-2 Cross section of non-metallic flat cable with square FRP rods & reinforced fiber ribbon

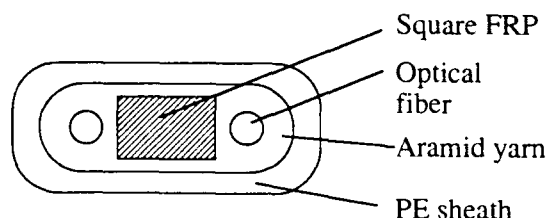


Fig.2-3 Cross section of non-metallic flat cable with square FRP rods & tight buffered fiber

### 3.1 Reinforced Fiber Ribbon

Prior to the manufacture of fiber-ribbon-type flat cable for indoor use, in order to improve the mechanical characteristics of the fiber ribbon itself, we reinforced it with a thin FRP rod, as shown in Figure 3, and integrated it with urethane acrylate resin to develop a reinforced fiber ribbon. Table 2 and Figure 4 show the evaluation results of a two-core single mode reinforced fiber ribbon with respect to the transmission and mechanical characteristics.

It was confirmed that, especially as for the tractive characteristics, the tensile strength at 0.2 percent elongation was improved up to ten times as same as that of fiber ribbon and as for the compressive characteristics the load value in which the transmission loss increases was also improved. Furthermore, good results were obtained with respect to the following items. As for the transmission loss, there was almost no fluctuation at a wavelength of 1.3  $\mu\text{m}$  around the reinforcement processing, and as for the temperature characteristics, the loss variation within the temperature range from  $-10^{\circ}\text{C}$  to  $+60^{\circ}\text{C}$  was less than 0.02 dB/km in length of 1,000 m as shown in Figure 4.

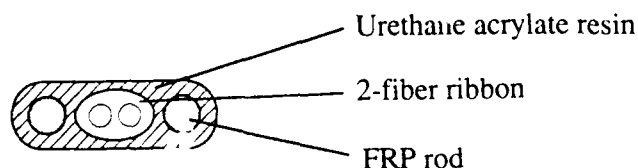


Fig.3 Cross section of 2-core reinforced fiber ribbon

Table 2 Characteristics of reinforced fiber ribbon

Item	Unit	2-fiber ribbon	After reinforcement
Size	mm x mm	0.6 x 0.4	1.6 x 0.5
Weight	g/m	0.27	1.0
Tensile breaking strength	kg	—	41
0.2% elongation strength	kg	—	2.8
Minimum bending diameter	mm	—	10
Thermal resistive bending diameter at $80^{\circ}\text{C}$	mm	—	24
Compressive strength	kg/50mm	—	150
Compressive strength at loss increase at 1.3 $\mu\text{m}$	kg/50mm	50	425
Flexural rigidity	$\frac{100\phi}{200\phi}$ g	—	4.0 1.5

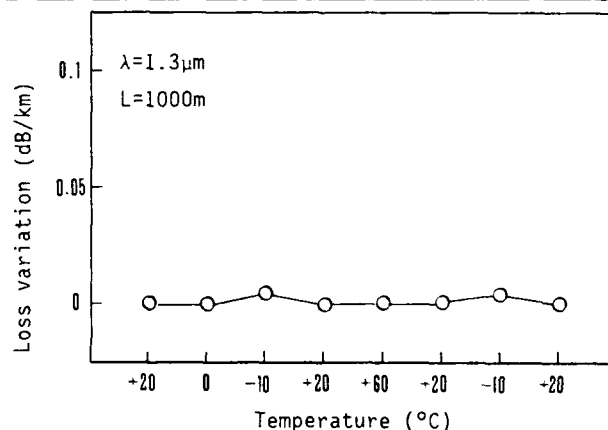


Fig.4 Temperature characteristics of 2-core single mode reinforced fiber ribbon

### 3.2 Fiber-Ribbon Flat Cable

To further improve the mechanical strength of the reinforced fiber ribbon that was introduced above, we designed and manufactured a non-metallic flat cable, as shown in Figure 2-2, in which a reinforced fiber ribbon is sandwiched at its top and bottom with the square-shaped FRP rods. If the top and bottom FRP rods are made of glass-fiber, their rigidity and elasticity increase due to the material. The overall bending rigidity increases and, at the same time, the compression force may be applied on the fiber ribbon because there is no mutual distortion clearance between the top and bottom FRP rods. Therefore, we manufactured a short length of prototype flat cable by using various materials for the top and bottom FRP rods and evaluated the various mechanical characteristics, as shown in Table 3. It was found from the experimental results, shown in Table 3, that the products using glass fiber and polyamid fiber together, or those using glass fiber and polypropylene together, are superior in mechanical characteristics to those of other combinations.



Table 3 Characteristics of ribbon-fiber flat cable with square-shaped FRP rod of various combination

FRP reinforcement fiber material (Position: Top)	Glass	Polyvinyl-alcohol	Polyvinyl-alcohol	Polyamide	Polypropylene	Glass	Glass	Glass
FRP reinforcement fiber material (Position: Bottom)	Glass	Glass	Polyvinyl-alcohol	Glass	Glass	Polyamide	Polypropylene	Polyamide
Minimum bending diameter (mm)	15	15	5	15	15	15	15	—
Bending diameter at loss increase at $1.3\ \mu\text{m}$ (mm)	700	650	210	<200	<200	<200	<200	<200
Compressive strength at loss increase at $1.3\ \mu\text{m}$ in the thickness direction (kg/50mm)	—	—	—	220	200	220	200	220
0.2% elongation strength(kg)	16.6	13.8	11.1	10.2	9.8	10.2	9.8	3.8
Flexural rigidity(g) $100\phi$ $200\phi$	— —	— 70	— —	47 17	50 34	40 34	66 32	21 9

Therefore, we manufactured a 600 meter length flat cable using glass fiber FRP and polyamid fiber FRP together and evaluated transmission and mechanical characteristics. Figure 5 shows the changes in the transmission loss before and after the cable was processed. Figure 6 shows the changes in transmission loss in the heat-cycle processing. Even though a slight increase in transmission loss caused by the compression force is seen in the fiber-ribbon by the ribbon winding on the reel after cable processing, almost stable characteristics are obtained. As for the temperature characteristics, there is almost no loss variation within the temperature range from 0 to  $60^\circ\text{C}$ . It was found that they have good characteristics in the indoor environmental conditions.

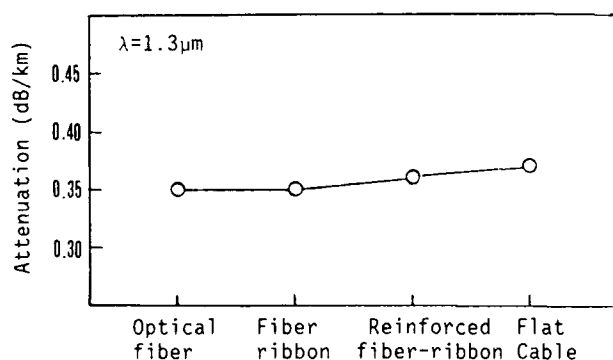


Fig.5 Attenuation of optical fibers in cable manufacturing for non-metallic flat cable with reinforced fiber ribbon

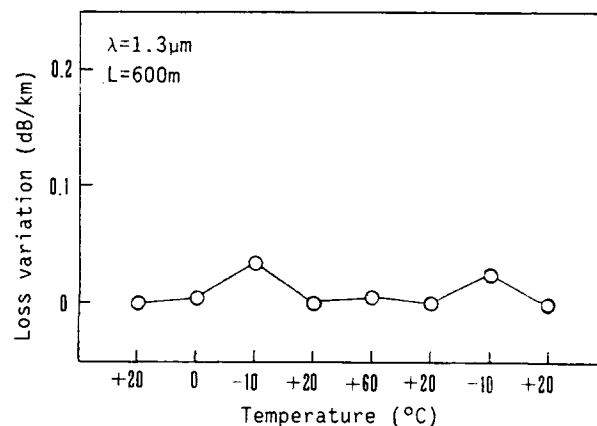


Fig.6 Temperature characteristics of non-metallic flat cable with reinforced fiber ribbon

Table 4 Cable performances of single mode 2-fiber ribbon flat cable with glass & polyamide based FRP rod

Item	Test results
Size	2.7mm x 2.7mm
Weight	6.7 g/m
Bend test	No loss increase was observed at 100mm bending diameter
Torsion test	No loss increase was observed at 10 turns in one direction in length of 1 m.
Heat cycle test	No loss fluctuation was observed in the temperature range from 0 ~ $60^\circ\text{C}$ .

### 3.3 Non-Metallic Flat Cable with Tight-Buffered Fiber

In order to further improve the handling characteristics of cables, we manufactured a flat cable by placing 2-core tight buffered single mode fibers, as shown in Figure 2-3, on both sides of the square-shaped FRP rod and filling up the remaining space with aramid yarn.

#### 3.3.1 Mechanical Characteristics of the FRP Rod

Prior to the manufacture of tight buffered type flat cable for indoor use, in order to prove the superiority of square-shaped FRP as a strength member, we evaluated the bending characteristics and compressive characteristic of the round-shaped FRP rod that has the same cross section and the tensile strength characteristics as those of the square-shaped FRP used this time. Table 4 shows their results. Remarkable improvement was recognized in the square-shaped FRP rod with respect to the mechanical characteristics.

Table 5 Mechanical characteristics of square & round FRP rods

Item	Unit	Square shape	Round shape
FRP size	mm	2.1 x 1.1	1.7 $\phi$
0.2% elongation strength	kg	21	21
Minimum bending diameter	kg	33	51
Flexural rigidity	100 $\phi$	280	440
	200 $\phi$	90	120
Compressive strength	kg/50mm	500	185

#### 3.3.2 Characteristics of Non-Metallic Flat Cable

Therefore, we manufactured and evaluated a flat cable with square-shaped FRP rod and tight buffered type optical fiber. Table 5 shows the mechanical characteristics of the cable and Figure 7 and Figure 8 shows the evaluation results of the transmission characteristic. There was almost no change in transmission loss during the processing. No loss variation was seen in the heat cycle within the temperature range of -10 to +60°C. Also good characteristics were obtained in the bending and compressive characteristics with respect to the mechanical characteristics. It was confirmed that the flat cable structure fully utilizes the excellent characteristics of the FRP rod.

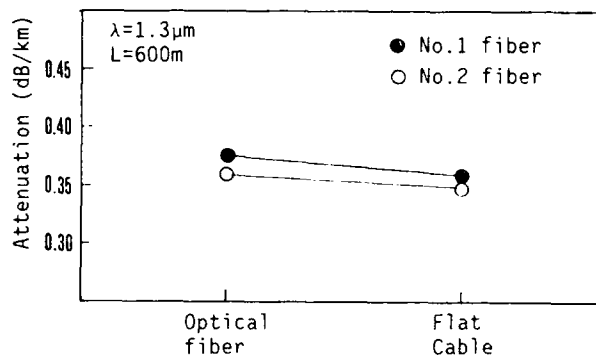


Fig.7 Attenuation of optical fibers in cable manufacturing for non-metallic flat cable with tight buffered fiber

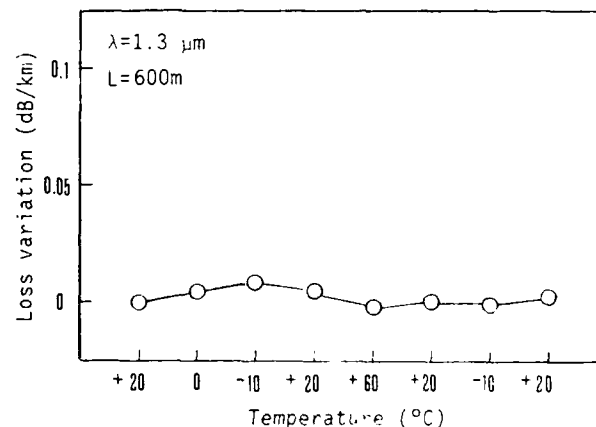


Fig.8 Temperature characteristics of non-metallic flat cable with tight buffered fiber

Table 6 Cable performances of 2-core single mode flat cable with tight buffered fiber

Item	Test results
Size	6mm x 3mm
Weight	15 g/m
0.2% elongation strength	40 kg
Minimum bending diameter	33 mm
Flexural rigidity	100 $\phi$ : 450 g 200 $\phi$ : 125 g 300 $\phi$ : 500 g
Compressive strength at loss increase at 1.3 $\mu$ m	500 kg/50mm
Torsion test	No loss increase was observed at 5 turns in one direction in length of 1 m.
Heat cycle test	No loss fluctuation was observed in the temperature range from -10 ~ 60°C.

#### 4. Conclusion

We developed FRP rods of various shapes, such as the square-and oval-shaped rods, and applied them to the non-metallic structure that fully utilizes the characteristics of optical fiber as strength members of indoor distribution fiber optic cable and manufactured and evaluated the thin non-metallic indoor distribution fiber optic cables that have a small diameter and flexibility by using their FRP rods.

The articles developed this time show excellent transmission and mechanical characteristics under indoor environmental conditions. It is expected that they will further expand the application range of non-metallic fiber optic cables.



Toku Ishii  
UBE-NITTO KASEI  
Co., Ltd.  
579-1, Yabuta  
Gifu 500, Japan

Toku Ishii received the B.E. degree in engineering from Kyoto Institute of Technology in 1984 and joined UBE-NITTO KASEI Co., Ltd. He has been engaged in research and development of fiber reinforced plastics in the optical fiber cables, and so on. He is now a Engineer of Gifu Factory.



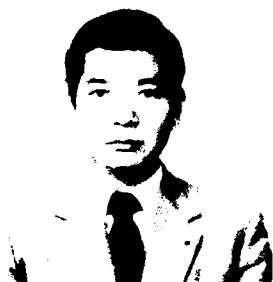
Yuji Kuwata  
Sumitomo Electric  
Industries, Ltd.  
1, Taya-cho,  
Sakae-ku,  
Yokohama 244, Japan

Yuji Kuwata received the B.E. degree in engineering from Waseda University in 1984 and joined Sumitomo Electric Industries, Ltd. He has been engaged in design and development of optical fiber cables. He is now an engineer of Fiber Optics Division.



Shigehiro Matsuno  
UBE-NITTO KASEI Co.,  
Ltd.  
579-1, Yabuta  
Gifu 500, Japan

Shigehiro Matsuno received the B.E. degree in engineering from Kyoto University in 1974 and joined UBE-NITTO KASEI Co., Ltd. He has been engaged in research and development of fiber reinforced plastics in the optical fiber cables, and so on. He is now a Chief Engineer of Gifu Research Laboratory.



Hiroaki Horima  
Sumitomo Electric  
Industries, Ltd.  
1, Taya-cho,  
Sakae-ku,  
Yokohama 244, Japan

Hiroaki Horima received the M.S. degree in engineering from Osaka University in 1972. He then joined Sumitomo Electric Industries, Ltd. and worked on the development of CATV coaxial cables, multipair PEF-insulated junction cables and low loss unbalanced type cables. Thereafter, concentrated on the development of optical fiber cables. He is now Manager of the Fiber Optics Engineering Department of Fiber Optics Division at Sumitomo Electric Industries, Ltd. He is a member of the Institute of Electronics, Information and Communication Engineers of Japan.

## EVOLUTION AND DESIGN OF FIBER OPTIC PREMISE CABLES

*Artis C. Jenkins, Don Mathis, Carla G. Wilson*

AT&T Bell Laboratories  
Norcross, Ga. 30071, USA

### ABSTRACT

Demand is escalating for optical fiber premise cable to be placed inside of buildings. This new demand has been highlighted in several publications on this subject (see references). These cables will be employed for telecommunication, data processing, data links, and computer networks. There are many requirements including flexibility, friction, small size, special materials, splicing ease, flammability and short lengths. This paper addresses the evolution and design of fiber optic premise cables.

### INTRODUCTION

"Premise" cable may be simply defined as cable designed to be placed inside of premises or buildings. These buildings may consist of small businesses occupying an office complex to large businesses in multifloor buildings. A generic premise distribution system is shown in Figure 1. While the requirements and applications of premise systems are certainly different from those of long-haul, interoffice trunking, and loop feeder applications, the same advantages of optical fiber which have made it the medium of choice in these outside plant applications are stimulating its use in the premises' market.

Premise cables are employed to transfer information between computers, PBX and terminal equipment located in different parts of a building which can evolve into Local Area Network (LAN) Systems. Typical cable configurations include single, duplex and multi-fiber arrangements. These configurations have evolved over the years to include multimode, single mode, dispersion shifted and polarization maintaining fiber types. The cables typically contain from one to thirty-six fibers. The current rules employed to design, manufacture, and

place outside plant cable must be modified for cables used in premise applications. The cable distribution facilities in buildings demand cable designs that are mechanically robust and at the same time easy to install and terminate. The unique characteristics of the building environment directly influence the fiber selection, materials, and ultimately the mechanical and optical performance characteristics.

Premise cables are divided into three sub-categories: backbone, distribution and interconnect cables which are defined by the typical required lengths. Backbone cables are usually installed in riser shafts and provide the source of all information coming into the building. The distribution and interconnect cables are then used to carry information to its specific destination. Distribution cables typically have lengths greater than 10 meters. They are used to connect the optical interconnection equipment to termination points in a subsystem. Interconnect cables typically have lengths less than 10 meters and are used in "point to point" connection such as connecting workstations to wall outlets. This paper will discuss the requirements for distribution and interconnect cables. New constraints dictate new designs as fiber optics evolves in the local loop and premise environment.

### APPLICATIONS OF PREMISES CABLES

Fiber optic premise cables are employed in numerous applications in premise distribution systems. One of the major reasons for its increased usage is that fiber optic systems have become cost competitive with metallic systems. The rapid deployment of fiber optic technology permits many applications including video (CATV, teleconferencing and image transmission), data, and voice transmission. One application is "point to point" datalinks in which two computers or a terminal and a computer are directly linked to each other or to another peripheral device. A more complicated application is the Local Area Network. In this application, the communication channels are not dedicated between devices and the need for flexible interconnection is great.

Fiber optic cables have several advantages over copper cables. One major advantage that fiber optic cable has over copper cable is its immunity to electromagnetic interference (EMI). For example, EMI may be a significant factor in a factory environment. Optical fiber cables may be employed as high capacity cables to eliminate coaxial cable in data communications systems, and to connect to the remote location of shared equipment in computer systems. The capability of one pair of fibers to replace these and other copper cables translates into much smaller cables and lower installation costs. This reduced cost and the alleviation of space congestion problems associated with the proliferation of large copper cables are two of the reasons that fiber optic cables are attractive in replacing copper cables.

Flexibility in upgrading the circuit capacity to accommodate future growth and changes without installing new cables is of great advantage. In addition, optical fiber cables provide for longer cable runs and support of many different communication schemes over the same cable.

Premise distribution systems vary from application to application. The application may change over a period of time even within a given building. For example, a collection of point to point datalinks may need to evolve over time into a Local Area Network.

## **REQUIREMENTS**

There are many qualification requirements for optical fiber premise cables. These requirements may be summarized as those required by the customers, Underwriter Laboratories and the local codes. The requirements may be further sub-divided into mechanical, optical and environmental. The premise cable environment is certainly not as severe as, for example, the buried service cable environment. Premise cable is designed for in-door application. However, the cable must be much more flexible for ease of installation and therefore be less robust than buried service cable. Although the cable is not plowed-in, it is sometimes pulled through ducts with 90 degree bends. Buried cable is usually not handled once it is in the ground. Premise cable, however, may be handled frequently if it is, for example, an interconnect cable in a central office. These requirements of flexibility and small size coupled with relatively high tensile strength and impact resistance, create design challenges.

Several organizations have set requirements for premise cable including Bellcore, ICEA, and EIA to name a few. The premise cable tests are given in "Generic Requirements for Intra-building Optical Fiber Cable" in Table I. Each one of these tests has different requirements depending on whether the cable is classified as "Riser (backbone)", "Plenum and General

Purpose (Distribution)", or "General Purpose (Interconnect)". The required testing load and energy level varies with each classification.

As the industry has matured, the operating temperature range as well as other requirements have increased. The environmental cycle is developed to ensure the optical integrity of the cable over its life time with an ageing cycle currently exceeding the one set for outside plant cable. A typical environmental cycle is shown in Figure 2. The duration of this test is a function of the required ageing time but is typically one month. Cables are cycled to -40° to simulate storage conditions.

In addition to these tests, other tests determine sheath strippability, flexibility, aesthetics, handling and ease of entry and splicing. Figure 3 shows a flexibility test which allows a quantitative estimate of a cable's bending stiffness. Some requirements for distribution cable may be completely opposite to requirements for interconnect cable. For example, customers require that the distribution cable have a low friction jacket for ease of installation. Interconnect cables require some friction for connectorization purposes.

It is educational to examine how premise cable requirements have evolved over the last 10 years. As the number of fiber optic cable installations have increased, smaller size has become important. Also optical interconnection cabinets have become smaller and there currently is a need for increased storage tray capacity. All of these have increased the need for smaller cables. However, cable mechanical requirements have not been relaxed. Tensile strength requirements have remained the same or increased. Impact strength requirements have done the same. This is evident on cables such as fiber optic jumpers and pigtails. An example of this can be seen in cordage and new minicord designs (see Figure 6c and 6d). The diameter has decreased about 46% and yet the new minicord must pass the same impact tests as the cordage design.

A technology that impacts directly on the cable industry is the connector industry. As time has passed, these connector designs have become smaller and yet their tensile requirements have remained the same or increased. This requires developing new cable designs which allow better coupling of the connector with the strength members in the cable.

In addition to performance requirements, the premise cables must also pass safety requirements. Codes have been developed to protect building occupants and equipment during a fire. These codes have set requirements based on flame spread and smoke density. Future directions could include toxicity and corrosion levels. Cables are rated based on their performance in selected tests. For example, to be "riser rated", a cable must pass the UL-1666 test; to be "plenum rated", a

cable must pass the UL-910 test. The Plenum test shown in Figure 4 is the most difficult to pass. Cables passing this test must meet stringent flame spread and smoke requirements. Although demand is escalating for nonhalogen designs, specifications have not defined what rates a product as nonhalogen. Therefore, development has been slow in this area.

Finally, the international markets have their own requirements for fiber optic cable. These requirements must be factored in with the American standards in order to satisfy the international and U. S. markets with one design.

### DESIGN CONSIDERATIONS

The premise environment has the potential for use of many cable designs. Increased usage has created a demand for generic, cost effective cables designed specially for the premise environment. There are certain constraints that dictate applicable designs. As has been stated, these include environmental, mechanical, customer and apparatus constraints.

A cross section of a generic premise cable design is shown in Figure 5. There are certain inherent features that each design must have. These include sufficient tensile strength, compressive strength and impact resistance to name a few. The exact value depends on the requirements set by the customer. Each design is composed of an outer jacket, strength members (normally aramid yarns), buffered fibers and sometimes spacers. The designer must package these components together to meet all requirements.

### ENVIRONMENTAL

A generic premise cable should be suitable for installation within the structure of a building as well as within electronic equipment. Often, this requirement heavily influences material selection. Cables placed in a plenum environment require materials with very high Limited Oxygen Index (LOI) such as fluoropolymers; consequently, these cables are often stiff and more expensive. Riser cables require materials with a sufficient LOI (such as PVC) but not as high an LOI as is required for a plenum cable.

One must know the intended life of the cable product. This requires knowledge of the thermal extremes at the location where the cable is installed. Any design must be able to function over the identified time period without deterioration. Therefore the response of all materials used in the cable to the temperature extremes must be known. Important properties include coefficient of thermal expansion, modulus of elasticity/material shrinkage, hydrolytic stability and oxidative stability.

Cables may be placed in extreme environments. The cables could be placed in tension in a high humidity environment. This could cause static fatigue of the glass fiber and possibly cause the fiber to break. Cables could be exposed to chemicals that could cause a cable to deteriorate over time. All of these environments must be considered in a cable design.

### MECHANICAL

Within any premise environment there are many mechanical constraints and mechanical considerations. The main purpose of the cable is to provide protection for the individual fibers. This is especially true during cable installation. Facilities with complex routing can cause high mechanical stresses in the cable during installation. It is important to isolate these stresses from the fibers. The cable should be as small as possible to conserve space in typically crowded ducts. The cable must have a jacket with low frictional properties and a core with sufficient robustness. Cable weight and bending stiffness are also important during installation.

### CUSTOMER

Since the customer specifies a particular fiber type, a design must be versatile enough to work with any of these fiber types. A cable design which contains single mode fiber must be robust enough to reduce macrobending loss at 1550nm wavelength. A Fiber proof strength dramatically affects the tensile rating and therefore, the size of the cable product. Cables with lengths on the order of 10 m or less are required to have low cut off wavelengths to reduce modal noise. Customers could require reliability tests which requires quantitative measurements of cable quality.

### APPARATUS

The indoor communication environment is apparatus intensive. Any cable design must be compatible with associated hardware. The sheath must be easy to enter and have low friction for installation. The fibers are required to be buffered and with identifiable colors for aid in relocation of fibers during system reconfiguration. Buffered fibers must also be strippable with standard mechanical stripping tools. The number of cable sizes must be minimized to reduce the amount of required apparatus.

### DESIGN CONFIGURATIONS

Figures 6 and 7 show typical configurations for interconnect and distribution cables seen in the premise cable environment respectively. Figure 7a and 7c

shows the buffered fiber designs. These designs are normally 2, 4, 6, 12, 18, 24 and 36 fiber count cables. Each fiber count often requires a different outer diameter. Figure 7b and 7d shows the breakout cable. This cable is similar to the buffered fiber cable but single fiber cables are employed in place of the buffered fibers. This cable is larger and more robust but is stiffer. Each subunit has sufficient robustness allowing the unit to be separated and run individually to desired locations without damage. Figure 6F shows ribbon interconnection cables. These cables are employed for backplane connections and point to point connection with computers and other peripheral equipment.

As fiber optics evolves more in the local loop and premise environment, new constraints will dictate new designs. Some additional new designs on the horizon include hybrid cables (designs containing a mixture of fiber types or media types), nonhalogen, flexible plenum, and indoor/outdoor cable designs.

### SUMMARY

Fiber optic cables are being rapidly deployed in the premise environment. This environment dictates many different cable designs including backbone, riser and interconnection cables. Requirements exist but are continuously being revised to ensure the successful installation and use of these designs as applications evolve. The challenge for manufacturers is to reduce the number of designs and at the same time provide the quality features and meet the full range of requirements set by the customers.

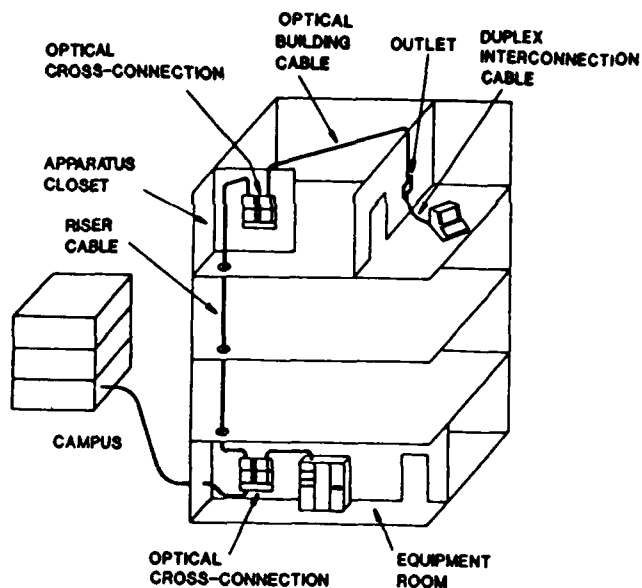


Figure 1: Fiber Optic Premises Distribution System

<p align="center"><b>Table I</b> <b>Generic Requirements For Premise Cables</b></p>			
<b>NO.</b>	<b>TEST DESCRIPTION</b>	<b>INTERCONNECT CABLE</b>	<b>DISTRIBUTION CABLE</b>
<b>1</b>	<b>Temperature Cycling</b>	EIA-455-3A 0°C to 50°C	EIA-455-3A 0°C to 50°C
<b>2</b>	<b>Aging</b>	EIA-455-3A Continuation of Temp. cycling 85°C, 336 hrs	EIA-455-3A Continuation of Temp. cycling 85°C, 336 hrs
<b>3</b>	<b>Fire Resistance</b>	VW1-UL 1666-UL-910	UL 1666-UL-910
<b>4</b>	<b>Strippability</b>	EIA-455-178 15mm (0.6) in ≤ 13.4N (3 lbf)	EIA-455-178 15mm (0.6in) ≤ 13.4N (3 lbf)
<b>5</b>	<b>Cyclic Flexing</b>	EIA-455-104 Mandrel Dia. = 20X Dia. 300 cycles	EIA-455-104 Mandrel Dia. = 20X Dia. 100 cycles
<b>6</b>	<b>Impact</b>	EIA-455-25 .74 N-M (.54 ft-lb), 20 cycles 150mm (5.9in)	EIA-455-25 2.9 N-M (2.2 ft-lb), 20 cycles 150mm (5.9in)
	<b>Twist</b>	EIA-455-85 Length = .3 meter (11.8 inches)	EIA-455-85 Length = 1 meter (3.3 feet)
	<b>Low &amp; High Temperature Bend</b>	EIA-455-37 Mandrel Dia. = 20X Dia./50mm(2.0 in) X kg, 10 Turns 0°C & 50°C	EIA-455-37 Mandrel Dia. = Dia./15.2cm(6 in) X kg, 10 Turns 0°C & 50°C
	<b>Compression</b>	EIA-455-41 10.16cm (4 in) Dia., 3.5 N/mm (20 lbf/in)	EIA-455-41 10.16cm (4 in) Dia., 10 N/mm (57 lbf/in)
<b>10</b>	<b>Tensile Strength</b>	EIA-455-33 220N (50 lbf)	EIA-455-33 ≤ 12f 444N (100 lbf), ≤ 12f 665N (150 lbf)
<b>11</b>	<b>Cable Jacket Shrinkage</b>	EIA-455-86 15 cm (6 in.)long, 0.6 cm (.24 in.)wide 121°C, 2 Hrs, Shrinkback ≤ 5%	EIA-455-86 15 cm (6 in.)long, 0.6 cm (.24 in.) wide 121°C, 2 Hrs, Shrinkback ≤ 5%

Single-Mode & Multimode change in loss should be ≤ 0.2 & 0.5 dB respectively.



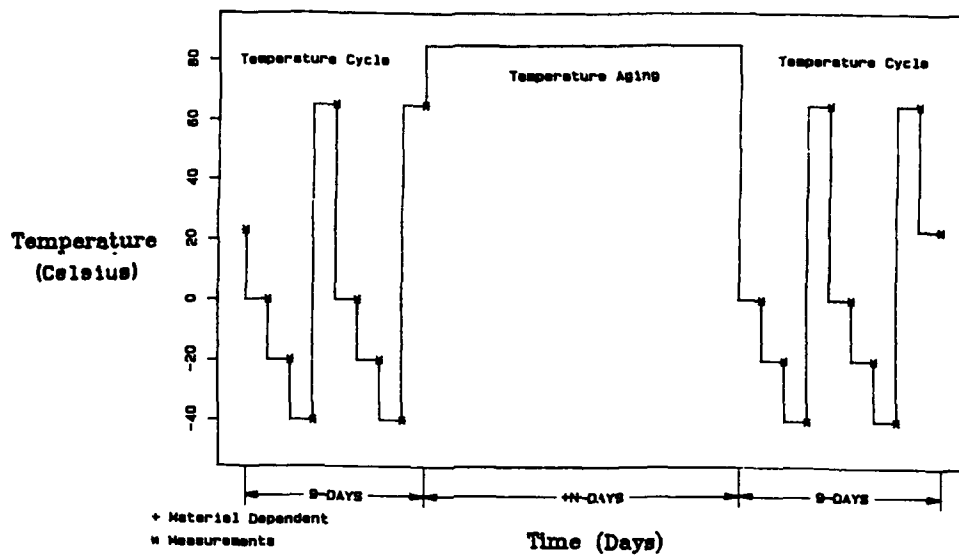


Figure 2: Generic Environmental Temperature Cycle

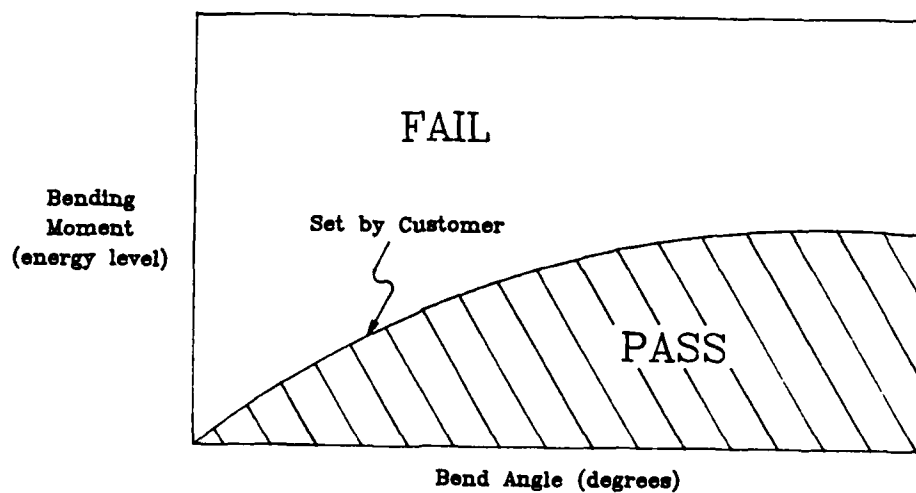


Figure 3: Flexibility Test

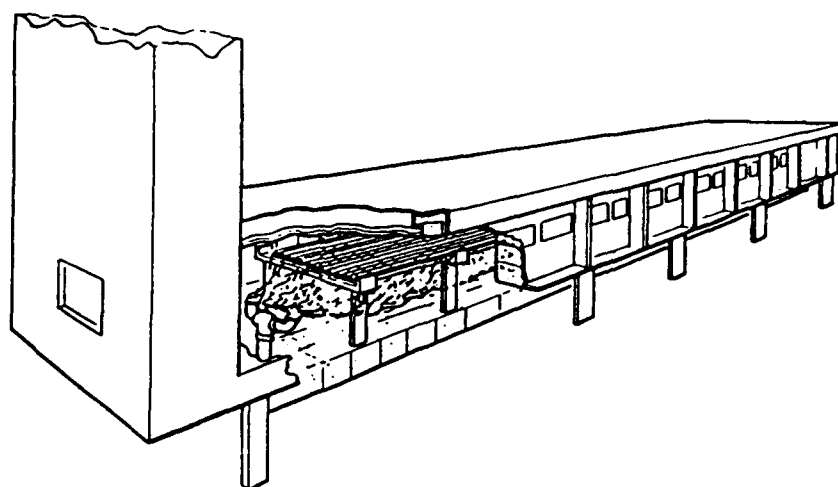


Figure 4: Plenum Cable Fire and Smoke Test (UL-910)

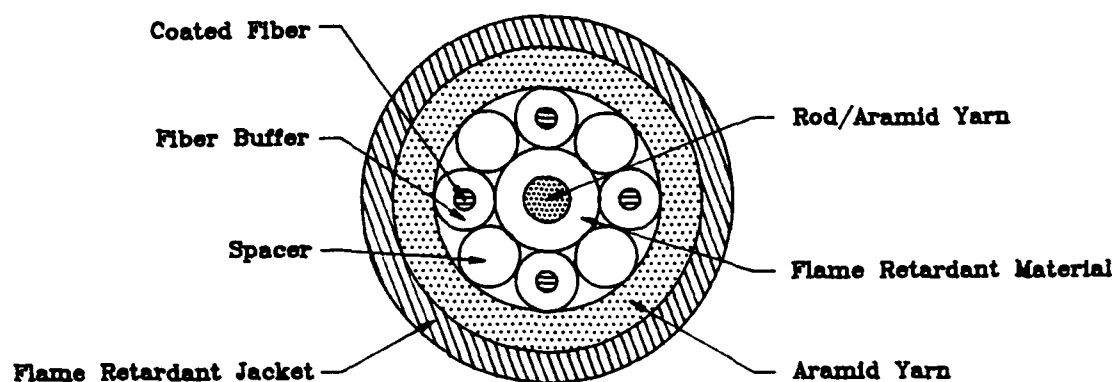
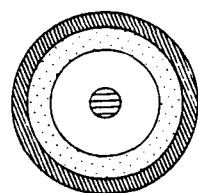
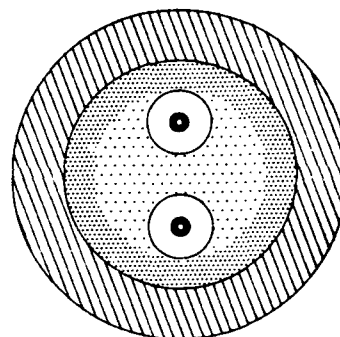


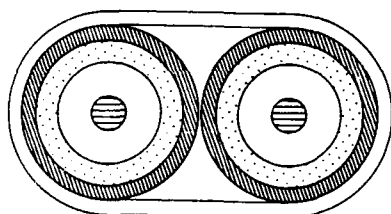
Figure 5: Generic Fiber Optic Premise Cable



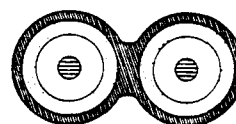
(a) Single Fiber  
(Cordage)



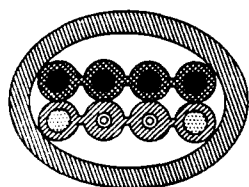
(b) FDDI  
(Fiber Distribution Data Interface)



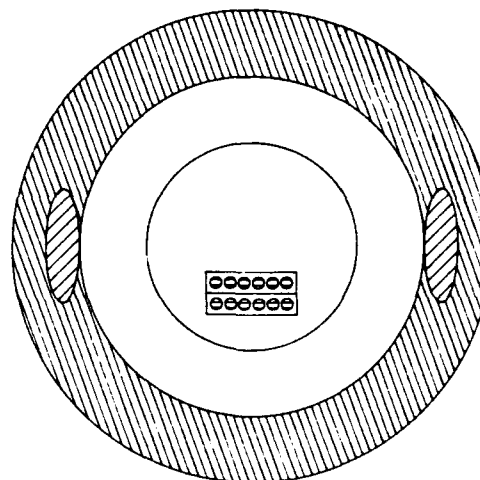
(c) Duplex



(d) Minicord Duplex

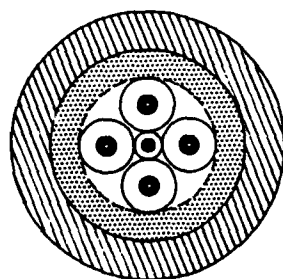


(e) Hybrid

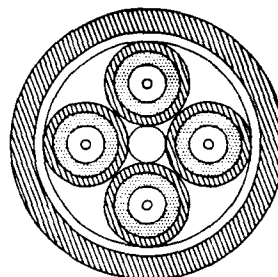


(f) Ribbon

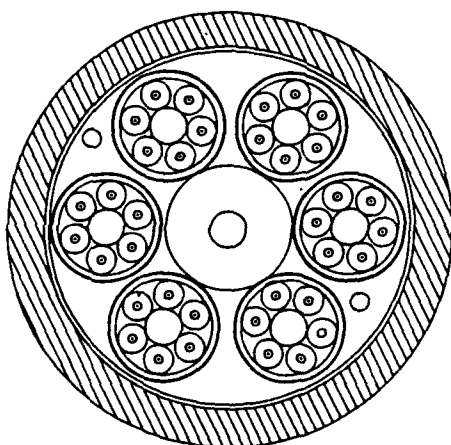
Figure 6: Fiber Optic Premise Interconnect Cables



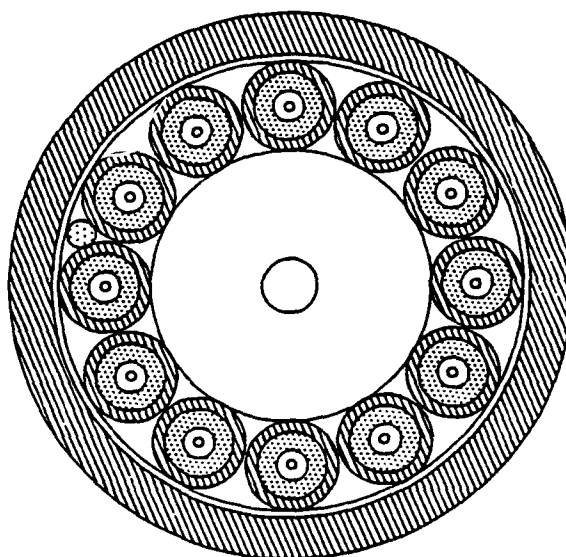
(a) Low Fiber Count  
(Buffer)



(b) Low Fiber Count  
(Breakout)



(c) High Fiber Count  
(Buffer)



(d) High Fiber Count  
(Breakout)

Figure 7: Fiber Optic Premise Distribution Cables

## REFERENCES

- H. Dunnenberger III, R. R. Frey.  
*"Fiber Optic Cables for the Intrabuilding Environment"*  
FOC/LAN 84, pp. 313-315
- J. T. Loadholt, T. M. Williamson  
*"Design of Custom Premises Fiber Optic Cables"*  
Proceedings of International Wire & Cable Symposium, 1984, pp.357-
- R. A. Cerny, A. B. Kasiewicz  
*"Combined Cable Technologies Challenge Coaxial for LAN Wiring"*  
Hard Copy, Nov. 1986, pp. 135-139
- J. L. Hardiman  
*User Considerations for the Use and Selection of Fiber Optic Cables In Premise Distribution Systems*  
IEEE 1985, pp. 1212-1216
- J. L. Ellis  
*"Practical Considerations in Determining the Established Cost of Lans, Optical Fiber Cables - Present & Future"*  
FOC/LAN 1984, pp. 147-152
- R. E. Jamison  
*"General Concerns for LAN Fiber Optic Cable Installation"*  
FOC/LAN 1984, pp. 168-173
- M. R. Gotthardt  
*"Lightguide LAN/Premises Product Integration"*  
FOC/LAN 1986, pp. 127-129
- J. P. Varachi, C. H. Hisz  
*"Distribution of Fiber Optic Facilities in Commercial Buildings"*  
IWCS 1987, pp. 169-174
- M. Hirai, M. Kawase, H. Kobaysha, Y. Kutsuyama  
*"Optical Fiber Cables for Local Area Network"*  
IEEE 1983, pp. 707-712
- R. Williams, P. Garner  
*"Fiber Optic Building Wiring System"*  
FOC/LAN 1984, pp. 301-304



Artis Jenkins is supervisor of the Fiber Optic Building Cable Group in the Fiber Optic Media Department at AT&T Bell Laboratories located in Norcross, Georgia. His group is responsible for the design of all fiber optic premise cable products including riser, plenum and indoor/outdoor.

Dr. Jenkins joined AT&T Bell Laboratories in 1980 and has designed outside plant, military and premise cables. He has been granted two patents and has written numerous papers on his work. He developed and taught a short course on cable design at IWCS 1990 and will conduct the same course at IWCS 1991.

Dr. Jenkins received his B.S. degree in Mechanical Engineering from North Carolina State University. He also has a Masters and Doctorate degree in Mechanical Engineering from the Georgia Institute of Technology.



Carla Wilson is a Member of Technical Staff in the Fiber Optic Media Department at AT&T Bell Laboratories in Norcross, Georgia. She is responsible for the design and development of optical fiber premise distribution and interconnect cables. Her current assignment emphasis is on plenum cable applications.

Ms. Wilson joined AT&T Bell Laboratories in 1975. She received her B.S. degree in Electrical Engineering Technology from Southern College of Technology in Marietta, Georgia.

She has been granted three patents on cable design with one more pending.



Don Mathis is a Member of Technical Staff in the Fiber Optic Media Department at AT&T Bell Laboratories in Norcross, Georgia. He is responsible for design of optical fiber service cables and premise cables.

Dr. Mathis joined AT&T Bell Laboratories in 1972. He has B.S. and M.S. degrees from Oklahoma State University, and a Ph.D degree in Mechanical Engineering from the University of Houston.

He has been granted seven patents with two more pending.

## DESIGN AND DEVELOPMENT OF STEAM RESISTANT FIBER OPTIC CABLE

Mahesh K. R. Vyas, Eric L. Buckland and Paul Neveux, Jr.

Sumitomo Electric Fiber Optics Corp., Research Triangle Park, NC 27709

### ABSTRACT

A systematic design and development of a novel Steam Resistant Loose Tube (LT) optical fiber cable is discussed. This design utilizes a hydrolytically and high temperature stable LT material. Moisture ingress into the cable core is highly suppressed by enclosing the optical core with a welded aluminum tube. Cable lifetime is increased substantially by using this design compared to standard polyethylene sheathed PBT LT cable designs. A mathematical model for the rate of change of MFI of PBT has been developed and used to justify this chosen cable design which meets all the mechanical and environmental requirements of Bellcore Technical document TR-TSY-000020, Issue 4, March 1990.

### 1.0 INTRODUCTION

Loose tube (LT) optical fiber cable designs have been widely used in industry to date. Polybutylene terephthalate (PBT) is commonly used as a preferred tube material because of its good mechanical and chemical characteristics, along with easy processibility.

Recently the deficiency of such an LT cable design was highlighted through the installation of such cables next to steam ducts in New York City and Cleveland. The underground steam ducts in these cities are approximately 80 - 100 years old and consequently are prone to steam leakage through aging and fatigue of steam pipes. In two specific instances, failure of steam pipes has been monitored recently. The average temperature and pressure of escaping steam is up to 400°F and 400 psi depending on the pipe size. (1) In both cases, the incipient failure resulted in the long term exposure of LT optical cable to such a harsh hot and humid

steam environment. The cumulative effect of such an exposure resulted in cable failures in both cases. A detailed examination of the failed cable sample revealed:

- (a) Catastrophic failure of PBT tubes (Fig. 1)
- (b) Swelling and degradation of fiber acrylate on-line coating (Fig. 2)



FIG.1. PHOTOGRAPH SHOWING DEGRADATION OF PBT TUBES IN A PLAIN SHEATH CABLE FIELD FAILURE.

The above scenario clearly highlighted the need for a more robust cable design which can be successfully used in such a hostile environment. In order to provide the high degree of reliability required for steam applications, cables must be designed using temperature and hydrolytically stable materials. Additionally, the UV acrylate coated fibers should be fully isolated from the ingress of moisture.

The aim of this investigation is to identify the engineering requirements

for steam environment applications. The study then identifies both tube and cable jacketing materials which are stable in such hostile environments. This paper discusses in detail the material compatibility studies undertaken along with the evolution of a new cable design based on a simple model and the results of experimental investigations.



FIG.2. PHOTOGRAPH SHOWING SWELLING AND DEGRADATION OF ACRYLATE ONLINE FIBER COATINGS.

## 2.0 THE STEAM ENVIRONMENT

The steam delivery systems in place in New York, Cleveland, Boston and elsewhere contain super-heated moisture at pressures to 150 psi or more, at temperatures to 400°F. Two modes of steam attack on fiber optic cables include the escape of steam through fractures in the antiquated piping system, or water external to the steam delivery system boiling on contact with the piping. For example, based on the thermodynamics of escaping steam from a 200 psi tunnel, at 400°F, it is estimated that the maximum exposure temperature to a neighboring cable is 250°F to 280°F. While this is an anticipated maximum exposure, practical experience indicates that the subject environment at the cable surface is below 212°F.

In order to get a comprehensive picture of the degradation of cable components in steam environments, the effects due to any chemicals used in these steam systems have to be quantified. Both in Cleveland and New York, the chemical constituents of steam are analyzed periodically. Table 1 shows such an analysis carried out for #2 and #4 steam canals of Cleveland. The chemical

constituents of steam are shown to be non-corrosive in nature. Similar data has also been obtained for steam canals in New York. Thus the degradation effects due to chemical constituents of steam are negligible and hence the primary degradation effects of concern in steam are mainly due to exposure to high temperature and humidity.

Table 1. Analysis of Chemical Constituents in City Water and Steam of Cleveland's #2 and #4 Main Steam Canals

Chemical Constituents (ppm)	City Water	Steam #2 Main Steam Canal	Steam #4 Main Steam Canal	Demineralized Water
Calcium	75	Nil	Nil	Nil
Magnesium	45	Nil	Nil	Nil
Sodium	20	10	5	5
Total Electrolyte	140	10	5	5
Bicarbonate	100	20	15	50
Carbonate	0	0	0	0
Hydroxyl	0	0	0	0
Sulfate	10	10	5	10
Fluoride	20	0	0	0
Chloride	30	20	20	30
Nitrate	0	0	0	0
Carbon Dioxide	0	0	0	0
pH	8.2	8.0	8.0	8.2
Conductivity	29.0	0.47	0.49	0.28
Silica	3	10	0	0
Iron	0	0	0	0
Turbidity	0	0	0	0
TDS	100	65	60	60
Color	0	0	0	0

Test data supplied by Cleveland Thermal Energy (courtesy of R. Henry Water Treatment Corp., Ohio)

## 3.0 MATERIAL REQUIREMENTS

The key issue is the survival of the delicate optical fibers when exposed long term to this high temperature steam. Since a high temperature steam environment is conducive to hydrolysis of both polyesters and acrylates, it is evident that standard PBT tubes in traditional loose tube cable constructions are inappropriate for the protection of optical fibers in this application. Alternative tube and/or jacket materials are therefore required. Ideal materials must fulfill four key requirements:

- 1) Materials must be stable to long-term exposure of at least 120°C.
- 2) Materials must be hydrolytically stable.
- 3) Materials must suppress moisture penetration to the vicinity of the optical fibers.
- 4) Materials should be readily processible using existing equipment.



Other key material attributes are good chemical and compressive resistance, high strength and low shrinkage.

### **3.1 Tube and Material Selection**

High performance polymers like fluoropolymers offer one obvious choice for tube and jacket materials. In all four tube materials were evaluated here, namely:

**Material A:** A PVDF-based material with a stable temperature rating of around 250°F (PVDF).

**Material B:** An amorphous Polyethersulphone with a stable operating temperature of greater than 300°F (PES).

**Material C:** This is a copolymer of Ethylene & chlorotrifluoroethylene with stable operation around 270°F (E-CTFE).

**Material D:** Improved hydrolytic stability PBT.

Some properties of these selected tube materials are shown in Table 2.

### **3.2 Tube Processing**

PVDF, PES and PBT are readily manufactured using standard LT Extrusion equipment. E-CTFE requires the use of a special Hestalloys Barrel and tooling. Excess fiber lengths are maintained in the desired range for PES, E-CTFE and PPT. However, PVDF material had lower melt strength and high post-extrusion shrinkage resulting in rather high and poorly controllable excess lengths. PVDF is therefore not acceptable candidate tube material at this time.

### **4.0 TUBE MATERIAL RELIABILITY TESTING**

A comprehensive program was conducted to evaluate the performance of these candidate tube materials. Test details are outlined below.

#### **4.1 Low Temperature Bend Test**

Low temperature bend is performed by wrapping each tube ten times around a mandrel the same size as tube O.D. at -20°C and observing for any kinks or cracks in the tubes. Minimum soak time for each tube was two hours.

#### **4.2 85°C/Jelly Aging Bend Test**

After test I is completed, tubes (secured around mandrel ten times) are placed in a pan of Naptel 851 jelly. The pan is then placed in a temperature cabinet at 85°C for 30 days. Tubes are

checked for further signs of cracks after 5, 15 and 30 days aging respectively.

### **4.3 High Temperature Stress Cracking Test**

Ten turns of samples of each material are wound on x 5.0 and x 10 mm mandrels respectively and aged for 30 days at 150°C/ambient air and 170°C/ambient air respectively. Samples were checked for cracks after 1, 7, 15 and 30 days aging respectively.

### **4.4 Tube Compression Test**

Tube samples of each of these materials are placed between compression plates in an Instron Tensilometer and compressed at steady rate until 2700N load was reached. Effective tube modulus and yield load are calculated from the slope of the compression curve.

### **4.5 85°C/94% R.H. Tensile Aging Test**

Dumbbell samples of materials are aged at 85°C/94% R.H. at different time intervals of 15, 31, 45 and 60 days, and tensile tested to evaluate degradation in material yield strength and elongation at yield.

### **4.6 PBT MFI Aging Test in 100°C Water**

Two meter cable samples containing PBT tubes are boiled in 100°C water with cable ends isolated from water. Melt flow index of standard PBT and hydrolytically stable PBT tubes is measured and compared after different aging time intervals.

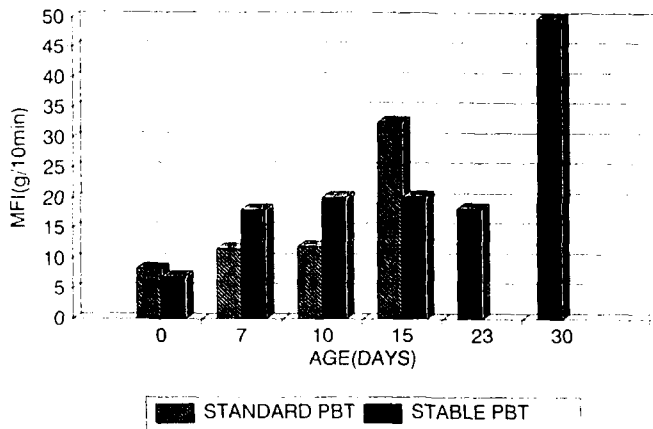
### **4.7 Tube Shrinkage Test**

2 m tube samples are soaked for 24 hours at 120°C and tube shrinkage measured.

Results of tests 4.1 to 4.4 are tabulated in table 3. Both polyethersulphone and E-CTFE are shown to be superior in performance than the hydrolytically stable form of PBT in cyclic cold bend flex tests. Furthermore, no stress cracking is observed up to 30 days exposure at 170°C in ambient humidity applications.

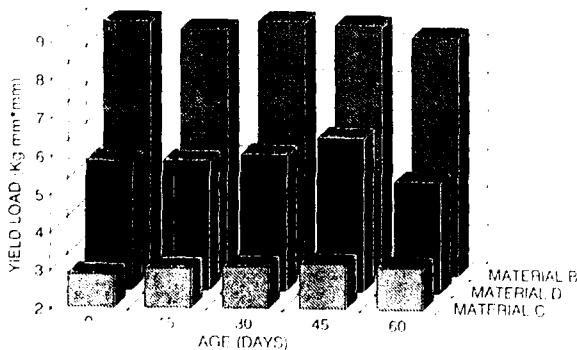
Fig. 3 shows the variation in MFI of the two types of PBT in 100°C boiling water conditions. It is clear that hydrolytically stable PBT shows an improvement but is still prone to hydrolysis at longer time interval and therefore it would be unsuitable for steam duct applications and is not considered further.

**FIG.3 MFI VARIATION OF PBT'S**  
100 DEG. C BOILING WATER



Tensile aging data is shown in figure 4. PES has approximately four times higher yield load as compared to E-CTFE even after aging for 60 days at 94% R.H. Tube shrinkage data in table 3 also shows that PES has the lower amount of shrinkage compared to E-CTFE. Low modulus and low shrinkage are beneficial in minimizing contraction which may cause attenuation increases at low temperature; both E-CTFE and PES are expected to perform well in cables.

**FIG.4 YIELD LOAD VERSUS AGING TIME**  
85 DEG.C & 94% R.H.



Based on the excellent mechanical properties then, the best choice of tube material is either PES or E-CTFE for steam environments.

## 5.0 CABLE DESIGN

In completing the design of a cable for steam duct application, the following criteria were established:

1. Ingress of moisture into the cable core and to the fibers must be either suppressed totally or otherwise retarded sufficiently for the fibers in the cable to operate for years without any adverse effects.
2. As stated earlier, the tube material selected must be hydrolytically and temperature stable up to 120°C.
3. The cable jacket should also be selected such that it is hydrolytically and temperature stable up to 120°C, although by a judicious design of intermediate moisture barriers surrounding the cable core, ordinary high density or medium density polyethylene (PE) is sufficient.
4. The cable should meet all other mechanical and environmental requirements normally expected of LT Fiber Optic Cables, i.e., as specified in Bellcore document TR-TS-20, Issue 4, (2).

## 5.1 Cable Design Iteration

In order to arrive at an optimized design based on the principles of multi-layer moisture barriers incorporated within the cable structure, a systematic experimental investigation was conducted. The starting point was a standard non-armored polyethylene sheathed PBT LT cable design. The performance of plain sheathed cable was compared to cables containing successively improved intermediate metallic barriers, utilizing LAP tapes, and welded aluminum tubing.

Cable performance was evaluated based on cable lifetime. Because of the known instability of PBT, Melt Flow Index (MFI) of cabled PBT tubes was used as the primary indicator of moisture ingress to the core. Additionally, Oxidation Induction Time (OIT) of the PE sheath was used to assess the external impact of the environment on the cable.

## 5.2 Experimental Cables

Four basic cable designs were evaluated, as shown in Fig. 5, i.e.

1. LT cable with polyethylene (PE) sheath
2. LT cable with "wet LAP" and PE sheath
3. LT cable with "dry LAP" and PE sheath

#### 4. LT cable with welded aluminum tube and PE sheath

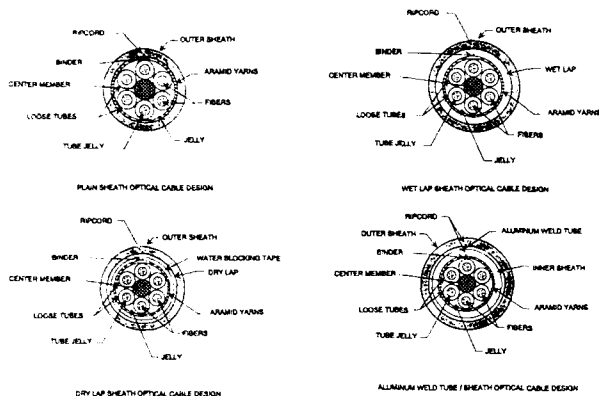


FIG. 5 DIFFERENT LOOSE TUBE OPTICAL CABLE DESIGN

The lap sheath cable utilizes a two side copolymer coated 0.008" aluminum tape longitudinally formed over the LT cable core. In the 'wet lap' version, the cable core floodant jelly is allowed to seep through the overlap of the aluminum tape. Axial water blocking is ensured, but at the expense of a good seal of the overlap. For the 'dry lap' version, a composite polyester/waterblocking tape is applied over the jelly impregnated core. This contained the jelly within the core thus improving the efficiency of the lap sealing process. The waterblocking tape then acts as a moisture barrier for any axial water flow.

During the aluminum welded tube process, an eddy current detector is used on-line to detect pinholes during the weld process. One hundred micron pinholes can be detected using this system. Any pinholes detected are filled in a second pass off-line process.

#### 6.0 CABLE PERFORMANCE AND RELIABILITY TESTING

Two parallel test plans are used to determine the performance capabilities of the intended steam resistant cable designs.

1. First, cable manufactured with the intended tube materials must be verified to meet as a minimum the performance specifications of Bellcore TR-TSY-000020, Issue 4.
2. Secondly, the cable must exhibit high reliability in the subject steam environment.

#### 6.1 Specification Testing

Dry Lap sheath cables housing each of the tube materials were subjected to the full Bellcore test schedule. Results are indicated in Table 4. The key result is that attenuation performance of the fibers over the -40°C to +70°C temperature range is excellent both before and after 85°C temperature aging. All mechanical test results also exceed the minimum requirements stipulated in the Bellcore document.

#### 6.2 Cable Lifetime Test Methods

In order to simulate a pseudo steam environment, and to facilitate testing in the laboratory, a 100°C boiling water test was developed. Cable samples were inserted in a 100°C water bath with cable ends isolated from the water. Top of the water bath is covered to reduce evaporation of water. Samples were aged for the following time intervals: 1 day, 7 days, 15 days, 30 days, 60 days, 90 days respectively. At each aging time interval, cable samples are removed after aging and then examined as follows:

1. Cable is dissected at the midsection of the submerged cable length and examined for any signs of degradation in cable components.
2. The Condition of PBT tubes was evaluated for visible signs of degradation or changes in handling characteristics.
3. Melt flow index (MFI) of PBT was measured according to ASTM D1238 using Tinius Olsen Extrusion Plastometer under the following conditions:

Test Temperature: 250± 1°C

Piston Weight: 1 kg

Preheat Time : 6 minutes plugged

Test Time : 0.25 or 0.50 minutes dependent upon flow rate

Orifice : standard stainless steel

A method for sample preparation was developed for obtaining repeatable MFI results on cabled PBT tubes (8).

4. The oxidation induction time (OIT) of polyethylene sheath of the aged cable sample was measured using a DSC module of Dupont TA-9900 thermal analyzer. Testing was conducted as follows:

Sample size: 5 - 10 mg

Container: open aluminum

Nitrogen purge: @ 50 ml/min.

Isothermal at ambient temperature for 5 minutes to stabilize equipment.

Equilibrate sample at 30°C

Ramp 20°C min.<sup>-1</sup> to 200°C

Equilibrate @ 200°C

Start oxygen purge: @ 50 ml/min.

Measure time to exotherm

### 6.3 EXPERIMENTAL RESULTS

#### 6.3.1 Melt Flow Index Variation

Polyester materials are well known to undergo hydrolysis reactions when subjected to high temperature and high humidity conditions (3,4). The hydrolysis reaction proceeds by scission of the main polymer chain at the ester linkage. This results in a reduction of molecular weight of the polymer and hence an increase in the melt flow index. The reduction in molecular weight also leads to a reduction in mechanical strength of the material and eventually leads to a catastrophic failure. Therefore MFI is a good aging indicator for PBT in high temperature humid environments and thus also a good indicator for moisture propagation through the outer sheaths.

We have used the value of the normalized melt flow index > 10 as a criterion to define cable lifetime. This value has been determined empirically to be indicative of the onset of cable failure, as demonstrated by increasing brittleness of PBT tubes. Fig. 6 shows variation in MFI for different aging time intervals under 100°C boiling water conditions for different cable samples. From the figure, the following inferences can be made:

1. A plain sheathed PBT LT cable degrades very quickly in a harsh steam environment. Based on a 100°C boiling water test, the lifetime is expected to be only 9 days.
2. An improvement is made by using metallic sheath as a moisture barrier. However, it is obvious that the condition of the seam, or LAP overlap, plays an important role in determining the

imperviousness of the cable structure to water.

3. It is clear that by using an Aluminum welded tube to enclose the cable core a substantial increase in cable lifetime is achieved. Furthermore, up to 30 days in 100°C boiling water there is no indication of hydrolysis induced degradation in PBT.

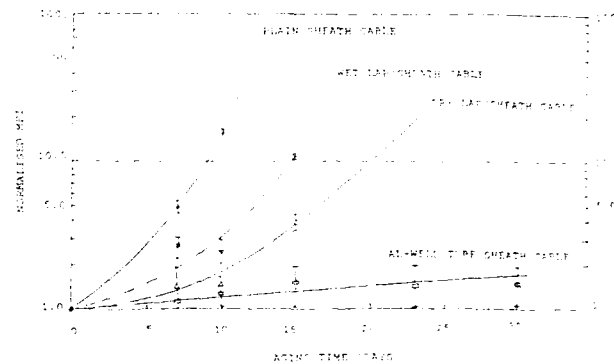


FIG. 6 MFI VARIATION FOR DIFFERENT CABLE DESIGNS.

Figures 7 and 8 show conditions of PBT tubes in both plain sheathed and aluminum welded tube cable designs for different aging times in 100°C water. There are no visible signs of degradation in PBT tubes for the Aluminum welded tube cable design.

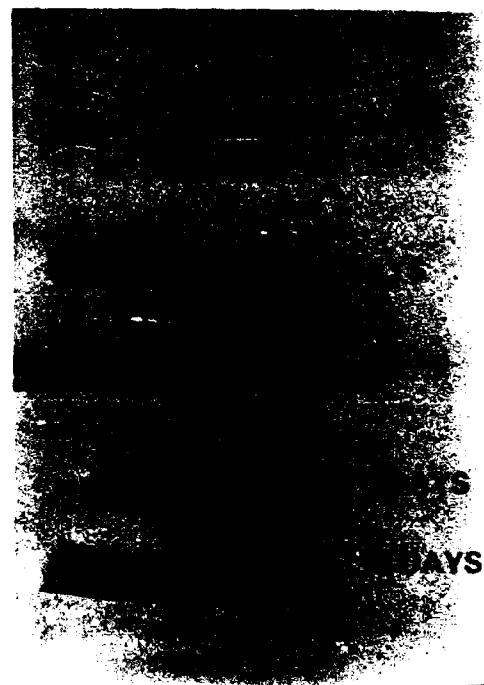


FIG 7 PHOTOGRAPH SHOWING CONDITION OF PBT TUBES IN PLAIN SHEATH CABLE

## ALUMINUM WELDED TUBE CABLE DESIGN

### CONDITIONS AFTER BOILING IN 100 DEG.C WATER

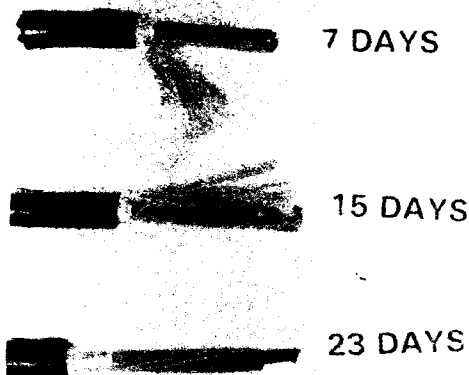


FIG.8 PHOTOGRAPH SHOWING CONDITION OF PBT  
TUBES IN ALUMINUM WELD SHEATH CABLE.

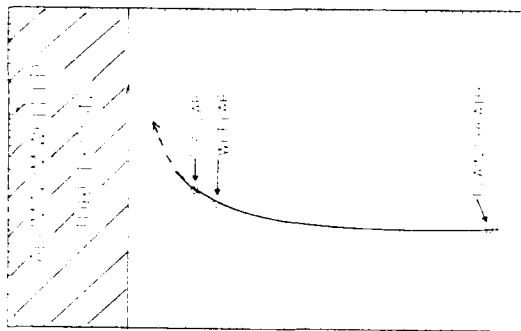
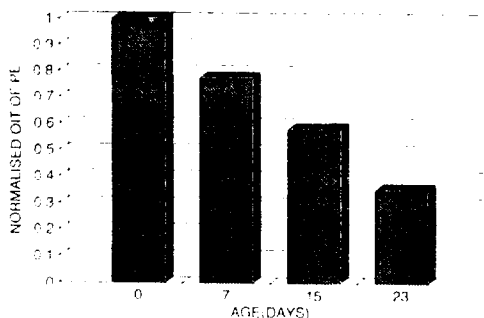


FIG.9 DESIGN CURVE FOR CABLE LIFETIME ESTIMATION

### FIG.10 NORMALISED OIT VARIATION OF PE IN 100 DEG.C WATER



### 6.3.2 OIT Variation of Polyethylene Sheath

The effects of steam exposure are felt more by the external Polyethylene Sheath. Oxidative indication time (OIT) was measured for polyethylene sheaths of cables aged in 100°C boiling water. The OIT value is defined as the time for oxidation to begin at an elevated temperature (typically 180 - 210°C) in a pure oxygen atmosphere (5,6). The OIT value is related to the stabilizer concentration for a given material and stabilizer package (7). Fig. 10 shows the variation in OIT of Polyethylene jacket with increased aging in 100°C boiling water. This reduction in OIT corresponds to depletion of stabilizers by the high temperature. There may be some migration of the stabilizer into the cable components.

### 7.0 PERFORMANCE MODEL

Figure 9 shows the cable lifetime design curve for different cable designs incorporating PBT tubes. An Aluminum welded tube design has therefore a predicted long lifetime in steam conditions, estimated to at least 14-times the lifetime of a plain sheath cable. It should be emphasized here that so far we have looked at PBT degradation to iterate a cable design. It can be further shown that by using PES or E-CTFE the longevity of the cable will be further enhanced since these materials do not hydrolyze or degrade in steam conditions. A dry LAP sheath cable was manufactured using these materials and aged in the 100°C boiling water test. There is no sign of brittleness or degradation in these materials, where in the same cable PBT was disintegrating within 20 days.

From Fig. 6, it is clear that the MFI of PBT follows a relationship of the form:

$$M = M_0 \exp (\phi t) \quad -- (1)$$

where  $M$  = MFI,  
 $M_0$  = MFI at  $t = 0$   
 $t$  = aging time  
 $\phi = A_0 \exp (-E_i/RT) * P^r$  expresses the Arrhenius dependence of the rate of degradation on temperature and a proposed power law dependence on the partial pressure of moisture available for reaction.

$A_0$  = constant

$E_i$  = activation energy for the scission reaction

$R$  = gas constant

T = aging temperature

P = partial pressure of water

r = power law exponent

Equation (1) yields the following equation for the rate of change of MFI under a constant temperature and external humidity condition.

$$\frac{d}{dt} \left\{ \log_e (M/M_0) \right\} = \phi P^r \left[ 1 + \left( \frac{r}{P} \right) \frac{dP}{dt} \cdot t \right] \quad \text{-- (2)}$$

where  $dP/dt$  = mass flow rate of water into the tube material.

By Fick's law

$$dP/dt = D (dc/dx) A_c \quad \text{-- (3)}$$

where D = Diffusivity of barrier layer,  $dc/dx$  = concentration gradient of water and  $A_c$  is the cross section for water flux propagation. Substituting equation (3) into (2) leads to:

$$\frac{d}{dt} \left\{ \log_e (M/M_0) \right\} = \phi P^r \left[ 1 + D A_c \left( \frac{r}{P} \right) t \frac{dc}{dx} \right] \quad \text{-- (4)}$$

Considering perpendicular flow through a uniform sheet of jacketing material into the core region,

$$\frac{dc}{dx} = \frac{C_0 - C_i(t)}{x} \quad \text{-- (5)}$$

where  $C_0$  is the equilibrium moisture concentration in the jacket,  $C_i(t)$  is the time variant moisture concentration in the core and x is the diffusion distance, i.e., jacket thickness. This equation assumes that immersed in water, the sheath reaches its equilibrium moisture concentration relatively quickly, so that  $C_0(t) = C_0$  is constant. Also in the case of PE plain sheathed

cables, the moisture concentration in the core presumably reaches saturation quickly, as indicated by the MFI test results.

If we assume for the case of moisture preventative cables instead that concentration  $C_i$  in the core is very low, as for the welded aluminum sheathed cable, then  $C_i(t) \ll 1$  and

$$\frac{dP}{dt} = \frac{D A_c C_0}{x} \quad \text{-- (6)}$$

$$\text{or } P(t) = \frac{D A_c C_0 t}{x} \quad \text{-- (7)}$$

By substituting equation (7) into equation (4), finally gives the equation for the rate of change of MFI as follows:

$$\frac{d}{dt} \left\{ \log_e (M/M_0) \right\} = \phi \left[ \frac{D C_0 A_c t}{x} \right]^r [1 + r] \quad \text{-- (8)}$$

The degradation can therefore be minimized by either reducing the cross section for moisture flux, for example by using the welded aluminum sheath, or by choosing a polymer jacket material with equally low permeabilities =  $DC_0$ . Unfortunately, polymeric materials tend to be inherently moisture permeable.

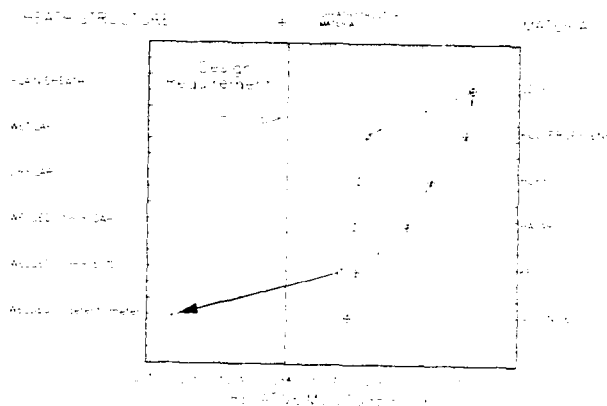


FIG. 11 DIAGRAM SHOWING RELATIVE MOISTURE FLUX FOR DIFFERENT SHEATH DESIGNS

Figure 11 shows the relative barrier strength obtained by choosing from a variety of polymers or through the use of hermetic metallic sheath, with values normalized to a non-metallic LDPE sheath. Nylon-6 is found to be one of the best choices for jacket material based on permeability, with a value of  $.138 \times 10^{13} \text{ (cm}^3 \text{ (stp) cm) / (cm}^2 \text{ s Pa)}$  (9). While almost three orders of magnitude better than PE, this level of barrier is not as good as even a poorly applied welded aluminum sheath.

For a welded aluminum sheath with an average 100µm square pinhole occurring every meter, the effective barrier is three to four orders of magnitude more effective than using a Nylon sheath with no metallic barrier. Practical experience indicates a pinhole rate of one per km level. Additionally, it is important to note that the polymer

permeabilities shown are at 25°C. Permeability increases exponentially with an activation energy with increasing temperature. Hence at steam temperatures, permeability of an optimum least permeable polymer will increase substantially thus negating its initial function as an effective moisture barrier.

## 8.0 CONCLUSIONS

A cable design study was undertaken to evaluate requirements for reliable operation of fiber optic cables exposed to high temperature steam environments. Two primary requirements are that the cable maintain mechanical integrity after long term aging in the environment and that the hydrolysis sensitive UV-acrylate coated optical fibers be isolated from moisture ingress.

Polyethersulfone and E-CTFE have both been shown to be suitable in terms of temperature and hydrolytic stability for use in the environment. Both materials have rated operating temperatures in excess of 140°C. PES, evaluated here for the first time for use in loose tube fiber optic cables, has exceptional mechanical characteristics and is readily processed on standard LT extrusion systems.

A model has been developed to demonstrate the effectiveness of moisture barriers in terms of polymer permeability and effective moisture flux cross section, as determined by gaps or pinholes in an applied metallic sheath. The best performance is achieved using a welded aluminum tube drawn down over the inner core. Such a sheath is expected to have diffusion rates into the fiber vicinity orders of magnitude lower than non-metallic polymer jackets.

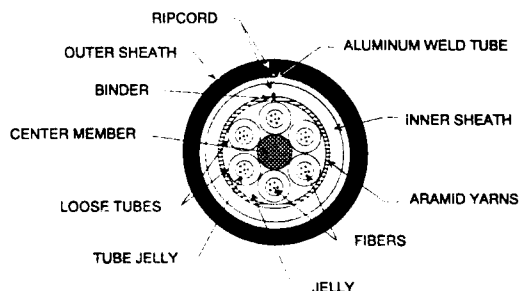


FIG12. STEAM RESISTANT OPTICAL CABLE DESIGN

This performance was verified in 100°C boiling water tests where the lifetime of PBT-tube cables under a welded aluminum sheath has an expected life approximately 14-times that of the same tubes in a plain sheath cable.

The preferred cable design shown in Figure 12 utilizes both the welded aluminum sheath and the high performance tube materials to provide the highest degree of protection for long term operation of the optical fibers in the steam environment.

## 9.0 REFERENCES

1. P.S.V. Madalli, Presentation to "Telecommunications Wire and Cable Standard Technical Advisory Committee (TWCSTAC)," New Orleans, May 1990.
2. Bellcore Technical Reference TR-TSY-000020, Issue 4, March 1990, "Generic Requirements for Optical Fiber and Optical Fiber Cable."
3. Martin S. R. and Gardner R.J., Polymer Engineering Science, 21 557 (1981).
4. K. Kishore and S. Sankaralingam, Polym. Eng. Sci, 24(13), 1043 (1984).
5. ASTM D 3895 -- Oxidative Induction Time for Polyolefins by Thermal Analysis," American Society for Testing of Materials, 1916 Race Street, Philadelphia, (1986).
6. T.N. Bowmer, Proceedings 37th I.W.C.S., p. 475 (1988).
7. T.N. Bowmer, R.J. Miner, IM Plitz, J.N. D'Amico and L.M. Hore, Proc. 39th I.W.C.S., p. 316 (1990).
8. P. Neveux, E. Buckland, to be presented at IWCS, Nov. 1991.
9. Polymer Handbook, 3rd Edition, J. Bandrup & E.H. Immergut, Wiley InterScience, NY (1989).

## 10.0 ACKNOWLEDGEMENTS

Thanks are due to all the members of the Lightwave and Materials Laboratories for their extensive testing support. Special thanks to Charles Boyer and Greg Tate for their continued support on material and cable reliability testing.

Material Property	Standard	Units	Material A	Material B	Material C	Material D
Density	ASTM D 792	g/cc	1.78	1.37	1.68	1.31
Melt Flow Index	ASTM D1238	g/10 min.	8	11.7	3	9
Ultimate Tensile Strength	ASTM D 638	psi	5510	12200	7000	7600
Elongation at Break	ASTM D 638	%	650	40-80	200	>= 50
Flexural Modulus	ASTM D 790	psi	55000	377000	240000	300000
Crystalline Melting Point	ASTM D 696	F (°C)	273 (134)	464 (240)	464 (240)	190 (254)
Linear Expansion Coefficient	ASTM D 696	F <sup>-1</sup>	6.1 x 10 <sup>-5</sup>	5.5 x 10 <sup>-5</sup>	1 x 10 <sup>-4</sup>	1.3 x 10 <sup>-4</sup>
Water Absorption (24 hrs. @ 23°C)	ASTM D 570	%	0.04	0.7	<0.1	0.45

Table 2. Properties of New Tube (Materials)

Test	RESULTS		
	Material B	Material C	Material D
I Low Temperature Cold Bend Test (-20 C) Mandrel Size = 2.5 mm 10 Turns	No cracks or kinks	No cracks or kinks	No cracks 5 kinks
II Bend/85 C Jelly Aging After 5 days After 10 days After 15 days	No further cracks or kinks No further cracks or kinks No further cracks or kinks	No further cracks or kinks No further cracks or kinks No further cracks or kinks	No further cracks or kinks No further cracks or kinks No further cracks or kinks
III Stress Cracking (1) 150 C/Ambient Air 30 days soak (2) 170 C/Ambient Air 30 day soak	No cracks No cracks	No cracks No cracks	
IV Tube Compression Compressive Modulus (N/mm) Yield Load (N)	5496 1002	3296 827	5359 1354
V Tube Shrinkage 120 C/24 hours	1.2%	2.8%	0.5%

Table 3. Tube Material Reliability Data

Test Item	Specification Requirement	Dry LAP Cable	Dry LAP Cable
Temperature Cycling -40 C to +70 C	All attenuation measurements at 1.55 um. (1) <= 0.20 dB/km maximum loss increase. (2) <= 0.10 dB/km mean loss increase. (3) 80% fibers <= 0.1 dB/km at 2nd -40 C.	All polyethersulphone tubes (1) <= 0.10 dB/km maximum loss increase. (2) <= 0.05 dB/km mean loss increase. (3) Pass	E-CTFE and PBT Tubes (1) 0.028 dB/km mean loss - mat. C tube 0.046 dB/km mean loss - PBT tube (2) Pass
Temperature Aging	(1) <= 0.4 dB/km maximum loss increase. (2) <= 0.20 dB/km mean loss increase. (3) 80% fibers <= 0.20 dB/km at 2nd -40 C.	Pass Pass Pass	Pass Pass Pass
Long Tensile and Bend Test	<= 0.10 dB loss at 600 lbs.	<= 0.05 dB loss	0.06 dB - Mat. C tube < 0.04 dB - PBT tube
Compression Test	<= 0.10 dB loss increase at 2200N load. No increase at release.	0.03 dB loss change for load up to 4.4 KN.	0.01 dB change in mat. C & D tubes at 2.2 KN.
Impact Test	<= 0.20 dB @ 4 kg load	2 samples at 6 kg - pass 0.02 dB change no damage to any cable components	0.01 dB change at up to 6 kg. no damage to any cable components
Flex. Test	<= 0.10 dB change at x 20 cable O.D. mandrel size	x 17 mandrel 0.02 dB change	x 25 mandrel - no damage or attenuation change with 6 kg.
Twist Test	<= 0.10 dB change	0.02 dB change No damage to sheath or tubes	0.03 dB change No damage to sheath or tubes

Table 4. Experimental Cables: Specification Testing Data





Mahesh Kumar R. Vyas  
Sumitomo Electric  
Fiber Optics Corp.  
78 Alexander Drive  
R.T.P., NC 27709

Mahesh Kumar R. Vyas graduated with an Honors degree in Electrical Engineering from Queen Mary College, University of London in 1970. He joined STC Technology Ltd. U.K. in July 1970, and he submitted a thesis on "Low Temperature Hall Measurements on <100> electrons in n-type GaAs" and gained an M.Sc. degree in Solid State Physics in 1973 from London University. He was a Senior Research Engineer and worked on R & D projects on various aspects of optical fiber and cable technology. He has published many papers and holds several patents.

He worked at Belden Engineering Center, Belden Wire & Cable Co. from 1989 - 1990 as a Senior Manufacturing Engineer with prime responsibilities for design and development of new cable manufacturing processes.

He is currently with Sumitomo Electric Fiber Optics Corp., Research Triangle Park, NC, which he joined in Jan. 1991 as a Senior Product Design Engineer, with main responsibilities for design and development of new materials and cable products. He is a senior member of the Society of Manufacturing Engineers and a corporate member of the Institute of Electrical Engineers (U.K.).



Eric L. Buckland  
Sumitomo Electric  
Fiber Optics Corp.  
78 Alexander Drive  
R.T.P., NC 27709

Eric L. Buckland obtained his B.S. degree in Physics in 1985 from North Carolina State University where he is nearing completion of his Master's Thesis studying issues in Analytic Photon Scanning Tunneling Microscopy. Since joining Sumitomo Electric Fiber Optics Corp. in 1985, he has been engaged in the research and development of optical fibers and cables. He is currently Manager of Product Design Engineering and the Sumitomo Laboratories. Mr. Buckland is a member of the Optical Society of America.



Paul E. Neveux, Jr.  
Sumitomo Electric  
Fiber Optics Corp.  
78 Alexander Drive  
R. T. P., NC 27709

Paul E. Neveux, Jr., obtained his double B.S. in Chemistry and Biology in 1979 from Antioch College, Yellow Springs, Ohio. After completing his Doctorate in Inorganic Photochemistry at the University of North Carolina at Chapel Hill, he held a post-doctoral fellowship investigating conducting liquid crystal polymers at Duke University in Durham, NC. In 1986, he joined Sumitomo Electric Fiber Optics Corp. and currently supervises the Materials Testing and Reliability Laboratory. Dr. Neveux is an active member in the Telecommunications Industries Association, American Chemical Society and Society of Plastics Engineers.

## RECENT ADVANCES IN THE DESIGNS OF RADIATING (LEAKY) COAXIAL CABLES

Sitaram Rampalli and Hugh R. Nudd

HELIAX® Engineering Division  
ANDREW CORPORATION, Orland Park, Illinois 60462, USA.

### **ABSTRACT**

*Radiating (Leaky) coaxial cables are used extensively for radio communications in tunnels, mines, and buildings where they improve signal transmission by acting as continuous antennas. This paper describes the characteristics of a design using two rows of apertures in the outer conductor, and barrier tapes to improve flame performance. In addition to improvement in attenuation, this design with appropriate non-halogenated jacketing meets stringent fire, smoke, and toxicity requirements. Characteristics of cables using halogenated materials are also discussed, and manufacturing techniques and system applications are presented.*

### **INTRODUCTION**

The terms "Radiating", "Leaky", and "Slotted" are used interchangeably in technical literature to describe any coaxial cable with either continuous or intermittent apertures (openings) in the outer conductor. Though there are substantial differences between various designs, these cables will all function as continuous antennas for radio and microwave communications. The use of radiating coaxial cables has increased several fold during the past decade,<sup>1</sup> for distributed communications systems. Typical applications are systems for subways and highway and rail tunnels,<sup>2-10</sup> high rise buildings,<sup>11-15</sup> and underground mines.<sup>16-22</sup> Additionally, leaky cables are finding use in more novel applications, such as soil moisture sensing,<sup>23</sup> and area access detection<sup>24</sup> for security systems.

Improvements in the performance of these systems are largely dependent on improvements in the overall design and performance of the radiating cables. The major considerations are fire safety, electrical transmission properties, and mechanical handling characteristics.

Radiating coaxial cables are frequently installed to implement communication systems in confined spaces such as subway tunnels, mines and buildings. Following a number of large scale fires, there are a number of national and international fire codes and other regulations that prohibit the use of electrical cables unless they meet certain flame spread, smoke, and toxicity requirements.

Optimum electrical transmission requires lowest longitudinal attenuation, which allows the system designer to maximize the distance between repeaters, and minimize system cost. Important mechanical performance parameters are adequate flexibility at sub-zero temperatures, and good resistance to abrasion, and resistance to various fluids and exhaust gases. Designs showing these desirable features must also, of course, be suitable for continuous manufacture at reasonable production speeds.

To meet these various technical challenges new radiating coaxial cables have been developed. This paper examines the various technical aspects of these new radiating cable designs, their performance characteristics, manufacturing methods, and some applications in systems.

### **DESIGN CONSIDERATIONS**

#### **Electrical Design Improvements**

The important electrical parameters for a radiating cable are, of course, attenuation and coupling loss.

Reflection levels (VSWR) may occasionally be of concern, but typical systems operate quite satisfactorily without particularly stringent VSWR requirements for the radiating cables. Adjustment of coupling loss to the desired level (typically in the range 60 dB to 85 dB down from the signal level in the cable) is readily achieved by adjusting the geometry of the radiating apertures. Improving the attenuation, however, implies improving the loss of the basic coaxial cable from which the radiating version is made.

### **Attenuation Improvement**

The choice of materials for such a cable will usually already be optimum. Thus high conductivity copper or copper-clad aluminum is used for the conductors, and electrical grades of polyethylene for the insulation. Now consider reduction in attenuation of a foam dielectric corrugated coaxial cable of given size (outer conductor diameter). The characteristic impedance, which is determined by the system, and the degree of corrugation (for flexibility), will also be fixed. The only way to decrease attenuation, then, is to reduce the quantity of dielectric material.

This reduces the cable loss in two ways. Firstly, the dielectric loss contribution is directly reduced by the decreased volume of material. Secondly, the size of the inner conductor must be increased for the increased cable velocity (lower dielectric constant) to maintain a constant characteristic impedance. This reduces the RF resistance, and hence the attenuation contribution, of the inner conductor. For the low-loss materials used in cable construction the magnitudes of the two effects are comparable.

In the past, radiating versions of typical foam dielectric coaxial cables, utilizing the so-called "standard density" foam dielectric (foams having densities in the range 0.4 to 0.5) were found to operate quite satisfactorily with a single row of radiating apertures along the length of the cable. This simple geometry, however, would not provide adequate performance for the "low density" dielectric cables (with foam densities around 0.2). Consequently, design enhancements were made to improve the performance of these low density radiating cables, as detailed later in this paper.

### **Fire Safety**

As noted previously, fire safety properties of leaky coaxial cables are important because of the nature of their applications. Conventional radiating coaxial cables are inherently limited in their degree of flame retardancy, because of the apertures in the outer conductor, especially when the outer sheathing is a halogen free polymer. This is because on exposure to fire, the flammable insulation melts, flows through the apertures and itself burns and increases the rate of flame propagation. Such a cable fails large scale fire tests.

There are various ways to arrest the flow of molten insulation. One is to use a fire retardant polymer as the insulation. A second approach is to crosslink the insulation thus preventing the melting and flowing of the insulation. However, use of a flame retardant polymer for insulation purposes is detrimental to the transmission characteristics of the cable due to the additives in the polymer, and crosslinking can also have adverse effects on the transmission properties, in addition to the high costs associated with this process.

To overcome the problem of enhanced flame spread due to the dielectric insulation, we have developed a radiating cable which uses a different approach. Our design utilizes a virgin polymer as the insulation, a non-halogenated polymer as the jacket material and a flame barrier tape between the outer conductor and the jacket.<sup>25</sup> The purpose of the flame barrier tape is to contain the molten plastic inside the cable, thus minimizing the flame spread. This type of design meets appropriate fire, electrical and mechanical performance criteria as detailed later in this paper.

## **EXPERIMENTAL METHODS**

### **Electrical Measurements**

Typical equipment the attenuation measurements is shown in Figure 1. These measurements are performed by a standard swept-frequency method, and an HP Model 8753 Network Analyzer may be used. The cable may be floor or wall mounted.

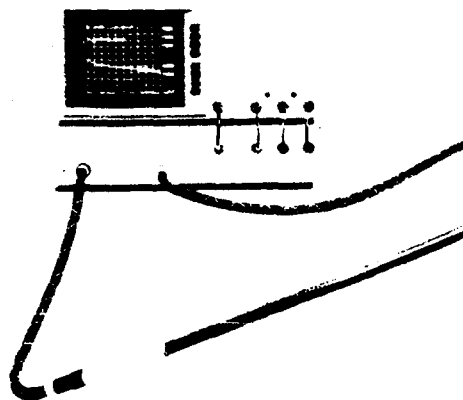


Figure 1  
Test Equipment for Measuring Cable  
Attenuation

Figure 2 shows a method for measuring the attenuation of the cable at various separations from a concrete surface.

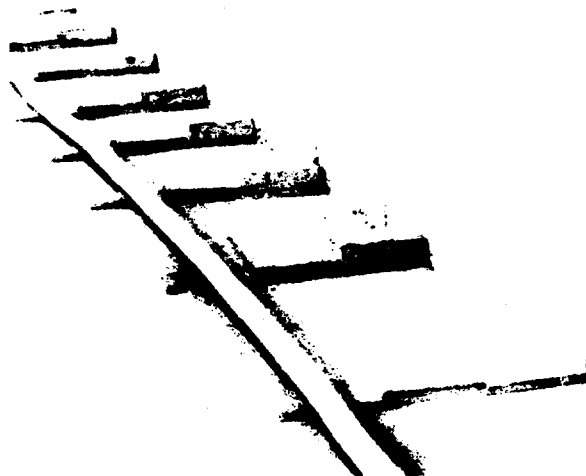


Figure 2  
Method for Measuring the Attenuation of the  
Cable at Various Separations from the  
Surface

Coupling loss measurements are performed by using an HP Model S562B Spectrum Analyzer, HP Model S350B Sweep Oscillator and a dipole antenna. Test equipment for coupling loss measurements is shown in Figures 3 and 4. The cable to be measured is mounted on the wall of the test area and connected to the spectrum analyzer (receiver). A "cart" carries the signal generator and transmit antenna, and moves parallel to the cable.

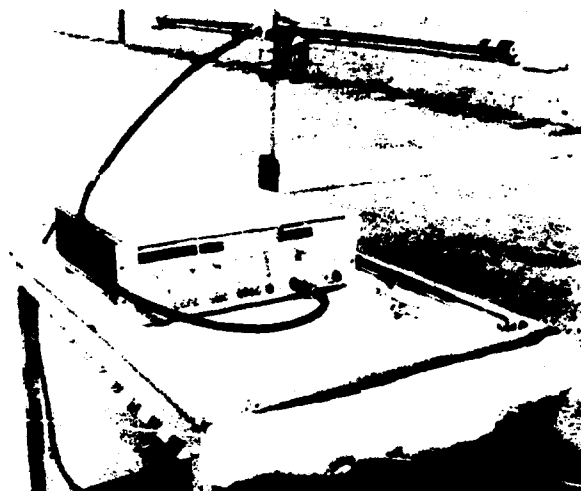


Figure 3  
Test Equipment for Coupling Loss  
Measurement  
Signal Generator and Transmit Antenna



Figure 4  
Test Equipment for Coupling Loss  
Measurement  
Spectrum Analyzer and Computer

Because of the phasing effects when combining the elemental signals received from all points of the cable, coupling loss characteristics at high frequencies ( $>100$  MHz) show considerable variation along the length of the cable. This effect is rather less pronounced when the measurements are performed indoors, where reflections from walls, floor and ceiling tend to fill in the deep nulls that are seen in outdoor measurements. For

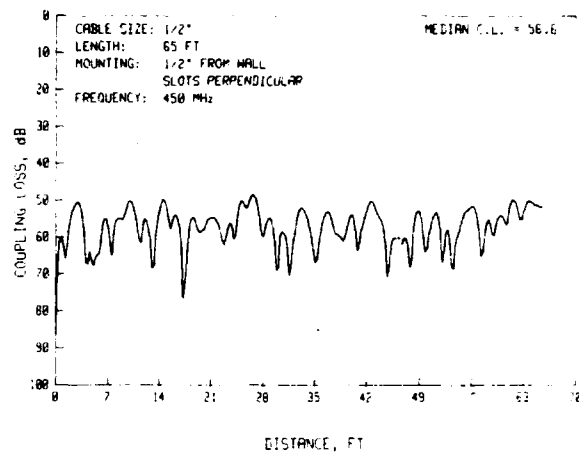
this reason, we use the results of indoor measurements for coupling losses, as these conditions more closely resemble the situations in typical systems.

Coupling losses are measured at a standard distance of 20 feet (6m) from the cable using a tuned dipole antenna at each frequency. After zeroing the receiver (spectrum analyzer) at the internal power level in the cable, measured levels directly indicate coupling losses relative to a dipole receive antenna. Figure 5 shows the mounting of a radiating cable on a wall for coupling loss measurements.



**Figure 5**  
Radiating Cable Mounted on a Wall for  
Coupling Loss Measurement

A digital data acquisition system stores coupling loss data as this varies along the length of the cable, and the median data point (50% probability point) is chosen as the resultant "coupling loss". Choosing the median point, rather than some mean value, also makes the coupling loss independent of the linearity of the amplitude display. A typical coupling loss plot is shown in Figure 6. All the above tests were done in-house by using the standard procedures.



**Figure 6**  
Typical Coupling Loss Plot

#### Fire Tests

Fire propagation characteristics of the cables were determined according to the methods described in the Underwriters Laboratories Standards and in the International Electrotechnical Commission (IEC) Standards. Cables were tested in the order of severity of flame test, as follows :-

UL VW-1 Vertical Wire Test  
UL 1581/IEEE 383/IEC 332-3 Vertical Tray Test  
UL 1666 Riser Test  
UL 910 Steiner Tunnel Test

A summary of the above fire test procedures is given in Tables 1 and 2. Diagrams of the actual test configurations are presented in a recently published article.<sup>26</sup>

All the fire tests were performed at the Underwriters Laboratories, Northbrook, Illinois.

#### Smoke and Toxicity Tests

Smoke and toxicity tests were performed at well recognized independent analytical laboratories. A summary of the various tests and the corresponding properties measured is shown in Table 2.

The NES 711 and ASTM E662 tests are performed on 3" x 3" sample plaques of jacket material and give a reasonable indication of the smoke intensity. The 3-meter cube test, by contrast, uses the actual cable samples. Because of this, the 3-meter cube test is generally considered to be the more realistic for measuring smoke generation.

## Mechanical Tests

The following mechanical tests were performed on the finished cable samples.

Cold bend at sub-zero temperatures  
Room temperature reverse bends  
Abrasion resistance  
Tensile properties of the jacket

All the above tests were done in-house using appropriate standard procedures.

TABLE 1

SUMMARY OF THE FLAME TEST PROCEDURES

Test	Procedure	Sample Fails Test If
VW-1	816°C Flame is applied for 15 sec. each application with 15 sec. between applications, or cessation of burning whichever is longer.	1. Cable supports flame longer than 60 sec. 2. Emits flaming drops which ignites the cotton on the floor.
UL 1581	A 70,000 Btu flame is applied for 20 minutes to cables on a vertical tray.	1. Cables are blistered and charred at 8 feet level.
UL 1666	A 512,000 Btu flame is applied for 30 minutes to cables in a test chamber.	1. Cables must not propagate flame to the top of the 12 foot high compartment.
UL 910	A 300,000 Btu flame is applied for 20 minutes to cables on a horizontal tray inside a tunnel with 240 fpm draft.	1. Flame travel exceeds 5.0 ft. 2. Peak smoke optical density exceeds 0.5 . 3. Average smoke optical density exceeds 0.15 .

TABLE 2

SUMMARY OF THE FLAME, SMOKE, TOXICITY, AND CORROSIVITY TESTS

TEST	MEASURED PROPERTY
VW-1	Flame Spread
IEC 332-1	Flame Spread
UL 1581	Flame Spread
IEC 332-3	Flame Spread
IEEE 383	Flame Spread
UL 1666	Flame Spread
UL 910	Flame Spread & Smoke Density
ASTM E 662	Smoke Density
NES 711	Smoke Index
3 Meter Cube	Smoke Density
NES 713	Toxicity Index
VDE 0472 Mil-C-28640	Acid Gas / Corrosivity pH

## RESULTS AND DISCUSSION

### Transmission Characteristics

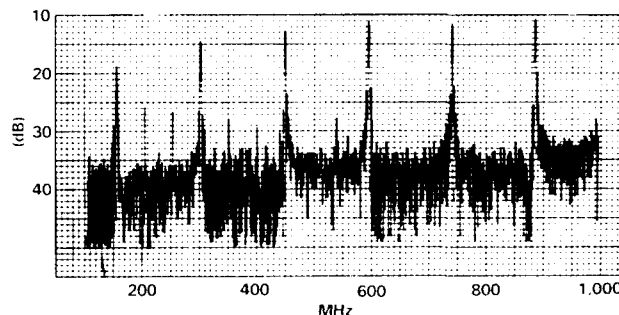
Measurements of Single Slotted Cables: Initial experiments with radiating versions of "low density" foam dielectric cables, with a single row of radiating apertures, showed unacceptable sensitivity of the attenuation to the proximity of certain mounting surfaces (conducting or electrically lossy), and excessive variation of attenuation with the orientation of the radiating apertures with respect to the mounting surface. These effects are shown in Figure 7 for an experimental 1-5/8" foam cable. For comparison, the attenuation of the unslotted coaxial cable is also shown in Figure 7. It is seen that in the worst case the actual losses for this configuration are large compared with the inherent or minimum loss to be expected.

This increased sensitivity to environment occurs with low density cables because the higher internal propagation velocity increases the coupling between the internal wave and external surface waves on the cable, which are responsible for the radiated fields.

In a first attempt to reduce this sensitivity to environment, some sample cables were manufactured with reduced numbers of radiating apertures, to reduce the coupling, the apertures being placed in groups separated by lengths of unperforated cable. This gave improvements in attenuation performance, but there were now unacceptably large VSWR "spikes" at frequencies related to the separation of the groups of apertures, as shown in Figure 8. Such large VSWR spikes also give correspondingly large increases in attenuation at these particular frequencies. Whilst individual cables made in this way can always have the slot geometry adjusted to "tune" the cable to an individual user's requirement for a single narrow frequency band, the presence of multiple VSWR spikes can present problems for multi-band or broad band systems.

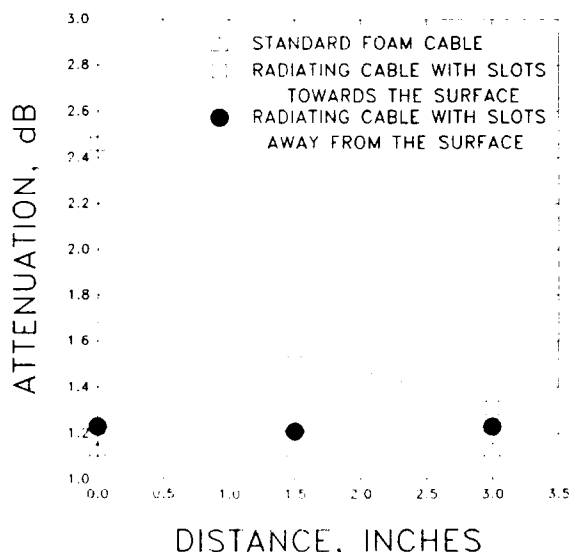
To avoid creating these VSWR spikes then, a continuous structure was needed for the radiating apertures (or quasi-continuous, as in our case of

closely spaced holes). A geometry of two rows of slots, separated by  $180^\circ$  around the circumference of the cable, was now tried.

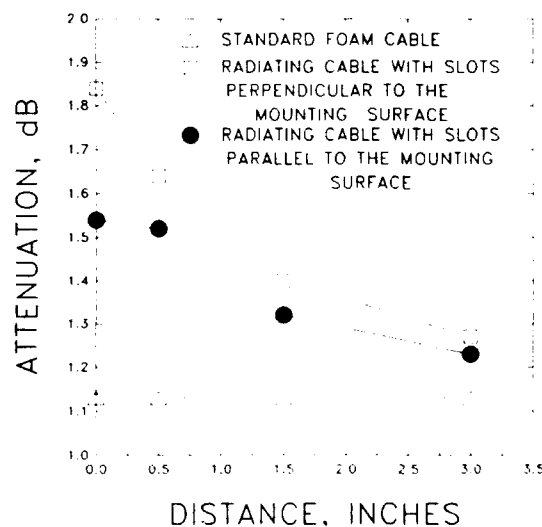


**Figure 8**  
Return Loss vs Frequency Plot  
for a Radiating Cable with  
Periodic Groups of Slots

Measurements of Double Slotted Cables: Variation of attenuation with distance from the mounting surface, and orientation of the radiating slots with respect to the mounting surface, are shown in Figure 9 for a 1-5/8" low density foam dielectric cable (of the same foam density as that of Figure 8). Again the unslotted coaxial cable attenuation is also shown. It is seen that there is substantial improvement over the initial results for the single slotted cable.



**Figure 7**  
Variation of Attenuation at 1700 MHz with  
Distance from Concrete Mounting Surface  
for a Single Slotted Radiating Cable  
Cable Size: 1.625"



**Figure 9**  
Variation of Attenuation at 1700 MHz with  
Distance from Concrete Mounting Surface  
for a Double Slotted Radiating Cable  
Cable Size: 1.625"

It would be inferred from the degree of improvement from the single-row slot geometry to the double-row, that using three or more rows would be even better. However, though a many-row geometry will show no orientation sensitivity, it poses difficulties in the manufacturing process. The design with two continuous rows of radiating apertures gives satisfactory electrical performance.

Effects of Exposure to Environment: Since radiating cables are often installed in road and rail tunnels, it is important to know the effects of salt or other chemicals that may be used for de-icing during winter. To simulate these effects, we subjected cable samples to a continuous salt spray for more than a year. Results of these tests are summarized in Table 3.

TABLE 3  
EFFECT OF SALT WATER ON  
CABLE ATTENUATION

CABLE TYPE	FREQ.	% CHANGE IN ATTENUATION	
FLAME RETARDANT	150	12	8
	450	11	14
	900	7	15
	1700	5	15
NON-FLAME RETARDANT	150	17	11
	450	16	18
	900	9	14
	1700	6	9

Most of the increase in attenuation occurs during the first week of exposure to salt spray, the amount of increase being up to 17%. This initial increase in attenuation is seen in both flame retardant and non-flame retardant jacketed cables. At 150 MHz, there is no measurable increase in attenuation after the first week for either cable type. However, at higher frequencies both cables showed continued increase in attenuation, even though the increase is not very significant. The increase was mainly due to the salt deposits over the jacket. When the cable was washed with distilled water, the attenuation was found to return to close to the original value.

Coupling Losses: Coupling losses were found to depend just on the slot sizes for these radiating cables, and essentially did not vary between different constructions where only details of flame barrier tape and jacket material were changed. This is to be expected when the dielectric loss factors of tapes and jacket materials are very small.

### Fire Propagation Characteristics

Cables with Halogen-Free Jacket: The results of flame tests of cables with halogen free jackets are presented in Table 4. The cable designs use a non-halogenated flame retardant polymer as the outer jacket and cellular insulation of virgin polyethylene. It can be seen from Table 4 that a sample with no flame barrier tape passed only the VW-1 test. When the apertures on the outer conductor of the cable are covered with a flame barrier tape, the cable meets the requirements of the vertical tray flame tests, i.e. UL 1581, IEEE 383, and IEC 332 Part 3. Utilizing double tapes (wrapping in clockwise and counterclockwise directions over the outer conductor) has provided additional fire resistance and these samples passed the UL 1666 riser test. However, the same cable would not pass the more severe UL 910 test, the "Steiner tunnel" test for plenum cables. This is expected of cables with halogen free jackets due to their low limiting oxygen index (LOI) values.

Cables with Halogenated Jacket: Though halogen free radiating cables are used in tunnels, subways, and elevator shafts for radio communications, their use elsewhere inside buildings is limited because halogen free cables are not presently capable of meeting the most stringent fire test, the UL 910 standard. At many locations in the USA, the building codes dictate that cables installed in plenums and ducts should pass this UL 910 test if they are to be used without conduit.

For plenum applications it is necessary to use fluoropolymer resin for both insulation and outer jacketing. A radiating cable sample so constructed passed the UL 910 test, as shown in Table 4. It is not necessary to use a flame barrier tape with this type of cable because of the inherently high level of flame resistance offered by the fluoropolymers. Radiating plenum cables are now increasingly used in hospitals for remote patient monitoring



systems, as well as in other large buildings for conventional radio communications.

**TABLE 4**  
**FLAME TEST RESULTS ON RADIATING**  
**COAXIAL CABLES**

**Sample:** Cable with a halogen-free jacket and cellular polyethylene insulation.

TEST	FLAME BARRIER TAPE	RESULT	REMARKS
VW-1	None	Pass	-
UL 1581	One tape	Pass	Flame Spread < 6 ft.
UL 1666	Two tapes	Pass	Flame Spread < 8 ft.

**Sample:** Cable with fluoropolymer jacket and cellular fluoropolymer insulation.

Test UL 910	Flame Spread (ft.)	Peak Smoke Density	Average Smoke Density
RESULT	3.5	0.25	0.07
REQUMT.	5.0	0.50	0.15

#### Cables with Flame and Moisture Resistance

Leaky coaxial cables are installed extensively in underground tunnels and in mines, where conditions can be very damp. Under these circumstances, the cable should be kept dry and protected from water ingress into the cable, to prevent undue increase in attenuation. For applications involving damp surroundings, then, the cables should have adequate moisture resistance in addition to flame retardancy. We have constructed prototype radiating cables having both flame and moisture resistance.

The design uses both a flame barrier tape and a water blocking tape over the outer conductor and a flame retardant jacket. The cable sample passed the UL 1581 Vertical Tray Flame Test. The sample was also tested for water migration using the method described in REA PE-39 and met the requirements.

#### National Electrical Code® Requirements

Under the Article 820 of the National Electrical Code, 1990<sup>27</sup> edition, all coaxial cables for radio and microwave applications, including radiating cables, are classified as CATV cables. The NEC classification of flame retardant cables for specific applications is shown in Table 5. The four levels of classification correspond to the four levels of flame test of Table 1.

**TABLE 5**  
**NATIONAL ELECTRIC CODE CLASSIFICATION OF**  
**CATV CABLES FOR RADIO AND MICROWAVE**  
**APPLICATIONS**

Designation	Type	Application
CATVX (VW-1)	CATV Cable Limited Use	For use in raceways and dwellings.
CATV (UL 1581)	CATV Cable	General purpose except in risers and plenum.
CATVR (UL 1666)	CATV Riser Cable	For use in vertical run in a shaft or from floor to floor.
CATVP (UL 910)	CATV Plenum Cable	For use in ducts, plenums, and other air handling spaces.

**Note:** CATVX, CATV, and CATV rated cables must be listed as being flame retardant. CATVP rated cables must be flame retardant and also should have low smoke producing characteristics.

Cables made to the designs described in this paper meet one of the two highest flame retardancy ratings, CATVR or CATVP. Thus cables with halogen free jackets and flame barrier tapes are rated as CATVR and those with halogenated materials for both jacket and insulation are rated as CATVP.

### Smoke, Toxicity, and Corrosivity

In addition to flame retardancy, users are now selecting cables based on the smoke and toxicity characteristics in the event of a fire. After studying the results of several fires, it has been found that the most damaging factors are often the smoke, toxicity, and corrosivity of the combustion products, rather than the actual fire intensity.

A non-halogenated radiating cable sample was tested for smoke, toxicity, and corrosivity according to the standard test methods described in Table 1. The results are summarized in Table 6.

**TABLE 6**  
**SUMMARY OF TYPICAL VALUES ON SMOKE, TOXICITY, AND CORROSIVITY OF FIRE GASES**

Property	Typical Value
Smoke Index	35.0
Smoke Density, $D_{\max}$	
Flaming Mode	67.0
Smoldering Mode	225.0
Smoke Test on a 7/8" Size Cable	
$A_o$ (On)	0.56
$A_o$ (Off)	1.12
Toxicity Index	0.465
Acid Gas Evolution	
Conductivity, $\mu\text{m}/\text{cm}$	14.0
pH	5.0

It is seen that the cable shows very low values for smoke index, smoke density and toxicity index. The cable also meets the current UK smoke standard for London Underground Limited (LUL) when tested according to the 3-meter cube test.

The results of the acid gas generation and corrosivity tests show that the gases evolved are not highly corrosive. They are only very weakly acidic, which is the major reason, of course, for using non-halogenated materials.

### Mechanical Performance

All samples were tested for their mechanical performance using standard procedures. The results showed that cables with halogen free outer jackets perform quite satisfactorily. Thus, for example, cables can be bent at  $-25^{\circ}\text{F}$  without developing cracks in the outer jacket. Jacket elongation was found to be approximately 110%, which is normal for a heavily filled halogen free polymer composition. Cables for plenum applications showed better mechanical performance, because unfilled virgin fluoropolymers are used in these constructions.

### MANUFACTURING TECHNIQUES

Continuous manufacture of this type of leaky coaxial cable involves the use of specialized tools and techniques.

The first step is to extrude the primary insulation onto a copper wire or tube (depending on the size of the cable). This is followed by addition of the outer conductor by a "seam welding" process, which forms a tube from a flat copper strip using a set of forming rolls. The edges of the strip are joined using Tungsten Inert Gas (TIG) welding, the cable is sized at a sizing station and finally is passed through a annular corrugating process.

The necessary apertures in the corrugated outer conductor are cut using a process which also ensures removal of all metal chips. The slots are cut just on the "crests" of the corrugations so that the foam insulation inside is not damaged.

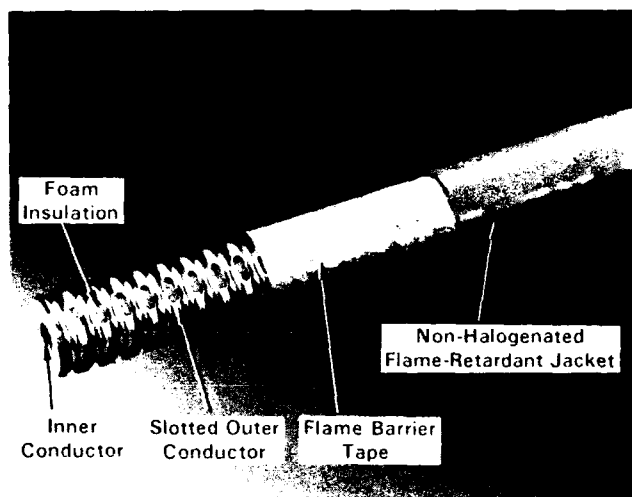
Application of the flame barrier tapes is performed using a standard taping machine. One tape is wrapped spirally clockwise and another counterclockwise. Adequate overlap is provided to ensure complete coverage of the apertures.

After taping, the cable passes through a conventional extruder, and a suitable halogen free flame

retardant jacketing compound is applied over the tape.

If the cable is intended for plenum applications, the sequence of manufacturing operations is similar, except that there is no flame barrier tape and the outer jacket is a fluoropolymer material.

Figure 10 shows a typical radiating cable with flame barrier tape and a halogen free outer jacket.



**Figure 10**  
**Radiating Coaxial Cable with a Flame**  
**Barrier Tape and a Non-Halogenated**  
**Flame Retardant Outer Jacket**

### **SYSTEMS APPLICATIONS**

Double-slotted low density foam dielectric radiating coaxial cables of the type described in this paper find wide application in conventional two-way radio systems for subways, tunnels, buildings etc., More recently, these cables have also been incorporated into similar systems to extend cellular radio coverage into buildings and tunnels.<sup>28</sup>

A typical system uses bi-directional amplifiers to compensate for the longitudinal attenuation of the cable, the separation of the amplifiers depending on the size (attenuation) of the cable, the amplifier gain, and the other system operating parameters. A full discussion of the system design considerations appears in the quoted reference.

This type of radiating cable has also been used extensively in a communication system for the construction phase of the English Channel Tunnel project.<sup>29</sup> Again, bi-directional amplifiers are used to compensate for the cable attenuation. The referenced article provides a comprehensive description of the system.

### **CONCLUSIONS**

In this paper we have presented some of the most recent advances in the designs of radiating (leaky) coaxial cables. Our primary conclusions from this work are:

1. Conventional high foam density, single slotted versions of radiating coaxial cables often showed higher levels of attenuation.
2. To reduce the attenuation, radiating cables with two rows of apertures separated by 180° on the circumference of the cable were developed. Cables of this design were found to be less sensitive to the effects of the mounting surface.
3. A continuously slotted geometry also exhibits no VSWR spikes. Designs with a periodic group of slots show large VSWR spikes.
4. Radiating cable designs with two flame barrier tapes and a halogen free outer jacket are listed as CATVR, for riser applications.
5. The non-halogenated radiating cable also showed very low levels of smoke, toxicity, and corrosivity.
6. Cables with fluoropolymer insulation and jacketing are listed as CATVP for plenum applications.
7. The new radiating cables are found to be working satisfactorily at various locations around the world.

## **ACKNOWLEDGEMENTS**

The authors would like to extend their sincere appreciation to Mr. V. K. Chopra, Engineering Manager and to Mr. R. Guipe, Vice President, HELIAX® Products, Andrew Corporation, for their support and encouragement during the writing of this paper. The authors also wish to thank several of their colleagues at Andrew Corporation who directly or indirectly helped during the various stages of this work. Special thanks to Messrs. Jeff Albrecht, Dan Bufanda and Jurgen Armbruster for making the cable samples and to Mr. Leonard Visser for valuable electrical developmental work.

Finally, the authors are grateful to the management of Andrew Corporation for granting the permission to communicate this paper.

## **REFERENCES**

1. P. Delogne, "Leaky Feeders and Subsurface Radio Communications"  
Peter Peregrinus Ltd., New York, 1982.
2. Anon  
Austral. Electronics Engg., **23**, 30-32 (1990)
3. L. Mariel  
Communications Intl., **16**, 70-71 (1989)
4. K. Matsumoto, Y. Yokoyama, S. Matsumoto, S. Arimura, and S. Fujita  
Mitsubishi Denki Giho, **64**, 11-17 (1990)
5. H. G. Haag, G. Thönneßen, and K. Schulze-Buxloh.,  
Proc. of the 38th Intl. Wire & Cable Symp., Atlanta, GA, USA., 286-294 (1989)
6. K. Matsumoto, Y. Yokoyama, M. Hanafusa, and T. Nakamura  
Mitsubishi Denki Giho., **63**, 64-69 (1989)
7. D. J. R. Martin and R. A. Sharp  
Proc. of the 39th Vehicular Technology Conference, San Francisco, CA, USA., 375-382 (1989)
8. W. Marek and H. Stockinger  
Electrotechnik und Informationstechnik, **106**, 203-205 (1989)
9. A. Bosshard  
Communications Intl., **12**, 52-62 (1985)
10. Q. V. DAVIS  
IEE Colloquim on "Propagation in Confined Spaces and Tunnels", London, UK., 2/1-4 March (1986)
11. T. Burke  
Telecommunications, **24**, 73-77 (1990)
12. K. J. Bye  
EUROCON 88: Proc. of the 8th European Conference on Electrotechnics, Stockholm, Sweden., 387-390, June (1988)
13. P. L. Camwell and J. G. McRory  
IEEE MONTECH '87: Montreal, Canada., 213-216, November (1987)
14. A. A. M. Saleh, A. J. Rustako, Jr., and R. S. Roman., IEEE Trans. on Commun., **35**, 1245-51 (1987)
15. D. A. Palmer and A. J. Motley  
Brit. Telecom Tech. J., **4**, 55-58 (1986)
16. B. A. Austin  
Proc. of the IEE Colloquium on "Electrically Small Antennas", London, UK., 3/1-5, October (1990)
17. M. Little  
Colliery Guardian, **234**, 492-98 (1986)
18. D. J. R. Martin, R. W. Haining, and A. B. Hunt.,  
Mining Engineer (London) **144**, 349-52 (1985)
19. R. J. Parsons  
Mining Engineer (London) **144**, 341-44 (1985)
20. T. Suzuki and N. Shikada  
Shigen (Japan) **1**, 29-34 (1989)

21. T. Suzuki, M. Satani, K. Yamaguchi, T. Isei, N. Shikada and M. Kinoshita  
Nippon Kogyo Kaishi, **101**, 1171 (1985)
22. J. Munro  
Aust. Coal Miner., Pages 5, 11, 27-28, 30, November 1983.
23. E. Bahar and J. D. Saylor  
IEEE MTT-S Digest, 362-64 (1984)
24. R. K. Harman and C. M. Bell  
Proc. of the Carnahan Conference on Security  
Technology: Electronic Crime Countermeasures, Atlanta, Ga, USA., 35-39 (1987)
25. S. Rampalli and H. R. Nudd  
US Patent, 4,800,351, Issued to Andrew Corporation, January 1989.
26. S. Rampalli and V. K. Chopra  
Wire J. Intl., **23**, 81-96(1990)
27. National Fire Protection Association, Quincy, MA.  
National Electrical Code® Handbook, 1990.
28. T. M. Burke  
Proc. of N.C.F, **43**, No. II, 892-900(1989)
29. M. A. Morgan and H. K. Sohner  
IEEE Vehicular Technology Conference, 368-374(1989)

Sitaram Rampalli is Materials Engineer associated with the HELIAX® Engineering Division, Andrew Corporation. He received his Ph. D. in Chemistry from the Indian Institute of Technology, Bombay, India, and M. S. Degree in Polymer Science from the University of Akron, Ohio. He is currently responsible for the selection, evaluation, and recommendation of polymers for wire and cable applications. He holds two US patents, and one Australian Patent and has several publications in scientific journals.

He is a Senior Member in the Society of Plastics Engineers, and a member in American Chemical Society.

Dr. Rampalli's research interests are in the characterization and analysis of polymers for cable applications, polymer degradation and structure-property relationship studies.



Hugh Nudd is Manager, Design Engineering, HELIAX® Products, with Andrew Corporation.

He graduated with honors degree in Physics from the University of Oxford, England in 1965 and joined the General Electric Company Ltd.(U.K.) to work on the design and development of microwave components, mainly for trunk radio systems. In 1975 he moved to Marconi Space and Defence Systems to work on microwave components and sub-systems for satellite communications.

He joined Andrew Corporation at their Lochgelly, Scotland, plant in 1978, transferring to the Orland Park, Illinois headquarters in 1982. Since 1983 he has been responsible for design engineering for the HELIAX® coaxial cable and waveguide product line.

# ADVANCED PAIR IDENTIFICATION TO ELIMINATE INTERFERENCE IN DATA SERVICES WITH AUTOMATIC CLASSIFICATION

Shuji Asakawa, Takafumi Sakaguchi\*, Satoshi Matsushashi

NTT Telecommunication Field Systems R & D Center

\* NTT Network Systems Development Center

## Abstract

Identification system for metallic twisted pairs requires interference-free identification for any services. There are many kinds of telecommunication services on metallic cables, such as telephone, analog data, digital data transmission and so on. On circuits of these services, identification need to be performed accurately and to give no intervention for all transmission. This paper addresses very effective technique to identify a pair without interference on services.

The functions above are all achieved without interference of any services.

Figure 1 shows the identification system. The system consists of central office and field units. Both units are controlled by the CPU and are connected to each other with a modem to exchange operation results and to proceed to the next steps. The main tasks of the C.O. unit are classifying circuits, generating tone signals and supervising field units. On the other hand, pair and tip/ring identification are the assignments for the field unit.

## 1. INTRODUCTION

In order to have efficient metallic cable replacement, a transfer splicing system should not cause any intervention in working loops, such as data transmission. An avoidable task in transfer splicing is pair identification. The splicing and pair identification need to be performed in such a way as to allow error-free for data transmission. The focus of this paper is a microprocessor-controlled pair identification system which is executed eliminating interference of data services. In this system, the most important operation is that the system classifies circuits and provides proper identification processes for various kinds of transmission.

## 2. Effective Identification System

To perform pair interference-free identification for various data transmissions, an identification system modifies its internal processes according to the transmitting circuits. The identification system described in this paper has the following functions;

- 1) Automatic circuits classification
- 2) Pair identification
- 3) Tip/ring identification
- 4) Imbalanced circuits identification

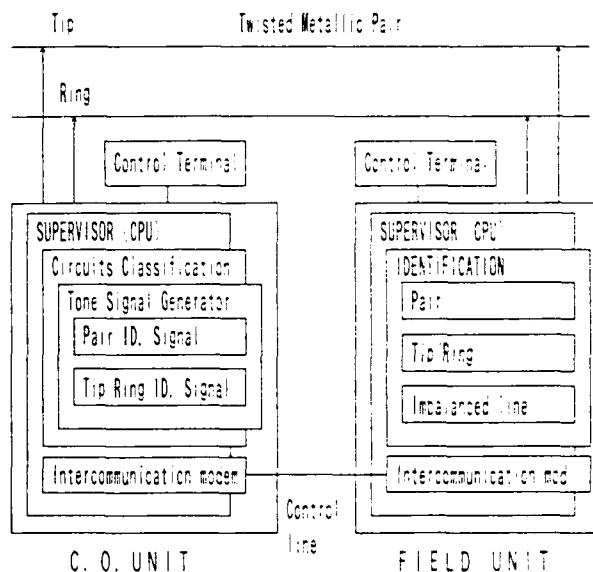


Figure 1. Identification system with automatic classification

### 3. Circuits Classification

Signal transmissions used on metallic twisted pairs are classified with terminated impedances, such as 600  $\Omega$ , which are for analog signal transmission, and 110  $\Omega$  for digital data transmission. There is a power loss of 7 dB for identification signals ( hereafter called tone signals ), when tone signals are applied to circuits that are terminated with different impedances between 600  $\Omega$  and 110  $\Omega$ . In the identification process, it is necessary that tone signals are detected at higher levels for all circuits terminated with different impedances, so that the identification process is performed accurately. The proposed identification system adjusts the power level of tone signals according to terminated impedances pair circuits. Tone signals in the system have no effect on data transmission because tone signals in tip/ring identification are applied as low as the noise level, -60 dBm. Detecting these tone signals needs an extremely intricate technique because of this low level. Basically, the process is done by examining and locking their phases in the phase of a reference signal so as to improve the signal-to-noise ratio. Therefore, at the beginning of identification, an initial adjustment is necessary to make the phase

difference between the tone and reference signals zero. Phase adjusting of the tone signal against the reference signal is done using a balanced circuit and holding it as initial data for tip/ring identification. In identifying imbalanced circuits, such as telephone lines not used by users, and circuits for security services, the above identification will not work because there is a phase adjustment violation. There is also interference in transmitting signals on imbalanced circuits with tone signals. For these reasons it is necessary for the identification system to notice or acknowledge the states of pairs, and to classify them. Classification categories are;

- a) Telephone services
- b) Data services
  - b-1) digital services
    - b-1-1) low speed
    - b-1-2) high speed
  - b-2) analog services
  - b-3) security services
- c) Open pairs

After classifying the above pairs, tone signals are applied at the proper transmitting level for them. Furthermore, if a circuit is imbalanced, a distinctive identifying process is provided. Figure 2 shows the classifying flow of the system.

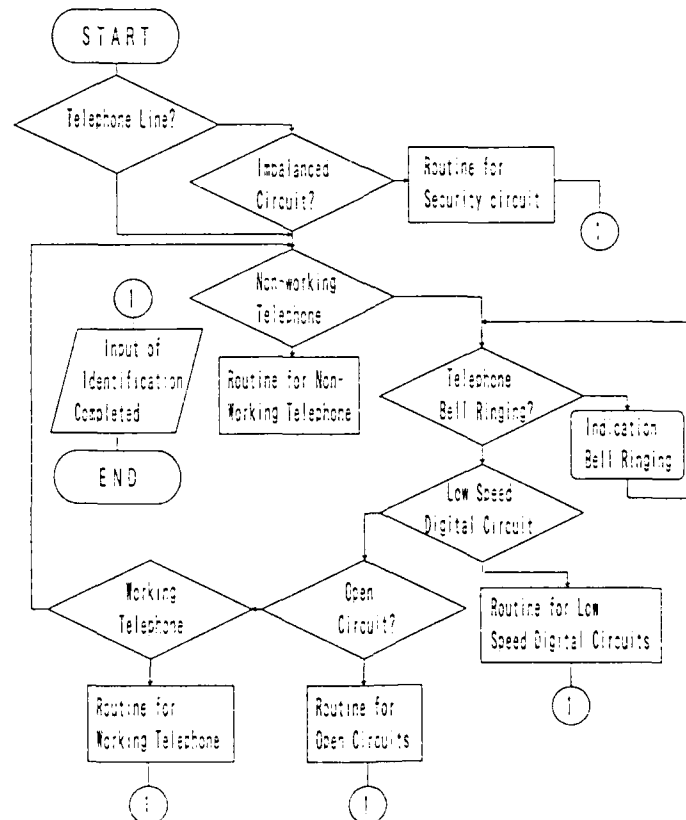


Figure 2. Classification flow

### 3.1 Classification

#### 3.1.1 Telephone Circuits

Telephone circuits that are not used by users are normally imbalanced circuits, such as when one of pair is connected to the ground line and the other is given DC -48 volts. The circuits are shown in Figure 3. To classify the circuit, tip and ring voltages must be measured.

The screening condition for these circuits is normally

$$\begin{aligned} \text{Tip (v)} &\geq -1 \text{ volts} \\ &\text{and} \\ \text{Ring (v)} &\leq -43 \text{ volts} \\ (\text{Above condition depends on ,.}) \end{aligned}$$

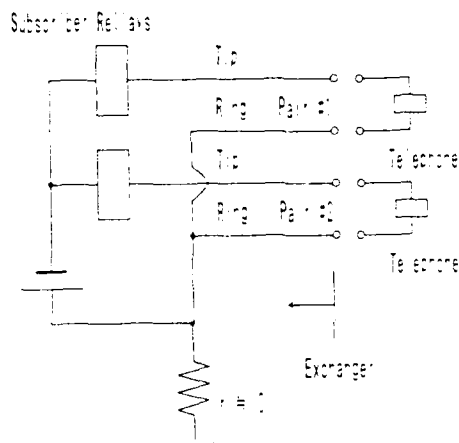


Figure 3. Non-working telephone circuits

In Figure 3, if a tone signal is applied to a pair, the signal will be flown thorough another pair either. They have the ground line as a common line. As a result, accurate identification is impossible. Also, since one of a pair is connected to the ground, tone signals have significant power loss, making identification difficult. To solve this problem, resistance is used to terminate telephone circuits after classifying them as non-working. ( This termination is called forced off-hook. ) While the forced off-hook is being performed, the system confirms whether termination has succeeded or not by detecting 400 Hz signals as dial tones from . If termination continues for more than 20 seconds, the will cause the lines to be busy, a hindrance for users. To avoid this, the forced off-hook by

the system is continued only for about 15 seconds.

There is also the possibility that users will use telephones while the system is identifying a pair terminating circuits. In this case, the tone signal intervenes with the circuits. The system must identify off-hook situations caused by users. Here, the system checks voltages of tip and ring to identify pairs. To distinguish between off-hook by users and the forced off-hook by the system, resistance for termination is chosen so as to cause different voltages from that of normal off-hook termination.

Moreover, when a telephone is ringing, the circuits is imbalanced. This can result in identification not being performed properly. In this situation, the system detects a 16 Hz signal which is for ringing, and stops identifying a pair during telephone ringing.

In all cases, the system regularly checks voltages of telephone circuits so as not to interfere with telephone lines for users.

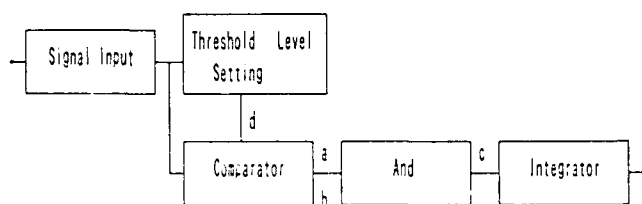
#### 3.1.2 Security (ground return ) circuits

Security services use imbalanced circuits where one of a pair is connected to the ground, or not terminated at the end of the circuits. The characteristic of circuits is that pulses are transmitted at 50 b/s between one of a pair and the ground. The remaining pair is not used, and is affected by induced noises where phases are the same as data signals. Therefore, identifying this circuit is easily executed by the outputs of two signals on the tip and ring, determined by adding their amplitudes. In this case the output is not zero. However, with this method, it is impossible to differentiate between security circuits and telephone circuits in ringing. As far as telephone circuits are concerned, ringing signals have very high amplitude, about  $200V_{rms}$ , which indicates that the threshold level for classifying can be set easily to identify security circuits. Moreover, in security circuits at 50 b/s speed data transmission, pulse intervals are about two seconds each. Hence, classification must be done for at least two seconds.

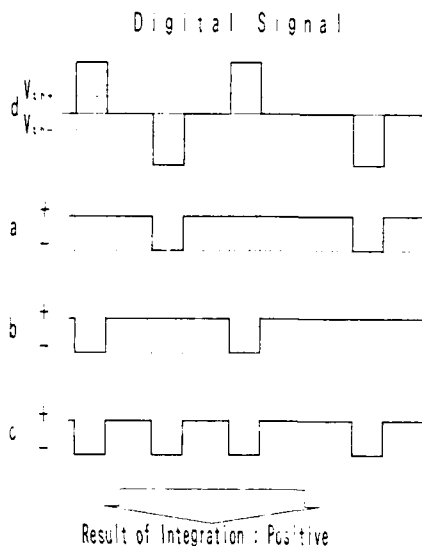
#### 3.1.3 Digital Circuits

Digital data services where pulses are transmitted at low speed, such as 3.2 kb/s of line-bit rate, have a power spectrum which affects the tone signal of the system. Furthermore, the power of tone signals varies by about 7 dB depending on the circuits in respect to terminated resistances ( 600  $\Omega$ , 110  $\Omega$  ). Tone signals have about 7 dB power loss when they are sent thorough circuits terminated with 110  $\Omega$ .

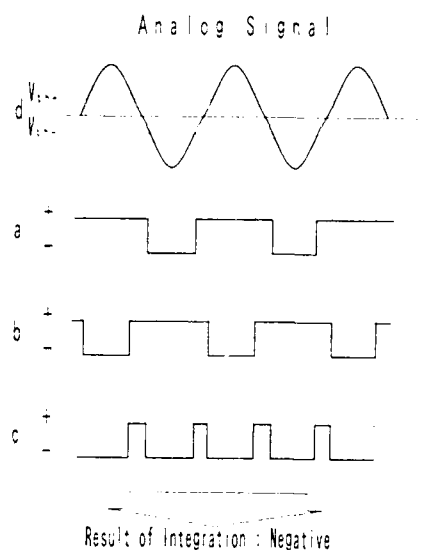




(a)



(b)



(c)

Figure 4. Classifying digital service

It is necessary to have proper gain adjusting of tone signals in digital circuits to hold the signal-to-noise ratio at a requested value ( -60 dBm ). The classification process of the system is performed by measuring the time when data signals are at zero volts. The classification is shown in Figure 4 (a). Threshold levels are set at nearly zero volts as  $V_{th+}$  and  $V_{th-}$ . Time is measured when data signals are between  $V_{th+}$  and  $V_{th-}$ . Integration of time can indicate whether the signals are pulses or waves. Figure 4 (b) and (c) show the difference of this integration.

### 3.1.4 Open Circuits ( No-User Lines )

Open circuits can be classified as both tip and ring are zero volts in DC. Any remaining circuits that cannot be identified belong to this category.

## 4. Pair Identification

There are a lot of pairs in a metallic cable. It is convenient to identify first a unit containing identifying pairs. A conventional pair identification method is used for the process of this system, but in the system, the same tone signals are applied to both the tip and ring respectively.

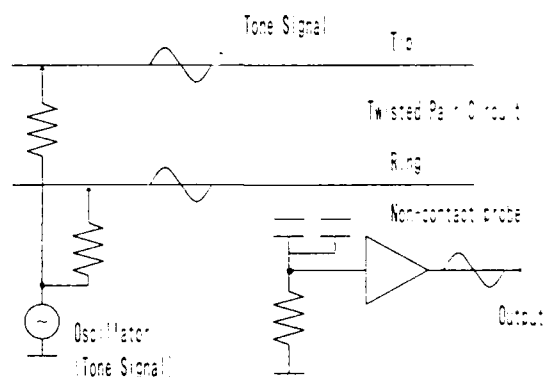


Figure 5. Pair identification

Figure 5 shows the pair identification circuit. Tone signals of the same phase and amplitude are input between the ground-tip and ground-ring. This means that tone signals do not cause any voltage differences between the tips and rings of pairs as far as balanced circuits are concerned. Therefore, this pair identification can be performed without any intervention of data services as balanced circuits. Since tone

signals are applied to both tips and rings, the tone signals can be set to a high power level. For this reason, tone signals can be detected with non-contact probes. However, inducing signals occur in other pairs, making precise tip and ring identification difficult. Therefore, there is tip/ring identification in this system to compensate for this disadvantage.

## 5. Tip and Ring Identification

### 5.1 Requirements for Identification

Pair identification is performed using the same tone signals for a pair. This method is not suitable, however for tip/ring identification, because it is impossible to differentiate between the tip and the ring. Therefore, different tone signals with the same amplitude but with a 180 degree shift in phase are applied to tip and ring of a pair. Since different tone signals are input for transmitting circuits, voltage differences normally occur between the tip and ring in a circuit. It is apparent that the voltage difference develops noises for data transmitting signals in balanced circuits. Therefore, a requirement is that tone signals must have very low transmitting power levels. To detect such low power signals at the detecting points, a unique technique to improve the signal-to-noise ratio is required. The following techniques are proposed to improve the s/n ratio.

- Synchronized addition in the time domain
- Using very narrow frequency band
- Synchronized addition in the frequency domain

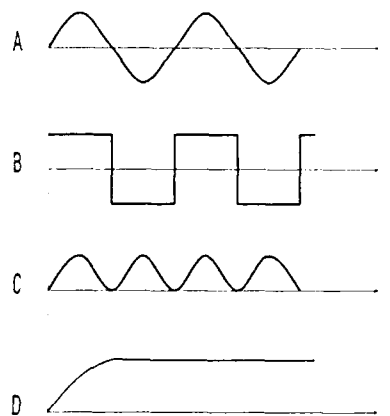
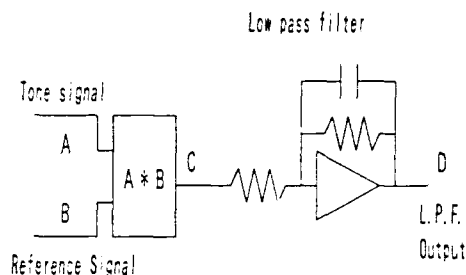


Figure 6. Principle of tip/ring identification

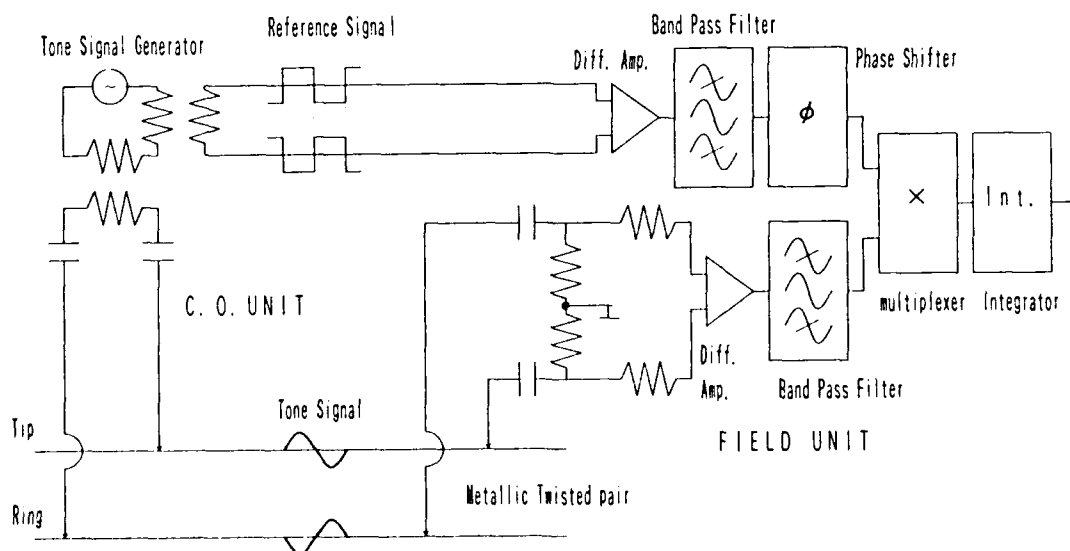


Figure 7. Tip/ring identification process

Here, methods a) and c) are not realistic because of cost. Therefore, method b) is used in the identification system. The basic principle of identification, shown in Figure 6, is based on the principle of Lock-in-amplifier. It is powerful enough to detect very low level signals.

Identification established on Lock-in-amplifier can be used for pair identification as well. But, since tone signals are very low level, non-contact probes cannot be used to identify pairs. They are not suitable because identification becomes quite inefficient. Figure 7 shows the identification process.

## 5.2 Principle of Tip/Ring identification

In Figure 6, let a tone signal be

$$E_i = e_i \times \cos(\omega t + \phi)$$

Here,  $\phi$  : Phase shift in a identifying circuit.

Let the reference signal  $E_r$  be

$$E_r = e_r \times \cos \omega t$$

Now the output  $E_o$ , which is obtained from multiplication of the tone signal by the reference signal, becomes

$$E_o = \frac{1}{2} \times e_i \times e_r + \frac{1}{2} \times e_i \times e_r \times \cos(2\omega t + \phi)$$

Hence, if phase  $\phi$  is adjusted as  $\phi=0$ , output  $E_o$  is

$$E_o = \frac{1}{2} \times e_i \times e_r + \frac{1}{2} \times e_i \times e_r \times \cos 2\omega t$$

Moreover, integration of  $E_o$  is

$$E_o = \frac{1}{2} \times e_i \times e_r$$

If the tone signal phase is delayed 180 degrees, the output becomes

$$E_o = -\frac{1}{2} \times e_i \times e_r$$

Therefore, the integration output can indicate the tip or ring of a pair. In the system, tip and ring tone signals have differences in phase. One of them is delayed 180 degrees. Their amplitudes are the same. Then, the integration of output  $E_o$  is the result of tip/ring identification of the system.

## 5.3 Frequency and Level of Tone Signal

To choose the frequency of tone signals, the following points are considered.

- The tone signal must hold its power to a detecting point at its frequency
- The frequency of tone signals does not exist near the spectrum of data transmission.

By the above reasons, the frequency of tone signals are determined as being lower than that of the voice bandwidth. ( The frequency is chosen 50 Hz ~ 300 Hz. )

The power level of tone signals is lower than -60 dBm for both cases in which circuits are terminated with 600  $\Omega$  and 110  $\Omega$ . ( Resistances of loops are neglected. )

## 5.4 Classifying for Identification

The above principle based on lock in amplifier works only for balanced circuits, since a phase adjustment is done on balanced circuits. It is necessary to classify circuits to determine whether identification is suitable or not. Also, the power level of tone signals is maintained at -60 dBm when classifying terminated impedances, such as 600  $\Omega$  and 110. In this point, digital and analog services are classified as mentioned in 3.1.3. After classifying circuits, the identification system modifies its identification processes.

### 5.4.1 Open Circuits Identification

Open circuits and non-working telephone circuits are imbalanced circuits. However, they can be balanced circuits if resistance such as 1 k $\Omega$  terminates a pair. The system first classifies these circuits, and terminates them to make them balanced. Then, the tip/ring identification is applied.

### 5.4.2 Low Speed Data Transmission

Digital data signals are classified to maintain tone signal level of tip/ring identification. But this is not enough for the accurate identification. Data signals transmitted at low speed, such as 3.2 kb/s at line bit rate have a spectrum near the frequency of tone signals. This disturbs tip/ring identification because the tone signals cannot maintain a better s/n ratio. To keep a proper s/n ratio, detecting circuits for tone signals eliminate data signals on pairs at a certain threshold level using clipper circuits. This process is shown in Figure 8.

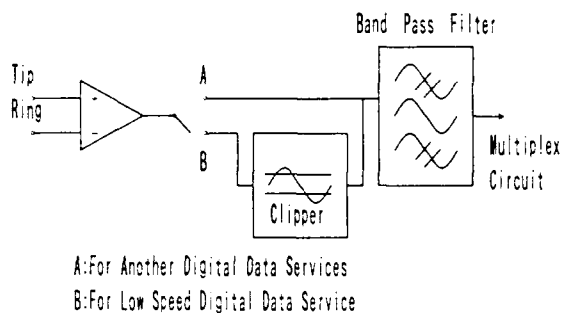


Figure 8. Clipping digital signal

### 6. Identification of Security Circuits

The identification methods employed in the system can be applied only to balanced circuits. However, imbalanced circuits such as security circuits also need to be identified. After the classifying process, a special identification technique is provided for imbalanced circuits. In general, security circuits use one of a pair and the ground line. The pattern of data signals is very simple. In the system, the character of signals is sampled and compared at both identifying points. In Figure 9 shows this identification.

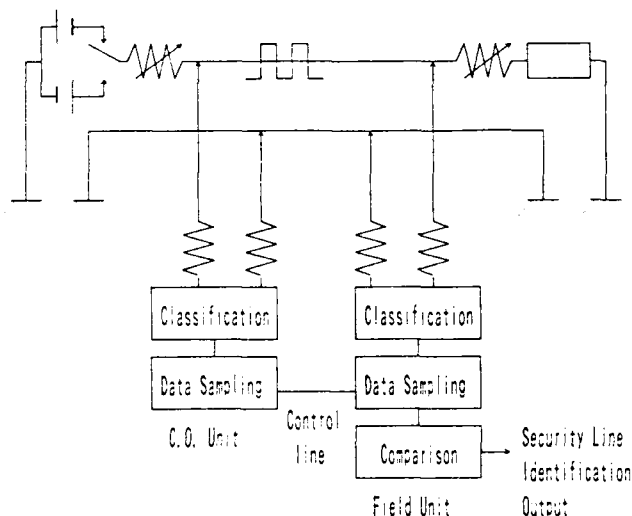


Figure 9. Security service identification

After classifying circuits as security service, the C.O. unit sends a start signal to sample data signals to the field units. At the identifying points, considering a delay time, the data signals are sampled by the C.O. unit. The data are compared with the sampling data of the field units. The identification result are right if the comparison is completely correct.

### 7. Performance of System

Using the proposed identification system, error-free identification is achieved for data services, as shown in Table 1. Both pair and tip/ring identification processes are performed without any interference in data transmission. In the table, the identification system can be applied to the fastest data service for twisted metallic pair, ISDN 320 kb/s. Even in this service, there is no error cause while the identification is performed. The tone signals are at quite low levels. However, the distances in which identification produced the correct results are desirably long. This is shown in Table 2.

Table 1. Identified data services in interference-free

MODEM	Transmission Speed	Modulation system
	1. 2 0 0 b/s	F S K
	2. 4 0 0 b/s	P S K
	4. 8 0 0 b/s	P S K
	9. 6 0 0 b/s	Q A M
D S U	Line bit rate	Transmission code
	3. 2 kb/s	D i g i t a l c o d e c A M I
	6. 4 kb/s	
	1 2. 8 kb/s	
	6 4 kb/s	
	3 2 0 kb/s	T C M ISDN 2B+D

Table 2. Maximum distance for identification

Gauge of conductor (mm)	0.4	0.5	0.65	0.9
Pair Identification (km)	1.5	2.2	2.6	2.8
Tip/Ring Identification (km)	1.5	2.5	2.8	3.5

Identifying Loop : Open circuit



Shuji Asakawa

NTT Telecommunication Field  
Systems R&D Center

1-7-1 Hanabatake, Tsukuba,  
Ibaraki, 305 Japan

Shuji Asakawa received his M.E. degree in electronics engineering from Ehime University in 1989. He joined NTT in 1989. He is engaged in the development of cable splicing technique at NTT Telecommunication Field Systems R&D Center, Japan..

## 8. Conclusion

An identification system should perform without intervention of services, including data transmission. To make an identification system suitable for all circuits, it is required that the identification process is adjusted properly according to miscellaneous service loops. The identification system introduced in this paper has automatic classification for services, and it prepares the suitable identifying process for them. In the identification process itself, the system has two-way identification, pair and tip/ring identification. Both are performed without any interference of services. In classifying service circuits services, the system adjusts its processes properly for efficient identification. Hence, the principle of Lock-in-amplifier is utilized for tip/ring identification, and tone signals are kept at a low power level. Therefore, the possibility of interrupting or causing an error in services is eliminated.



Takafumi Sakaguchi

NTT Network Systems  
Development Center

2-1 Uchisaiwai-cho,  
1-chome, Chiyoda-ku,  
Tokyo, 100 Japan

Takafumi Sakaguchi received his B.E. degree in mechanical engineering from Kyusyu University in 1987. He joined NTT in 1987. He is engaged in the development of cable splicing technique at NTT Network Systems Development Center, Japan.



Satoshi Matsuhashi

NTT Telecommunication Field  
Systems R&D Center

1-7-1 Hanabatake, Tsukuba,  
Ibaraki, 305 Japan

Satoshi Matsuhashi is a Senior Engineer at NTT Telecommunication Field Systems R&D Center, Japan. He received his B.E. degree in electronics engineering from Hokkaido University in 1981. He joined NTT in 1981. He is engaged in the development of aerial cable installation technique and cable splicing technique. Mr. Matsuhashi is a member of the Institute of Electronics, Information and Communication Engineers of Japan.

# Template Testing at DS1 and DS3 Line Rates for Transmission Studies of Twisted Pair and Coaxial Cables

Wing Eng, Jr.

Pacific Bell  
2600 Camino Ramon  
San Ramon, CA 94583

## Abstract

Template testing at DS1 (1.544 Mb/s) and DS3 (44.736 Mb/s) digital rates are standard within Bell Operating Companies for systems typically utilizing a high rate optical multiplexer, metallic cable and cross-connect equipment. This paper addresses the test criteria and test methodology for qualifying cables for use in these cross-connect circuits. Particular attention is focused on the usefulness of these tests for verifying the transmission performance of newly designed, shielded, twisted pair cables and smaller diameter mini-coaxial cables.

## 1. Introduction

Pacific Bell has been evaluating the transmission performance of many newly designed twisted pair and coaxial cables as the needs for the reduction of cable congestion in overhead racks and the introduction of DS1 and DS3 services for small size business customers have been addressed. This paper focuses on the construction, electrical characteristics and intended use of each type of cable tested. It also outlines the rationale behind DS1 and DS3 testing from a systems point of view. Details of the templates are given that precisely define the upper and lower limit boundaries.

Cables which meet the DS1 or DS3 template become qualified for use in cross-connect systems that will nominally provide  $10^{-9}$  or better bit error rate (BER) service. The test template is the Fourier Transform representation of the quantifiable electrical transmission performance parameters of the cable.

This paper details the validity of the template test in relation to a "standard" test cable. A discussion of the test methodology is given involving the DS source, the cable under test, the automated, software driven, digital oscilloscope and the interpretation of the test results.

Template testing is presented in this paper as being a reasonably low cost method for the evaluation of cables that are intended for digital use in Bell Operating Companies. It is an especially useful test method for the evaluation of new or redesigned metallic cables.

## 2. Background

Due to the increasing concentration of digital equipment in central offices, cable manufacturers have been developing smaller, more compact, twisted pair and coaxial cables for DS1 and DS3 cross-connect installations. The DSX is a manual cross-connect point to interconnect DS1 or DS3 signals in a central office and has become a well documented and standardized interface. The traditional cable used for DS1 (1.544 Mb/s) cabling between equipment and cross-connect frame has been 22 AWG ABAM, while the corresponding cable used for DS3 (44.736 Mb/s) applications has been 20 AWG coaxial cable.

### 3. Features: Paired and Coaxial Cables

The following four tables display the physical and electrical features of typical twisted pair and coaxial cables.

#### DS1 Cable: Comparison of Physical Features for Twisted Pair Cable

Table 1 compares the physical features of ABAM with two representative samples of reduced outer diameter DS1 cables.

**Table 1**

	ABAM paired	RD24 paired	RD26 paired
Conductor Gauge(AWG)	22	24	26
Insulation Materials	PE/PVC	PE/PVC	XPE/PVC
Diameter over Dielectric (in.)	0.049	0.040	0.032
Maximum Twist Length (in.)	5.0	6.0	1.0
Shield Material	Alum. Foil(X1)	Alum. Foil(X1)	Alum. Foil(X2)
PVC Jacket	Outer Only	Outer Only	Inner & Outer
Outer Diameter (in.) 25 pair	0.70	0.43	0.43

#### DS3 Cable: Comparison of Physical Features For Coaxial Cable

Table 2 compares the physical features of 20 AWG coaxial cable with two representative samples of reduced outer diameter DS3 cables.

**Table 2**

	20 AWG coax	RD26 coax	RD29 coax
Conductor Gauge(AWG)	20	26	29
Conductor Material	solid copper	silver-plated copper	silver coated copper-covered steel
Dielectric Type	FRPE	XFRPE	Solid Poly-tetra-fluoro-ethylene
Diameter Over Dielectric (in.)	0.150	0.077	0.060
Shield	80% braid over 3 mil alum. foil	90% braid over 3 mil alum. foil	Double Braid (90%)
Jacket Material	PVC	PVC	PVC
Outer Diameter (in.)	0.236	0.125	0.121

**DS1 Cable: Comparison of Electrical Characteristics for Twisted Pair Cable**

Table 3 compares the electrical features of ABAM with two representative samples of reduced outer diameter DS1 cables.

**Table 3**

	ABAM paired	RD24 paired	RD26 paired
Characteristic Impedance at 772 kHz(ohms)	100	100	120
Attenuation at 772 kHz(dB/kft)	4.6	5.7	5.9
Worse pair near end power sum crosstalk at 772 kHz(dB)	38	42	48
Meets DSX-1 Template?	yes	?	yes
DSX-1 cabling distance - maximum length (ft)	655	450-600?	450

**DS3 Cable: Comparison of Electrical Features for Coaxial Cable**

Table 4 compares the electrical features of 20 AWG coaxial cable with two representative samples of reduced outer diameter DS3 cables.

**Table 4**

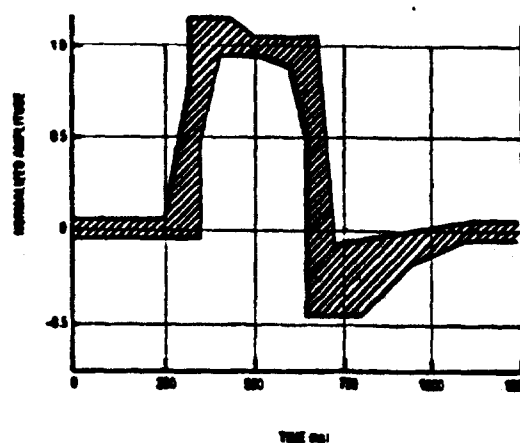
	20 AWG coax	RD26 coax	RD29 coax
Nominal Impedance (ohms)	75	75	75
Relative Dielectric Constant	1.60	1.60	2.10
Attenuation at 22.368 MHz(dB/kft)	11.5	21.8	30.9
DSX-3 Cabling Distance - maximum length(ft)	450	250	150

**4. Definition of DSX Template**

The DSX template tests in Bell Operating Companies are intended to measure the suitability of DS1 (1.544 Mb/s) or DS3 (44.736 Mb/s) transmission equipment for installation in central offices. In particular, the digital line rate generators at DS1 or DS3 speeds are accepted or rejected based upon DSX template test results.

Figure 1, below, illustrates the DS1 template, with maximum and minimum curve definitions for twisted pair cable.

note: Pulse voltage must be between 2.4 and 3.6 volts at the cross-connect (DSX-1) cabling distance.



TIME (ns)	0	20	30	40	50	60	70	80	90	100
NORMALIZED AMP. (V)	0.00	0.00	0.0	1.0	1.0	1.0	1.0	0.5	0.0	0.0

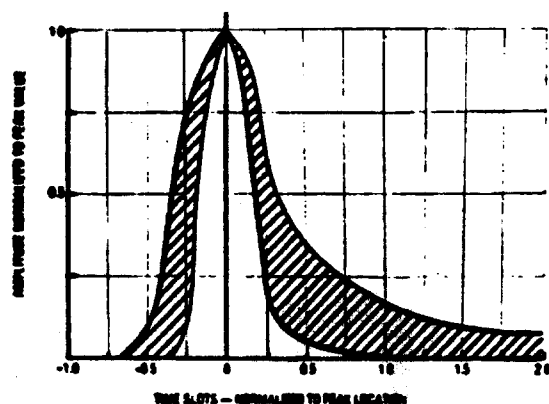
TIME (ns)	0	20	30	40	50	60	70	80	90	100
NORMALIZED AMP. (V)	-0.5	-0.5	0.0	0.0	0.0	0.0	0.0	-0.5	-0.5	-0.5

**DSX-1 twisted pair template**

**Figure 1**



Figure 2, below, illustrates the DS3 template, with maximum and minimum curve definitions for coaxial cable. note: Pulse voltage must be between 0.36 and 0.85 volts at the cross-connect (DSX-3) cabling distance.



LOWER CURVE	TIME (ns)	NORMALIZED AMPLITUDE
	$7.5 \leq t \leq 0$	0
	$-0.25 \leq t \leq 0.25$	$0.5(1 + \sin(\pi(t + 0.25)))$
	$0.25 \leq t$	$0.5(1 + \cos(\pi(t - 0.25)))$
UPPER CURVE	TIME (ns)	NORMALIZED AMPLITUDE
	$7.5 \leq t$	1
	$-0.25 \leq t \leq 0.25$	$0.5(1 + \sin(\pi(t - 0.25)))$
	$0.25 \leq t$	$0.5(1 + \cos(\pi(t - 0.25)))$

DSX-3 defined pulse template

Figure 2

## 5. Set-up of DSX Template Tests

The previously defined DS1 and DS3 templates per figures 1 and 2, respectively, may be used to test digital line rate transmitters for acceptance of use in cross-connect circuits. The two following figures illustrate these tests.

Figure 3, below, is a set-up illustration of a DS1 template test.

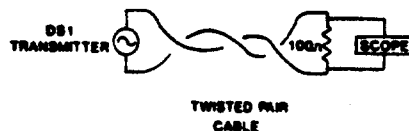


Figure 3

## DSX-1 Pulse Template Test Set-Up

Figure 4, below, is a set-up illustration of a DS3 template test.



Figure 4

## DSX-3 Pulse Template Test Set-Up

It is generally preferred to have an automated oscilloscope that displays the DS1 or DS3 pulse mask and shows any points of template non-conformance.

It must also be understood per figures 3 and 4 that template tests must be made with "standard" twisted pair and coaxial cables. This is true since a template test "failure" does not indicate whether a sub-par transmitter or cable (or both) is at fault.

When cable meets the insertion loss and insertion phase (non-linear only) characteristics per figures 5 and 6, for twisted pair cable, or figures 7 and 8, for coaxial cable, it becomes qualified for testing purposes as a "standard" cable. Any qualified and acceptable DS1 or DS3 equipment transmission pulse will now lie totally within the DS1 (see figure 1) or DS3 (see figure 2) pulse template when tested with a qualified "standard" cable. The equipment-cable system will now also meet a bit error rate (BER) of  $10 \times 10^{-9}$  or better.

Figures 5 and 6, below, illustrate the insertion loss and insertion phase features of "standard" acceptable twisted pair cable (ABAM).

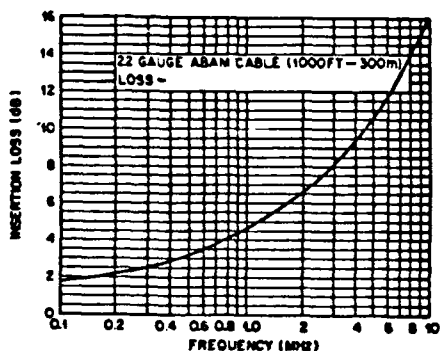


Figure 5  
Insertion Loss ABAM

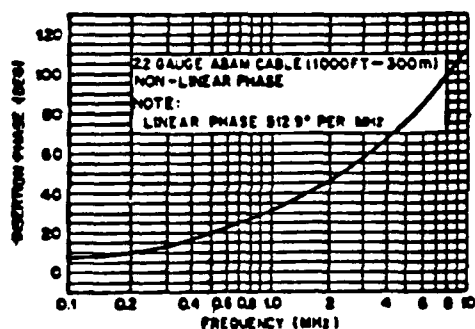


Figure 6  
Insertion Phase ABAM

Figures 7 and 8, below, illustrate the insertion loss and insertion phase features of "standard" acceptable 20 AWG coaxial cable.

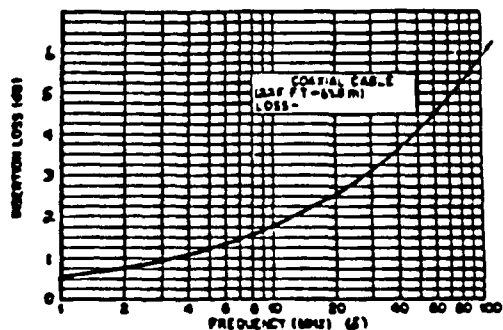


Figure 7  
Insertion Loss 20 AWG Coax

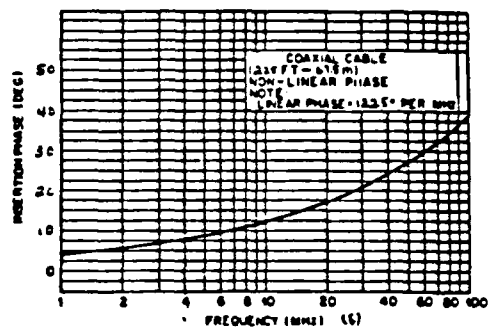


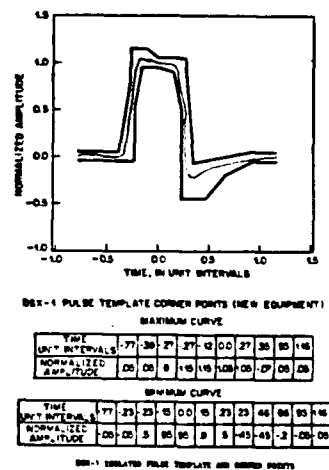
Figure 8  
Insertion Phase 20 AWG Coax

An important method is now available for comparing a qualified "standard" cable's test template with the test template of other, reduced diameter, cables. Of course, the maximum lengths at which these reduced diameter cables will meet the DSX template will now be less than 655 feet in the case of twisted pair cable and less than 450 feet in the case of coaxial cable.

## 6. Test Results

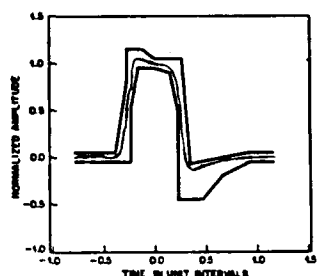
### DS1, Twisted Pair

The figures, below, illustrate test results using a "standard" ABAM, DS1, reference cable and 26 AWG reduced diameter cable.



Maximum ABAM DS1 Template  
Length is 655 feet

Figure 9  
DSX-1 Pulse Template - ABAM



DSX-1 PULSE TEMPLATE CORNER POINTS (NEW EQUIPMENT)

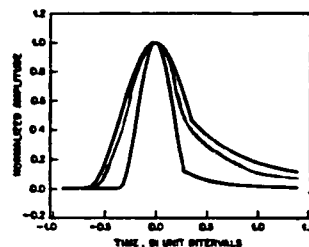
MAXIMUM CURVE												
TIME UNIT INTERVALS	77	23	27	27	12	00	27	30	85	115		
NORMALIZED AMP. VALUE	0.0	0.5	0.8	1.0	1.0	0.5	0.2	0.0	0.0			

MINIMUM CURVE												
TIME UNIT INTERVALS	77	23	23	15	00	23	23	46	86	90	115	
NORMALIZED AMP. VALUE	-0.0	-0.0	0.5	0.5	0.5	0.5	-0.5	-0.5	-0.5	-0.0	-0.0	

DSX-1 ISOLATED PULSE TEMPLATE AND CORNER POINTS

Maximum RD26 DS1 Template  
Length is 450 feet

Figure 10  
DSX-1 Pulse Template - RD26



DSX-3 PULSE TEMPLATE BOUNDARIES

CURVE	TIME UNIT INTERVALS	NORMALIZED AMP. VALUE
MAXIMUM CURVE	$T_S - 0.85$ $-0.85 \leq T \leq 0.35$ $0.35 \leq T$	$0.5 \left[ 1 + \sin^2 \left( 14 \pi \frac{T}{0.35} \right) \right]$ $0.05 + 0.40 \pi^2 (0.35 - T)^2$
MINIMUM CURVE	$T_S - 0.35$ $-0.35 \leq T \leq 0.35$ $0.35 \leq T$	$0.5 \left[ 1 + \sin^2 \left( 14 \pi \frac{T}{0.35} \right) \right]$ $0.14 + 0.42 (T - 0.35)$

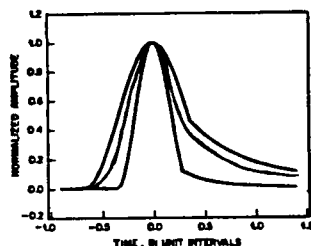
DSX-3 ISOLATED PULSE TEMPLATE AND BOUNDARIES

Maximum RD26 Coax DS3  
Template Length is 250 feet

Figure 12  
DSX-3 Pulse Template - RD26 Coax

### DS3, Coaxial Cable

The figures, below, illustrate test results using a "standard" 20 AWG, DS3, reference cable and 26 AWG and 29 AWG reduced diameter cable.



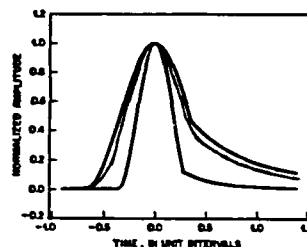
DSX-3 PULSE TEMPLATE BOUNDARIES

CURVE	TIME UNIT INTERVALS	NORMALIZED AMP. VALUE
MAXIMUM CURVE	$T_S - 0.85$ $-0.85 \leq T \leq 0.35$ $0.35 \leq T$	$0.5 \left[ 1 + \sin^2 \left( 14 \pi \frac{T}{0.35} \right) \right]$ $0.05 + 0.40 \pi^2 (0.35 - T)^2$
MINIMUM CURVE	$T_S - 0.35$ $-0.35 \leq T \leq 0.35$ $0.35 \leq T$	$0.5 \left[ 1 + \sin^2 \left( 14 \pi \frac{T}{0.35} \right) \right]$ $0.14 + 0.42 (T - 0.35)$

DSX-3 ISOLATED PULSE TEMPLATE AND BOUNDARIES

Maximum 20 AWG Coax DS3  
Template Length is 450 feet

Figure 11  
DSX-3 Pulse Template - 20 AWG Coax



DSX-3 PULSE TEMPLATE BOUNDARIES

CURVE	TIME UNIT INTERVALS	NORMALIZED AMP. VALUE
MAXIMUM CURVE	$T_S - 0.85$ $-0.85 \leq T \leq 0.35$ $0.35 \leq T$	$0.5 \left[ 1 + \sin^2 \left( 14 \pi \frac{T}{0.35} \right) \right]$ $0.05 + 0.40 \pi^2 (0.35 - T)^2$
MINIMUM CURVE	$T_S - 0.35$ $-0.35 \leq T \leq 0.35$ $0.35 \leq T$	$0.5 \left[ 1 + \sin^2 \left( 14 \pi \frac{T}{0.35} \right) \right]$ $0.14 + 0.42 (T - 0.35)$

DSX-3 ISOLATED PULSE TEMPLATE AND BOUNDARIES

Maximum RD29 Coax DS3  
Template Length is 150 feet

Figure 13  
DSX-3 Pulse Template - RD29 Coax

## 7. Conclusions

Template testing using DS1 and DS3 cables has traditionally been used to qualify DS1 and DS3 transmission equipment in BOC central offices.

This paper has stated the application of a "standard" DS1 or DS3 cable for the purpose of qualifying reduced diameter cables for use in congested central offices.

It should be understood that a "borderline" or marginal template failure will normally still ensure  $10 \exp -9$  Bit Error Rate (BER) performance.

Oscilloscopes are available that are software driven to perform DS1 and DS3 template measurements. These scopes are becoming increasingly common in many central offices and their relative low cost, compared to other automated electrical parameter testing equipment, makes sense for BOCs to pursue template testing on existing and new-type cables.

The test results presented in this paper are intended only as illustrations of the process of comparing standard and reduced diameter cable DS1 and DS3 templates and do not endorse the use of any manufacturer's cable products.

## 8. Acknowledgments

I would like to thank the following people who have assisted me in the preparation of this paper: Mr. R. H. McVey, Mr. M. A. Wright, Mr. J. C. Martinez, Mr. A. G. Eriksen, Mr. M. D. Egeland, Mr. J. H. Benjamins, and Ms. E. M. Healy. All except Mr. Wright (retired from Pacific Bell) are current Pacific Bell employees.

## REFERENCES

1. M. L. Fuller, "A Compact Cable for Within Building 1.544 Mb/s Digital Transmission", 1987 International Wire and Cable Symposium Proceedings, pp. 492-498.
2. A. LaSelle and D. Burroughs, "Technical Report to T1 Standards Project; Mathematical Modeling of DS1, DS1A, DS1C, DS3, and DS4NA Waveshapes", 1988, pp. 1-17.
3. J. H. Benjamins, "PE/PVC Terminating Cable Specification", Issue 2, 1987, Attachment 5.
4. J. H. Benjamins, "Double Shielded, Close Tolerance 75 Ohm R.F. Coaxial Cable Specification", Issue 2, 1987, Attachment 2.
5. M. A. Wright, Private Communication



W. Eng, Jr.

Pacific Bell

2600 Camino Ramon

San Ramon, CA 94583

Wing Eng, Jr., joined Pacific Bell in 1981. He has worked in the testing and evaluation of metallic cables for the past 4 years. Mr. Eng received his BA in Astronomy and MS in Physics from UCLA in 1972 and 1974, respectively.

# AN EVALUATION OF MEASUREMENT TECHNIQUES FOR DETERMINING COPPER CABLE STRUCTURAL EFFECTS

H. W. Friesen

AT&T Bell Laboratories  
Norcross, Georgia 30071

## Abstract

The frequently used methods of evaluating structural variation often focus on single-ended measurements such as input impedance variation and structural return loss (SRL). Through-the-cable techniques which evaluate excess loss and delay jitter regions in the frequency domain, appear more closely aligned with end-to-end transmission objectives. This work reviews the various measurement techniques focusing on LAN frequencies where relatively inexpensive unshielded multipair cables are being used at higher frequencies than ever before. The use of excess loss as a roughness test offers the advantage of effectively examining a longer length of cable than SRL, which is heavily weighted by the end portion of the sample under test.

Numerical evaluations as well as measurements on actual samples are used to show that periodic structural variation at a given level is considerably more threatening to transmission performance than the same amount of random variation. Also of interest is that the SRL of pairs tends to decrease with frequency at a rate similar to near end crosstalk. Increased loss due to random roughness exhibits a frequency dependence similar to dielectric loss along with some amount of roughness.

## I. Introduction

A recent IWCS paper by this author discusses data processing techniques for extracting characteristic impedance information from what are in many cases rough input impedance\* scans versus frequency. It advocates distinguishing between the input impedance and the characteristic impedance of twisted pair structures<sup>1</sup>. In one of the procedures described in that paper an impedance-like function is least squares fitted to the input impedance scan spanning the applicable frequency range. The desired smooth characteristic impedance estimate is obtained devoid of the structural variations that occur along the length of the pair. Figure 1 reviews a typical input impedance scan fitted with such an impedance function. One criticism of that work, recognized at the time it was done, has been that structural roughness must also be quantified. This paper explores the various single-ended and through-the-cable

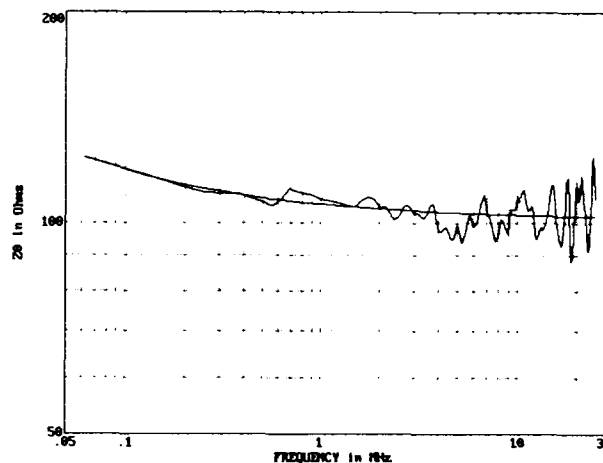


Fig. 1 Input Impedance Scan Least Squares Fitted with Smooth Impedance Function

techniques for doing that, keeping in mind that the current local area network (LAN) interest is continuing to focus on unshielded twisted pair (UTP) cable. These UTP cables typically exhibit random structural effects, compared to more controlled structures such as coaxials, which may have insignificant random structural variations but can exhibit periodic structural effects if a particular manufacturing process is not well controlled.

Roughness effects on transmission due to random variations tend to increase with frequency. Like crosstalk, as the move to higher frequencies continues, the demands on transmission performance through the medium increase. Cables with very adequate smoothness to 16 MHz may not look as good when examined for 100 Mbit/s operation. Later in this paper the rate of decrease of structural return loss (SRL) resulting from random variation will be evaluated. Comparisons will be made between the reflection mechanism and near end crosstalk coupling.

A number of techniques for determining structural variation along the length of a cable pair will be considered. The traditional input impedance and return loss techniques are reviewed both by numerical modelling and by means of actual examples. A distinction is drawn between structures which have periodic structural roughness throughout the whole length

\* The term "input impedance" as used in this paper means the impedance obtained from open and short circuit measurements according to  $Z_{in} = \sqrt{Z_o Z_s}$  which is the basis for impedance measurements on electrically long as well as short lengths.

and those where the roughness is random. In the second main section consideration will be given to using through-the-cable measurement of excess transmission loss. One of the examples serves to point out that through-the-cable measurements generally are more capable of detecting structural effects within the given span than are single-ended measurements.

Other aspects of this work deal with the frequency dependence of SRL traces and input impedance variation with frequency. Recognizing the frequency dependence leads to some suggestions about a standards model for input impedance limits which are more in keeping with actual twisted pair behavior. An area of concern is the extent to which SRL can deteriorate as the frequency range of interest is extended to 100 MHz. Fortunately, much of the excess loss due to random structural effects exhibits a uniformly increasing with frequency kind of behavior and can be tolerated as long as loss objectives are met.

## II. Input Impedance and Structural Return Loss Variation with Frequency

### 2.1 Basic Premise is Random Variation

Support for the idea that structural variation in twisted pair cable varies more in a random way than in a periodic manner, comes from the cable cutting experiment discussed in Reference 1. A 500 foot length of a standard UTP design was tested as a whole length. It was subsequently cut into 10 foot segments

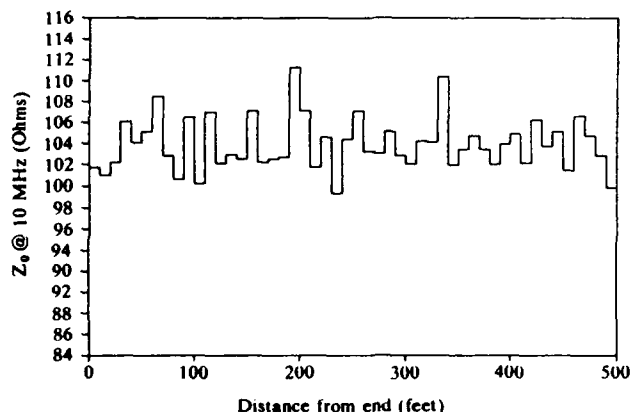


Fig. 2 Impedance Variation with Length Found in Cable Cutting Experiment

to determine how much the characteristic impedance varied on a segment by segment basis. It was reported that the impedance of the segments varied as much as 11 Ohms. Figure 2 is a replica of Figure 4 of Reference 1 showing the variation from segment to segment. It shows that much of the variation is of a random nature with perhaps some periodic effects being prominent at the right end. In general the impedance for one segment cannot be predicted from knowledge of the value for an adjacent segment. Some cable samples may exhibit periodic behavior along with random variation. Figure 2 does exhibit

some periodicity on the right end. In the vast majority of cases though, when input impedance or  $s_{11}$  data is transformed to the time domain or distance domain as effected here, largely random variation is observed.

The impedance variation shown in Figure 2 is thought to be the result of variation with distance of physical parameters such as wire separation, which might happen during the final cable assembly operations. Figure 3 represents the situation where

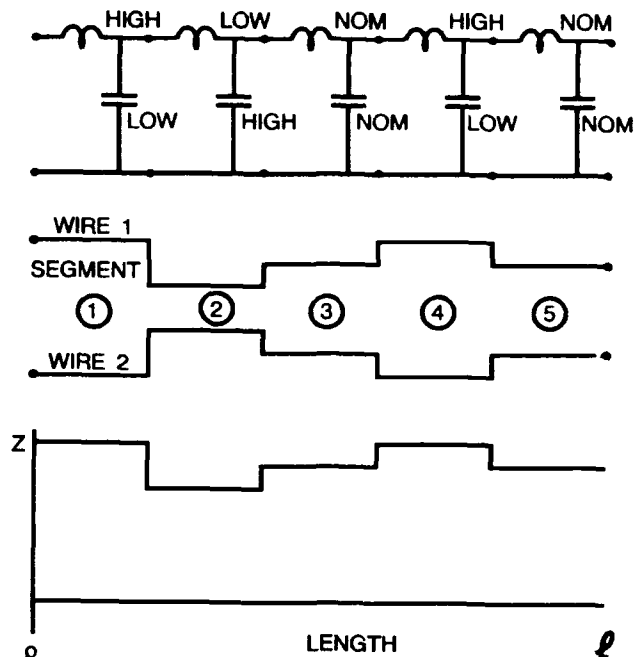


Fig. 3 Structural Variation Associated with Impedance Variation

segment by segment variation of impedance is the result of variation in wire separation. Separation of wires 1 and 2 of a pair are shown to vary from the nominal separation represented by the third segment with segment 1 showing increased separation and segment 2 reduced separation over nominal. The discrete element circuit representing short pair segments shows a high value for inductance and a low value for capacitance compared to nominal for the first segment. This will result in this segment having a high characteristic impedance. Segment two has low inductance and high capacitance resulting in a low impedance value compared to nominal.

The eleven Ohms of impedance variation shown in Figure 2 corresponds to about 5 mils of wire separation variation which is considerable compared to the approximately 32 mil insulation diameter for a design of this type. Wire separation in this design probably varies from insulation diameter on the low side to insulation diameter plus 5 mils on the high side with nominal being half way in between. The concept of wires in twisted pair cable not being in constant contact is not new. It was discussed by A. S. Windeler almost three decades ago.<sup>2</sup> Other types of variation such as conductor diameter, insulation

diameter and eccentricity and in the case of expanded insulation, variation of insulation density are also possible. The ways in which different pairs interact within the bundle of pairs leads to variation as well.

## 2.2 Numerical Evaluation of Structural Effects

The relationship between a given amount of structural variation and the effects on input impedance, SRL, insertion loss and delay can be approached either analytically or with numerical techniques. Analytical approaches exist and can be found in the literature. A paper by Karbowski<sup>3</sup> develops the behavior of non-smooth transmission lines in a familiar manner where expressions are arrived at for first and second order effects. First order effects involve a single reflection, second order effects pertain to two reflections, etc. Bolinder is frequently referred to with regard to relating these phenomena to Fourier Transforms<sup>4</sup>. These equations are useful for demonstrating that periodic structural variation relates to poor return loss at a frequency corresponding to the round trip delay associated with the structural period. Point discontinuities periodically spaced can also be evaluated. Handling random structural variation with these equations results in somewhat more complicated analysis and often having to do numerical evaluations anyway. It becomes difficult to look at the expressions and visualize the end result when the variation is not periodic.

The approach to be taken here is one of starting out by numerically evaluating a transmission line on a circuitual basis using many segments similar to those in Figure 3. Series resistance and shunt conductance are included. The calculation starts with nominal primary (R, L, G, and C) line parameters

$$\Delta V = \frac{YZ}{2} V_1 - [Z + \frac{YZ^2}{4}] I_1 \quad (1)$$

$$\Delta I = \frac{YZ}{2} I_1 - YV_1 \quad (2)$$

used on functional fits to actual cable measurements for the frequency range of interest. The actual circuit segment used is the balanced T circuit. Equations 1 and 2 describe the changes in voltage and current occurring in each segment.  $Z$  and  $Y$  represent the series impedance ( $R + j\omega L$ ) and shunt admittance ( $G + j\omega C$ ) respectively for the segment. A length of cable pair consists of many segments where the segment length is very short compared to a wavelength. Segment lengths on the order of 2 to 3 inches are used to represent a pair for frequencies extending up to 100 MHz (6 ft. wavelength). When such small increments are used for the case where the line is smooth, very close agreement is obtained between resultant secondary transmission parameters  $Z_0$  and  $\gamma$  and those computed directly from the nominal R, L, G and C values.

The advantage of the numerical approach is that rather arbitrary assignments can be made to the individual segments. The segments are allowed to take on values deviating from nominal as depicted in Figure 3. Various kinds of departures from a

smooth line such as the continuously varying periodic, periodic point, and random variation and combinations of these can be simulated. Most of the study discussed here has been along the lines of modelling variation in wire separation which affects both inductance and capacitance. For random variations a random number generator can be used to generate examples of random structural variation.

## 2.3 Typical Results Obtained from Difference Equations

We proceed to examine an input impedance trace based on random variation seeking to determine whether it is similar to traces obtained from actual cable measurements. The irregular

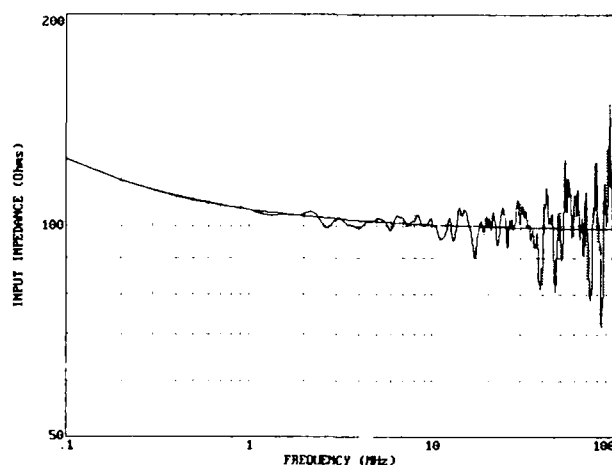


Fig. 4 Impedance Trace Calculated from Random Structural Sequence

trace in Figure 4 is a plot of an input impedance result obtained when a random number generator is used to generate a sequence of deviations. This trace shows an input impedance trace typical of actual cable pairs such as the one shown in Figure 1. Here the calculated trace extends to a frequency of 100 MHz, which is in keeping with present day interest in using copper pairs for FDDI bit rates. Since this example is based on a given set of smooth cable parameters we can also calculate the smooth or average characteristic impedance. The smooth trace also plotted in Figure 4, is well aligned with the input impedance trace at low frequencies and passes through what appears to be the middle of the input impedance trace at high frequencies. The amplitude and structure of this response are typical of UTP data cables in manufacture today.

The input impedance trace of Figure 4 is the response to the impedance deviation sequence  $W(x)$  shown in Figure 5. As indicated earlier this trace was generated with a random number generator. The peak deviation is 4 Ohms with about 830 different impedance sections constituting this random sequence which simulates 500 ft. of cable. This number of sections is large enough to allow individual sections to be electrically short at the highest frequency. The total number of segments used in this example was larger, 2500, with each randomly

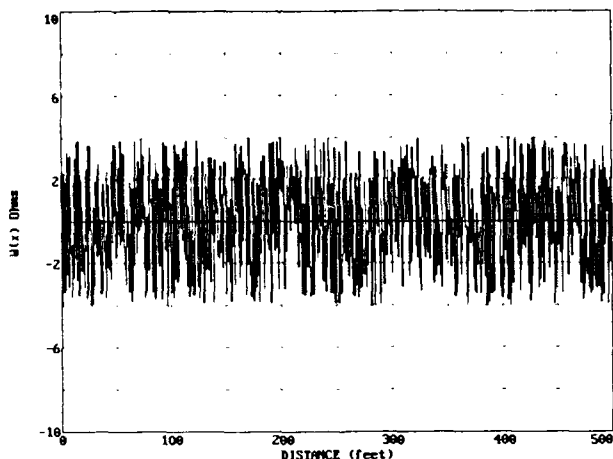


Fig. 5 Structural Impedance Deviation from Nominal Versus Length

generated impedance section being represented by three line segments. Letting each line segment be 2.4 inches in length resulted in the difference equations for the individual segment representing smooth line solutions with sufficient accuracy when variation was set to zero. Figure 4 shows that impedance departures in the frequency domain are smaller than the peak impedance value of 4 Ohms showing in Figure 5 at frequencies below 10 MHz. This is due to the considerable averaging that takes place at those frequencies. At high frequencies the opposite is true. Here different sections of  $W(x)$  reinforce each other when the phasing is right.

#### 2.4 Computing the Structural Return Loss from Input Impedance and Characteristic Impedance

A return loss trace can be obtained directly from a network analyzer with an S-parameter unit. It gives us a result which is relative to the calibrating impedance. Of interest is the ability to calculate the SRL. SRL focuses only on departure from the average characteristic impedance which is based on the through-the-cable total inductance and capacitance at high frequencies according to the equation  $Z_0 = \sqrt{L_T/C_T}$ . In this simulated example the characteristic impedance is readily

$$SRL = -20 \log \frac{Z_{in} - Z_0}{Z_{in} + Z_0} \quad (3)$$

available. Equation 3 can be used to compute the SRL from the input impedance and the characteristic impedance. We next consider the SRL trace calculated for this example.

A trace resulting from the procedure just discussed is plotted in Figure 6. The relationship between this measure of roughness and input impedance is one of rectification. In Figure 4 deviations show on both sides of nominal whereas here the display represents only magnitude. The irregularities with regard to the sign of the deviations in the particular input

impedance trace (for instance in the 50 to 70 MHz range) shown in Figure 4 are not a part of the SRL trace.

A most important aspect of this trace is that it shows marked degradation with frequency. The SRL for this simulated response is quite high in the 1 MHz vicinity (about 45 dB) but degrades with increase in frequency to about 15 dB at 100 MHz. There appears to be a marked similarity between the slope and structure of this trace and near end crosstalk traces which also worsen with increase in frequency exhibiting a 15 dB/decade slope.

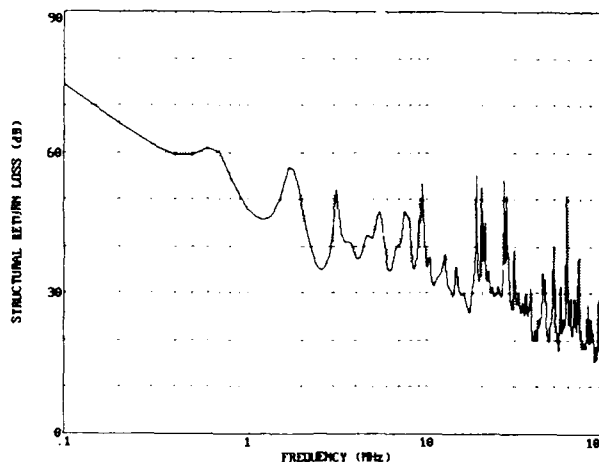


Fig. 6 Structural Return Loss Calculated from Random Structural Sequence

#### 2.5 Input Impedance Behavior Based on Single Reflections

Earlier we indicated that analytical approaches to the evaluation of structural effects result in expressions for single and double reflections, etc. It is of interest to determine if results obtained from numerically solving the difference equations and the single reflection model agree. The equation representing only single reflections is given by Equation 4. This equation states that the reflected to input voltage ratio as a function of frequency

$$s_{11}(\omega) = \frac{\gamma(\omega)}{Z_0(\omega)} \int_0^l W(x) e^{-2\gamma(\omega)x} dx \quad (4)$$

is equal to the  $\gamma/Z_0$  ratio multiplying the integral. The integral represents a summation over the whole cable length of the characteristic impedance deviation function of distance,  $W(x)$ , multiplied by the round trip propagation effect to the point of reflection and back. The ratio of the propagation constant to characteristic impedance  $\gamma/Z_0$  is really the shunt admittance of the transmission line consisting of the conductance and capacitive reactance ( $G + j\omega C$ ). This up front term has first power of frequency dependence if the dielectric constant of the pair is not frequency dependent.

The reflection ratio equation appears quite similar to the near



$$N(\omega) = j\omega \int_0^l U(x) e^{-2\gamma(\omega)x} dx \quad (5)$$

end crosstalk equation included here as Equation 5. The only differences are that here radian frequency shows in front of the integral in place of the  $\gamma/Z_0$  ratio and that coupling unbalance as a function of position,  $U(x)$ , replaces  $W(x)$ . This equation dates back to early in this century<sup>5</sup>. It has been studied extensively<sup>6</sup> and is thought to accurately represent first order coupling between pairs.

We seek now to determine how well results from the reflection expression, Equation 4, and the difference expressions, Equations 1 and 2, agree. Figure 7 shows SRL results based on Equation 4 for the same example used in Figures 4, 5 and 6. Overlaid is the result obtained earlier with excellent agreement showing. While the computation based on the difference equations represents the total effect, if done with sufficiently fine incremental line segments, the equation representing single reflections yields virtually the same result. This is obviously only one supportive example but additional computer runs have been made, each one with a different random sequence, with similar levels of agreement.

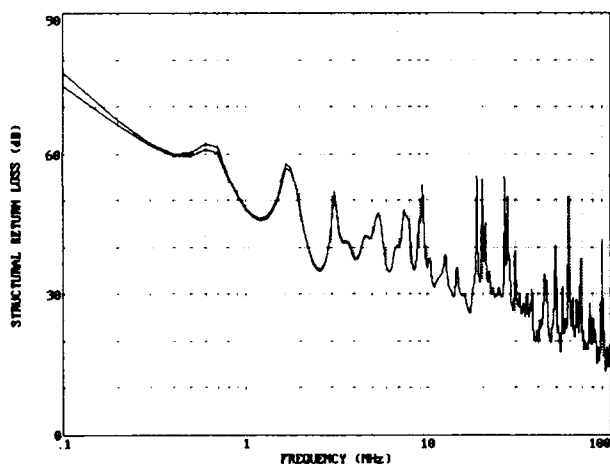


Fig. 7 SRL Computed from Single Reflection Equation

## 2.6 Near End Crosstalk Slope Analysis

Recognizing the similarity between Equations 4 and 5 is useful in that it allows us to borrow further from crosstalk analysis. We turn to Cravis and Crater<sup>7</sup> who in Appendix A of their BSTJ paper derive proof for the 15 dB/decade slope of infinite length near end crosstalk. Their derivation does not apply to individual combinations or the worst crosstalk among all combinations in a cable as a function of frequency, but rather the mean square crosstalk obtained for many crosstalk scans over a range of frequencies.

Several assumptions are important in their derivation. One is that the process represented by the coupling functions be what

is termed stationary in a statistical sense. This implies that all crosstalk observations being considered as data come from a time invariant process. It implies taking data on the very same type of combination from many cable samples. Considering data representing the universe of all combinations from one cable would not meet this condition since the different twist ratios and pair separations in a single cable would generally have inherently different levels of crosstalk performance associated with them.

Another important assumption in that derivation is that the coupling function  $U(x)$  of Equation 5 have a short correlation length. That means that points of coupling along the span of a combination of pairs separated by more than an electrically short length be uncorrelated. This condition is generally met by combinations of pairs made with different twist lengths properly chosen to avoid troublesome ratios but is not met by pairs with the same twist length. Like twists pairs can exhibit a coupling function  $U(x)$  substantially constant for considerable lengths of cable.

These conditions are ones that are probably representative of the structural variations found in well made cable pairs. We cable manufacturers, if we're doing our job, seek to eliminate processing problems which cause significant periodic variation because these are associated with very poor return loss regions at associated frequencies and excess transmission loss at those frequencies as well. The result of our efforts is that we end up with random variation whose amplitude depends on how inherently good the process and the design are. A parallel in the crosstalk arena is that we choose different twist lengths as much as possible to achieve nominally small coupling amplitudes. We know from experience that adjacent like twists are typically 20 dB worse than different twists so we separate like twists in the cable cross-section.

## 2.7 SRL Results for Actual Cables

Returning to actual cable data to examine SRL behavior, we consider a typical example from a medium grade data cable where the frequency range extends to 100 MHz. We start by examining a typical single return loss trace shown in Figure 8 knowing that it does not strictly decrease at the 15 dB/decade rate with frequency. Rather, it exhibits a frequency domain structure that is transform related to the way the structural deviation  $W(x)$  of Equation 4 varies. This example comes close to showing a 15 dB/decade reduction in SRL in the two decades extending from 1 MHz to 100 MHz. Much of the structure above 8 MHz conforms to the slope of the line added to Figure 8. The return loss is markedly less than the trend line at the low frequency end. This is largely the result of the network analyzer giving us return loss where input impedance is in effect being compared to the 100 Ohm resistor used in calibration. A calibrating network representing the actual through-the-cable characteristic impedance shape instead of a constant 100 Ohms would allow a better direct display rendition. There would still be the problem of the nominal pair impedance typically being different from that of the network by

REF LEVEL 0.000dB /DIV 5.000dB MARKER 3 152 278.000HZ MAG (UDF) -31.065dB

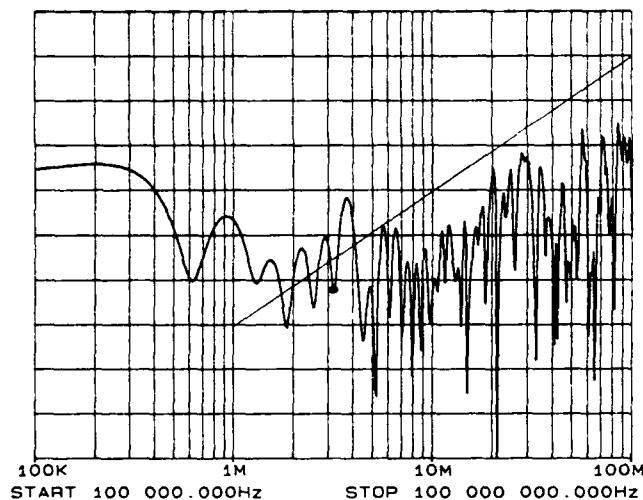


Fig. 8 Return Loss Trace Obtained Directly from Network Analyzer

several Ohms. Even so, this return loss trace comes close to displaying the 15 dB/decade trend with frequency that is a subject of interest here.

We turn now to processing  $s_{11}$  parameter data in a manner similar to what was done with the numerically simulated results shown in Figure 6 to obtain actual estimates of the SRL values. The computation procedure used in this case is that of fitting a characteristic impedance like function of frequency to the input impedance data, which is the data processing procedure described in Reference 1 that is most useful in this application. This procedure is used here to obtain values for both the magnitude and angle of the characteristic impedance as a function of frequency. With characteristic impedance values in

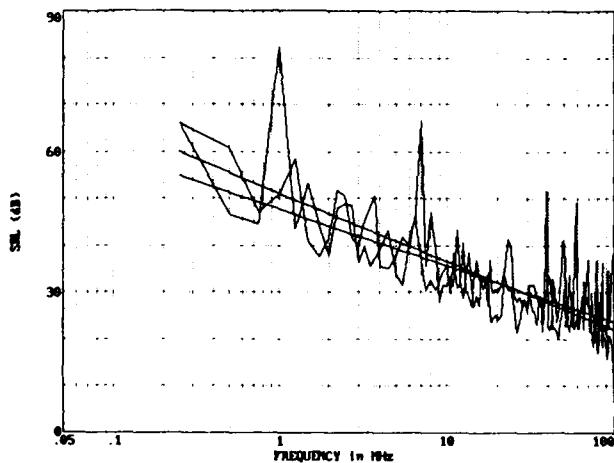


Fig. 9 Structural Return Loss Values Calculated for Input Impedance Data

hand Equation 3, where the impedances are complex quantities, is used to compute the SRL for the pair.

SRL traces obtained for the two ends of a 500 foot length of pair resulting from this procedure are shown in Figure 9. These traces exhibit the 15 dB/decade slope quite well if one lays a straight edge along the minimums. Least squares fitting a straight line to these traces yields two different slopes with the value of one being 12.0 and the other 14.6 dB/decade. This demonstrates that individual traces are fairly independent with regard to slope as well as structure. At the high end of the frequency scale each trace mainly represents the 100 ft. of cable closest to the end, since the round trip 100 MHz loss of a 100 ft. length of these pairs is about 12 dB.

The traces from the two ends of the pair in Figure 9 differ from each other just as cutting a few feet from a sample results in a substantially different trace. What is common to these two traces is the characteristic impedance deviation function  $W(x)$  of Equation 4 which can be computed from the SRL (magnitude) and the associated angle information. This computation, which may be of interest in a cable design evaluation, is discussed for near end crosstalk data in Reference 6.

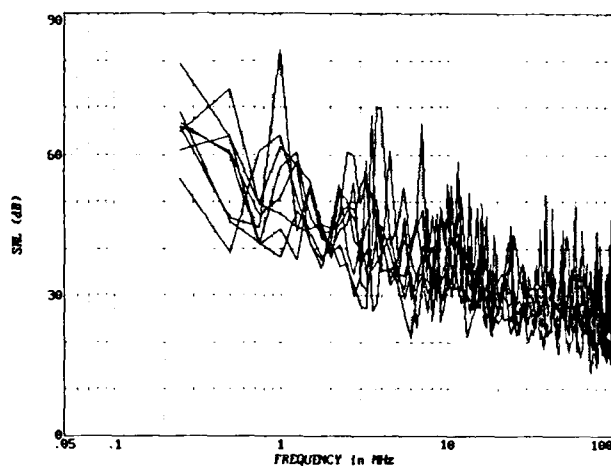


Fig. 10 Return Loss Values Calculated for Eight Traces from a Four Pair Cable

We continue our examination of impedance data by considering the eight traces obtained from both ends of a four pair cable. Figure 10 displays these on a common graticule. The eight traces all appear to exhibit the similar decreasing trends versus frequency. This set of traces collectively exhibits somewhat less than 15 dB of negative slope per decade, more like 13. The eight individual traces when fitted with a straight line exhibited minimum, average and maximum slopes of 11.1, 13.2 and 16.9 dB/decade respectively.

Figure 11 shows the rms result and straight lines fitted to the minimum, rms and average return loss values computed for the data shown in Figure 10. With only a few traces compared to the many combinations typically encountered in crosstalk data, the fitted lines along with one of the statistics being fitted are

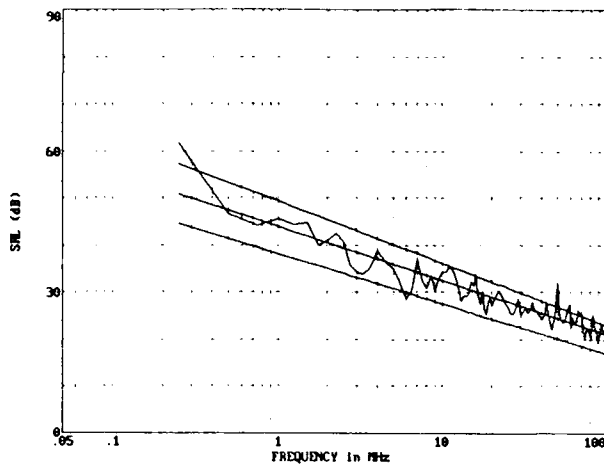


Fig. 11 Straight Lines Fitted to Average, RMS and Minimum SRL Values in Four Pair Cable

easier to view on this scale. We conclude that here, as is typical in crosstalk data, all three lines exhibit about the same slope. The average line has a little higher slope than the other two lines. The three slope values for minimum, rms and average are 10.6, 11.4 and 13.0 dB/decade respectively. While the derivation in Reference 7 only applies to the rms of near end crosstalk power it can be seen that here, as with crosstalk, the other measures exhibit similar slope values. Of the three sloping lines the minimum is bound to be the most volatile indicator with the rms and average being more reliable.

While this set of data exhibits close to the 15 dB/decade SRL slope, other examples may vary. All input impedance traces examined to date, most of which extend only to 25 MHz, exhibit the high frequency flair effect evident in Figure 1. SRL was computed for many of these data sets were found to have slopes in the 10 to 15 dB range. There probably are differences between the crosstalk and the reflection mechanisms. The coupling function  $U(x)$  of Equation 5 has strong high mechanical frequency structure going right up to the vicinity of the twist frequencies. The impedance deviation function  $W(x)$  of Equation 4 does not necessarily have those same mechanical frequency components. The auto correlation function for  $W(x)$ , while somewhat like an impulse function of mechanical frequency, is probably wider than what is encountered in crosstalk. While a cable with low SRL slope would be in our favor when we think of extending transmission to higher bit rates, we probably need to recognize that 15 dB/decade slopes can occur. The alternative to a lower slope is moving the whole SRL curve to a higher level of performance to the extent that this is possible.

## 2.8 On the Need for SRL or Input Impedance Limits that Recognize Frequency Dependence of the Media

Much of the standards work with regard to the permitted characteristic impedance ranges has resulted in two parallel horizontal lines for the upper and lower limits extending from

1 MHz to the upper frequency limit covered by the specification. These limits extend upward with decrease in frequency as indicated in Figure 12 for frequencies less than 1 MHz to accommodate the higher impedances in this frequency range. The concept of parallel limits possibly applying to input impedance for frequencies above 1 MHz goes back to the 150 Ohm IBM™ Type 1 LAN cable design<sup>8</sup>. For that design input impedance could be interpreted as characteristic impedance with only a few Ohms error resulting, for frequencies up through those applicable for 16 Mbit/s Token Ring, because of the inherent electrical smoothness of the shielded balanced pair design. Closer examination of Type 1 pairs (Reference 1 shows an input impedance trace going to 25 MHz) shows that input impedance variation increases and consequently SRL decreases with increase in frequency for these pairs as well.

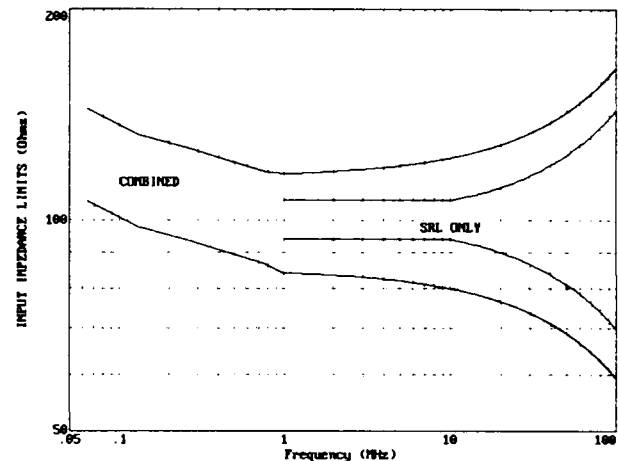


Fig. 12 Input Impedance Limits Allowing for Both Characteristic Impedance Variation and Structural Effects

A favored viewpoint concerning parallel, horizontal impedance limits, such as those in the EIA/TIA 568 specification where the permitted range for 1 MHz through 16 MHz is 100 Ohms  $\pm 15\%$ , is that they need to apply to the characteristic impedance (not the input impedance). One of the purposes of this part of this paper has been to demonstrate that SRL of UTP degrades at rates up to 15 dB per decade. An input impedance standard applying to both the characteristic impedance and structural effects is workable but needs to accommodate the structural frequency dependence demonstrated in this work. Most cable manufacturers and users today recognize that near end crosstalk degrades with frequency in a fairly predictable manner. We also need to recognize that input impedance varies more as frequency increases.

For SRL the limits might take a two segment approach with a flat portion at low frequencies and a negative 15 dB/decade slope for high frequencies. The level of the flat region and the corner frequency should be set at a level appropriate for the level of data cable performance being addressed. Equivalent input impedance limits are represented by the "SRL only" curves in Figure 12 shifted upward so as to be centered around

100 Ohms. The corresponding SRL is flat at 30 dB up to a 10 MHz corner frequency. Input impedance limits addressing structural effects and making an allowance for characteristic impedance variation would be separated further to represent the combined effects. The upper and lower limits shown here trace the EIA/TIA horizontal limits up to the point where the flair sets in. The transition to the flair occurs at 1 MHz in this case. The  $100 \pm 15\%$  limits are operated on by the "SRL only" limits in a multiplicative manner with the flair shape assumed throughout the two decades. These limits, which are intended to be illustrative at this point, appear to be consistent with input impedance data for products associated with Level 4 of the Anixter Twisted Pair Level Program.

### III. Excess Loss in Twisted Pair Insertion Loss

#### 3.1 Loss Computed from Difference Equation Model

The analytical evaluation of structural variation includes expressions for the effects on attenuation through the pair. A second reflection redirecting some of the energy headed back to the transmit end to the intended receiver plays a role with regard to the effect on attenuation. The difference equations stated earlier can be used to evaluate the transfer function  $s_{21}$  for the lumped element line in a manner similar to that for input impedance. The evaluating procedure is straight forward for arbitrary impedance deviation functions. Two examples, one for the periodic case where the structural variation is sinusoidal and the other for random variation, are considered here. The periodic result is calculated for sinusoidal deviation with a 1 Ohm peak (2 Ohms peak-to-peak) excursion and a 5.3 foot (60 MHz) period. The result shown in Figure 13 is for a 500 foot length of 24 gauge pair where only the center 250 feet of the 500 foot length has sinusoidal variation. Both the loss for the rough pair as indicated and for a smooth pair with the same average characteristics are plotted. The difference between the two traces which indicates the excess loss is shown

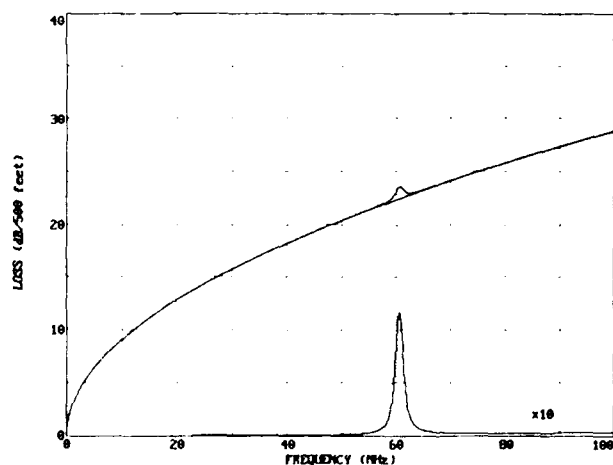


Fig. 13 Calculated Loss Response Resulting from Periodic Variation

at the bottom of the graticule with x10 magnification. The difference trace shows strong excess loss only in the narrow band of frequencies which corresponds to the round trip time of the periodicity. Here the calculated pair loss peaks at just over 1 dB over what shows on either side of the 60 MHz peak.

The nature of the excess loss region for a truly periodic structure is that it peaks at a frequency that is consistent with the period of the variation. Many cycles of the periodicity (47 in this example) are present, giving the response some sharpness. If periodic variation had been present for the whole 500 ft. length the peak would have exhibited twice as much amplitude. If the peak amplitude of the variation had been 2 Ohms instead of 1 Ohm the excess loss would have been four times ( $2^2$ ) as large. This example shows that a small but periodic 2 Ohm peak-to-peak variation over only half of the length can result in just over 1 dB of excess loss. A dB of excess loss (20 dB S/N when the only interference is excess loss) is a frequently used tolerance level relative to the total loss for the system length, in a system where equalization may have been carried out to a fraction of a dB and other interference such as crosstalk does not have to be provided for. This example just fails the one dB rule of thumb.

This periodic example was chosen with only the center 250 ft. of the 500 ft. length being permitted to vary, to illustrate that the excess loss approach to finding a periodic structure works when single ended measurements do not. With the periodic variation being only 125 ft. in from either end the SRL was at the 23 dB level. It would have been masked in moderate random variation such as that exhibited in Figure 6. Had the periodicity been at the measurement end the SRL exhibited would have been prominent at about 8 dB. This example demonstrates that the excess loss approach is capable of detecting a periodicity present only in midspan which would probably go undetected with single ended measurements when moderate random variation is present.

Cable length plays a role in through-the-cable measurements. Measurements should be made on lengths representative of the intended application. The examples in this section are based on 500 ft. This round number length is about half way between one pass through the 100 meter maximum horizontal run found in most building wiring, and two passes through a 100 meter run as found in ring architecture with passive concentrators. This length very likely will not allow 100 MHz bi-directional capability when near end crosstalk is a consideration.

The effect is different when random variation is present. Only moderate peaking occurs. Figure 14 shows a loss trace for the same random sequence  $W(x)$  first considered in Figure 4 where the peak deviation was 4 Ohms. As in Figure 13 we have calculated the loss for a rough transmission line, a smooth line representation placed next to it, and the x10 expanded difference plot showing at the bottom of the graticule. This set of loss traces shows some added loss due to roughness. No single loss peak stands out above the others. The peak excess loss just exceeds 1 dB but our 1 dB rule of thumb doesn't apply to the peak excess loss calculated for this simulation example.

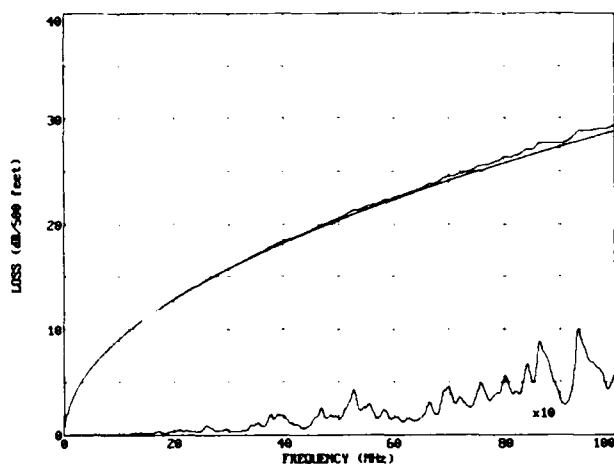


Fig. 14 Calculated Excess Loss Resulting from Random Structural Variation

Rather it applies to the peak-to-peak variation which is about .7 dB in the 90 MHz range for this 500 foot example; so this pair passes. Typically, the difference between adjacent excess loss maxima and minima is about half of the peak excess loss in calculated examples such as this one. Much of the excess loss builds systematically with frequency.

### 3.2 Analytic Expression for Rough Line Transmission Loss

- Frequency dependence of random excess loss can be explored by considering Equation 6 which results when a second reflection is taken into account. In this case a double integration is indicated whereas Equation 4 only involved a single

$$s_{21} = e^{-\gamma(\omega)l} \left[ 1 - \frac{\gamma(\omega)^2}{Z_0(\omega)^2} \int_0^l W(x) e^{2\gamma(\omega)x} \int_x^l W(y) e^{-2\gamma(\omega)y} dy dx \right] \quad (6)$$

integration. A possible cause for concern is that this equation contains  $\gamma^2$  (indicating  $f^2$  behavior) where Equation 4 only shows  $\gamma$  to the first power. How fast the loss builds with frequency can be better seen for the example at hand by replotting the traces shown in Figure 14 using logarithmic scaling for both axes. Figure 15 shows the results. The excess loss calculated from the difference equations shows frequency squared dependence in the 10 to 100 MHz range for this example. Several runs made with different  $W(x)$  sequences indicate this example has about the highest slope observed thus far. The several examples that were examined were found to have frequency dependence in  $f^{1.5}$  to  $f^2$  range. The smooth and rough loss traces showing  $f^5$  dependence are included in this figure as well. They practically overlay on this 4 decade logarithmic scale.

It appears in Figures 14 and 15 that much of the excess loss due to random roughness can masquerade as dielectric loss but may have a stronger frequency dependence than the first power of frequency rate associated with dielectric loss. A functional

fit for the excess loss trace as shown in Figure 15 can be approximated readily. Using the more significant 10 to 100 MHz portion of the frequency range results in a  $0.00007 \times f^2$  (frequency in MHz) fit, keeping in mind that the excess loss trace in these two figures has been expanded by a factor of ten (moved up a decade in Figure 15). This means the constantly increasing portion of the excess loss is only 0.007 dB at 10 MHz and is about 0.7 dB at 100 MHz for this numerical example which is for a fairly smooth pair. Peak loss deviations at the high frequency end appear to be about 0.35 dB. The vertical range of the excess loss variation on the log scaled plot is about the same in all regions of this frequency range. This means the ratio of maximum to minimum excess loss variation is constant (about 2 to 1) over this range.

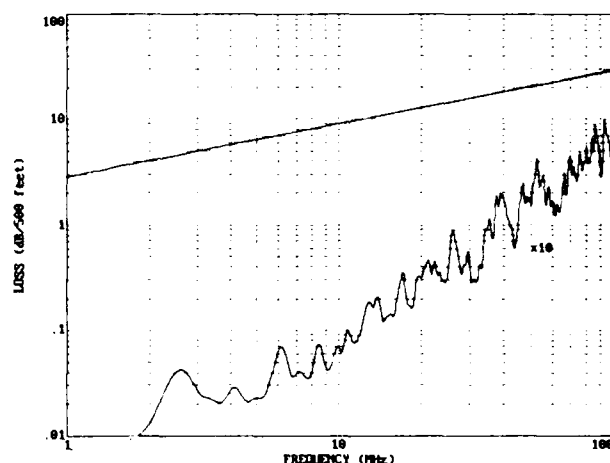


Fig. 15 Calculated Excess Loss Replotted using Logarithmic Scaling

Summarizing what we see in the calculated excess loss example obtained from the difference equations, is that while the quality twisted pair designs may feature materials resulting in negligible dielectric loss, when sufficient random roughness is present, what appears to resemble dielectric loss accompanied by some roughness, can be present. We find that the excess loss consists of two parts, a constantly increasing component which appears to increase at a rate faster than frequency (perhaps as fast as frequency squared) and the varying part which has a fairly constant maximum to minimum ratio over this frequency range. The added loss represented by a constantly increasing component, although not desirable, does not prevent product like this from transmitting at high bit rates provided that the total loss objective is met. The peak-to-peak amplitude of the varying component is of concern if too large. This study appears to indicate that the loss behavior is departing some from  $\sqrt{T}$  loss behavior when a dielectric material with a low dissipation factor is assumed, as was the case in this simulation. A final point is that random excess loss can be fairly modest when SRL appears rather poor. This example which is based on modelling has a 100 MHz SRL of about 14 dB.

### 3.3 Fitting a Loss Function to Cable Pair Loss Data to Evaluate Roughness

Figure 16 takes us back to actual cable loss data seeking to relate it to the difference equation results in Figure 14 where the impedance deviation function  $W(x)$  was allowed to vary in

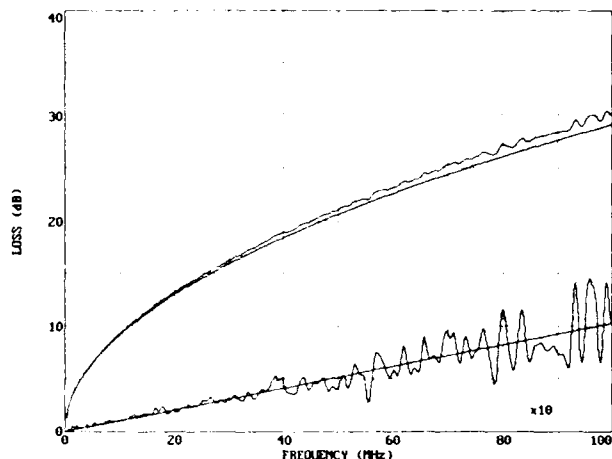


Fig. 16 401 Loss Data Points with Least Squares Function Fit

a random manner. Both the actual data and the calculated results show variation increasing with frequency. In both cases most of the loss is copper loss represented by the smooth trace just below the rough trace. The dissipation factor for the pair represented by Figure 16 is low so the difference between the total loss and the copper loss is thought to be due mostly to roughness. The structure of the added loss due to roughness in Figure 16 is also similar to the simulated result shown in Figure 14 in that it consists of both a varying component and a constantly increasing with frequency component where the varying component is of greatest concern. The maximum variation showing in the  $\times 10$  difference trace is .8 dB in the above 90 MHz frequency range, so this pair passes the 1 dB roughness rule of thumb. This pair was also found to have quite good SRL with values at 10 MHz being in the just above 30 dB range.

$$\text{Loss} = K_1\sqrt{f} + K_2f \quad (7)$$

The smooth line fitted to the difference trace indicates a good fit. The  $K_1$  and  $K_2$  coefficients for the fit to the loss data were found to be 2.91 and .010 for this 500 foot length of 24 gauge cable pair where frequency is in MHz. Equation 7 is one of a family of loss equations that might be fitted to loss data. Other forms of the loss equation might include higher frequency components such as  $f^{1.5}$  or  $f^2$ . Experience dictates that simpler equations which are closely tied to theoretical performance are often best. Goodness of fit criteria is usually based on the root of the mean square of the deviations. This criterion is mainly quantifying the roughness in this application. The example considered here was found to have a lack of fit rms of 0.13 dB

when fitted with Equation 7 over this frequency range. The concept of fitting a loss equation to loss data for purposes of detecting excess loss variation is not limited to random kinds of variation. Excess loss due to periodic variation can readily be quantified via this procedure by scanning the loss deviations for peak values.

The copper loss for the data in Figure 16 was computed by two methods. The first method consists of using the value obtained for  $K_1$  in Equation 7 to calculate the copper loss. A second approach involves obtaining the copper loss from data for the phase constant  $\beta$ . Equation 8 is an expression showing  $\beta$  as a

$$\beta = \omega\sqrt{L_e C} + \frac{\omega L_i}{2} \sqrt{\frac{C}{L_e}} \quad (8)$$

function of radian frequency  $\omega$ , the internal and external inductance ( $L_i$  and  $L_e$ ) and capacitance  $C$ . The internal reactance  $\omega L_i$  actually increases as  $f^{1.5}$  because of internal inductance decreasing with frequency. This reactance is equal to the a.c. resistance of the pair, which means that the second term of Equation 8 represents the copper loss (in nepers) of the pair. The copper loss coefficient obtained via the phase data agreed with that obtained from the loss data to within a fraction of a percent lending credence to the data fitting procedures.

### 3.4 Correlating Excess Loss Variation with SRL Results

Comparing results obtained from through-the-cable measurements with those obtained from single-ended measurements is of interest at this point. Measurements of both types have been made for several cables for the range of frequencies extending from .1 MHz to 100 MHz. The single ended measurements started with S-parameter data processed to obtain the SRL as indicated in Section 2.6. Straight line least squares fits such as those shown in Figure 9 were obtained for pairs from several cables. The coefficients for the fits appear in Table I as the 1 MHz SRL and SLOPE values. The values for 10 MHz were calculated from the fit coefficients. The values in the RMS LOSS column were values obtained when loss data for these pairs was fitted with Equation 7.

Table I contains results for two four pair cables with SRL values obtained from both ends. The first eight rows of values are for cable A, the next 8 rows for cable B, and the last row is for the example calculated from the difference equations. The SRL values do not represent worst values for the individual traces but rather an average as indicated in Figure 9. Similarly the RMS loss deviation values do not represent the peak deviation but rather the rms deviation from the fitted function where deviations increase with frequency. This table shows that individual slope values vary considerably from -7.4 to -15.3 dB/decade which is consistent with results in Section 2.7.

Table I: Comparison of SRL and Excessive Loss Variation

PAIR	1 MHz SRL	SLOPE	10 MHz SRL	RMS LOSS DEVIATION
1-A	38.1	-15.3	22.8	.349
1-A	36.2	-12.6	23.6	.349
2-A	43.5	-9.7	33.8	.236
2-A	44.4	-13.2	31.3	.236
3-A	44.1	-12.2	31.8	.284
3-A	46.4	-12.8	33.5	.284
4-A	38.5	-12.6	25.9	.381
4-A	37.4	-13.2	24.1	.381
1-B	46.6	-11.8	34.8	.137
1-B	49.2	-13.0	36.3	.137
2-B	41.3	-7.4	34.0	.130
2-B	48.3	-13.4	34.9	.130
3-B	38.8	-8.0	30.8	.210
3-B	41.0	-11.2	29.8	.210
4-B	48.9	-11.1	37.8	.190
4-B	48.0	-11.7	36.3	.190
1-C	50.0	-13.8	36.2	.118

Figure 17 plots the fitted SRL values against the loss fit rms deviation values. The two cables are represented by the A and B symbols and the example calculated by means of the difference equations by symbol C. The scatter plot shows that high and low SRL values can be associated with small and large loss fit rms deviation values respectively. The two cables can readily be distinguished as being of different quality. The best A cable pairs come close to being like the B cable pairs. There appears to be continuity between the two sets of data. The calculated result fits in well and is in the "better than" good

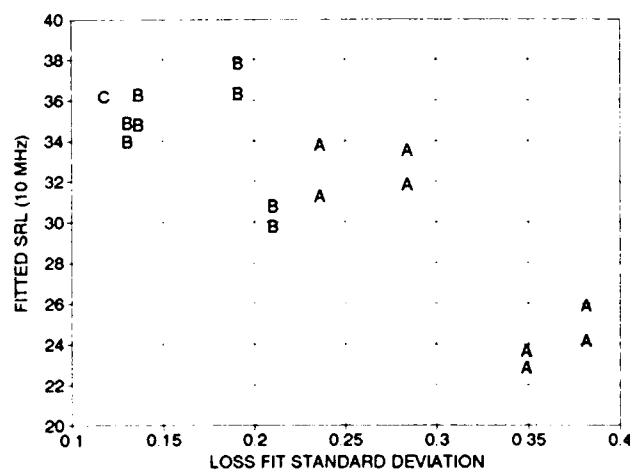


Fig. 17 SRL Results and Loss Fit RMS Deviation Scatter Plot

cable region. Differences between the SRL values obtained from the two ends of any given pair are as high as 3 dB indicating that single-ended measurements are sensitive to the measurement end section of the cable being measured.

#### IV. Conclusion

This document is a sequel to the one presented a year ago which dealt with the measurement and data processing required to obtain reliable characteristic impedance results. The need for evaluating structural effects was recognized in the first paper. In this paper the single-ended measurements for structural effects were discussed first. It was pointed out that simply using a network analyzer to measure the  $s_{11}$  parameter may not be adequate. Processing of the data can yield better information for determining acceptance or rejection of product.

In the case of single ended measurements it was demonstrated that one can start with S-parameter data, proceed with computing the characteristic impedance, and then compute either the SRL or impedance variation about the characteristic impedance. The SRL plot has an advantage over the input impedance plot approach because it exhibits a trace which can be fitted with a straight line on a dB versus log frequency graticule. Input impedance deviation plots yield results which typically flair open on the high frequency end.

Present day impedance standards with the parallel limits should apply only to the smooth impedance. A considerable portion of a 20 to 30 Ohm range is required for pairs with different twist lengths and to accommodate  $Z_0$  decrease with frequency in this range. Structural effects add to the other variation requiring additional allowance at the high frequency end.

Recognizing that twisted pairs typically exhibit random structural variation with length and that a given amount of this type of structural variation is not nearly as damaging as the same amount of periodic variation leads to the concept of using excess loss variation as a criterion for cable acceptance testing. For randomly varying structures the excess loss consists of a smooth with frequency component and a component that varies. Only the amount of variation is of concern if the total loss objectives are being met. This method of testing which looks for departures from a smooth swept frequency loss trace, readily intercepts structural effects which are of a periodic nature. The results for two cables differing in quality as discussed in the previous section show that SRL and excess loss variation correlate well.

There are advantages and disadvantages to both method for measuring structural effects. Advantages for single-ended measurements are that the  $s_{11}$  data may be taken anyway if it is needed to determine the characteristic impedance. SRL results exhibit frequency scaling that is fairly consistent allowing a straight line function to be fitted readily. If the evaluation proceeds no further than input impedance, then a combined specification making allowance for both the characteristic impedance variation about a nominal design value and

structural variation can possibly be used. A disadvantage for the single-ended measurements is that, with interest in frequencies up to 100 MHz, we are dealing with a measurement technique that evaluates a rather short sample at the high end where 12 dB round trip attenuation corresponds to a cable length of only 100 feet or less. Even taking data from both ends only evaluates several hundred feet out of a shipping length typically 1000 ft. long or longer. Another disadvantage is that measurement technique is more demanding for single-ended measurements. The end effects at the point of measurement are severe if the fanned out region is not kept to a few inches. The high impedance of the exposed portion of the pair affects the observations made on the intact portion. Lastly, single-ended measurements other than a low frequency capacitance value may not be needed at all if the delay-capacitance method is used to obtain characteristic impedance and loss measurements can be used to determine structural effects.

High on the list of advantages for through-the-cable measurements is the idea that the whole length receives equal emphasis. The effects for the length are integrated into a total effect. An important advantage is that periodic variation in the center of the section is more likely to be detected. Through-the-cable results are more akin to what is of most interest, transmission from point A to point B. Another advantage is that loss measurements are sure to be on the list of measurements being done anyway. A scan of loss data extending over the desired frequency range can be taken with little more effort than that involved for a few discrete frequencies. A computer can readily process the data to determine the level of excess loss variation using fairly basic loss functions. A disadvantage for the through-the-cable approach is that while 500 ft. lengths can readily be measured at frequencies up to 100 MHz, even a 1000 ft. length of 24 gauge 100 Ohm pair can have 100 MHz loss in excess of 60 dB. Crosstalk in the measurement equipment may have to be guarded against. Measurements on cable lengths shorter than those being shipped or curtailment of the frequency range may be necessary if interference is too severe.

Ancillary results that were demonstrated included showing that, as in near end crosstalk, the single reflection equation (single point of coupling in crosstalk) and results obtained from using the difference equations agree well. Another result was that SRL degrades by as much as 15 dB/decade when the structure varies in a random manner. Showing that structural return loss degrades at a considerable rate with frequency led to proposing an input impedance limit form that widens with increasing frequency. Simulation was used to show that excess loss due to roughness consists of two components. One appears to increase continuously with frequency with a slope somewhere in the 20 to 40 dB/decade range (direct observations of this component are often obscured by dielectric loss in actual cable data). This component of excess loss is tolerable provided that the overall loss objectives are being met. The other exhibits variation with frequency increasing at a minimum of 20 dB/decade based on actual data. This is the component of random structure excess loss found to be troublesome if the fluctuations are severe enough.

## References

1. Friesen, H. W., "An Improved Characteristic Measurement Technique", 39th International Wire & Cable Symposium Proceedings, 1990, pp 608-617.
2. Windeler, A. S., "Design of Polyethylene Insulated Multipair Telephone Cables", Bell Telephone System Technical Publications, Monograph 3574, 1960.
3. Karbowiak, A. E., "Investigation of Signal Distortion in Cables Caused by Imperfections in Cable Manufacture", Proc. IEE, Vol 121, No. 6, June 1971.
4. Bolinder, F., "Fourier Transforms in the Theory of Inhomogeneous Transmission Lines", Transactions of the Royal Institute of Technology, Stockholm, Sweden, No. 48, 1951.
5. Campbell, G. A., "Dr. G. A. Campbell's Memoranda of 1907 and 1912", BSTJ, Vol.14, October, 1935, pp. 558-572.
6. Friesen, H. W., "Experimental Verification of Near End Crosstalk Equation for Balanced Telephone Cable Pairs", National Communication Conference 73 Proceedings, Nov., 1973, pp. 8C-1 to 8C-11.
7. Cravis, H. and Crater, T. V., "Engineering of T1 Repeated Lines", BSTJ, Vol. 42, March, 1963, pp 431-486.
8. Abramson, P., "Design of a Twisted Pair Cable for a Token Passing Local Area Network", 32nd International Wire & Cable Symposium Proceedings, 1983, pp 268-270.



HAROLD W. FRIESEN  
AT&T Bell Laboratories  
Norcross, GA

Harold W. Friesen is a Distinguished Member of Technical Staff at AT&T Bell Laboratories. He has been a part of the Transmission Media Laboratory since 1963. He received a BSEE degree from the University of Colorado in 1963 and a MEE degree from New York University in 1965. Hal has been involved in cable design, the development of fabrication methods and cable measurement techniques. He holds four patents in this area. He is a member of the IEEE.



## Development of Electronic Wire Harness for Mainframe (PTS Cable)

T. Yamamoto, S. Ashida, T. Hirahara, K. Ueda, H. Zako, Y. Nakagawa

— Fujikura Ltd.

### Abstract

Electronic Wire Harness for major computer wiring system (PTS-Cable ; called by a customer) has been developed by new application of fine conductor cable with FEP material, high density shielded connector and card connector with built-in printed circuit board (PCB). In order to get very high quality and reliability with many characteristics, we have developed new connection system including the above mentioned cable and connectors, and the connecting methods between them. In this, it has been certified that newly developed crimping methods for solid conductor will be very effective for connection of fine sized conductor with high-productibility and high-reliability.

We have manufactured many products and have made various severe tests including reliability test. After the statistical evaluation, it has been certified that PTS-Cable has excellent quality and high reliability and will be very available for major computer wiring system.

### 1. INTRODUCTION

Electronic wire harness has been applied extensively to connect electronic devices and their inner wiring system.

In them, the electronic wire harness for computer wiring system has to satisfy various requirements in order to be applied to such transmission lines as equal to other important component parts of electronic devices. Recently, along with this trend the demands of smaller size, higher density and higher transmission speed for electronic wiring harness are rapidly increasing. Therefore, it is desired to develop proper cables, termination components and connecting methods that satisfy the above requirements and realize cost reduction also.

To get these requirements, it has to be investigated the following items. At first, the cable should be fine and should be required excellent mechanical and electrical characteristics. Fluororesin like FEP has been used to get very thin insulation thickness and high insulation resistance. At the second, for terminated parts as

connector and connecting method, it is needed to develop the fine and compact size of connector, high reliability of connection method.

In this paper, it is reported that we have developed new connecting system including new cable and new connectors, and the connecting method between them. For the purpose to evaluate, we have manufactured many products and have made various tests including reliability qualification. As results, it is verified that the newly developed electronic wire harness has excellent quality and high reliability for a computer wiring system.

### 2. CONCEPT FOR PTS-CABLE

PTS-Cable is required the excellent electrical, mechanical properties and high reliability which is to achieve the zero defect over an operating life of 100,000 hrs. The requirements and specification of it and the developed contents are shown as follows.

#### 2.1 Requirements

In case of application to the signal transmission line, it is afraid to occur exothermic phenomena caused by cycling current application as power on-off, and rounding pulse wave of signal caused by vibration during operating term. Therefore, it is very important to investigate them and develop a new termination method for a solid conductor and a new connector and their good connecting condition to get high reliability.

On the other side, it is needed to examine that suitable material and construction against mechanical force to prevent the abrasion of contact due to insertion or withdrawal of connectors and the breaking of conductor caused by flexing at a strain relief portion.

To certify the performance for new application, initial peculiar tests and reliability tests based on operating and non-operating service conditions in the

practical applied environments has been made.

## 2.2 Specification

The external appearance of PTS-Cable is shown in Figure 1.

### 2.2.1 Cable

This cable has a solid conductor, AWG 30 and silver plated oxygen free copper. For insulation and outer jacket material fluoro-ethylene propylene is used. It has high strength against mechanical force, low dielectric constant and high electrical transmission characteristics. The cable is composed by two insulated conductors, aluminum mylar tape with a drain wire for shield.

The major feature of this cable is to reduce its diameter.

### 2.2.2 High density shielded connector

On condition to mate to the existing mount header connector on printed circuit board of the mainframe, the new connectors have been developed. The new connectors consist of 10, 26 and 44 contacts plugs and 26, 44 contacts headers. The contacts are arranged in two rows in each connector, and the adjacent distance between contacts (pitch) is 2.54 mm (0.1inch). A aluminum die cast is used for connector covers which has sufficient stiffness to get the mechanical property and has the good shielding property also.

On the other hand, for connection of solid conductors and contacts, the new crimping method has been developed.

### 2.2.3 Card connector with printed circuit board

This connector consist of a glass epoxy printed circuit board and two plastic

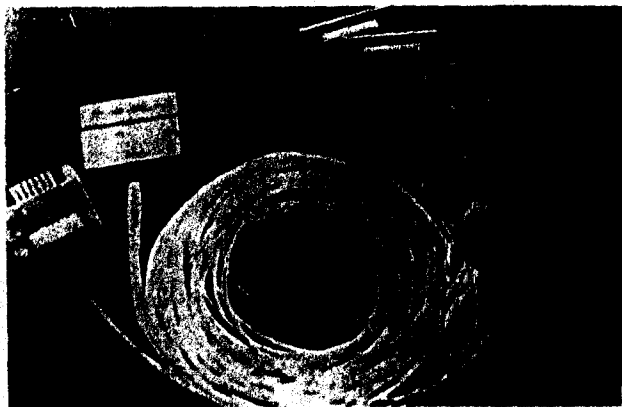


Figure 1. PTS-Cable

covers. This connector is very thin and available to put into spring contact equipped boards, and has a life of 50 times insertion. Individual conductor is bonded to the gold-plated contact of the printed circuit by multi-conductors soldering method using solder pad and heating machine. The soldered assembly is partially enclosed with two plastic covers which are bonded ultrasonically each other. Clear hot melt is served to the exposed area which is available for visual check the condition of connection.

## 3. Developments of main parts and assembling procedure

### 3.1 Development of crimping method for solid conductor

Generally, the connecting methods are considered as follows. 1) Soldering method, 2) Insulation displacement connection method, and 3) crimping method. In case of solid conductor, For 1), it is difficult to connect and to ensure reliability as conductor size is so fine. For 2), it is difficult to make parallel arrangement of insulated conductors for mass-termination due to FEP insulation, and to get contact reliability for solid conductor. Therefore, we have adopted the crimping methods. It is easy to get high reliability, high productibility and cost reduction also.

#### 3.1.1 Construction

Crimping appearance and its cross section are shown in Figure 2 and 3. Contact is made with Be-Cu, and has nickel underplate and gold overplate. For conductor barrel, we have developed double leaves holding of a conductor without gnawing. Good results are shown in Figure 3.

#### 3.1.2 Reliability test

Crimping resistance between the crimped contact and conductor was measured at the initial and after the following test.

The measured values after test were compared with the initial values.

##### 3.1.2.1 Flexing test

Crimped contacts must be capable of being flexed  $30 \pm 10$  degrees in an angle once each to left, to right, up, and down.

##### 3.1.2.2 Thermal shock test

Crimped contact were subjected to thermal shock as plus 89 degree C 18 hours and minus 15 degree C 30 minutes.

##### 3.1.2.3 Vibration test

Contacts to 20 minutes of broad-band

random vibration.

The conditions of vibration are 0.02, 0.2, 0.2 and 0.02 grams squared per Hz for loads at 10, 40, 250 and 300 Hz for frequencies, respectively. All frequencies should be applied simultaneously.

#### 3.1.2.4 Accelerated aging test

Contacts are subjected to five cycles of the 24 hours test. For step 1, 4 hours at 25 degree C and 60% relative humidity and 2 hours maximum transition time to step 2. For step 2, 4 hours at 75 degree C and 90 to 95% relative humidity and 1 hour maximum transition time to step 3. For step 3, 11 hours at 75 degree C and 40% relative humidity and 2 hours maximum transition time to step 1. Figure 4 shows crimping resistance test results after each test increased a little. But the increasing satisfied sufficiently the required value to be less than 1.71 m-ohm.

From the result of these tests, it is confirmed that this crimping method for solid conductor is very effective.

#### 3.2 Development of high density shielded connector

The new connectors consist of plug type and header type with thin shielding covers of aluminum die cast. It is designed to meet the electromagnetic interference prevention requirements specified in FCC standard. Figure 5 shows the construction of these connectors. The housing has the resilient lances. Thereby it enables the contacts to be easily inserted by low insertion force and to be held securely also. The header type connector is the plug type connector with grounding covers and locking levers

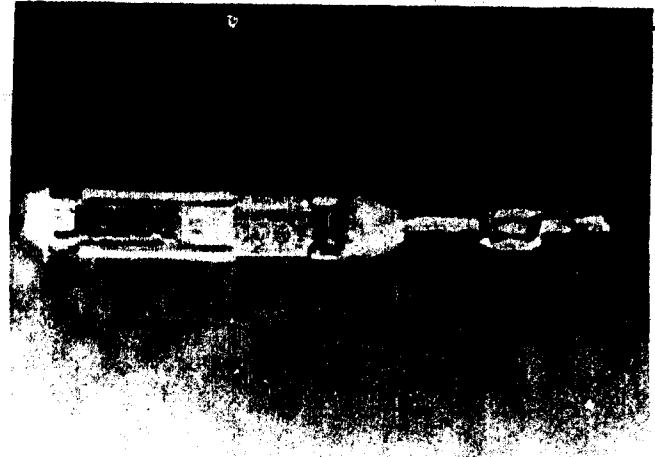


Figure 2. Crimping of solid conductor

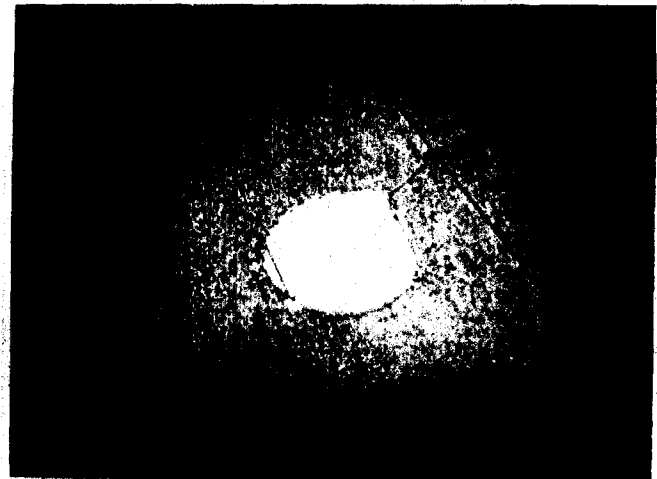
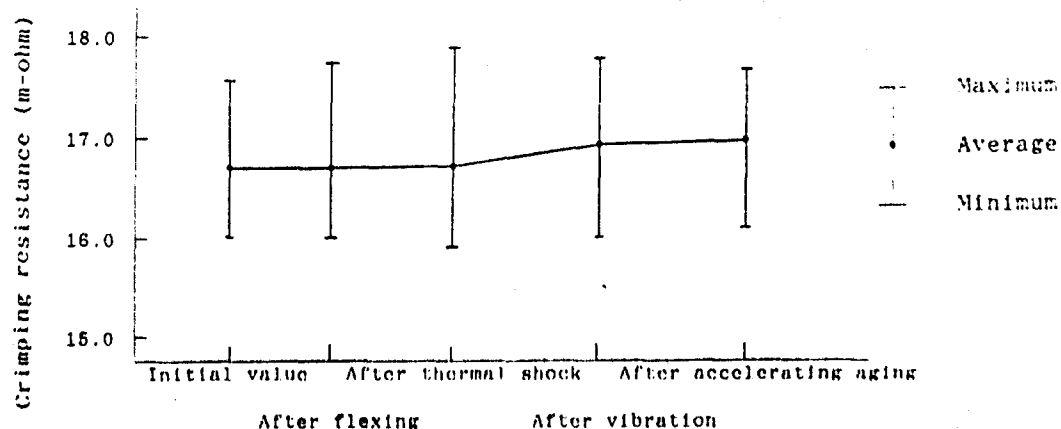


Figure 3. Crimping cross section



Change in crimping resistance

Items	(Unit : m-ohm)				
	Initial	Flexing	Thermal shock	Vibration	Accelerating aging
Average	16.72	0.07	0.17	0.30	0.36
X ± 5.48 S	-	0.20	0.66	0.80	1.07

Figure 4. Results of environment tests crimping

additionally. When the plug connector is inserted to header connector, they are securely connected by two locking levers. The grounding covers of the header connector make a grounding circuit link between the plug and the header. The test methods and results are shown in Table 1. As results, it is confirmed to put a thing to practical use.

### 3.3 Multi-conductors soldering method for card connector

Figure 6 shows the construction of card connector. An applied printed circuit board is made with glass epoxy with 0.2mm thickness and its printed lines are made with copper with 35 micron m. On contact surface, hard gold and soft gold with 5 micron m of

total thickness are plated. For the termination method between a printed circuit and solid conductors of cables, the multi-conductors soldering method is adopted shown in Figure 7. The conductors are arranged on the contacts served with solder pad previously over them of the printed circuit board and soldered by the heating machine at the same time. The feature of this method is that it could realize good soldering condition and high reliability, and could reduce assembly cost as the soldering condition can be easily controlled and it was very speedy. In addition, we have developed an arranging tool of conductors over the board in the fixed pitch of 1.83 mm between each adjacent conductor shown in Figure 8.

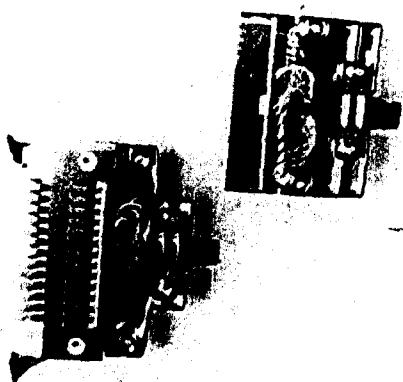


Figure 5. Construction of high density shielded connector

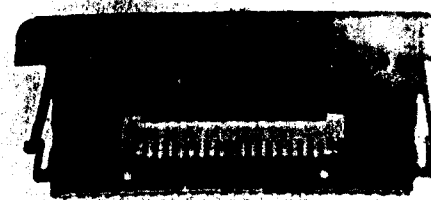


Figure 6. Card connector

Table 1. Test items and results of high density shielded connector

Test item	Requirements	Results (X - KS)	Sample size ( n )
Cable flexing	X - 4.7 S > 10 cycles	12.1	47
Cable retension	X - 2.5 S > 0.9 Kg	1.35	226
Connector retension	Along cable axis X - 4.0 S > 9 Kg	41.6	6
	Radially around cable X - 4.0 S > 4.5 Kg	39.3	6
Incompatibly keyed strength	X - 4.0 S > 10 Kg	23.2	6
Header latch strength	X - 4.0 S > 5.4 Kg	6.87	6
Contact retension after thermal shock test	X - 3.0 S > 0.27 Kg	1.24	20
Initial withdrawal force of contact after thermal shock test	X - 2.7 S > 28.0 g	89	55
Withdrawal force after thermal shock test and 25 times insertions	X - 2.7 S > 25.0 g	70	55

X : Average value

#### 4. Reliability tests

It is important to evaluate the reliability of the developed products. The following is test methods and results based on statistical evaluation.

##### 4.1 Current/thermal cycling test

To confirm the effect to crimping point and contact area caused by exothermic phenomena. To subject the test specimens to the condition, 3000 on/off cycles at intervals of 12 minutes on and 12 minutes off, with a current of 1 mA. Any change (dR) in contact resistance of the crimping point is determined during or after this test. The results are shown in Table 2. As results, dR is less than 10 m-ohm, confirmed to the good condition.

##### 4.2 Temperature/humidity Test

To confirm the corrosion of metal portion such as contacts and shielding covers, and the effect of change of contact resistance. Cable terminated connectors are subjected to

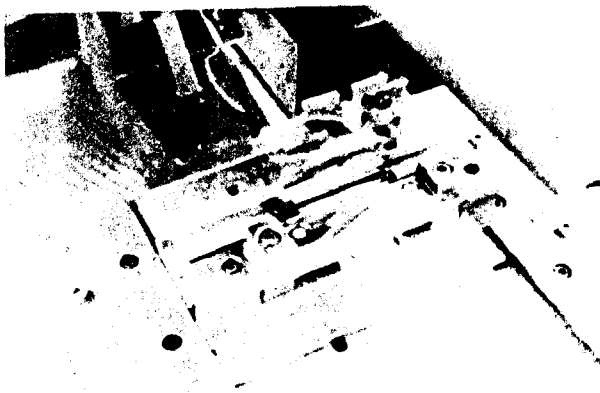


Figure 7. Multi-conductor soldering method

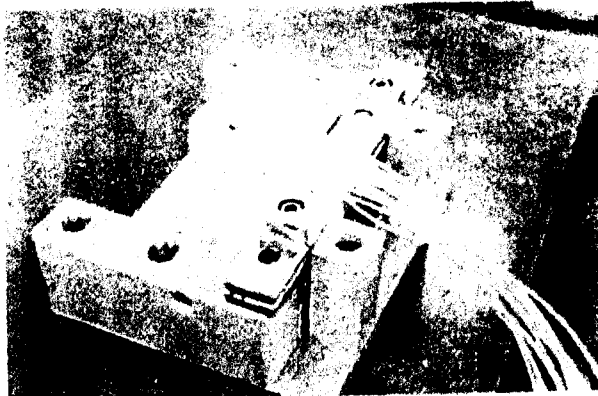


Figure 8. Wire arrangement tool

50 cycles of the condition based on Figure 9. Two specimen groups are used : 1) mated to other connectors during test term, 2) A total 25 cycles of mating and unmating were conducted five times every 10 days during test term (50 days). Figure 10 shows the change dR of contact resistance measured. As Figure 10, the contact and this crimping method were found to be stable at the stress condition.

##### 4.3 Aging test

To confirm the performance of spring construction and material of contact, the specimens were subjected to the condition of 140 degree C for 50 days. For contact normal force that should not be less than 25 grams. It has been realized that the initial value

Table 2. Results of current thermal cycle test

Items	Requirements	Results (X - KS)	Sample size (n)
Contact resistance			
Initial	$X + 2.7S < 10$	6.81	140
After test	$X - 2.7S < 10$	9.14	140

X : Average value

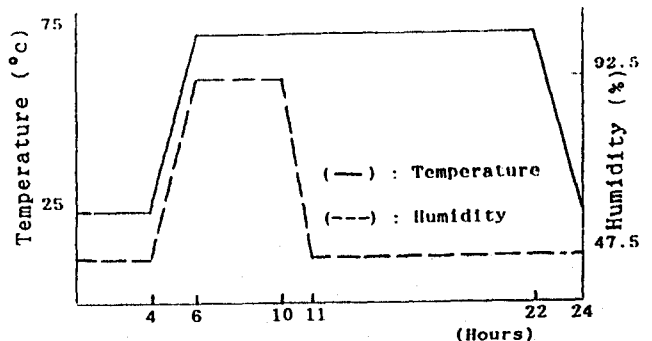


Figure 9. Condition of high temperature and high humidity cycle test

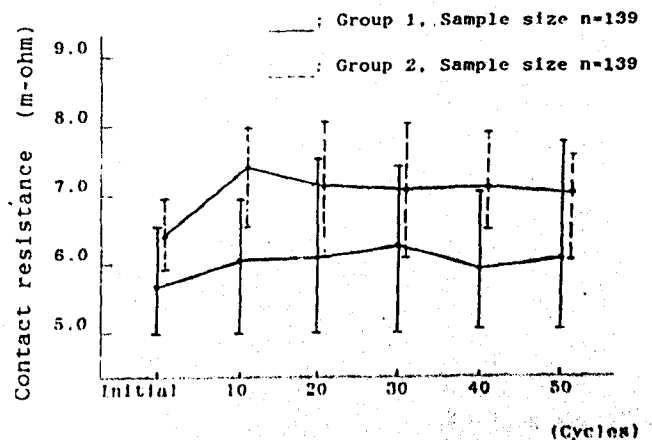


Figure 10. Results of high temperature and high humidity cycle test

Table 3. Initial properties of PTS-Cable

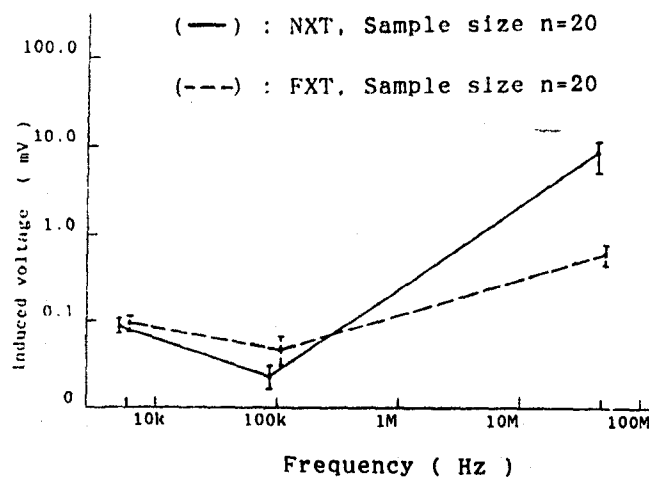
Test items	Requirements	Results (X - KS)	Sample size ( n )
Insulation resistance	X - 4.6S > 100 M-ohm	23 k	55
Dielectric strength	AC 500V -1 Minute	good	60
Latch flexing test for card connector	X - 3.0S > 20 Cycles	2828	20
Pull/electrical test	X - 3.0S > 2.7 Kg	4.22	20
Peeling strength for soldered joint	X - 2.7S > 0.15 Kg	0.22	55
Ultrasonic bond strength for plastic covers	X - 3.0S > 4.1 Kg	4.7	20

X : Average value

is 70.5 grams and the value after test is 68.8 grams.

#### 4.4 Cross talk test

Cross talk test was conducted by applying 10 volts (peak to peak) of sine wave to the signal line at the frequencies 8k, 100k and 50 MHz. Near-end crosstalk(NXT) and Far-end crosstalk (FXT) were measured. The equipment under the test was installed on a copper plate within shielded enclosure and the cable harnesses were separated from the top of table by minimum of 25 mm. The results are shown in Figure 11. As results, the induced voltage satisfied the required value at each frequencies. It is considered it depends on twisting of insulated conductors in a very short pitch and enough shielding with metal covers of the connector.



#### Required performances

- X + 3.0 S < 0.12 mV, at 8 kHz
- X + 3.0 S < 0.87 mV, at 100 kHz
- X + 3.0 S < 30 mV, at 50 MHz

Figure 11. Results of cross talk test

#### 4.5 Peculiar performance

The results of peculiar performance are shown in Table 3. These satisfied the required properties enough.

#### 5. Conclusion

In order to satisfy the many requirements including high reliability for wire harness of mainframe, we have developed a new cable, high density shielded connectors, card connectors and their assembly (wire harness called PTS-Cable). As results, it has been confirmed that PTS-Cable has excellent quality and high reliability and is very available to mainframe wiring system. The new developed crimping method for solid conductor and multi-soldering method for card connector are very effective to get high quality and cost reduction.

#### ACKNOWLEDGMENT

The authors would like to acknowledge their thanks to N.Akise and Y.Ichimiya of Electrical Parts Engineering System Products in a customer for their continuous encouragement.



Tomohiro Yamamoto

Fujikura Ltd.

1440, Mutsuzaki,  
Sakura, Chiba, 285,  
Japan

Mr. Yamamoto, a member of the Institute of Electrical Engineers of Japan, received B.E. degree in electrical engineering from Kyushu University in 1967. He joined Fujikura Ltd. has been engaged in engineering and manufacturing of electronic wires and cables. He is now a General Manager of electronic component division.



Koji Ueda

Fujikura Ltd.

1440, Mutsuzaki,  
Sakura, Chiba, 285,  
Japan

Mr. Ueda, a member of the Institute of Electronics and Communication Engineers of Japan, received M.S. degree in electronic engineering from Ohita University in 1986. He joined Fujikura Ltd. has been engaged in engineering of electronic cable assembly. He is now an Engineer of electronic component engineering department.



Shigeru Ashida

Fujikura Ltd.

1440, Mutsuzaki,  
Sakura, Chiba, 285,  
Japan

Mr. Ashida graduated in mechanical engineering course from Industry and Commerce High school in 1967. He joined Fujikura Ltd. has been engaged in engineering and manufacturing of electronic cable assembly. He is now a Manager of electronic cable assembly engineering section.



Hideki Zako

Fujikura Ltd.

1440, Mutsuzaki,  
Sakura, Chiba, 285,  
Japan

Mr. Zako received the B.E. degree in mechanical engineering from Musashi Institute of Technology in 1986. He joined Fujikura Ltd. has been engaged in engineering of electronic cable assembly. He is now an Engineer of electronic component engineering department.



Tsuyoshi Hirahara

Fujikura Ltd.

1440, Mutsuzaki,  
Sakura, Chiba, 285,  
Japan

Mr. Hirahara graduated in electrical engineering course from Syowa Daiichi Technical high school in 1964. He joined Fujikura Ltd. has been engaged in manufacturing of electronic cable assembly. He is now a Manager of electronic component engineering section.



Yasushi Nakagawa

Fujikura Ltd.

1440, Mutsuzaki,  
Sakura, Chiba, 285,  
Japan

Mr. Nakagawa received the B.E. degree in chemical engineering from Nagaoka University of Technology in 1989. He joined Fujikura Ltd. has been engaged in engineering of electronic cable assembly. He is now an Engineer of electronic component engineering department.

# PREFABRICATED CABLE SYSTEMS FOR THE "TRANSRAPID" MAGNETIC LEVITATION (MAGLEV) TRAIN

Siegfried Richter

KABELMETAL ELECTRO GmbH, Special Cable Division  
Nürnberg / Germany

## Abstract

This report gives three examples for prefabricated, ready to install cable systems for the newly developed Transrapid train for

- power cables
- data and control cables
- sensor cables.

## 1. Introduction

The "Transrapid" is a contactless, electromagnetically supported, guided and powered magnetic levitation train, intended for travelling speeds between 400 km/h and 500 km/h. A test facility for the operation of Transrapid trains was built in the north of Germany. The installed length of the track is about 32 km. The function of the magnetic systems for support and track is based on the principle of magnetic levitation. Magnets are installed in the train and in the track, holding the train at a permanent distance of approx. 10 mm above the surface of the track. Other magnets guide the train in keeping it laterally on the track. The contactless propulsion system consist of a synchronous long-stator linear motor.

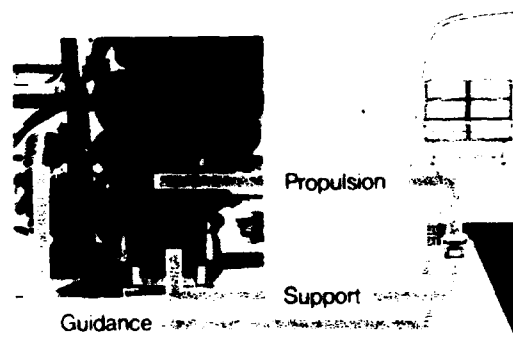
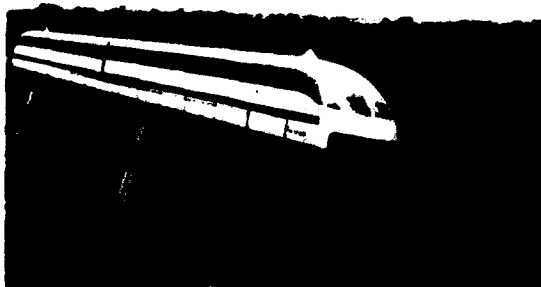


Fig.: 2 Function of the Transrapid  
Maglev System

## 2. Stator windings

The stator packs of the three-phase synchronous long stator linear motor are installed underneath the track on both sides of the track support. No electrical contact are necessary between track and train. The electro magnetic field lifts the train and electro magnetic travelling waves running along the horizontally extended stator pull the train forward.

The stator packs are individual bundles of laminations underneath the track platform. The three phase windings of the stator consist of flexible rubber insulated cables for a nominal voltage of 6/10 kV with copper or aluminum conductors. Depending on the energy which is needed in the individual sections of the route, in the test facility cables were installed having either 185 mm<sup>2</sup> or 300 mm<sup>2</sup> copper or 300 mm<sup>2</sup> aluminum cross-section.

The conductors are not stranded as is usual for highly flexible cables, but are a slightly-compacted rope strand of 58 wires made of soft annealed



copper or hard drawn aluminum which is annealed after stranding.

The conductors are covered by a conductor screen, an extruded semi-conductive compound based on ethylene propylene rubber (EPR).

The insulation meets the electrical and mechanical properties required in IEC-Publication 502. The nominal wallthickness is in accordance with the nominal voltage of 6/10 kV, i.e. 3.4 mm for all conductor sizes.

A semi-conductive, carbon-black loaded EPR compound is extruded over the insulation (insulation screen).

Conductor screen, insulation and insulation screen are extruded and vulcanized in line with three extruders in tandem. The length of the production line is 180 m and the steam pressure to vulcanize the EPR-compound is 22 bars maximum.

Cable type 1, used in the first section of the test facility, is fitted out with a metallic screen consisting of 40 wires each of 0.7 mm diameter. There is no counter helix applied over the wires of the screen, to avoid an increase of the eddy current losses in the magnetic circuit of the stator winding, and also in order not to impede the propagation of the travelling waves. The distance of adjacent wires must be accurately maintained and the wires must not touch each other, to avoid an increase of eddy current losses.

The jacket consists of a very tough weather proof rubber compound based on polychloroprene. This compound has a very high tear resistance to withstand the high stresses during shaping and installation of the winding. The jacket must be also abrasion resistant and it must insulate the screens of adjacent cables against each other as well as against ground.

Cable type 2 has no metallic screen, but a semi-conductive jacket directly extruded over the insulation. This serves to reduce eddy current losses. It is possible to replace the metallic screen by a semi-conductive elastomer jacket, provided that the distance of the ground fault current within the jacket from the spot of damage or break down to the next ground connection is very short, so that the conductivity of the jacket

is sufficient. In order to achieve this result, the design of the winding was changed.

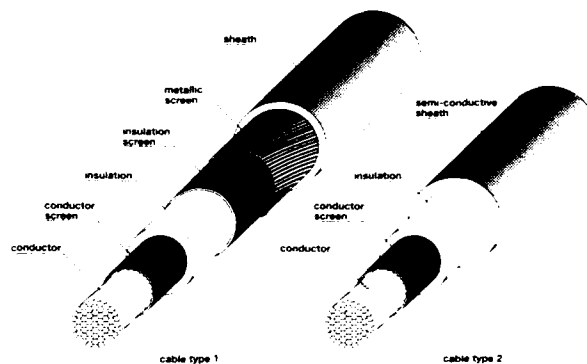


Fig.: 3 Design of cable types 1 and 2

To prove the safety of such a system and to determine the necessary resistivity of the semi-conductive jacket compound extensive test have been made with

- stable ground fault currents up to 10 A
- instable ground faults

All tests have been carried out in the laboratory on single phase windings with the original cables and the original winding carriers.

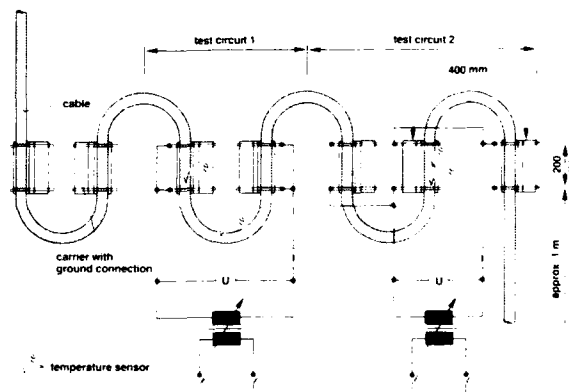


Fig.: 4 Principle of test circuits

The stable ground fault were produced by a nail, 3 mm in diameter, connecting the conductor and the outer conductive layer.

The instable ground faults were initiated by a hole of 3 mm diameter drilled through the insulation down to the conductor. The ignition of the electric arc started at approx. 4 kV.

The test results in brief are :

- In case of a ground fault current up to 2 A (with the current stabilized over 15 min) only a light corona and a little smoke were observed.
- With the ground fault current higher than 2 A, the behavior of both cable types was different:
- Cable type 1 (metallic screen): The electric arc was limited to the spot of damage or break down and extinguished itself within a few seconds.
- Cable type 2 (semi-conductive jacket): The electric arc may move to the next ground connection point and can burn down the cable over the entire distance.

The surface resistivity of the semi-conductive compound depends on the temperature. The resistance of the jacket of cable type 2 for a length of 400 mm in the range from 20°C to 120°C varies from 40 Ohms to 80 Ohms.

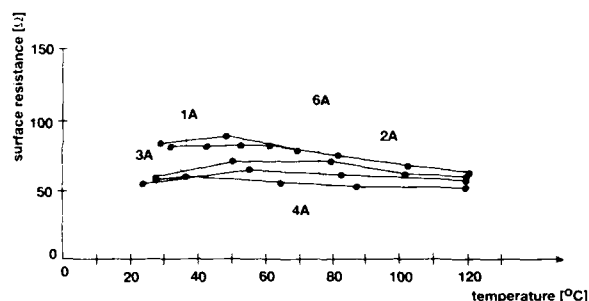


Fig.: 5 Surface resistance versus temperature

The temperature rise as a function of the current load was determined with two other cycles. The principal test dimensions were the same as before. The temperature was measured :

- in the heads of the windings, outside the winding carrier. The length of the active cable was 400 mm.
- within the winding carrier. The length of the active cable was 200 mm.

The load current limits for the semi-conductive jacket are :

- the ampacity at which the cable jacket starts burning. This is to

be expected for currents approx. 20 % higher than the values given in Fig.: 6 for 120 °C. when the conductivity is destroyed and the jacket at the fault location becomes insulating, i.e. the resistivity increases, the fault current decreases and the fuse will not respond. This is not expected because the compound used has a negative temperature coefficient.

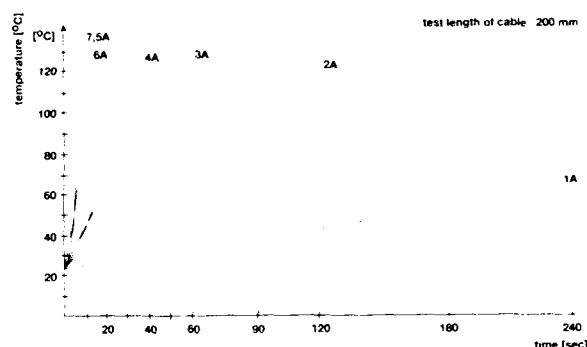


Fig.: 6 Load current versus time

The prefabricated stator winding consists of

- 3 rubber insulated flexible cables.
- polymer carriers.
- 2 flexible ground conductors.
- 2 mounting straps.

The cables are manufactured in lengths of 240 m or multiples thereof supplied on separate reels. They are individually bent and shaped in a meander-like manner by means of pneumatic tools in an equipment the principle of which is shown in the Fig.: 7. The length of such an equipment is approx. 25 m.

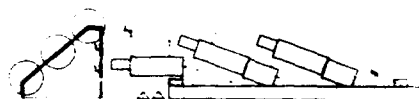


Fig.: 7 Principle of the assembly plant for the stator windings

The shaped cables are installed separately in carriers made of a carbon compound. Outside form and dimensions of the carriers match the

channels in the laminated stator packs, so that at the construction site the prefabricated stator winding can be easily-inserted into the already installed laminated stator packs underneath the track and fixed in place by snap closures only.

On the bottom of the carriers are two flexible, braided tapes, made of thin, tinned copper wires which are running longitudinally along both sides of the carriers. These ground conductors provide a secure connection to the ground potential of the structure. Two stainless steel tapes running longitudinally on the upper side fix the cables in place. The assembly is now comparable to a chain, easy to bend. Two stator windings - each 100 m in length - are wound on a shipping reel with a 4 m diameter.



Fig.: 8 Assembly plant for the stator windings

Due to transportation requirements, the shipping length is limited. Therefore for the future it is planned to mount the assembly equipment for the production of the stator windings on a movable platform which runs along the track. This will allow to produce much longer length of the stator windings, which can then be directly installed. In this way also the number of joints can be reduced.

Finally in the plant the stator windings are terminated with compression type sleeves for easy and quick splicing and terminating on the construction site.

At the construction site the reels with the stator windings are inserted into a specially designed laying

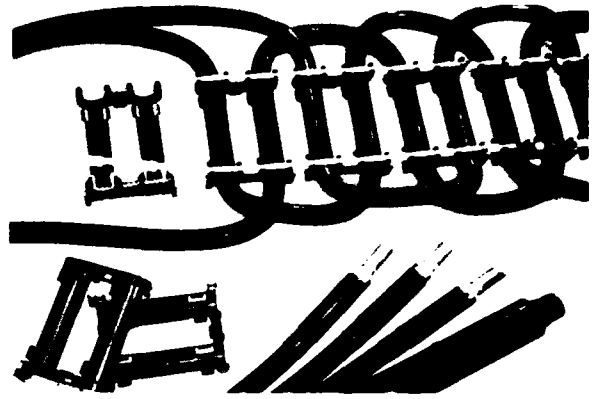


Fig.: 9 Carriers, ground connectors, fixing tapes and terminators of the stator winding

vehicle, which moves along the track, placing the stator winding below the track. The stator windings are precisely aligned with the channels in the previously installed laminated stator packs. The windings are then pressed into the channels where they are fixed by snap closures only, a process which is comparable to a zipper fastener. The laying speed is approx. 2 m/min.

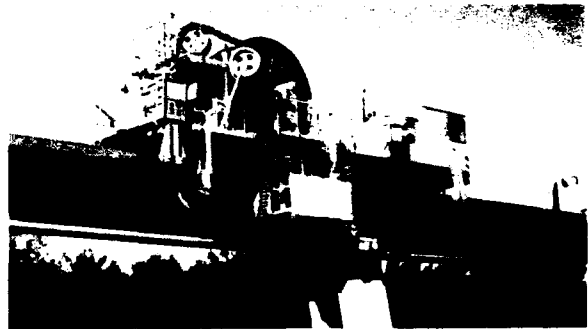


Fig.: 10 Laying vehicle

To connect the individual stator windings and to make connections with the power supply, the prefabricated compression type connectors need only to be inserted into the pre-installed receptacles and to make the ground connection.

### 3. Data- and Control cables

For the safety of the service, it is of great importance to assure high availability and reliability as well as good riding comfort. In order to provide secure data and voice transmission special cables are used.

These cables must be resistant against :

- mechanical stresses
- effect of oil, greases, hydraulic fluids or fire.
- (In case of fire, the cables must not develop corrosive gases and they must remain functional for a certain period of time.)

Fig.: 11 shows a typical hybrid data and control cable used in the Trans-rapid. The copper conductors have a double insulation wall of silicone rubber and crosslinked polyethylene. The two optic fibers are of the 100/140  $\mu\text{m}$  type, covered with polyurethane.

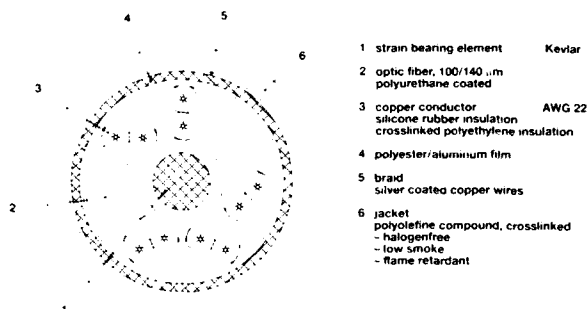


Fig.: 11 Data and control cable

The conductor pairs and the optic fibers are stranded over a central strength member made of Kevlar, covered with a flame retardant, halogen-free, low smoke polyolefin compound. An aluminum tape and a braid of tinned copper wires over the cable core serve as screens and the same time provide increased the flame resistivity. The jacket is made of a flame retardant, halogen-free, low smoke polyolefin compound, cross-linked by irradiation.

Cables of the described type and various other combinations can be found all over the train. The cables passed fire resistance tests for three hours according to IEC 331. They must withstand three hours without break down. The increase in attenuation of the optic fibers was about 0.1 dB. The cables also met the requirements for smoke development, bending behavior, abrasion resistance and resistance to chemical attack.

In order to facilitate maintenance work and changes during the test operations all cables were fitted with prefabricated plugs, ready for installation. To avoid contamination

of the optical connectors, plugs with integrated optical/electrical transmitters have been used. In view of the narrow and difficult conditions inside the train angular plugs are required. Due to the expected mechanical damage during maintenance these plugs and in particular the single fibre optic cables running from the plugs must be protected. This was realized by using cast aluminum boxes for the plugs and shaped copper tubes for the single core fiber optic cables.



Fig.: 12 Cable set ready for installation with optical data and control cable

In Fig.: 12 an open plug box is illustrated and also the optical plugs on the other end. To avoid magnetic coupling inside the plug box the copper conductor leads are as short as possible. The optical fibers in the plug box are fitted out with optical plugs of the SMA-type and are then connected with the optical outlet of the transmitter.

These cable harness which were assembled under clean conditions ensure secure and quick installations and maintenance.

#### 4. Abrasion sensor

For test with sliding skids an abrasion sensor was developed. This sensor is built into the skids. It controls the remaining thickness of the skids during the tests. Because the surface temperature of the skid and the sensor may reach temperatures up to 700 °C the sensors must be heat resistant.

A mineral insulated (MI) cable is suitable to withstand temperatures up

to 1000 °C or even higher, because it is insulated with compacted ceramic powder and enclosed in a copper or stainless steel sheath. Such single core cable having an outer diameter of 2.6 mm, was bent around a mandrel 12 mm in diameter, as shown in Fig.: 13. The MI-cable loop is introduced into a stainless steel cylinder which is filled with a ceramic compound. Because this compound is not moisture resistant its surface has to be protected by an epoxy resin. This moisture barrier can be used only for storage because it is not heat resistant. The tails of the MI-cables are about 200 mm long. They are connected to PTFE insulated coaxial cables of the RG 1789 B/U type. This is necessary because the stiff MI-cables can not be connected directly to the plug due to the strong vibrations during operation, which would soon destroy the plug.

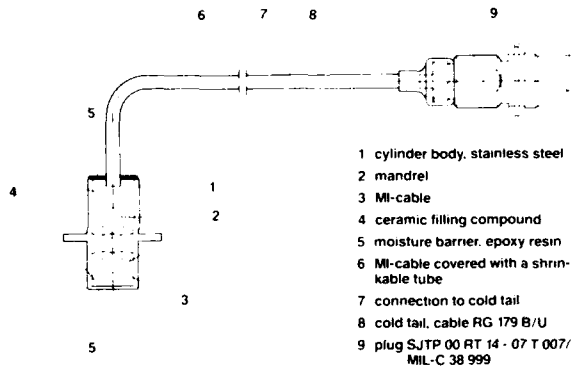


Fig.: 13 Principle of abrasion sensor cable set

During the a heat test - the sensor was placed on a hot plate with a surface temperature of 700 °C. 20 minutes after the temperature had stabilized in the whole assembly the following temperatures were measured:

- surface of the plate 700 °C
- surface of the cylinder 700 °C
- outer copper conductor at the entrance of the cylinder 170 °C
- outer copper conductor at the MI/RG cable joint 70 °C

The function of this sensor is as follows:

In operation, both the skid and the cylinder of the sensor are abraded. After a certain amount of abrasion, the surface of the MI-cable will likewise be scraped off. During the

test, the insulation and the conductor resistance is controlled. In this way it can be determined when the outer conductor of the MI-cable is damaged and later on the central conductor is interrupted. Because the sensor is placed in a very precise position it is possible to determine the remaining thickness of the skid during test operation.



Fig.: 14 Open head of abrasion sensor before filling with ceramic powder

#### Acknowledgment

The author wishes to thank the Transrapid International Gesellschaft für Magnetbahnsysteme, München, and his colleagues at KABELMETAL ELECTRO, division Special Cables, Nürnberg for assistance in preparing this report.



Siegfried Richter  
KABELMETAL ELECTRO GmbH  
Special Cable Division  
Nürnberg / Germany

### Biography

Siegfried Richter was born in 1929.

He studied Electrical Engineering and received an engineering degree in 1952. Until 1958 he developed power cables in the East German cable industry. In 1958 he joined Hackethal Draht- und Kabelwerke in Hannover (West Germany), which is now a part of KABELMETAL-ELECTRO. There he worked in cable design and production planning for power and telecommunication cables. In 1985 he transferred to the Nürnberg plant of KABELMETAL ELECTRO where he is responsible for the development of special cables. He is now chief engineer of the Special Cable Division.

Richter is involved in national and international standardization for power and special cables. He is a delegate to numerous committees of VDE, CENELEC and IEC.

CHARACTERISTIC IMPEDANCE TEST METHODS  
AT LAN FREQUENCIES: UTP-STP CASE

ROBERT D. KENNY

DAVID N. KOON

COOPER INDUSTRIES  
BELDEN DIVISION

**Abstract**

Discerning the proper test method for characteristic impedance of transmission lines at LAN frequencies (.1 to 100 MHz) has been subject to debate for many years. Several methods are in common practice today. They include the following:

- 1) Delay and fixed capacitance method
- 2) Impedance measurements via vector wave analysis: open and shorted transmission line
  - a) on short lengths (under a quarter wave)
  - b) on long lengths (330 to 1000 feet)
- 3) Impedance measurements via reflected wave analysis: loaded transmission line
  - a) on long lengths (330 to 1000 feet)

Naturally, each method has advantages and disadvantages. Only when the pros and cons of each is fully understood can the correct method versus application be realized.

**I. Introduction**

Transmission lines consist of four basic properties; series resistance, series inductance, shunt capacitance, and shunt resistance. These parameters, when viewed collectively, offer valuable insight towards the understanding of transmission lines as a whole. Below is the transmission line model. It is made up of an array of small sections of capacitors

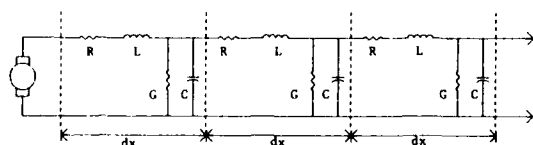


Figure 1: Transmission Line Model

and inductors (reactive components), and series resistors and shunt resistors (resistive components). Circuit analysis of the transmission line with its respective components is obtainable by letting each section ( $dx$ ) of the model be equivalent to one another. The resulting analysis produces a parameter which contains both real and imaginary parts, and is referred to as the "characteristic" impedance of the cable.<sup>1</sup> In real life, however, each section is rarely equivalent to one another, and a different approach to normal circuit analysis must be examined. One alternative is to look at what is happening at some point along the transmission line - perhaps by means of S-parameter technique or incident/reflected wave analysis. This type of impedance is often called "input" impedance.

It is the purpose of this document to consider how one can obtain useful results for LAN applications whether it be characteristic impedance or input impedance. In accomplishing this, several testing techniques will be explored using modern network analyzers and computer programming.

The following cables will be used throughout the document to aid in the understanding of the various impedance methods.

- 1) 150 ohm STP cable (Type 1)
- 2) 100 ohm UTP cable in which great care was taken to insure processing consistency throughout the length
- 3) 100 ohm UTP cable in which process measurements varied as much as  $\pm 7.5\%$  (i.e. insulated conductor diameter).

\* Since cables are not perfectly matched throughout the transmission line, it is often preferred to express cable impedance as "input" impedance rather than characteristic impedance. This will be addressed more thoroughly within the document.

## II. Test Methods and Results

### 2.1 Delay and Fixed Capacitance Method

The delay and fixed capacitance method is most often used for cables employing stable and predictable dielectrics (such as polyethylene and FEP). This technique relies on the notion that capacitance will not change with frequency. This is advantageous in that only one value of capacitance is needed for calculating cable impedance over the LAN frequency range. To better understand how capacitance and delay are related to impedance, analysis is given below.

Since at high frequencies the reactive components dominate, the following relationships can be obtained.

$$Z_o = \sqrt{\frac{L}{C}} \quad (1) \text{ Impedance Magnitude}$$

$$\beta = \omega \cdot \sqrt{LC} \quad (2) \text{ Phase Constant}$$

Where  $\omega$  is the radian frequency, L and C are inductance and capacitance respectively, and  $v$  is the phase velocity, all expressed in conventional units.

By combining the following equation with that of (2),

$$\beta = \frac{\omega}{v} \quad (2a)$$

the phase velocity can be expressed as follows.<sup>2</sup>

$$v^2 = \frac{1}{LC} \quad (2b)$$

It then becomes possible to express  $Z_o$  in terms of phase velocity and capacitance via equations (1) and (2b).

$$Z_o = \frac{1}{vC} \quad (3)$$

Therefore, assuming capacitance to be constant with frequency as this method does, the impedance will inversely correlate with the phase velocity. This

relationship becomes directly proportional when expressing phase velocity in terms of phase delay.

However, the assumption used by this method of a constant capacitance over the desired frequency range can create problems. When using such unstable dielectrics as PVC, capacitance can vary significantly over the swept frequency range. This variance will in turn cause invalid results in  $Z_o$ . Even stable dielectrics such as polyethylene shows some variation. Therefore, any results obtained by this method should be interpreted with caution.

### 2.2 Open/Short Vector Wave Analysis

As noted in the beginning of this document, open/short vector analysis technique can be applied to both short and long length transmission lines. Although their results will be shown to be different, the concept remains the same for both cases. Therefore, a brief overview of the basis behind the open/short vector technique will first be investigated.

#### 2.2.1 Wave Analysis

Assuming a sinusoidal voltage source as the input, a forward voltage is introduced upon the transmission line. Because of its sinusoidal nature, it will contain both magnitude and phase. If the line contains variations or mismatches along its length, some of the energy will be reflected back towards the source. This reflection will also contain both magnitude and phase. The relationship of these two voltages (which are travelling as "waves" in opposite directions to each other) can be used to express the impedance of a transmission line.

When looking at the case of only one mismatch occurring at the termination end of the cable, a relationship can be derived between the impedance looking into the transmission line, the load impedance, and the impedance of the transmission line itself. It is acquired through utilization of both the forward and reflected wave.

$$Z_{input} = Z_o \cdot \frac{Z_{load} - Z_o \cdot \tanh(\gamma \cdot \text{length})}{Z_o + Z_{load} \cdot \tanh(\gamma \cdot \text{length})} \quad (4)$$

Where gamma is the propagation constant containing both magnitude and phase ( $\gamma = \alpha + j\beta$ ).<sup>1</sup>



However, it is common knowledge that the impedance of a practical transmission line is **not** uniform and contains many mismatches throughout the cable length. In this case, the equation becomes even more complex since each mismatch and its resulting effect must be examined separately, including the mismatch occurring at the load.

When trying to isolate the behavior of just the transmission line without the influence of the load termination, a technique has been developed via use of an open and short circuited transmission line. This technique is especially advantageous when examining a short length of transmission line where the load termination could mask reflections of the cable itself. To see how this is done, the analysis of the open and short circuited transmission line must first be discussed.

The equations for both the open and short circuited input impedances (lossless transmission line) are illustrated below

$$Z_{sc} = jZ_o \tan (\beta * length) \quad (5)$$

$$Z_{oc} = -jZ_o \cot (\beta * length) \quad (6)$$

where  $Z_o$  is the characteristic impedance and  $\beta$  is the frequency divided by the velocity.<sup>2</sup> This result can be verified by simply letting  $\alpha = 0$  and  $Z_{load} = 0$  or infinity within equation (4).

By multiplying equations 5 and 6 together, it is ultimately found that;

$$Z_o = \sqrt{Z_{sc} * Z_{oc}} \quad (7)$$

Therefore, if one were to place a cable on a network analyzer and performed separate swept frequency input impedance measurements of an open and short circuited load, the characteristic impedance would be obtainable by the relationship shown in equation (7).

### 2.2.2 Open/Short Vector Wave Analysis: Short Length Case

Measuring electrically short cable lengths (under a quarter wave length) is advantageous due to low

preparation time and traces which are smooth and easy to interpretate. When calculating the correct sample size for a quarter wavelength, the following formula should be used.

$$\frac{\lambda}{4} = \frac{9.84 * 10^8 * v_p}{4 * 100 * f} \quad (8)$$

where  $v_p$  is the velocity of propagation of the dielectric in percentage.

For example, if someone desired to test a cable using polyethylene (assume 66% velocity) up to 20 MHz and wanted to avoid quarter wavelength oscillations, the calculation would be:

$$\frac{\lambda}{4} = \frac{9.84 * 10^8 * 66}{4 * 100 * 20 * 10^6} = 8 \text{ feet}$$

So the user should choose a sample length close to but not equal or greater than 8 feet.

Figure 2 illustrates the impedance oscillations seen when a sample length exceeds a whole number multiple of the quarter wave length.

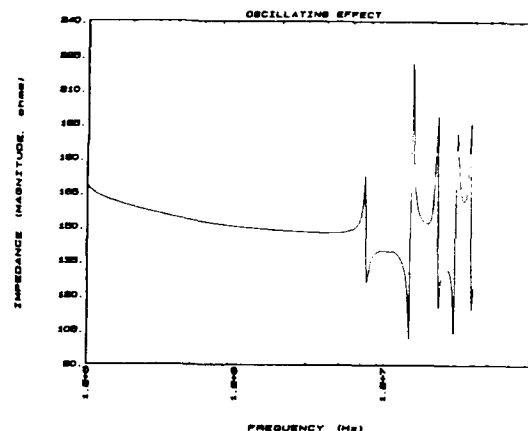


Figure 2: Oscillating behavior at multiples of the quarter wave

When placing short lengths of the two UTP cables and one STP cable defined in the introduction upon a network analyzer, the following traces are realized (since the equipment is measuring the magnitude and phase of the voltage and current at the input of the cable, it is actually input impedance being measured).

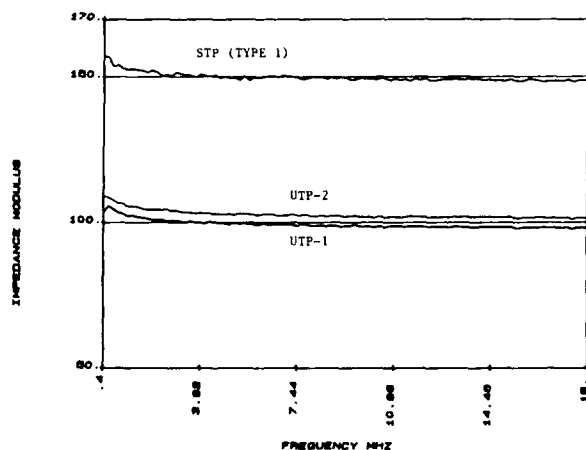


Figure 3: UTP-1, UTP-2, and STP Type 1: 4 feet

As one can ascertain, all three impedance traces show a smooth response over the frequency range. When analyzing a sample of this length, however, certain drawbacks must be mentioned. First, it is quite possible that the sample being tested represents only a very small percentage of the actual cable which was manufactured. Statistically, one sample says nothing about the impedance variation that will be experienced throughout the cable run. The only way to determine this would be to choose a sample size large enough (say, twenty or more 8 foot samples, for example) to fully understand what kind of variance could be expected with the impedance. Notice above that the two UTP cables would appear to have a different impedance. However, as stated previously, variations in the cable impedance cannot be realized with just one sample. Therefore this conclusion might very well be incorrect. Another disadvantage to electrically short length samples is that the additive structural effects of processing inconsistencies will not be readily seen. Remember that since capacitance is dependent on conductor separation via the dielectric, any variation in insulation thickness will ultimately change the impedance.

### 2.2.3 Open/Short Vector Analysis: Long Length Case

One method used to help understand how variations in manufactured cables relate to the input impedance is by application of long length samples. To better perceive why this is the case, an example is given below.

The following illustration is a ladder diagram similar to that of Figure 1, except with equivalent impedances  $Z_1$ ,  $Z_2$ , ect. replacing the distributed



Figure 4: ladder network with input impedance

components. For this case, it is assumed that the impedances  $Z_1$ ,  $Z_2$ , ect. are not equivalent to each other. Because of this, any forward or incident wave introduced upon the transmission line media will encounter mismatches as it propagates along it. Further, each mismatch will result in a reflected wave which will propagate back towards the input.

When an analyzer measures cable input impedance via open/short vector analysis (whether it be an electrically short or long length sample), it does so by correlating the input generated wave to the reflected wave returned. This is achieved by vectorially summing the reflected energy (vectorially since the reflections are complex containing both magnitude and phase) and comparing it to the incident energy at the input.

One point that must be addressed is that of multiple reflections and the distance they occur from the input. When the incident energy encounters mismatches along the line, energy is reflected back towards the input. Generally speaking, the bigger the mismatch, the greater the reflection. As these mismatches occur further and further distances from the input, the reflected energy is increasingly attenuated due to series losses and re-reflections as it returns towards the input. Since this method determines impedance by comparing the incident wave to the reflected wave *at the input*, different magnitudes and phases will in turn cause different levels of impedance. Therefore, if a mismatch occurring 20 meters from the input was changed to occur only 10 meters from the input, it will have a greater effect on the input impedance of the cable. One immediate conclusion that can be drawn from this

is that a long length vector impedance measurement does not represent an average of combined short length vector impedance measurements performed on the same cable.

Another effect which is unique to long length measurements is that of an impedance spike. Reflected energy of cyclical structural variations can cause an additive effect of this energy. In this case, there is no one point in the cable to where the spike is contributed, but rather a multitude of periodic reflections adding in phase causing a spike to occur. As will be seen, these "spikes" and other variations can have an effect on a cable's performance.

Interpreting these variations or spikes could become important when reflections from mismatches travelling towards the input are re-reflected back towards the load; conceivably adding to the forward or trailing edge of the incident signal. The result of this could be an increase in the amount of jitter incurred. It should be noted, however, that the mismatch needed to significantly effect jitter is fairly large in most cases. This is due to the fact that the reflected wave must be re-reflected back in the direction of positive propagation and not completely attenuate before it reaches the load.

Below are actual test results when measuring impedance via long length open/short vector analysis. The cables shown are the same as discussed in the introduction. As can be clearly seen, UTP-1 and UTP-2 are now quite different, with the latter showing increased variation with respect to frequency. This effect was not evident when the electrically short sample was tested (refer back to section 2.2).

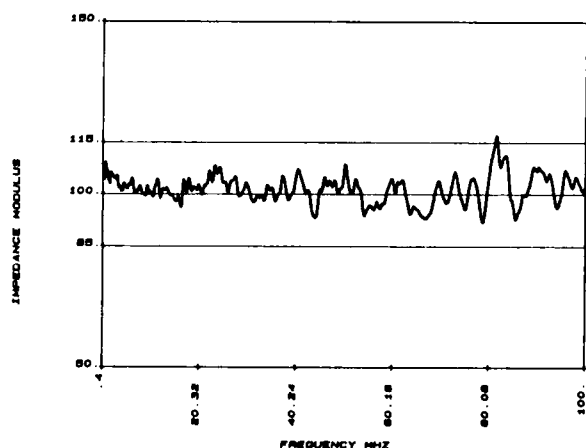


Figure 5a: UTP-1: 1000 feet

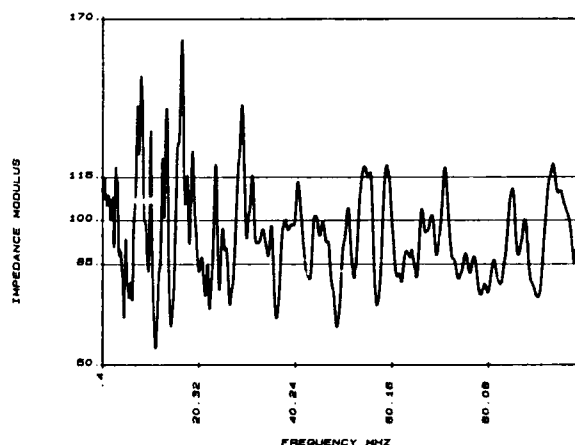
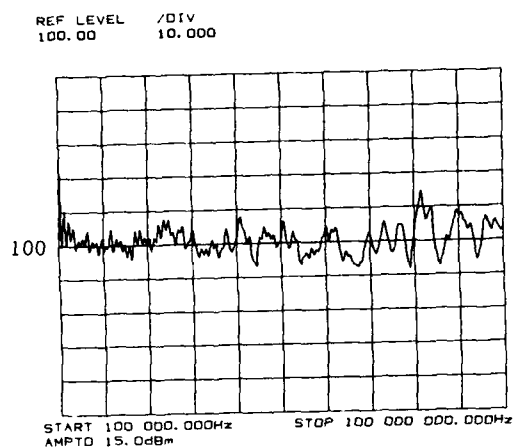


Figure 5b: UTP-2: 1000 feet

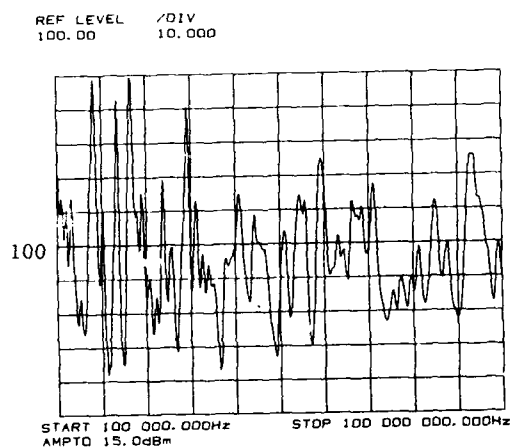
### 2.3 Reflected Wave Technique With Load Termination: Long Length

LAN cables are normally terminated with some type of load. When the load is not matched to the characteristic impedance of the cable, energy is reflected back towards the source. If the load is distant enough from the input, the reflected energy will have almost no effect on the swept impedance measurement being taken due to attenuation effects. In this case, the cable is said to be self terminating. Therefore, when the cable self terminates, the results from an open/short measurement and a matched load termination should be the same.

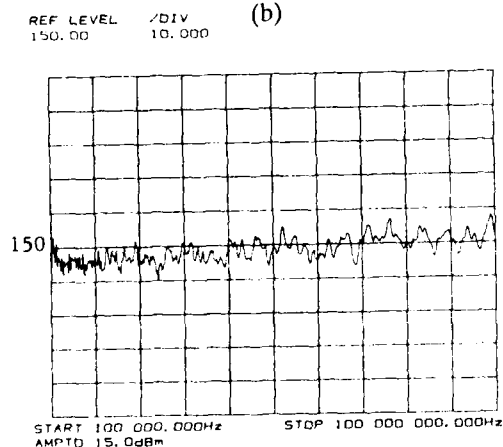
The following graphs are the results from a swept impedance measurement of the UTP-1, UTP-2, and STP Type 1 transmission lines. Both UTP cables were terminated with 100 ohm resistive loads, with the STP type 1 being a 150 ohm resistive load. As expected, the graphs are extremely similar to that shown for the open short vector technique (ignoring the minor scale differences). It is important to understand that both the open/short vector technique and the matched load terminated reflected wave technique use the same basic concept of wave analysis. It is only the mathematics and equipment data manipulations which are different. It can then be concluded that for electrically long lengths (*preferably* 500 to 1000 feet for LAN frequencies) that both methods produce similar results.



(a)



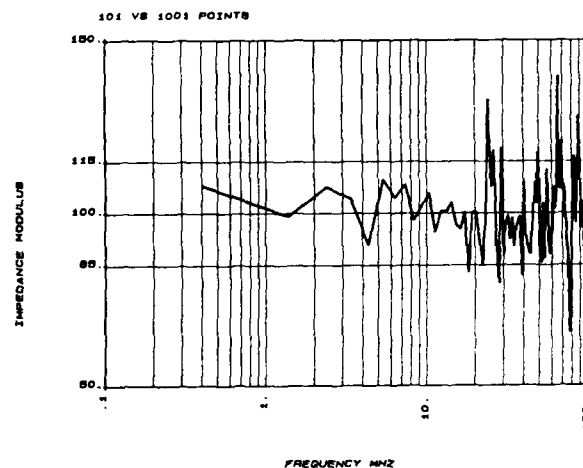
(b)



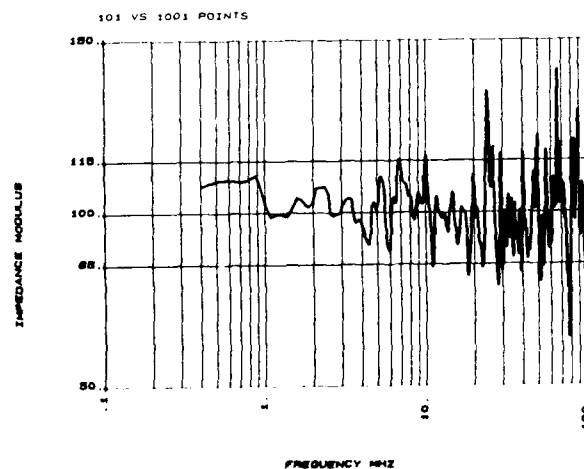
(c)

Figure 6: (a) UTP-1, (b) UTP-2, (c) STP Type 1

Finally, one minor warning should be given in regards to long length measurement interpretation - whichever technique is used. Results given in this document use a frequency resolution of either 401 or 1001 data points (depending upon analyzer utilized). If fewer points of resolution are employed, lower frequencies will tend to be deceptively smoother than that of higher frequencies, especially when looking at a logarithmic scale. Therefore, at least 200 points per decade should be used. Also, the sweep time in correlation with the number of points of resolution should be slow enough to capture all of the energy response reflected back to the input (typically 20 seconds).



(a)



(b)

Figure 7: (a) 101 vs (b) 1001 points (log scale)

### III. Conclusion

This document discussed 3 methods for determining impedance of a transmission line at LAN frequencies - delay and fixed capacitance, open/short circuit load via reflected wave analysis, and terminated load via reflected wave analysis. However, as noted in this document, methods discussed produced very different results.

In the delay and fixed capacitance method, phase delay is used to obtain the impedance of the transmission line. This method is advantageous due to its simplicity. However, there are several drawbacks. First, capacitance is measured at just one frequency within the voice range. It is then utilized to determine impedance for the entire swept frequency range. As is known, however, capacitance does vary with frequency. Therefore, any variation in capacitance will result in error being introduced into the calculation of impedance (since this method cannot account for this effect). Additionally, the two port measurement technique used to evaluate delay produces a deceptively smooth trace, not exhibiting many of the variations that would normally be seen with delay over a swept frequency.

The technique of using an open/short circuited load via vector wave analysis can be applied to both electrically short and electrically long lengths of cable. When a short length is implemented, it yields a very smooth trace with respect to frequency. Additionally, sample preparation time is negligible. What a short length does not show is structural effects due to process variations along the cable length. However, when testing long length samples, structural effects are evident. These effects are displayed in the form of variations on the swept impedance trace. If the variations are cyclical, their reflections will be additive hence creating a spike along the trace. One drawback to long length measurements is the lengthy sample preparation time. Furthermore, a long length measurement does not treat successive mismatches along the cable length equally as explained in section 2.2.3.

The third method utilizes reflected wave analysis with a terminating load. This method has been shown to yield the same results as the long length vector impedance technique, with the added advantage of needing only one measurement per sample as opposed to two measurements.

### References

1. Matick, R., Transmission Lines for Digital and Communication Networks, McGraw-Hill Inc., New York, NY, 1969
2. Liboff, R., Transmission Lines, Waveguides, and Smith Charts, Macmillan Publishing Co., New York, NY, 1985



Robert D. Kenny received his B.S. degree in electrical engineering from Ohio Northern University, Ada, OH in 1988. He joined Cooper Industries, Belden Division at that time as a product development engineer. He is presently involved in the development of LAN products.



David N. Koon received his B.S. degree in electrical technology from Purdue University, West Lafayette, IN. in 1985. Since that time, he has been with AT&T, TRW, and Cooper Industries, Belden Division. His earlier work concerned the analyzing and programming of data acquisition systems and the development of electronic circuitry. More recently, Dave is involved with the automation of the engineering laboratory and the development of test methods. He is a member of IEEE.

# HIGH-SPEED COATING OF OPTICAL FIBERS WITH UV CURABLE RESINS

K. Kobayashi, K. Tsurusaki, Y. Sato, and S. Araki

Fujikura Ltd.

1440, Mutsuzaki, Sakura-Shi, Chiba, Japan

## ABSTRACT

High-speed curing UV resins for primary and secondary have been developed, and an optical fiber drawing rate of 1300m/min has been achieved using these UV curable resins. The coated fibers drawn at 1300m/min have stable mechanical properties and transmission characteristics. The slot-type optical fiber cable manufactured on trial had excellent mechanical properties and temperature characteristics.

## 1. INTRODUCTION

The demand for optical fibers has recently been on the rise. It is important for manufacturers to decrease the production cost of optical fibers. Increasing the optical fiber drawing rate may prove to be the most effective technique.

However, if you attempt to increase the drawing speed by using conventional UV curable resin, you have to use several UV curing systems. To use more curing systems is an obstacle to the design of economical drawing towers. Therefore, it is necessary to develop UV curable resin with a higher curing rate.

In this paper, we report on our results as follows;

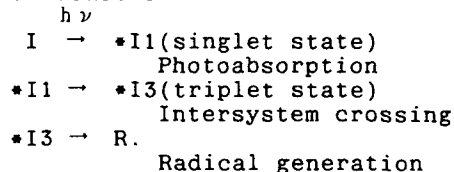
- 1) We discussed the UV resin molecular design to increase the curing speed of UV curable coatings for optical fibers.
- 2) Using the high-speed curing UV resins, we prepared optical fiber drawn at 1300m/min, and we investigated the appearance of the coating layers, fiber strength, and transmission loss characteristics of these fibers, respectively.
- 3) We evaluated the mechanical properties and temperature characteristics of a slot-type 100-fiber cable manufactured as an experiment.

## 2. DEVELOPMENT OF HIGH-SPEED CURING UV RESINS

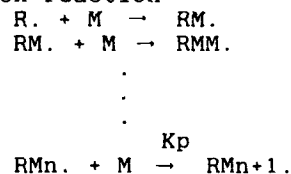
### 2-1 MOLECULAR DESIGN OF HIGH-SPEED CURING UV RESINS

The curing reaction of UV curable resin is given as the following formulae:<sup>(1)</sup>

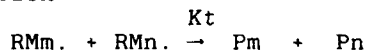
Initiation reaction



Propagation reaction



Termination



The rate of polymerization ( $R_p$ ) is expressed by the following formula:

$$R_p = \{M\} \cdot K_p (R_i / K_t)^{1/2}$$

where,

$$R_i = K_d \cdot F \cdot I \cdot \{PI\}$$

$K_p$ : Velocity constant of propagation reaction  
 $R_i$ : Velocity of initiation reaction  
 $K_t$ : Velocity constant of termination  
 $\{M\}$ : Concentration of double bond  
 $K_d$ : Photoabsorption coefficient of initiator  
 $F$ : Frequency of photoinitiation reaction

$$= f \cdot \Phi$$

f: photoinitiator efficiency  
 $\Phi$ : Quantum efficiency  
 I: Ultraviolet radiation intensity

$$=I_0 \exp(-\alpha L)$$

$\alpha$ : Ultraviolet absorption coefficient of UV resin  
 L: Coating thickness

{PI}: Concentration of photoinitiator

To increase the curing speed of UV resin, a molecular design with the following characteristics is required:

- 1) Photoinitiators have a high ultraviolet absorption coefficient, easily rise to intersystem crossing, and have a high radical generation efficiency (quantum efficiency).
- 2) Monomers have a high  $K_p$  value, i.e., a high double bond reactivity.
- 3) Monomers and oligomers have low absorbance, and the overlap of absorption spectra between them and the photoinitiator is small.
- 4) Absorption spectra of photoinitiators and the spectrum of a UV lamp overlap as much as possible.

## 2-2 CHARACTERISTICS OF THE HIGH-SPEED CURING UV RESINS

On developing UV curable resins for high-speed drawing, we considered the molecular design for the high-rate curing UV resins mentioned above, in addition to physical properties (Young's modulus, elongation, strength), thermal properties, resin's viscosity, and so on. Table 1 shows the differences between the composition of the high-rate curing resins and that of the conventional resin.

Table 1 The compositions of the resins

	Conventional resin	Primary A	Secondary A
Photoinitiator	a	b	b
Monomer	$\alpha$	$\beta$	$\gamma$
Oligomer	x	y	z

The ultraviolet absorption spectra of the oligomers "x" and "y," and photoinitiators "a" and "b" are shown in Fig.1. Fig.2 shows the radiation spectrum of the UV lamp used in this study. As seen from the figures, the following facts have been found.

- 1) Oligomer "y" has a lower absorbance than oligomer "x."
- 2) The overlap between the absorption spectrum of photoinitiator "b" and that of oligomer "y" is not so large in comparison with the overlap between photoinitiator "a" and oligomer "x."
- 3) Photoinitiator "b" has a higher absorbance than photoinitiator "a."
- 4) Photoinitiator "b" has another absorption in the region of nearby 360nm. The wavelength of 360nm is the main radiation wavelength of the UV lamp.

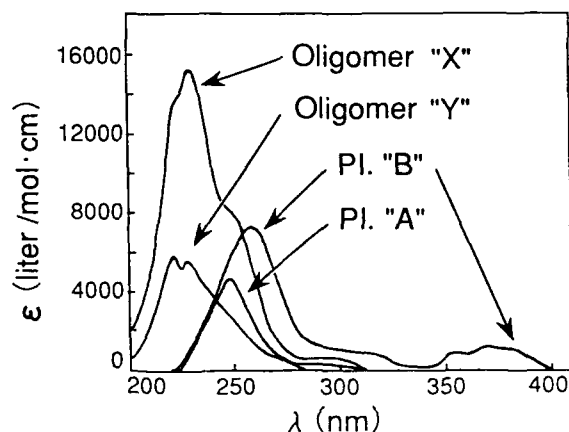


Fig.1 Absorption spectra of oligomers and photoinitiators

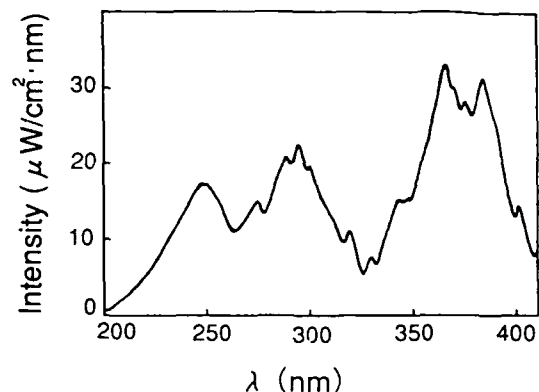


Fig.2 Radiation spectrum of the UV-lamp

To estimate the curing speed for Primary A and Secondary A, we measured the gel fractions, the Young's moduli, and the unreacted double bond contents for these resins at several different UV doses. In addition, we compared these resins with conventional resins under the same conditions. Fig.3, Fig.4, and Fig.5 show the changes of the gel fractions, the Young's moduli, and the unreacted double bond contents for Primary A and Secondary A, respectively. For these measurements, we prepared the cured sheet specimens with a thickness of about 100 $\mu$ m. We also measured the unreacted double bond contents according to the FT-IR method. Double bond content was calculated by the following formula:

$$\text{Unreacted double bond content (\%)} = 100 (R_s/R_o)$$

where,

$$R_o: \frac{\text{Absorbance}(1410\text{cm}^{-1})}{\text{Absorbance}(1730\text{cm}^{-1})} \text{ for UV resin before curing}$$

$$R_s: \frac{\text{Absorbance}(1410\text{cm}^{-1})}{\text{Absorbance}(1730\text{cm}^{-1})} \text{ for UV resin after curing}$$

As shown in Fig.3 - Fig.5, both Primary A and Secondary A have been fully cured at half the UV dose required for the conventional UV resins. Therefore, these resins cure about twice as fast as the conventional resins.

### 3. HIGH-SPEED DRAWING

First, we determined the temperature of an uncoated fiber surface needed to obtain uniform coating layers in a high speed drawing process. Next, we determined the pressure value needed for a pressurized coating applicator at a drawing speed of 1300m/min.

#### 3-1 TEMPERATURE OF THE FIBER

In a fiber drawing process, the temperature of the fiber has to be low enough to prevent fluctuations in the coating diameter and bubble formation in the coating layer. Normally, the faster the drawing speed is, the higher the fiber temperature at the coating applicator is. Therefore, increasing the fiber drawing speed causes some problems with respect to fiber coating. Fig.6 shows the relation between the temperature( $T_f$ ) of the fiber surface and the distance( $x$ ) from the bottom of the drawing furnace. The fiber temperatures were measured with an IR thermometer. In the case of natural air cooling, the temperature ( $T_f$ ) is about

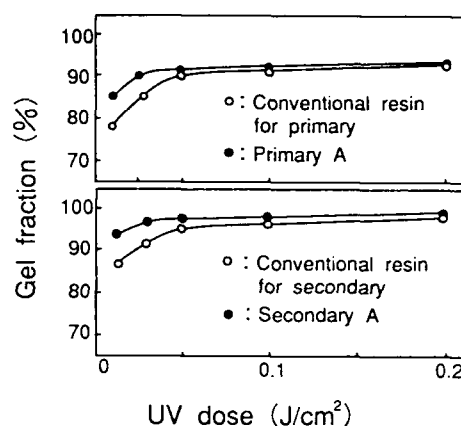


Fig.3 Dependence of UV dose on gel fraction

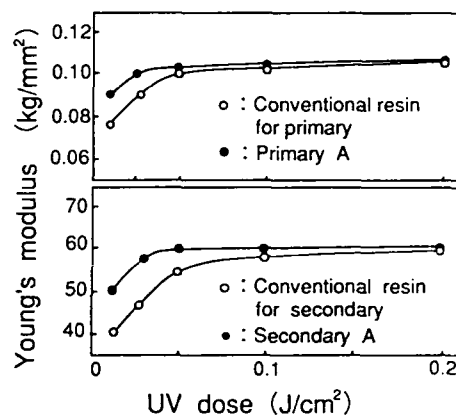


Fig.4 Dependence of UV dose on Young's modulus

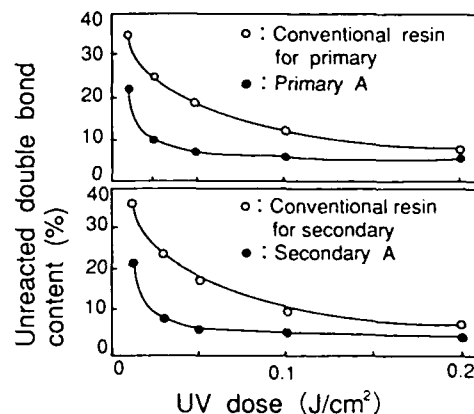


Fig.5 Dependence of UV dose on unreacted double bond content



400 °C, at a drawing rate ( $V_f$ ) of 1300m/min(21.7m/sec), and the distance ( $x$ ) of 5m. The temperature of the fiber just before coating of the primary resin should be controlled below 80 °C in order to obtain a bubble-free concentric coating layer. We therefore, set a cooling device between the furnace and the coating applicator for the primary resin. By using forced cooling of the fiber, we can draw the coated fiber at 1300m/min.

### 3-2 PRESSURE VALUE FOR THE PRESSURIZED COATING APPLICATOR

In general, a pressurized coating applicator is used for high-speed drawing.<sup>(2)</sup> We investigated proper pressure values for the pressurized applicator used in our experiments. Fig.8 shows the relation between the pressure values and the coating diameters at a drawing speed of 1300m/min. The fluctuations in the primary and secondary coating diameters are rather large at pressures below 2kg/cm<sup>2</sup>. Thus, when drawing fibers at 1300m/min, we set the pressure at 3 - 4 kg/cm<sup>2</sup>. As shown in Fig.7, fluctuations in coating diameter can be controlled within  $\pm 1 \mu\text{m}$  when the pressure value is 3 - 4kg/cm<sup>2</sup>.

## 4. CHARACTERISTICS OF COATED FIBERS

We prepared 100km coated fibers at a drawing speed of 1300m/min using Primary A and Secondary A. Fig.8 shows a cross section of the coated fiber. The fiber is Germanium-doped silica-core SM fiber with a MFD of 9.5 $\mu\text{m}$  and a cutoff wavelength of 1.22 $\mu\text{m}$ . The diameter of the fiber and the dual coatings are 125 $\mu\text{m}$  and 250 $\mu\text{m}$ , respectively.

### 4-1 APPEARANCE

At first, we observed the internal state of the coating layers. It is well known that bubble in the coating layer causes the degradation of the transmission characteristics of the coated fiber.<sup>(3)</sup> So, we prepared a specimen at 10km intervals from the start point in drawing to the end of the coated fiber, and observed the inside of the coating with a microscope. Photo.1 shows the observations of the coated fiber. No bubble is found in any specimen of the coated fibers. Thus, it is confirmed that the coated fibers have high coating stability.

Fig.9 shows the typical result of the changes in the primary and secondary diameter during the fiber drawing. Fluctuations in the coating diameters are within  $\pm 1 \mu\text{m}$ . And so, the dimensional stability of the coated fiber is equal to that of the fibers drawn at conventional speed.

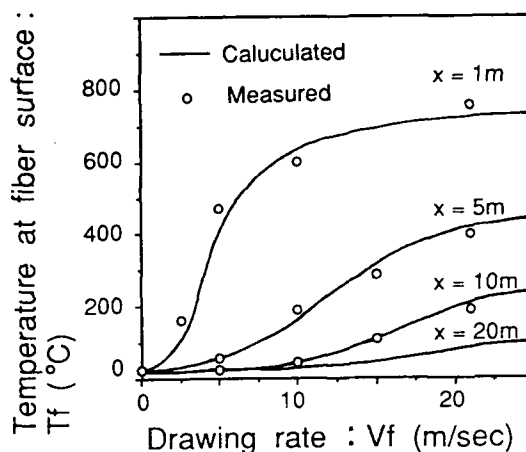


Fig.6 Drawing rate vs. temperature of the fiber surface

$$T_f = 27 + 800 \exp(-3.18x/V_f)$$

$x$ : Distance from the bottom of the furnace

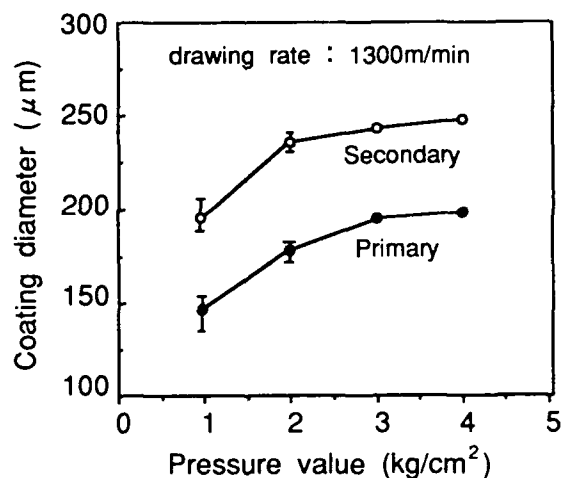


Fig.7 Relation between the pressure values and the coating diameters

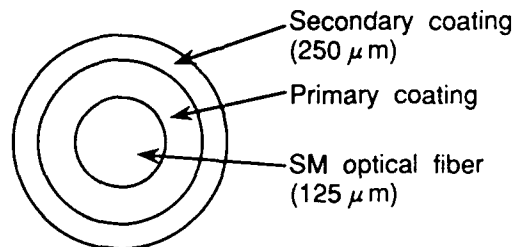


Fig.8 Structure of the optical fiber

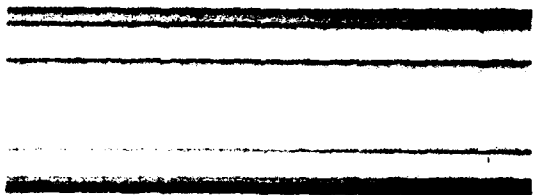


Photo.1 Observation of the coated fiber

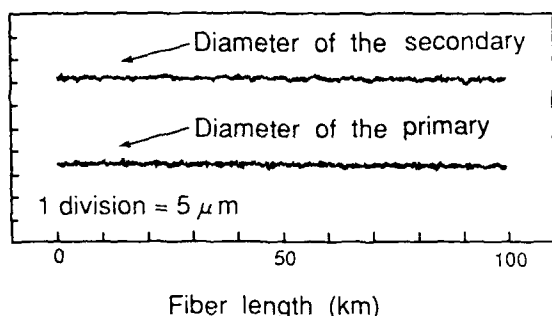


Fig.9 Changes of the primary and secondary diameter during the fiber drawing

#### 4-2 CURING DEGREE

Table 2 lists the measured results of gel fractions, Young's moduli, and unreacted double bond contents of the coating materials. For these measurements, the coating materials were prepared by peeling off the coated fibers.

As shown in the table, we verified that the curing degrees of both the primary layer and secondary layer had reached completely saturated values.

#### 4-3 FIBER STRENGTH

We examined the fiber strength of the coated fibers. We took samples at 10km intervals on the coated fibers and measured the fiber strength at room temperature (20 °C). We used the gage length of 10m, with a 10%/min strain rate. The number of specimens for each sample was 50.

Fig.10 shows the changes of tensile strength for the coated fibers along the fiber length. The median strength value is 5GPa or more. Breakage at low strength levels was not observed.

#### 4-4 TRANSMISSION CHARACTERISTICS

We tested the transmission characteristics of the coated fibers. The fiber for measurement was in a free coil about 30cm in diameter and 1000m in length. The fiber coil was subjected to the atmosphere at temperatures of -40 °C and +60 °C. And we measured the spectral transmission loss for the coated fiber at high and low temperatures. Fig.11 shows the results of the test. As shown in Fig.11, the transmission loss after drawing is 0.34dB/km at 1.3μm and 0.20dB/km at 1.55μm, and loss increases at low and high temperatures are negligible at both 1.3μm and 1.55μm. These results indicate that the coated fibers have the stable transmission characteristics.

Table 2 Gel fractions, Young's moduli, and unreacted double bond contents of the primary and the secondary of the coated fiber

	gel fraction (%)	Young's modulus (kg/mm <sup>2</sup> )	double bond content (%)
primary	90	--	5
secondary	96	61	4

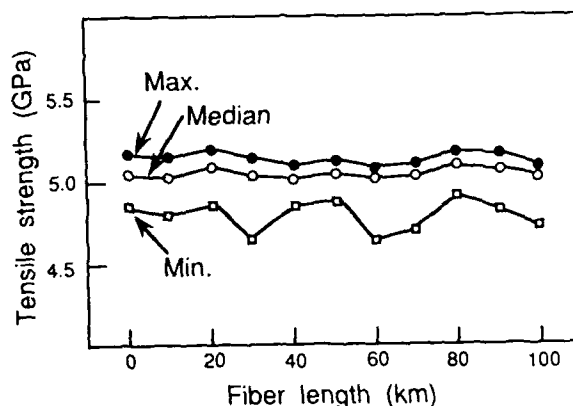


Fig.10 Changes of tensile strength for the coated fiber along the fiber length

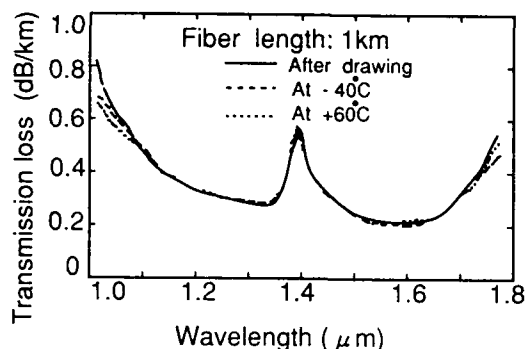


Fig. 11 Spectral transmission loss of the coated fiber

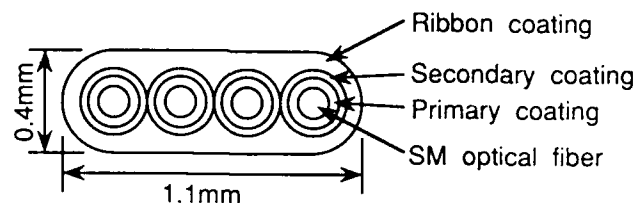


Fig. 12 Structure of the manufactured 4-fiber ribbon

## 5. CHARACTERISTICS OF SLOT-TYPE CABLE MANUFACTURED ON TRIAL

We used the coated fibers to make 4-fiber ribbon, and manufactured a ribbon slot-type 100-fiber cable. Fig. 12 and 13 show the cross section of the fiber ribbon and the cable.

### 5-1 TRANSMISSION LOSS

Fig. 14 shows the transmission loss during the manufacturing process. The average loss increase was less than 0.02dB/km. This result indicates that the cable can be manufactured with excellent transmission loss stability.

### 5-2 MECHANICAL PROPERTIES

In our investigation of the mechanical properties, we subjected the cable to various mechanical tests. The test conditions and results are listed in Table 3. In all tests, no additional transmission loss was observed.

### 5-3 TEMPERATURE CHARACTERISTICS

Fig. 15 shows the transmission loss stability during a temperature cycle from -40 °C to +60 °C. Added loss was minimal, 0.02dB/km at -40 °C and 0.03dB/km at +60 °C.

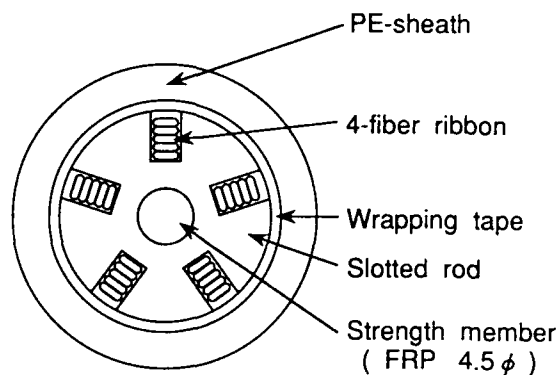


Fig. 13 Structure of the manufactured 100-fiber cable

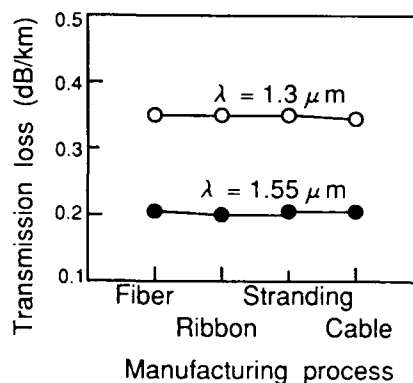


Fig. 14 Transmission loss during the manufacturing process

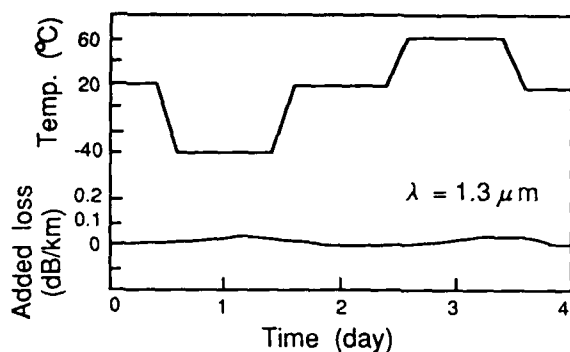


Fig.15 Transmission loss change of the 100-fiber cable during a temperature cycle

## 6 CONCLUSION

Based on the experimental results described above, we reached the following conclusions:

- 1) The newly developed UV resins Primary A and Secondary A have twice the curing speed of conventional resins.
- 2) We used the developed resins to make coated fibers at a drawing rate of 1300m/min. Then, the curing levels of the coating materials, the appearance of the coating layers, the fiber strength, and the transmission loss characteristics were investigated. In this manner, we were able to confirm the excellent characteristics of the coated fibers.
- 3) The slot-type 100-fiber cable manufactured on trial also has the excellent mechanical properties and temperature characteristics.

Our study confirmed that an optical fiber drawing rate of 1300m/min can be achieved by using the newly developed UV resins. These techniques can be expected to contribute to the reduction of fiber production costs in the future.

## References

- 1) T. Kokubun, Y. Katsuyama, K. Hogari, and S. Hatano: Journal of Lightwave Technology, vol. 7, NO. 5, pp 824, May 1989
- 2) S. Sakiguchi and T. Kimura: OFC '85, Technical Digest, pp 18, February, 1985
- 3) C. M. G. Jochem and J. W. C. van der Ligt: IOOC-ECOC '85, pp 515, 1985

Table 3 Mechanical properties of the 100-fiber cable

Test item	Condition	Result
Lateral pressure	300kg/50mm x 1min	< 0.01dB at 1.3 $\mu$ m
Bending	R=10D x 10cycles D:Cable outer diameter	< 0.01dB at 1.3 $\mu$ m
Tensile	T=200kgf, L=10m	< 0.01dB at 1.3 $\mu$ m
Impact	1kg x 1m height (25mm colum )	< 0.01dB at 1.3 $\mu$ m
Squeezing	R=250mm, T=200kgf, L=100m	< 0.01dB at 1.3 $\mu$ m
Tortion	$\pm 180$ deg./m	< 0.01dB at 1.3 $\mu$ m



Kazunaga Kobayashi

Fujikura Ltd.  
1440 Mutuzaki,  
Sakura, Chiba,  
285, Japan

Mr. Kobayashi was born in 1961. He joined Fujikura Ltd. after his graduation from Gunma University with the M.E. degree in 1985. He has been engaged in research and development of optical fibers and optical fiber coatings. He is now an engineer of Telecommunication Cable Material Section and a member of IEICE of Japan.



Yoshiyuki Sato

Fujikura Ltd.  
1440 Mutuzaki,  
Sakura, Chiba,  
285, Japan

Mr. Sato was born in 1963. He joined Fujikura Ltd. after his graduation from Tohoku University with the M.E. degree in 1988. He has been engaged in research and development of optical fiber cables. He is now an engineer of Telecommunication Cable Section and a member of IEICE of Japan.



Koji Tsurusaki

Fujikura Ltd.  
1440 Mutuzaki,  
Sakura, Chiba,  
285, Japan

Mr. Tsurusaki was born in 1963. He joined Fujikura Ltd. after his graduation from Hiroshima University with the M.E. degree in 1988. He has been engaged in research and development of optical fibers and optical fiber coatings. He is now an engineer of Telecommunication Cable Material Section and a member of IEICE of Japan.



Shinji Araki

Fujikura Ltd.  
1440 Mutuzaki,  
Sakura, Chiba,  
285, Japan

Mr. Araki was born in 1950. He joined Fujikura Ltd. after his graduation from Tokyo Metropolitan University with the B.E. degree in 1974. He has been engaged in research and development of optical fibers and optical fiber coatings. He is now the chief of the Telecommunication Cable Material Section and a member of IEICE of Japan.

# EVALUATION OF TECHNIQUES FOR DETERMINING THE EXTENT OF CURE OF OPTICAL FIBER COATINGS

Rolf A. Frantz\*, Irene M. Plitz\*\* and Steven R. Schmidt†

\*Bellcore, Morristown, NJ; \*\*Bellcore, Red Bank, NJ; †DSM Desotech, Des Plaines, IL

## ABSTRACT

Proper curing of optical fiber coatings is necessary to ensure that the glass fiber is protected from environmentally-induced stresses. In this paper we examine a wide range of techniques for measuring the extent of coating cure, including several not previously referenced in the fiber coating literature. Data are presented for six fibers representing two different coatings with varying extents of cure. Our studies show that these techniques fall into three categories: (1) those that are insufficiently sensitive to warrant further study (e.g., measurements of dielectric properties); (2) those that identify different cures but have some inadequacy (e.g., abrasion resistance); and (3) those that are sensitive and reproducible (e.g., Differential Photocalorimetry). The latter warrant additional, broader-based work to develop standard test procedures for use by fiber manufacturers and users.

## INTRODUCTION

Many properties of an optical fiber coating (for example, its tensile modulus) depend upon its extent of cure or crosslink density.<sup>[1]</sup> In a previous paper<sup>[2]</sup>, we demonstrated that the long term mechanical properties of optical fibers are affected by the extent of cure of the coating. Lower extents of cure result in lower median strengths, broader strength distributions, and lower resistance to static and dynamic fatigue. This increases the susceptibility of the fiber to failure under high stresses that may occur during installation or under residual stresses present throughout the fiber's service life. The measurement of coating cure is therefore of concern not only for manufacturing operations, but also for assuring the reliability of a finished fiber optic cable.

Unfortunately, the industry has not agreed on a definition of "full coating cure" and lacks a standardized technique for measuring the extent of cure. In this paper we review a wide range of techniques that are applicable to measuring the extent of cure. These include qualitative measures such as color and residual odor as well as specific thermo-chemical analyses that focus on measuring the extent of the crosslinking reaction and/or the fraction of residual unreacted material. All techniques were compared using the four fibers with different extents of coating cure whose mechanical characteristics (dynamic tensile and bending strength and fatigue) were reported in [2]; these fibers were coated with Desolite® 950-008, a hard, high-modulus single-coat coating. The more successful techniques were also applied to sample fibers coated with Desolite® 950-133, a soft, low-modulus single-coat coating, using two different extents of cure.

After describing the preparation of the sample fibers, we explain the various measurement techniques and present data for the sample fibers. We compare and discuss the advantages and disadvantages of the techniques and the significance of the results and we conclude with comments on the possible standardization of several measurement techniques.

## SAMPLE PREPARATION

All samples were prepared in Bellcore's experimental fiber drawing tower. Two single-coat coatings were selected that represent the extremes available with polyurethane acrylate coatings. As shown in Table 1, Desolite® 950-008 is similar to a secondary coating, with a high tensile modulus and strength, a high glass transition temperature, and low adhesion to glass; its modulus varies relatively slowly with temperature. In contrast, Desolite® 950-133 (Table 1) has a low tensile modulus and strength, a lower glass transition temperature, and high adhesion to glass; its modulus is ten times more sensitive to temperature than that of 950-008.

TABLE 1. PROPERTIES OF CURED COATING FILMS

Property	950-008	950-133
Tensile Modulus (23°C)	620 MPa	32 MPa
Tensile Modulus (-40°C)	1520 MPa	850 MPa
Tensile Strength (23°C)	26 MPa	9 MPa
Glass Transition Temperature	52°C	34°C
Adhesion to Glass (50%RH)	10g	150g

Curing is a function of the ultra-violet (UV) dose, which is directly proportional to the UV lamp intensity and inversely proportional to the draw speed. The UV curing lamps in the draw tower are 12-inch long, 200 W/in medium pressure mercury vapor quartz lamps from Canrad-Hanovia. Two different power settings were used, as shown in Table 2. The draw speed in the tower is continuously variable from less than 5 m/min to over 60 m/min; the best control is obtained in a range from 20 to 50 m/min. Full use was made of this range in drawing the sample fibers (Table 2).

TABLE 2. DESCRIPTIONS OF FIBER SAMPLES

Fiber Sample	Draw Speed	Lamp Power	Coating Diameter	Weight Fraction
950-008 #1	23 m/min	3500W	233 µm	58.0%
950-008 #2	38 m/min	3500W	244 µm	59.0%
950-008 #3	50 m/min	3500W	262 µm	64.5%
950-008 #4	50 m/min	2500W	261 µm	64.5%
950-133 #1	40 m/min	3500W	240 µm	56.0%
950-133 #2	40 m/min	2500W	230 µm	56.0%

As detailed in [2], we pulled UV-sensitive labels through the draw tower to estimate the doses seen by the coating at various draw speeds and lamp powers. The drawing conditions in Table 2 were selected by comparing the color changes of these labels with those of identical labels exposed in a UV conveyor belt system to known doses as measured by a radiometer.

The fibers were drawn from fire-polished fused silica rods to a diameter of  $123 \pm 1 \mu\text{m}$ . The outer diameter of the coating (Table 2) is controlled by the die in the coating cup; the die wore considerably from other uses between the first and last pairs of 008-coated fibers, so a new die was used for the 133-coated fibers. The weight fraction of each coating is determined by the die diameter, since the glass diameter is constant; Table 2 shows the weight fractions as determined by stripping the fiber and by thermogravimetric analysis (TGA).

## MEASUREMENT TECHNIQUES

### Infrared Spectroscopy

The extent of cure of a UV-curable polyurethane acrylate coating can be characterized by its degree of acrylate unsaturation. The magnitude of the acrylate absorption peak at  $810 \text{ cm}^{-1}$  indicates the degree of unsaturation; it can be measured using Fourier Transform Infrared (FTIR) Spectroscopy - Attenuated Total Reflectance (ATR) techniques. Lengths of coated fiber are mounted on opposing faces of the crystal through which the infrared beam is passed; energy is absorbed by the coating at each of the multiple reflections from the coating/crystal interface. The greater the extent of cure of the coating, the the lower the degree of unsaturation and the smaller the total absorption peak compared to that of the liquid resin. The decrease in unsaturation from the liquid resin to the cured coating is normalized to an internal standard and is used to calculate the percent reacted acrylate unsaturation (%RAU). Table 3 gives the %RAU for the four 008-coated fibers and the two 133-coated fibers.

### Differential Photocalorimetry

The extent of cure of a fiber coating can also be measured by determining the amount of residual crosslinking reaction. Differential photocalorimetry (DPC) measures the heat of reaction when a partially cured coating is re-exposed to UV light and the curing reaction is carried to practical completion. The heat of the residual reaction in Joules per gram of coating material (J/g) can be compared to the heat of reaction when the liquid resin is cured to the same stage of completion under the same UV source. In each case, a small sample (of resin or coated fiber) is placed in a pan in a differential scanning calorimeter; it is exposed to a UV light of known intensity for a controlled time period, and the heat of the (residual) curing reaction is measured. Full curing of the

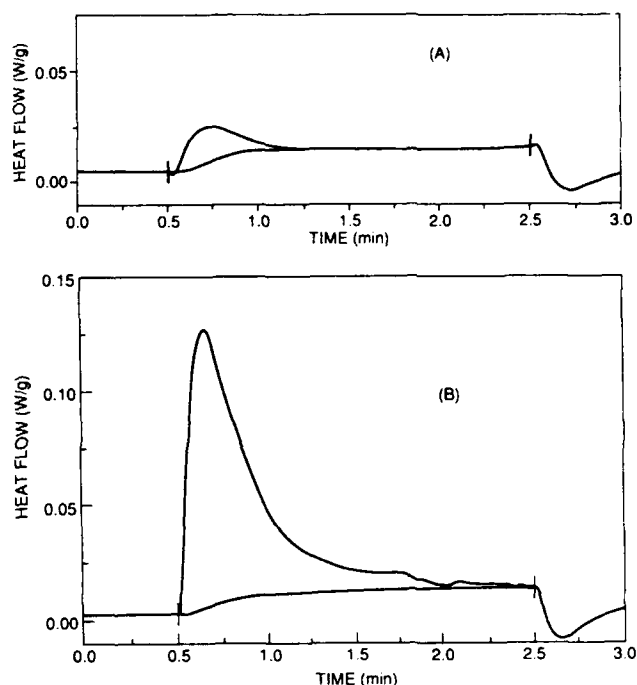


FIGURE 1. HEAT FLOW OF RESIDUAL CURING REACTION  
(A) 950-008 #1; (B) 950-008 #4

008 resin generates a heat of reaction of  $100.9 \text{ J/g}$ , while the 133 resin generates  $61.9 \text{ J/g}$ . The values for the residual reactions for the four 008-coated fibers and the two 133-coated fibers are given in Table 3 and constitute only a few percent of the total curing reaction for the liquid resin. Figure 1 compares the heat flow curves for typical high and low cure coated fibers, in this case the highest and lowest cured 008 coatings; the offset from zero that develops during the test is an artifact of the heat emanating from the UV source.

### Evaporation Rate Analysis

Increasing the extent of cure of a polymeric coating increases its crosslink density, which lowers its permeability to and absorption of solvents. In evaporation rate analysis (ERA), a solvent or a solvent blend containing minute amounts of a radioactive tracer is applied to a sample of coated fiber and evaporated by an air stream directed over the sample. The higher the extent of cure, the faster the rate of evaporation, since less solvent is absorbed and retained in the coating. The rate of evaporation is monitored by detecting emissions from the radioactive tracer. The ratio of the highest detected count (the peak solvent concentration) to the count at the end of the

TABLE 3. MEASUREMENTS OF EXTENT OF COATING CURING REACTION FOR SAMPLE FIBERS

Property	950-008 #1	950-008 #2	950-008 #3	950-008 #4	950-133 #1	950-133 #2
Reacted Acrylate Unsaturation	95%	96%	86%	70%	97%	95%
Residual Reaction	0.45 J/g	0.30 J/g	1.97 J/g	3.13 J/g	1.33 J/g	3.10 J/g
ERA Cure Index	458	177	164	150	103	101
Total Count	545	2218	3626	4602	4443	5291
Extractables	1.77%	2.08%	6.21%	9.24%	6.25%	9.28%

test (when most of the solvent has evaporated) gives a measure of the extent of coating cure. In particular, a "cure index" is often used which is proportional to the ratio of the log of the count for the highest 30-sec interval to the count for the last 30-sec interval in a three-minute test.<sup>[3]</sup> A high cure index corresponds to a rapid evaporation of solvent and a high extent of cure. The total count of detected emissions is also sometimes helpful in assessing extent of cure; in this case, highly cured coatings result in rapid evaporation of the solvent and tracer, so low total counts correspond to high extents of cure. Table 3 gives the cure index and total count for all sample fibers.

### Extraction

Another measure of the extent of cure of a crosslinked coating is the amount of material that can be extracted from the coating through immersion in a solvent. Fiber Optic Test Procedure FOTP-10<sup>[4]</sup> specifies a procedure using soxhlet extraction that can be used to assess varying extents of cure of a given coating, though not to compare different coatings. Samples of fiber are soaked repeatedly in freshly distilled warm methyl ethyl ketone (MEK) solvent for a period of at least 15 hours; extracted material is periodically flushed away in the extraction apparatus. The resulting weight loss, due to the removal of unreacted coating resin and possibly some residual photoinitiator, is used as a measure of cure. Higher weight losses correspond to lower extents of cure. The results for all six sample fibers are shown in Table 3.

### Dielectric Measurements

As the curing reaction proceeds in a coating, its dielectric properties change. While the raw resin is somewhat conductive due to the readily reactive material, the cured coating develops a high resistivity as the reactive sites are consumed in the ongoing crosslinking reaction. Similarly, the dielectric constant  $\epsilon$  changes as dipole moments in the molecular structure are frozen in place by the reaction. Dielectric analysis, sometimes referred to as dielectrometry, can be used to measure these changes and assess the extent of cure.<sup>[5]</sup>

Changes in  $\epsilon$  are most readily measured by using the material as the dielectric in a capacitor. Coated fiber is particularly unsuited to this; a layer of fibers placed between the plates of a capacitance sensor contains both air and glass dielectrics as well as the coating. Both materials affect the measured value of  $\epsilon$ , and the variability in the open spaces in a layer of fibers results in very poor reproducibility of the measurements. It was quickly apparent that we could not measure differences in dielectric constant among the sample fibers.

The resistivity of fiber samples is more readily determined. We used three different instruments to assess the resistivity by measuring: (1) the resistance in  $m\Omega$  of lengths of coated fiber over a frequency range from 100 Hz to 100 kHz; (2) the leakage current in  $\mu A$  under ac stresses up to 4 kV; and (3) the insulation resistance under dc stresses up to 1 kV. A sampling of the results of these measurements for the four 008-coated fibers is shown in Figure 2. We chose not to apply these tests to the 133-coated fibers because of the difficulty in differentiating among the various extents of cure of the 008-coated fibers.

### Physical Characteristics

Differences exist between the sample fibers that allowed at least some of the spools to be identified without reading the labels. These observable differences are summarized in Table

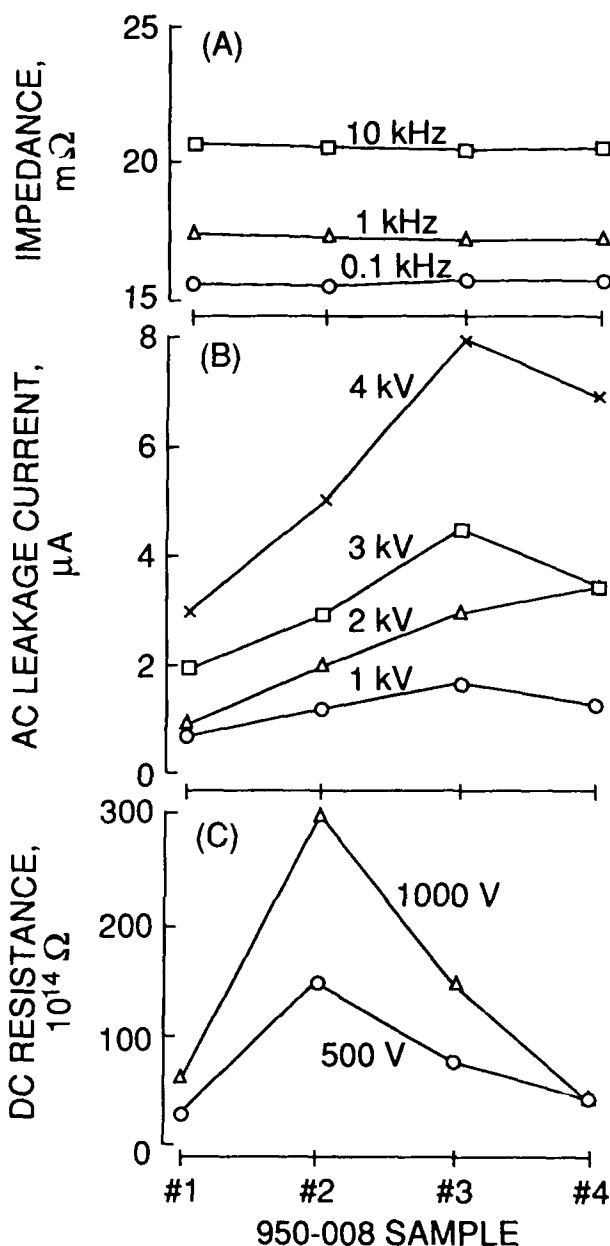


FIGURE 2. DIELECTRIC MEASUREMENTS ON FIBERS  
(A) Impedance at Various Frequencies  
(B) Leakage Current at Different AC Voltages  
(C) Insulation Resistance at Different DC Voltages

4. The colors of the 008 coatings with the highest and lowest extent of cure could be differentiated from all other samples. The 133-coated fibers had a slight residual acrylate odor that gradually faded with time; for the 008-coated fibers, this was only observed with the fiber with the lowest extent of cure. The 133-coated fibers had soft surfaces as opposed to the hard outer surface of the 008-coated fibers. Again, the lowest-cured 008-coated fiber was distinct in having a very slight tackiness to its surface, but this caused no problems in spooling or handling the fiber, indicating that this represents the least-cured sample that might inadvertently slip through a manufacturer's quality control screening.



TABLE 4. PHYSICAL CHARACTERISTICS OF FIBER SAMPLES

Fiber Sample	Color	Odor	Surface
950-008 #1	Dull Yellow	None	Hard, Brittle
950-008 #2	Clear	None	Smooth
950-008 #3	Clear	None	Smooth
950-008 #4	Very Slight Milkiness	Noticeable Acrylate	Very Slight Tackiness
950-133 #1	Clear	Slight Acrylate	Soft
950-133 #2	Clear	Lingering Acrylate	Soft, Uneven

The color measurement can be quantified using a chromameter, which locates colors in three-dimensional space (brightness, red/green hue, and yellow/blue hue). Measured colors for the 008-coated fibers are shown in Figure 3 (the red/green components of color are negligible). The perceived yellowness of fiber #1 is readily confirmed; for all practical purposes, however, the other fibers are indistinguishable.

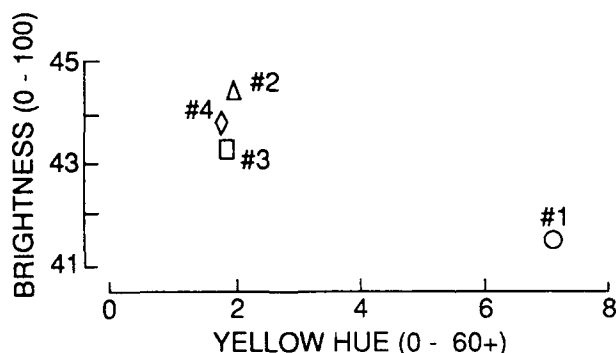


FIGURE 3. MEASURED COLOR OF 008-COATED FIBERS

### Hydrogen Generation

Another potential method for assessing the relative extent of cure of a coating is measuring the amount of hydrogen gas generated when the coated fiber is subjected to accelerated aging. The quantity of hydrogen evolved from UV-curable coatings depends upon the choice of photoinitiator and oligomer type. Hydrogen generation generally decreases with higher extents of cure. However, UV doses in excess of the manufacturer's recommendation can increase the amount of hydrogen evolved.

We used two similar methods to measure the amount of hydrogen generated. In both, coated fiber samples were aged in capped headspace vials, using 1g of sample per 20 ml of vial volume. In the first test, fibers were aged at 80°C in an argon atmosphere; after 24 hours, samples of the headspace gas were injected into a calibrated Key-Med Exhaled Hydrogen Monitor. In the second test, the fibers were aged at 100°C in air. In accordance with proposed FOTP-182<sup>[4]</sup>, the vials were flushed after 72 hours; after an additional 24 hours of aging, gas samples were injected into a calibrated gas chromatograph equipped with a thermal conductivity detector. These hydrogen concentrations represent a steady state condition, rather than an initial burst; similar results were obtained when the first method was extended to this longer aging period. All data were converted into microliters of hydrogen evolved per gram of coating and are given in Table 5.

### Weight Loss

To the extent that a coating is undercured, a greater amount of volatile material is released when the fiber is heated. The weight loss due to volatilization can be measured using TGA. We performed two types of experiments. In one, the stacked fibers in the sample pan were heated from 50°C to 600°C at a rate of 20°C/min. The weight losses of the various samples were compared at each of several temperatures for evidence of differences in the extent of cure. The data at 200°C are given in Table 5. In the other test, samples were held isothermally at 200°C and the weight losses measured after 30 minutes. Other samples run at 150°C and 250°C confirmed the 200°C data. These data are also given in Table 5.

### Oxidation Onset

Different crosslink densities in a polymer coating should change its susceptibility to oxidation. Samples of coated fiber were heated in a differential thermal analyzer (DTA) in oxygen at a rate of 10°C/min to 250°C. The onset of oxidation was defined as the temperature at which the extrapolated oxidation exotherm intersected the baseline. Data for the 008-coated samples is given in Table 5. This procedure was not applied to the 133-coated samples because of its inability to differentiate among the various extents of cure.

### Water or Solvent Soak

One function of a fiber coating is to protect the glass from water and solvents that can cause stress-induced corrosion. As noted above, the permeability of a polymeric coating varies with its extent of cure. Recent work<sup>[6]</sup> has shown that water absorption by a coating is a dynamic process, with an initial weight gain followed by a weight loss due to slow extraction of unreacted material. A modification of this test was applied to

TABLE 5. CURE MEASUREMENT BY HYDROGEN GENERATION AND THERMAL ANALYSIS TECHNIQUES

Property	950-008 #1	950-008 #2	950-008 #3	950-008 #4	950-133 #1	950-133 #2
H <sub>2</sub> Generation <sup>①</sup>						
Key-Med	0.5 µl/g	0.4 µl/g	<0.1 µl/g	<0.1 µl/g	1.2 µl/g	1.4 µl/g
Chromatograph	0.8 µl/g	<0.3 µl/g	<0.3 µl/g	<0.3 µl/g	0.6 µl/g	0.7 µl/g
TGA Weight Loss						
Ramp at 200°C	1.8%	- - -	- - -	2.2%	1.3%	5.3%
Isothermal at						
150°C	0.46%	- - -	- - -	1.7%	- - -	- - -
200°C	0.69%	0.83%	1.0%	2.3%	3.3%	7.7%
250°C	3.0%	- - -	3.3%	- - -	- - -	- - -
Oxidation Onset	191°C	192°C	204°C	191°C	- -	- - -

<sup>①</sup>See text for comparison of the two methods.

the 008-coated fibers. Samples were immersed in deionized water at 20°C and 85°C and in MEK at 20°C. The samples were weighed immediately after being removed from the liquid and again after being reconditioned in a 20°C, 45% RH environment. Both the amount of water or MEK absorbed by the coating and the amount of coating material extracted due to immersion were thus assessed. Typical plots of weight gain or loss as a function of time are shown in Figure 4.

#### Abrasion Resistance

The coating also protects the glass fiber from abrasion - nicks and scratches due to spooling, cabling, and handling. This measure of comparative performance among coatings can also be used to measure the extent of cure of a specific coating. The higher crosslink density of a highly cured coating increases its toughness and hence its abrasion resistance. We measured abrasion resistance using the procedure of FOTP-66[4] in which a falling abrasive impinges on a tensioned fiber sample. The average amount of abrasive required to break each of the sample fibers is given in Table 6.

#### Coating Strip Force

The ability of the coating to adhere to the glass, yet be stripped off (e.g., for splicing), is another measure of performance that can be used to monitor the extent of cure. FOTP-178[4] specifies a standard stripping tool mounted in a universal tensile testing machine to measure the force required to strip the coating from the glass. We performed this test at 50 cm/min using a 3-cm gauge length for all samples. We also repeated the test on the 008-coated fibers using a gauge length of 1 cm to determine the sensitivity to gauge length. The results of all tests are shown in Table 6.

#### Pull-Out (Coating Adhesion)

The adhesion of the coating to the glass is only one factor that affects the strip force. A more direct measure of adhesion is the force required to pull the glass out of a length of coating. Proposed FOTP-105[4] provides a standard technique for making this measurement. A 1-cm length of fiber is bonded to a substrate, the coating is nicked, and the glass is pulled out of the anchored length of coating. Recognizing that this FOTP is still under development, we applied it to the 008-coated fibers in an effort to learn about both the procedure and the fibers. Although we had some problems and identified necessary refinements in the method, we also obtained useful data, which is summarized in Table 6.

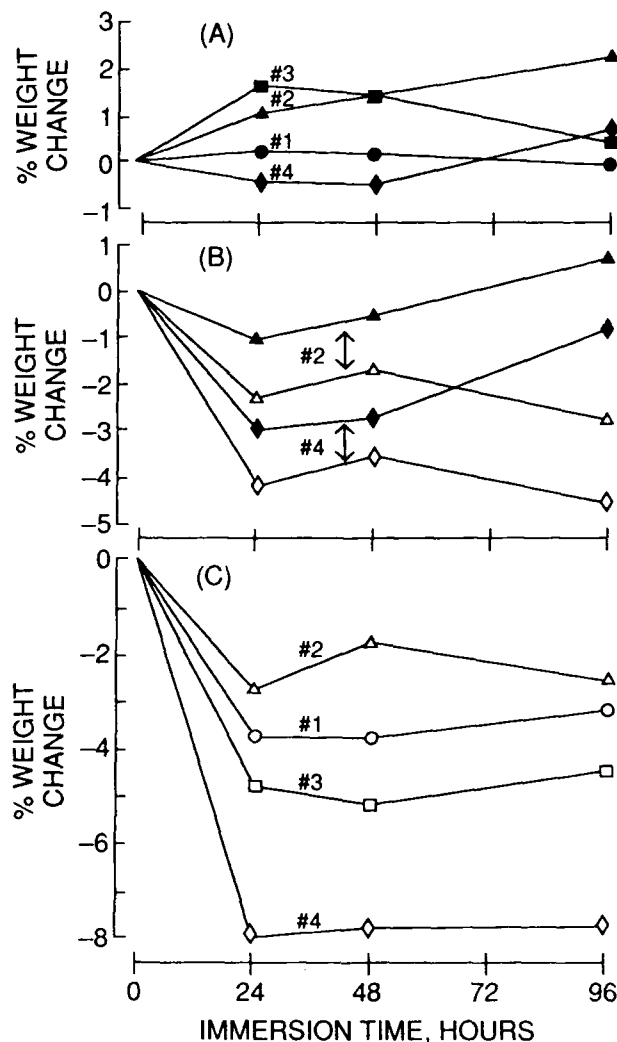


FIGURE 4. WEIGHT GAIN /LOSS FOR 008-COATED FIBERS  
(A) At Removal from 20°C DI Water  
(B) At Removal and after Reconditioning from 80°C DI Water  
(C) After Reconditioning from 20°C MEK

TABLE 6. MECHANICAL MEASURES OF EXTENT OF CURE FOR SAMPLE FIBERS

Property	950-008 #1	950-008 #2	950-008 #3	950-008 #4	950-133 #1	950-133 #2
Abrasion Resistance	1.662 kg	2.041 kg	2.349 kg	1.973 kg	1.834 kg	0.527 kg
Strip Force (3 cm gage)	6.63N	5.84N	5.66N	6.32N	3.35N	2.42N
Strip Force (1 cm gage)	5.92N	5.48N	4.97N	5.71N	---	---
Pull-Out (Adhesion)	13.24N	①	28.04N	22.55N	---	---
Median Tensile Strength	4399 MPa ②	4034 MPa ②	3834 MPa ②	3758 MPa ②	4454 MPa	4447 MPa

① Adhesive bond or fiber itself broke for all samples.

② Strain rate 2.5%/min (see [2]).

## **Fiber Strength**

Fiber strength is another performance parameter that might serve to measure the extent of cure. In [2], we demonstrated that the strength and fatigue resistance of the 008-coated fibers in both tension and bending changed with the extent of coating cure; typical results are given in Table 6. We also performed tensile strength tests on the 133-coated fibers as specified in FOTP-28B[4]. These results are also in Table 6.

## **DISCUSSION**

The data above show that several of the techniques are not sufficiently sensitive to use for measuring the extent of coating cure. The impedance of the coating is insensitive to the extent of cure over a wide range of frequencies (Figure 2A). The ac leakage current (Figure 2B) is found by subtracting the leakage without a sample present from that with a sample in place; both values are around 100  $\mu$ A and the subtraction yields very poor reproducibility for the measurement. The insulation resistance of the coating (Figure 2C) is exceptionally sensitive to the surroundings, resulting in wide swings on the meter; this again leads to very poor reproducibility. One factor contributing to these problems is the high surface-to-volume ratio of the coating. Volume properties that are most affected by differing extents of cure can be masked by outer surface effects, where the extent of cure differs less and environmental effects can be significant.

Similarly, the physical characteristics of the coating are poor indicators of the extent of cure. Coatings with very high and very low extents of cure might be identified by color or odor (Table 4), but these are subjective judgements. Even quantifying the color measurement fails to differentiate among samples with very different cures (Figure 3). Experienced shop personnel should be immediately aware of and act to correct a problem in the manufacturing process indicated by such gross changes.

Hydrogen generation is poorly suited to determining the extent of cure of polyurethane acrylate coatings that currently dominate the market. Coating manufacturers have emphasized reduced hydrogen evolution, so that present coatings release very little hydrogen, even when 'overcured' or 'undercured'. The subtle differences among different extents of cure cannot be reliably measured using currently available instruments.

The onset of oxidation does not distinguish highly cured (008 #1), moderately cured (#2), and poorly cured (#4) fibers (Table 5). This technique is therefore unsatisfactory and not worth further investigation as a measure of extent of cure.

The pull-out or adhesion test presents a unique situation. Our experience indicates a number of difficulties with the test procedure, but the proposed FOTP is still in the draft stage. With better controls and instructions, it could become a useful and meaningful test, and it does warrant further exploration.

It should be noted here that our test program, while extensive, was not all-inclusive. Differential scanning calorimetry (DSC) should distinguish among different extents of cure by differences in the glass transition temperature,  $T_g$ ; however, initial efforts to use this technique gave such poor results that we chose not to pursue it. Also, although we have not yet pursued thermal mechanical analysis (TMA), either static or dynamic measurements could have sufficient sensitivity to differentiate among various extents of coating cure.

While none of the tests we performed are without drawbacks, many of them appear to be sensitive and reproducible. Both FTIR and DPC involve relatively expensive apparatus - in the case of DPC, a specialized instrument with limited uses in a manufacturing facility. The ERA apparatus is less expensive, but the results appear to be strongly dependent upon the characteristics of the coating. All of these tests can give answers in a matter of minutes using less than 1m of fiber, although repetitive testing to increase confidence takes longer. Similar advantages in speed, sample size, and sensitivity apply to the TGA weight loss test, although again a relatively expensive piece of apparatus is required. The extraction test, in contrast, uses relatively inexpensive apparatus but consumes up to 250m of fiber for each test. Also, several days may be required to prepare, condition, extract, dry, and recondition the samples, which could be unacceptable in a manufacturing environment.

The water/solvent soak technique for measuring weight gain or loss suffers from similar problems. Although different extents of cure can be identified, the ability to rank order the samples depends upon the solvent, duration, temperature, and the time allowed for reconditioning (Figure 4). Two to five days may be necessary to precondition, soak, and recondition the samples. In addition, the small changes in weight necessitate either a very sensitive balance or relatively large volumes of fiber (and appropriately large soak baths).

Abrasion resistance and strip force tests both provide results in about an hour for multiple samples, and both use only a few meters of fiber. Both relate to field performance, since they measure characteristics that are significant when the fiber is handled, e.g., for splicing. A significant drawback is that they do not distinguish highly cured from poorly cured coatings. Abrasion resistance decreases at the extremes (Table 6) due to brittleness at high cure and softness at low cure. Strip force increases at low cure (Table 6) because the coating buckles, rather than sliding off as a rigid tube. If it is necessary to determine whether the cure is high or low (for example, to control process parameters), additional tests are necessary.

Fiber strength, while clearly affected by the extent of coating cure, has varying sensitivity for different coatings (Table 6). Because of its relevance to long-term fiber performance, it would be premature to discontinue study of this technique. Test environments more stressful than ambient temperature and humidity, different rates for applying stress or strain, and bending (and/or torsion) all warrant further exploration.

The data indicate that measurements of the curing reaction (FTIR, DPC, ERA, and extraction) offer the most promise. Aside from TGA weight loss, these provide the only values that increase (or decrease) monotonically with cure dose. All measurements 'saturate' at high extents of cure: 008 sample #2 was exposed to about 60% of the UV dose for #1, yet both samples give comparable values for % RAU, residual J/g, and % extractables (Table 3). The ERA data show saturation for the 133 samples, although not for the 008 samples. For TGA weight loss, reduced sensitivity extends to 008 #3 as well. Figure 5 plots %RAU, residual J/g, ERA index and total count, strength, and % extractables for 008 samples 2 - 4 (plotted proportional to their relative doses). All data show apparent linearities, indicating that linear relationships may exist among these cure indicators and with long-term fiber strength. However, data must be collected for a wider range of coatings before any correlation is used in a predictive manner.

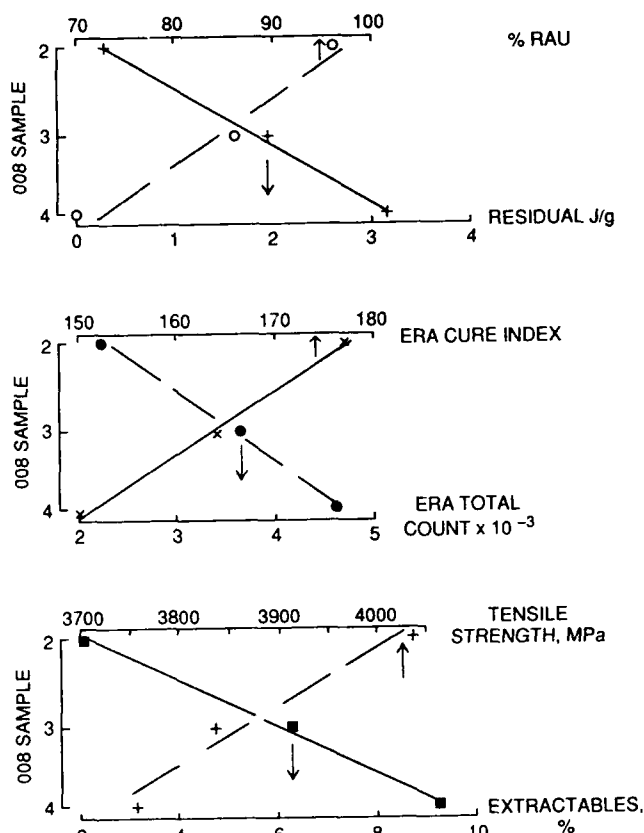


FIGURE 5. EXTENT OF CURE INDICATORS VS. DOSE FOR 008-COATED FIBERS

### CONCLUSIONS

Our data indicate that the techniques used to evaluate the extent of cure of fiber coatings fall into three categories. Dielectric measurements, hydrogen generation, and oxidation onset are among those that lack the sensitivity to differentiate among varying extents of cure, even for very different UV doses. Water/solvent soak, abrasion resistance, and strip force have adequate sensitivity; however, the first requires the accurate measurement of small and variable changes, while the latter cannot differentiate highly cured from poorly cured coatings. FTIR, DPC, ERA, and solvent extraction form the third category, offering promise for providing sensitive and reproducible measures of the extent of cure; in fact, a standard extraction procedure already exists. While the dependence of the test results upon UV cure dose must be established independently for individual coatings, our data indicate that the remaining techniques should be actively pursued with a goal of developing additional industry-standard test procedures.

### ACKNOWLEDGEMENTS

We gratefully acknowledge the following for their assistance: Trevor Bowmer, for many helpful suggestions; Hakan Yuce, for the strength and strip force data; Matt Andrejco, for drawing the sample fibers; Jim Julian, for the FTIR data; and Ron Domingo, for the hydrogen generation data.

### REFERENCES

1. Pasternak, G., Anderson, D. G., Johnson, R. W., Leo, A. F., and Cutler, O. R., "Property Measurements of Acrylate Based Radiation Curable Coatings", *RADCURE '86 Conference Proceedings*, September 1986, p. 17-1.
2. Yuce, H. H., Plitz, I. M., Frantz, R. A., and Andrejco, M., "The Effects of Coating Cure on the Mechanical Characteristics of Optical Fibers", *Proceedings of the 39th International Wire and Cable Symposium*, November 1990, p. 715.
3. "Technical Manual for the Con-Trol-Cure® Ink Cure Analyzer™", Con-Trol-Cure, Inc., Chicago, IL, 1990.
4. Fiber Optic Test Procedures are available by number from the Electronic Industries Association, Engineering Department, 1722 Eye Street, N. W., Washington, DC 20006.
5. Venkataswamy, K., and Waack, R., "Rapid cure monitoring by microdielectrometry", *Plastics Engineering*, February 1988, p. 43.
6. Chawla, C. P., Bishop, T. E., Szum, D. M., and Murray, K. P., "New test method for determining the water sensitivity of optical fiber coatings", *Optical Engineering*, Volume 30, Number 6, June 1991, p.763.

**Rolf A. Frantz** is a Distinguished Member of Technical Staff in the Fiber Distribution and Reliability District at Bellcore. He holds BS and MS degrees from Cornell University and a PhD in engineering mechanics from Brown University. He joined Bell Laboratories, where his major responsibilities were in the field of electrical insulation, an area in which he continued to work upon joining Bellcore in 1983. Since 1988, he has focused on optical fiber coatings, particularly extent of cure, aging, and coating durability.



**Irene M Plitz** is a Member of Technical Staff in Bellcore's Polymer Chemistry and Engineering District. She received her BS in chemistry in 1970 from Morgan State University and directly joined Bell Laboratories. Since coming to Bellcore in 1984, her interests have centered on chemical and structural analyses of polymers with special focus on optical fiber coatings and cable materials.



**Steven R. Schmid** is a Technical Team Leader at DSM Desotech, Inc. He holds BS and MS degrees in chemistry from the University of Illinois and the University of Houston, respectively, and an MBA from the Illinois Institute of Technology. Since joining DeSoto in 1976, he has held positions in research, international licensing, market development, and product management. The radiation curing group of DeSoto was purchased by DSM in 1990. He is now responsible for coordinating the development of new radiation curable materials for optical fiber and cabling applications.



# "EFFECT OF CHEMICAL ENVIRONMENTS ON UV CURABLE OPTICAL FIBER COATINGS"

Chander P. Chawla, David M. Szum

DSM Desotech Inc.  
1700 S. Mount Prospect Rd.  
Des Plaines, IL 60017.

## Abstract

Optical fiber is being increasingly used in the subscriber loop and on customer sites, where it can be exposed to a wide variety of chemicals. These chemicals can affect the physical properties of protective inner and outer primary coatings, thereby endangering the mechanical reliability of the optical fiber. The effect of nine common chemical environments on the dynamic mechanical properties of ultra-violet (UV) light curable inner and outer primary coatings was studied. The glass transition temperatures of most of the coatings were found to increase in most of the environments. The equilibrium moduli were largely unaffected for most of the coatings in most of the environments. Dynamic weight change revealed that some inner primary coatings swelled considerably compared to the outer primary coatings. From the dynamic weight change and dynamic mechanical data, approximate values of solvent-coating interaction parameters were calculated for two coatings.

## INTRODUCTION

Stringent demands are being placed on optical fiber coatings to protect the relatively fragile glass fiber. As fiber to the home becomes reality, it is important for organic coatings to protect fiber after exposure to some common household chemicals.<sup>1</sup> The effects of hydrocarbon gels and other cable filling compounds on the coating and fiber has been reported.<sup>2,3</sup> While much work has been done on the effects of water on coatings<sup>4</sup> and glass fibers<sup>5-8</sup>, not much work has been published on the effects of various other chemicals on fiber optic coatings.

This paper focuses on the changes of coatings after exposure to various common chemicals. These changes were monitored by Dynamic Mechanical Analysis (DMA) and by a dynamic weight change test. Chemicals for this test were chosen to encompass as broad a range of polarities and solvent properties as possible. The DMA test was chosen because any  $T_g$  or crosslink density changes can be easily recognized by this extremely sensitive test. The weight change test was included to illustrate the affinity of the chemicals for the coatings. Dual coat construction, which includes a low modulus inner primary and a high modulus outer primary coating, is a widely used fiber structure. For this study, both types of materials were studied. Both commercial and developmental coatings are included in the study.

## EXPERIMENTAL

### Coating Preparation

All coating formulations were prepared in a similar manner using reactants and diluents obtained from the manufacturers without further purification.

The oligomers were weighed into eight-ounce lined steel cans. The remaining ingredients were added and the cans placed in a 60°C oven for one hour. The contents were then blended with an air mixer for fifteen minutes on a hot plate. Each solution was filtered through an extra-fine ADTEC filter cone into a new, cleaned, lined steel can and was centrifuged at 1500 rpm for five minutes to remove bubbles.

See Table I for a list of coatings that were tested and the approximate equilibrium moduli of the resulting cured films.

Table I. List of Coatings Used in the Study and Their Approximate Moduli

Coating #	Type	Equilibrium modulus, Mpa
1	Inner Primary	2.1
2	Inner Primary	2.2
3	Inner Primary	1.2
4	Inner Primary	2
5	Inner Primary	1.1
6	Inner Primary	2.5
7	Inner Primary	3.1
8	Outer Primary	24
9	Outer Primary	22
10	Outer Primary	36
11	Outer Primary	21
12	Outer Primary	23
13	Outer Primary	26
14	Outer Primary	13

### Film Preparation

Each coating was drawn down on a clean 9" x 12" glass plate using a Pacific Scientific Automatic Drawdown Apparatus and either a Gardner 3 mil or 6 mil bird bar film applicator. The higher modulus coatings were drawn down to a nominal thickness of 3 mils while the lower modulus coatings were drawn down to a nominal thickness of 6 mils. The coatings were cured to 100% of their ultimate moduli using a Fusion Systems Model K523/2 Fusion Unit. Two films were prepared for each coating sample.

### Dynamic Mechanical Analysis

One film for each coating sample was cut into ten to twelve 0.5" x 8" rectangular strips for Dynamic Mechanical Analysis (DMA). All strips were preconditioned at 60°C for one hour to minimize any water present in the coatings from the atmosphere humidity. The following chemical substances were used in the test:

WD-40 Lubricant Spray

Unleaded Gasoline

Acetone

1,1,1 Trichloroethane

Isopropyl Alcohol

Deionized Water

5.25% Bleach Solution

3.5% Ammonia Solution

Xylene Based Wasp and Ant Spray (Inner Primaries)

Water Based Wasp and Ant Spray (Outer Primaries)

One strip from each coating was submerged in a different chemical substance for a length of time dependent on the modulus. Low moduli coatings were exposed for 24 hours while high moduli coatings were exposed for 32 hours. The higher moduli coatings were submerged for a longer time to compensate for the higher crosslink densities and thus the longer diffusion times. One strip from each coating was used as an unexposed control. After exposure, all strips were postconditioned at 60°C for one hour to minimize any volatile chemicals left after submersion.

DMA data was obtained using a Rheometrics Linear Rheometer (Model RDSLA). The frequency was set at 1.0 radian/second.  $E'$ ,  $E''$ , and  $\tan \delta$  values were printed and plotted at two degrees intervals.

Before starting a DMA run, the sample was preheated to 80°C for a minimum of five minutes in the dry nitrogen atmosphere (1% RH) of the rheometer's environmental chamber to remove water or residual solvent that may have been present and could have acted as a plasticizer.

### Dynamic Weight Change of Coatings Submerged in Chemicals

The method used for this test was similar to the one presented by Chawla et al<sup>9</sup> except that other chemical substances were used in addition to distilled water. One film from each coating was used to measure the amount of a specific chemical substance that was absorbed by that coating. The following chemical substances were tested:

Water

Acetone

Gasoline

Isopropanol

WD-40

Three 1" x 1" samples were cut from the film for each chemical substance tested. Samples were dried in a 65°C oven for one hour and then cooled in a desiccator for ten minutes. Each sample square was weighed to the nearest 0.1 mg and then submerged in the chemical substances. The weight change was monitored at intervals after surface chemical was removed by patting dry with a Kim-Wipe tissue. This weight gain is recorded as a percentage of the initial dry weight of the sample.

### RESULTS AND DISCUSSION

A chemical can have two or three general types of behavior on a crosslinked polymer coating. The chemical may leach out any unbound material in the coating reducing plasticization. This would increase the apparent  $T_g$  of the polymer causing an undesirable change in the coating performance (any change after manufacture is an undesirable change).

The chemical may have an extreme affinity to the coating causing a plasticization effect. This could result in swelling or even delamination of the coating from the glass surface. In an extreme case, the chemical could actually attack the coating, thus causing a change in the cross-linked network of the coating matrix. In order to conduct a study of chemical effects on optical fiber coatings, it is desirable to have a test method which can detect all three of these possible effects. Dynamic Mechanical Analysis (DMA) was used to measure any change in glass transition temperature or crosslink density.

The ultra-violet (UV) light cured inner and outer primary optical fiber coatings are chemically cross-linked. They also contain some residual material (e.g. unreacted photoinitiator or monomers) which do not become a part of the cross-linked network. This material generally acts as a plasticizer and depresses the  $T_g$  of the cured coating. When a cured coating is immersed in a chemical substance, the non-cross-linked plasticizer material can be extracted out, thereby raising the  $T_g$  of the coating. It is expected that the amount of extractable material is in direct proportion to the increase in the  $T_g$ . The other effect of immersion of cured coatings in different chemical substances is the possible chemical attack on the coating material which may affect the cross-link density and hence the equilibrium modulus ( $E_0$ ) of the coating.  $E_0$  is directly proportional to the cross-link density<sup>10</sup>. Large shifts in  $E_0$  indicate a chemical attack on the coating.

In addition to changes in  $T_g$  and  $E_0$  (which are measured after the solvent has been evaporated by reconditioning), the UV curable coating can swell when placed in a solvent. The swelling is a result of absorption of solvent material. The swelling of a cured coating in a particular solvent will depend upon the cross-link density of the coating and the solvent-polymer interaction parameter<sup>11</sup>. The dynamic weight change of the cured coatings is a measure of swelling in various solvents. In general it is expected that, given the same basic polymer structure, the value of the cross-link density will be in direct inverse proportion to the amount of solvent absorbed by a coating.

The chemicals used in this study cover a wide range of environments with which the optical fiber may come in contact. These include polar (acetone, isopropanol, water), non-polar (unleaded gasoline,

WD-40), alkaline (liquid ammonia solution), and biologically and chemically active (wasp and ant spray, bleach solution) environments. The optical fiber coatings studied include very soft, low modulus, low cross-link density, and low glass transition temperature ( $T_g$ ) inner primary coatings; and very high modulus, high cross-link density outer primary coatings.

### Effect of Household Chemical Exposure on the Dynamic Mechanical Properties of Inner Primary Coatings

Glass Transition Temperature ( $T_g$ ) Changes The results of the DMA analysis for inner primary coatings are summarized in Table II.  $T_g$  changes are measured as changes in the maximum of the tan delta peaks. The error of the measurement is approximately  $\pm 4^\circ\text{C}$ .

Table II.  $T_g$  Changes for Inner Primary Coatings in Different Household Chemicals.

Coating #	$T_g$ Shifts ( $^\circ\text{C}$ ) in different household chemicals								
	WD-40	UG	Acn.	TCE	IPA	DI H <sub>2</sub> O	Bleach	NH <sub>3</sub>	W&A Spray
1	-3	+4	+5	+5	+4	0	0	0	+2
2	+2	+4	+5	+4	+5	+1	+1	+2	+4
3	-7	+2	+3	+2	+1	+1	+2	-1	+2
4*	-3, +3	+2, +6	-2, +6	0, +5	0, +7	+2, +5	+2, +5	+4, +5	+2, +5
5	-26	+20	+20	+22	+20	+7	+5	+5	+16
6	-15	+2	+3	+3	0	+1	-1	-2	-3
7		+6	+8			+3			

UG	Unleaded Gasoline
Acn.	Acetone
TCE	1,1,1 Trichloroethane
IPA	Isopropanol
DI H <sub>2</sub> O	Deionized Water
Bleach	5.25% Bleach Solution
NH <sub>3</sub>	3.5% Ammonia Solution
W&A Spray	Wasp and Ant Spray (Xylene based)

\* Coating 4 exhibited two tan delta peaks. Both value changes are recorded.

Most of the coatings exhibited increases in  $T_g$  after exposure due to the extraction of non-cross-linked material. Figures 1 and 2 have been included as examples of  $T_g$  shifts. Figure 1 shows the DMA curve for coating 4 before immersion, and Figure 2 shows the DMA curve after immersion in isopropanol and then reconditioning. A shift in the tan delta curve is observed, indicating a corresponding change in the  $T_g$ .

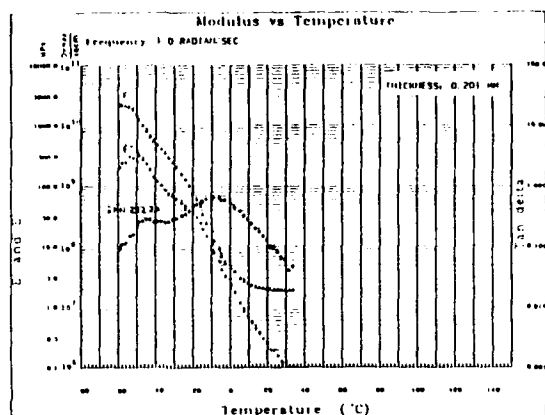


Figure 1. DMA Plot for Coating 4 Before Immersion in Isopropanol.

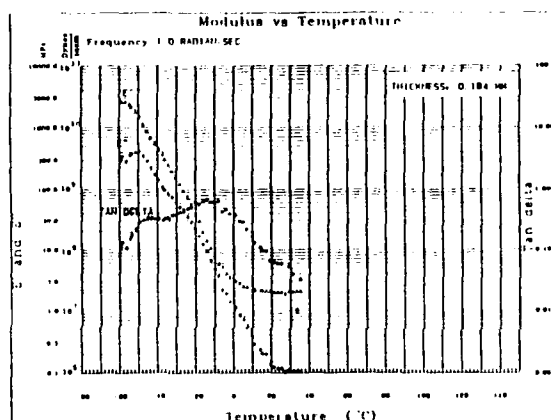


Figure 2. DMA Plot for Coating 4 After Immersion in Isopropanol and Reconditioning.

The only exception to the general shift to higher  $T_g$  after exposure were those coatings exposed to WD-40. Due to the lower volatility of this material it is not fully removed from the coating upon reconditioning. The coating is plasticized by residual WD-40 resulting in a lower  $T_g$  (as evidenced by the observed shift in the tan delta curves).

The inner primary coatings tested included very low water absorbing coatings 5 and 6. Compared to coating 6, coating 5 contains a large amount of extractables. Both of these coatings show a relatively large decrease in the  $T_g$  in WD-40, which could be due to high absorption and retention of WD-40 by these coatings due to their hydrocarbon nature.

The changes in the  $T_g$  for most of the coatings were very small after exposure to all of the household chemicals indicating the presence of relatively small amounts of extractable materials. Coating 5, however, shows a large increase in the  $T_g$  in most of the chemical substances implying the presence of large amounts of extractable materials.

Coating 4 exhibits interesting behavior. Two separate  $T_g$ 's are observed implying the presence of a two phase system, with each phase having its own glass transition temperature. The shifts in the  $T_g$  for both the phases are slightly different. The lower  $T_g$  phase shows somewhat smaller changes compared to the higher  $T_g$  phase. One possible explanation of this behavior is that most of the extractable material is present in the higher  $T_g$  phase.

**Equilibrium Modulus ( $E_0$ ) Changes** The results of  $E_0$  measurements for inner primary coatings are summarized in Table III. The changes in  $E_0$  were found to be much smaller compared to the changes in the  $T_g$ .  $E_0$ , as discussed earlier, is directly proportional to the cross-link density of a material. Exposure to household chemicals does not seem to be affecting the cross-link density. Thus it appears that these coatings exhibit good stability in the presence of household chemicals.

Table III.  $E_0$  Changes for Inner Primary Coatings in Different Household Chemicals.

Coating #	$E_0$ Shifts (MPa) in different household chemicals								
	WD-40	UG	Ac.	TCE	IPA	DH <sub>2</sub> O	Bleach	NH <sub>3</sub>	W&A Spray
1	+0.15	+0.1	+0.1	+0.1	+0.15	+0.05	+0.05	+0.2	+0.1
2	-0.2	-0.15	-0.25	-0.15	-0.2	-0.3	-0.25	-0.25	-0.3
3	-0.3	0	-0.05	0	-0.05	-0.15	-0.15	-0.15	-0.1
4	-0.25	-0.15	-0.1	-0.1	+0.1	-0.15	-0.15	-0.15	-0.15
5	+0.1	+0.05	+0.05	+0.05	+0.1	+0.05	+0.15	-0.1	0
6	0	+0.2	+0.05	0	0	0	+0.4	+0.2	-0.1
7		+0.1	+0.15			+0.1			

UG	Unleaded Gasoline
Ac.	Acetone
TCE	1,1,1 Trichloroethane
IPA	Isopropanol
DH <sub>2</sub> O	Deionized Water
Bleach	5.25% Bleach Solution
NH <sub>3</sub>	3.5% Ammonia Solution
W&A Spray	Wasp and Ant Spray (Xylene Based)

**Effect of Household Chemical Exposure on the Dynamic Mechanical Properties of Outer Primary Coatings**

**Glass Transition Temperature ( $T_g$ ) Changes** The results of  $T_g$  measurements of outer primary coatings are summarized in Tables IV. As with the inner



primary coatings, the  $T_g$ 's were found to increase after exposure to household chemicals due to the extraction of the non-cross-linked material. The glass transition temperatures of most of the outer primary coatings either remained constant or showed a slight decrease after exposure to WD-40 compared to some of the inner primary coatings which showed a large decrease in  $T_g$  after exposure to WD-40. This difference can be explained by the fact that the outer primary coatings have a tighter network structure and thus high molecular weight components of WD-40 are absorbed at a greatly reduced rate.

Table IV.  $T_g$  Changes for Outer Primary Coatings in Different Household Chemicals.

Coating #	$T_g$ Shifts ( $^{\circ}\text{C}$ ) in different household chemicals								
	WD-40	UG	Ac.	TCE	IPA	DI H <sub>2</sub> O	Bleach	NH <sub>3</sub>	W&A Spray
8	-5	+3	+2	0	0	-1	-3	0	-5
9	0	+4	+3	+2	+4	0	+2	+2	-4
10	0	+3	+4	+3	+4	+2	0	+9	-1
11	+2	+8	+8	+7	+10	+4	+4	+9	-2
12	-3	+3	+2	+1	+3	-1	0	+2	-5
13	0	+4	+10	+4	+9	+1	0	0	-5
14	+4	+7	+17	+8	+12	+6	+4	+8	+3

UG Unleaded Gasoline  
 Ac. Acetone  
 TCE 1,1,1 Trichloroethane  
 IPA Isopropanol  
 DI H<sub>2</sub>O Deionized Water  
 Bleach 5.25% Bleach Solution  
 NH<sub>3</sub> 3.5% Ammonia Solution  
 W & A Spray Wasp and Ant Spray (Water Based)

Coatings 11 and 14 show a comparatively large change in the  $T_g$ 's after exposure to the household chemicals indicating the presence of a large amount of extractable material. The other coatings tested show relatively small changes (if any) indicating relatively low extractable contents.

**Equilibrium Modulus ( $E_0$ ) Changes** The results of the  $E_0$  measurements for outer primary coatings are shown in Table V. The changes in  $E_0$ , just as for primary coatings, are very small for most of the coatings. This implies no change in cross-link density and no chemical attack on the coating. Coatings 10 and 11 are exceptions, and show a very significant change in  $E_0$  upon immersion in bleach solution. This indicates that these coatings are chemically attacked by the bleach solution and the cross-link density is significantly increased. Figures 3 and 4 show DMA curves of coating 10 before and after immersion, in the bleach solution.

Table V.  $E_0$  Changes for Outer Primary Coatings in Different Household Chemicals.

Coating #	$E_0$ Shifts (MPa) in different household chemicals								
	WD-40	UG	Ac.	TCE	IPA	DI H <sub>2</sub> O	Bleach	NH <sub>3</sub>	W&A Spray
8	0	0	-1.0	-1.5	-1.0	-0.5	-0.5	0	0
9	-0.5	0	-2.0	-1.5	-1.5	0	+2.5	+0.5	-1.0
10	-0.5	0	-2.5	-1.0	0	-2.0	+32.5	+4.5	-2.0
11	+2	+1.0	+0.5	+1.0	+1.5	0	+8.0	+2.0	-0.5
12	+0.5	+0.5	-1.0	-0.5	+0.5	-0.5	+0.5	+1.0	+0.5
13	-1.0	-1.5	-0.5	-1.5	-1.0	-1.0	-2.0	-1.0	-2.0
14	+1.0	-0.5	-1.5	+0.5	0	-0.5	0	+1	0

UG Unleaded Gasoline  
 Ac. Acetone  
 TCE 1,1,1 Trichloroethane  
 IPA Isopropanol  
 DI H<sub>2</sub>O Deionized Water  
 Bleach 5.25% Bleach Solution  
 NH<sub>3</sub> 3.5% Ammonia Solution  
 W&A Spray Wasp and Ant Spray (Water Based)

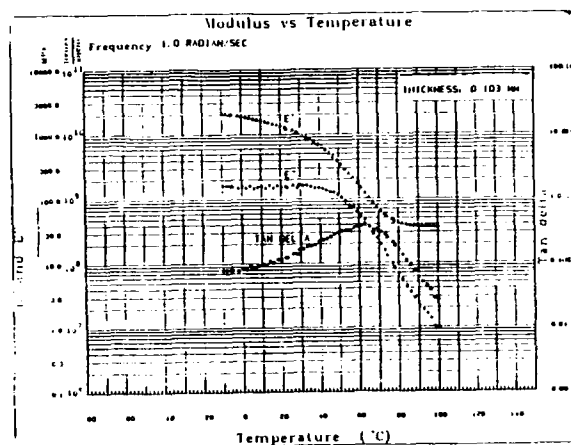


Figure 3. DMA Plot for Coating 10 Before Immersion in Bleach Solution.

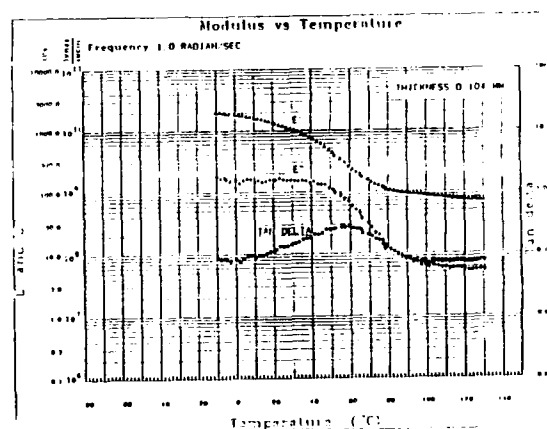


Figure 4. DMA Plot for Coating 10 After Immersion in Bleach Solution and Reconditioning.

## Summary of the Effect of Household Chemical Exposure on the Dynamic Mechanical Properties of Optical Fiber Inner and Outer Primary Coatings

Most of the inner and outer primary coatings tested showed good resistance to most of the household chemicals. Inner primary coating 5 showed the presence of a large amount of extractable material (large  $T_g$  shifts) in almost all the test materials. Inner primary coating 4 also showed comparatively larger  $T_g$  shifts. Among the outer primary coatings, 14 (and coatings 11 and 13 to some extent) showed the largest  $T_g$  shifts. Outer primary coatings 9 and 10 showed unusually large changes in  $E_o$  in the bleach solution.

### Dynamic Weight Change Study

A dynamic weight change study of some of the inner and outer primary coatings was undertaken to get an idea of the physical state or swelling of these coatings in different household chemicals (Tables VI and VII). The inner primary coatings showed up to ~90% weight increase in acetone and gasoline. This increase in weight was very rapid. The outer primary coatings on the other hand showed up to ~30% weight increase in both the solvents. The weight increase was rapid in acetone and much slower in gasoline for the outer primary coatings. The data presented in Tables VI and VII is only approximate for acetone and gasoline due to the inaccuracies involved in measuring the weight change of the coatings in volatile solvents. The smaller weight increase for the outer primary coatings is due to a higher cross-linked density ("tighter network") and a more rigid structure, which resists solvent absorption and swelling. The inner primary coatings, on the other hand, have a much lower cross-link density.

Table VI. Maximum Weight Change of Some Inner Primary Coatings in Some Household Chemicals

Coating #	Maximum Weight Change, %				
	Water	Acetone	Gasoline	IPA	WD-40
1	1.15	61.6	35.1	28.3	27.3
3	6.42	73.7	66.3	-	-
4	2.75	66.2	71.3	-	-
7	2.14	67.9	27.3	63.1	31.9

Table VII. Maximum Weight Change of Outer Primary Coatings in Some Household Chemicals

Coating #	Maximum Weight Change, %				
	Water	Acetone	Gasoline	IPA	WD-40
9	1.95	23.1	19	13.0	4.6
10	4.53	26.3	14.7	8.5	3.4
13	1.83	26.7	19.5	-	-
14	7.12	28.4	28.2	-	-

Another factor affecting the solvent absorption is the solvent-coating interaction parameter. The weight changes of an inner and an outer primary coating were measured in isopropanol and WD-40 (Tables VI and VII). These household chemicals were chosen for their relatively low volatility. Isopropanol is a relatively polar solvent and WD-40 is a relatively non polar substance. Figures 5 and 6 show the plots of weight change versus time of the inner primary coating 7 and the outer primary coating 10, respectively. Inner primary coating 7 (Figure 5) exhibits a rapid weight increase in the first few hours followed by a weight decrease due to extraction. The outer primary coating 10 (Figure 6), shows similar behavior albeit a much less significant increase in isopropanol.

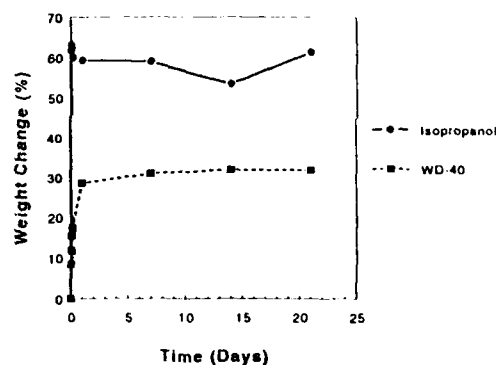


Figure 5. Weight Change Versus Time for Coating 7 in Isopropanol and WD-40.

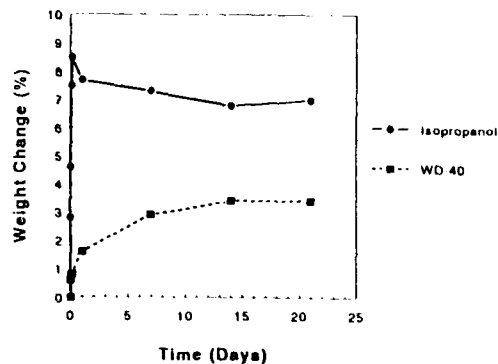


Figure 6. Weight Change Versus Time for Coating 10 in Isopropanol and WD-40.

Both inner and outer primary coatings show a significant amount of extractable material thus explaining the  $T_g$  increase discussed earlier. The weight change in WD-40 is much lower for both the coatings compared to that in isopropanol. Inner primary coating 7 absorbs significantly more WD-40 than outer primary coating 10. Again, due to the higher molecular weight components of WD-40, the diffusion is much slower through a polymer network resulting in a slower increase of the weights of the coating than in isopropanol. Both of the coatings showed increased weights upon reconditioning after 3 weeks immersion in WD-40. The increase is much larger for the inner primary coating 7 (15%) compared to the outer primary coating 10 (1.2%). This is reflected in the large decrease in  $T_g$  for the inner primary coatings and the minimal decrease for the outer primary coatings.

The data for weight change in water are also presented in Tables VI and VII. The comparatively lower weight gains are due to lower affinity of these coatings to water.

#### Solvent-Coating Interaction Parameter Calculation

The extent of swelling of a coating depends on the cross-link density and the solvent-polymer (coating) interaction parameter. The Flory-Rehner equation shown below, relates swelling, cross-link density, and solvent-polymer interaction parameter<sup>10</sup>.

$$-(\ln(1 - v_2) + v_2 + X_1 v_2^2) = V_1 n (v_2^{1/3} - v_2/2) \quad (1)$$

where  $v_2$  is the volume fraction of the polymer in the swollen mass,  $V_1$  is the molar volume of the solvent, and  $X_1$  is Flory-Huggins interaction parameter.

$$n = \rho_2 / M_c \quad (2)$$

where  $\rho_2$  is the polymer (coating) density and  $M_c$  the molecular weight between cross-links. Assuming tetrafunctional cross-links

$$n = 2 C_x \quad (3)$$

Equation (1) can be rewritten as

$$-(\ln(1 - v_2) + v_2 + X_1 v_2^2) = V_1 \cdot 2 \cdot C_x (v_2^{1/3} - v_2/2) \quad (4)$$

Volume of the swollen polymer is given by the following equation<sup>12</sup>

$$V_s = w_0 / \rho_2 + (w_s / \rho_1 - w_0 / \rho_1) \quad (5)$$

where  $w_0$  = weight of the cured coating sample  
 $w_s$  = weight of the swollen coating sample  
 $\rho_1$  = density of the solvent

From the dynamic weight change method, the peak absorption gives the maximum amount of solvent that can be absorbed by the coating (assuming no extraction). The equilibrium modulus of the coating from DMA gives the cross-link density of the coating. Knowing the densities of the solvent and coating, and knowing the molar volume of the solvent, an approximate value of the interaction parameter can be calculated. Generally a value of 0.5 for the interaction parameter would indicate no solvent-polymer interaction (i.e. no swelling and the solvent acts as a theta solvent). Values below 0.5 would indicate some solvent-coating interaction. The smaller the decrease below 0.5, the larger the interaction (swelling).

Based on DMA and dynamic weight change data, interaction parameters for primary coating 4 and secondary coating 10 in isopropanol were calculated and found to be 0.77 and 1.40 respectively. The maximum value of interaction parameter is supposed to be 0.5 for most solvent-polymer combinations. Though higher than expected, these numbers still give a good comparison between the inner and outer primary coating behavior in isopropanol. The larger positive number for the outer primary coating indicates a lesser affinity for isopropanol than the inner primary coating.

#### CONCLUSIONS

As optical fiber to the home becomes a reality, there is a potential for exposure to many household chemicals. This study shows that UV curable coatings can be formulated to resist the effects of many household chemicals. Exposure effects can be measured by DMA free film testing and plasticizer loss can be distinguished from chemical attack on the coatings. To be most resistant, coatings should be formulated to have very low extractable content and should also be resistant to different chemical environments with which they can come in contact with. The dynamic weight change study shows that primary coatings absorb significantly more solvent than the secondary coatings due to their low cross-link densities. The cross-link density data from DMA and swelling data from dynamic weight change can give a rough idea about the solvent-coating interaction parameter.

## Acknowledgements

The authors would like to acknowledge Steven Schmid and Kevin Murray for their valuable suggestions. The authors would also like to acknowledge Dr. Robert Johnson for the DMA work; and Roger Salvesen and Andrew Hickman for assistance in the dynamic weight change experiments.

## References

1. H. H. Yuce, *Optical Fiber Communication Conference Technical Digest*, 1, 171(1990).
2. O. S. Gebizlioglu, and I. M. Plitz, *Optical Engineering Journal*, 30, No.6, 749(1991).
3. Y. Yamzaki, H. Horima, H. Igarashi, and K. Niikura, *Proceedings of the 39th Int. Wire and Cable Symp.*, 190(1990).
4. D. M. Szum, C. P. Chawla, T. E. Bishop, K. P. Murray, and J. M. Zimmerman, *Proceedings of the 39th Int. Wire and Cable Symp.*, 703(1990).
5. T. T. Wang, and H. M. Zupko, *J. Mater. Sci.*, 13, 2241(1978).
6. H. H. Vazirani, H. Schonhorn, and T. T. Wang, *Optical Society of America*, Topical Meeting on Optical Transmission, Williamsburg, VA February 22-24, 1977.
7. T. T. Wang, H. M. Zupko, H. H. Vazirani, and H. Schonhorn, *J. rad. Curing*, 10, 22(1977).
8. T. T. Wang, H. N. Vazirani, H. Schonhorn, and H. M. Zupko, *J. Appl. Polym. Sci.*, 23, 887(1979).
9. C. P. Chawla, T. E. Bishop, D. M. Szum, and K. P. Murray, *Optical Engineering Journal*, 30, No.6, 763(1991).
10. L. H. Sperling, "Introduction to Physical Polymer Science", John Wiley and Sons, 1986.
11. P. J. Flory, "Principles of Polymer Chemistry", Cornell University Press, 1983.
12. E. A. Collins, J. Bares, and F. W. Billmeyer, "Experiments in Polymer Science", John Wiley and Sons, 1973.



Chander P. Chawla received his Ph.D. in polymer science from the University of Southern Mississippi in May 1990. He obtained a master's degree in polymer science and technology from the Indian Institute of Technology, New Delhi, in 1984, and a master's degree in chemistry from the University of Delhi, New Delhi in 1982. He has been working in the area of fiber optic coatings since October 1989. He is currently a senior research chemist in the optical fiber coatings group of DSM Desotech Inc.



David M. Szum received an MS in Chemistry from the University of Illinois at Chicago. He is currently a research chemist for DSM Desotech Inc. He has been engaged in research and development of coatings for optical fibers since January 1989. He is also a member of EIA/TIA working committees 6.6.7, fiber coatings, and 6.6.8, fiber reliability.

# UV RESISTANCE PROPERTY OF UV-CURED RESIN COATED OPTICAL FIBER

T. Hosoya and Y. Matsuda

Sumitomo Electric Industries, Ltd.  
1, Taya-cho, Sakae-ku, Yokohama, Japan

## Abstract

Ultra violet (UV) resistance property of UV-cured resin coated optical fiber was studied. For appropriate indices to evaluate UV degradation, weight change, glass transition temperature ( $T_g$ ) and hydrogen generation were proposed. Measuring the  $T_g$  change ( $\Delta T_g$ ) of the coating by mechanical  $\tan \delta$  method, we studied the relationship between  $\Delta T_g$  and low temperature excess loss of an exposed fiber. And it was found that the degree of the excess loss could be excellently estimated by the value of  $\Delta T_g$ .

The UV cut-off effect of ink layer overcoating was studied using this method. In result, UV-cured ink showed high performance to protect UV-cured resin coating from UV-degradation.

## 1. Introduction

With the progress of the optical fiber network for subscriber requirements, the possibility that the fiber has taken the weathering degradation (especially UV degradation) is certainly increasing. UV-cured resins, such as urethane-acrylates, are very widely used for optical fiber coatings today, however it is also well known that some of them are adversely affected by exposure to UV-light, and in the worst, suffer fatal damages with decomposition-reactions.

In spite of these circumstances, there are much less data of the UV resistance properties of UV-cured resin coated optical fibers, because of the difficulty to treat very thin and weak coating sample. Moreover, the simulation test using resin sheet has also other difficulty. We must keep the thickness of the resin sheet sample equal to that of the fiber coating if we need a quantitative experiment, because UV degradation property of a resin shows large thickness dependence. However,

traditional test methods measuring tensile modulus or elongation are not suitable for these small and thin samples.

Under these situations, we investigated alternative evaluation methods for UV degradation from a viewpoint of the sensitivity to decomposition of resin structure, and developed some new practical methods which could apply to the thin and small sample and have high sensitivity to UV degradation.

## 2. Mechanism of UV degradation

UV degradation reaction of UV-cured resin, especially polyurethane resin, is widely investigated.<sup>1,2)</sup> The most popular model for degradation is that the main damage occurs through the scission of C-H, C-C, C-O and C-N bond in the urethane groups. An assumed scheme of the bond scission is shown in Fig. 1.

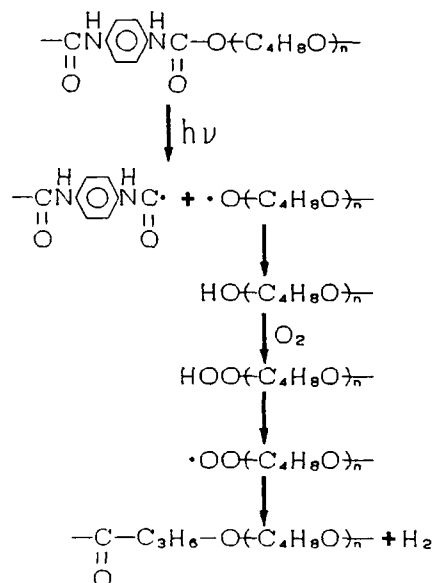


Fig. 1 Main-chain Scission of Urethane-acrylates

C-O bond which connects polyether and isocyanate is easily cut off UV light, and the auto-oxidation of polyether follows, which leads the hydrogen abstraction and the generation of  $H_2$ .

These urethane bond scission reactions cause decrease of the cross-linking density, which leads  $T_g$  change, and finally the decomposition of the resin.

For these reasons, we examined the possibility that hydrogen generation increase,  $T_g$  change and weight decrease could be applied to the index of UV degradation.

### 3. Evaluation of UV-cured resin sheet

UV degradation reaction occurs on the surface of the resin at first, and progress to the deep area little by little. Under the heterogeneous degradation like this, mechanical tests, tensile modulus or elongation for example, can not be in use for the correct evaluation.

This is the reason why mechanical tests are very insensitive in UV degradation compared with other environmental degradation such as heat or humidity. Moreover, in order to consider the thickness dependence, we have to keep test samples very thin, ordinary at  $10\text{--}30\text{ }\mu\text{m}$  which value corresponds to the thickness of optical fiber coating.

This restriction also makes the mechanical test very difficult. In this sense, measuring Weight change is one of the possible practical method using UV-cured resin sheet sample.

We applied a UV-gravimetry method for these samples and obtained proper data in wide thickness range of a sample.

Fig. 2 shows the relationship between the thickness of initial sample and the weight decrease ( $\Delta W$ ) of a UV-cured resin. Samples which have various thickness between  $25$  and  $200\text{ }\mu\text{m}$  were prepared by spin-coating method, and exposed to UV-light by Sunshine-weather-o-meter.

From the thickness- $\Delta W$  curve in Fig. 2, it is clear that  $\Delta W$  is almost independent on the sample thickness, though it have a good correlation with UV dose. This result proves that UV degradation is essentially a heterogeneous degradation where the surface reaction is dominant. As the degradation progress, there can be seen the tendency that thinner sample shows slower down of weight decrease speed. We think it is for the saturation of UV degradation reaction, because the weight decrease reaches more than 10% of initial value at thinner sample.

Fig. 3 shows the time degradation curve of a resin at  $25$ ,  $50$  and  $100\text{ }\mu\text{m}$  thickness. It seems that thicker sample shows better UV durability compared to thinner sample.

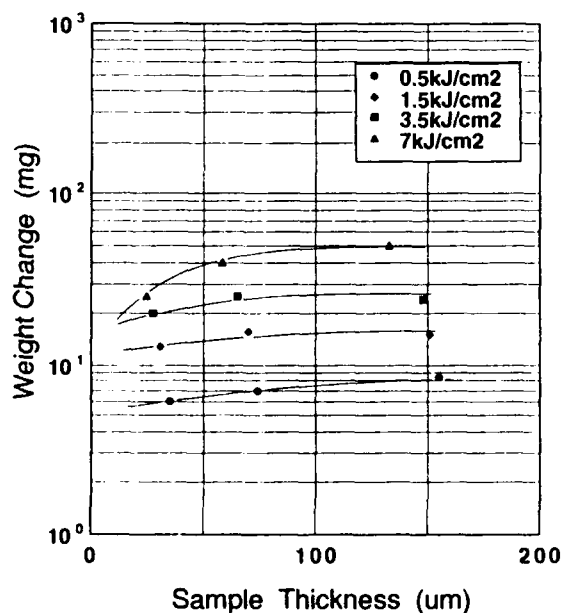


Fig. 2 UV Degradation Curve of UV-cured Resin Sheet

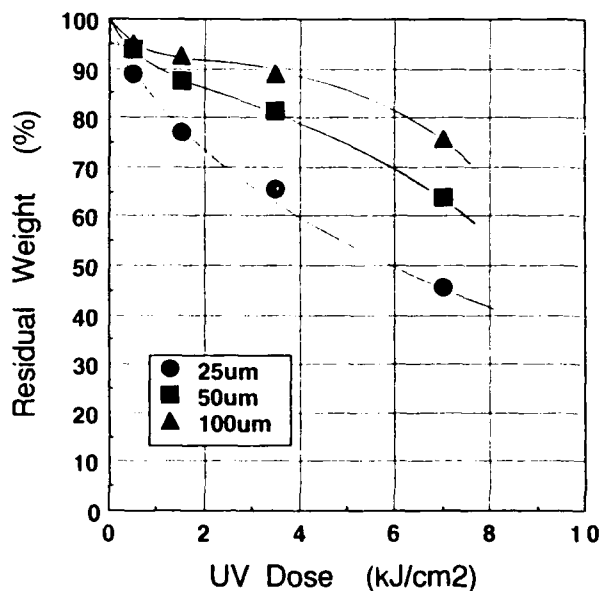


Fig. 3 Time-Degradation Curve of UV-cured Resin Sheet

#### 4. Evaluation of fiber coatings

##### 4-1. Measuring method

UV-gravimetry is a very useful method to evaluate the UV durability of UV-cured resin sheet. However, this method is not suitable for a very small sample or the sample which was exposed at outside for an environmental test, because of the increase of measuring error derived from the sample size or the outer contamination such as dust.

Recently, dynamic mechanical measurement is widely used for the analysis of the mechanical behavior of polymer-glass composite.<sup>3)</sup> In this study, we newly developed the Tg evaluation method by measuring Tan  $\delta$  peak temperature of optical fiber coating.<sup>4)</sup>

As explained at Fig. 1, UV degradation of UV cured resins such as urethane-acrylates involves the main-chain scission reaction, which decreases Tg of resins. We measured mechanical Tan  $\delta$  of the UV-cured resin coating in a certain temperature range to get the value of Tg.

The measurement was achieved by using a dynamic mechanical analyzer with a glass-removed coating sample (Fig. 4).

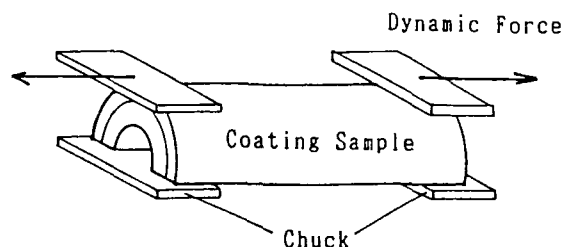


Fig. 4 Figure of a Sample

The instrument used for measuring is Rheovibron dynamic viscoelastometer. The block diagram of the instrument essentially consists of a drive amplifier, a strain and stress detector, a high and low temperature chamber, a stress detector, a tension controller and a process control unit. In this system, a vibration displacement of sine wave is applied on the sample under the constant-amplitude control. This instrument detects the vibration load signal of the sine wave to define the dynamic property.

##### 4-2. Non inked fiber

Typical Tan  $\delta$  -Temperature curve of the coating is shown in Fig. 5. The peak at 90°C correspond to Tg of outer layer coating of a dual coated optical fiber ('A'). Two dotted lines in Fig. 5 are Tan  $\delta$  -Temp. curves after the fiber was exposed to sun light for 7 and 60 days (maximum dose is approximately 500J/cm<sup>2</sup>).

A distinct decrease of Tg can be observed after UV irradiation, which means decrease of the cross-linking density of the resin. After the 60 days exposure,  $\Delta T_g$  reaches to  $\sim 60^\circ\text{C}$  and the figure of Tan  $\delta$  - Temp. curve is greatly distorted, which indicates the fatal damage of main-chain in the resin.

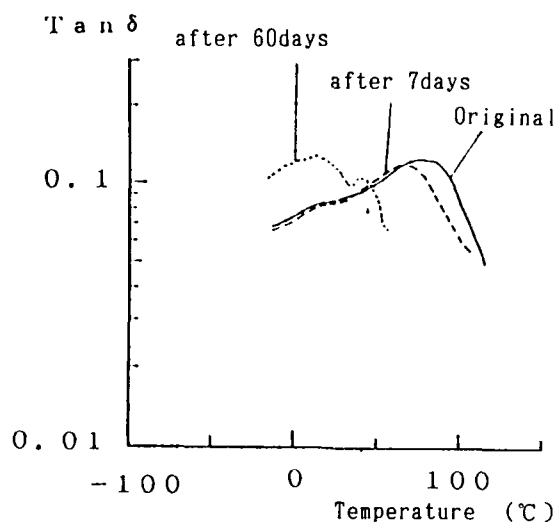


Fig. 5 Tan  $\delta$  -Temp. Curve of Fiber Coating 'A'

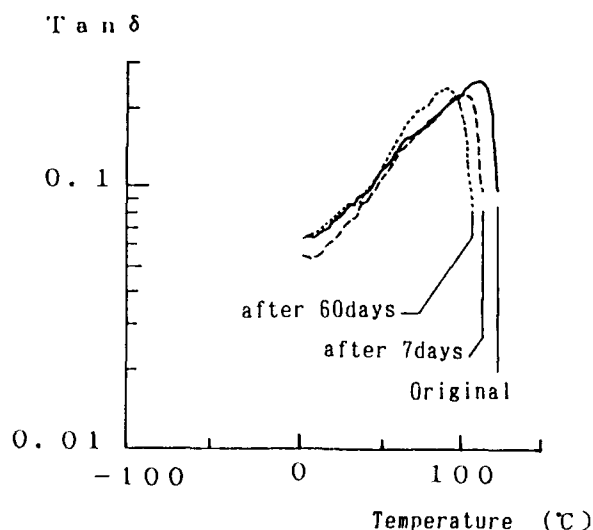


Fig. 6 Tan  $\delta$  -Temp. Curve of Fiber Coating 'B'

Fig.6 shows another  $\tan \delta$ -Temp curves of the fiber coating ('B') which has excellent UV transmissivity and UV durability. In this case, after 60 days there is little  $T_g$  change of the coating. The transmission loss and the low temperature excess loss of these fibers before and after UV dose were measured (Table1). For the fiber 'A' which has  $-60^\circ\text{C}$  of  $\Delta T_g$ ,  $+0.024\text{dB/km}$  of  $-40^\circ\text{C}$  excess loss was observed, while there is no excess loss was seen for the sample 'B' whose  $\Delta T_g$  is equal to  $-19^\circ\text{C}$ .

Table 1  $-40^\circ\text{C}$  Excess Loss after UV Irradiation

Fiber	$T_g$ ( $^\circ\text{C}$ )		$-40^\circ\text{C}$ Excess Loss ( $\Delta\text{dB/km}$ at $1.55\mu\text{m}$ )	
	original	60days	original	60days
A	75	15	$\pm 0.000$	$+0.024$
B	111	92	$\pm 0.000$	$\pm 0.000$

In order to shorten the degradation time, we studied the relationship between the sun light irradiation and the accelerated irradiation using UV-carbon-arc lamp.

Fig.7 shows the curve of  $T_g$  decrease of resin 'B' under the environment of both sun light and UV-carbon-arc lamp. From this result, the accelerate coefficient of UV-carbon-arc lamp is proved to be estimated to 20 times of sun light.

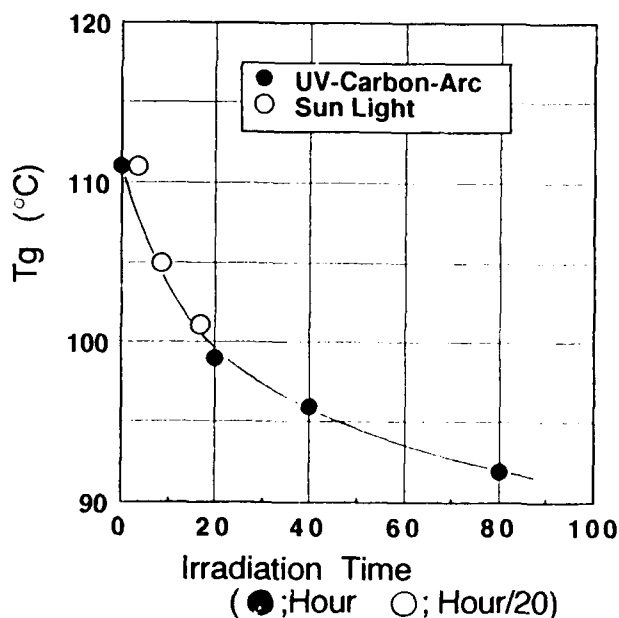


Fig.7  $T_g$  Degradation Curve

#### 4-3. Inked fiber

Overcoating with ink is one of the best way to protect fiber coating from UV because of its excellent UV cut-off effect. In order to evaluate this effect, two types of ink, solvent-type ink and UV-cured ink, were overcoated on the optical fiber 'A' with  $\Delta T_g$  of  $-60^\circ\text{C}$ .

The result is shown in Fig.8.  $T_g$  decrease was greatly improved in the case of inked optical fibers. Observed  $\Delta T_g$  was  $-8^\circ\text{C}$  on the solvent-type ink and only  $-4^\circ\text{C}$  on the UV-cured ink after  $500\text{J/cm}^2$  UV irradiation. This value is almost equal to that of the fiber whose coating has excellent UV durability.

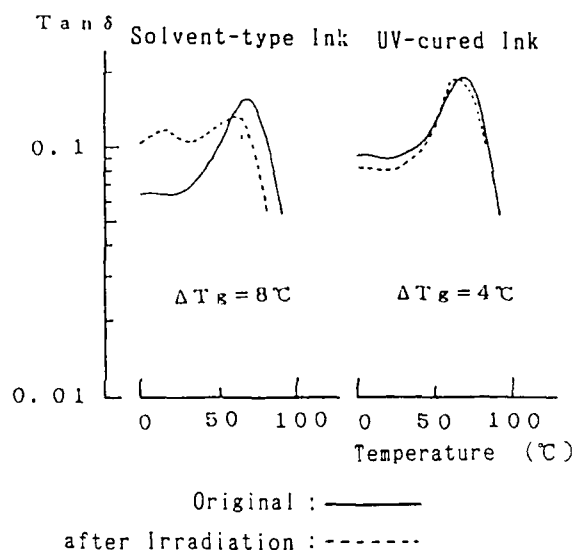


Fig.8  $\tan \delta$ -Temp. Curve of Inked Fiber Coating

These effects were concluded to be derived from the UV cut-off effect of the pigment in the ink, and the difference between the UV-cured ink and the solvent type ink was explained by that of the coating thickness of ink.

Table2 shows low temperature property of inked optical fibers, both before and after UV-irradiation. The effect of overcoating by UV-cured ink can be also seen in the data of low temperature excess loss.

Table 2 Transmission Loss of Inked Fiber

Overcoat Layer	Transmission Loss at $1.55\mu\text{m}$ (dB/km)			
	Original		500J/cm <sup>2</sup> Irradiation	
	23 $^\circ\text{C}$	-40 $^\circ\text{C}$	23 $^\circ\text{C}$	40 $^\circ\text{C}$
Solvent type Ink	0.20	0.20	0.20	0.22
UV-cured Ink	0.20	0.20	0.20	0.20



## 5. Hydrogen generation

As the UV-cured resin suffers UV irradiation, the volume of hydrogen generation increases in proportion to the UV dosage exposed to the UV-cured resin. Because the increase of hydrogen generation directly affects the transmission loss of optical fiber, it is important to estimate the volume of H<sub>2</sub> generation after UV irradiation.

We defined the rate of H<sub>2</sub> generation from a coated optical fiber as the time to reach 10<sup>-3</sup> ml/m of H<sub>2</sub> concentration at 120 °C, and measured the rate after exposure of various UV dose.

Theoretically, the rate must be in proportion to the powers of the UV dose amount. But the experiment data indicate the equation as follows:

$$1/v = A - B \cdot \log(x)$$

where  $v$ : H<sub>2</sub> generation rate     $x$ : UV dose  
A, B: coefficient

Fig. 9 shows the relationship between H<sub>2</sub> generation rate and UV dose. In the UV dosage range of 0 ~ 10000 mJ/cm<sup>2</sup>, this equation seems to be valid.

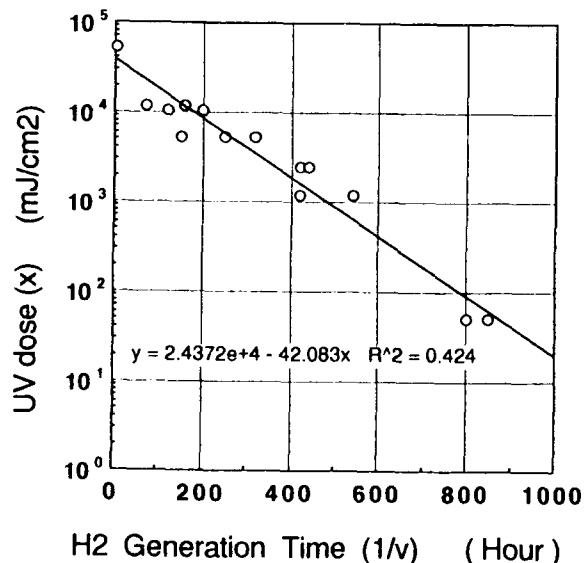


Fig.9 The Relationship between H<sub>2</sub> generation rate and UV dose

## 6. Conclusion

New methods to evaluate the UV resistance property of the optical fiber coating easily and correctly were studied. We proposed three sorts of indices for an proper judgement of UV resistance property as follows and evaluated the characteristics of them:

- (1) weight decrease
- (2) change of glass transition temperature
- (3) increase of hydrogen generation

Weight decrease of resin sheet was measured by UV-gravimetry method. In this experiment, the resin which had higher transmissivity was proved to show excellent UV durability.

In order to evaluate the UV degradation of optical fiber coating sample with high sensitivity, we developed  $\Delta T_g$  method by dynamic viscoelastometer.

Using this method, the effect of ink overcoating was clearly observed. Especially UV-cured ink was proved to have a good UV cut-off efficiency to protect inner coating.

As to hydrogen generation, new equation was proposed to estimate the generation amount from the UV dose.

## Reference

- 1) V. Rek and M. Bravar  
"The Effect of Ultraviolet Irradiation on Polyurethane Solution and on Solid Polymer"  
J. Elastomers and Plastics, 12, 245, (1980)
- 2) M. E. Abu-Zeid, E. E. Nofal and L. A. Tahseen,  
"Photoacoustic Study of UV, UV-Thermal, and Weathering Degradation of Rigid Foam Polyurethane"  
J. Appl. Pol. Sci., 29, 2443, (1984)
- 3) T. Hosoya and S. Masuda, "Analysis of Transmission Characteristics of Dual Coated Fiber by Dynamic Mechanical Method", 14th ECOC, Brighton, United Kingdom, Tech Digest, vol. 1, 522-525, (1988)
- 4) T. Hosoya, N. Akasaka, Y. Matsuda, T. Yamanishi and S. Ito, "UV Degradation Characteristics of UV Resin Coated Optical Fiber", 1990 Autumn National Convention Record, The Institute of Electronics, Information and Communication Engineers, Part 4, 8-679, (1990)



Toshifumi Hosoya

Sumitomo Electric  
Industries, Ltd.

1. Taya-cho, Sakae-ku,  
Yokohama 244, Japan

Toshifumi Hosoya received the M. S. degree in Reaction Chemistry from Tokyo University in 1985. He joined Sumitomo Electric Industries, Ltd in 1985, and has been engaged in research and development of optical fiber and cables. Mr. Hosoya is a member of Chemical Society of Japan and Material Life Society of Japan.



Yasuo Matsuda

Sumitomo Electric  
Industries, Ltd.

1. Taya-cho, Sakae-ku,  
Yokohama 244, Japan

Yasuo Matsuda received the M. S. degree in Industrial Chemistry from Tokyo University in 1978. He joined Sumitomo Electric Industries, Ltd in 1978, and has been engaged in research and development of optical fiber and cables. Mr. Matsuda is now a chief research associate of Transmission Media R & D Department.

# LONG-TERM RELIABILITY OF A CARBON COATED OPTICAL FIBER CABLE

T. Akiyama, Y. Kawada, H. Hiramatsu, and K. Hirabayashi

The Furukawa Electric Co., Ltd.

6, Yawatakaigandori, Ichihara, Chiba, 290, Japan

## Abstract

A harsh field test was conducted in order to confirm the long-term reliability of a carbon coated fiber cable. A ribbon/slot cable, in which water was intentionally injected to generate hydrogen inside the cable, was installed in aerial condition for about 1.5 years and the loss change was measured periodically. As a result, it was revealed that no loss increase in carbon coated fibers was detected even after 1.5 years. The test data clearly show that carbon coating protects completely optical fibers from the generated hydrogen and UV coatings have high performance against microbending in actual installation condition. This promising results are expected to further advance the optical fiber technology toward the practical use of carbon coated fibers.

## I. Introduction

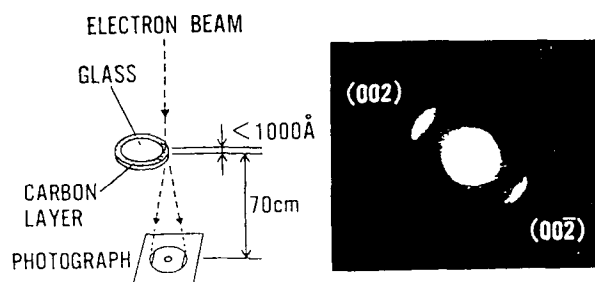
Carbon coated fiber is known to have excellent characteristics ever found for preventing permeation of hydrogen and in fatigue. In recent progress, problems preventing carbon coated fibers from the practical application, were almost solved, which were related to the coating speed<sup>1,2</sup>, the initial strength, and fusion splice<sup>3,4</sup>. And carbon coated fiber is expected to be a hopeful candidate applied to the undersea, aerial, and other special cables which are subjected to harsh environments, and has been attracting great attention as practical fibers that drastically enhance long-term reliability of cables.

On the final stage toward its practical use, we conducted a harsh field test, where water was forcibly injected into the cable and it was installed in aerial condition for about 1.5 years. This paper describes the field test results including the initial characteristics of the cable and also superior fatigue and hydrogen resistance of carbon coated fiber itself.

## II Characteristics of carbon coated fiber

### 1. Microstructure of carbon

The carbon coating layer is a single composition of carbon that doesn't contain impurities and is nearly amorphous. Nevertheless, a more detailed examination by electron beam diffraction and other techniques has shown that the layer structure actually contains a fixed amount of graphite. Fig. 1 shows an electron diffraction photograph of the carbon coating. In addition to a hollow pattern peculiar to the amorphous structure, a clear Debye-Sherrer ring due to (002) lattice plane shows that the graphite crystalline plane is positioned C-axis orientation to the optical fiber surface. This structure is more conspicuous with carbon layer exhibiting more resistance against permeation of hydrogen. These results have indicated the importance of the crystalline structure of carbon coating layer.



ACCELERATION VOLTAGE ; 200kV  
BEAM DIAMETER ; 0.1 $\mu$ m

Fig. 1 Electron Diffraction Photograph of Carbon Coating

## 2. Fatigue and strength

It is well known that the standard fiber exhibits the fatigue behavior particularly in the presence of moisture. The static fatigue plots are shown in Fig. 2. Although the breakage of all the standard fibers occurred at a strain of over 3.3% in water within 400 hours, the carbon coated fibers have survived for more than 3 months. From Fig. 2, fatigue parameter  $n$  for carbon coated fiber have not yet been determined, but it is estimated to be more than 500 by alternate dynamic fatigue test. This result suggests that the carbon coating on optical fiber prevents water reaching the silica surface, thus the

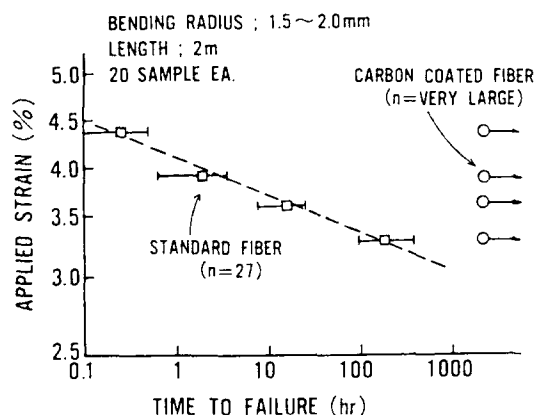


Fig. 2 Static Fatigue of Fiber in Water

carbon coated fiber exhibits negligible strength degradation caused by stress corrosion.

And now the strength of the carbon coated fiber is approximately 6kgf(4.8GPa) which is just the same as that of the standard fiber.

## 3. Hydrogen resistance

The carbon coated fiber can greatly improve fiber reliability by preventing hydrogen induced loss increase.<sup>4),5)</sup> As described by Lemaire,<sup>6)</sup> the concentration of  $H_2$  in the core position as a function of time can be expressed by Eqs. (1) and (2), assuming that the diffusivity of  $H_2$  is much higher in silica than that in the carbon coating:

$$(C-C_i)/(C_r-C_i)=t/\tau_r \quad (1)$$

Where  $C$  is the concentration in the fiber,  $C_i$  is the initial concentration, and  $C_r$  is the final concentration. The characteristic time constant,  $\tau_r$ , is given by:

$$\tau_r=r\delta/2D_cK_{cs} \quad (2)$$

Where  $r$  is the fiber radius,  $\delta$  is the carbon coating thickness,  $D_c$  is the diffusivity of the solubility of  $H_2$  in the carbon coating, and  $K_{cs}$  is the ratio of the solubility of the carbon coating to that in silica.

We apply this model to our carbon coated fibers. Fig. 3 shows the loss increase at 1.24  $\mu$ m tested in  $H_2$  of 1atm at elevated temperatures. The Arrhenius plots of the calculated values for  $\tau_r$  are shown in Fig. 4. Using an estimated activation energy of 95.3kJ/mol,  $\tau_r$  is given by:

$$\tau_r(\text{days})=2.1 \times 10^{-15} \exp(95.3\text{kJ} \cdot \text{mol}^{-1}/RT) \quad (3)$$

From Eq. (3), it is possible to estimate the loss increase under various conditions. For example, the estimated loss increases at 1.3 and 1.55  $\mu$ m operating windows are both less than 0.001dB/km after 20 years in a hydrogen atmosphere of 1atm at 5  $^{\circ}$ C. (On the other hand, the loss increases the standard fiber under the same conditions are estimated to be 0.3 and 0.4dB/km at 1.3 and 1.55  $\mu$ m, respectively)

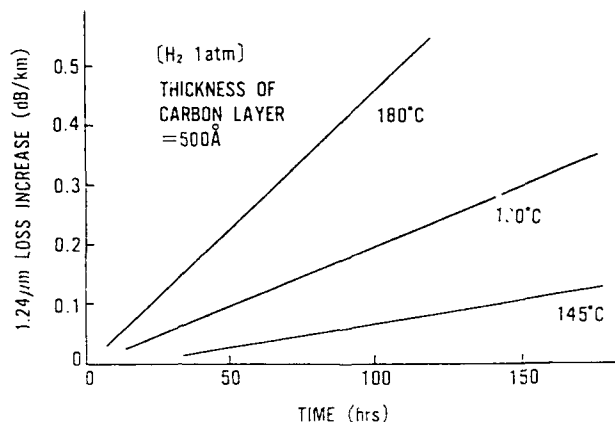


Fig. 3 Growth of Interstitial Peak at  $1.24 \mu\text{m}$  Wavelength in  $\text{H}_2$  1atm at Elevated Temperature

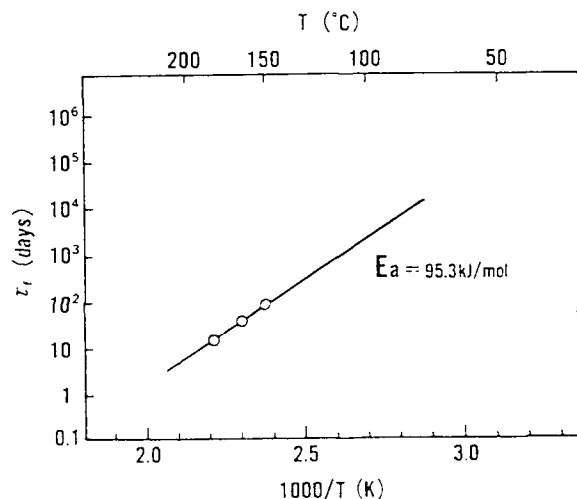


Fig. 4 Arrhenius Plots of Calculated Values for  $\tau$

### III. Characteristics of tested cable

The carbon coated fiber is expected to exhibit no strength deterioration even if it is left with a high applied stress and no transmission loss increases even if hydrogen generates around it. Therefore, carbon coated fiber is a promising candidate to be used in submarine cables and other purposes which require high long-term reliability. Moreover cable structure can be simplified if carbon coated fibers are used.

### 1. Structure of cable

We selected a ribbon/slot structure as a carbon coated fiber cable for a field test. Fig. 5 shows the cross-sectional structure of the tested cable. Single mode optical fibers for  $1.3 \mu\text{m}$  use were used in the cable. In one slot groove, five ribbons were alternately stacked by the carbon coated fiber ribbon and the standard fiber ribbon as reference. Steel wire 1.4mm in diameter was used as the strength member. A wrapping tape was wound on the slot and LAP (Laminated Aluminum Polyethylene) sheath was extruded on the wrapping tape. The cable outside diameter was 13mm and the cable weighed 170kg/km.

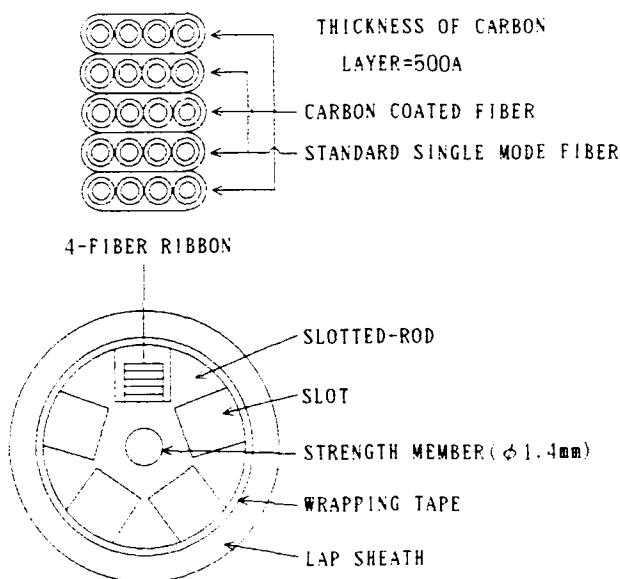


Fig. 5 Structure of the Cable

### 2. Initial characteristics

Fig. 6 shows the transmission loss variation in the processes of the cable production. The loss variations due to processing were not found for both carbon coated fibers and standard fibers.

Fig. 7 shows temperature cycling test of the cable. Loss changes within the temperature range between  $-30$  and  $+60^\circ\text{C}$  were  $0.05\text{dB/km}$  maximum, which presents no problems in actual use.

Bending, lateral pressing, torsion, squeezing and impact tests were conducted to evaluate the mechanical characteristics of the carbon coated fiber cable. Table 1 presents the conditions and results of these tests. As the table indicates, the cable showed no loss increases in all these tests for both carbon coated fibers and standard fibers.

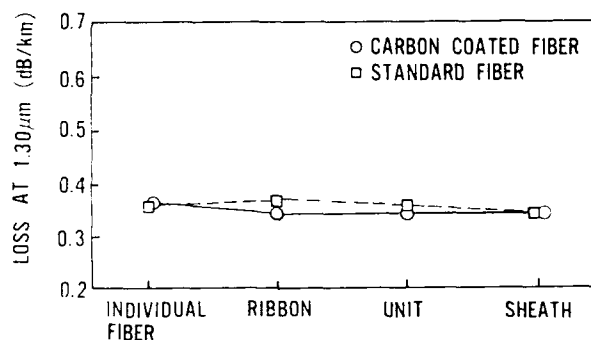


Fig. 6 Loss Variation in Cabling Process

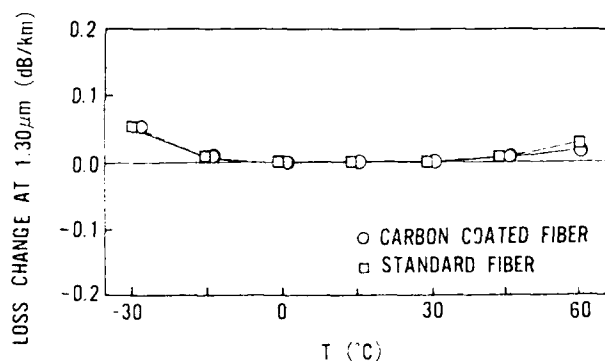


Fig. 7 Result of Temperature Cycling Test

### 3. A field test

An installation experiment was conducted using the test cable to check the long-term reliability of carbon coated fibers. In order to accelerate the environmental damage, we forcibly injected water into the cable and blew it by  $N_2$  gas for 24 hours. Then keeping the inside of the cable moist, both ends of the cable were sealed. 500m of the cable was installed in aerial condition for 1.5 years. The attenuation change with wavelength was measured periodically, as shown in Fig. 8. The attenuation in the standard fiber was gradually increased with the installation time. Especially the increase at around  $1.24 \mu m$  wavelength due to hydrogen diffusion was significant, since hydrogen was generated by corrosion or galvanic reaction with water and aluminum in the LAP sheath or steel wire as the strength member. One year after installation, the loss increases had reached about 16dB/km, which was estimated to be approximately 2atm in the hydrogen partial pressure inside the cable. On the other hand, in spite of this harsh environment, no detectable attenuation increase was observed in the carbon coated fibers. And no fiber breakage occurred even for the standard fibers due to static fatigue in a moisture environment under the installation.

Moreover, in order to clarify the reliability of the carbon coated fiber cable, hard environmental tests

Table 1 Mechanical Characteristics of the Cable ( $\lambda = 1.3 \mu m$ )

Item	Condition	Loss change
Bending	Bending radius: 130mm $\times$ 10 times	< 0.01dB
	75mm $\times$ once	Sheath defects
	R.T. and -30°C	not found.
Lateral pressing	100kg/50mm	< 0.01dB
Torsion	$\pm 180^\circ$ /2m	< 0.01dB
Squeezing	Tension 20kg	
	Cable 125m, Tension 100kg	< 0.01dB
	Curved guide radius 600mm	Fiber strain
Impact	Squeezed twice	max. 0.29%
	Cylinder 1kg weight 25mm	< 0.01dB
	diameter dropped on cable from 1m height.	

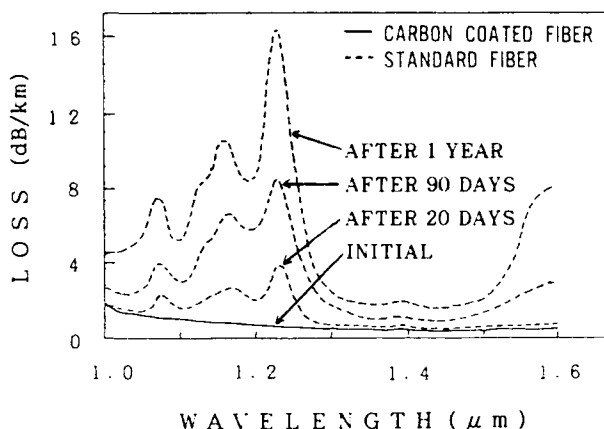


Fig. 8 Attenuation Spectrum

were carried out on the carbon coated fiber and the carbon coated fiber ribbon themselves. No attenuation increase was also observed due to microbending.

The long-term reliability evaluation indicated that neither transmission characteristics nor mechanical strength of carbon coated fibers would deteriorate at all even if water entered inside the cable.

#### IV. Conclusion

A field installation test was conducted to evaluate reliability of carbon coated fiber cable. In spite of harsh environment, no loss increase was observed after 1.5 years installation. The long-term reliability of optical fiber cable in transmission and mechanical characteristics drastically improve by applying carbon coated fibers which have the excellent characteristics.

#### References

- 1) C.M.G. et al., OFC'89, PD8-1.
- 2) Y.KATSUYAMA et al., IWCS(1990) pp.197-503.
- 3) N.YOSHIZAWA et al., J.Lightwave Technol.1991.4, pp. 117-121.

4) R.G.Huff et al., OFC'88, TUG2(1988).

5) K.E.Lu et al., OFC'88, PD1-1.

6) P.J.Lemaire et al., Electr.Lett.24,1323(1988).

7) N.YOSHIZAWA et al., IWCS(1989) pp.603-610.



Tsutomu AKIYAMA

The Furukawa Electric  
Co., Ltd.

6,Yawatakaigandori,  
Ichihara,Chiba,290,Japan

Mr. Akiyama was born in 1966. He received B.S. degree in electric engineering from Waseda University in 1989 and joined The Furukawa Electric Co., Ltd.. He has been engaged in development of optical fiber cables.

He is a member of The Institute of Electronics, Information and Communication Engineers of Japan.



Yukihiro KAWADA

The Furukawa Electric  
Co., Ltd.

6,Yawatakaigandori,  
Ichihara,Chiba,290,Japan

Mr. Kawada was born in 1962. He received B.S., M.S., and Ph.D. degrees in chemical engineering from Niigata University in 1985, 1987, and 1990, respectively. Then he joined The Furukawa Electric Co., Ltd.. He has been engaged in development of optical fiber cables.

He is a member of The Institute of Electronics, Information and Communication Engineers of Japan.



Hideyo HIRAMATSU

The Furukawa Electric  
Co., Ltd.  
6, Yawatakaigandori,  
Ichihara, Chiba, 290, Japan

Mr. Hiramatsu was born in 1959. He received B.S. degree in electric engineering from Kyoto University in 1984 and joined The Furukawa Electric Co., Ltd.. He has been engaged in development of optical fiber cables.

He is a member of The Institute of Electronics, Information and Communication Engineers of Japan.



Kazuto HIRABAYASHI

The Furukawa Electric  
Co., Ltd.  
6, Yawatakaigandori,  
Ichihara, Chiba, 290, Japan

Mr. Hirabayashi was born in 1962. He received B.S. degree in engineering from Tokyo University in 1987, and joined The Furukawa Electric Co., Ltd.. He is now working on engineering of optical fiber production.

He is a member of The Institute of Electronics, Information and Communication Engineers of Japan.



# Carbon-Coated Polarization Maintaining Fibers for Compact Optical Gyro Module

Kazuto Hirabayashi Masayuki Nishimoto Yoshikazu Matsuda

THE FURUKAWA ELECTRIC CO., LTD.

## (ABSTRACT)

Carbon-coated polarization maintaining optical fibers have been highly upgraded in fatigue properties. It is revealed that the fatigue parameter "n" of the carbon-coated fibers go over 500, which enables the fibers to coil up in a diameter below 30mm, tolerating strain over 0.4%.

## 1. INTRODUCTION

It can serve to the purpose in miniaturizing an optical fiber gyroscope, to shorten a diameter of sensing coils, which used to be some 60 mm. As for a phase modulator and such, a bending diameter below 30mm is required of the wiring. To date, it has been well known as a typical means to select a smaller diameter (about  $80\mu\text{m}$ ) than the conventional one (about  $125\mu\text{m}$ ).<sup>1,2</sup> However, fibers of  $80\mu\text{m}$  diameter are susceptible to lateral pressure and unable to be fused into fibers of  $125\mu\text{m}$  diameter. As the alternative, it is recommended to apply "Carbon coating method", to polarization maintaining fibers, because the method assures long-term reliability on mechanical strength, resistance against lateral pressure,<sup>2,3</sup> and readiness for fusion splicing as a conventional method.<sup>3,4</sup> This report details the characteristics of carbon-coated polarization maintaining fibers for a compact optical gyro module.

## 2. Experimental Procedure

Fig.1 schematically shows the drawing process of carbon-coated polarization maintaining optical

fibers. A fiber of  $125\mu\text{m}$  diameter is drawn out of the preform rods with a stress-applying parts, and passed through a CVD reactor for carbon-coating, being jacketed with UV curable resin thereafter, to form the outer diameter into  $250\mu\text{m}$ . The thickness of carbon layers may be measured by an in-line conductivity monitor over the entire length. Therefore, it is revealed to be about  $500\text{\AA}$  on the average.

The tensile strength test and fatigue test were carried out for the assurance of long-term reliability of carbon-coated fibers. The tensile test resulted in a strain rate of 5%/min with a gauge length of 200mm at  $25^\circ\text{C}$  and 60% in humidity. Through with the tensile test over 25 specimens, the value corresponding to failure probability of 50% was assumed to be the failure strength. Dynamic fatigue test was performed to obtain fatigue parameter "n".

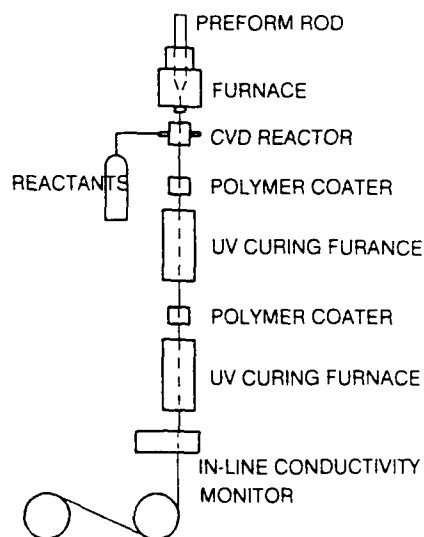


Fig. 1 A SCHEMATIC SHOWING  
THE DRAWING PROCESS

Moreover, carbon-coated and non-carbon-coated fibers were coiled around mandrels of 2.3~3.2mm and 10 specimens were prepared for one type of strain. They were left in both water and air at a room temperature for the examination on static fatigue. Sensing coils of carbon-coated fibers were prepared for vibration test, impact test, and heat cycle test. As to the vibration and impact test, increase in loss and degradation in crosstalk were determined. By the way, variation of crosstalk was observed from the heat cycle test.

### 3.Results and Evaluation

Table.1 shows the detailed properties of carbon-coated polarization maintaining optical fibers. There are seen a spread in specific refraction indexes, 1%, cutoff wave length,  $0.7\mu\text{m}$ , transmission loss at  $0.85\mu\text{m}$ , 2.0dB/km, birefringence,  $4.5\times 10^{-4}$  and crosstalk, -35dB at 1km.

Table 1. The properties of the carbon-coated polarization maintaining optical fibers

Fiber diameter	$\mu\text{m}$	125
Thickness of carbon layer	$\text{\AA}$	500
Coating diameter of resins	$\mu\text{m}$	250
Relative refractive-index difference	%	1.0
Cutoff wavelength	$\mu\text{m}$	0.70
Transmission loss at $0.85\mu\text{m}$	dB/km	2.0
Birefringence	-	$4.5\times 10^{-4}$
Crosstalk	dB at 1km	-35
Failure strength	GPa	4.71

The Weibull distribution in strength of carbon-coated polarization maintaining optical fibers, is plotted in figure.2 by contrast with the case of non-carbon-coated ones. The failure strength ( the value at 50% in failure probability ) of carbon-coated fibers was 4.7GPa, resulting in an increase by 0.24GPa compared to non-carbon-coated ones'.

Figure.3 shows the dynamic fatigue characteristics of the carbon-coated polarization maintaining fibers, by contrast with the case of conventional fibers in non-carbon-coating. A fatigue parameter "n" (>500) of the carbon-coated fibers is far greater than the conventional fibers' (24.8).

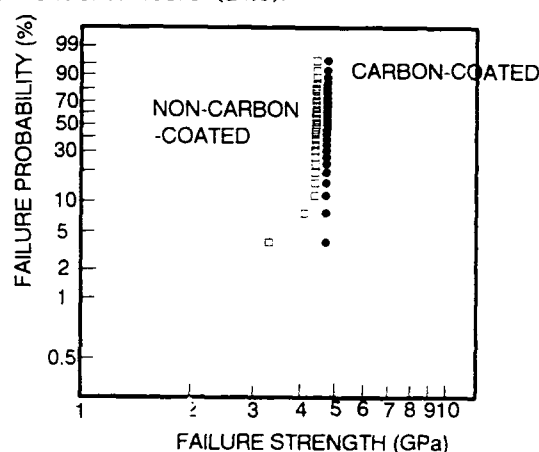


Fig.2 WEIBULL PLOTS OF CARBON-COATED AND NON-CARBON-COATED POLARIZATION MAINTAINING FIBERS

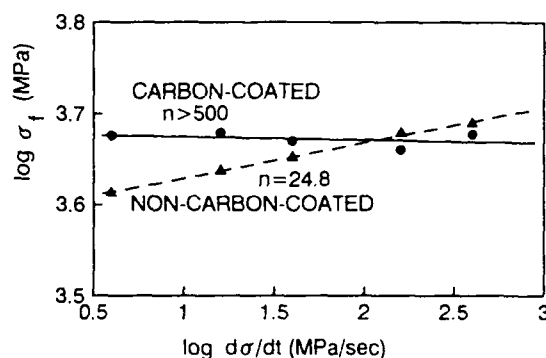


Fig.3 The dynamic fatigue properties of carbon-coated and non-carbon-coated polarization maintaining optical fibers

Figure.4 shows the static fatigue properties of carbon-coated fibers, by contrast with the fibers in non-carbon-coating. As for static fatigue parameters of the non-carbon-coated fibers, there are figured out 29.5 in the air and 27.4 in water. It is impractical to wind carbon-coated fibers around a mandrel smaller than 2mm in diameter. At that, no breakage was, in reality, found on the fibers wound around a mandrel of 2.3mm diameter, even though the fibers had remained wound over half a year. Consequently, the static fatigue parameter "n" seems to be quite a large one. From the Weibull distribution plots in strength and the fatigue properties, it is definitely interpretable that carbon-coated fibers far excel conventional fibers of non-carbon-coating, in enduring reliability on mechanical strength.

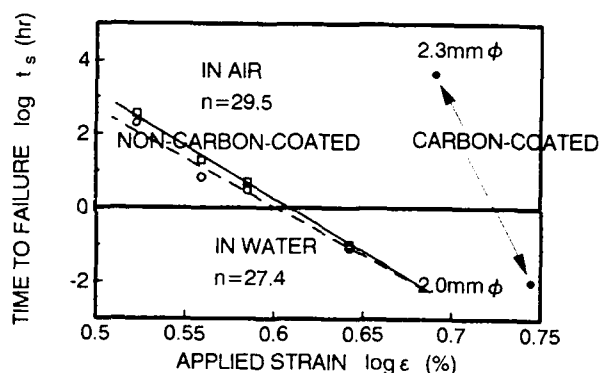


Fig. 4 The static fatigue properties of carbon-coated and non-carbon-coated polarization maintaining optical fibers

Figure.5 shows the appearance of a sensing coil and a phase modulator of carbon-coated polarization maintaining optical fibers. The properties of the sensing coil are epitomized in Table.2.

In figure 6, shown is the relationship winding diameter and crosstalk property of carbon-coated polarization maintaining fibers comprising the sensing coil and phase modulator. No degradation was observed from the crosstalk property up to 10mm in either way of winding length.

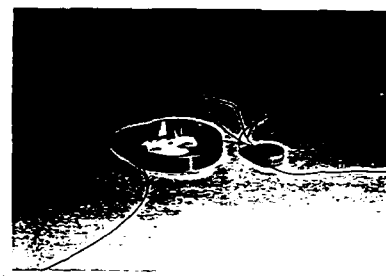


Fig. 5 Appearance of the coil and phase modulator made out of the carbon-coated polarization maintaining of optical fiber

Table 2. The properties of the carbon-coated fiber coil

Diameter of the coil	mmφ	74
Width of the coil	mm	12
Diameter of phase modulator	mmφ	27
Fiber length	m	150
Transmission loss	dB	0.5

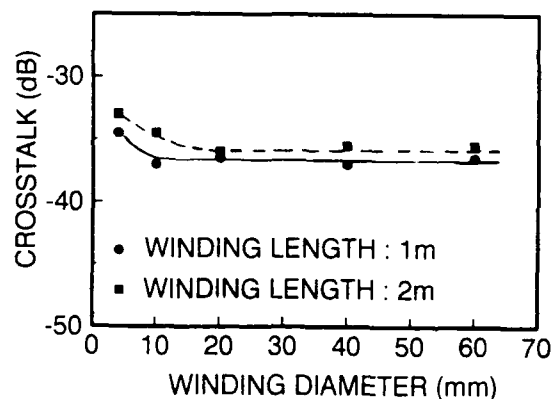


Fig. 6 Crosstalk of carbon-coated polarization maintaining optical fiber

Figure.7 shows the state, where the changes in crosstalk during the heat cycle test on the sensing coil of carbon-coated polarization maintaining optical fibers. After heat cycle was repeated four times over the range of  $-40 \sim 60^{\circ}\text{C}$ , no prominent deterioration was seen on the crosstalk property.

Table.3 shows the conditions and results from impact and vibration tests on the sensing coil of carbon-coated polarization maintaining optical fibers. Neither increase in loss nor degradation of crosstalk property was observed from both of tests.

As a result, it becomes clear that coils made out of carbon-coated fibers, have excellent resistance against impact and vibration, which is level with that of conventional non-carbon-coated ones.

Eventually, on the basis of the obtained value of fatigue parameter "n" value, we inferred the failure probabilities over 10 years on coiled carbon-coated fibers. As described by Mitsunaga<sup>4)</sup>, F, failure probabilities, can be expressed as follows,

$$F = 1 - \exp\left\{-\alpha N_p \frac{B_p/E^2(\epsilon_s^n t_s)^\beta}{(B/E^2) \epsilon_p^n t_p} \cdot L_o\right\} \quad (1)$$

$$\alpha = m/(n_p - 2)$$

$$\beta = (np - 2)/(n - 2)$$

F; Failure probability of optical fibers

$N_p$ ; The number of times of failure during proof tests

$L_o$ ; Length of optical fibers

$\epsilon_s$ ; Applied strain for use

$\epsilon_p$ ; Applied strain for proof test

$t_s$ ; period for use (=10 years)

$t_p$ ; period for strain for proof test to be applied (=1sec)

$m$ ; constant obtained from Weibull plots (=5)

$n$ ; fatigue parameter for use

$n_p$ ; fatigue parameter for proof test (=n)

$B$ ; constant defined by environment for use and materials

$B_p$ ; constant defined by conditions of proof tests (=B)

$E$ ; Young's modulus of optical fibers

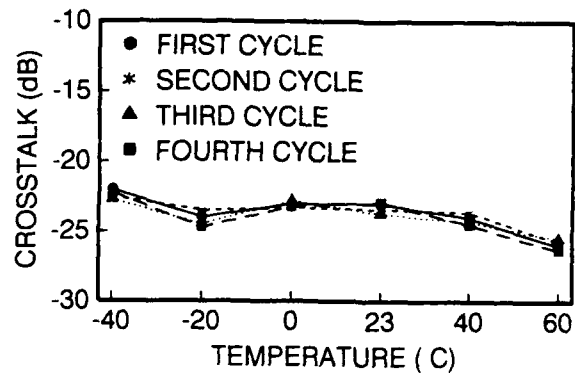


Fig. 7 Changes in crosstalk of the fiber coil during heat cycle test

Table 3. The results of impact tests and vibration tests of carbon-coated fiber coil

	Impact test	Vibration test
Test conditions	15G 11msec sine wave 3 times along every axes	5G 5~2000 Hz
Loss increase	>0.1 dB/km	>0.1 dB/km
Crosstalk degradation	>0.5 dB	>0.5 dB

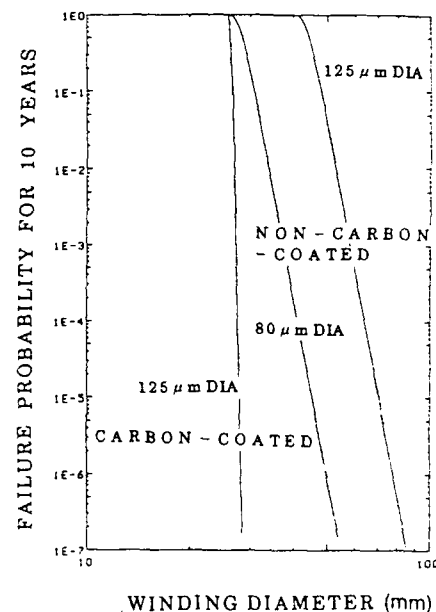


Fig. 8 Failure probability of carbon-coated and non-carbon-coated fiber coils

Figure 8 shows the results from the calculation of failure probabilities over 10 years on carbon-coated fibers of 125  $\mu\text{m}$  diameter and non-carbon-coated fibers of 80  $\mu\text{m}$  and 125  $\mu\text{m}$  diameter, throughout the range of winding diameter.

Through with the review of Figure.8, we have reached the conclusion that coils made out of carbon-coated polarization maintaining optical fibers excel ones made out of conventional non-carbon-coated fibers in lifespan.

#### 4.CONCLUSION

We developed carbon-coated polarization maintaining optical fibers, and analyzed the various properties. In conclusion, it is clarified that carbon-coated fibers enable a winding diameter of coils to go under 30mm, tolerating as much as 0.4% or over, while causing no degradation of polarization maintaining properties.

#### ( REFERENCE )

- 1) Nakamura et al., IEICEJ'88 Autumn National Convention Record C-267
- 2) K. Hirabayashi et al., IEICEJ Technical Report Vol.91 No.61 CS 91-16
- 3) Dary Inniss et al., OFC'91 ThG4
- 4) Y. Mitsunaga et al., J. Appl. Phys., Vol.53, 4847, 1982



Kazuto Hirabayashi was born in Wakayama, Japan, on July 13, 1962. He received the B.E. degree in engineering from Tokyo University, Japan, in 1987. In 1987 he joined The Furukawa Electric Co. Ltd., where he has been engaged in research on fabrication of fiber cables. Currently, he is working on engineering of optical fiber production.

Mr. Hirabayashi is a member of the Institute of Electronics and Communication Engineers of Japan.



Masayuki Nishimoto was born in Chiba, Japan, on January 25, 1943. He graduated from Narutoh High School, Chiba, Japan in 1961.

In 1963 he joined The Furukawa Electric Co. Ltd., and he has been engaged in research on fabrication and characterization of fiber cables. Currently, he is working on sensor systems and fabrication of special fibers for sensors.

Mr. Nishimoto is a member of the Institute of Electronics and Communication Engineers of Japan.



Yoshikazu Matsuda was born in Tokyo, Japan, on August 25, 1942. He received the B.S. and M.S. degrees in applied physics from Keio University, Kanagawa, Japan, in 1964 and 1966, respectively.

In 1966 he joined The Furukawa Electric Co. Ltd., and he has been engaged in research on fiber cables and fiber optic devices. Currently, he is working on fiber sensors.

Mr. Matsuda is a member of the Institute of Electronics and Communication Engineers of Japan.

# Low loss metal-coated optical fibers for heat resistant cables

Masahide KUWABARA\*, Kunio KOKURA\* and Seiji Ikegami\*\*

\*The Furukawa Electric Co., Ltd. 6, Yawatakaigandori, Ichihara, Chiba, 290, Japan

\*\*The Kyowa Electric Wire Co., Ltd. 2-5, Kusune-kitamachi, Neyagawa, Osaka, 572, Japan

## ABSTRACT

A novel process was developed to continuously form metal coatings for silica optical fibers by electroless plating and electroplating. The metal-coated optical fibers fabricated through our new process, excels in mechanical strength, fatigue resistance, and transmission loss.

Additionally, a trial model cable which was made out of the metal-coated optical fibers, exhibited significant improvement in heat resistance.

## 1. INTRODUCTION

Recently, as low loss optical fibers are extensively employed in a variety of fields, the need for high mechanical strength, excellent resistance to hydrogen permeation, and improved tolerance to heat becomes apparent. Some examples include applications for the fire-protection systems where optical fibers be exposed to high temperature for extended period of time. However, plastic coatings as conventional means burn to decompose under fire so that optical fibers would be broken easily. Thus, the use of metal coatings on optical fibers is required.

Several researchers have attempted coating fibers with metal coatings such as aluminium<sup>(1)</sup>, lead, and tin. It is well known as a conventional method for forming metal coatings for optical fibers, to pass optical fibers through a bath containing metal melt in fiber drawing process. This dipping method, however, suffers from a disadvantage of a generation of a microbent, which causes an increase of a transmission loss. Besides, the degradation of the fiber strength is caused by the reaction between molten metal and silica fiber surface. Thus, the dipping method has not yet found wide acceptance.

In order to solve such problems, we have developed a novel metal-coating process. This paper describes in detail the characteristics of our metal-coated fibers, and the experimental result of the heat resistant cable made out of these fibers.

## 2. METAL-COATED OPTICAL FIBERS

### 2.1 METAL-COATING PROCESS

The optical fiber is drawn without plastic coating and wound up on the bobbin. This fiber is dipped into container filled with electroless plating solution of nickel and phosphorus at about 70°C as shown as Fig.1. Nickel able to be easily electroless plated, having a contact with the fiber surface, is most preferably used as the primary coating material. Following electroless plating, various metal coatings such as copper, silver, gold, and nickel are applied over the thin primary Ni-coating by electroplating.

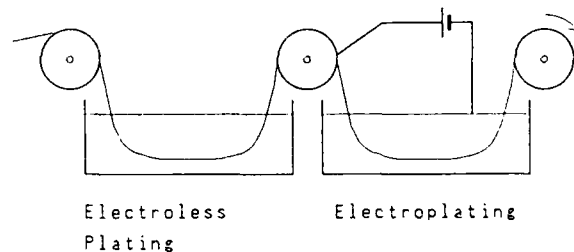


Fig.1 Metal-Coating Process

In this study, Ni-coating was only prepared for a single-mode optical fiber due to the fact that Ni can serve fairly well as a means of resisting heat, compared to other materials. The phot.1 shows the SEM photograph of the cross-section of the Ni-coated fiber. The Ni-coating having a thickness of 3~5  $\mu\text{m}$ , is quite uniform in thickness. Additionally, the surface of Ni-coating looks very smooth as shown as the phot.2.

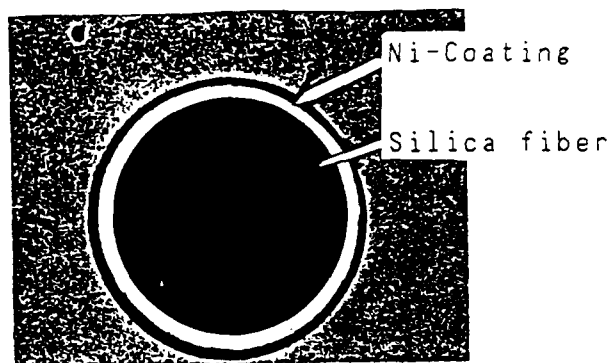


Photo.1 Cross-sectional Structure of Ni-Coated Fiber



Photo.2 SEM of Ni Coated Fiber (400 X)

## 2.2 STRENGTH AND FATIGUE

The failure strength of Ni-coated optical fiber was measured by dynamic bending test<sup>(2)</sup>. Fig.2 shows the typical strength distribution of the Ni-coated fiber. The strength at 50% failure probability is approximately 5.0 GPa which is just the same as that of the conventional plastic coated fiber. Also, the portion of low strength cannot be located in the Weibull plot.

To characterize the fatigue resistance of Ni-coated fiber, the static fatigue behavior was examined using the fibers wound on small diameter mandrels. The maximum bending stress for the fibers was 3.0 GPa. Under the stress of such magnitude, the Ni-coated fiber has been survived for more 3 months. It was found that the Ni-coated fiber exhibits negligible strength degradation caused by stress corrosion.

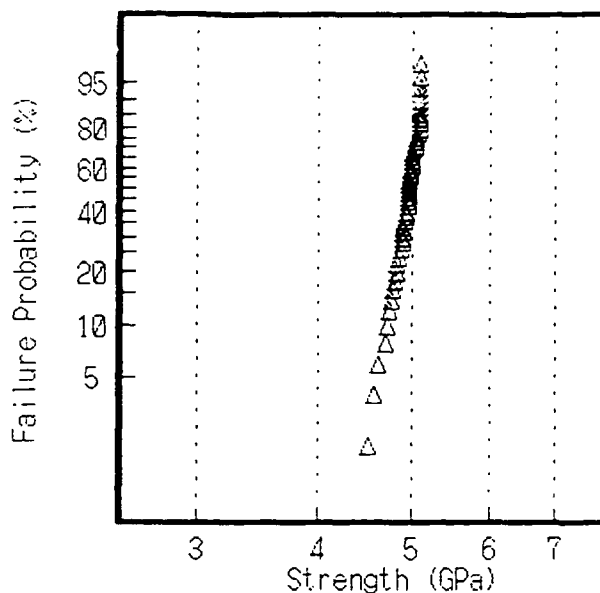


Fig.2 Strength of Ni-Coated Fiber

## 2.3 TRANSMISSION LOSS

Fig.3 shows the loss spectra of the Ni-coated single-mode fiber fabricated through our new process. This fiber shows lower loss (0.7 dB/km at 1.3  $\mu\text{m}$ ) than those in the conventional metal coated fiber by the dipping process. In the case of dipping process, the remarkable microbending loss increase is caused by the shrinkage of the fiber which is generated on cooling from melting temperature (about 700 °C for aluminium) to room temperature. On the other hand, electroless plating and electroplating, which can be done at a much lower temperature (70-90 °C), are free from such shrinkage.

Table.1 Characteristics of Ni-coated Fiber

fiber type	single mode
MFD ( $\mu\text{m}$ )	9.0
cladding dia. ( $\mu\text{m}$ )	125
Ni coating dia. ( $\mu\text{m}$ )	130
optical loss at 1.3 $\mu\text{m}$ (dB/km)	0.7



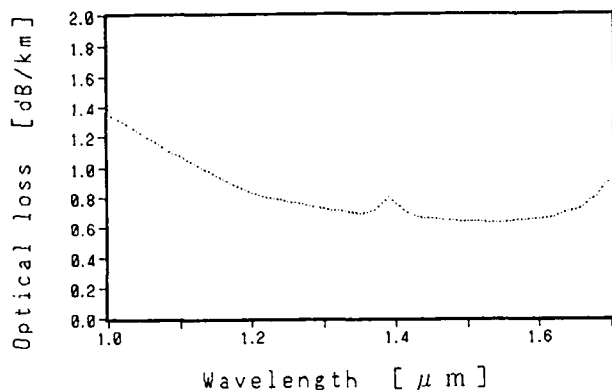


Fig. 3 Initial Optical losses of Ni-Coated Fiber

#### 2.4 TEMPERATURE CYCLING TEST

Fig. 4 shows the temperature characteristic of Ni-coated fiber. In a heat chamber, a fiber line was strung over a distance of 500m, and a temperature repeated to cycle from  $-80$  to  $+90^{\circ}\text{C}$  at intervals of 8.5 hours. The transmission loss was monitored at  $1.3\ \mu\text{m}$ , where a negligible change of loss was observed.

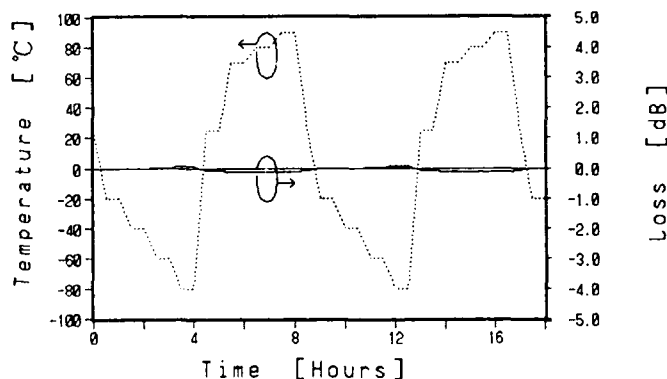


Fig. 4 Temperature Cycling for Ni-Coated Fiber at  $1.3\ \mu\text{m}$  [ $L=500\text{m}$ ]

### 3. NEW HEAT RESISTANT CABLE

#### 3.1 CABLE CONSTRUCTION

A most modern heat resistant cable is designed, by taking full advantage of Ni-coated optical fiber and described as follows.

The structure of the referenced cable is shown in Fig. 5. The cable core is prepared by thrusting Ni-coated optical fibers into stainless steel tubes, which have an outer diameter of 1.2 mm and the inner of 0.8 mm. Then, they are stranded and bound up around a galvanized steel wire. The outer sheath comprises flame-retardant polyethylene containing magnesium hydroxide<sup>(3)</sup>. Also, the cable diameter is 7.0 mm.

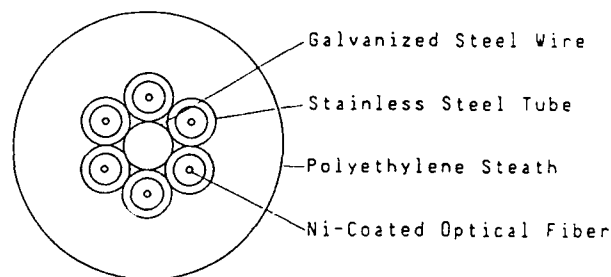


Fig. 5 Cross-section of Tested Cables

#### 3.2 HEATING CONDITIONS

The test method for flame resistance meets Regulation No. 7 of Fire Defence Agency of Japan (FDAJ): "Testing Standard of Fire-Proof Cables".

The test went as follows. As shown in Fig. 6, test cables were set straight on a pearlite board. Fig. 7 shows a furnace compatible with Specification JIS A 1305. These samples were heated for 30 minutes, following the temperature curve specified in Japanese Industrial Standard (JIS) A 1304, which simulates a temperature-shift in fire<sup>(4)</sup>.

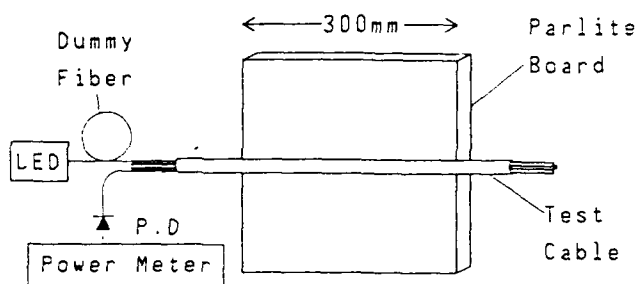


Fig.6 Measurement Method of Heating Test  
(In compliance with Japanese  
Industrial Standard JIS A 1305)

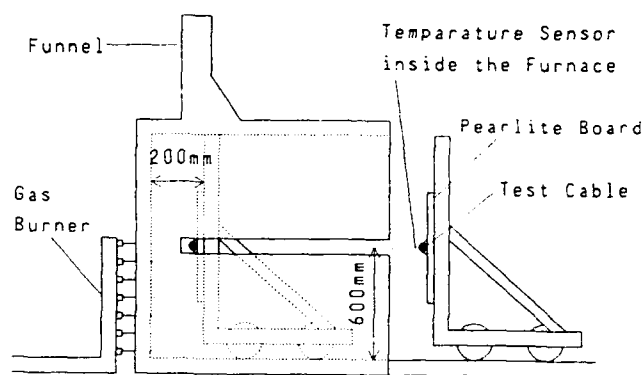


Fig.7 Apparatus of Flame Resistance Test

### 3.3 RESULT

Fig.8 shows the sensed temperature, and the transmission loss change of the test fiber. The temperature of fiber rises slowly due to its heat-insulation. Throughout the 30 minutes, there was neither breakage of optical fiber nor an remarkable increase of loss to be observed. Also, the Ni-coating on the optical fiber remained sound.

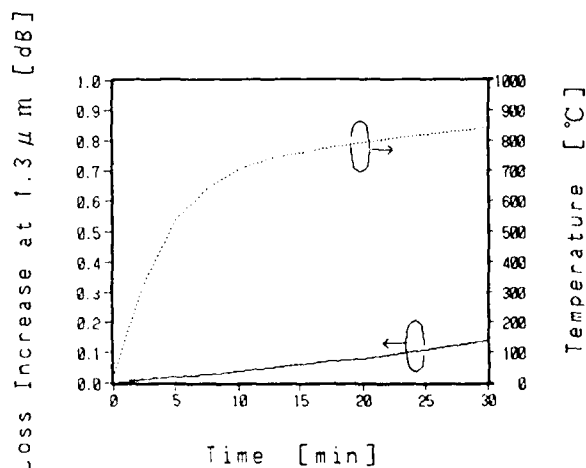


Fig.8 Optical Loss vs Temperature  
for Heat Resistant Cable

### 4. CONCLUSION

In this study, a new metal-coating process by electroless plating and electroplating, has been developed. The Ni-coated optical fiber fabricated through our new process provided excellent performances in mechanical strength, fatigue resistance, transmission loss.

Additionally, using the Ni-coated optical fibers, a trial model cable was prepared and examined. As the result, we confirmed the excellent heat resistance.

### REFERENCES

- (1) D.A.Pinnow, J.A.Wysocki and G.D.Robertson, "Hermetically sealed high strength fiber optical waveguides", IOOC'77 P335-338
- (2) G.S.Glasemann, et al., "Dynamic fatigue data for resistant fiber in tension vs bending." OFC'89 WA3
- (3) S.Shimizu, et al., "A study on fire-retardant optical cable." 39th IWCS Preceedings 683 (1990)
- (4) Y.Kikuchi, et al., "Characteristics of heat and flame resistant optical fiber cables." 32th IWCS Preceedings 348 (1983)



Masahide KUWABARA

The Furukawa Electric  
Co.,Ltd.  
6, Yawatakaigandori,  
Ichihara, Chiba, 290,  
Japan

Masahide Kuwabara was born in Gifu, Japan, on July 13, 1963. He received the B.S. degree in inorganic chemistry from Kyoto University, Kyoto, Japan, in 1987.

He joined The Furukawa Electric Company, Ltd., Chiba, Japan, in 1987, and has been engaged in researches on fabrication and characterization of optical fibers. Mr. Kuwabara is a member of the Institute of Electronics, Information and Communication Engineers of Japan.



Seiji IKEGAMI

The Kyowa Electric Wire  
Co.,Ltd.  
2-5, Kusune-kitamachi,  
Neyagawa, Osaka, 572,  
Japan

Seiji Ikegami was born in Kyoto, Japan, on Sep 21, 1946. He received the B.S. degree in chemistry from Kyoto Institute of Technology, Kyoto, Japan, in 1969.

He joined The Kyowa Electric Wire Company, Ltd., Osaka, Japan, in 1974, and has been engaged in researches on fabrication and characterization of optical fibers. Mr. Ikegami is a member of the Institute of Electronics, Information and Communication Engineers of Japan.



Kunio KOKURA

The Furukawa Electric  
Co.,Ltd.  
6, Yawatakaigandori,  
Ichihara, Chiba, 290,  
Japan

Kunio Kokura was born in Kanazawa, Japan, on May 4, 1954. He received the B.S. degree in inorganic chemistry from Kyoto University, Kyoto, Japan, in 1978.

He joined The Furukawa Electric Company, Ltd., Chiba, Japan, in 1978, and has been engaged in researches on fabrication and characterization of optical fibers. Mr. Kokura is a member of the American Ceramic Society.

# AERODYNAMIC FORCE OF AERIAL CABLES

Tokio KAWANABE, Satoshi MATSUHASHI, Isao FUJIBAYASHI

NTT Telecommunication Field Systems Research and Development Center.  
Tsukuba, Ibaraki, 305, JAPAN

## ABSTRACT

It is already known that self-supporting cables and lashing cables undergo galloping oscillation mode in strong winds.

However, in actual fact, this galloping oscillation generally occurs in a direction which is not perpendicular to the wind direction. Therefore, model cables with various cross-sectional shapes are tested using wind tunnel experiment equipment and the discrimination equation which gives the occurrence conditions of galloping oscillation except for that perpendicular to the wind direction. The experimental results agree with aerial cable oscillation under wind pressure during actual conditions and this discrimination equation proves valuable if the direction of oscillation is inclined from a perpendicular direction to the wind direction.

Moreover, it is confirmed that galloping oscillation can be prevented by inserting a cable twisting.

## 1. INTRODUCTION

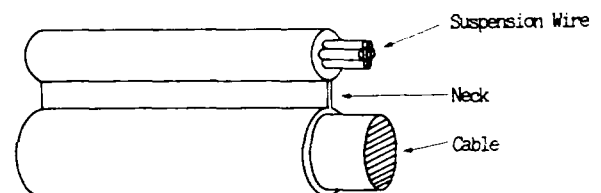
As aerial cables are constructed outside, they are exposed to the elements. It is necessary to consider various fatigue factors such as temperature changes, strong winds, and uv rays when designing the cables. In particular, since fatigue of the cable due to strong wind tends to cause snapping, this important factor must be taken into consideration.

Figure 1 shows the structure of a self-supporting cable and a lashing cable. Nowadays, these cables are generally used as telecommunication lines because of their advantages in construction. Self-supporting cables containing strands and the cable itself are manufactured with polyethyren. Lashing cables use united suspension type wire with the cable part consisting of a spiral stainless steel wire. As the structure of each cable has a figure-8 section as shown in the figure, self-supporting cables and lashing cables tend to suffer galloping oscillation when exposed to strong winds.

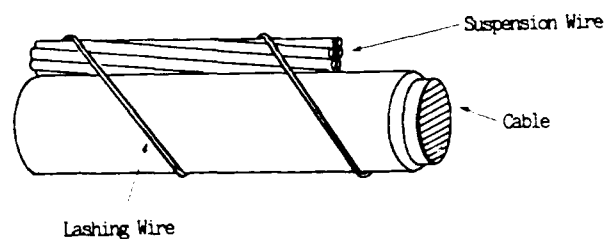
It has been reported that in most cases, for example, oscillation of iced-up electric power cables was studied

using the elliptic model cables in detail. (1) However, there are very few examples regarding this type of research, because the aerodynamic force of the figure-8 cross-section is very special.

So, in this study, the aerodynamics of model cables having various cross-sectional shapes were measured and analyzed, and unstable regions which bring about the possibility of oscillation are calculated using a special equation which gives the occurrence conditions of galloping oscillation of a various directions.



(a) Self-supporting Cable



(b) Lashing Cable

Fig. 1 Self-supporting Cable and Lashing Cable

## 2. INITIAL DIRECTION OF MOTION OF GALLOPING OSCILLATION

Figure 2 shows a dynamic model, when a cable is exposed to wind pressure. This figure shows that the cable cross-section inclines only at  $\beta$  from the horizontal direction, when cable is subjected to horizontal wind velocity  $U$ . At this time, the drag and lift forces  $D, L$  can be expressed using the drag and lift coefficients  $C_D, C_L$  as follows.

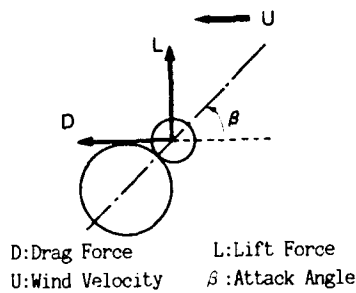


Fig. 2 Dynamic Cable Model

$$D = 0.5 C_D \rho U^2 (a + b) \ell \quad [1]$$

$$L = 0.5 C_L \rho U^2 (a + b) \ell \quad [2]$$

where,

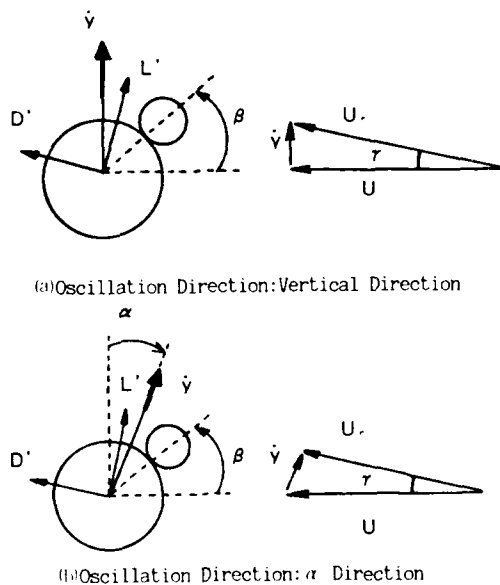
a: Suspension wire diameter

b: Cable diameter

$\ell$ : Cable length

$\rho$ : Air density

The conditions under which galloping oscillation occurs are described under the early stage of the galloping oscillation. Outline is given using Fig. 3.



$y$ : Oscillation Direction

$\gamma$ : Relative Direction Angle of the Wind

$\alpha$ : Oscillation Direction Angle

$U_r$ : Relative Wind Velocity

$L'$ : Lift Force

$D'$ : Drag Force

Fig. 3 Definition Of Oscillation Direction

This figure expresses the force direction vector when the cable begins to oscillate due to a strong wind. At first, this paper explains the case with a very small oscillation perpendicular to the wind direction which Den Hartog et al. have investigated. (1) In the case of Fig. 3(a), the oscillation direction is shown in the figure, and the occurrence conditions for galloping have been analyzed by Novak et al.. (2)

At the start, the cable begins oscillation in the  $y$  direction at velocity  $\dot{y}$ . Therefore, the relative wind velocity is  $U_r$  ( $U/\cos \gamma$ ) and drag force  $D'$  and lift force  $L'$  are shown as in Eqs. [3], [4].

$$D' = 0.5 C_D \rho (U/\cos \gamma)^2 (a + b) \ell \quad [3]$$

$$L' = 0.5 C_L \rho (U/\cos \gamma)^2 (a + b) \ell \quad [4]$$

Where,  $C_D$  and  $C_L$  are considered to be a function of the attack angle such as  $\beta$ . However, since  $\dot{y}$  is very small at the beginning of galloping oscillation, it is assumed that  $\gamma = \beta$  and in the case of the attack angle being  $\beta < \gamma$ , the same  $C_D$  and  $C_L$  should be used.

Force  $F$ , acts on the direction of oscillation  $y$  and aerodynamic force coefficient  $C_F$ , is defined by Eq. [5] as follows.

$$F = 0.5 C_F \rho U^2 (a + b) \ell \\ = D' \sin(\gamma) + L' \cos(\gamma) \quad [5]$$

When Eq. [5] is rearranged by substituting Eqs. [3] and [4], the aerodynamic force coefficient  $C_F$ , is considered to be a function of the drag coefficient  $C_D$ , lift coefficient  $C_L$  and the relative direction angle of the wind  $\gamma$ . The result is shown as follows.

$$C_F = (C_D \tan \gamma + C_L) / \cos \gamma \quad [6]$$

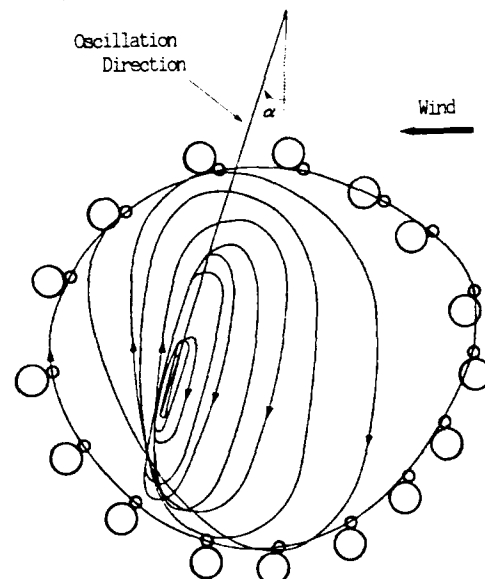


Fig. 4. Growing Process of Galloping Oscillation  
(by Ito et al.)

The typical growth process of galloping oscillation for an aerial cable having a figure-8 cross-section, has been observed by Ito et al.. The example is shown in Fig. 4. (1) This figure indicates the cable locus in the cable cross-section plane. From this figure one can see that when the amplitude in the initial stages of oscillation is low it gathers within a certain area.

However, after the amplitude of the oscillation reaches a certain level, oscillation containing other directions increases and starts rotating around the suspension wire and cable oscillation is stabilized in an elliptical or close-to-circular locus as shown in Fig. 4. It is interesting that the initial direction of galloping oscillation is neither vertical nor in the angle direction of the wind attack.

It has been reported that this oscillation direction angle is found in all cases to be smaller than the angle of wind attack. (2) Angle of oscillation direction in case of Fig. 3 (b) is shown in Fig. 4. Tsuruta et al. have analyzed galloping oscillation in the case of the inclines for  $\alpha$  from the vertical direction. (3) The aerodynamic force coefficient  $C_F$ , is shown as Eq. [7] by Tsuruta et al..

$$C_F = \frac{\cos^2 \alpha \{ C_D \sin(\alpha - \gamma) - C_L \cos(\alpha - \gamma) \}}{\cos^2(\alpha - \gamma)} \quad [7]$$

Here, if  $\alpha$  is 0, Eq. [7] agrees with Eq. [6]. The distinctive equation of the occurrence of galloping oscillation is derived from Eq. [7] and the results are shown as Eq. [8].

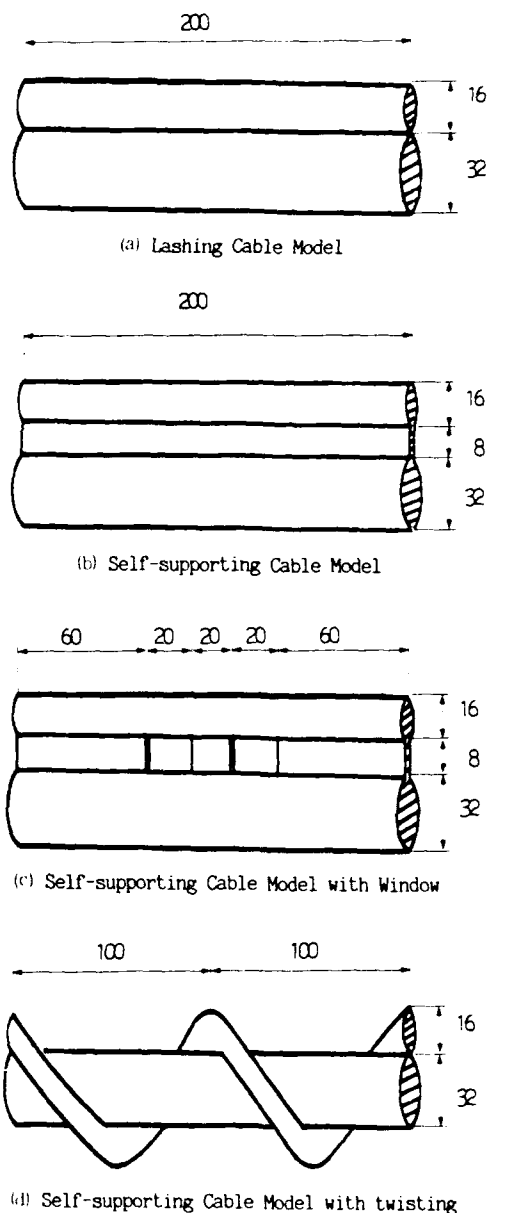
$$\begin{aligned} S &= (dC_F / d\beta) \\ &= (dC_D / d\beta) \sin \alpha \cos \alpha - (dC_L / d\beta) \cos^2 \alpha \\ &\quad + C_D \cos^2 \alpha - C_L \sin \alpha \cos \alpha - 2C_D > 0 \end{aligned} \quad [8]$$

Equation [8] is the distinctive equation of the occurrence of galloping oscillation and was obtained by extending the Den Hartog theory.

### 3. WIND TUNNEL EXPERIMENT

#### 3.1 MODEL CABLES

To measure the aerodynamic force of the cables, four types of model cables as shown in Fig. 5 were manufactured. Here, because aerodynamic force, which is the issue in the discrimination of the occurrence of galloping oscillation, is due to the cross-sectional shape of the cable, it is measured using a 2-dimensional wind tunnel experiment. For this reason, longitudinal tensile rigidity in the cable was ignored, so the cable models were manufactured as a rigid body. The ratio of shape is defined by the ratio of suspension wire diameter to the cable diameter with the ratio being 1:2.



(Unit:mm)

Fig. 5 Cross Section Shape of Model Cables

Type (a) assumes the self-supporting cable in actual service. Both cable and suspension wire are made of steel pipe with a neck provided between the cable and suspension wire.

Type (b) uses a lashing cable, with steel pipe being used in the same way as in type (a) but type (b) does not have a neck.

Type (c) cable model was made of steel pipe and a window is provided between the cable and suspension wire using a plate. This type has been not used for telecommunication lines.

Type (d) assumes the self-supporting cable (type (a)) with inserted twisting as during service. The cable was made of steel pipe and the suspension wire was made of a vinyl hose filled with resin and twines around the cable.

### 3.2 EXPERIMENTAL METHOD

The aerodynamic force was measured using the large Gottingen type wind tunnel at the Building Research Institute. The experiment equipment is shown in Fig. 6. Working section size is  $2\text{m} \times 1.5\text{m}$ , and the equipment has an edge plate, in order to subject uniform velocity wind in the longitudinal direction of the model cables. The ends of the model cables pass through the edge plate and connect with the load cell, as shown in Fig. 6. Wind velocity was measured by a pitot tube fixed at the blow-out duct.

Experiments were carried out under a steady wind force with a wind velocity of  $13\text{m/s}$  for almost all model cables. The attack angle of the model cables was varied from  $0^\circ$  to  $90^\circ$  when drag force and lift force were measured by the load cell, and then drag coefficient and lift coefficient were calculated from eqs. [1], [2].

### 3.3 EXPERIMENTAL RESULTS

Unstable regions were determined by the measurement results of the drag coefficient and lift coefficient of model cables as shown in Fig. 5.

At first, measured values of the lift coefficient were closely approximated with the 4-dimensional Fourier series in the range of  $0 < \theta < 2\pi$  and the results are shown as Eq. [9].

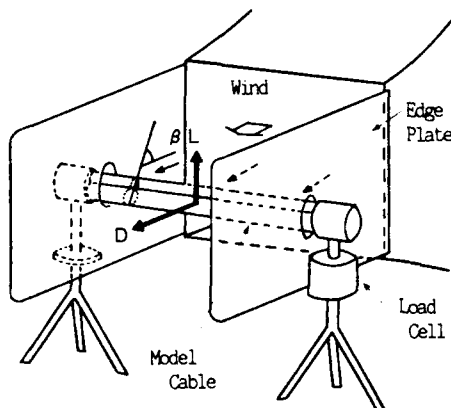


Fig. 6. Experimental Equipment

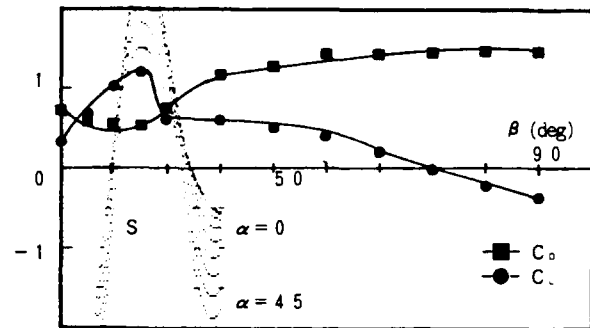


Fig. 7 Experimental Result  
(a) Lashing Cable Model

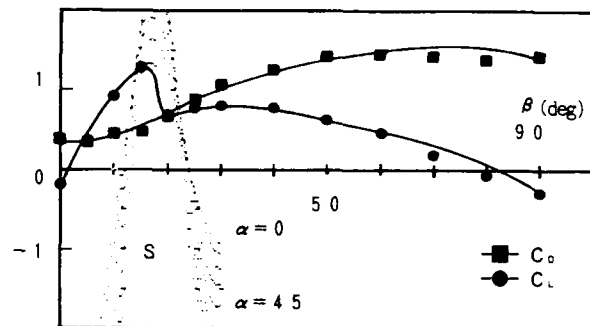


Fig. 8 Experimental Result  
(b) Self-supporting Cable Model

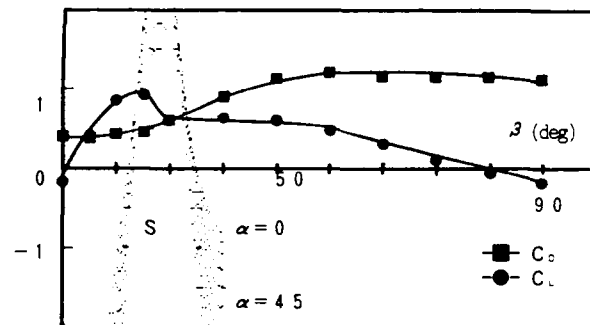


Fig. 9 Experimental Result  
(c) Self-supporting Cable Model with Window

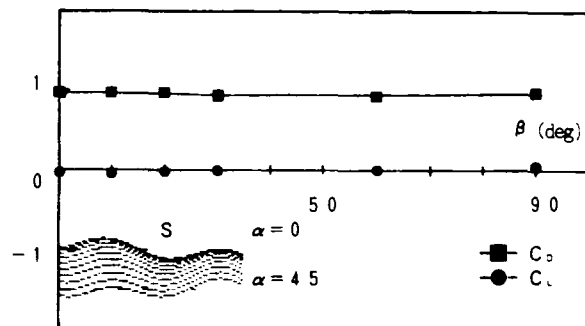


Fig. 10 Experimental Result  
(d) Self-supporting Cable Model with Twisting

$$C_D = f(\theta) = A_0 + A_1 \cos \theta + A_2 \cos 2\theta + A_3 \cos 3\theta + A_4 \cos 4\theta \\ + B_1 \sin \theta + B_2 \sin 2\theta + B_3 \sin 3\theta + B_4 \sin 4\theta \quad [9]$$

Because the range of  $\beta$  is  $0 < \beta < \pi/2$ , as follows:  
 $\theta = 4\beta$ ,  $d\theta/d\beta = 4$ .

Therefore,  $C_D/d\beta$  is expressed as Eq. [10].

$$C_D/d\beta = (d\theta/d\beta)(dC_D/d\theta) \\ = 4 \{ df(\theta)/d\theta \} \\ = 4 \{ (B_1 \cos 4\beta + 2B_2 \cos 8\beta + 3B_3 \cos 12\beta \\ + 4B_4 \cos 16\beta) - (A_1 \sin 4\beta + 2A_2 \sin 8\beta \\ + 3A_3 \sin 12\beta + 4A_4 \sin 16\beta) \} \quad [10]$$

The lift coefficient is also approximated by Eq. [10].

In addition, the angle of oscillation direction  $\alpha$  was in the range of  $0^\circ$  to  $45^\circ$  with an interval of  $5^\circ$ , the drag coefficient  $C_D$ , the lift coefficient  $C_L$  and  $S$  calculated by Eq. [8], are shown in Figs. 7~10.

Figure 7 shows the measured results of the lashing cable model (type (a)) and that a large negative slope exists on the  $C_L$ -curve. Due to this, an unstable region exists nearby with a range of  $10^\circ$  to  $25^\circ$ , mostly. The experimental results showed that it is difficult to deny the possibility of galloping oscillation occurring. This fact agrees with the result that the occurrence of galloping oscillation has been confirmed by Ito et al. using a 3-dimensional model cable in a wind tunnel experiment.

Next, the results of the self-supporting cable model (type (b)) are shown in Fig. 8 and the self-supporting cable with window model (type (c)) is shown in Fig. 9. These results are similar to those of the lashing cable model (type (a)) shown in Fig. 7 and it is recognized that an unstable region exists nearby. It is shown that the neck or window between suspension wire and cable does not affect aerodynamic force so much.

The results of the self-supporting cable with twisting (type (d)) are shown in Fig. 10 and it is seen that the lift coefficient is almost constant in spite of the size of attack angle. No unstable region exists and the effect of twisting is observed.

These results are also proved by the fact that after inserting a twist every 10m. On self-supporting cables there have been no incidences of snapping at this stage.

#### 4. CONCLUSION

At this time, the measured results of aerodynamic force agree with the actual oscillation conditions of aerial cables in the wind which are used at present time.

It clarified that the occurrence distinction of galloping oscillation is estimated by calculating the unstable region which is the purpose of this investigation.

However, the relation between the number of twists and occurrence conditions of galloping oscillation is not clear. Hereafter, the authors intend to verify the above-mentioned relation using the 3-dimensional model cables.

#### ACKNOWLEDGEMENT

The authors wish to thank Prof. Ito and Prof. Fujino who belong to the Dept. of Civil Engineering, University of Tokyo for their help with the experiments and valuable advice.

#### REFERENCES

- (1) Den Hartog, J.P.: Mechanical Vibration, McGraw-Hill, 1934.
- (2) Milos Novak: Aeroelastic Galloping of Prismatic Bodies, Proc. of ASCE, EM1, February 1969.
- (3) Ito, M., Fujino, Y and Yamaguchi, H: Wind study on galloping oscillations of suspend figure-8 telecommunication cables, Proc. of JSCE, Structural Eng./Earthquake Eng., Vol.2, No.1, pp.193s-201s, April 1985.
- (4) Tsuruta, I.: Aeroelastic Instability Oscillations of Suspend Figure-8 Telecommunication Cables, Master's Thesis, Dept. of Civil Eng., Univ. of Tokyo, 1983 (in Japanese).



Tokio KAWANABE  
 NIPPON TELEGRAPH AND TELEPHONE  
 CORPORATION  
 1-7-1 Hanabatake, Tsukuba city,  
 Ibaraki 305 JAPAN

Tokio KAWANABE was born in 1952.  
 He received his B.E. degree in Information engineering from Ibaraki University in 1977 and joined NIPPON TELEGRAPH AND TELEPHONE CORPORATION. He is now a Senior Engineer Supervisor of the Aerial Cable Installation section in Telecommunication Field Systems R&D Center.





Satoshi MATSUHASHI  
NIPPON TELEGRAPH AND TELEPHONE  
CORPORATION  
1-7-1 Hanabatake, Tsukuba city,  
Ibaraki 305 JAPAN

Satoshi MATSUHASHI is a Senior Engineer at NTT Telecommunication Field Systems R&D Center, Japan. He received his B.E. degree in electronics engineering from Hokkaido University in 1981. He joined NIPPON TELEGRAPH AND TELEPHONE CORPORATION 1981. He is engaged in the development of Aerial Cable Installation Technique and Cable Splicing Technique. Mr. MATSUHASHI is a member of the Institute of Electronics, Information and Communication Engineers of Japan.



Isao FUJIBAYASHI  
NIPPON TELEGRAPH AND TELEPHONE  
CORPORATION  
1-7-1 Hanabatake, Tsukuba city,  
Ibaraki 305 JAPAN

Isao FUJIBAYASHI was born in 1964. He received his B.E. degree in mechanical engineering from Chiba University in 1986 and joined NIPPON TELEGRAPH AND TELEPHONE CORPORATION. He is now a staff development engineer of the Aerial Cable Installation section in Telecommunication Field Systems R&D Center.

$$C_D = f(\theta) = A_0 + A_1 \cos \theta + A_2 \cos 2\theta + A_3 \cos 3\theta + A_4 \cos 4\theta \\ + B_1 \sin \theta + B_2 \sin 2\theta + B_3 \sin 3\theta + B_4 \sin 4\theta \quad [9]$$

Because the range of  $\beta$  is  $0 \leq \beta \leq \pi/2$ , as follows:  
 $\theta = 4\beta$ ,  $d\theta/d\beta = 4$ .

Therefore,  $C_D/d\beta$  is expressed as Eq. [10].

$$C_D/d\beta = (d\theta/d\beta)(dC_D/d\theta) \\ = 4 \{ d f(\theta) / d\theta \} \\ = 4 \{ (B_1 \cos 4\beta + 2B_2 \cos 8\beta + 3B_3 \cos 12\beta \\ + 4B_4 \cos 16\beta) (A_1 \sin 4\beta + 2A_2 \sin 8\beta \\ + 3A_3 \sin 12\beta + 4A_4 \sin 16\beta) \} \quad [10]$$

The lift coefficient is also approximated by Eq. [10].

In addition, the angle of oscillation direction  $\alpha$  was in the range of  $0^\circ$  to  $45^\circ$  with an interval of  $5^\circ$ , the drag coefficient  $C_D$ , the lift coefficient  $C_L$  and  $S$  calculated by Eq. [8], are shown in Figs. 7~10.

Figure 7 shows the measured results of the lashing cable model (type (a)) and that a large negative slope exists on the  $C_L$  curve. Due to this, an unstable region exists nearby with a range of  $10^\circ$  to  $25^\circ$ , mostly. The experimental results showed that it is difficult to deny the possibility of galloping oscillation occurring. This fact agrees with the result that the occurrence of galloping oscillation has been confirmed by Ito et al. using a 3-dimensional model cable in a wind tunnel experiment.

Next, the results of the self-supporting cable model (type (b)) are shown in Fig. 8 and the self-supporting cable with window model (type (c)) is shown in Fig. 9. These results are similar to those of the lashing cable model (type (a)) shown in Fig. 7 and it is recognized that an unstable region exists nearby. It is shown that the neck or window between suspension wire and cable does not affect aerodynamic force so much.

The results of the self-supporting cable with twisting (type (d)) are shown in Fig. 10 and it is seen that the lift coefficient is almost constant in spite of the size of attack angle. No unstable region exists and the effect of twisting is observed.

These results are also proved by the fact that after inserting a twist every 10m. On self-supporting cables there have been no incidences of snapping at this stage.

#### 4. CONCLUSION

At this time, the measured results of aerodynamic force agree with the actual oscillation conditions of aerial cables in the wind which are used at present time.

It clarified that the occurrence distinction of galloping oscillation is estimated by calculating the unstable region which is the purpose of this investigation.

However, the relation between the number of twists and occurrence conditions of galloping oscillation is not clear. Hereafter, the authors intend to verify the above-mentioned relation using the 3-dimensional model cables.

#### ACKNOWLEDGEMENT

The authors wish to thank Prof. Ito and Prof. Fujino who belong to the Dept. of Civil Engineering, University of Tokyo for their help with the experiments and valuable advice.

#### REFERENCES

- (1) Den Hartog, J.P.: Mechanical Vibration, McGraw-Hill, 1934.
- (2) Milos Novak: Aeroelastic Galloping of Prismatic Bodies, Proc. of ASCE, EM1, February 1969.
- (3) Ito, M., Fujino, Y and Yamaguchi, H: Wind study on galloping oscillations of suspend figure-8 telecommunication cables, Proc. of JSCE, Structural Eng./Earthquake Eng., Vol.2, No.1, pp.193s-201s, April 1985.
- (4) Tsuruta, I.: Aeroelastic Instability Oscillations of Suspend Figure-8 Telecommunication Cables, Master's Thesis, Dept. of Civil Eng., Univ. of Tokyo, 1983 (in Japanese).



Tokio KAWANABE  
 NIPPON TELEGRAPH AND TELEPHONE  
 CORPORATION  
 1-7-1 Hanabatake, Tsukuba city,  
 Ibaraki 305 JAPAN

Tokio KAWANABE was born in 1952.  
 He received his B.E. degree in Information engineering from Ibaraki University in 1977 and joined NIPPON TELEGRAPH AND TELEPHONE CORPORATION. He is now a Senior Engineer Supervisor of the Aerial Cable Installation section in Telecommunication Field Systems R&D Center.

### III CABLE DESIGNS AND CALCULATIONS

Two cable structures were designed to meet the end-users requirements.

Both structures employ loose tubes as the cabling elements. The reason for this selection is that it is easier to design a larger strain-free margin for the fibres in a loose tube structure compared to other conventional cable structures. A strain-free margin implies that the optical fibres remain stress-free up to a certain amount of cable strain when the cable is stretched. This feature is important in an aerial cable as the cable is subject to permanent tension during its service life.

The short span version can accommodate up to 40 single mode optical fibres. A typical cross-section for a 24 fibre cable is shown in Fig. 1. It consists of a number of loose tubes and polymeric fillers stranded around a glass fibre reinforced plastic (GRP) rod. The principle strength member is two layers of aramid yarns contra-helically applied between the inner and outer sheaths of the cable. The GRP rod is used to provide compressive stiffness to prevent buckling.

Fig. 1 SHORT SPAN CABLE

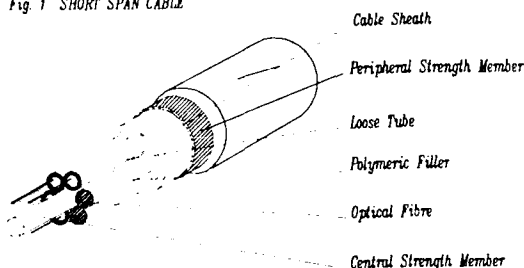


Table I - Short Span Cable

PARAMETER	VALUE
Cable Overall Diameter	14.5 +/- 1 mm
Cable Mass	165 kg/km
Strain-free Window	0.40% (min.)
Maximum Allowable Stress	5.9 KN
Minimum Breaking Load	19 KN
Effective Cable Cross-Sectional Area	121 mm <sup>2</sup>
Effective Modulus of Elasticity	12.6 GPa
Co-efficient of Thermal Linear Expansion	3.3 X 10 <sup>-6</sup> /°C

The long span version can accommodate up to 24 fibres and has an identical optical core to the short span design. A typical cross-section for a 24 fibre cable is shown in Fig. 2. The principle strength member is a layer of GRP rod stranded over the inner sheath of the cable. As well as providing tensile strength, the layer of GRP rods also provide improved crush performance by its 'bird-caging' effect.

Fig. 2 LONG SPAN CABLE

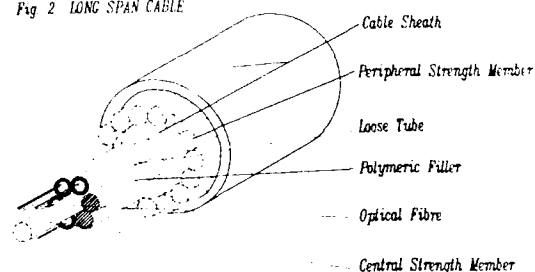


Table II - Long Span Cable

PARAMETER	VALUE
Cable Overall Diameter	17.5 +/- 1 mm
Cable Mass	310 kg/km
Strain-free Window	0.25% (min.)
Maximum Allowable Stress	23.1 KN
Minimum Breaking Load	90 KN
Effective Cable Cross-Sectional Area	220 mm <sup>2</sup>
Effective Modulus of Elasticity	18.0 GPa
Co-efficient of Thermal Linear Expansion	7.7 X 10 <sup>-6</sup> /°C

Both designs exhibit a high degree of versatility in the sense that the amount of strengthening can be varied to suit different span lengths and different climatic conditions with very little change to the cable diameter. For example, the short span version can be designed for a 250 metre span with 130 km/hr wind loads<sup>2</sup>.

From the stranding pitch of the loose tubes and using the 'rule of mixtures'<sup>3,4</sup>, the amount of strain-free margin, effective modulus, effective cross-sectional area and the coefficient of linear thermal expansion of the cables can be calculated. Together with other relevant cable parameters, these calculations are summarized in Tables I and II for the short span and long span cables respectively. These composite parameters form the basis of sag-tension calculations required for accurate stringing in the field. In Section V we will describe tests conducted to confirm the validity of these calculations.

#### IV OPTICAL PERFORMANCE OF THE CABLES

The distribution of the attenuation coefficients of the optical fibres at 1300 and 1550 nm are shown in Figs. 3 and 4, for the short span cable. These results represent over 1500 km of cable manufactured in nominal 5 km drum lengths. Minor differences in pre-cabbling and post-cabbling attenuation results, shown in Table III, is attributed to measurement tolerance.

Table III - Summary of Attenuation for Short Span

N = 4058

PROCESS	1300 nm (dB/km)		1550 nm (dB/km)	
	MEAN	S.D	MEAN	S.D
Before Cabling	0.346	0.011	0.196	0.009
After Cabling	0.335	0.013	0.193	0.009

S.D. denotes Standard Deviation

A smaller volume of long span cables have been manufactured. However, their attenuation results are almost identical to those for the short span. These values represent the state-of-the-art manufacturing statistics for single mode optical fibre cables.

#### V STANDARD OPTO-MECHANICAL TESTS

Both cable structures were manufactured and subjected to a series of opto-mechanical tests in accordance with IEC 794-1 and EIA 455 POTP. Results for both cables are shown in Table IV. The crush resistance of these cables is superior to those cables designed for underground deployment to ensure that the cable core is unaffected by crushing at the pole attachment points.

Due to the service condition of these cables, the tensile performance of the cable is considered to be the most critical parameter. This parameter is measured in two ways. The first method is to terminate both ends of a 50 metre cable length in an epoxy matrix. All the strength members and optical fibres are potted. During the test, the load, cable and fibre elongations are recorded. The fibre elongation is measured using a phase delay technique<sup>5</sup> where a laser is modulated at 100 MHz and the fibre strain is deduced directly from the measured phase shift.

The results are presented graphically in Figs. 5 and 6 for the short and long span cables. Since this arrangement approximates very closely the assumptions made in the design calculations, the results can be directly compared to the design value as a check on the design calculations. From the gradients of the applied force versus cable extension plots in Figs. 5 and 6, the average modulus of the cables are 13.3 GPa and 19.6 GPa respectively. These figures are in good agreement with the 'rule of mixture' results shown in Tables I and II. Notice that hysteresis is more evident in the short span cable than in the long span. This is typical of cables which incorporate aramid yarns as the principle strength member.

The second method requires the cable to be terminated with dead-ends identical to those used in the field. This method simulates worst case conditions in the installed environment and ensures that the modulus used for estimating sag-tension values leads to correct specifications for stringing.

Table IV

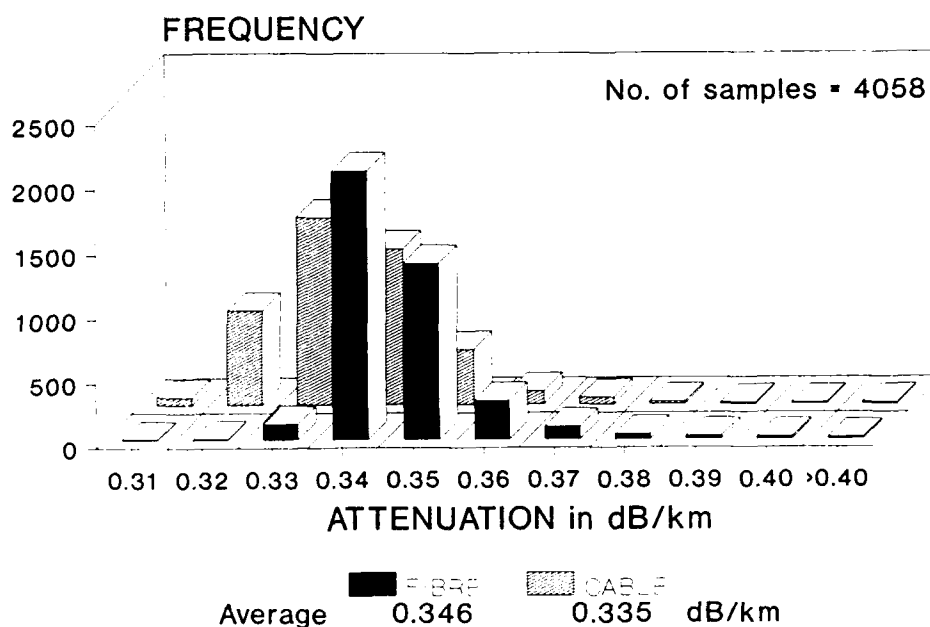
PARAMETER	TEST METHOD	RESULTS	
		SHORT SPAN	LONG SPAN
Crush Resistance	794-1-E3 or 455-41	>3.5 KN/100 mm	>6.0 KN/100 mm
Impact	794-1-E4 or 455-25	50 drops, 9N-m	50 drops, 25N-m
Twist	794-1-E7 or 455-85	>4.0 turns/m	>2.0 turns/m
Repeated Bend	794-1-E6 or 455-104	15 X OD mm	15 X OD
Temperature *	794-1-F1 or 455-3A	-20 to +70°C	-20 to +70°C
Water Penetration	794-1-F5 or 455-82	Pass	Pass**

OD is the outer diameter of the cable.

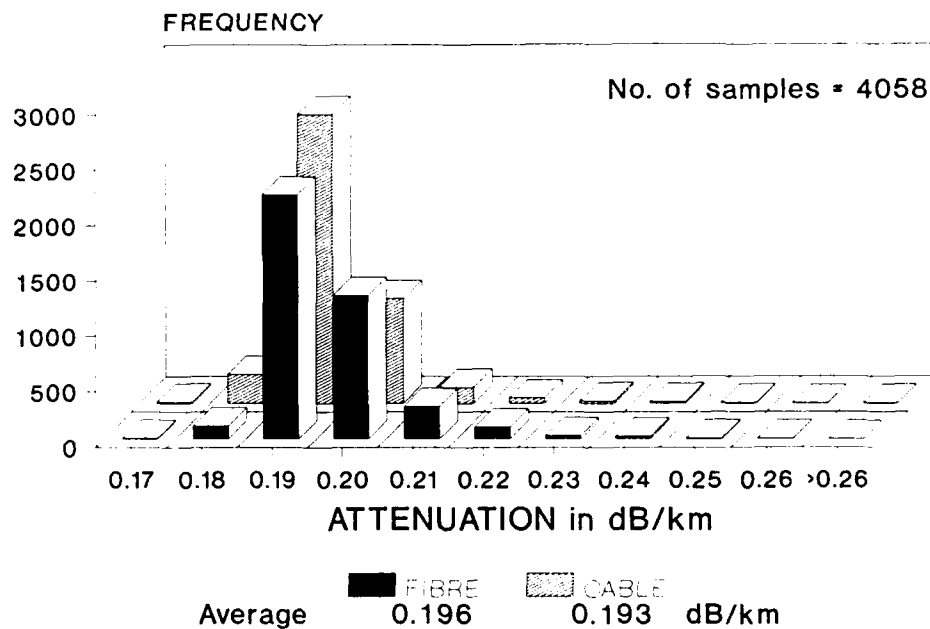
\* Criterion for Test: less than 0.1 dB attenuation increase at 1550 nm.

\*\* No leakage is used to judge Pass/Fail.

**FIG. 3 AERIAL - SHORT SPAN CABLE  
TYPICAL ATTENUATION at 1300 nm**



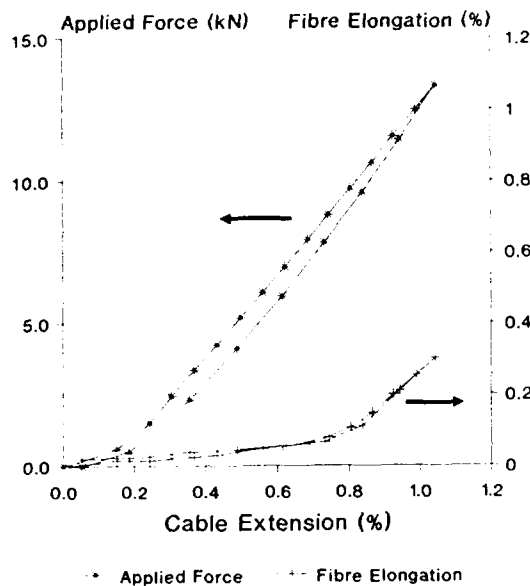
**FIG. 4 AERIAL- SHORT SPAN CABLE  
TYPICAL ATTENUATION at 1550 nm**



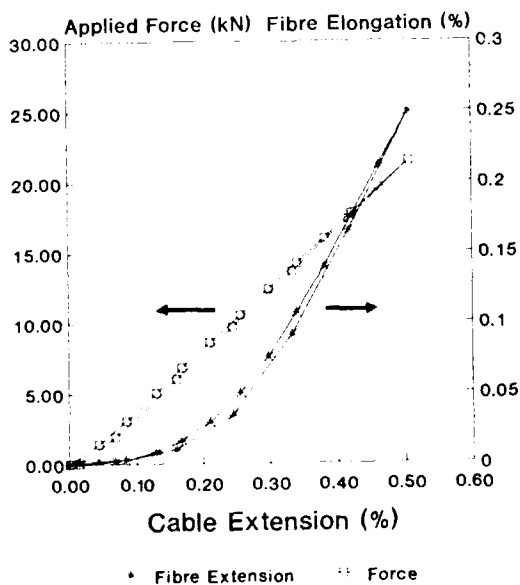
CABLE TERMINATIONS

The method of attaching preformed helical aluminium-steel dead-end fittings on optical fibre cables is a relatively new technique. To validate the performance of the cable plus hardware we carried out a tensile test in accordance with IEC 794-1 (except that the cable is terminated with dead-ends). The optical fibres are concatenated to form a continuous loop for both attenuation and strain measurements. To simulate the effect of cyclic loads on the cable and hardware, the load-hold-unload cycle is repeated three times to determine the optical and stress-strain characteristics. The results exhibited in Fig. 7 lead us to conclude that after a settling-in strain of 0.1% attributed to the relaxation of the hardware (no slippage between cable and hardware was observed), the stress-strain curves stabilize to a value which is consistent with the earlier curves obtained from epoxy termination. The optical attenuation captured in Fig. 8 shows extremely stable 1550 nm transmission characteristics up to 15 kN, a factor of three higher than the rated maximum load. These two important operating features of aerial self-supporting cables have been achieved with judicious design of the strain margin and cable hardware. In an installed cable, this test ensures that stable sag and transmission performance will be sustained over the service life of the cable.

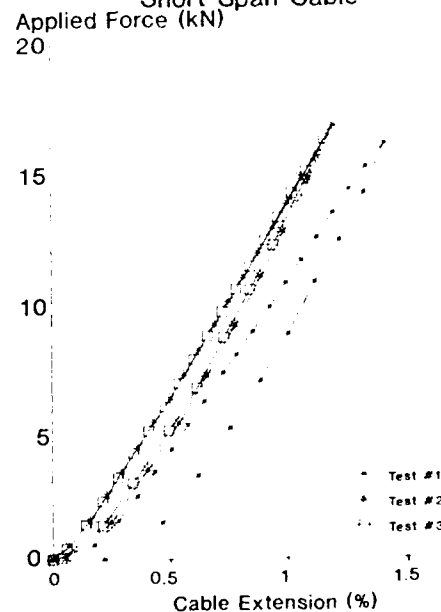
**FIG. 5 AERIAL SHORT SPAN CABLE  
Typical Tensile Test**



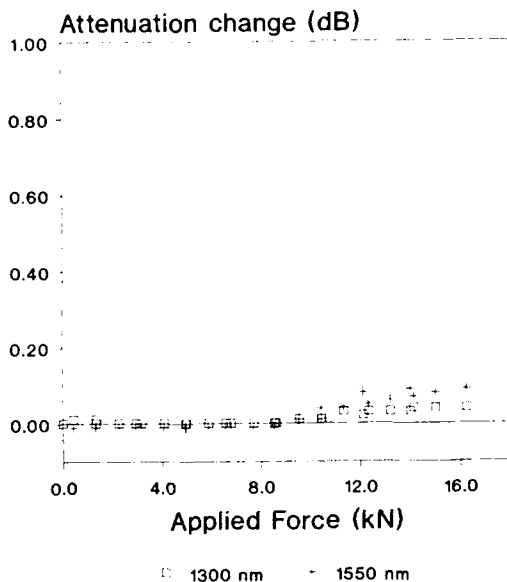
**FIG. 6 AERIAL LONG SPAN CABLE  
Typical Tensile Test**



**FIG. 7 TENSILE TEST WITH DEAD-ENDS  
Short Span Cable**



**FIG. 8 AERIAL SHORT SPAN CABLE  
Attenuation vs Applied Force**



are organized into splice cassettes within the dome with fibre loop diameters exceeding 60 mm. This ensures that the residual stress and excess attenuation at 1550 nm is kept below accepted industry standards.



**FIGURE 9a:** Dead-end termination fittings seen in a typical field setting.

#### VII CABLE ATTACHMENTS AND ACCESSORIES

To minimize the occurrence of faults and cost of maintenance of the cable system, the attachments and accessories that form an integral part of the system must be equally reliable. This is achieved by testing these components to recognised standards.

The dead-ends (Fig. 9a) and suspension clamps (Fig. 9b) were tested to Australia Standards 1154<sup>6</sup> to ensure that the holding and breaking strengths are in accordance to user specifications. Aeolian vibration activity is a stress mechanism for most dielectric cables with circular cross-section. Thus, vibration dampers shown in Fig. 9c are normally fitted close to each cable termination or clamp to reduce any stress that may build up at these critical locations. Vibration testing is a topic that is currently being addressed by an IEEE Sub-Committee with feedback from the manufacturer of cable fittings<sup>7</sup>.

Due to the above-ground deployment of self-supporting cables, the method of jointing is best achieved using pole mounted joint enclosures as shown in Fig. 9d. Here the major concerns are mechanical robustness, temperature and humidity ratings. These parameters are determined from testing to major end-user specifications, for example, Telecom Australia<sup>8</sup>. The excess optical fibres



**FIGURE 9b:** Demonstration of deployment of a suspension clamp.

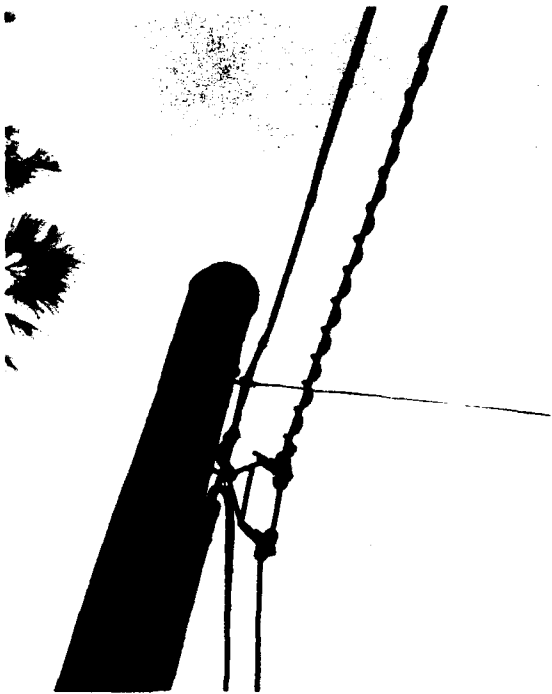


FIGURE 9c: Vibration damper (spiral) seen in actual use.

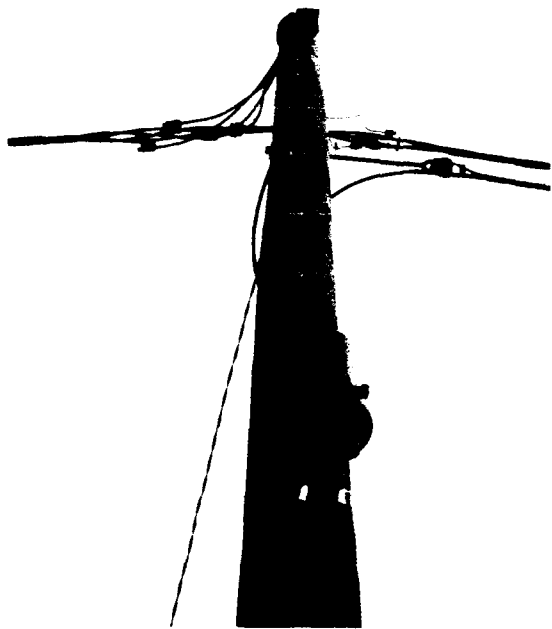


FIGURE 9d: Pole-mounted joint enclosure.

#### VIII

#### CONCLUSION

Through proper design and extensive laboratory and simulation testing of key design and operational parameters of self-supporting cables, associated attachments and accessories we have shown that these components will meet the required service conditions expected over their lifespan. The concept of building up a cable network using self-supporting cables is a reliable and economically viable option. If adopted, this technique lends itself to very rapid installation compared to established underground methods.

#### IX

#### ACKNOWLEDGEMENT

The authors wish to thank the General Manager of MM Cables - Communication Products for permission to publish this paper.



X

# REFERENCES

1. G. Mahlke and P. Gossing "Fibre Optic Cables", J. Wiley & Sons, 1987, pp117.
2. S.V. Chung "Self-Supporting Non-Metallic Aerial Optical Fibre Cables", Asia Pacific Telecommunity Journal, Vol. 3, No. 1, Jan 1991, pp 39.
3. T.A. Lenahan, "Thermal Buckling of Dual Coated Fibre", AT & T Technical Journal, Vol. 64, No. 7, Sept 1985, pp 1570.
4. M.A. Anderson, Phillips Cables Ltd, Engineering Report 87, 36 OE, Aug 1987, Private Communication.
5. B.T. de Boer, R.W.A. Ayre and R.B. Schuster "Cable Design and Installation Technique for Direct Buried Non-Metallic Optical Fibres", 34th International Wire and Cable Symposium, 1985, pp 385.
6. Australian Standard 1154, 1985 "Insulator and Conductor Fittings for Overhead Power Lines, Part 3 - Performance and General Requirements for Helical Fittings".
7. D.C. Sunkle and R.J. Champa "Testing of Fittings and Aerial Fibre Optic Cable", Distribution 2000, 1991, pp 205.
8. Telecom Australia Schedule MS 5053.



Su-Vun Chung

MM Cables -  
Communication  
Products

71 Whiteside Road  
Clayton, Victoria  
Australia. 3168

Su-Vun Chung (Member, IEEE) was born in Kuching, Malaysia in 1960 and holds B.E. (Electrical and Computer Systems) and Ph.D. Degrees (Fibre Optics) from Monash University, Australia. He has over four (4) years experience in the optical fibre cable industry with responsibilities in the areas of Product Design/Development and Technical Sales Support. He currently holds the position of Product Manager (Telecom), MM Cables - Communication Products.



Lian Ding

MM Cables -  
Communication  
Products

71 Whiteside Road  
Clayton, Victoria  
Australia. 3168

Lian Ding (Member, IEEE) graduated in 1979 with M.Sc. (Communication Engineering) and B.E. (Electrical). He has over ten (10) years experience in the optical fibre cable technology. He is responsible for cable design and liaison with customers on all technical aspects relating to cable and cable-related products. Currently he holds the position of Technical Marketing Manager in MM Cables - Communication Products.

# SHORT- AND LONG-SPAN, SELF-SUPPORTING, NON-METALLIC AERIAL FIBER OPTIC CABLE

S. Kloepper, B. Menze, J. Schulte, G. Maltz  
Kabelmetal Electro GmbH  
P.O. Box 260, 3000 Hannover 1, Germany

F. Teucher  
ABB Energiebau  
P.O. Box 74, 8012 Dresden, Germany

## Abstract.

A self-supporting, non-metallic aerial fiber optic cable suitable for diverse applications is presented. Short span lengths as well as long span lengths, up to 500 m, can be achieved. Its special design enables the cable to carry high mechanical loads and it presents complete protection of the fibers by providing for adequate excess fiber length and excellent resistance to axial compression. Furthermore, the selected design permits an assured stress transfer between the anchoring or supporting fittings and the strength members without shift of the jacket and without slippage of the fittings. Conventional overhead line fittings may be used thus making for simple and rapid installation.

## Introduction.

In many cases the use of directly buried cables or cables installed in ducts is neither technically feasible nor economical. This holds particularly true in rural areas with low population density or in regions with rocky grounds or in mountains. In these cases the use of aerial cables is indicated. A non-metallic design is highly desirable in areas that are subject to frequent lightning discharges or electrical interference. A non-metallic, self-supporting aerial cable can also be incorporated in high voltage transmission lines. This kind of cable must be designed to meet the stringent mechanical requirements for these applications and lend itself to easy installation.

## Mechanical requirements for aerial cables.

The installed aerial cable is constantly subjected to a tensile load. This leads to cable elongation. A fiber optic aerial cable must be designed so that the elongation, under normal operating conditions and over its design life, will not result in fiber elongation. Ice and wind loads must also be considered as normal operating conditions. However, in the case of extreme, rarely encountered

conditions (i.e.: extremely heavy ice loads) one may allow a maximum fiber elongation at a 30% screen test level. On this premise, the life expectancy of the fiber is not yet affected. Of course, an unacceptable attenuation increase must not be allowed under any circumstances.

During installation, the cable is subject to elongation as a function of span, sag, cable weight and of its design load. The elongation thus arrived at varies with the wind velocity, temperature and the ice deposition on the cable. Eq. 1<sup>1</sup> is the fundamental equation for the calculation of different environmental and load conditions. Starting from this equation, the cable elongation can be derived:

$$\epsilon = \frac{a^2}{24} \left[ \left( \frac{w_x}{F_x} \right)^2 - \left( \frac{w_0}{F_0} \right)^2 \right] - \frac{F_x - F_0}{E \cdot A} - \alpha (T_x - T_0) \quad (1)$$

wherein:

A	= cable cross-section	(mm <sup>2</sup> )
a	= span length	(m)
α	= linear expansion coefficient	(1/K)
E	= modulus of elasticity of the cable	(N/mm <sup>2</sup> )
s	= cable sag	(m)
w	= cable weight per unit length	(N/m)
w <sub>0</sub>	= initial cable weight per unit length (with or without additional load)	(N/m)
w <sub>x</sub>	= cable weight per unit length under the observed load condition	(N/m)
w <sub>z</sub>	= cable weight per unit length of the additional load	(N/m)
F	= tensile force	(N)
F <sub>0</sub>	= initial tensile force	(N)
F <sub>x</sub>	= tensile force under the observed load condition	(N)

$T_o$  = initial temperature (°C)  
 $T_x$  = temperature at the observed load condition (°C)

The cable sag is derived from the following equations (see 1):

without additional load:

$$s = \frac{a^2 \cdot w}{8 \cdot F} \quad (m) \quad (2)$$

with additional load:

$$s = \frac{a^2 (w + w_2)}{8 \cdot F} \quad (m) \quad (3)$$

According to VDE specifications<sup>2</sup>, a single ice load, referred to cable length, may be calculated using Eq. 4:

$$w_i = 5 + 0.1 d \quad (N/m) \quad (4)$$

wherein  $d$  = cable diameter (mm)

Depending on local conditions, it may be necessary to take into account a multiple of this ice load. Experimental results covering ice loads are reported in the section "Ice Deposition on Aerial Cables" of this paper.

The wind load, referred to cable length is<sup>2</sup>:

$$W_w = c \cdot q \cdot d \quad (N/m) \quad \text{for } a \leq 200 \text{ m} \quad (5)$$

$$W_w = c \cdot q \cdot d \left( \frac{80}{a} + 0.6 \right) \quad (N/m) \quad \text{for } a > 200 \text{ m}$$

$c$  = aerodynamic shape factor  
 (1.00...1.2 for cables with circular cross-section)

$$q = \text{dynamic pressure} \frac{v^2}{1600} \quad \text{in } kN/m^2,$$

wherein  $v$  = wind velocity in m/s

The linear expansion coefficient of the cable must be determined either experimentally or calculated from the contributions of individual cable components to:

$$\alpha_k = \frac{\sum \alpha_i E_i A_i}{\sum E_i A_i} \quad (6)$$

The temperature range in Europe is typically specified between -40°C and +60°C.

The breaking load of an aerial cable is:

$$F_B = \sigma_B \cdot A \quad (N) \quad (7)$$

wherein  $\sigma_B$  is the tensile strength of the supporting elements (N/mm<sup>2</sup>)

The maximum permanent load capacity is:

$$F_{LT} = F_B / 3 \quad (N) \quad (8)$$

#### Ice Deposition on Aerial Cables.

For over 25 years East Germany has established a measurement network for the experimental determination of deposited ice masses. This network encompasses different typical climatic situations. The following equation serves as the basis for ice deposition calculations<sup>3</sup>:

$$m_g = m_g' \cdot k_h \cdot k_d \quad (9)$$

wherein:

$m_g$  = ice deposition for a given component (kg/m)

$m_g'$  = statistical base value for the reference gauge (vertical, non-rotatable, fixed yardstick 35mm diameter, 1 m long) located 2 m over ground level (kg/m) (Fig. 1).

$k_h$  = height factor for the conversion of the ice deposition from 2 m to the actual height (Table 1)

$k_d$  = diameter factor for the conversion of ice deposition from the reference gauge to the actual component (Table 2).

This calculation corresponds to the method proposed in IEC 11 (CO) 28.

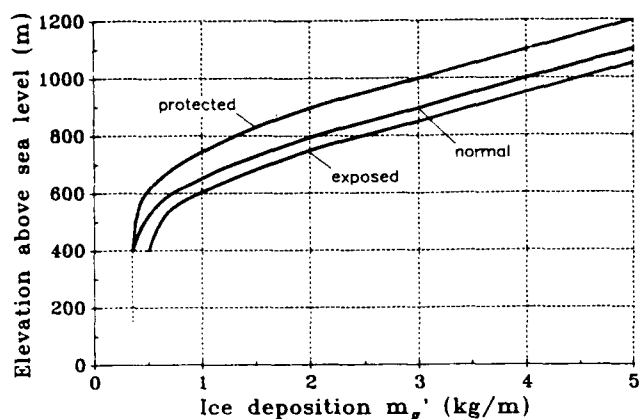


Fig. 1 Ice deposition  $m_g'$  for a recurring 5-year period, as a function of elevation and relative exposure to wind

Type of location:	Conductor height above ground (m)								
	2	6	10	15	20	25	30	40	50
normal or exposed	1.0	1.5	1.9	2.4	2.8	3.1	3.4	3.9	4.2
protected	1.0	1.3	1.5	1.7	1.8	2.0	2.1	2.3	2.5

Table 1:  $k_h$  factor (NOTE: the location refers to the relative exposure to wind)

Conductor dia. (mm)	Ice deposition $m_g'$ $k_h$ (kg/m)				
	1.0	2.0	3.0	4.0	5.0
27.0	1.25	1.10	1.05	1.00	0.95
21.7	1.20	1.05	1.00	0.95	0.90
15.7	1.10	1.00	0.95	0.90	0.85
10.0	1.00	0.90	0.85	0.80	0.75
5.0	0.80	0.70	0.65	0.60	0.55

Table 2:  $k_d$  factor

The base value  $m_g'$  is determined from yearly maximum ice deposition values.

A number of monitoring stations in selected locations rendered possible the experimental determination of the  $k_h$  and  $k_d$  factors for application to overhead conductors. For determination of the height factor  $k_h$ , the average height over ground level is considered. This means that in the case of aerial cables having short spans (100 m) the actual height of the cable suspension must be considered. In the case of long spans (500 m), a weighted mean value of the difference in height between the suspension point and the deepest sag must be taken into account.

The  $k_d$  factor was derived from measurements on 1 m long conductor or aerial cable samples which were anchored so that they could not rotate. It was recognized a short time ago that thinner conductors and cables which are more easily twisting in the span field are more receptive to heavier ice deposition than thick conductors of higher torsional strength which have hitherto been the main subjects of investigation.

For a closer investigation of ice deposition on aerial cables we installed such a cable (15.5 mm dia.) in a test range on a crest of the Erzgebirge Mountains in East Germany at an altitude of 1,200 m over sea level during the winter of 1990/91. The installation consists of a span field of two 50-m lengths. In view of the high frequency of ice deposits (an average of 70% of the days during the six months cold period) and their intensity it will be possible within the next 2 to 3 years to issue specific statements with authoritative statistical value. Along with the aerial cable, an overhead AlSt 380/50 (steel-covered aluminum 27 mm dia.) conductor was suspended. The following experience has been gained from these tests:

- ice formation on the aerial cable and on the steel rope occurs more readily on the side exposed to the wind (Fig. 2a);
- this ice formation, which takes on the shape of an inverted airfoil, is more pronounced on the steel rope than on the aerial cable. This is explained by the fact that the non-metallic aerial cable is twisted more easily than a steel conductor. The leverage effect due to gravity of the one-sided ice deposit causes the aerial cable to twist about its longitudinal axis. This may happen, for example, as a one-quarter rotation in the middle of the span, that is, less than 1°/m. Further ice formation occurs on top of the already deposited ice (Fig. 2b.). Thus, the ice deposition on the aerial cable finally takes on a near-circular cross-section. This behavior is most noticeable in the middle of the span.
- ice drop-off occurs when the temperature rises above 0°C and from the influence of the wind. The one-sided ice deposit on the steel conductor causes the ice to drop off sooner than on the fiber optic cable with its near-circular ice deposit.

- data gathered up to now for an ice mass of about 1.5 kg/m yield an average value of 0.96 for the ratio of the ice weight of the AlSt rope vs. the ice weight of the aerial cable;

According to Table 2 this ratio should be about 1.15 because of the smaller diameter of the aerial cable. The reason for the higher ice load on the aerial cable is its increased twist, as described above. The ice load on the non-metallic F.O. aerial cable must therefore be assumed to be 20% higher than for conventional overhead bare conductors. Data collected until now provide this conclusion for Central Europe up to elevations of about 500 m above sea level. The effect of higher ice deposit on the thin fiber optic aerial cable seems to be even more pronounced at higher elevations.

- The sway of the aerial cable under strong wind conditions has not been examined in detail until now. A few observations confirm the calculated values. A wind velocity of about 60 km/h results in a sway of about 50°.
- ice formations observed during the test period represent extreme environmental conditions with respect to locations at elevations up to 500 m above sea level. No unusual effects have been noticed on the fittings. Cable slippage or cable creep has not occurred in the fittings.

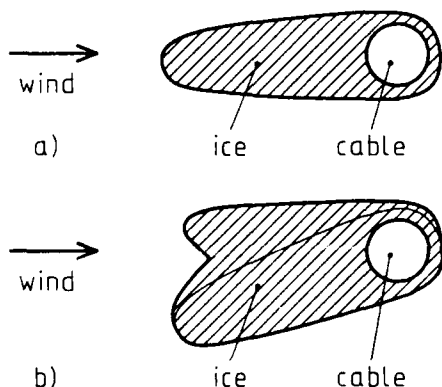


Fig. 2 Schematic representation of ice deposition

- a) on cables without torsion
- b) on cables under torsion

## Aerial Cable Construction.

### Basic Design.

The aerial cable which we developed is shown in Fig. 3. Its basic design is illustrated in the diagram of Fig. 4. The number of individual components and their dimensions can be adapted to specific requirements.



Fig. 3 Self-supporting, non-metallic, fiber optic aerial cable

The core consists of loose tubes each containing, for example, two fibers. The tubes are stranded around a central strength member of fiber-reinforced plastic (FRP). Dummies replace unneeded loose tubes. This type of construction assures that the maximum cable elongation encountered in operation does not lead to elongation of the fibers. The selection of loose tube dimensions, stranding radius and lay length is such that the required fiber excess length is available without affecting the minimum allowable fiber bending radius.

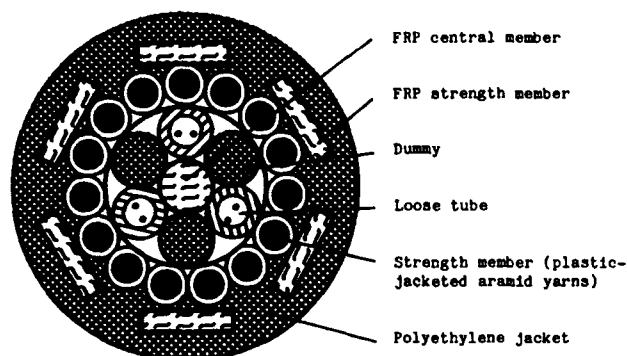


Fig. 4 Cross-section of a self-supporting, non-metallic, fiber optic aerial cable with 6 fibers

The armoring is carried out in two layers. The first layer consists of stranded, plastic-jacketed aramid yarn elements. The second layer consists of fiber-reinforced plastic flat profiles which are stranded in opposite direction to the first layer. They cover the aramid element layer to about 70%. The two-layer, inversely-stranded strengthening design results in torsion compensation. It is so designed that the cable elongation remains low, even at high additional loads. This feature permits minimum sag.

The outer jacket consists of modified, pressure-extruded hard polyolefin. As a result of the gaps in the second armoring layer, the material is pressed into the interstices of the first layer. This results in an interlocking action between the jacket and the two armoring layers. In the installed cable the tensile forces are directly transmitted from the suspension and span fittings through the cable jacket to the strength members. The interlocking action of the jacket, together with the two armoring layers, is also effective in preventing sliding or elongation of the outer jacket, even in the presence of strong stresses and high temperatures.

In general, self-supporting fiber optic aerial cables exhibit bad axial compression resistance. This may lead to increased attenuation when the cable is in unloaded condition, that is, when it is not suspended and there is no tensile force acting on it. The cable presented in this paper exhibits excellent resistance to axial compression. It is therefore also suitable, for example, for use as a short drop-off cable from the aerial cable route, thus rendering unnecessary a splice box between the buried cable and the aerial cable. An additional advantage of this compression-resistant cable is the fact that the core is not compressed

during take-up on a reel. As a result, there is no increase in attenuation after the cable is put on a reel, even at low temperatures.

#### Design Examples.

Table 3 illustrates two examples of this design for cables containing up to twelve fibers. Either single-mode or multi-mode fibers may be used. A larger number of fibers is possible, for example, if larger diameter loose tubes are used.

cable type	A	B
cable outer diameter (mm)	13.0	19.7
cable weight (kN/km)	1.45	3.20
number of fibers	up to 12	up to 12
span (m)	200	500
operating temperature (°C)	-40...+70	-40...+70
min. bending radius (mm)	130	200
breaking load (kN)	40	127
max. tensile load before fiber elongation (kN)	8.5	42.0
max. tensile load (0.2% fiber elongation) (kN)	13.0	- *

\* 1/3 breaking load is limiting the tensile load to 42kN

Table 3: Specifications of two typical F.O. aerial cable samples

Type A is suitable for short to average span lengths (200 m) with moderate additional loads. Its design tensile force is 8.5 kN. It finds typical application in the lowlands of Central Europe at average span heights (average cable height, for example, 10 m above ground). These locations are also classifiable as "not exposed" in accordance to Fig. 1.

For this application we get  $\pi_g = 0.35$  kg/m from Fig. 1,  $k_h = 1.9$  from Table 1 and  $k_d = 1.05$  from Table 2 (interpolation for a 13 mm cable diameter). Adding a 20% increase yields a value for  $\pi_g = 0.64$  kg/m. An equivalent, uniform ice layer around the cable would have 13.5 mm thickness. Under this ice load the tensile load on the cable is 7.7 kN.

At 13 kN, Type A shows 0.2% fiber elongation. This means that occasional, short-term extreme loads up to 13 kN do not affect the fiber lifetime as long as fibers with adequate screen test level are used. The increase in attenuation at 13 kN is still insignificant, permitting uninterrupted operation of the cable.

Type B is suitable for very long span lengths (500 m) under high additional loads; it is designed for a tensile force

of 42 kN. Its maximum tensile load is limited by the fact that  $F_{LT}$  (Eq. 8) may not be exceeded. There is no elongation of the fibers up to this level.

Type B can be used in locations up to 500 m above sea level. Fig. 1 shows that  $m_j = 0.5$  kg/m in places in Central Europe up to 500 m above sea level (including "exposed" locations). According to Table 1,  $k_d = 2.8$  (average cable height over ground level: 20 m). Table 2, through interpolation, yields a value for  $k_d$  of 1.11. Adding 20%, results in a value for  $m_g = 1.87$  kg/m. Thus, Type B is designed to carry almost 3 times the VDE-rated ice load (Eq. 4).

Tables 4 and 5 list the values of tensile force and sag under various conditions of wind and ice loads for the cable types listed in Table 3. The ice load is computed by Eq. 4 and the wind load by Eq. 5.  $t_{ice}$  is the thickness of a uniform ice jacket corresponding to the ice load. For both cables the assumption is made that the sag corresponds to 1% of the span length at  $-5^\circ\text{C}$  without wind or ice load.

Temp. °C	Wind km/h	Ice N/m	$t_{ice}$ mm	Tensile Load kN	Sag m
-5	0	0	0.0	3.6	2.0
-5	0	6.3	11.1	6.8	5.7
-5	0	12.6	17.5	9.4	7.5
-5	0	18.9	22.6	11.6	8.7
-5	60	6.3	11.1	7.7	5.0
-5	60	12.6	17.5	10.2	6.9
-5	60	18.9	22.6	12.4	8.2
+5	120	0	0.0	7.7	0.9

Table 4: Tensile load and sag of cable type A under various conditions

Temp. °C	Wind km/h	Ice N/m	$t_{ice}$ mm	Tensile Load kN	Sag m
-5	0	0	0.0	19.6	5.0
-5	0	7.0	10.0	26.1	12.1
-5	0	14.0	16.4	32.6	16.4
-5	0	21.0	21.6	38.6	19.6
-5	60	7.0	10.0	27.3	11.6
-5	60	14.0	16.4	33.8	15.9
-5	60	21.0	21.6	39.7	19.0
+5	120	0	0.0	26.7	3.7

Table 5: Tensile load and sag of cable type B under various conditions

Type A (Table 4) is designed for a single ice load, as defined by VDE, and for a wind load corresponding to a wind velocity of 120 km/h. Even under a combined load of a single VDE ice load and wind velocity of 60 km/h the tensile force in the cable remains below the maximum allowable force of 8.5 kN.

With an ice load of three times the VDE-rated value (even with a wind velocity of 60 km/h) the tensile force stays below 13 kN. As mentioned above, it is therefore admissible for short time periods.

Cable type B (Table 5) is laid out for triple VDE-rated ice loads, even at 60 km/h wind velocity. Without ice, the 120 km/h wind velocity causes a load which is well below the permissible load. No fiber elongation occurs in Cable B under the stated wind and ice loads.

In both cables a comparison of the numerical values of tensile load and sag at  $-40^\circ\text{C}$  and  $-5^\circ\text{C}$  shows only a slight deviation. The same holds true for a comparison at  $+60^\circ\text{C}$  and  $+5^\circ\text{C}$ .

#### Testing.

The results of mechanical tests for Cable type A using single-mode fibers are shown in Table 6.

For tensile strength tests the cable was attached to dead-end spirals of the same kind as those used for the installation. Fig. 5 represents the tensile force/elongation diagram measured on Cable Type A. The cable shows a linear elongation behavior even under low tensile forces. This confirms that the strength members are fully effective as soon as the cable is elongated. Fiber elongation begins at 8.5 kN at which point the cable elongation has already reached 0.4%.

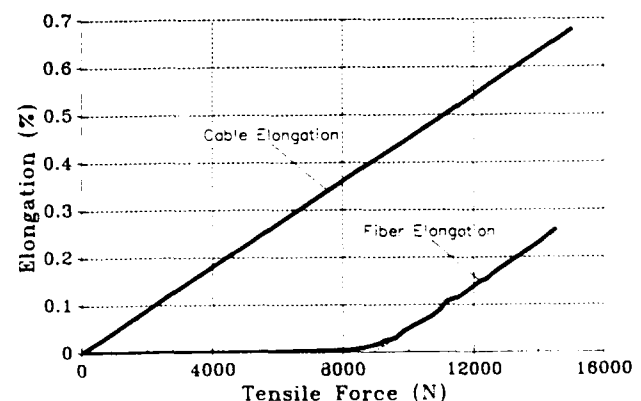


Fig. 5 Tensile force/elongation diagram for Cable Type A (in accordance with Table 3)

Item	Test conditions	Test results
Impact resistance (IEC 794-1-E4)	impact energy: 22Nm anvil radius: 12.5mm wavelength: 1550nm one impact at three different places spaced more than 500mm apart	no change in attenuation after impact; no fiber breakage; no damage to the jacket or cable elements
Repeated bending (IEC 794-1-E6)	bending radius: 135mm load: 324N cycle duration: 2s wavelength: 1550nm	no change in attenuation after 500 cycles; no damage to the jacket or cable elements
Cable bend (IEC 794-1-E11)	diameter of mandrel: 270mm number of turns per helix: 5 number of cycles: 3 wavelength: 1310 and 1550nm	change in attenuation during the test less than 0.05dB; no permanent change in attenuation
Torsion (IEC 794-1-E7)	length under test: 1m load: 324N number of turns: $\pm 1$ number of cycles: 5 wavelength: 1310 and 1550nm	change in attenuation during the test less than 0.01dB; no permanent change in attenuation; no fiber breakage; no damage to the jacket or cable elements
Tensile strength (IEC 794-1-E1)	length under tension: 200m fiber length under tension: 400m tensile load: 13kN wavelength: 1310nm	no damage to the jacket or cable elements; change in attenuation during the test less than 0.02dB (less than 0.05dB/km)
Temperature cycling (IEC 794-1-F1)	cable length: 2km high temperature: +70°C low temperature: -40°C number of cycles: 2 cycle duration: 96h wavelength: 1310 and 1550nm	maximum change in attenuation at both wavelengths: 0.03dB/km
Crush resistance (IEC 794-1-E3)	length under pressure: 100mm load: 5000N (= 50kN/m) duration of load: 15min wavelength: 1550nm	change in attenuation during the test less than 0.05dB; no damage to the jacket or cable elements
Breaking load	length under tension: 8m anchoring: protection and dead end spirals	breaking load: 40kN
Fitting creep	length under tension: 8m anchoring: protection and dead end spirals; temperatures: -40°C, +20°C, +60°C load: 20kN, 30min	no slippage of the spirals
Long-term span test	length under test: 160m anchoring: protection and dead end spirals; load: 1/3 breaking load, 1 yr	no change in attenuation; no slippage of the spirals
Vibration test	length under tension: 30m number of cycles: 10 <sup>5</sup> anchoring: protection and dead end spirals, supporting fitting;	no damage to the jacket or cable elements

Table 6: Test conditions and results for Cable type A



An increase in the attenuation is not noticed until fiber elongation occurs. At 13 kN the increase in attenuation is less than 0.05 dB/km (Table 6). The experimentally-determined breaking load is 40 kN (Table 6). A one-year span test using a 160 m length of cable with a tensile load equal to 1/3 of the breaking load was conducted. No change in attenuation was measured. No sliding or creeping of the fittings was noticed.

The results of additional tests are shown in Table 6.

#### Installation.

The installation of the cable presented in this paper utilizes conventional fittings that are in common use in aerial cable construction. Fig. 6 shows the dead-end spiral (a) and the supporting fitting (b). The manufacturer matches the dimensions of these components to the particular diameter of the cable to be used.

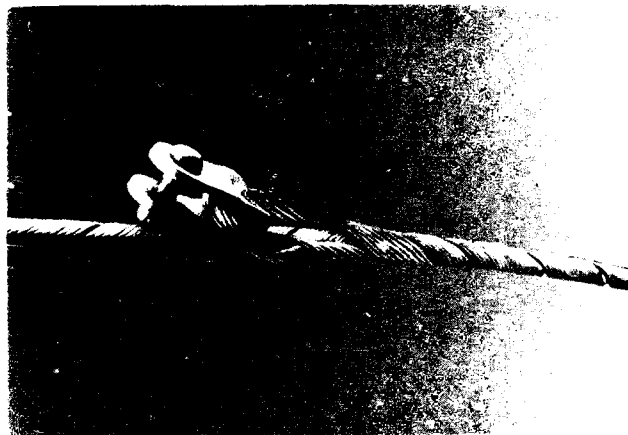


Fig. 6a Dead-end spiral for the F.O. aerial cable

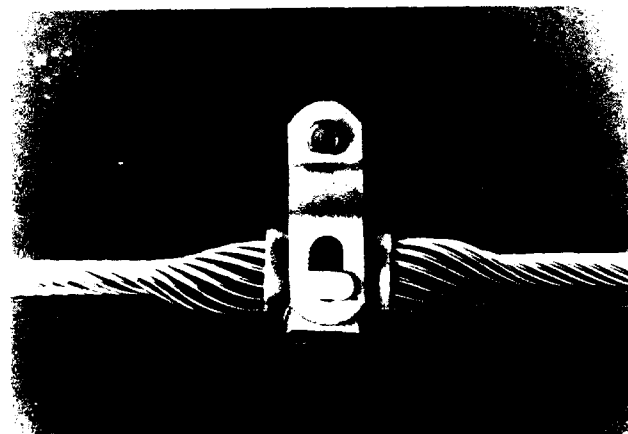


Fig. 6b Supporting fitting for the F.O. aerial cable

#### Conclusion.

The design for self-supporting, non-metallic fiber optic aerial cables presented in this paper suitable for short and very long span lengths (500 m) fulfills all requirements: ability to carry high mechanical load, complete fiber protection through adequate excess length and excellent resistance to axial compression, firm transfer of forces between the anchoring components and the strength members in the cable, without slippage or elongation of the outer jacket and without slippage or creeping of the fittings. Single-mode fibers (also in the 1550  $\mu$ m wavelength range) and multi-mode fibers may be used. We examined the ice load which is the most significant additional load in the design of aerial cables and we quantified it for Central European locations up to 500 m above sea level. Tests of manufactured cables show excellent results. The installation calls for standard fittings for conventional overhead lines which permit simple and rapid installation.

#### Acknowledgment.

The authors wish to thank Mr. H. Hofheimer of Cable Consultants Corp., Larchmont NY for his valuable assistance in preparing this paper.

#### References.

1. DIN 0800, part 4
2. DIN VDE 0210
3. F. Teucher, K. Kartschall, "Eislastuntersuchungen in der DDR und ihre praktische Anwendung" ("Ice load investigations in the GDR and their practical application") *Energietechnik*, 38, 6 (1988)
4. W. Wenski, B. Menze, J. Schulte, "Fiber strain during cable pulling: An important factor in cable design", *Proc. 38th IWCS*, 1989, pp. 368-373



Stefan Kloepper received his degree in electrical engineering from the Technical University Braunschweig in 1990. During the same year he joined Kabelmetal Electro GmbH, where he is active in cable development, with particular emphasis on fiber optic aerial cables.



Bernd Menze obtained his degree in Physical Technology from the Fachhochschule Luebeck in 1986, when he joined Kabelmetal Electro GmbH. As a development engineer he is active in the field of cable design and measurement techniques for fiber optic cables.



Johann Schulte received his physics degree in quantum optics in 1981 and his Ph.D. in engineering in 1986 from the Technical University Hannover. After a research fellowship at IBM, Yorktown Heights NY, he joined Kabelmetal Electro in 1987, where he has been engaged in the development of fiber optic cables.



Georg Maltz received his degree in communication engineering from the Technical University Hannover in 1958. During the same year he joined Kabelmetal Electro GmbH. Since 1965 he is responsible for research and development of telephone and carrier frequency cables and, since 1978, also in R & D of fiber optic cables.



Frank Teucher completed his studies in electrical power technology at the Technische Hochschule Ilmenau in 1970. He obtained his Ph. D. degree in the field of gas turbine power generation in 1973. He joined ABB Energiebau Dresden in 1973 where he has been active in the development and planning of overhead power transmission lines. The emphasis of his work dealt with the mechanical impact of climatic conditions, such as wind and ice loads, in particular.

## PORTABLE BYPASS OPTICAL CABLE SYSTEM FOR AERIAL INSTALLATION

by Y. Komaki\*, H. Tanji\*\* and Y. Moriya\*\*\*

\*Tohoku Electric Power Co., Inc. 3-7-1, Ichibanchō, Aoba-ku, Sendai 980, Japan

\*\*Sumitomo Electric Industries, Ltd. 1, Taya-chō, Sakae-ku, Yokohama 244, Japan

\*\*\*Kitanihon Electric Cable Co., Ltd. 1-2-1, Kōriyama, Taihaku-ku, Sendai 982, Japan

### ABSTRACT

There are two main approaches to route switching of fiberoptic cables installed on power distribution lines: (1) removal of a unit length (between joint closures) of cable from the existing route and its relocation to the new route, a method which realizes efficient re-use of existing fiber cables, and (2) preinstallation of a fiber cable along the new route before removal of the existing cable, a method which minimizes interruption of service. Each approach has its own advantages and disadvantages. Using a temporary fiberoptic bypass cable for the purpose of such rerouting, we are able to realize the advantages of both approaches. It can also be used as a temporary bypass during cable failure. It is a thin, light, non-metallic, 6-fiber cable (outer diameter: 6 mm, weight: 30 kg/km) with multi-fiber connectors at both ends. With the need for repetitive use in mind, installation and withdrawal methods were investigated. The required equipment and tools (reels, carriers, joint boxes, sheaves, cable clamps, and portable winches) were developed and the feasibility of the overall system was demonstrated through field tests.

### 1. Introduction

Regarding optical transmission lines installed on power distribution lines of electric power companies in Japan, it is increasingly necessary to change the routing of these lines because of the rerouting of electric poles. There are two approaches to route switching of fiberoptic cables: (1) removal of a unit length (between joint closures) of cable from the existing route and its relocation to the new route, and (2) preinstallation of a fiber cable in the new route prior to removal of the existing cable. These two approaches are selected according to the requirements of individual cases.

In the first method, fiberoptic cable can be effectively utilized, but the line is out of service for a considerable time, usually 1 - 2 days. On the other hand, with the second method, interruption of service is shorter, but re-utilization of the removed fiberoptic cable is seldom realized.

To overcome the disadvantages of these two methods, the most effective approach seems to be the modification of the first method; namely, a trans-

portable bypass cable (hereinafter referred to as "temporary fiberoptic cable") is temporarily installed during removal of the existing fiber cable and its reinstallation along the new route. By such procedure, route switching and installation work can be carried out more flexibly.

Such temporary fiberoptic cable can also be used for the restoration of service after emergencies in which the existing fiberoptic cable system is damaged due to natural calamities, fire, etc.

Based on the above background, the authors developed temporary fiberoptic cable and the equipment and materials necessary for its installation. Such cable can contribute to the shortening of service interruption consequent with route switching of fiberoptic cable system and to the effective utilization of fiberoptic cables. This cable can also be used for emergency restoration.

### 2. Procedures and materials for the system

Table 1 summarizes the process of work involved in the newly developed transportable aerial fiberoptic cable system and the material to be used in each of these processes.

### 3. Temporary fiberoptic cable

#### 3-1 Structure of temporary fiberoptic cable

Handling and maneuverability in transport, installation and withdrawal are very important factors for temporary fiberoptic cable, and the cable must be lightweight and small in diameter. The cable is designed to weigh 30 kg/km or less based on the necessity of transportability and working efficiency assuming a unit length of about 1,000 m. Single-mode (SM) 6-fiber is employed in this fiberoptic cable so that the existing line presently in use can be covered.

For stringing of the fiberoptic cable to overhead distribution poles, self-supporting type cable with messenger wire (MW) is conventionally used or round cable is suspended on the MW, which has been pulled into place in advance. The former approach is inferior to the use of round cable in terms of weight and handling efficiency, while the latter method is not suitable for simple and quick installation.

Table 1. Work processes and materials

(Work processes)		(Materials and equipment)
Pulling	Mounting of sheaves and traction rope	----- Traction rope used to pull cable (wound on reel) Cable (with connectors at both end; wound on reel) Reel carrier Sheaves with fixing band Capstan & winding drum
	Cable pulling	
Tension, clamping	Tensioning and clamping of cable	----- Cable clamp
Joining	Mounting of excess length of cable	----- Reel hanger Suspension hardware Field assembly type connector Joint box
	Connection with the existing cable immediately after cutting it	
Main restoration (existing cable)	Removal of the existing cable and its reinstallation with regular joint along the new route	
Withdrawal	Withdrawal and winding of cable	----- Capstan & winding drum Auxiliary rope for applying back-tension Rod for removal of fixing band

As the simplest aerial installation method, we decided to clamp the round cable directly onto the electric pole without MW; the round cable was designed under the assumption that it would be used for a short period (less than about one week).

Round cable must be small in diameter and as lightweight as practical, and fiber elongation must be 0.3% or less under the condition of a maximum span of 75 m, an initial dip of 0.5 - 1 m and a maximum wind velocity of 20 m/s. Thus, the round cable having the structure shown in Fig. 1 was adopted.

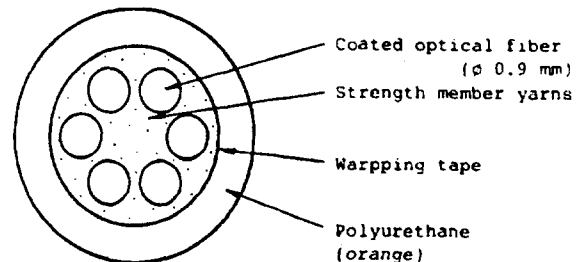


Fig. 1 Structure of temporary fiberoptic cable. (6-fiber nonmetallic type; outer dia., 6 mm; weight, 30 kg/km)

This cable does not contain a hard tension member such as steel wire or FRP at the core and is fully flexible and highly resistant to lateral pressure. Highly wear-resistant polyurethane was adopted as sheathing to insure endurance with repeated use of the cable. Orange was used as the color of the sheath to facilitate easier identification of the cable for temporary use.

### 3-2 Characteristics of temporary fiberoptic cable

Mechanical and temperature characteristics of temporary fiberoptic cable were evaluated.

#### (1) Mechanical characteristics

Temporary fiberoptic cable has satisfactory mechanical characteristics for normal operation as shown in Table 2. The results of tensile tests of cable is shown in Fig. 2.

#### (2) Temperature characteristics

Heat cycle testing was performed for the temperature range of -30 to 60°C. Results showed the change of transmission loss to be lower than 0.01 dB/km (measured wavelength: 1.3  $\mu$ m).

### 3-3 Applicability to aerial installation

In order to define the application conditions when temporary fiberoptic cable is installed on overhead distribution lines without using messenger wire, dip was calculated. One example of the results is shown in Table 3.

The results of dip calculation reveal that, in case cable is installed with an initial dip of 0.5 - 1 m over a maximum span of 75 m, fiber elongation at a wind velocity of 20 m/s is 0.20 - 0.25%, and dip is 1.5 - 1.9 m. The cable can be used for wind velocity at this value or lower.

## 4. Method of cable jointing

### 4-1 Connection between temporary fiberoptic cables

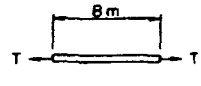
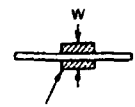
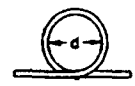
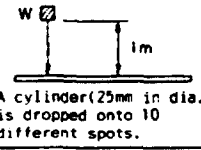
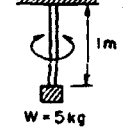
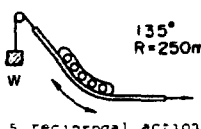
Temporary fiberoptic cables are mutually connected and extended when necessary according to the section length, and thus easy connection at site is desirable.

Accordingly, a waterproof 6-fiber connector (plug) was mounted at the cable terminal so that the cable could be connected at the adaptor by a single action. A general connection loss value of a 6-fiber connector is 0.7 dB or lower (SM type).

### 4-2 Connection with the existing fiberoptic cable

It is necessary to provide a means for connecting the ends of the temporary fiberoptic cable, to each of the fiberoptic cores of the existing fiberoptic cable. For this purpose, a joint box, as shown in Fig. 3, was adopted. Employing a built-in receptacle, the 6-fiber connector of the temporary fiberoptic cable is separated into single core cords, and single core connectors are mounted at the tips. At the installation site, field assembly type connectors requiring neither polishing nor

Table 2 Mechanical characteristics of temporary fiberoptic cable

Item	Test conditions	Test results
Tensile performance	 T = 0 - 200 kgf	$\Delta\alpha = 0$ Relation between tension and elongation: Fig. 2
Crush	 Plate plate 50 mm wide	Up to W = 200 kg: $\Delta\alpha = 0$ W = 500 kg: $\Delta\alpha \approx 0.01$ dB
Mandrel winding	 Wound 3 turns	Loss increase when d = 80 mm or less
Impact	 A cylinder (25mm in dia.) is dropped onto 10 different spots.	W = 1 kg: $\Delta\alpha = 0$ W = 1.5 kg: Sheath damaged
Torsion	 W = 5kg	$\pm 5$ turns, 1 m: $\Delta\alpha \approx 0$
Squeezing	 135° R = 250mm W 5 reciprocal actions	Up to W = 80 kg: $\Delta\alpha \approx 0$ W = 100 kg: $\Delta\alpha \leq 0.5$ dB After test: $\Delta\alpha \approx 0$

$\Delta\alpha$ : Total transmission loss increment with 6-fiber loop connection [dB] (wavelength, 1.3  $\mu$ m)

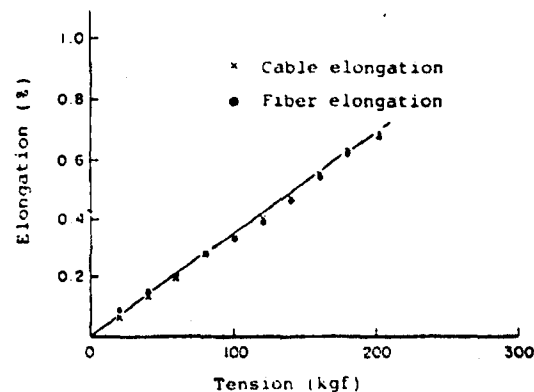


Fig. 2 Results of tensile tests of cable (Relation between tension and elongation)

Table 3. Results of dip calculation for temporary fiberoptic cable

Span (m)	Initial dip (m)	Condition Item	Initial stage (no wind)	Wind velocity 10 m/s	Wind velocity 20 m/s
75	0.5	Dip (m)	0.50	0.73	1.53
		Tension (kgf)	42.2	46.1	70.4
		Fiber elongation (%)	0.15	0.16	0.25
	1.0	Dip (m)	1.00	1.22	1.90
		Tension (kgf)	21.1	27.7	56.6
		Fiber elongation (%)	0.07	0.10	0.20

adhesive are mounted on the fiberoptic cores of the existing cable and are connected to the single core connectors. This type of field assembly connector can be used repeatedly, and general connection loss is 1.0 dB or less (SM type; with index matching material).

By adopting such a connecting methods, it is possible to separately execute connection with the existing fiberoptic cable and pulling of temporary

fiberoptic cable. Accordingly, work efficiency is improved, and work time is also shortened because both operations can be performed in parallel.

Considering the future increase in fiber count of existing fiberoptic cable, two 6-fiber receptacles are placed in the joint box. By installing two lines of temporary fiberoptic cable, an existing cable with up to 12 cores can be connected.

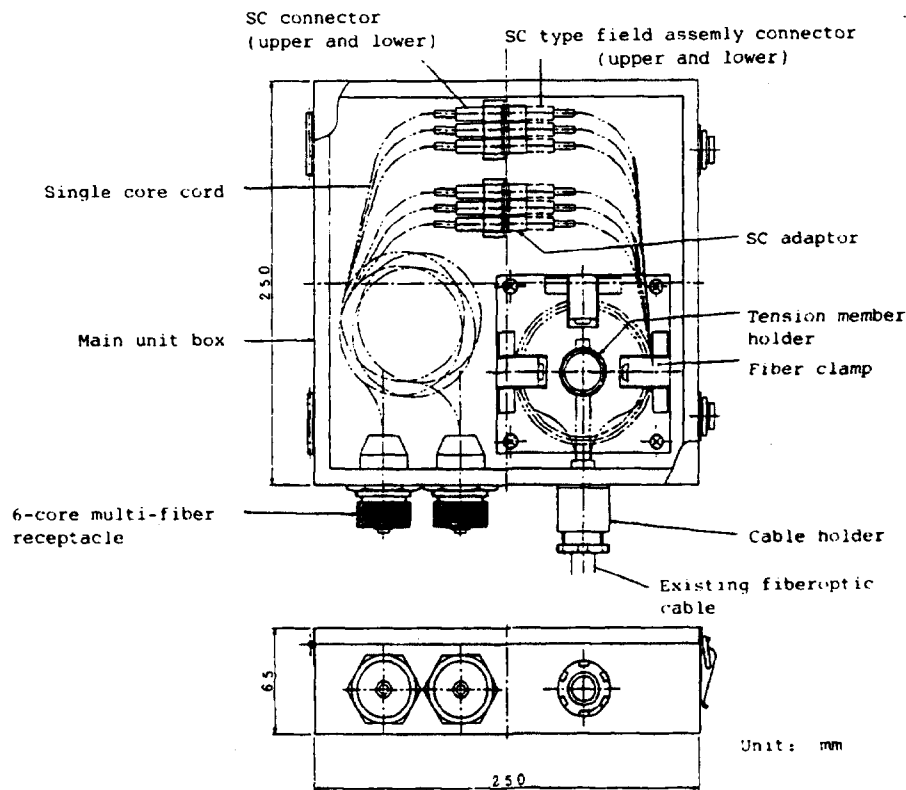


Fig. 3 Joint box with existing fiberoptic cable (for 12-fiber connection)

Connection loss of temporary fiberoptic cable and the existing fiberoptic cable (maximum value) is as follows: 0.7 dB (6-fiber connector) + 1.0 dB (field assembly type connector) = 1.7 dB per joint box; 3.4 dB (SM type) at both ends. Because the transmission loss of the cable itself is almost offset between the existing fiberoptic cable and temporary fiberoptic cable, the maximum line loss margin due to the application of temporary fiberoptic cable is  $3.4 \text{ dB} + 0.7 \text{ dB} \times n$  ( $n$ : the number of connections between temporary fiberoptic cables).

#### 4-3 Mechanical characteristics of cable terminal connector

Mechanical test for tension, bending (60 mm dia.;  $\pm 180^\circ$ ) and twisting ( $\pm 5$  turns/1 m) were performed on a sample of temporary fiberoptic cable mounted with a 6-core multi-fiber connector. As a result, satisfactory characteristics were obtained and there was almost no change in transmission loss.

Particularly, in tension testing, the application of the tension of 0 – 60 kgf (maintained for one minute) was repeated 10 times with no increase in loss. This reveals that the connector end can be directly pulled if the pulling tension in the field is 60 kgf or lower.

#### 5. Method of installation and materials

Most of the new routes resulting from rerouting of electric poles are along roads. Because route switching may also be carried out in cities,

special care should be taken that the cable installation does not hinder or interfere with vehicle or pedestrian traffic nor with conditions around buildings. Furthermore preparations should also be made for quick restoration in case of natural calamities, accidents, etc. Taking these factors into account, a method installation procedures and necessary materials and equipment have been developed.

#### 5-1 Cable installation method

##### (1) Pulling

For the pulling of temporary fiberoptic cable, a method suitable for the work of 1 crew (4-5 persons) and for convenient traffic safety has been adopted. It is the same method of fixed carrier aerial pulling as employed in the conventional method. (Cable supply side is fixed, and the tip of the cable is pulled through sheaves on top of the pole.)

Temporary fiberoptic cable is wound on an aluminum reel and this is mounted on a carrier for easy transport and paying out.

In fixed carrier aerial pulling, as shown in Fig. 4 (a), the multi-fiber connector of temporary fiberoptic cable is directly pulled with using a traction rope by a transportable winding drum (See 5-2). In case cable on two or more reels is installed, it is continuously pulled by means of multi-fiber connectors. After pulling, the connector joint is left on the span as is.

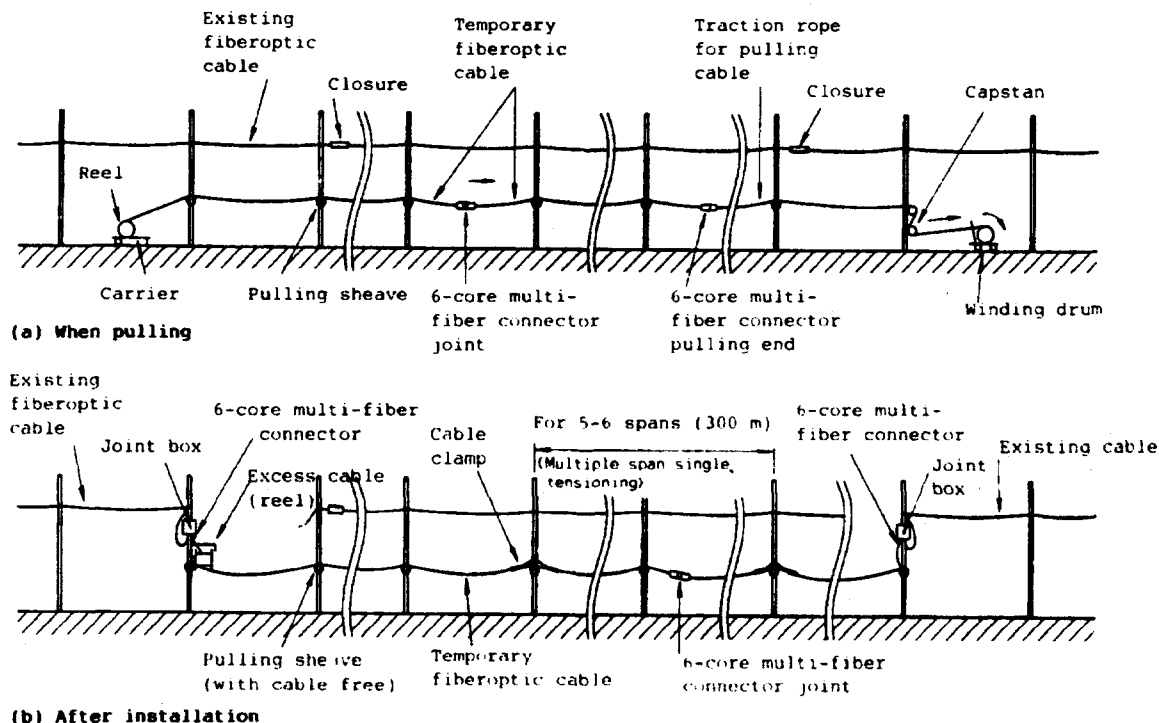


Fig. 4 Installation method for temporary fiberoptic cable (fixed carrier aerial pulling)

As sheaves for pulling to be mounted on each electric pole, the sheaves suitable for small diameter cable, as shown in Fig. 5, have been developed. They are connected with easily removable or attachable fixing bands on electric pole.

## (2) Tensioning

To increase work efficiency and shorten work time, tensioning of the cable after pulling by fixed-type carrier is performed for every 5 - 6 spans (approx. 300 m) as shown in Fig. 4 (b), and no processing of the intermediate clamp is performed. (Cable is left in a free condition within the pulling sheave.)

In case the cable is installed for a short section by the moving carrier method in emergency restoration, pulling and tensioning are carried out for each span (Fig. 6). When the cable clamp is mounted on each pole, the pulling sheave (Fig. 5) to be used at withdrawal is mounted. Therefore, the difference between fixed carrier and moving carrier aerial pulling after installation is only the difference between multiple span single tensioning or single span tensioning, and the equipment and materials used are the same.

Tensioning is performed by adjusting the dip at 0.5

- 1.0 m according to span length (50 - 75 m) so that tensioning can be carried out manually.

For clamping of the cable, special care should be taken with regard to fiberoptic characteristics (increase of optical loss due to bending and/or lateral pressure). As shown in Fig. 7, a wedge type clamp has been developed, which clamps fiberoptic cable over its total periphery by a single action.

## (3) Mounting of excess length of cable.

In case the length of temporary fiberoptic cable is longer than the length of the route to be installed, the excess length of cable left in the reel after pulling and tensioning is fixed on the pole using reel hanger to prevent accidents.

## (4) Connection with the existing cable.

After the installation of temporary fiberoptic cable is completed (or in parallel with the installation of temporary fiberoptic cable), the existing fiberoptic cable is cut near the closure at both ends, and the cable is connected (mounting of field assembly type connector) using a joint box. Then the joint box is mounted on the pole, and the 6-core multi-fiber connector of the temporary fiberoptic cable is inserted into the receptacle of the joint box. Thus, the line connection for the temporary cable is completed. (See Fig. 4(b))

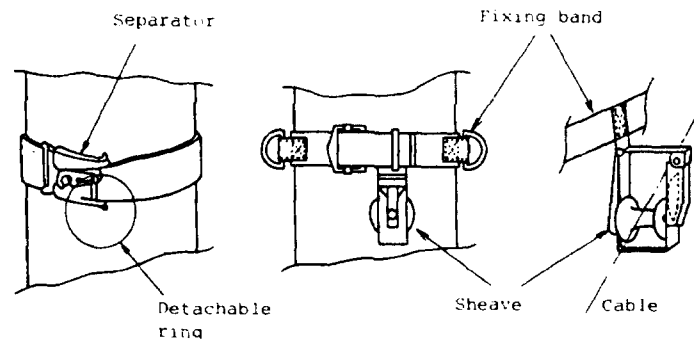


Fig. 5 Pulling sheave with fixing band

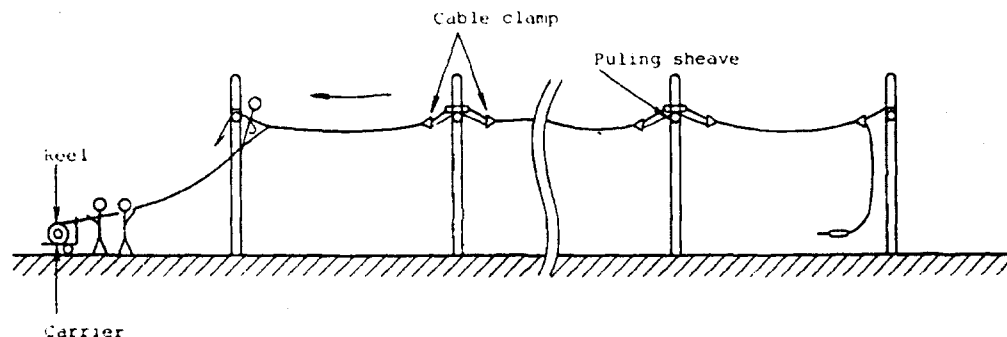


Fig. 6 Installation of temporary fiberoptic cable (moving carrier method; single span tensioning)



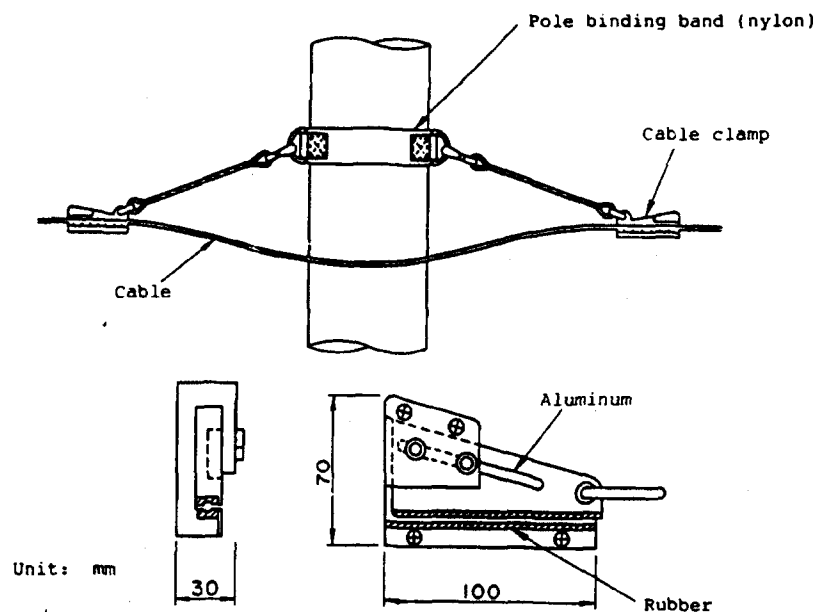


Fig. 7 Cable clamp (wedge type)

#### 5-2 Withdrawal of cable

After the regular splicing (closure joint) of the fiberoptic cable has been completed on the new route, the temporary fiberoptic cable must be removed. To remove and withdraw the temporary fiberoptic cable, the cable clamps are opened, the pulling sheaves used for the intermediate suspending are utilized, and aerial traction is performed. In this case, to prevent cable sag, auxiliary rope for withdrawing the cable is mounted on the rear end of the cable, and back tension is applied.

The cable thus removed is continuously taken up on the reel mounted on the winding drum. For this purpose, a transportable capstan & winding drum capable of being set and controlled at the required speed and torque has been newly developed. Further, as shown in Fig. 8 and Fig. 9, a new system has been adopted to facilitate well-aligned winding so that direct load is not applied to the take-up reel by the driving capstan mounted on the pole.

After cable withdrawal, the sheave can be removed by pulling the detachable ring mounted on the fixing band from the ground using a removal rod.

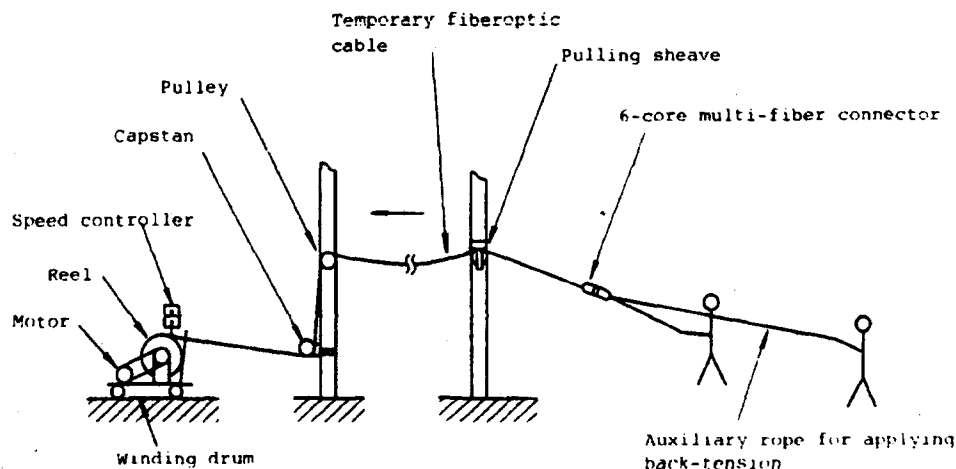


Fig. 8 Withdrawal of temporary fiberoptic cable



Fig. 9 Take-up of temporary fiberoptic cable (capstan & winding drum)

#### 6. Verification by field tests

##### 6-1 Verification of installation and withdrawal of cable

To verify the work efficiency of cable installation and withdrawal for long distances, field tests were performed. On a distribution line of about 1,300 m, temporary fiberoptic cable (800 m x 2 reels) was used, and pulling, tensioning and withdrawal were performed.

As a result, all operations could be carried out

smoothly as shown in Table 4. It has been confirmed by ITR that there was no sign of abnormal transmission loss of fiberoptic cable after pulling, tensioning and withdrawal.

For checking the reliability of cable clamping, the cable was clamped on the poles and left for 3 months; it showed no sign of abnormality.

The conditions of the field test are summarized in Figs. 10 to 13.



Fig. 10 Paying out of temporary fiberoptic cable (when pulling)

Table 4. The results of field tests

Operation	Test results
1. Mounting of traction rope and sheave for pulling	- Time required: 30 min./1,300 m (4 workers)
2. Cable pulling (800 m x 2 reels; continuous pulling)	- Pulling speed: 40 - 50 m/min. - Pulling tension: an average of 20 kgf (30 kgf max.)
3. Cable tension and clamping	- Tension: approx. 10 kgf - Time required: approx. 40 min./1,300 m (2 workers)
4. Withdrawal and winding of cable	- Back tension: 5- 10 kgf - Withdrawal speed: approx. 30 m/min. Time required: Removal of cable clamp: approx. 20 min./1,300 m Cable withdrawal: approx. 60 min./1,300 m
5. Removal of pulling sheave (operated and withdrawn from the ground)	- Time required: approx. 30 sec./point



Fig. 11 Pulling of temporary fiberoptic cable (connector joint)

#### 6-2 Verification of cable connection

The work efficiency has been verified for the connection with the existing fiberoptic cable and the mounting of excess length of cable. As shown in Table 5, it has been confirmed that the time required (in the case of a 6-core connection) for the connection and mounting of a joint box at each point is about one hour.



Fig. 12 Intermediate cable clamp.

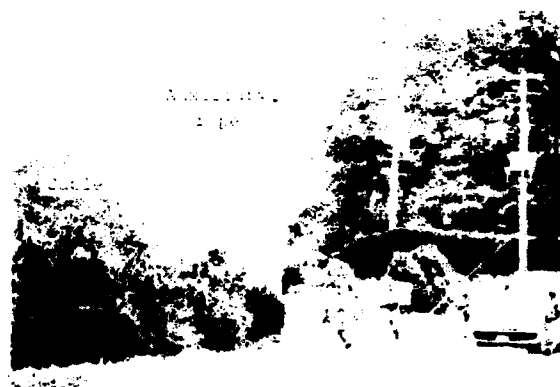


Fig. 13 Withdrawal of temporary fiberoptic cable. (Application of back tension by auxiliary rope)

Table 5. The time required for connection with existing cable and for mounting on pole.

Type of work		Work time
Connection with existing cable (joint box)	- Cable end preparation (jacket removing of existing fiberoptic cable)	7 min.
	- Mounting of field assembly type connector, accommodation of excess length of fiber	30 min. (5 min./core x 6 cores)
	- Mounting of joint box, coiling of excess length of existing fiberoptic cable and fixing	10 min.
Mounting of excess length of temporary fiberoptic cable	- Mounting of reel hanger	7 min.
	- Mounting of reel on pole	8 min.
Total		62 min.

Fig. 14 shows the mounting conditions of such a joint box and excess length of cable (reel).

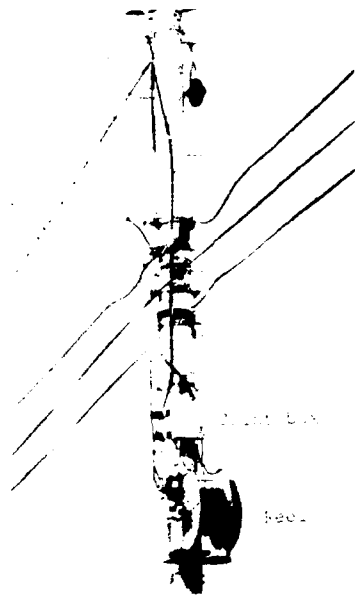


Fig. 14 Mounting conditions of joint box and excess length of cable (reel).

## 7. Conclusion

In order to facilitate the route switching operation of fiberoptic cable for distribution line associated with the rerouting of electric poles, lightweight 6-core nonmetallic type fiberoptic cable with a small diameter has been developed as temporary bypass cable. Also, under the assumption that this cable would be repeatedly used, technical methods and materials and equipment for simple and quick installation of this cable have been developed. This lightweight, compact and transportable fiberoptic system is characterized by high work efficiency and by aerial pulling. It can be widely applied for distribution lines in various areas including cities.



Yoichi Komaki  
Tohoku Electric  
Power Co., Inc.  
3-7-1, Ichibanchō,  
Aoba-ku, Sendai  
980, Japan

Yoichi Komaki graduated from Kamaishi Technical School in 1960. He then joined Tohoku Electric Power Co. Inc., and has been engaged in engineering of electric distributions. He is now a supervisor of telecommunications engineering section, and engaged in engineering of optical fiber communications system.



Yoshihiro Moriya  
Kitanihon Electric  
Cable Co., Ltd.  
1-2-1, Kōriyama,  
Taihaku-ku, Sendai  
982, Japan

Yoshihiro Moriya received his B.E. degree in engineering from Tohoku University in 1973 and joined Kitanihon Electric Cable Co., Ltd. He had been engaged in the development and design of power cables, and thereafter, worked on the development and production engineering of optical fiber cables. He is now Section Manager of the Technical Department at Kitanihon Electric Cable Co., Ltd.



Hisashi Tanji  
Sumitomo Electric  
Industries, Ltd.  
1, Taya-chō, Sakae-ku,  
Yokohama, 244, Japan

Hisashi Tanji received his B.S. and M.S. degrees in communication engineering from Tohoku University in 1981 and 1983, respectively. He then joined Sumitomo Electric Industries and has been engaged in the development of fiberoptic cables and accessories. He is a member of the Institute of Electronics, Information and Communication Engineers of Japan.

# Self Supporting Optical Fibre Aerial Cable Constructions and Related Fibre Parameters for the Transmission at $\lambda = 1550 \text{ nm}$

Helmut G. Haag, Georg F. Hög, Michael Hoffart, Ronald G. Sommer, Jörg v. Wienskowski,  
Peter E. Zamzow

AEG KABEL Aktiengesellschaft  
Mönchengladbach, Federal Republic of Germany

## 1. Abstract

Optical fibre aerial cables have been constructed for nearly 15 years. By a new technology fibres can be inserted into a tube of high quality stainless steel and this fibre filled tube substituted for an element in a metallic ground or phase wire.

The thus created new aerial cable changes in its mechanical characteristics only unimportantly. With these cables the individual fibre characteristics are most important in order to avoid any degradation of the attenuation performance of the fibre. The fibre MAC number which determines the macrobending characteristic of the fibre is an essential criterium for the selection of fibres for such cables.

Construction, test and first field experiences will be reported.

characteristics are unchanged under all environmental conditions, there is only little future for those cables because the outer sheath of such cables is destroyed over time in the case of high voltage lines.

Therefore, since 1986 some hundred kilometre of optical fibre aerial cables with metallic armouring are laid annually in the network of the German power utilities.

## 2. Introduction

The transmission technique of optical fibres in self supporting aerial cables is of great interest for power utilities. The transmission tasks such as data transmission, ISDN and protection signals are more and more digital. Moreover with this transmission medium no electromagnetic interference occurs and the broadband characteristics of the optical fibres together with the low attenuation allows fast data transmission, an enormous increase of available transmission channels, and long repeater spacing. This contribution describes a new generation of self supporting optical fibre aerial cables.

The first optical fibre aerial cable was installed in 1978 on a 110 kV line. This metal armoured aerial cable consisted of 3 star quads and 2 optical fibres. This 1.6 km long length was installed in two pieces at the lower traverse of the towers. Since that time this route is in service without any difficulties. In further projects double armoured aerial cables were further installed on 20 kV up to 380 kV lines.

Totally dielectric self supporting aerial cables were installed since the beginning of the '80's on 20 kV, and since 1984 on high tension towers up to 380 kV. Even if the optical transmission



Fig. 1 Installation of Self Supporting Optical Aerial Cable

Fundamental to the cable technology for the described here new ground wire with optical fibres are the requirements:

- the same diameter as the corresponding ground wire (ice/windload)
- the same weight as conventional ground wire (pylon stress)

This is achieved by the introduction of a metal loose buffer for up to 12 optical fibres with a diameter adapted to that of the other wires of the aerial cable. For this aerial cable design technical data for elongation under tension as well as fibre reserve and fibre bending radius issues are discussed. It is shown that for this type of cable construction the fibre MAC number, which characterizes the fibre macrobending sensitivity, is a critical parameter for transmission at 1550 nm. The MAC number technique is shown valid for depressed-inner-clad fibre.

### 3. Self-Supporting Optical Aerial Cable Construction

Self-supporting aerial cables with optical fibres are nowadays the backbone of the communication networks of German and other power utility companies. Optical fibres used in aerial cables are mostly single mode fibres with attenuation 0.36 dB/km at 1310 nm and 0.25 dB/km at 1550 nm in cable, i.e. double window fibres. These single mode fibres are designed for 1300 nm use. The dispersion is lower than 3.5 ps/(nm x km) between 1280 nm and 1320 nm. The cables are metal armoured with a first layer of aluminium alloy (aldrey) and aluminium clad steel (stalum) wires and a second layer of aluminium alloy wires in order to fulfill their grounding function. They are installed like normal conductor wires (Fig. 1).

Optical aerial cables have to be designed such that while operating over a wide temperature range (-30°C ...+60°C), and under large load, for example ice, the fibres within the cable are kept free from microbending, macrobending and elongation which would increase attenuation and reduce lifetime of the fibres. The best way to prevent the optical fibres from mechanical stress is to give them enough space for free movement. Therefore, the loose buffer technique is favoured. Depending on the total number of fibres required for a cable up to 12 can be put in one tube.

In order to prevent moisture from reaching the primary coated fibres, and in order to prevent physical contact between buffer and fibre, a jelly filling is included. Figure 2 shows typical self supporting optical aerial cable designs with either plastic or steel tube.

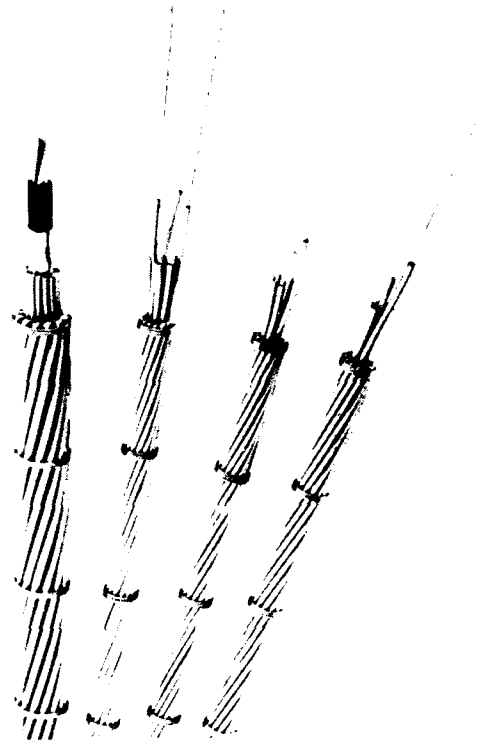


Fig. 2 Optical Aerial Cables with Plastic and Steel Buffers

Power companies request that the total design cable elongation must be more than 5% for the following reasons:

- |  |      |
|--|------|
| ◦ Laying the cable and fixing to the towers      | 1%   |
| ◦ Setting of the two layer armouring             | 1.5% |
| ◦ Elongation for temperature and mechanical load | 1.5% |
| ◦ Safety margin                                  | 1%   |

In the conventional cable construction the fibre buffers are stranded around a central FRP strength member. The pitch length for these constructions is chosen so that both elongation and contraction of the cable under operating conditions do not adversely affect the fibres. A too short pitch length gives a small bending radius and an increase of attenuation at  $\lambda = 1550$  nm may occur. A high pitch length results in a total admissible cable elongation of less than 5%.

For choosing optical fibres, especially for the aerial cables, the MAC number technique is of great interest and helpful. This technique is discussed in the next chapter.

In Figure 3 an overview with the technical data is given of some typical aerial cables with plastic and stainless steel tubes.


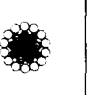
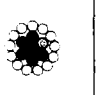

Construction	Plastic tube ASLH-D2Y0b 6x2E9/125 (AY/AW 13/21-13.5)	ASLH-D2Y0b 3x2E9/125 (AY/AW 44/28-4.7)	Steel tube ASLH-D2Y0b 1x6E9/125 (AY/AW 52/30-5.5)	ASLH-D2Y0b 1x12E9/125 (AY/AW 84/44-8.9)
				
Core	1.8	3.7 AW	2.6 AW	3.2 AW
Plastic tube	mm 1.2/1.7 (2E)			
Armoring	10x2.0 AW-5x2.0 AY	6x1.8 AW + 1x1.4/1.7 (2E)	5x2.5 AW + 1x2.1/2.5 (6E)	5x3.0 AW + 1x2.5/3.0 (12E)
Steel tube	14x3.25 AY	14x2.0 AY	13x2.25 AY	12x3.0 AY
<b>Technical aerial cable data</b>				
Cable diameter	mm 18.7	11.3	12.1	15.2
Cable weight	kg/km 648	310	356	544
Supporting cross-section	mm <sup>2</sup> 163	70	82	128
Aluminum cross-section	mm <sup>2</sup> 132	44	52	84
Steel cross-section	mm <sup>2</sup> 31	26	30	44
Ultimate tensile strength	kN 73	44	46	69
E-modulus	kN/mm <sup>2</sup> 76	95	94	92
Nominal short time current (T=20 °C)	KA 1 sec 13.5	4.7	5.5	8.9

Fig. 3 Technical Data of Optical Aerial Cables with Plastic and Steel Buffers

For the case of plastic tubes the cable core is protected by an extruded polyethylene sheath which forms the foundation for the two layer armouring. The ratio of steel to aluminium is 1:4 to 1:6. In this construction the aerial cable consists of two separate parts: The inner part, i.e. the cable core, is made of plastics and protects the fibres against mechanical stress. The outer part is made of metal to fulfill the grounding requirements.

Using a metal tube the fibres are incorporated into the cable as in an earth wire. Taking a wire such as Al/St 50/30 mm<sup>2</sup>, one wire of the inner armouring layer is replaced by a metal tube with up to 6 fibres. For larger wires, tubes with up to 12 fibres are used. Cable constructions with steel tubes of outer tube diameters of 1.7, 2.5 or 3.0 mm were developed.

Figure 4 shows an overview of the possible cable constructions with the various tube diameters together with stalum and aldrety wires for replacing conventional Al/St earth wires. The great advantage of aerial cables with steel tubes is the reduction of diameter and weight in comparison to the conventional cables with plastic tubes. With plastic tubes it is not possible to make cable constructions with a diameter on the order of 11 mm for transmission at  $\lambda = 1550$  nm and fibre excess lengths of more than 5 %. The designs are based on standard stalum and aldrety wires with 0.25 mm steps in diameter.

Aerial Cable with Steel Tube					Ground Wire			
ASLH-D2Y0b Type No	Number and Steel tube diameter mm	max fibre number	Cross section AY AW mm <sup>2</sup>	Cable diameter mm	Weight kg/km	Short Time current kA 1 s	AL ST Cross section mm <sup>2</sup>	Rope diameter mm
1.1	3x1.4 1.7	6	42 10	10.1	193	4.1	44 32	11.2
1.2	3x1.4 1.7	6	66 10	12.0	262	6.4	70 12	11.2
1.3	3x1.4 1.7	6	44 26	11.3	310	4.7	44 32	11.2
2.1	1x2.1 2.5	6	52 30	12.1	356	5.5	50 30	11.65
2.2	1x2.1 2.5	6	59 30	12.6	377	6.2	50 30	11.65
2.3	1x2.1 2.5	6	83 30	14.1	445	8.4	95 15	13.6
2.4	1x2.1 2.5	6	99 30	15.1	491	9.9	120 20	15.46
2.5	1x2.1 2.5	6	121 30	16.6	569	12.5	125 30	16.21
2.6	1x2.1 2.5	6	147 30	17.6	626	14.4	150 25	17.1
2.7	1x2.1 2.5	6	158 30	18.1	656	15.4	150 25	17.1
2.8	1x2.1 2.5	6	168 30	18.6	684	16.3	170 40	18.9
2.9	1x2.1 2.5	6	202 30	20.1	782	19.5	210 35	20.27
2.10	1x2.1 2.5	6	216 30	20.6	819	20.7	210 35	20.27
2.11	1x2.1 2.5	6	227 30	21.1	852	21.8	230 30	20.9
3.1	1x2.6 3.0	12	84 44	15.2	544	8.9	95 55	16.0
3.2	1x2.6 3.0	12	174 36	19.2	747	17.0	170 40	18.9
3.3	1x2.6 3.0	12	212 44	21.2	904	20.7	210 50	21.0
3.4	1x2.6 3.0	12	225 44	21.7	943	22.0	230 30	20.99
3.5	1x2.6 3.0	12	238 44	22.2	979	23.2	240 40	21.84
3.6	1x2.6 3.0	12	267 44	22.7	1044	25.3	265 35	22.43
3.7	1x2.6 3.0	12	382 44	27.2	1383	36.5	380 50	27.0
4.1	1x2.3 2.7	12	95 12	13.9	394	9.2	95 15	13.6

AY Aldrey, aluminium alloy  
AW Stalum, aluminium clad steel  
Al Aluminium  
ST Steel

Fig. 4 Optical Aerial Cables with Various Steel Buffers

For old towers aerial cables with steel tubes are especially preferred. They are thinner than any other aerial cables.

#### 4. MAC Number Technique

The sensitivity of optical fibres to macrobending at 1550 nm is critical to their performance in cables, especially as bending radii reduce to the order of 50 mm to 60 mm. Thus to be able to forecast what possible increase in attenuation may occur from macrobending in the described self supporting aerial cable design is essential in order to ensure loss remains below 0.25 dB/km at 1550 nm. A simple criterium to exclude fibres which would have unacceptably high macrobending loss is necessary.

In 1988 S.V. Chung /1/ developed the "MAC" number technique of characterizing macrobending loss. The MAC number is the ratio of the measured fibre mode field to the measured fibre cutoff. A MAC number of less than 8.5 in order to ensure a bending loss of less than 0.1 dB over 50 turns on a 60 mm mandrel at 1550 nm was recommended for matched clad (MC) single mode fibre optimized for 1300 nm use. This 0.1 dB value is the total loss increase over this short length of fibre at a bending radius ( $R_c$ ) of 30 mm. A lower MAC number boundary value was expected for the depressed inner clad (DIC) fibre design, but could not be experimentally verified.



For the described self supporting aerial cable constructions it was preferred to develop a test which characterized the potential macrobending loss for each and every fiber over its entire long length at a radius approximately that to be expected in cable. A type test which is made only for a limited number of samples, and which only sees the macrobending in a short length of fiber, was considered not precise enough. The resulting criterium is thus very severe in comparison to what would be normally expected of optical fibre with respect to potential macrobending loss for standard cables.

The method has been to derive a MAC number prediction from theory and to verify that the prediction is in good agreement with experiment. MAC number boundary values for both MC and DIC fiber designs were the result of this study. To date the model has been verified only for DIC. It is used to exclude DIC fibres which could have potentially high macrobending loss in the described self supporting aerial cable constructions.

From theory /2/, and taking into account the stress induced increase in refractive index with macrobending, the attenuation increase from macrobending at some test radius  $R_c$  for a particular wavelength can be predicted. This prediction is made in terms of the fibre core diameter  $2a$ , the core refractive index, and additionally, in the case of DIC, in terms of the depressed inner cladding refractive index, and the ratio of the diameter of the depressed inner cladding to that of the core ( $b/a$ ). The measured fibre mode field and measured fibre cutoff relate to these index and geometrical parameters. (We use the Petermann II definition of mode field and measure with far-field scan.) The measured fibre cutoff is the effective cutoff in a 2 meter bent fibre length as defined by CCITT G.652.

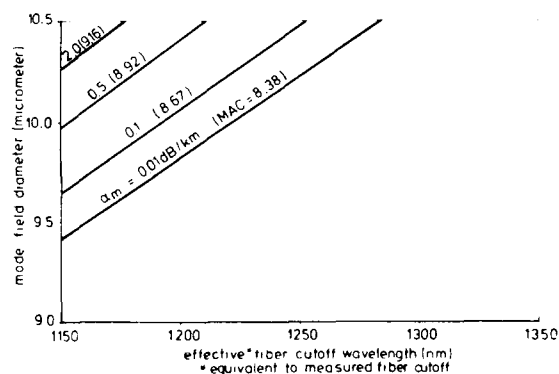


Fig. 5 Macrobending loss Boundary for MC Fibres

In the DIC fibre design it is known that the effective fibre cutoff is dependent on the magnitude of both the index depression in the inner cladding and the ratio  $b/a$  /3/. Thus this factor is included also in the model for the case of DIC in order to ensure that the predicted macrobending loss is in terms of a MAC number which correlates with the measured fibre cutoff.

Shown in Figures 5 and 6 are a series of forecast macrobending loss boundary curves for typical MC and DIC, respectively, in terms of mode field and effective fiber cutoff for a bending radius of 50 mm. A boundary MAC number value corresponds to each macrobending loss boundary curve. For the DIC case the depression index in the inner cladding is 1.2 times ten to the minus three and  $b/a$  is 6.5.

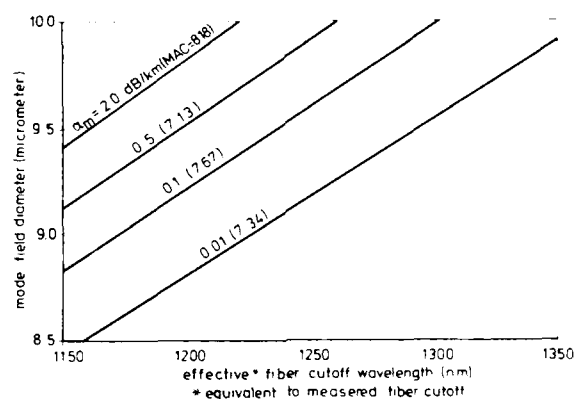


Fig. 6 Macrobending loss Boundary for DIC Fibres

The boundary values for DIC would linearly decrease somewhat as either or both index depression and  $b/a$  increase.

For the MC case, it can be seen that for a nominal mode field of  $10.0 \mu\text{m}$ , an effective cutoff greater than 1195 nm is necessary in order to reduce the 1550 nm macrobending loss over the entire fiber length at a bending radius  $R_c$  of 50 mm to below 0.1 dB/km. This means a MAC number of less than 8.67. This value is comparable to the value reported by S.V. Chung /1/ for 1300 nm optimized MC. For the DIC case, for a nominal mode field of  $9.5 \mu\text{m}$ , an effective cutoff greater than 1240 nm is necessary in order to reduce the 1550 nm macrobending loss over the entire fiber length at a bending radius  $R_c$  of 50 mm to below 0.1 dB/km. This means a MAC number of less than 7.67.

In order to verify the correctness of the forecast MAC number boundary values for DIC an experiment was performed. The increase in loss at 1550 nm on winding in long lengths on approximately 50 mm radius spools was determined and related to the measured mode fields and cutoffs for a large number of fibres. This loss increase is not necessarily purely macrobending, but is in practice a convenient test. In fact, an application advantage for DIC is its lower sensitivity to microbending, so a test with DIC is most suitable.

The result is displayed in Figure 7.

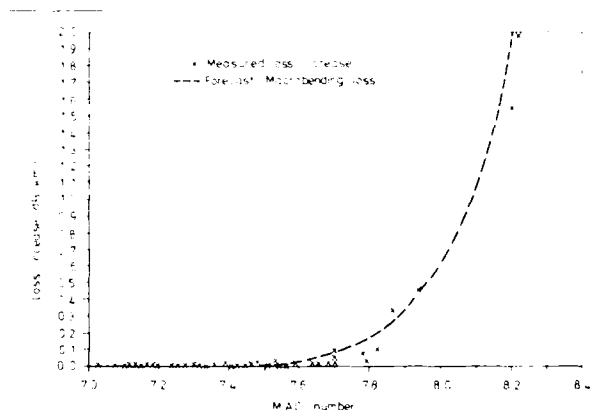


Fig. 7 MAC Number Versus loss Increase

The agreement to model is excellent. From these results we confidently chose a MAC number boundary value of 7.5 for DIC. This simple criterium is used to exclude potentially high macrobending loss DIC fibres from the described self supporting aerial cable constructions.

#### 5. Test Results for the Optical Fibre Aerial Cable

In the following chapter the most important test requirements and results for self supporting aerial cables with optical fibres are described. Only cable constructions with optical fibres in stainless steel tubes are discussed. In earlier papers aerial cables with plastic tubes were sufficiently reported on /4/.

The decisive tests for aerial cables with steel tubes are:

- o Temperature
- o Mechanical damping
- o Short time current
- o Torsion
- o Tension
- o Elongation over lifetime

For the various tests the measurement equipments that were used and the cable performances are described. As an typical example the cable type ASLH-SD 3x2E9 (44/26-4.7) corresponding to Figure 4 in chapter 3 is discussed. Figure 8 shows a cross sectional photograph of the tested cable.

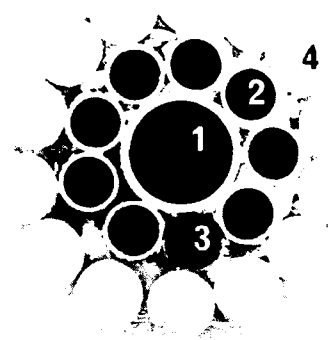


Fig. 8 Cross Section of the Aerial Cable with Steel Tube

- 1 ACS-Wires
- 2 ACS-Wires
- 3 Steel Tube with optical fibres
- 4 Al-Wires

#### Temperature

Generally aerial cables with optical fibres in steel tubes are less sensitive to temperature changes over a wide range in comparison to cables with plastic tubes. This is because the temperature expansion coefficient of steel is lower than that of polyamide or polyester, which are the common materials for the plastic buffer. Therefore, the problem of too much fibre excess length at low temperatures ( $-40^{\circ}\text{C}$ ) and too less excess length at high temperatures ( $+80^{\circ}\text{C}$ ) is not significant.

Temperature tests of some cables with steel tubes between  $-40^{\circ}\text{C}$  to  $+80^{\circ}\text{C}$  have verified this.

The changes in attenuation at  $\lambda = 1310 \text{ nm}$  and  $\lambda = 1550 \text{ nm}$  were lower than  $0.05 \text{ dB/km}$ .

#### Torsion

An important criterium for laying the aerial cables at the top of the towers is the torsion performance of the cable. In the case of a high torque, fibre excess length is loss.

This may result in an increase of attenuation, especially at  $\lambda = 1550 \text{ nm}$ , which is independent of fibre characteristics. In order to optimize the torque behaviour of the cable a special torque measurement is used. Figure 9 shows the construction of the equipment.

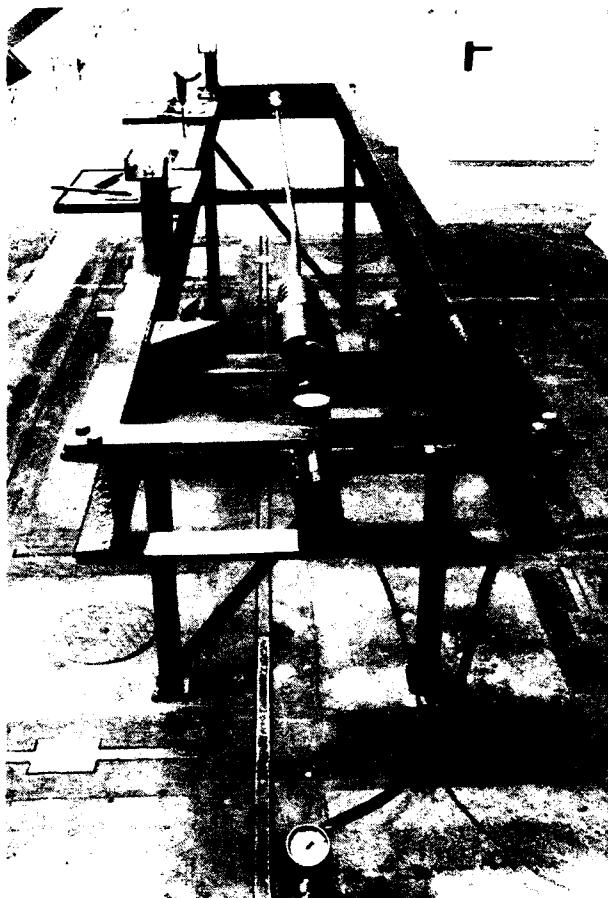


Fig. 9 Torsion Measurement

By means of this test equipment, it is possible to analyse the behaviour of the cable armouring in respect to the number of the wires and their diameter, the pitch length ratio and the preforming of the single wires. With the results of the test it is possible to optimize the cable armouring in such a way, that during the cable drawing no torque occurs and no fibre excess length is loss.

Figure 10 shows for the mentioned cable the torque as a function of the tensile load for the not optimized and the optimized cable.

The optimized cable shows in the tension test (100 m length) almost no torque. For other aerial cables with steel tube design corresponding to those in Figure 4 for armouring optimisation the same test is necessary.

In the text below the influence of torsion is no longer discussed as this factor has been shown not a concern with the described cable design.

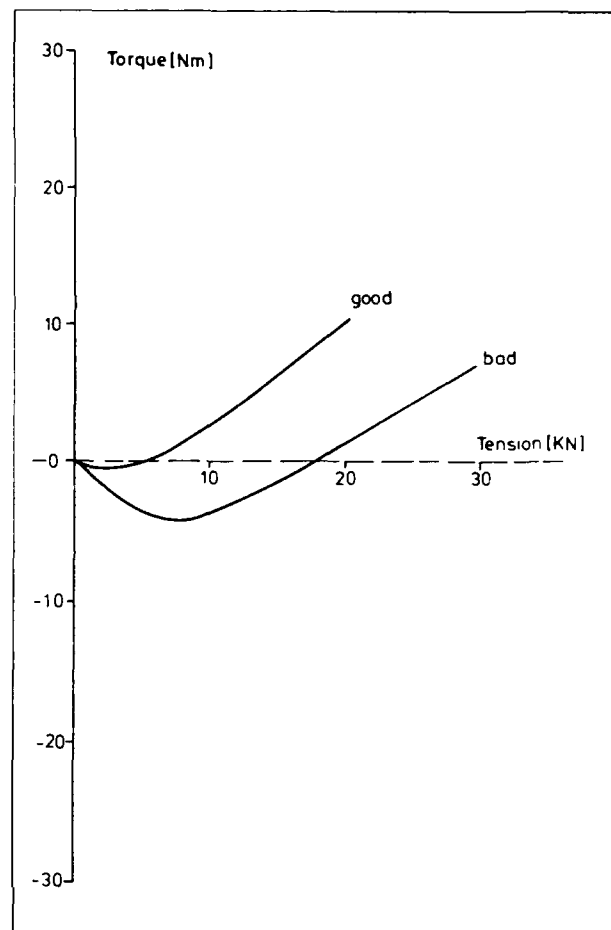


Fig. 10 Torque Behavior of the Aerial Cable

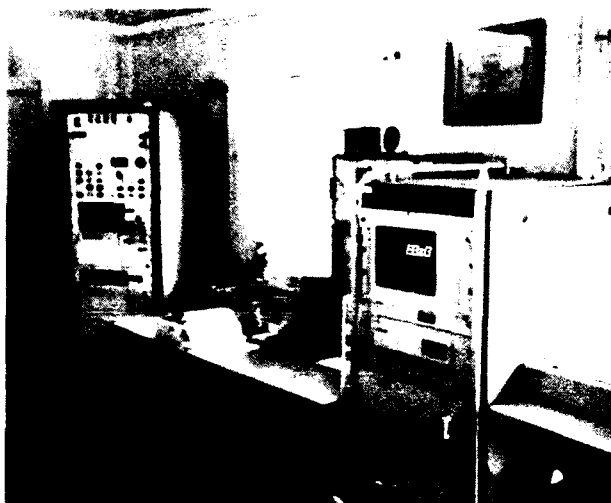
#### Tension

For self supporting aerial cables with optical fibres the most decisive factor is the tension load as no change of attenuation is allowed upto this load. This tension load is specified by the maximum continuous permissible strain. This load is for the described cable 30.5 kN. The fibres in the cable must have - specified by the customer - more than 5% excess length, i.e. no fibre strain is allowed at the mentioned tensile load. This value can be obtained by choosing a correct pitch length of the steel tubes and the armouring wires, or by putting a defined fibre excess length into the steel tube. An important criterium for the latter situation is the fibre bending radius in the aerial cable.

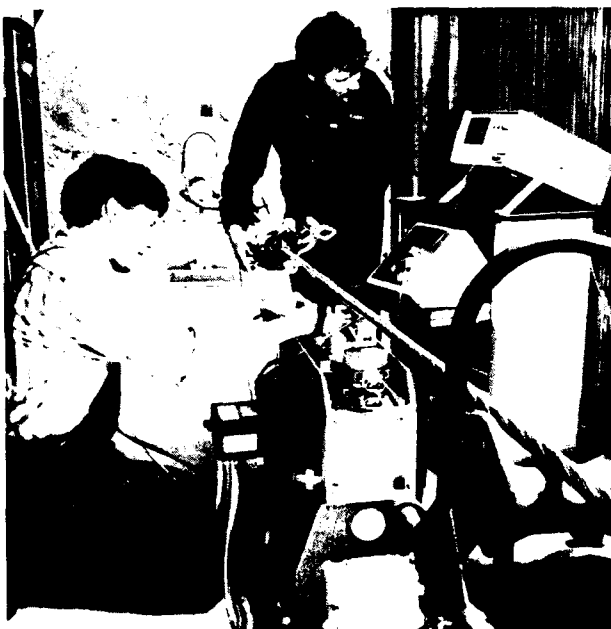
For the described cable construction the following values were chosen:

Number of fibres in steel tube	2
Number of steel tubes	3
Diameter of steel tube	1.4/1.7 mm
Pitch length	82 mm
Excess length in steel tube	2%
Total excess length in cable	8.9%
Fiber bending radius	69 mm

The tension test - see Figures 11 and 12 for the equipment - was made with a 100 m long cable sample.

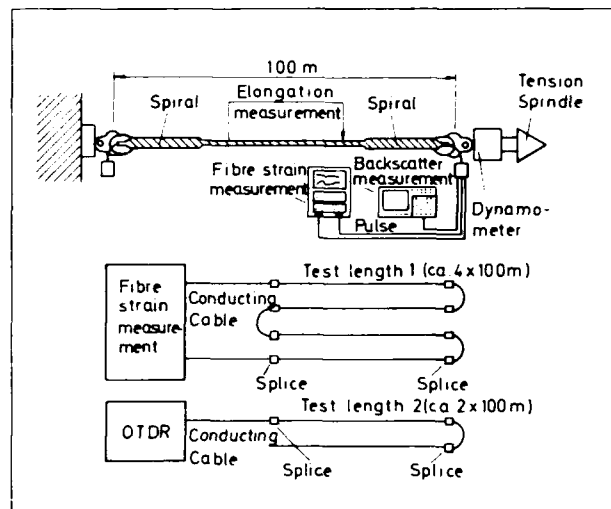


**Fig. 11** Tension Test Equipment Measurement



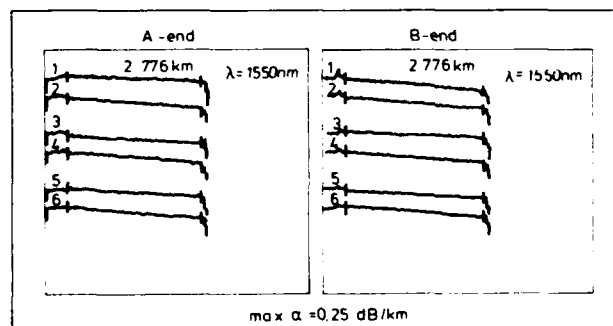
**Fig. 12** Preparation for Tension Test (100 m)

Figure 13 shows the measurement principle. Three fibres in this cable sample were spliced together for the OTDR measurements, and the other three similarly spliced for the fibre strain measurements.



**Fig. 13** Principle of OTDR and Fibre Strain Measurement

The results in Figure 14a (OTDR) and 14b (left: fibre strain in steel tube, right: fibre strain in the finished cable) show that up to the calculated ultimate tensile load of 44 kN no change of attenuation at  $\lambda = 1550$  nm, and no fibre strain, occurs.



**Fig. 14a** OTDR Results on the Aerial Cable with Steel Tube

The measured fibre reserve in the cable corresponds with the theoretical value of about 9%. Even after the completion of this tension test, the cable still had tight armouring of usable quality.

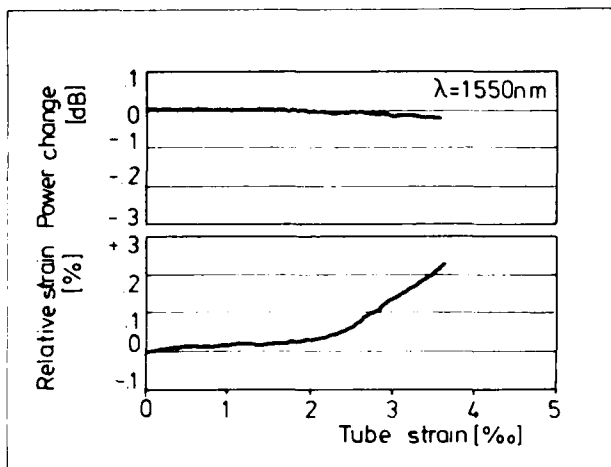


Fig. 14b Fibre Strain in the Single Steel Tube

#### Elongation over lifetime

For conventional Al/St ground wires it is known that the extrapolated elongation at a lifetime of 30 years is between 1‰-2‰.

The appropriate tests should show if this performance is also valid for ground wires with integrated fibre optics.

Figure 15 shows the test equipment for the measurements.

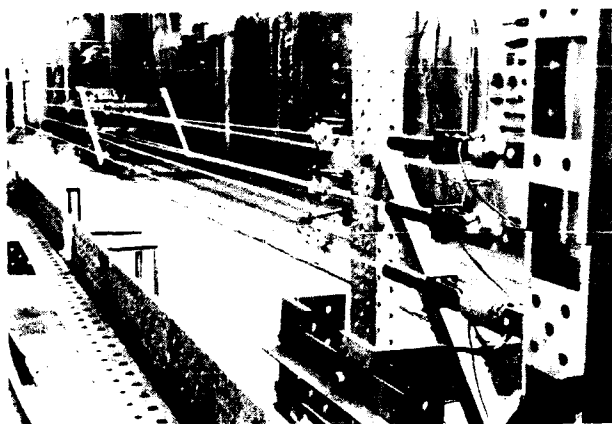


Fig. 15 Elongation Measurement

The tests were made over 4000 hours and then an extrapolation was made to 30 years.

In total three samples of the described cable were tested with tensile loads as follows:

Sample 1: 17% calculated ultimate tensile load  
110 N/mm<sup>2</sup> tensile load

Sample 2: 39% calculated ultimate tensile load  
250 N/mm<sup>2</sup> tensile load

Sample 3: 60% calculated ultimate tensile load  
380 N/mm<sup>2</sup> tensile load

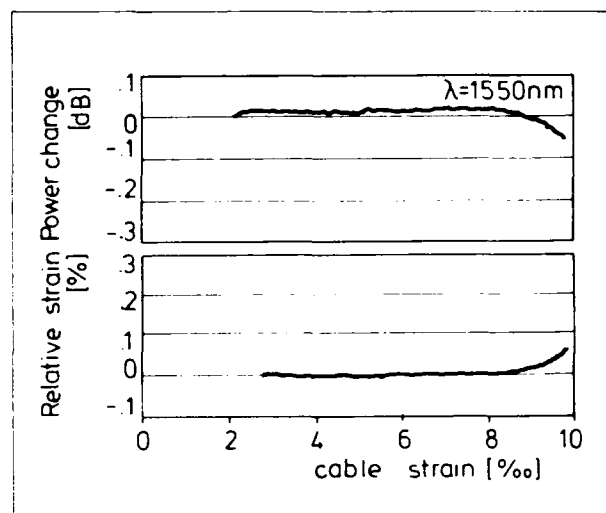


Fig. 14b Fibre Strain in the Cable

The diagrams of performance against time are shown in Figure 16.

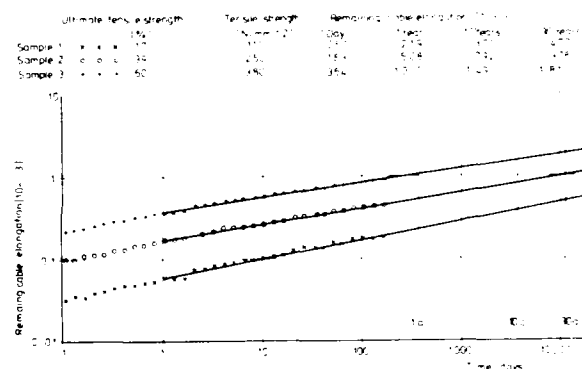


Fig. 16 Lifetime Elongation Results

The extrapolated cable elongations at 30 years are:

Sample 1: 0.48‰

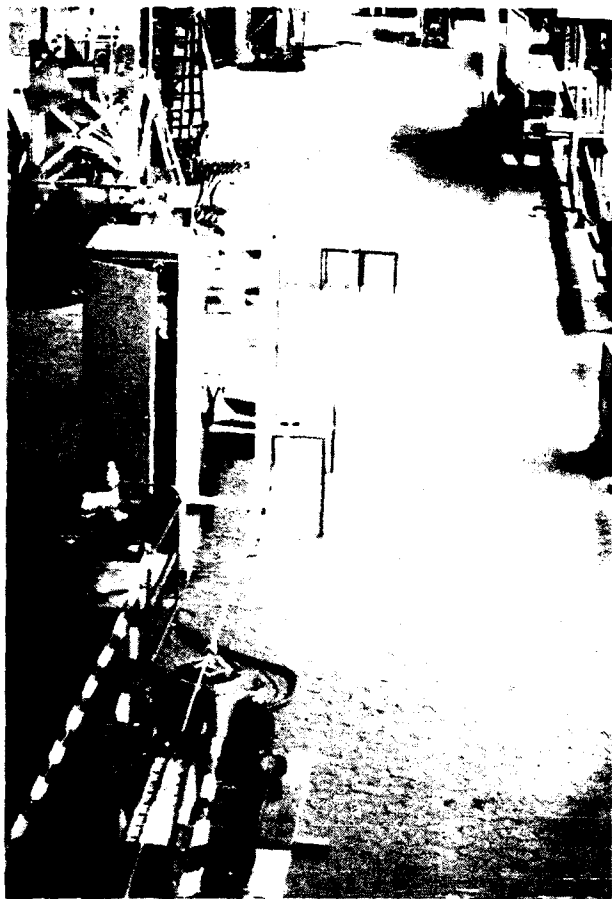
Sample 2: 0.98‰

Sample 3: 1.81‰

These results are nearly the same as for a conventional ground wire.

#### Self damping

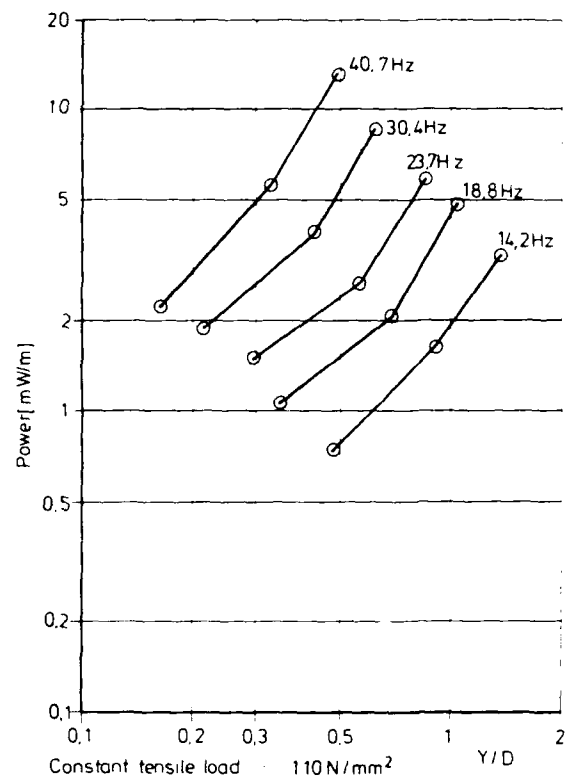
With this test it should be found whether or not the aerial cable with steel tubes needs damper clamps. The tests were made in accordance with the "Guide on Conductor Self-Damping Measurements" of the CIGRE Study Committee No 22 /5/ (Figure 17).



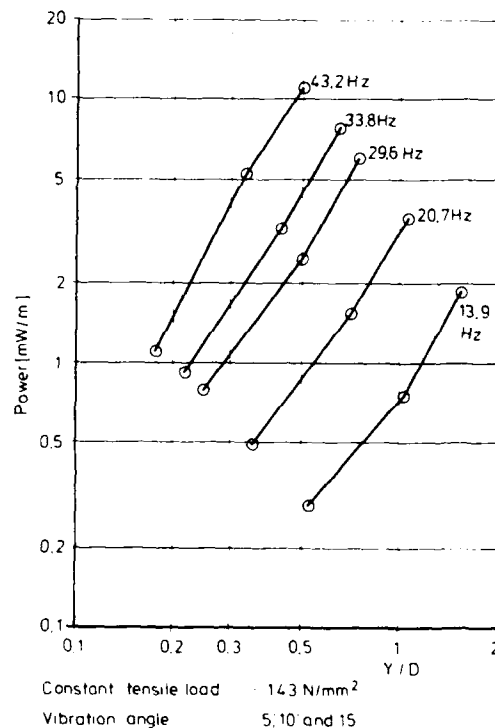
**Fig. 17** Self Damping Measurement

The tests for the aerial cable ASLH-SD 3x2E9/125 (44/2.-4.7) were made with two tensile loads (7.4 kN and 10 kN) and three vibration angles (5', 10' and 15'). The self damping measurements were made at five frequencies between 10 Hz and 50 Hz. The Figures 18a and 18b show the test results. In Figure 18a the damping powers of the aerial cable with tensile loads of 110N/mm<sup>2</sup> and 143N/mm<sup>2</sup> versus Y/D (Y: maximum amplitude of vibration, D: Cable diameter) are shown.

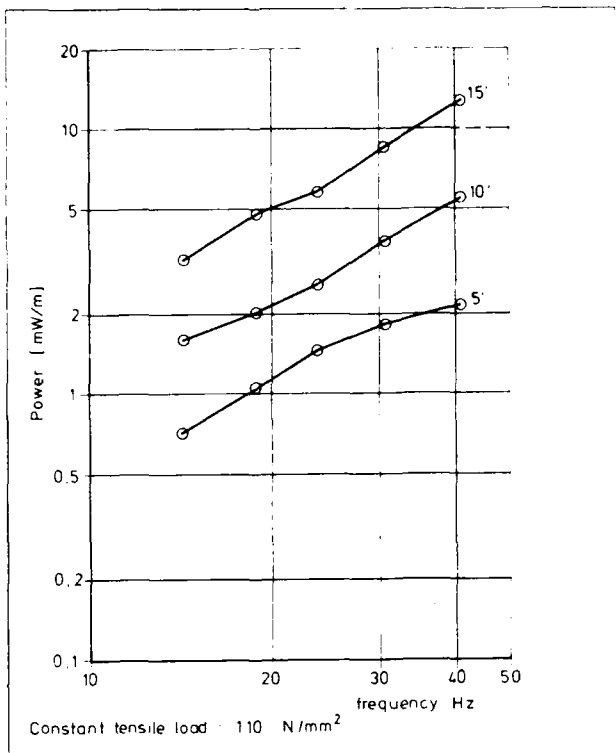
In Figure 18b the damping powers versus vibration frequency are shown for the two tensile loads. From these results clamps are needed for this cable design.



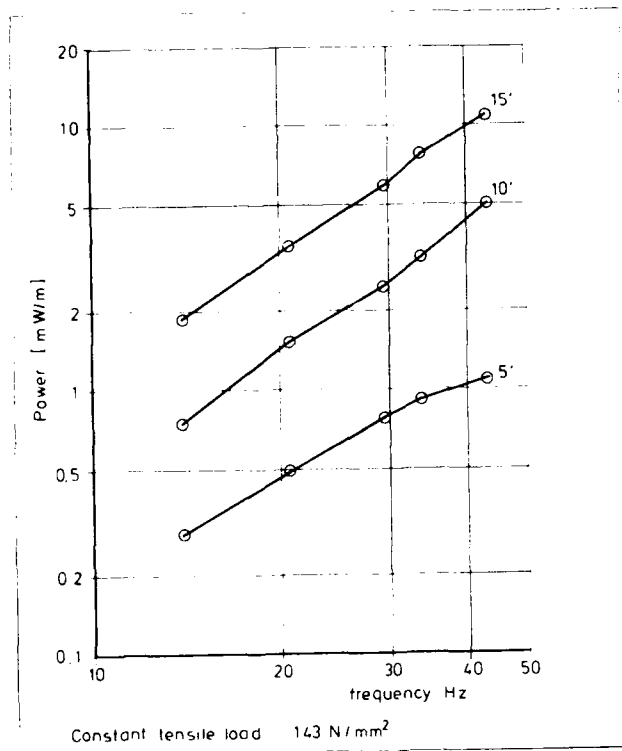
**Fig. 18a** Damping Power Versus Vibration Amplitude (110 N/mm<sup>2</sup>)



**Fig. 18a** Damping Power Versus Vibration Amplitude (143 N/mm<sup>2</sup>)



**Fig. 18b** Damping Power Versus Frequency (110 N/mm²)



**Fig. 18b** Damping Power Versus Frequency (143 N/mm²)

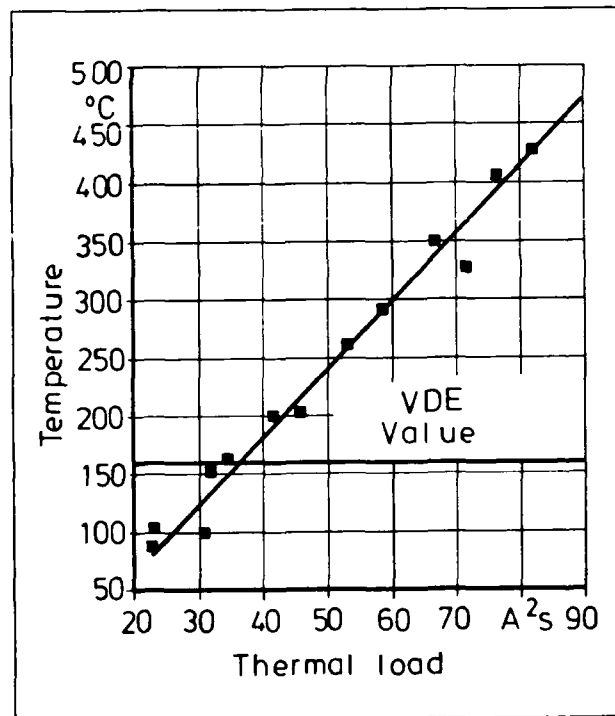
### Short Time Current

After the completion of the tension test, the short time current measurement was made on the same test sample. In this test the cable is loaded for 1 sec with the specified value for short time current, i.e. for the described cable a value of 4.7 kA. The temperature limit for the cable is 160°C. In actuality the optical and mechanical function of the aerial cable was tested at higher thermal load up to its destruction.

To do this test, a sample of 30 m length was hung suspending the air and connected to a 220 KV source and a current I applied for a time t to the cable. Thermoelements were present in the inner and outer layer of armouring so that the temperature could be observed after the current surge.

Attenuation at  $\lambda = 1310$  nm was monitored throughout the entire test.

With a current of  $I = 4.75$  kA over  $t = 1$  sec the temperature increased from 20°C to 92°C. No change of attenuation was recorded. If the  $I \cdot t$  load was increased by a factor of 2.6 against that of the above test, a change in attenuation of less than 1/100 dB per 160 m test length with a temperature increase to 295°C in the outer layer was observed. At a factor of 3.9 the temperature increased to 430°C (Figure 19). The fibres went dark. At this higher load the aerial cable was mechanical destroyed.



**Fig. 19** Short Time Current Results

With this test it was shown that the aerial cable with optical fibres in steel tube satisfies the specification at high thermal loads.

Thus a self supporting optical fibre aerial cable with stainless steel tubes fulfills the requirements placed on a conventional Al/St ground wire.

Corresponding tests are in progress at the moment for cables with 6 and 12 fibres per steel tube and are expected to be finished at the end of 1991.

#### **6. Future trends**

An important trend for the further development of aerial cables with steel tubes is corrosion prevention. Early tests have revealed that a standard bare steel tube in combination with aluminium or stalum wire corrodes slightly. However, a range of tests with salt water sprays and simultaneous mechanical dynamic stress did not show any intensive corrosion of the surface of the steel tubes. At this time whether or not it is necessary to protect the steel surface from corrosion is not clear. Nor at this moment, if protection is necessary, is it clear which method would be the best choice.

The described here new aerial cable meet the increasing demand for communication of all subscribers in the near future period.

It will be the successful third generation of aerial cables. The complete cable range will be covered by a maximum of two tube dimensions.

The choice of these two dimensions will come out of further developments. The described technique for steel tubes will be extended to higher fibre counts than 12 by techniques such as ribbons and solid mini bundles in order to increase fibre packing density.

MAC-number will be a necessary technique for the development of such cables.

#### **7. Acknowledgement**

Dr. R. Yang, in an industrial postdoctoral position at AEG KABEL AG, did the mathematical calculations.

SAG (Starkstrom-Anlagen-Gesellschaft, Langen, Germany) did the self damping and lifetime strain tests.

#### **8. References**

1. S. V. Chung, 'Macrobend loss of 1300 nm optimized single mode fibre at 1550 nm', International Wire and Cable Symposium Proceedings, 1988, pp. 704-709.

2. R. Yang and L. Wetenkamp, 'Bending loss of depressed clad fibres', Fifth National Symposium on Optical Fibres and Their Applications, Warsaw, February 1989, pp. 422-426.

3. R. Yang, M. Hoffart, H. Schürmann, R.G. Sommer, 'Profile dependence with empirical model for effective cutoff in depressed inner cladding fibre', Electron. Lett., 1989, 16, pp. 1070-1071.

4. H. Haag, G. Hög, P. Zamzow 'New generation of self supporting optical fibre aerial cables' IWCS 1990.

5. CIGRE Study Committee

No. 22-Electra no. 62(1979) Guide on Conductor Self-Damping Measurements.



Helmut G. Haag  
AEG KABEL AG  
Sales Division for Telecommunications  
Mönchengladbach, Germany

Helmut G. Haag (43) is Manager of Sales Division for Telecommunications. After reaching his Dipl.-Physiker-degree from the University of Stuttgart he joined AEG KABEL in 1975 for the development of coaxial cables. Later he has been also responsible for the development of optical fibre cables. From 1980 to 1983 he built up the production plant for these cables. In autumn 1983 he took over the Technical Sales Division and in Jan. 1990 the total Sales Division.



Georg Hög  
AEG KABEL  
Mönchengladbach, Germany

Georg Hög (41) is head of the Development Group for Optical Fibre Cables. He reached his Dipl.-Ing.-degree from the University of Aachen and joined AEG KABEL in 1977. After being engaged in the development of symmetrical telecommunications cables he got the responsibility for this group in 1980. Since 1985 he covers his present position.





Michael Hoffart  
AEG KABEL AG  
Mönchengladbach, Germany

Michael Hoffart (35) is General Manager of the Optical Fibre Plant. He received his Dipl.-Ing.-degree from the "Bergische University" Wuppertal in 1983. He joined AEG KABEL on graduation and has been engaged in the field of optical measurement technique and telecommunication cables.

Ronald G. Sommer  
AEG KABEL AG  
Mönchengladbach, Germany

Ronald G. Sommer (47) is Manager for Optical Fibre Development. He received a Ph. D. in Physical Chemistry from the University of Iowa in 1974. He has since then continually worked in the area of optical fibres, joining AEG KABEL in 1987 after prior employment in the USA and the UK.



Jörg H.W. von Wienskowski  
AEG KABEL AG  
Mönchengladbach, Germany

Jörg H. W. von Wienskowski (47) is head of the Sales Department for Overhead Aerial Cables. He got his diploma degree as Dipl.-Phys. and his Ph.D. degree at the Technical University Aachen. In 1982 he joined AEG KABEL for optical fiber and optical fiber cable development. Starting in 1984 he was responsible for the production of those products. He joined the sales division in 1988 and since 1990 he covers the present position.



Peter E. Zamzow  
AEG KABEL AG  
Telecommunication Development  
Mönchengladbach, West Germany

Peter E. Zamzow (51) is director of the Telecommunication Development Division. After finishing his postgraduate studies in telecommunications in Munich and Graz as Dipl.-Ing. he joined AEG KABEL in 1970. He has been engaged in development and production of telecommunication cables. In 1980 he became head of the fiber optic division at AEG KABEL and in 1982 he was nominated as a senior engineer. Since 1985 he has covered his present position.

## DESIGN AND OPERATION OF AN AERIAL FIBER-OPTIC CABLE FOR RAILROAD COMMUNICATIONS

A. Bidinger

German Federal Railroad/ Central Administration  
Friedrich-Ebert-Anlage 43-45, D-6000 Frankfurt a.M. 1, Germany

W. Lynen and R. Ney

Lynenwerk GmbH & Co. KG, Postfach 1280, D-5180 Eschweiler, Germany

### Summary.

The technical problems connected with the application of fiber-optic data communications over long distances can be considered as solved. There exist a sufficient number of networks in operation which substantiate the validity of this claim. Hitherto, the cables used were mainly buried. The application of aerial cables for this purpose was considered problematical, based on prior experience which revealed a deterioration of the transmission characteristics and lifetime of optical fibers under mechanical load. In cooperation with the Deutsche Bundesbahn (German Federal Railroad) the development of a non-metallic, fiber-optic aerial cable was started in 1987. This cable is suspended from the masts carrying the contact wire. It is suited for free spans up to 100 m (300 ft). The important novel feature of the cable design is a polyethylene jacket with embedded glass yarn bundles which combines high tensile strength and light weight. The evaluation of the cable presented in this paper took place along the railroad track between Reutlingen and Tuebingen, Germany. After three years of successful operation, the test is considered completed.

### Aerial Cables for Long-distance Communications along Electrified Railroad Tracks.

With the advance of electrification, the economical aerial cables were displaced by buried cables. The main reason for this is that the electromagnetic interference generated by the electrical traction system can, in practice, not be eliminated by conventional cable design techniques. Another limiting factor is the lack of space for installing heavy shielded cable in proximity of the track. These conditions changed when non-metallic, fiber-optic aerial cables became available. Furthermore, it was determined that suspension of the light-weight cables from the masts carrying the contact wire for the

electrical traction system does not affect the masts or the operation of the railroad (Fig. 1).



Fig. 1 Track section with fiber optic cable (arrow)

The design requirements for this kind of F.O. aerial cable are mainly derived from the properties of optical transmission. Their principal component is the optical fiber which, when compared to conventional copper conductors, is extremely sensitive to tensile and compression stresses. Special designs are therefore needed to protect the delicate optical fiber in the cable core after installation from excessive stresses caused by varying climatic conditions.

### Design Considerations.

□ Six optical fibers were required between the Reutlingen and Tuebingen railroad stations for an over-all length of 15.38 km (9.6 mi), including drop-offs to three intermediate stations. A copper conductor star-quad had to be included in the cable core for occasional operational use.

□ The round fiber-optic cable had to be suspended from and braced to the overhead line masts in such a manner that its system transmission characteristics as well as the railroad operation were not adversely affected by temperatures between  $-40^{\circ}\text{C}$  and  $+60^{\circ}\text{C}$ , snow loads of 2 kg/m (1.34 lb/ft) at  $-5^{\circ}\text{C}$  or wind velocities up to 104 km/h (64.6 mph) at  $+5^{\circ}\text{C}$ .

□ Trees that might collapse in proximity of the line must be caught by the cable in a manner resilient enough that does not permanently affect the transmission characteristics. In case of tree collapse between masts, the stored slack in the cable must suffice to enable the tree to fall and force the cable to the ground, without damaging it (Fig. 2).



Fig. 2 Tracks exposed to potential tree impact

□ The basic design of the cable core should utilize proven techniques of buried cables.

□ The required non-metallic tension relief system must be integrated into the cable jacket, so as to permit the use of traditional laying techniques using dead-end spirals and support rollers.

#### Characteristics of the Reutlingen-Tuebingen Railroad Track Section.

When we first started our project, the overall 48.76 km (30.3 mi) track section between Plochingen and Tuebingen, corresponding to an actual cable length of 53.61 km (33.31 mi) was nearing completion. During the 1984-88 period, the 34.72 km (21.58 mi) section between Plochingen and Reutlingen (cable length: 38.23 km = 23.76 mi) was rebuilt, using paper-insulated, buried copper cables of type AI-PLb2Y 64(8/18/38).

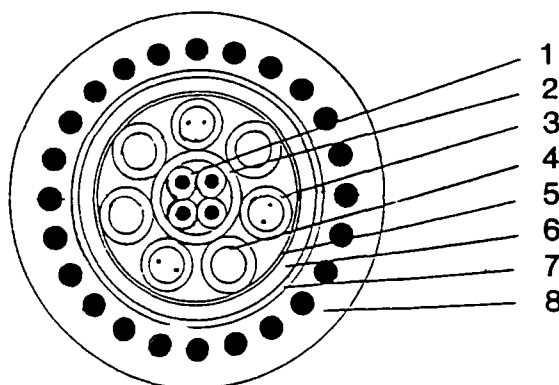
The use of a F.O. aerial cable between Reutlingen and Tuebingen permitted a meaningful comparison of both techniques. This track section crosses populated areas, woods and open terrain (see Appendix 1).

A total of 217 supporting structures of conventional design were available for the suspension of a F.O. aerial cable. The cable route required two crossings of the tracks for connection to stations located on the far side of the selected spur.

#### Characteristics of the F.O. Aerial Cable.

##### Cable Construction and Production.

The cable used single-mode fiber pairs (colored red and green, respectively) longitudinally water-proofed, placed in polyamide tubes. During fabrication of these so-called fiber bundles of 2.2 mm (0.087") outer dia. and 1.3 mm (0.051") inner tube diameter, the excess fiber length was set between 0 to 0.1% with respect to the straight polyamide tube. The bundles were filled with a petroleum jelly whose water-blocking characteristics remain stable between  $-40^{\circ}\text{C}$  and  $+70^{\circ}\text{C}$  (Fig. 3).



##### Cable Construction

- 1 - Star quad
- 2 - 3 ea. foamed polypropylene tapes
- 3 - Optical fiber bundle
- 4 - Dummy
- 5 - Polyester tape
- 6 - Polyethylene inner jacket
- 7 - Polyester tape
- 8 - Polyethylene jacket with 24 ea. embedded, reinforcing glass yarn fiber bundles

Fig. 3 Fiber optic cable (cross-section)

The core of the cable consists of a 0.6 mm conductor dia. (#23 AWG) star-quad with a foam-skin insulation of 0.35 mm (0.014") wall thickness. This component was specified by the user in order to have available an operational copper cable during and after laying. The quad was surrounded by a cushioning layer. The diameter of this layer is 3.9 mm (0.15").

Seven F.O. bundles were stranded over the core with a relatively short lay, starting with a red-colored bundle. Seen in the clockwise direction, we stranded a dummy element (neutral color), a yellow-colored bundle, a dummy element, a yellow bundle, followed by two dummies. The dummies are made from polyamide, similar to the buffer tubes. However, their outer dia. is 2.4 mm (0.095").

The cable core, which was prepared with greatest care, is covered with polyester tapes. It has a  $9.5 \pm 0.1$  mm ( $0.374 \pm 0.004$ ") diameter, prior to the application of the inner jacket. The inner jacket consists of translucent high-density polyethylene with a 0.6 mm (0.024") wall thickness.

As a final step, a glass-fiber reinforced cable jacket, developed by Lynenwerk, was extruded over the inner jacket. Without stress, the difference between the inner jacket diameter and the inner diameter of this outer jacket is 0.2 mm (0.008").

The so-called "LYNIPOORT" jacket (Fig. 4), made from black high-density polyethylene, has a total wall thickness of 2.8 mm (0.11"). A ring of 24 glass yarn bundles, each of which consists of 6 glass yarns, is located in the center portion of the jacket. The wall between the inner diameter of the jacket and the glass bundles is 0.5 mm (0.020") and the wall between the glass bundles and the outer jacket diameter is 1.0 mm (0.039"). The glass fiber bundles are tightly locked within the polyethylene jacket, thus providing the necessary mechanical strength to the cable.

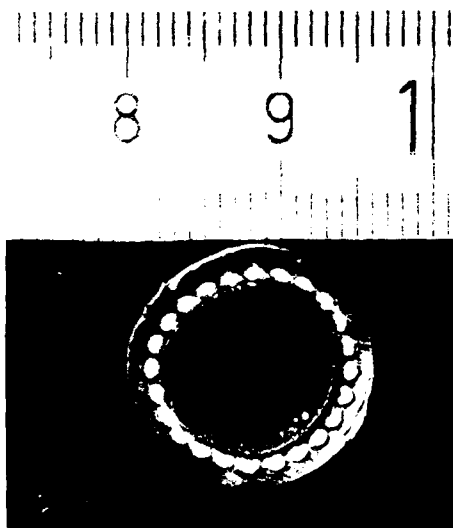


Fig. 4 Lyniport jacket cross-section (metric scale)

The outer diameter of the cable is  $15.9 \pm 0.2$  mm ( $0.626 \pm 0.008$ "). The finished cable bears a white-colored identification, specified by the user, including continuous footage markings.

The ordered production quantity was delivered in twelve individual lengths, including a spare, varying from 1,200 m to 2,100 m (3,937 to 6,890 ft).

Table 1 shows only those specification requirements that are characteristic for the special application of this cable. Of primary concern is the stability of the optical transmission characteristics under varying conditions of tension/elongation and temperature. The results of special tests are summarized below.

### Cable Laying

#### Laying and Suspension Techniques.

The masts for the contact wires which provide the traction power for electrified railroads are well suited for the suspension of F.O. aerial cables. Initial apprehensions by the technical services of the Bundesbahn regarding mast loading and operational security of the telecommunications have revealed themselves to be unfounded. The laying and suspension techniques used in this case are identical to those practiced with copper-conductor aerial cables along non-electrified railroad tracks. Each suspension section contains as many spans as possible.

To brace the cable we used dead-end spirals of the kind that have an established track record for the bracing of round cables or overhead power conductors (Fig.5).



Fig. 5 Mid-span break-out with 2 dead-end spirals

#### Fiber dimensions

Mode field diameter (at 1300 nm):	9 $\mu\text{m}$
Tolerance:	$\pm 1$ $\mu\text{m}$
Cladding diameter:	125 $\mu\text{m}$
Tolerance:	$\pm 3$ $\mu\text{m}$
Jacket: deviation from round (max.):	2.5 $\mu\text{m}$
Concentricity deviation between core and cladding:	1 $\mu\text{m}$

#### Cable dimensions and mechanical characteristics

Fiber bundle diameter:	2.2 mm
Dummy diameter:	2.4 mm
Core diameter:	3.9 mm
Stranded diameter:	8.7 mm
Diameter over the tape:	9.5 mm
Inner jacket wall thickness:	0.6 mm
Inner jacket diameter:	10.7 mm
Outer jacket wall thickness:	2.6 mm
Overall diameter (= D):	15.9 mm

Cable weight:	200 kg/km
Weight of glass yarn stress relief elements:	32.7 kg/km
Modulus of elasticity:	400 kp/sq.mm
Temperature elongation coefficient:	0.000018/ $^{\circ}\text{C}$

#### Transmission properties of the fibers

Attenuation coefficient (betw. 1285 - 1330 nm):	0.4 dB/km
Dispersion (betw. 1285 - 1330 nm):	3.5 ps/nm/km
Cutoff wavelength:	between 1100 and 1280 nm

#### Mechanical properties and temperature behavior

Min. tensile stress/max. elongation:	
Test limits:	12000 N/1.5%
Max. load to rupture:	10000 N/1.2%
Rupture:	20000 N/2%
Permissible attenuation change*:	
under tensile stress,	
up to a test load of:	0.05 dB/100 m (loaded)
under bending stress**:	$\pm 0.01$ dB/100 m
Temperature variation stress:	
at $0^{\circ}\text{C}$	$\pm 0.1$ dB/km max.
at $-20^{\circ}\text{C}$	$\pm 0.5$ dB/km max.
at $+60^{\circ}\text{C}$	$\pm 0.5$ dB/km max.
Attenuation change at $-40^{\circ}\text{C}$ with respect to room temperature:	$\pm 0.5$ dB/km max.

\* the change must be reversible

\*\* one-time bending without tensile stress (bending radius = 10D)

Table 1. Fiber Optic Aerial Cable: Dimensions and properties.

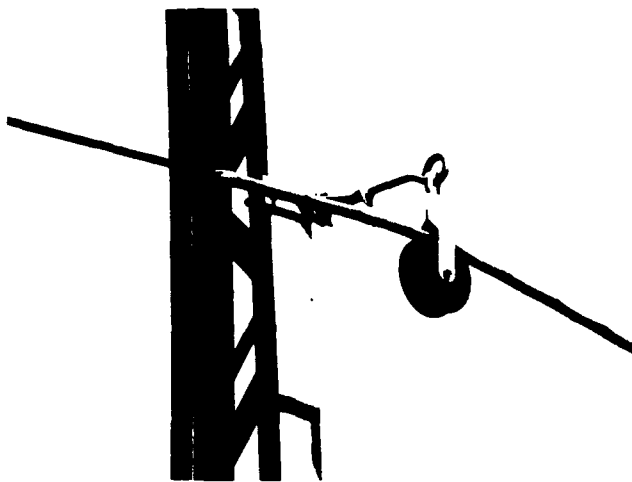


Fig. 6 Supporting roller with oscillation-suppressing spiral

Between suspension points we installed rollers on the masts for the purpose of supporting the cable (Fig. 6). Except for ice and wind loads, the masts are therefore supporting only the relatively light weight of the cable. Special pole braces and brackets for the installation of the spirals and supporting rollers had to be developed for the aerial cable. During the planning stage, the type and size of these accessories were determined based on considerations of railroad operational safety and proper overall installation of the cable. Special attention was given to:

- Possible wind loads, including those generated by the passing trains;
- Ice and snow loads;
- Danger of collapsing trees;
- Safe distances to perform maintenance work on cable fittings.

The cable was suspended at a height of about 5 m (15 ft) from the top of the rail. The distance between masts varied between 60 m (180 ft) and 80 m (240 ft).

#### Installation Techniques, Slack Adjustment.

The use of supporting rollers simplified the installation of the cable. It took place at walking speed with a maximum of six technicians for the actual pulling operations. The pulling of a suspension section starts with the mounting of a dead-end spiral to a mast. The cable length ahead of the spiral must be adapted to the required conditions. If a mid-span break-out is required within a given cable length, as in the case of grade or track crossings, it becomes necessary to form a loop (Fig. 7).

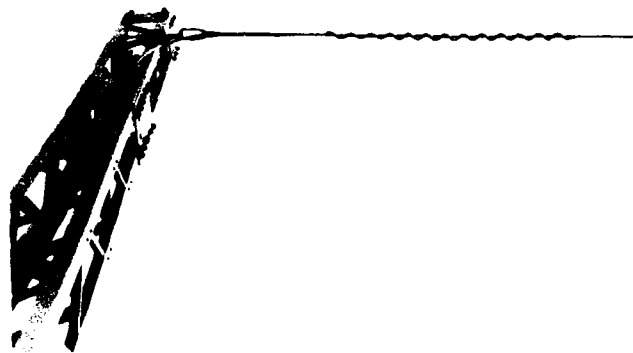


Fig. 7 Mid-span break-out at beginning or end of span with plastic damping spiral

The sag is set to amount to between 0.8 to 1.5% of the distance between masts based at a temperature of  $-5^{\circ}\text{C}$ . The setting of the desired sag determines the pulling force in all spans.

#### Vibration Considerations.

During the summer of 1990 we had to take the following preventive measures, after we observed slight oscillation of the cable in certain spans at near-freezing temperatures and under calm wind conditions:

- An oscillation-suppressing spiral was attached to each suspension point. This component has the additional benefit of reducing the pressure on the cable jacket at the suspension roller.
- Special plastic damping spirals were installed in several selected spans (Fig. 8).

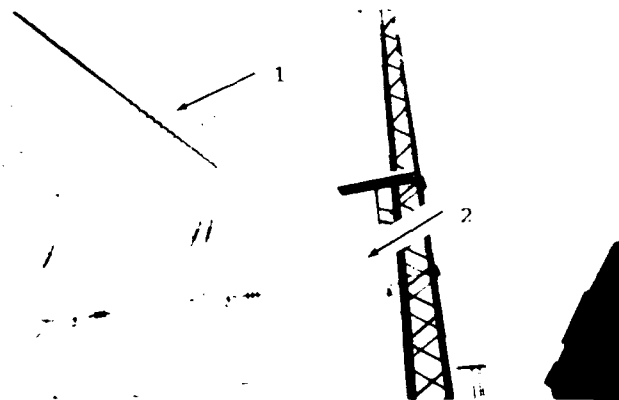


Fig. 8 Support point with oscillation-suppression (1) and plastic damping spirals (2)

## Results and Experience Gained.

### Pertinent Cable Properties.

Attenuation. The measured attenuation coefficient on a length of cable of 2,055 m (6,742 ft), for each of the six fibers, was between 0.33 dB/km and 0.35 dB/km at 1,300 nm. The specification requirement was for 0.4 dB/km max. OTDR measurements over the complete 15.175 km (9.43 mi) length of the line yielded the following readings:

Fiber No. 1: 5.47 dB

Fiber No. 2: 5.51 dB

Fiber No. 3: 5.40 dB

Fiber No. 4: 5.69 dB

The line includes 10 splice boxes.

Attenuation as a Function of Temperature. This property was measured on bundled fibers between  $-40^{\circ}$  and  $+60^{\circ}\text{C}$ . The fibers were wound on 630 mm (24.8") flange dia. reels. Fig. 9 illustrates the test results which confirm that the fibers embedded in the petroleum jelly exhibit the expected temperature dependence. The attenuation change as a function of ambient temperature is more meaningful as we shall explain further (see Fig. 13).

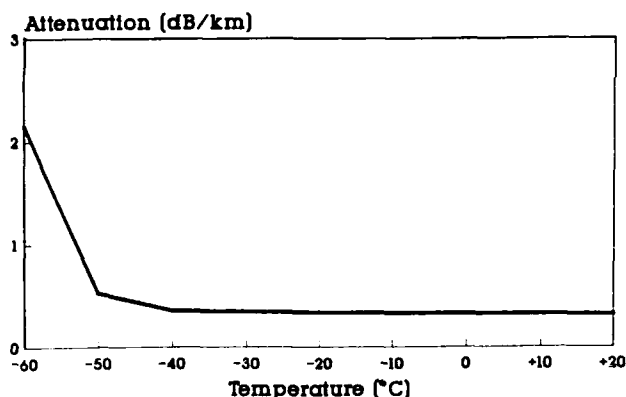


Fig. 9 Attenuation as a function of temperature

Conventional test procedures to determine changes of attenuation as a function of ambient temperature variations between  $-40^{\circ}\text{C}$  and  $+60^{\circ}\text{C}$  were not used, as we do not consider them useful for the evaluation of the transmission characteristics of F.O. aerial cables. In our opinion these tests are primarily meaningful for the determination of the suitability of shipping and storage of the cable on reels.

Stress-Elongation Diagram. The stress behavior must be investigated as a function of cable elongation. The results of the tensile test are useful, among other, for the determination of the modulus of elasticity of the cable construction, as it affects considerably the sag behavior of the aerial cable. It should be mentioned that a temperature dependence of the modulus of elasticity of the described cable construction, although present, may be neglected for the purpose of sag calculations. The uneven rise of the stress-elongation curve is an indication of the variation of the modulus of elasticity when placing the cable under load. This property must be considered for a precise computation of sag (Fig. 10).

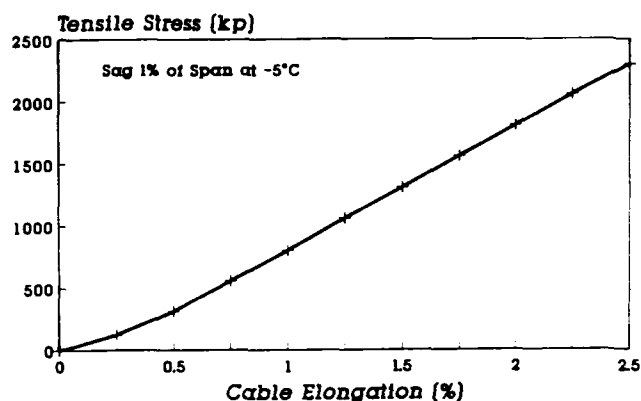


Fig. 10 Stress-elongation diagram

Attenuation under Tension/Elongation. First of all, the attenuation change of the cable under elongation is of interest, whereby the elongation of the optical fibers is also considered. Fig. 11 illustrates the relative dependency of the parameters. The figure also provides the answer to the question: what is the maximum load that the cable can be subjected to before the transmission characteristics are impaired? It also illustrates the aging of the fibers as a result of elongation.

For a maximum allowable fiber elongation of 0.20%, the cable in the span may be loaded up to 9,000 N. In this case, the cable elongation is 1.1% and the changes in attenuation are: 0.009 dB/100 m (@ 1,300 nm) and 0.11 dB/100 m (@ 1,550 nm).

The described F.O. aerial cable is not used in the third window. However, in case of such a potential application, it would be proper to set lower limits for the acceptable cable elongation.

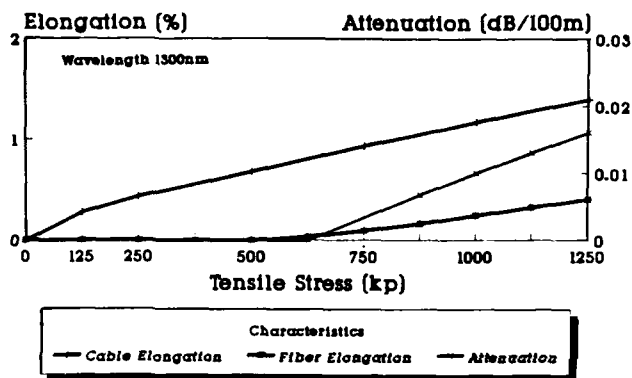


Fig. 11 Attenuation change and fiber elongation under stress

Temperature Behavior in the Span. The temperature elongation coefficient of the aerial cable is of particular importance for this feature for the entire cable length. This value which characterizes cable construction is determined on the completed cable. We measured a value of  $0.000018/^{\circ}\text{C}$ .

#### Conditions along the Track and Special Events.

Tensile Stress and Sag. During installation of the line, special attention was given to the basic sag calculations. Fig. 12 shows tensile stress and sag as a function of temperature and span lengths.

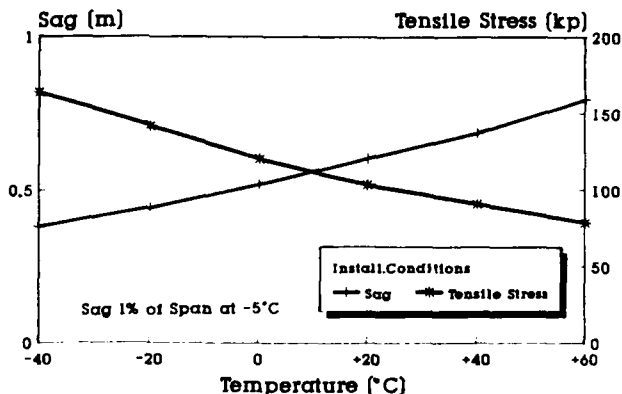


Fig. 12 Tensile stress and sag as a function of temperature

Environmental Effects on the Transmission Quality. Attenuation as a function of ambient temperature was measured daily between January 1989 and the summer of 1990. This test consisted of the continuous monitoring at the two ends of two spliced optical fibers in a bundle for

the total 30 km (18.6 mi) length in the cable. Recordings were made of attenuation and outside temperature in addition to extraordinary meteorological events. As evidenced by Fig. 13 no effects to disturb the transmission characteristics were recorded during periods of large temperature changes.

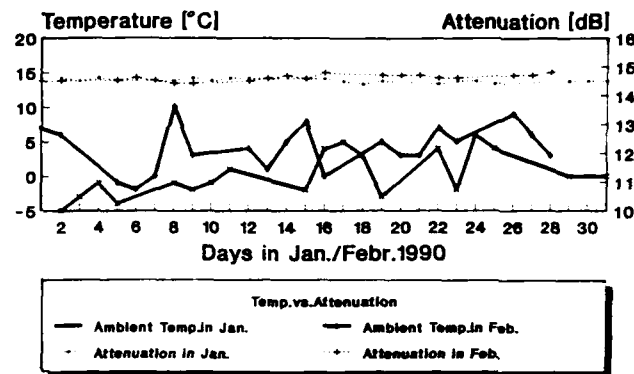


Fig. 13 Attenuation as a function of ambient temperature

Effects of Railroad Operation on the Transmission Quality. We examined the failure rates in the switched PCM 480-system over a 22-hr. period beginning on March 5, 1990. The results lie within acceptable tolerances of CCITT.

Formation of Ice Loads. Following several heavy snow falls during the 1988/89 winter, we observed ice loads on the cable in several spans. The diameter of the ice formation was estimated at about 30 mm (1.18"). It corresponds to a load of 3.9 kp/m (2.62 lb/ft), that is, a twenty-fold increase of the weight of the cable. Prevailing calm resulted in a quadrupling of the sag in the 80 m (262 ft) spans. It was observed that a sudden release of the ice load from an individual span resulted in reducing the sag only in this particular field (to a lesser extent than that which would have been caused only by a change in temperature due to the increased tensile strength). (Fig. 14).

Collapsing Trees. A few days after the installation strong winds caused a spruce located in the vicinity of the line to break and impact directly into a span and simultaneously into the overhead line, causing the latter to rupture. The aerial cable was forced to the ground by the tree, taking advantage of the slack offered by the span lengths without suffering any damage. Once the tree was removed, the cable bounced back to its normal slack.



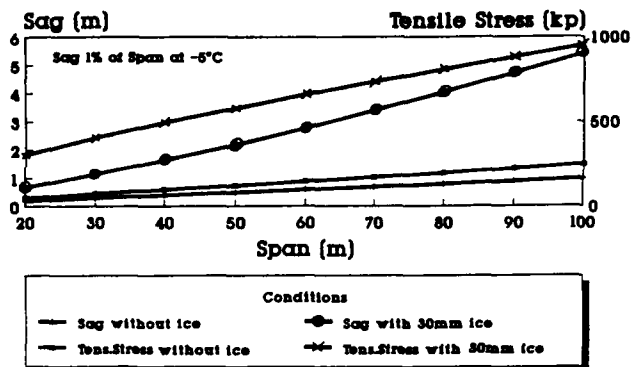
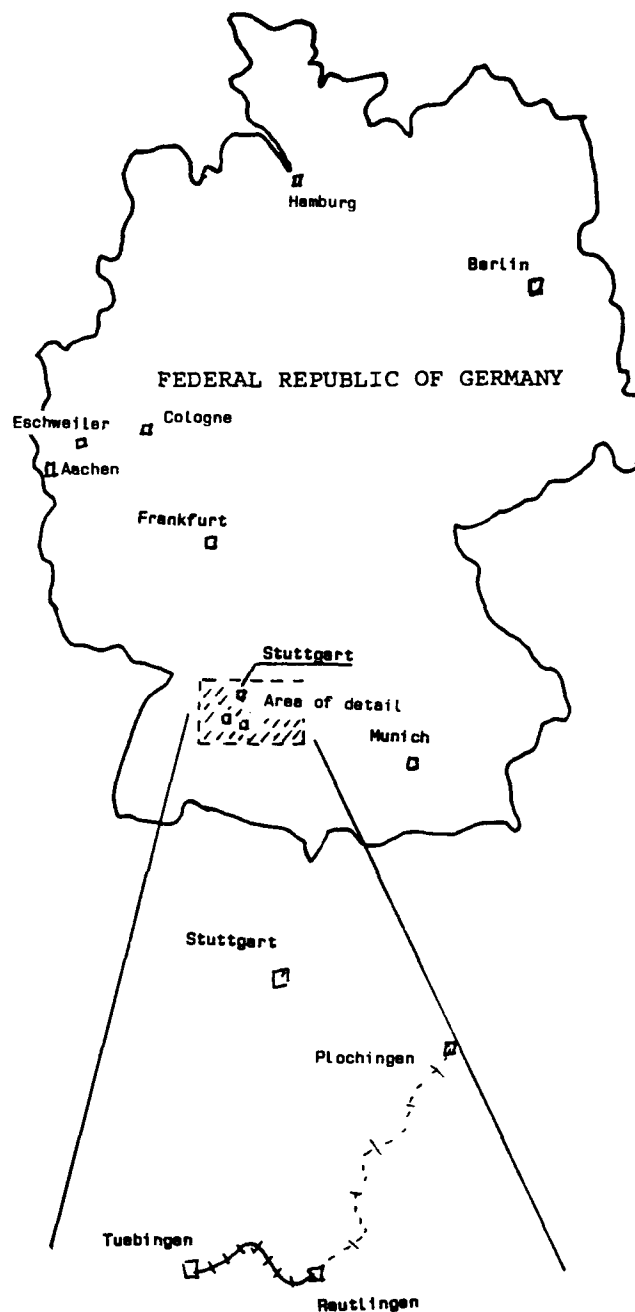


Fig. 14 Tensile stress and sag as a function of span length at  $-5^{\circ}\text{C}$  and 30 mm thick ice formation

Observed Cable Oscillation in the Cable Spans. During the winter of 1989-90 oscillation of the cable was observed in individual cable spans over a period of several minutes while the temperature was around freezing under virtual calm wind conditions. The oscillation frequency was estimated at 25 Hz with amplitudes of about 20 mm (0.8"). Oscillation nodes and maxima, spaced about 600 mm (2 ft) apart, were easily recognizable. Upon consultation with oscillation experts, we installed the oscillation damping devices previously described in the most affected areas during the summer of 1990. Experience gained to-date with these damping devices confirms that the inclusion of oscillation suppressing spirals at the contact points of the support rollers is adequate.

#### Summary and Outlook

The F.O. aerial cable which was installed in 1988 has proven to be reliable. An optical fiber pair has been switched with a PCM 480-system (34 Mbit) since the beginning of 1989. The system has worked without interruption. Following the positive experience made during the summer of 1990, the Deutsche Bundesbahn has issued a general approval for the installation of F.O. aerial cables along electrified railroad tracks, using for suspension the overhead masts carrying the contact wire. At the present time the installation of F.O. aerial cables along several new sections of track is under construction or in the planning stage. Meanwhile, the German Bundespost (German PTT) decided to use the same F.O. cable in their communications network. The first aerial cable connection was installed in May 1991 within the framework of the new telecommunication link between Berlin and Bayreuth.



Appendix 1 Location diagram of the Tuebingen - Reutlingen track section within the Tuebingen - Stuttgart main railroad line

### Acknowledgment.

The authors wish to thank Mr. H. Hofheimer of Cable Consultants Corp., Larchmont NY for his valuable assistance in preparing this paper.

### References

1. Lynen W. and Ney R., "A new Cable Jacket Design with Built-in Axial Stress Relief". Proceeds. 26th IWCS, Nov. 15-17, 1977, pp. 312-320.



Albert Bidinger is the Head of the Signal and Communications Department of the Deutsche Bundesbahn Central Office. He studied at the Stuttgart University where he obtained his degree in Electrical Engineering in 1972. He has been with the Deutsche Bundesbahn since 1973.



Wolfgang Lynen received his MBA degree from the University of Fribourg, Switzerland, in 1967. After further studies at the University of Oklahoma, Norman, he was employed by Monsanto Co., first in St. Louis, then in Brussels. He joined Lynenwerk, cable works, Germany, in 1973. He is managing director since 1975 and primarily responsible for all marketing activities.



Robert P. Ney is technical director of Lynenwerk, where he heads the R & D effort. He graduated from the universities of Aachen and Cologne as mechanical and electrical engineer. Mr. Ney has been primarily responsible for the development of the new cable.

# Development of optical composite messenger wire

Shigeo SHIMIZU, Tsutomu AKIYAMA and Akihiro OTAKE

The Furukawa Electric Co., Ltd.

## Abstract

In the case of CATV, which serves the distributed same signal source to customers, the small-count cable is enough for trunk lines as the long-distance and high-capability transmission. The conventional method for overhead optical cable installation was to hang it on a messenger wire. However, installation of small-count cables by this method increased the installation cost per core. Therefore a small-count optical composite messenger wire has been developed with a central metal tube containing optical fibers. The cable can be installed by the same method as for messenger wires.

## 1. Introduction

When using optical fiber cables in systems that distribute the same signal source to many users as in CATV systems:

1) Optical fiber cables are suitable for trunk lines in accomplishing long-distance and large capacity transmission. And because branching does not have to be considered, the small number of optical fibers are sufficient for it.

2) In systems that distribute to end users, diverse branching and amplifiers will be needed. When the overall cost is taken into consideration, coaxial cable systems are less expensive at present.

Hybrid systems using optical fiber cables in trunk lines and using coaxial cables in distribution lines are considered to be economical. In these systems overhead optical fiber cables, whose installation cost is low, are required for trunk lines.

In the past, overhead optical cables have been installed by suspending them on messenger wire. When the number of optical fibers in cable is small, this installation method increases the instal-

lation cost per fiber.

We have developed an overhead optical fiber cable that is an optical composite messenger wire. It is low in cable cost and in installation cost for routes that require a few optical fibers. The transmission, mechanical and installation characteristics of this cable have been evaluated. Suspending another cable on the new cable has also been evaluated.

## 2. Cable design

In designing the cable, the following points were taken into consideration.

(1) Replace one of the messenger wire strands by an metal-jacketed optical fiber that a metal tube contains optical fibers.

(2) Put the metal-jacketed optical fiber in the center of 1 x 6 array to prevent collapse by the nose suspension hardware.

(3) The metal tube should be of a size that can contain a small number of optical fibers such as two to eight fibers.

(4) Taking corrosion into consideration, the metal tube material must be not less electropositive than zinc and iron.

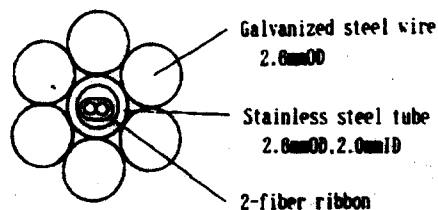


Figure 1 Cross-sectional structure of the cable

(5) Because of the following conditions, optical fiber ribbons are used.

1) Optical fibers must be unitized as much as possible to minimize the difference of excess lengths of several optical fibers in a metal tube.

2) The number of optical fibers can be constructed in multiples of two for the two-fiber two-way communications in a reduced weight.

### 3. Cable structure

Figure 1 shows the cross-sectional structure of the tested cable.

The stainless steel tube 2.6mm in outer diameter and 2.0mm in inner diameter contains a two-fiber ribbon using  $1.3 \mu\text{m}$  single-mode optical fibers. Six galvanized steel wires were wound around the stainless steel tube.

### 4. Characteristics

#### 4.1 Metal-jacketed optical fiber

##### (1) Tensile test

Figure 2 shows the relationship among the tensile load, metal tube elongation and optical fiber elongation. Young's modulus of the stainless steel tube was  $14000\text{kg/mm}^2$ . The initial excess length of the optical fiber was 0.06%.

##### (2) Lateral pressure test

Figure 3 shows the deformation quantity of stainless steel tube and optical-fiber loss variations when lateral pressure was applied. The metal tube suddenly started to deform under a load larger than  $400\text{kg/50mm}$ , causing the metal tube to plastically deform or collapse. Optical fiber transmission losses started to increase at more than  $900\text{kg/50mm}$ .

From the result of the deformation quantity of stainless steel tube, optical fiber losses are seemed to increase after the inner surfaces of the tube started to contact the optical fibers.

##### (3) Bending test

The metal-jacketed fibers were wound around a mandrel of 50mm in diameter four turns. Stainless steel tube collapsing or deformation or optical fiber loss increases could not be detected.

The cable was repeatedly bent 50mm in diameter and  $\pm 90^\circ$ . The stainless steel tube did not break after it was bent nine times back and forth. And it broke after it was bent ten times or more.

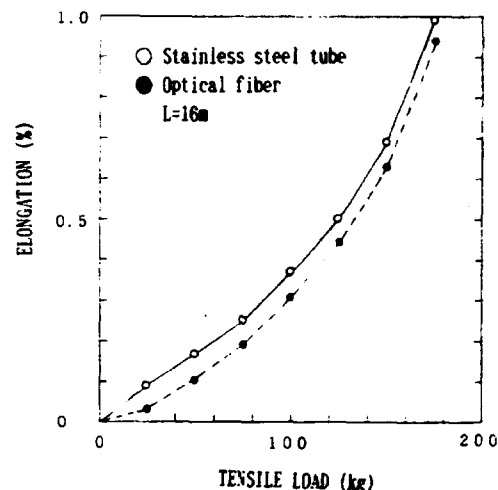


Figure 2 Tensile test results

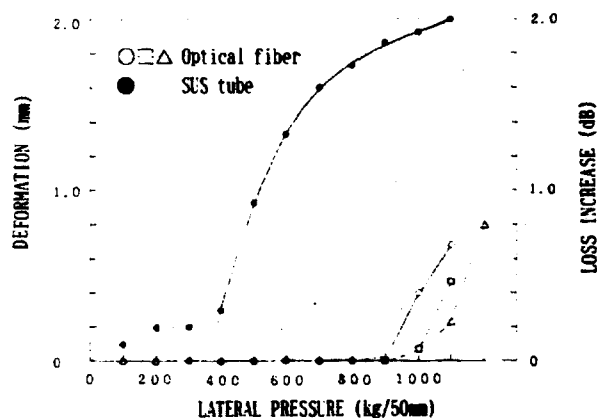


Figure 3 Lateral pressure test results

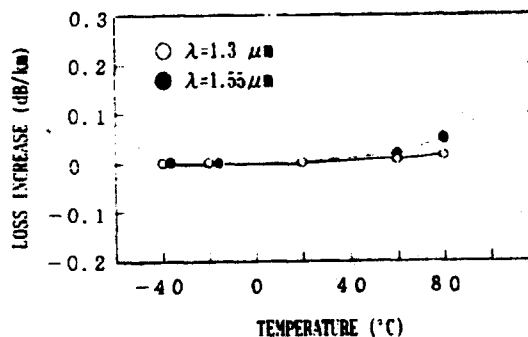


Figure 4 Loss increase with temperature

#### (4) Loss increase with temperature

Figure 4 shows the transmission loss variations with temperature when the metal-jacketed optical fibers were wound on a bobbin 300mm in diameter. Loss variations within the temperature range of  $-40$  to  $+80^{\circ}\text{C}$  were less than  $\pm 0.02\text{dB/km}$  and  $\pm 0.05\text{dB/km}$  in the wavelengths of  $1.3\ \mu\text{m}$  and  $1.55\ \mu\text{m}$ , respectively.

#### 4.2 Optical composite cable

##### (1) Tensile test

Figure 5 shows the relationship among the tensile load, cable elongation and optical fiber elongation. The galvanized steel strand slackened  $0.004\%$ . The cable elongated  $0.17\%$  under the tension of  $1000\text{kg}$ . Young's modulus calculated based on the cross section of the galvanized steel strand without including the stainless steel tube was  $18500\text{kg/mm}^2$ . The excess length of the optical fiber was  $0.006\%$ .

##### (2) Lateral pressure test

Figure 6 shows cable deformation, optical fiber loss variations and residual deformation quantity of stainless steel tube when lateral pressure was applied using  $50\text{mm}$ -width flat board. Optical fiber losses did not increase at lateral pressure of  $1000\text{kg}/50\text{mm}$ . Compared with stainless steel tube alone, the same tube was well protected against collapse by the galvanized steel wire around it.

##### (3) Loss increase with temperature

Figure 7 shows the variation of transmission loss with temperature when the cable was wound on a drum. The loss variations within the temperature range of  $-40$  to  $+80^{\circ}\text{C}$  were less than  $\pm 0.03$  and  $\pm 0.05\ \text{dB/km}$  in wavelengths of  $1.3$  and  $1.55\ \mu\text{m}$ , respectively.

#### 5. Overhead installation characteristics

##### 5.1 Collapse by nose suspension hardware

"L" and SS nose suspension hardware are generally used when fixing messenger wire on telephone poles. The collapsing conditions of the stainless steel tube when the cable was clamped by those nose suspension hardware was tested. The results of this test are shown in figure 8.

The stainless steel tube collapsed when the bolt tightening torque of the "L" nose suspension hardware surpassed  $2.5\text{kg}\cdot\text{m}$ , indicating that it is impossible

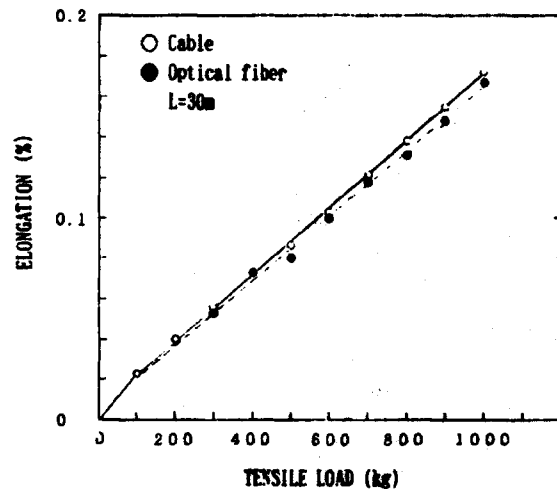


Figure 5 Tensile test results of cable

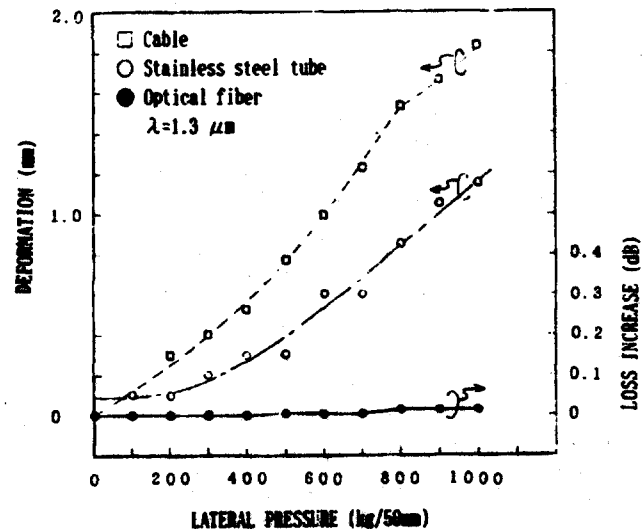


Figure 6 Lateral pressure test results of cable

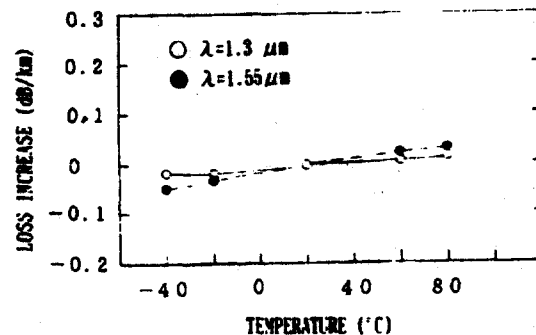


Figure 7 Loss increase with temperature

to be clamped sufficiently.

The SS nose suspension hardware did not cause collapse till the torque reached 9kg·m, indicating that it can be clamped sufficiently.

Therefore, SS nose suspension hardware has to be used when fixing the cables on poles.

### 5.2 Midspan tensile test

The tension, cable sag and optical fiber strain when the cable was installed between poles in span 45m were measured.

The optical fibers were fixed onto the stainless steel tube at both ends of the cable. The cable weighed 277g/m.

A coaxial cable in outer diameter 15.3mm and weight 198g/m was suspended on the cable using hangers to evaluate effects when a light weight cable was installed.

Figure 9 shows the test method. A load cell was attached on the fixed end side and another end side was pulled by a winding machine.

Figure 10 shows the test results. Measured and theoretically calculated values of cable sag well coincided. The tensile strain of the optical fiber did not occur under a tension below 400kg. Under tension of more than 400kg, optical fiber strain when a coaxial cable was suspended was greater than when the cable alone was installed.

Although the optical fiber elongated 0.07% under a tension of 400kg in the tensile test mentioned in section 1.2, the optical fibers did not elongate by a mid span tensile test because an apparent excess length occurred due to cable deflection and clearance of the optical fiber ribbon inside the stainless steel tube.

### 5.3 Overhead installation test

Fluctuation of optical fiber strain when the optical fiber cable was installed in three spans, span length was 45m, were measured to evaluate overhead installation performances of the cable. Both ends of optical fibers were free against the cable. Figure 11 shows the test method.

Figure 12 shows fluctuation of optical fiber strain measured during the test.

(1) When one end of the cable was fixed on a pole and the cable was slacked till it reached the ground, the initial value of the optical fiber strain was set to zero.

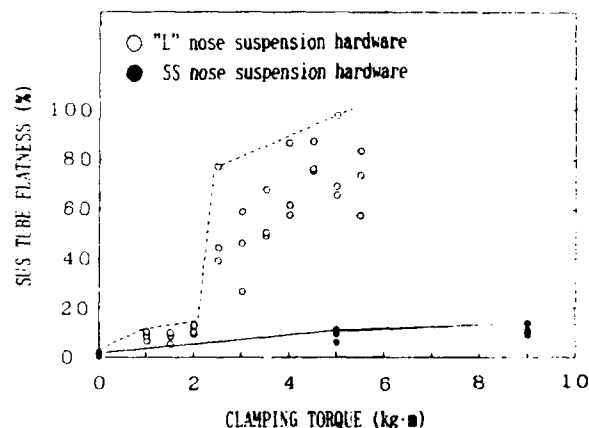


Figure 8 Deformation by nose suspension hardware

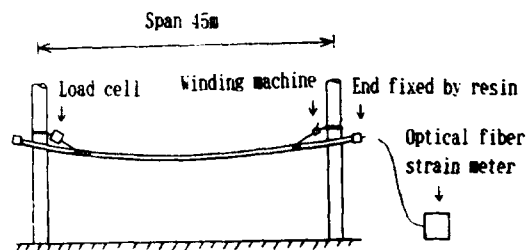


Figure 9 Midspan tensile test method

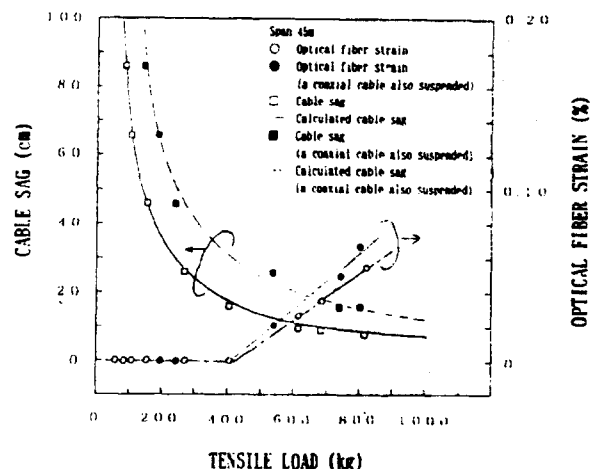


Figure 10 Results of midspan tensile test

(2) The other end of the cable was pulled by a winding machine and the cable sag was adjusted to be 16cm. The maximum optical fiber strain fluctuation occurred during installation work while pulling the cable by the winding machine and it was 0.04%. The tension of approximately 800kg was estimated to have been caused during pulling by the winding machine.

(3) At the intermediate poles the cable was fixed by SS nose suspension hardware. And the pulling end was fixed by a clamp. The final cable sag was 17cm on the fixed end side and at the intermediate part and was 22cm at the pulling end side. After installing the cable, the residue of the optical fiber strain was nil.

(4) After fixing the optical fiber cable on the poles, a coaxial cable was hanged on the optical cable in one span on the fixed end side. The maximum optical fiber strain fluctuation was 0.02% on average for three spans(135m). Assuming that all the strain was caused in one span(15m), the strain would be 0.06%.

(5) The cable sag of this part after suspending on the hanger was 31cm. Optical fiber strain of 0.01% remained after hanging a coaxial cable.

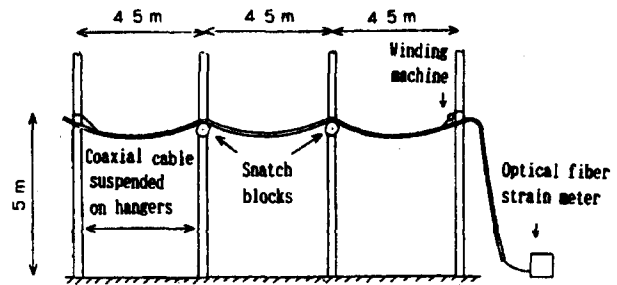


Figure 11 Midspan installation test method

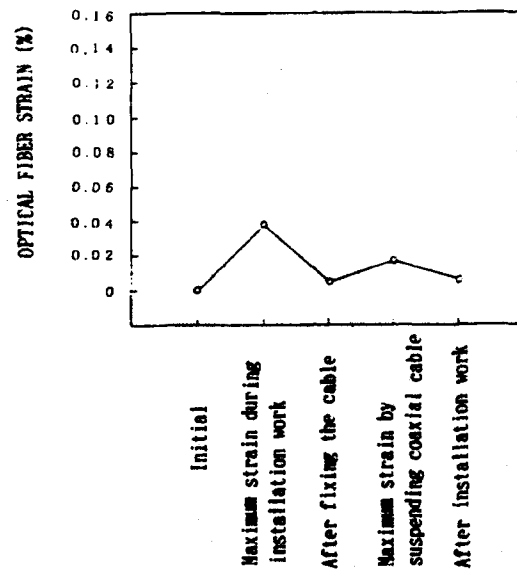


Figure 12 Results of overhead installation test

## 6. Wind pressure load evaluation

Calculations were made to evaluate optical fiber strains which would be applied under wind pressure load conditions shown in table 1 and for the following four cases because of the combinations of installation and operating conditions.

Case	Installation season	Operating environment
1	Winter	Summer (Case A)
2	Winter	Winter (Case B)
3	Summer	Summer (Case A)
4	Summer	Winter (Case B)

The tension during installation was used as the parameter.

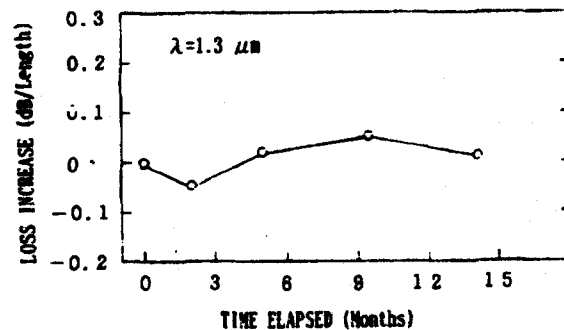


Figure 13 Transmission loss variations of installed cable

The following equation was used to calculate the optical fiber strains. The initial excess length of the optical fiber was set to zero.

$$\varepsilon = T / (E \cdot A) + \alpha \cdot (t - t_0)$$

where

- $\varepsilon$  : Optical fiber strain
- $T$  : Cable tension
- $E$  : Young's modulus of the cable (19000kg/mm<sup>2</sup>)
- $A$  : Cross-sectional area of galvanized steel strand (31.88mm<sup>2</sup>)
- $\alpha$  : Linear expansion coefficient of the cable ( $1.25 \times 10^{-5} \text{ deg}^{-1}$ )
- $t$  : Ambient temperature in operation
- $t_0$  : Normal temperature (25°C)

Figure 14 and 15 plot Case 3 and 4 which showed large calculated values for optical fiber strain.

The tension during installation, in which the optical fiber strain was maintained to be below 0.2% in all cases were as follows:

Ambient temperature: -15 ~ +60°C

The new cable alone  $\leq 900\text{kg}$

When a light cable was suspended  $\leq 800\text{kg}$

Ambient temperature: -40 ~ +85°C

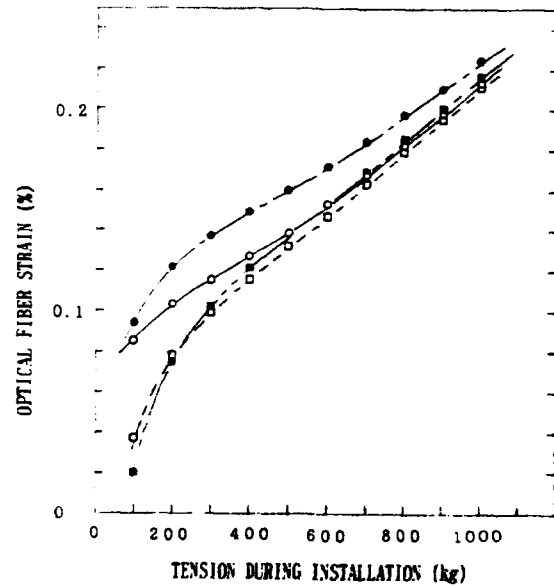
The new cable alone  $\leq 700\text{kg}$

When a light cable was suspended  $\leq 600\text{kg}$

It shows that the tensile strain applied to optical fibers would be able to be maintained below 0.2% by adjusting the installation tension to the ambient temperature during installation.

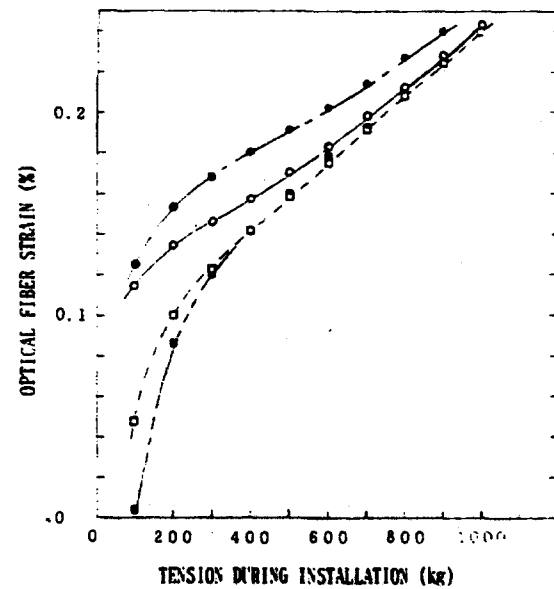
Table 1 Calculation conditions of wind pressure load

Ambient temperature	1) Winter : -15°C , Summer : +60°C 2) Winter : -40°C , Summer : +85°C
Installation condition	1) New cable alone 2) A light weight cable is suspended (Outer diameter 15.3mm, weight 196g/m)
Wind pressure condition	1) Case A : Summer Wind pressure 100 kg/m <sup>2</sup> 2) Case B : Winter Wind pressure 50 kg/m <sup>2</sup> Snow fall 6mm in depth 0.9 g/cm <sup>3</sup>



Installation In operation Cable alone with a light weight cable suspended  
 season  
 Summer → Summer(Case A) ○ ●  
 Summer → Winter(Case B) □ ■

Figure 14 Optical fiber strain under wind pressure (Ambient temperature: -15 ~ +60°C)



Installation In operation Cable alone with a light weight cable suspended  
 season  
 Summer → Summer(Case A) ○ ●  
 Summer → Winter(Case B) □ ■

Figure 15 Optical fiber strain under wind pressure (Ambient temperature: -40 ~ +85°C)



The tensile strain applied to the optical fiber can be relaxed by providing an excess length of the optical fiber in the metal tube. An apparent excess fiber length caused by the installed cable deflection and clearances between the optical fiber and the metal tube also relaxes the tensile strain.

#### 7. Conclusion

Optical fiber composite messenger wire cable was developed and tested.

The cable transmission and mechanical characteristics were fully satisfactory as optical fiber cable.

The installation experiment results confirmed the following:

The optical fiber cable can be installed on poles using SS nose suspension hardware.

Strain applied to optical fibers during installation was of a level that would present no practical problems.

From the results of the wind pressure load of case A and B at the temperature range from -40 to +85°C, optical fiber strain can always be maintained below 0.2% by adjusting the installation tension to the ambient temperature. Optical fiber strain can likewise be always maintained below 0.2% even if a light weight and thin cable (below approx. 200g/m in weight and approx. 15mm in outer diameter) such as coaxial cables and other optical fiber cables is suspended on the optical cable.

From these results, it was confirmed that this cable can be installed overhead by the same method as that for messenger wire.



Shigeo SHIMIZU

The Furukawa Electric Co., Ltd.

6, Yawatakaigandori,  
Ichihara, Chiba, 290, Japan

Mr. Shimizu was born in 1957. He received B.S. degree in nuclear engineering from Nagoya University in 1980 and joined The Furukawa Electric Co., Ltd.. He has been engaged in development of optical fibers and cables.

He is a member of The Institute of Electronics, Information and Communication Engineers of Japan.



Tsutomu AKIYAMA

The Furukawa Electric Co., Ltd.

6, Yawatakaigandori,  
Ichihara, Chiba, 290, Japan

Mr. Akiyama was born in 1966. He received B.S. degree in electronics from Waseda University in 1989 and joined The Furukawa Electric Co., Ltd.. He has been engaged in development of optical fiber cables.

He is a member of The Institute of Electronics, Information and Communication Engineers of Japan.



Akihiro OTAKE

The Furukawa Electric Co., Ltd.

6, Yawatakaigandori,  
Ichihara, Chiba, 290, Japan

Mr. Otake graduated from Tohoku University and joined The Furukawa Electric Co., Ltd. in 1974. He has been engaged in research and development of optical fiber cables and those accessories.

He is now a manager of optical fiber transmission research section.

# NEW EXPANSION TECHNOLOGY OF INSULATED CORE WITHOUT CHLOROFLUOROCARBON (CFC)

K. SAKAMOTO M. SUGIMURA I. KOBAYASHI & S. HAYASHI

THE FURUKAWA ELECTRIC CO., LTD.  
CHIBA JAPAN

## Abstract

CFC (Chlorofluorocarbon) had been useful as foaming agent for high expansion insulated core of thin wall thickness and toughness. But it shall be surely abolished within coming a few years caused by decomposition of ozone. Therefore we have been developing the substitute for CFC.

There were much relations between boiling point, viscosity of organic solvent and expansion ratio, deformation ratio respectively. And only alcohol had different expansion actions against to other solvents, and each solvent were classified by expansion actions such as expansion ratio, deformation ratio (toughness), surface appearance and number of cells in the insulation.

We had not developed new independent solvent replace of CFC which had satisfied both high expansion ratio (more than 60%) and low deformation ratio (less than 10%). However we had discovered especially new combined solvent that had enough satisfied above-mentioned properties, and so it could be got prospects of utilization for CFC.

## 1. Introduction

CFC (Chlorofluorocarbon) gas foamed processing technology has been carried out for more than 20 years, resulting for wire and cable industrial applications such as insulated core in the wire/cable used for computer wiring, CATV transmission line and common communication line etc.

In fact, this gas foamed technology had become a especially necessary method to the high speed propagation coaxial cable producing as it offers more advantage and more effectiveness over the conventional cable's properties.

The most important properties of such cables are velocity of propagation (VOP) and characteristic impedance ( $Z_0$ ). And recently, we have made requests to coaxial cables and wires for higher VOP and lower  $Z_0$ . VOP and  $Z_0$  are given as follows,

$$VOP = \frac{1}{\sqrt{\epsilon_r}} \times 100 \quad (\%) \quad (\text{eq.1})$$

$$Z_0 = \frac{138.2}{\sqrt{\epsilon_r}} \times \log \frac{d}{d_i} \quad (\Omega) \quad (\text{eq.2})$$

where,  $\epsilon_r$ : Effective relative dielectric constant  
(~)

$d$ : Outer diameter of conductor (mm)

$d_i$ : Insulated core diameter (mm)

Then in order to be satisfied higher VOP and lower  $Z_0$  need it for lower  $\epsilon_r$  (i.e., higher expansion ratio), smaller insulated core diameter (i.e., thinner wall thickness) and more toughness of insulated core (i.e., lower deformation ratio). If so, we are able to use more useful and effective high speed propagation coaxial cable. Then toughening insulated core is especially necessary to prevent the mechanical damage from manufacturing on each process.

CFC generates minute and many cells in the insulation, so it has been available for such a insulated core manufacturing. But it is regretted that utilization of this technology by CFC should be cut-down immediately for the prevention of environment pollution.

Concretely speaking as you may know well that CFC decomposes ozone at the stratosphere, it shall be surely abolished coming a few years. So we present you epochal new gas foamed technology without CFC.

## 2. Requirements for Cable and Insulated core

### 2.1. Requirements for a Cable

- (1) High speed propagation property
  - Velocity of propagation (VOP)  $\geq 85\%$
- (2) Low characteristic impedance ( $Z_0$ )
  - $Z_0: 50 \sim 90 \Omega$

### 2.2. Requirements for a Insulated core (experimentally)

(so as to satisfy above-mentioned requirements for the cable)

- (1) Low effective relative dielectric constant ( $\epsilon_r$ ) i.e., High expansion ratio (E.R.)
  - $\epsilon_r \leq 1.43$  E.R.  $\geq 60\%$
- (2) Small outer diameter of a insulated core (O.D.)
  - O.D.  $\leq 1.0 \text{ mm}$
- (3) Low deformation ratio (D.R.)
  - D.R.  $\leq 10\%$

### 3. Previous Foaming Technology without CFC

#### 3.1. HCFC (Hydrochlorofluorocarbon)

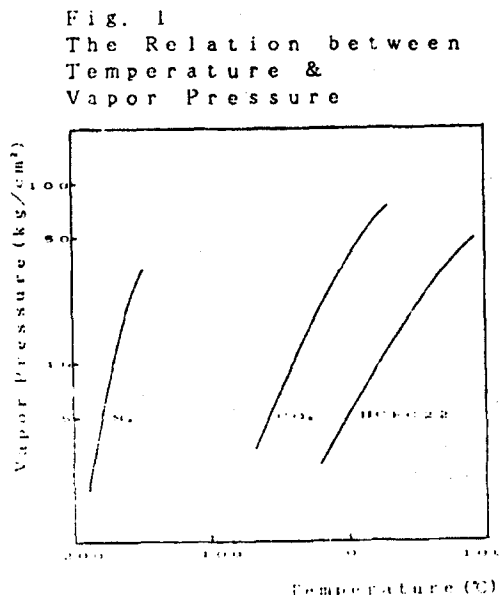
HCFC22, one of HCFC group, generates minute and many cells in the insulation as CFC, and it is recommended to substitute for CFC. But HCFC also decomposes a little ozone, and will be abolished coming in a few years. So we should not use HCFC even no-abolishment.

#### 3.2. N<sub>2</sub>, CO<sub>2</sub>

N<sub>2</sub> (Nitrogen gas) and CO<sub>2</sub> (Carbon dioxide) have been used for the foaming agent based on its harmlessness, safety and cheapness. But they are not able to generate minute cells in the insulation and not to be injected precisely caused on the measurement their injection volume by a gas flow meter or a pressure regulator. If vapor pressure of gaseous foaming agent is low, they are liquefied with comparative low pressure and is able to inject precisely with a precision pump. But the vapor pressure of N<sub>2</sub> and CO<sub>2</sub> is very high (shown in Fig. 1), therefore, N<sub>2</sub> and CO<sub>2</sub> are no use for a thin wall thickness and high expanded insulation.

#### 3.3. Organic solvent

Organic solvent has been also used for foaming agent. But there is no report that organic solvent realized an insulated core with high expansion ratio, thin wall thickness and toughness. However we have expected that organic solvent shall be substitute for CFC.



### 4. Experimental Results

We have used organic solvents in place of CFC foaming agent which were comparative low cost and easy treatment. But there were some noxious and/or dangerous solvents, therefore we had to select more innocuous and safer one. And we used low density polyethylene as base polymer.

#### 4.1. Single solvent

At first, we examined expansion actions of single solvent. Fig. 2 shows the relation between the expansion ratio and the deformation ratio with each solvent, but there was no solvent satisfied both the expansion ratio of more than 60% and the deformation ratio of less than 10% (The expansion ratio described in this paper is the maximum value with such single solvent. And the deformation ratio described in this paper is the value of specimen having the maximum expansion ratio. And methods of measuring the expansion ratio and the deformation ratio shall be described in the following items 5.)

But, when we used CFC as foaming agent, the expansion ratio would be more than 60% and the deformation ratio would be less than 10%.

Then, we investigated the expansion actions of single solvent minutely, and it was clear boiling point and viscosity of solvent influenced expansion ratio and deformation ratio. Fig. 3 shows the relation between boiling point and expansion ratio, Fig. 4 shows the relation between boiling point and deformation ratio, Fig. 5 shows the relation between viscosity and expansion ratio, and Fig. 6 shows the relation between viscosity and deformation ratio.

It was suggested that the higher boiling point of viscosity realized the large expansion ratio or deformation ratio. But the correlation coefficients (absolute value) were not so large (shown in Table. 1), especially in case of viscosity. But if we stratified alcohol from others, the correlation coefficients were large (absolute value).

Therefore it was clear that there were correlation between boiling point, viscosity, expansion ratio and deformation ratio, and then only alcohol had different expansion actions among the solvents, that is, the high expansion ratio was given by alcohol even if the viscosity was rather high, notwithstanding, such high expansion ratio was never given by other solvent of rather high viscosity.

Fig. 7 shows the relation between boiling point and viscosity of solvent we examined. It was also clear only alcohol had different actions.

Then we classified the solvent to some types according to the expansion actions which were surface appearance of insulated core, number of cells, expansion ratio and deformation ratio (toughness). And the types were Type A, Type B and Type C. And Type B was further classified to Type B I (without alcohol) and Type B II (only alcohol), based on the differences between boiling point and viscosity of Type B I and Type B II, and the expectation that alcohol and others were going to cause different expansion actions in case of mixed solvent.

The characteristics of each Type were shown in Table 2.

Fig.8 shows the classification each solvent to Type A, B I, B II and C, and Photo.1-4 show the representative cross section of each Type, and Photo.5 shows the comparative cross section of CFC.

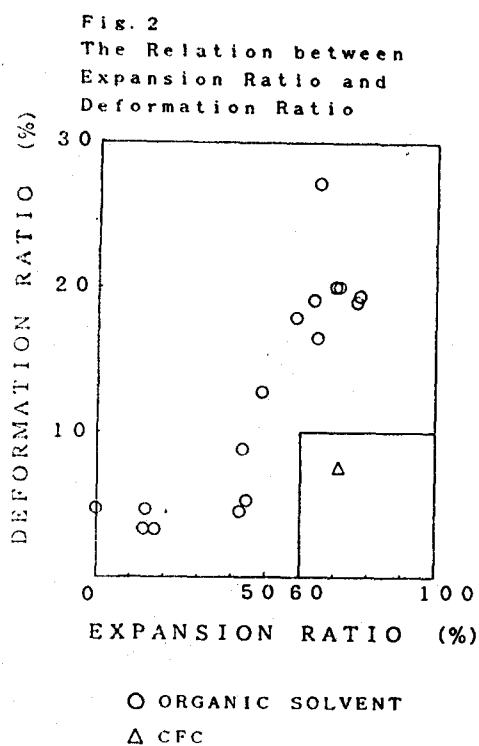


Table 1.  
Correlation Coefficient  
between each Variable

Variable		Total	Alcohol	Without Alcohol
B. P.	E. R.	-0.75	-0.95	-0.86
B. P.	D. R.	-0.57	-0.85	-0.81
Vis.	E. R.	-0.26	-0.80	-0.76
Vis.	D. R.	-0.13	-0.77	-0.63

B. P. : Boiling Point  
Vis. : Viscosity  
E. R. : Expansion Ratio  
D. R. : Deformation Ratio

Table 2  
Expansion Actions of Single Solvent

	Appearance	Number of Cells	Expansion Ratio (%)	Deformation Ratio (%)
A	Smooth	Minute & Many	O 60~70	x 15~20
B I	Rough	Rather large	O 60~70	x 15~20
B II		& Many		
C	Smooth	Minute & Few	x 0~30	O <10

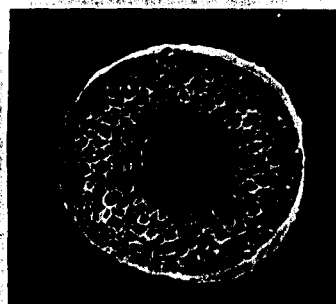


Photo 1  
Type A



Photo 2  
Type B I

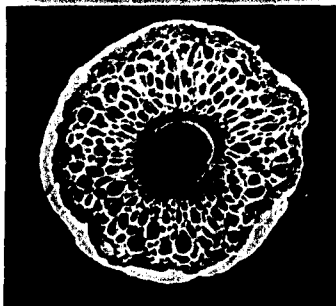


Photo 3  
Type B II

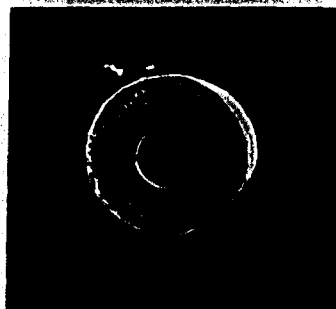


Photo 4  
Type C

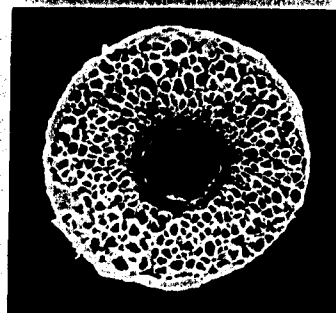


Photo 5  
CFC

Fig. 3  
The Relation between  
Boiling Point and  
Expansion Ratio

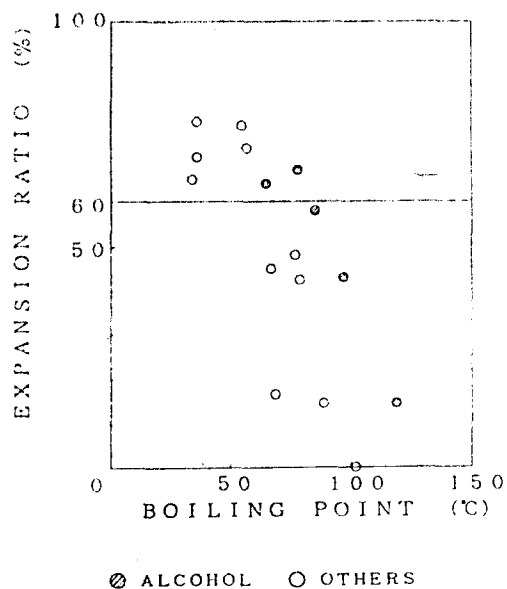


Fig. 5  
The Relation between  
Viscosity and Expansion Ratio

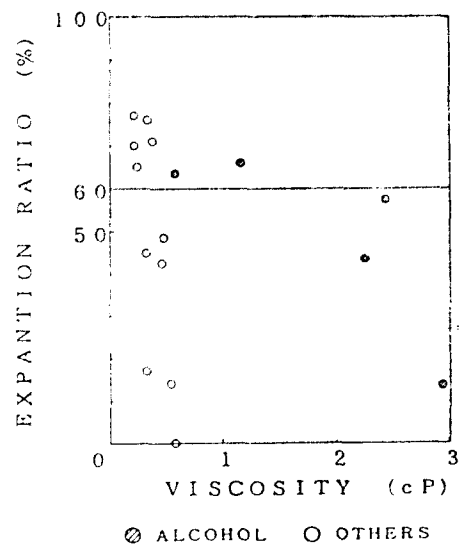


Fig. 4  
The Relation between  
Boiling Point and  
Deformation Ratio (at 23°C)

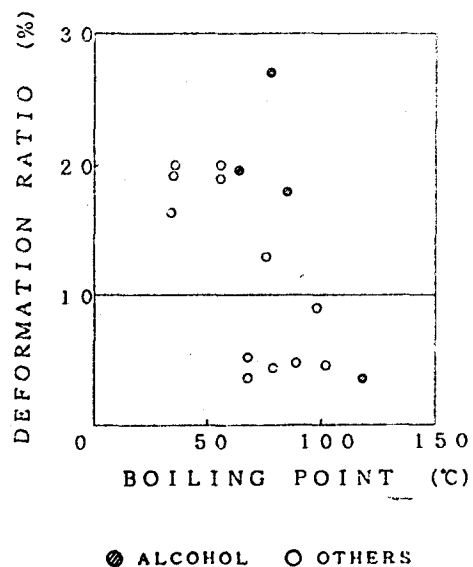


Fig. 6  
The Relation between  
Viscosity and  
Deformation Ratio (at 23°C)

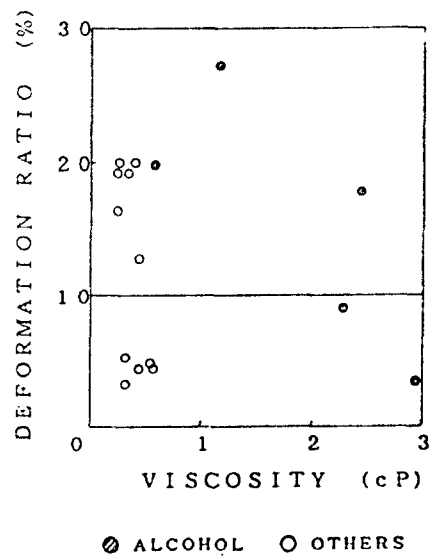


Fig. 7  
The Relation between  
Boiling Point and Viscosity

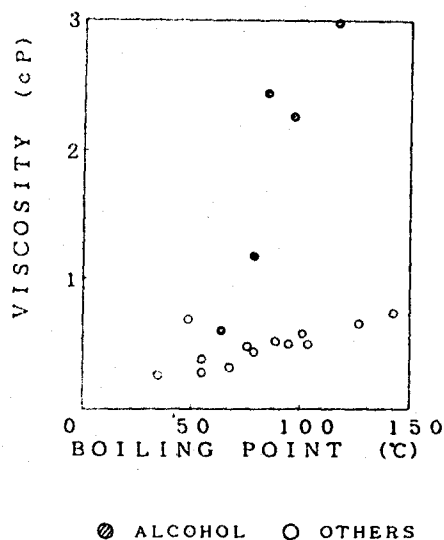
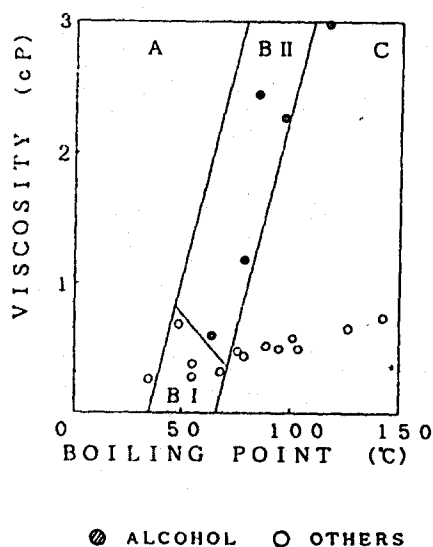


Fig. 8  
The Relation between  
Boiling Point and Viscosity



#### 4.2. Mixed Solvent

Next we examined the expansion actions of mixed solvent that was the combination of two kinds of equal mole solvent. There were nine combinations of each solvent and they were shown as in Table 3 (No.1-No.9). The combination of two kinds of Type A did not exist in our experiment caused by only one solvent belonging to Type A.

The results of expansion actions of each combination are shown in Table 3. And we got the following understanding through our test products:

- (1) Only No.1 (Type A-Type B I) gave an insulated core satisfied all of our requirements.
- (2) No.4 (Type B I-Type B I, where, two Type B I means two kinds of Type B I) and No.6 (Type B I-Type C) satisfied almost enough our requirements except the expansion ratio was a little low.
- (3) The solvent belonged to Type B II was available for high expansion ratio (more than 65%), but not available for deformation ratio and surface appearance of insulated core.
- (4) The solvent belonged to Type C was not available for high expansion ratio based on the existence of very few cells.

Photo.6-14 show the representative cross section of each combination.

Table 3.

Expansion Actions of Mixed Solvent

No	Combination	Appearance	Number of Cells	E. R. (%)	D. R. (%)
1	A B I	Smooth	Many	>40	<10
2	A B II	Rough	Many	>45	>15
3	A C	Smooth	Few	<40	<10
4	B I B I	Smooth	Many	40~60	<10
5	B I B II	Rough	Many	>45	40~15
6	B I C	Smooth	Many	40~60	<10
7	B II B II	Rough	Many	>45	40~15
8	B II C	Rough	Many	>40	>15
9	C C	Smooth	Few	<40	<10

E. R. : Expansion Ratio  
D. R. : Deformation Ratio

#### 4.3. Considerations

##### (1) Single Solvent

The high expansion ratio was given by the solvent Types A, B I and B II, based on the existence of many cells in the insulation. All these solvents have low boiling point and viscosity.

The low deformation ratio was given by only Type C, based on low expansion ratio.

This low deformation property was not given by Types A, B I and B II

Smooth surface appearance of insulated core was given by Types A and C, based on existence of very minute size of cells in the insulation.

##### (2) Mixed Solvents

The reason No.1 (Type A-Type B I) satisfied all of our requests was caused by the arrangement of many two size of cells densely and properly in the insulation. We understood the actions of solvents as follows:

Type A generated minute and many cells and Type B1 generated rather large and many cells. The difference of diffusion speed of Type A and Type B1 was not so large.

No.2 (Type A-Type BII) did not satisfy low deformation ratio and smooth appearance, which is based on excess expansion by Type BII, even though No.2 was expected to satisfy such properties owing to the similarity of expansion actions between Types B1 and BII.

## 5. Appendices

The measuring methods of expansion ratio and the deformation ratio were given as follows:

### (1) Expansion Ratio

Measuring coaxial capacitance of an expanded insulated core and calculating effective relative dielectric constant by equation 3, then calculating expansion ratio by equation 4.

$$\epsilon_s = \frac{C}{24.13} \times \log \frac{d_2}{d_1} \quad (\text{eq.3})$$

$$F = \frac{(2\epsilon_s + \epsilon_a)(\epsilon_a - \epsilon_s)}{3\epsilon_s(\epsilon_a - \epsilon_s)} \times 100 (\%) \quad (\text{eq.4})$$

where,  $\epsilon_s$ : Effective relative dielectric constant (-)

$\epsilon_a$ : Relative dielectric constant of insulation material (-)

$\epsilon$ : Relative dielectric constant of air (-)

C: Coaxial capacitance (PF/m)

$d_1$ : Conductor outer diameter (mm)

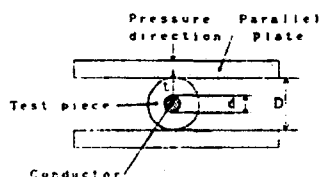
$d_2$ : Insulated core diameter (mm)

### (2) Deformation Ratio

Measuring the thickness of insulation before weighting. Placing the insulated core between the parallel plates of the measuring apparatus, applying the weight of 500g on it, and elapse of 15 minutes measuring the thickness of insulation. Calculating the diminution factor from the thickness of before weighting to that after weighting from the following equation 5. The measuring temperature is 23°C.

$$\text{Deformation Ratio (\%)} = \frac{\text{Thickness before weighting (mm)} - \text{Thickness after weighting (mm)}}{\text{Thickness before weighting (mm)}} \times 100 \quad (\text{eq.5})$$

Fig. 9  
Measuring Method of  
Deformation Ratio



Weight=500(g)

Pressure Time=15(min)

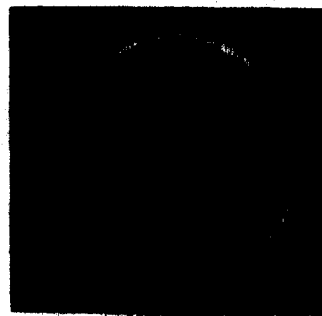


Photo 6  
Type A - Type B1

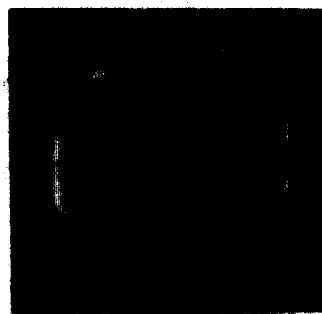


Photo 7  
Type A - Type BII



Photo 8  
Type A - Type C

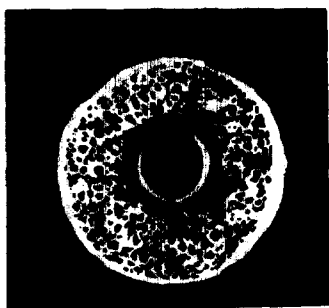


Photo 9.  
Type BI - Type BI

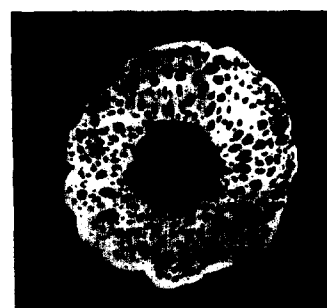


Photo 12  
Type BH - Type BH



Photo 10  
Type BI - Type BH



Photo 13  
Type BH - Type C



Photo 11  
Type BI - Type C



Photo 14  
Type C - Type C





KAZUHIDE SAKAMOTO  
The Furukawa Electric  
Co., Ltd.  
6-Yawata-Kaigandori  
Ichihara, Chiba 290  
Japan

Mr. Sakamoto graduated from Waseda University with a master of engineering degree majoring in organic chemistry in 1982. Then he joined The Furukawa Electric Co., Ltd. and has been engaged in research and development of plastics insulation material and manufacturing methods of expansion insulated core.

He is now an assistant manager of 1st Production Engineering Section of Electronic Appliance Wire Division.



ISAMU KOBAYASHI  
The Furukawa Electric  
Co., Ltd.  
6-Yawata-Kaigandori  
Ichihara, Chiba 290  
Japan

Mr. Kobayashi graduated from Tokyo Denki University majoring in analytical chemistry in 1989. Then he joined The Furukawa Electric Co., Ltd. and has been engaged in research and development of manufacturing coaxial cables and expansion insulated core.

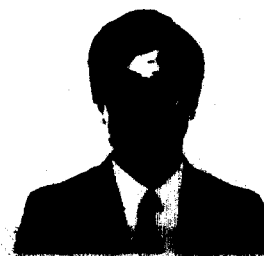
He is now a member of 1st Production Engineering Section of Electronic Appliance Wire Division.



MASANOBU SUGIMURA  
The Furukawa Electric  
Co., Ltd.  
6-Yawata-Kaigandori  
Ichihara, Chiba 290  
Japan

Mr. Sugimura graduated from Shibaura Institute of Technology majoring in electronics engineering in 1986. Then he joined The Furukawa Electric Co., Ltd. and has been engaged in research and development of manufacturing methods of flatcables and coaxial cables.

He is now a member of 1st Production Engineering Section of Electronic Appliance Wire Division.



SHINJI HAYASHI  
The Furukawa Electric  
Co., Ltd.  
6-Yawata-Kaigandori  
Ichihara, Chiba 290  
Japan

Mr. Hayashi graduated from Numazu Technology College majoring in mechanical engineering in 1972. Then he joined The Furukawa Electric Co., Ltd. and has been engaged in research and development of manufacturing wires and cables.

He is now an assistant manager of 1st production Engineering Section of Electronic Appliance Wire Division.

# PROPERTIES OF WATER ABSORBENT GELS FORMULATED FOR USE AS FILLING COMPOUNDS FOR COPPER TELECOMMUNICATIONS CABLE AND AS SPLICE CASE ENCAPSULANTS

Alvin C. Levy  
Alvin C. Levy & Associates, Inc.  
Norcross, Georgia

Steven C. Welch  
California State University San Marcos  
San Marcos, California

Peter V. Croft  
Waterguard Cable Products  
Channelview, Texas

## ABSTRACT

A new class of water absorbent materials developed for use as copper cable filling compounds and as splice case encapsulants has been investigated. These materials incorporate superabsorbents into more conventional products to give compounds capable of providing superior waterproof performance. In addition, these new materials possess the unique ability to heal shorts which can occur if small flaws are present in the conductor insulation.

The formulation technology and the mechanisms by which these materials function are explained. The properties investigated include the ability to withstand various water heads, short elimination as a function of flaw size, dielectric constant stability in the presence of moisture, the capacitance stability of twisted pairs immersed in the filling compound at 60°C, the oxidative induction time of conductor insulation in aged cables, and other properties important to cable and splice performance.

## INTRODUCTION

For a number of years, both ETPR and PEPJ compounds have been used to fill the cores of copper telecommunications cables designed for buried applications. Splice case encapsulants have consisted primarily of two-part polyurethanes. Although referred to as "waterproof," these systems are in reality only "water resistant." For example, current cables cannot always meet the industry three foot water head requirement, even while work continues to achieve the objective of withstanding a twelve foot water head.

In the past several years water absorbent materials, often referred to as superabsorbents, have come into use as a means of blocking the ingress and flow of water in telecommunications cable.<sup>1-5</sup> Such materials have included tapes impregnated

with superabsorbents, water absorbent fibers, and now water absorbent thixotropic gels (ATGs). The ATG products, developed and marketed by Waterguard Cable Products, exist in slightly different forms, dependent on whether their intended use is as a copper cable filling compound, as a flooding compound for optical fiber cable or as a splice encapsulant. Functionally, ATGs combine the technological advantages of both traditional filling compounds and superabsorbents to give a significantly improved "waterproof" system.

The purpose of this paper is to examine the properties of ATG compounds both in terms of existing industry requirements as well as potential product performance advantages. Where possible, explanation of behavior mechanisms is given.

## HOW ATGS WORK

As mentioned above, ATGs combine the advantages of traditional filling compounds and superabsorbents. Traditional filling compounds such as ETPR and PEPJ block water by void exclusion. Superabsorbents swell to form a rigid gel which blocks further water ingress. ATGs function in both the above manners to provide two methods of blocking water ingress. Additionally, ATGs have the ability to eliminate shorts which occur when water comes into contact with small pin holes or flaws in conductor insulation. This property, referred to as self-healing, is discussed in more detail later in the paper.

## FORMULATION CHEMISTRY

The water absorbent gels which are the subject of this paper more closely resemble the filling compounds for optical fiber cable in their chemistry and rheological properties than they do either ETPR and PEPJ filling compounds or the two-part polyurethane encapsulants. These new compounds, like optical fiber cable filling compounds, are thixotropic. The

primary components are a petroleum based oil, a thixotrope and a constituent that is commonly referred to as a superabsorbent. The superabsorbents are in the same class of crosslinked polyacrylate copolymers used in water blocking tapes elsewhere in the cable industry. In addition to the above components, other minor ingredients are added to provide the property balance required.

In the gel matrix, the superabsorbent remains as a particulate as opposed to being in solution. Trapped in this manner, the absorbent remains uniformly distributed. However, because the superabsorbent exists as a particulate, it is of primary importance that the particulates be small enough to prevent size exclusion during the cable filling process. Also, because of the particle nature of the absorbent, the molecule has limited mobility and therefore does not contribute significantly to the dielectric constant. This latter property is extremely important in copper cable filling compounds.

From the above description, one might assume that a simple blend of an optical fiber type filling compound with a superabsorbent would suffice as a water absorbent gel. This, however, is not the case. Such a compound would not absorb water. What is further required is a means of getting the water to the surface of the absorbent through the hydrophobic grease surrounding the individual absorbent particles. To achieve this property without allowing water to rapidly wick through the gel and without increasing the dielectric constant, is an important property of these materials.

#### PROPERTY CHARACTERIZATION

This section contains ATG characterization data relevant to properties that are measured external to the cable environment. The topics covered include: (1) a discussion of the physical properties generally included in a materials specification, (2) an examination of the self-healing phenomena, (3) data demonstrating the inherent water absorption capability of ATGs, and (4) testing relevant to the stability of the dielectric constant in the presence of moisture.

#### SPECIFICATION PROPERTIES

Typical properties for the encapsulant and filling compound are given in Table I. As can be seen from viscosity and penetration data, the encapsulant is significantly stiffer than the filling compound. The greater stiffness of the

encapsulant assists in limiting water penetration into the splice. In the cable configuration, the tightly packed conductors in conjunction with the filling compound limit water penetration at high water heads. As a result, the filling compound does not need to be as rigid as the encapsulant. Experimental data illustrating the above is given in the section on water penetration. It should also be noted that both compounds remain soft at low temperature. This property is important in low temperature handling.

TABLE I  
ATG PROPERTIES

Property	ATG FILL. CPD.	ATG ENCAP.	ETPR
Dielectric Constant (DC measurement)	2.25	-3.0	2.06
Dielectric Constant @ 1MHz (ASTM D150)	-	-	2.27 <sup>a</sup>
Dissipation Factor @ 1 MHz (ASTM D150)	-	-	0.0000 <sup>a</sup>
Volume Resistivity @ 1 MHz (ASTM D150)	-	-	1.2 x 10 <sup>15a</sup>
Viscosity, scale read. @ RT (Brookfield RVT, TD, 0.5 rpm)	35-43	>100	na
Penetration, dmm (ASTM D217)			
@ RT	315	230	124 <sup>a</sup>
@ 0°F	220	155	93 <sup>a</sup>
Oil Separation, % (1hr @ 15,000 rpm)	nil	nil	na
Water Absorption, min. (10g water by 15g ATG in Al weigh pan)	6	4	na
Oxid. Ind. Time, min.			
@ 200°C	-	-	17
@ 220°C	>50	-	-

-----  
a. A.C. Levy & R. Sabia, 31st IWCS (1982), p.313

The electrical properties for the filling compound are in the range of what is obtained for ETPRs. However, ETPRs are, on the average, lower in dielectric constant than is the ATG filling compound. As a result, the mutual capacitance in cables made with ATG could be ~1 nF/mile higher than an ETPR cable with the same construction.

With thixotropic gels one does not have to worry about high temperature cable drip if there is no syneresis (oil

separation). Such behavior occurs because thixotropic materials are temperature insensitive as compared with thermoplastics. However, syneresis can be problem. The data in Table I would indicate excellent performance by both ATG products. To put these numbers in perspective, thixotropic gels used to fill optical fiber cable characteristically exhibit much higher oil separation than ATGs.

Water absorption data given in Table I is typical of product which has been found to be functional in cable and splice tests. No standards for performance have been set for this property.

The oxidation induction time (OIT) for ATG products is excellent. The OIT for ETPR is generally measured at only 200°C whereas these data are reported at 220°C.

### SELF-HEALING

Self-healing provides a dimension to filling compound and encapsulant functionality that is not available with traditional materials. The mechanism is as follows.

When water comes into contact with a flaw in the conductor insulation, a short occurs. The water is then taken up by the superabsorbent in the ATG to form a rigid gel around the flaw. The superabsorbent at the same time starts to electroplate<sup>6</sup> on the conductor which functions as the anode. The water previously bound by the now deposited superabsorbent must find a new home. It therefore flows away from the area of the flaw into the balance of the superabsorbent/gel matrix. As a result there is now a void (air or gas gap) around the flaw (not water) and the short terminates. Elimination of the short is due to both insulation of the exposed copper with deposited absorbent layer as well as formation of the air gap. The degree to which each mechanism participates has not been determined. Experimental data illustrating the above sequence is presented in Figures 1 and 2.

The test cell configuration was as follows. Filling compound was placed in a shallow plastic pan to a depth of about 1 cm. The flaw area of an insulated conductor was placed at the surface of the filling compound. This wire was connected to the positive terminal of a 48 volt battery. A second length of wire having one inch of bare copper was used to provide the cathode. The cathode was connected to the battery in series with a microammeter. In Figure 1, the flaw was a cut end (cross-section) of a 22 gauge insulated conductor. In Figure 2, the flaw consisted of ~2mm of insulation removed from the circumference of the conductor.

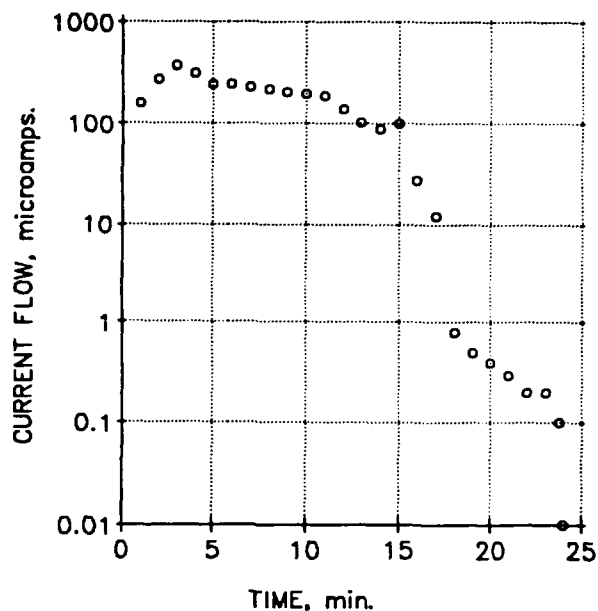


Figure 1. SELF-HEALING TEST - 22 GAUGE CROSS-SECTION FLAW

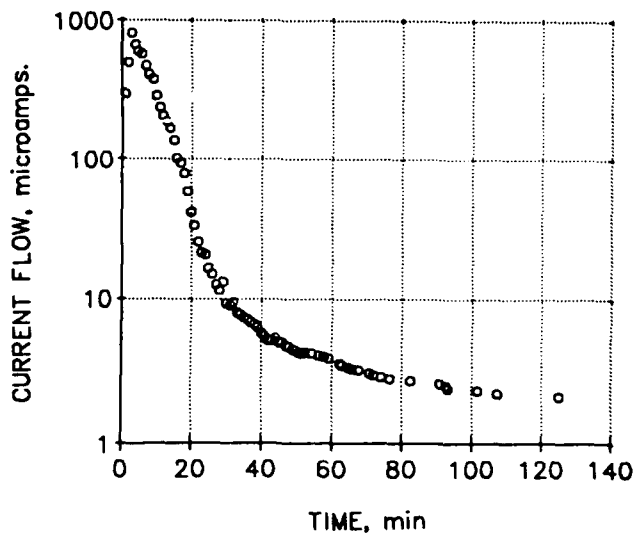


Figure 2. SELF-HEALING TEST, 2MM FLAW

To start the test, deionized water was added to the cell to a depth of approximately 3/4 cm. As ions were provided to the water by superabsorbent, the current increased as shown in the figures. At approximately five minutes into the test, the water was gelled and the current began to drop. At that time, a blue deposit was also visible at the surface of the flaw. This deposit is the copper salt of the superabsorbent molecule. With the smaller of the two

flaws, Figure 1, current ceased to flow in ~ 20 minutes. With the 2mm flaw, the current flow was 2 microamps at 120 minutes. In both cases, small voids around the flaw could be seen. Whether or not the flaw would completely heal in the second test was not determined. In a third test, 11 mil thick, 1x5 cm copper strips were used as the electrodes. In this case the size of the strip was sufficient to totally remove the gel, thereby exposing the electrode covered by the deposited blue layer. The weight loss (lost copper) of the electrode in this case was 0.25%.

What is apparent from the data is that the ability and time required to eliminate a flaw depends on the size of the flaw. The larger the flaw, the more difficult it is to complete the void required to terminate current flow. However, based on these data, the self-healing would be complete for any flaw exclusive of what might exist in the case of major cable damage.

#### WATER ABSORPTION

As previously mentioned, the manner in which superabsorbents function is to rapidly swell when contacted with water to form a rigid, instantaneous block. However, as long as an excess of water under pressure remains in contact at the block point there must be a slow diffusion of water through the absorbent or absorbent containing matrix. Figures 3-5 illustrate such data. The inside diameter of the tube in all tests is 5/16 in. The penetration number reflects visible movement of the boundary between the water swelled layer and the test compound.

Figure 3 illustrates how water moves through ATG as a function of water head. As can be seen there is a significant difference as both a function of head and type of compound. The encapsulant performs better than the filling compound because it is a stiffer product.

Figure 4 shows the penetration rate at 12 feet in several test configurations. The purpose of this figure is to illustrate the effect of packing of the conductors in the cable on water penetration into the cable core. Curve A is the control which is also shown in Figure 3. The test structure of curve B has a 1 inch depth of 20-30 mesh sand placed on top of the filling compound. Condition B represents a tighter packing than Condition A. In test C, pure superabsorbent is used in the tube. This test is still in progress.

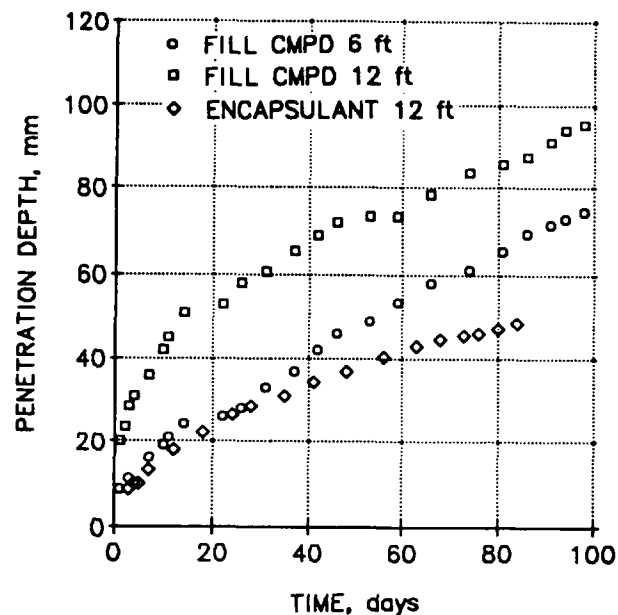


Figure 3. WATER PENETRATION FOR FILLING COMPOUND AND ENCAPSULANT

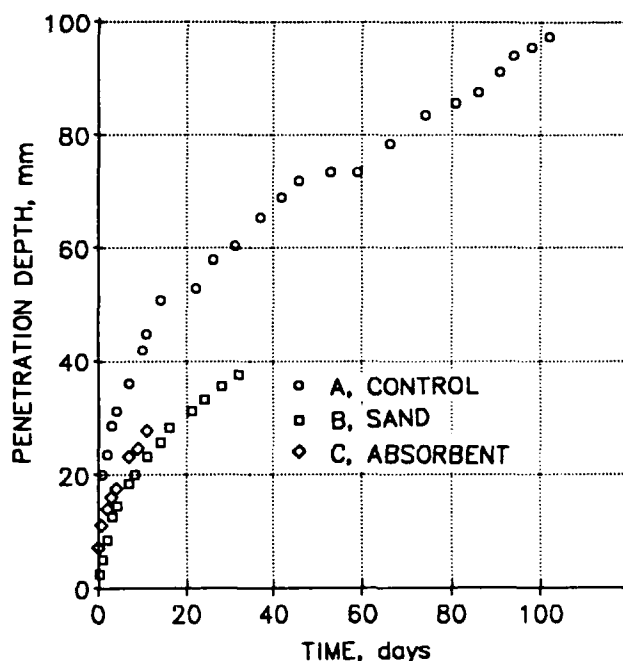


Figure 4. WATER PENETRATION AT 12 FOOT WATER HEADS

What is demonstrated in Figure 4 is that as the packing increases, the tendency for the superabsorbent to become trapped in the packing material increases and the result is a lower rate of movement of the boundary layer. In the case of a cable, the packing is so tight that the rate of penetration is much reduced over any of the tube test cases. For example, a cable kept under a 20 foot head for 7 months showed ~ 65 mm water penetration. In the worst case tube test, the equilibrium penetration rate is ~12mm (0.5 in.)/month. Keep in mind that to pass the industry's proposed 12 foot water head test, water is not permitted to flow more than 8 feet in 24 hours (~240 feet/month). It is also interesting to note that movement of water through the pure superabsorbent is intermediate between the encapsulant and filling compound.

Figure 5 illustrates the case in which a small head of water, in this case 30 mm, is placed on top of the ATG and then capped with aluminum foil. The penetration into the filling compound is then measured as a function of time. The data indicate that penetration rate for the filling compound drops below 1mm/month after about 4 months. The rate for the encapsulant is slightly higher.

Based on these data, one could expect true "waterproof" performance with ATGs under any water head that might occur in the terrestrial plant.

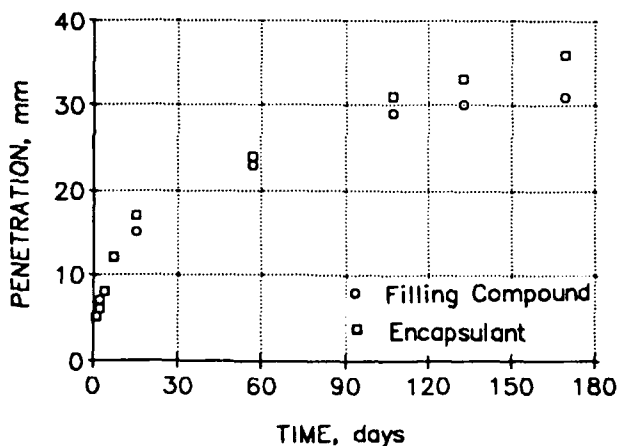


Figure 5. WATER PENETRATION IN A CLOSED SYSTEM

#### DIELECTRIC CONSTANT STABILITY

Of primary importance in the filling compound application is the stability of the dielectric constant under the various moisture and temperature environments that

the cable is likely to see. For example, the question as to whether or not water migrates to any degree past the front where swelling is apparent must be asked. Two tests were conducted to answer this question; one intermediate term at high temperature and high humidity, and the other long term at room temperature in contact with water.

In the first test, an aluminum pan filled with the filling compound was placed in a 70°C/ 95% RH environment for 21 days. The dielectric constant was then measured as a function of depth below the surface. The test was also run on the encapsulant. Data are plotted in Figure 6. In the second test, the dielectric constant was run on the filling compound after conclusion of the test described for Figure 5 data.

The data in Figure 6 show a rapid drop off of the dielectric constant at only a slight depth below the surface. The effect is more pronounced with the filling compound. In the second test, the dielectric constant was measured at a depth of ~3mm below the surface of the boundary between the water swelled and normal appearing layers. The value of 2.29 that was determined is essentially the same as the initial dielectric constant, 2.27.

Both of the above tests indicate that the dielectric constant of the bulk is stable and unchanged several mm beyond the swell boundary.

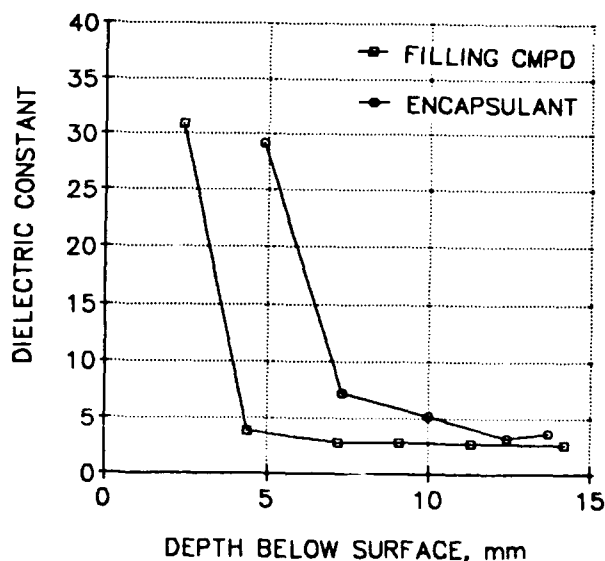


Figure 6. DIELECTRIC CONSTANT AFTER 21 DAYS @ 70C, 95%RH

## CABLE PERFORMANCE CHARACTERIZATION

This section contains discussion and data relevant to cable properties which are influenced by the filling compound or encapsulant. These properties include the effect of cell filling on the capacitance of twisted pairs having foam-skin insulation, the oxidative stability of conductor insulation in contact with the filling compound, cable electrical data, and finally the results of compatibility testing. Cable performance under water head is discussed above in the section on Water Absorption.

### CAPACITANCE STABILITY

In recent years, there have been a number of papers given with respect to cell filling of foam-skin insulation with the oils in ETPR type filling compound.<sup>7,8</sup> Work by Mitchell showed that the degree of cell filling was dependent on the type of filling compound and that in the actual cable environment, the degree of capacitance change associated with that cell filling was not significant.<sup>8</sup> However, since ATGs represent a new type of compound, it was thought advisable to repeat these studies.

Figure 7 shows plots of capacitance increase versus time for twisted pairs of 26 gauge foam-skin immersed at 60°C in beakers of three different filling compounds, two commercial ETPRs and the ATG filling compound. As can be seen the ATG is more stable than the two ETPRs. Reference to Mitchell's work shows the ATG to be similar to the more stable ETPRs in performance. However, a sample of that latter material was not available for testing.

The above performance of ATG compound might be related to differences in the oils used in ATGs and ETPRs. Also the above data is an indication of the stability of ATG with respect to dielectric constant when exposed to elevated temperature.

Finally, the capacitance of the blue-white pairs of two 25 pair cables with 24 gauge solid insulation, one with ATG and the other with ETPR filling compound were measured as a function of temperature. The data is shown in Figure 8. As can be seen, the capacitance of the ETPR filled cable decreases with increasing temperature. This decrease occurs because the cable and resultant spacing between conductors expand with increasing temperature. On the other hand, the capacitance of the ATG filled cable remains level with increasing temperature. Functionally, this behavior occurs because there is a slight temperature dependence (increase with

temperature) in the dielectric constant of ATG which offsets the capacitance decrease associated with thermal expansion.

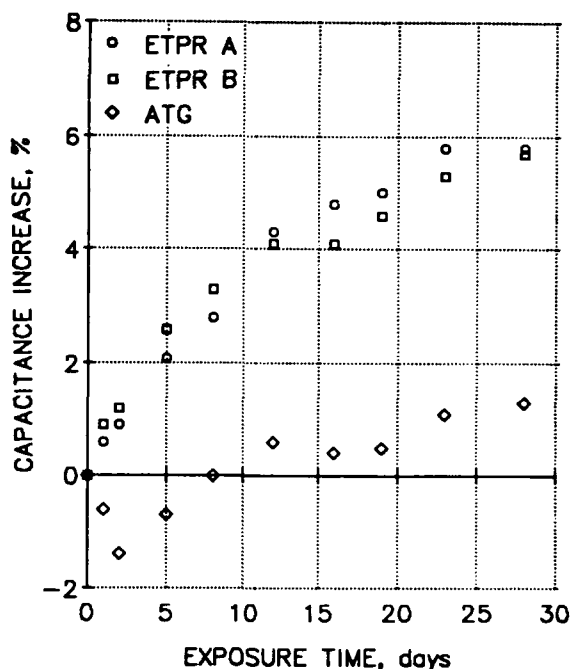


Figure 7. CAPACITANCE STABILITY OF 26 GAUGE FOAM-SKIN @ 60C

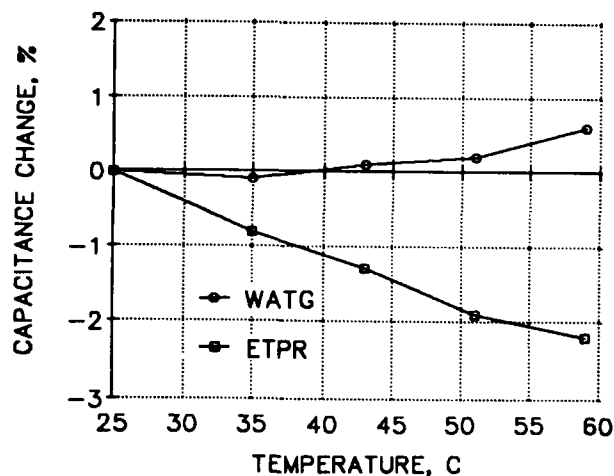


Figure 8. CABLE CAPACITANCE STABILITY AS A FUNCTION OF TEMPERATURE

## INSULATION STABILITY

No issue in filled copper cable has received more attention in the past several years than the cracking of the foam-skin polyethylene used to insulate copper conductors.<sup>9-12</sup> This cracking is a function of both the stabilization package in the insulation and the properties of the filling compound. In order to determine whether or not ATG filling compound performed satisfactorily in this respect, cables filled with ATG were aged for various periods and the oxidation induction time (OIT) measured. The test instrument was a Perkin-Elmer DSC4 using the Model 3700 Data Station. The test procedure was per Bellcore specification TA-NWT-000421.

In the first test, a 50 pair 24 gauge foam-skin cable was aged for four weeks at 70°C. OIT was determined at 200°C before and after aging. The type of stabilization package used in the insulation is not known, nor is the cable's prior thermal history. In the second test, three cables, one filled with ATG and two with different ETPRs, were evaluated at 200°C after aging two weeks at 70°C. All three cables were 50 pair, 26 gauge foam-skin insulated conductors. The insulated conductors in all three cables were from the same wire production run. Again, the stabilization packages are not known. The data for both tests are shown in Table II. All values reported represent the average of one run on each of the ten color insulations. Variation of OIT between different color insulations in the same cable, as indicated by the standard deviations, are consistent with data reported by Hershkowitz and Hore<sup>12</sup>.

TABLE II

OXIDATIVE INDUCTION TIME OF FOAM-SKIN  
INSULATION @ 200°C

	TEST # 1		TEST # 2	
	4 Weeks Aging		2 Weeks Aging	
	@ 70°C		@ 70°C	
	INDUCTION TIME, min. @ 200°C			
	Av.	Std. Dev.	Av.	Std. Dev.
Filling <u>Compound</u>				
ATG	53.7	7.4	64.1	4.6
ETPR I	-	-	53.5	8.7
ETPR II	-	-	46.3	6.3

Comparison of OIT performance of ATG filled cable aged for two versus four weeks at 70°C shows the expected relative performance. No precise analysis can be made because the insulation stability packages may not be the same. However, comparison of ATG performance versus the ETPRs in test 2 is clear. ATG offers improved performance relative to the ETPRs. Several possible explanations are possible for this improved performance. They are as follows.

- Lower extraction of stabilizers from the insulation with ATG because of differences between compound oils in the two product types.

- Lower stabilizer extraction with ATG because of lower cable filling temperatures with ATG versus ETPR (room temperature versus 110°C).

- Better stabilization of ATG versus the ETPRs.

- Less severe thermal history with ATG because of lower temperature blending and storage.

- Combinations of the above mechanisms.

## CABLE ELECTRICAL DATA

Table III contains the electrical data for the 50 pair super-unit of a AFMW 200 cable containing ATG filling compound. These data are typical of filled cable. For instance, the mutual capacitance requirement for filled cable is 83 +/- 4 nF/mile. The data reported in Table 3 comfortably fit in this range. The value of R/C Ratio for the cable was 0.0173 (0.0200 is passing).

TABLE III

ELECTRICAL DATA FOR AFMW 200  
ATG FILLED CABLE SUPER-UNIT

	Average	Stand. Dev.	Ind. Max.	Ind. Min.
Mutual Cap. (nF/mile)	83.53	1.37	86.20	80.99
Attenuation (dB/kf)	5.30	0.04	5.41	5.21



## COMPATIBILITY AND OTHER TESTING

ATG encapsulant was tested in splices having polycarbonate connectors. No evidence of stress cracking was observed.

Both ATG encapsulant and filling compound were tested in contact with Caschem 126 Encapsulant as was an ETPR control. Testing was at room temperature and 70°C for 7 days. No evidence of oil formation at the interface between the 126 Encapsulant and any of the test compounds was found. ATG encapsulant was evaluated in contact with ETPR at room temperature. No significant oil formation was seen at the boundary between the materials after 30 days at room temperature.

Cable drip tests were performed at 80°C per Bellcore TA-TSY-000421, Issue 2, dated September 1989. None of the cables tested dripped.

ATG filling compound and encapsulant were tested in accordance with ASTM G21-70 and found not to support fungus growth.

## SUMMARY AND CONCLUSIONS

A wide range of test data relevant to the performance of superabsorbent thixotropic gels, ATGs, as filling compounds and encapsulants in the outside copper plant have been presented. A brief summary of that performance is as follows:

- Superior waterproof performance relative to existing filling compounds and encapsulants.
- Self-Healing of electrical shorts due to small flaws in the conductor insulation.
- Improved oxidative stability of conductor insulation versus ETPR.
- Stable dielectric properties of the compounds in advance of the water swell.
- Stable cable capacitance as a function of time and temperature, equal to or better than ETPR filled cable.
- Satisfactory 80°C cable drip performance.
- Other ATG properties meet industry requirements and are comparable in performance to other commercial filling compounds and encapsulants.

## REFERENCES

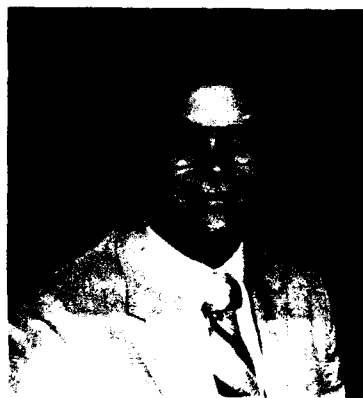
1. H. Hiramatsu, N. Ishii, and K. Nagai, "Development of Dry-Type Water-Blocking Optical Fiber Cable Using Swelling Material, Proceed., 38th Int. Wire & Cable Symposium, p.463 (1989)
2. S. Kukita, et al, "A New Nonmetallic and Waterproof Optical Fiber Cable with Absorbent Polymer Ribbon," Proceed., 36th Int. Wire & Cable Symposium, p.357 (1987)
3. P. D. Patel, et al, "LXE - A Fiber-Optic Cable Sheath Family with Enhanced Fiber Access," Proceed., 37th Int. Wire & Cable Symposium, p.72 (1988)
4. C. J. Arroyo, et al, "A High Performance Nonmetallic Sheath For Lightguide Cables," Proceed., 36th Int. Wire & Cable Symposium, p. 344 (1987)
5. K. Kathiresan, et al, "Fiber-Optic Cable Shipboard Systems," Proceed., 37th Int. Wire & Cable Symposium, p. 303 (1988)
6. C. S. Freeman and K. M. Freeman, U. S. Patent 4,711,022, Dec. 8, 1987
7. A. W. Stratton, T. J. Roessing, and J. D. Burkhard, "A Comparative Stability Study Related to the Performance of PE/PJ and ETPR Filling Compounds," Proceed., 36th Int. Wire & Cable Symposium, p.322 (1987)
8. D. M. Mitchell, "The Effect of Filling Compound on the Capacitance of Foam-Skin Insulation: Laboratory Simulation vs. Cable Performance," Proceed., 37th Wire & Cable Symposium, p.500 (1988)
9. L. P. Beltz, "Factors That Influence PIC Degradation of Filled Foamskin Telephone Cable," Proceed., 38th Int. Wire & Cable Symposium, p.123 (1989)
10. K. Dye et al, "Analysis of Stabilizer Concentrations In Polyolefin Cable Materials, Proceed., 38th Int. Wire & Cable Symposium, p.98 (1989)
11. T. N. Bowmer, "Cracking of Foam-Skin Polyethylene Insulations in Pedestals," Proceed., 37th Int. Wire & Cable Symposium, p.475 (1988)
12. E. E. Hershkowitz and L. M. Hore, "Variations of Oxidative Induction Times of Polyolefin Insulated Conductors," Proceed., 39th Int. Wire & Cable Symposium, p.479 (1990)



Alvin C. Levy received his Ph.D. in physical chemistry from the Georgia Institute of Technology. Since 1987, he has been President of Alvin C. Levy and Associates, a R&D laboratory specializing in the development of adhesives, coatings, and sealants. His prior work experience includes product development with AT&T Bell Laboratories and E.I. Du Pont. Dr. Levy holds patents on filling compounds for both copper and optical fiber cable and on coatings for optical fiber.



Peter V. Croft is the President of WaterGuard Cable Products, Inc., Channelview, Texas and has been since its incorporation in April of 1990. No stranger to the wire and cable industry, Mr. Croft has been involved in the development, manufacture, and marketing of cable compounds while serving as Sr. Vice President, Pennzoil Products Company and President of Pennzoil's Penreco Division.



Steven C. Welch is Chairman and Professor of Chemistry at the California State University, San Marcos. He received his Ph.D. in synthetic organic chemistry from the University of Southern California in 1968. He has been a member of the American Chemical Society since 1965. Dr. Welch has 45 research publication on subjects ranging from new reagent materials to the synthesis of complex organic substances. He has been associated with Waterguard Products from their inception.

# Temperature Effect on High Frequency Data Transmission Through Plenum Wires

L. M. Hore

Belcore, New Jersey, USA

## Abstract

This paper presents a short overview of the general properties of the dielectric materials used in plenum wires and the effect of elevated temperatures on the dielectric properties and consequently on the transmission parameters of the wires. The purpose of this paper is to supplement the limited scientific data published by resin manufacturers for wide varieties of insulating materials now being used in plenum wires for applications in high frequency and high temperature areas. To evaluate the temperature effects on the transmission of wires, samples made of different insulation/jacket combinations currently being used in plenum wires are stabilized at room temperature (RT) ranging from 70°F to 73°F, 110°F and 150°F before the transmission parameter measurements are performed on the wires. The results will show the temperature effects on attenuation, near end crosstalk, characteristic impedance and mutual capacitance to a varied degree. Based on this study, temperature coefficients of attenuation ( $T_c$ ) of the wires insulated with FEP, ECTFE, PVC and PE are computed for different frequency and different temperature range. Ideally, the temperature coefficient of attenuation of the plenum wires should be 0.0010/dB/°F same as the reference cable with PE insulation. From this standpoint, FEP insulation meets the above expectation in the frequency range up to 40 MHz and the temperature range up to 150°F, the maximum limits of the current measurements. PVC insulated cables should be avoided in applications where high frequency signals and higher than room temperature environments are expected. While not as poor a choice, ECTFE insulation may also create some problems in the higher frequency band.

## 1. Introduction

The ANSI X3T 9.5 FDDI (Fiber Distributed Data Interface) Committee set up an ad hoc working group in 1990 to investigate the implementation of FDDI through a low cost media - shielded twisted pairs (STP) and unshielded twisted pairs (UTP). At the time of preparing this paper there are at least three known companies claiming that 100 megabits/sec (Mbps) data transmission is possible over twisted pairs<sup>(1)</sup> for practical distances. There are also a number of companies who report to have developed transceivers that would transmit 100 Mbps signals through the media which is being called TPDDI (Twisted Pair Distributed Data Interface).<sup>(2)</sup> It is expected that the ANSI ad hoc working group will prepare a standard to cover transmission parameters, viz., mutual capacitance, attenuation, near end crosstalk, characteristic impedance, etc. suitable for transmission up to 100 Mbps.

The transmission parameters of the twisted wires depend on the design criteria, materials used in the wire, and the

environmental conditions of the wire during its service life. Normally plenum wire operates at room temperature (RT) because it is located in air return plenums. In some buildings, however, wire and cable could run parallel to steam pipes or may be exposed to other heat sources and thereby become heated above ambient temperature, especially in cold weather. In some other buildings, cable could be placed in wiring closets and other non-plenum areas where there is no air conditioning provided and where temperature can rise during summer. With this scenario in mind, the twisted wires exposed to elevated temperatures will be measured and analyzed to determine the suitability of the dielectric materials used in plenum wires.

## 2. General Properties of Dielectric Materials

The properties affecting the behavior of insulating materials in service can be classified under the sub-heading of (i) mechanical, (ii) electrical, (iii) thermal, (iv) chemical, (v) environmental and miscellaneous. Of all these properties, we are interested in dealing with the electrical properties only, and a brief review of the factors affecting the electrical properties of dielectric materials is stated below.

The electrical properties that influence the design of wires are (i) dielectric constant, (ii) dissipation factor or loss factor, (iii) insulation resistance, (iv) volume and surface resistivity, (v) dielectric strength, (vi) surface breakdown strength, (vii) liability to track, (viii) temperature coefficients and frequency dependency of these properties.

The insulating materials are used over the entire electromagnetic spectrum from zero frequency to radar frequencies of at least 30 GHz. There are only a few materials whose dielectric constant and dissipation factor are approximately constant over this frequency range. The change in dielectric constant and loss factor with frequency are produced by a phenomenon called dielectric polarization.<sup>(3)</sup> It is beyond the scope of this paper to go into the detailed aspects of dielectric polarization. It can be said, however, that starting at the highest frequency, each succeeding polarization, dipole or interfacial, adds its contribution to dielectric constant, with the result that dielectric constant has its maximum value at zero frequency. Each polarization furnishes a maximum of dissipation factor. The frequency at which dissipation is maximum is called the relaxation frequency for that polarization.

The major electrical effect of temperature on an insulating material is to increase the relaxation frequency which is the reciprocal of relaxation time ( $\tau$ ) of its polarization.

The relaxation time  $\tau$ <sup>(4)</sup> is defined as,

$$\tau = 10^{-14} \cdot e^{\frac{E}{kT}} \text{ seconds} \quad (1)$$

where,

E : energy in electron volt (e.v.)

K : a constant

T : absolute temperature

The difference of 40 seconds to one day would be caused by a temperature change of 60°C at constant barrier height of 1 e.v.

### 3. Experimental Samples

The various twisted pair samples used for transmission measurements are,

Sample No.	Pair/AWG	Insul./Jkt.
Insulation: ECTFE		
1	4/24	ECTFE/ECTFE
2	4/24	ECTFE/ECTFE
6	3/24	ECTFE/PVDF
8	3/24	ECTFE/ECTFE
Insulation: FEP		
3	4/24	FEP/ECTFE
4	4 Cond./24 SQ	FEP/ECTFE
Insulation: PVC		
7	4 Cond./24 OQ	PVC/PVC
9	4/24	PVC/PVC
Insulation: PE		
12	12/22 Shielded Pair	PE/PVC

NOTE:

ECTFE - Ethylene Chloro Tetra Floro Ethylene Copolymer  
 PVDF - Poly Vinylidene Fluoride  
 FEP - Fluorinated Ethylene Propylene Copolymer  
 PVC - Poly Vinyl Chloride  
 PE - Polyethylene  
 SQ - Star Quad,  
 OQ - Oscillating Quad

To measure the transmission parameters of the above wires, two different measuring sets were employed - a DCM model CMS-2PCX Computerized Automatic Cable Measuring System to measure mutual capacitance (C) and capacitance unbalance at 1 kHz, attenuation, characteristic impedance ( $Z_0$ ) and near end crosstalk (NEXT) from 64 kHz to 8 MHz and a HP 4194A Impedance Analyzer to measure attenuation, NEXT, characteristic impedance and phase angle from 64 kHz to 40 MHz.

### 4. Cable Parameters Relations

The following transmission equations can be found in any textbook on transmission lines. The propagation constant ( $\gamma$ ) is a complex number comprised of a real part ( $\alpha$ ) and imaginary part ( $\beta$ ) as shown,

$$\gamma = \alpha + j\beta \quad (2)$$

$$\gamma = \sqrt{ZY} \quad (3)$$

The real part ( $\alpha$ ) is called the attenuation constant and the imaginary part ( $\beta$ ) is called the phase shift.

The characteristic impedance ( $Z_0$ ) is related to the primary constants of a transmission line by the following equation:

$$Z_0 = \sqrt{\frac{Z}{Y}} = \frac{\sqrt{R + j\omega L}}{\sqrt{G + j\omega C}} \quad (4)$$

where,

$Z = R + j\omega L$  = series impedance, ohms per mile  
 $Y = G + j\omega C$  = parallel admittance, mhos per mile  
 $R$  = series resistance, ohms per loop mile  
 $L$  = series inductance, henrys per loop mile  
 $G$  = parallel conductance, mhos per mile  
 $C$  = mutual capacitance, farads per mile  
 $\omega = 2\pi f$  (where  $f$  is the frequency in Hz)  
 $\alpha$  = attenuation, nepers per mile  
 (dB per mile = 8.686  $\times$  nepers per mile)  
 $\beta$  = phase shift, radians per mile

At high frequencies,

$$Z_0 \approx \sqrt{\frac{L}{C}} \quad (5)$$

$$\alpha \approx \frac{1}{2} R \sqrt{\frac{C}{L}} + \frac{1}{2} G \sqrt{\frac{L}{C}}, \text{ nepers/mile} \quad (6)$$

$$\approx 4.343R/Z_0 + 4.343 G \cdot Z_0 \text{ dB/mile} \quad (7)$$

The first term of the equation (7) is due to conductor loss and the second term is due to dielectric loss. The loss due to conductor resistance ( $R$ ) vary as the square root of frequency and it consists of dc resistance, increment due to skin effect, increment due to proximity effect, and increment due to eddy currents in other pairs and the sheath, if present.<sup>(5)</sup> In the second term the parallel conductance ( $G$ ) is expressed by,

$$G = \omega C \tan \delta \quad (8)$$

$$= 2\pi f \cdot C \cdot \tan \delta$$

where,

$f$  - frequency in Hz

$C$  - mutual capacitance in farads/mile

$\tan \delta$  - dissipation factor of the dielectric

The loss due to conductance ( $G$ ) can be of significant importance at higher frequencies if the dissipation factor increases with frequency.

The mutual capacitance ( $C$ ), shown in the above equations is related to the size of the conductor, insulation thickness, dielectric constant of the insulation and the interstitial medium and is given by the following approximate expression,

$$C \approx \frac{0.019415 \pi \epsilon \times 10^{-6}}{\log_{10} \frac{2S}{d}} \text{ farads per mile} \quad (9)$$

where,

$\epsilon$  : effective dielectric constant of the cable medium

$S$  : center to center conductor spacing in inches

$d$  : wire diameter in inches

## 5. Attenuation versus Temperature

Attenuation of all nine wire samples is measured using the DCM test set up to 8 MHz. In addition, the HP Impedance Analyzer is employed to measure the attenuation of four selected samples up to 40 MHz to represent the various insulation/jacket combination of ECTFE/ECTFE, FEP/ECTFE, ECTFE/PVDF and PVC/PVC. The only sample with PE insulation and PVC jacket covers measurements up to 8 MHz. The attenuation data up to 40 MHz at room temperature (RT), 110°F and 150°F are shown in Tables 2, 3, 4, 5 and 6. The analysis of the data is covered in Section 9.

TABLE 1 Avg. Mutual Capacitance (C) vs. Temperature

Sample No.	Pair/AWG	Ins/Jkt	Avg. C, nF/kft @			ΔC (%)	
			RT	110°F	150°F	(1)-(2)	(1)-(3)
			(1)	(2)	(3)		
Insulation: ECTFE							
1	4/24	ECTFE/ECTFE	18.29	18.28	18.33	-0.1	0.2
2	4/24	ECTFE/ECTFE	18.10	18.12	18.17	0.1	0.4
6	3/24	ECTFE/PVDF	18.84	18.87	18.99	0.2	0.8
8	3/24	ECTFE/ECTFE	17.65	17.62	17.70	-0.2	0.3
Insulation: FEP							
3	4/24	FEP/ECTFE	15.08	14.98	14.92	-0.7	-1.1
4	4 Cond./24 SQ	FEP/ECTFE	12.15	12.13	12.09	-0.2	-0.5
Insulation: PVC							
7	4 Cond./24 OQ	PVC/PVC	13.03	13.29	13.43	2.0	3.1
9	4/24	PVC/PVC	20.12	24.01	28.64	19.3	42.3
Insulation: PE							
12	12/22 Shielded Pair	PE/PVC	21.38	21.24	21.19	-0.7	-0.9
Note:							
ECTFE - ethylene chlorotetrafluoro ethylene copolymer							
PVDF - poly vinylidene fluoride							
FEP - fluorinated ethylene propylene copolymer							
PVC - poly vinyl chloride							
PE - polyethylene							

### Average Attenuation (α) vs. Frequency

TABLE 2 No. 1 4 Pair/24 AWG (ECTFE/ECTFE)

Freq. (kHz)	Avg. α, dB/Kft. @		
	70°F	110°F	150°F
64	2.30	3.38	2.60
256	3.31	4.15	3.57
512	4.99	5.91	5.33
772	6.28	7.27	6.71
1000	7.20	8.24	7.72
1600	9.33	10.49	10.02
4000	15.38	17.01	16.69
6300	19.83	21.91	21.70
8000	22.80	25.16	25.08
10,000	25.81	28.47	28.54
16,000	35.12	38.84	38.97
20,000	39.10	43.72	44.09
30,000	49.46	56.32	57.05
40,000	59.14	67.38	67.98

TABLE 3 No. 3 4 Pair/24 AWG (FEP/ECTFE)

Freq. (kHz)	Avg. α, dB/Kft. @		
	70°F	110°F	150°F
64	2.43	2.62	2.75
256	3.11	3.26	3.37
512	4.07	4.26	4.39
772	5.22	5.46	5.63
1000	5.91	6.16	6.38
1600	7.51	7.83	8.10
4000	11.83	12.37	12.79
6300	14.92	15.65	16.18
8000	16.76	17.63	18.21
10,000	18.74	19.72	20.34
16,000	23.99	25.33	26.03
20,000	26.82	28.36	29.17
30,000	33.84	35.63	36.48
40,000	38.57	41.17	41.79

TABLE 4 No. 6 3 Pair/24 AWG (ECTFE/PVDF)

Freq. (kHz)	Avg. α, dB/Kft. @		
	70°F	110°F	150°F
64	2.31	2.51	2.63
256	3.39	3.50	3.61
512	5.23	5.29	5.38
772	6.61	6.67	6.76
1000	7.67	7.19	7.82
1600	10.06	10.15	10.17
4000	17.39	17.69	17.47
6300	22.72	23.54	23.09
8000	26.37	27.62	27.11
10,000	30.24	32.12	31.40
16,000	40.65	44.58	44.10
20,000	46.37	51.79	51.71
30,000	61.79	69.94	70.32
40,000	71.73	84.49	87.67

TABLE 5 No. 9 4 Pair/24 AWG (PVC/PVC)

Freq. (kHz)	Avg. α, dB/Kft. @		
	70°F	110°F	150°F
64	2.46	2.69	2.84
256	3.66	4.35	5.08
512	5.46	6.60	7.75
772	6.83	8.34	10.00
1000	7.88	9.77	11.85
1600	10.21	12.82	15.92
4000	17.18	22.14	28.87
6300	22.61	29.39	38.93
8000	25.92	34.03	45.59
10,000	29.83	39.37	52.82
16,000	39.87	53.51	72.65
20,000	48.59	62.54	84.73
30,000	60.67	83.84	111.74
40,000	73.09	99.43	118.45

TABLE 6 No. 12 12/22 Shielded Pair (PE/PVC)

Freq. (kHz)	Avg. $\alpha$ , dB/Kft. @		
	71°F	110°F	150°F
64	1.52	2.05	2.14
256	3.31	3.40	3.85
512	5.88	5.88	5.94
772	7.93	8.06	8.21
1000	9.91	10.11	10.15
1576	13.70	13.95	14.02
4000	23.44	24.17	24.10
6300	29.72	30.41	30.34
8000	33.70	34.17	34.10

## 6. Temperature Coefficient of Attenuation ( $T_c$ )

The resistance of conductors increases with the increase in temperature and therefore will increase the first term of the attenuation equation (7), assuming the characteristic impedance ( $Z_0$ ) is unchanged with temperature. Similarly, if the conductance (G) which is also temperature dependent for certain dielectric materials increases with the rise of temperature, the second term of the equation (7) will be increasing with the increased temperature. The temperature coefficient of attenuation in the above situation can be expressed by,

$$T_c = \frac{\alpha_T - \alpha_{RT}}{\alpha_{RT} (T - RT)} \quad (10)$$

where,

$\alpha_{RT}$  : attenuation at RT°F

$\alpha_T$  : attenuation at T°F

By measuring the attenuation of wires at RT, and at 110°F and 150°F, the temperature coefficient of attenuation ( $T_c$ ) for wires insulated with ECTFE, FEP, PVC and PE are computed between RT and 110°F and between RT and 150°F.

The temperature coefficient of attenuation ( $T_c$ ) values of all the samples are computed using both the DCM and HP data and averaged under each category of insulation, viz., FEP, ECTFE, PVC and PE. The computed  $T_c$  values are shown in Table 7 and plotted in Figure 1.

## 7. Near End Crosstalk (NEXT)

The near end crosstalk between two pairs inside a cable is dependent on the attenuation of the wires and the length of the wires, unless the wire is sufficiently long. The attenuation and length dependency of NEXT is expressed by the following equation:<sup>(6)</sup>

$$\text{NEXT, dB/kft} = \text{next}_\ell + 10 \log \left[ \frac{1 - 10^{-\frac{\alpha \ell}{5}}}{1 - 10^{-\frac{\alpha}{5}}} \right] \quad (11)$$

where,

$\text{next}_\ell$  = measured value of NEXT for length  $\ell$  ft.

$\alpha$  = attenuation, dB/kft

Since the wire samples have temperature coefficients of attenuation, the wires show different attenuation values at different temperatures. The length correction factor shown

TABLE 7

Temperature Coefficient of Attenuation ( $T_c$ ) vs. Frequency

$$T_c = \frac{\alpha_T - \alpha_{RT}}{\alpha_{RT} (T - RT)}$$

where,

$\alpha_{RT}$  = attenuation at RT°F

$\alpha_T$  = attenuation at temperature, T°F

Freq. (kHz)	$T_c$ (%/dB/°F)							
	RT to 110°F				RT to 150°F			
	FEP	ECTFE	PVC	PE	FEP	ECTFE	PVC	PE
64	0.24	0.34	0.38	0.22	0.20	0.28	0.28	---
256	0.16	0.15	0.46	0.07	0.10	0.09	0.47	0.20
512	0.03	0.11	0.39	0	0.06	0.06	0.45	0.01
772	0.05	0.14	0.46	0.05	0.07	0.05	0.50	0.04
1000	0.10	0.11	0.50	0.05	0.09	0.07	0.54	0.03
1600	0.08	0.11	0.54	0.05	0.09	0.07	0.62	0.03
4000	0.15	0.18	0.68	0.08	0.12	0.09	0.79	0.04
6300	0.12	0.15	0.67	0.06	0.11	0.10	0.81	0.03
8000	0.10	0.16	0.67	0.04	0.09	0.10	0.83	0.02
10,000	0.13	0.21	0.80	---	0.11	0.09	0.96	---
16,000	0.14	0.25	0.85	---	0.11	0.13	1.03	---
20,000	0.14	0.30	0.72	---	0.11	0.15	0.93	---
30,000	0.15	0.34	0.95	---	0.11	0.18	1.05	---
40,000	0.17	0.40	0.90	---	0.10	0.24	0.78	---

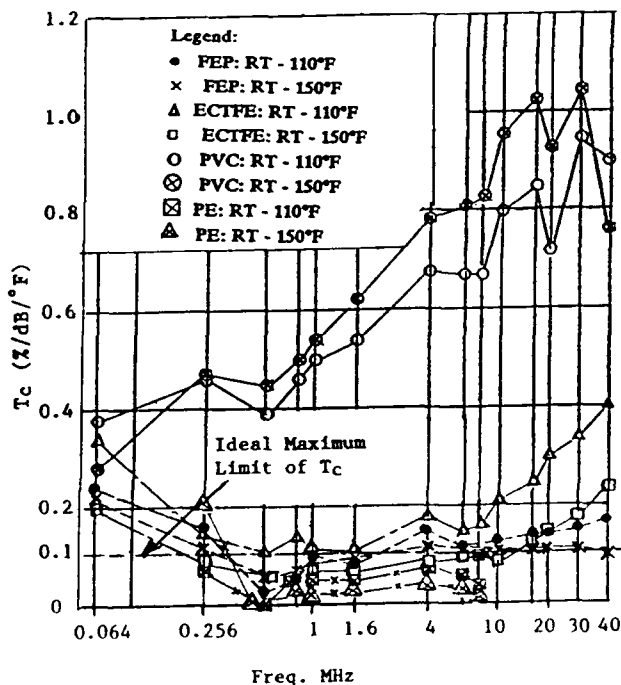


Fig. 1. Temperature Coefficient of Attenuation ( $T_c$ ) vs. Frequency

in the second term of the equation (11) therefore, has different values for different temperatures. Since the attenuation of the wires at RT is already high, no significant changes in the correction factor will be noticeable for the higher attenuation values at 110°F and 150°F.

The average near end crosstalk (NEXT) and the worst pair NEXT values of the representative samples of ECTFE/ECTFE, FEP/ECTFE, PVC/PVC and PE/PVC wires at RT, 110°F and 150°F are presented in Table Nos. 8, 9, 10 and 11. As expected no pattern was noticed except in the case of shielded pair wire (No. 12 12/22). The NEXT values of this wire are measured significantly higher than those of the other unshielded samples.

#### NEXT vs. Frequency and Temperature

TABLE 8 No. 1 4 Pair/24 AWG (ECTFE/ECTFE)

Freq. (kHz)	NEXT, dB/Kft. @					
	70°F		110°F		150°F	
	Avg.	Worst	Avg.	Worst	Avg.	Worst
64	79	63	65	64	81	65
256	63	54	63	54	64	55
512	56	52	56	51	57	53
772	55	50	54	46	55	50
1000	52	50	51	45	53	50
1600	52	45	52	41	53	48
4000	42	33	45	35	45	36
6300	40	35	43	36	44	37
8000	41	35	39	33	40	36
10,000	41	28	38	31	38	31
16,000	35	32	36	27	40	27
20,000	36	32	37	27	40	33
30,000	34	26	33	27	33	26
40,000	32	27	30	25	31	25

TABLE 9 No. 3 4 Pair/24 AWG (FEP/ECTFE)

Freq. (kHz)	NEXT, dB/Kft. @					
	70°F		110°F		150°F	
	Avg.	Worst	Avg.	Worst	Avg.	Worst
64	71	64	72	56	71	66
256	60	55	60	50	61	56
512	55	52	56	42	56	50
772	51	41	50	37	51	42
1000	50	37	51	37	51	38
1600	45	35	46	37	46	38
4000	44	39	44	37	44	34
6300	35	29	42	25	43	37
8000	36	26	39	25	37	25
10,000	39	28	36	25	37	25
16,000	33	24	32	24	32	24
20,000	31	21	31	24	31	24
30,000	30	18	31	21	31	21
40,000	32	20	29	25	29	23

TABLE 10 No. 9 4 Pair/24 AWG (PVC/PVC)

Freq. (kHz)	NEXT, dB/Kft. @					
	70°F		110°F		150°F	
	Avg.	Worst	Avg.	Worst	Avg.	Worst
64	77	65	77	64	74	65
256	64	56	63	55	66	54
512	61	52	62	52	60	51
772	59	46	59	49	57	49
1000	57	52	58	52	56	52
1600	52	47	52	45	55	49
4000	46	35	47	35	49	45
6300	41	34	42	33	47	39
8000	34	33	45	34	43	32
10,000	44	32	43	34	47	37
16,000	39	33	42	33	42	32
20,000	41	33	42	31	40	28
30,000	39	25	37	29	34	25
40,000	29	18	29	19	33	24

TABLE 11 No. 12 12/22 Shielded Pair (PE/PVC)

Freq. (kHz)	NEXT, dB/Kft. @					
	71°F		110°F		150°F	
	Avg.	Worst	Avg.	Worst	Avg.	Worst
64	94	78	93	79	94	80
256	86	73	85	73	86	73
512	85	74	85	72	85	72
772	85	72	84	72	85	73
1000	85	72	84	73	85	74
1576	87	73	85	72	86	72
4000	86	71	84	65	85	64
6300	85	73	83	61	84	60
8000	78	65	77	59	77	59

## 8. Estimate of Transmit Distances

In Hore and Thuraisamy's paper,<sup>(7)</sup> it has been shown that near end crosstalk (NEXT) and loss characteristics are dominant factors for high speed transmission through twisted copper wires. In the same paper, various impairments, i.e., inductive noise, echo, intersymbol interference, impulse noise were discussed and their effects in limiting the transmit distance were presented. Based on engineering judgement, a margin of 12 dB is considered acceptable for various impairments for theoretical studies. For laboratory studies and performance evaluation, 6 dB is adequate.

In digital transmission for a Bit Error Ratio (BER) of one error in ten million ( $10^{-7}$ ), a signal having binary code requires a peak Signal-to-Noise Ratio (SNR) of 14.3 dB.<sup>(8)</sup> For higher frequency digital transmission, SNR values need to be worked out.

Considering all conditions, i.e., impairments, Signal-to-Noise Ratio, and other factors, such as bridged-taps, and subtracting the total margin from the NEXT values, an estimate could be made of the available dB budget for transmission with desired bit error ratio. From the available dB budget, the transmit distances can be worked out dividing

the dB values by the attenuation (dB/kft) of the wire, only if there is no bridged-tap. To have longer transmit distances, crosstalk separation should be high and/or the attenuation of the wire should be lower. High temperature coefficient of attenuation produces higher loss at higher temperatures, thereby reducing the effective transmit distances.

## 9. Characteristic Impedance ( $Z_0$ )

Presently the EIA 41.8.1 committee is working to develop requirements for wire and cable parameters. Of these parameters, measurement of characteristic impedance is a challenging one. Various methods have been outlined in Friesen's paper.<sup>(9)</sup> One method is based on open circuit and short circuit measurements. When the length of the wire is short (under a quarter wave length), the characteristic impedance  $Z_0$  can be defined by the following relation.

$$Z_0 = \sqrt{Z_{sc} \cdot Z_{oc}} \quad (12)$$

where,

$$Z_{sc} \text{ (short circuit impedance)} = Z_0 \tanh \gamma l \quad (13)$$

and

$$Z_{oc} \text{ (open circuit impedance)} = Z_0 \coth \gamma l \quad (14)$$

The characteristic impedance value, can be expressed by the primary constants, R, L, G and C shown in equation (4). At

high frequencies,  $Z_0 \approx \sqrt{\frac{L}{C}}$  and it depends on two parameters, L and C. At around 1 MHz and above,  $Z_0$  tends to maintain approximately a constant value as shown in Figures 2 thru 13 for four representative sample numbers 1, 3, 9 and 12. The average  $Z_0$  values at 1 MHz are shown in Table 12 for the above samples at three temperatures, 70°F, 110°F and 150°F. Of these four samples, the greatest changes in  $Z_0$  take place in sample number 9 with PVC insulation. In the temperature range of 70° to 110°F, the change in  $Z_0$  is -6% and 70° to 150°F, the corresponding change is -11%. This result can be explained from the observation of the increased mutual capacitance (C) of sample No. 9 (see Table 1 and Figure 14). The reason for the decrease in  $Z_0$  at higher temperatures is primarily due to the increase in C as evident from the expression for  $Z_0 = \sqrt{\frac{L}{C}}$ , assuming inductance L is constant. Changes in  $Z_0$  values for other samples up to 4% may be attributed to the measurement variability.

Sample No. 1 4/24 ECTFE/ECTFE T- 70°F

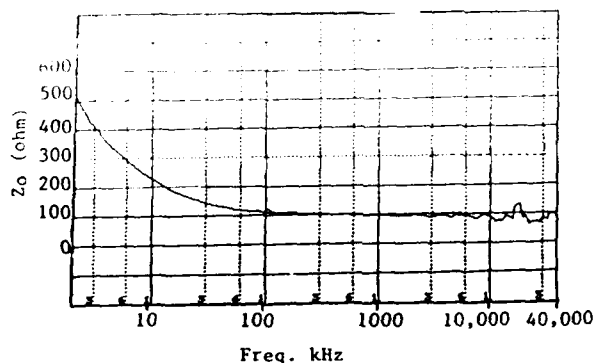


Fig. 2. Characteristic Impedance ( $Z_0$ ) vs. Frequency

$Z_0$  vs. Freq. No. 1 T- 110°F

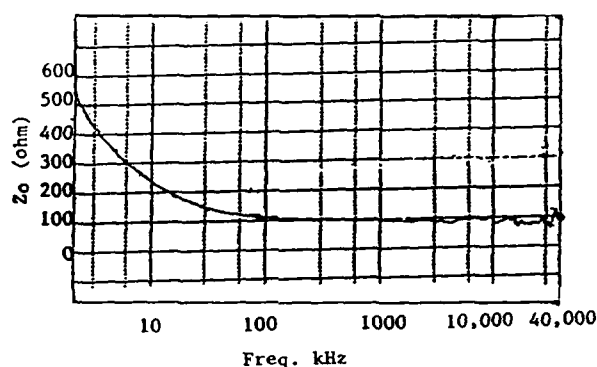


Fig. 3. Characteristic Impedance ( $Z_0$ ) vs. Frequency

Sample: 4/24 ECTFE/ECTFE

$Z_0$  vs. Freq. No. 1 T- 150°F

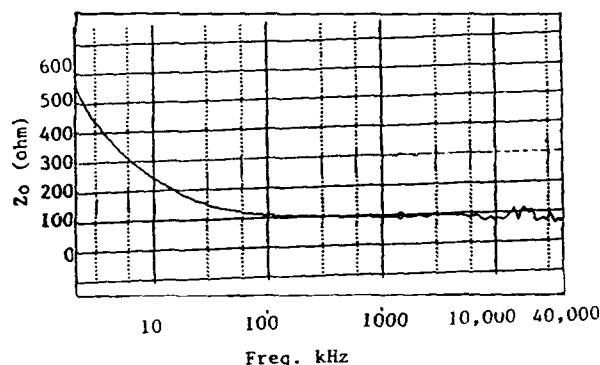


Fig. 4. Characteristic Impedance ( $Z_0$ ) vs. Frequency

Sample: 4/24 ECTFE/ECTFE

$Z_0$  vs. Freq. No. 3 T- 70°F

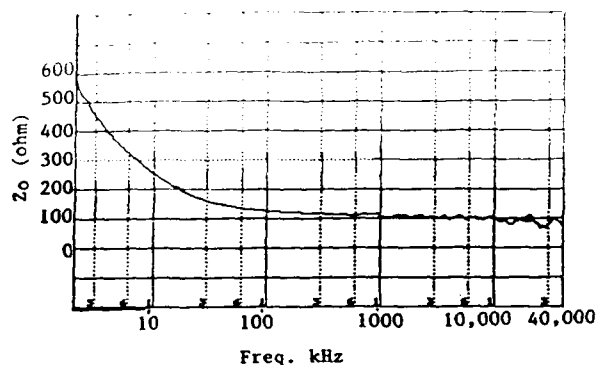
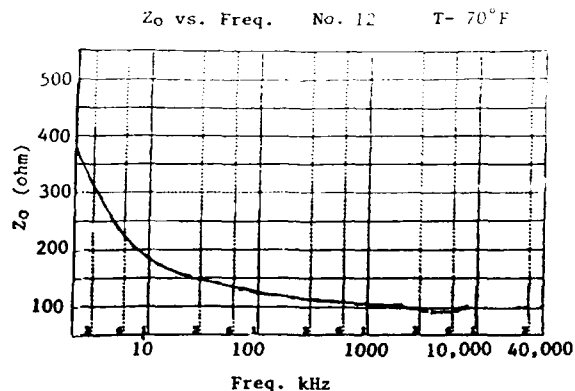
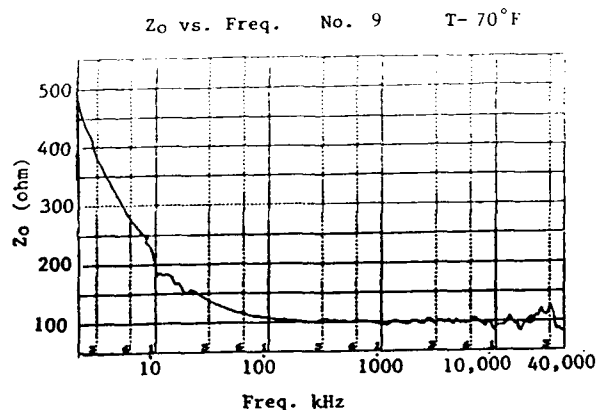
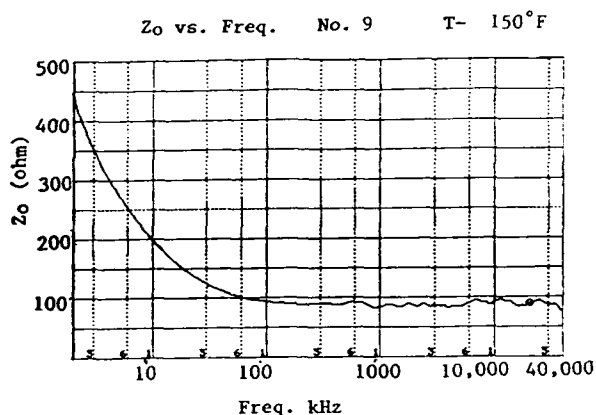
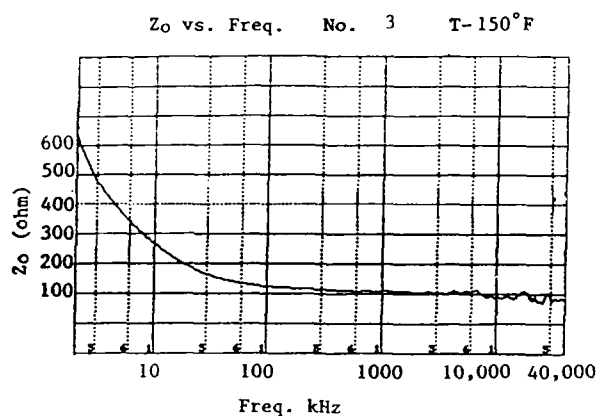
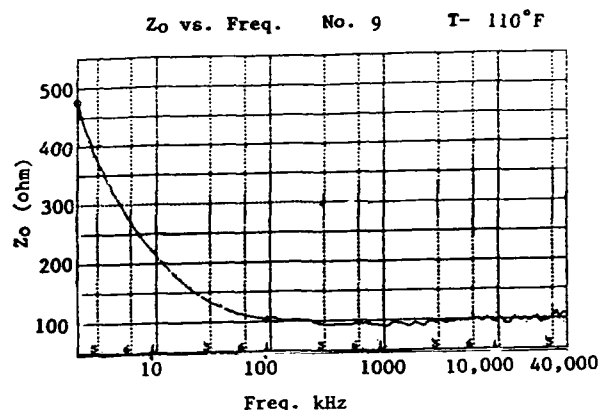
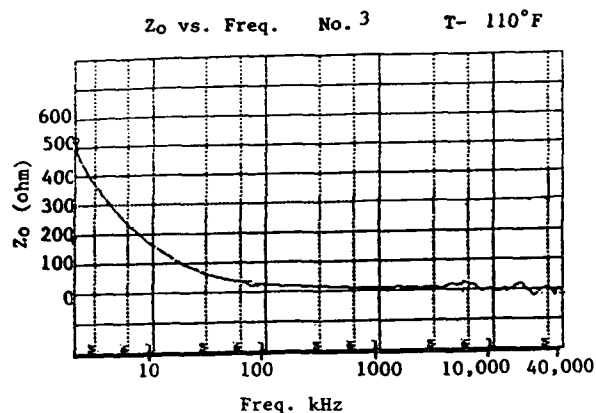


Fig. 5. Characteristic Impedance ( $Z_0$ ) vs. Temperature

Sample: 4/24 (FEP/ECTFE)





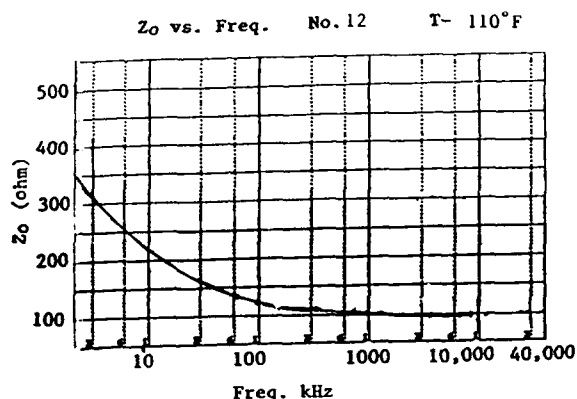


Fig. 12. Characteristic Impedance ( $Z_0$ ) vs. Temperature

Sample: 12/22 Shielded Pair (PE/PVC)

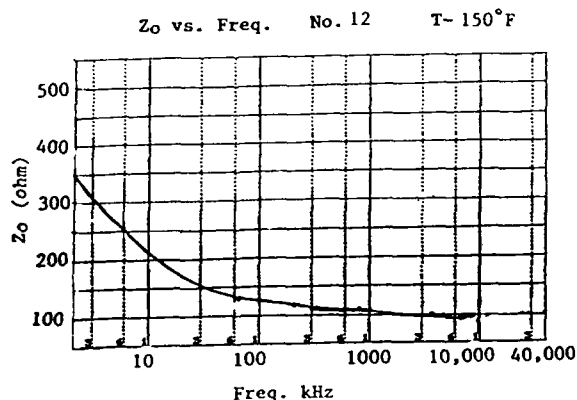


Fig. 13. Characteristic Impedance ( $Z_0$ ) vs. Temperature

Sample: 12/22 Shielded Pair (PE/PVC)

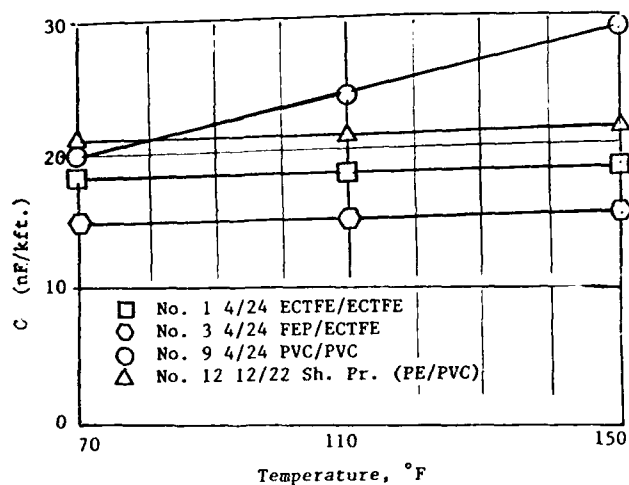


Fig. 14. Mutual Capacitance ( $C$ ) vs. Temperature

## 10. Discussion

The attenuation measurements on various wire samples up to 40 MHz at different temperatures, i.e., RT,  $110^\circ\text{F}$  and  $150^\circ\text{F}$  clearly indicate that some of the insulating materials produce a significant increase in attenuation due to high conductive (G) loss. The temperature coefficients of attenuation ( $T_c$ ) computed from the attenuation data can be used as a yardstick for selection of dielectric materials as insulation when high frequency and high temperature applications are warranted. Ideally, a temperature coefficient ( $T_c$ ) of 0.0010/dB/ $^\circ\text{F}$  maximum should be the target. Any values above the limit of 0.0010/dB/ $^\circ\text{F}$  should be avoided by making proper selection of insulating materials (see Figure 1).

Near end crosstalk of individually shielded pairs is significantly higher than the rest of the samples made without any shield by a factor of about two (see results in Table Nos. 8 thru 11). Because of high attenuation values at higher frequencies, the crosstalk values are not noticeably affected due to the temperature rise.

Characteristic impedance ( $Z_0$ ) values are reasonably constant for each sample at the three temperatures, RT,  $110^\circ$  and  $150^\circ\text{F}$  except the sample with the PVC insulation (see Table 12). At  $150^\circ\text{F}$ , PVC insulation produces about 11% lower  $Z_0$  value in comparison to the RT data. This result is expected due to the increase in mutual capacitance ( $C$ ) of the PVC insulated sample #9 over the RT value by 42% (see Table 1). Since  $Z_0$  is inversely proportional to  $\sqrt{C}$ , 42% increase in  $C$  produces about 19% decrease in  $Z_0$  value. The difference between the measured 11% against the theoretical 19% cannot be precisely explained.

The increase in  $C$  value at higher temperature, raises an interesting topic of the dielectric constant of the insulating material vs. temperature. In equation (9),  $C$  is found directly related to the dielectric constant of the media (consisting of PVC insulation and interstitial air space). Since the center to center spacing ( $S$ ) and the wire diameter ( $d$ ) are expected to remain reasonably constant, the increase in  $C$  can be attributed to the increase in the dielectric constant of the PVC insulation due to the temperature rise.

In summary, manufacturers, users and designers of the plenum wiring system should be aware of the limitations of some of the insulating materials intended for use in high frequency and high temperature applications.

TABLE 12

Sample No.	Average $Z_0$ @ 1 MHz vs. Temperature			$\Delta Z_0$ (%)	
	$Z_0$ @ 1 MHz $70^\circ\text{F}$	$Z_0$ @ 1 MHz $110^\circ\text{F}$	$Z_0$ @ 1 MHz $150^\circ\text{F}$	$70^\circ\text{F}-110^\circ\text{F}$	$70^\circ\text{F}-150^\circ\text{F}$
1 (ECTFE/ECTFE)	95.8	96.2	94.4	0.4	-1.5
3 (FEP/ECTFE)	110.0	109.6	108.5	-0.4	-1.4
9 (PVC/PVC)	96.5	90.7	86.1	-6.0	-10.8
12 (PE/PVC)	108.6	104.2	104.4	-4.1	-3.9

## 10. Empirical Relations for Attenuation versus Temperature

After analyzing the temperature coefficient ( $T_c$ ) data shown in Table 7, the following approximate empirical relations for attenuation vs. temperature ( $T$ ) have been developed.

### RT to 110°F

#### A. Insulation: FEP

64 kHz to 40 MHz Range:

$$\alpha_T \cong \alpha_{RT} [1 + 0.0011 (T - RT)] \quad (15)$$

#### B. Insulation: ECTFE

64 kHz to 8 MHz Range:

$$\alpha_T \cong \alpha_{RT} [1 + 0.0014 (T - RT)] \quad (16)$$

8 MHz to 40 MHz Range:

$$\alpha_T \cong \alpha_{RT} [1 + 0.0030 (T - RT)] \quad (17)$$

### 110°F - 150°F

#### A. Insulation: FEP

64 kHz to 40 MHz Range:

$$\alpha_T \cong \alpha_{RT} [1 + 0.0010 (T - RT)] \quad (18)$$

#### B. Insulation: ECTFE

64 kHz to 10 MHz Range:

$$\alpha_T \cong \alpha_{RT} [1 + 0.0008 (T - RT)] \quad (19)$$

10 MHz to 40 MHz Range:

$$\alpha_T \cong \alpha_{RT} [1 + 0.0018 (T - RT)] \quad (20)$$

For polyethylene, the temperature coefficient ( $T_c$ ) is well established within wide frequency and wide temperature range. This value is 0.0010/dB/°F.

Ideally, the temperature coefficient of attenuation ( $T_c$ ) of the plenum wires should be 0.0010/dB/°F. From this standpoint, FEP insulation meets the above expectation in the temperature range of RT to 150°F, and the frequency range of 64 kHz to 40 MHz, the maximum limits of the current measurements.

For PVC, ( $T_c$ ) values are ever increasing with the increase in frequency and no attempt has been made to develop empirical relations. In simple language, PVC insulated cables should be avoided in applications where high frequency signals and higher than room temperature environments are expected.

While not as poor a choice, ECTFE insulation may also create some problems in the higher frequency band (see Figure 1 and Table 7).

## 11. Acknowledgement

The author would like to thank Mr. A. J. Gambardella for his help in measuring the transmission parameters of the plenum wires and Messrs. E. P. Hjorth and M. A. Schwartz in reviewing the manuscript and offering valuable suggestions.

## References

1. D. Greenfield, "FDDI - It's Not Just for Fiber Anymore", Data Communications, September 1990.
2. C. Medford, "Firms Offer FDDI Over Twisted-Pair", MIS Week, June 1990.

3. E. J. Murphy and S. O. Morgan, "The Dielectric Properties of Insulating Materials," Bell System Technical Journal, Vol. 16, October 1937, pp 493-512.
4. Willis Jackson, "The Insulation of Electrical Equipment," pp 46.
5. G. S. Eager, Jr., L. Jachimowicz, I. Kolodny, D. E. Robinson, "Transmission Properties of Polyethylene Insulated Telephone Cables at Voice and Carrier Frequencies," Communications and Electronics, published by American Institute of Electrical Engineers, November 1959.
6. ANSI-ICEA S-84-608-1988 Standard for "Telecommunications Cable, Filled, Polyolefin Insulated, Copper Conductor Technical Requirements", June 1989.
7. L. M. Hore and V. Thiraisamy, "High Speed Transmission Through Twisted Pair Wire," Thirty-Seventh International Wire and Cable Symposium, 1988.
8. "Transmission Systems for Communications," 5th Edition, Published by Bell Telephone Laboratories, 1982.
9. H. W. Friesen, "An Improved Characteristic Impedance Measurement Technique," Thirty-Ninth International Wire and Cable Symposium, 1990.



Lal M. Hore  
Bellcore  
445 South St.,  
Morristown,  
NJ 07962

Lal Hore is responsible for the preparation of Bellcore's Technical Requirements for Outside Plant Cables and the development of high speed transmission requirements for wire products. After receiving a M.Sc. Tech. degree in Applied Physics from the University of Calcutta and a Dr. Tech. degree from the Technical University of Budapest in Electrical Engineering, he joined Bell Northern Research in 1970 to design and develop communications cables. In 1972, Lal moved to General Cable Company where he worked as a manager in the Communications Cable Section and next as a Staff Project Manager in the Applications Engineering Section until 1987 when he joined Bellcore.

Dr. Hore has authored numerous technical papers on dielectric materials and telecommunications wire and cable and holds a number of patents on telecommunications cables.

# NEW EXTRUSION MATERIALS FOR HIGHLY EXPANDED INSULATIONS FOR COAXIAL CABLES

Yukio Morita    Nobuyoshi Matsuda    Kaneharu Suga    Takuma Takai

Mitsubishi Cable Industries, Ltd.  
Itami, Japan

## ABSTRACT

Highly expanded insulation materials for coaxial cables are composed of base resin, nucleating agent and blowing agent. Development of new materials had been necessary to solve problems arising from productivity of cables, quality of insulation and world environment. Mechanical strength, dissipation factor at high frequency and foaming extrusion processability of various materials were evaluated, and it was found that followings are suitable for new substitute materials; polypropylene as a better base resin than the conventional high density polyethylene, boron nitride as an nucleating agent, and HCFC22 as a blowing agent owing to environmental compatibility and good processability.

## 1. INTRODUCTION

In accordance with a growing demand for coaxial cables with highly expanded insulation, high productivity and product quality improvement, in particular, higher mechanical strength and lower electrical loss of insulation, have become necessary. It has also been required to find a new blowing agent to replace chlorofluorocarbons (CFC12, CFC114), because it causes environmental pollution such as ozone depletion.

Problems of conventional materials and relating material properties are summarized in Table 1. To solve these problems, we have conducted R & D on the development of a new base resin, nucleating agent and blowing agent as improved materials for expanded insulation.

## 2. EXPERIMENTAL

### 2.1. Materials

#### 2.1.1. Nucleating Agent

Instead of azodicarbonamide (ADCA) which produces nucleating gas for physical foaming extrusion process by chemical decomposition, low polarity and finely divided powder of inorganic compounds such as aluminum oxide, magnesium oxide, zirconium oxide and boron nitride were used as new nucleating agents. These nucleating agents were added to base resins in a varied amounts.

#### 2.1.2. Base Resin

High density polyethylene (HDPE) and low density polyethylene (LDPE) were the conventional base resins. For the experiment, polypropylene copolymer (PP) which was expected to yield high mechanical strength, low dissipation factor at high frequency<sup>1</sup> and good foaming extrusion processability<sup>2</sup> was used as an alternative base resin. Properties of base resins are compared in Table 2.

#### 2.1.3. Blowing Agent

Chlorofluorocarbons (CFC12, CFC114) used as conventional blowing agents are now undesirable for industrial use, because they cause environmental pollution such as ozone depletion. Four hydrochlorofluorocarbons (HCFC22, HCFC123, HCFC141b, HCFC142b) which have low ozone depletion potential ratings and hydrofluorocarbon (HFC134a) which has zero ozone depletion potential were used as alternative blowing agents. These blowing agents were added to molten resin (mixture of the base resin and the nucleating agent) from a blowing agent inlet formed separately in an extruder. Properties of the blowing agents are shown in Table 3.

## 2.2. Materials Screening Tests

### 2.2.1. Dissipation Factor

It is very difficult to evaluate dissipation factor ( $\tan \delta$ ) of a base resin and a nucleating agent at high frequency by sheet test. Therefore, coaxial cable method was used. A Base resin or a mixture of a base resin and a nucleating agent was supplied in a 30-mm diameter extruder and extruded on a 0.8-mm diameter annealed copper wire to form insulated wire having a insulating layer 5-mm in outer diameter. Then, copper wire braid and PVC sheath were applied to the outside of insulating layer. Further, high frequency of 1.0 GHz was applied on the coaxial cable at room temperature and  $\tan \delta$  was calculated from damping attenuation.

### 2.2.2. Mechanical Strength

Mechanical strength of a base resin was evaluated by flexural modulus according to ASTM D790.

### 2.2.3. Foaming Extrusion Processability

A mixture of a base resin and a nucleating agent was feeded into a 30-mm diameter extruder and foam extruded on a 1.2-mm diameter annealed copper wire while adding blowing agent from a blowing agent inlet formed separately in the extruder, to produce insulated wire having foamed insulating layer 10-mm in outer diameter. Void fraction (occupied fraction of foams) varied greatly depending upon the injected blowing agent. After foaming extrusion, maximum void fraction and foam structure of foamed insulating layer were evaluated.

## 2.3. Manufacturing a CATV Cable Using New Materials

Standard size CATV cable with about 80-% void fraction was manufactured by a coaxial cable extrusion line with highly expanded insulation using new materials. Then, electrical and mechanical properties of cable were evaluated. The extrusion line is shown in Fig. 1.

## 3. RESULTS AND DISCUSSIONS

### 3.1. Materials Screening Tests

#### 3.1.1. Nucleating Agent

Conventional 4,4'-oxybis(benzene-sulfonylhydrazide) (OBSh) and ADCA are relatively good nucleating agents owing to excellent foaming extrusion processability, but for OBSh drying of insulation is necessary to remove moisture formed by chemical decomposition reaction. ADCA has bad electrical properties with high  $\tan \delta$  because its decomposition products are polar molecules. In order to improve productivity by eliminating moisture-drying process and product quality by reducing electrical loss, dissipation factors and foaming extrusion processabilities of nucleating agents were evaluated first.

Nucleating agents were added to high density polyethylene in varied amounts and  $\tan \delta$  of mixtures at 1.0 GHz were calculated from damping attenuation by coaxial cable method. The results are shown in Table 4. There were almost no increase in  $\tan \delta$  caused by increased mixing amounts of boron nitride, zirconium oxide and magnesium oxide fine powders, while  $\tan \delta$  increased along with increased mixing amounts of aluminum oxide and ADCA. Therefore boron nitride, zirconium oxide and magnesium oxide have satisfactory electrical insulation property. Foaming extrusion processabilities of mixtures of nucleating agents and high density polyethylene were also evaluated. In this experiment, HCFC22 was used as a blowing agent and the results are shown in Table 5. It is noted that foamed insulating layers had uniform, fine structures and high void fractions when boron nitride and ADCA were used. Foam structures were giant, when zirconium oxide and magnesium oxide were used.

These results suggest that boron nitride having a good electrical property (low  $\tan \delta$ ) and a good foaming extrusion processability is an excellent nucleating agent. It is possible to omit dry treatment of foamed insulating layer and improve electrical loss of insulation.

#### 3.1.2. Base Resin

It is very important to decrease electrical loss and to increase mechanical strength of expanded insula-

tion. Therefore, dissipation factor, flexural modulus and foaming extrusion processability were evaluated.

Dissipation factors of the conventional high density polyethylene and new polypropylene at 1.0 GHz were calculated from damping attenuation by coaxial cable method. The results are shown in Table 6. Dissipation factor of new polypropylene was lower than that of polyethylene, as had been already reported<sup>1</sup>.

Flexural moduli of high density polyethylene, mixture of high density polyethylene and low density polyethylene, low density polyethylene, and polypropylene were determined. The results are shown in Table 7. Flexural modulus of polypropylene was higher than that of the conventional polyethylene, indicating that an effect of increased compressive strength of foamed insulating layer can be obtained.

The conventional high density polyethylene and novel polypropylene were compared in foaming extrusion processability test. In this test, boron nitride which has good electrical property and foaming extrusion processability was used as a nucleating agent, and HCFC22 was used as a blowing agent. The results were shown in Table 8. Void fraction of polypropylene foamed insulating layer was higher than that of polyethylene foamed insulating layer. Furthermore foamed insulating layer had uniform and fine structure when polypropylene was used.

These results show polypropylene has lower dissipation factor, higher mechanical strength and better foaming extrusion processability than the conventional high density polyethylene. By using polypropylene as base resin, highly expanded coaxial cables with product quality improvement, in particular, higher mechanical strength and lower electrical loss of insulation can be obtained.

### 3.1.3. Blowing Agent

Chlorofluorocarbons (CFC12, CFC114) were widely regarded as the preferred blowing agents for the manufacture of highly expanded insulations for coaxial cables. The success of chlorofluorocarbons as blowing agents is due to their unique properties such as adequate solubility in the molten polyethylene resin, appropriate volatility,

low order of toxicity and nonflammability. Recent concern over environmental issues including ozone depletion and greenhouse effect has focused attention on the use of large quantities of chlorofluorocarbons<sup>3</sup>.

By using boron nitride as a nucleating agent and polypropylene as a base resin, several alternative compounds were evaluated as replacements for CFC12 and CFC114. The results are listed in Table 9. Void fraction of insulating layer when HCFC22 was used was as high as that of insulating layer when the conventional CFC12 or CFC114 was used. Furthermore foamed insulating layer had uniform and fine structure when HCFC22 was used.

HCFC22 has also such advantages as low ozone depletion potential ratings, low greenhouse potential ratings, nonflammability, cost-effectiveness due to its lower molecular weight (HCFC22: 87, CFC12:121, CFC114:171) and commercial availability. Therefore, HCFC22 was selected as the most favorable blowing agent.

### 3.2. Manufacturing a CATV Cable Using New Materials

It is important to apply laboratory test results to actual commercial cable manufacturing, by using new materials.

Polypropylene, boron nitride and HCFC22 were selected as base resin, nucleating agent and blowing agent respectively, according to the materials screening tests results. As polypropylene does not have good oxidative stability especially in the presence of copper, copper inhibitor and antioxidant were added.

A standard size 8C CATV cable with about 80% in void fraction, 2.04-mm in inner conductor diameter and 9.55-mm in outer conductor diameter were manufactured without moisture-drying process of insulation.

The cross section of foamed insulation is shown in Fig. 2. It had uniform and fine structure.

Cable structures, electrical properties and mechanical properties of the cable are shown in Table 10. These properties of the cable were excellent and satisfied the specification of JIS C3503 (CATV Coaxial Cables).

Frequency characteristics of attenuation constants and structural return loss are shown in Fig. 3 and Fig. 4. Attenuation constants are equal to those of cables manufactured by using the conventional materials with moisture-drying process of insulations. The structural return loss charts show excellent properties.

Comparison between the foamed insulation made by the conventional materials and that made by new materials is shown in Table 11. Hardness (mechanical strength) of the foamed insulation prepared by new materials is larger than that of the insulation by the conventional materials. Further, oxidative stability of foamed insulation used new materials is excellent.

These results show that high quality coaxial cables with high mechanical strength and low electrical loss can be produced under high productivity without environmental destruction by use of alternative blowing agent.

#### 4. CONCLUSIONS

New extrusion materials for highly expanded insulations for coaxial cables were developed. Polypropylene, boron nitride and HCFC22 proved to be the best base resin, nucleating agent and blowing agent, respectively. By using these new materials, high quality coaxial cables can be produced under high productivity without environmental destruction.

#### 5. ACKNOWLEDGMENTS

The authors wish to thank Mr. T. Kaide, Y. Fujiwara and T. Yoshida for their many enlightening discussions and helpful hints. The authors also wish to thank Ms. M. Yamagishi and Mr. S. Takeshita for their invaluable assistance in the developmental work.

#### 6. REFERENCES

- 1) D.H. Buerkle et al., "Electrical Properties of polypropylene homo- and copolymers at high frequencies", 26th International Wire and Cable Symposium, p110-117 (1977).
- 2) M.B. Bradley and H.M. Phillips, "Novel Polypropylenes for Foaming on Conventional Equipment", *Plastics Engineering*, P82-85, March (1991).
- 3) P.S. Zurer, "Studies on Ozone Destruction Expand Beyond Antarctic", *C & EN*, p18-25, May 30 (1988).

Table 1 Problems of Materials for Highly Expanded Insulations for Coaxial Cables

Material	Conventional material	Problem	Property related to material
Base resin	•HDPE •HDPE/LDPE	•Lowering electrical loss •Increasing mechanical strength of insulation	• $\tan \delta$ •Flexural modulus •Foaming extrusion processability
Nucleating agent	•OBSh,ADCA(Organic) •Talc(Inorganic)	•Lowering electrical loss •Productivity improvement	• $\tan \delta$ •Foaming extrusion processability
Blowing agent	•CFC12 •CFC114	•Environmental pollution	•Ozone depletion potential rating •Foaming extrusion processability

Table 2 Properties of Base Resins

Base resin	High density polyethylene	Low density polyethylene	Polypropylene
Density (g/cm <sup>3</sup> )	0.945	0.920	0.90
Melt flow rate (g/10min.)	0.9	2.0	1.8

Table 3 Properties of Blowing Agents

	Blowing agent	MW (-)	BP (°C)	Ozone depl. pot. (-)	Flammable limit in air (% by Vol.)	Mfg. process	Est. cost
Possible alternative	HCFC22	87	-41	0.05	No	Yes	1×
	HCFC123	153	28	0.02	No	Yes	2×
	HFC134a	102	-27	0.00	No	No	5×
	HCFC141b	117	32	0.10	6.4~15.1	No	2×
	HCFC142b	101	-9	0.06	6.7~14.9	Yes	2×
Conventional compound	CFC12	121	-30	1.00	No	Yes	1×
	CFC114	171	4	1.00	No	Yes	1×



Table 4 Dissipation Factors of Mixtures of High Density Polyethylene and Nucleating Agents by Coaxial Cable Method

Nucleating agent	Nucleating agent (%)	$\tan \delta$ at 1.0GHz(-)
BN	0.5	$1.6 \times 10^{-4}$
	1.0	$1.6 \times 10^{-4}$
	2.0	$1.5 \times 10^{-4}$
ZrO <sub>2</sub>	0.5	$1.6 \times 10^{-4}$
	1.0	$1.7 \times 10^{-4}$
	2.0	$1.6 \times 10^{-4}$
MgO	0.5	$1.6 \times 10^{-4}$
	1.0	$1.5 \times 10^{-4}$
	2.0	$1.5 \times 10^{-4}$
Al <sub>2</sub> O <sub>3</sub>	0.5	$1.6 \times 10^{-4}$
	1.0	$1.9 \times 10^{-4}$
	2.0	$2.3 \times 10^{-4}$
ADCA	0.5	$2.1 \times 10^{-4}$
	1.0	$2.5 \times 10^{-4}$
	2.0	$3.6 \times 10^{-4}$
None	0.0	$1.6 \times 10^{-4}$

Table 5 Foam Extrusion Results of Nucleating Agents (Base Resin: High Density Polyethylene, Blowing Agent: HCFC22)

Nucleating agent (%)	Foam extrusion result	
	Void fraction (%)	Foam structure
BN 1.0	80	Uniform and fine Giant
ZrO <sub>2</sub> 1.0	70	
MgO 1.0	73	
ADCA 0.5	80	Uniform and fine

Table 6 Dissipation Factors of Base Resins Measured by Coaxial Cable Method

Base resin	$\tan \delta$ at 1.0GHz(-)
High density polyethylene	$1.6 \times 10^{-4}$
Polypropylene	$1.1 \times 10^{-4}$

Table 7 Flexural Moduli of Base Resins

Base resin	Flexural modulus (kg/mm <sup>2</sup> )
HDPE	61
HDPE/LDPE=70/30	44
HDPE/LDPE=50/50	36
HDPE/LDPE=30/70	29
LDPE	15
Polypropylene	76

Table 8 Foam Extrusion Results of Base Resins (Nucleating Agent: Boron Nitride 1.0 %, Blowing Agent: HCFC22)

Base resin	Foam extrusion result	
	Void fraction (%)	Foam structure
High density polyethylene	80	Uniform and fine
Polypropylene	86	

Table 9 Foam Extrusion Results of  
Blowing Agent (Nucleating  
Agent: Boron Nitride 1.0 %,  
Base Resin: Polypropylene)

Blowing agent	Foam extrusion result	
	Void fraction (%)	Foam structure
HCFC22	86	Uniform and fine
HCFC123	79	Uniform and fine
HFC134a	73	Uniform and fine
HCFC141b	77	Uniform and fine
HCFC142b	87	Uniform and fine
CFC12	83	Uniform and fine
CFC114	85	Uniform and fine

Table 11 Comparison of Foamed Insulation  
Properties

		New	Conven.
Material used	Base resin	PP	HDPE
	Nucleating agent	BN 1.0 %	ADCA 0.5 %
	Blowing agent	HCFC22	CFC114
Void fraction (%)		80	81
Hardness (Shore D)		70	62
DSC OIP at 220 °C (min.)		16	11
Aging test at 120 °C, 100 days		No cracks	No cracks

Table 10 Properties of CATV Cable Manufactured by Using New Materials

		8C CATV cable	Specification of JIS C3503
Cable structure	Diameter of inner conductor (mm)	2.04	2.1±0.08
	Diameter of core (mm)	8.2	8.5
	Diameter of outer conductor (mm)	9.6	9.5±0.3
	Diameter of PE jacket (mm)	11.7	11.9±0.6
Electrical property	Attenuation constant at 200 MHz (dB/Km)	45	under 52
	Capacitance (pF/m)	52	-
	Velocity of propagation (%)	88	-
	Characteristic impedance (Ω)	74	75±3
	Dielectric constant (-)	1.2	-
	Dissipation factor to frequency of 1.0GHz (-)	0.65×10 <sup>-4</sup> ~ 1.10×10 <sup>-4</sup>	-
Mechanical property	Pull-out strength		
	Outer conductor to insulation (kgf/m)	190	over 20
	Inner conductor to insulation (kgf/m)	110	-
	Bending test [Note]	No cracks	-

[Note] Bending diameter: 200mm, Bending angle: ±180°/cycle, Number of bending: 3 cycles

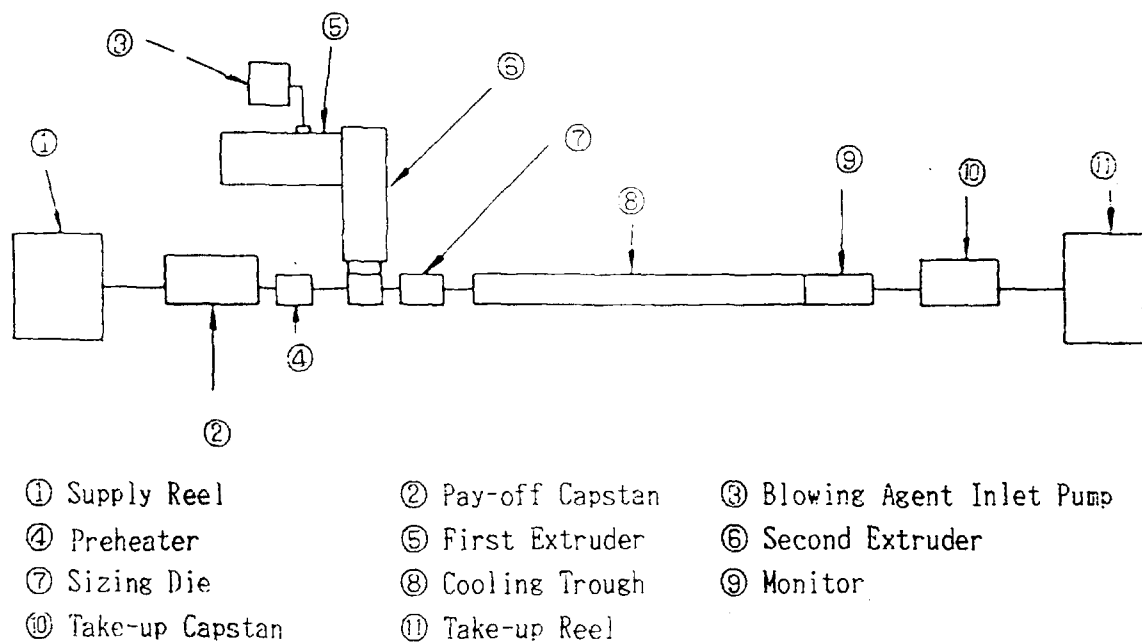


Fig. 1 Extrusion Line for Coaxial Cable Core with Highly Expanded Insulation

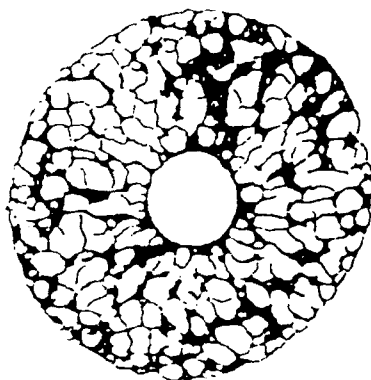


Fig. 2 Cross Section of Highly Expanded Insulation Using New Materials

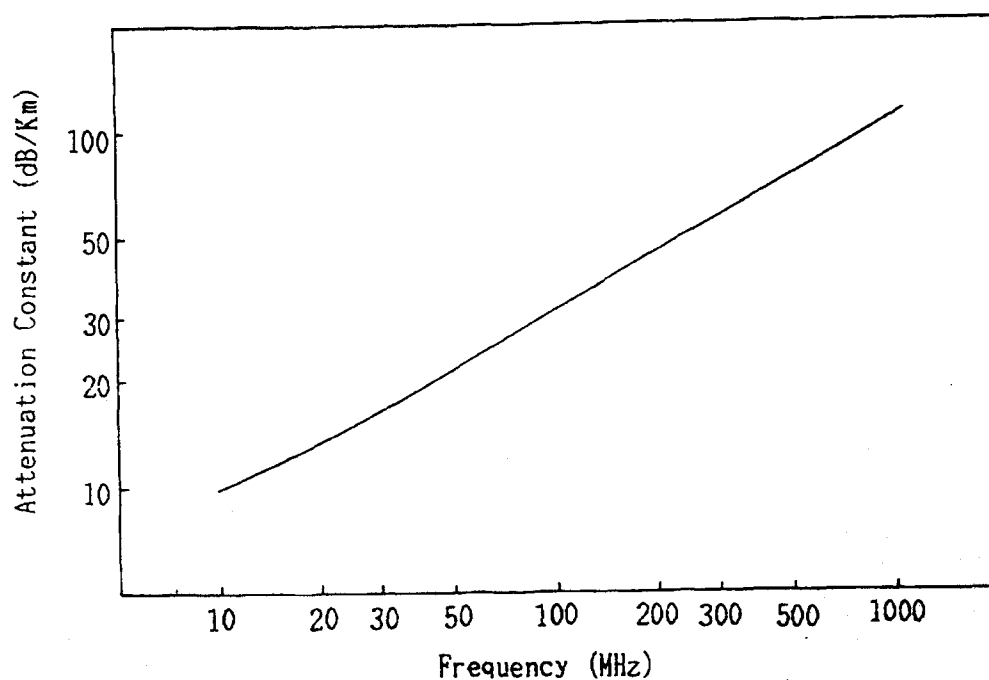


Fig. 3 Attenuation Constant vs Frequency Characteristics of CATV Cable

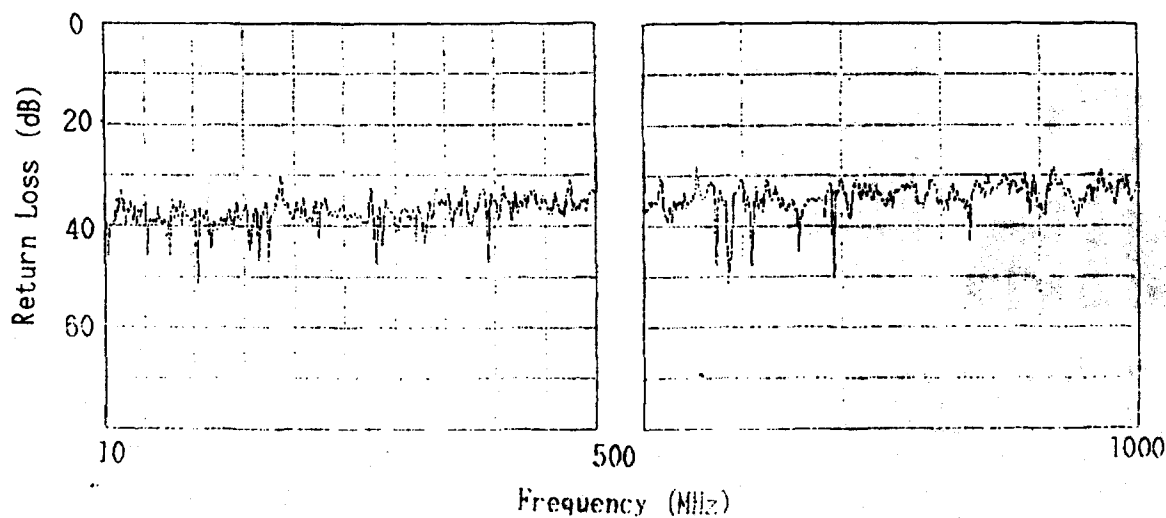


Fig. 4 Structural Return Loss Characteristics of CATV Cable



Yukio Morita

Mitsubishi Cable  
Industries, Ltd.  
4-3, Ikejiri  
Itami-City  
Hyogo-Pref  
Japan

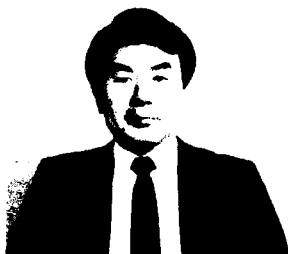
Mr. Y. Morita graduated from Osaka University majoring in applied chemistry in 1973. Then he immediately joined Mitsubishi Cable Industries, Ltd. and has been engaging in the research and development of plastic materials for communication cables. Mr. Morita is now senior engineer of Materials Research Dept.



Kaneharu Suga

Mitsubishi Cable  
Industries, Ltd.  
4-3, Ikejiri  
Itami-City  
Hyogo-Pref  
Japan

Mr. K. Suga graduated from Amagasaki Industrial High School majoring in TV technology in 1967. Then he immediately joined Mitsubishi Cable Industries, Ltd. and engaged in the quality control of high frequency communication cables. Mr. Suga is now a member of Itami Works.



Nobuyoshi Matsuda

Mitsubishi Cable  
Industries, Ltd.  
4-3, Ikejiri  
Itami-City  
Hyogo-Pref  
Japan

Mr. N. Matsuda graduated from Sasebo Industrial High School majoring in electrical engineering in 1961. Then he immediately joined Mitsubishi Cable Industries, Ltd. and has been engaging in test plant and communication cable production. Mr. Matsuda is now a manager of Itami Works.



Takuma Takai

Mitsubishi Cable  
Industries, Ltd.  
8, Nishinocho  
Higashimukaijima  
Amagasaki-City  
Hyogo-Pref  
Japan

Mr. T. Takai graduated from Waseda University majoring in mechanical engineering in 1971. Then he immediately joined Mitsubishi Cable Industries, Ltd. and engaged in production engineering of communication cables. Mr. Takai is now a manager of Mechanical Equipment & Engineering Center.

## High Speed Transmission Coaxial Cable by A New Polyolefin Material

Toshiya Tanaka<sup>1</sup>, Shoji Yamamoto<sup>1</sup>, Makoto Kado<sup>2</sup> and Ryoichi Shimizu<sup>2</sup>

1. The Furukawa Electric Co., Ltd.

2. Ube Industries Ltd.

CHIBA, JAPAN

### Summary

Recently, miniature coaxial multi-flat cables with highly expanded insulation are required to achieve the more short operation time and to get more intensification in density of computer systems. So we have developed a new material to get highly expanded thin insulation wire. By studying of relationship between rheological parameters and expansive properties of polymer, we have found that melt tension and ultimate draw rate influence greatly on the expansive properties. If both parameters are suitable, the polymer have a good expansive properties in spite of the thin thickness of insulation. Also examining the mechanical and electrical properties of polymer, we have developed a new material. The multi-flat cable with this material has 87% velocity of propagation and accurate pitches between conductors.

### 1. Introduction

With amounts of signal and speed of operation time in signal processors such as large computers, magnetic core storages and communication equipment increasing, there is also a growing demand for finer and multi - core type cables possessing high speed transmission characteristics, which are wired inside those facilities. In the meantime, automatic terminal processors have begun to be adopted as a way to process cable terminals in view of reliability on high density multi terminal connectors and also from viewpoint of economy. For that reason, every parts of a cable, including its pitch between signal lines requires high dimensional accuracy. To meet such requirements, Rectangular Jacket typed High Speed Cable has been developed.<sup>1</sup> Since this type of cable has narrow line - to - line pitch of 1.27mm and its transmission delay time is as high as 3.80ns/m, over 70% highly expanded insulation is needed for a cable with less than 0.3mm insulation thickness. Such a highly expanded insulation with thin thickness is very difficult to be obtained from conventional polyolefin (such as LDPE, HDPE or PP, for instance), and at the same time, double layer simultaneous extrusion was required for getting it.<sup>2</sup>

The Furukawa Electric Company and Ube Industries, Ltd. jointly developed new polyolefin

material being able to make highly expanded insulation with thin thickness even in single layer insulation, which has conventionally been considered to be difficult to get. The material also has favorable expansion characteristics to a double layers insulation and is optimum for afore - mentioned cables.

In the development of the material, it was found out, as a result of a study made on the relationship between expansion characteristics of the material in thin thickness and rheological parameters, that its expansion characteristics are greatly influenced by melt tension and ultimate draw rate of the material, both of which were unknown characteristics by that time and that the material possessing suitable values of above characteristics shows favorable expansion characteristics in spite of thin thickness.

This report describe the result of our study on those characteristics and a small coaxial multi - flat cable, in which the material is used.

### 2. Development of Material for Expansion

Conventionally, various kinds of material have been used for insulations of expanded insulation cables, depending on size of cable, expansion ratio of insulation and circumstances, under which it is used. The kinds of material are roughly divided into two categories, i.e. fluorine polymer and polyolefin.

Among polyolefins, LDPE, HDPE or PP, all of which possess excellent electric property is used alone or after they are blended. Among these substances, a blend of LDPE and HDPE has been used as material for high expansion.<sup>3</sup> Using the material for high expansion, it is possible to get 70% highly expanded insulation, when its thickness is large, that its outer diameter is over 1.15mm. However it is impossible to get over 70% high expansion and smooth extruded surface, when insulation thickness is thin, that is less than 1mm outer diameter insulation, which is used for small coaxial multi - flat cables. That means that the material is suitable for getting expansion, which has relatively large cell whereas it is inadequate for getting expansion having thin thickness, where small cells are densely contained.

Rheological property of material is of importance for expansion. It is important to obtain a proper condition by taking balance between pressure of expanding gas and melt elasticity of polymer in a cell, in order to obtain a wire with high expansion insulation with smooth surface. Up to present, much studies have been made on the relationship between melt elasticity of polymer and its expansion characteristics. Those studies have focused on MI and swell ratio and have discussed the relationship between those terms and expansion characteristics. However, as the subject of those studies is large thickness insulation and large cell size, it is difficult to directly apply the result of studies to thin thickness type. In order to overcome the difficulty, we made a detailed study on the relationship between rheological property of material and its expansion characteristics. The result could prove their relationship to some extents and found a rheological area, in which high expansion can be obtained even at thin thickness.

Based on the results of the study, new polyolefin material was development by taking account of electrical and mechanical properties, which need for insulation.

## 2.1 Evaluation of Characteristics of Material

Various terms have been known as indicators of rheological property of material. For example, some of them are MI, swell ratio, melt viscosity and its dependence on temperature and shear rate, and melt tension.

Among those terms, our study focused on swell ratio, melt tension and ultimate draw rate, all of which are relatively easy to be measured, and our study was made on the relationship between them and expansion characteristics. Melt tension and ultimate draw rate were measured with a device shown in Fig. 1. Melt tension is specified as tension which is added to extruded polymer, when it is taken up by a bottom roller, and ultimate draw rate is specified as speed when the polymer is fracture. In addition to above study, a detailed study was made on rheological properties and morphology of typical specimens to investigate into which properties of the material allow to obtain high expansion, even in thin thickness.

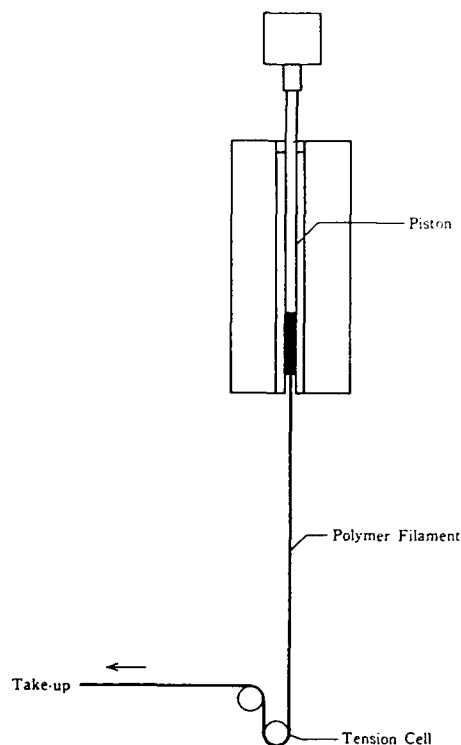


Fig. 1 Schematic Diagram of Apparatus

## 2.2 Evaluation of Expansion Characteristics

Expansion characteristics of material was evaluated by the expansion ratio and surface of expanded wire, which was obtained after it was actually processed by expansion extrusion. Used extruder was a single extruder with 25mm $\phi$  with 25 of L/D, and Freon gas, an inactive gas, was used as an expansion agent. A 0.16mm diameter conductor was covered with expanded insulation by using pressurized extrusion. The expanded insulation wire has outer diameter of 0.6mm (insulation thickness 0.22mm).

## 2.3 Characteristics of Material and Result of Extrusion

The kinds of material we used for our study are 7 kinds of polyolefin material, which can be extruded to get smooth surface.

Both Sample A and B are a blend of LDPE and HDPE and sample from C to G are polyolefin blends, which were newly prepared for studies. The polyolefin blends were prepared, because they might have possibility to show high expansion even in this thickness. Each kind of material is adjusted to possess different characteristics by changing kind of base material and blend ratio. Characteristics of material and obtained expansion ratio of extruded material are shown in Table 1. The results shown in Table 1 clearly indicate that high expansion of about 80% is obtainable, when polyolefin blend is used.

Table 1 Characteristics of Material and Result

Sample	Material	MI	Swell	Melt Tension	Ultimate Draw Ratio	Expansion Ratio
		g/min	%	g	m/min	%
A	LDPE+HDPE	0.35	85	6.6	34	60
B	LDPE+HDPE	4.10	57	1.2	170	58
C	Polyolefin Blend	2.10	76	2.9	105	78
D	Polyolefin Blend	2.00	87	4.1	64	80
E	Polyolefin Blend	2.00	86	2.9	159	79
F	Polyolefin Blend	1.20	85	3.3	164	74
G	Polyolefin Blend	1.40	88	1.6	313	50

## 2.4 Discussion about Melt Characteristics and Expansion Characteristics

### 1) Relationship with Swell Ratio

Fig. 2 shows the relationship between swell ratio and expansion ratio. As is clear by Fig. 2, no correlation is observed between swell ratio and expansion ratio, that is, Specimen A, D, E, F, and G all show their swell ratio of about 85%, whereas, their expansion ratio changes considerably in the range of between 50 and 80%. Contrary to conventional theory that swell ratio has correlation with expansion characteristic on large thickness type, no relationship was observed between them. A likely reason is that in large thickness type, cells grow larger in balance with melt elasticity and expansive gas pressure, in such case, relationship exist between swell ratio and elasticity whereas, such relationship does not exist in thin thickness type as those specimens used this time because this type needs to form a lot of minute cells.

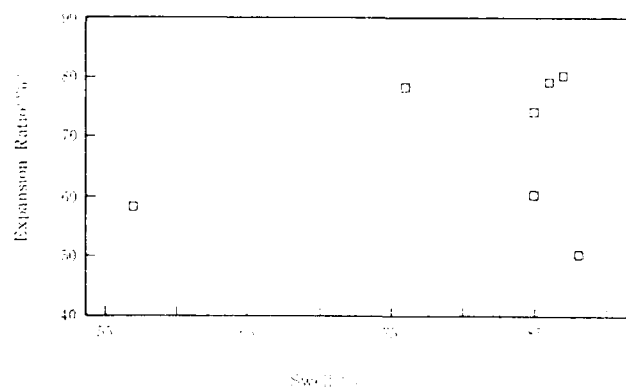


Fig. 2 Relationship between Swell and Expansion Ratio

### 2) Relationship with Melt Tension

Fig. 3 shows relationship between melt tension and expansion ratio. This figure shows that the area, where over 70% high expansion is obtainable, corresponds to the area of about 3 ~ 4 gr of melt tension. Material possessing such a range of melt tension has such melt elasticity that high expansion can be got even in thin thickness type, and it could be material, in which large quantity of expansion nucleus is generated and then they form a thin wall so that they do not make open cells after they grow and are assembled.

It is estimated that when value of melt tension of material is lower than that indicate by the area, the material's melt elasticity is too low to overcome pressure of expansion gas and because of it, expansion gas tends to go out of material easily. On the other hand, when value of melt tension of material is larger than that indicate by the area, the material's melt elasticity is too high for cells in polymer to overcome gas pressure and keep growing.

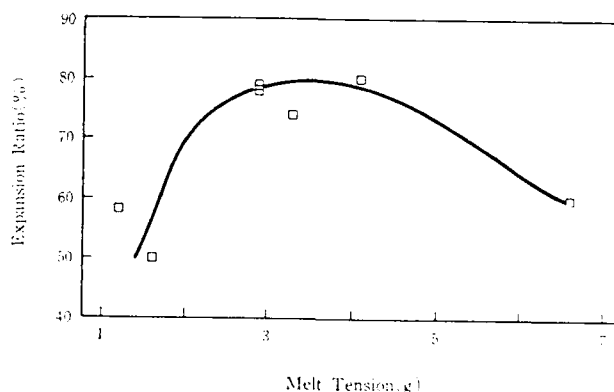


Fig. 3 Relationship between Melt Tension and Expansion Ratio



### 3) Relationship with Ultimate Draw Rate

Fig. 4 shows relationship between ultimate draw rate and expansion ratio. Although, the relationship is not clearer than that between melt tension and expansion ratio, it can be said that region of 50~200m/min is favorable.

Although it is difficult to discuss the effect of ultimate draw rate alone because there is negative correlation between melt tension and ultimate draw rate of specimens, which were used this time as shown in Fig. 5, above relationship suggests that ultimate draw rate is also one of indicators in selecting material.

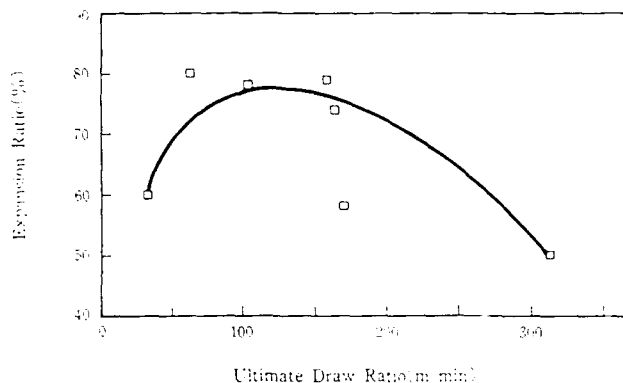


Fig. 4 Relationship between Ultimate Draw Ratio and Expansion Ratio

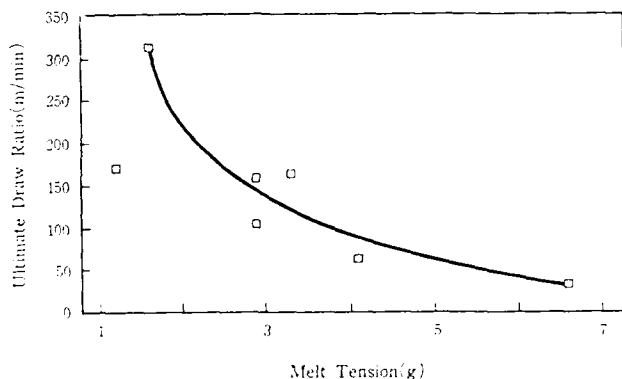


Fig. 5 Relationship between Ultimate Draw Ratio and Melt Tension

### 4) Study of Viscosity

Fig. 6 shows viscosity's dependence on shear rate of specimen A to D.

As this figure clearly proves, there exists proper viscosity region where high expansion is obtainable, and high expansion can not be got outside the region.

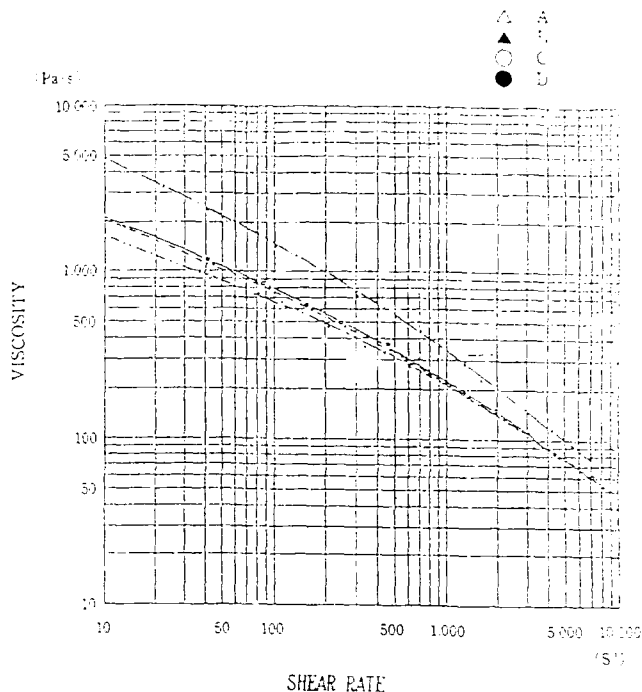


Fig. 6 Comparison of Viscosity vs. Shear Rate for Sample A,B,C and D

### 5) Study of Morphology

To study difference of each of samples that have good or bad expansive characteristics was observed under transmission electron microscope (TEM). As shown in Fig. 7, the structure of highly expanded specimen looks like small islands uniformly distributed in sea, while that of poorly expanded specimen looks like big islands which are formed by condensation of composition of small islands, that is, it can be understand that when composition of the islands is uniformly distributed in small form in the sea, the composition serves for high expansion, but when small islands coalesce into big islands, the composition of the island does not serve for expansion. Accordingly, it is important to make a study on the combination and mixing ratio of polyolefin so as to get finely distributed micro phase separation, when polyolefin blend is used.

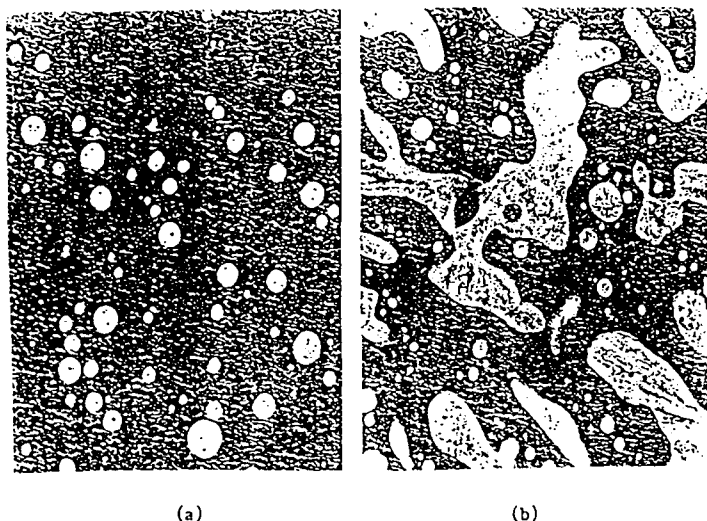


Fig. 7 TEM photograph of Polyolefin Blend  
(x15,000)  
(a) good expansive (b) bad expansive

## 2.5 Study of Electrical Property and Mechanical Property

Studies having been made so far has proved that over 75% highly expanded material such as C~E is obtainable. In order to select optimum one among these for a small coaxial multi - flat cable, attention was focused on their electrical and mechanical properties. Especially, a highlight was shot to their own dielectric constant (at unexpanded state), because low effective dielectric constant is needed for high speed signal transmission. Adding to such property, the material should be hard and be resistant to deformation, since it undergoes outer force, when insulation cables are made into a coaxial cable. Therefore, their tensile modulus was also studied as a part of their mechanical properties. Results are shown in Table 2. Material D is optimum for the purpose, as it has the lowest dielectric constant of 2.40 and the highest tensile modulus of 470 kgf/mm<sup>2</sup>.

Table 2 Comparison of Dielectric Constant and Tensile Modulus

Sample	Dielectric Constant	Tensile Modulus kgf/mm <sup>2</sup>
C	2.81	283
D	2.40	470
E	2.75	312

## 2.6 Developed Material and Its Property

Properties of Material D are shown in Table 3. The material allows to use gas and/or thermal decomposition type expansion agent. In every

case, some 80% expansion ratio can be obtained. The material can satisfy thermal resistivity of UL 80°C, when an adequate antioxidant is added to it. Fig. 8 shows a cross section of an expanded insulation cable, in which the material is used. The cable has possibility toward time delay of 3.60ns/m because it achieved effective dielectric constant of less than 1.20.

Table 3 Properties of New Polyolefin Material

Item	Unit	Value
Melt Index	g/10min	2.03
Density	g/cm <sup>3</sup>	0.921
Tensile Strength	kgf/mm <sup>2</sup>	1.78
Elongation	%	615
Brittleness Temperature	°C	-60<
Dielectric Constant		2.40
Dielectric Loss Tangent		3.40×10 <sup>-1</sup>
Volume Resistivity	Ωcm	4.1×10 <sup>10</sup>

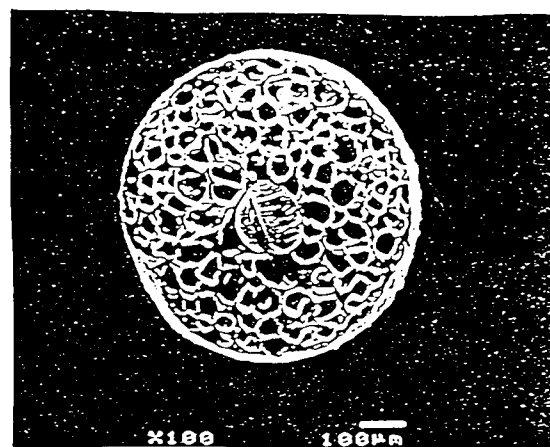


Fig. 8 Cross Section of Expanded Polyolefin Insulation

## 3. Small Coaxial Multi - Flat Cable

Small coaxial multi - flat cable will be introduced in the following, in which newly developed polyolefin D is used.

### 3.1 Structure

Miniature coaxial multi - flat cable for wiring peripheral equipment of computers has structure as shown in Fig. 9. An expanded insulation cable with skin layers is covered with a PVC jacket after it is loaded together with drain wire inside an aluminum - polyester laminated tape. Then, each of coaxial cores undergoes intermittent bonding by heat.

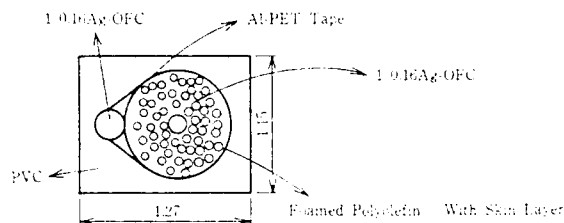


Fig. 9 Structure of Miniature Coaxial Cable

### 3.2 Insulation Wire

Material D, Polyolefin material for expansion, which was developed this time, is capable of being used in either one layer insulation or double layers insulation which has an unexpanded skin layer on its outside, and in both cases, it shows favorable expansion characteristics. A small coaxial multi - flat cable adopted a double layers insulation by taking account of mechanical properties and reliability of both of one and double layer insulation. The insulation cable is that of about 80% of expansion ratio, which has 0.70mm outer diameter with 0.16mm center conductor and its outer layer has 0.05mm skin layer. To manufacture the cable, one process was required in which a common head consisted of two extruders was used. Photograph of its cross section is shown in Fig. 10.



Fig. 10 Cross Section of Two Layers Insulation

### 3.3 Jacket and Bonding by Heat

In order to get precise pitches, bonding by heat is preferable. To hold characteristics'

change minimum level during process of bonding by heat, it was carried out at a relatively low temperature, and to meet the condition, a special PVC was developed, which can undergo bonding by heat at a relatively low temperature. Using it, a small coaxial multi - fiat cable was manufactured, which showed favorable assembling and high accuracy of its pitch length.

### 3.4 Properties of Small Coaxial Multi - Flat Cable

Properties of a typical small coaxial multi - flat cable are shown in Table 4. It possesses 1.27mm pitch between signal lines and a signal transmission velocity of 87% of light velocity.

Table 4 Typical Properties of Miniature Multi Flat Cable

	Item		Detail
	Center Conductor		Material Silver Coated Oxygen Free Copper Size 1.016mm
Structure	Insulation	Inner Layer	Material Irradiated Polyolefin Outer Diameter 0.6mm
		Outer Layer	Material Irradiated Polyolefin Thickness 0.05mm
		Drain Wire	Material Silver Coated Oxygen Free Copper Size 1.018mm
	Shield Tape		Material Al-PET Laminate Tape
	Sheath		Material PVC Size 1.27X1.13mm
Electrical Properties	Pitch between Conductor		1.27±0.05mm
	Average Pitch between Conductor		1.273mm
	Conductor Resistance of Center Conductor		863.0Ω/m
	Conductor Resistance of Drain Wire		318.0Ω/m
	Insulation Resistance		3248.0Ω/m
	Characteristics Impedance		79.5Ω
	Propagation Delay		3.80ns/m

### 4. Conclusion

New polyolefin material was developed for small coaxial multi - flat cable. In its development, the following subjects were found out.

1) At thin thickness type, melt tension and ultimate draw rate have of more importance than swell ratio. On the conditions of 3~4 gr melt tension and 50~200 m/min ultimate draw rate, the material shows high expansion even at thin thickness.

2) A small coaxial multi - flat cable of a double layers insulation core, to which the material was applied, possesses signal transmission velocity of 87% of light velocity and excellent accuracy of its pitch.

3) Dielectric constant of less than 1.2 could be obtained by one layer insulation cable, in which the material was used, and the material has possibility toward time delay of 3.6ns/m, which is desired for mainframes in the next generation.

#### REFERENCE

1. K. kadoya, A. Mori, T. Abe, K. Tanaka  
IWCS Proceedings, PP. 499 - 503, 1984.
2. F. Suzuki, T. Komura, A. Mori  
IWCS Proceedings, PP. 300 - 307, 1984.
3. K. Sakamoto, S. Yamamoto, T. Kato,  
K. Negishi, K. Akimoto  
IWCS Proceedings, PP. 483 - 491, 1987.



TOSHIYA TANAKA  
The Furukawa Electric  
Co., Ltd.  
6-Yawata-kaigandori,  
Ichihara, Chiba Japan

Mr. Tanaka graduated from Tokyo Institute of Technology with a master of engineering majoring in organic and polymeric materials in 1987. Then he joined The Furukawa Electric Co., Ltd. and has been engaged in research and development of foamed plastic insulation.

He is now a member of Chiba Research Laboratories of Research and Development Division.



SHOJI YAMAMOTO  
The Furukawa Electric  
Co., Ltd.  
6-Yawata-kaigandori,  
Ichihara, Chiba Japan

Mr. Yamamoto graduated from Hakodate Technical College majoring in industrial chemistry in 1972. Then he joined The Furukawa Electric Co., Ltd. and development of flame retardent plastics and manufacturing method for foamed plastic insulation.

He is now a senior engineer of Chiba Research Laboratories of Research and Development Division.



MAKOTO KADO  
Ube Industries Ltd.  
8-1-Goi-minamikaigan,  
Ichihara, Chiba Japan

Mr. Kado graduated from Kannabe High School majoring in foods technical in 1970. Then he joined Ube Industries Ltd.

He is now a member of Chiba Technical Section Polyethylene Group of Research and Development Dept.



RYOICHI SHIMIZU  
Ube Industries Ltd.  
8-1-Goi-minamikaigan,  
Ichihara, Chiba Japan

Mr. Shimizu graduated from Miura High School majoring in electrical engineering in 1965. Then he joined Ube Industries Ltd.

He is now a assistant manager of Chiba Technical Section Polyethylene Group of Research and Development Dept.

# METHODS OF DETERMINING THERMAL STABILITY OF POLYOLEFIN INSULATIONS

E. D. Nelson

AT&T Bell Laboratories, Norcross, GA 30071

## Abstract

Thermal stability of polyolefin (DEPIC) insulation is determined using pedestal tests. Pedestal tests are used to physically measure cracking intervals of wire insulation at 90°C. Time/temperature profiles are shown for several pedestal tests. These profiles emphasize the uniformity and accuracy of the temperature control. Results of pedestal tests on two novel DEPIC wire insulations are shown. Both insulations easily pass the 260 day/90°C requirement in Bellcore's pedestal test (TA-TSY-000421). One of these insulations is shown to survive more than 1 year at 90°C.

## INTRODUCTION

Polyolefin insulated conductors (PIC) have been used in the wire and cable industry for more than 40 years. Without adequate antioxidants, the wire insulations were susceptible to premature oxidation.<sup>[1]</sup> As a result, much work was done on improving the oxidative stability of polyethylene for PIC insulation.<sup>[2] [3] [4] [5]</sup> Early versions of PIC cable used low density polyethylene (LDPE) as the wire insulation. This wire insulation evolved into high density polyethylene (HDPE). In addition, the stabilizer package used in wire insulations also evolved over time. Santonox® antioxidant was first used in LDPE. Then Irganox 1010 antioxidant and OABH (copper deactivator) were used in place of Santonox®. The same stabilizer package was used in HDPE. Finally, the current antioxidant package being used since the mid 1970's consists of Irganox 1010 together with a metal deactivator.<sup>[3]</sup> The principal metal deactivator used was Irganox 1024.

A recent report<sup>[6]</sup> predicts cracking patterns of foamed skin polyethylene insulation in pedestals in various areas of the country. This report used oxidation induction time (OIT) as a qualitative measure of the amount of remaining stability in wire insulation that was retrieved from field environments. The OIT is obtained by heating the sample at 200°C

under oxygen. Using a thermal analyzer, time to degradation is observed as an exothermic reaction in the calorimeter plot.

It is widely believed that the single most important variable that affects insulation oxidation is temperature. Other factors such as stress, humidity, ultraviolet radiation, etc. are considered secondary contributors to PIC cracking. Interaction with blowing agents can also be important and some data have been obtained.<sup>[7] [8]</sup> Also, contact of insulation with cable filler is known to affect stability.<sup>[8] [9] [10]</sup> Chan et al<sup>[8]</sup> suggest that the failures in foam skin insulation is related to the susceptibility of the foam layer to oxidation by the copper conductor. The currently accepted test method for evaluating longevity of polyethylene wire insulation is the Bellcore pedestal test.<sup>[11]</sup> This test is a variation on the pedestal test used by AT&T in the development of HDPE insulation.<sup>[12]</sup> The Bellcore pedestal test requires that cable should be preaged in an oven for 28 days/70°C, the insulation coiled and then the insulation is placed in a PC/6 telephone pedestal for thermal aging at 90°C and 110°C. Time for first crack to occur is measured. It was suggested<sup>[13]</sup> that 350 days at 90°C in the pedestal test without cracking occurring is equivalent to 40 years under field conditions. This has since been adjusted by Bellcore to 260 days at 90°C.<sup>[14]</sup>

The pedestal test was used to evaluate multiple wire insulation formulations. This includes improvements in both wire insulation and filling compound. The evaluation was done at temperatures ranging from 50 to 110°C in 10°C increments. Arrhenius plots were made with the test results.

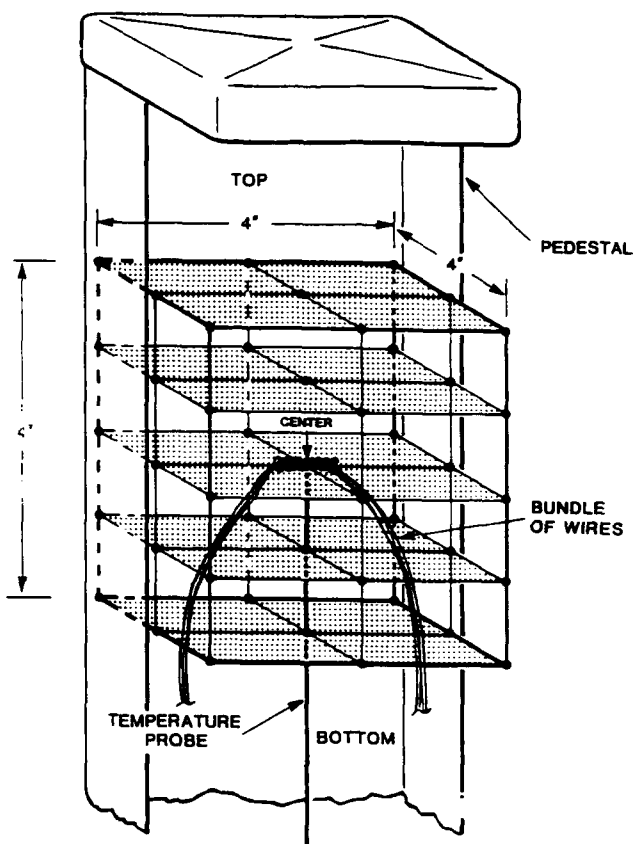
## EXPERIMENTAL

The samples tested were DEPIC (Dual Expanded Plastic Insulated Conductor) wire insulation obtained from filled cable. Two DEPIC insulations are labeled A, and B. Each insulation contained a different stabilizer package. The cables containing the insulation were preaged for 28 days/70°C in a forced air oven.

## Belcore Pedestal Test

Belcore has issued a technical document (TR-TSY-000421) which includes a section called "Pedestal Thermal Oxidation Stability Performance Test". An early version of TR-TSY-000421 is issue 2, June 1988. In this issue, there was no 28 day/70°C preage requirement for the pedestal test. Also, the insulated conductors were not required to be stressed (coiled). TR-TSY-000421 was later revised (Issue 2, June 1988, Revision 1, March 1989) to include preaging and insulation coiling. To pass the pedestal test, insulated wire must be aged in the pedestal for 1 year at 90°C and 45 days at 110°C without any cracking occurring. TR-TSY-000421 is still evolving. Technical Advisory TA-NWT-000421, Issue 2, November 1990, Supplement 1, April 1991 has been issued. This Advisory requires the insulation wire to be aged for 260 days (instead of one year) at 90°C. No more than one cracked insulation is permitted. Also, the 110°C/45 day requirement has been eliminated. Standard PC/6 telephone pedestals are used. Face plates, liners and brackets are removed from the interior of the pedestals. A heating mantle is placed over the pedestal to bring the interior of the pedestal to the desired temperature. The mantles are obtained from Glas-Col Apparatus Co., Terre Haute, Indiana. Each mantle is 12 inches long and rated at 260 watts. The temperature control system must be capable of maintaining the temperature of all the insulated conductor coils inside the pedestal within  $\pm 2^\circ\text{C}$  of the specified test temperature.

The temperature control system used by AT&T Bell Labs - Norcross is different from that proposed by Belcore. Belcore uses two temperature sensors (probes). One is in the middle to monitor temperature and one is on the side of the pedestal to control the temperature. The temperature controller used at AT&T Bell Labs is a Barber-Colman AT-PLUS. Our pedestal apparatus uses a single probe to both monitor and control temperature. A schematic of the pedestal set-up (without heating mantle) is shown in Figure 1. Included in the schematic is the solitary temperature probe and the general location of wires. The pedestal test calls for placing 50 wires (5 of each color) in the pedestal. Time for first cracks to occur was measured.



LOCATION OF INSULATED WIRES IN PEDESTAL  
FIGURE 1

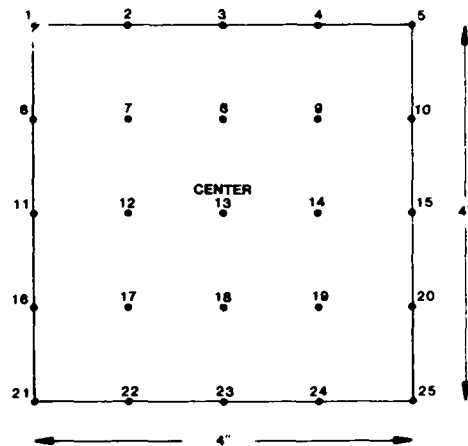
## PEDESTAL TEMPERATURE PROFILE

A thorough temperature profile was obtained on the inside of a PC/6 telephone pedestal in the Belcore pedestal test at control temperatures ranging from 50° to 110°C. This profile is performed in three dimensions and shows the temperature variations at different locations in the pedestal. Figure 2 shows a typical PC-6 pedestal with 25 thermocouples placed at various locations. Figure 3 shows a schematic (top view) of where the 25 thermocouples are located in the pedestal. Each thermocouple is attached to a 1/8" diameter wooden rod held in place with a 1" long steel spring. The thermocouples are spaced 1" apart permitting temperature measurements every inch over a 4" x 4" plane. When temperatures above or below this plane were desired, the thermocouples were simply raised or lowered accordingly such that temperatures were obtained through a 4" x 4" x 4" volume. The temperature measurements were made using an AT&T 6300 personal computer interfaced with a Metabyte DAS-8 and EXP-16 I/O cards.



PC-6 PEDESTAL WITH 25 THERMOCOUPLES

FIGURE 2



SCHEMATIC OF THERMOCOUPLE LOCATIONS  
ACROSS A PLANE IN THE PEDESTAL (TOP VIEW)

FIGURE 3

## RESULTS AND DISCUSSION

### Pedestal Temperature Profile

Figures 4-10, show isometric views of the temperature profiles in pedestals at temperatures ranging from 50 to 110°C, respectively. The center point in the figure is the tip of the monitor and control probe. This is the recommended location for insulated wires in the Bellcore pedestal test. The temperatures in each horizontal plane above and below the center are also shown. For clarity, only 9 of the 25 temperature measurements made in each plane are represented in the figures. The temperature probes at 90°C and 110°C (Figure 8 and Figure 10) show a 7°C and 9°C increase in temperature, respectively one inch above the recommended center. One inch below the center is a 2°C and 4°C temperature decrease, respectively. When wires are tested, the thickness of the bundle is ~ 0.5 inch. This assures that the coils are within the  $\pm 2^\circ \text{C}$  temperature zone specified by Bellcore.



Figure 1 is a schematic diagram of a temperature probe array. The array is a 6x6 grid of temperature probes. The central probe is labeled "70 CENTER 76 (70°C)". The probes are numbered 63 through 84. The array is mounted on a pedestal. A 4-inch scale bar is shown. A label "TEMPERATURE PROBE" points to one of the probes. A label "PEDESTAL" points to the base of the array.

### TEMPERATURE PROFILE (70°C)

### TEMPERATURE PROFILE (60°C)

### TEMPERATURE PROFILE (80°C)

280 International Wire &amp; Cable Symposium Proceedings 1991



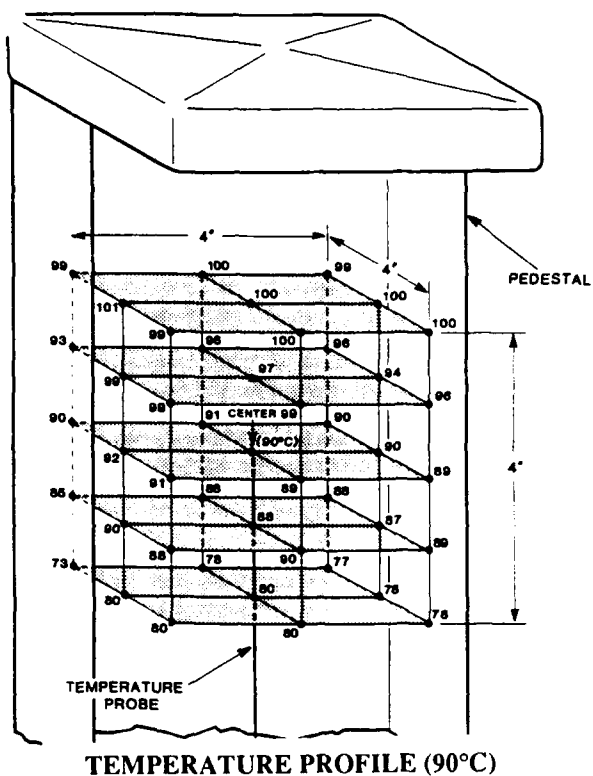


FIGURE 8

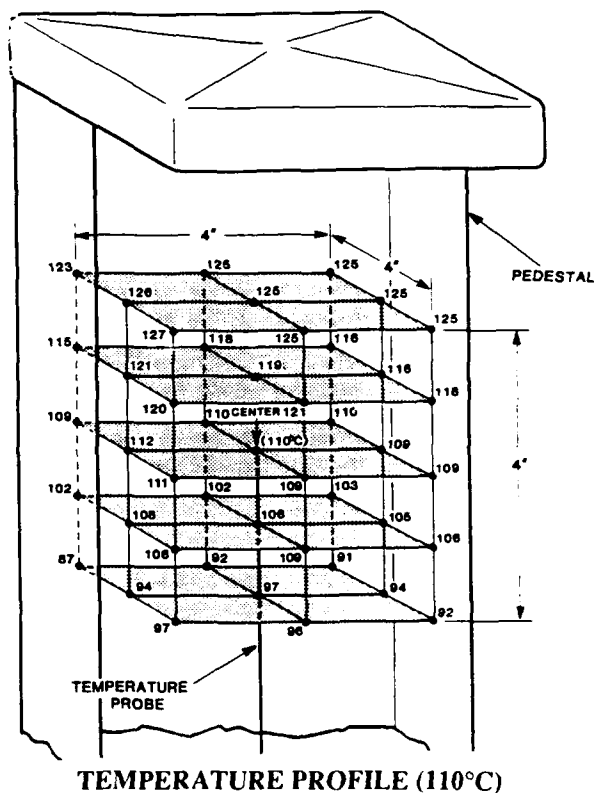


FIGURE 10

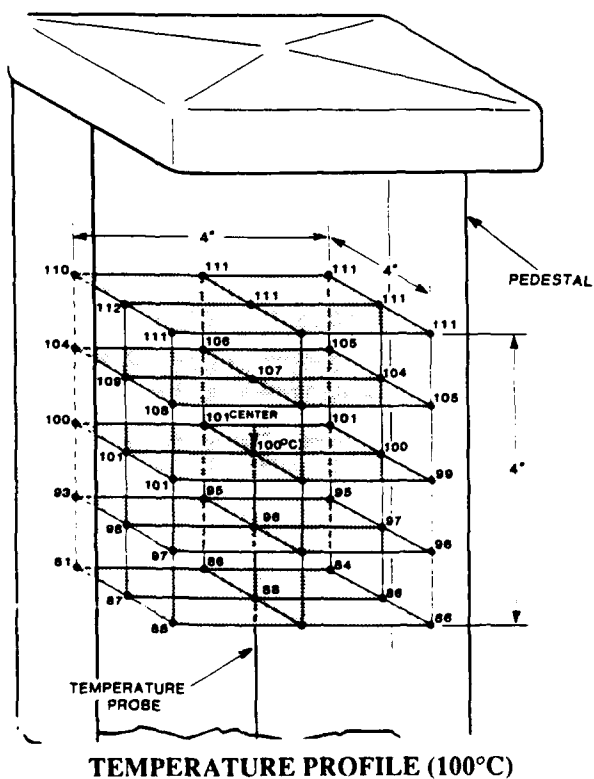


FIGURE 9

Figures 11 and 12 show the excellent temperature control achieved. These figures are time/temperature plots obtained every hour for both the 110°C/45 days (Figure 11) and 90°C/one year test (Figure 12). The temperature was measured at the top of the wire bundle. The profiles are within the  $\pm 2^\circ\text{C}$  Bellcore requirement for this test. The spikes in Figure 12 are inspection intervals. When the pedestal is opened, temperature control is temporarily halted until the test is restarted.

#### PEDESTAL #1 (DEPIC CABLE), 2E-30

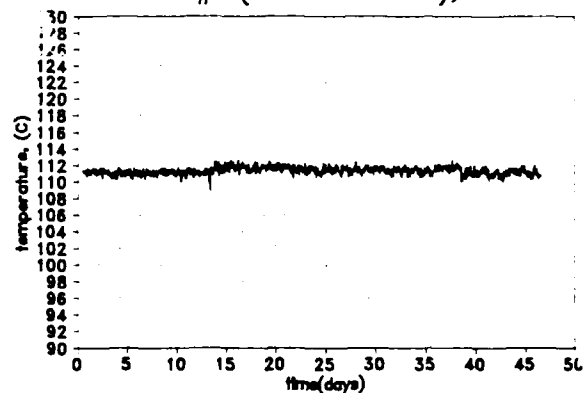


FIGURE 11 - 110°C TEMPERATURE CONTROL

# PEDESTAL #61 (DEPIC CABLE)

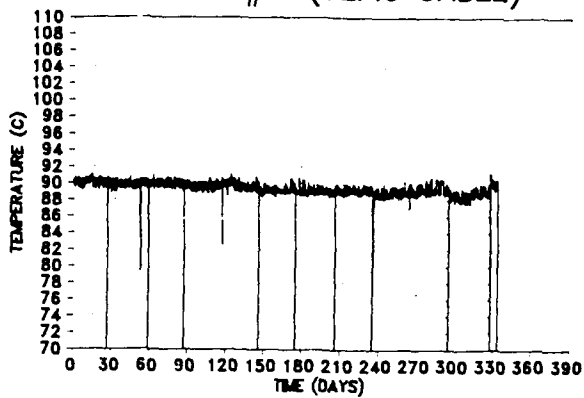


FIGURE 12 - 90°C TEMPERATURE CONTROL

## NEW DEPIC INSULATION

Table I and Figures 13-14 show Arrhenius plots from pedestal tests of insulation of new DEPIC cable designs. These test results are compared to the industry standard as of 1988. Again, test temperatures were 50-110°C. As seen in the Table and Figures, both of the improved designs are greatly superior to the industry standard. One design has achieved more than 1 year at 90°C. Both the designs exceed 260 days (the new Bellcore requirement) at 90°C. The reason that the 1988 insulation performed so poorly is because this insulation was designed to meet the June, 1988 Bellcore Technical Reference TSY-000421 which did not contain preaging or coiling.

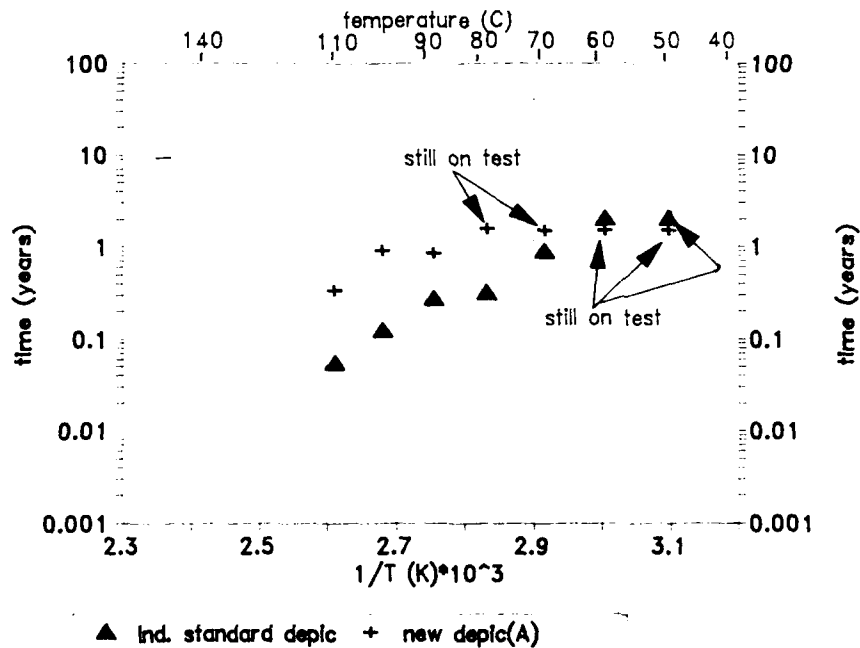
TABLE I

PERFORMANCE OF NEW DEPIC WIRE INSULATION IN EPIC TEST

Temperature, °C	Time to First Crack (Days)		
	A*	B**	1988 Cable
110	126-137	115-123	0-20
100	339-360	370-391	28-45
90	318-338	391-451	89-101
80	>581	>490	105-117
70	>560	>490	299-329
60	>560	>490	633-752
50	>560	>490	>752

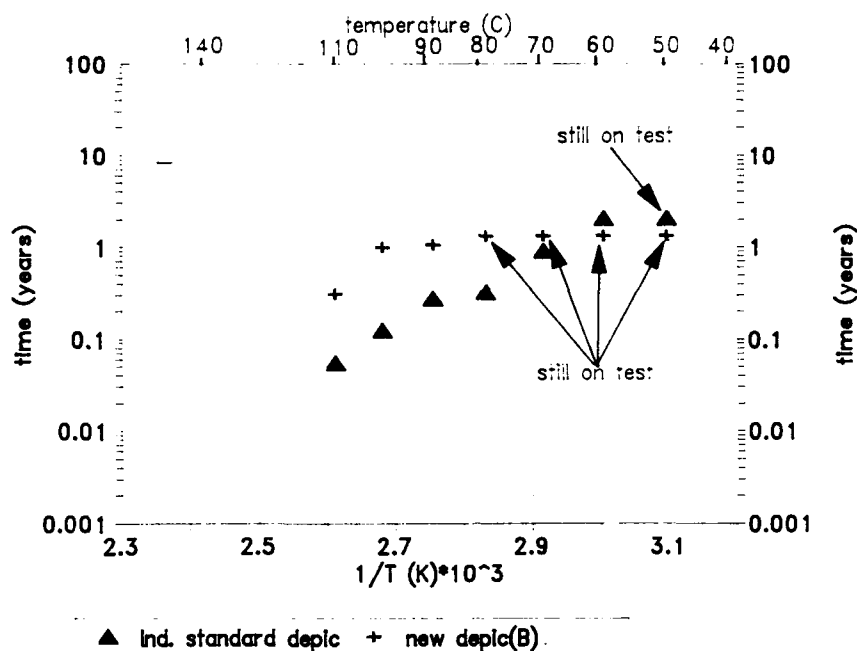
\* AT&T Current Product

\*\* AT&T Experimental Design



Arrhenius Plot - 1988 Insulation Vs. Insulation A

FIGURE 13



Arrhenius Plot - 1988 Insulation Vs. Insulation B

FIGURE 14

## CONCLUSIONS

The currently accepted test method for evaluating longevity of polyethylene wire insulation is the Bellcore pedestal test. A thorough temperature profile of the interior of a PC/6 telephone pedestal conforming to the temperature requirements of the Bellcore test is completed. This temperature profile is obtained through the control temperature range of 50-110°C. At the critical temperature of 90°C, it was found that a one inch deviation in placement of the wire samples above the recommended position represents a 7°C increase in temperature (from 90 to 97°C). One inch below the recommended level, the temperature drops to 88°C.

Evaluation of two improved DEPIC cable designs in the pedestal test shows both designs are far superior to the 1988 industry standard. Both designs easily pass the 260 day/90°C requirement in Bellcores pedestal test (TA-TSY-000421). One of these designs (Cable B) even surpasses one year at 90°C in the pedestal test.

## REFERENCES

1. J. B. Howard, "Stabilization Problems with Low Density Polyethylene Insulation," *Proceedings of the 21st International Wire and Cable Symposium*, 329 (1972).
2. B. D. Gesner, J. W. Shea and F. R. Wight, "Establishing Longevity Criteria from Thermo-Oxidative Cracking Measurements of Polyolefin Insulations," *Proceedings of the 22nd International Wire and Cable Symposium*, 7-20 (1973).
3. M. G. Chan, "High Density Polyethylene for PIC Insulation: Oxidative Stability," *Proceedings of the 23rd International Wire and Cable Symposium*, 34-41 (1974).
4. H. M. Gilroy, "Thermal Oxidative Cracking of Polyethylene Insulation on Telephone Conductors," *Proceedings of the 23rd International Wire and Cable Symposium*, 42-45 (1974).
5. M. G. Chan, H. M. Gilroy, L. Johnson, W. M. Martin, "Copper Deactivators for Polyolefin Insulation," *Proceedings of the 27th International Wire & Cable Symposium*, 99-106 (1978).

6. T. N. Bowmer, "Cracking of Foam-Skin Polyethylene Insulations in Pedestals," *Proceedings of the 37th International Wire and Cable Symposium*, 475-483 (1988)
7. D. D. O'Rell and A. Patel, "Oxidative Stability Studies on Cellular High Density Polyethylene Insulation for Communication Wire," *Proceedings of the 24th International Wire and Cable Symposium*, 231-236, (1975)
8. M. G. Chan, V. J. Kuck, F. C. Schilling, K. D. Dye, L. D. Loan, "Stabilization of Foamed Polyethylene Communication Cable over Copper Conductors," *International Conference on Advances in the Stabilization and Degradation of Polymers*, May 22-24, 1991 (P11-21).
9. Geoffrey D. Brown and Lawrence E. Davis, "Evaluation of Materials for Improved Life Expectancy of Foam Skin Insulation," *Proceedings of the 36th International Wire and Cable Symposium*, 734-743, (1987).
10. Geoffrey D. Brown, "Performance of HDPE Insulation Antioxidants in Filled Telephone Cable Applications," *Proceedings of the 36th International Wire and Cable Symposium*,
11. Bellcore Technical Advisory TA-NWT-000421, "Generic Requirements for Metallic Communication Cables."
12. E. T. Kokta, "Comparison of Test Methods for Determination of Stability of Wire and Cable Insulation," *Proceedings of the 24th International Wire and Cable Symposium*, 220-224, (1975).
13. T. N. Bowmer, "Thermal Stability Tests for Polyolefin Insulations," *Proceedings of the 39th International Wire and Cable Symposium*, 316-327 (1990).
14. Bellcore Technical Advisory TA-NWT-000421, "Generic Requirements for Metallic Communication Cables," Issue 2, November 1990, Supplement 1, April 1991.



E. D. Nelson is a Member of the Technical Staff at AT&T Bell Laboratories, Norcross, GA. He is currently a member of the Chemistry Group in the Materials Engineering Department. He received a B.S. degree in Chemistry from St. Francis College and a M.S. degree in Engineering Science from the Newark College of Engineering. His interests include fire and smoke properties as well as oxidative stability of polymeric materials.

# NONBLOCKING $100 \times 100$ OPTOMECHANICAL MATRIX SWITCH FOR SUBSCRIBER NETWORKS

Toshiaki KATAGIRI, Yahei KOYAMADA, Masao TACHIKURA  
and Yutaka KATSUYAMA

NTT Telecommunication Field Systems R&D Center  
Tokai-mura, Naka-gun, Ibaraki-ken, 319-11, Japan

## Abstract

A nonblocking optomechanical matrix switch has been developed, that can be arbitrarily switched between two ferrule-terminated-fiber groups by automatic reconnection and disconnection. The fabricated  $100 \times 100$ , 3-mm-ferrule-pitch,  $630^{\mu} \times 570^{\mu} \times 550^{\mu}$  (mm) switch exhibits a mean insertion loss of about 1 dB (1.3- $\mu$ m wavelength LED). The developed switch is applied to a subscriber model switching system and its effectiveness is confirmed.

## 1. Introduction

Optical switching plays an important role in terms of maintenance reduction and long-term system reliability in optical communication systems. Optomechanical switches offer advantages for practical use in the near future because of their excellent optical performance. In subscriber transmission lines, nonblocking switches are required that have a large matrix in a small size. They also need to be latching type switches without holding electric power, economical and highly reliable.

One type of large matrix optomechanical switch that has been developed is the moving beam nonblocking  $100 \times 100$  switch.<sup>1</sup> However, the use of this switch is restricted to multimode fibers because of its poor misalignment tolerance. The matrix size of non-mechanical switches<sup>2</sup> is small, for example  $8 \times 8$ . Both types of switch need holding electric power for latching.

With moving fiber matrix switches, it is essential to align each fiber individually to prevent fibers from crossing each other. Methods have been proposed to eliminate the need for fiber alignment. However, conventional methods<sup>3,4</sup> have a large splitting loss at the optical power input side.

When constructing a large matrix  $N \times N$  crossbar interconnection network using small matrix switches, the required number of small switches is approximately proportional to  $N^2$ , and the maximum insertion loss increases approximately in proportion to  $N$ . Furthermore, when small switches are joined under the restriction of the upper limit of the fiber bending radius, there are problems of the increase in switch dimensions and the sum of jointing losses.

This paper describes a large matrix, latching type, nonblocking optomechanical switch which we have developed and an example of its application to a remote controlled, subscriber model switching system.

## 2. Structure and switching mechanism

Figure 1 shows the proposed nonblocking matrix switch construction method. The ferrules on one side can move in the matrix row direction and those on the other side in the column direction. Using this method, each ferrule can be independently and arbitrarily positioned along every row or column. As a result, facing ferrules can be arbitrarily joined between two ferrule-terminated-fiber groups.

Figure 2 is a simple representation of the fabricated switch, which is based on the switch construction method shown in Fig.1. Slitted alignment sleeves are fixed on the ferrules of either fiber group with adhesive. One ferrule is attached to a slider and the other to a linear guide supported by a slider with compression springs between the ferrule and the slider or the guide. The ferrules on both sides move along rails set at right angles to each other.

As shown in Fig.2, the ferrule-group with sleeves and linear-guides is referred to as the Z-side group and the other group is the W-side group.

A fiber-accumulator maintains tension in the fiber spanned between the slider and the accumulator. The fiber is wound a few times around two pulleys. Both axes of the pulleys are supported by a tension spring so that their axes are kept apart. The distance

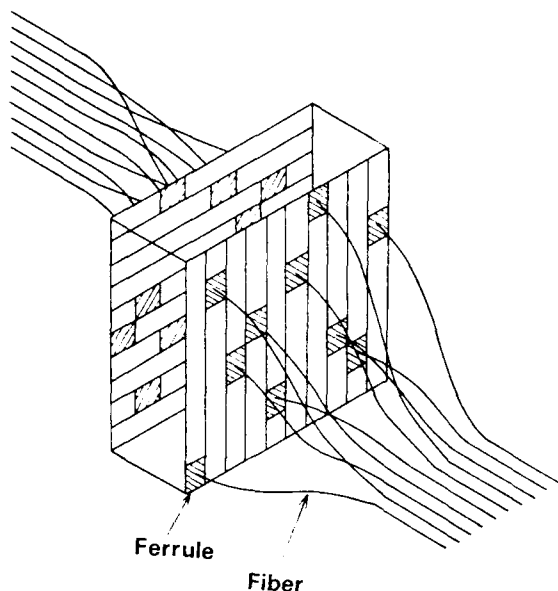


Fig. 1 Nonblocking matrix switch construction method

between their axes can be changed dependent on the length of fiber drawn out from the accumulator. This enables each fiber to be aligned along the rails. The ferrule positioning mechanism can move freely. The fiber bending radius and the fiber tension, which are related to fiber life and the bending loss, are all kept within their designed values.

The switching motion is as follows. Ferrule positioning is accomplished by 3-D positioning mechanisms on both sides of the switch, that position the operation rod attached to the linear guide or the slider. One ferrule is connected to a facing ferrule with the slitted alignment sleeve and then a hook on the operation rod attached to the linear guide is positioned against the rail by rotating it. This then applies a ferrule-end load by the action of the compression spring. At the same time, the reaction force in the ferrule-axial direction causes friction between the slider and the rail, so that the slider position is fixed.

The accumulator, drawn with broken lines in Fig.2, is described in 3-1(4) and the laser beam sensor to detect the sleeve is described in 3-2.

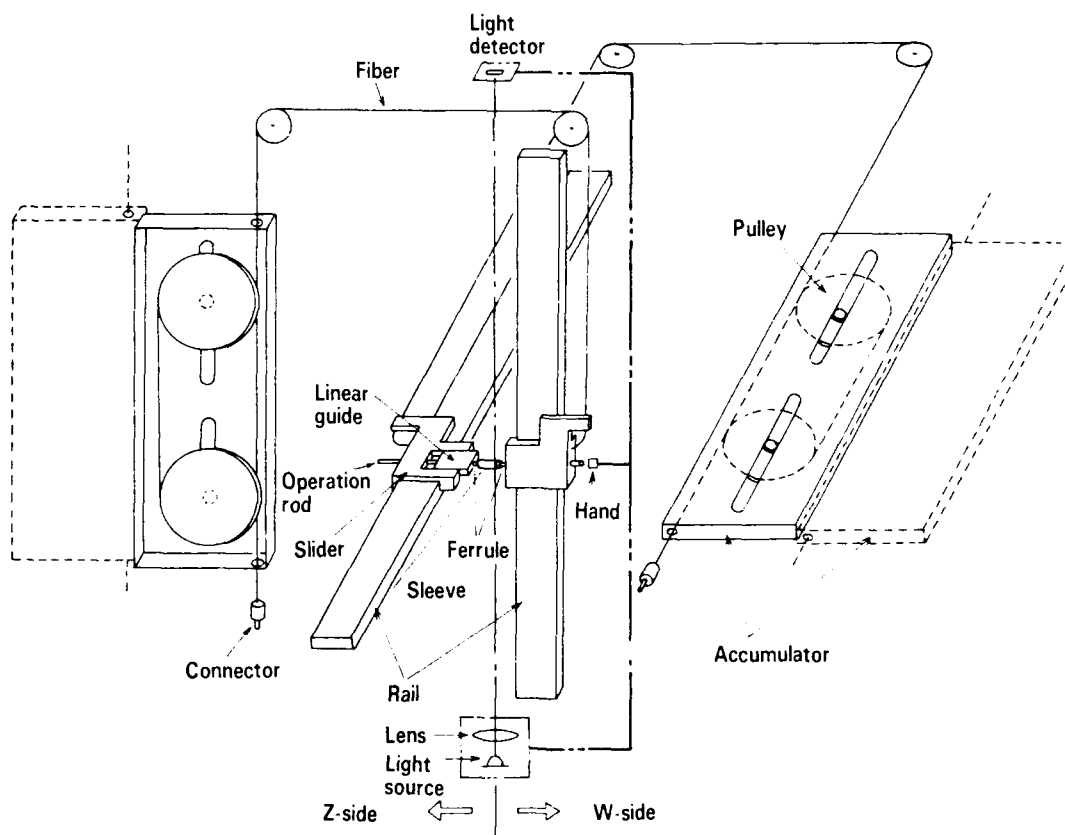


Fig. 2 Switch structure

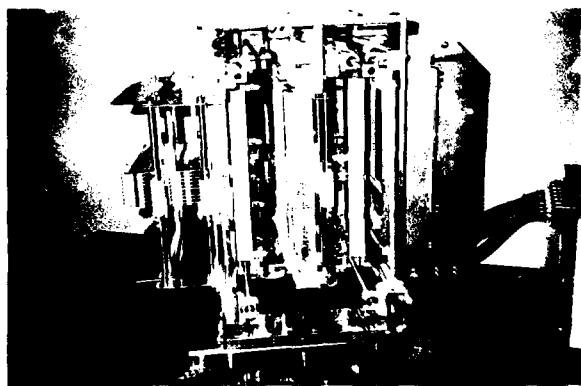


Fig. 3 Photograph of developed switch

Table 1 Switch performance

Matrix size	100×100 (designed)
Dimensions	630 <sup>w</sup> ×570 <sup>d</sup> ×550 <sup>h</sup> mm
Switching time	< 1.3 min. (estimated)
Mean insertion loss	~ 1 dB
Driving power	< 140 watt

Table 2 Parameters of fiber, ferrule and sleeve

Fiber	10/125 $\mu$ m, single-mode mode field diameter: 9.4 $\mu$ m
Ferrule	zirconia ceramic, 2.0 $\phi$ (od)×7.5 <sup>l</sup> mm
Sleeve	zirconia ceramic, 2.7 $\phi$ (od)×10.4 <sup>l</sup> mm

### 3. Developed switch

#### 3-1 Switch features

Figure 3 shows a photograph of the developed switch. The practical fabricated switch has a small 20×20 matrix in the center of a 100×100 matrix. Table 1 summarizes the switch performance. Table 2 lists the parameters of the fibers, ferrules, and slitted alignment sleeves. The features of the switch are as follows.

(1) The switch consists of a ferrule reconnection-disconnection mechanism and its controller (425<sup>w</sup>×410<sup>d</sup>×245<sup>h</sup> mm) equipped with an RS-232C interface.

(2) The pitch between ferrules is 3 mm. This pitch dimension is close to the mechanical fabrication limit of the slider parts.

(3) The switch dimension in the ferrule-axial direction becomes smaller with decreases in fiber bending radius. High-strength carbon-coated optical fiber<sup>5</sup> was used in order to minimize the fiber bending radius. The minimum radius was determined to be 10 mm, taking into consideration of the bending loss increase due to deviations in the fiber index profile of

commercially available fiber.

(4) The thickness of accumulator was greater than the 3mm-pitch between the ferrules. For this reason, the accumulators are constructed with two stage as shown in Fig.2. The minimum fiber tension is designed to be 0.3 N. The fiber tension was maintained at the maximum slider speed of 32.5 mm/sec.

(5) The master driver (3-D positioning mechanism) and the slave mechanism (ferrule reconnection-disconnection mechanism) were designed to be able to be separated from each other. This enables the master driver to be applied to many slave mechanisms.

#### 3-2 Positioning compensation by laser beam sensor

The final relative position between a ferrule-tip and a sleeve-tip is important when ferrules are joined. For the Z-side sliders with linear guides, in particular, the position of the sleeve-tip fluctuates in the slider moving direction because of the clearances of the movable mechanical parts. Furthermore, the allowable positioning error in the slider moving direction is estimated to be within 0.2 mm of the mechanical clearance and corner-plane-off of the ferrule-ends. For this reason, the Z-side sliders in the slider moving direction were positioned using a laser beam sensor, attached to the W-side 3-D positioning mechanism, in addition to the encoder coupled to the motor-rotating-axis. In other words, the final position of Z-side sliders was compensated for by detecting Z-side sleeve-tips on the basis of the position of W-side ferrules to be joined. Figure 2 illustrates this.

The fluctuation magnitude of stationary positions on the linear guides of the Z-side sliders was measured with a digital micro-gauge. The desired moving distance was set at 250 mm for the Z-side sliders and at 200 mm for the W-side sliders. Figure 4-1 shows the results of measurements made without the laser beam sensor and Figure 4-2 shows those made with it. In Fig.4-1, the fluctuation difference between the sliders is considered to be dependent on the clearance of each slider and guide. When standard deviations  $\sigma$  and maximum fluctuations  $\Delta$  in Fig.4-1 are compared with those in Fig.4-2, it can be seen that the laser beam sensor reduces fluctuations in the slider moving direction. The sensor contributes to stable ferrule jointing.

Additionally, the fluctuation in the stationary positions of the W-side sliders was also measured with the digital micro-gauge. Figure 4-3 shows the measured results. The laser beam sensor is not adopted for W-side positioning. In Fig.4-3, it can be seen that the fluctuation of the W-side sliders is much smaller than that of the Z-side sliders. This is because the influence of mechanical clearance is small.

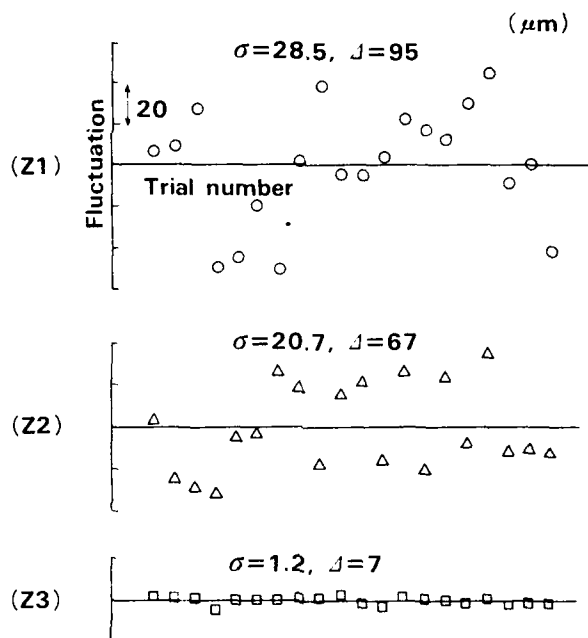


Fig. 4-1 Fluctuations of Z-slider without sensor

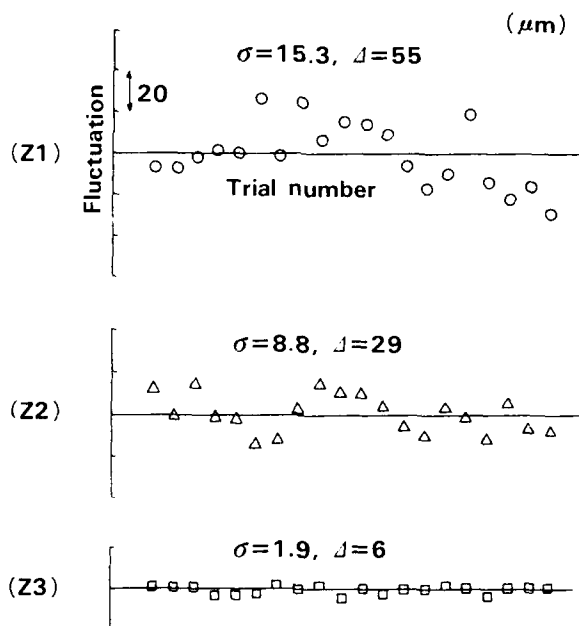


Fig. 4-2 Fluctuations of Z-slider with sensor

### 3-3 Loss measurement

Figure 5 shows the insertion loss measurement setup. A 1.3 μm wavelength LED was used. The measured loss is the sum of the loss at the connector<sup>6</sup> on the switch input-side and the loss at the ferrule-

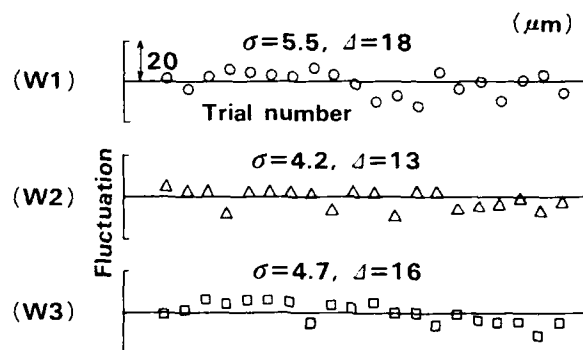


Fig. 4-3 Fluctuations of W-slider

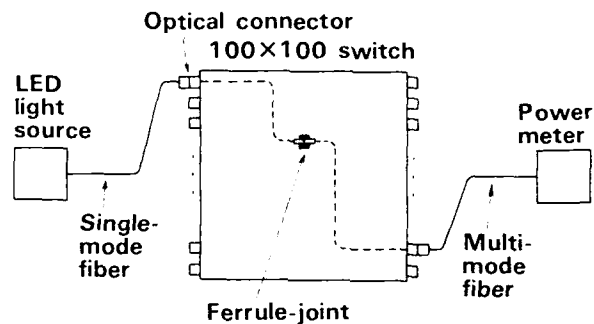


Fig. 5 Loss measurement setup

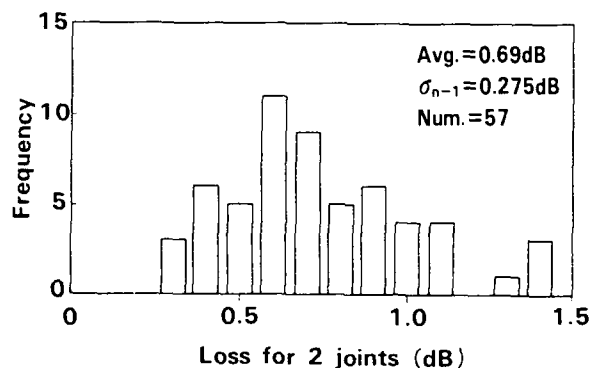


Fig. 6 Loss histogram

joint in the switch. Index-matching material was not used at the joint portions. Figure 6 shows the measured loss histogram for the two above mentioned joints. The mean loss was 0.69 dB/2 joints. The mean switch insertion loss was approximately 1 dB assuming a loss of 0.35 dB/joint. Each fiber had a bending loss for a 3/4 turn of the radius of 10 mm, but the influence of this loss on the switch insertion loss is considered to be small.



Table3 Measurement examples of switching time

Switching condition	Switching time
Z1&W1: start position on rail	
Z1 to W1: jointed	~ 31 sec
Z20&W20: start position on rail	
Z20 to W20: jointed	~ 32 sec
Z1 to W1& Z20 to W20: jointed	
Z1 to W20: jointed	~ 72 sec

### 3-4 Switching time

Table 3 summarizes the switching time measurements under several switching conditions. The switching time was always measured after the operation rod hand had returned to its home position because the switching time depends on the initial position of the hand. The maximum switching time for the 100×100 matrix was about 1.3 min. This was estimated from the slider moving speed. The switching time includes approximately 5 sec. due to the positioning compensation of the Z-side sliders via laser beam detection.

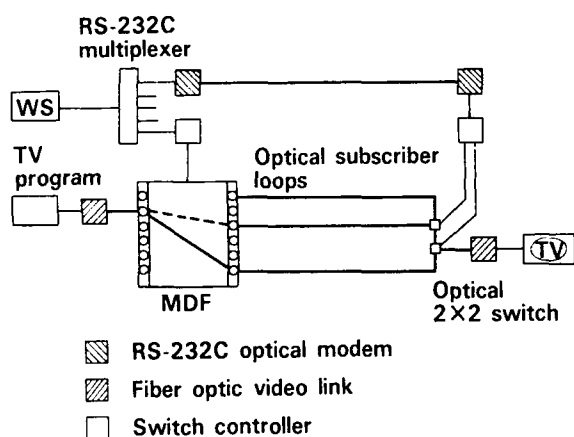


Fig. 7 Subscriber model switching system

### 4. Subscriber model switching system

Figure 7 shows a remote controlled, subscriber model switching system. The remote switches in subscriber transmission lines are operated from the workstation (WS) when service order or fiber trouble occurs. The developed matrix switch was used as the MDF (main distribution frame) and 2×2 mechanical switches were used as remote nodes. The switching command signal was transferred to the remote switches with an RS-232C multiplexer and a pair of RS-232C optical modems. The TV video signal was transferred to the user TV by means of a fiber optic

video link.

When fiber trouble occurred, protection switching was achieved from the workstation. The switching result was easily confirmed by observing the TV picture. The remote control switching function contributes to service improvement, ease of system operation and maintenance reduction.

### 5. Conclusion

A nonblocking optomechanical matrix switch has been developed. A 100×100-matrix-size and 3-mm-ferrule-pitch was confirmed to be mechanically available. It is a latching type switch without holding electric power. The transmission characteristics and reliability of the joint components are as good as conventional optical connectors because both employ the same jointing method.

The developed switch was applied to a subscriber model switching system and its effectiveness was successfully confirmed.

### Acknowledgment

The authors wish to thank K. Ishihara, Manager of Optical Subscriber Cable Systems Laboratory in NTT Telecommunication Field Systems R&D Center, for his encouragement.

### Reference

- (1) J. BAINERMAN : 'Piezoelectrics Switch Optical Signals', Lasers & Applications, pp.49-51, December, 1984.
- (2) H. A. ROBERTS : 'Optical switching - Ready for switching', Proc Natl Comm Forum, **43**, pp.827-831, 1989.
- (3) F. BLANC, A. CASAL, P. FAUGERAS, G. OULLET and J. SOURGENS : 'Multiservice subscriber connection made with an optomechanical switching equipment', ECOC Proceeding, pp.264-265, 1984.
- (4) A. R. DIAS, R. F. KALMAN, J. W. GOODMAN and A. A. SAWCHUK : 'Fiber-optic crossbar switch with broadcast capability', Optical Engineering, **27**, pp.955-960, 1988.
- (5) N. YOSHIZAWA and Y. KATSUYAMA : 'High-strength carbon-coated optical fiber', Electron.Lett., **25**, pp.1429-1431, 1989.
- (6) E. SUGITA, R. NAGASE, K. KANAYAMA and T. SHINTAKU : 'SC-Type Single-Mode Optical Fiber Connectors', J. Lightwave Technol, **7**, pp.1689-1696, 1989.



Toshiaki KATAGIRI  
NTT Telecommunication  
Field Systems R&D Center  
Tokai, 319-11, Japan

He was born in Gifu Prefecture, Japan, in 1949. He received the B.E. degree in mechanical engineering from Toyama University, the M.E. and Ph.D. degrees in precision engineering from Tohoku University, Toyama, Sendai, Japan, in 1972, 1974 and 1989, respectively. He joined NTT Electrical Communications Labs., Ibaraki, Japan, in 1974. From 1974 to 1981, he was engaged in construction machinery. Since 1982, he has been engaged in developmental research on optical fiber joint and switching technology. Dr. Katagiri is a member of the Institute of Electronics, Information and Communication Engineers of Japan.



Masao TACHIKURA  
NTT Telecommunication  
Field Systems R&D Center  
Tokai, 319-11, Japan

He was born in Ibaraki Prefecture, Japan, on September 10, in 1950. He received the B.E., M.E. degrees in mechanical engineering from Kyoto University, Kyoto, Japan, in 1974 and 1976, respectively. He joined NTT Electrical Communications Labs., Tokyo, Japan, in 1976. Since then, he has been engaged in research and development on optical fiber splicing and switching technology. Mr. Tachikura is a member of Optical Society of America, the Institute of Electronics, Information and Communication Engineers of Japan, and the Japan Society of Applied Physics.



Yahei KOYAMADA  
NTT Telecommunication  
Field Systems R&D Center  
Tokai, 319-11, Japan

He was born in Mie Prefecture, Japan, on September 15, 1947. He received the B.S., M.S. and Ph.D. degrees in electrical engineering, all from Osaka University, Osaka, Japan, in 1970, 1972 and 1978, respectively. He joined NTT Electrical Communications Labs., Tokyo, Japan, in 1972. From 1972 to 1977, he was engaged in research on surface acoustic wave devices. Since 1978, he has been engaged in developmental research on optical fiber cables and measuring equipment. Dr. Koyamada is a member of IEEE and the Institute of Electronics, Information and Communication Engineers of Japan.



Yutaka KATSUYAMA  
NTT Telecommunication  
Field Systems R&D Center  
Tokai, 319-11, Japan

He was born in Kyoto, Japan, in 1949. He received the B.S., M.S. and Ph.D. degrees in mechanical engineering, all from Kyoto University, Kyoto, Japan, in 1971, 1973 and 1981, respectively. He joined NTT Electrical Communications Labs., Ibaraki, Japan, where he has been engaged in the research and developmental work on design and characterization of optical fiber cables. Dr. Katsuyama is a senior member of IEEE, and a member of Optical Society of America and the Institute of Electronics, Information and Communication Engineers of Japan.

# A LOW LOSS FOUR-FIBER 1X2 OPTICAL SWITCH

Y. Nomura      K. Jimbo      H. Yokosuka

Fujikura Ltd. Chiba, Japan

## ABSTRACT

We developed a high performance 1x2 optical switching device capable of mechanically switching four-fiber ribbon.

The newly developed optical fiber switching device is applicable to 1.55  $\mu\text{m}$  zero-dispersion shifted fibers. It features an extremely low insertion loss with a remarkably high switching speed considering that it is a mechanical switch. It has been tested in strict conditions simulating severe environmental environment and in all the tests its performance was found to be highly repeatable.

The reliable and high performance of the optical switching device makes it suitable for use in optical networks.

## 1. INTRODUCTION

Optical fiber networks are expanding rapidly on the global scale. In order to construct and operate the optical fiber networks efficiently, a switching mechanism capable of switching from one network to another at branching or connection points is essential. As the number of optical fibers in optical fiber cables increases, use of multi-fiber ribbons is becoming increasingly extensive for their high efficiency in integration. Moreover, as the transmission distance becomes longer, the trend sees accelerated use of cables with multi-fiber ribbons using 1.55  $\mu\text{m}$  zero-dispersion shifted fibers which are suitable for long distance transmission. Earlier work[1] has reported the basic structure of multi-fiber mechanical switches.

We have developed an optical fiber switching device capable of high speed operation with low loss for multi-fiber ribbon comprising 1.55  $\mu\text{m}$  zero-dispersion shifted fibers.

The newly developed optical fiber switching device has the following characteristics.

### **Multi-fiber switching:**

The device is capable of simultaneously switching four-fiber ribbon.

### **Low loss:**

The device has an insertion loss of 0.4dB or lower on the average, which is extremely low for a switching device for multi-fiber ribbon using 1.55  $\mu\text{m}$  zero-dispersion shifted fibers.

### **High speed switching:**

The device has a switching time of 2 ms or less which is extremely fast for a mechanical switching device.

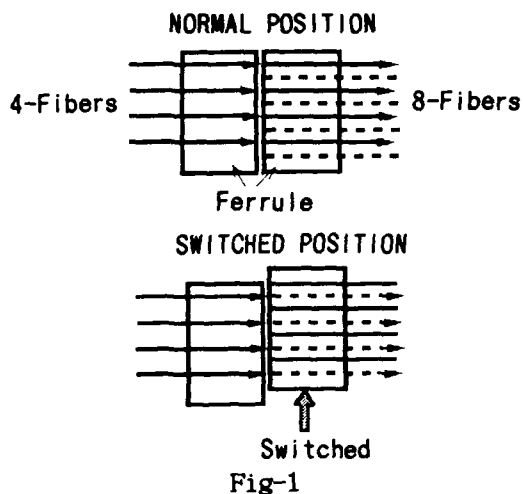
### **High reliability:**

The device has a highly stable switching performance with loss fluctuation of  $\pm 0.2$  dB or less in switching tests repeated 10,000 times.

## 2. STRUCTURE

### 2-1. Switching Principle

As shown in Fig. 1, a ferrule containing four optical fiber is mated against a ferrule containing eight optical fibers, and one of the ferrules is shifted to switch the fiber connections.



## 2-2. Structure of the Ferrules

Positioning of the movable ferrule plays a critical role in the present switching device. As shown in Fig. 2, positioning is achieved as the alignment pins built in the device move in the enlarged V-grooves until they hit against the respective side walls of the grooves.

A pair of ferrules to be mated against each other are assembled, and one of the ferrules is formed with alignment pins. The movable ferrule is formed with V-grooves which are wider to allow it to move by  $250\text{ }\mu\text{m}$  (fiber pitch).

Thus, the fiber pitch and the V-grooves must be processed with a high precision. The fiber pitch precision in the switching device is within  $\pm 0.5\text{ }\mu\text{m}$ . The precision of the V-grooves is also within  $\pm 0.5\text{ }\mu\text{m}$ . These precisions enabled the low connection loss to be achieved.

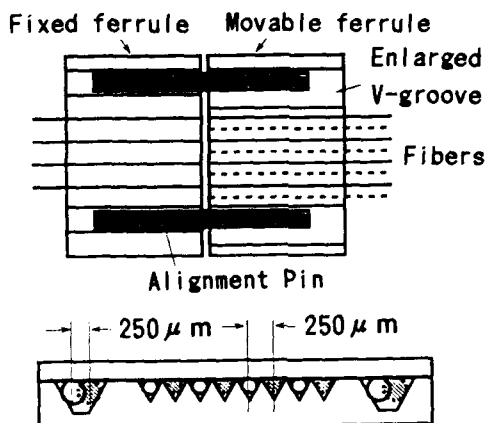


Fig-2

## 2-3. Structure of the Driving Unit

The driving unit for shifting the ferrule comprises a bistable type solenoid as shown in Fig. 3. The ferrule to be shifted is switched by means of push pins linked to the solenoid.

Coil springs are arranged in parallel at the back of the movable ferrule to press the ferrules against each other at a given pressure, keeping the faces at the respective ends of the ferrules in contact even when one of the ferrules is shifted. This in turn allows the optical waveform to be less fluctuating, and ensures stable operation.

The solenoid is a latching type (bistable type) and is capable of maintaining the ferrule at either position without consuming electric-power. The device therefore consumes only minimal power during operation.

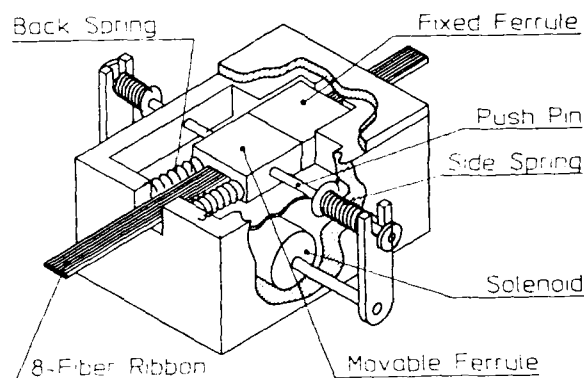


Fig-3

## 3. OPTICAL CHARACTERISTICS

### 3-1. Insertion Loss

Insertion loss of the new switching devices were measured using a  $1.55\text{ }\mu\text{m}$  light source.

As shown in Fig. 4, a very low connection loss of  $0.35\text{ dB}$  on the average was obtained in the 2,000 fibers (500 devices) that were tested. There is no significant difference in the average insertion loss between the two switching position, demonstrating a highly stable performance.

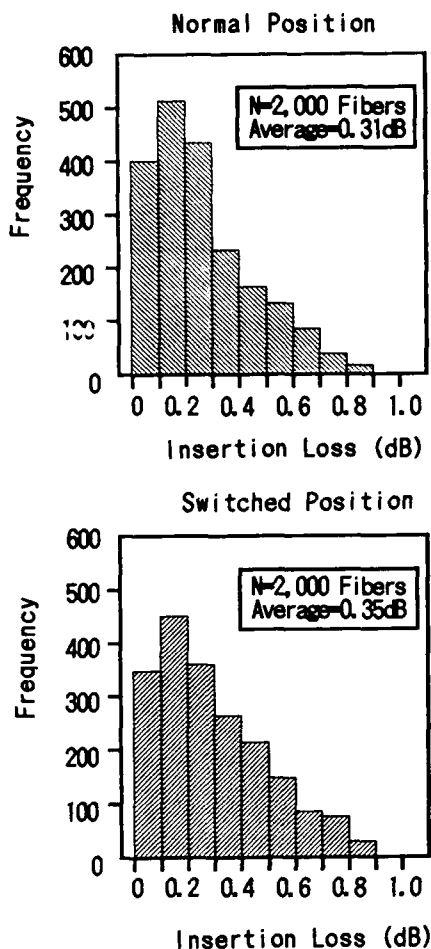


Fig-4

### 3-2. Switching Time

Switching characteristics of the devices were measured with a digital oscilloscope. The typical waveforms obtained in the measurement are shown in Fig. 5.

T1 and T2 in Fig. 5 represent the following:

T1: The duration from the time an optical fiber is disconnected from one fiber to the time it is reconnected with the next fiber.

T2: The duration from the time the device is triggered to the time the fiber is reconnected (switching operation is completed).

The average switching time (T1) of 500 devices was 1.4 ms, which is extremely high for a mechanical switching device.

The average time required from triggering until completion of switching (T2) was 4.5 ms or less, which is also very fast.

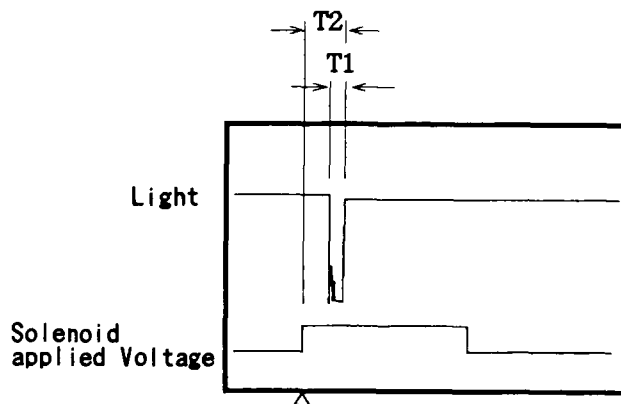


Fig-5

### 3-3. Return Loss

Using a 1.55  $\mu\text{m}$  light source, reflection at the mating face of a switching device was measured with a power meter using a coupling/branching filter. The other end of the switching device is made non-reflective by immersing the end fiber in refractive index matching oil. The return loss measured was more than -40 dB.

## 4. RELIABILITY TESTS

In order to verify the reliability of the switching device, we conducted various evaluation tests and confirmed that the switching device was satisfactory for practical application.

### 4-1. Repeated Switching Test

The switching devices were repeatedly operated for 10,000 times to measure the fluctuation in the insertion loss. A typical result is shown in Fig. 6.

As is clear from Fig. 6, loss fluctuation under repeated operation was less than  $\pm 0.1$  dB, indicating an extremely high stability.

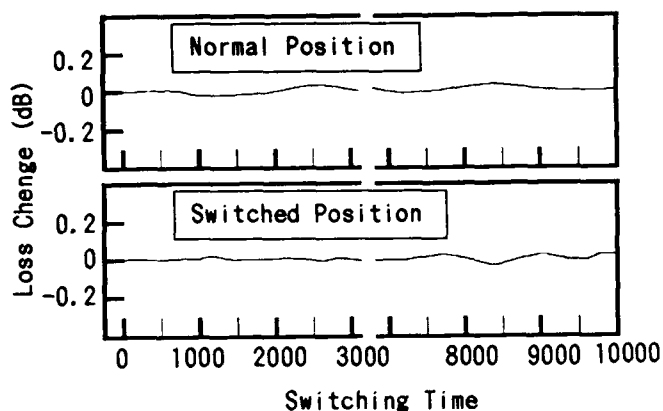


Fig-6

#### 4-2. Heat Cycle Test

Heat cycle tests were conducted to measure the changes in the insertion loss with changes in temperature.

Temperatures ranging from  $-10^{\circ}\text{C}$  to  $+60^{\circ}\text{C}$  for four hours was repeated 10 times, and changes in the loss when the switching devices were under static condition were measured. As is clear from Fig. 7, the fluctuation in the loss was less than  $\pm 0.1$  dB.

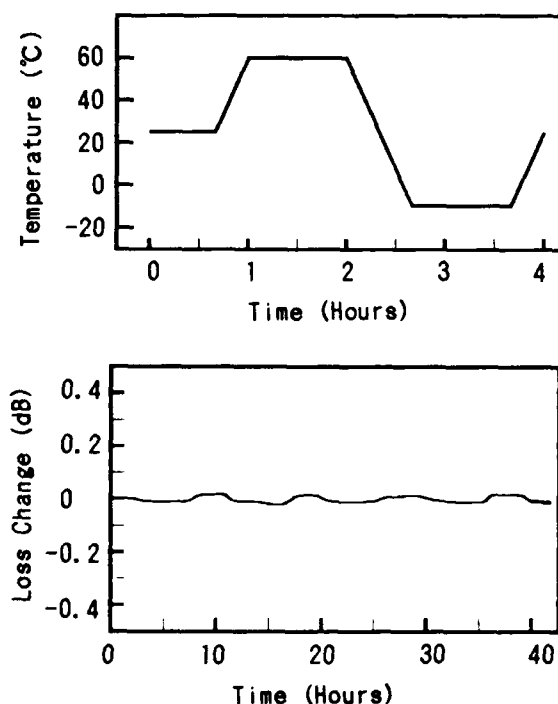


Fig-7

#### 4-3. Vibration Test

The optical switching devices were subjected to vibration test. The test was conducted under the below-mentioned conditions.

Vibration frequency: 10 - 55 Hz

Amplitude: 1.5mm

Direction: Three directions

Duration: Two hours in each direction

The connection characteristic (fluctuation in insertion loss) were measured. The fluctuation in insertion loss at the normal position was within 0.05 dB. No marked difference in the switching performance (waveform at the time of switching and switching time) observed before and after the test.

#### 4-4. High Temperature Test

High temperature tests of the optical switching devices were conducted using a constant temperature testing apparatus in the laboratory. The switching devices were maintained at  $+60^{\circ}\text{C}$  for four hours, and were subjected to switching operations repeated for 100 times to measure the connection characteristic (fluctuation in the insertion loss) and the switching performance (waveform at the time of switching and switching time). Insertion loss changes at the normal position were within 0.15 dB. No fluctuation was observed in the switching performance.

#### 4-5. Low Temperature Test

Low temperature characteristics of the optical switching devices were measured using a constant temperature testing apparatus in the laboratory. The switching devices were maintained at  $-10^{\circ}\text{C}$  for four hours, and were subjected to switching operations repeated 100 times. The connection characteristic (fluctuation in the insertion loss) and the switching performance (waveform at the time of switching and switching time) were measured. The fluctuation in the insertion loss at the normal position was within 0.15 dB. No fluctuation was observed in the switching performance.

#### 4-6. Switching Test under Heat Cycle

The static characteristics of the devices during heat cycle were measured in Section 4-2. Dynamic characteristics of the devices under heat cycle were also measured using a heat cycle test apparatus. A heat cycle test at temperatures ranging from 0°C to +60 °C for four hours was repeated twice, while the devices were switched 100 times to measure the switching performance (waveform at the time of switching and switching time). The fluctuation in the loss in the normal position was within +0.15 dB. No difference was observed in the waveform or the switching time.

#### 5. CONCLUSION

The newly developed optical fiber switching device is extremely low in loss and highly efficient in switching performance for a device of this type using 1.55  $\mu\text{m}$  zero-dispersion shifted fibers.

The results of the reliability tests demonstrate that the device is adequate for practical applications and has high reliability. We believe the device can be used in optical fiber network to achieve a more efficient network operation.

#### REFERENCE

- [1] S. Nagasawa et al., "A low-loss multifiber mechanical switch for 1.55 $\mu\text{m}$  zero-dispersion fibers", Trans. IEICE, Vol. E73, P. 1147-1149, 1990.



Yoshikazu Nomura

Opto-Electronics  
Laboratory  
FUJIKURA LTD.

1440, Mutsuzaki,  
Sakura-shi, Chiba, 285  
Japan

Yoshikazu Nomura was born in 1951. He graduated in mechanical engineering from Shinsyu University. He has been engaged in research and development of telecommunication cables and accessories. He is now a chief of the fiber and cable Accessory Department of Fujikura Ltd.



Kunihiko Jimbo

Opto-Electronics  
Laboratory  
FUJIKURA LTD.

1440, Mutsuzaki,  
Sakura-shi, Chiba, 285  
Japan

Kunihiko Jimbo was born in 1958. He graduated from Tokyo Denki University in 1981. He has been engaged in research and development of telecommunication cable and accessories. He is a member of the Institute of Electronics and Communication Engineers of Japan.



Hiroshi Yokosuka

Opto-Electronics  
Laboratory  
FUJIKURA LTD.

1440, Mutsuzaki,  
Sakura-shi, Chiba, 285  
Japan

Hiroshi Yokosuka graduated in mechanical engineering from Tokyo Metropolitan Technical Junior College in 1967. He has been engaged in development of telecommunication cables and accessories. He is now a Manager of the Fiber and Cable Accessory Department of Fujikura Ltd. He is a member of the Institute of Electronics and Communication Engineers of Japan.

## High-Speed, Low-Loss Connection Techniques for High-Count Pre-Connectorized Cables

Tadashi HAIBARA, Shigeru TOMITA, Michito MATSUMOTO  
and Tetsuro YABUTA

NTT Telecommunication Field Systems R & D Center  
Tokai, Naka, Ibaraki, 319-11 JAPAN

### Abstract

High-speed, low-loss connection techniques are indispensable for construction of optical subscriber cable networks because many cable connections are required. We have designed two types of high-count pre-connectorized cables. One is an array connector type to join ultra-high count (more than 1000 fibers) cables in single step. The other is a fiber-ribbon unit connector type to join high-count (less than 1000 fibers) cables. Connection times of 90 min. for the array type and 20 min. for the fiber unit type are achieved for both types of pre-connectorized cables. Average connection losses of about 0.35 dB for both types are achieved.

### 1. Introduction

Recently, ways to construct optical subscriber networks have been discussed. In Japan, NTT has a plan to construct optical subscriber cable networks to be called "Fiber-to-the-Home" (FTTH) by the year 2015 (OFL'21)<sup>(1)</sup>. Many different methods and approaches have been proposed in order to realize FTTH networks. For example, "Fiber-to-the-Curb" (FTTC) is proposed as a first step in the construction of FTTH, and active or passive double-star configurations are investigated to minimize the initial construction outlay. However, the infrastructure of the optical subscriber network must be able to cope promptly and flexibly with diverse and changable future demands.

Therefore, we started to develop technologies to construct a simple optical subscriber network in which each

customer can be connected to a central office through his own optical transmission line. The network formed by single-star configuration is adaptable to various kinds of services and can flexibly respond to future service expansion. In construction of these networks, very high count optical cables are required, and it is important to reduce the cable installation and splicing cost. Presently, 1000 fiber cables<sup>(2)</sup>, mechanically transferable (MT) connectors<sup>(3)</sup> and techniques for their connection are being used in subscriber networks in NTT. Therefore, higher speed and lower loss connection techniques are required to increase the flexibility and performance of the networks.

In this paper, we describe designs and performance for pre-connectorized high-count optical cables which can be simply connected at high speed with low connection loss.

### 2. Present joining techniques

Presently, we use the two technologies of mass-fusion splicing and MT connectors for optical fiber cable joining. Each of these techniques has its own advantages (Table 1). Mass-fusion splicing can achieve low splice loss, and the reliability of the spliced portion is very high. On the other hand, MT connector are fast and can be rapidly transferred from one ribbon to another by using a transferring system. Consequently, MT connectors have been used at connecting points where transferring will occur in the near future and mass-fusion splicing has been

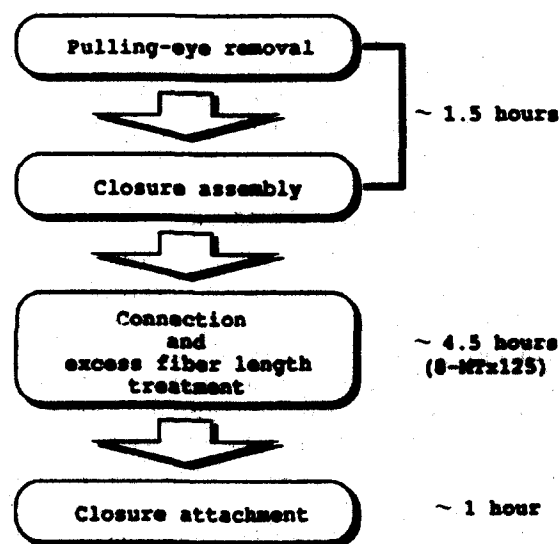


used at splicing points where transferring will not occur.

Figure 1 shows the connecting procedures for conventional pre-connectorized cable and the time required to connect the cable. In the case of MT connectors, whereby high-speed connection can be accomplished, it takes about one work day to join a 1000-fiber cable using conventional techniques. Therefore, it takes a huge amount of time to join the ultra-high-count optical cable<sup>(4)</sup> which has been considered in the construction of FTTH networks.

**Table 1 Features of Mass-fusion Splice and MT Connector Joining Techniques**

	Mass-fusion splice	MT Connector
Splice loss	Ave. 0.1 dB	Ave. 0.35 dB
Splice time	5 min./ ribbon	1 min./ ribbon
Loss change in heat-cycle test	< 0.05 dB (-40 °C ~ 60 °C)	< 0.2 dB (-40 °C ~ 60 °C)



**Fig.1 Connecting procedures for conventional pre-connectorized cable**

### 3. Design of new pre-connectorized cables

#### 3.1 Concepts for future joining technologies

NTT has started to develop an ultra-high-count cable having 4000 fibers for optical subscriber networks, so joining techniques for this new cable must be developed. In this case, optical cable joining technics should be simplified and the joining time should be extremely reduced. In order to satisfy these requirements, it is necessary to develop high-count pre-connectorized cables. In developing the high-count pre-connectorized cables, it is important to be able to connect many fibers in one connector and to simplify the treatment of excess fiber length in the junction box.

Therefore, we have developed high-count pre-connectorized cables by: (1) the development of stacked multiple-connectors; (2) the enlargement of fibers contained in multiple-connectors.

Of course, low connection loss must be maintained in these approaches. Moreover, it is necessary to reduce the connection loss, because of the high number of connecting points in subscriber loops.

#### 3.2 Structure of pre-connectorized cables

In developing high-count pre-connectorized cables, there is an important requirement which is related to installation condition. The inner diameter of conventional conduit is 75 mm. So, the pulling head including the connector protection, must be smaller than this. In considering this requirement, to confirm the limits on connection time, we studied new pre-connectorized cables of both the fiber ribbon unit connection type and the array connection type.

(1) Fiber ribbon unit connector type for high-count cables

We considered two types of connectors which have been used in these pre-connectorized cables. Figure 2 shows the structure of these connectors.

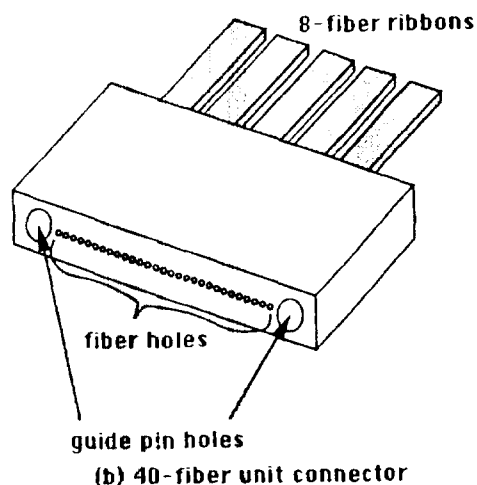
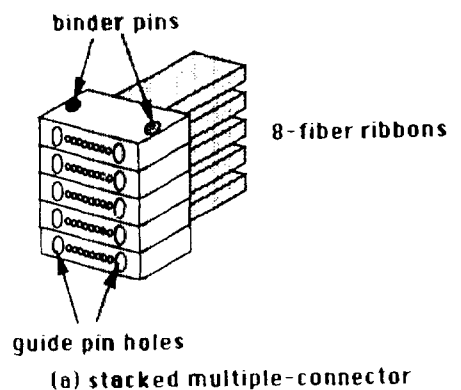


Fig.2 Structure of Fiber Ribbon Unit Connector

Figure 2(a) shows a stacked multiple-connector which is composed of 8-fiber-connectors, like the conventional 8-MT connector, and two pins to combine twelve 8-fiber-connectors. Each connector in the stacked connector is aligned by guide pins. Figure 2(b) shows a 40-fiber unit connector to which five 8-fiber ribbon were attached. The structure of 200-fiber pre-connectorized cable to which 40-fiber unit connectors were attached, and the connecting procedures are shown in Fig.3. The connecting procedures are as follows.

- (a) The pulling-eye is removed.
- (b) The under cover is attached.
- (c) Unit connectors, packaged in easy-access trays, are pulled out removed from the trays.
- (d) All unit connectors are connected.
- (e) Excess fiber lengths of unit connectors are pushed into the trays.
- (f) The upper cover is attached last.

The main feature of this type is easy fiber access and handling.

## (2) Array connector type for ultra-high-count cables

In the array connector type, it is important to arrange many connectors densely and to align them simultaneously. The cable-end structure of the 1000-fiber cable is shown in Fig.4. 125

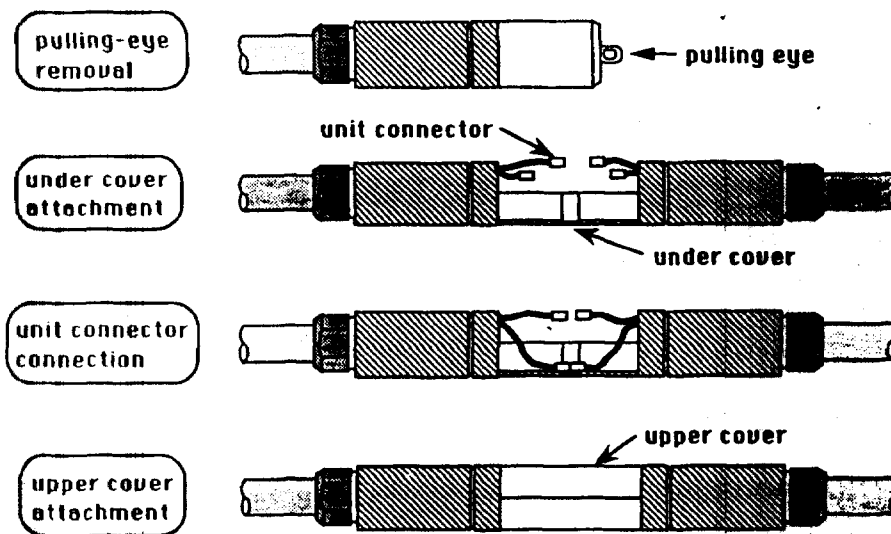


Fig.3 Cable-end structure of unit connection type, and connecting procedures

conventional 8-MT connectors are arranged in an array on each cable end. The cable end also has two large pins acting as cable guides. These pins are used to align the cable-end face. Connectors are aligned by guide pins which are held by each connector. The connecting procedures are as follows.

- (a) The pulling-eye is removed.
- (b) The cable-ends are butted together and fixed tightly by universal joint.

The main feature of this type is that all connectors can be connected in one action when the cable-ends are joined.

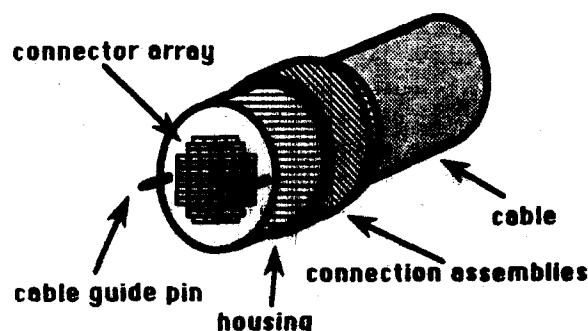


Fig. 4 Cable end structure of array connection type

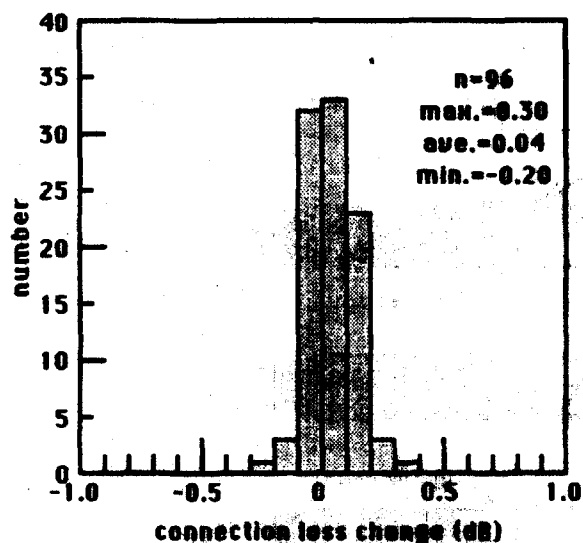


Fig. 5 Difference between stacked 8-fiber connector loss and each 8-fiber connector loss

#### 4. Performance

##### 4.1 Connection loss

Connection losses of stacked 8-fiber connectors relate to each 8-fiber connector's loss. So, we evaluated the connector loss of stacked connectors, comparing them with 8-fiber connector loss. Figure 5 is the histogram of the difference between stacked 8-fiber connector loss and 8-fiber connector loss. The average of increasing loss is about 0.04 dB. The influence of

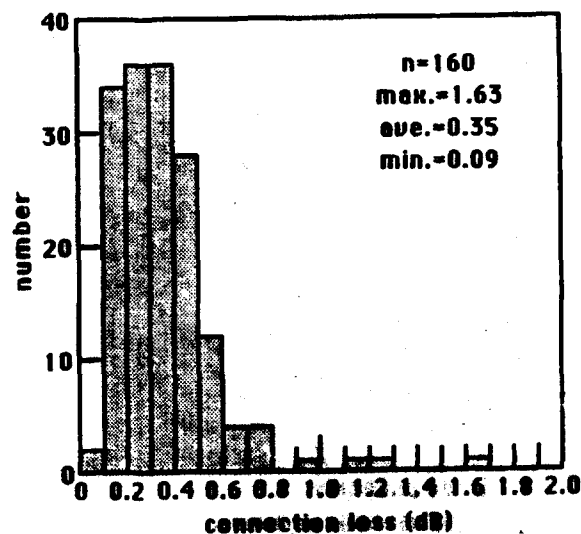


Fig. 6 Connection loss of pre-connectorized cable with 40-fiber unit connectors

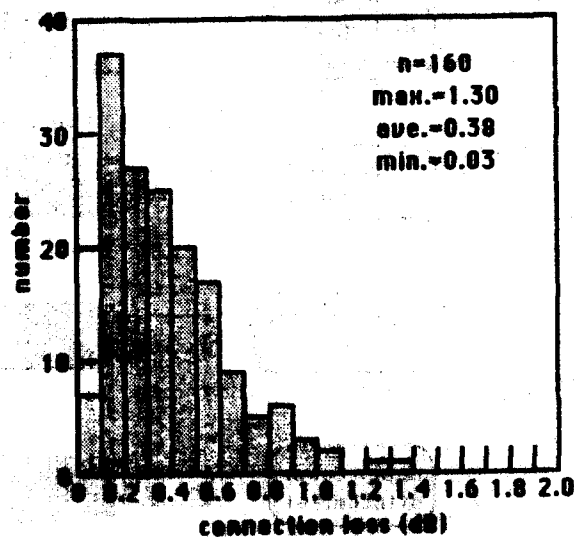


Fig. 7 Connection loss of 40-fiber unit connectors

stacking is sufficiently suppressed.

The connection loss histogram of pre-connectorized cable with 40-fiber unit connectors is shown in Fig.6. An average loss of 0.35 dB is achieved. Figure 7 is the loss histogram when 40-fiber connectors are connected with other 40-fiber connectors at random. The average loss is about 0.38 dB. These loss levels are the same as that of conventional 8-MT connector.

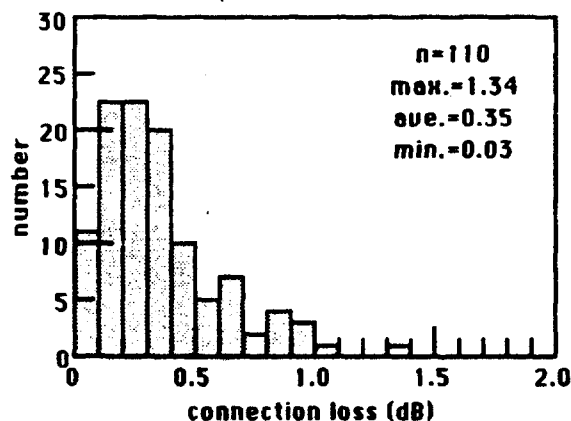


Fig.8 Connection loss histogram of array connection type

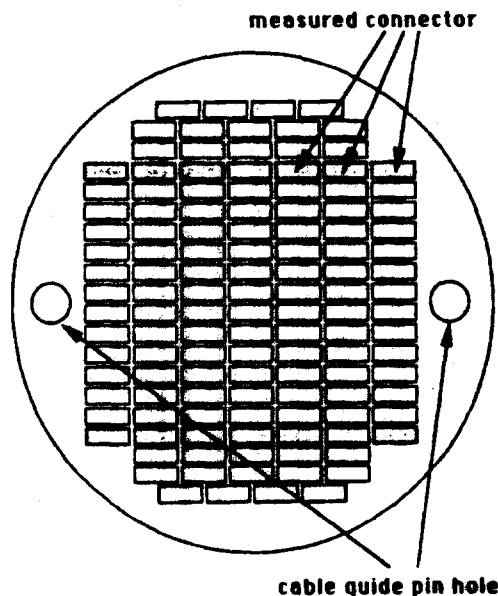


Fig.9 Measured connectors in array type

Figure 8 shows the connection loss histogram of the array connection type. Measured connectors are arranged in an array as shown in Fig.9. The average loss is 0.35 dB. In this array connection type, conventional 8-MT connectors were used, with an average loss of about 0.35 dB.

As described above, both types have sufficient performance to enable the construction of subscriber networks.

#### 4.2 Connection time

The processing time of pre-connectorized cable with 40-fiber unit connectors is shown in Fig.10. Connection time of about 20 minutes for 200-fiber cable is achieved. This is about 10 times faster than the speed attained by conventional connecting techniques. In this first trial, the fiber pitch of the 40-fiber connector is 0.25 mm. A higher-density unit connector is expected to be developed by decreasing fiber pitch. Consequently, a high-speed connection will be also achieved for more than 1000-fiber cables by combining higher-density unit connector and stacked multiple-connector techniques.

The processing time for the array connector type is shown in Fig.11. Connection time is about 90 minutes for

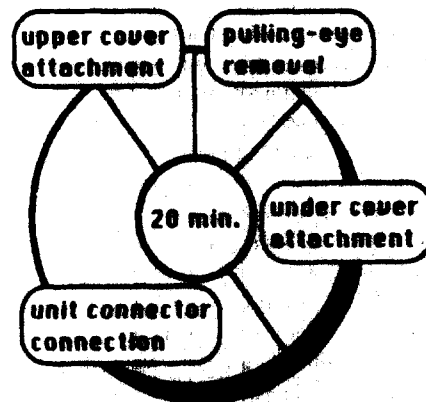


Fig.10 Processing time of unit connection type

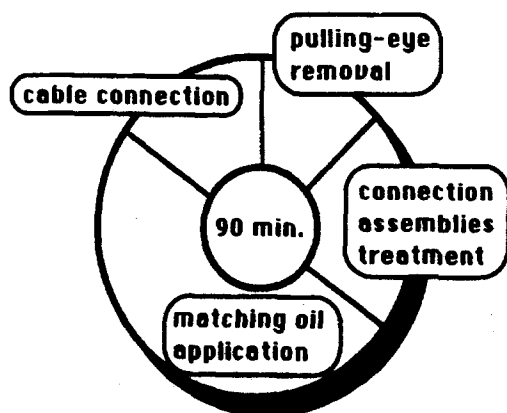


Fig.11 Processing time of array connection type.

1000-fiber cable. The main reason for the longer connection time of the array connector type, compared to the fiber unit connector type, is the connector end treatment, including oil application and insertion of many connector guide pins. This connector type can also be used for more-than-1000-fiber cables by using higher-density unit connectors.

### 5. Conclusions

We began to develop simple, high-speed and low-loss connection techniques which are indispensable for construction of optical subscriber cable networks for FTTH. We proposed new high-count pre-connectorized cables and evaluated the performance as a first step in the development of future joining technologies. The following results have been obtained with the new pre-connectorized cables.

- (1) Cables of 1000 fibers and 200 fibers can be connected in about 90 min. and about 20 min., respectively.
- (2) Average connection losses of 0.35 dB for array connection and about 0.35 dB for fiber unit connection are achieved.

These results show the newly proposed connection techniques to be useful in achieving FTTH.

### ACKNOWLEDGMENT

The authors express their sincere appreciation to Dr K. Ishihara and T. Uenoya for their helpful discussion and suggestions.

### REFERENCES

- (1) T. Uenoya, "The Optical Fiber Loop 21 Plan", OEC'90.
- (2) M. Kawase, T. Fuchigami, M. Matsumoto, S. Nagasawa, S. Tomita, and S. Takashima, "Subscriber Single-Mode optical fiber ribbon cable technologies suitable for mid-span access", J. of Lightwave Technology", Vol.7, No.11, November, 1989.
- (3) T. Haibara, S. Nagasawa, M. Matsumoto and M. Kawase, "Single-mode multifiber joining techniques for high-density high-count subscriber cables", Proceedings of 37th IWCS, 1988.
- (4) S. Tomita, M. Matsumoto, T. Yabuta and T. Uenoya, "Preliminary Research into Ultra High Density and High Count Optical Fiber Cables", to be submitted to 40th IWCS, 1991.

**Tadashi HAIBARA**

NTT  
Telecommunication Field  
Systems Research &  
Development Center  
Tokai, Ibaraki,  
319-11, JAPAN



Tadashi Haibara is a Senior Research Engineer of Telecommunication Field Systems Research and Development Center. He was born in 1956 and received B.E. and M.E. degrees in precision engineering from Hokkaido University in 1979 and 1981, respectively. He received Ph.D. degrees in precision engineering from Hokkaido University in 1989.

He joined NTT in 1981. Since 1990 he has been engaged in research on High-density and Pre-connectorized optical fiber cable.

Dr. Haibara is a member of IEEE.

**Shigeru TOMITA**

NTT  
Telecommunication Field  
Systems Research &  
Development Center  
Tokai, Ibaraki,  
319-11, JAPAN



Shigeru Tomita is a Research Engineer.

He was born in 1960 and received a B.E. degree in electrical engineering from Nihon University in 1983.

He joined NTT in 1983. Since 1990 he has been engaged in research on High-density and Pre-connectorized optical fiber cable.

Mr. Tomita is a member of IEEE.

**Michito MATSUMOTO**

NTT  
Telecommunication Field  
Systems Research &  
Development Center  
Tokai, Ibaraki,  
319-11, JAPAN



Michito Matsumoto is an Executive Research Engineer.

He was born in 1952 and received B.E. degree in electrical engineering from Kyushu Institute of Technology. He received M.E. and Ph.D. degrees in electronics engineering from Kyushu University in 1977 and 1987, respectively.

He joined NTT in 1977. Since 1990 he has been engaged in research on High-density and Pre-connectorized optical fiber cable.

Dr. Matsumoto is a member of IEEE.

**Tetsuro YABUTA**

NTT  
Telecommunication Field  
Systems Research &  
Development Center  
Tokai, Ibaraki,  
319-11, JAPAN



Tetsuro YABUTA is an Executive Research Engineer.

He was born in 1949 and received B.E. and M.E. degrees in electronics engineering from Tokyo University in 1972 and 1974, respectively. He received Ph.D. degrees in mechanical engineering from Tohoku University in 1984.

He joined NTT in 1974. Since 1990 he has been engaged in research on High-density and Pre-connectorized optical fiber cable.

Dr. Yabuta is a member of IEEE.

## AUTOMATED MOUNTING OF CONNECTORS TO FIBER OPTIC CABLES

Johann Schulte

Kabelmetal Electro GmbH  
Postfach 260, 3000 Hannover 1, Germany

### Abstract.

Fiber optic cable installations require cables terminated with connectors. The ever-increasing demand for these products calls for automation of the presently used manual assembly methods, so as to ensure cost reduction and the attainment of a uniform quality level. This requires consideration of the specific properties of fiber optic cables and optical connectors: most of the fiber optic cables contain tough and hard-to-cut aramid yarns, the fiber is extremely delicate and the assembly of optical connectors requires a certain degree of dexterity. This paper will describe how a specially-developed process renders possible the automated mounting of fiber optic connectors.

### Introduction.

The growth of fiber optic cables in local networks<sup>1</sup> and in the subscriber loop<sup>2</sup> places the connection techniques into increasing focus. While telecommunication trunk links which make up today's major part of fiber optic applications have distances between connections on the order of several tens of km, the corresponding interval in these new applications shrinks to the order of 1 km (0.6 mi) and to substantially less than that, in LANs. With interconnections assuming an increasing portion of the overall costs, it has become necessary to concentrate on reducing the cost of the connectors as well as the cost of their assembling and testing without affecting their optical properties.

The assembling of cables with connectors can be carried out either on-site or through the use of pre-connectorized cables or by splicing-on connectorized pigtails. Although some connectors were developed to facilitate on-site installation, this procedure which requires measurement of the optical properties continues to be cumbersome and prone to failure. A further problem connected with on-site installation is the

required assembly time. The installation of a LAN, for example, may interfere considerably with the normal business activity of a customer.

Connectors are assembled and installed under optimal conditions in a factory environment. Quantity production can result in cost-effectiveness without sacrificing the demanding requirements placed on the optical characteristics. Automated assembly ensures a reproducible and reliable manufacturing process. As far as we know, the market provides no satisfactory solution for the automated mounting of optical connectors. We therefore investigated the possibility of automated assembly and this paper reports the results of our work.

### Optical Connectors and the Mounting of Optical Connectors.

We limit our description to the mounting of single-fiber connectors to cables whose single fiber has the following dimensions:

Cladding dia.:	125 $\mu\text{m}$
Primary coating dia.:	250 $\mu\text{m}$
Secondary coating dia.:	900 $\mu\text{m}$

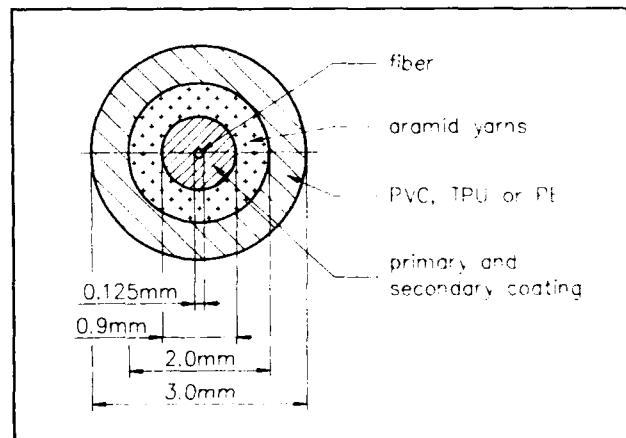


Fig. 1 Indoor cable containing one optical fiber (cross-section)

The secondary coating may be "loose" or "tight". Our cable design utilizes aramid yarns as strength members and a PVC, PE or TPU outer jacket. The outer diameter of the cable is between 2.2 and 3.5 mm (0.087" and .138"). Fig. 1 shows a typical cross-section.

The market offers a great number of different optical connectors for either single-mode or multi-mode fibers. We shall limit our description to connectors that utilize a ferrule to guide the fiber. These are distinguished by the following features:

- their design, which allows for the lateral adjustment between the cores of adjoining fibers;
- their ability to allow for physical contact or no physical contact between adjoining cores;
- the design of their mechanical coupling mechanism;
- the manner in which the cable is secured;
- the number of component parts and their assembly;
- the use of adhesives and their curing;
- the finishing of the ferrule face (polishing).

The lateral alignment of the fiber extremities may make use of active methods (i.e.: the fiber end is fine-positioned and tied down under the microscope) and of passive methods, in which high-precision ferrules are used to guide the fiber. The automated mounting of the connectors is greatly simplified using the passive method. We are limiting ourselves to the implementation of this type of connector.

The cable is attached to the connector body by crimping a sleeve to the back part of the connector, whereby the aramid yarns are seized at the same time. Occasional use is also made of adhesives. We utilize connectors which secure the cable by crimping without the use of adhesives. Only in the ferrule is the fiber secured by an adhesive for which we generally use a two-component epoxy.

The most popular connectors consist of anywhere between two and eight component parts, including the boot. For the automated mounting procedure we have considered only those connectors which are simple to assemble. They consist of three parts:

- connector body;
- crimp sleeve;
- boot.

One such connector, for example, is the EC-connector which is described in another paper of this Symposium<sup>3</sup>. For automated mounting this connector can be purchased with a pre-mounted barrel. Fig. 2 illustrates its component parts.

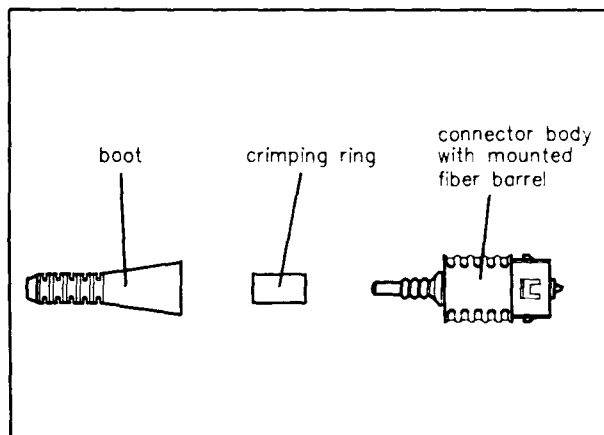


Fig. 2 EC-connector (parts break-down)

The curing of the epoxy which secures the fiber in the ferrule and the polishing of the tip of the ferrule are time-consuming steps. The best way to treat them is to process several connectors at a time, ten for example, using special equipment made available by connector manufacturers for this purpose.

#### Automated Connector Mounting.

The following assembly sequence must generally be observed:

#### Cable Preparation.

The cable must be cut to length from its reel and the jacket must be stripped back to a prescribed dimension. The exposed aramid yarns must be seized and cut back. The primary and secondary coatings must then be removed neatly to the prescribed length for the particular connector.

#### Affixing the Connector Component Parts to the Cable.

The assembly sequencing depends on the type of connector used. In general, the following steps are required: the boot and the crimp sleeve must be threaded onto the cable. The connector body is then filled with an epoxy and the fiber is inserted into the connector and ferrule. Finally, the crimp sleeve is crimped down to provide strain relief and the boot is attached.



### Curing the Epoxy.

Most connectors utilize a two-component epoxy for bonding the fiber to the ferrule. This epoxy cures in several minutes at elevated temperature. For this step a number of assembled connectors are jointly placed onto a specially-adapted hot plate.

### Polishing the Ferrule Tip.

Once the epoxy has hardened, that part of the fiber which protrudes from the ferrule must be scored and snipped off. Next, the tip of the ferrule must be polished according to a specified procedure. The polishing, too, is conducted simultaneously on a certain number of connectors.

### Testing of Assembled Connectors.

The success of the connector mounting operation is verified through measurement by comparing the insertion and reflection losses to the specified values.

### Principal Steps in Automated Connector Mounting.

Automatic or semi-automatic devices for cutting the cables to length, for the adhesive curing and for the polishing of the ferrule tip are commercially available. Fig. 3 illustrates schematically our automated connector mounting sequence. The concept includes several work stations for the preparation of the cable ends and for attaching the connector.

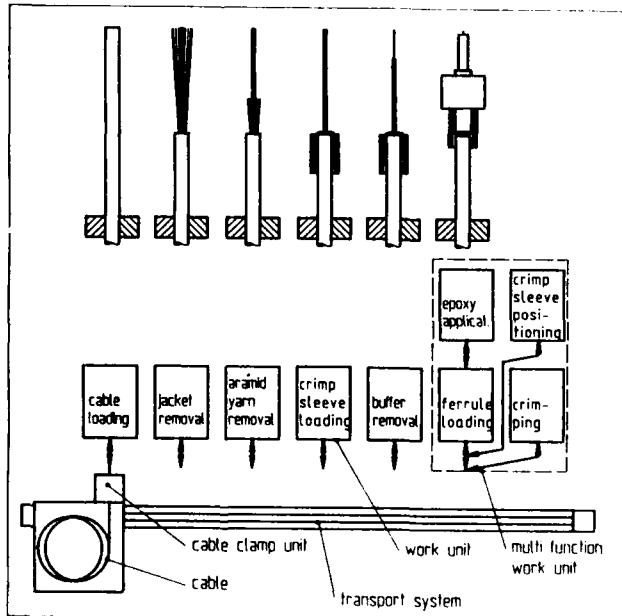


Fig. 3 Principle of the automated connector mounting set-up

The cable is transported between individual work stations on a support which rests on a moving belt. Fig. 3 also shows the condition of the cable end after each process step. The following explanation provides details of these individual steps:

Cable Loading. The cable end is manually loaded into the cable loading station. An automatic grip mechanism ensures that the end of the cable protrudes from the cable retainer of the transport system by a predetermined length. Thereupon the cable is moved on to the next station.

Jacket Removal. Two blades are passed over the cable end for the purpose of scoring and removing the jacket. The aramid yarns are now exposed.

Aramid Yarn Removal. As a first step, the aramid yarns which adhered slightly to the secondary coating are now freed. Next they are stretched into a defined position before being cut back to the required length.

Crimp Sleeve Loading. The required crimp sleeve is now pulled over the cable in such a manner that the aramid yarns are pushed back over the jacket. This prevents them from interfering with further processing.

Buffer Removal. Two precisely adjusted blades cut into the coating and pull it off. Additionally, the coating may be softened by heating. On cable types with which we have experience, the optical fiber is free from any residue following this step. It is possible that additional cleaning may be required with other cable types.

Connector Mounting. In the last work station several steps are carried out in sequence:

- the connector is subjected to a precisely metered epoxy application through a hollow needle (Fig. 4);
- the connector is then placed over the cable end at a preset speed through a linear drive motor (ferrule loading) (Fig. 5);
- the aramid yarns are loosened and the crimp sleeve together with the aramid yarns are placed over the rear portion of the connector (crimp sleeve positioning) (Fig. 6).
- finally, the sleeve is crimped.

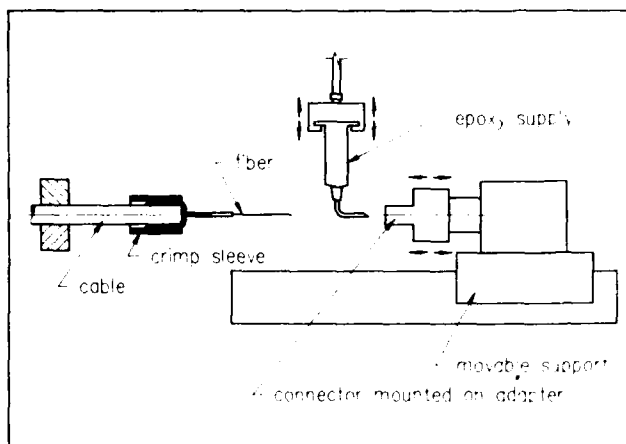


Fig. 4 Epoxy application to the connector

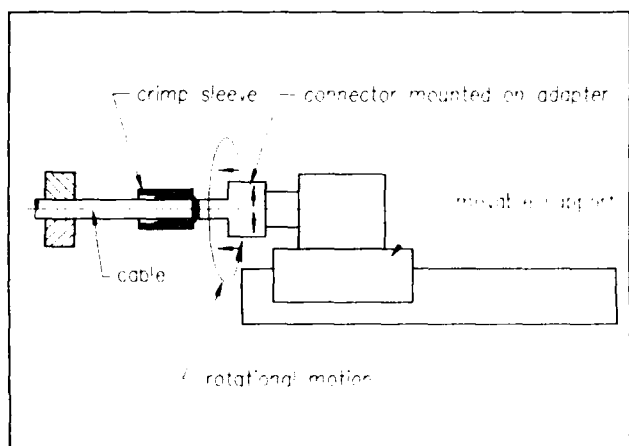


Fig. 5 Applying the connector to the fiber

This last step completes the mounting of the connector and the terminated cable may now be removed from the device. For the required curing of the epoxy and the ensuing polishing of the face of the ferrule several connectors may be gathered together for simultaneous processing.

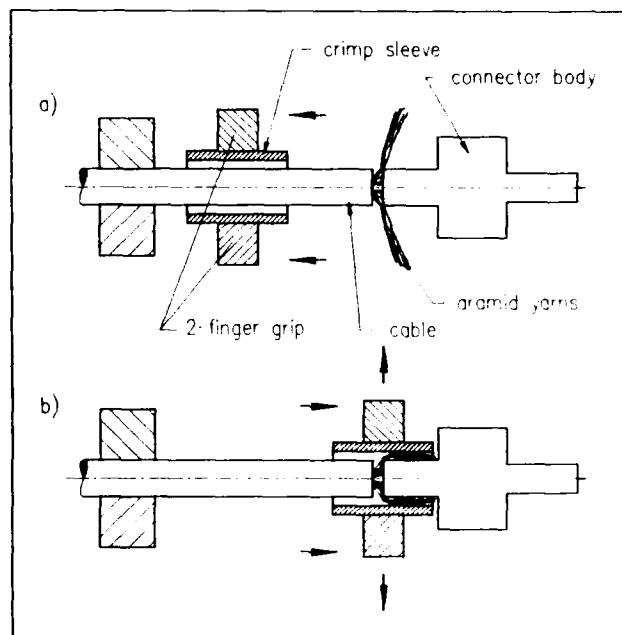


Fig. 6 Positioning of the crimp sleeve

### Results.

Experience gained with this system, using the EC-connector, confirmed that the automated mounting of fiber optic connectors is possible. The various cable members can be cut to the exact length with the required degree of precision and the fiber can be introduced mechanically into the connector body. It is therefore necessary that the connector ferrule be provided with an internal bore hole that corresponds to the diameter of the particular fiber. Fig. 7 illustrates the strip-back dimensions required for the connector mounting operation.

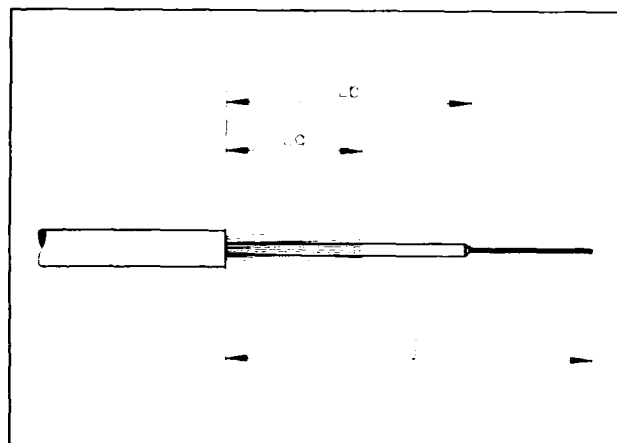


Fig. 7 Definition of individual strip-back dimensions

The following definitions refer to Fig. 7:

$L_j$  = jacket strip-back length  
 $L_j^a$  = remaining length of the aramid yarn  
 $L_b^a$  = remaining length of the coating

The results achieved on one-hundred (100) cables are shown in Figs. 8a through 8c. The standard deviation ( $s$ ) of these values is on the order of 0.5 mm. This value is less than that normally experienced with manual mounting and therefore entirely satisfactory. The epoxy filling, the introduction of the fiber and the crimping operation show results comparable to those experienced with manual connector mounting.

Table 1 illustrates the time required for the execution of the individual steps. The present state of development of this technique leads to a cumulative total assembly time of about one minute. It is felt that this can still be reduced.

It may become necessary to alter the details and the sequencing of the individual assembly steps, depending on the type of cable or connector used. Once the connector is assembled, the epoxy must still be cured and the face of the ferrule must be polished.

#### Summary.

We have demonstrated that the automated mounting of connectors to fiber optic cables is possible. The time required at the present stage of development is about one minute. The curing of the epoxy and the polishing of the face of the ferrules must be carried out in parallel on batches of connectors. Thus, 480 connectors can be mounted in about eight hours. It is possible to increase the efficiency of the process if the work stations are set up for simultaneous operation on the cable ends, that is, if several cable ends are being worked on at the same time. This permits the actual mounting of the connector to be divided over several work stations, thus lowering the time cycle.

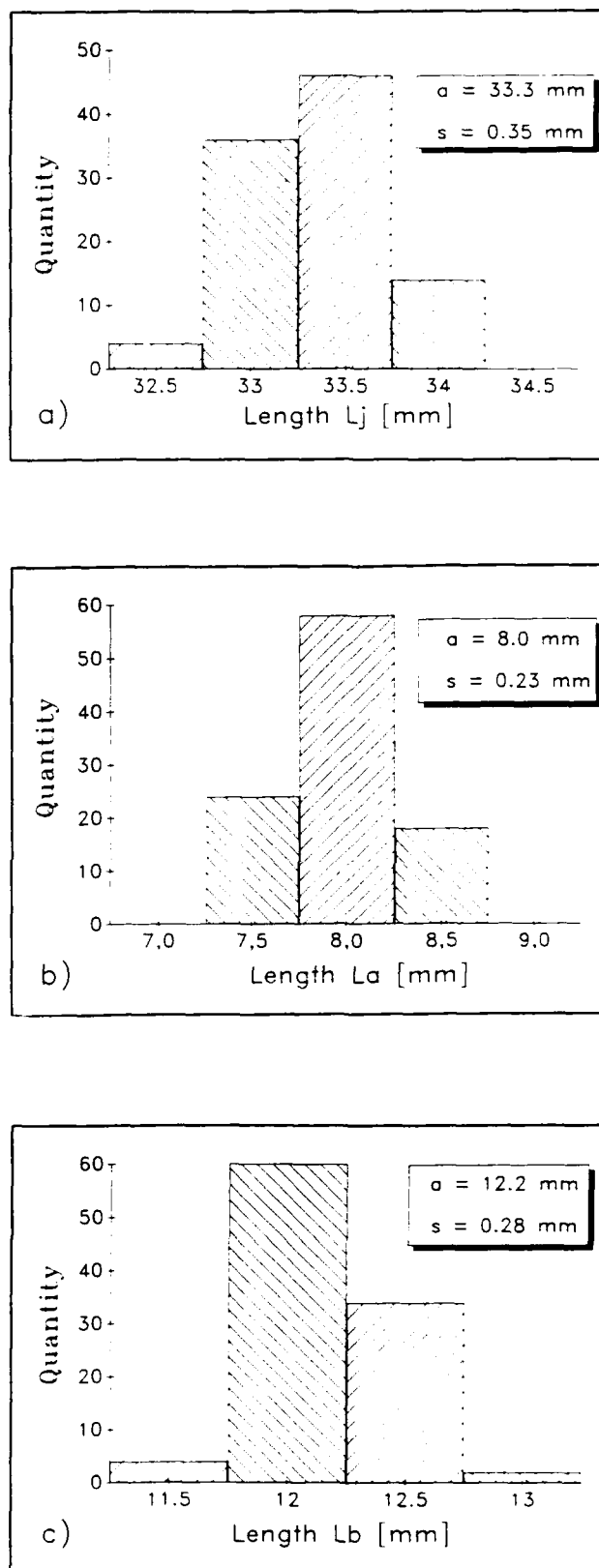


Fig. 8 Statistical distribution of measured strip-back lengths

Operation:	Elapsed time (sec.)
Cable transport	5
Load cable	4
Strip back jacket	2
Cut aramid yarns	4
Place crimp sleeve	4
Remove coating	6
Mount connector	35
	----
Total time:	60

Table 1: Automated fiber optic connector mounting. Required time for individual operations.

#### Acknowledgments.

The work described in this paper was promoted by the European Community within the framework of the LOOP (Low-Cost Optimized Optical Passive Components) Project as part of the RACE (Research and Development in Advanced Communications Technologies in Europe) Program. The author wishes to thank Mr. H. Hofheimer of Cable Consultants Corp., Larchmont NY for his valuable assistance in preparing this paper.

#### References.

1. G.Evers, "Light for Data Communication", to be published in "Electrical Communication".
2. C. Tenzer, "Glasfaser bis zum Haus/ Fiber to the Home", R. v. Decker's Verlag, Heidelberg, 1991.
3. H. Deharde, J. Schulte, G. Billet, H. B. Yin, S. Crico, J.J. Crosnier, M. Lincot, A. Fielding, J. S. Leach, "High Performance and Low Cost Passive Optical Components for the Subscriber Loop", Proceeds. IWCS 1991.



Johann Schulte received his physics degree in quantum optics in 1981 and his Ph. D. in engineering in 1986 from the Technical University Hannover. After a research fellowship at IBM, Yorktown Heights NY, he joined Kabelmetal Electro in 1987, where he has been engaged in the development of fiber optic cables.

# LONG-TERM RELIABILITY ASSURANCE FOR MASS-FUSION SPLICED FIBER RIBBON

Masahiro HAMADA

Isamu FUJITA

Keiji OSAKA

Yasuo ASANO

Optomechatronics systems R&D Dept., Yokohama Research Labs.,  
Sumitomo Electric Industries, LTD.

## Abstract

In order to assure long-term reliability for fusion spliced fiber, it is necessary to eliminate weak splices by a screening test before reinforcement. This paper explains the failure mechanism of mass-fusion spliced fibers and the theory concerning the failure strength for mass-fusion spliced fiber ribbon. Thus it was demonstrated that the failure strength for mass-fusion spliced fiber ribbon can be estimated well using numerical simulation. Based on the conventional screening theory, the appropriate tensile load during the screening test is derived from failure strength for any number of mass-fusion spliced fibers in a ribbon. In case of 12 fibers, it is sufficient to apply a tensile load of 0.3kg in order to keep the failure probability lower than  $10^{-7}$  for 20 years.

## 1. Introduction

Recently, high-count, high-density optical fiber cables were introduced into subscriber networks, thus the mass-fusion splicing technologies have been developed for the purpose of joining optical fiber ribbon quickly and economically.

It was reported that an automatic splice machine capable of mass-splicing up to 12-fiber ribbons with loss lower than 0.1dB was developed<sup>[1]</sup>. While the theory of long-term reliability for the fusion spliced single-fiber was reported<sup>[2]</sup>, it has not been discussed in detail so far for the mass-fusion spliced fiber ribbon.

In this paper, firstly the failure mechanism of mass-fusion spliced fibers is cleared. Next a theory of failure strength for mass-fusion spliced fiber ribbon is proposed. Lastly the appropriate tensile load to assure a long-term reliability is calculated using an equation based on the experimental results. In the present mass-fusion splicer, the number of fibers in a ribbon can be selected from 1 to 12. The machine automatically realizes the optimum fusion condition. For such

a splicer, a decision of an appropriate tensile load is important.

## 2. Screening theory for spliced single-fiber

An optimum reinforcement method increases the initial reliability in spliced points. However, as there may be some defective splices, weak points among spliced portions must be eliminated through a screening test with appropriate tensile load from the viewpoint of long-term reliability assurance. Usually a screening test is performed after splicing and before reinforcement. It is very difficult to find the fault with the reinforced fibers, especially with mass-fusion spliced fiber ribbon. For the reason, it is important to decide the appropriate tensile load.

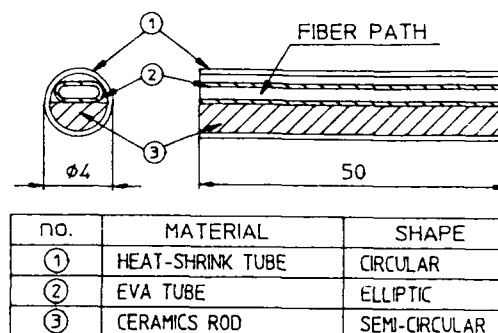


FIG.1 CURRENT REINFORCEMENT STRUCTURE FOR MASS-FUSION SPLICED FIBER

Fig.1 shows the structure of a typical protection sleeve for reinforcement after splicing. It is composed of 3 elements, a heat-shrink tube, a hot-melt adhesive tube of EVA and a tension member. The protection sleeve is inserted over the spliced portions and heated. After this process, the splice protection is

exposed under various environments. Thermal stress,  $\sigma_s$ , caused in fibers is one of the major factors for long term reliability. Thermal stress in a fiber, which is caused by the difference of thermal expansion coefficient among the elements of protection sleeve and the fiber, is given by the following equation:

$$\sigma_s = \frac{(\alpha_2 - \alpha_1)A_2E_2 + (\alpha_3 - \alpha_1)A_3E_3}{A_1E_1 + A_2E_2 + A_3E_3} \epsilon_1 \Delta T \quad (1)$$

where  $\alpha$ ,  $A$  and  $E$  denote the thermal-expansion coefficient, cross-sectional area, and Young's modulus, respectively and subscripts 1, 2, and 3 indicate fiber, adhesive resin (EVA) and tension member, respectively.

Concerning the spliced single-fiber, it was reported the relationship between thermal stress and tensile load during screening test to assure a long-term reliability<sup>(2)</sup>. According to the paper, in order to keep the failure probability lower than  $10^{-7}$  for 20 years, tensile load four times as large as the maximum thermal stress must be applied. Therefore, in case a fluctuation range of temperature  $\Delta T$  is from  $-40$  to  $70^\circ\text{C}$  and the tension member is stainless steel rod, which is used conventionally, the thermal stress is calculated at  $9\text{kg/mm}^2$  using Eq.(1). Thus tensile load becomes  $36\text{kg/mm}^2$  ( $=9\text{kg/mm}^2 \times 4$ ), that is equivalent to the strength of  $0.45\text{kg}$  for a fiber (its diameter is  $125\mu\text{m}$ ). Recently, instead of stainless steel rod, ceramics rod is being used as a tension member. As the thermal-expansion coefficient of ceramics is closer to that of fiber, the thermal stress calculated by Eq.(1) is reduced to  $0.8\text{kg/mm}^2$ . Consequently it is sufficient to apply  $3.2\text{kg/mm}^2$ , that corresponds to  $0.04\text{kg}$  per one fiber, as a tensile load in order to assure the failure probability  $10^{-7}$  for 20 years. The relationship between tensile load and failure probability is shown in Fig.2. As a result, a ceramics tension member needs 1/11 tensile load compared with a stainless steel tension member.

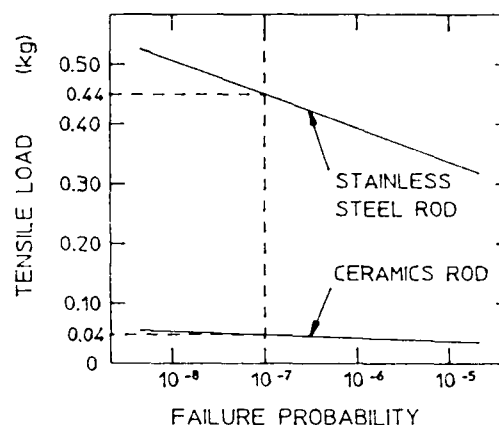


FIG.2 RELATIONSHIP BETWEEN FAILURE PROBABILITY AND TENSILE LOAD FOR SPLICED SINGLE-FIBER

### 3. Screening condition for mass-fusion splicing

#### 3-1 Theory of failure strength

In the present mass-fusion splicing procedure, jacket removing, cleaving are done simultaneously to the fibers in a ribbon. After the cleaving, each fiber in a ribbon is placed face to face on each V-groove, and mass-fusion spliced with an electric arc (Fig.3). However after mass-fusion splicing, the fibers in a ribbon does not break simultaneously but they may break one by one by an accident.

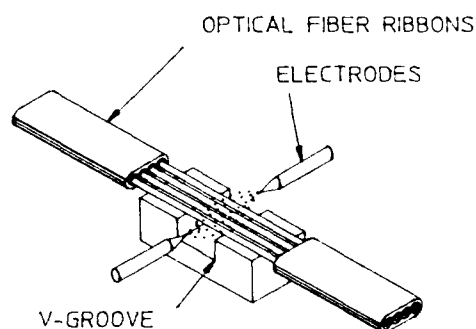
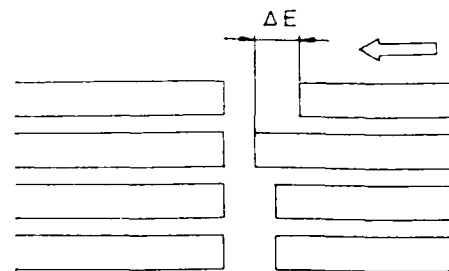
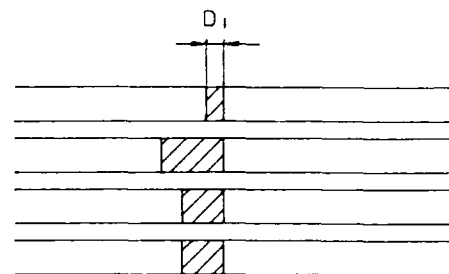


FIG.3 MASS-FUSION SPLICING

Accordingly we analyzed the failure mechanism of mass-fusion spliced fibers at first. In a mass-fusion splicing, it was uncertain whether the fusion conditions for every fiber were uniform. For the purpose, Thus it is important to know the effect of fusion conditions to failure strength of each mass-fusion spliced fibers. Two particular fusion conditions over mass-fusion splicing are considered. One is the difference of the arc power applied to the fiber placed on the each V-groove. This may be caused by thermal distribution of electric arc. Fig.4 shows the failure strength distributions of individual fibers taken from the mass-fusion spliced 12-fiber ribbons. The failure strength did not depend on the position of fibers. The other is the difference of stuffing stroke of each fibers after arc as illustrated in Fig.5. The allowable variance of cleaved length is pre-set  $30\text{ }\mu\text{m}$  on one side of the fibers to be spliced. Thus the difference of the stuffing stroke is occurred from 20 to  $80\text{ }\mu\text{m}$ . Finally after splicing, all fibers become the same length, and never show the curving or bending. Fig.6 shows the relationship between the failure strength and stuffing stroke of each fibers. The failure strength was found independent of the difference of stuffing stroke either. From these results, it was clarified that the failure strength of mass-fusion spliced fibers were scarcely affected by the slight difference of fusion conditions. At the same time, the average failure strength of individual fiber is obtained at  $0.6\text{kg}$ .



(a) FIBERS BEFORE SPLICING



(b) FIBERS AFTER SPLICING

FIG.5 DIFFERENCE OF STUFFING STROKE FOR EACH FIBERS

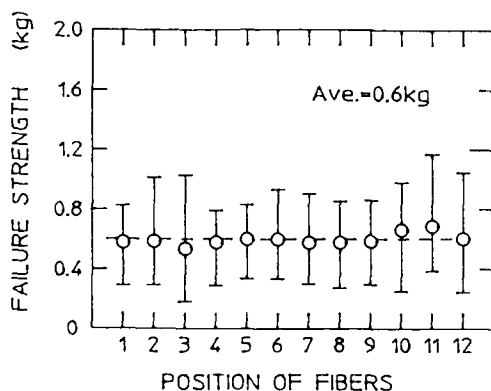


FIG.4 INDIVIDUAL FAILURE STRENGTH OF FIBER ON EACH V-GROOVE

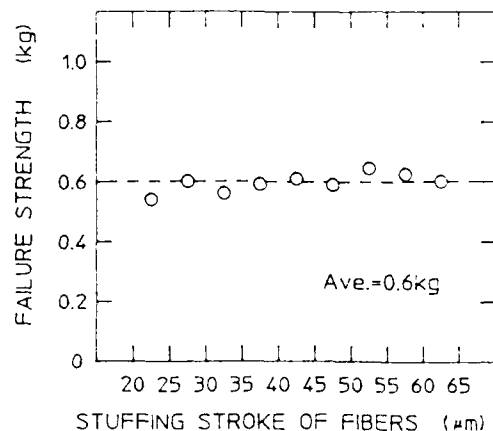


FIG.6 PLOT OF FAILURE STRENGTH VS. STUFFING STROKE

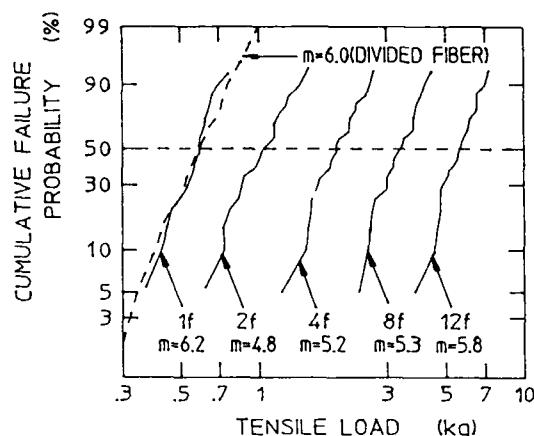


FIG.7 WEIBULL PLOTS OF FAILURE PROBABILITY OF MASS-FUSION SPLICED FIBER (DASHED LINE IS FIBER DIVIDED FROM 12-FIBERS RIBBON)

Next, in order to clear the failure mechanism of mass-fusion spliced fibers in more detail, we measured the failure strength of the mass-fusion spliced fiber ribbon. Here, the failure strength of mass-fusion spliced fiber ribbon is defined as the load when the first breakage occurred in spliced fibers in a ribbon by increasing tensile load. Fig.7 shows the distribution of failure strength for each number of the mass-fusion spliced fibers in a ribbon on the Weibull chart. 1f, 2f, ..., 12f in the figure mean the number of mass-fusion spliced fibers in a ribbon. The  $m$  value derived from the gradient of approximated line on Weibull chart does not depend on the number of fibers. Furthermore, the failure strength distribution of individual fibers taken from mass-fusion spliced fiber ribbon, as indicated by the dashed line in Fig.7, is almost the same inclination as the distribution for spliced single-fiber. Therefore it is clear that one spliced fiber taken from the mass-fusion spliced fiber ribbon is equivalent to the spliced single-fiber chosen at random. Based on these results, we introduced the following theory<sup>(3)</sup>;

— The distribution of failure strength for  $N$ -fiber ribbon is calculated using the minimum failure value in  $N$  samples that are extracted at random from the distribution of failure strength of a spliced single-fiber. —

Here,  $N$  indicates the number of fibers in a ribbon. This is explained in Fig.8. The upper figure shows the distribution of the failure strength for spliced single-fibers. When  $N$  samples,  $A_1$  ( $i=1, 2, \dots, N$ ), are extracted from

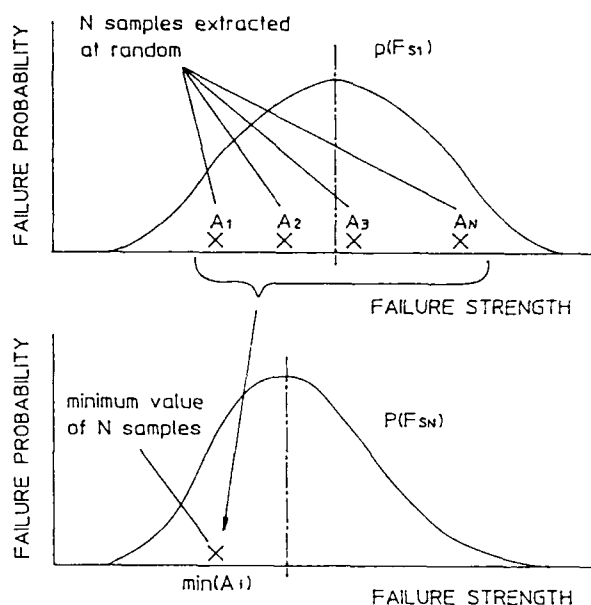


FIG.8 DISTRIBUTION OF FAILURE STRENGTH PER ONE FUSION-SPLICED FIBER

this group at random, it is treated that a set of  $N$  samples is equivalent to a  $N$ -fibers ribbon. In case that a tensile strength  $F_S$  applies to  $N$ -fibers in a ribbon, it is considered that the  $F_S/N$  is equally applied to each fiber until first breakage. Therefore the failure strength of mass-fusion spliced fiber ribbon is dominated by the weakest fiber in a ribbon. In other words,

the failure strength per one fiber among mass-fusion spliced fibers is calculated by the minimum value of  $N$ -samples as is shown in the lower figure.

In case the above theory is expressed by numerical equation, the distribution of failure strength  $P(F_{SN})$  for mass-fusion spliced fibers is as following:

$$P(F_{SN}) = N \cdot p(F_{S1}) \left\{ \int_{F_{SN}}^{\infty} p(F_{S1}) dF_{S1} \right\}^{N-1} \quad (2)$$

where  $p(F_{S1})$  is the distribution of failure strength for spliced single-fibers. Fig.9 shows the mean values of failure strength calculated by Eq.(2) and actually measured for up to 12-fiber ribbon. It is apparent that the failure strength for mass-fusion spliced fiber ribbon was estimated well. Consequently, the above theory is justified.



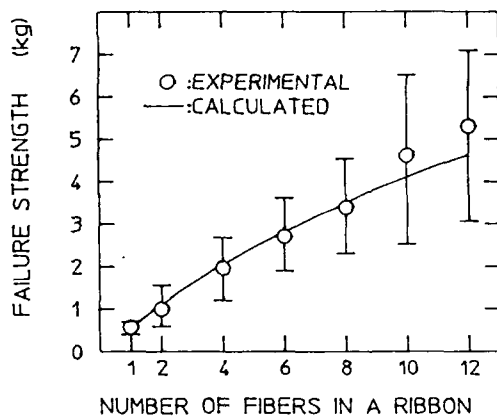


FIG.9 RELATIONSHIP BETWEEN FAILURE STRENGTH AND NUMBER OF MASS-FUSION SPLICED FIBERS IN A RIBBON

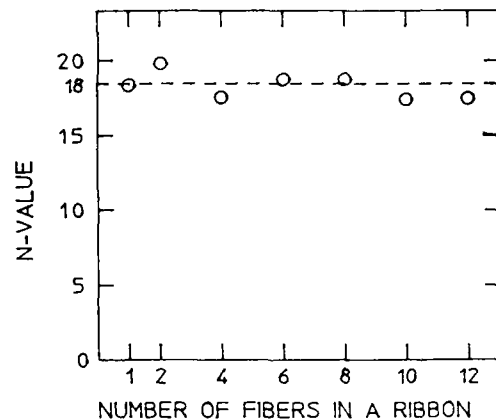


FIG.10 RELATIONSHIP BETWEEN DYNAMIC FATIGUE PARAMETER (N VALUE) AND NUMBER OF FIBERS IN A RIBBON

### 3-2 Appropriate tensile load during screening test

According to Ref.[2], when the thermal stress,  $\sigma_s$ , is applied to a fusion spliced portion after a screening test, failure probability,  $F_s$ , is expressed by the following equation in case of a spliced single-fiber.

$$F_s = 1 - \exp \left[ -N_P \cdot \frac{m_1}{n_1 - 2} \left( \frac{\sigma_s}{\sigma_p} \right)^{n_1} \cdot \frac{t_s}{t_p} \right] \quad (3)$$

where  $\sigma_p$  is tensile load,  $t_p$  is tensile duration,  $t_s$  is time-to-failure,  $N_P$  is failure probability during screening test,  $n_1$  and  $m_1$  are constants. This  $m_1$  value is derived from Weibull distribution shown in Fig.6 and the  $n_1$  value indicates the dynamic fatigue parameter. Fig.10 shows the relationship between measured  $n$  values and the number of mass-fusion spliced fibers in a ribbon. It was found that the  $n$  values did not depend on the number of mass-fusion spliced fibers. Thus it is possible to use common  $m_1$  and  $n_1$  values for any number of fibers in Eq.(3). Using the following parameters:  $n_1=18$ ,  $m_1=5$ ,  $t_p=1\text{sec}$ ,  $t_s=20\text{years}$ ,  $F_s=10^{-7}$ , tensile load,  $F_L(N)$ , is obtained by the following equation:

$$F_L(N) = (4 + 0.5 \log N) \cdot \sigma_s \left\{ \frac{P(F_{SN})}{p(F_{S1})} \right\}^{0.7} \quad (4)$$

where  $p(F_{S1})$  is the mean of failure strength for spliced single-fiber,  $P(F_{SN})$  is the mean of failure strength for  $N$ -fiber, which is calculated from Eq.(2), and  $\sigma_s$  is the thermal stress described in section 2 for spliced single-fiber, in this case ceramics tension member is used.

Fig.11 shows the tensile load which can be calculated by Eq.(4) for any number of mass-fusion spliced fibers.

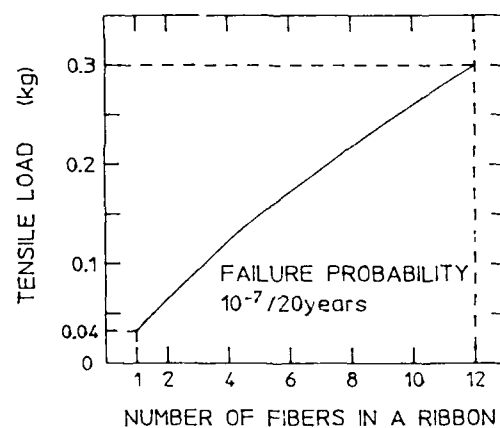


FIG.11 FAILURE PROBABILITY DEPENDENCY ON THE NUMBER OF MASS-FUSION SPLICED FIBERS IN A RIBBON

#### 4. Result of static fatigue test

The static fatigue of mass-fusion spliced fiber ribbon was tested by applying a static load for a long period. If a static load,  $\sigma_s$ , equivalent to thermal stress to the spliced portion, is applied after the screening test, time-to-failure,  $t_s$ , is expressed as follows<sup>[5]</sup>

$$\log t_s = -n' \cdot \log \sigma_s + \log k_s \quad (5)$$

where  $n'$  and  $k_s$  are constants, determined by material and ambient conditions. It is known that  $n'$  is equivalent to dynamic fatigue parameter,  $n$ , obtained from the experiments.

It was confirmed through the experiments that there was no breakage for 20 samples during a period of 3 months ( $10^5$  min.), in case the applied static load,  $\sigma_s$ , is 0.30kg for fibers after screening test. As the relationship between the time-to-failure and the static load is shown in Fig.12 derived from Eq.(5), it is estimated that the life time of spliced fibers under a static load of 0.22kg, which is bigger than the thermal stress discussed in section 2, is longer than 20 years ( $10^7$  min.).

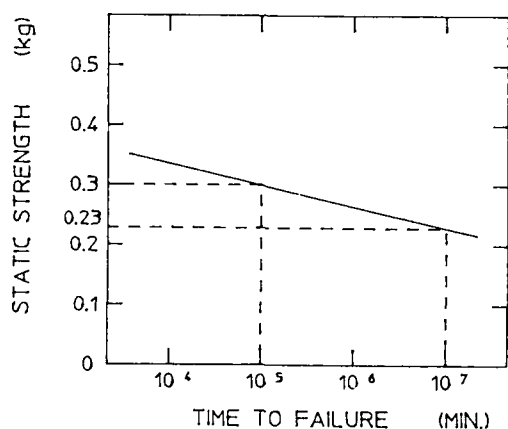


FIG.12 RELATIONSHIP BETWEEN STATIC STRENGTH AND TIME-TO-FAILURE

#### 5. Conclusion

The failure mechanism of mass-fusion spliced fibers was investigated. The tensile load on screening test to assure a long-term reliability for mass-fusion spliced fiber ribbon was described. The main results were as follows:

(1) It is demonstrated that the failure strength of mass-fusion spliced fibers is scarcely affected by the slight difference of fusion conditions.

(2) It is clarified that the distribution of failure strength for mass-fusion spliced fiber ribbon fit well to Weibull plot and the  $m$  value ( $\approx 6$ ) hardly depends on the number of mass-fusion spliced fibers in a ribbon.

(3) The failure strength for mass-fusion spliced fiber ribbon was estimated well by a numerical simulation using the failure strength results for spliced single-fibers.

(4) The appropriate tensile load to assure a long-term reliability was calculated using an equation based on previous results. The equation is applied to any number of mass-fusion spliced fibers in a ribbon.

(5) In case of 12 fibers, it is sufficient to apply a tensile load of 0.3kg during the screening test before reinforcement in order to keep the failure probability lower than  $10^{-7}$  for 20 years.

#### Acknowledgment

The authors wish to thank to N.Yoshizawa and M.Matsumoto from Field Systems R&D Center, NTT for their advices and informative discussions.

#### References

- [1] Osaka et al., Sumitomo Electric Tech. Review, No.29, p85, 1990
- [2] Matsumoto et al., J. Lightwave Tech., vol.LT-3, No.2, p.322, 1985
- [3] Hamada et al., OEC'90, 12b3-5
- [4] Katsuyama et al., Appl. Opt., vol.19, No.24, p.4200, 1980
- [5] Kalish et al., J. Am. Ceram. Soc., vol.61, p.518, 1978



Masahiro Hamada

Sumitomo Electric  
Industries, Ltd.

1, Taya-cho, Sakae-ku  
Yokohama, Japan

Masahiro Hamada was born in 1962 and received his M.S. degree in electronic engineering from Saitama University in 1987. He joined Sumitomo Electric Industries the same year and has been engaged in research and development of fusion splicing technologies for optical fibers. He is a member of the Institute of Electronics, Information and Communication Engineering of Japan.



Keiji Osaka

Sumitomo Electric  
Industries, Ltd.

1, Taya-cho, Sakae-ku  
Yokohama, Japan

Keiji Osaka was born in 1955 and received his M.S. degree in precision mechanical engineering from Kyoto University in 1981. He joined Sumitomo Electric Industries the same year and has been engaged in research and development of high NA optical fiber fabrication and fusion splicing technologies for optical fibers. He is now a senior engineer of Optomechatronics Systems R&D Dept. Yokohama Research Labs. and a member of Electronics, Information and Communication Engineering of Japan.



Isamu Fujita

Sumitomo Electric  
Industries, Ltd.

1, Taya-cho, Sakae-ku  
Yokohama, Japan

Isamu Fujita was born in 1965 and received his M.S. degree in mechanical engineering from Tokyo University in 1990. He joined Sumitomo Electric Industries the same year and has been engaged in research and development of fusion splicing technologies for optical fibers. He is a member of Japan Society of Mechanical Engineers.



Yasuo Asano

Sumitomo Electric  
Industries, Ltd.

1, Taya-cho, Sakae-ku  
Yokohama, Japan

Yasuo Asano received his B.S. degree in mechanical engineering from Waseda University in 1968. He joined Sumitomo Electric Industries in 1971 has been engaged in development of jointing technologies for coaxial cables and optical fiber cables. He is now a manager of Optomechatronics Systems R&D Dept. Yokohama Research Labs. and a member of Japan Society of Mechanical Engineers and the Institute of Electronics, Information and Communication Engineering of Japan.

## NEW COMPACT, EASY TO OPERATE FIBER OPTIC CONNECTOR COMPATIBLE WITH EXISTING COUPLINGS

J. C. Huber, N. H. Cubukciyan, A. Gennaro, J. T. Puchhammer, M. T. Stender, T. Szostak

3M Company, Austin TX and Eatontown NJ

### ABSTRACT

A new connector has been developed that is fully compatible with the ST (AT&T trademark) coupling and also is compact, robust and inexpensive. Connection and disconnection do not require finger access near the mounting bulkhead. Connectors are mountable nearly in side-by-side contact. Connectors are gangable in duplex format and polarized so that transmit and receive fibers are not mis-connected. Pulling on the cable (both axial and radial) does not cause physical disconnection. Pulling on the cable (both axial and radial) does not cause optical disconnection.

### DESIGN CRITERIA

Until fairly recently the most common applications for fiber optic connectors have been in higher revenue and physically protected locations. In telephony, the major uses have been in long distance lines, interoffice trunks and recently in feeder links. In data communications, the major uses have been in Local Area Network backbone links. These applications tend to have nearly continuous usage, fairly long lengths (500 m to 5 km), and are located in secured areas.

Recently fiber optics has begun to be used in lower revenue and physically exposed locations. In telephony, there are a number of field trials in fiber to the home or fiber to the curb. In data communications, the Fiber Distributed Data Interface (FDDI) has brought fiber to the desktop and there are a number of proprietary links between computers and high speed peripherals.

These new applications may require new features and designs for fiber optic connectors. To discover the design criteria, a survey of leading edge users was performed. Table 1 lists the design criteria.

TABLE 1

DUPLEX	Separate connectors for transmit and receive are too expensive, too time consuming and too prone to misconnection.
COMPACT	3.5 inch wide printed circuit cards have become popular. Two duplex connectors must not be wider than 3.0 inches. Space available on electronic equipment and patch panels becomes smaller with time.
PUSH-PULL	Most common electrical connectors have push-pull operation. Fiber optic connectors should also.
ROBUST	It must not readily disconnect, mechanically or optically. These new environments are not as protected from accidental abuse. This applies to both axial pull and lateral pull.
STANDARD	There are at least five incompatible connectors designs in common use in telephony and in data communications. In both telephony and data communications there are millions of standard receptacles and couplings already installed but not yet in service. Any new connector should be backwards compatible to the most commonly accepted standard.
SIMPLE	It must be easy to install in the field, whether at the wall outlet or at the home/curb by ordinary people. The more like an electrical connection, the better.
AVAILABLE	It must be available from several sources. No large user wants to be dependent on one supplier.

As in most new product design criteria, these are not very specific and somewhat contradictory. Rendering them into a design is the art of new product development. For only a specific design can be effectively evaluated by users to determine if it meets their requirements.

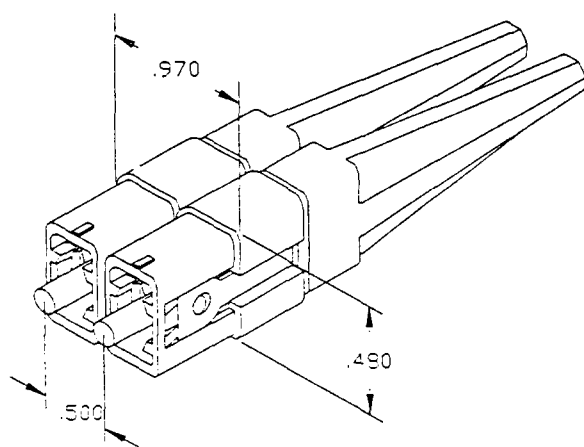
## DESIGN

On a worldwide basis, the most common data communications connector is the ST (AT&T trademark). It is a commonly accepted standard in the North America, Europe and South East Pacific countries. According to Kessler Marketing Inc (1), there are over 10,000,000 ST couplings and receptacles installed worldwide for data communications. The ST format has been in use for at least five years from at least four large suppliers and has demonstrated an excellent level of reliability, optical performance, simple installation and attractive price. Moreover, recently there have been at least four ST connectors introduced that greatly simplify installation. These connectors use fast acting adhesives or crimp and cleave designs. These designs are especially useful on the back side of a duplex wall outlet where their simplicity outweighs the value of a duplex connector.

In its previous designs, the ST did not satisfy the requirements of duplex, push-pull and robust, as was true of most other connector designs. The compactness requirement is dependent on the duplex design details.

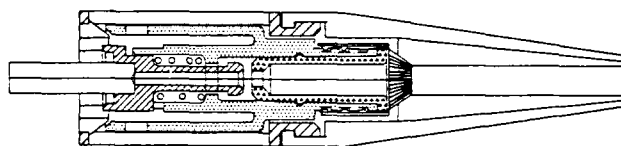
Thus the challenge was to add these features to the ST connector while still maintaining the ones inherent in the native design.

Figure 1 is an exterior perspective view of the resulting design. Figure 2 is a longitudinal cross section view.



PUSH-PULL CONNECTOR (PERSPECTIVE VIEW)

FIGURE 1



PUSH-PULL CONNECTOR (SECTION VIEW)

FIGURE 2

Firstly, the connector mates with all ST couplings and receptacles that comply with the draft EIA/TIA 6.3 specification. This is indicated by the 2.5 mm ceramic ferrule and the concentric interior surface of the outer shell.

Secondly, the connector latches on the ST coupling lugs with a simple pushing operation. The latches are simple cantilever arms parallel to the ferrule with ramps on the leading edges. When the connector is inserted into the coupling, these ramps urge the latches outward until the bayonet lug mates with the hole in the latch arm, whence the latch snaps closed. The connector unlatches from the lugs with a simple pulling operation. The outer shell is pulled backward and reverse orientation ramps engage the latches, urging them outward until the lug is free of the latch hole, whence the connector pulls free. Latching and unlatching can be accomplished by pushing and pulling, respectively, on the shell or on the boot.

Thirdly, the push-pull operation allows two simplex connectors to be easily joined to form a duplex connector. This is easily accomplished with a simple bridge or yoke attachment device, as shown in Figure 1. Different yokes can provide duplex designs with different ferrule spacings, different connector key orientations and field-changeable versus factory-fixed simplex/duplex conversion.

Fourthly, the compact outer shell allows the connector to be compact. Ferrule spacing of .50 inch (12.7 mm) is readily obtained. The simple push-pull operation requires less finger access space and is therefore more compact. Operation from the boot requires no extra space; connectors can be mounted in a close-packed configuration, as in a recessed outlet.

Fifthly, the connector features a ferrule that is not rigidly attached to the cable. Yet the cable is rigidly attached to the coupling through the connector backbone. So axial and radial disturbances to the cable and connector shell are insulated from the ferrule. In addition, the coupling shell is gripped both externally and internally by the

connector, providing further rigidity of attachment. Thus the connector is both pull-proof and side-pull-resistant.

Sixthly, the materials are chosen to be compatible with fast-acting adhesives, specifically hot melt adhesive. Hot melt adhesive greatly reduces installed cost without compromising performance (2). An accurate amount of adhesive is preloaded in the ferrule in the factory. This eliminates the time, mess and chance for error of loading epoxy in the field. And it shortens the polishing time because the adhesive bead is smaller. And it shortens the adhesive curing time because hot melt adhesive cures in less than four minutes, compared to epoxy, which takes twenty minutes. The installed cost of hot melt connectors is approximately 40% less than epoxy connectors (3).

Lastly, this connector uses a zirconia ferrule. Zirconia has been discussed by Carter (4) as having superior physical properties which lead to superior optical and mechanical performance in use.

### SPECIFICATIONS

Table 2 lists the specifications for this new connector. The performance has been specifically designed to meet the requirements of the ANSI X3T9 Low Cost FDDI and Fiber Channel committees. The design lends itself to meeting a wide variety of requirements and the specifications can be modified.

PUSH-PULL ST COMPATIBLE CONNECTOR SPECIFICATIONS		
Test Requirement	ANSI Goal	Push-Pull ST Spec
<b>MECHANICAL CHARACTERISTICS</b>		
Axial Pull Force	90 N (20 lb)	90 N (20 lb)
Plug Insertion Force	20 N (4.5 lb)	9 N (2 lb max)
Plug Withdrawl Force	20 N (4.5 lb)	9 N (2 lb max)
Cable/Connector Axial Pull	140 N (30 lb)	140 N (30 lb min)
Side Pull Load	not specified	9 N (2 lb min)
Ferrule to Ferrule Spacing	12.7 mm (.50")	12.7 mm (.50")
Lateral Connector Pitch	25.4 mm (1.0")	25.4 mm (1.0")
Component Profile Height	12 mm (.47")	12.5 mm (.49")
<b>ENVIRONMENTAL CHARACTERISTICS</b>		
Operating Temperature	0 to 60 deg C	-40 to 60 deg C
and Relative Humidity Range	5 to 95% RH	5 to 95% RH
Storage/Shipping Temperature	-40 to 85 deg C	-40 to 80 deg C
and Relative Humidity Range	5 to 100% RH	5 to 100% RH
Cable Flammability	UL Listed	UL 94V-0
<b>RELIABILITY CHARACTERISTICS</b>		
Frequent Mating	250 min	250 min
Product Life	100K hours	100K hours min
Optical Repeatability	.3 dB max	.2 dB max
Cross Plug Repeatability	1.0 dB max	1.0 dB max
Return Loss	30 dB	30 dB
Insertion Loss	not specified	.2 dB typical .6 dB max

TABLE 2

### CONCLUSIONS

A new compact, easy to operate fiber optic connector compatible with existing couplings has been designed. It meets the requirements of a large number of end users for both the enhancement of existing networks and also new applications, such as fiber to the home/curb and fiber to the workstation.

- 1 "U.S. Markets for Fiber optics in Point-to-Point Data Communications," Feb 1990, Kessler Marketing Intelligence, Newport RI
- 2 Lee, Nicholas A., "A Fast, Epoxiless Bonding System for Fiber Optic Connectors," SPIE Proceedings 1365, OE Fibers 1990
- 3 Huber, John C., "Installed Cost of Fiber Optic Connectors on Various Fiber Sizes," International Wire and Cable Symposium, Nov 1991
- 4 Carter, H. Robert, "Zirconia: A High Performance Material for Fiber Optic Ferrules," Optical Fiber Conference OFC, Feb 1989

All the authors hold positions in the TelComm Products Division of 3M Company. They are principally engaged in fiber optic connector development. Huber's address is PO Box 2963, Bldg A144-2N-01, Austin TX 78769. All the other authors' addresses are 10 Industrial Way East, Eatontown NJ 07724.

## "HIGH PERFORMANCE AND LOW COST PASSIVE OPTICAL COMPONENTS FOR THE SUBSCRIBER LOOP"

G. BILLET - S. CRICO - J.J. CROSNIER - A. FIELDING - J. LEACH  
C. LINCOT - J. SCHULTE - H.B. YIN

BNRE - KABELMETAL - RADIAL - SIRT - SOURIAU

### Summary

The implementation of high capacity broadband optical networks for the distribution of integrated services and data requires the development of a range of passive interconnection components. These single mode components must be low cost, high performance, low reflectivity and wavelength independent to allow future evolution to multiwavelength and coherent systems.

This paper describes five key components which have been developed in a joint European project, sponsored in part by the Commission of European Communities through the programme RACE. These components include connectors (including automated assembly), re-enterable splices and branching devices.

### Introduction

A successful implementation of optical fibre in the subscriber loop is closely linked to the cost of optical networks compared to more traditional copper ones. Since interconnect and branching passive components represent an important contribution to the overall cost of an optical network, the European Community has decided to specifically address the points of cost reduction and performance improvement of passive optical components through its programme RACE (Research and Development in Advanced Communications technologies in Europe).

Five components developed for that purpose are described :

. The single way connector is a push-pull type, field mountable offering 0.25 dB mean loss and a worst case return loss of -60 dB. The high return loss is achieved with a unique solution involving a silicone based index matching membrane, thus avoiding 'physical contact' of the fibres. A set-up for automating the cable stripping and connector mounting of this (and other) connector(s) has been investigated offering a cost reduction in connector assembly of up to 80% at high volumes ;

. The single-way re-enterable splice also has a push-pull mechanism and incorporates a rigid plastic moulded 'v' groove as alignment feature offering 0.14 dB mean loss and return losses better than -40 dB;

. The push-pull multi-way connector includes a high precision 5 or 10 fibre ribbon moulded 'v' groove module which integrates a direct solid glue transfert for an easy assembly;

. The fan-out connector enables a direct connection between multi-fibre units on one side and single fibres on the other side. This permits an easier, faster and therefore cheaper installation as well as more reliable connections with the use of factory assembled components;

. Finally 1 x 19 and 19 x 19 branching devices which are both wavelength and polarisation independent have been fabricated. These devices are based on radiative coupling between bundles of fibres and the technique can be extended to very large port count splitters eg 64 x 64. Reflection suppression up to -60 dB has been achieved.

### Singleway connector

The aim of this work is to develop a low-cost, high-performance singleway connector for subscriber distribution networks, which can be easily mounted in the field with simple tools and in the factory with automatic mounting.

It has been identified that the main element of the connector cost is the ferrule. The precision required for the ferrule is related to its shape, and hence to the alignment concept ; and for one type of ferrule, the achievable tolerances depend upon the manufacturing processes. The cost is evidently a function of the ferrule design and its manufacturing technologies.

For cylinder to cylinder alignment (FC, ST, SC, etc...) 3 tolerances of less than 1  $\mu\text{m}$  are required for the ferrule. The three tolerances of lower than 1  $\mu\text{m}$  required for a cylindrical ceramic ferrule cannot be obtained directly from extrusion or moulding due to the large shrinkage variations. Successive and costly grinding processes are needed.

In the case of a conical ferrule, only the I.D and the concentricity are to be controlled within 1  $\mu\text{m}$  tolerance. High precision metal machining technology has been developed for producing singlemode conical ferrules at half the cost compared to the cylindrical ceramic ferrules.

It has been shown that high return loss is necessary for high bit-rate transmissions, analog systems such as CATV, bidirectional transmissions and coherent communications. Various techniques (such as "physical contact") have been proposed in the past to obtain low reflections, but they do not meet all of the current requirements.

We have found an original solution which uses oblique polishing of fibre endfaces and a silicone based membrane fixed inside the adaptor (Fig. 1). The thickness of the membrane in its central region is approximately 20  $\mu\text{m}$ . The gap distance between the two fibre endfaces is controlled by polishing. The compression ratio of the membrane is between 20 and 50 %. The ferrule tip and the form of the silicone membrane are designed so that when compressed the membrane has ideal deformations. The endurance test of 500 mating cycles shows the repeatability is better than 0.1 dB. Very small loss variations (< 0.1 dB) have been observed for a temperature range from - 40° to + 85° C. No long-term degradations were recorded during high temperature endurance testing.

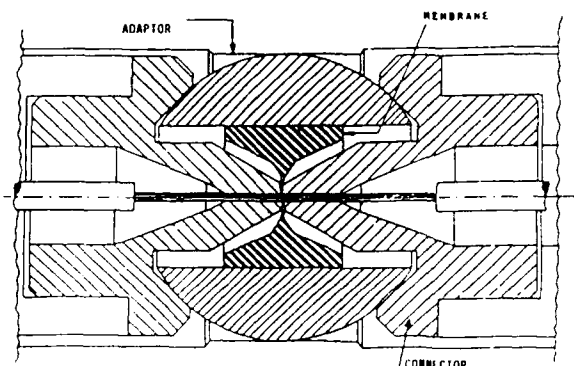
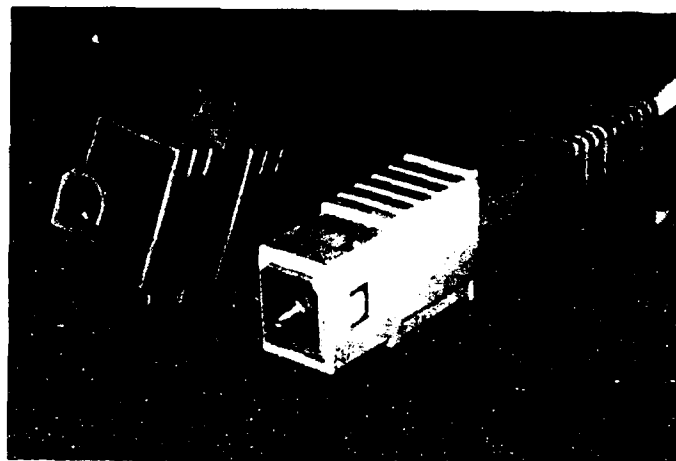


Fig.1 : Optical interface

Very high return loss (worst case 60 dB) and low insertion loss (mean 0.25 dB, max 0.5 dB) have been obtained. Only a conventional polishing process with very simple tools is needed. Equipment for automating the cable stripping and connector mounting has been produced offering a cost reduction in connector cabling of up to 80 %.

The singleway connector has a keyed push pull system with plastic housing (Fig. 2). Other features of this connector named "EC" are :

- non interruption of the signal when the cable is pulled back or bent
- modular design with high density multi-adaptor convenient for panel mounting of the adaptor
- low cost, low reflection active device receptacle design
- low cost, low reflection attenuator design



Automation of connector assembly

The EC connector has been designed such that it can easily be assembled in the field and also in a plant using automated assembly. Automation makes mounting of big quantities of connectors very cost effective. Factory mounting also makes tight quality assurance possible.

Automated mounting can of course be used for the manufacture of jumper cables and pigtails. But also drop cables for the subscriber loop and cables used in the cabling of buildings can be pre-connectorized in the factory using automated mounting. In these cases the cables have a connector on one end and they are spliced on the other end.

The automation of connector assembly comprises the automation of cable preparation (stripping), the automation of the actual mounting of the connector on the cable and fibre as well as the automation of the final polishing. We have set up a system, which performs automated cable preparation and connector mounting. Details of the system and its performance are described in a separate contribution presented at this symposium<sup>1</sup>.

#### Singleway re-enterable splice

It has been identified that a low-insertion loss and low cost singleway re-enterable splice would be needed for subscriber network interconnections, especially at Branching boxes. At these points, one needs a demountable connection giving some flexibility of installation and testing, but the number of mating/unmatings is expected to be very low (< 20 cycles).

The re-enterable splice developed consists of two plugs and one adaptor (Fig. 3). All the pieces are plastic moulded. The adaptor incorporates in its center a rigid moulded V-groove as the alignment reference of the two fibres. The coated fibre is fixed in the plug ① by clamps ③. The plug has an automatic fibre protector ② and a push pull coupling mechanism. The form of the plug body at its front part looks like a fork, allowing the two plugs to be butted against each other when they are coupled to the adaptor.



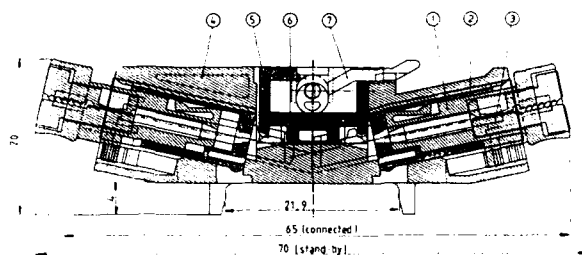


Fig.3 : Singleway re-enterable splice

The fibre with its extremity stripped is first inserted into the plug body and fixed by clamp. Then the fibre will be cleaved by a simple tool to a certain length. When the two plugs are coupled to the adaptor, the bare fibres will be automatically laid in the V-groove and butted against each other. The fibres will be slightly buckled. A plastic fibre holding device ⑤ with a leaf spring presser to be lowered by a can mechanism ⑦, assures that the fibres are pressed on the V-groove and the plugs are locked into the adaptor. To minimize the reflection, index-matching gel is used. Part ⑥ is the reservoir for the gel.

A mean loss of 0.14 dB (max. 0.28 dB) has been obtained with identical fibres. Return losses are better than 40 dB. This value can be improved by oblique cleaving of the fibre end. The performances are stable in mechanical and climatic tests.

#### Multiway connector

The introduction of single mode fiber optic for customer connexion starting with professional customers and the evolution toward passive optical networks have pushed cable manufacturer to develop high fiber count cables based on elementary ribbon of fibers. When such cables have to be connectorized single way connectors are not suitable and multiway connectors are preferred.

Several types of products are already available such as silicon etched splices and MT Japanese product. These connectors are expensive and the mounting operation is complicated.

Within the framework of the LOOP RACE PROJECT a new approach has been made to develop a low cost solution for multiway connector. To reach this target the effort has been focussed on plastic moulding process to manufacture high precision pieces.

A vee groove structure as shown on figure 4 has been preferred to other possible shapes to limit the precision requirement to a single surface of the piece.

For such a piece only symmetry and reproducibility of the shape has to be mastered within one micron.

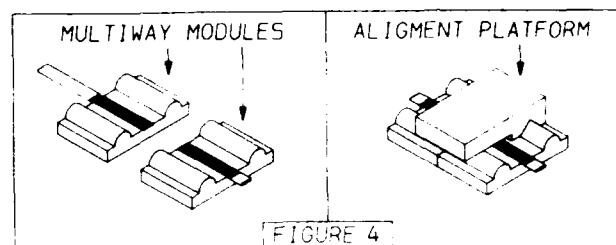


Fig.4

The moulding tools, the material and the moulding parameters have been optimized to produce pieces with the adequate tolerance.

Fiber ribbon are pressed and glued on the multiway modules (using room temperature glue) and then the front end of the modules are polished manually (using a specific jig to guarantee perpendicularity) see fig.5.

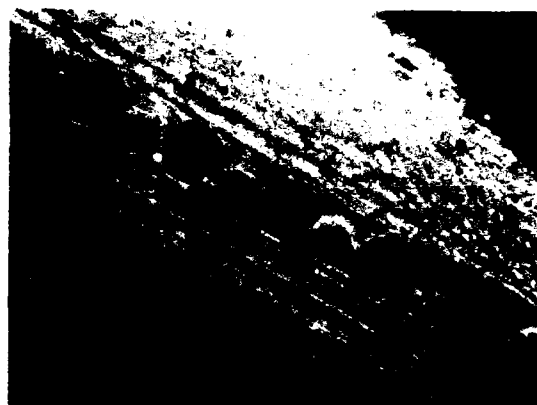


Fig.5

The first results obtained with moulded modules are very encouraging :

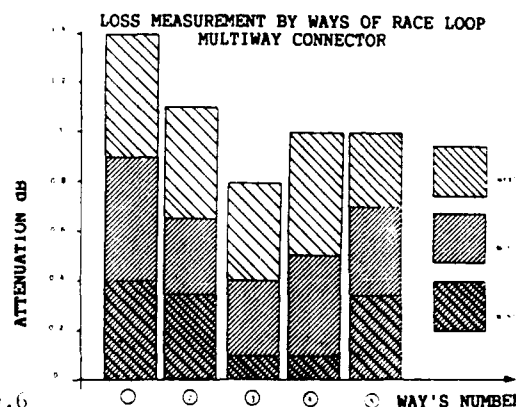
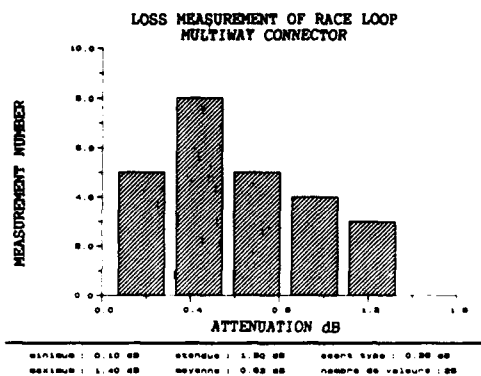


Fig.6



A splice housing built around the alignment platform has been designed. Taking into account the low cost target this housing is made of a self locking single moulded piece that is folded around the modules and insures all the mechanical functions (see figure 8).

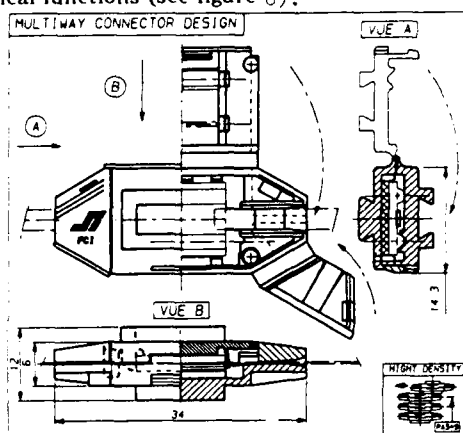


Fig.8

#### Fan-out connector

Subscriber lines are obtained by connecting high, medium and low fiber count cables at many points between Central Offices and Subscriber Premises. The relevant number of interconnecting points and the use of a variety of different cable counts and structures imply the adoption of cost effective interconnecting technologies.

Between the different types of interconnecting components an important role will be played by fan-out connectors.

The fan-out connector is a fully passive component enabling a direct transition from multifiber units on one side to individual fibers on the other side. This transition is obtained using multifiber connectors or splices on one side of the component and individual connectors on the other side.

The advantage of fan-out connectors is that they offer better handling, lower cost of component parts and lower mounting time per fiber than other solutions. Therefore these components are particularly useful to provide quick and reliable mass fiber termination of high and medium

fiber count cables. If it is required a network flexibility at individual fiber level (any individual feeder fiber can be cross-connected to any secondary distribution fiber) fan-out terminations have to be preferred.

Different possible configurations of fan-outs were studied within the project, considering the usefulness of having pig-tails on both ends of the component versus a more compact shape and a smaller size. The most promising solution was considered the compact one (see figure ...) taking also into account the number of different possible choices on the multi-fiber side (connector, re-entenable mechanical splice, fusion splice).

Performances of fan-outs are usually similar or slightly worse than fusion technique. The results obtained are in the area of 0.5 dB as typical insertion loss and 35 dB as typical return loss.

The performance drawback is highly compensated by the time saving allowed by fan-out connector terminations. Fan-out connectors can be fitted to interface cable fibers to the equipment any time there are requirements for further subscriber activations. This can be done with very simple tooling and with no active control of performance. Mass splice or multifiber connector which lie on the multifiber side of the fan-out shall both be factory and field installable. Factory installation has to be preferred, whenever possible, for lower cost and better performance. Nevertheless field assembly is a mandatory requirements as it is not possible to factory pre-terminate all cable lengths (uncertainties on exact cable route length is the main limiting factor).

The result of a field trial has given a gain of 20% in installation-time saving using the fan-out technique with the drawback of a higher cost because of the higher number of components. This will anyway lead to an economic advantage due to the higher cost of man-power versus the components.

As a conclusion, fan-out connectors appear to be strategic products which have a number of potential applications. Their use will contribute to enhance both flexibility and reliability and they will play an important role in the future subscriber network.

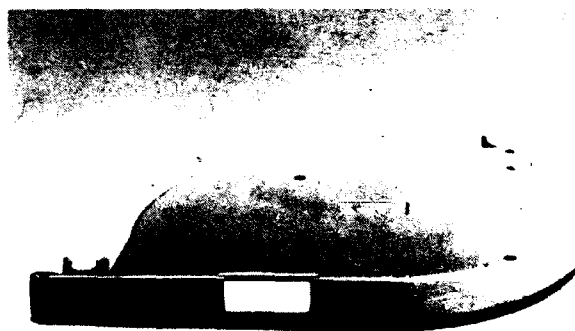


Fig.9

### Branching devices

A novel technique aimed at fabricating large port count (64-way) wavelength independent branching devices has been developed and 19-way components have been demonstrated. The component is based on a radiative coupling mechanism and consists of co-axial, polished arrays of close packed, tapered single mode fibre as shown in figure 10.

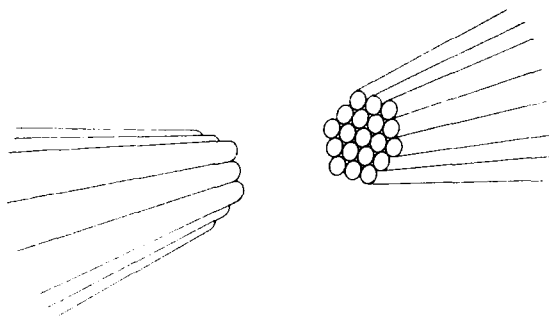


Fig.10: General Arrangement of 19 x 19 tapered fibre bundles

Using a Gaussian field approximation to the fundamental mode, a model has been derived which analyses the radiative coupling between individual fibres in the two arrays<sup>2</sup>. Using this model, it is possible to optimise the geometry to minimise the worst case insertion loss at a given wavelength by ensuring that each tapered fibre is focused towards the centre of the opposing array.

To increase the packaging fraction of the fibre bundle, and therefore reduce the loss and uniformity of the device, an externally clad single mode fibre designed and produced at BNR Europe is used. This allows the fibre to be tapered down further than conventional fibre, whilst maintaining the same spot size.

To fabricate the 19-way components, 19 fibres are prepared and twisted into a close packed configuration, and then tapered and lightly fused in a single operation. The tapered fibre bundle is then encapsulated prior to being sawn, lapped and polished. This technique for producing the tapered fibre bundles can be extended to devices with higher port count, with only relatively minor modifications to current jigging. The components for the branching device are then bonded into a silica v-groove and the complete assembly packaged in a dural box.

Reflection suppression using angled ends and adhesive bonded facet windows reduce directivity and return loss to < -60 dB.

For the 19 x 19 device, worst case loss over 300 nm was only 25.0 dB with a uniformity of 6 dB. The spectral response of a single port-port combination is shown in figure 11. The variation over 300 nm is < 1 dB.

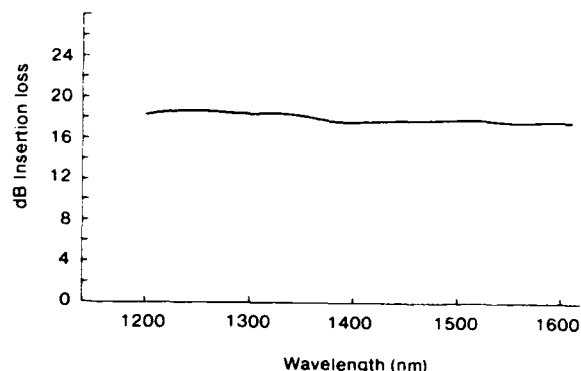


Fig.11: Spectral Response

For a 1 x 19 device, the worst case loss over 300 nm was 20.5 dB with a uniformity of 4.5 dB. Both devices are polarisation insensitive (< 0.1 dB).

Further work is now being carried out to implement the radiative coupling technique in Silica-on-Silicon planar technology. These devices will be aimed at medium port count applications (< 20) where they are more efficient than the fibre version. This is because integrated optics waveguides can have a much smaller core/cladding ratio (increasing the packing fraction) than even tapered fibres and radiative coupling in two rather than three dimensions is less lossy.

### Conclusion

In this paper have been presented a range of components able to comply with every foreseen evolution of an optical network, because all of them :

- are wavelength independent (including the branching devices), so they will be transparent to the likely evolutions of transmission systems in the network,
- show low reflection and allow therefore bi-directional communications and the use of fibre amplifiers or DFB lasers without isolators loss and cost penalties,
- are cost effective and therefore reinforce the competitiveness of optical networks in the subscriber loop.

This work carried out in direction of performance improvement and cost reduction should enable an earlier lay-out of evolutive and economically viable optical networks.

### References

- 1) J. Schulte, "Automated mounting of connectors to fiber optic cables" Proc. IWCS, 1991.
- 2) S.J. Wilson, T. Bricheno, "Broadband single-mode optical fibre couplers". Optics Communications, Feb. 1990, 75, 2 pp 106-110.

**A. FIELDING** received his BSc (Hons) in Applied Physics in 1981 from Sunderland Polytechnic. In 1982 he received an MSc in Lasers and their Applications from Essex University and in the same year joined BNR Europe Limited in Harlow. Since then he has been engaged in the development of fibre optic components particularly tapered fibre devices. He is currently Activity Leader of the Coupler Technology Group.



**A. FIELDING**  
BNR EUROPE LTD  
London Road  
Harlow  
Essex CM17 9NA  
ENGLAND

**J. LEACH** received his BSc from Southampton University before joining STL in 1969. He is currently manager of the Fibre Based and Integrated Components Department at BNR Europe Limited (Formerly STC Technology Ltd). He is a Member of the Institute of Physics and a Chartered Physicist.



**J. LEACH**  
BNR EUROPE LTD  
London Road  
Harlow  
Essex CM17 9NA  
ENGLAND

**J SCHULTE** received his physics degree in quantum optics in 1981 and his Ph.D. in engineering in 1986 from the Technical University Hannover. After a research fellowship at IBM, Yorktown Heights NY, he joined Kabelmetal Electro in 1987, where he has been engaged in the development of fiber optic cables.



**J. SCHULTE**  
KABELMETAL  
ELECTRO GmbH  
P.O Box 260  
3000 Hannover 1  
GERMANY

**G. BILLET** was born in 1953 and graduated from Ecole Nationale Supérieure des Arts et Métiers in 1975 and started his professional experience with ALCATEL. He joined RADIAL in 1979 and worked as R & D manager for the Microwave Division. He is currently the Director of the Fibre Optic Division.



**G. BILLET**  
RADIAL SA  
Dept Fibre Optique  
81, Bd Denfert  
Rochereau  
B.P 328  
38509 Voiron Cedex -  
FRANCE

**H.B YIN** was born in Tchong King, China, in 1944. He received his university degree in Physics in 1966 from the Hang Tcheou University in China and the doctoral degree in Physics in 1985 from the University of Franche-Comté (Besançon) in France.

He joined RADIAL in 1983 as an engineer and was engaged in the R & D of fibre optic passive components. In 1988 he was appointed R & D Manager of the Fibre Optic Division.



**H.B YIN**  
RADIAL S.A  
Dept Fibre Optique  
101, rue Ph. Hoffman  
93116 Rosny sous Bois -  
FRANCE

**J.J CROSNIER** is an engineer from Ecole Supérieure de Physique et Chimie de Paris (1975) and Doctor Engineer from the University of Paris (1976). After two years' work as Design Engineer in electronics he joined SOURIAU (1978) where he was successively Design Engineer, Design and Production Manager and Director of the Fiber Optic Division.

**J.J CROSNIER**  
SOURIAU  
Division Fibres Optiques  
3, Av. du Maréchal Devaux  
91150 Paray-Vieille-Poste  
FRANCE

C. LINCOT received a Technical University Degree (1982), he is an engineer from Centre d'Etudes Supérieures des Techniques Industrielles (1985) with a material speciality from Institut Supérieur des Matériaux et de la Construction Mécanique (1986) and a "Diplome d'Etudes Approfondies" in dynamical structure (1986). After seven months of research in Renault Sport Society he joined SOURIAU (1986) where he was successively Production Engineer, Multiproduct Design Manager of the electrical division and Design and Development Manager of the Fiber Optic Division.

**C. LINCOT  
SOURIAU**

Division Fibres Optiques  
3, Av. du Maréchal Devaux  
91150 Paray-Vieille-Poste  
FRANCE

S. CRICO was born in MILANO in 1959. He received his University degree in Nuclear Engineering from the Politecnico of MILAN in 1984. He passed 1 year between (1982-83) for an EURATOM stage at the "Laue-Langevin" Institute in Grenoble (FRANCE).

In 1985 he joined FIAR in the Defence Group, Electro-Optics Department, where he was manager of the IR sensors engineering.

In 1988 he joined SIRTl, cables and optical technology department, where he was involved in passive optical component design and in manufacturing and characterization techniques for almost two years. During this period he has been involved in standardization activity as a member of CECC and EIA working groups on connectors.

In 1990 he got the responsibility of the marketing of Optical Components and Accessories within SIRTl.

He is author of 5 papers.



**S. CRICO**  
**SIRTl SPA**  
Direz Ricerce E  
Tecnologie  
Via Vida 19  
20127 Milano  
ITALY

**The Use of Superabsorbent Materials  
in Optical Fiber Cable Design**  
**C. John Arroyo, Jim J. Sheu, and W. J. Paucke**  
**AT&T Bell Laboratories and Network Cable Systems**  
**Norcross, Georgia 30071**

The present global demand for optical fiber cables has required a reevaluation of present cable designs to insure quality in every aspect of cable design and manufacturing. In order to provide quality water-blocking capabilities in optical fiber cable sheaths, an investigation was initiated to study the prevention of water ingress and migration in cable sheaths. Tests were designed and/or modified to study the movement of water under pressure at different sheath interfaces. Superabsorbent materials in three different configurations were found to outperform other materials. As a result of this development, superabsorbents have been incorporated into all optical fiber outside plant cable sheaths, with consistent reliable performance.

## INTRODUCTION

With the global increase in optical fiber cable demand, customers are requiring greater performance reliability, and zero maintenance at lower costs. The technology of preventing the ingress and migration of water inside cables has progressed from gas-pressurized systems to filling and flooding compounds. Gas-pressurized systems have difficulty providing long term reliability and the maintenance costs are prohibitive. Flooding compounds require the use of an organic solvent at termination. Another commonly used material is a 'sticky' atactic noncrystalline polypropylene flooding material. These flooding compounds are difficult to apply during cable manufacturing and are not craft-friendly during termination in the field.

An alternative and more efficient water-blocking provision has been accomplished by use of 'superabsorbents'. Developed in 1966 by the United States Department of Agriculture, and appropriately called 'Super Slurper', superabsorbents have been extensively used in the incontinent market.<sup>[1]</sup> In 1975, superabsorbent laminated tapes were first offered in Europe for the cable industry, and in 1977, a

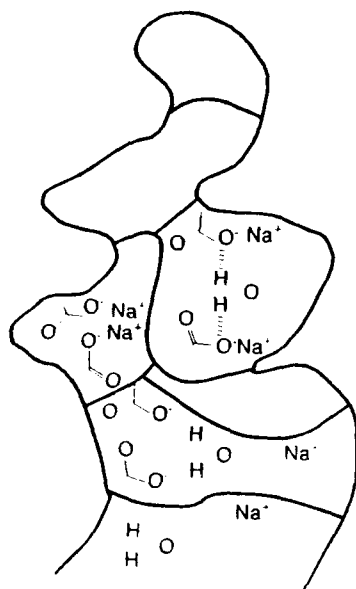
superabsorbent powder in loose form was first introduced into a copper cable design. Since then all major cable manufacturing companies have experimented and/or introduced superabsorbents in various forms into their cable designs. This paper will discuss the chemistry and application of superabsorbents in fiber optic cables.

## SUPERABSORBENT POLYMERS

The significance of providing water-blocking protection in cables is to eliminate the possibility of water entering the splice closure. In freezing environments, such an occurrence could induce microbending in optical fibers, resulting in fiber degradation or increased loss. One of the first documented uses of the term "superabsorbent" was by R. E. Erickson of Dow Chemical in 1980.<sup>[2]</sup> A superabsorbent is a dry material which rapidly absorbs about 1000 times its own weight in distilled water to form a gel with a corresponding volume increase.<sup>[1]</sup> While undergoing these changes, the material retains its original identity. This means that the basic chemical structure of the superabsorbent is not changed. Recently, J. R. Gross of Kimberly-Clark Corp.<sup>[3]</sup> suggested a term "Xerogellant." The prefix "xero" means a dry material while gellant, contraction of gelling agent, describes the behavior of the material. The new term, although applicable to the incontinent market, is not general enough to cover materials produced in wet form, such as many water soluble polymers which can be crosslinked to produce superabsorbent polymers (Figure 1). For the cable industry, superabsorbent polymer (SAP) seems to be a more popular term.

The mechanism by which SAP absorbs and retains water can be described in two ways, physical and chemical. On the physical level, aqueous fluid wets the surface of SAP and is physically distributed into and throughout the network (or matrix) of SAP. Since the aqueous fluid is moving in columns of continuous fluid, the physical absorption of SAP depends upon factors such as pore size, specific gravity, viscosity, surface tension and contact angle. The last two factors actually affect the wettability of SAP.

## Crosslinked Superabsorbent Polymers Figure 1



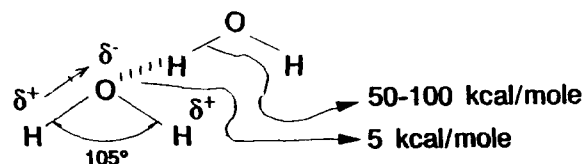
The other type of absorbency is chemical, which occurs on the molecular level. The aqueous fluid interacts with the polymer chains via solvation and hydrogen bonding. Since energy associated with this process is relatively high, the aqueous fluid has been described as "bond" water. The bulk of fluid chemically bonded to SAP does freeze with some difficulty but does not easily escape out of the network (matrix) of SAP.

The SAP at this stage look like gels, and are generally described as "hydrogels." Factors such as hydrogen bonding, hydration (solvation), diffusion, porosity of network, electrostatic attraction and repulsion affect the chemical absorption of SAP. Overall, if the matrix (network) of SAP is considered as a separated entity from the surrounding aqueous fluid, a pressure gradient can exist between the two entities. Physically, such a pressure gradient is in effect an osmotic pressure gradient. This is why people attribute the absorbency of SAP to osmotic pressure.

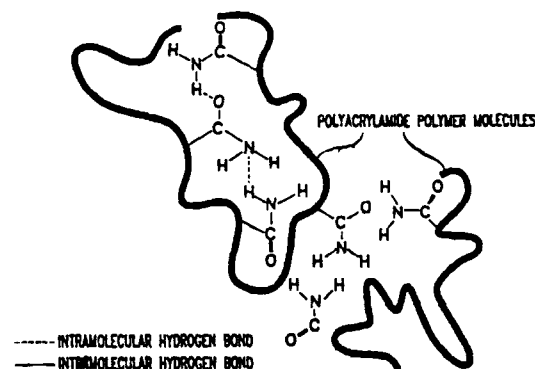
Whether the SAP absorb aqueous fluid via a chemical an/or physical process, the most important driving force for these processes appears to be the high energy hydrogen bonding. In water, the energy for hydrogen bonding has been found to be about 5 kcal/mole (Figure 2). This energy is very significant considering the very strong covalent bond energy of 50-100 kcal for the O-H bond in water. Furthermore, there are numerous hydrogen bonds among the superabsorbent molecule and water molecules.

## Figure 2 HYDROGEN BONDING (H-BONDING)

A Hydrogen Atom Serves as a Bridge between Two Electronegative Atoms, Holding One by a Covalent Bond and the Other by Purely Electrostatic Forces



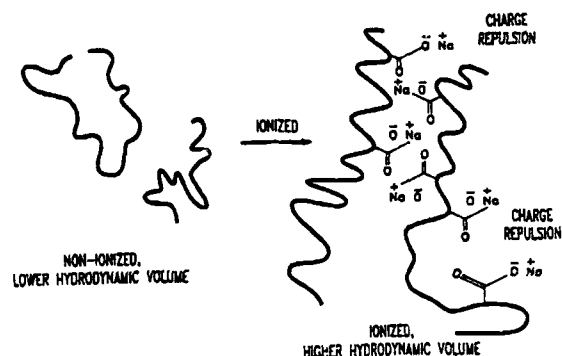
- Special kind of Dipole-Dipole Attraction



## Hydrogen Bonding of Polyacrylamide Figure 3

SAP generally are made in several ways as in crosslinked polyacrylates. Crosslinking controls the nature of network of SAP and makes the polymer insoluble in water. Chemically, the major functional groups in polyacrylates are carboxylates. The carboxylates group will absorb water through hydrogen bonding. Other types of functional groups such as amides can also have hydrogen bonding with water. Using water soluble polymer, polyacrylamide, as an example (Figure 3) the polyacrylamide polymer chains once dissolved in water will have two types of hydrogen bonding, intra and intermolecular. The intramolecular hydrogen bonding tends to pull the individual molecular chain together, thus the individual polymer chain becomes folded and curled. The molecular volume of such polymer in water is small. The volume which the polymer chains occupy in aqueous solution, is called the hydrodynamic volume. The smaller the hydrodynamic volume, the closer the viscosity of polymer solution approaches that of water. In other words, the polymer's influence on the water is small if the hydrodynamic volume of that polymer is small. In the case of polyacrylamide, the

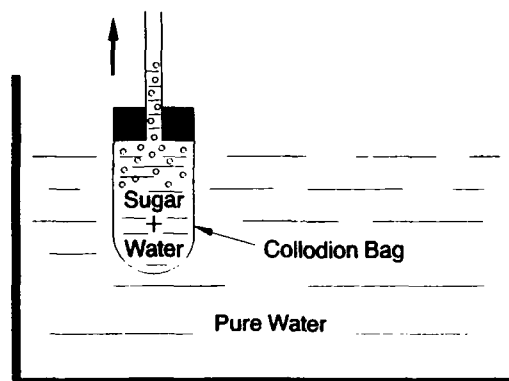
intermolecular hydrogen bonding also pulls the polymer chains together. Interestingly, polymer chains not only curl or coil by themselves, they also bundle together. The effective hydrodynamic volume of polyacrylamide is therefore low resulting in low viscosity. If the amide groups in polyacrylamide were hydrolyzed to carboxylate groups (i.e., the same functional groups in polyacrylates, or SAP), shown in Figure 4, intermolecular as well as intramolecular charge repulsion exist between polymer chains. These repulsions extend the hydrodynamic volume of polyacrylates and result in a much higher viscosity. In fact, some low molecular weight polyacrylates are used as thickeners due to this phenomenon. Carboxylates also have higher ability than amides in polyacrylamides to form hydrogen bonding with water molecules. Having numerous hydrogen bonding with water molecules, SAP absorbs and retains water into its matrix.



**Volume or Size of a Non-Hydrolyzed Polyacrylamide Molecule vs. That of a Partially Hydrolyzed Polyacrylamide**  
Figure 4

At macroscopic level, the net result is an osmotic phenomenon. As shown in Figure 5, just as a reminder, sugar solution inside the collodion bag has higher solute concentration than that of the pure water outside the bag. The concentration gradient results in osmotic pressure gradient which drives water into the collodion bag. The sugar solution and collodion bag can be considered as the matrix of a SAP. Since SAP has many functional groups such as carboxylates (electrolytes) dissolved in water, the concentration of these groups is higher inside the SAP matrix. The concentration gradient results in osmotic pressure gradient. The osmotic pressure gradient between the network of SAP and surrounding aqueous fluid therefore, drives the water into the network of SAP.

The way the network of SAP is constructed has a great impact on the absorbency of SAP. The network of SAP is generally built via crosslinking of polymer chains.



**FIGURE 5. OSMOTIC PRESSURE**

The amount of crosslinking is important and must be maintained at an optimum level depending on the application, such as the rate of absorption and total amount of water absorbed, for example. The crosslinking determines the space in the network of SAP, thus the total volume of SAP, which in turn influences the concentration of functional groups in the network. As mentioned before, concentration gradient affects the osmotic pressure gradient and thus the absorbency of SAP.

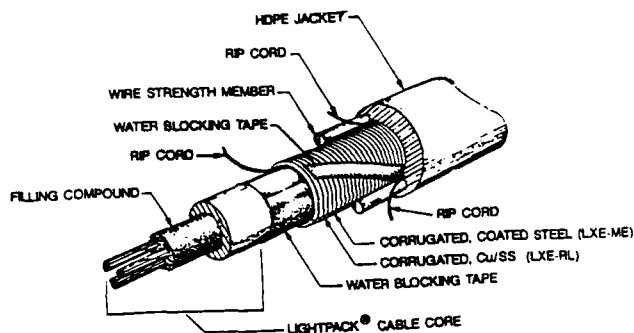
#### MATERIAL CONSTRUCTION

When incorporating SAPs into a cable design one must consider the ability of the SAP to quickly swell into a gel consistency and longitudinally block water paths along different sheath interfaces or within difficult to reach interstices. The ability of the formed gel to reactivate after drying is also critical. Three constructions were investigated; laminates that contain the SAP between two layers of nonwoven materials; coated SAP onto spunbonded nonwovens and onto synthetic aramid fibers; and SAP fibers which are made into yarns.

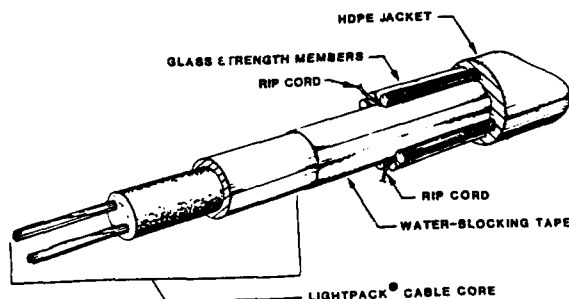
#### CABLE CONSTRUCTION

The incorporation of superabsorbents in optical fiber cables can best be explained by actual cable design. Figure 6 presents both a metallic and dielectric Lightguide Express Entry (LXE) optical fiber cables. In both designs, laminated SAP tapes are longitudinally applied in the sheath interface. In the metallic version the laminated SAP tape is located between the core tube and the corrugated armor, and an additional helically wrapped SAP laminated tape is introduced as insurance against the possibility of water migration along the metallic wires and the corrugated armor interface. In the dielectric version, the laminated SAP tape is located between the inner core tube and the outer jacket. These tapes prevent water migration within the cable in the event of a breach in the jacket due to rodents, lightning or accidental mechanical damage.



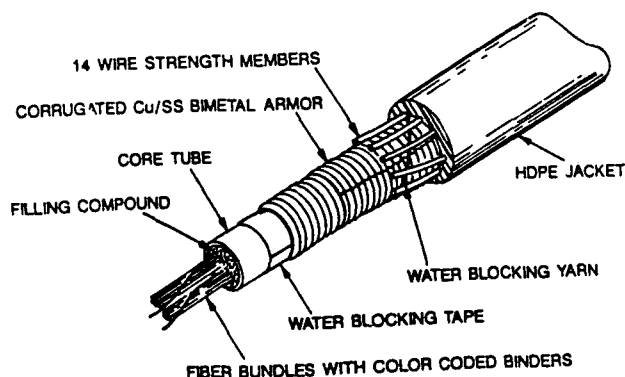


**LXE-ME (Metallic) Sheath**



**LXE-DE (Dielectric) Sheath**  
**Figure 6**

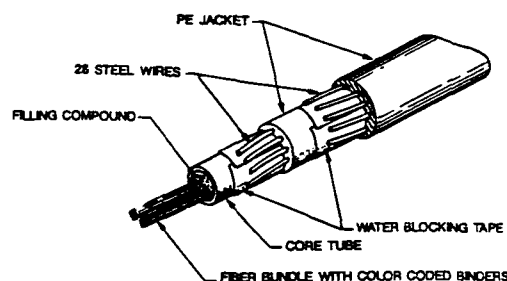
Figure 7 presents another SAP application in the form of a swellable yarn. The Primary Rodent Lightning (P-RL) optical fiber cable design incorporates a longitudinal laminated SAP tape between the inner core tube and the corrugated metal interface. It also contains a swellable superabsorbent yarn helically applied between the corrugated armor and the strength members, to prevent the possibility of water migration along this interface.



**Primary Rodent-Lightning Sheath**  
**Figure 7**

Figure 8, presents another SAP application. In this Metallic Crossply optical fiber sheath design, it was important that the cable outside diameter not be increased with the introduction of the SAP tape. Therefore, the nonwoven spunbonded polyester tape originally used was impregnated with a SAP coating that impregnated the spunbonded matrix with only a one mil increase in the tape thickness. Since the tape remained compressible, there was no increase in the cables' outside diameter.

The scope of this paper does not allow for all the varied cable applications in both optical fiber and copper cables that have been successfully designed, and that are presently commercially available. However, the SAP material selection is vitally important and will next be discussed.



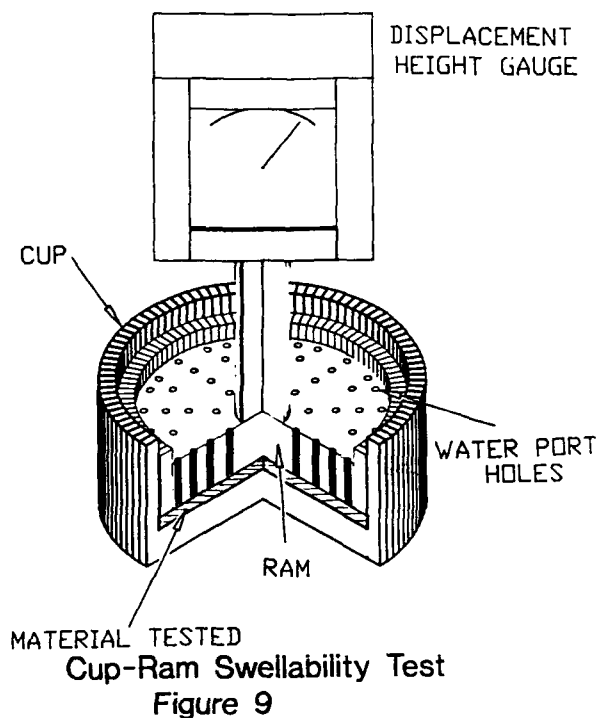
**Crossply Sheath**  
**Figure 8**

#### **MATERIAL SELECTION**

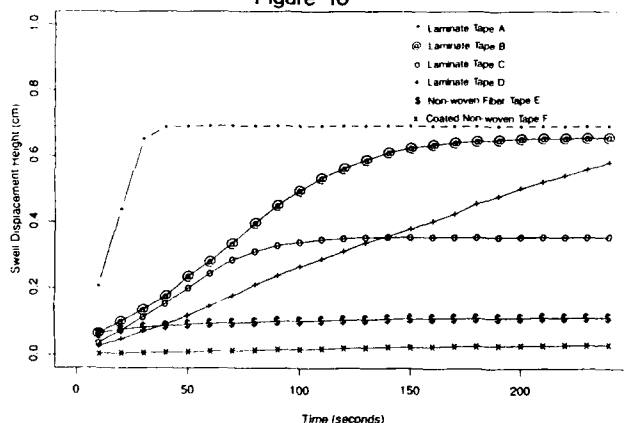
The current commercial state-of-the-art SAP tests evaluate the material's absorbency or ability to absorb water, and are applicable for the incontinent market. For the cable industry a more straightforward approach is to measure a material's swellability in terms of swell height, rate-of-rise and gel retention.

The Lantor BV, Cup-Ram swellability test was modified to measure the effects of radial swelling. This test as seen in Figure 9, measures a material's swellability by monitoring the free vertical movement of a ram, as water is added to the cup. Figure 10 shows the swell displacement height in centimeters vs time in seconds for superabsorbent tapes. This test provides information on effects of different water types i.e., distilled-brackish-sea water, SAP loading and chemistry, carrier porosity-thickness-adhesion, as well as the effects of wetting agents and physical tape construction.

Figure 10 demonstrates the above effects using four similar SAP laminated tapes (A to D) from different manufacturers, as well as a SAP nonwoven fiber tape E and a SAP coated nonwoven tape F. The swellability of tape laminates A through D can be explained as one analyzes the individual components and tape structures.



Cup-Ram Swellability Test Results  
**Figure 10**



The swellability of the nonwoven fiber tape E depends on the amount of layered swellable fibers per unit area. The swellability of the nonwoven tape F depends upon the amount of solids in the coating applied to the spunbonded nonwoven material. Although the swelling of the last two materials is not as impressive, swelling does occur within their matrix, and both have demonstrated exceptional gel retention.

These materials were also evaluated in a Hydraulic Pressure test. This test, while affected by the above characteristics, also measures the effects of a laminates' rate-of-rise and gel retention. While the product literature is full of different hydraulic pressure tests, the interpretation of results differs. It is therefore important to correlate the results to actual cable performance by dissecting the cable tested.

Table I shows the effects of tape thickness. The gap simulates the radial expansion within which the material is allowed to expand inside the cable, the travel represents the longitudinal migration due to a set pressure at the selected time in days and is a measure of gel retention. It should be noted that the travel length in Table I represents the maximum travel after one day, although the test was continued for a five day period.

Test Length- 30.5 cm Water Pressure- 1.0 meter				
Material	Thickness (cm)	Gap (cm)	Swell %	Travel @ 5 Days (cm)
Laminated tape A	.036	.102	283	10.6
Laminated tape B	.025	.102	408	14.8
Laminated tape C	.025	.076	304	13.0
Laminated tape D	.033	.102	309	26.0
Nonwoven Fiber tape E	.071	.254	358	20.6
Coated Nonwoven tape F	.020	.064	320	13.3
#7 cc Swellable Yarn	759 Denier	.064		15.9
#1.67 cc Swellable Yarn	3183 Denier	.127		14.9
#.67 cc Swellable Yarn	7933 Denier	.254		16.8
Coated Aramid Yarn	2130 Denier	.064		14.8
Aramid/Swellable Fiber Yarn	2130 Denier/ 3183 Denier	.216		17.5
Coated Glass Roving	.102	.140	137	24.8

cc = cotton count

Comparing the matrix of the first four laminated tapes, the designer can make certain comparisons that would assist in material selection. i) Comparing tapes A & B, if the travel distance is deemed comparable, then tape B would be preferred because it is thinner, and has a higher percent (408% vs 283%) swell. ii) Comparing tapes B & C, if the travel length is deemed comparable, then tape B would be preferred since it has a higher percent swell. iii) Tape D is considered the worst performer on the basis of its' longer water migration (26 cm.), even though its' 309% swell is comparable to tapes A and C.

Tapes E and F are not laminates; E is a nonwoven SAP fiber tape, while F is an SAP coated spunbonded nonwoven tape. Both tapes perform well considering their thicknesses and gap constraints. It should be noted that compared to the results in figure 10, these two materials show better performance than anticipated. This underscores the value of understanding test results and their relevance to the application under investigation.

The SAP swellable yarns were evaluated in three different sizes and in combination with an aramid fiber for added strength. Also, SAP coated aramid and glass rovings were evaluated, and although having lower percentage swell, they had comparable gel retention to SAP tapes.

It should be noted that changes in SAP loading, type chemistry, gap size, water pressure and duration will change these results. However, these results are indicative of the expected performance in actual cable designs.

## IMPACT

Presently, all of our outside plant optical fiber cables have one or two types of SAP waterblocking materials, with maintenance free performance over the last five years. These materials are also making inroads into copper outside plant products. Also, additional applications are being discovered for SAPs such as in foams and compounding into elastomers. They've even been compounded into filling compound for added performance. It is clear that superabsorbents present a whole new generation of materials in providing maintenance free water blocking provisions in cable design. What is needed is a set of industry standards to assist cable designers in selecting and implementing these superabsorbent materials.

## CONCLUSIONS

The use of superabsorbents present a radical departure from the traditional means of providing water blocking in cable design. An attempt at explaining the physical and chemical mechanisms of SAPs has been presented. Also bench-type tests to evaluate material performance have been outlined. Additionally, since SAP materials are compatible with all other cable processing materials, the ease of manufacturing presents yet another attribute not discussed in this paper. Tests have been developed to evaluate the performance of these materials and cables dissected to ascertain correlation with these results. As a result, all of our outside plant optical fiber cables, over the last five years have been designed with one or two types of superabsorbent materials.

## ACKNOWLEDGEMENTS

The authors would like to acknowledge the many contributions from members of AT&T Bell Laboratories and AT&T Network Cable Systems.

## REFERENCES

1. Obenski, B. J., *New Developments in Super-Absorbents in the United States, Europe and Japan, Proc. pp 1-2, INDA-TEC (1986).*
2. R. E. Erickson, *Proc. Absorbent Prod. Conference, Sect. VI (1980) U/TS, Kalamazoo, Mich.*
3. J. R. Gross, "The Evolution of Absorbent Materials," p. 3, *Absorbent Polymer Technology*, Ed. Lisa Brannon-Peppas and Ronald S. Harland, Elsevier (1990).



\*\*\*\*\*

John Arroyo joined AT&T Bell Laboratories in Whippany, New Jersey in 1969, and has worked in research and development of copper and fiber optic cables at Norcross, Georgia since 1978. As a Member of the Technical Staff, his responsibilities include fiber optic cable development concepts, sheath design, standardization of lightning tests and cable specifications. John received the Design News Journal "Excellence in Design Award" in 1981, for a "Helical-Wrap Peel Strength Test". He co-authored the "Outstanding Technical Paper", at the 30th IWCS, November, 1981, and received the 'Fiber Optic Award' from AT&T International in July, 1990, for his contributions in fiber optic technology. John has co-authored seven technical papers and received seventeen patents related to cable design.



\*\*\*\*\*

Jim Sheu joined the Materials Engineering Department at AT&T Bell Laboratories in Norcross, Georgia in 1990. He is responsible for the research and development of materials including water blocking materials, used in fiber optic cables and apparatus.

Dr. Sheu received his M. A. and Ph. D. degrees in Chemistry from Rice University in 1973 and 1975 respectively. He did postdoctoral research at Harvard University on a fellowship. His areas of research included synthesis and application of superabsorbent polymers, water soluble polymers and specialty chemicals. In 1984, he also taught graduate chemistry courses at the University of Houston.

Dr. Sheu is a member of American Chemical Society and Society of Petroleum Engineers.



\*\*\*\*\*

Walt Paucke joined AT&T Baltimore Works in 1963 and worked in the Plastic Insulation Area before being transferred to the Atlanta Works in 1969. He has worked in Fiber Optic Sheathing since 1984. A Member of the Technical Staff, Walt is a graduate from Penn State Technical Institute, with a degree in Machine and Tool Design.

# THE RELIABILITY OF WATER PROOF OPTICAL CABLE WITH A PLASTIC SHEATH AND WATER SWELLABLE MATERIALS.

Hiroyuki SAWANO, Yoshiyuki SATO and Matsuhiro MIYAMOTO.

Fujikura Ltd.

Sakura-shi, Chiba-ken, 285 Japan

## ABSTRACT

Water swellable materials composed of water absorbent polymers are widely used in trunk and subscriber networks in Japan. A plastic sheath protects the cable core from outer forces and environmental effects in and after installation.

A one-hundred-fiber optical cable and a one-thousand-fiber optical cable were subject to the several examinations, such as mechanical, environmental tests. Especially, aqueous vapor permeation through the plastic sheath into the cable was investigated.

It was clarified that the aqueous vapor permeation into the cable depends on the temperature and water absorbent polymer in the cable. However, the aqueous vapor permeated can scarcely affect the transmission characteristics and fiber strength.

## 1. Introduction

Optical fiber networks are being constructed widely in the world and play very important role as an infrastructure of the society to realize the high speed digital transmission. Accompanied by it, many structures of optical cables that accommodate the climates and social conditions are developed. Among them, slotted core structure and loose tube structure using mono fibers or fiber ribbons are very popular because of their capability of highly dense fiber packaging and easiness of cable connection and their superior transmission characteristics<sup>1,2</sup>.

In Japan, nonmetallic water proof cable has been introduced to the trunk line, because it can protect workers from the trouble due to electron-magnetic induction<sup>3,4</sup>. In the subscriber network, one-thousand-fiber water proof cable has been adopted in metropolitan area<sup>5</sup>. These cables have one or several slotted rods and water swellable tapes and yarns as core wrappings and fillings. One-thousand-fiber water proof cable was originally a metallic cable that has a laminated aluminum polyethylene sheath and a steel central strength member<sup>6,7</sup>.

However, the laminated aluminum sheath has changed to polyethylene sheath<sup>8</sup>.

In designing the optical cable, it is important to prevent the cable from water penetration, because water degrades the optical fiber strength and increases the transmission loss due to hydrogen generated by the chemical reaction between water and metallic materials. So, optical cables are protected by two methods from water penetration. One is to use the gas pressurized system and the other is to use the water blocking compound like jelly or water swellable materials. When water swellable materials are applied to plastic sheath cable as the water blocking materials, aqueous vapor penetration should be checked because the aqueous vapor also plays the same role as water.

## 2. Water swellable materials.

### (1) Structures of water swellable materials.

As water blocking materials, water swellable tape and yarn were developed.

They consist of unwoven tape, yarn, absorbent polymer and adhesive. Absorbent polymer is attached by adhesive on the base unwoven tape or plastic yarn. Fig.1 shows the structures of water swellable tape.

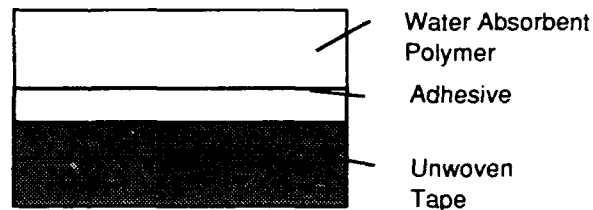


Fig.1 Cross Section of Water Swellable Tape.

When water penetrates into the cable, water absorbent polymer expands its volume more than one hundred times as large as that of its original volume. Then, absorbent polymer is released from the base tape and fills the vacancy in the cable.

## (2) Mechanism of water absorption.

There are two mechanisms of water absorption. One is the aqueous vapor absorption and the other is water absorption. These two mechanisms are described as follows<sup>9</sup>:

In the case of aqueous vapor absorption:

$$\ln(p/p_0) = \ln(1-v) + (1-1/n) + \chi v^2 \quad \text{--- (1)}$$

In the case of water absorption:

$$\begin{aligned} & (1/v)^{5/3} \\ & = [(i/2v_u s^{0.5})^2 + (1/2 - \chi)/v_1] / (n_e/v_0) \end{aligned} \quad \text{--- (2)}$$

Where:

$p$  = Aqueous vapor pressure.

$p_0$  = Aqueous vapor pressure at standard condition.

$v$  = Volume fraction of absorbent polymer.

$n$  = Segment number.

$\chi$  = Interaction parameter that expresses the affinity between the absorbent polymer and aqueous vapor.

$i$  = Product of degree of ionization and ionic charge number.

$v_u$  = Molar volume of structural unit.

$s^u$  = ionic strength of water.

$v_1$  = Molar volume of water.

$n_e$  = Effective chain number of net in absorbent polymer.

$v_0$  = Volume of absorbent polymer before water absorption.

From equation (1), it is recognized that the aqueous vapor absorption will be dominated by the relative vapor pressure and interaction parameter. Temperature dependence is included in relative vapor pressure.

On the other hand, equation (2) shows that the water absorption depends upon the degree of ionization, ionic strength and degree of crosslink but has no dependence on temperature. The large water absorption of absorbent polymer is explained by the first term of equation (2).

## (3) Experimental results of water absorption of water absorbent polymer.

Fig.2 shows the relation between the aqueous vapor absorption and the relative humidity. Aqueous vapor absorption increases as the relative humidity.

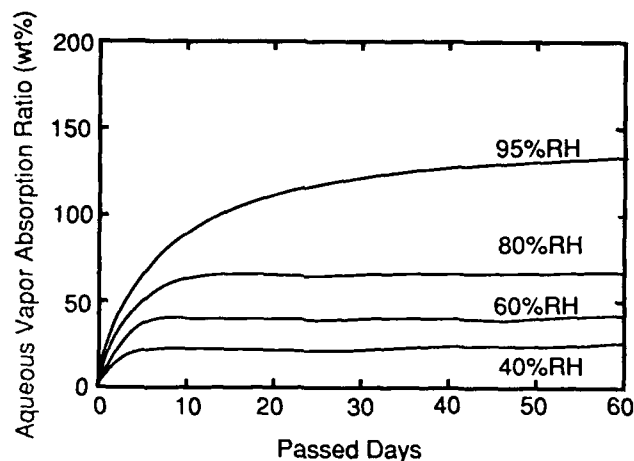


Fig.2 Humidity Dependence of Aqueous Vapor Absorption.

Fig.3 shows the temperature dependence of saturated aqueous vapor absorption. With the increase of temperature, the aqueous vapor absorption becomes large because the absolute humidity is large in high temperature.

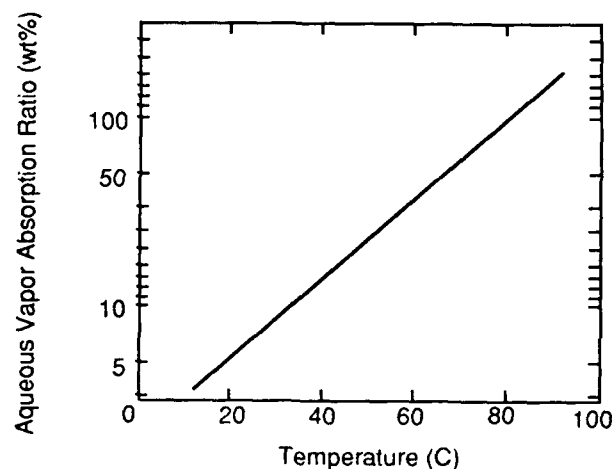


Fig.3 Temperature Dependence of Saturated Aqueous Vapor Absorption.

In Fig.4-6, the relations between water absorption and temperature, pH and concentration of salts are shown. Temperature and pH dependence of water absorption are scarcely observed but the salts in aqueous solution degrade the water absorption extremely.

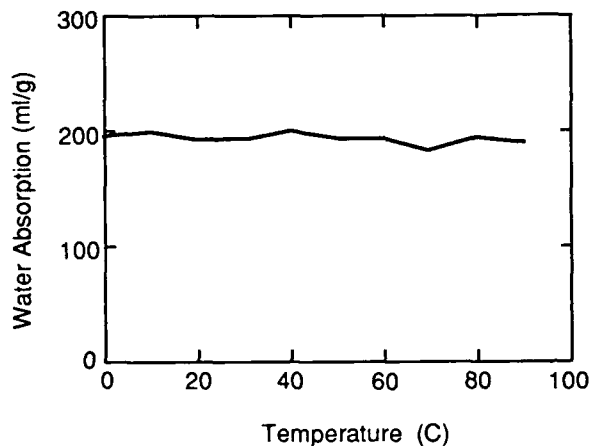


Fig.4 Temperature dependence of Water Swelling Ability.

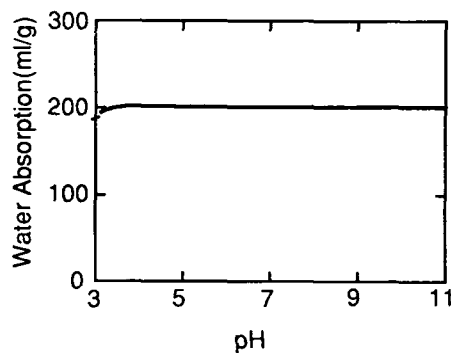


Fig.5 pH dependence of Water Swelling Property.

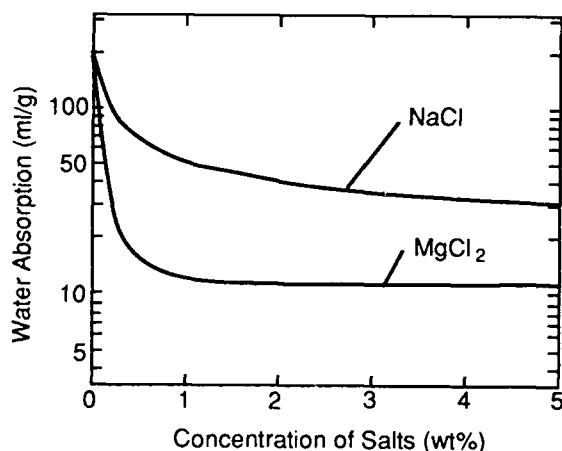


Fig.6 Salt Concentration Dependence of Water Absorption.

Thus, the amount of aqueous vapor absorption is the order of water absorbent polymer weight, but the amount of water absorption is more than hundred times as large as that of aqueous vapor.

### 3. Water permeation into the cable.

#### (1) Theoretical discussion.

Water penetration into the cable is the diffusion of water through the sheath and dominated by the permeability of water through the polyethylene sheath.

Water can diffuse through the plastic sheath very slowly. The amount of water that can pass through can be calculated assuming the initial concentration within the cable is negligible using<sup>10</sup>:

$$Q = 2D\pi / \ln(b/a) \quad \text{--- (3)}$$

where:

Q = The amount of water passing through the sheath per unit length.

D = Penetration rate of water through the sheath.

t = Time.

a = Internal diameter of the sheath.

b = Outer diameter of the sheath.

In addition, it is considered that the temperature dependence of water permeation through the sheath can be described in the same form as diffusion using<sup>10</sup>:

$$Q = Q_0 \exp(-E/RT) \quad \text{--- (4)}$$

Where:

$Q_0$  = Constant.

E = Activation energy of diffusion.

R = Gas constant.

T = Temperature.

Fig.7 illustrates the mechanism of water permeation. In the case of water proof cables, it is considered that the aqueous vapor that passes into the cable will be absorbed by water swellable materials, so the aqueous vapor pressure in the cable is smaller than the ordinary plastic sheath cable. This aqueous vapor absorption makes the aqueous vapor difference between outside and inside of the sheath larger than ordinary plastic sheath cable.

Due to this aqueous vapor pressure difference, the water permeation of the cable that has water swellable materials becomes larger than the ordinary plastic sheath cable.

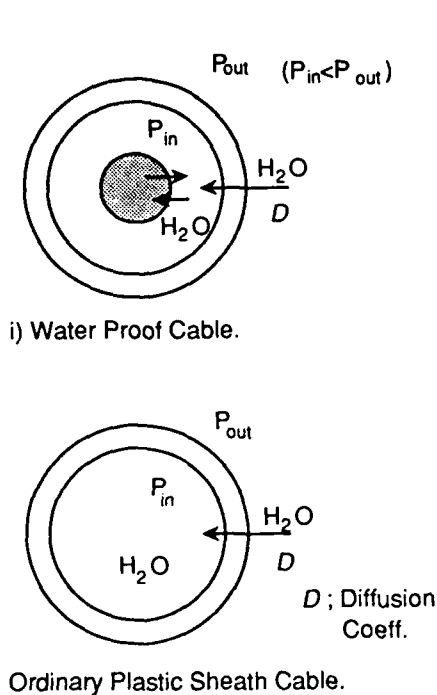


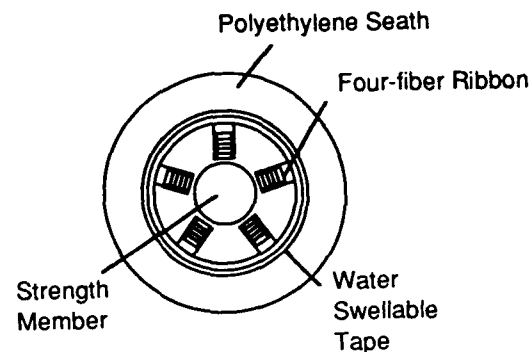
Fig.7 Mechanism of Water Penetration into the Cable.

## (2) Sample cable

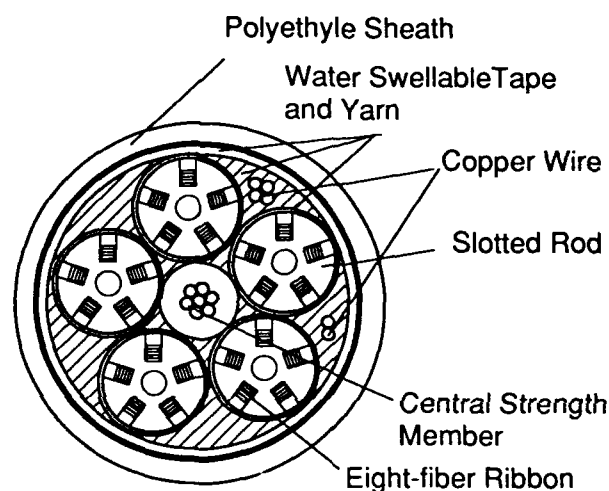
Cables used to research the aqueous vapor absorption are shown in Fig.8. One is a one-hundred-fiber nonmetallic optical cable composed of single mode four-fiber ribbons and a slotted core that has a aramid FRP rod as a strength member. The other is a one-thousand-fiber optical cable which has eight-fiber ribbons and five two-hundred-fiber units and a steel central strength member. Each cable has water swellable materials and low density polyethylene sheath. The amounts of water absorbent polymer contained in each cable are 4.5g/m and 45g/m.

## (3) Water permeation tests.

Samples are listed in table 1. Samples were cut in 30cm long and desiccated by vacuum pump at 80C for 24 hours. Then, their ends were sealed by fused polyethylene to avoid water penetration. These samples were immersed in waters at 40C, 60C and 80C.



(a) One-hundred-fiber Nonmetallic Water Proof Cable.



(b) One-thousand-fiber Water Proof Cable.

Fig.8 Crossectional View of investigated Water Proof Cables

Table 1 List of Sample Cables.

Sample	Cable	Sheath	O.D. I.D.	Amount of Polymer
A,B,C	nonmetallic 100 fibers	LDPE	17mm 13mm	4.5g
D	nonmetallic 100 fibers	LDPE	17mm 13mm	0g
E	metallic 1000 fibers	LDPE	40mm 35mm	45g



Fig.9 shows the temperature dependence of low density polyethylene sheath. The amount of absorbed water at 80C was about 7-8 times as large as that of at 40C. From the equation (4), the amount of aqueous vapor permeation can be estimated 1/22 as much as that of at 80C. This temperature dependence is almost equal to the polyethylene itself. Moreover, the weight increase of water proof cable is larger than the plastic sheath cable.

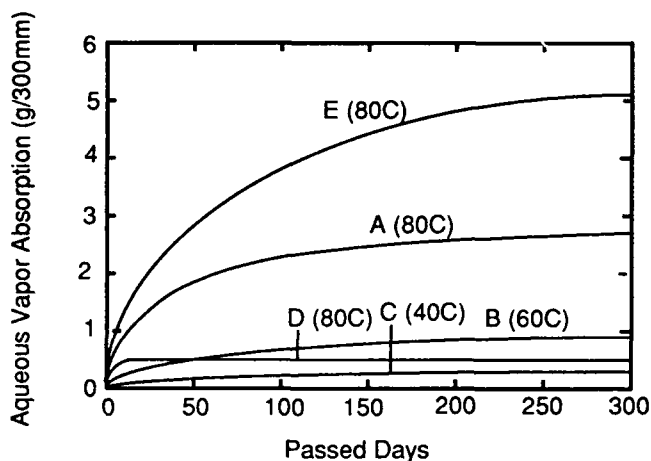


Fig.9 Aqueous Vapor Absorption of Cables.

The saturation time of aqueous vapor is determined by the amount of saturated aqueous vapor absorption and the amount of aqueous vapor permeation into the cable per unit time.

From Fig.3, the saturated aqueous vapor absorption at room temperature is about 5% of the weight of water absorbent polymer. In the case of 30cm long one-hundred-fiber nonmetallic cable, its value is about 0.15g. On the other hand, aqueous vapor permeation at room temperature is estimated about 0.06g/year, so it takes about 2.5 years to reach the saturation of aqueous vapor permeation. This value is 150 time as large as that of ordinary plastic sheath cable.

In the case of one-thousand-fiber water proof cable, the amount of permeated water was larger than that of one-hundred-fiber nonmetallic optical cable. This is caused by the difference of dimensions. The difference between these two kinds of cable is illustrated by equation (3).

To investigate the humidity in the cable, two kinds of polyethylene tubes were prepared. One had the water swellable tapes. Fig.10 shows the humidity in the tubes. The tube which had no water swellable tape was 98% of relative humidity but the tube with water swellable tape was 65% of relative humidity after 30 day's water immersion at 40C.

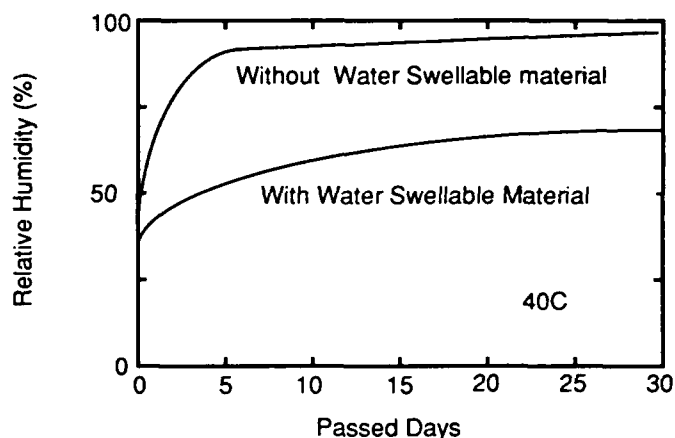


Fig.10 Humidity in the Polyethylene Pipe.

From the results of above examinations, aqueous vapor permeation of water proof cable is larger than the ordinary plastic sheath cable but the relative humidity in water proof cable is smaller than that of ordinary plastic cables. This means that the aqueous vapor permeated into the cable is absorbed by water swellable materials and the humidity is kept low for long term. So, it can be expected that the degradation of transmission characteristics and fiber strength of water proof cable is smaller than the ordinary plastic sheath cable.

#### 4.Cable properties.

A one-hundred-fiber nonmetallic water proof cable was immersed in water for 1.5 years at room temperature. Absorbed water was 0.35g/m. The amount of absorbed water was a little less than the estimated value.

This cable was subject to the researches of transmission loss and mechanical properties.

### (1)Transmission characteristics.

Fig.11 shows the loss changes of at 1.3um, 1.55um and 1.38um. The loss changes were less than 0.02dB/km.

Temperature dependence of transmission loss is shown in Fig.12. The investigated temperature range is from -40C to 60C. The loss increases at -40C and 60C were 0.03dB/km and 0.02dB/km, respectively. These loss changes were similar to those of soon after the cable fabrication.

As a result of these researches, it can be said that the transmission loss was not affected by permeated aqueous vapor.

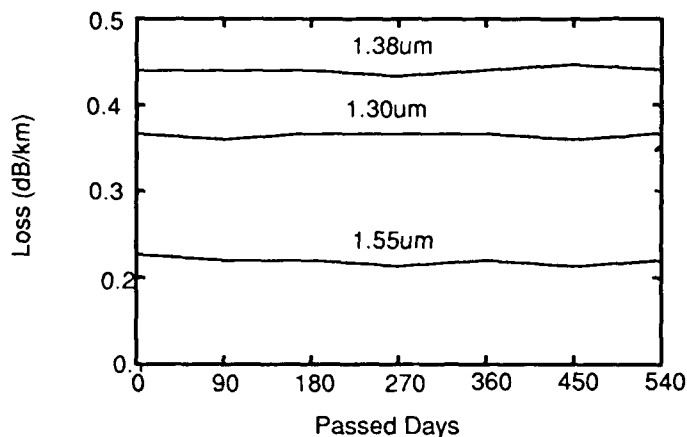


Fig.11 Loss Change of Water Immersed Cable.

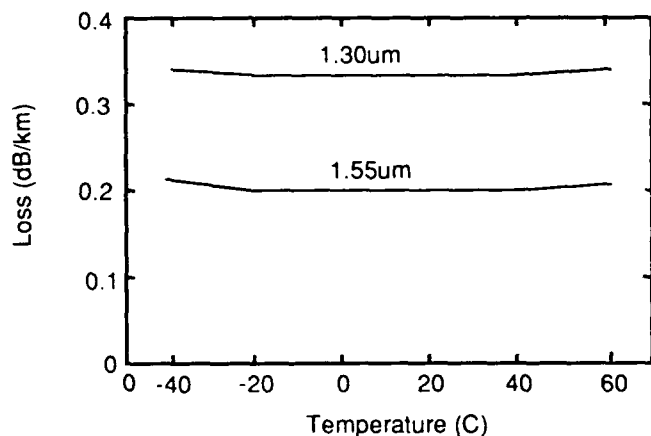


Fig.12 Temperature Characteristics of Water Immersed cable.

### (2)Mechanical properties.

In table 2, mechanical properties are shown.

Crush, bending, stretching, squeezing, vibration and impact tests were carried out. Against these tests, no degradation of transmission characteristics or cable strength was observed.

Table 2 Mechanical Properties of 100-fiber Nonmetallic Water Proof Cable.

Item	Condition	Result
Bending	R=200mm, 1turn	less than 0.01dB/turn
Stretching	up to 0.2% elongation	less than 0.01dB/100m
Crush	up to 2500N/50mm of lateral force	less than 0.01dB/50mm
Vibration	10Hz, 5mm of amplitude, 1 million times	less than 0.01dB/m
Impact	1kg, 1m height	less than 0.01dB
Squeezing	R=200mm, up to 0.2% elongation	less than 0.01dB/100m

### (3)Fiber strength.

Weibull plots of fiber breaking strength before and after the water immersion are shown in Fig.13. The fiber strength does not decrease after 1.5 year's water immersion.

This result seems that the water absorbent polymer acts as desiccating agent in the cable so the aqueous vapor pressure is not so large around the optical fibers.

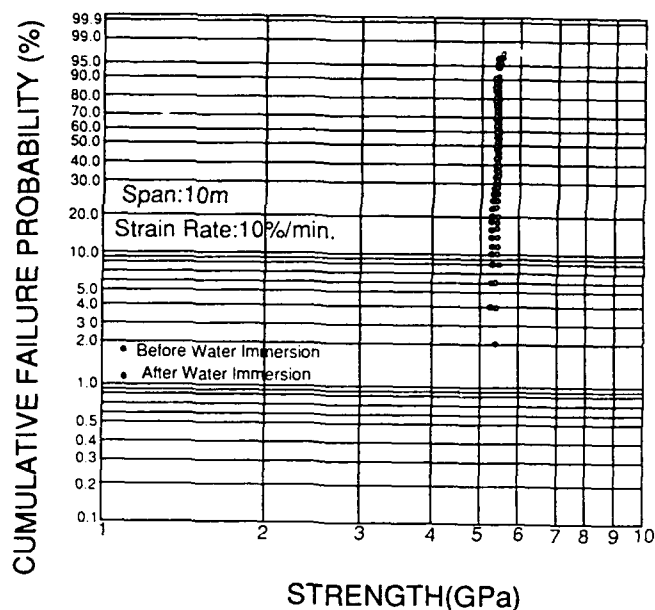


Fig.13 Weibull Plot of Fiber breaking strength before and after Water Immersion Test.

### 5.Conclusion.

A one-hundred-fiber non-metallic optical cable and a one-thousand-fiber water proof cable were subject to the research of aqueous vapor permeation into the cable. The aqueous vapor permeation into the cable becomes large at high temperature and under the existence of absorbent polymer. However, the humidity in the cable is smaller than the ordinary plastic sheath cable. The amount of water permeation at 20C can be estimated 1/22 time as large as that of at 80C.

The cable properties against temperature change and fundamental mechanical tests were similar to that of soon after the cable fabrication. In addition, optical fiber strength was kept in the initial level.

### Acknowledgment.

Authors would like to express their sincere appreciation to Dr. Inada for his helpful discussions and suggestions and other members who engaged in this work with patience.

### References

1. M. Kawase, T. Fuchigami, M. Matsumoto, S. Nagasawa, S. Tomita and S. Takashima, "Loop-Network Configuration for Subscriber Loops and Single-mode Optical Fiber Cable Technologies Suitable for Mid-span Access," 37th IWCS 1988.
2. H. Sawano, Y. Kikuchi, K. Kobayashi, N. Okada, N. Misono, H. Suzuki and N. Sato, "One-thousand-fiber Cable Composed of Eight Fiber Ribbons," 38th IWCS 1989.
3. S. Kikuta, T. Nakai, A. Hayashi and H. Koga, "A New Nonmetallic and Waterproof Optical Fiber Cable with Absorbent Polymer Ribbon," 36th IWCS 1987.
4. S. Kikuta, T. Nakai, A. Hayashi and H. Koga, "Design and Performance of Nonmetallic Waterproof Optical Fiber Cable Using Water-Absorbent Polymer," IEEEJ. Lightwave Tech., LT-7, No. 4, 1989.
5. M. Kawase, S. Tomita, N. Kasahara and T. Uenoya, "Optical Subscriber Loops by Nonpressurized Optical Fiber Cable," Transactions of the IEICE, Vol. J73-B-I No. 10, 1990.
6. S. Tomita, F. Ashiya and M. Kawase, "1000-Fiber Water Blocking Cable," Transactions of the IEICE, Vol. E73, No. 9, 1990.
7. Y. Kikuchi, H. Sawano, Y. Sato, K. Kobayashi, K. Okamura, H. Suzuki and N. Sato, "Characteristics of One-thousand-Fiber Water Proof Cable," 39th IWCS 1990.
8. F. Ashiya, K. Hogari and K. Omoto, "A Water-Blocking Optical Fiber System for Subscriber Networks," NTT REVIEW Vol. 3 No. 1, 1991.
9. P. J. Flory, "Polymer Chemistry," Chapter 12 and 13, Maruzen 1967.
10. T. Kuwabara and S. Mochizuki, "Permeance Properties of Plastic Sheaths and Their Improvement for Telecommunication Cables," Transactions of the IEICE, Vol. J66-B, No.5, 1983.



Hiroyuki SAWANO

Opto-Electronics  
Laboratory  
Fujikura LTD.

1440 Mutsuzaki,  
Sakura-shi, Chiba-ken  
285 Japan

Mr. SAWANO was born in 1955. He joined Fujikura LTD. after his graduation from Hokkaido University with a M.S. Degree in 1983 and has been engaged in research and development of optical cables. He is now an engineer of Telecommunication Cable Section and a member of IEICE of Japan.



Yoshiyuki SATO

Opto-Electronics  
Laboratory  
Fujikura LTD.

1440 Mutsuzaki,  
Sakura-shi, Chiba-ken  
285 Japan

Mr. SATO was born in 1963. He joined Fujikura LTD. after his graduation from Tohoku University with a M.E. Degree in 1987 and has been engaged in research and development of optical cables. He is now an engineer of Telecommunication Cable Section and a member of IEICE of Japan.



Matsuhiro MIYAMOTO

Opto-Electronics  
Laboratory  
Fujikura LTD.

1440 Mutsuzaki,  
Sakura-shi, Chiba-ken  
285 Japan

Mr. MIYAMOTO was born in 1953. He joined Fujikura LTD. after his graduation from Tokyo Institute of Technology with a M.S. Degree in 1978 and has been engaged in design and research of optical fibers and cables. He is now a senior engineer of Telecommunication Cable Section and a member of IEICE of Japan.

## Cable Polymer Reliability Testing

Paul E. Neveux, Jr. and Eric L. Buckland

Sumitomo Electric Fiber Optics Corp., Research Triangle Park, North Carolina, 27709

### ABSTRACT

An improved model for the degradation of PBT used in loose tube fiber optic cables has been developed based on an acid catalyzed hydrolysis reaction. An improved class of PBTs was studied, and through the use of a carboxylic end group determination test, it was found that while the lifetime of the new materials does significantly improve, the basic degradation mechanism remains the same. It is found through MFR testing that the degradation rate follows a power law dependence with moisture concentration, with an exponent of 2.8. The new materials offer a predicted 3x improvement in lifetime, making them more suitable for use in the pedestal environment.

### I. INTRODUCTION

With the introduction of fiber optic cables in the distribution loop, the long term reliability requirements for cable components have become more stringent. All of the materials will be expected to withstand the pedestal environment where much higher temperatures and humidity conditions prevail, compared to buried service cable. In choosing the materials to be used in fiber optic cables, the materials must:

- (1) Meet Customer Specification
- (2) Have Intercomponent Compatibility
- (3) Perform Reliably under Field Service Conditions

For all three conditions to be met, extensive testing is preformed to insure that each material is suited for the application in which it will be used. The last criteria, however, is the most time consuming and rigorous since the results of the testing must prove that the material will function adequately for the lifetime of the cable. Reliability testing involves aging the materials under various conditions much more severe than would be normally encountered in the field to shorten the amount of time required to observe some loss of performance. In order to predict the time to failure of a cable component it is also necessary vary the exposure conditions, *e.g.* temperature, humidity, light, *etc.*, to determine the *rate* at which the material degrades with the severity of the exposure. Especially important is a knowledge of the material itself, its degradation mechanisms and which physical and/or chemical properties should be monitored to assess the extent of degradation.

Table 1 shows some typical polymer types which are currently used in many fiber optic cable types. In conducting reliability tests for these materials and others in a cable, various physical parameters can be followed to determine the extent of

degradation. The allowable change tensile characteristics of the polymers is often used in customer specifications since they are easily measured. While mechanical characteristics might be appropriate to determine a performance endpoint, it is difficult to predict long-term behavior using these tests, especially when the results are catastrophic rather than gradual. For long term reliability testing, analytical test methods are performed in addition to physical tests.

Table 1. Some Typical Polymers Used in Cables

Polymer Type	Function
U.V. Acrylates	Fiber Coatings Ribbon Matrix
Poly(esters)	Loose Tubes Binder & Ripcord
Poly(amide)	Loose Tubes Tight Buffer
Poly(aramid)	Fiber Strength Elements; Ripcord
Poly(acrylic acid)	Water Blocking Agent
Poly(olefins)	Loose Tube Material Filler Rods CSM Upjacket Steel Tape Coating Sheathing Material
Poly(vinyl chloride)	Tight Buffer Riser Sheathing

There are a number of advantages for choosing an analytical method to perform reliability testing. While physical tests yield bulk property information, a correctly chosen analytical method will give important structural information about state of the polymer. In addition, most analytical tests, *e.g.* Fourier Transform Infrared Spectroscopy (FTIR), require very little sample compared to physical tests, *e.g.* tensileometry, which at the very least requires a sample big enough to grip. This last advantage is especially important when actual field samples need to be evaluated: the sample need not be intact.

Ideally, the analytical method should meet the following criteria:

- (A) Detects Degradation *Before* Mechanical Failure Occurs
- (B) Sensitive to Concentration of Polymer Degradation Products
- (C) Immune to Interfering Compounds

Not all analytical methods yield the same amount of information compared with other methods for the same material. For example, it has been shown that Melt Flow Index, when properly done, will increase as the poly(ester), poly(butylene terephthalate) or PBT, degrades.<sup>1</sup> In addition, the degradation mechanism must be known for an appropriate analytical method to be chosen. Table 2 gives a summary of typical physical and analytical methods and the polymer types which can be tested by them.

Recently, some new grades of hydrolysis resistant poly(butylene) terephthalates (PBT) were introduced onto the market. This paper focuses on comparing these new grades of PBT to standard grades and how hydrolysis resistance, if any, is achieved. Each compound was examined for its resistance to hydrolysis by examining both the mechanical and chemical changes after aging.

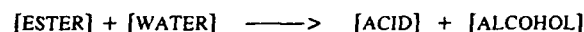
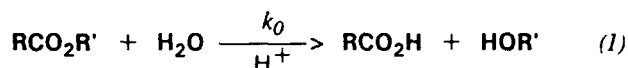
**Table 2. Test Method vs. Polymer Type**

Polymer Type	Method
All Polymers	Tensilemetry
	Compression Resistance
	Minimum Bend
	Stress Cracking
	Thermal Analysis, <i>e.g.</i> Differential Scanning Calorimetry (DSC)
Poly(esters)	FTIR
	Nuclear Magnetic Resonance
	Melt Flow
Poly(olefins)	Carboxylic Acid End Group Titration
	Oxidation Induction Time

## II. THEORY

### A. Degradation Mechanism for PBT

The primary mode of degradation for PBT and most other poly(esters) is hydrolysis:



where R and R' are the polymer chain continuing on either side.

In the reaction a molecule of water is introduced into the ester bond to produce the starting materials: a carboxylic acid and an alcohol. While there are other degradation pathways, they typically occur at temperatures not normally experienced in the field for fiber optic cables.<sup>2</sup> Note that simple esterification reactions are known to be acid catalyzed and further, that a carboxylic acid end group can catalyze the esterification, or de-esterification in this case, of an adjacent ester linkage.<sup>3</sup> The reaction rate equation must then reflect the effect of the concentration of carboxylic acid end groups on the overall reaction rate.

### B. The Rate Equation

Rather than use the number average degree of polymerization to follow the rate of degradation, as is often done,<sup>4</sup> the rate of formation of the carboxylic acid end group was observed, both directly and indirectly, through melt flow results. The rate hydrolysis of an ester linkage, including the catalytic effect of an adjacent carboxylic acid end group, can be expressed simply as the rate of formation of carboxylic acid end groups:

$$d[\text{RCO}_2\text{H}]/dt = k_0 [\text{H}_2\text{O}]^\alpha [\text{RCO}_2\text{R}']^\beta \quad (2)$$

$$k_0 = k_w + k' [\text{RCO}_2\text{H}] \quad (3)$$

where  $k_w$  is the rate of hydrolysis in the absence of acid and  $k$  is the acid catalyzed rate. In order to simplify the equation, two basic assumptions were made:

- (1)  $k_w \ll k'$ , *i.e.*, the acid catalyzed rate is much faster than the uncatalyzed rate
- (2)  $d[\text{RCO}_2\text{R}']/dt \approx 0$ , *i.e.*, the *change* in the concentration of [ESTER] linkages with hydrolysis is very small, therefore the reaction is can be made "psuedo-zero order" in ester concentration and  $\beta = 0$

These assumptions simplify the equation to:

$$d[\text{RCO}_2\text{H}]/dt = k' [\text{H}_2\text{O}]^\alpha [\text{RCO}_2\text{H}] \quad (4)$$

By keeping the water concentration constant for the series of PBT compounds, the equation is further simplified to:

$$d[\text{RCO}_2\text{H}]/dt = k [\text{RCO}_2\text{H}] \quad (5)$$

$$\text{where } k = k' [\text{H}_2\text{O}]^\alpha$$

Note that  $\alpha$  must be determined experimentally.

Rearranging the equation and taking the integral of each side:

$$\int d[\text{RCO}_2\text{H}]/[\text{RCO}_2\text{H}] = \int k dt \quad (6)$$

and integrating both sides from time = 0 to time =  $t$ ,

$$\text{Ln}([\text{RCO}_2\text{H}]_t) = kt + \text{Ln}([\text{RCO}_2\text{H}]_0)$$

Since, for a given PBT, the melt flow rate is proportional to the number average  $\text{MW}^5$  and the number average molecular weight is proportional to the number of carboxylic acid end groups in the polymer, the relationship of melt flow rate (MFR) with time can be expressed in a similar fashion:

$$\text{Ln}(\text{MFR}_t) = kt + \text{Ln}(\text{MFR}_0)$$

The temperature dependence of the reaction rate,  $k'$ , is described by the familiar Arrhenius equation:

$$k' = A \exp(-E_a/RT)$$

where  $A$  is a constant,  $E_a$ , the energy of activation for the reaction,  $R$  is the gas constant, and  $T$  is the temperature in degrees Kelvin. The value of  $E_a$  which was used in this paper is 26 kcal/mol.<sup>6</sup>

### C. The Concentration of Water Vapor

In an earlier work, the rate of degradation was correlated with the percent relative humidity.<sup>7</sup> What was not taken into account was that relative humidity is a function of temperature, i.e., 50% RH at 25°C is far less water vapor than 50% RH at 50°C. The maximum concentration of water vapor (partial pressure in mm Hg) at any given temperature below 100°C and at 1 atmosphere (760 mm Hg) is given approximately by:

$$P_{\text{max}} (\text{mmHg}) = \exp(20.5 - 5167/T)$$

To calculate % RH, the actual partial pressure of water is divided the maximum and multiplied by 100:

$$\%RH = P_{\text{act}} / P_{\text{max}} \times 100$$

The relationship between Partial Pressure of water vapor,  $P$ , and relative humidity is shown graphically in Figure 1. As can be seen by the isotherms, 50% RH corresponds to  $\approx$  340 Torr at 95°C,  $\approx$  90 Torr at 65°C, and  $\approx$  25 Torr at 35°C. In this work the concentration of water in mm Hg, or Torr, is used in the calculations of the rate of hydrolysis of the PBT's.

## III. EXPERIMENTAL

### A. Humidity Aging

Aging of PBT pellets, loose tubes and tensile bars was performed in Thermotron humidity chambers. Samples were variously aged at 85°C at 37% (160 Torr), 65% (282 Torr), 85% (367 Torr), and 94% RH (408 Torr). 94% RH was especially difficult to control with the results that the humidity was closer to 100% RH than 94% RH.

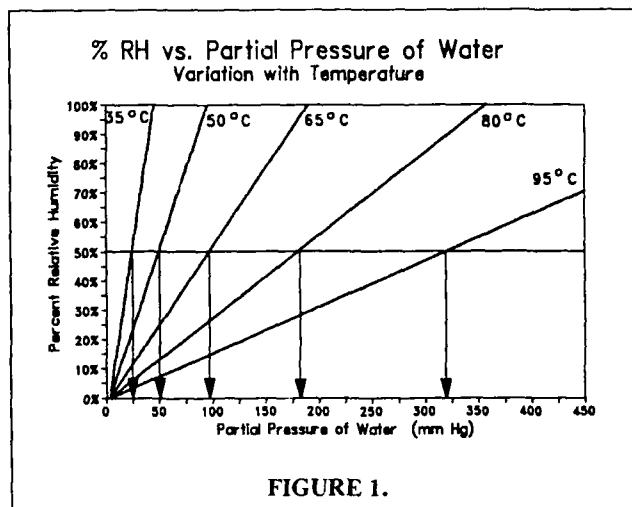


FIGURE 1.

### B. Melt Flow

Melt Flow was determined using a Tinius-Olsen Melt Plastometer following ASTM D 1238. In addition to using 2160 g load, a 1000 g weight was also used to keep the flow below 50 g/10 min for highly degraded samples (see below for details). The temperature was the standard 250°C. All samples were dried in a desiccator for 24 hours prior to testing.

### C. Mechanical Tests

Tensile testing was performed using an Instron Model 2100.

A Minimum Bend Test was performed using mandrels 1X, 2X, and 5X the diameter of the PBT tubes.

### D. Carboxylic Acid End Group Determination

A modified titration method by Kohl<sup>8</sup> was used.

## IV. RESULTS and DISCUSSION

### A. General Considerations

As previously mentioned, both the formation of esters and the hydrolysis of esters is catalyzed by the presence of acid.<sup>9</sup> The product of the hydrolysis of an ester is a carboxylic acid and an alcohol. For PBT, the carboxylic acid is held in place by the remaining polymer chain and can hydrolyze an adjacent ester bond. Hence the reaction is "autocatalytic". Reducing the amount of carboxylic acid end groups initially present in the polymer should significantly reduce the rate of hydrolysis and extend the lifetime of the polymer.

Reducing the amount of carboxylic acid end groups (CEG's) can be accomplished a number of ways. One way is to increase the molecular weight of the polymer chain: the higher the molecular weight for a specific PBT the fewer the carboxylic acid end groups. Another way might be to "cap" the acid end groups with a molecule which "inactivates" the acid.<sup>10,11</sup> Since it is not known how the CEG numbers were reduced in either of the low CEG PBT's, no attempt was made to reach a conclusion as to the relative advantage of either method of reducing CEG number.

Since CEG is so important to the lifetime of a PBT, the change in CEG with aging was compared for three PBT's. PBT A was a standard unfilled grade and PBT's B and C were "low CEG" - hydrolysis resistant grades. In addition, melt flow rates were also determined and correlated with CEG.

## B. Mechanical Results

In order to determine what MFI or CEG value corresponded with failure tensile bars of each PBT was aged at 85°C and 94% RH and measured for Percent Elongation at Yield, Strength at Yield, and Modulus at 2% strain. As can be seen, with PBT A the % elongation and strength at yield both drop dramatically after 30 days. For the hydrolysis resistant PBT's, however, these parameters fall after 60 days. The modulus at 2% did not significantly change at all during this time period. Note, for PBT B, that there is an increase in % elongation and strength at yield before the drop at 60 days and the loss of elongation and strength is nearly half as great as PBT C.

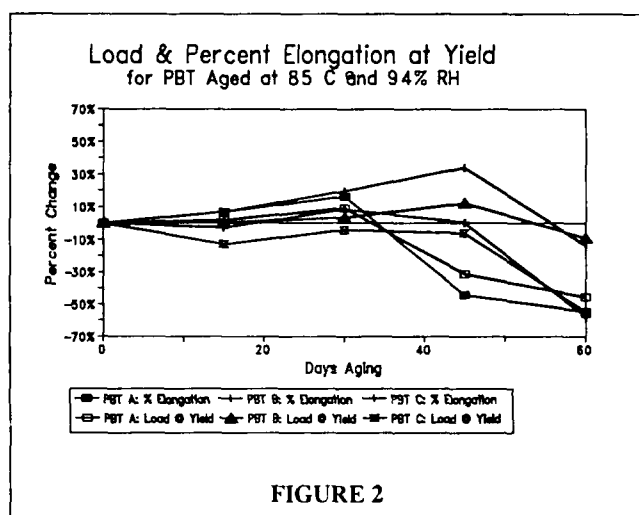


FIGURE 2

In the aging of PBT's, the tensile bar samples became brittle even before a change was seen in the tensile testing. Therefore, a Minimum Bend Test devised which would reflect the brittleness of the PBT and the extent to which it might be handles in the field. Tubes of each PBT were aged and then wrapped around mandrels which were 1X, 2X, and 5X the diameter of the tubes. Failure was considered that point when the tube cracked as it was applied around the mandrel. Table 4 shows the results of the Minimum Bend Radius Testing.

Table 4.  
Minimum Bend Results after 85°C/95% RH Aging

Sample	30 Days			45 Days		
	1X	2X	5X	1X	2X	5X
PBT A	Pass	Pass	Pass	Fail	Fail	Fail
PBT B	Pass	Pass	Pass	Pass	Pass	Pass
PBT C	Pass	Pass	Pass	Pass	Pass	Pass

It is clear from the results that the mechanical failure for PBT occurs catastrophically, whether testing via a tensiometer or a mandrel and that there is a critical molecular weight after which the material loses its mechanical integrity. These results are consistent with previous studies which show that tensile strength and elongation of thermoplastics are insensitive to changes in molecular weight only above a limiting value.<sup>12</sup>

## C. Melt Flow

One problem which was quickly realized when performing melt flow on aged PBT samples was the relatively short time it took to reach 50 g/10 min, the maximum flow recommended by the ASTM. Beyond this point, non-newtonian flow is expected and the viscosity - molecular weight relationship becomes non-linear. In order to extend the useful "lifetime" of the test method, the load weight was reduced from the normal 2160 g to 1000 g. As can be seen in Figure 1 which shows the results of using the 2160 g load weight, PBT A could only be tested up to 20 days and PBT B, up to 45 days. By decreasing the load to 1000 g, and hence the shear rate, the useful aging time for PBT A was increased to 30 days and for PBT's B and C, to 60 days.

Note that the slope of Ln(MFR) vs. Days Aging for PBT A is nearly twice the rate of PBT's B and C, which are themselves, very similar. Also, the initial melt flow rate of PBT B is higher at time zero than PBT A.

## D. Carboxylic Acid End Group Determination

For each of the PBT's aged at 85°C and 85% RH, the carboxylic acid end group concentration (in milliequivalents per kg of polymer) was determined. Figure 5 shows the results. What is immediately obvious is that all of the rates are very nearly equal, within experimental error. This result confirms that the mechanism by which each of the PBT's hydrolyze is the same, a conclusion which could not have been reached with the MFR results. This assumes that the change in the hydrolysis rate with temperature, as given by  $E_a$  (via the Arrhenius equation) is the same. The CEG test is, unlike MFR, insensitive to the type of PBT, since it gives the absolute concentration of carboxylic acid end groups. This allows the determination of the age of any field sample, regardless of the source. Although methods have been developed to determine the MFR of cable samples,<sup>13</sup> only

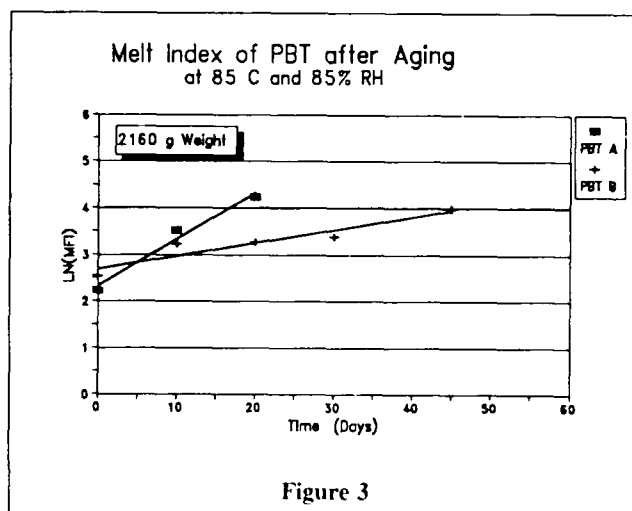


Figure 3



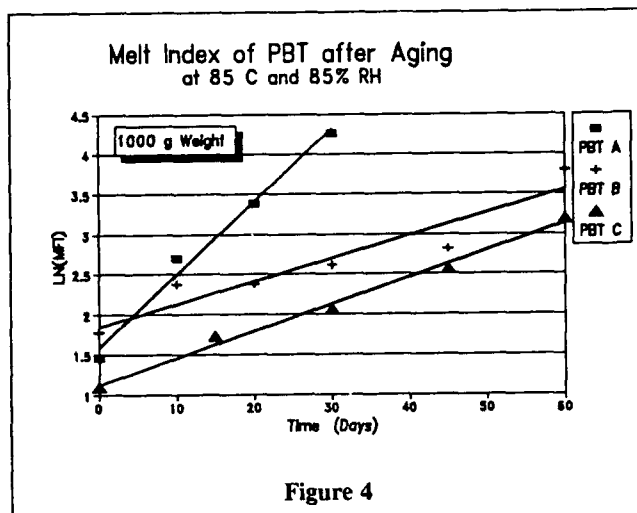


Figure 4

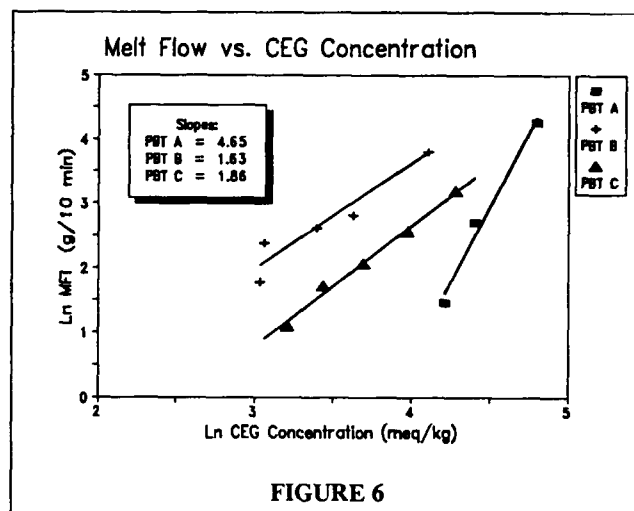


FIGURE 6

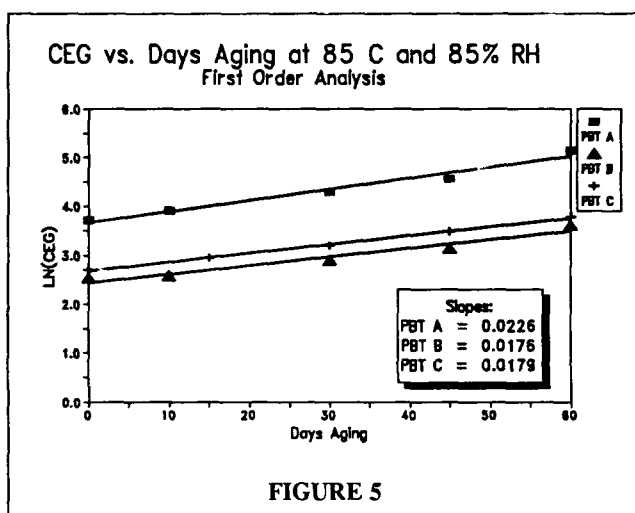


FIGURE 5

relative results, *i.e.* compared to unaged cable samples, could be obtained. It is infrequent when field samples can be compared to their unaged counterparts.

Shown in Figure 6 is the relationship between CEG and MFR for the PBT's aged at 85°C and 85% RH. The graph clearly points out the difference between PBT A and the hydrolysis resistant PBT C and D.

#### E. Dependence of Hydrolysis Rate on Humidity

Since the energy of activation for hydrolysis,  $E_a$ , has already been established (Ref. 7), the dependence of the rate of hydrolysis with water vapor concentration for PBT A and PBT B was determined. With the temperature maintained at 85°C, the rate of change in melt flow rate with humidity was monitored. It was originally desired to also include the change in the rate of CEG number with humidity aging,

however, that testing is still in progress. Table 4. shows the results of  $k$ , derived from  $\ln(\text{MFR})$  vs. Time regressions, vs. Concentration of Water Vapor in Torr (mm Hg). Table 5. and Graph 7 shows the results of the change in rates. Note that the rate of hydrolysis with water vapor concentration is three (3) times greater for PBT A than for PBT B.

Table 5.  
The Rate Constant,  $k$ , vs. Water Vapor Concentration

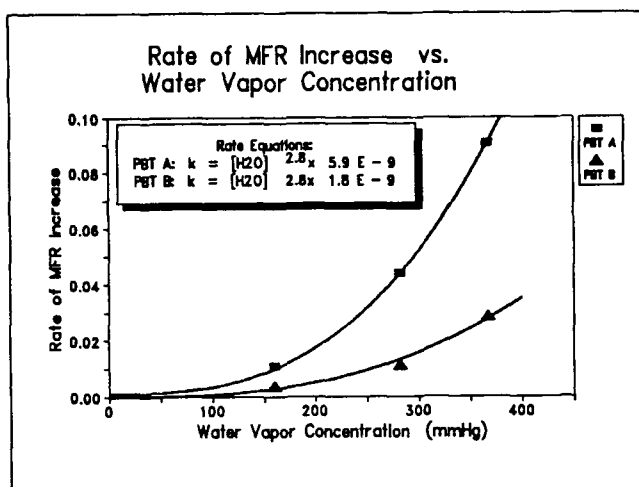
%RH at 85°C	Water Concentration (Torr)	PBT A Rate, $k$	PBT B Rate, $k$
37%	160	$1.1 \times 10^{-2}$	$0.35 \times 10^{-2}$
65%	280	$4.4 \times 10^{-2}$	$1.1 \times 10^{-2}$
85%	410	$9.1 \times 10^{-2}$	$2.8 \times 10^{-2}$

The order of the reaction was determined by performing a least squares analysis optimizing for  $\alpha$  in Equation 4 and assuming a zero intercept. In determining constants for the best fit, the order was varied from one (1) to three (3). What is most significant in these results is the calculated order of the reaction: the rate changes with  $[\text{H}_2\text{O}]^{2.8}$  vapor concentration, *i.e.*, there is a very strong dependence on the concentration of water vapor. Several factors could account for the high order of reaction. It is known that water causes the PBT to swell and this could enhance the reactivity. The additional water could also act to solvate the proton (acid) from the carboxylic acid group and allow its transport to an adjacent ester linkage.

Table 4. Humidity Matrix Results

Sample	Rate, $k'$	Order, $\alpha$
PBT A	$5.9 \times 10^{-9}$	2.8
PBT B	$1.8 \times 10^{-9}$	2.8

Caution should be used in applying these values because of the relatively small number of  $k$  rates used to obtain them. It does appear, however, that the order is indeed greater than at least 2, but further humidity studies are needed to confirm these results. CEG numbers currently being obtained with all PBT's should help better define the order of the reaction,  $\alpha$ .



#### F. Lifetime Prediction

Using the results above one can roughly approximate the lifetime of PBT given a set of typical field conditions. In the pedestal environment, it is expected that temperatures as high as 60°C (140°F) may be possible at times and with ground moisture as a nearly constant source of water vapor humidities may easily reach 85%. Using 60°C and 85% RH as a starting point to determine the lifetime, the first step is to convert %RH to absolute water concentration:

$$P_{act} = \%RH \times P_{max}/100$$

$$P_{act} = .85 \times 149 \text{ Torr} = 127 \text{ Torr}$$

Applying this value to the equation for  $k$  at 85°C,

$$k_{85} = 5.9 \times 10^{-9} \times 127^{2.8} = 4.6 \times 10^{-3}$$

The value for  $k_{85}$  is then entered into the Arrhenius equation:

$$\ln k_{60} = -Ea/R (1/T_{60} - 1/T_{85}) - \ln k_{85}$$

where  $\ln k_{60}$  is the rate of change in MFR at 60°C and 85% RH,  $Ea$  is the energy of activation for hydrolysis,  $R$  is the gas constant (1.987 cal/mol), and  $T_{60}$  and  $T_{85}$  are the temperatures in degrees Kelvin for 60°C and 85°C degrees, respectively.

The final step is to enter the rate,  $k_{60}$  into the rate equation for the change in MFR with time:

$$\ln(\text{MFR}_t) = k_{60} t + \ln(\text{MFR}_0)$$

or

$$t (\text{days to failure}) = \ln(\text{MFR}_t/\text{MFR}_0) / k_{60}$$

Before the final result can be obtained, the critical normalized MFR,  $\text{MFR}_t/\text{MFR}_0$  must be obtained from the mechanical

reliability results, where **MFR**, is the melt flow rate at failure. In the present case a value of 10 was used. Since the Ln of 10 is 2.303, the equation becomes:

$$t (\text{days to failure}) = 2.303 / k_{60}$$

Table 6. shows the results of these calculations.

Sample	Temperature	Humidity	[H <sub>2</sub> O]	Lifetime
PBT A	60°C	50%	75 Torr	46 years
	60°C	85%	127 Torr	17 years
PBT B	60°C	50%	75 Torr	150 years
	60°C	85%	127 Torr	55 years

#### V. CONCLUSIONS

Cable polymer reliability testing is an integral part of product development. Various physical and analytical methods are used to establish failure modes and assessing failure rates for critical materials under severe application environments. As a component in direct proximity to fragile optical fibers, PBT tubes are an especially important candidate for reliability studies. Two new commercially available hydrolysis resistant PBTs were compared with a standard grade of unfilled PBT.

A model was proposed for the hydrolysis degradation, based on an acid catalyzed reaction with a power law dependence on water concentration. Through physical tests, a normalized MFR of 10 was found to be indicative of failed PBT. After following the MFR rate vs. moisture, in Torr, PBT failure was found to proceed to the power of 2.8 of the water vapor concentration.

By using the mechanism specific CEG test, the failure mechanism for each of the PBT's was found to be the same, regardless of the method used to achieve the improvement in hydrolysis resistance. However, because the initial concentration of carboxylic acid end groups, which acts as an "autocatalyst", is much lower, the new hydrolysis resistance PBTs exhibit a significant improvement in lifetime expected to be at least three (3) times that of previous standard grade PBT's.

From these results, it is reasonable to expect reliable service of standard PBT in typical buried service cable environments. As movement toward the loop and pedestal environments continues, additional advantage in reliability are provided by the new generation of PBTs. Note that the power law dependence of water vapor still makes PBT unsuitable for the most severe environments, such as steam ducts.

#### Acknowledgments

The authors would like to thank Mr. Stuart Woods and Mr. Greg Tate for conducting the experiments.

- <sup>1</sup> Kelleher, P. G.; Wentz, R. P.; Falcone, D. R.; *Polymer Engineering & Science*, **1982**, 22(4), 260.
- <sup>2</sup> Zimmerman, H. in *Developments in Polymer Degradation*, Vol. 5, pp 79-119, N. Grassie, ed.; Applied Science Publ., London/New York, 1984.
- <sup>3</sup> Goldschmidt, H., *Ber.*, **1896**, 29, 2208; Rolfe, A. C.; Hinshelwood, C. N., *Trans. Faraday Soc.*, **1934**, 30, 935.
- <sup>4</sup> Rodriguez, F.; *Principles of Polymer Systems*, p 320, Hemisphere Publishing Corporation, New York, 1989.
- <sup>5</sup> Kelleher, P.G., Wents, R.P., Falcone, D.R., *SPE 39th ANTEC, Tech. Papers*, **1981**, 27, 95.
- <sup>6</sup> Kelleher, P.G., Bobbington, G.H., Falcone, D.R., Ryan, T.J., *SPE 37th ANTEC, Tech. Papers*, **1979**, 25, 527.
- <sup>7</sup> Gardner, R.J., Martin, J.R., *J.Appl. Polymer Science*, **1980**, 25, 2353.
- <sup>8</sup> Kohl, H. A.; *Analytical Chemistry*, **1954**, 26(10), 1614.
- <sup>9</sup> Flory, P.J., *Principles of Polymer Chemistry*, pp 79-91, Cornell University Press, Ithica, NY, 1953
- <sup>10</sup> Rothwell, R.E., Rowan, H.H., Dunbar, J.J., "Polyester Fibers with Improved Stability", U.S. Patent # 4,374,960.
- <sup>11</sup> Matthies, H.G., et al, "Poly(ethylene terephthalate) with Increased Hydrolysis Resistance", Ger. Offen. DE 3,132,371
- <sup>12</sup> Martin, J.R., Johnson, J.F., Cooper, A.R., *J.Macromol.Sci.Rev.Macromol. Chem.*, **1972**, 8(1), 57.
- <sup>13</sup> Neveux, Jr., P. E., *unpublished results*
- <sup>14</sup> Vyas, M. K. R., Buckland, E. L., Neveux, Jr., P. E., *IWCS Proceedings*, 1991.



**Paul E. Neveux, Jr.** obtained his double B.S. in Chemistry and Biology in 1979 from Antioch College, Yellow Springs, Ohio. After completing his Doctorate in Inorganic Photochemistry at the University of North Carolina in Chapel Hill, he held a post-doctoral fellowship investigating conducting liquid crystal polymers at Duke University in Durham, North Carolina. In 1986, he joined Sumitomo Electric Fiber Optics Corp. and currently supervises the Materials Testing & Reliability Laboratory. Dr. Neveux is an active member in the Telecommunications Industries Association, American Chemical Society and Society of Plastics Engineers.



**Eric L. Buckland** obtained his B.S. degree in Physics in 1985 from North Carolina State University where he is nearing completion of his Master's Thesis studying issues in Analytic Photon Scanning Tunneling Microscopy. Since joining Sumitomo Electric Fiber Optics Corp. in 1985, he has been engaged in the research and development of optical fibers and cables. He is currently Manager of Product Design Engineering and the Sumitomo Laboratories. Mr. Buckland is a member of the Optical Society of America.

## CORROSIVITY TEST METHODS FOR POLYMERIC MATERIALS

Stephen L. Kessel

James G. Bennett, Jr.

Charles E. Rogers

Quantum Chemical Corporation,  
USI Division

GE Plastics

Union Carbide Chemicals &  
Plastics Company, Inc.

### ABSTRACT

This is the first in a series of papers published by the Polyolefins Fire Performance Council, a unit of the Society of the Plastics Industry, Inc., to investigate corrosivity test methods. In this paper, 25 polymeric materials were evaluated for smoke corrosion using the proposed ASTM E05.21.70 test standard. These commercially available polymeric materials cover a broad range of compositions used for wire and cable insulation and jacketing.

The samples were decomposed in the proposed ASTM apparatus and a copper probe was subsequently exposed to the combustion gases. The corrosive potential, as defined by metal loss in angstroms, was determined for each material. The data demonstrate that the ASTM E05.21.70 test protocol does differentiate corrosive potentials of polymeric materials. Some refinement in this test method is warranted to better develop it as a standard for measuring corrosivity.

Further work is underway to evaluate other test methods as standardized corrosivity methods. This future work will focus on the proposed CNET ISO TC61/SC4/WG2 test, the DIN 57472 acid gas test, and the cone calorimeter (DyGST) corrosivity test under review by ASTM D09.21.04.

### INTRODUCTION

The effects of smoke and corrosive gases released in a fire are gaining increased attention. While tests to determine smoke release have been standardized, only now are tests to define smoke corrosivity being developed. Recent fire events have underscored the need for standardized tests that measure corrosivity, as corrosion is particularly important with fires around electronic equipment. And, as computer and telecommunications equipment usage is increasing, there is a need to prevent equipment from being out of service. The concern over corrosion extends to building structures, too, as corrosive gases can damage load-bearing girders and concrete structures.

To better define test methods that measure smoke corrosivity of plastic materials and products, the Polyolefins Fire Performance Council (PFPC) initiated a program to investigate several test protocols. The specific goal of this program is to determine the suitability of proposed test methods for measuring corrosive potential. This council has been an operating unit of the Society of the Plastics Industry, Inc. since 1988. It consists of the nine member companies listed in Table I.

BP Chemicals

Dow Chemical Company

EXXON Chemical Company

GE Plastics

Himont Inc.

J. M. Huber Corporation,  
Solex Division

Lonza Inc.

Quantum Chemical Corporation,  
USI Division

Union Carbide Chemicals and  
Plastics Company Inc.

Table I. Member companies of the Polyolefins Fire Performance Council. Carl F. Tripp is Managing Director.

To accomplish the program goal, the PFPC decided to evaluate four test methods currently under consideration for standardization, the CNET test, a DIN test, the cone calorimeter (DyGST) corrosivity method, and the ASTM radiant combustion test method. The CNET test is a combustion corrosivity method under consideration by ISO TC61/SC4/WG2. Results from this apparatus are being obtained from a round robin test program involving three laboratories worldwide. The DIN test selected is an acid gas test, VDE 57472 part 813, similar to the IEC 754-1 test, which measures pH and aqueous conductivity changes. The cone calorimeter test involves a protocol currently under review by ASTM D9.21.04, which uses the cone calorimeter as a method for generating combustion gases. This proposed test method has also been referred to as the dynamic gas sampling test (DyGST).

In this first of a series of papers, several polymeric materials are evaluated with the static, radiant combustion method currently under review by ASTM E05.21.70. A protocol for this test, defined as the Radiant Combustion/Exposure Smoke Corrosivity Test, has been prepared by this ASTM task group under the auspices of the ASTM Committee E-5 on fire standards. The polymeric materials list consists of a wide and balanced selection of wire and cable coatings and other materials. It contains non-halogenated filled polyolefins, high temperature thermoplastics, unfilled polyolefin base resins, and halogenated materials, with a Douglas fir reference material.

While this work was aimed at evaluating the current, proposed ASTM E05.21.70 test protocol, minor variations in the test protocol were investigated. Two different probes and two sample sizes were used in some experiments. All experiments were performed under identical conditions so that the data could be directly compared. These results add to the database

using this apparatus and test procedure, and they build on published results.<sup>1,2</sup>

In subsequent publications, the other three test methods will be evaluated with the same list of polymeric materials. These next papers are targeted for publication in 1992, and will permit a direct comparison of the four different corrosivity test methods. It is particularly important, as corrosivity test methods are standardized, to determine whether each test gives the same relative results in terms of ranking materials by their corrosive potentials. It is also important to determine which test methods are precise, meaning reproducible, as well as accurate.

#### EXPERIMENTAL

The ASTM E05.21.70 test method measures the corrosion of a suitable target, specifically a copper probe, which is exposed to combustion gases generated by burning materials. The resistance of the copper is actually measured, initially and at select time intervals during the experiment. The resistance increases, as the copper is corroded, and the resistance changes are defined in terms of copper thickness changes. Thus, the corrosion is expressed as average copper metal loss in angstroms over measured time periods. Copper is the material of choice, since most printed circuit boards contain copper circuits.

The ASTM E05.21.70 corrosivity method was developed so that the corrosion susceptible target, or copper probe, could be exposed to a sequenced environment similar to that which occurs in actual fires. Parameters important to the chemistry of corrosion, such as relative humidity and time, were factored into the test protocol. Essentially, there are four phases that would occur before, during, and after an actual fire:

Phase I (Pre-fire) - Prior to a fire, computers, control panels, and other electronic instruments would be at some normal, ambient temperature and humidity.

Phase II (Smoke Exposure) - Combustion gases from a fire in an area contact corrosion sensitive equipment. Combustion gases from a fire remote to the enclosed area may also enter the area through ventilation systems or corridors. The temperature of the combustion gases may vary from slightly to significantly above ambient. Moisture as a product of combustion will cause the moisture content of the environment to rise. Heat from the fire will energize sprinkler systems, if present, and at some point fire fighters will likely add moisture to the environment.

Phase III (Early Post Fire) - After the fire is extinguished, the humidity level will persist for some period of time. Instruments in the enclosed area will experience high relative humidity and continue to corrode.

Phase IV (Late Post Fire) - The building or room will be ventilated and the environment will begin to dry out. Chemical and particulate matter deposited onto equipment will remain, and even though the relative humidity will decrease, corrosion may continue.

The procedure used in this paper, which is the protocol prepared by ASTM E05.21.70, was structured to simulate such a scenario. It must be recognized, though, that other scenarios are possible, as the critical fire parameters will vary depending on the actual fire conditions. Carefully controlling the test parameters is critical, however, so that different materials can be reliably compared.

#### Apparatus

The test apparatus (Figure 1) used in this work is the Radiant Combustion/Exposure Apparatus designed and built by Southwest Research Institute. This apparatus was originally developed for the National Institute of Building Sciences for animal toxicity tests.<sup>3</sup> It consists of a 5 in. diameter cylindrical quartz combustion cell connected to a 200 L exposure chamber by a vertical stainless steel flue.

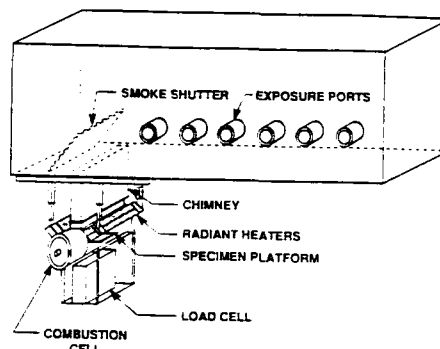


Figure 1. Schematic drawing of Radiant Combustion/Exposure Apparatus.

The test specimen is supported in the center of the combustion cell on a horizontal pan connected to a load cell, permitting a continuous measurement of specimen weight loss during the test. A uniform heat flux is applied to the specimen by four tungsten-quartz radiant heat lamps situated on either side of the flue. Combustible gases are ignited by a continuous spark.

The flue is divided into three vertical channels which induce the products of combustion and pyrolysis to travel up the center channel into the exposure chamber. Air from the exposure chamber is then induced to circulate, countercurrently, down into the combustion cell.

The exposure chamber is made of polymethylmethacrylate (PMMA) to minimize absorption of combustion gases while allowing a view of the smoke build up, circulation, and decay. Two doors at each end of the chamber permit easy access for cleaning and maintenance. There are six access ports at mid-height in the chamber side, and these are used for probe instrumentation wires and gas sampling tubes. One additional port is used for a 49 L plastic expansion bag. This expansion bag is essential to the operation, as the gases generated from sample combustion would otherwise build up considerable pressure inside the 200 L chamber.

A shutter is used to cover the exit of the flue at the end of the specimen irradiation period. This shutter consists of a stainless steel plate covered with a disposable aluminum foil.

### Test Specimens

For this program, most test specimens were 2 x 2 x 1/8 in. plaques. This 2 x 2 in. size was selected to insure that the oxygen level in the exposure chamber remained significantly high so that sample combustion was not oxygen limited. Samples PFPC-17 and 18 (Table II) were run with 1 x 1 x 1/8 in. specimens because of safety concerns expressed by the testing laboratory. These safety concerns about the toxicity of the combustion gases were alleviated by running the smaller specimens, so that only 1/4 the size of the standard specimen was used. Sample PFPC-19 was run with 1 x 1 x 1/8 in. and 2 x 2 x 1/8 in. specimens to investigate the response of the 2500 Å probes to both specimen sizes.

### Target Probes

Copper corrosion probes manufactured by Rohrbach-Cosasco were used as targets. Corrosion is expressed as average metal loss in angstroms ( $1 \text{ Å} = 39.37 \times 10^{-9} \text{ in.}$ ) as determined by the resistance increase of the probe. This calculated metal loss assumed uniform thickness loss over the plane of the probe.

The probes used were constructed of copper metal in two thicknesses. The high sensitivity probe, Model 610 (Figure 2), generally used to measure low levels of corrosion is nominally 5000 Å copper sputtered onto a glass substrate. The lower sensitivity probe, Model 600 (Figure 3), used to measure high levels of corrosion is nominally 50,000 Å thick copper foil applied to a glass substrate. These probes have a linear response over approximately 2500 and 25,000 Å, respectively, as defined by Rohrbach-Cosasco. Since these copper thicknesses distinguish the probes, they are identified throughout the course of this study by their respective thicknesses. These thicknesses represent the maximum metal loss that each probe could experience, beyond which they are off-scale.

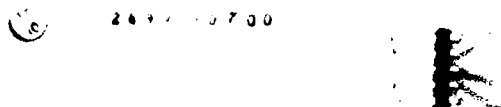


Figure 2. Model 610, 2500 Å probe from Rohrbach-Cosasco.



Figure 3. Model 600, 25,000 Å probe from Rohrbach-Cosasco.

Each probe consists of a reference copper leg and an operating copper leg. The reference copper leg is coated with a clear polymeric coating, so that only the operating copper leg can corrode. So, both probes have a leg protected from corrosion to provide temperature compensation during the sample combustion. The copper strips of each leg are separated by approximately 1.5 mm to prevent polymer decomposition particles from bridging the copper circuit and causing erroneous results.

### Test Procedures

Each test specimen was placed on the specimen holder and the combustion chamber was closed. The probe was placed in the approximate center of the 200 L exposure chamber with the copper surface horizontal and facing upwards. This exposure chamber was closed and the relative humidity brought to 60% at room temperature.

The radiant heaters were turned on at a power level to yield 50 kW/m<sup>2</sup> and a spark ignitor was turned on for a 15 min. period. The spark ignitor was left on for the entire 15 min. combustion period to promote complete combustion. Even with the spark ignitor being left on, a few specimens did not completely combust, as is discussed later in this paper. Samples ignited at different times and combusted at different rates because of the different sample compositions.

The power was adjusted during the irradiation period to maintain a constant heat flux based on a pre-run calibration with a radiometer replacing the specimen. Irradiation was terminated after 15 min. and the flue was closed. The probe was then left in the chamber with the combustion gases for an additional 45 min.

During this 1 h total irradiation/exposure period, the temperature, relative humidity, oxygen, carbon monoxide, and carbon dioxide levels in the chamber were allowed to vary as driven by the heat release and products of combustion. The target probe was not actively cooled. The following measurements were made during this irradiation/exposure period:

- Time to visible smoke
- Time to specimen ignition
- Time of flame out
- Probe resistance change (converted to metal loss)
- Specimen mass loss
- Chamber temperature
- Chamber oxygen level
- Chamber carbon monoxide level
- Chamber carbon dioxide level

At the end of this 60 min. period, the probe was moved to a chamber maintained at 75% relative humidity at room temperature. The probe was maintained in this chamber for a period of 24 h, after which it was moved to an environmental chamber maintained at 35% relative humidity at room temperature. The probe remained for 6 additional days in this lower relative humidity environment. Measurements of resistance change were made at 2-3 min. intervals during the first hour, at the end of the 24 h period, and again at the end of the 6 day period. These resistance changes were actually measured on a scale of 0 to 1000 resistance units, with 1000 units equalling the upper copper thickness for which the probe had a linear response. This maximum thickness, or span, was around 2500 Å or 25,000 Å, depending on which probe model was used. The exact span value for each probe was established by the manufacturer.

For each sample, three specimens were tested on separate runs except as noted in Table III. Sample PFPC-21 was tested six times, meaning that six specimens were evaluated, to provide statistical data on reproducibility. A separate probe was used for each specimen that was decomposed.

## RESULTS AND DISCUSSION

### Materials Evaluated

Table II lists the 25 polymeric materials evaluated for smoke corrosivity. These resins and compounds represent a broad sampling of polymeric materials, particularly materials that are used in wire and cable jacketing/insulation applications. They are all commercially available.

PFPC NO.	COMPANY	PRODUCT DESIGNATION	MATERIAL DESCRIPTION
1	BP	EXP 839	XL OLEFIN ELASTOMER WITH METAL HYDRATE FILLER
2	DOW	5435-30-11	BLEND OF HDPE AND CHLORINATED PE ELASTOMER
3	DOW	5348-40-1	CHLORINATED PE WITH FILLERS
4	EXXON	EX-FR-100	EVA POLYOLEFIN WITH ATH FILLER
5	GEP	NORYL <sup>®</sup> PX1766	POLYPHENYLENE OXIDE/POLYSTYRENE BLEND
6	GEP	ULTEM <sup>®</sup> 1000	POLYETHERIMIDE
7	GEP	SILTEM <sup>®</sup> STM1500	POLYETHERIMIDE/SILOXANE COPOLYMER
8	HIMONT	ASTRYN <sup>®</sup> AA36H	INTUMESCENT POLYPROPYLENE
9	LONZA		NYLON WITH MINERAL FILLER <sup>*</sup>
10	UCC&P	UNIGARD-RE <sup>™</sup> DFDA-1736NT	POLYOLEFIN COPOLYMER WITH MINERAL FILLER
11	UCC&P	UNIGARD-RE <sup>™</sup> HFDA-1393BK	XL POLYOLEFIN COPOLYMER WITH MINERAL FILLER
12	QUANTUM	PETROTHENE <sup>®</sup> XL 7403	XL POLYOLEFIN COPOLYMER WITH ATH FILLER
13	QUANTUM	PETROTHENE <sup>®</sup> YR 19535	XL POLYOLEFIN COPOLYMER WITH ATH FILLER
14	QUANTUM	PETROTHENE <sup>®</sup> YR19543	EVA POLYOLEFIN WITH MINERAL FILLER
15	UCC&P	UCARSIL <sup>®</sup> FR-792ONT	POLYOLEFIN WITH MINERAL FILLER
16	BP	POLYCURE <sup>™</sup> 798	XL POLYETHYLENE COPOLYMER WITH CHLORINATED ADDITIVE
17		COMMERCIAL SAMPLE	A POLYVINYLIDENE FLUORIDE MATERIAL
18		COMMERCIAL SAMPLE	A POLYTETRAFLUOROETHYLENE MATERIAL
19		COMMERCIAL SAMPLE	A PVC MATERIAL
20		COMMERCIAL SAMPLE	A PVC BUILDING WIRE COMPOUND
21	UCC&P	DGDK-3364NT	POLYETHYLENE HOMOPOLYMER
22	-----	-----	DOUGLAS FIR
23	QUANTUM	ULTRATHENE <sup>®</sup> UE 631	EVA POLYOLEFIN COPOLYMER
24	NYLET	P50	NYLON 6.6
25	UCC&P	UNIGARD-HP <sup>™</sup> HFDA-6522NT	XL POLYETHYLENE COPOLYMER WITH BROMINATED ADDITIVE

Table II. Materials evaluated for smoke corrosivity.

This material list covers polymeric materials that retard flame spread by several means. Some materials contain hydrated mineral fillers compounded with polyolefin resins or resin blends. So, they would be expected to retard flame spread by endothermic water-of-hydration release.

Sample PFPC-3 is an intumescent polypropylene compound containing a phosphorus flame retardant additive. This material retards flame spread by formation of a char barrier, and its flaming characteristics are different from the others listed in this table.

Some samples are halogenated flame retardant materials. They can be divided into compounds containing halogenated additives and materials that have halogen atoms chemically bonded to the polymer backbone. The brominated and chlorinated materials deter flame spread by halogen release and subsequent formation of flame poisoning radicals. As such, they act in the vapor phase to extinguish flame, often through the synergistic action of halogenated species with antimony oxide. The fluoropolymers are halogenated materials, which have very high limiting oxygen index values and retard flame spread by being difficult to ignite.

This table includes three high-heat, non-halogenated flame retardant materials. One of these materials contains a phosphorus flame retardant additive and the other two are unfilled resins. These materials are also considered difficult to ignite, so that they also retard flame spread by resisting ignition.

Also included are three unfilled base resins from different suppliers. The two polyolefin materials were selected so that an accurate comparison of filled materials with their respective base resins could be accomplished.

Finally, Douglas fir, sample PFPC-22, was included as a standard since it is well used in flame testing materials for the building industry. The Douglas fir represents the only non-synthetic polymeric material used in this study.

### Typical Corrosion Response

A typical corrosion response is illustrated in Figure 4, which details the metal loss for specimens 1, 2, and 3 of sample PFPC-25, a bromine containing polyolefin. These curves were obtained by combusting 2 x 2 x 1/8 in. specimens according to the proposed ASTM E05.21.70 protocol. As can be seen in this figure, there are two main features of interest: the total metal loss resulting from each specimen and the time required for the metal loss to occur. Corrosion could be defined as both the absolute metal loss and the time to achieve this metal loss. In this paper, total metal loss is considered to be the barometer of corrosion.

Figure 4 illustrates the metal loss that occurred over the 60 min. exposure period. The three specimens completely combusted over the 15 min. ignition period, as indicated by their appearance and weight loss. For these specimens, as for all specimens evaluated, the weight loss was measured to ensure that decomposition occurred.

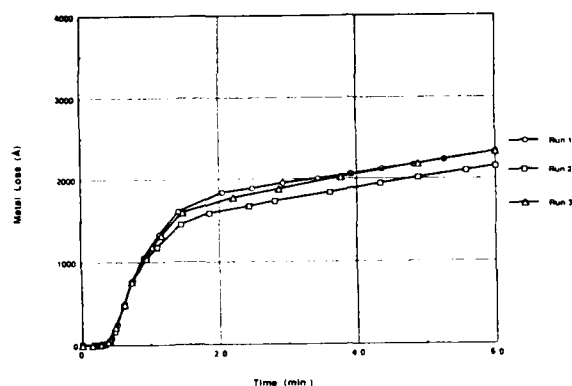


Figure 4. Corrosion caused by combustion of sample PFPC-25 ( $2 \times 2 \times 1/8$  in. specimens, 2500 Å probes).

This issue of decomposition is important for test methods measuring the corrosive potential of polymeric materials. If the sample does not decompose, then the actual corrosive potential would not be measured. Consequently, the heat flux was maintained at  $50 \text{ kW/m}^2$  and the ignitor was left on for the entire 15 min. combustion period. This same procedure was used for all samples evaluated, to ensure that decomposition occurred. As mentioned previously, the fluoropolymers and high heat materials are difficult to ignite, and some of these samples did not actually ignite.

#### Total Metal Loss Results

Corrosion data for all 25 samples are tabulated in Tables III and IV and highlighted results for 12 samples are illustrated in Figure 5. These 12 samples are representative of the different materials evaluated and they, rather than the entire 25 materials, are illustrated for the sake of brevity.

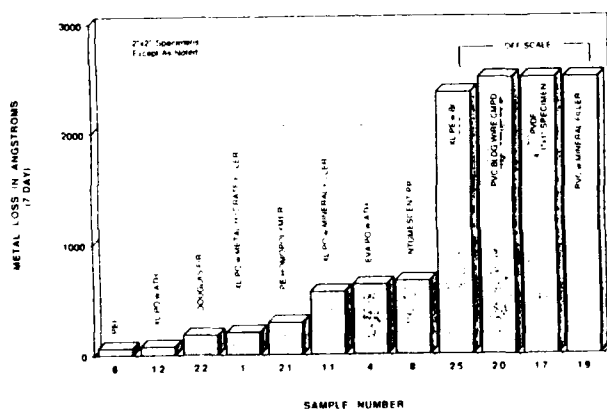


Figure 5. Corrosion caused by combustion of representative samples (2500 Å probes).

PFPC NO.	SAMPLE	METAL LOSS(Å)			AVE. METAL LOSS(Å)
		RUN 1	RUN 2	RUN 3	
6	POLYETHERIMIDE	17	189	12	66
12	FILLED POLYOLEFIN	31	42	166	76
23	EVA COPOLYMER	61	26	191	93
5	PPO / PS	149	308	30	162
22	DOUGLAS FIR	19	281	231	177
7	PEI / SILOXANE	447	12	93	184
1	FILLED OLEFIN ELASTOMER	267	290	57	206
13	NYLON 6, 6	39	396	-	198
24	FILLED POLYOLEFIN	598	14	44	219
21	POLYETHYLENE	62	26	784	291
14	FILLED EVA	173	1048	24	415
11	FILLED POLYOLEFIN	557	373	775	568
4	FILLED EVA	15	504	1362	627
8	INTUMESCENT PP	828	386	775	663
15	FILLED POLYOLEFIN	1264	519	207	663
10	FILLED POLYOLEFIN	420	381	2289 <sup>a</sup>	1023
25	POLYETHYLENE WITH Br	2409	2280	2424 <sup>b</sup>	2362
2	CI POLYOLEFIN	2498 <sup>b</sup>	2590 <sup>b</sup>	-	2500 <sup>b</sup>
3	CI POLYOLEFIN	2515 <sup>b</sup>	2564 <sup>b</sup>	-	2500 <sup>b</sup>
16	POLYETHYLENE WITH CI	2616 <sup>b</sup>	2423 <sup>b</sup>	2567 <sup>b</sup>	2500 <sup>b</sup>
17	A PVdF <sup>a</sup>	2447 <sup>b</sup>	2492 <sup>b</sup>	2575 <sup>b</sup>	2500 <sup>b</sup>
18	A PTFE <sup>a</sup>	2468 <sup>b</sup>	2589 <sup>b</sup>	2419 <sup>b</sup>	2500 <sup>b</sup>
19	A PVC	2324 <sup>b</sup>	2312 <sup>b</sup>	2444 <sup>b</sup>	2500 <sup>b</sup>
20	A PVC	2545 <sup>b</sup>	2647 <sup>b</sup>	2545 <sup>b</sup>	2500 <sup>b</sup>

<sup>a</sup>  $1 \times 1 \times 1/8$  IN. SPECIMENS WERE TESTED. ALL OTHER SPECIMENS WERE  $2 \times 2 \times 1/8$  IN.  
<sup>b</sup> METAL LOSS WENT OFF-SCALE. PROBE COMPLETELY CORRODED.

Table III. Corrosion as defined by metal loss after complete test period. 2500 Å probes were corroded.

Table III lists the total metal loss, expressed in angstroms, for each material run in triplicate with 2500 Å probes. The metal loss for the 60 min. exposure period, the 24 h high humidity period, and the 6 day low humidity periods are added to reach the total metal loss. Thus, the total metal loss over the entire 1 h and 7 day test is tabulated for each of the three test specimens of each sample.

The data show that the samples can be differentiated as to their corrosive potentials. The polyetherimide (PFPC-6), metal hydrate filled polyolefins (PFPC-12, 1, 11, and 4), intumescent polypropylene (PFPC-8), polyolefin resin (PFPC-21), and Douglas fir (PFPC-22) all gave relatively low corrosive results. The metal loss for these samples ranged from 66 to 663 Å. The metal loss values greater than a few hundred angstroms suggest that some minor amounts of corrosion occurred. For example, PFPC-11, 4, and 8 appear to produce some minimal corrosion, since the metal loss averaged around 500 Å. This would need to be substantiated by repeating the runs and using statistical data analysis to decide if these slight corrosion values are meaningful.

The other materials illustrated in Figure 5, PFPC-25, 17, 19, and 20, gave high corrosion values. They caused considerable metal loss, as they went off-scale, often before the first 60 min. had expired. The values tabulated for these materials are the maximum readings permissible for the probes, as calibrated by the manufacturer. So, in most cases, the data are tabulated as simply greater than the upper detectable probe limit.



All samples in Table III were run as 2 x 2 x 1/8 in. plaques, except for samples PFPC-17 and 18, which were run as 1 x 1 x 1/8 in. plaques. The reduced specimen size was used because of safety concerns expressed by the testing laboratory, specifically regarding the toxicity of the combustion gases. Even with the reduced specimen size, this polymeric material gave very high corrosion.

#### Metal Loss During Each Test Period

Table IV lists the percent corrosion that occurred during the 3 experimental time periods for the samples. The percent corrosion is tabulated for: 1) the 60 min. period that the probe was exposed to the combustion gases, 2) the 24 h at 75% relative humidity, and 3) the 6 days at 35% relative humidity. These data show considerable differences as to when the corrosion occurred for each sample.

PFPC NO.	SAMPLE	AVE. METAL LOSS (Å)	% METAL LOSS DURING		
			60 MIN	24 H	6 DAYS
8	POLYETHERIMIDE	66	31	38	31
12	FILLED POLYOLEFIN	76	67	17	16
23	EVA COPOLYMER	93	66	22	12
5	PPO/PS	162	31	49	20
22	DOUGLAS FIR	177	75	10	15
7	PEI/SILOXANE	184	22	45	33
1	FILLED OLEFIN ELASTOMER	205	38	47	15
24	NYLON 6,6	198	88	6	6
13	FILLED POLYOLEFIN	219	61	24	15
21	POLYETHYLENE	291	23	27	50
14	FILLED EVA	415	63	18	19
11	FILLED POLYOLEFIN	568	17	30	55
4	FILLED EVA	627	20	29	51
8	INTUMESCENT PP	663	82	13	5
15	FILLED POLYOLEFIN	663	13	47	40
10	FILLED POLYOLEFIN	> 1023	70	22	8
25	POLYETHYLENE WITH Br	> 2362	96	2	2
2	Cl POLYOLEFIN	> 2500 <sup>b</sup>	100	-	-
3	Cl POLYOLEFIN	> 2500 <sup>b</sup>	100	-	-
16	POLYETHYLENE WITH Cl	> 2500 <sup>b</sup>	100	-	-
17	A PVdf <sup>a</sup>	> 2500 <sup>b</sup>	100	-	-
18	A PTFE <sup>a</sup>	> 2500 <sup>b</sup>	100	-	-
19	A PVC	> 2500 <sup>b</sup>	100	-	-
20	A PVC	> 2500 <sup>b</sup>	100	-	-

<sup>a</sup> 1 x 1 x 1/8 IN. SPECIMENS WERE TESTED. ALL OTHER SPECIMENS WERE 2 x 2 x 1/8 IN.  
<sup>b</sup> METAL LOSS WENT OFF-SCALE. PROBE COMPLETELY CORRODED.

Table IV. Percent of corrosion occurring during test periods.

In general, the high corrosion materials show nearly complete corrosion of the 2500 Å probe during the 1 h exposure period. In fact, many of the high corrosion samples in Table IV exceeded the corrosion limit of the probe within the first 60 min. This might be expected due to the highly corrosive hydrogen halides formed, which react with the moisture in the atmosphere to form hydrochloric, hydrobromic, or hydrofluoric acids. These acids would be expected to rapidly and severely corrode the copper probes.

Other low corrosive samples, however, show that a significant percent of the corrosion occurred within the 75% relative humidity time period. In some samples, a large portion of the corrosion occurred during the 6 day, lower humidity period. Samples PFPC-21 and 11, for example, exhibited over half of their corrosion during the 6 day period. Sample PFPC-6, on the other hand, exhibited equal amounts of corrosion during the 60 min. exposure, the 24 h at 75% relative humidity, and the 6 days at 35% relative humidity. It should be emphasized that the total corrosion for these samples was minimal, so that when the corrosion occurred is not as meaningful as the total corrosion values. These results do demonstrate that running a corrosion experiment for only a short period may not indicate the entire corrosive potential of the polymeric material.

#### Evaluation of Different Probes

While most of the corrosion results were obtained with 2500 Å probes, several specimens were evaluated with 25,000 Å probes. This was primarily done to measure the corrosion of the samples that completely destroyed the 2500 Å probes. The data for these runs are tabulated in Table V. Figure 6 illustrates the corrosion for sample PFPC-20, in which both 2500 Å and 25,000 Å probes were used. The two probes generally correlate, as there appears to be a linear relationship between them.

PFPC No.	SAMPLE	Metal Loss (Å)			Ave. Metal Loss (Å)
		RUN 1	RUN 2	RUN 3	
16	POLYOLEFIN WITH CL	2275	1100		1688
20	A PVC	1825	2175		2000
2	CL POLYOLEFIN	2582	2483		2522
19	A PVC	4213	2176	1982	2790
3	CL POLYOLEFIN	3463	3275	2063	2934

Table V. Corrosion as defined by metal loss after complete test period. 25,000 Å probes were corroded.

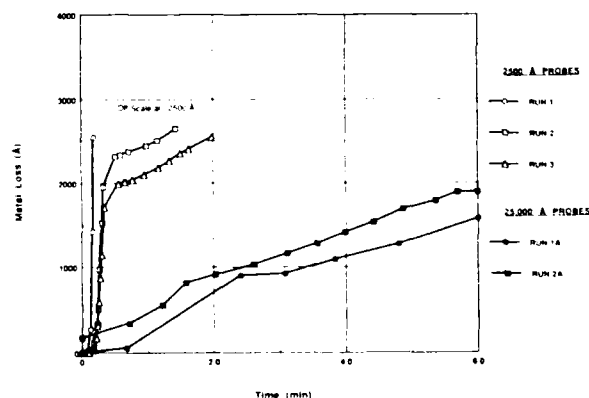


Figure 6. Corrosion caused by combustion of sample PFPC-20 (2500 Å probes versus 25,000 Å probes).

Corrosion occurred more slowly with the 25,000 Å probes than the 2500 Å probes for this sample. This may be explained by the different copper film morphologies for the two probes. The 2500 Å probes consist of copper films on glass that are formed by a physical vapor deposition technique known as sputtering. Copper films produced in this manner often display large columnar crystals perpendicular to the plane of the sputtered substrate, in this case the glass base. The bulk density of such a film is always lower than the bulk density of copper metal, due to the cracks and fissures, or lattice defects, in the copper film.

The 25,000 Å probes are constructed of copper foil on circuit board substrates. The copper foil has the same bulk density as copper metal, as there are less lattice defects in the film. These thicker probes, then, would be expected to corrode at a slower rate than the sputtered, 2500 Å probes. In addition, the lattice defects in the 2500 Å probes make these probes more susceptible to spot corrosion. Should this occur, the resistance change of the probe would be substantial, even though only a small portion of the copper probe would have actually been corroded.

#### Influence of Sample Size

To investigate the effect of specimen size, sample PFPC-19 was evaluated as 1 x 1 x 1/8 in. plaques and also as 2 x 2 x 1/8 in. plaques. As illustrated in Figure 7, the larger specimen more readily corroded the 2500 Å probe. However, even the 1 x 1 x 1/8 in. plaque completely corroded the probe before the full 60 min. exposure period. Also, it should be pointed out that the larger specimen, although 4 times the mass of the smaller specimen, did not corrode the probe 4 times as much or 4 times as fast. More experimental work is needed to quantify the absolute effect of specimen size. These results in Figure 7 do show, however, that sample PFPC-19 is highly corrosive, even at the smaller specimen size.

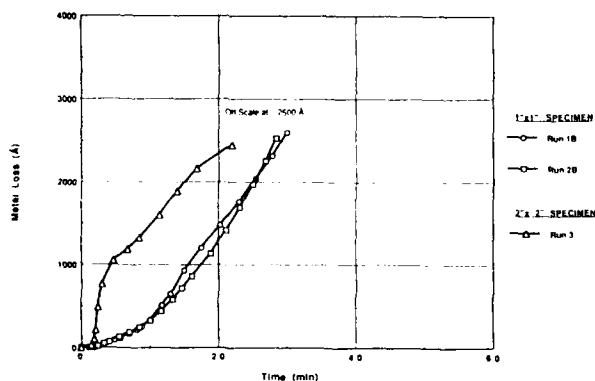


Figure 7. Corrosion caused by combustion of sample PFPC-19 (1 x 1 x 1/8 in. versus 2 x 2 x 1/8 in. specimens, 2500 Å probes).

#### Weight Loss

The average weight loss for the three specimens of each sample is listed in Table VI. These results were collected to measure the amount of decomposition for each specimen. All samples showed extensive decomposition, although some did not actually combust in a flaming mode.

PFPC No.	Ave. Mass Loss (%)	Minimum O <sub>2</sub> (%)	Maximum CO (ppm)	Maximum CO <sub>2</sub> (%)
1	69.0	16.8	2730	3.4
2	90.6	16.2	5580	3.4
3	74.3	18.3	2980	2.1
4	59.6	15.3	850	4.2
5	97.1	16.3	6900	3.1
6	83.5	16.8	3840	2.9
7	80.5	17.3	3910	2.6
8	89.1	13.6	1200	5.0
10	54.1	16.6	300	3.2
11	56.9	16.4	490	3.5
12	65.4	17.4	690	2.5
13	65.0	16.1	760	3.6
14	65.0	17.2	380	2.9
15	56.3	16.7	180	3.1
16	81.7	15.6	3640	3.6
17 <sup>a</sup>	78.5	20.6	2540	0.2
18 <sup>a</sup>	51.4	20.8	- <sup>b</sup>	0.1
19	68.1	19.5	3420	1.1
20	90.3	18.3	5070	1.7
21	96.2	14.3	2850	4.5
22	98.4	18.1	2930	2.7
23	99.5	16.2	1570	3.4
24	100.0	16.1	1870	3.7
25	76.6	17.4	4320	2.3

<sup>a</sup> 1 x 1 x 1/8 in. specimens were tested. All other specimens were 2 x 2 x 1/8 in.  
<sup>b</sup> No CO was detected.

Table VI. Percent mass losses and analysis of exposure chamber gases.

Sample PFPC-21 exhibited nearly 100% weight loss, as expected, since it does not contain fillers that could leave ash after combustion. Sample PFPC-12, though, contains a mineral filler and it was expected to show some, but not complete, weight loss. This was indeed the case with this material.

It should be noted that for seven of the nine 1 x 1 in. specimens, flaming combustion was either not visually observed or was uncertain. It is not clear whether this is a function of the material tested, the specimen, or the observers ability to detect the flame. Still, the weight loss data for these specimens show that significant decomposition did occur. The weight loss data for all samples tested generally show the results expected, knowing the composition of each material.

#### Analysis of Exposure Chamber Gases

The minimum oxygen percents observed during decomposition are listed in Table VI. The oxygen level remained sufficiently high so that the combustion characteristics were not changed during each run. The mean oxygen level for all 2 x 2 x 1/8 in. specimens was 16.5% with a sample average range of 13.6 to 18.3%. The lowest oxygen level observed on any single 2 x 2 x 1/8 in. specimen was 12.7% for specimen 2 of sample PFPC-21. The mean value for the three

specimens of this sample was 14.3%. Carbon monoxide and carbon dioxide levels were also determined during each experimental run and the average values are listed in Table VI.

#### Reproducibility of Results

The reproducibility of any test method being prepared for standardization should be determined. Consequently, the data collected were scrutinized to determine any variation, and the results show that the precision, or reproducibility, of this proposed ASTM E05.21.70 test could be improved. This comment should be tempered, though, by acknowledging that the test method was developed to define a broad corrosion range. The thin 2500 Å probes, in particular, are designed to show large differences in corrosive potential from sample to sample. So, a small amount of data scatter would be anticipated for this test method.

Still, the causes of variation in data should be investigated, as the scatter is larger than desired. Some samples did give relatively consistent metal loss with different specimens, although other samples showed considerable variation. For example, samples PFPC-12, 6, and 22 gave relatively similar results with different specimens. Sample PFPC-4, however, gave somewhat variable results, as the total metal loss ranged from 15 to 1362 Å, a very wide spread for three specimens. Even sample PFPC-21, the standard unfilled polyethylene homopolymer, gave some spread in the results.

There are several potential causes of the scatter in the data which merit further investigation. An implicit assumption in this test method is that the copper film is corroded uniformly throughout the experiment. Any spot corrosion of the copper film would dramatically alter the resistance. This would lead to inaccurate, high results in the observed metal loss, which is recorded as the average copper loss over the entire probe.

All probes were visually examined after each test, and no catastrophic spot corrosion was observed. So, the assumption of uniform corrosion seems to be valid for most of the corrosion experiments. Copper films produced by sputtering are not as dense as bulk copper, as already mentioned, so the possibility of microscopic spot corrosion is possible. Detailed electron microscopy studies would need to be performed to determine whether spot corrosion had occurred.

If lattice defects in the copper film were the cause of spot corrosion and subsequent data variation, this should be eliminated or reduced by using the 25,000 Å probes. Samples PFPC-16 and 19, which were combusted with 25,000 Å probes, also showed considerable scatter in the data, however. This suggests that the sputtered film is not the sole cause of the data scatter. A complete statistical analysis of repeated runs would be needed to definitively assess the effect of the copper film morphology.

Pyrolysate matter generated during combustion could lead to uneven results, especially since the probes were positioned face-upward in the exposure chamber. Indeed, many of the probes were coated with a layer of particulate matter after specimen decomposition. The individual copper legs comprising the circuit of the Rohrbach-Cosasco probe are separated by approximately 1.5 mm, which makes bridging between the copper legs difficult. Bridging thus does not seem to be a problem with these

probes. Single combustion particles contacting the copper legs could give high spot corrosion and cause reproducibility problems. No severe spot corrosion from smoke particles was visually observed, however, suggesting that this was not a problem.

While differences in specimen preparation can always cause experimental error, this does not appear to be a main source of data scatter in this study. To limit this type of experimental error, specimens were prepared from the same lots of materials. The specimens of each sample were prepared at the same time and under the same laboratory conditions. In most cases, the 2 x 2 in. specimens were cut out of larger single plaques to minimize the effects of sample preparation.

Differences in combustion do not seem to be the cause of differences in run to run. Decomposition parameters were closely controlled, as described, and kept constant for all experiments. In addition, the mass losses recorded are fairly consistent with a given sample set, so this does not seem to explain the data variation.

To better define the reproducibility of this test, sample PFPC-21 was run 6 times, so that a reasonable statistical treatment of the data could be performed. The total metal loss data for these runs are detailed in Table VII. The average total metal loss was 170 Å and the standard deviation was 303 Å. Excluding the data from run 3, which was very high, the average metal loss was 47 Å and the standard deviation was 42 Å. These values were only determined for one sample, and standard deviation would not need to be determined for all samples evaluated in this study to best determine the reproducibility of this test.

<u>RUN NO.</u>	<u>TOTAL METAL LOSS (Å)</u>
1	62
2	26
3	784
4	115
5	16
6	17
Average = 170 = 47 *	
Standard Deviation = 303 = 42 *	

\* Excluding run 3.

Table VII. Metal loss and standard deviation for PFPC-21.

#### CONCLUSIONS AND RECOMMENDATIONS

The test protocol being proposed by ASTM E05.21.70 does differentiate the corrosive potentials of polymeric materials. The 25 samples evaluated in this study exhibited a wide range of corrosivity, demonstrating that this radiant combustion test method does have the desired sensitivity to distinguish materials.

An important feature of this test method is that different types of polymeric specimens can be evaluated. In this work, the corrosive potentials of polymeric specimens in the form of plaques were determined. Other work has shown that corrosive potentials of electric cable specimens can also be determined.<sup>2</sup>

The reproducibility of this test merits some attention, as the results show some scatter in the data. Test parameters, such as the sample size and the positioning of the probe in the exposure chamber, could be investigated further to improve the test method. The copper probes used deserve particular attention, as more precise knowledge of the copper thicknesses and more in-depth understanding of the resistance change as defined in metal loss are warranted.

The 25 polymeric materials evaluated in this study will next be evaluated with the CNET ISO TC61/SC4/WG2 corrosivity test, the DIN 57472 acid gas test, and the cone calorimeter corrosivity test (DyGST) being proposed by ASTM D09.21.04. As a long range goal, the Polyolefins Fire Performance Council intends to investigate total risk assessment of fire situations, by including the smoke corrosivity results obtained in this program.

#### REFERENCES

1. Grand, Arthur E., "Evaluation of the Corrosivity of Smoke from Fire Retarded Products," pp 44, Journal of Fire Sciences, Vol. 9 No. 1, January/February 1991.
2. Keogh, M.J., Rogers, C.E., Schmidt, G.A., "Polyolefin Resin Blends and Additive Technology: Advanced Non-Halogen Flame Retarded Compounds," Fire Retardant Blends, Alloys and Thermoplastic Elastomers, Joint Meeting of Society of Plastics Engineers and Fire Retardant Chemicals Association, March 17-20, 1991.
3. Grand, A.F. "Development of a Product Performance Smoke Toxicity Test," Final Report on SWRI Project No. 01-1744 for National Institute of Building Sciences, July 1990.



Dr. Stephen L. Kessel received his B.S. degree in Chemistry from Eastern Illinois University in 1974. He then attended the University of Illinois where he received his M.S. and Ph.D. degrees in Inorganic Chemistry while obtaining a minor in Chemical Engineering. He joined Monsanto Company in 1979 as a Senior Research Chemist in petrochemicals research. During his employment at Monsanto company, he investigated metal-polymer adhesion science. In 1989 he joined Quantum Chemical Corporation, USI Division as a Section Leader in polymer materials, Basic Research and Development. He is a member of the American Chemical Society, the American Institute of Chemical Engineers, Materials Research Society, and the Society of Plastics Engineers.



Dr. Jim Bennett is Principal Scientist at GE Plastics Selkirk, N.Y. He received his B.S. degree in Chemistry from State University of New York in Albany in 1954 and his Ph.D. degree in Organic Chemistry from Rensselaer Polytechnic Institute in Troy, N.Y. in 1959. After employment at Parke Davis and Huyck Felt Company, he joined GE Plastics in 1963. A pioneer in the GE Plastics Noryl® Business, he holds 38 patents and has published 7 journal articles. Dr. Bennett is active in both the American Chemical Society and the Society of Plastics Industry.



Charles E. Rogers is a Senior Research Scientist with the Polyolefins Division of the Union Carbide Chemicals and Plastics Company, Inc. He is a member of the Flame Retardant Wire and Cable Materials Group involved in product research and development. Mr. Rogers received his B.S. degree in Mechanical/Aeronautical Engineering from Syracuse University in 1956 and his M.S. degree in Aeronautical Engineering from Rensselaer Polytechnic Institute in Troy, N.Y. in 1960. After a 20 year career in the Aerospace Industry, he joined the Linde Division of Union Carbide Corporation in 1976. He joined the Polyolefins Division in 1988. He is active in the ASTM(D09.21 - Electrical and Electronic Insulating Materials, Fire Performance Standards sub-committee and E05 Fire Standards Committee), the Society of Plastics Engineers and the National Fire Protection Association.

## PLENUM CABLE FOR THE 90'S - NEW CONCERNS FOR NEW DEMANDS

by

Richard J. Rockosi

Ausimont USA Inc.  
PO Box 1838  
Morristown, New Jersey 07962-1838

### ABSTRACT

Historically, the primary consideration for selecting an insulation material for use in plenum areas has been its flame and smoke performance when tested for compliance to UL 910 (the Steiner Tunnel Test) and UL 444 requirements.

With the increased use of these UTP cables for high speed data transmission as well as telephone communications, factors in addition to smoke and flame performance must be considered to assure system integrity.

This paper describes the results of a series of environmental tests designed to evaluate the electrical stability of typical plenum cables at elevated temperatures.

The plenum wiring concept, as we know it today, was established 14 years ago as a FIRE SAFETY and LIFE SAVING measure. This concept developed as a result of a near disastrous fire which occurred in a Telephone Company office in the early 1970's.

During the early stages of plenum development, the only materials meeting the critical low flame spread and smoke generation requirements for these cables were the high temperature, fluoropolymer materials such as ECTFE, FEP and PVDF.

As material development grew more sophisticated, other, more temperature dependent materials such as PVC and SMOKEGUARD® were permitted for plenum applications - usually with fluoropolymer jacketing.

During the 1980's the many of these cables were used for telecommunications and some low speed data transmission in the kilobit range.

Today and into the 90's, the widespread use of UTP cables for data as well as telephone communications is making transmission quality - as effected by electrical stability - more critical.

UTP plenum cables now support a large number of high speed data systems. Among these are:

DEC Connect

HP

IBM Type 3

Protecn 3

Synoptics

10 BaseT & STARLAN 10

Wang Net

3 COM

T1 - DS1 Rate

Token Ring 4 MHz

Token Ring 16 MHz

Cabling for these systems meet attenuation and other requirements for frequencies up to 16 MHz.

Industry specifications currently in the draft stages are extending frequency ranges to 100 MHz.

These increased performance requirements will place more demands on the cable design engineer in the future. They will also place added responsibilities upon the specifier or purchaser as they will not be just specifying plenum cables that meet the code (National Electric Code - NEC). They must also meet the performance requirements of current as well as future systems.

Because of the critical demands of high speed data transmission, more than flame, smoke, and even base electrical requirements must be considered when selecting cables.

For instance, the electrical properties of some dielectric materials are known to become unstable or change dramatically when exposed to elevated temperatures such as may be encountered in plenums and other wiring spaces.

Industry specifications such as IEEE 802.3<sup>1</sup> and EIA/TIA 568<sup>2</sup> contain engineering notes calling attention to the increase in attenuation loss when using cables containing temperature dependent materials such as PVC at elevated temperatures.

#### **DRAFT SUPPLEMENT TO IEEE STD. 802.3 TYPE 10 BASE-T**

##### **Para: 14.4.2.1 Attenuation**

"NOTE: Multi-pair PVC insulated 0.5 mm (24 gauge) cable typically exhibits an attenuation of 8 to 10 dB per 100 m at 20 C. The loss of PVC insulated cable exhibits significant temperature dependence. At temperatures greater than 40 C, it may be necessary to use less temperature-dependent cable, such as most plenum rated cables."

#### **ETA/TIA STANDARDS PROPOSAL NO. 1907B (EIA/TIA 568) PROPOSED NEW STANDARD "COMMERCIAL BUILDING TELECOMMUNICATIONS WIRING STANDARD"**

##### **Para. 10.2.1.2.5 Attenuation**

"NOTE: The attenuation of some UTP cables, such as PVC insulated cables, exhibit a significant temperature dependence. A temperature coefficient of 1.5% per degree celsius is not uncommon for such cables. In particular installations where the cable will be subjected to higher temperatures, a less-temperature dependent cable may be required."

To measure the effect of temperature and frequency on the electrical stability of cable insulating materials, Ausimont conducted a series of tests at GTE Testmark Laboratories in Lexington, Kentucky on typical plenum cables at several temperatures and transmission frequencies.

Twenty-seven four pair plenum cable constructions were tested for attenuation, characteristic impedance and near-end crosstalk at temperatures of 23°C, 40°C, 50°C, and 67°C.

All cables tested were 24 AWG, 1000-foot lengths purchased randomly. The cables utilized PVC, Smokeguard, and fluoropolymer materials as insulation. All cables were tested concurrently, on reel, in the same environmental chamber.

#### **Results**

The following graphs show the results of attenuation vs. temperature at 1, 4, 10, and 16 MHz.

As test temperatures increased, attenuation values for the non-fluoropolymer materials increased dramatically. At 1 MHz, the attenuation increased 23% from 23°C to 50°C compared to less than 5% for the fluoropolymer insulated cables. At 67°C, attenuation values increased between 34% and 48% compared to a 7% increase obtained on the fluoropolymer insulated cables.

More dramatic increases in attenuation for the non-fluoropolymers were exhibited at higher frequencies. For example, at 16 MHz and 23°C, the difference in attenuation between non-fluoropolymers and the fluoropolymers was 14 db. At 23°C and 1 MHz, the differences were only 2 db illustrating the effects of higher frequencies when compared to fluoropolymer materials.

Attenuation values recorded at the highest temperature and frequency tested (67°C & 16MHz) demonstrate the significant combined impact of temperature and frequency on transmission signals carried by non-fluoropolymer insulating materials. Attenuation values for the non-fluoropolymer materials were in the range of 70 db. At the same conditions, the maximum value recorded for the fluoropolymer insulating materials was 36 db - still significantly below the industry standard of 40.

#### **CONCLUSIONS**

From these studies, it is clear that the attenuation levels of many non-fluoropolymer materials are severely affected by temperature, and that this impact is magnified as temperature and frequency increase.

Random temperature excursions affecting signal quality can lead to system problems not easily detected such as increased bit error rate and system slowdown. This can lead to excessive system down time along with additional costs related to system trouble shooting.

Concern for electrical stability at elevated temperatures has been recognized by the IEEE 802.5 Plenary Committee and the EIA/TIA work group responsible for establishing Premise Wiring requirements in EIA/TIA 568. Articles appearing in recent issues of various trade magazines have also referred to consequences of attenuation losses related to elevated temperature exposure.

As the emphasis on increased operating frequencies for UTP plenum data cables continues into the 90's, the effects of elevated temperature on the transmission media must be taken into account.

To insure that the end user is receiving the quality of cabling demanded of the 90's we would encourage you as end users, government and commercial agencies as well as manufacturers, to solicit and support required elevated temperature testing as part of specification requirements for all categories of cable used for data transmission.

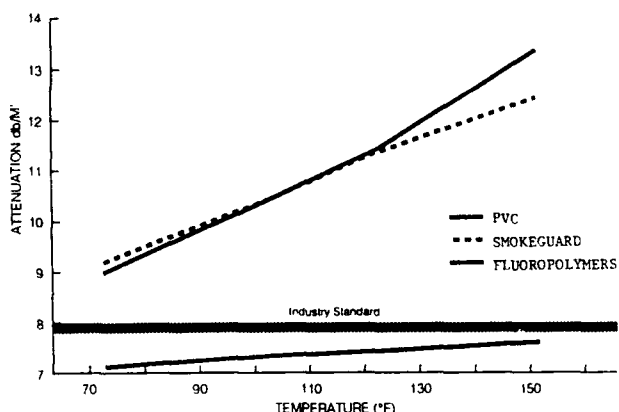
## REFERENCES

1. ANSI/IEEE STANDARD 802.3-1985 ISO/DIS 8802/3, Institute of Electrical and Electronic Engineers Inc., New York, N.Y.
2. EIA/TIA STANDARD Commercial Building Telecommunication Wiring Standard EIA/TIA 568, 1991.

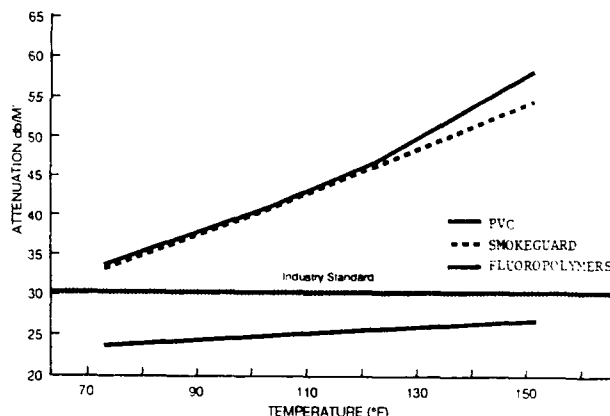
\* SMOKEGUARD is a registered trademark of Gary Corporation for a patented insulation and jacketing material supplied by Gary Corporation, Leominster, Ma.

# ATTENUATION VS TEMPERATURE

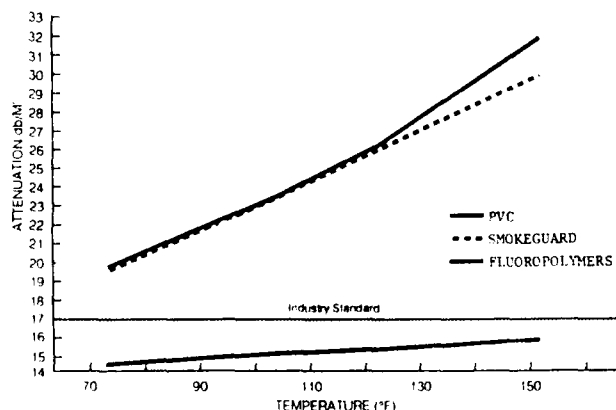
1 MEG HZ



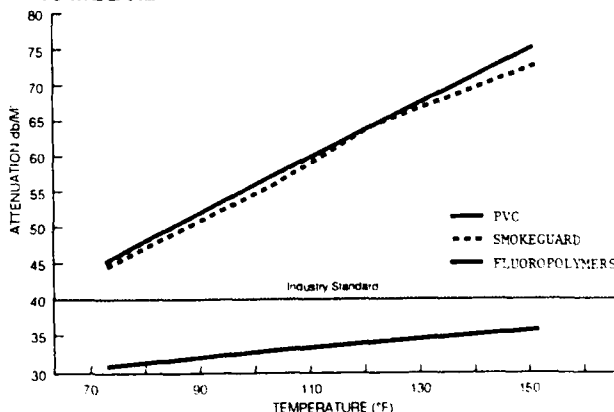
10 MEG HZ



4 MEG HZ



16 MEG HZ





AUSIMONT USA Inc.  
P.O. Box 1838  
Morristown, N. J.  
07962-1838

Richard J. (Dick) Rockosi graduated from Fairleigh Dickinson University with a B.S. Degree in Management Science. He is presently a Technical Service Engineer with Ausimont USA Inc. located in Morristown, New Jersey. He was employed in the Wire and Cable industry for 15 years prior to Joining Ausimont.



## Improved PVC Based Jacket Compound For Plenum Cable Applications

Paul W. Kroushl

Cooper Industries / Belden Division

### Abstract

Traditionally, fluoropolymer based jacketing materials have been used over constructions for plenum cable applications. However, recent advances in PVC flame and smoke suppression technology have enabled PVC based compounds and alloys to replace fluoropolymers in many of these applications. The first PVC compounds developed for the plenum jacket applications were major breakthroughs and found acceptance in many plenum cable constructions. However, as with any new breakthrough, there were some constructions which would not meet the requirements for plenum cable when these first generation PVC compounds were used as the jackets. Other areas of weakness also became apparent as these compounds gained wider use, including physical properties that were marginal for some applications and processing variability in extruding these new materials. Therefore, a development project to improve the physicals, flame and smoke properties and consistency of plenum rated PVC jacket materials was undertaken. This paper describes that project and its results.

### Introduction

The plenum area referred to in this paper is the space between the drop ceiling and the floor above found in most of today's modern office buildings. This area is commonly used as a horizontal network for office wiring systems. The ease of cable installation in these areas, coupled with the ability to quickly reconfigure cable networks located in these areas, has led to an increase in popularity for plenum cable products. In 1975, the National Fire Protection Association, via the National Electric Code, began adopting standards for the installation of cable in plenum spaces. Initially, all cables located in plenum areas had to run through metal conduit. In 1978 the regulations were altered to permit certain cable constructions to be installed in plenum areas without conduit. This change was instrumental in the development of today's plenum cable market.

The NEC code called for a construction to meet the Underwriters Laboratory Standard UL 910 in order to qualify for use in a plenum without being placed in a conduit. This standard is a modified ASTM E84 Steiner Tunnel test. The

test uses the Steiner Tunnel with a tray for the cables placed inside. The test is for 20 minutes instead of the 10 minutes called for in E84. The Tunnel itself is a chamber 25' long, 18" wide and 12" high. The tray is 25' long by 11.25" wide. The cables are placed side by side on the tray and subjected to a 300,000 BTU/hr flame for 20 minutes. A 240 cubic ft./min. airflow is maintained in the chamber throughout the test. When the test begins, the flame engulfs the first 4.5' of the cable. The distance the flames travels past this point is noted by the operator and recorded over the time period. The Tunnel is also instrumented to record the smoke generated and this is recorded over the time of the test. To qualify for use in a plenum the cables being tested must convey the flame less than 5' past the point where the burner impinges on the cable, have a peak smoke of less than 0.5 and an average smoke of less than 0.15. These last two values correspond to 70% and 30% light transmission respectively.

When this standard was first adopted, the only materials capable of being used in cable constructions which met the requirements of the standard were fluoropolymer based materials. Although these materials worked quite well as far as their flame and smoke properties were concerned, they were stiff and difficult to install in certain situations. They were also expensive and an overkill as far as temperature requirements were concerned.

Originally polyvinylchloride (PVC) based formulations were not even considered for plenum cable constructions. This was because although PVC has better flame retardant properties than many polymers, it generated large amounts of smoke when involved in a fire. New smoke suppressants, flame retardant plasticizers and alloying techniques led to the development of PVC based materials which could be used as jackets on some constructions and would meet the requirements of the UL 910 standard. Installers found the PVC jacketed cables easier to install and work with than the fluoropolymer jacketed cables.

As is usual with new developments, the first PVC's developed for this application had some drawbacks. They could not be used in all the constructions to replace the fluoropolymer jacket materials, their physical properties were borderline in meeting the requirements, and they were prone to be difficult to process. That is they lacked the consistency desired to

make manufacturing cables using them a routine event. Development was undertaken to improve on these first generation materials in the areas mentioned above.

#### Experimental

Two screening tests were chosen to aid in the development of an improved PVC plenum formulation. To determine the smoke characteristics, the NBS Smoke Chamber was used to measure the degree of flame retardancy and the Limited Oxygen Index (LOI) was measured. Many experimental formulations were mixed, most of these formulations were rejected before being screened by these tests because of poor physicals or poor agings. Examples of some of these trials are shown in Table I below. Formulations were tried using some blending of PVC with other polymers such as chlorinated polyethylene (CPE) and chlorinated polyvinyl chloride (CPVC). However, due to difficulty in mixing, poor physicals and the advent of better smoke and flame suppressants for these applications the final trials were concentrated on only PVC based resin.

TABLE I

#### PRELIMINARY FORMULATIONS

INGREDIENT-PHR	1	2	3
PVC Resin	100	100	80
Chlorinated Polyethylene	-	25	-
Chlorinated PVC	-	-	20
Phosphate Plasticizer	5	-	30
Epoxidized Soybean Oil	-	5	10
Chlorinated Paraffin	5	-	-
Phthalate Plasticizer	35	-	-
Clay	31	-	-
Ammonium Octamolybdate	31	10	30
Lead Phthalate	5	-	-
Tribase E	-	5	7
Stabilizer	-	-	2
Wax	-	-	0.5
Antimony Oxide	3	3	3
Aluminum Trihydrate	-	-	30
Zinc Borate	-	2	10
Tensile Strength (PSI)	2640	2300	2400
Elongation (%)	240	225	225

Table II shows some of the final trial formulations, their smoke values and their LOI values. The control is a first generation PVC plenum formulation. Formulations 5 and 6 utilize slightly different smoke suppression technologies. Formulation 5 was based on standard PVC flame and smoke technology obtained through patent and literature searches. Formulation 6 is similar to formulation 5 but includes some newly developed smoke and flame suppressants.

TABLE II

#### SECOND TRIAL FORMULATION

Ingredient-PHR	4	5	6
PVC Resin	F	100	100
Phosphate Plasticizer	I	0	30
Plasticizer	R	42	0
Brominated Plasticizer	S	0	20
Phosphorous Plasticizer	T P	15	0
Epoxidized Soybean Oil	L	3	3
Aluminum Trihydrate	G E	30	30
Ammonium Octamolybdate	E N	30	30
Lead Phthalate	N U	7	7
Stearic Acid	E M	0.5	0.5
Wax	R	0.5	0.5
Experimental Ingredient A	A	0	7
	T		
	I		
	O		
	N		
LOI (%)	52.8	40	49.1
Smoke Density (DM/G)	21	38	20

Each showed good enough values that they were extruded as a jacket over RG 6 type coaxial cable with a fluoropolymer dielectric. The first generation plenum PVC was also extruded as a jacket on the same construction to determine what improvements there were. These cables were then sent to Underwriters Laboratory and subjected to the UL 910 test. This was necessary because the NBS smoke chamber is only a screening tool and correlation between it and results in the UL 910 test is not always predictable.

Table III shows the results of the UL 910 test on these three cables. The data shows that formulation 6 had equivalent results to the first generation material.

TABLE III

#### UL 910 Results of RG 6 Cables

Jacket Compound	Flame	Peak Smoke	Average Smoke
Formula 5	4.5'	0.33	0.13
Formula 6	2.0'	0.25	0.08
1st Generation	2.0'	0.25	0.08

This equivalency was done with an improvement in physical properties and a perceived improvement in processability. After analyzing these results, some minor modifications were made to formulation 6, the result of which was labeled formulation 7. Table IV shows the formulation change which was made as well as the LOI and NBS smoke results.

TABLE IV

<u>Ingredient-PHR</u>	<u>6</u>	<u>7</u>
PVC Resin	100	100
Phosphate Plasticizer	30	30
Plasticizer	0	0
Brominated Plasticizer	20	20
Phosphorous Plasticizer	0	0
Epoxidized Soybean Oil	3	3
Aluminum Trihydrate	30	30
Ammonium Octamolybdate	30	30
Lead Phthalate	7	7
Stearic Acid	0.5	0.5
Wax	0.5	0.5
Experimental Ingredient A	7	-
Experimental Ingredient B	-	10
LOI (%)	49.1	45
SMOKE DENSITY (DM/G)	20	18

The addition of the one extra smoke suppressant resulted in an improved smoke generation according to the NBS smoke chamber, while also improving the LOI. This formulation was then extruded as a jacket over a more complex construction which is known as an IBM Type II cable. The first generation compound was also extruded over the same construction and both were subjected to the UL 910 test. The results of that test are shown in Table V. Both samples passed the requirements although the newest formulation 7 passed with a little wider margin than the control.

TABLE V

## UL 910 Results of IBM Type II Cables

<u>Jacket Compound</u>	<u>Flame</u>	<u>Peak Smoke</u>	<u>Average Smoke</u>
Formula 7	2.0'	0.33	0.12
1st Generation	2.0'	0.38	0.14

Based on these results the newly developed PVC formulation was applied as a jacket on a variety of constructions which had previously used the first generation jacket material. The new PVC met all the requirements for these constructions. This new material had better physical properties and, during preliminary extrusion trials, was more consistent in its extrusion characteristics than the first generation material.

Until the advent of this latest formulation, there was a reluctance to submit multi-pair fluoropolymer insulated singles jacketed with a PVC jacket for plenum rating. The new formulation had flame and smoke properties which were felt to be good enough to try this material as a jacket over fluoropolymer insulated singles in plenum applications. A one pair and a twelve pair construction of fluoropolymer insulated singles were jacketed with the improved formulation and submitted to Underwriters Laboratory for the UL 910 test. The results of those tests are given in Table VI.

TABLE VI

## UL 910 Results of Multipair Cable

<u>Number of Pairs</u>	<u>Flame</u>	<u>Peak Smoke</u>	<u>Average Smoke</u>
1	4.0'	0.40	0.06
12	2.0'	0.24	0.11

Both constructions met the requirements of the UL 910 test. This allowed a new product line with good sales potential to be introduced to the marketplace at a critical time.

As pointed out earlier, the first generation of plenum PVC compounds had a significant problem with consistency. Lot to lot or batch to batch variation in these materials was greater than acceptable in a quality manufacturing environment. Processing parameters such as extrusion speeds, heat zones and tip and die combinations would have to be adjusted for extrusion of each new batch. Sometimes these changes would also adversely affect the physical properties and the cable constructions would fail the Underwriters Laboratory requirements for these properties. The new compound development was aimed at solving these problems by developing a compound which had inherently better physicals so there was a wider margin for error. The processing variability was brought under closer control by carefully specifying the attributes of the raw materials which made up the new compound and precisely controlling the mixing cycle for this new compound. Although processing variability is sometimes hard to pin down, a trial run was made with the new compound compared to a typical lot of the first generation compound. The extrusion trial was performed on the jacketing operation of the IBM Type II cable mentioned previously as part of the evaluation of this new formulation. This trial consisted of measuring the extrusion speed which gave an acceptable product based on a measurement of the number of blows per thousand feet. The blows resulted from "burned" compound which was found in the jacket. This burned compound can be the result of a variety of problems, most of which are related to the mix consistency of the compound.

TABLE VII

## Extrusion Trials

<u>Compound</u>	<u>Line Speed - ft/min.</u>	<u>Blows/1000'</u>
Formula 7	360	0.14
1st Generation	210	0.46
Rated First Generation	300	0.50

Table VII gives the results of this processing trial. These results show that the new formulation resulted in higher extrusion speeds than the first generation formulations were rated to extrude and that this particular batch of the first

generation material had to be run slower than its rated speed. This second item is attributed to the variability involved with this material.

Although this is the only run where the two materials were compared on a side-by-side basis, the manufacturing facility has reported less variability with the second generation material with the formulation as it has been introduced into the manufacturing environment.

The PVC jacket plenum constructions offer greater ease of installation than fluoropolymer jacketed counterparts but one of the concerns about these materials has been their abrasion resistance. The fluoropolymer jacketed constructions do have very good abrasion resistance. The first generation of plenum PVC jackets had acceptable abrasion resistance. There was a concern that the proposed second generation PVC plenum formulation might have a poorer abrasion resistance. An RG 6 coaxial cable construction was made using both jackets, and the abrasion test described in Underwriters Laboratory specification UL 1581, was performed on the two constructions. Ten tests were run on each construction and the average number of cycles/mil until failure are shown on Table VIII.

TABLE VIII  
Abrasion Test Results

<u>Compound</u>	<u>Cycles/mil</u>
Formula 7	3.54
1st Generation	3.05

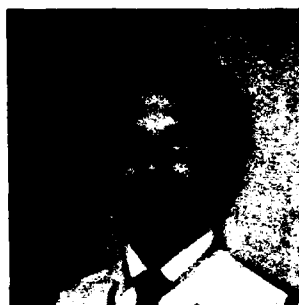
From the results, it can be seen that the new formulation is as good as the first generation material and may be interpreted as showing a slight improvement.

### Summary

The efforts to develop a second generation of PVC plenum jacket materials resulted in a new formulation which had improved flame and smoke properties. These improvements were sufficient to allow for the application of PVC plenum jackets to constructions which had previously consisted of fluoropolymer jackets. The lot to lot variation was improved to the extent that faster extrusion speeds were realized in the manufacturing process. The physical properties were improved to provide a wider margin of safety in meeting the required physical properties. The abrasion resistance of the second generation PVC jacket was equal or superior to the abrasion resistance of the first generation PVC plenum material. Based on these facts, this development project was considered a solid technological success.

### References

1. Glew, Charles A. "A National Electrical Code (NEC) Update". Wire Technology. Mar. 1989, pp. 41-45.
2. Mitchell, L.C. (to Ethyl Corp.), U.S. Patent 3,821, 151 (June 28, 1974).
3. McRowe, A.W. (to B.F. Goodrich Co.), U.S. Patent 3,822,234 (July 2, 1974).
4. Mitchell, L.C. (to Ethyl Corp.), U.S. Patent 3,846,372 (Nov. 5, 1974).
5. McRowe, A.W. (to B.F. Goodrich), U.S. Patent 3,862,086
6. Mathis, T.C., and Morgan, A.W. (to Monsanto), Bel. Patent 808,824, (Dec. 19, 1973).
7. Syntex Corp., German Patent 2,307,387 (Feb. 15, 1973).
8. Kroenke, W. J. (to B.F. Goodrich), U.S. Patent 3,883,480 (May 13, 1975).
9. Kroenke, W.J. (to B.F. Goodrich), U.S. Patent 3,883,482 (May 13, 1975).
10. Flame Retardancy Smoke Reduction - for the First Time You Can Have Both - with Arapahoe DFR-121, Tech., Bull., Arapahoe Chemicals, Inc., Boulder Colo.
11. Bonsignore, P.V., and Claassen P.L., J. Vinyl Technol., 2(2), 114 (1980).
12. Moore, F.W., and Church, D.A., Molybdenum Compounds as Flame Retardants and Smoke Suppressants for Polymers, presented at the International Symposium on Flammability and Flame Retardants, Toronto, May 7, 1976.



Paul W. Kroushl received a BS in Chemistry from Northern Illinois University in 1986. He is a Compound Development Engineer at the Belden Engineering Center specializing in PVC compound development.

# **A NON-METALLIC WATER PROOF OPTICAL FIBER CABLE WITH HALOGEN FREE FIRE RESISTANCE**

**Hideo Suzuki   Yoshlyuki Sato   Nobuyasu Sato**

**Opto-Electronics Laboratory  
Fujikura Ltd.  
Sakura-shi, Chiba-ken 285 Japan**

## **Abstract**

A non-metallic water proof optical fiber cable with halogen free fire resistance has been developed. This cable completely consists of non-metallic material, and has a water proof property by using water swellable materials. Furthermore this cable has the fire resistant property to meet IEEE 383 VTFT.

This paper presents the cable structure, the new component materials and the characteristics of the cable.

## **Introduction**

Optical fiber cables begin to be widely used for subscriber networks, and requirements for optical fiber cables are changing. Now customers need economical and safety optical fiber cables with easiness to handle, as general purpose optical fiber cables.

A non-metallic water proof optical fiber cable with halogen free fire resistance has been developed. This cable completely consists of non-metallic material, and has a water proof property by using water swellable materials.<sup>1,2</sup> Furthermore this cable has the fire resistant property to meet IEEE 383 VTFT.

The cable structure of this cable is a single slotted rod with 4-fiber ribbons. The cable consists of a slotted rod, 4-fiber ribbons, a water swellable tape, a halogen free fire resistant wrapping tape, and a halogen free fire resistant compound. Number of fibers in the cable is 100, and the strength member of the slotted rod is fiber reinforced plastics.

The cable simultaneously meets four major conditions as general purpose optical fiber cables. These conditions are a noninductive property, minimization of hydrogen generation, a water proof property and a halogen free fire resistant property.

It is very difficult for optical fiber cables to meet the four major conditions mentioned above at the same time. Especially the compatibility in fire resistance and other properties, such as a noninductive property, a water proof property and mechanical properties, has been a very difficult subject. Several new materials, such as a halogen free fire resistant wrapping tape and a water swellable tape, have been introduced to develop the new optical fiber cable. This cable meets same specification for mechanical properties as conventional one in spite of a non-metallic optical cable.

This paper presents the cable structure, the new component materials and the characteristics of the cable.

## **Cable Structure**

The developed cable consists of 4-fiber ribbons accommodated tightly in a single slotted rod. The cross sectional structure of the cable is shown in Fig. 1. The slotted rod is made of pure high density polyethylene by extrusion technique, and the strength member of the slotted rod is fiber reinforced plastics.

An optical fiber ribbon is composed of four coated fibers aligned in parallel, and coating materials for fibers and a 4-fiber ribbon are UV curable resin. The thickness and the width of the 4-fiber ribbon are 0.4 and 1.1 mm, respectively.

Coated single mode fibers having 250  $\mu\text{m}$  in outside diameter are used in the 4-fiber ribbons. The mode field diameter and the effective cut off wavelength of the fibers are 9.5  $\mu\text{m}$  and 1.10~1.29  $\mu\text{m}$ , respectively. These fibers have 125  $\mu\text{m}$  in fiber diameter.

Five 4-fiber ribbons are stacked tightly in each of the five rectangular slots. The slotted rod is wrapped with a water swellable tape and a halogen free fire resistant wrapping tape. This cable core

is covered with a halogen free fire resistant compound. This cable is 19 mm in diameter and 0.29 Kg/m in weight.

This cable completely consists of non-metallic material, and has an unfilled structure. Therefore its weight is equal to a conventional one and no special treatment is required for a cable joining in spite of a water proof cable.

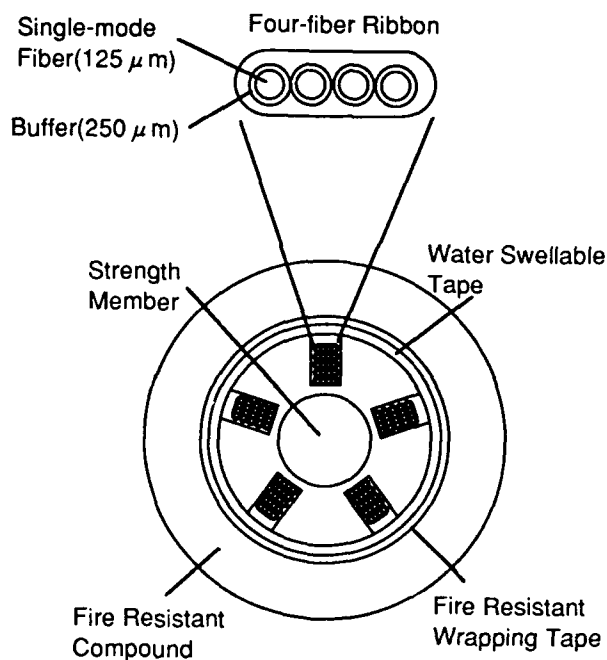


Fig. 1 Cross Sectional Structure of the Cable.

#### Component Materials

##### Water Swellable Tape

The water swellable tape is composed of unwoven cloth and water swellable powder. The water swellable powder is adhered to unwoven cloth. Fig. 2 shows the principle of water blocking mechanism. When water reaches the inside of the cable, water meets with the water swellable tape. The water swellable powder is disconnected from the unwoven cloth, and fill the vacancy in the cable. The water swellable powder absorbs water, and swells to stop a flow of water.

It is an important factor for the water proof property of the cable that the swelling velocity of the water swellable tape is rapid. Fig. 3 shows the method of measurement for the swelling velocity of

water swellable tapes. Changes of thickness of water swellable tapes were measured to know the swelling velocity of water swellable tapes with a differential transformer. The water swellable tapes were immersed in artificial sea water. The results of the measurement are shown in Fig. 4. The swelling velocity depends on the composition of water swellable tapes. The selection of the water swellable tape for the developed cable was based on this results.

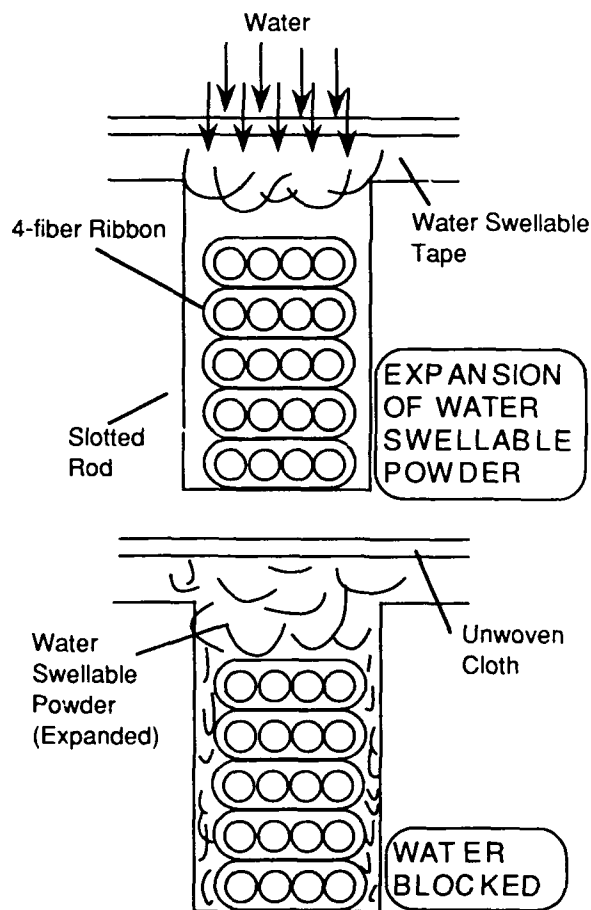


Fig. 2 Principle of Water Blocking Mechanism.

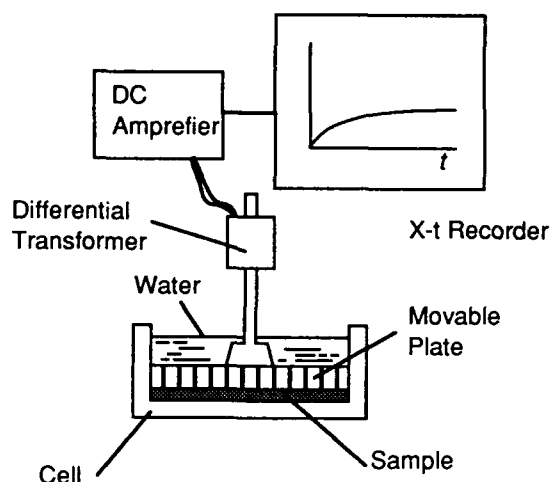


Fig. 3 Apparatus for Swelling Velocity Measurement.

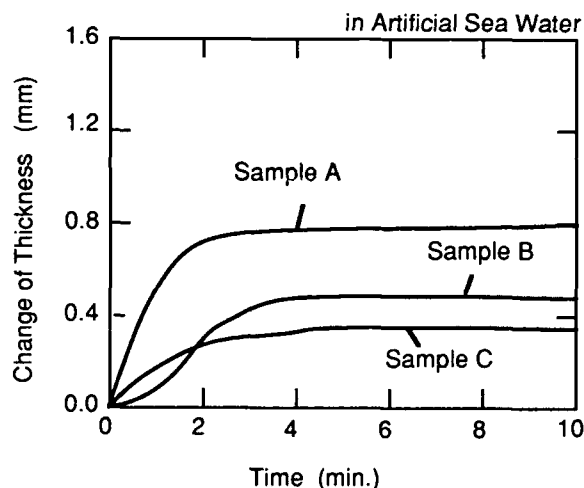


Fig. 4 Water Swelling Velocities of various kinds of Water Swellable Tapes.

#### Halogen Free Fire Resistant Wrapping Tape

A flame barrier layer under a cable jacket is used to suppress the temperature rise in a cable for a thermal isolator in fire. Flame barrier layers made of non-metallic material were investigated to complete the fire resistant property of the developed cable. Five kinds of wrapping tapes were investigated for a flame barrier layer.

- 1) Polyester unwoven cloth
- 2) Kraft paper
- 3) Fire resistant Kraft paper
- 4) Mixed paper with aluminum hydroxide
- 5) Halogen free fire resistant tape

The five kinds of fire resistant optical fiber cables were manufactured experimentally. The each wrapping tape mentioned above were wrapped separately on the cable cores of same structure. The fire resistant properties of the manufactured cables were evaluated according to the vertical tray flame test specified in the standard IEEE 383 (VTFT).

Fig. 5 shows the test results of the VTFT. A halogen free fire resistant tape is suitable as a flame barrier layer as shown in Fig. 5. It is of importance that the flame barrier layer prevents melted polymeric materials from gushing out, and flammable gases from escaping. Polyester unwoven cloth is not suitable as a flame barrier layer, because it melts by heat. Cellulose materials such as Kraft paper are suitable for a flame barrier layer, because they don't be melted by heat, and they form a carbonized ablative layer in reduced oxygen conditions.

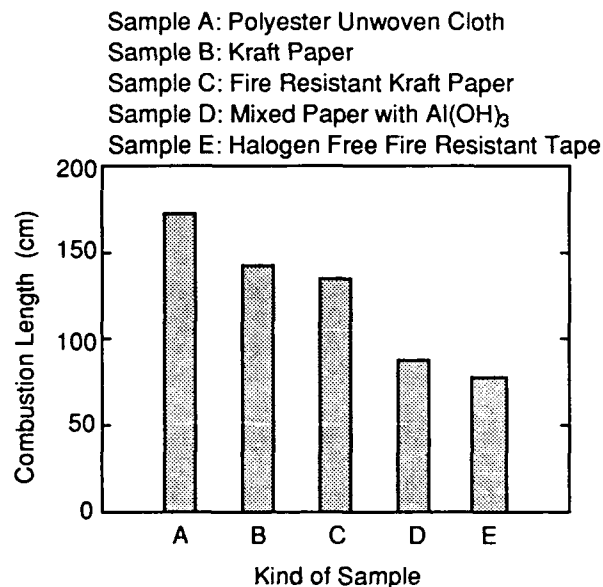


Fig. 5 Results of Vertical Tray Frame Test.

The halogen free fire resistant tape is the best choice for a flame barrier layer among the cellulose papers. The halogen free fire resistant tape is composed of a base tape and a halogen free fire resistant compound. The compound is coated on the base tape made from cellulose material. The halogen free fire resistant tape is used for a wrapping tape in the developed cable.

### Halogen Free Fire Resistant Compound

The halogen free fire resistant compound used in the developed cable is designed to maintain good thermal isolation as well as good physical characteristics for a jacket. The compound absorbs thermal energy by the reaction of a metal hydroxide during a fire. After the reaction, the compound forms hard and foamed char that is a good thermal isolator.

The typical properties of the halogen free fire resistant compound are shown in Table 1. The compound exhibits optimum balance of LOI, brittleness temperature and hardness.

Table 1 Typical Properties of the Halogen Free Fire Resistant Compound.

Property	Unit	Test Method	Typical Value
Tensile Strength	MPa	ASTM D368	12.7
Elongation at Break	%	ASTM D368	500
Melt Index	g/10min.	ASTM D1238	0.3
Limited Oxygen Index	-	ASTM D2862	33
Environmental Stress	$F_0$ -hrs	ASTM	
Crack Resistance		D1693	>1000
Brittleness	$F_0$ °C	ASTM	
Temperature		D764	-40
Smoke Density	Ds	NBS(NF)	90
Density	g/cm	ASTM D1505	1.4
Volume Resistivity	ohm-cm	ASTM D257	$1 \times 10^{16}$
Hardness (Shore D)	-	ASTM D2240	50

## Characteristics of The Cable

### Water Proof Property

Fig. 6 shows the method of measurement of water proof property. The water proof property of the developed cable was measured. The height of water is 1m, and artificial sea water is used. Only a jacket of 25 mm length is stripped.

Table 2 shows the results of the measurement of the water proof property. The water proof properties with temperature were measured, and the water proof properties with time were measured. The penetration length of water is about 0.8m at each result. The temperature dependence and the time dependence of the water proof property of this cable are scarcely observed.

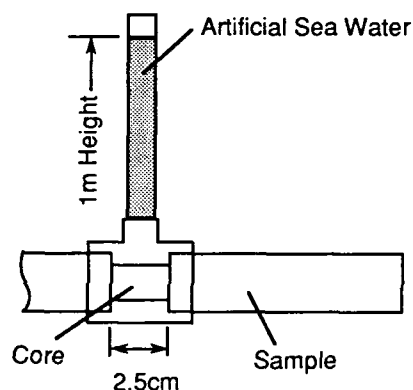


Fig. 6 Method of Waterproof Property Measurement.

Table 2 Characteristics of Water Penetration Length in Cable.

Treatment	80°C	60°C	40°C	20°C
3days	0.6m	0.8m	0.9m	0.7m
10days	0.7m	1.0m	0.8m	0.6m
1month	1.0m	0.7m	0.9m	0.9m
3months	0.8m	0.6m	0.7m	0.7m
6months	0.8m	0.7m	0.6m	0.9m

in Artificial Sea Water



## Fire Resistant Property

The fire resistant property of the developed cable was evaluated according to the vertical tray flame test specified in the standard IEEE 383 (VTFT). The cable passed satisfactorily the standard IEEE 383 as shown in Photo. 1. The combustion length of the cable after the test is less than 1m.

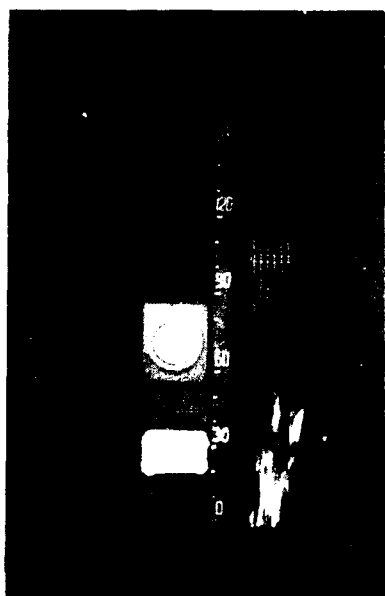


Photo. 1 Test Result of VTFT

## Mechanical Properties

Table 3 shows the mechanical properties of the developed cable. This cable meets same specification for mechanical properties as a laminated aluminum jacket cable in spite of a non-metallic cable.

Fig. 7 shows the method of measurement of the abrasion property of the developed cable. This abrasion test was carried out to simulate the damage of the cable under an actual installation. The tested cable was rubbed with a fixed pulley having rough surface. The bending angle of the cable on the pulley was 90 degrees. The applied tension was 300 Kgf. The surface of the cable jacket was only slightly damaged.

Table 3 Mechanical Properties of the 100-fiber Fire Resistant Cable.

Item	Condition	Result
Crush	up to 250kgf/50mm of lateral force	<0.01dB
Bending	R=250mm, 180deg. 10 times	<0.01dB
Tensile	up to 300kgf, l=100m	<0.01dB
Squeezing	R=250mm, T=300kgf, l=100m	<0.01dB
Impact	1kgf, 1m height	<0.01dB
Torsion	360deg., l=1m	<0.01dB

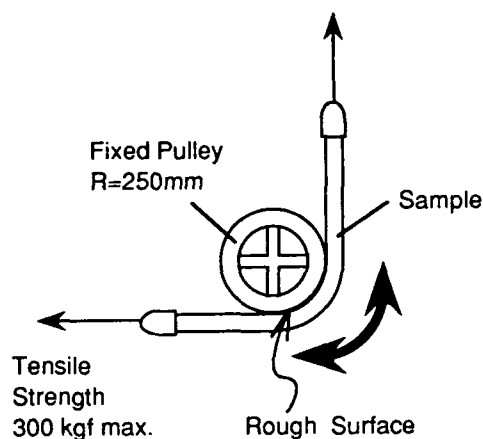


Fig. 7 Method of Abrasion Test.

## Hydrogen Generation

The component materials of the developed cable scarcely generate hydrogen, because the cable completely consists of non-metallic material. The loss changes of the cable after water penetration were measured to investigate the loss increase due to the generated hydrogen in the cable. The cable core of the cable was immersed in artificial sea water along the full length, and then the immersed core was covered with a halogen free fire

resistant compound. The cable after penetration was treated at 80 degrees centigrade, and measured the loss.

Fig. 8 shows the result the loss changes after the treatment of 6 months at 80 degree centigrade. There is no loss change due to hydrogen generation. Fig. 9 shows the loss histogram of the developed cable.

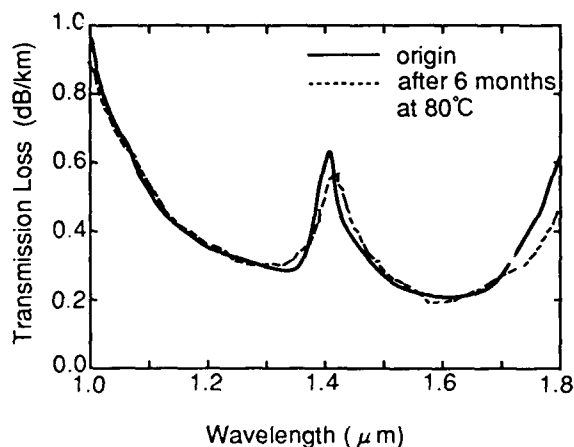


Fig. 8 Effect of Hydrogen Generation in Cable.

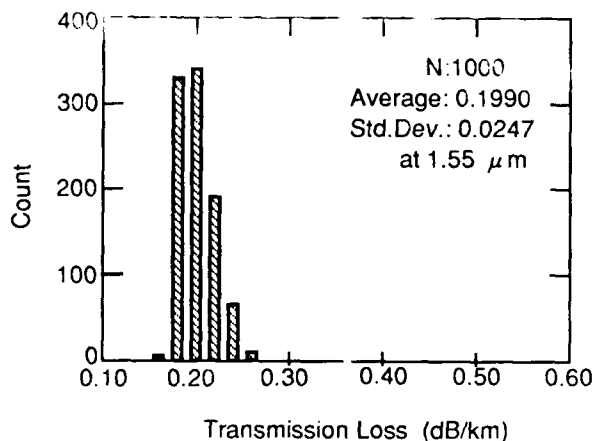


Fig. 9 Transmission Loss of the 100-fiber Cable.

## Conclusion

The non-metallic water proof optical fiber cable with halogen free fire resistance has been developed. The cable completely consists of non-metallic material, and has a water proof property by using water swellable materials. Furthermore this cable has the fire resistant property to meet IEEE 383 VTFT.

The cable is very convenient for the design of subscriber networks, because the cable can comply with several demands for subscriber networks at the same time, such as maintenance free cables, induction free cables, and halogen free fire resistant cables. The cable is a water proof optical fiber cable by using water swellable materials, so the cable is easy to handle at cable connection because of the omission of wiping jelly compound out. The cable will be useful for the construction of subscriber networks.

## Acknowledgment

The authors express their sincere appreciation to Dr. K. Inada for his helpful discussions and suggestions.

## Reference

1. S. Kukita, T. Nakai, A. Hayashi and H. Koga, "A New Nonmetallic and Waterproof Optical Fiber Cable with Absorbent Polymer Ribbon," 36th IWCS 1987
2. F. Ashiya, K. Hogari, and K. Omoto, "A Water-Blocking Optical Fiber System for Subscriber Networks," NTT REVIEW Vol. 3 No. 1, 1991
3. S. Kukita, T. Nakai, A. Hayashi and H. Koga, "Design and Performance of Nonmetallic Waterproof Optical Fiber Cable Using Water-Absorbent Polymer," IEEEJ. Lightwave Tech., LT-7, No. 4, 1989
4. M. Kawase, T. Fuchigami, M. Matsumoto, S. Nagasawa, S. Tomita, and S. Takashima, "Loop-Network Configuration for Subscriber Loops and Single-mode Optical Fiber Cable Technologies Suitable for Mid-span Access," 37th IWCS 1988
5. M. Kawase, S. Tomita, N. Kasahara and T. Uenoya, "Optical Subscriber Loops by Nonpressurized Optical Fiber Cable," The Transactions of the IEICE, Vol. J73-B-I No. 10, 1990
6. K. Omoto, K. Hogari, F. Ashiya, "Optical Loss Characteristics of High-Fiber-Count Water-Blocking Optical Cables," Spring National Convention Record B-867

IEICE, 1991

7. S. Tomita, F. Ashiya, M. Kawase, "1000-Fiber Water Blocking Cable," The Transactions of the IEICE, Vol. E73, No. 9, 1990

8. H. Sawano, Y. Kikuchi, K. Kobayashi, N. Okada, N. Misono, H. Suzuki and N. Sato, "One-thousand-fiber Cable Composed of Eight Fiber Ribbons," 38th IWCS 1989

9. Y. Kikuchi, H. Sawano, Y. Sato, K. Kobayashi, K. Okamura, H. Suzuki and N. Sato, "Characteristics of One-thousand-fiber Water Proof Cable," 39th IWCS 1990



Hideo Suzuki

Opto-Electronics  
Laboratory  
Fujikura Ltd.

1440 Mutsuzaki  
Sakura-shi, Chiba-ken  
285 Japan

Mr. Suzuki was born in 1948. He joined Fujikura Ltd. after graduation from Gunma University with a B.E. in 1971 and has been engaged in research and development of telecommunication cables. He is now the manager of Telecommunication Cable Section. He is a member of IEICE of Japan and The Society of Polymer Science, Japan.



Yoshiyuki Sato

Opto-Electronics  
Laboratory  
Fujikura Ltd.

1440 Mutsuzaki  
Sakura-shi, Chiba-ken  
285 Japan

Mr. Sato was born in 1963. He joined Fujikura Ltd. after his graduation from Tohoku University with a M.E. in 1987 and has been engaged in research and development of optical cables. He is an engineer of Telecommunication Cable Section and a member of IEICE of Japan.



Nobuyasu Sato

Opto-Electronics  
Laboratory  
Fujikura Ltd.

1440 Mutsuzaki  
Sakura-shi, Chiba-ken  
285 Japan

Mr. Sato was born in 1943. He joined Fujikura Ltd. after graduation from Tohoku University with a B.E. in 1966 and has been engaged in research and development of transmission cables. He is now the manager of Transmission Line Department and a member of IEICE of Japan.

SEMI-CONDUCTIVE AND HALOGEN-FREE FLAME RETARDANT CABLE COMPOUNDS  
ADVANCED COMPOUNDING TECHNOLOGIES

Peter Franz  
Tim Kelly

Buss AG, Basel Switzerland  
Buss (America) Inc., Bloomington, Ill. 60608 - USA

ABSTRACT

Data established on lab, pilot plant and commercial lines for the compounding of semi-conductive and halogenfree flame retardant cable grades are evaluated summarizing theoretical aspects, physical phenomena and field experiences. The data prove the theory: Moderate shear rates, short residence times, narrow residence time distribution and an outstanding distributive and dispersive mixing efficiency are the key factors to improve the quality of semicon and flame retardant cable compounds either thermoplastic or crosslinkable. This advanced compounding technology based on a rotating and simultaneously axially oscillating screw type machine proves to be a most powerful tool for those looking into super-smooth qualities. Stimulated by the positive results achieved R&D work was initiated to develop the "Direct Extrusion Process", an innovative contribution to the economic manufacture of cables.

1. INTRODUCTION

1.1 Semi-Conductors

Within the wide variety of cable materials (Table 1) the semi-conducting compounds represent a specific category of cable compounds as there is a must for power cable shields (as screen) at all voltages above 600 volts, i.e. in the medium and high voltage application range. Semi-conductors improve the dielectric strength of a cable insulation. As semi-conductors initially fibrous tapes impregnated with conductive carbon blacks were used. These were discontinued when it became known that fibrous protrusions from these tapes caused treeing and hence cable failure. As substitute semi-conductive extrudable polyethylenes were developed (1). The semi-conducting characteristics are based on the conductivity of carbon black. The conductivity of the carbon black depends on the carbon black's.

- particle size
- porosity or specific surface
- structure
- oxygen groups on the particle surface

The conductivity of carbon black improves with the particle size and the number of oxygen groups decreasing and with the specific surface and the structure increasing.

("structure" may be understood as the number of primary carbon black particles being lined up or agglomerated to a chain. The larger this number of lined-up particles, i.e. the longer the carbon black chain the higher the structure.)

The particle size of conductive carbon blacks typically are in the range of 15 to 30 (nm) and the specific surface is 150 to 260 (m<sup>2</sup>/g).

The conductivity of a semi-conducting compound in addition depends on the carbon black loading ranging from 12-20% and 30 to 40% by weight.

Within the past decade much progress has been made in semi-conductive compounds:

- as vehicle or matrix co-polymers like EVA, EEA, EBA and EPDM are used rather than the pure PE because their extrudability suffers less from the high loading of carbon black
- in addition to the standard conductive carbon blacks - which typically are loaded at 30-40% by weight to a polymer - special carbon blacks as the Ketjen EC were developed requiring an addition of 12-20% by weight only.
- conductive carbon blacks for super-smooth quality were made available; a major progress regarding especially the high voltage application and inner shielding.

Nowadays, semi-conducting extrudable compounds are used - either thermoplastic or crosslinkable - for inner and outer shields and strippable outer shields.

1.2 Flame Retardant Compounds

The vast increase in gross national product of the industrialised nations resulted in increased wealth, living standards and concentration of both population and materials. This concentration of industry, commerce, high value products and population increased the risk of fire and exponentially increased the compensation paid by insurances as e.g. Fig. 1 shows for the Federal Republic of Germany (2).

These factors initiate a steadily increasing public conscientiousness regarding fire protection and in consequence generate respective regulations

claiming for fire resistant materials.

In addition the public domain gets more and more concerned about halogen containing polymer compounds. These aspects also relate to LV, MV and HV power cables, building wires, wire and cables for apparatus, telecommunication, electronics, transportation and others as well (Table 1).

In 1990 the US and Canadian polymer consumption for wire and cable applications totaled 1895 mio lbs or about 860'000 tons in which PVC and LDPE/HDPE/Thermosets take a share of 38% and 53% respectively (Fig.2) (3). Within the next decade export and domestic regulations make the share of fire retardant cable compounds increase to a considerable volume. It is well known that PVC is self-extinguishing immediately after the ignition source is removed as the hydrogen chloride (HCl) molecules generated remove hydrogen and hydroxy radicals which support combustion and shield the PVC from further attack by oxygen.

But plasticised PVC - as used for wire and cable insulation and sheathing - may continue to burn depending on the type and quantity of plasticiser incorporated. Thus even PVC compounds may be subject to fire retardance regulations, i.e. to the replacement of the filler or part of the filler by flame retardants.

The major volume of polymers used for wires and cables are LDPE, HDPE and the co-polymers as EVA, EEA and EPDM. They are missing the self-extinguishing characteristics of PVC. Hence according to current and future standards they have to be fitted out with flame retardants. Typically 60-70% by weight of a flame retardant are added to a polymer. Containing no halogenes (F, Br, Cl, I) in their chains these polymers are the vehicle or matrix for halogen-free flame retardant wire and cable compounds.

A fire or a combustion process can only happen if simultaneously three elements are present at a time (Fig.3) (4):

- combustible material e.g. organic matter as polymers
- oxygen e.g. supplied from the ambient air
- ignition source e.g. excessive heat or a flame

If one of these three elements is missing a combustion process cannot take place.

A flame retardant inhibits or suppresses a combustion process either by physical and/or chemical action. It should get active within the temperature range the polymer start to decompose. For wire and cable compounds this range typically is 180°C up to about 300°C.

The most widely used halogen-free flame retardant is aluminium hydroxyde (ATH). It is low cost and as an inorganic compound it serves as filler.

At temperatures of 180°C to 200°C the ATH starts to convert to aluminium oxide (Fig.4). This reaction is endothermic and hence removes heat from the wire or cable. As a by-product water is created which evaporates and in addition to the endothermic conversion removes heat. One kilogram of ATH thus may remove about 5000 kJ.

The water vapour dilutes the ambient gas phase,

i.e. displaces oxygen and generates a protective gas layer over the wire or cable surface. Furthermore, the aluminium oxide forms a protective mineral layer on the surface of the wire and cable preventing oxygen from penetrating further into the combustible cable compound.

In recent years magnesium hydroxyde has been used as an alternative. It acts similarly to ATH but its decomposition temperature of about 260°C to 300°C is significantly higher. Experiences indicate that it promotes char formation and reduces smoke development; a positive aspect when looking into low smoke compounds.

Due to their specific characteristics blends of ATH and magnesium hydroxyde are used for some applications.

### 1.3 Compounding

Within the last decade important progress and improvements have been made regarding raw materials and formulations. In parallel the quality requirements increased steadily. Evidently, it was recognized that besides the raw material characteristics and the formulations the way of compounding interferes significantly regarding the quality achievable for semi-conductors or flame retardant wire and cable compounds.

## 2. FUNDAMENTAL PHENOMENA

At a first glimpse it looks like semi-conductors and flame retardant compounds would not have anything in common at all. But from a processing point of view they do have very much so:

Both categories represent polymer compounds with a high loading of inert components like carbon black or flame retardants.

This high loading makes dramatically increase the melt viscosity; an aspect that has to be considered for the proper design of both the compounding and the extrusion equipment.

In addition to the distributive and dispersive mixing taking place during compounding the surface of the carbon black or the flame retardant particles have to be "wetted" or coated thoroughly otherwise the mechanical characteristics of the extrudate would be below standard.

Hence the higher the loading and the larger the specific surface of the carbon black or the flame retardant the more polymer melt sticks to the particle surfaces being no longer as fluid as without filler. Thus the melt viscosity increases. Fig.5 may visualise this influence:

The lower and the upper diagram have the same abscissa "Mrel" i.e. the number of square meters one gram of polymer has to coat. With increasing addition of carbon black or flame retardant the number of square meters one gram of polymer has to coat increases. This is shown in the lower diagram of Fig.5 plotted vs the carbon black or the flame retardant loading "cfil" (% by weight). Based on analytical data made up by computer regression and splining the upper diagram of Fig.5 represents a master curve, i.e. the function of the relative Melt Volume Index "MVIrel" vs Mrel.

(MVIrel is the ratio of the specific MVI and the MVI of the pure polymer.)  
At low loadings, i.e. small numbers of square meters one gram of polymer has to coat there is minor influence on the viscosity. At about 2m<sup>2</sup> per g polymer the master curve starts to drop dramatically, i.e. the melt viscosity increases dramatically. It is just this area of the steep decline which is interesting for semi-conductors and flame retardant wire and cable compounds. To get the compounds conductivity carbon blacks with a particle size and structure resulting in specific surfaces of 150-260 m<sup>2</sup>/g have to be added at 12-40% by weight. For flame retardance 60-70% by weight of flame retardants have to be incorporated. Fortunately their specific surface of typically 2-12 m<sup>2</sup>/g is significantly smaller than that of carbon black thus compensating for the high loading.

#### Conclusion 1:

Obviously it is very important that carbon black or flame retardants are accurately metered as errors of a few percent change the melt viscosity significantly and consequently change the extrudability of a compound.

#### Conclusion 2:

Carbon black or flame retardants have to be homogeneously distributed in a compound otherwise the surface finish of an extrudate may suffer due to locally different melt viscosities.

It is common knowledge that the viscosity is one of the key factors determining the level of stress a viscous stock is subject to when sheared. As polymer melts are non-Newtonian fluids the mathematical functions for the shear stress might be rather complex. It is the Ostwald-de Waele function which best helps to understand the correlations:

$$\tau = \eta * \gamma^m$$

i.e. the shear stress "tau" equals the viscosity "eta" (which in itself is a function of temperature and shear rate) times the shear rate "gamma" raised to the power "m" (the exponent m is a characteristic figure for a specific compound).

Hence, the higher the viscosity and the higher the shear rate the higher are the shear stresses generated. To achieve the conductivity of a semi-conductive compound the addition of carbon black is set, i.e. the melt viscosity is set. As discussed in paragraph 1.1 the conductivity of the carbon black depends on its structure. This structure is sensitive to shear stress as it may easily be reduced, i.e. the carbon black chains may easily be broken apart when getting over-stressed. This would reduce the conductivity of the compound.

#### Conclusion 3:

The brittleness of the conductive carbon blacks limits the shear rates admissible.

It may be shown mathematically that the specific kneading energy "e", i.e. the energy imparted to

a mass unit is proportional to the shear stress "tau" and inverse proportional to the melt density "rho":

$$e \propto \tau / \rho$$

Now, the thermodynamic laws show that the energy imparted transform into heat, i.e. into a temperature raise:

$$e = c * \Delta T$$

Thus, the higher the melt viscosity and the higher the shear rates, the higher the shear stress will be, resulting in a high specific kneading energy and consequently in a high delta T.

The flame retardant in a compound set stringent temperature limits during processing. In addition most of the polymers used as a matrix may degrade or decompose when exposed to excessive heat, i.e. to too high temperatures. The degradation of polymers not only depends on temperature but also on the period of time exposed to it.

#### Conclusion 4:

Temperature sensitivity of both flame retardants and polymers set stringent limits to the shear rates generated during processing.

#### Conclusion 5:

Polymer degradation calls for short residence times and a narrow residence time distribution (RTD) during processing.

Summarizing the fundamental phenomena and the conclusions it is obvious that semi-conductive and flame-retardant compounds have to be processed at gentle shear rates, short residence times and a narrow RTD. Accurate metering of the components also is imperative. The need for a perfect distributive and dispersive mixing is superimposed to these aspects.

### 3. ADVANCED COMPOUNDING TECHNOLOGIES

#### 3.1 Basic Aspects

In order to optimally fulfill the requirements derived from the fundamental phenomena and in order to achieve the high quality level required in terms of distributive and dispersive mixing, consistency and reproducibility within the last decade there is a significant trend for the use of continuously operating equipment rather than the batch wise operation.

For the continuous compounding screw machines are used. These screw type machines can be broken down into three major categories:

- Single Screw Extruders (SSE)
- Twin Screw Extruders (TSE)
- Buss-Kneaders

These three categories distinguish from each other by their operating principle and the shear rates generated (Fig.6): Common single screw extruders generate very low shear rates limiting their ability for the homogenous distributive and disper-

sive mixing and high filler loadings as required when compounding semi-conductive and flame-retardant cable compounds.

TSE (for dispersive mixing co-rotating twin screws are used) generate high shear rates which may be a limiting factor when processing highly filled compounds, i.e. high viscosity melts.

The third category, the Buss-Kneader, generates moderate shear rates a most promising aspect regarding the fundamental phenomena discussed in paragraph 2.

### 3.2 Buss-Kneader

The Buss-Kneader (Fig.7) is a single screw design. But its operating principle is so unique that it represents a specific category within the screw machines:

The normally continuous spiral of a single screw extruder with the Buss-Kneader system is interrupted by three gaps per revolution resulting in the so called kneading flights (Fig.8). So called kneading teeth individually inserted in the barrel co-operate as stationary tools with these kneading flights. When the screw rotates the kneading flights and the kneading teeth form shear gaps where energy is imparted to melt the polymers and to perform a distributive and dispersive mixing. Each shear gap may be considered to be an incremental two roll mill summing up to an integral mixing system. Superimposed to the rotation the screw simultaneously axially oscillates. This makes the kneading teeth travel through the gaps between the kneading flights. Hence the polymer melt gets divided and then partially recombined and divided further like in a static mixer. Thus the axial oscillation generates an axial mixing effect superimposed to the radial one (5).

The stock is gently stressed in the shear gaps and relaxes in the gaps between the kneading flights. The alternate stressing and relaxation leads to a high degree of reorientation increasing the interfacial area in the melt, the key factor for good mixing (6,7,8,9). The interfacial area can be expressed in terms of the striation thickness. This striation thickness for a length of 4L/D of a Buss-Kneader was calculated to (10):

$$N_s = 2^{48} = 2.8 \cdot 10^{14}$$

which means that the mixing operation can be accomplished within a very short length, i.e. within a short residence time.

Additionally, the axial mixing effect smoothes out variations in the feed rate. Using the "Frequency Response Analysis" it could be shown that with the Buss-Kneader operating principle input variations can be smoothed out to an output variation of one-tenth even at long variation cycles of 30 seconds and more, i.e. at low variation frequencies of 2 per minute and lower. This contributes successfully to a consistent and uniform composition of a compound (11).

### 3.3 Compounding Technology

3.3.1 Semicon for the compounding of thermoplastic semicon formulations (Fig.9) the polymer(s)

like LDPE, EVA, EEA, EPDM etc. and additives are individually and continuously metered by corresponding gravimetric feeders into the first feed port of the Buss-Kneader. In the first zone shear energy is imparted to melt the polymer and to homogenize the polymer melt and the additives. The conductive carbon black is continuously added to the polymer melt by gravimetric feeders. At carbon black loadings of up to 30% all carbon black is fed via the second feed port. For carbon black loadings higher than that the carbon black is split into two fractions, the two fractions being fed individually via the second and the third feed port of the Buss-Kneader.

The shear energy imparted to the stock in the second and third zone of the Buss-Kneader accomplishes the dispersive and distributive mixing of the polymer melt and the carbon black.

The homogeneous melt finally is devolatilised, i.e. volatiles as moisture are removed from the stock by pulling vacuum at the degassing port located in the final zone of the Buss-Kneader.

A melt pump flanged into the discharge of the Buss-Kneader builds up the melt pressure necessary for passing an automatic screen changer and the hot face pelletizing die. The screen removes contamination eventually incorporated in the raw material components. Typically screens or filters of 120 up to 300 mesh are used.

The melt strands emerging the die plate are cut by rotating knives. By the impact of the knives and by gravity the still viscous pellets are falling down in a whirlpool generated by water in the lower section of the collector hood. The water immediately removes heat from the pellets so that they no longer are sticky. A centrifuge separates the pellets from the water which is recycled to the collector hood. The pellets are conveyed pneumatically to the pellet dryer and cooler which in parallel removes moisture sticking to the pellet surface and cools down the pellets to the bagging or storage temperature.

The barrel zones, the Buss-Kneader screw and the melt pump are individually temperature controlled by liquid heat transfer media (LHTM). LHTM can add or remove heat. Hence, the use of LHTM results in an accurate temperature control free of any hot spots. Each individual feeder is controlled by an automatic control loop to its set point. All feeders are integrated to a whole feeding system by a master/slave mode.

#### 3.3.2 Halogenfree, Flame Retardant Compounds.

The compounding technology for halogenfree flame retardant compounds is identical to that for semicon except for the addition of the flame retardant (Fig.10). Again the flame retardant is split into two fractions which are individually fed to the Buss-Kneader. But as the flame retardants are not sensitive to compaction as it is true for carbon blacks the first fraction of flame retardant can be added into the first feed port of the Buss-Kneader, i.e. into the melt zone together with the polymer(s) and additives.

3.3.3 To get crosslinkable semicon compounds mainly two alternatives are used:

- Peroxyde crosslinkable semicons:  
After pelletizing and cooling the pellets pass a mixer where the liquid or melted peroxyde is sprayed in so that it gets absorbed by the pellets. This "absorption process" neither sets limits to the type of peroxyde used nor to the mesh size of the screen or filter.
- Silane crosslinkable FR compounds:  
To get silane crosslinkable compounds organosilanes have to be grafted into the polymer chain prior to the incorporation of flame retardant. To accomplish this a liquid silane/peroxyde compound is injected via an injection tooth into the first Buss-Kneader zone where the grafting reaction takes place (Fig.11).  
As crosslinking only takes place by moisture and time not by heat (as it is true for peroxyde crosslinkable compounds) after grafting the compound is chemically inert and not thermoplastic. Thus there are no limitations for the use of a screen changer and the mesh size of the screen.

#### 4. FINDINGS AND FIELD EXPERIENCES

In the early 80th, i.e. about 10 years ago, R&D work started for the compounding of semi-conductive and flame retardant cable compounds either thermoplastic or crosslinkable. Many tests for a wide variety of formulations have been carried out so far on lab, pilot plant and commercial size Buss-Kneaders.

The data established like this are completed by field experiences gathered from plants commercially operated worldwide since about 5 years. In this paragraph, as far as proprietorship allows, the findings are discussed and compared to the targets to meet according to the fundamental phenomena (paragraph 2).

##### 4.1 Residence Time Distribution

The RTD was investigated on a commercial size dia 200mm Buss-Kneader processing LDPE (0,918 kg/dm<sup>3</sup>, MFI 2). A very stringent method was used (12).

To get an extremely high resolution the rare earth SmO was fed as tracer. To "contaminate" the whole system thoroughly the tracer was added during one hour. The tracer then was stopped and specimens collected at intervals of 15 seconds. The specimens were irradiated and their radioactivity checked. Fig.12 shows a dimensionless plot of the findings. (To get the dimensionless radioactivity the activity of an individual specimen was divided by the activity of a probe containing the total addition of tracer. The dimensionless residence time is the "specimen time" minus the systems "response time" divided by the average residence time).

Compared to the dashed line which represents data for single screw extruders the straight line for the Buss-Kneader at the beginning shows a smaller slope. This confirms the axial mixing effect stipulated by theory. At a dimensionless residence time of about 0.5 the radioactivity of the Buss-

Kneader specimens starts to decline dramatically where as the dashed line keeps on with its moderate slope. This again proves the high level of axial and radial mixing in the Buss-Kneader system and its efficiency in wiping clean all metal surfaces being contacted by the polymer. Fig.8 may visualise this effect as there is no area left which is not wiped by the kneading teeth and the kneading flights.

At a dimensionless residence time of about 1.1 the residence time "tailing" starts and clearly ends at 2.3. The dashed line keeps on still showing tracer. (Not yet published findings of a European University indicate that even TSE follow the dashed line rather than the straight line of the Buss-Kneader).

When opening the split barrel after the dimensionless residence time of 2.3 no tracer could be detected anymore, i.e. the tailing with a Buss-Kneader system absolutely ends at 2.3 or in other words a particle longest can stay in the Buss-Kneader for a time of 2.3 times the average residence time. After that time it definitely will be exchanged. For the compounding of cable grades the average residence time in a Buss-Kneader typically is 60-70sec. Therefore the longest time a particle may stay in the system is 2-3min. Obviously the Buss-Kneader fulfills the condition of a short residence time and a narrow RTD optimally.

##### 4.2 Metering Accuracy

In order to evaluate the accuracy of the feeders and the consistency of the composition a non-stop production run in a commercial line compounding LDPE with 40% of carbon black was carefully sampled during five days. The carbon black content of each sample was analysed. The statistical analysis revealed a two-sigma or two-standard deviation of plus/minus 0.25% absolute, i.e. at a probability of 95.44% the carbon black loading varies between 39.75% min and 40.25% max only.

This impressive accuracy confirms the quality of feeders used and the axial mixing effect of the Buss-Kneader which smoothes out input variations (see paragraph 3.2).

##### 4.3 Dispersion

The dispersion of the carbon black in an EVA based semicon cable compound was checked by automatically counting the number of categorised particle sizes on extrudates. Compared to samples obtained with the traditional compounding technology the samples compounded using the advanced technology of paragraph 3.3 showed a significantly narrower particle size distribution, the number of larger size particles being reduced by a factor of 6.5. This narrow particle size distribution is a key factor when looking into super-smooth semicon quality. This analysis also reveals that the advanced compounding technology disperses the carbon black to a degree which optimally develops the conductivity of the carbon black added. Experience shows that it is even possible to reduce the carbon black addition by 5-10%rel without loss to conductivity.



According to paragraph 2 and Fig.5 this may help to improve the extrudability of a semicon compound.

#### 4.4 Temperature Profiles

To read out the stock temperature, as a standard, thermocouples are inserted into kneading teeth along the Buss-Kneading axis.

Fig.13 shows the temperature profiles for semicon compounds based on EVA, EBA or EEA at carbon black loadings of 35-40%. The specific kneading energy of typically 0.18-0.22 (kWh/kg) raises the stock temperature to its discharge temperature of 175-215°C.

Fig.14 shows the temperature profiles for halogen-free flame retardant cable compounds based on EVA at ATH loadings of 55-60%. The specific kneading energy of 0.17 (kWh/kg) imparted to the stock raises its discharge temperature to 175-180°C.

It is interesting to note that the temperature after the ATH addition is lower than that of the polymer melt passed on to the feed zone for the ATH. This confirms that the large amount of ATH added cools the polymer melt by 5-20°C.

Experience shows that the temperature profiles achieved by the advanced compounding technology are by 20-30°C lower than those of the traditional compounding technology. This confirms the positive influence of the moderate shear rates.

According to the flow diagrams 10 and 11 the homogenized compound continuously is passed on to a melt pump flanged on to the discharge of the Buss-Kneader. This melt pump builds up the pressure necessary to push the melt through the screen changer and the die plate. Pressurizing the melt by means of a separate equipment like a melt pump or a discharge extruder releases the compounding extruder from this duty. Hence, the process parameters for compounding are independent of those for the pressure build-up; an important fact as passing the melt via a screen changer the head pressure varies during time. In addition the pressure build-up equipment can be designed for minimal energy impartation to the stock, i.e. for optimal pressure build-up efficiency. Thus, at a pressure build-up efficiency of 85% and a head pressure of 200 bars the energy imparted to the stock results in a temperature rise on about 4°C only.

#### 4.5 Electrical and Mechanical Properties

##### 4.5.1 Semi-conductive Compounds

The key criterion for the quality of semicon compounds is the dispersion of the carbon black which was discussed in paragraph 4.3. Mechanical and electrical properties are secondary aspects as there are no internationally approved standard methods and the characteristics depend very much on the design of a cable. As a rule of thumb the elongation at break after aging should be equal or higher than 100% and the specific resistivity should reach the order of magnitude of  $10^2$  (ohm\*cm). The specific resistivity very much depends on the temperature; with increasing temperature the resistivity increases according to an exponential function. Hence, it is virtually impossible to develop international standard methods to check these properties conclusively on a specimen made out of a compound. Therefore quality control relies primarily on checking the dispersion what moves back to paragraph 4.3.

##### 4.3.2 Halogenfree Flame Retardant Compounds

As these compounds are used for insulation or as sheath, i.e. at gauges larger than those for semicon conclusive standard methods were developed to check the properties.

Fig.15 summarizes the most interesting mechanical properties of two EVA based halogenfree flame retardant compounds. As flame retardants ATH and magnesium hydroxyde were added. Compared to the actual standards the samples processed with the advanced compounding technology discussed in this paper show significantly higher figures both for the tensile strength at break and the elongation at break.

#### 5. SUMMARY

An advanced compounding technology has been investigated for the compounding of both semi-conductive and halogenfree flame retardant cable compounds. Data established on lab and commercial size machines follow the theoretical aspects derived from the physical phenomena. They also prove that processing at moderate shear rates, narrow RTD and low stock temperature profiles - characteristics inherent to the Buss-Kneader used for this technology - obviously are key factors to improve the quality of semicon and flame retardant cable compounds.

#### 6. OUTLOOK

Stimulated by the positive results achieved with the advanced compounding technology three years ago R&D work started to develop the "Direct Extrusion Process".

With this process PVC or flame retardant cable grades are compounded on a Buss-Kneader as discussed in this paper. The pressure generated by the melt pump no longer is used for pelletizing but for the direct extrusion on the homogenized stock via a cable coating die (Fig.16).

This Direct Extrusion Process does not aim at a total replacement of the compounding and pelletizing technology but feasibility studies showed that it might be an alternative to improve the economic manufacture of some cables.

Further work shall prove the promising results achieved during lab tests is going on a commercial size pilot plant. Results will be reported in due time (13,14).

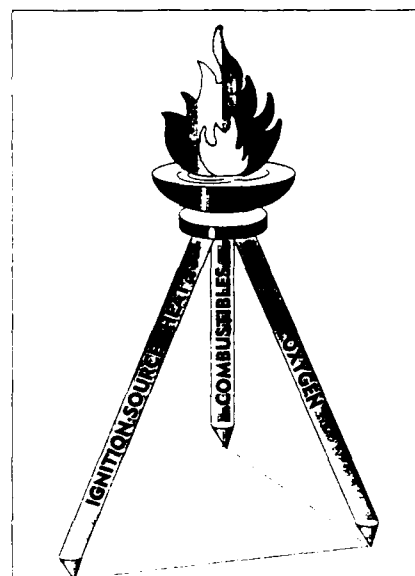
## REFERENCES

- ( 1 ) J.Kennth Gillet, Michael M.Suba: Electrical Wire Handbook, The Wire Association International, Inc. Guilford Connecticut, 1983
- ( 2 ) J.Troitzsch: International Flammability Handbook 2nd Edition, Hanser Publishers, Munich, Vienna, New York, 1990
- ( 3 ) J4 Communications, Inc: The Wire and Cable Industry in North America, Copyright Buss (America) Inc., Bloomingdale, Illinois, 1991
- ( 4 ) H.W.Emmons: Heat Transfer (1973) p.145
- ( 5 ) P.Franz: Devolatilisation of Plastics, VDI-Verlag GmbH, Düsseldorf, FRG, 1980
- ( 6 ) Y.Yabushita, R.Brzoskowski, J.L.White, N.Nakajima: Experimental Studies of the Flow of a Rubber Compound in a Pin Barrel Extruder, APEC, University of Akron, Ohio
- ( 7 ) R.Brzoskowski, J.L.White, W.Szydlowski, N.Nakajima, K.Min: Modelling Flow in Pin-Barrel Screw Extruders APEC/PERC 10, University of Akron, Ohio
- ( 8 ) R.Brzoskowski, J.L.White: Further Considerations of Simulation of Flow in Pin Barrel Extruders and in Screw Extruders with Sliced Flights, APEC, University of Akron, Ohio
- ( 9 ) R.Brzoskowski, T.Kumazawa, J.L.White: Modelling Flow in the Mixing Section of a Kneader (Buss), APEC, University of Akron, Ohio
- (10) S.Jakopin, P.Franz: Flow Behavior in Continuous Kneader and its Effect on Mixing, AICHE Diamond Jubilee, Washington, D.C., 1983
- (11) P.Franz: Dosieren in der Kunststofftechnik, VDI-Verlag GmbH, Düsseldorf, FRG, 1978
- (12) P.Franz: Der Buss-Ko-Kneter in der Extrusionstechnologie, Zucker- und Süßwaren Wirtschaft, Heft 10 und 11, 1984
- (13) P.Franz:Direktverarbeitung - Integration von Aufbereitung und Verarbeitung, VDI-Verlag GmbH, Düsseldorf, FRG, 1990
- (14) P.Franz: Silane Crosslinkable Polyethylene - from Raw Material directly to the Cable or Tube, Kautschuk + Gummi, Kunststoffe, Heft 6/91, p.566-570, Dr.Alfred Hüthig Verlag, Heidelberg, FRG, 1991

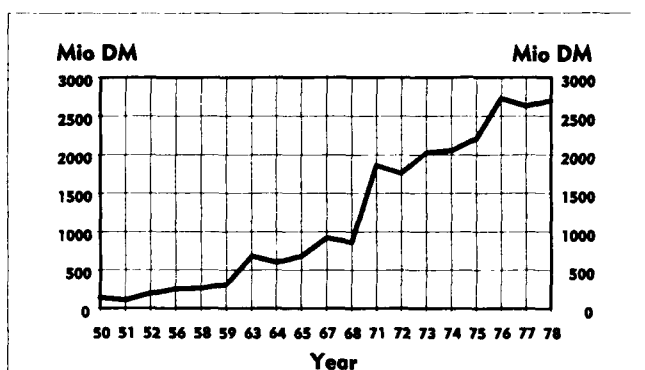
		POWER			BUILDING	TELECOM	APPARATUS	ELECTRONICS
		LV	MF	HV				
INSULATION	PVC	○	○	○	○	○	○	○
	POLYURETHANE	○	○	○	○	○	○	○
	ELASTOMER	○	○	○	○	○	○	○
SHEATHING	PVC	○	○	○	○	○	○	○
	POLYURETHANE	○	○	○	○	○	○	○
	ELASTOMER	○	○	○	○	○	○	○
SHEATHING	PVC	○	○	○	○	○	○	○
	POLYURETHANE	○	○	○	○	○	○	○
	ELASTOMER	○	○	○	○	○	○	○
FILMS	PVC	○	○	○	○	○	○	○
	POLYURETHANE	○	○	○	○	○	○	○
	ELASTOMER	○	○	○	○	○	○	○

○ THERMOPLASTIC  
○ THERMOPLASTIC, HEAVILY HALOGENATED FLAME RETARDANT  
○ HEAVILY CROSSLINKED  
○ CROSSLINKED ONLY  
○ HEAVILY CROSSLINKED & HALOGENATED FLAME RETARDANT  
○ CROSSLINKED ONLY, HEAVILY HALOGENATED FLAME RETARDANT

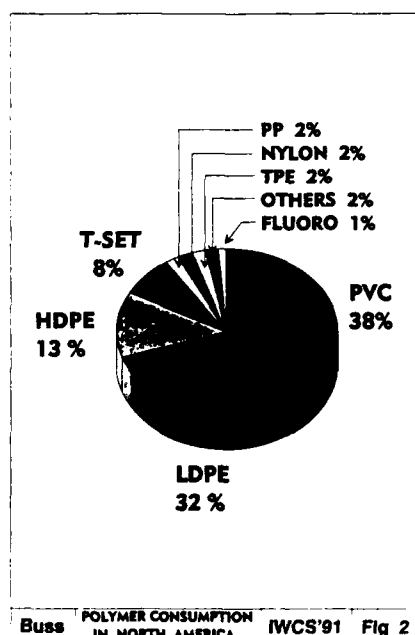
Buss WIRE AND CABLE SEGMENTS & COMPOUNDS IWCS'91 TABLE 1



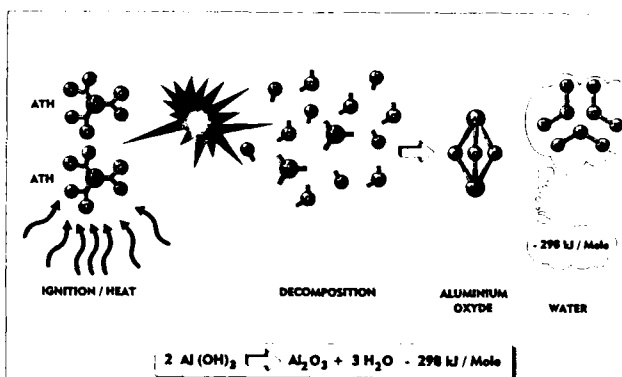
Buss FIRE TRIPOD IWCS'91 Fig 3



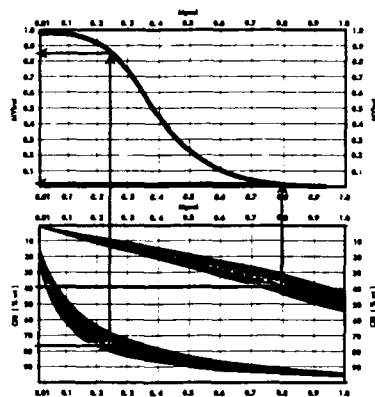
Buss COMPENSATION PAID BY FIRE LOSS IN THE FRG IWCS'91 Fig 1



Buss POLYMER CONSUMPTION IN NORTH AMERICA IWCS'91 Fig 2



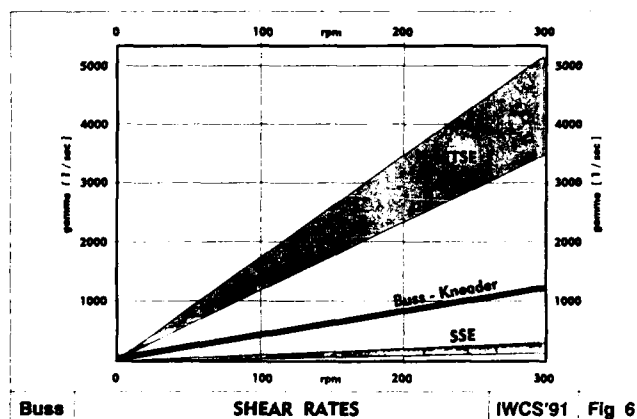
Buss DECOMPOSITION OF ALUMINIUM TRI-HYDROXYDE (ATH) IWCS'91 Fig 4



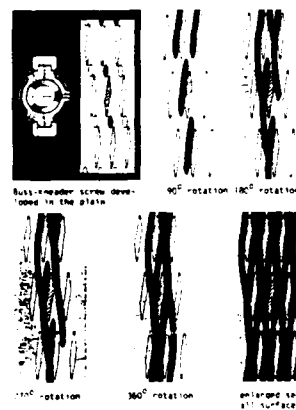
Buss RELATIVE MV1 vs FILLER LOADING IWCS'91 Fig 5



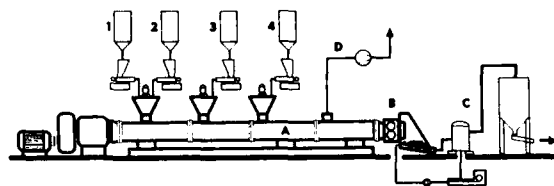
Buss Buss - KNEADER IWCS'91 Fig 7



Buss SHEAR RATES IWCS'91 Fig 6

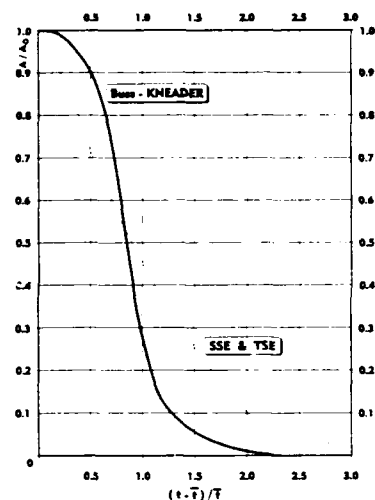


Buss - KNEADER OPERATING PRINCIPLE IWCS'91 Fig 8

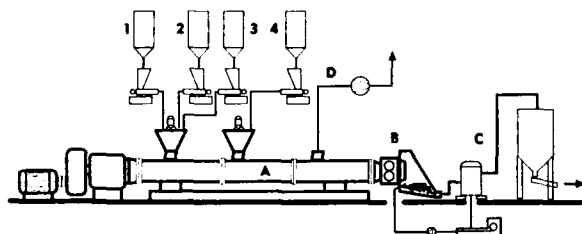


- |                |                             |
|----------------|-----------------------------|
| 1 POLYMER      | A Buss - KNEADER            |
| 2 ADDITIVES    | B PELLETIZER                |
| 3 CARBON BLACK | C PELLET DEWATERING /       |
| 4 CARBON BLACK | COOLING / DRYING            |
|                | D VACUUM / DEVOLATILIZATION |

Buss THERMOPLASTIC SEMI-CONDUCTIVE CABLE COMPOUNDS IWCS'91 Fig 9

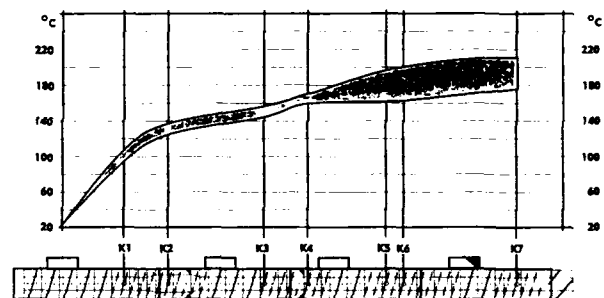


Buss RTD IWCS'91 Fig 12



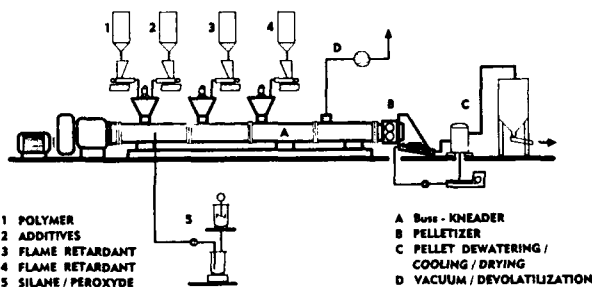
- |                   |                             |
|-------------------|-----------------------------|
| 1 POLYMER         | A Buss - KNEADER            |
| 2 ADDITIVES       | B PELLETIZER                |
| 3 FLAME RETARDANT | C PELLET DEWATERING /       |
| 4 FLAME RETARDANT | COOLING / DRYING            |
|                   | D VACUUM / DEVOLATILIZATION |

Buss HALOGENFREE FLAME RETARDANT CABLE COMPOUNDS IWCS'91 Fig 10



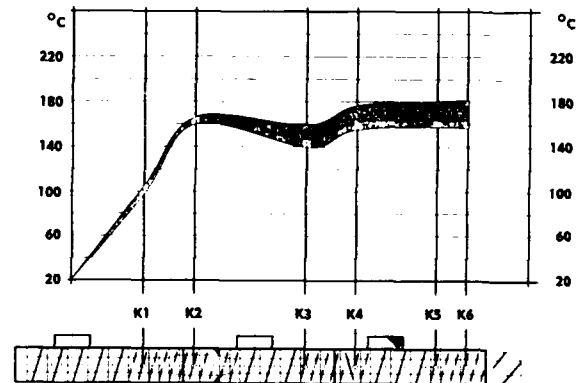
EVA + 35 - 40 % CARBON BLACK

Buss TEMPERATURE PROFILES FOR SEMICON CABLE COMPOUNDS IWCS'91 Fig 13



- |                     |                             |
|---------------------|-----------------------------|
| 1 POLYMER           | A Buss - KNEADER            |
| 2 ADDITIVES         | B PELLETIZER                |
| 3 FLAME RETARDANT   | C PELLET DEWATERING /       |
| 4 FLAME RETARDANT   | COOLING / DRYING            |
| 5 SILANE / PEROXYDE | D VACUUM / DEVOLATILIZATION |

Buss SILANE CROSSLINKABLE FLAME RETARDANT CABLE COMPOUNDS IWCS'91 Fig 11

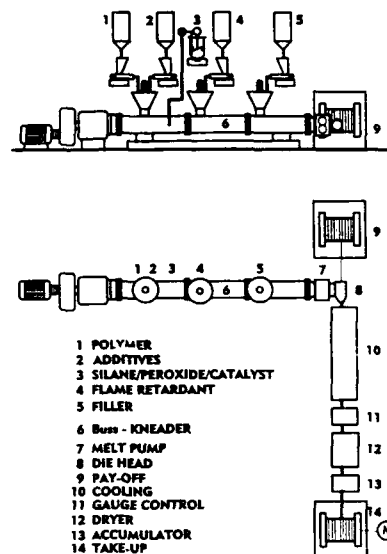


Buss TEMPERATURE PROFILES FOR HALOGENFREE FR CABLE COMPOUNDS IWCS'91 Fig 14

SHEATHING COMPOUND				
EVA	22	wt%		
Mg (OH) <sub>2</sub>	67	wt%		
ADDITIVES	1	wt%		
QUALITY				
	UNIT	STANDARD	Buss - KHEADER	
TENSILE STRENGTH AT BREAK	MPa	4 - 4.5	5.5	
ELONGATION AT BREAK	%	125	500	

SHEATHING COMPOUND				
EVA	36	wt%		
Al <sub>2</sub> (OH) <sub>3</sub>	63	wt%		
ADDITIVES	1	wt%		
QUALITY				
	UNIT	STANDARD	Buss - KHEADER	
TENSILE STRENGTH AT BREAK	MPa	10	12.5 - 16.5	
ELONGATION AT BREAK	%	125	440	

Buss QUALITY OF HALOGENFREE  
FLAME RETARDANT GRADES IWCS'91 Fig 15



Buss DIRECT EXTRUSION PROCESS FOR HALOGENFREE FR CABLES IWCS'91 Fig 16

# Dry Cure Simulation with Shrinkback Minimizing for XLPE Insulation

Pekka Huotari

Nokia-Maillefer Oy

## Abstract

One of the major difficulties in the control of the cross-linkable power cable dry cure process is the lack of the on-line measurement of the insulation temperature and the degree of cross-links. This has been solved by numerical simulation of the process. The simulation opens an artificial window into the process by estimating the cable temperature and the progress of cross-linking along the CV-line. Together with process optimization it has proved to be an essential part of the CV-line automation system.

The decreasing specific volume of the insulation material during the cooling phase creates internal stresses inside the cable insulation. This results as shrinkback, which complicates the cable insulation. This results as shrinkback, which complicates the cable joining and terminating. The shrinkback can be reduced by thermal relaxation. A new method is introduced, where the relaxation is combined into the CV-line. Numerical simulation is used to estimate the effect of the new relaxation method.

## Introduction

Measurement of product properties is essential for the control of continuous manufacturing processes. Often the measurement can be made on-line but there still exist many properties which can be found only in laboratory analysis. Laboratory analysis always means delay in the feedback control and non-acceptable results cause product rejection and often significant economical losses.

The described problem is familiar in the production of power cables with cross-linkable insulation and semiconductives. A single production line may produce tens of cable types. No measure of the cable temperature or the progress of the cross-linking is available inside the CV-tube. The production is quite expensive and rejected reels are extremely undesirable.

Computer based simulation is one solution for this problem. It gives an artificial window to the production phase allowing the user to see the development of cable properties along the production line. The time history of the temperature and the progress of the degree of cross-links can continuously be predicted.

However, simulation alone does not give any suggestions for which might be good production line settings. It only gives knowledge of what happens if the process is run according to the tentative settings. What is still needed is an optimization package, which finds the proper production settings for different products under given limitations and product requirements. Typical limitations for a power cable dry cure process are maximum output

rates of the extruders, maximum speeds of the capstans and caterpillars and physical limitations like the maximum pressure or temperature of the CV-tube. Requirements for the insulated conductor are specified by general standards and company specifications.

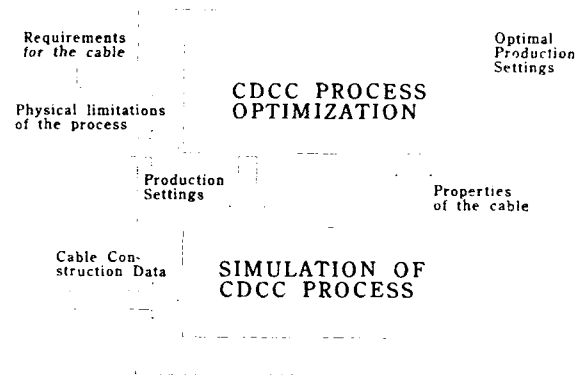


Figure 1. Optimization of the XLPE insulated power cable production. The optimization procedure iterates optimal production by using the dry cure simulation module to test succeeding tentative steps. The requirements for the insulated cable and the limitations of the dry cure CV process as well as the construction of the insulated conductor are inputs and the optimal production settings are results.

Numerical simulation of cable extrusion has been utilized for the last two decades. Boysen has used the finite difference method in his studies of the CV process of power cables (1) and contraction voids due to thermal stresses in PE insulations (2). Numerical analysis was used for research purposes.

Simulation of XLPE-insulated power cable curing process was quite active during the first half of 1980ies. One reason for that was the breakthrough of radiant curing in XLPE insulated power cable production. An automation system utilizing numerical simulation and optimization was on market 1981 and reported later 1983 (3), (4) by Huotari. This system was developed for a minicomputer controlling CDCC-line. The optimization program calculated a recipe for each production run and stored it on a floppy disc, where it was loaded from at the start of the production. Parallel work has also been done by universities

(5), (6) and material suppliers (7).

The specific volume of the LDPE insulation material decreases when the insulated conductor is cooled down. The shrinkage continues also below the crystallization temperature resulting in internal stresses in the insulation. All the three stresses, axial, radial and tangential, define together, how much shrinkback there exists, when a cable is joined or terminated. The shrinkage can not be avoided, but it can be minimized by correct cooling. The amount of stresses can also be estimated with numerical simulation. (2), (4), (8). Later in this paper a new method is presented, which minimized the shrinkback.

#### Numerical Simulation of Dry Cure Process

Numerical simulation of the CDCC process estimates the cable temperature and the degree of cross-links from the extruder cross-head to the end seal of the CV-line and computes also the remaining internal stresses. Dry curing consists physically of heat transfer to and from the cable, heat conduction inside the cable layers and cross-linking reaction.

The heat transfers in the curing section both by heat radiation and free convection. In the cooling section the heat transfer mechanism is forced convection and also heat radiation, if nitrogen is used for cooling.

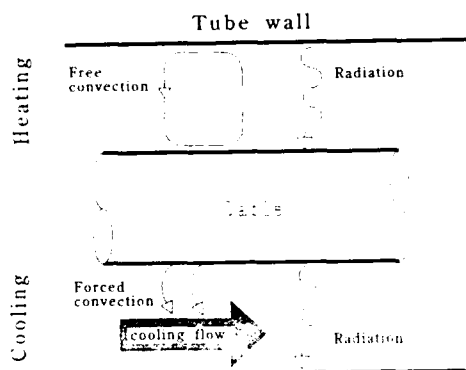


Figure 2.  
Heat transfer to and from the cable. Heat is transferred by heat radiation and free convection in the curing section, and by forced convection and heat radiation in the cooling section.

To solve the temperature field inside the cable in each part of the CV-line a small element of the cable is followed through the line. The insulation and the semiconductive layers of this element are divided into concentric cylinders, as is seen in Fig. 3. The temperature, the degree of cross-links and the dimensions of each cylinder are computed step by step starting from the extruder cross-head and ending to the end seal of the CV-line. The initial values are the layer extrusion temperatures and the conductor temperature when it enters the cross-head. The first computed values are got one time step further, next values two time steps further and so on.

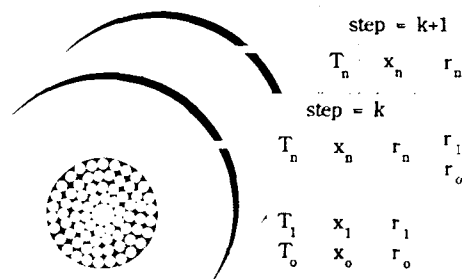


Figure 3.  
Concentric cylinder elements of the cable. Recursive equations are derived for each cylinder and for the conductor. The computation of the temperatures ( $T_n$ ), the degrees of cross-links ( $x_n$ ) and the cylinder dimensions ( $r_n$ ) progresses one time step in each round.

As a result the temperature of the cable and the degree of cross-links are got as graphical curves. A typical output of the simulation is shown in Fig. 4, where the user of the simulation program can see the temperature of the conductor, the surface and the mid point of the insulation and the degree of cross-links of the insulation in the vicinity of the inner semiconductive.

The temperature equations are derived from thermal balance of the cylinders and the computation of the curing kinetics is based on the familiar Arrhenius formula. The temperature dependence of the specific heat and the thermal conductivity of the layer materials as well as the thermal expansion is taken into account in the simulation model. To validate the model the real temperature of several cables has been measured and the heat transfer parameters adjusted according to the results.

#### Application of Simulation for Process Automation

The insulation phase of the power cable production can be described as a two-step process. The first step finds the best production parameters for the cable. The second step produces the cable according to these parameter settings. The set of the production parameters for CDCC-line is called as a cable recipe. The recipe includes the necessary data to produce a cable from the start-up phase to the shut-down phase. The first step is called as recipe generation and it includes the numerical simulation model of the cable production and the optimization part, which seeks the optimized parameters for the production.



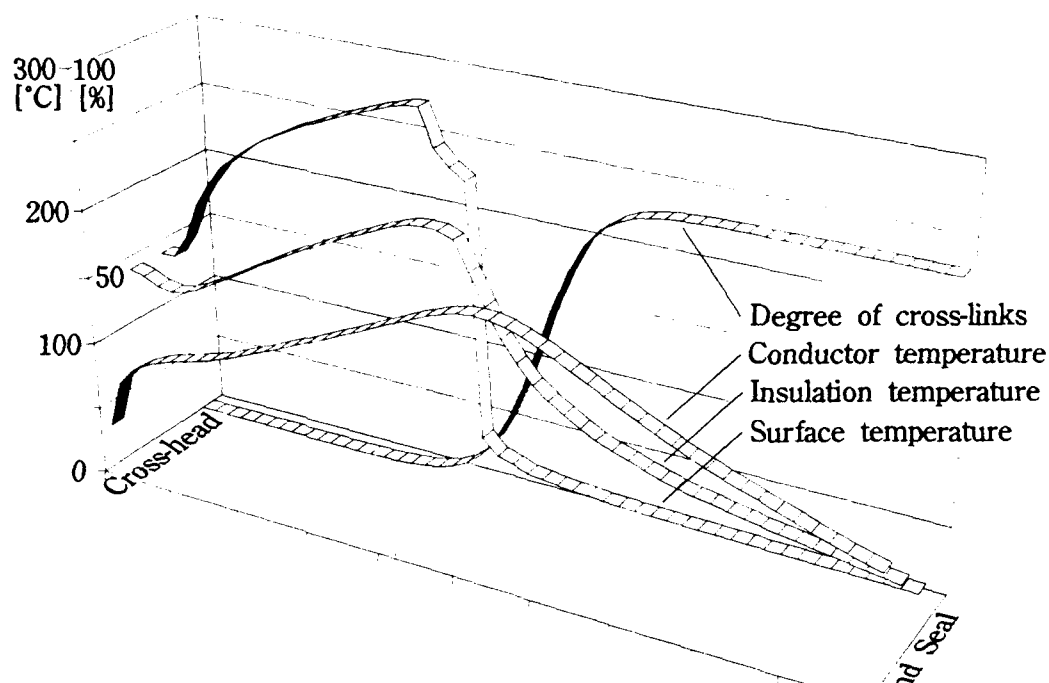


Figure 4. Typical output of the dry cure simulation. The user can see the temperature and the degree of cross-links of the cable.

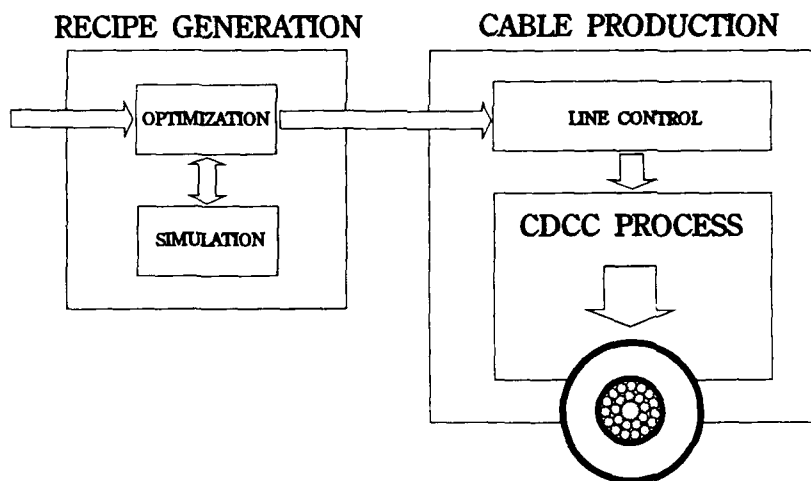


Figure 5. The two steps of the insulation phase of XLPE insulated power cable production. The first step generates a production recipe for the second step, which then produces the cable.

The automation system of the CDCC-line consists of three separate units; the recipe generator, the line control PLC and the line supervisor. The recipe generator is an executable program running under MS-DOS in industrial standard PCs. An advanced PLC has been applied to the line control unit.

The line supervisor, which is based on a commercially available control system, is running in the same PC as the recipe generator. The line supervisor activates the recipe generation and sends the completed recipe to the PLC via serial line. Fig. 6. shows the principle of the hardware solution.

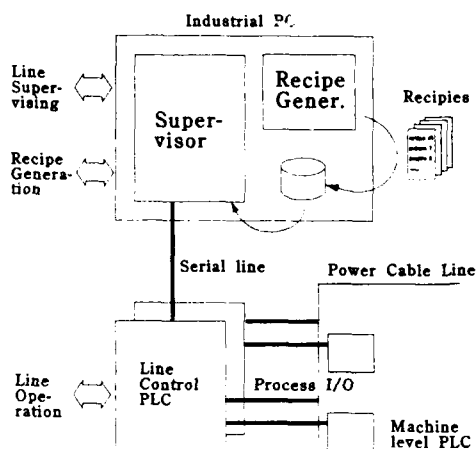


Figure 6.  
Automation system of the CDCC-line. The supervisor together with the recipe generator is located in the same industrial standard PC and communicates with the line control PLC via serial line.

#### Shrinkback Minimizing

The outer cylinders of the cable insulation cools very rapidly at the entry of the cooling part and the diameter of these cylinders remains rather large after crystallization, because the inner cylinders of the insulation are still hot and expanded and prevent the shrinkage of the outer cylinders. This results decreased radial stress towards the conductor and increases axial shrinkback. A steam path can be used to decrease the shrinkback, but it means an additional processing phase and extra investments. A new solution is relaxation zone in the middle of the cooling section. The surface of the cable is heated over the melting temperature

Surface temperature  
Insulation temperature  
Conductor temperature

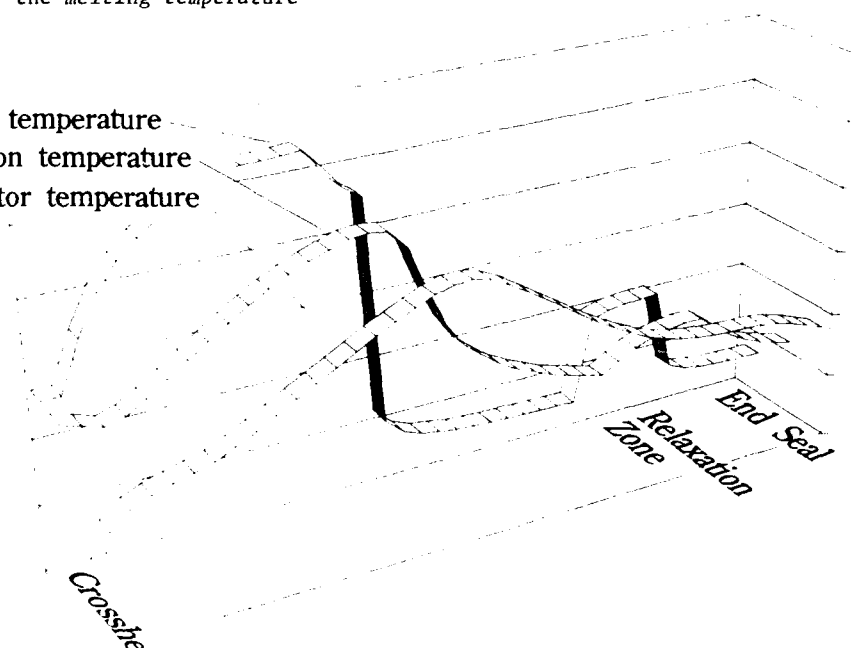


Figure 7.  
Use of the relaxation zone. The surface of the cable is heated over the melting temperature. The outer diameter is now smaller during the final crystallization.

achieving a rather even radial profile of the cable temperature during the final crystallization. Fig. 7 shows the temperature of the cable, when the relaxation zone is used.

The smaller outer diameter reluts increased stress towards the conductor and decreases axial stress. The increased pressure towards the conductor produces higher friction between the conductor and the inner semiconductive resists the shrinkback. Fig.8 shows simulation results of the remaining stresses with and without the use of the relaxation zone. The example is a medium voltage cable with 95 mm<sup>2</sup> aluminium conductor.

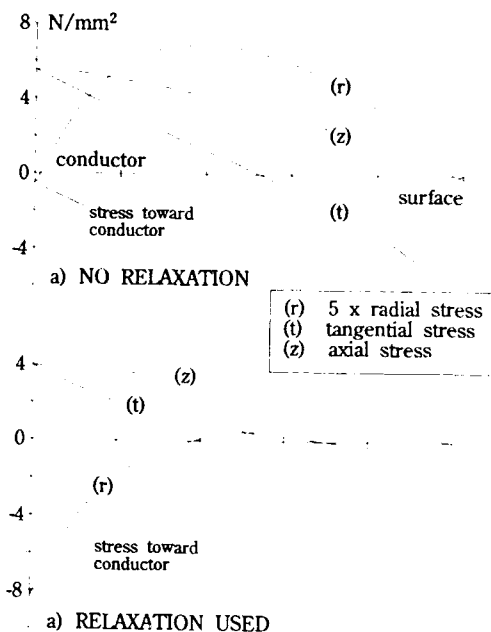


Figure 8. Thermal stresses of a XLPE insulated power cable. Case a) is without the relaxation zone and case b) is with it. The cable is a medium voltage one with aluminum conductor of 95 mm<sup>2</sup>.

From the Fig. 8. one may see that the use of the relaxation zone increases significantly the radial stress towards the conductor. In principle the result is the same as with a separate heat relaxation.

#### Conclusion

Numerical simulation and optimization are today used effectively in the automation of power cable CV-lines and as CAD tool for CV-line design. Today almost every CDCC-line includes the simulation based recipe generator and the corresponding design package is always used in the design of new CDCC-lines.

A new method, based on the tandemization of the power cable insulation process and the heat relaxation of the internal stresses, has been presented. Simulation shows clearly, that the additional relaxation zone in the cooling section of the CV-line increases the radial stress needed to resist the shrink back.

#### References

- (1) Boysen, R. L.: An analysis of the continuous vulcanizing process for polyethylenes, IEEE Summer Power Meeting and EHV Conference. Los Angeles, Calif., July 12-17, 1970, pp. 926..933
- (2) Boysen, R. L.: Contraction void prediction by thermal stress analysis. 22nd International Wire and Cable Symposium. Atlantic City, New Jersey, Dec. 1973, pp. 336...342

- (3) Huotari, P.: With computer simulation of power cable continuous vulcanizing to higher quality and maximized output rate. Research and development in the Nokia Group, August 1983, pp. 20...22
- (4) Huotari, P.: Voimakaapelin vulkanointiprosessin mallinnus, Tampere, Finland: Tampere University of technology, 1983. Licentiate thesis (in Finnish)
- (5) Franzkock, B.: Analyse eines neuen Verfahrens zur Herstellung vernetzter Polyäthylenkabel. Institut für Kunststoffverarbeitung (IKV), TH Aachen, 1979. 187 pp. Dissertation
- (6) Menges, G., Bolder, G., Rudolph, K., Meier, M.: On-line calculation of cross-linking of XLPE cables. Wire World International v. 28 n. 9-10, Sep-Oct 1986, pp 160...162
- (7) Schirato, P., Fretier, P.: Optimization of cable crosslinking process on dry curing lines. B 4.8 JICABLE 87
- (8) Robinson, J. E., Normanton, J.K.: Extrusion processing of polyethylene compounds for large-diameter communication cable insulation. Conference on Plastics in Telecommunication II London 18-20 Sep. 1978, pp. 115...120.

## LONG-TERM SERVICE DEGRADATION OF POLYETHYLENE AND RUBBER INSULATED POWER CABLES

Joseph H. Groeger and Matthew S. Mashikian

Electrical Insulation Research Center  
University of Connecticut  
Storrs, CT 06269-3136 USA

### ABSTRACT

Cables used for medium voltage power applications (4kV - 35kV) are available with various combinations of shielding and insulating materials. Several jacketing designs are also available for cable protection. When exposed to the conditions of field-aging, cable components deteriorate through processes that reflect the materials, designs, and specific aging conditions involved. Manufacturing defects may also contribute to premature aging of these cables. This paper cites examples of case studies of cable failures, presents selected laboratory research results, and indicates how historical trends in cable materials development have improved cable performance.

### INTRODUCTION

Service-aging of power cables involves complex interactions between the cable materials, thermal stress, electrical stress, and water with its associated impurities introduced from the local environment. The choice of cable materials and the type of cable construction play a significant role in the rate of degradation of power cable insulation. During the past ten years, the authors have used a number of specially-developed diagnostic methods [1] to characterize the deterioration of medium voltage power cable insulation removed from many utility systems throughout the United States. Cables ranging in age from less than one year through as many as 60 years have been included in these studies. These results have been analyzed in the context of laboratory tests specifically designed to simulate the aging of cable materials in controlled, systematically-varied environments. The investigations have clearly indicated that medium voltage power cables that can be expected to perform reliably for more than twenty years will require clean construction materials and designs

that mitigate the intrusion of water and ions into the cable insulation. Through an enhanced understanding of the aging performance of various cable materials/design combinations, the electric utility companies can make more informed decisions as newer cable materials, for example, become available. Results of this research have influenced trends in the cable materials supply industry, further improving the products presently manufactured.

### BACKGROUND

The cables and materials addressed in this report apply principally to medium voltage (from 4kV through 35 kV) power distribution applications. Historically, a number of cable designs have been available, each with its own virtues and associated costs. Figure 1 summarizes various construction features of a typical distribution cable. Conductors may be either aluminum or copper, stranded or solid. The interstices of stranded conductor cables may contain a polymeric filler which is intended to exclude the introduction and longitudinal migration of moisture should the end of the cable be exposed to water during storage, installation, or repair operations. The semiconducting shields are present to provide a uniform distribution of electrical stresses at the interface with the insulation. Since the mid 1970's the semiconducting shield layers have been extruded rather than applied as tapes as previously done. The shield materials are typically thermoplastic polymers such as ethyl-ethylene acrylate (EEA) or ethylene vinyl acetate (EVA). Crosslinked elastomers, such as ethylene-propylene rubber (EPR) may also be used in some cases. The insulation is typically crosslinked polyethylene or a crosslinked rubber copolymer or terpolymer such as EPR or ethylene-propylene diene monomer (EPDM), respectively. Grounded neutrals, in the form of stranded conductors, tapes, or flat straps are included over the insulation shield for the purpose of providing a ground potential return path for the

current. Over the neutral conductors, a polymeric jacket is typically added to offer protection of the neutrals during installation, to limit their corrosion, and to reduce the effects of moisture from the environment. In some cases, a lead sheath is applied over the insulation shield to provide complete protection against ambient moisture.

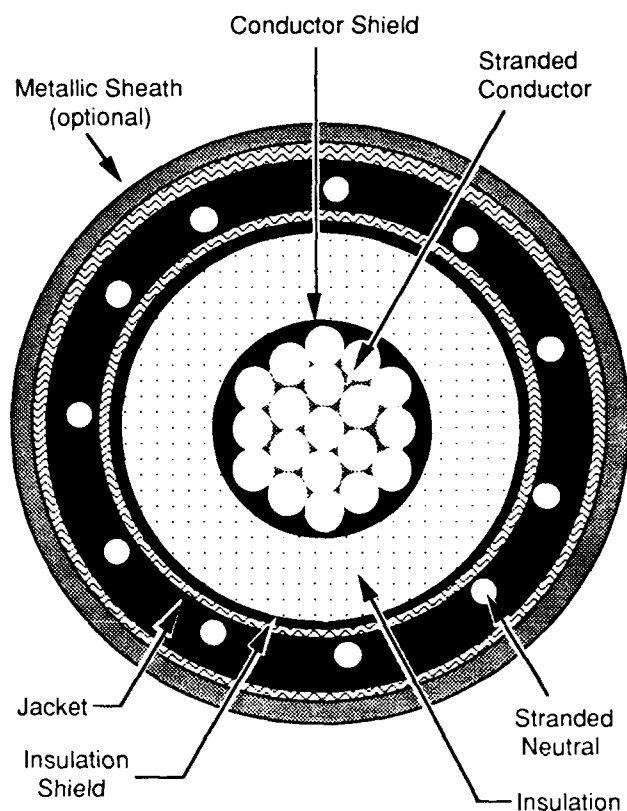


Figure 1. Major Construction Features of Medium Voltage Power Distribution Cables

#### ROLE OF INSULATIONS: CASE STUDIES OF FIELD-AGED CABLES

##### Example 1

Fifty butyl rubber insulated, lead-sheathed cables were removed from a major urban service area for the purpose of determining the cause of their increasing number of dielectric failures. These had been in service between 20 and 40 years in very wet, high salt concentration areas. Dielectric breakdown tests were conducted on cables near fault sites, on adjacent non-faulted areas of the same cable, and on adjacent, non-faulted phases from the same circuit. Table 1 summarizes the breakdown test results for these cables. As indicated, the breakdown strengths were found to be significantly lower in the areas where the faults occurred. Figure 2 shows one such area. As shown in this

Figure, the lead sheath on this cable has been severely damaged resulting in exposure of the underlying insulation. Metallurgical inspection of the lead indicated that it had been peeled back on the cable so long ago that the slow, natural relaxation of this material had obliterated its surface features. The peeled surfaces were also covered with a thick oxide film. This evidence suggested that the sheaths had been damaged during installation of the cables.

TABLE 1  
Summary of Breakdown Tests of Field-Aged Cables, Comparing Various Locations

circuit	cable	breakdown strength (V/mil)	
		near fault	remote
1	QA	42	145
1	QB	--	165
1	QC	--	185
2	QA	20	320
2	QB	--	340
2	QC	--	300
3	QA	32	285
3	QB	--	230
3	QC	--	245



Figure 2. Lead Sheath Damage On 40 Year Old Distribution Cable

Several analytical tools were used in an effort to determine why the damaged jackets should have allowed an increased rate of deterioration of the underlying cable insulation. Elemental analysis of the cable insulation was conducted with X-ray emission spectroscopy [1, 2, 3, 4, 5]. As shown in Table 2, the composition of the insulation varied considerably between the sites where the lead was intact and other areas of the same cable where the lead sheath had been damaged. The elements shown in bold type correspond to the

contaminants that were introduced into the insulation. As noted previously, the cables were exposed to salt (chlorides of sodium, potassium, and calcium) water environments. The damaged lead sheath allowed the ingress of salts from this water into the insulation. Many salts are known to be strong promoters of water treeing [7]. Due to their ionic nature, these salts also increase the local dielectric losses and the resulting thermal energy may increase the rate of degradation.

TABLE 2  
Elemental Analysis Results, Comparing  
Insulation Compositions from Various  
Locations and Cables

circuit	cable	elements
1	ΦA (at fault)	C, O, Al, Si, Cl, K, Pb, Zn
1	ΦA (remote)	C, O, Al, Si, Pb, Zn
1	ΦB	C, O, Al, Si, Pb, Zn
2	ΦA (at fault)	C, O, Na, Al, Si, Cl, K, Pb, Zn
2	ΦA (remote)	C, O, Al, Si, Pb, Zn
3	ΦA (at fault)	C, O, Mg, Al, Si, Cl, K, Ca, Pb, Zn
3	ΦA (remote)	C, O, Mg, Al, Si, Pb, Zn

#### Example 2

An EPR insulated cable failed while energized but not loaded in a 6.9kV delta system at a power plant in a non-critical application. The cable had been in service for approximately five years and was installed in a conduit that became water-filled. The cable featured jacketed construction and a 133% insulation level as defined in the AEIC specifications [6]. The entire length of the faulted cable and its adjacent non-faulted phase B and C conductors were removed from the conduit. Fortunately, a non-aged section of the same cable was obtained from a warehouse.

The dielectric losses of the insulation from various sections of each cable were measured over a wide frequency range using time domain dielectric spectroscopy (TDDS) [8]. As shown in Table

3, the low frequency losses were highest near the fault site of the failed cable (phase A). These losses were lower for the same cable about 10 ft. away from the fault site. As shown in Table 3, the dielectric losses were also lower for the adjacent, non-faulted phase and for the non-aged cable obtained from the warehouse. The losses above 1.0 Hz were nearly identical for all cables and locations.

TABLE 3  
Dielectric Loss (Tangent Delta) vs.  
Frequency for Various Locations and Cables

cable	frequency, Hz			
	10 <sup>-3</sup>	10 <sup>-2</sup>	10 <sup>-1</sup>	1.0
ΦA (at fault)	.0612	.0267	.0121	.0071
ΦA (remote)	.0593	.0224	.0109	.0064
ΦB	.0561	.0227	.0114	.0064
non-aged	.0562	.0226	.0115	.0065

Chemical tests were conducted on the cable insulation and on water removed from the conduit in which the cable had been located to attempt to determine why the local dielectric losses were higher near the fault site. Conductivity and pH tests on the water indicated that it was nearly neutral and had low electrical conductivity. Sections of the insulation from the various cable sections were immersed in distilled, deionized water for 48 hours at 60°C to extract soluble, conductive (ionic) material(s), if present. Conductivity and pH measurements were made on these water extractions and they, too, indicated normal pH (7.2) and low electrical conductivity (158μS/cm).

Figure 3. Structure of Insulation from  
Non-Aged Cable. 100x magnification

The insulations from these cable sections were then prepared cryogenically into thin sections so that they could be examined microscopically with transmitted

illumination. Figure 3 shows the insulation characteristics for the non-aged cable obtained from the warehouse. The insulation is shown to be homogeneous, with uniform dispersion of the ingredients (clay, red lead, zinc oxide, others). The insulation from the field-aged, non-faulted cable section appeared to have identical characteristics. Microscopic examination of the insulation near the fault site of the failed cable, however, indicated the presence of atypically large particles of what appeared to be inorganic material, as shown in Figure 4. Following polarized optical measurements of some of the crystalline properties of these particles [9] they were identified as Kaolin, a silicate clay used in most EPR cable insulation compounds.




Figure 4. Structure of Insulation Near Fault Site of Failed Cable. 100x magnification

#### Example 3

Repeated failures of a crosslinked polyethylene insulated medium voltage cable, following six years in service, prompted an investigation into their cause. The cable appeared to be of good quality construction, it had not suffered abusive in-situ testing procedures, nor were any apparent defects present in the materials. A section of this cable was removed from service and prepared into thin sections for microscopic analysis. Optical microscopy of stained sections revealed the presence of a large number of bowtie electrical trees, as shown in Figure 5. It was noted that these initiated at sites where inhomogeneities existed within the crosslinked polyethylene (XLPE) insulation. Optical characterization indicated that these were not typical contaminants for a cable of that vintage. Historically, contaminants have included oxidized polyethylene, catalyst residue, various minerals, and others. Infrared micro-

spectrophotometry [1, 2] was used to identify the sites where tree initiation had occurred. Spectra obtained from these sites, when compared to a suitable reference [10], indicated that the insulation antioxidant (an amine stabilized phenol) was segregated at these sites. Analyses of a non-aged section of the same cable confirmed that this inhomogeneity resulted during manufacturing of the cable rather than as a consequence of aging.




Figure 5. Bowtie Tree and its Initiation Site in a Field-Aged XLPE Cable

#### Example 4

From the early 1960's through the mid-1970's, medium voltage power cables were available with a mineral-filled polyethylene insulation. These cables met with mixed experience by the utility companies [12]. Some were plagued with failures following less than 7 years in field service, while others continue to perform reliably to the present time, following more than 25 years in service. Several analytical tools were used to determine why some of these cables suffered premature degradation while others did not. Optical microscopy was first used to examine cables that had proven unreliable. These were stained and examined for the presence of trees and other features that might have affected their performance. Figure 6 shows trees in one of these cables and Figure 7 shows a common defect associated with sites of localized degradation. Polarized microscopy indicated that these sites consisted of agglomerates of Kaolin clay, the mineral filler used for this type of insulation compound. Cables that did not experience a high incidence of failures were found to contain insulations with well dispersed clays and appear much the same as the EPR insulation shown in Figure 3.

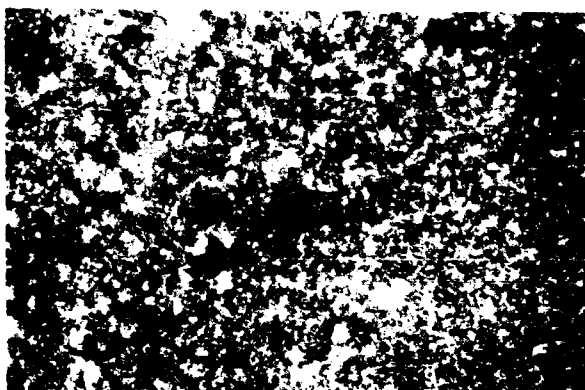


Figure 6. Bowtie Tree in Filled Polyethylene Insulation



Figure 7. Clay Agglomerates in Defective Filled Polyethylene Insulation

Gas chromatography (GC) and mass spectrometry (MS) [1, 2] were used to comparatively analyze specimens of "good" and "bad" mineral-filled polyethylene insulations to try to understand why the differences in dispersion existed. Sections of insulation from these cables were prepared under clean conditions, then placed into stainless steel containers and heated to approximately 175°C. The gases evolved from the specimens were directed with a stream of high purity nitrogen gas into the GC/MS system and analyzed. When the resulting spectra were compared, the well dispersed insulation compound was found to contain a low moisture concentration (800 ppm, or less) and a vinyl-silane compound. The latter is commercially used as a clay surface treatment agent to promote the formation of chemical bonds between this material and the polyethylene matrix. The bad insulation was found to contain no traces of the vinyl-silane compound and a significantly higher moisture concentration (>4000 ppm).

The latter data suggested that the good cables contained clays that had been sufficiently heated (calcined) to remove the water of hydration. This is known to promote better mixing and is a process that is presently used for EPR insulation compounding.

#### Example 5

Corrosion of copper concentric neutrals in underground distribution systems is a recognized problem, most prevalent with non-jacketed cables, that has received sporadic research attention. Traditionally, bare copper has been relatively corrosion-free in this application while "tinned" neutrals have often suffered severe corrosion damage. Some utility companies have employed anodic or cathodic protection schemes to reduce the rate of neutral corrosion. An investigation [11] was undertaken to comparatively explore the mechanism of corrosion on bare and coated neutral conductors. Failure of the neutrals can introduce operational difficulties, failures due to discontinuous grounding, and safety concerns.

Exposure tests for periods of up to one year were performed on samples of both bare and tin-coated copper neutral wire obtained from a medium voltage power cable manufacturer. These were immersed in an electrolyte with a standard biological culturing medium to simulate a soil environment. Electrical environments were provided by application of a 60 Hz current to the wire samples. In the absence of an ac voltage, tin has a negative potential (anodic) with respect to copper. This condition cathodically protects the underlying copper from corrosion. The application of an ac voltage reverses the relative potentials making copper the more negative (anodic). In addition, tin coatings are typically imperfect leading to small areas of copper (anode) exposed to a large area of tin (cathode). These combined factors initiate local attack on the exposed copper. Once pitting begins, the reaction becomes autocatalytic, that is, the corrosion process itself creates a local environment within the pit which stimulates further corrosion, as shown in Figure 8. This self-perpetuating mechanism can rapidly lead to failure. Since this degradation is localized, it may not be recognized when accessible areas of cables are inspected.

The root cause of concentric neutral corrosion has been identified as a synergism between the copper/tin galvanic cell (resulting from the imperfect coating), a corrosive environment, and the applied ac current. It is this particular combination of parameters that experience



enhanced rates of corrosion. Copper or tin alone in a typical soil environment, with or without ac voltage, is comparatively immune to corrosion. Tin-coated copper in the soil environment without ac current (i.e., spare, non-energized cable) is also relatively immune. (Although this is a galvanic couple, the corrosion rate is low because the anode, tin, has a much larger exposed area than the cathode, copper.) Application of ac to this system, however, passivates the tin, rendering it cathodic with respect to the copper. The copper, now the anode, has a small exposed area relative to the tin, therefore it corrodes rapidly. Once initiated, these local corrosion cells experience autocatalytic propagation. The tin-coated copper neutrals, as received, will experience rapid, localized corrosion when energized in soil. These results suggest that tinned copper neutrals will corrode at a greater rate than bare copper under the same conditions.

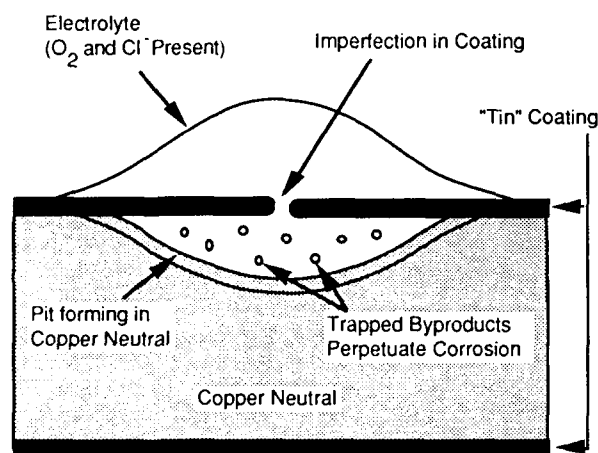


Figure 8. Schematic of Tinned Neutral Conductor Corrosion Process

#### ROLE OF CABLE JACKETS AND SHEATHS

During the past six years, a number of reports have clearly indicated the need to protect cable insulation from the deleterious effects of underground water and its associated impurities [i.e., 3, 4, 5, 13, 14]. The authors have pioneer chemical analyses of field-aged cable insulation indicating the migration of impurities into cable insulation, such as the example shown in Figure 9. As further shown by the data in Table 4, the rate and extent of intrusion of these impurities is directly related to the type of cable construction and the materials chosen for its protection. These data compare the performance for cables jacketed with polyvinyl chloride (PVC), high density polyethylene (HDPE), and lead. While

polymer jackets are indicated to retard the ingress of environmental contaminants, particularly when compared to those cables that were aged without jackets, none offers complete, long-term protection of the underlying cable.

TABLE 4  
Ion Concentration in Cable Insulations,  
Showing Effectiveness of Various Jacketing  
Materials

<u>cable/condition</u>	<u>jacket</u>	<u>water-soluble ion conc.</u>
1, non-aged	PVC	125 ppm
1, aged, intact	PVC	850 ppm
1, aged, punctured	PVC	1300 ppm
2, non-aged	HDPE	220 ppm
2, aged, intact	HDPE	1100 ppm
2, aged, punctured	HDPE	1000 ppm
3, non-aged	none	300 ppm
3, aged	none	1800 ppm
4, non-aged	lead	240 ppm
4, aged, intact	lead	260 ppm
4, aged, punctured	lead	2100 ppm

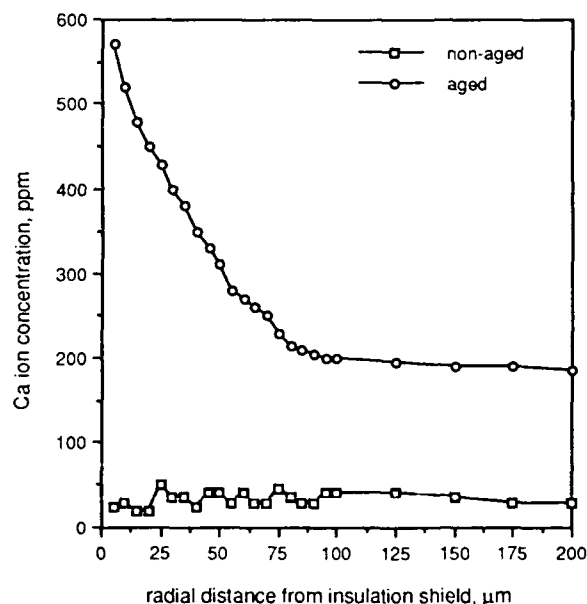


Figure 9. Migration of Calcium Ions from Soil Environment Into Underlying Cable Insulation, Comparing Aged and Non-Aged Sections of Same Cable

While limited published data are available to indicate the relative diffusivities of water through some common polymers [15, 16], none have indicated the performance of the polymers that are commercially used for cable jacketing purposes. To better assess the performance of these materials, the rates of water

diffusion were measured using thin strips of cable materials in which the moisture uptake was measured gravimetrically over approximately 6 months immersion in tap water at temperatures of 25°C, 60°C, and 80°C, following the examples of Crank [15]. Table 5 summarizes these results. Equation 1 indicates how this data can be used to estimate the rate of moisture diffusion into a cable with a jacket of known material. It should be noted that the measured diffusivities can vary according to the processing conditions of a given polymer.

$$(1) \quad \text{flow rate} = F = \frac{D_0 \Delta C}{l}$$

where:  $l$  = section thickness

$\Delta C$  = concentration gradient

$D_0$  = diffusion coefficient

TABLE 5  
Experimentally Determined Diffusion  
Coefficients for Commercial Cable Jacketing  
Materials

material	$D_0$ (cm <sup>2</sup> /sec)
crosslinked polyethylene	$330 \times 10^{-5}$
polyvinyl chloride	$600 \times 10^{-5}$
low density polyethylene	$450 \times 10^{-5}$
linear low density polyethylene	$300 \times 10^{-5}$
Nylar	$5 \times 10^{-5}$
Teflon	$2 \times 10^{-5}$
Lead	0

#### ROLE OF SEMICONDUCTING SHIELDS

Cable shields have been shown to contribute to the treeing process through two principal mechanisms; (1) they are known sources of water-soluble ionic materials and (2) they may contain solid particulate material that leads to the formation of sharp protrusions at the shield/insulation interfaces where electrical stresses may be locally concentrated.

The need for clean shielding compounds was systematically indicated through a study supported by the U.S. Department of Energy, with the cooperation of a major cable materials supplier [18]. Shield compounds consist of a host polymer, typically EVA or EEA, which is filled with approximately 40 wt% carbon black. The carbon black may be produced through a variety of pyrolysis processes from a range of raw materials. The starting materials vary in their purity levels and this directly affects the cleanliness of the resulting carbon black [20, 21]. While

impurities may also exist in the base polymer and its associated antioxidant, the carbon black has been shown to be the most significant contributor of the impurities that have been linked to the formation of water trees. Recently, a comprehensive program was undertaken to determine what cleanliness levels could be achieved using improvements in processing technology and feedstock controls [19]. It is now felt that state-of-the-art cleanliness has been achieved by using carbon blacks produced through the furnace or acetylene pyrolysis processes. Carbon blacks produced today contain less than 10% of the impurities present ten years ago [20]. Removal of the impurities has also improved the smoothness of these compounds since the irregularities were caused by the impurities.

#### DISCUSSION

Through experience gained by analyses of field-aged cables, laboratory-aged cables, and laboratory-aged cable materials, an improved understanding of the aging processes has been realized. Associated with this improved level of knowledge has been a dramatic improvement in the materials from which cables are made, cable designs, and the choice of materials used for cable construction.

Filled insulation systems now exclusively use surface-treated, calcined fillers to promote improved dispersion. Non-filled insulations are now considerably cleaner than those produced ten years ago. Optical inspection devices can be incorporated to exclude polyethylene pellets that include visible impurities or discolorations. Owing to improved antioxidant selection and improved concentration control, agglomerates of antioxidants are seldom encountered.

One major supplier of cable jacketing materials has recently introduced an improved semiconducting jacketing compound that offers moisture resistance comparable to that of an insulating jacket.

The industry has moved dramatically toward cleaner shielding compounds. As a result, the sources of tree-inducing ions has been greatly reduced, while smoothness of the shield/insulation interfaces has been realized as an associated benefit.

Higher technology jacketing materials are becoming available. Several manufacturers have developed cable jackets that incorporate integral thin lead films so that complete moisture resistance can be achieved. This design offers the exterior protection provided by a conventional lead sheath but has the added advantage of having a minimal effect on the outer diameter of the cable.

Historically, most utility companies have purchased cables on a competitive bidding basis, with contracts being awarded on the basis of lowest cost. As results of cable aging studies have become available, many utilities have come to recognize that a premium price for a longer lasting cable may be a better bargain in the long run. This has led some companies to develop specifications that stipulate certain materials, designs, and performance features. Some have further developed a policy of having their own inspectors present in the plants when their cables are being made and/or inspected.

#### ACKNOWLEDGEMENT

Many of the examples cited in this report resulted from projects that were supported by individual utility companies including Boston Edison Company, Potomac Electric Power Company, and Northeast Utilities. The Cable Data Bank project is supported by the Empire State Electric Energy Research Corporation and Northeast Utilities. The Cabot Corporation and Union Carbide were instrumental in supplying materials, support, and technical expertise in some of the cited research. The support of these companies and organizations is gratefully acknowledged.

#### REFERENCES

- [1] "Diagnostic Techniques for Cable Characterization", Technical report EL-6207, Electric Power Research Institute, February, 1989.
- [2] "Evaluation of Sensitive Diagnostic Techniques for Cable Materials Characterization", Technical report EL-7076, vol. 1, Electric Power Research Institute, December, 1990.
- [3] M.S. Mashikian and J.H. Groeger, "Ionic Impurities In Extruded Cable Insulation: Analytical Detection Techniques, Sources, Nature, and Effects", Proceedings of the Jicable Conference, Versailles, 1987.
- [4] A. Bulinski, S. Bamji, and J. Densley, "Wavelength and Energy Dispersive X-ray Studies of Contaminants In Water-Treed Insulation", Proceedings of the IEEE Conference On Electrical Insulation and Dielectric Phenomena, pp. 78-85, 1988.
- [5] J.H. Groeger, J. Henry, and A. Garton, "Location and Concentration of Ionic Impurities In Polymeric Cable Insulation", Conference Record of the IEEE International Symposium On Electrical Insulation, pp. 300-305, 1988.
- [6] Specifications for Ethylene Propylene Rubber Insulated Shielded Power Cables Rated 5 Through 69 kV, Specification CS5-87, Association of Edison Illuminating Companies, New York, 1987.
- [7] E.F. Steennis and F.H. Krueger, "Water Treeing In Polyethylene Cables" IEEE Transactions On Electrical Insulation, vol. 25, 5, pp. 989-1028, October, 1990.
- [8] U. Gafvert and B. Nettleblad, "Measurement Techniques for Dielectric Response Characterization at Low Frequencies", Proc. of the Nordic Insulation Symposium (NORD-IS), Lyngby, Denmark, June 1990, pp. 7:1:(1-10).
- [9] H.U. Bambauer, F. Taborszky, and H.D. Trochim, Optical Determination of the Rock Forming Minerals, Part 1. E. Schweitzerbart'sche Publ. Stuttgart, Germany, 1979.
- [10] The Infrared Spectra Atlas of Polymer Additives, Volume 2 (Protective Materials), Sadtler Laboratories, 1987.
- [11] O.J. Van Der Schijff, Aspects of Concentric Neutral Corrosion In Underground Rural Distribution Systems, PhD thesis, University of Connecticut, December, 1990.
- [12] J.H. Lawson and W.A. Thue, "Summary of Service Failures of High Voltage Extruded Dielectric Cables in the United States", Record of the IEEE International Symposium On Electrical Insulation, 1980.
- [13] E. Ildstad, J. Sletbak, S. Hagen, and H. Faremo, "Examination of Defects In XLPE Cable Insulation", Proceedings of the Sixth International Symposium On High Voltage Engineering, New Orleans, 1989.
- [14] C.G. Richardson and G. Matthey, "Ion Migration In Aged Power Cables", Proceedings of the JICABLE International Conference on Polymer Insulated Power Cables, pp. 259-266, Versailles, 1991.
- [15] J. Crank and G.S. Park, Diffusion In Polymers, Academic Press, 1968.
- [16] Polymer Permeability, J. Comyn, editor, Elsevier Science, 1985.
- [17] M.S. Mashikian, J.H. Groeger, S. Dale, and E. Ildstad, "Role of Semiconducting Shield Compounds On the Premature Aging of XLPE Cable Insulation", Conference Record of the IEEE International Symposium On Electrical Insulation, pp. 314-320, 1988.
- [18] Interfacial Aging Phenomena In Power Cable Insulation Systems, U.S. Department of Energy, Oak Ridge National Laboratory (ORNL) subcontract 19X-27424C, 1985-1990.

- [19] S.D. Lefebvre, J.H. Groeger, W. Sifleet, and M. Tomme, "Wet Electrical Aging Characteristics of various Furnace Carbon Blacks", Proceedings of the JICABLE International Conference on Polymer Insulated Power Cables, pp. 1-7, Versailles, 1991.
- [20] Minutes of the IEEE Insulated Conductors Committee, Subcommittee 5-29, November, 1990.
- [21] A. Belhadfa et al, "Impurities In Semiconductive Compounds Used As High-Voltage Cable Shields, IEEE Trans On Electrical Insulation, vol. 24, 4, pp. 709-712, 1989.



Matthew S. Mashikian (M'63, SM'84) received his B.E. degree in Electrical Engineering with honors, from the American University of Beirut in 1958, his M.S.E.E. degree from Wayne State University in 1966, and his Doctor of Engineering degree from the University of Detroit in 1976.

From 1958 to 1963, he was employed by ASEA first in Lebanon and, subsequently, in Vasterås, Sweden, where his last position was that of applications engineer for lightning arrestors. From 1963 to 1979, he was employed in the Engineering Research Department of Detroit Edison where he rose to the position of Supervisor for the Electrical Equipment and Instrumentation Section. In 1979, he founded his own consulting organization, Mashikian and Associates, Inc., and, since 1983, he has been a professor of Electrical and Systems Engineering and Director of the Electrical Insulation Research Center at the University of Connecticut.

Dr. Mashikian holds seven U.S. patents covering high voltage cable terminations and joints, insulating devices, a partial discharge locating method, and zinc chloride battery systems. He is a registered professional engineer, a member of Eta Kappa Nu, and the IEEE Power and Insulation Societies. He is a member of the Administrative Committee of the Dielectrics and Insulation Society (DEIS), past Chairman of the Publications and Publicity Committee of CEIDP, Chairman of the DEIS Education Committee, and Chairman of Transnational Activities of the Insulated Conductors Committee. He is also a U.S. delegate to Working Group 15-06 of CIGRE.



Joseph H. Groeger (M'85)

Mr. Groeger received his BSME/Materials degree from the University of Connecticut in 1976 and is pursuing a PhD degree in materials science at the University of Connecticut.

Mr. Groeger has published extensively in the field of engineering dielectrics, with over 40 publications to date. He has been the recipient of the IEEE Best Technical Publication Award and has made invited presentations to the Electric Council of New England and the Southeast Electric Exchange, among others.

Mr. Groeger is a member of the Insulated Conductors Committee and the Dielectrics and Electrical Insulation Society. He is Associate Director of the Electrical Insulation Research Center at the University of Connecticut where he directs research projects for the electric utility companies, their representing organizations, and the utility supply industry.

# COMPOUNDING NEW SPECIALTY LINEAR POLYMERS FOR LV & MV CABLES

Lawrence Spenadel and Monica Hendewerk

Exxon Chemical Company - Baytown, TX

## Abstract

Exact™ polymers, produced via new single-site catalyst technology developed at Exxon Chemical Company(1), features narrow distributions of molecular weight and chemical composition. Control of these parameters can be used to tailor the molecular architecture of ethylene polymers to produce low and medium voltage cables with improved performance.

This paper discusses the applicability of tailoring polymer structure to meet both power cable applications and low voltage wire requirements. Minimization of the high and low MW tails of the new specialty linear polymers (SLP), and uniform distribution of its comonomer can be desirable for achieving optimum performance properties. In addition, polymer properties affected by MW, MWD, and compositional distribution (CD) were studied. Finally, polymer properties such as crosslinkability, filler acceptance, tree retardancy, etc. and how they relate to cable performance are discussed.

## Introduction

As a result of the development of unique catalyst and process technology at Exxon Chemical Company(1), a new class of ethylene polymers, which will be referred to in this paper as specialty linear polymers (SLP), are available in a broad range of densities: from plastomers(2) (0.870-0.899 g/cm) to VLDPE (0.900-0.914 g/cm) to LLDPE ( $\geq 0.915$ ) and a broad range of melt indices (0.2 to 30+ dg/min). They have the required physical and electrical properties to make them suitable for use in the total construction of a power cable, i.e. insulation, insulation shields, and jacketing. In addition, the SLP's have good filler acceptance and compounding latitude and could be used in low voltage specialty wires.

With this unique class of specialty linear polymers, it is possible to have the electrical and physical properties associated with low density polyethylene and the tree retardancy and flexibility associated with EP rubber.

In this paper, the influence of polymer properties (density, molecular weight, molecular weight distribution, compositional distribution) on performance attributes such

as crosslinkability, physical properties, filler acceptance, tree retardancy, and processability are discussed. The electrical properties and physical performance characteristics of the new specialty linear polymers are demonstrated relative to low density polyethylene and ethylene-propylene rubbers.

## I. General Polymer Properties

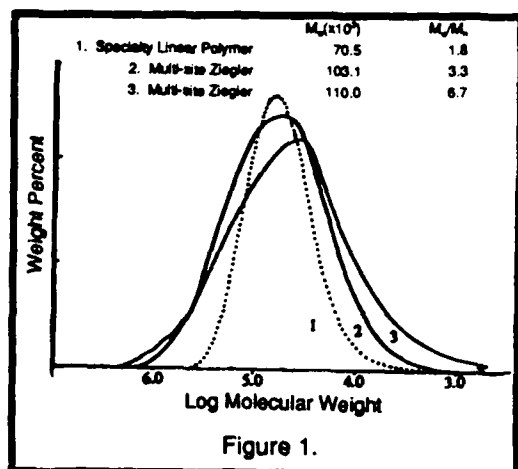
Two very important properties of polyolefins, critical to their success for wire and cable application, are physical properties and processability. Producing a high level of performance in these two properties and an optimum balance between them has long been the focus of efforts in the industry.

The key to accomplishing this is control of the molecular structure of the basic polymer molecules and with the discovery of single-site catalysis this is now possible. In particular, two aspects of the molecular structure are of primary importance. These are the control of the high molecular weight and low molecular weight tails of the molecular weight distribution and the control of the comonomer distribution among the polyolefin molecules(3,4).

The influence of these structural features on polymer performance relative to the requirements for wire and cable applications are the focus of this paper.

## Molecular Weight and Molecular Weight Distribution

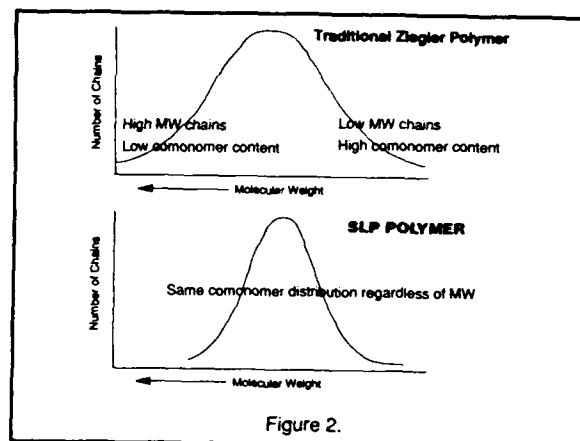
Molecular weight and molecular weight distribution play a significant role in melt processability as well as in the level and balance of physical properties achievable. The MWD's of three linear backbone polymers are shown in Figure 1: a single-site Ziegler catalyzed resin (SLP) with narrow MWD ( $M_w/M_n \sim 2.0$  (most probable distribution)) and two multi-site Ziegler type resins which have broader MWD's ( $M_w/M_n = 3.3$  and  $6.7$ )(5). Of particular note is the much lower concentration of both low MW and high MW components in the SLP resin.



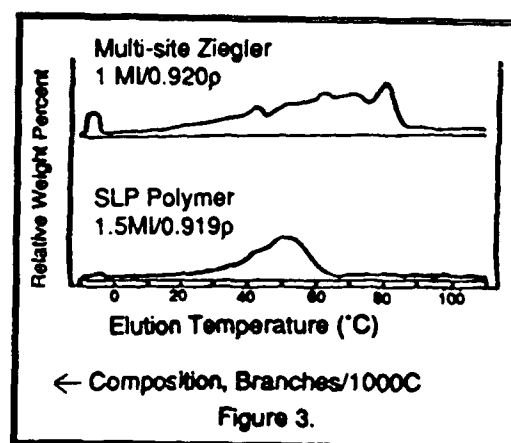
Because there is no low MW tail in the SLP polymers, the materials are much less tacky than conventional broader MWD polyolefins(5). This has a number of consequences. Firstly, even the very low density polymers with a density around  $0.880 \text{ g/cm}^3$  (plastomers) are easily pelletized and the pellets require no dusting to prevent agglomeration. Elimination of the low MW tail also means less volatiles during processing (lower hexane solubles). Secondly, the absence of the high molecular weight tail allows lower processing temperatures because the melting point of the polymer will be lower. The missing high MW tail also means less shrinkback. The NMWD also creates the potential for melt fracture.

#### Composition Distribution

Composition distribution (CD) refers to the distribution of comonomer between polymer molecules - i.e. an intermolecular effect. This feature relates directly to polymer crystallizability, hexane extractability, toughness properties and many other important properties including filler acceptance at a given density and crosslinkability. The polymers under consideration here possess narrow CD - i.e. all of the polymer molecules (chains) tend to have the same comonomer content throughout the entire resin sample regardless of the MW of the chain. In contrast, resins made from multi-site Ziegler catalysts tend to have a very disparate CD: low MW molecular chains have high comonomer content while the high molecular weight chains are very low in comonomer content. This is demonstrated in Figure 2.



The composition distribution of these polymers was determined using a proprietary fractionation method. The graph shown in Figure 3 compares one of the new copolymers with a multi-site Ziegler catalyzed resin. The multi-site Ziegler catalyzed resin has a broad CD containing copolymer molecules with very low comonomer content on the one side and copolymer molecules with very high comonomer content on the other. The new resin by contrast is a very narrow CD material with the copolymer molecules clustered tightly around a single comonomer content. These differing CD's influence a number of important properties.



#### Combined MWD / CD Effects

The true value of the SLP polymers is realized through a combination of narrow MWD, narrow CD, and product cleanliness. Narrow MWD/CD resins have a balance of

physical and melt flow properties that are well suited for many applications. Properties can be significantly altered by tailoring the MWD and/or CD. This is illustrated in Table I below. Both polymers have a density of 0.920 and a melt index of 5.0. In the first example polymer properties of 68 g/mil tear strength and 22% hexane insolubles were achieved. The Type II example shows a dramatic difference in properties obtained by tailoring the MWD and CD. Tear strength was significantly increased (150 → 530 lb/in) and hexane solubles significantly decreased (22% → 3%).

Table I. Polymer Properties as a Function of MW/CD Combinations.

Sample	Tear Strength	Hexane Solubles
Type I	68 g/mil (150 lb/in)	22%
Type II	240 g/mil (530 lb/in)	3%

### Melting Point

Having a narrow CD leads to a narrow melting point range and to a lower peak melting point than a resin of similar melt index and density made with a multi-site Ziegler catalyst. Illustrated in Figure 4 are the DSC curves for two polymers with equivalent density and identical comonomer type. The new SLP copolymer has a peak melting point of about 100°C while the multi-site Ziegler resin has a peak melting point of about 120°C, even though the density is equivalent.

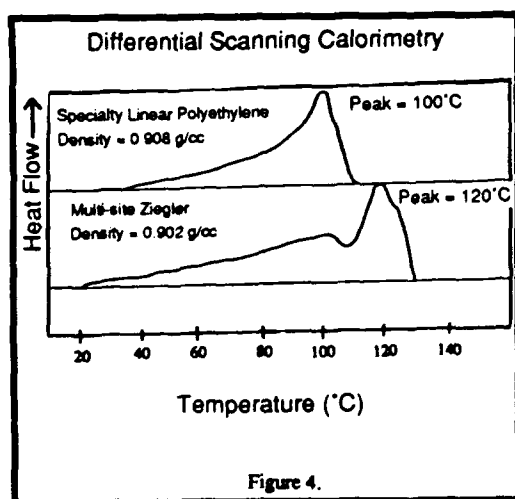


Figure 4.

### Melting Point / Density Relationships

The melting point as a function of polymer density is plotted in Figure 5 for both multi-site Ziegler polymers and the new SLP polymers. Multi-site Ziegler products tend to retain a high melting peak over a wide density range, because the high molecular weight tail determines the peak of the melting point curve and because the high molecular weight tail contains lesser amounts of comonomer. On the

other hand the peak melting point of the single-site resins varies uniformly with resin density because of the narrow MWD and more uniform CD. The melting point can be adjusted to meet the requirements of a given application by altering density or combining narrow CD polymers. As you move to lower densities the copolymers may start processing more like elastomers than plastics, i.e. large L/D ratios (extruder length to diameter) and high temperatures are not necessary. This can provide a larger processing window to operate without scorching, and requires less energy.

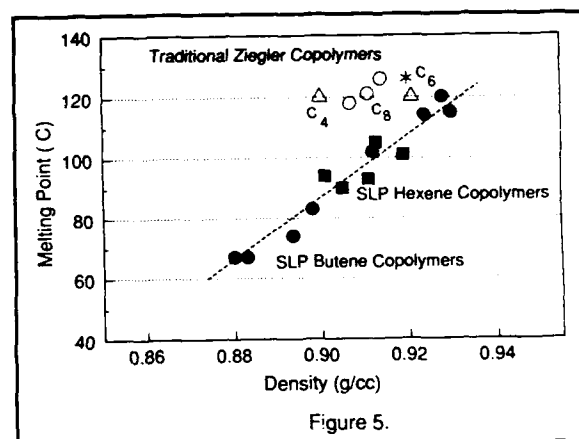


Figure 5.

## II. Polymer Attributes for Power Cables

The following sections describe attributes of the new class of polymers which can be translated into performance attributes desirable for components in the construction of a power cable. A list of the ASTM methods used to obtain the data in this section is given in reference (6).

### Crosslinkability

These new polymers can be crosslinked by both peroxide and radiation curing. The peroxide response of two of the SLP polymers as well as a crystalline EPDM and an LDPE are shown in Figure 6. Torque values (a measure of modulus build-up) are plotted against peroxide concentration. The top curve represents one of the SLP polymers which contains residual unsaturation. The middle lines show an equivalent response of a saturated SLP polymer to EP, both being better than LDPE in an environment of equivalent peroxide levels.

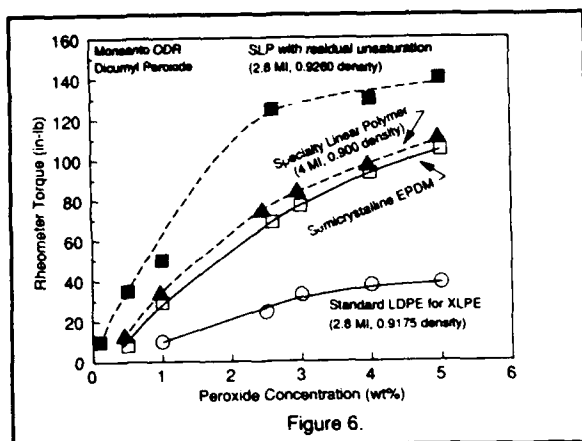


Figure 6.

The radiation response of one of the new polymers relative to a LDPE is shown in Figure 7. The polymers have similar MI and density. Again, the new class of polymers show significantly greater crosslinking response in an environment of equivalent radiation levels as evidenced by the greater levels of torque measured by ODR.

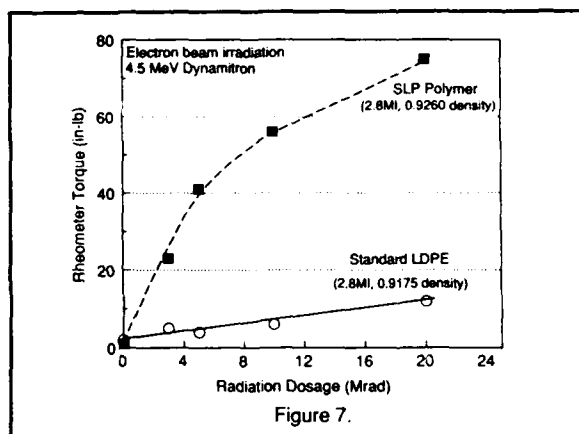


Figure 7.

The excellent cure response of the new specialty linear polymers to either peroxide or radiation makes them attractive for use in both medium or low voltage wire constructions. It is also anticipated that this class of new polymers will be responsive to silane grafting and moisture crosslinking.

### Tree Retardancy

One of the most interesting attributes of these new polymers is their tree retardance. Tree retardancy tests were performed at an independent laboratory (National Research Council of Canada) using the following methods. A 75mil plaque containing the polymer, peroxide and stabilizer were pressed at 175°C then cut into 1" circles. Three small areas were sandblasted onto the surface of the circles to accelerate tree initiation. The samples were stressed at 6kV, 1000Hz using the apparatus and procedure in reference(7). After

3,500 hours the specimens were removed from the test and analyzed. The "degree of treeing" was determined by slicing the sample vertically through two of the sandblasted areas and then measuring the length of the trees relative to the thickness of the sample (stress is proportional to the thickness). The method is shown in Figure 8. All samples were tested in triplicate.

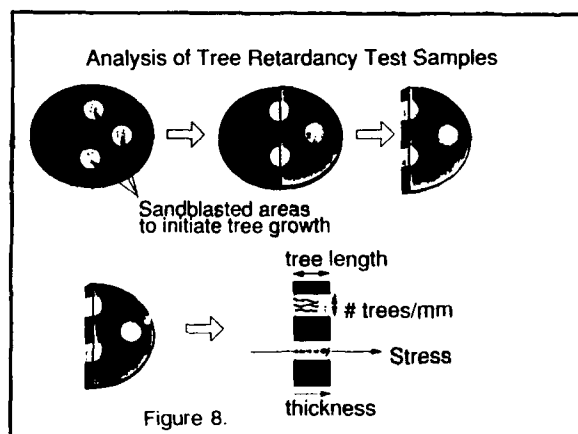


Figure 8.

The tree retardancy test involved 34 types of samples which included the leading commercial materials which are available today, both tree retardant and basic XLPE and EPR compounds. The tree rating (0-100) for each of the samples was determined as described above. The samples were then ranked in performance in four qualitative groups (excellent, good, fair, poor) according to natural breaks in the data. The results are summarized in Table II.

Table II Tree Retardancy Performance

Sample	Tree Rating*	Performance Rating	Comments
MV EPR compound	1	Excellent	Clay filled insulation compound w/ additives
Exact™ SLP-4009**	6	Excellent	No tree retardant additives, no filler
Exact™ SLP-4003**	16	Good	No tree retardant additives, no filler
Commercial tree retardant XLPE	22	Good	Tree retardant additives, no filler
LDPE (XLPE standard)**	68	Poor	No tree retardant additives, no filler

\*Tree rating = tree length divided by sample thickness x 100.

\*\*Samples were crosslinked with 2.6% Dicum R and contained a small amount of stabilizer.



The Exact™ polymers, with no tree retardant additives and no filler, performed very well against the commercial crosslinked compounds currently being used for tree retardant insulation. These properties are a result of the unique architecture of these polymers. Future work will include testing of full size power cables(8) to verify these laboratory results.

#### Electrical Properties

The electrical properties of the new class of polymers are compared in Table III with a semicrystalline EP rubber, both in a filled crosslinked MV insulation compound.

With Filler:

Table III. Electrical Properties of Polymers in a Filled Compound.

	MV Insulation SLP4003 Compound	MV Semi- crystalline EPR Compound
<u>Dielectric Constant</u>		
+ Original	2.64	2.75
+1 Day/90°C Water	2.40	2.50
+7 Days/90°C Water	2.44	2.51
+30 Days/90°C Water	2.42	2.52
<u>Dissipation Factor, %</u>		
+ Original	0.21	0.21
+1 Day/90°C Water	0.78	0.74
+7 Days/90°C Water	0.52	0.56
+30 Days/90°C Water	0.50	0.48

As shown in Table III, the new SLP polymer in a filled compound has electrical properties equal to a semicrystalline EPR. This result is expected since the electrical properties are dominated by filler type and filler loading.

Without filler:

Without filler, these new polymers perform equal to the best LDPE polymers in an XLPE formulation, see Table IV.

Table IV. Electrical Properties of Neat Crosslinked Polymers.

	SLP-4003	XLPE
<u>Dielectric Constant</u>		
+ Original	2.30	2.37
+1 Day/90°C Water	2.15	2.16
+7 Days/90°C Water	2.12	2.15
+30 Days/90°C Water	2.12	2.14
<u>Dissipation Factor, %</u>		
+ Original	0.035	0.037
+1 Day/90°C Water	0.032	0.034
+7 Days/90°C Water	0.037	0.038
+30 Days/90°C Water	0.037	0.036

#### Mechanical Properties

The SLP polymers have excellent physical properties which combined with the previously shown electrical properties makes them highly suitable for many power cable applications. Table V shows a comparison of the physical properties of a semicrystalline EP and a low density polymer (plastomer) made with the single-site catalysts.

Table V. Mechanical Properties of Filled Crosslinked Polymer Formulations.

	Filled Plastomer (0.880p)	Filled EPR Insulation
100% Modulus, psi	1185	685
300% Modulus, psi	2290	1650
Tensile Strength, psi	2555	1710
Elongation, %	405	320
Aged 7 Days, 150°C		
% Tensile retained	100	105
% Elongation retained	92	94

The data in Table V demonstrate the excellence of mechanical properties of the new class of polymers. These properties make the plastomers highly attractive as an EPR alternative. The modulus, tensile strength, and elongation both before and after aging are significantly greater than for a filled semicrystalline EP formulation.

In Table VI, the mechanical properties of the specialty linear polymers, are compared with a commercial LDPE formulation. In each case, the polymers were crosslinked and did not contain filler.

Table VI. Mechanical Properties of Unfilled Crosslinked Polymers.

	Crosslinked SLP VLDPE (0.902p)	Commercial XLPE	Crosslinked SLP Plastomer (0.880p)
Tensile Strength, psi	3200	2400	2475
Elongation, %	540	550	520
Aged 7 Days	150°C	136°C	150°C
% Tensile retained	92	95	98%
Elongation retained	99	95	98

The mechanical properties of these new NMWD polymers are also attractive and make them interesting in XLPE power cable applications. Because of the NMWD, the new polymers have very good mechanical properties. Therefore, SLP's with lower density than XLPE can meet the mechanical performance criteria required in today's XLPE applications, but add more flexibility. Because of the unique comonomer distribution and MWD, these polymers exhibit exceptional tensile strength. Even the 0.880p plastomer has a tensile strength equivalent to XLPE. The

new polymers retain tensile and elongation properties even when aged at a temperature higher than XLPE can withstand.

### Tensile Set

Tensile set measurements were conducted to test the new polymers in a standard EPR test. The samples contain a base stabilization package and no filler. After cure, by either radiation or peroxide, samples were elongated to 200%, held 10 minutes, allowed to relax for 10 minutes, and then measured to determine the extent to which the samples had recovered their original length.

Data after radiation comparing an amorphous EPR, several of the new polymers, and a crosslinked LDPE are shown in Figure 9.

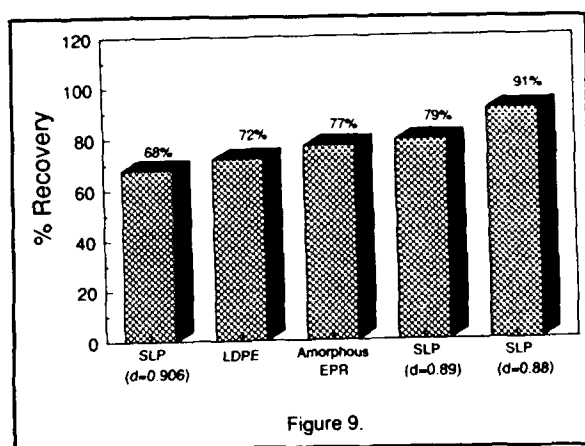


Figure 9.

The peroxide data comparing a semicrystalline EPR, an amorphous EPR, several of the new polymers, and a crosslinked LDPE are shown in the next figure.

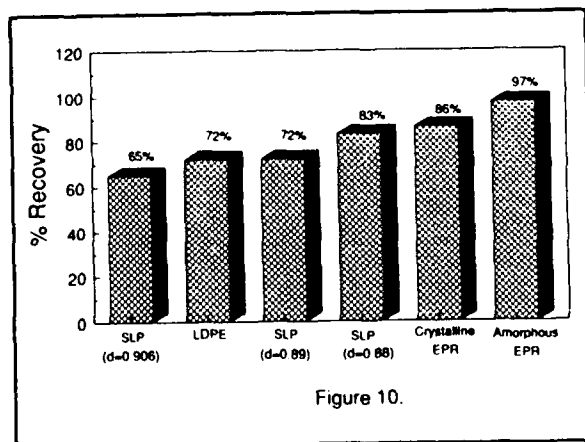


Figure 10.

Again, these data demonstrate that the SLP polymers cure well and have excellent modulus after cure.

### Filler Acceptance

For purposes of economics in the manufacture of low voltage wires, it is usually desirable to load the polymer with high levels of fillers. EP rubbers have the ability to accept large quantities of filler, in fact, the filler has the function of reinforcing the EPR and thereby imparting to it a desirable level of physical properties. Polyethylene polymers, on the other hand, do not readily accept fillers above the 25% level. The SLP polymers have good filler acceptance of both carbon black and Kaolin-clays. This ability of the SLP polymers to accept loadings of filler at 100 phr or even higher levels is a result of its almost uniform comonomer distribution.

In Figures 11 and 12, the effect of filler loading on tensile strength and elongation of two SLP polymers are shown. As expected, the tensile strength of the 0.90 density polymer is higher than the lower density more flexible 0.88 density polymer. However, the plastomer processed better showing no signs of melt fracture during extrusion.

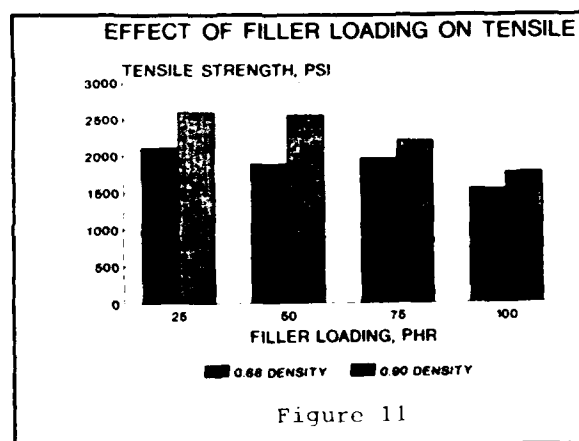


Figure 11

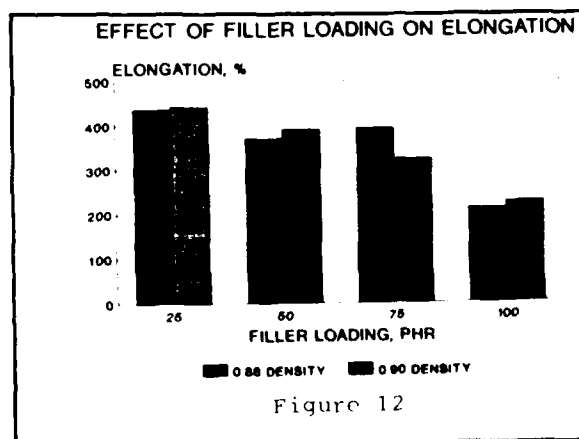
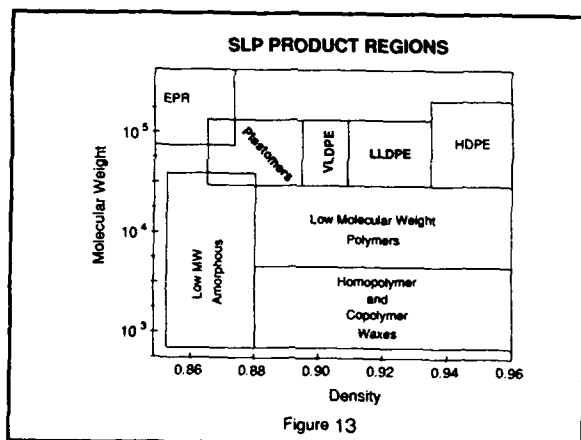


Figure 12

## Product Regions (Plastomers, waxes, VLDPE, etc.)

These ethylene based polymers span a wide range of molecular weight and comonomer content - ranging from extremely viscous high molecular weight resins to low molecular weight liquids, from highly crystalline, stiff materials to low modulus, amorphous polymers. A graphic illustration of the wide range of products available using single-site catalysis is shown in Figure 13. The resins of principal focus in this paper were those of higher molecular weight, MI = 0.2 - 30, and in the linear low and low density areas,  $\rho = 0.930 - 0.870$  because those are the polymers with the most obvious uses in power cable construction.



## Conclusion

Initial laboratory studies show that Exact™ polymers are suitable for many components in power cable construction. Excellent crosslinkability with both peroxides and radiation, making the polymers suitable for both MV and LV insulation applications, has been demonstrated. With the appropriate polymer architecture, the low density plastomers have good tree retardance without tree-retardant additives and have good filler acceptance making them attractive for both MV and LV insulation applications. The higher density materials exhibit excellent mechanical properties and may be useful for jacketing applications. The good combination of electrical and physical properties make this new class of polymers interesting candidates for both XLPE and semicrystalline EPR insulation applications.

## Acknowledgment

The authors of this paper would like to acknowledge the many technical contributions made by Aspy Mehta which are contained in this paper.

## References

- 1) H.C. Welborn, et.al., U.S. Patent 4,937,299, "Process and Catalyst for Producing Reactor Blend Polyolefins".

- 2) The term "plastomer" refers to ethylene-based copolymers with density  $< 0.900 \text{ g/cm}^3$  down to  $\sim 0.865 \text{ g/cm}^3$  with a MW level  $> \text{Mw } 20,000$  ( $\sim 200 \text{ MI}$  and lower)  $\rightarrow$  between PLASTICS (LL/VLDPE) and ethylene/alpha-olefin elastOMERS in amount of ethylene crystallinity.
- 3) A.K. Mehta, C.S. Speed, et.al., "Structure/Property Relationships in Exxpol™ Polymers", SPE Retec Southwest Section, Houston, TX. February 25, 1991.
- 4) M.P. Jeffries, "Exxpol™ Technology", SPE Southwest Section, December 10, 1990.
- 5) J. Boor, Jr., "Ziegler Natta Catalysts and Polymerization", Academic Press Inc., 1979.
- 6) ASTM methods used for the tests conducted throughout this paper are: Shore A Hardness, ASTM C886; Secant Modulus, ASTM D790; Tensile/Elongation, ASTM D638; Dielectric Constant/Dissipation Factor, ASTM D150; Dielectric Strength, ASTM D149; ODR, ASTM D2084.
- 7) A.T. Bulinski, S.S. Bamji, R.J. Densley, J.-P. Crine, B. Noirhomme, B.S. Bernstein, "Water Treeing in a Heavily Oxidized Cross-linked Polyethylene Insulation," Proceedings of the Sixth International Symposium on High Voltage Engineering, New Orleans, LA. August 28 - September 1, 1989. In press.
- 8) R. Lyle, J.W. Kirkland, "An Accelerated Life Test for Evaluating Power Cable Insulation", IEE Winter Power Meeting, Atlanta, GA., 1981



**Lawrence Spenadel** was born in Brooklyn, N.Y. and received his Ph.D. in Chemistry from the University of Cincinnati in 1957. He has more than 30 years service with Exxon Chemical Company and has worked in the wire and cable area since 1970. He has 28 patents and 17 publications.



**Monica Hendewerk** was raised in the heart of the Rocky Mountains in Salida, Colorado. She received her B.S. degree in chemistry from the University of Colorado, Boulder in 1981 and her Ph.D. from the University of California, Berkeley in 1985. She has been with Exxon Chemical Company, in Houston, Texas for the past 6 years.

## MEETING THE DEMANDS OF EVOLVING PREMISES NETWORKS

Donald R. Coover

AT&T

An explosive growth in information exchanged electronically and optically within offices places a high premium on connectivity. Information managers are demanding far more of the copper and fiber optic cable systems that pipe voice, data, video, security monitoring, temperature regulation, lighting control, and other signals throughout a building or campus. They want premises distribution systems that accommodate equipment from any vendor, and expect such systems to handle new technologies such as the Fiber Distributed Data Interface (FDDI), fiber to the desk, synchronous optical transmission, and intelligent building systems.

Building wiring has truly become the fourth utility. Information managers, building owners and occupants must consider the connectivity requirements of both their existing and future building systems (heating/ventilation, air conditioning, security, fire-life-safety, etc.) as well as building services (voice, data, video and Local Area Networks) for new construction as well as retrofit projects.

My presentation this afternoon centers around the impact of building wiring on the emerging "Intelligent Building", uniform versus non-uniform premises wiring schemes and a suggested approach to implementing premises wiring.

### TYPICAL INTELLIGENT BUILDING CHARACTERISTICS

The definition of an "Intelligent Building" as viewed by the Intelligent Buildings Institute (Fig. #1) is one of the most comprehensive descriptions I have seen concerning what I would consider as typical Intelligent Building characteristics.

In my opinion, all the characteristics of an Intelligent Building must be considered when designing and implementing premises wiring in support of existing and future Intelligent Building systems and services.

Rapid deployment of technology and systems integration are driving market demand for open protocols, and industry standard interfaces between various manufacturers' equipment on a global basis. Customers want and are beginning to demand the capability to purchase hardware and software from vendor A and have it communicate with hardware and software provided by vendor B. This ability to mix and match different vendors equipment and devices using standard interfaces allows customers the ability to procure the best performance for the lowest cost.

### CAPITALIZE ON INVESTMENT

Premises wiring is a large capital and operational investment for building developers, owners and managers. From their perspective, there is a need to capitalize on that investment. Traditionally, telecommunications system wiring costs (labor and material) for a telephone system, range from 20 - 40% percent of the total systems cost.

In discussions with several major building control vendors, they agreed that the labor and materials required to connect a typical building management system average at least 33 percent of the systems initial cost.

Imagine the impact if a single integrated low voltage premises wiring system could be installed in an Intelligent Building or Campus that would provide connectivity and transparent information flow between telecommunications, data processing, and traditional building automation systems.

From a building owner or managers perspective the benefits include lower material and labor costs, the ability to evolve to new technologies and protection of their current investment in premises wiring, reduced physical space requirements, lower relocations (moves & changes) expenses, lower maintenance and administration costs, and the ability to migrate and integrate new technologies with greater ease, less risk and lower costs.

From the manufacturers perspective the potential ability to reduce connectivity costs, the emergence of global protocol and connectivity standards and the capability to provide their "added value" to larger integrated systems solutions could have a dramatic impact on their future.

For the vendors, there are many choices when considering premises connectivity requirements. The decision to incorporate the correct media, i.e., 18 AWG, coaxial, unshielded or shielded twisted pair copper or fiber optic wiring and cables, and adherence to building wiring standards (Fig 2) and open protocols when developing future systems and products may directly impact the success of that vendor in the evolving market-driven Intelligent Building environment of the 90's.

## INTEGRATED NETWORKS AND SYSTEMS

The impact of technology on business in the past decade has been tremendous. Remember that prior to 1980, the personal computer did not exist, there were no digital PABX telephone systems and the building controls industry was primarily based on pneumatic technology.

Advancing technology in the Intelligent Building field has certainly had a dramatic effect on how business is conducted throughout the world; however, these technologies have been primarily based on stand alone systems and for the most part can be considered "islands of automation" (Fig 3). The need to integrate these existing "islands of automation" will increase as we enter the 1990s. The need is developing to integrate building support systems that monitor and control energy usage, fire safety, lighting, security and process control with the telecommunications and office automation systems found in modern structures. Just as office communications systems have migrated from proprietary connecting schemes to structured uniform wiring systems handling voice and data, building automation systems will evolve to support open systems connectivity. This will allow the evolution from proprietary connecting schemes to integrated wiring systems that connect telecommunications, office automation and building automation systems, devices and applications.

In my opinion, the emerging "Intelligent Building and Campus" will not rely on outlets in offices, but on "smart access points" to provide integrated information pathways. By utilizing this integrated information pathway approach, communications, data and support systems and devices can share common backbone and administration systems allowing building owners and managers to reduce installation and system administrations costs.

Such integrated system solutions allow customers to move and manage all the information within a building using a common and open wiring architecture based on global standards.

The Intelligent Building Institute is addressing this issue and has endorsed unshielded twisted pair copper wire and 62.5 micron, multimode fiber optic cable for Intelligent Building/Campus distribution of low voltage signals.

#### MULTI-VENDOR ENVIRONMENTS

Certainly the two most important pieces of information I have learned over the past 10 years is that advancements in technology are happening almost on a daily basis and customers are demanding integrated, multi-vendor solutions to their business problems. Customers are no longer satisfied with the concept of "locking in" by purchasing vendor specific solutions from major manufacturers, instead they are beginning to deploy systems integrator to solve their business problems. Systems integrator have the ability to mix and match various devices and applications into unique solutions designed around specific customer needs and desires.

Currently, multi-vendor environments exist in both the telecommunications and data processing industries and, as they evolve, will have a major impact on the traditional building automation and control industry. The need for large centralized building management, security, and fire-life-safety systems from large vendors will certainly continue; however, niche manufacturers will begin to position their devices within these larger systems utilizing emerging standard protocols and interfaces.

#### HIGHER DATA SPEEDS AND BANDWIDTH

The requirements for increased data speeds and higher bandwidth will continue to grow. Fifteen years ago, 1,200 Bits per second (Bps) was considered state of the art data communications when connecting computers with various peripheral devices. In 1990 it is common to have Local Area Networks (LANs) installed that transmit from 1 Million to 16 Million bits per second (Mbps).

In my opinion, 1992 will be the beginning of the Information Age and by coupling the ever increasing computer power that is being developed and the next generation of networking technology like the Fiber Distributed Data Interface (FDDI) standard that currently operates at 100 Million bits per second, Intelligent Buildings linked together with Public and Private Intelligent Networks will become common place throughout the world by the mid-90's.

#### NON-UNIFORM AND UNIFORM WIRING APPROACHES

Premises wiring can be classified into two approaches: non-uniform and uniform. Non-uniform wiring utilizes separate wiring schemes for the various building systems and services found in a structure.

In non-uniform environments, it is typical to have as many as seven or eight separate wiring plans within a facility. In addition, these independent wiring schemes utilize various media (coaxial, shielded, unshielded copper and fiber optics) to support the various systems and devices found in the building.

Various levels of support exist for non-uniform building wiring and are usually dependent on the individual equipment provider. Since these vendors are generally not "premises wiring companies", one must consider what happens when something goes wrong with the wiring, who does the customer call and what kind of support can be expected.

The advantages of non-uniform wiring include generally lower individual system installation costs. In addition, it is a mature way of wiring buildings and accounts for 80 to 90 percent of the building wiring that exists today.

Some of the major disadvantages involved with the non-uniform approach include the requirement for separate wiring to support voice, data, image, energy management/control and security systems, limited support of emerging multi-vendor environments and generally no logical administration or labeling methods or procedures. Additionally, the non-uniform approach is not well suited for future technologies requiring higher bandwidth and faster speeds.

The uniform wiring approach is based on the EIA/TIA-568 (Fig 4) standard and consists of a single integrated wiring system designed to support various voice, data, video and building automation systems utilizing a standard interfaces and media. Uniform structured wiring utilizes a subsystem approach comprised of the following:

Work Location System

Horizontal System

Administration System

Backbone (Riser) system

Equipment/Network Interface System

Campus System

In addition, integrated uniform wiring systems generally adhere to existing standards and are positioned to conform with future standards as they emerge. They provide transparent connectivity between various vendors' systems and equipment. This feature provides the customer with the capability to mix and match various devices and systems. From a vendors perspective, transparent connectivity allows them to retain proprietary features, operating systems and functions to market their individual system advantages without developing and supporting proprietary wiring schemes.

Utilizing the subsystem approach, uniform wiring systems can be modified and easily upgraded to support future technologies when they are required.

The perceived disadvantage of the uniform wiring approach is the higher individual system wiring installation costs. This is clearly offset by the ability to integrate and connect several or all of a building's systems over a single wiring plan; however, the customer must understand the economies of scale that the uniform wiring approach provides.

#### SUGGESTED APPROACH TO PREMISES WIRING

**WIRE ONCE!** In my opinion, this is the most important aspect to consider when planning and implementing building wiring. The incremental material cost and labor expense incurred in implementing a uniform wiring system to support existing and future requirements is minimal when compared to the high labor expense involved in upgrading and rewiring an existing structure.



Donald R. Coover (Don)  
AT&T Network Cable Systems  
111 Madison Avenue  
Morristown, NJ 07962-1970

Don Coover is with AT&T Network Cable Systems as the Manager for AT&T's SYSTIMAX(tm) Premises Distribution System (PDS). He has more than 24 years experience in the telecommunications, data processing and building controls industries. Previously, he has held positions with IBM, the U.S. Treasury Department and New Jersey Bell Telephone Company. Mr. Coover's present responsibilities include evaluating potential requirements for premises wiring by the Building Controls Industry and managing AT&T's SYSTIMAX PDS system to provide connectivity for various energy management, security, fire/life/safety, telephone, video, local area network (LAN) and data communications systems in intelligent building environments. His other responsibilities have included developing and managing AT&T's Integrated Services Digital Network (ISDN) and Fiber Distributed Data Interface (FDDI) premises wiring plans.

Mr. Coover currently serves on the Board of Directors of the Intelligent Buildings Institute and has previously served on the LAN and ISDN committees of the Building Industry Consulting Service International (BICSI) organization.

Mr. Coover has made numerous international presentations to the Building Owners and Managers' Association (Toronto Canada), United Kingdom Telecommunications Managers' Association (London, UK), Premises Wiring Seminar (Stockholm, Sweden), A/P Buro '90 International Intelligent Building, Office Environment & Business Automation Event (Singapore) and the Telecommunications Managers Association (Bangkok, Thailand).

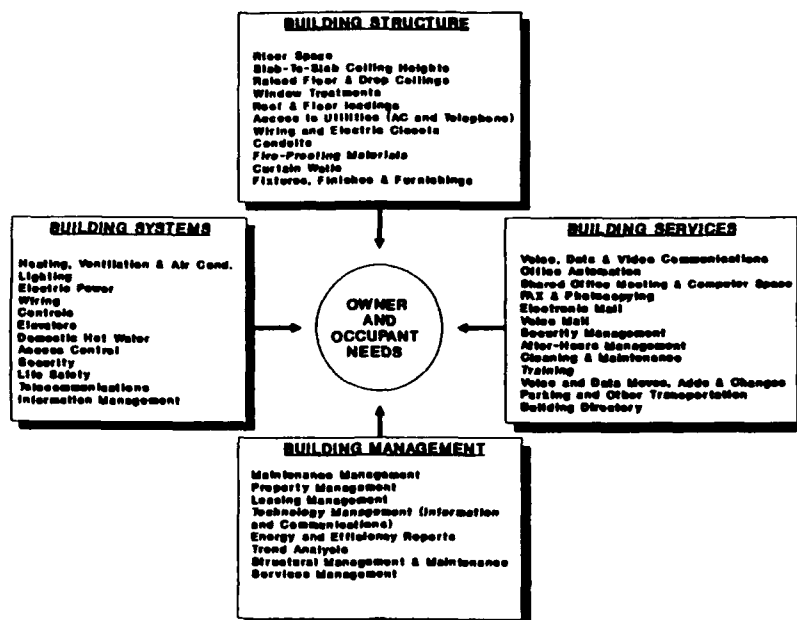


FIG. 1

## STANDARDS

- EIA/TIA - 568 - COMMERCIAL BUILDING WIRING STANDARD
- ISO/IEC JTC1/SC25/WG3
- IEEE - 802 - LOCAL AREA NETWORKS
- ANSI - FDDI - FIBER DISTRIBUTED DATA INTERFACE

FIG. 2



## Islands Of Automation

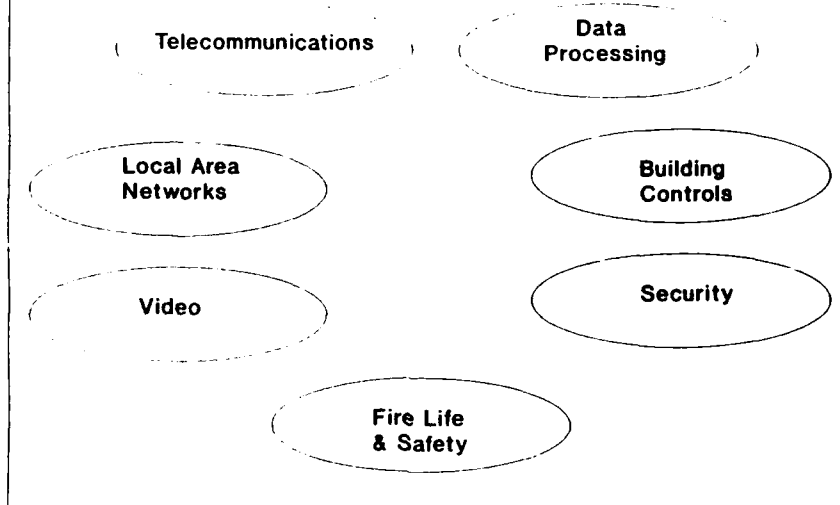


FIG. 3

## SYSTIMAX® PDS STANDARDS EIA/TIA-568

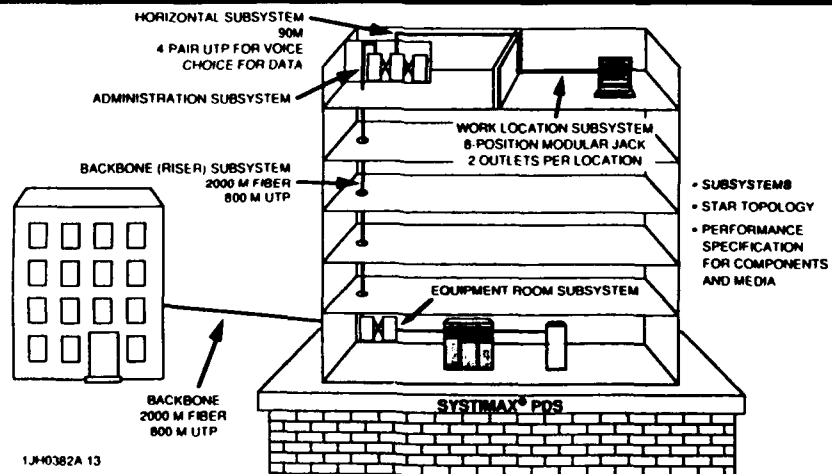


FIG. 4

## SYSTEM INTEGRATOR'S VIEW OF INTELLIGENT BUILDINGS

Ronald Sumski

### Electronic Systems Associates

The Systems Integrator is charged with the responsibility of linking low voltage systems together to form a synergy. He or she views the Intelligent Building as a friendly environment that supports these various systems. Further, he or she is concerned that there are adequate pathways for linking systems with standard wire and cable.

Recently, there have been standards developed for horizontal and vertical cable. These standards include Fiber Distributed Digital Interface (FDDI). Consultative Committee on International Telephone and Telegraph (CITT) and Integrated Systems Digital Network (ISDN).

These standards will, in most cases, dictate how new buildings will be cabled for all communicating processors.

Careful planning of a building's ability to support technology must take place. This

planning must begin in the design phase of the project. Traditionally, electronic systems have been attached to buildings nearing completion. The Intelligent Building has technology built into the infrastructure in the same fashion that heating, air conditioning, ventilation, electric and plumbing are.

The Systems Integrator views the Intelligent Building as a structure designed to support a variety of electronic systems. The electronic systems are similar in their respective technical characteristics; yet diverse in their functional objective.

The Intelligent Building provides a multitude of electronic services to the occupants and building management. They are:

- A. Telecommunications-Voice and Data
- B. Security
- C. Fire Detection and Life Safety Services
- D. Audio/Visual Services
- E. Video Broadcast Services
- F. Building Systems Instrumentation and Control

The single most important factor that distinguishes the Intelligent Building from others is that electronic systems are successfully imbedded in the infrastructure not attached to it.

Electronic systems are defined as hardware, software, wire & cable all working in concert. Therefore, a building must be designed and constructed with a view towards ensuring a symbiotic environment for electronic systems.

All who are involved with computer based systems know that these systems are becoming capable of performing more functions and working at faster speeds. Therefore, two very important factors that must be considered, when planning for electronic system infrastructure, are bandwidth capacity and transmission speed capability.

The wider the bandwidth capacity and faster the speed, the less likely an infrastructure will have to be modified in the future.

There are many groups and individuals involved with the planning and construction of a building. They are:

- A. Owner
- B. Architect
- C. Engineer
- D. General Contractor
- E. Sub Contractor
- F. Specialty Consultants

These groups and individuals, are generally bound together as a Project Team when a new building is built or major renovation work occurs.

In order to be successful, the Systems Integrator strives to have the project team plan, and build an environment that is System Friendly. System Friendliness is comprised of two categories. They are Tactical Elements and Support Elements.

#### Tactical elements

The infrastructure must be flexible in order to meet changing technology requirements for the life of the building. The proper time to address flexibility is during the planning stages of the building project. There is a cost associated with

flexibility. The cost is low during initial build when compared with renovation after building completion.

Tactical elements concern themselves with locations and sizes. They are:

- A. Building entry points for electronic utilities such as:
1. Telephone Company Service Cables
  2. Cable TV Company Cables
  3. Fiber Optic Cables
  4. Private Cables

In many cases, the owner or tenants will desire alternate entry points on opposite sides of the building for redundancy or disaster prevention purposes.

These entry points are usually in the building basement. The routing of the cables must be carefully coordinated with the other utilities penetrating the foundation walls such as, high voltage electric, steam, water and sewer.

- B. Riser Shafts - In the traditional building, there are separate risers for telecommunications, security, control systems, fire, radio page, etc. Each specifically must find its own vertical path through the building core. With growth factored in, these risers (when added together) take a considerable amount of space. The Intelligent Building should have common electronic systems risers. Respective vertical cables then share the same space.

The riser shaft should pass through the Technology Room on each floor. This arrangement allows for the maximum of flexibility while exercising the maximum amount of control.

- C. Technology Rooms-Historically, electronic systems were located in separate spaces. The security system electronics were in one closet, control systems in another, telephone in a third, fire detection in a fourth, etc. (see figure 1). The Intelligent Building should have at least one common technology room located on each floor. This room should have separate power, and emergency power, adequate air conditioning. In short, the room should look much like a mini-data center. The advantages are:
1. Cost - The cost of constructing one room per floor is less than construction costs for many (one UPS circuit, one air duct, one

card reader).

2. Control-The room would be at the same location on each floor (in the building core). Maintenance personnel will not be wandering through the core area.
  3. Standardization-Connecting cables can be routed to the same geographical hub regardless of the application. Coordination with other trades is easier. The same riser shaft can be shared by all low voltage utilities. It is possible to share the same riser cable (if territorial disputes can be mediated).
- D. Uniform Cable-The Systems Integrator strives to apply the least common denominator to electronic systems with protocols, computer language, space and cable. During the 1980's and 1990's, industry wide standards were, and continue to be introduced and refined. Most multiplexers, regardless of the system involved, transmit over 62.5 micron, multi-mode, dual window fiber optic cable. The most common form of horizontal media is multi-wire, 24 AWG, unshielded twisted pair cable. The new high quality cables can carry data transmission speeds of up to 100 MBS at distances of up to 100 meters. It makes the most sense to install this type of cable to any low voltage communications point. This point can be anything from a telephone to an electronic door strike. The electronic system driving the system can be a highly sophisticated PBX Telephone System or a lighting control computer turning the lights off after the staff leaves for the night.
- The real value in a standard intelligent building cable is that the electronic engine can be changed without opening walls and ceilings.
- E. Standard Protocols-The ultimate in Intelligent Buildings will not be enjoyed until there is a standard protocol that all electronic systems manufacturers employ. Today, there is minimum data sharing between low voltage systems. The telephone system cannot talk to the building control system. The security system cannot monitor the fire detection system unless they are hard wired together.

The truly intelligent building will have linked systems. Whether the ultimate solution is one master system controlling sub-systems, or several independent systems with a synergistic link, remains to be seen.

- F. Rooftop Coordination-Many companies have a need to place microwave and satellite dishes on the roof of the building. The Systems Integrator seeks assurances that lines of sight are not impaired by other roof structures such as water tanks and cooling towers. Additionally, there should be adequate structural strength to support these antennae.

Building owners and developers should take into account the future placement of a variety of antennae that do not conflict with one another. Provisions should also be made for the location of radio rooms that are located on the top floor. The Systems Integrator often must compete for this space with the company executives who want offices with the best view.

Support Elements is the other factor that enhances a building's System Friendliness. They are:

- A. Documentation-Careful attention must be paid to how well cable ends and system components are labeled and inventoried. This information must be kept current and correct at all times. Computers are most often used to manage this information.

Once the data is correctly entered, a variety of functions can be performed, depending on the sophistication of the Management System. Repair requests can be generated, available capacity recorded, inventory managed, troubles isolated, etc.

- B. Patchability-By terminating all wire ends in patch panels the requirement for technicians, schooled in the intricacies of hard wire installation, can be eliminated. Instead, non-technical personnel can make most wire and cable moves and changes. The cost advantages are obvious.

- C. Operating and Maintenance Manuals-By providing a well written set of documents, the Intelligent Building Owner is assured that the incremental systems can be managed and maintained in the most efficient and cost effective manner regardless of any personnel changes that occur.

From a Systems Integration perspective, the truly intelligent building is still in the future. There are several events that must take place. They are:

- A. Developers and Owners must be willing to invest the capital and planning necessary to build a flexible technology infrastructure into , not on-to, the building.
- B. Systems Manufacturers must agree on a mutually acceptable common protocol for

operating systems.

- C. Cable Manufacturers must continue to develop transmission media that meet a wide variety of system performance criteria. In fact, the cable manufacturers must gain an agreement that their cables will be certified as acceptable by systems manufacturers.
- D. Cable Termination and Connection Component Manufacturers must also continue to develop products that are certifiable by both cable manufacturers and systems manufacturers.

Once the aforementioned events take place, we will see system integration development and intelligent building development occurring at a much more rapid rate.

Mr. Sumski is a Regional Vice President with Electronic Systems Associates located in New York City, he has been planning, designing and implementing electronic systems for over 24 years. Mr. Sumski spent a total of twelve years with the Bell System as a major account manager. The remainder of his time has been spent working for Consulting Firms in the New York Area.



## FDDI TECHNOLOGY AND IMPLEMENTATION

Margot A. Botelho, Senior Applications Engineer

Corning Incorporated

This paper provides an overview of FDDI applications, the technology, and the fiber-related issues that you should consider when implementing a network.

Corning's fiber network, which was recently upgraded to FDDI, is used as a case study. Originally installed in 1985, the network is being upgraded simply by means of changes in the electronics; the existing cable plant will remain intact, with new optical cable added only to connect new buildings.

Companies are actively preparing for -- or implementing -- networks that can take full advantage of the potential of FDDI and will support increasing numbers of users and more sophisticated applications.

### FDDI Applications

FDDI was designed to function as a high-speed "backbone" to join existing local-area networks, such as Ethernet and Token Ring. FDDI systems linking lower-speed LANs are found today both in interbuilding backbones and intrabuilding risers.

Other applications for FDDI include the interconnection of mainframes, file servers, peripherals and controllers, or providing high-performance networking for work

groups.

FDDI networks are installed and operational at a number of locations today. In addition, many companies are using optical fiber with FDDI capability to support lower speed networks in anticipation of upgrading to FDDI in the future.

### FDDI Technology

FDDI is the highest-speed -- and potentially the most powerful -- standard available for private-premises communications today. Developed specifically for use with optical fiber, the FDDI standard takes advantage of the medium's high bandwidth, supporting data rates of 100 megabits per second (Mbps).

At the logical level, FDDI is a fiber-optic, token-passing ring network. Network nodes are connected in a closed path and data travels around the network in opposite directions on one of two rings.

The primary ring carries data, while the secondary ring serves as a redundant path, increasing network reliability. The secondary ring can be used to carry data, or can be used to back up the primary ring.

The recommended physical topology for FDDI is a dual ring of trees, with each connection a duplex link pair. Peer-to-peer connections are constructed from the trunk ring by means of concentrators that serve to protect the trunk ring from faults that occur in the nodes attached to the tree.

FDDI LANs using multimode optical fiber support up to 500 nodes, located up to two kilometers (km) apart. The maximum total ring circumference is 100 km.

While the standard calls for 62.5 micron multimode fiber with a

bandwidth of 500 MHz.km at 1300 nanometers (nm), the standard also permits use of 50 micron and other multimode fiber sizes. It's also possible to use single-mode fiber for FDDI; single-mode fiber dramatically increases the maximum allowable distance between stations -- to as much as 60 km -- and offers even higher bandwidths.

#### Fiber Specifications

The Physical Layer Medium Dependent (PMD) standard defines the fiber performance required for FDDI as the following:

Core diameter:	62.5 microns
Cladding diameter:	125.0 $\pm$ 3.0 microns
Numerical aperture:	0.275
Minimum modal:	500 MHz.km
bandwidth @ 1300 nm	
Maximum Attenuation:	Not specified

(Attenuation of multimode fiber, before cabling, typically is in the range of 0.6 to 1.0 dB/km at 1300 nm.)

The PMD also specifies the limits for zero dispersion wavelength and zero dispersion slope.

The PMD specifications ensure the network can support link distances of up to two km using 62.5/125 micron fiber. When other common fiber sizes, such as 50/125 micron and 100/140 micron are used, their different attenuation and bandwidth characteristics will change the distance capabilities of the system, so it is important to understand the ramifications of your fiber choice.

#### FDDI Implementation

Understanding how each of the specifications listed above

determines system performance can help you select a fiber that provides a long-term solution based on the needs of your network.

This section of the paper discusses the parameters that affect system bandwidth and system loss budgeting: fiber bandwidth, chromatic dispersion, attenuation and fiber geometry.

#### Fiber Bandwidth

Fiber bandwidth and chromatic dispersion determine overall system bandwidth.

Fiber, or modal, bandwidth is a measure of the dispersion, or signal pulse broadening, that occurs as the different modes of light travel through the multimode fiber.

Each mode of light follows a slightly different path and arrives at the receiver at different times. When the pulse broadening causes the pulses of light to overlap, they cannot be distinguished by the receiver, thus limiting the system data rate.

To support link distances of up to two km, the PMD document calls for a minimum fiber bandwidth of 500 MHz.km at 1300 nm. However, if longer distances between stations are required, or if you plan to add more users or eventually run at higher data rates than FDDI, a higher-bandwidth fiber may be necessary. In those cases, you must ensure that the fiber and transmitter characteristics still comply with the FDDI standard.

#### Chromatic Dispersion

Another source of pulse broadening, chromatic dispersion is caused by the different wavelengths of light traveling at different speeds through the fiber.

Chromatic dispersion can be minimized by operating near 1300 nm, where glass optical fibers exhibit minimal chromatic dispersion.

Choosing LEDs with narrow spectral widths helps decrease chromatic dispersion because the range of wavelengths propagating through the fiber is smaller. However, whenever LEDs are used, chromatic dispersion is an important parameter to consider because it limits total system bandwidth.

#### Attenuation

Fiber attenuation contributes to the amount of light power lost in the cable plant and, therefore, sets limits on the link lengths in the network through its impact on the link loss budget. It is a measure of decreasing optical power over the length of the fiber resulting from light absorption, light scattering and fiber bending.

The total system loss budget is determined by losses caused by connector and termination points and by fiber attenuation. Systems with many connections will suffer greater losses and will be more sensitive to losses caused by fiber attenuation.

The PMD document specifies that total end-to-end attenuation between stations must be 11 dB or less at 1300 nm. That number includes all contributions to optical power loss -- cabled fiber attenuation, connectors, splices, and any other items in the cable plant that cause light loss.

Low cabled fiber attenuation is desirable because it provides more flexibility in the end-to-end power budget, facilitating future network rearrangements or additional splices or connections.

#### Fiber Geometry

Fiber geometry, or the physical dimensions and shape of the fiber, also contributes to the total loss budget through its impact on connector and splice losses. In addition, it determines the ease and efficiency of connectorization.

Important parameters to consider are cladding diameter and core and cladding non-circularity, both of which affect the fiber's ability to fit into standard ferrule-type connectors and mechanical splices; and core to cladding offset (concentricity), which impacts the amount of light lost at a connection.

#### Corning's ACORN Network

A network at Corning Incorporated's world headquarters in Corning, N.Y. provides an example of how fiber can be installed to run at lower data rates and then upgraded to FDDI at a later date.

In 1985 we installed a fiber-optic network that ran at 10 megabits per second (Mbps); that is, Ethernet data rates. This year we're upgrading to FDDI rates simply by upgrading the electronics. The existing cable plant will remain intact, avoiding network downtime and other disruptions.

We already are running at FDDI rates over a single-mode fiber nine-km link between our R&D facility and a satellite office building, and over multimode fiber between our R&D facility and the computer system, located at another site. The rest of the network is scheduled for completion between now and 1993.

Our network, dubbed ACORN -- Advanced Corning Optical Regional Network -- links manufacturing, research, and office buildings at more than five sites in and around

our headquarters in Corning, N.Y.

The original network was designed to support voice, data and electronic messaging capabilities, as well as video-conferencing between two of the five facilities.

Our decision to upgrade to FDDI was based on heavy network traffic and the increased use of such high-bandwidth applications as CAD/CAM. FDDI also offers improved network management capability and more reliability -- provided by FDDI's dual-ring topology.

The new network supports data rates of 100 Mbps. In addition to the existing applications, we also are considering installing fiber-to-the-desk in some facilities. In those cases, we plan to take advantage of optical cable's small size and light weight by installing all the cable under raised floors. This will eliminate the need to run cables down from the ceiling and make it a non-plenum installation.

#### ACORN Specifications

In the ACORN network, Corning installed a combination of Corning 50/125 micron multimode fibers and Corning single-mode fibers for all interbuilding connections.

In 1985, 50 micron fiber was the predominant fiber for premises networks and was compatible with then-available electronics. Although 62.5 micron fiber now is the most common fiber used in premises communications, Corning continues to use its 50 micron fiber in new interbuilding cables added; the cable offers enough bandwidth to support FDDI data rates and allows Corning to leave the rest of its cable plant intact.

Corning is considering using its 62.5 micron fiber for the proposed fiber-to-the-desk applications because with currently available electronics, it offers the lowest insertion loss.

The single-mode fibers were installed for future upgradability. While they mostly remained "dark" for the first five or six years, that foresight already has paid off; Corning already is using the single-mode cable to support parts of its FDDI network.

The Corning 50/125 micron fibers installed have modal bandwidths greater than 600 MHz.km at 850 nm and greater than 1.0 GHz.km at 1300 nm. Initially the multimode fibers were

used at 850 nm, but now are used at 1300 nm to comply with the FDDI specification. Because of long link distances, the network is powered by a 1300 nm laser.

The link distances in the ACORN network range from 0.5 to 9.4 km. Each loose tube cable contains 12 or 24 each of Corning single-mode and 50 micron multimode fibers, depending on the number of buildings at each site location.

#### Planning for the Future

In 1985, when Corning installed its first fiber network, FDDI specifications were not yet available to help network planners design a system. The fact that we are able to upgrade our system without replacing the existing cable plant -- and disrupting our entire network -- is a testament to our network planners, who specified fiber with enough bandwidth to meet more than just our current needs.

The FDDI standard is playing an important role in facilitating the use of optical cable in networks. The standard is critical in establishing equipment compatibility and determining the performance parameters required to support the application.

However, when selecting the technology and implementing your network today, it's always important to keep the future in mind. Already people are talking about the possibility of networks with higher data rates than FDDI, so planning ahead now will help you take advantage of the technology of the future.



Margot A. Botelho  
Senior Applications Engineer  
Opto-Electronics Group  
Corning Incorporated

Margot A. Botelho is a senior applications engineer in the North American Applications Engineering Department, responsible for providing engineering support to Corning's cabler customers and end-users.

Botelho joined Corning's Electronics Products Division in 1980, manufacturing facilities before assuming her current responsibilities.

Botelho has a bachelor's degree in mechanical engineering from Purdue University.



# Cabling Systems for Industrial Applications

Timothy K. Cahall

## AT&T Network Systems

### Abstract

The industrial marketplace is rapidly accepting fiber optic cable as the communications media of choice. However, the hostile environments which characterize a factory present some unique challenges to fiber optic cabling manufacturers. This paper is a discussion of some of the environmental considerations which are pivotal to the success of a fiber optic communications system in an industrial environment.

=====

The industrial marketplace is quickly standardizing on fiber optic cable as the media of choice. While a large number of copper based solutions continue to be installed, this number is diminishing rapidly. The hostile environments which are typical in a factory are ideal for fiber optic cable, however, these hostile environments pose unique challenges for manufacturers of fiber optic cable and apparatus.

The manufacturing environment typically has numerous hazards which must be bridged to ensure a successful installation. ElectroMagnetic Interference (EMI) is the most common environmental hazard in a factory environment and is the driving force behind the manufacturing industry's move toward fiber optics. While fiber optic cable manufacturers do not have to be

concerned with EMI's effect on communications signals, a wide range of environmental hazards such as distance, heat, dust, induced currents, lightning, rodents, corrosives and physical damage are primary concerns. Each of these hazards has a distinct effect on lightguide cable and apparatus design.

Fiber optic cable is uniquely suited to cope with the relatively large campus environments which are typical of a factory. However, unlike long haul cabling solutions, factories usually do not have straight, clear right of ways in which a single cable can be run. In addition, it is common for a fiber optic cable to pass through several, varied environments between cross connect locations. This puts unique pressures on both cable and apparatus design.

Fiber optic cables are typically designed to enhance one or several capabilities. These capabilities may be light weight, bend radius, pulling strength, plenum, etc. While these designs are optimized for certain environmental situations, it is common for different, and seemingly opposed, requirements to be present in a single long cable run. An example of this would be a single cable which is required to run through a plenum air passage from a computer room to a building exit

point two hundred meters away. Upon exiting the building this same cable will be run aerially for a kilometer before entering a production facility. Upon entering the production facility this cable will be exposed to 500 meters of a rodent infested, possibly corrosive environment. Obviously, it is nearly impossible for a single cable to suit all of these needs. However, in order to service the widest possible market, a new family of cables which is capable of surviving a wider range of environments is required.

Rather than seek the perfect fiber optic cable, a typical installation in an industrial environment will utilize cable splices to change cable types where needed. This has the effect of increasing the demands placed upon lightguide apparatus manufacturers to create lower cost, higher performance splices and enclosures which can be installed and survive in increasingly hostile environments. In order to take advantage of the significant industrial marketplace, lightguide apparatus must increase its reliability and performance while decreasing the cost and complexity of installation.

The relatively long, complex cable runs which typify a factory environment are well suited to fiber optic cabling solutions. However, in order to capitalize on this growing marketplace, fiber optic cable and apparatus manufacturers must be able to support the diverse environments which are common in an industrial facility.

Heat represents one of the most difficult environmental hazards to overcome in a manufacturing environment. Many primary manufacturing functions, such as steel,

aluminum and glass, generate enormous amounts of heat during the manufacturing process. Often, hardened control systems which are capable of residing very close to these extremely hot manufacturing processes have been installed. Even when control systems are located a distance from the actual manufacturing process, the physical layout of a factory often requires that these extremely hot environments be traversed by fiber optic cables. Often, lightguide cable for many industrial environments must be able to survive limited exposure in proximity to temperatures in excess of 1000 degrees Celsius and extended exposure to temperatures in excess of 100 degrees Celsius. While alternative routes can often be located for fiber optic cable runs, high temperature cables will be required in order to support the increasingly complex process control systems which are being planned for the future.

Lightguide apparatus manufacturers must also be able to survive in extremely high temperature environments. As process control equipment moves closer to the actual manufacturing process, the need for high temperature connectors and enclosures increases. Operating ranges for lightguide apparatus are similar to those of fiber optic cable. However, care must be taken to dissipate heat which is transferred from end point equipment and surrounding housings. In order to aggressively address the growing manufacturing marketplace, lightguide apparatus capable of a wider range of temperature operation is required.

High temperature is an exceptionally challenging and complex problem for a manufacturer. While many

other hazards can be avoided or shielded, heat is endemic to many manufacturing processes and unavoidable if the full capability of a fiber optic communications system is to be tapped. In order to capture a significant share of the growing industrial marketplace, fiber optic cables and apparatus capable of surviving in a wide range of temperatures is required.

Dust is a significant hazard to lightguide apparatus and, to a lesser extent, lightguide cable in an industrial environment. Unlike typical office environments, in which dust is a manageable problem, dirty, oily dust is common in a factory environment. This dust can block light transmission between connectors, fill cross connects and place tremendous weight strains upon fiber optic cables.

Lightguide apparatus is most vulnerable to the dirty environment which is found in a factory. While current fiber optic communications systems installations enjoy the protection of high performance industrial enclosures, this will not continue into the future. In current installations, optoelectronic equipment must be adequately protected. Accordingly, expensive enclosures are installed to protect electronic equipment. Cross connect apparatus is installed in this same cabinet. As more process control equipment providers integrate optoelectronic components into their hardened product offerings, lightguide apparatus will be required to survive in dusty, dirty environments. Current lightguide installations in factory environments typically utilize industrial enclosures to protect both electronic equipment and lightguide apparatus. As

optoelectronics become more widely integrated in process control equipment, a new family of industrially hardened lightguide apparatus will be required.

Lightguide cable is also at risk from dust and dirt in an industrial environment. One primary metals manufacturer with a coaxial cable based network required work crews to remove soot from the cabling on a quarterly basis to relieve weight strain. This removal was done by beating the cable with baseball bats. Obviously, this is not a solution for a fiber optic cable. However, it does point out the need for fiber optic cables which are capable of supporting relatively high weight loads for long periods of time. The additional weight which is added to a fiber optic cable through the accumulation of dust and dirt in an industrial environment can have a significant impact on overall cable design and life span.

Dust is a significant hazard in an industrial environment. While many of the dust problems which are encountered currently are being overcome with specialized enclosures, the affordability of these enclosures will drop over time as optoelectronics are incorporated into hardened process control equipment.

Induced currents are a significant concern in an industrial environment. The electrically noisy environment which exists in a factory will induce currents in metallic armour and strength members in a fiber optic cable. While proper grounding will negate these problems, factories often have difficulty establishing a good ground plane. It is not uncommon to find several volts present on the ground plane and

sustained currents of over thirty volts have been recorded. The difficulty in establishing a ground plane in a factory demands that lightguide cabling systems make very limited use of metallic armour and strength members in a factory environment. In order to avoid induced currents in industrial environments, stronger, non-metallic cables will be required in the future.

Lightning is a common environmental hazard in many industrial locations. Due to the campus environment which is common in a factory, fiber optic cables are often installed aerially. While fiber optic cable does not attract lightning, metallic armour, strength members and supporting stringers do attract lightning. This requires that lightning protected cables be installed. Unfortunately, lightning protected cables are subject to the same grounding considerations which are a concern for induced currents. Ideally, self supporting, non-metallic cables should be used for all aerial installations in an industrial environment.

Rodents are a significant concern in a manufacturing environment. While significant efforts are made by most factories to control rodents and other pests, this is extremely difficult in the large, open environments which are common to the industrial workplace. The presence of rodents in the manufacturing environment demands that designers of both lightguide cable and apparatus address this significant problem.

Often lightguide cables are installed underground in tunnels or conduit and are subject to immersion in water and other fluids. In addition, these same cables often transition between buried, aerial and office

environments. Existing rodent protected cables work well in industrial environments. However, the varied environments through which these cables must pass call for a wide range of operating temperatures and tolerances to caustics and immersion.

Fiber optic apparatus is commonly exposed to rodent infestation. While lightguide cables are a common victim of gnawing by rodents, lightguide apparatus is a common nesting place for rodents. In order to prevent rodents from using lightguide apparatus as a nesting place, lightguide apparatus must be developed which is capable of preventing rodents from entering the unit. While this is common in splice enclosures, this capability is much less common in cross connect equipment.

Rodents pose a significant threat to lightguide cables and apparatus. Current technologies for rodent protection for fiber optic cable and apparatus is extremely useful in an industrial application. However, as manufacturers move fiber optics into increasingly hostile environments, rodent protection will become even more important.

Corrosives are common in many factory environments. Most notable are chemical processing facilities and refineries where large quantities of petrochemicals may be present in underground cable trays and tunnels. In addition, it is common to install fiber optic cables and apparatus very close to chemical processing equipment. In these environments it is not unusual to have corrosive materials splash on lightguide cables and apparatus.

Exposure to corrosive materials is common in an industrial environment. While efforts, such as conduit and avoidance of particularly hostile areas, can assist in protecting lightguide cables from exposure, it is a requirement of many industrial installations that fiber optic cables be capable of long term immersion in caustic and corrosive materials. This requirement places unique pressures on lightguide cable manufacturers to develop cable jacketing materials for the industrial marketplace which are resistant to the widest possible range of corrosive materials. While exposure to corrosive materials is not unique to the industrial marketplace, the predominance of these materials in a factory demands that special considerations be taken both in the manufacture and installation of lightguide cables in these environments.

Lightguide apparatus is often exposed to the same corrosives as lightguide cable. As manufacturers drive fiber optic communications systems closer to process control equipment, and as optoelectronic equipment is incorporated into process control equipment, lightguide apparatus will be required which is easily enterable and reconfigurable, yet capable of withstanding constant exposure to corrosive and caustic materials.

Corrosive materials pose significant threats to both lightguide cable and apparatus in an industrial environment. While great efforts are normally taken to contain caustic materials, it is not unusual for cables and enclosures to come in contact with these materials. In order to provide the level of support which the industrial marketplace will require in the future, higher

levels of resistance to corrosive materials must be achieved.

Physical damage is a common occurrence in an industrial environment. Physical damage generally falls into two separate categories. Those categories are incidents in which a fiber optic cable is expected to survive and those disasters in which it is unreasonable to expect any cabling to survive. Each of these situations places unique demands upon the lightguide cable developer.

Survival of physical damage is difficult in a factory environment. As previously mentioned, the use of metallic strength members in lightguide cable is suboptimal in a factory environment. However, fiber optic cable is expected to survive significant impacts which result from small industrial accidents and vandalism. While all accidents in a factory are not survivable, industrial customers are increasingly demanding communications systems which are capable of sustaining some level of impact without permanent damage. The requirement of survivability for lightguide cables, without the inclusion of metallic armour or strength members, places unique challenges before the designers of lightguide cables for the industrial marketplace.

Lightguide apparatus is being exposed to increasingly dangerous environments in factories. As manufacturers increasingly utilize fiber optic cabling solutions for direct process control, lightguide apparatus is being mounted extremely close to the process. This exposes the apparatus to impacts from personnel, falling

materials, automatic guided vehicles (AGVs) and material movement equipment. While all of these impacts are not survivable, it is critical that lightguide apparatus be capable of surviving a wide range of impact damage with little or no long term effect.

It is not possible to protect a fiber optic cable from all possible damage which can occur within a manufacturing facility. Damage from extremely large or heavy objects, or explosions, will occur from time to time. While it would be ideal to design a fiber optic cable which is capable of surviving any impact, this is an unreasonable expectation. However, when disasters do occur, it is critical that lightguide cable facilitate repair or replacement by allowing rapid entry for splicing or retermination.

Lightguide apparatus is a common victim of crushing blows in an industrial environment. While these accidents cannot be prevented, it is extremely important that lightguide apparatus be able to sustain significant impacts. Just as in automobiles, impact survivability is a critical concern for lightguide apparatus. It is impossible to predict or prevent the damage of lightguide apparatus. However, if lightguide apparatus is designed to protect fiber optic cable and connectors, the loss of the apparatus itself is less important. Just as in automobiles, it is critical that lightguide apparatus protect its valuable contents from damage, even at the expense of the apparatus itself. By protecting the lightguide fibers and connectors during a crushing impact, lightguide apparatus will greatly enhance the survivability of an industrial fiber optic communications system.

Physical damage represents the second most common cause (after electronics failure) of an industrial fiber optic network. While it is impossible to design lightguide systems which are capable of surviving all damage, it is critical that industrial cabling systems survive as wide a range of damage as possible. When a non-survivable impact does occur, lightguide cable and apparatus for the industrial marketplace must facilitate the rapid restoration of service.

The industrial environment is a hostile environment. Distance, temperature, dust, induced currents, lightning, rodents, corrosive materials and physical damage represent the most significant threats to a fiber optic communications system. While all of these situations may not be present in every manufacturing facility, it is common to have three or more of these conditions simultaneously. It is this simultaneity which poses the greatest challenge to the developer of fiber optic cable and apparatus.

The design of fiber optic cable for the industrial marketplace is a case of satisficing. While it may be possible to build fiber optic cable capable of surviving most, or all, of the environmental considerations which are present in a factory, it is likely that this cable would be extremely expensive and little used. Rather, it is critical that a wide range of fiber optic cables and apparatus be developed which are capable of supporting combinations of environmental concerns. For example, one cable may be developed which is capable of surviving rodents and caustic materials while another cable may be capable of surviving

caustic materials and high temperatures. By providing the widest possible selection of lightguide cable constructions to the industrial marketplace, a cable manufacturer will be able to address the majority of the environments which are present in a factory.

As with lightguide cable, lightguide apparatus must be capable of withstanding a wide range of environmental considerations. It is unreasonable to expect a single enclosure to meet all of an industrial customer's requirements for size, fiber count and mounting options in addition to a wide range of environmental concerns. However, by building a family of industrial enclosures which is capable of surviving within certain classes of environmental considerations, the industrial marketplace will be able to select the appropriate apparatus for a given situation.

The industrial workplace is inherently a dangerous environment for lightguide communications systems. However, lightguide cable is uniquely suited to the requirements of an industrial customer. While existing fiber optic cables and apparatus are currently being adapted to meet the needs of industrial customers, there is a significant gap between the requirements of the industrial marketplace and current lightguide communication systems offerings. By developing a broad based family of lightguide cables and apparatus suited to the particular needs to the industrial marketplace, lightguide cable and apparatus manufacturers will be able to take advantage of this significant and growing market.



Timothy K. Cahall is Manager, Fiber Optic Systems Engineering - Europe for AT&T Network Systems. He has over ten years of experience designing and installing industrial control systems and cabling systems in industrial environments. He resides in Hilversum, The Netherlands and is responsible for the deployment of AT&T's Industrial Distribution System in Europe.

## OVERVIEW OF WIRELESS BUILDING SYSTEMS FOR VOICE AND DATA COMMUNICATIONS

John Pryma

Anixter Bros., Inc.  
Skokie, Illinois

### ABSTRACT

Wireless voice and data systems address those installations where hard wiring is difficult to accomplish or where mobility of the equipment is a key consideration. Wireless can solve problems in buildings containing asbestos, historic structures which can't be modified and modern buildings where cableways have been filled.

Cordless telephones, wireless PBX ports and personal communications systems are voice applications. For data communications, wireless links may be used to bridge information between two buildings and to connect wireless nodes to Ethernet or Token Ring local area networks.

There are three types of wireless data systems: Infrared transmits line of sight; Microwave is configured in a microcell arrangement; and Spread Spectrum is very effective in transmitting data between and throughout buildings.

### Wireless Communications

Wireless communications are now being seriously evaluated for various voice and data applications. Installation is relatively easy, since hard wiring, if not completely eliminated, is significantly diminished. This makes for quick set up and almost instantaneous moves and changes.

#### Voice

Approaches for handling voice communications include cordless telephones, wireless PBX ports and various types of personal communications systems. These are described below:

Cordless Telephone: This is similar to the current home cordless phone but with more technological sophistication. The base station needs to be hard wired to the telephone system, but each of the cordless handsets can be used within several hundred feet of the base station. All of the extensions can be cordless, thus saving the cost of wiring each room with a phone jack.

For multiple dwelling units the base station can be at the curb, with each tenant having one or more cordless telephones.

Wireless PBX: For business applications the private branch exchange switch would have a number of wireless ports on it. This would allow a customer service representative or an executive to walk around the facility and make and receive telephone calls using a cordless handset.

Personal Communications: The cordless handset used at home, or in the office, could be carried about the city. Within convenient areas, telepoint locations would exist where an outgoing call could be made. This is analogous to a wireless pay telephone.

The above applications are illustrated in Figures 1-3. Table 1 compares range of service and cost of the customer premises equipment and the air time.

	PCN	VS.	CELLULAR
NETWORK	\$500/SUBSCRIBER		\$1000/SUBSCRIBER
INSTALLATION			
LIMITATIONS	20 MPH OR NO HAND-OFF		FULL SPEED HAND-OFF
PHONE NO.	UNIVERSAL		SEPARATE RESIDENTIAL/ CELLULAR NOS.
CELL SIZE	420 METERS MAX		10 MILE TYPICAL
PHONE COSTS	\$50-75 EST.		\$200 - \$600
CHARGES	\$20/MO.		\$30/MO.
	10-15 CENTS/MIN.		20-40 CENTS/MIN.

TABLE 1 - COST COMPARISON OF VOICE WIRELESS SYSTEMS

#### Data

If one can have a telephone conversation over a wireless connection, why not send data in the same manner? The answer to this question has spurred the development of wireless local area networks. These



networks are defined by two parameters. One parameter is the type of data, which can range from a 230 kb/s RS-232 serial interface to 10 Mb/s Ethernet and 16 Mb/s Token Ring. The other parameter is the wireless technology used, which typically is infrared, spread spectrum or microwave. These are defined below:

**Infrared:** This is a line-of-sight application using light emitting diodes for transmitting and photodiodes for receiving. Distances of 80 feet can be accommodated in an open office environment. The transmitter/receiver modules are positioned sufficiently high above the partitions, or suspended from the ceiling, so that the path is not inadvertently interrupted.

**Microwave:** The microcell approach is similar to cellular but is accomplished at microwave frequencies, which are much higher. Range is typically 40 feet, dependent on whether interior walls need to be penetrated or not.

**Spread Spectrum:** This is a radio technology which takes a high power transmitter output but broadcasts it over a very wide frequency spectrum. Figure 4 compares spread spectrum with conventional radio technology. Consequently, with spread spectrum, the signal is so spread out that at any frequency its signal strength at the receiver is almost in the noise level. Range is several hundred feet in an open office, warehouse or factory environment.

Figures 5-7 illustrate the topology of these networks. Table 2 compares per node costs.

	INFRARED	MICROWAVE	SPREAD SPECTRUM
BASE UNIT	\$2995	\$3995	\$2000
MAX USERS	6	32	30
REMOTE UNITS	0	5	30
REMOTE UNIT COST		995	1500
REMOTE UNIT COST TOTAL		4975	45000
TOTAL COST	\$2995	8970	\$47000
COST PER USER	\$500	\$299	\$1567

TABLE 2 - COST COMPARISON OF WIRELESS LOCAL AREA NETWORKS

#### Assigned Spectrum

Assigned spectrum is a very real consideration for wireless systems because radio frequencies are a very scarce commodity. Since the FCC only regulates

radio frequency spectrum, infrared systems can operate without licensing. This allows for worldwide implementation of this approach. On the other hand, the 18 GHz microwave approach requires licensing from the FCC. Spectrum is currently available in the U.S. and allocations are being considered in Canada and in several European countries. The availability of licensed spectrum precludes interference from other users, since there can only be one licensee in any particular location. Spread spectrum is a mixture of the two scenarios. The 902-928 MHz band has been allocated in the U.S., and very recently also in Canada, for industrial, scientific, and medical applications. This band can be utilized without licensing. Because spread spectrum transmits over a very broad frequency, interference with adjacent users is minimized. As a matter of fact, spread spectrum techniques were developed by the military to avoid eavesdropping on technical communications. A spread spectrum signal, when monitored by a receiver that is not part of the system, looks just like noise. Because of the above factors, all of the wireless systems discussed have a certain level of security associated with them and encryption can be provided for those applications where the utmost in security is required.

#### Local Area Networks

There are three factors driving the rapid commercial deployment of local area networks. These are the increasing computing power available on personal computers, the growth of the number of nodes connected into local area networks and standards activity, which has allowed for enterprise connectivity solutions.

The MIPS (millions of instructions per second) capability of computers is literally exploding. In 1989 computers had a capability of 1.8 MIPS and by 1993 this is projected to grow to 8 MIPS. At the same time the number of computers hooked into a local area network will grow from an average of 12 to an average of 30. This quadrupling of instructional and processing capability, coupled with the tripling of the number of users on a network, will result in an order of magnitude larger information transfer requirements across the network. In the near future 10 Mb/s Ethernet and 16 Mb/s Token Ring will not be enough and networks will evolve to run at Fiber Distributed Data Interface (FDDI) speeds of 100 Mb/s.

Successful wireless systems will conform to existing industry specifications, such as IEEE 802.3 for Ethernet and IEEE 802.5 for Token Ring. A separate standards group, IEEE 802.11, has been formed to develop wireless standards. Properly engineered

wireless systems are completely transparent to the user, which is an advantage, because only the hard to wire nodes need to be wireless.

### Conclusion

Since wireless communications, by nature use some portion of our scarce frequency spectrum, government regulations are usually involved. Hopefully, the 1992 World Administrative Radio Conference (WARC) will reach some harmonized standards, but currently available frequency allocations vary from country to country. Thus a wireless technique available in one country may not be available in another due to licensing restrictions.

To be successful, a technology needs real business applications. For the next several years projections are that wireless will be a niche market. It will replace wire in those applications which are difficult or very costly to wire. Until large volumes are reached, chip costs will be high, licensing considerations will inhibit growth and the bias towards hard wiring will need to be overcome. However, due to its flexibility wireless may be a very significant part of the wiring market by the end of this decade.

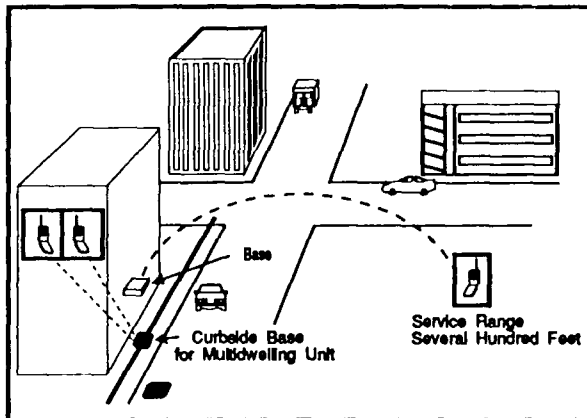


Figure 1 - Cordless Telephone

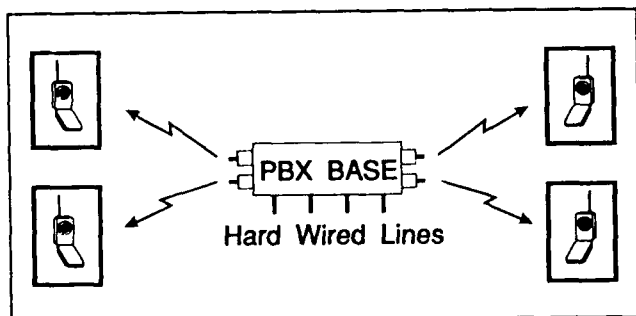


Figure 2 - Wireless PBX

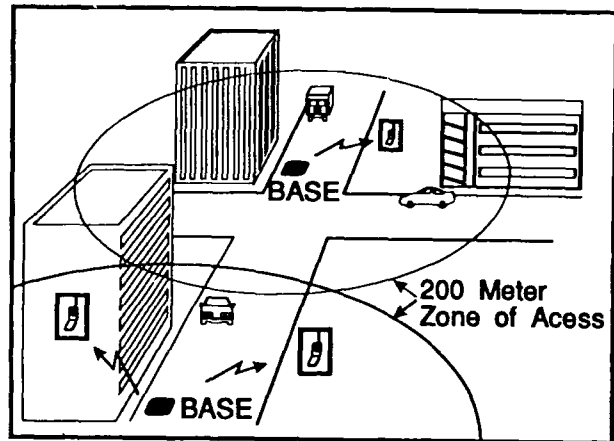


Figure 3 - Personal Communications

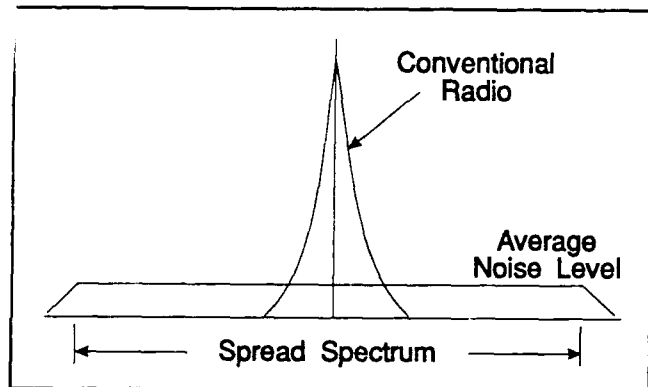


Figure 4 - Comparison between Conventional and Spread Spectrum Radio

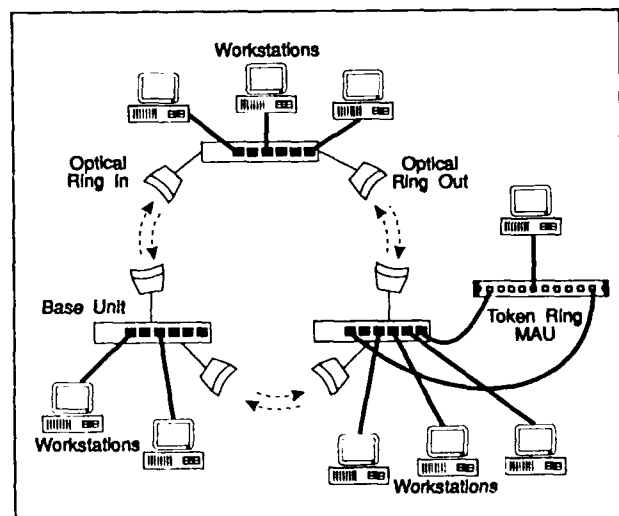


Figure 5 - Infrared Token Ring Network

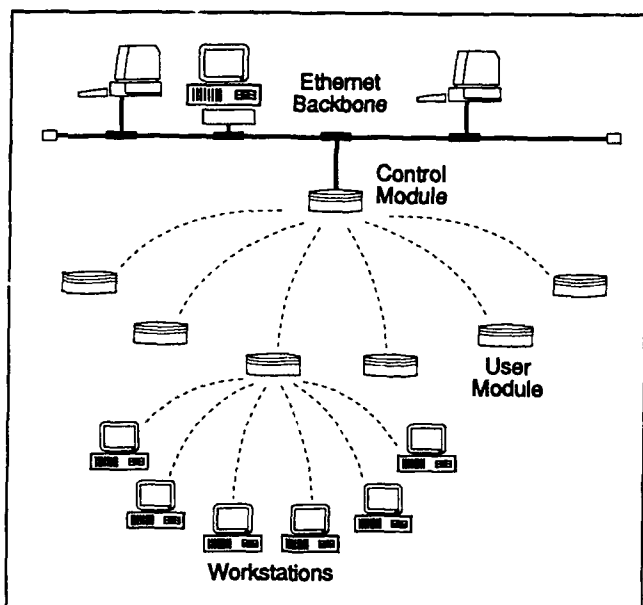


Figure 6 - Microcell Local Area Network



John Pryma is Vice President of New Technology for Anixter Bros., Inc., a worldwide wiring systems specialist for voice, video, data and power. John is responsible for evaluating new technologies and recommending those that provide state-of-the-art solutions for Anixter's customers. He holds a BS and an MBA from Illinois Institute of Technology, is a Registered Professional Engineer in Illinois and is an active member in ACUTA, BICSI, IEEE and TIA.

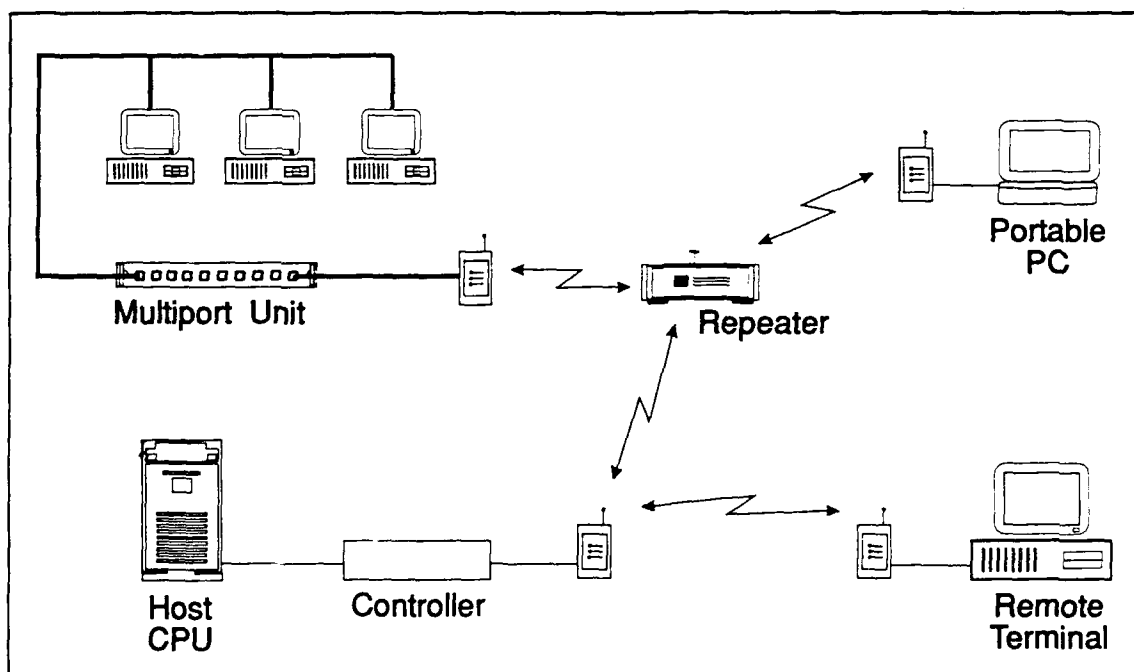


Figure 7 - Spread Spectrum Local Area Network

## WEAR RESISTANCE OF OPTICAL FIBER COATINGS USING A MODIFIED FALLING SAND TESTER

T. K. Vethanayagam

J. L. Smith

D. L. Taylor

Corning Incorporated, Corning, NY

### Abstract

As fiber-optic technology moves into the local-loop environment, the mechanical performance requirements of optical fiber coatings will become more stringent. Coatings will be required to withstand much more rigorous mechanical action such as rubbing, scraping, chipping or erosion during subsequent handling, installation, use and service.

Currently, the wear resistance of optical fiber coating is measured using a modified falling sand tester. The falling abrasive powder provides a range of eroding actions, from vertical impinging wear to tangential abrasive wear. This paper discusses the test procedure, and the parameters that affect the measurement results. Any deviation from the correct apparatus setting alters the measured values for wear resistance. The use of control fibers or metal wires to ensure measurement consistency is recommended.

### Introduction

Wear resistance of optical fiber coating is an indicator of the protective coating's ability to resist damage during subsequent processing, installation, use and service. Industry currently uses a modified ASTM falling sand test<sup>1</sup> to determine the wear resistance of optical fiber coatings. The method<sup>2</sup> has been recognized by the Telecommunications Industries Association (TIA) as a procedure for comparing wear resistance of optical fiber coatings.

There are two types of wear,<sup>3</sup> namely abrasion and impact. Wear by abrasion removes material by scratching or scoring; impact removes material by peening, mushrooming, cracking, chipping and spalling. The falling sand method tests optical fiber coatings for wear resistance under simultaneous actions of both abrasion and impact. The end product, namely the optical fiber, is tested under a simulated service condition. Abrasion refers to wear or loss of material caused by movement of an abrading material parallel to the surface. Abrasion resistance is improved either by introducing a very hard surface, or by introducing a soft and elastic, but tough, material that will deform rather than score. Impact is the type of wear that results from hammering effects perpendicular to the surface. Resistance to wear

by impact requires toughness, hardness, and strength.

The paper discusses the various parameters that influence the test results and highlights precautions necessary to ensure measurement consistency.

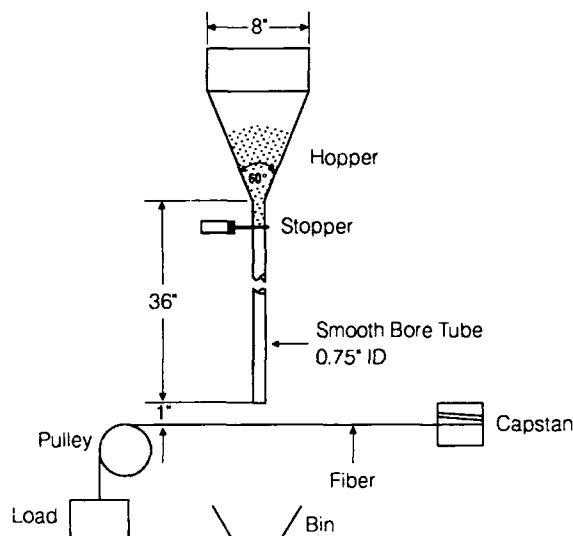


Figure 1: Schematic of the Modified Falling Sand Tester

### Experimental Procedure

A schematic of the testing apparatus is shown in Fig. 1. A hopper holds the alumina abrasive, and a guide-tube is attached to the hopper to allow for controlled abrasive flow. A stopper valve is used to open and close the flow of abrasive. The fiber sample is attached to a capstan and placed under the guide-tube in tension by hanging a load. A bin is placed right below the guide-tube to collect the falling abrasive.

Upon opening the stopper valve, a thin stream of abrasive falls on the taut fiber sample. The

Table 1: Frictional loss at the pulley for a 1000 gram load

Material	Diameter	Axle Type	Age	Fiber Tension (g)
Teflon®	1 inch	Teflon shaft	8 months	630
Aluminum	1 inch	Teflon shaft	New	860
Aluminum	4 inches	Ball-bearing	New	1000

abrasive flow constitutes both perpendicular and parallel streams with respect to the fiber. The test measures the amount of alumina abrasive required to abrade through the protective coating and cause failure of the fiber. The measurement is based on the wear mechanism that first damages the coating layer sufficiently to cause breakage of the underlying glass fiber. Apart from the fundamental properties of the coating, the measured wear resistance also is influenced by the mechanism of the coating removal, heat developed during the test, and friction between the abrasive and the coating. The size and material of the abrasive greatly influences the wearing process. It has been determined that, for the commercially available current coatings, an ANSI grit size #24 yields wear resistance values within a manageable 10 pounds.

The test parameters that may influence the final results fall into three categories, namely, fixable, verifiable, and uncontrolled. The fixable parameters include guide-tube material and size, stopper location, abrasive material and size, sample gauge length, and tension load. Fixable parameters have been standardized in an effort to minimize the variables. The verifiable parameters include frictional loss at the pulley, guide-tube verticality, fiber position in the stream, and temperature and humidity. Verifiable parameters are monitored to ensure reliability. The uncontrolled parameters include abrasive size distribution and shape, abrasive breakdown resistance, abrasive stream size and flow pattern, variations in abrasive characteristics from lot to lot and from supplier to supplier, and operator variability (the human factor). The uncontrolled parameters pose serious concerns in terms of achieving repeatable and reproducible results. This mandates the use of either control or reference samples in order to normalize data.

The effects of the various test parameters and the ways to account for them are discussed below. As far as the fixable parameters are concerned, the experiments were performed at set conditions. The verifiable parameters were tested to demonstrate the degree of their impact on the final results. A normalization procedure is recommended in order to compensate for the measurement variability due to the uncontrolled parameters.

#### Experimental Results and Discussion

The guide-tube material and size, stopper location, abrasive material and size, sample gauge length, and tension load were kept the same throughout this investigation. The test parameters that were analyzed included frictional loss at the pulley, guide-tube verticality, fiber position in the stream, abrasive size, abrasive suppliers, and humidity.

The mechanism of fiber failure is based on the flaw generated on the bare glass after coating removal. A load of 1000 grams (g) is equivalent to a tension of about 25 kpsi on the fiber. At this tension, a flaw of about 20 micrometers ( $\mu\text{m}$ ) on the surface will cause the glass to fail. Such flaws are easily formed on the glass by the falling alumina abrasive with an average particle size of about 750  $\mu\text{m}$ . Table 1 contains the data that illustrates the occurrence of frictional loss at the pulley. A sealed ball-bearing provides complete transfer of load to the fiber. In fact, it has been observed that the frictional loss did not affect the measured mean of coating wear resistance significantly, although the measurement sigma was higher for a lower load of 500 grams.

Two important characteristics of the abrasive stream that influence the measured value are the momentum of the particles and the stream density. The abrasive falling down the guide-tube experiences both sliding action along the tube walls and free falling in the core region. The sliding action, though retarding the speed of flow, has a tendency to cause a flow of higher density. In other words, the momentum of the particles is reduced but the number of particles striking the fiber is increased, resulting in contrary bias on the measured value of wear resistance. Figure 2 shows the effect of guide-tube verticality on the measured coating wear resistance for grit #24 and #30. It is believed that the guide-tube verticality is an important factor, although its effect appears to be slight. All the data reported in this paper were made at the vertical position. The verticality is checked with a level

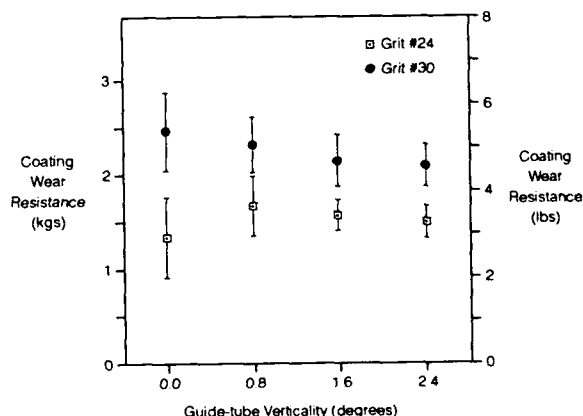


Figure 2: Effect of Guide-tube Verticality on the Measured Coating Wear Resistance

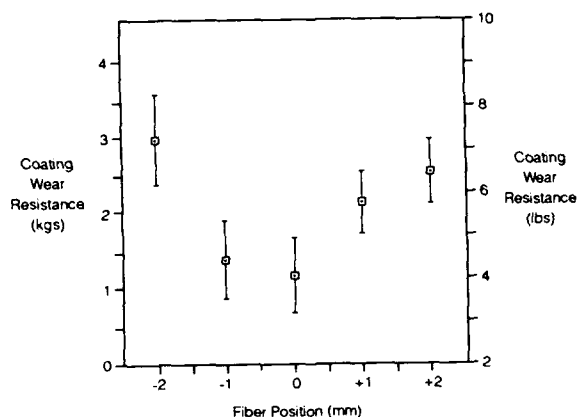


Figure 3: Across-the-stream Mapping to Determine the Center of the Stream

prior to testing.

The surfaces of the falling abrasive are rough and will touch only a limited number of small, discrete areas. The real area of contact is generally very much smaller than the apparent geometric area. The stream falling on the fiber is about 6 millimeters in diameter. The fiber's position in the stream significantly influences the measured value. Figure 3 illustrates the trend over the cross-section of the stream. The point of minimum is taken as the center of the stream, and all the tests were performed at that setting.

Figure 4 contains information on the effects of grit size. The finer grit (#30) results in higher values for the wear resistance. Again, there is a trade-off between the momentum and stream density, leading to the observed differences. Figure 5 addresses the variations observed using abrasives from various suppliers. The differences in size distribution and particle shape contribute to the observed differences in the measured coating wear resistance. Table 2 contains information on the size distribution for abrasives from three commercial suppliers. Continuous usage of the abrasive leads to abrasive size break down and shape changes. Table 3 contains data on the break down performance of a commercial abrasive. Based on the coating wear resistance values obtained from the abrasives after repeated use, it appears that a batch of abrasive is reusable up to nearly 500 times. Figure 6 demonstrates the usefulness of this technique to compare optical fiber coatings for their wear resistance

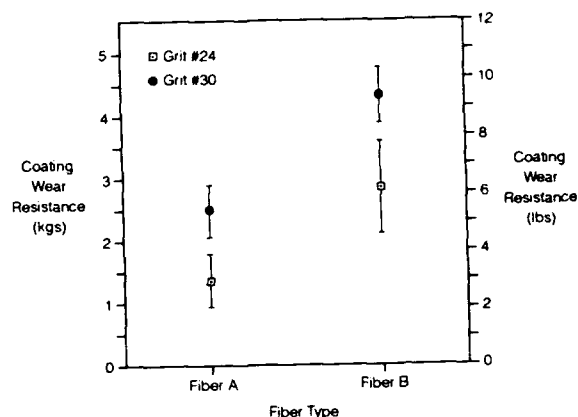


Figure 4: Coating Wear Resistance for Different Abrasive Sizes from Supplier B

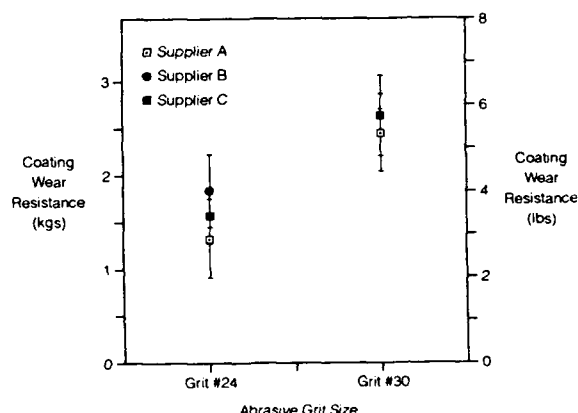


Figure 5: Comparison of Coating Wear Resistance of Fiber A for Abrasives from Various Suppliers

performance. Fiber B displays a higher resistance than fiber A. The ratio of their resistances is about 1.8.

The effect of humidity on the measured coating wear resistance was investigated from 30 to 80% RH. This range includes the standard ambient prescribed by the Electronics Industries Association<sup>5</sup>. The samples were preconditioned at the specified humidity, and tested at ambient. Figure 7 contains the data. It is evident that

Table 2: Size distribution of grit #24 for various suppliers (given in %)

	+18 mesh	+20 mesh	+25 mesh	+40 mesh	-40 mesh
ANSI Spec	0 - 25	35 - 65	25 - 55	10 - 40	< 5
Supplier D	0	23.2	61.3	15.4	0
Supplier E	0.1	9.4	33.0	53.4	4.2
Supplier A	0	8.9	47.8	43.3	0

Table 3: Break-down characteristics of abrasives on repeated use (given in %)

	+18 mesh	+20 mesh	+25 mesh	+40 mesh	-40 mesh
ANSI Spec	0 - 25	35 - 65	25 - 55	40 - 40	< 5
Supplier A (as-received)	0	8.9	47.8	43.3	0
Supplier A (after 300 uses)	0	8.1	49.9	41.8	0.1

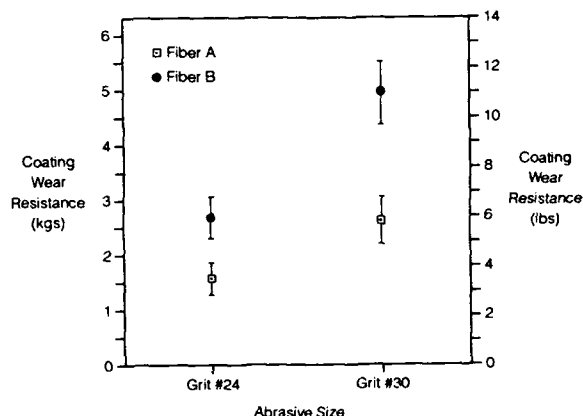


Figure 6: Comparison of Coating Wear Resistance of Fiber A & B using Abrasives from Supplier C

the mean of the tested fiber (fiber A) was not influenced by the humidity; however, the higher humidity resulted in higher measurement sigma<sup>6</sup>.

Only relative (non-absolute) information is possible due to the measurement variability introduced by the uncontrolled parameters. Control samples with an assigned wear resistance must be used in order to normalize the measured

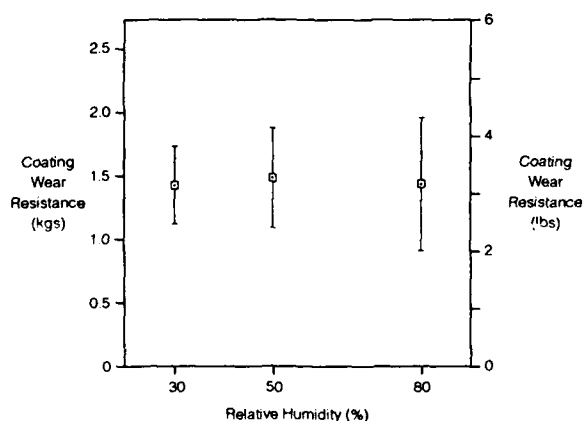


Figure 7: Effect of Humidity on the Measured Coating Wear Resistance of Fiber A

data within a laboratory. The authors<sup>7</sup> have previously published data, using a linear normalization procedure, on the effect of various aqueous and thermal environments on the coating wear resistance of Corning Titan<sup>®</sup> fiber. However, for the purposes of comparing data between laboratories, it is essential to establish a calibration procedure. Corning has evaluated metal wires as potential calibration markers. Table 4 includes the observations made on three metal wires. The diameter and the tensile strength of the metal wires coupled with the wear resistance determine the amount of abrasive required to cause failure of the wires.

Table 4: Abrasion resistance of metal wires at a 1000 gram load

	Mean (kgs)	95% C.I. (kgs)
Molybdenum, 127 $\mu$ m	> 8	--
Tungsten, 75 $\mu$ m	0.62	0.22
Tungsten, 100 $\mu$ m	8.56	0.53
Nichrome, 143 $\mu$ m (Ni:Cr:80:20)	5.45	0.68

In order to ensure that the load is transferred to the wire, the frictional loss at the pulley is critical. As suggested before, a sealed ball-bearing provides negligible loss.

In any given situation, the relative importance of the different processes causing abrasion and impact will depend on the conditions of operation to which the fibers are subjected. It is important to recognize that the falling sand tester checks the fiber for only the worst of the two failure modes, namely, abrasion and impact. Abrasive wear losses<sup>8</sup> are most pronounced when the particles slide against rough surfaces where plastic flow may lead to microcutting and viscoelastic deformation. This can result in tearing, cracking, or fatigue. At the other extreme, when the particles slide against smooth surfaces (interfacial sliding), frictional work is dissipated in a very narrow interfacial zone. Both viscoelastic deformation and interfacial sliding processes lead to heat generation that may ultimately result in surface oxidation, thermal degradation, or actual melting. Thus, the main complication during abrasive wear is the energy transfer that often occurs from the abrasive particles to the polymer coating; the amount and type of transfer depend on the conditions of

abrasion imposed (momentum of particles, stream density and temperature).

The impinging particles (impact wear) cause viscoelastic and plastic deformation of polymeric materials. Material is worn away due to tearing off of the lips and fibrils produced by the impinging particles. Brittle materials splinter when subjected to this kind of particle bombardment. Deformable polymers are generally more resistant to this type of wear because they have more elastic deformability.

#### Conclusion

The modified falling sand test checks the optical fiber coatings for the worst of the two failure modes, namely, abrasion and impact resistance. This test is a good tool to compare optical fiber coatings for wear resistance. However, control fibers should be used to ensure wear resistance values that can be used for the purposes of comparison. Use of metal wires as calibration (reference) markers is a possibility to compensate for the existing measurement variability between laboratories, and render measurement reproducibility.

#### Acknowledgement

The authors wish to thank Leslie Branigan and Stuart Saikkonen for their assistance in making this work possible.

#### References

1. "Abrasion resistance of coatings of paint, varnish, lacquer, and related products by the falling sand method", D 968, American Society for Testing and Materials, Philadelphia, Pa. 1990.
2. "Test method for measuring relative abrasion resistance of optical waveguide coatings and buffers", EIA RS-455-66, Electronics Industries Association, Washington, D.C.
3. "Mechanical characteristics of materials" in Materials in industries, ed. W. J. Patton, Prentice-Hall, Inc., Englewood Cliffs, NJ, 1988, 1984.
4. "Specifications for the size of abrasive grain - grinding wheels, polishing and general industrial uses", B74.12, American National Standards Institute, Inc., New York, NY, 1982.
5. EIA/TIA-455A, "Standard test procedure for fiber optic fibers, cables, transducers, sensors, connecting and terminating devices, and other fiber optic components", EIA Standards Promotion, 2001 Eye Street, N.W., Washington, D.C.
6. D. R. Dreyer, S. L. Saikkonen, T. A. Hanson and B. A. Linchuck, "The impact of relative humidity on mechanical test results for optical fiber", Fiber Optics Reliability: Benign and Adverse Environments, ed. R. A. Greenwell and D. K. Paul, volume 1366, pp 372-79, SPIE - The International Society of Optical Engineering, Bellingham, WA, 1990.
7. T. K. Vethanayagam, B. A. Linchuck, D. R. Dreyer, J. R. Toler, L. G. Amos and D. L. Taylor, "Mechanical performance and reliability of Corning Titan<sup>SM</sup> SMF CPC5 fiber after exposure to a variety of environments", *ibid.*,

1366, pp 343-50, 1990.

8. "Abrasion and wear" in Encyclopedia of polymer science and engineering, ed. J. Kroschwitz, 2nd edition, volume 1, John Wiley & sons, NY, pp 1-35, 1985.



Thirukumar Vethanayagam is a senior product engineer responsible for coating-related performance testing of optical fibers. He joined Corning in 1990 and has worked on projects involving the long-term environmental effects on fiber performance. He also is participating in the efforts of the Telecommunications Industry Assoc-

iation (TIA) Working Group 6.6.7 in developing the coating abrasion resistance test procedure, of which he is the author. Vethanayagam holds a doctorate degree in ceramics from Alfred University, and received both the master's and bachelor's degree in metallurgical engineering from Indian Institute of Technology. He is a member of American Ceramics Society, Society of Photo-Optical Instrumentation Engineers, American Society of Metals and Materials Research Society.



Jeffrey L. Smith is an electro-optic technician responsible for research projects related to environmental and mechanical performance of optical fiber products. He joined Corning in 1989 and has been involved with the development, design, implementation and documentation of new or enhanced environmental and mechanical test methods and equipment. Smith holds an associate's degree in electronics technology from Pennsylvania College of Technology and currently is pursuing a bachelor's degree in electrical engineering.



Donna L. Taylor is manager of Waveguide Product Engineering Laboratory. During her 20 year career with Corning, she has held a variety of positions. She is the author of numerous research papers summarizing her work on static fatigue, tensile testing and water integrity of optical fibers. Taylor holds a bachelor's degree

in ceramic science from Alfred University. She is president of the Twin Tiers chapter of the Society of Women Engineers, and a member of SPIE and the American Ceramic Society (ACS).



## COST EFFECTIVE LIGHTNING PROTECTION FOR FIBER OPTIC BASED COMMUNICATION SYSTEMS

CHARLES DAVIS

ROY B. CARPENTER, JR.

ENTERGY CORPORATION  
NEW ORLEANS, LOUISIANA

LIGHTNING ELIMINATORS & CONSULTANTS, INC.  
BOULDER, COLORADO

**Abstract** - Fiber optic based communications systems are very attractive to the electric utility industries, because they can be deployed along with existing right-of-ways where transmission systems already exist. One of the more cost-effective ways of implementing a system, particularly for new construction, is to use a wire commonly known as Optical Ground Wire (OPGW). This concept involves the encasement of the optical fibers within a wire jacket which is also used for "static line" or overhead shielded wire.

Over the past few years, more and more of these systems are being implemented. As more are installed, a significant weakness is manifesting. The optical fibers are failing, predominately as the result of lightning activity; the higher the isokeraunic number for a given area, the greater the failure rate. In some areas, the problem is so significant that the system may have to be replaced. The situation is a classic paradox. The shield is deployed to intercept the strikes, but the strikes cause damage to the optic fibers therein.

This paper describes the concept used to prevent lightning damage to static lines enclosing OPGW and the results achieved by this approach.

### INTRODUCTION

In 1987, Mississippi Power & Light rebuilt thirty-six miles of 115 kV transmission line north of Jackson, Mississippi, upgrading it to 230 kV. The old conductors were used to pull in the new conductors and the thirty year old 5/16 inch shield wire was used to pull in a new 7/16 inch EHS galvanized strand in the static wire position.

In 1989, this same technique was proposed for installation of overhead fiber optic ground wire (OPGW) along the original 115 kV system west of Jackson, Mississippi. This method would have reduced installation cost of the fiber optic cable when compared to the costs of removal and separate installation.

The installation contractor and Mississippi Power & Light engineers quickly discovered that the 5/16 inch galvanized high strength steel static line had sustained substantial damage. Numerous failures of the static line occurred during the initial installation of the OPGW on the east end of the project and it was necessary to change the installation method. The old static wire was removed span-by-span and pull ropes were used to install the fiber optic wire.

During the great ice storm of 1989, there were seven static line failures involving 5/16 inch galvanized HSS wire in the same geographical areas as the OPGW route. Investigation of these failures showed evidence of substantial overheating as would occur with high current lightning strokes.

Service personnel and residents in the area reported witnessing heavy, long duration lightning strokes to the static wires. Occasional failures of the old bail-type Hulett insulators had shown evidence of flashovers which were thought to be lightning related. A study by the State University of New York, which operates the EPRI Lightning Detection Network, showed that in this area there were a greater number than average strikes per square kilometer and higher than average first stroke intensity, which correlated with the previously stated observations.

It appeared that the static wire was functioning as designed, that it was intercepting lightning strokes, many of which were striking at mid-span. The fiber optic cable had been specified to match the characteristics of the existing 5/16 inch HSS galvanized strand based on the performance of the previously mentioned shield wire north of Jackson.

There was concern that lightning damage might penetrate the alumoweld strands and the aluminum tube surrounding the fiber optic strands. Consequently, the fiber optic network would become unreliable. Removing the existing OPGW and replacing it with a higher 12T cable was considered but the estimated cost was \$700,000. The decision was made to go with a lightning protection system.

### Discussion

Not all lightning strikes cause damage to the overhead shield wire. In fact, only a small percentage of them seem to be of sufficient magnitude to influence the encased fibers. From Figure 1, it is obvious that the high energy strikes occur less frequently. Further, the higher the energy, the less frequently a strike will occur. In spite of this fact, history has proven that the risk of a damaging strike may be far too high to be considered acceptable.

The risk of damage to a fiber optic line from a direct strike is a function of at least four factors:

1. The isokeraunic number for the area. (This is the number of thunderstorm days per year.)

2. The length of the encased fiber optic line.
3. The energy withstanding capability of the line.
4. The energy contained within the strike collected by the encased fiber optic line.

These factors fall into two categories:

1. The probability of a strike to the line.
2. The probability of damage to the fiber optic line given that a strike to the line has occurred.

The risk of a strike is directly proportional to the isokeraunic number and the length of the line.

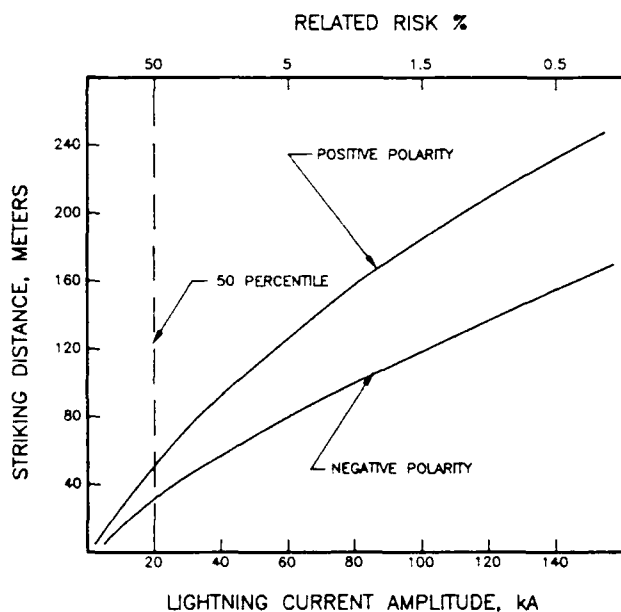


FIGURE 1. STROKE CURRENT RISK ASSESSMENT

The probability of damage to a fiber optic line, given that a strike has occurred, is directly proportional to the energy in the stroke and inversely proportional to the heat dissipation capability of the given wire. For example, consider a wire that has been qualified to function without failure up to a 60,000 ampere peak current. Since the average U.S. location will receive 100 strikes for a 100 mile length of line, we can expect five of these to be potentially damaging strikes. Texas, Louisiana, Mississippi, Georgia and the Carolinas will have twice that number, and central Florida will have three times as many. The risk incurred is obviously far too high if 60,000 amperes is the maximum peak energy that can be tolerated. If the maximum safe energy is increased to 100,000 amperes peak current, the risk of damage is still at least three damaging strikes per year for each 100 miles of fiber optic line in

the South and Eastern United States. The risk can be three times this number in other parts of the world.

From these data, it becomes obvious that there is a significant risk that lightning will strike the transmission line static wire and that an unacceptable number of these strikes will contain enough energy to induce damage to the line. The risk may be considered acceptable in the northern latitudes but must be reduced or eliminated in about fifty percent of the U.S. and other areas of equal or greater risk.

The protection problem centers around the primary purpose of the fiber carrier, the static line. Its purpose is to be a preferential strike termination in order to protect the nearby phase conductors. Therefore, strokes are to be expected and indeed encouraged to terminate thereon.

From the foregoing discussion, it is apparent that only the very high energy strikes are a threat. The lower energy strikes, those below the line tolerance level, are of no concern to the optical fibers as well.

One obvious protection option is to increase the withstanding capability of the static line itself by adding more steel strands. Unfortunately, the cost of so doing rises exponentially with the associated reduction in risk. As the static line size increases, its weight also increases, and the static and dynamic loads on the supporting structures increase. This option is not economically acceptable.

Recent developments within the lightning protection industry have provided a solution to this problem:

The Spline Ball Ionizer<sup>®</sup> (SBI<sup>™</sup>) is a UL listed device designed to dissipate the storm induced energy from a facility by the "Point Discharge" mechanism, thus reducing the probability of a strike to that facility. It is based on the Dissipation Array<sup>®</sup> System which collects and dissipates the storm induced charge in the area of concern, slowly, through point discharge or ionization. Unlike the Dissipation Array System which prevents all strikes to a facility, the SBI prevents most strikes but in an intense storm will act as a "collector/diverter". The SBI thus serves two functions in the protection of fiber optic line, i.e., (1) it greatly reduces the probability of a strike and, (2) should it fail to prevent a strike, the SBI, rather than the fiber optic line, will become the terminus of the potentially damaging stroke. Figure 2, depicts a typical Spline Ball Ionizer module.

Lightning rod performance data indicates that the following factors must be present to assure 100% effectiveness as an air terminal in collecting strikes (refer to Figures 3 and 4):

1. The air terminal generates a streamer which moves toward the step leader.
2. The streamer must enter the strike zone.
3. The streamer must be predominate within the strike zone.

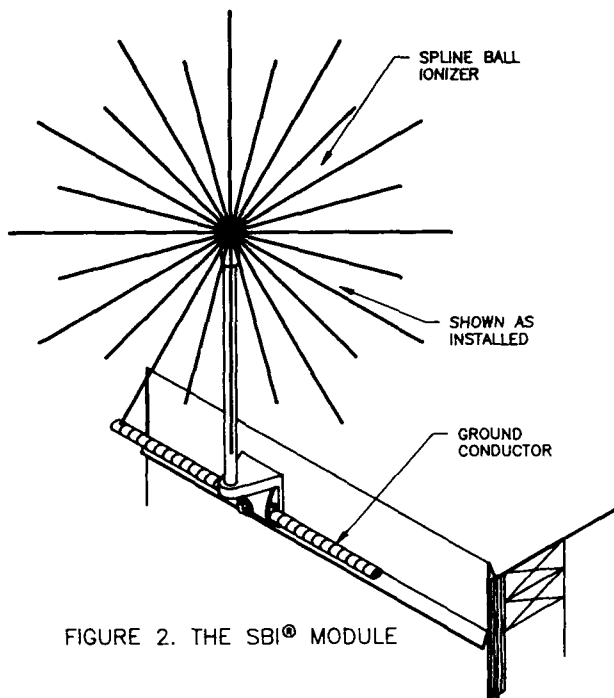


FIGURE 2. THE SBI® MODULE

4. To generate the required streamer, the air terminal must present a point oriented toward the leader; efficiency is related to the angular difference between the point of the air terminal and the leader.

Because the SBI provides a point oriented at least every five degrees and a full 120 degrees in elevation, it will collect lightning leaders from any azimuth or elevation angle within its sphere of influence if it is within the strike zone. Given the foregoing premise, the next step is to define the SBI "Sphere of Influence" in the collection mode. To that end, we can draw upon the work of several atmospheric physicists who claim that the lightning leader follows a random or unpredictable path until it reaches a point above earth called the "Point of Discrimination" as illustrated in Figure 4. At that point, the strike target has been selected. The voltage on the leader tip is approximately  $10^8$  volts. The related field strength can exceed 100 kV/meter of elevation above earth or between the leader tip and an object on the earth that it will strike. Upward moving streamers from several sources "reach" toward the leader and compete for it. The first streamer to reach the leader closes the circuit and receives the stroke. The question is, how far will the streamers reach and/or how far will the stroke reach?

Again, the atmospheric physicist has provided some answers[2]. Photographs taken over a period of years by various researchers indicate that the downward moving leader usually travels between 30 to 40 percent of the last step (or strike distance) before being joined by the successful upward moving streamer. They also indicate that the "step distance" can vary from a low of about ten meters to a high of 160 meters for the common negative

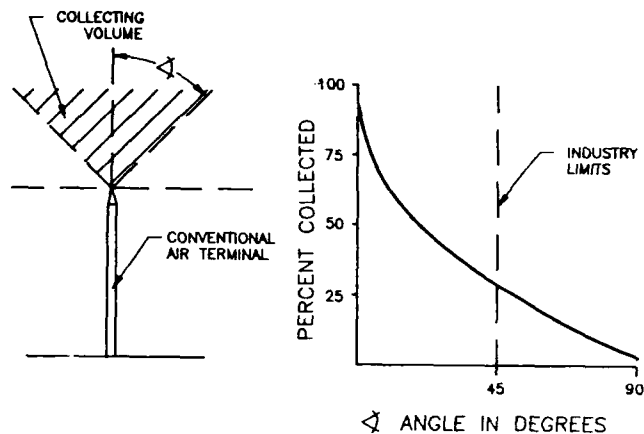


FIGURE 3. STROKE COLLECTION EFFICIENCY, CONVENTIONAL AIR TERMINALS

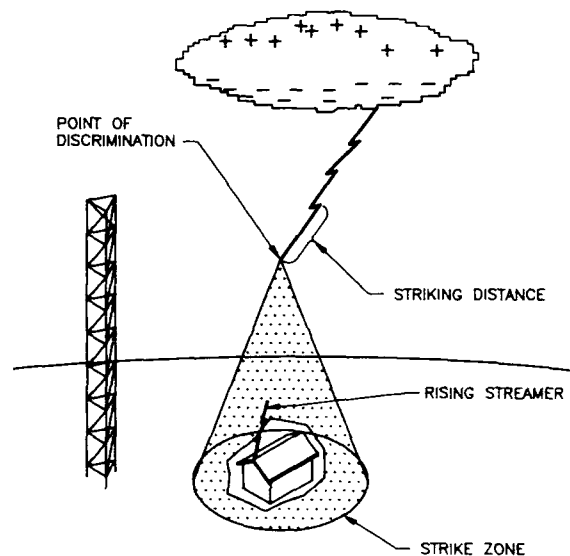


FIGURE 4. STRIKE ZONE FACTOR

stroke, or as much as 240 meters for the unusual positive stroke. Refer again to Figure 1.

(Note: Lightning leaders move in steps from the cloud toward earth, therefore, the "step distance" is the length of one step. The length of those steps is a function of the energy in the descending leader. Refer again to Figure 4.)

From these data, we find that the "Striking Distance" is approximately equal to the "Step Distance" and is also a function of the energy in the leader.

In summary, the body of available scientific data suggest that the higher the energy in a downward moving step leader the farther the Point of Discrimination is from the earth's surface, or the longer its reach. The lower energy leaders have a limited reach, often as low as ten to fifteen meters.

Since only the higher energy strokes are of concern to fiber optic systems, the short range, lower energy strokes can be neglected. From the

foregoing factors, it is now obvious that there is a requirement for a protective system that will augment the protection provided by the static line and will divert the higher energy strikes to a preferred terminal, thus preventing them from terminating on the OPGW static line. As mentioned earlier, the Spline Ball Ionizer® accomplishes this objective by presenting a streamer point every five degrees in both azimuth and elevation from which a lightning leader can enter its sphere of influence.

To illustrate this application, consider the results of the 60,000 ampere stroke discussed earlier. Although the probability of exceeding this level is less than five percent, it is still too high. Figure 1, indicates that strokes of this magnitude and greater will reach or have a striking distance of at least 250 feet.

The Spline Ball Ionizer will collect the 60,000 ampere stroke and those of greater magnitude from a range of 250 feet or greater provided there is no preferential streamer point to compete with it. As illustrated in a prior paper[4], if there are many pointed objects or sharp objects within the strike zone, they will compete for the leader. The longer streamer, or the closest of these to the leader, usually wins the competition and collects the stroke.

## CONCLUSIONS

Since installation of the lightning protection system described in this paper, Mississippi Power & Light has not experienced a lightning related fiber optic outage for the past two years.

It seems evident that a properly deployed SBI (or SBI's) can provide the required protection for OPGW lines. At the very least, it will significantly reduce the probability of damage. The exact impact is a function of installation parameters, e.g., number of SBI's or their distance apart. Figure 5, presents an example which illustrates the impact of implementing the system on a transmission line where the spans are approximately 600 feet in length.

Using a conservative estimate for the radius of the SBI collective mode sphere of influence and a conventional transmission line, these data indicate that at least 500 feet of typical 600 foot span length would be protected by the use of one module installed in the center of each supporting structure. This indicates that less than 100 feet of that span would be exposed to a damaging strike if the withstanding limit of the static line was 600,000 amperes. Strokes significantly above that level would also be collected because of their extended strike zones, leaving less exposure to those strokes.

It is interesting to note that the Grand Gulf Nuclear Plant, which is served by this fiber optic route, had previously experienced lightning related outages. There has not been a lightning related outage at the plant since the installation of a Dissipation Array® System two years ago.

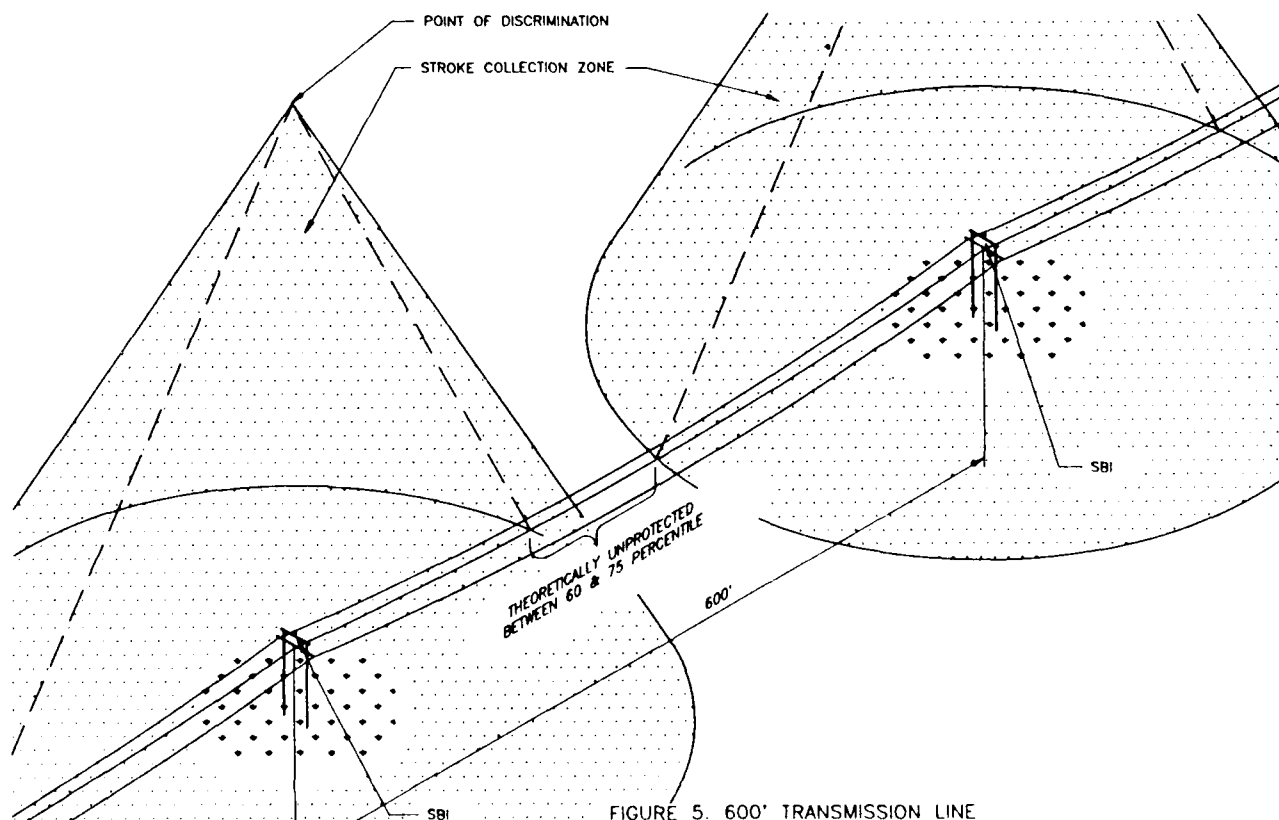


FIGURE 5. 600' TRANSMISSION LINE

#### REFERENCES

- [1] R.H. Golde , Lightning Protection, Edward Arnold Publishers, 1973.
- [2] Journal of the Franklin Institute, Vol. 283, No. 6, June 1967.
- [3] Martin A. Uman, et al, Lightning, McGraw-Hill, 1969.
- [4] Martin A. Uman, The Lightning Discharge, 1987.



Roy B. Carpenter, Jr. is Chief Executive Officer and Consultant of Lightning Eliminators & Consultants, Inc., Boulder, Colorado, U.S.A. Mr. Carpenter has had more than 44 years of education and experience in electrical engineering and systems engineering, devoting the past 19

years to lightning protection and grounding systems. He holds many patents, and his previous job titles have included Chief of Apollo Reliability, Director of Reliability and Maintainability for the Air Force Electronics Systems Division, and Technical Advisor to the USAF NATO Advisory Group. He is a life member of IEEE and has authored many papers on systems engineering, safety, grounding, lightning protection, and power and data line conditioning.



Charles R. Davis was born in Shreveport, Louisiana. He received his B.S.E.E. from Louisiana Tech University in 1973 and is a candidate for an M.S.I.E. from Mississippi State University in December 1991. He is the Manager of Transmission Line Project Engineering for Entergy Corporation in New Orleans, Louisiana. He has experience with HV and EHV substation equipment, power system protection,

and transmission line design and construction. His research interests include cost reduction and organizational efficiency. Mr. Davis is a member of the I.E.E.E. and is a Registered Professional Engineer.

# Dynamic Stress Analysis of Optical Fibers in Splice Closures in the Aerial Plant

P. B. Grimado and R. A. Frantz

Bellcore, Morristown, New Jersey, USA

## ABSTRACT

A nonlinear dynamic finite element model has been developed to examine mechanical reliability issues for optical fiber configurations in splice tray organizers. Vibration testing of splice closure assemblies is typically conducted at high frequencies and low acceleration levels. However, it was found in a previous study that splice closures can experience large inertial loads at low frequencies (0.5 - 5 Hz) when deployed in the aerial plant. The finite element model was verified by comparing computed and experimentally obtained mode shapes at high frequencies. The model was then used to analyze optical fiber structures found in several commonly used splice closure assemblies when exposed to low-frequency, high acceleration excitations. The examined fibers were proven to be sufficiently robust to prevent any mechanical fiber failures. However, in some splice tray organizers large displacement excursions occur and could be a source of some handling difficulties if excess fiber becomes tangled and intertwined.

## 1. Introduction

The dynamic environment experienced by the aerial plant represents one of the most stringent scenarios for imparting high inertial loads and mechanical stress to fiber optic cables. In a previous paper [1], the dynamic characteristics of aerial fiber optical cables (FOC) were evaluated for a number of different conditions capable of inducing periodic motions of the aerial plant. An ice-covered strand/FOC configuration was considered for wind galloping in a steady 64 KMH (40 MPH) crosswind. Another plausible scenario involved the breaking of a support pole 6 feet above the ground as a result of vehicular impact.

It was determined from these analyses that the pole removal scenario imposes the most severe acceleration levels on splice closures attached to the support strand. A peak acceleration of 13g is immediately realized just as the severed pole impacts the ground. This acceleration, as shown in Fig. 1, is heavily damped, reaching insignificant levels after about 20 seconds. A spectral analysis of this acceleration is given in Fig. 2. The dominant frequency is 0.8 Hz with a significant component at 2.5 Hz.

An issue not addressed in these analyses is the fate of the optical fibers contained in aerial splice closures where the fibers are arranged in splice tray organizers. It is important to examine the effect of dynamic inertial loads arising from the aforementioned disturbance on the mechanical integrity of these fibers.

A typical vibration test specification [2] imposes a steady state vibration in the frequency range 10-55 Hz with an amplitude of 0.077 cm (0.03 in). This translates into a maximum acceleration of 9.3g at the maximum frequency of 55 Hz. In the aerial plant, however, higher accelerations at lower frequencies can be encountered. Low frequency, high acceleration testing entails large

amplitude displacements and can be cumbersome and costly. Consequently, a dynamic optical fiber finite element program was developed to analyze the response of optical fiber configurations in typical splice trays. The program accounts for the nonlinear behavior associated with large displacements and the restricted movement of the fibers within the dimensional constraints of the splice tray organizers.

Mock-ups of the splice tray organizers used in the analysis were constructed, fiber was installed, and the assemblies were subjected to vibration over the range 10-60 Hz. However, by using an amplitude of 0.19 cm (0.075 in), accelerations up to 27g were obtained. The 13g peak acceleration cited above was obtained at a frequency of 42 Hz. Both high-speed stop-action photographs and time exposures were taken at several frequencies (accelerations).

In this presentation a description of the finite element model is given in Section 2. In Section 3, the optical fiber structures found in splice tray organizers and the idealization of these geometries to the finite element model are presented. The results of computer simulations at 27g and 60 Hz are compared with photographs of actual vibration tests in Section 4. Section 5 contains the results of computing the state of stress of optical fiber configurations contained in splice tray organizers when subjected to the high accelerations at low frequency that can arise in the aerial plant. Vibrational mode shapes, swept areas, and maximum tensile stress histories are presented for several fiber configurations. Finally, Section 6 includes a summary and conclusions.

## 2. Finite Element Model

The optical fiber configuration is considered an elastica with small deformations and large displacements. Initial optical fiber configurations with curvature are constructed by a series of straight beam elements oriented end-to-end approximating the curve.

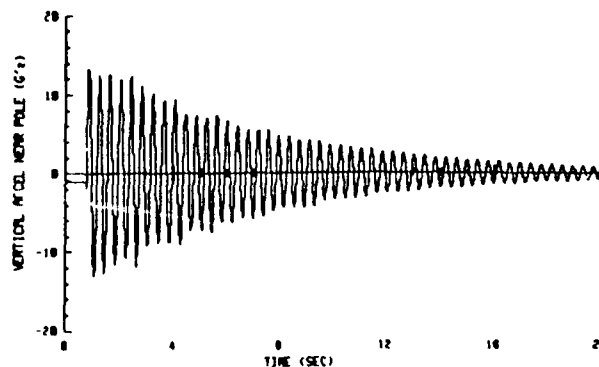


FIG 1: VERTICAL ACCELERATION OF AERIAL SPLICE CLOSURE FOR POLE REMOVAL

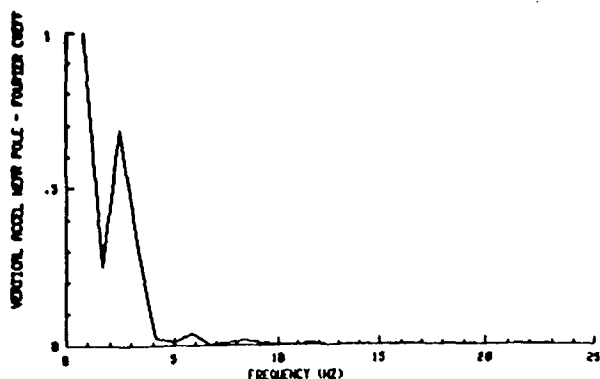


FIG. 2: SPECTRAL DISTRIBUTION OF VERTICAL ACCELERATION FOR POLE REMOVAL

A single beam element, Fig. 3, is two-dimensional having 2 nodes, one at each end, and 3 degrees of freedom per node - an axial extension, a transverse deflection and a rotation. The corresponding nodal forces are an axial force, a bending moment and a shear force. The expression for the total energy,  $\Gamma$ , of the beam element is

$$\Gamma = \int_{x_A}^{x_B} \left\{ \left( \frac{EI}{2} \right) \left( \frac{d^2 w}{dx^2} \right)^2 + \left( \frac{AE}{2} \right) \left( \frac{du}{dx} \right)^2 + C \left( \dot{u}u + \dot{w}w + \dot{\phi}\phi \right) + \rho \ddot{u}u + \rho \ddot{w}w - f_x u - f_y w \right\} dx \quad (2.1)$$

$$- P_A u_A - V_A w_A - M_A \phi_A - P_B u_B - V_B w_B - M_B \phi_B,$$

where a dot over a variable indicates partial differentiation with respect to time and

- $w(x)$  = transverse deflection
- $u(x)$  = axial displacement
- $\phi(x)$  = angular rotation
- $EI$  = beam bending stiffness
- $AE$  = axial stiffness
- $C$  = damping coefficient
- $\rho$  = mass per unit length
- $f_x$  = external axial load per unit length
- $f_y$  = external transverse load per unit length
- $w_A, w_B$  = transverse deflection at node points A and B
- $u_A, u_B$  = axial displacement at node points A and B
- $\phi_A, \phi_B$  = angular rotation at node points A and B
- $V_A, V_B$  = shear force at node points A and B
- $P_A, P_B$  = axial force at node points A and B
- $M_A, M_B$  = bending moment at node points A and B

To perform the integration of (2.1),  $u(x)$  and  $w(x)$  are represented by algebraic polynomials in the  $x$ -coordinate. These special polynomials, called shape functions [3, 4], have the unique distinction that the nodal displacements appear as coefficients. The shape function for the axial displacement is simple:

$$u(x) = u_A (x_B - x)/(x_B - x_A) + u_B (x - x_A)/(x_B - x_A). \quad (2.2)$$

On the other hand, the shape function for the transverse deflection is:

$$w(x) = w_A \psi_1(x) + w_B \psi_2(x) + \phi_A \psi_3(x) + \phi_B \psi_4(x), \quad (2.3)$$

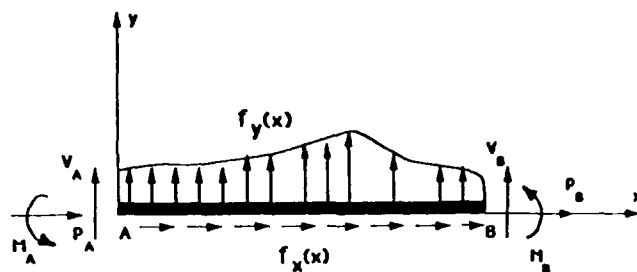


FIG. 3: TWO DIMENSIONAL BEAM ELEMENT

where:

$$\psi_1(x) = 1 - 3(x - x_A)^2/(x_B - x_A)^2 + 2(x - x_A)^3/(x_B - x_A)^3,$$

$$\psi_2(x) = 1 - 3(x_B - x)^2/(x_B - x_A)^2 + 2(x_B - x)^3/(x_B - x_A)^3$$

$$\psi_3(x) = (x - x_A) - 2(x - x_A)^2/(x_B - x_A) + (x - x_A)^3/(x_B - x_A)^2$$

$$\psi_4(x) = -(x_B - x) + 2(x_B - x)^2/(x_B - x_A) - (x_B - x)^3/(x_B - x_A)^2.$$

The  $\psi_i(x)$  polynomials represent beam deflection curves when each of the nodes is displaced or rotated independently a unit amount in a positive sense. Substituting (2.2) and (2.3) into (2.1) and integrating produces an expression relating the total energy in the beam element to the six unknown nodal displacements, i.e.,  $u_A, u_B, w_A, w_B, \phi_A$  and  $\phi_B$ . For equilibrium, the total energy  $\Gamma$  is a stationary function; therefore, the partial derivatives with respect to the nodal displacements must vanish, i.e.,  $\frac{\partial \Gamma}{\partial u_A} = \frac{\partial \Gamma}{\partial u_B} = \frac{\partial \Gamma}{\partial w_A} = \frac{\partial \Gamma}{\partial w_B} = \frac{\partial \Gamma}{\partial \phi_A} = \frac{\partial \Gamma}{\partial \phi_B} = 0$ . Performing this operation produces six equations for determination of the six unknown nodal displacements. These six equations in matrix notation become:

$$[M_\ell] [\ddot{u}_\ell] + [C_\ell] [\dot{u}_\ell] + [K_\ell] [u_\ell] = [F_\ell] + [P_\ell] \quad (2.4)$$

where:

$$[u_\ell] = [u_A, u_B, \phi_A, \phi_B, w_A, w_B]^T$$

is the nodal displacement vector in local coordinates, the superscript  $T$  indicates the transpose of the vector obtained by exchanging rows and columns.

$$[K_\ell] = \begin{bmatrix} \frac{AE}{L} & 0 & 0 & -\frac{AE}{L} & 0 & 0 \\ 0 & \frac{12EI}{L^3} & \frac{6EI}{L^2} & 0 & -\frac{12EI}{L^3} & \frac{6EI}{L^2} \\ 0 & \frac{6EI}{L^2} & \frac{4EI}{L} & 0 & -\frac{6EI}{L^2} & \frac{2EI}{L} \\ -\frac{AE}{L} & 0 & 0 & \frac{AE}{L} & 0 & 0 \\ 0 & -\frac{12EI}{L^3} & -\frac{6EI}{L^2} & 0 & \frac{12EI}{L^3} & -\frac{6EI}{L^2} \\ 0 & \frac{6EI}{L^2} & \frac{2EI}{L} & 0 & -\frac{6EI}{L^2} & \frac{4EI}{L} \end{bmatrix}$$

is the stiffness matrix in the local coordinate system,  $L = x_B - x_A$  is the length of the beam element.

$$[M_t] = \rho \begin{bmatrix} \frac{L}{3} & 0 & 0 & \frac{L}{6} & 0 & 0 \\ 0 & \frac{13L}{35} & \frac{11L^2}{210} & 0 & \frac{9L}{70} & -\frac{13L^2}{420} \\ 0 & \frac{11L^2}{210} & \frac{L^3}{105} & 0 & \frac{13L^2}{420} & -\frac{L^3}{140} \\ \frac{L}{6} & 0 & 0 & \frac{L}{3} & 0 & 0 \\ 0 & \frac{9L}{70} & \frac{13L^2}{420} & 0 & \frac{13L}{35} & -\frac{11L^2}{210} \\ 0 & -\frac{13L^2}{420} & \frac{L^3}{140} & 0 & -\frac{11L^2}{210} & \frac{L^3}{105} \end{bmatrix}$$

is the mass matrix in local coordinates, and  $[C_t] = \alpha [M_t] + \beta [K_t]$  is the Rayleigh damping matrix [3].

$$[F_t] = [f_x L/2, f_y L/2, f_y L^2/12, f_x L/2, f_y L/2, -f_y L^2/12]^T$$

and

$$[P_t] = [P_A, V_A, M_A, P_B, V_B, M_B]^T$$

are the applied force and the nodal reaction force vectors in local coordinates, respectively.

In addition, for thin structures with bending stiffness very small compared with axial stiffness, such as cables and thin beams, which obviously include the optical fibers considered here, stress stiffening must be taken into account [5]. Stress stiffening, also known as geometric stiffening, is the stiffening (or weakening) of a structure due to its stress state. This is effected in the model by constructing an additional stiffness matrix,  $[K_t^*]$  called the "stress stiffness matrix". This matrix in local coordinates for the beam element considered assumes the form [5]:

$$[K_t^*] = \frac{T}{L} \begin{bmatrix} 0 & 0 & 0 & 0 & 0 & 0 \\ 0 & \frac{6}{5} & \frac{L}{10} & 0 & -\frac{6}{5} & \frac{L}{10} \\ 0 & \frac{L}{10} & \frac{2L^2}{15} & 0 & -\frac{L}{10} & -\frac{L^2}{30} \\ 0 & 0 & 0 & 0 & 0 & 0 \\ 0 & -\frac{6}{5} & -\frac{L}{10} & 0 & \frac{6}{5} & -\frac{L}{10} \\ 0 & \frac{L}{10} & -\frac{L^2}{30} & 0 & -\frac{L}{10} & \frac{2L^2}{15} \end{bmatrix}$$

where  $T$  is the axial load on the element obtained from the previous iterative cycle.

This stiffness matrix is added to the previously determined matrix,  $[K_t]$ . It should be understood, that hereafter, reference to the stiffness matrix  $[K_t]$  includes  $[K_t^*]$ , i.e.,  $[K_t] = [K_t] + [K_t^*]$ . This is the matrix referenced in equation (2.4).

The beam element matrix equation (2.4) is valid for the local coordinate system, i.e., a coordinate system fixed to the beam as depicted in Fig. 3. However, when forming geometric shapes using many beam elements at varying orientations, all nodal displacements and forces are referenced to a fixed common coordinate system known as the global coordinate system. The global displacements and forces are derived from the local quantities through the direction cosine matrix:

$$[u_g] = [\lambda]^T [u_t], [P_g] = [\lambda]^T [P_t], [F_g] = [\lambda]^T [F_t],$$

where:

$$[\lambda] = \begin{bmatrix} \frac{\Delta x}{L} & \frac{\Delta y}{L} & 0 & 0 & 0 & 0 \\ -\frac{\Delta y}{L} & \frac{\Delta x}{L} & 0 & 0 & 0 & 0 \\ 0 & 0 & 1 & 0 & 0 & 0 \\ 0 & 0 & 0 & \frac{\Delta x}{L} & \frac{\Delta y}{L} & 0 \\ 0 & 0 & 0 & -\frac{\Delta y}{L} & \frac{\Delta x}{L} & 0 \\ 0 & 0 & 0 & 0 & 0 & 1 \end{bmatrix}$$

is the direction cosine matrix,  $\Delta x$  and  $\Delta y$  are the difference in the global  $x$  and  $y$  coordinates of the beam element node points, respectively,  $[u_g]$  is the global displacement matrix,  $[P_g]$  is the global reaction force matrix, and  $[F_g]$  is the global applied load matrix.

The matrix equation of motion for the beam element in the global coordinate system is reached through use of the transformation of the mass, stiffness and damping matrices [4]:

$$[M_g] = [\lambda]^T [M_t] [\lambda], [K_g] = [\lambda]^T [K_t] [\lambda] \text{ and}$$

$$[C_g] = [\lambda]^T [C_t] [\lambda];$$

consequently, Equation (2.4) is written as:

$$[M_g] [\ddot{u}_g] + [C_g] [\dot{u}_g] + [K_g] [u_g] = [F_g] + [P_g]. \quad (2.5)$$

The reaction forces at internal nodes cancel when assembling an entire structure comprised of many elements and therefore the matrix equation of motion for the whole structure is:

$$[M] [\ddot{u}] + [C] [\dot{u}] + [K] [u] = [F]. \quad (2.6)$$

where  $[M]$ ,  $[C]$ ,  $[K]$  are the mass, damping and stiffness matrices, respectively, of the whole structure in global coordinates,  $[u]$  is the nodal displacement matrix of the whole structure in global coordinates and  $[F]$  is the applied load per unit length in global coordinates.

A non-linear transient dynamic analysis technique numerically integrates (2.6) starting with a known initial state at  $t = 0$ . Equation (2.6) is converted from the general form to that specialized at time  $t_n$ :

$$[M] [\ddot{u}_n] + [C] [\dot{u}_n] + [K] [u_n] = [F(t_n)]. \quad (2.7)$$

The acceleration  $[\ddot{u}_n]$  and velocity  $[\dot{u}_n]$  are approximated by finite difference equations derived from a consideration of Lagrange's interpolation formula [6]:

$$[\ddot{u}_n] = \frac{1}{(\Delta t)^2} \left\{ 2 [u_n] - 5 [u_{n-1}] + 4 [u_{n-2}] - [u_{n-3}] \right\}. \quad (2.8)$$

$$[\dot{u}_n] = \frac{1}{6(\Delta t)} \left\{ 11 [u_n] - 18 [u_{n-1}] + 9 [u_{n-2}] - 2 [u_{n-3}] \right\}.$$



where:

$[u_n]$  = displacement at time step  $t = t_n$  and

$\Delta t = t_n - t_{n-1}$ , a constant time step.

Substituting equations (2.8) into (2.7) produces:

$$\begin{aligned} & \left\{ \frac{2}{(\Delta t)^2} [M] + \frac{11}{6\Delta t} [C] + [K] \right\} [u_n] = \\ & \left\{ \frac{5}{(\Delta t)^2} [M] + \frac{3}{\Delta t} [C] \right\} [u_{n-1}] \\ & - \left\{ \frac{4}{(\Delta t)^2} [M] + \frac{3}{2\Delta t} [C] \right\} [u_{n-2}] \\ & + \left\{ \frac{1}{(\Delta t)^2} [M] + \frac{1}{3\Delta t} [C] \right\} [u_{n-3}] + [F(t_n)]. \end{aligned} \quad (2.9)$$

This results in an implicit time integration procedure. At each point in time, the unknown  $[u_n]$  is calculated using an efficient Gauss elimination routine.

Equation (2.9) can be used whenever the displacements are small. However, when displacements are large, such that the geometric shape of the structure changes considerably from one iteration cycle to the next, it is necessary to compute incremental displacements. At each cycle, the global mass, damping and stiffness matrices are re-evaluated to reflect the altered geometry. This results in the following dynamic equation for handling geometric non-linearities:

$$\begin{aligned} & [M_{n-1}] [\ddot{u}_n] + [C_{n-1}] [\dot{u}_n] + [K_{n-1}] [\delta u_n] = \\ & [F(t_n)] - [S(t_{n-1})], \end{aligned} \quad (2.10)$$

where  $[M_{n-1}]$ ,  $[C_{n-1}]$  and  $[K_{n-1}]$  are the mass, damping and stiffness matrices, respectively in the global system established from the geometric properties of the structure at the previous iteration,  $[S(t_{n-1})] = \sum_{i=1}^{n-1} [K_i] [\delta u_i]$  is the matrix of the total internal nodal resisting forces and bending moments at the previous iteration and  $[\delta u_n] = [u_n - u_{n-1}]$  is the incremental change in displacement from the previous iteration. The difference equation for numerically determining  $[\delta u_n]$  is similar to (2.9) with obvious modification.

For the optical fiber configurations addressed, an additional non-linearity presents itself. This concerns the restricted movement of the optical fiber within the finite dimensional constraints of the splice tray organizers. This finite element program contains logic, not generally found in many programs of this nature, that checks the location of each node point every cycle for contact with the sides of the organizer. When contact is indicated, the affected node or nodes are fixed to the boundary. At that time, subsequent iteration cycles involve, in general, two iterations per time cycle. The first iteration is performed to check the status of the nodes in contact with the boundary. This calculation is carried out assuming the affected node or nodes are free. If this computation indicates continued boundary intrusion, the cycle is repeated with the nodes fixed to the boundary, otherwise, the results of the iterative cycle are accepted.

### 3. Optical Fiber Geometries in Splice Tray Organizers

Three splice tray organizers are considered in this paper. Schematics are given in Fig. 4. The splice tray organizer designated as A permits the fibers to assume a snugly fitted oval in compartments that are approximately 7.7 cm x 16 cm (3 in x 6.25 in) on either side of the splice holder. Splice tray organizers B and C are similar in shape and function but differ in size. Splice tray B has an overall dimension of approximately 13 cm x 30 cm (5.2 in x 12 in) and a splice holder dimension of approximately 3.8 cm x 11.5 cm (1.5 in x 4.5 in). Splice tray C is approximately 15.4 cm x 35.9 cm (6 in x 14 in) in overall dimension and has a splice holder approximately 6.4 cm x 25.6 cm (2.5 in x 10 in). Unlike splice tray A, the fibers in trays B and C enter from the same side and are joined after making at least one complete loop around the splice holder. This configuration resembles a "race track" oval.

The worst case orientation, as far as inducing mechanical stress, is when the fiber is loaded in the plane of the loop. Therefore, it is assumed that the dynamic loads are applied in the plane of the fiber loops, that the splice tray is rigid, i.e., there is no dynamic coupling between the fibers and tray, and the sides of the tray are smooth. In general, there will be many fiber loops to provide sufficient slack for maintenance and restoration. A minimum of 60 cm (23.6 in) of slack is required [2]. However, the mechanical response of the fibers in the organizer is assessed by analyzing a single fiber loop. It is therefore tacitly assumed that there is minimal interaction between the fiber loops and that each loop experiences the stress state of the single fiber loop modeled. In addition, the details of the actual splice (fusion or mechanical) and holder assembly are not considered.

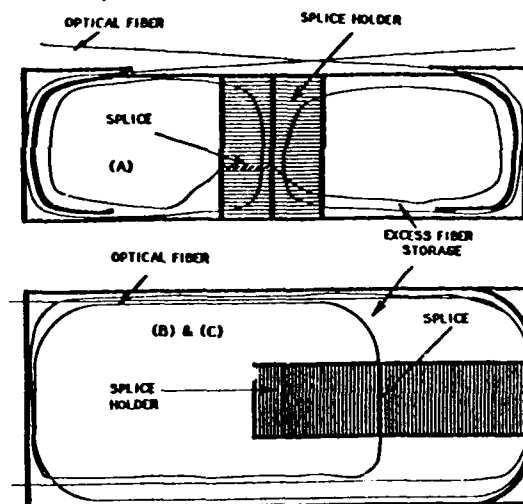


FIG. 4: FIBER OPTIC SPLICE TRAY ORGANIZERS

### 4. Experimental Verification

The finite element model was verified by constructing mock-ups of the splice tray organizers, adding fiber loops, and testing them on a laboratory vibration table. Frequencies from 10 to 60 Hz were used; a peak-to-peak displacement of 0.38 cm (0.15 in) resulted in a maximum acceleration of 27g at 60 Hz. The 13g acceleration generated by support pole impact was obtained at 42 Hz.

The motions of the fibers in the different splice tray organizer mock-ups were recorded on videotape for comparison to the computer simulations at both full-speed and slow-speed playback. Still photographs were taken at shutter speeds up to 1/2000 sec to "freeze" the fiber motions and allow direct comparisons to the computer-generated mode shapes. Figures 5(a) and (b) show the deflection of the fiber at 27g (60 Hz) in the mock-up of the splice tray organizer A; the distorted curves in the fiber at the left and

right sides of the picture (a) agree with the shapes predicted by the computer analysis (b). Figures 5(c) and (d) also show the more complex modes obtained in splice tray organizer C. In the photograph (c) the curve at the left end of the fiber is distorted, the fiber no longer makes continuous contact with the long sides of the tray, and the fiber crosses over itself twice at the top of the picture. All of these deformations, however, are consistent with the computer predictions as shown in the plot (d) from the analysis of the 27g, 60 Hz conditions.

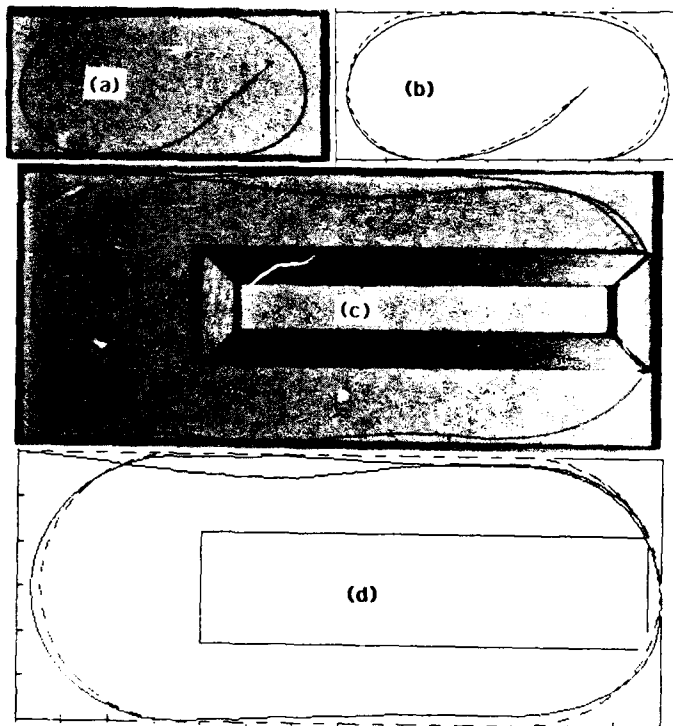


FIG. 5 : THEORETICAL AND EXPERIMENTAL MODES IN SPLICE TRAY ORGANIZERS (A) AND (C)

The consistent agreement between the computer plots and the photographs for all three splice tray organizers over a range of accelerations demonstrate the validity of the computer model. It can thus be used with confidence to predict fiber responses under conditions outside the range of laboratory experiments.

##### 5. Dynamics of Aerial Optical Fibers

Computer simulations of the splice tray organizer configurations shown in Fig. 4 were conducted by approximating the input acceleration of Fig. 1 by a damped sinusoid with a maximum acceleration of  $1g$  and frequency  $0.8$  Hz:

$$A(t) = 13 \text{ Exp } (-0.135t) \text{ Sin } (5.026t).$$

Vibration mode shapes of the optical fiber loops in all three splice trays are shown in Figure 6. The dashed figure in each frame depicts the original fiber position. The total area swept by the vibrating fiber loop is an interesting feature useful for correlating experimental data and assessing clearance issues. These areas are plotted in Fig. 7. Only a small fraction of the open area is ever occupied by the fiber in the case of splice tray organizer A while the opposite is true for both the B and C fiber arrangements. The maximum computed tensile stresses realized during the vibration are presented in Fig. 8. The maximum tensile stress is lowest - less than  $30$  ksi - for fiber arrangement A; for both B and C it does not exceed  $50$  ksi. These stress levels do not exceed the fiber proof stress and therefore are not expected to produce either instantaneous or future fiber failures.

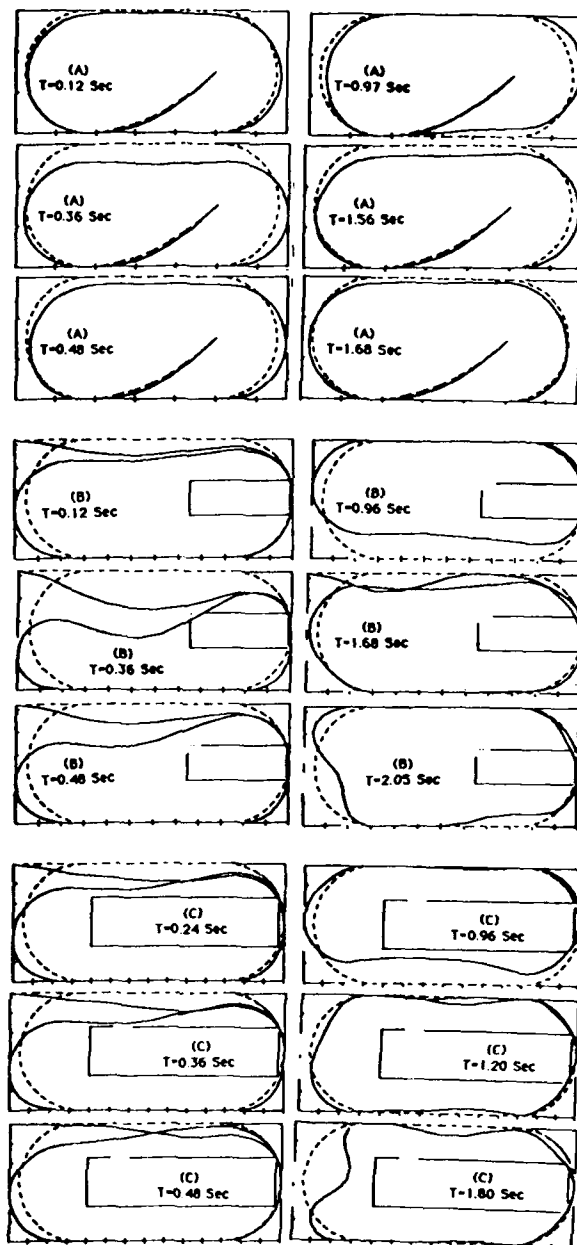


FIG. 6: VIBRATION MODES FOR  $13g, 0.8\text{Hz}$  DAMPED SINUSOID FOR SPLICE TRAYS (A), (B) & (C)

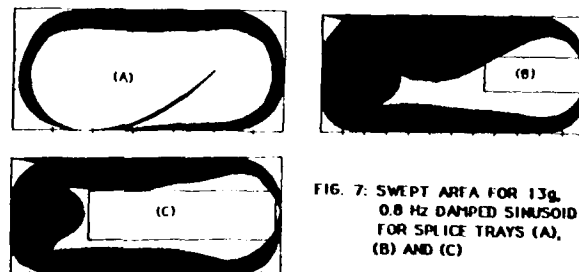


FIG. 7: SWEEP AREA FOR  $13g, 0.8 \text{ Hz}$  DAMPED SINUSOID FOR SPLICE TRAYS (A), (B) AND (C)

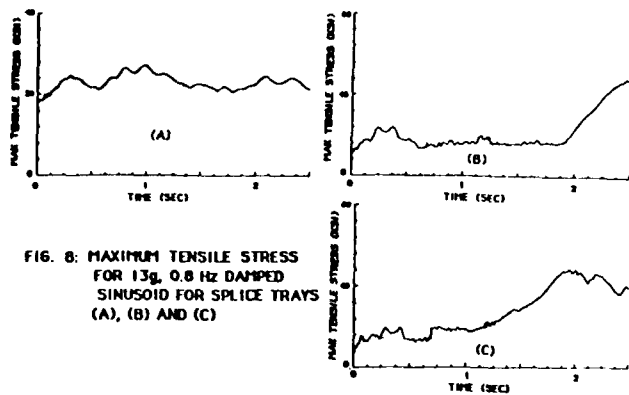


FIG. 6: MAXIMUM TENSILE STRESS FOR 13g, 0.8 Hz DAMPED SINUSOID FOR SPLICE TRAYS (A), (B) AND (C)

## 6. Summary and Conclusions

The dynamic response of aerial optical fiber configurations located in optical splice organizers has been explored using a recently developed nonlinear finite element computer program. The accuracy of the model was verified by comparing vibration mode shapes produced with actual vibration experiments.

Reference 2 stipulates vibration tests at frequencies 10-55 Hz at relatively low acceleration levels - 0.3g at 10 Hz, 2.7g at 30 Hz and 9.3g at 55 Hz. However, when splice enclosures are deployed in the aerial plant, higher accelerations at lower frequencies can be encountered. Peak accelerations as high as 13g at 0.8 Hz can be achieved when a support pole is suddenly removed [1].

In this paper, numerical experiments have been conducted to investigate the mechanical reliability of optical fibers arranged in optical splice organizers when exposed to aerial plant conditions calculated in [1]. Fiber optic loop arrangements germane to several popular vendor products form the basis for exploring the potential susceptibility to the aerial plant dynamic excitations. Each of the fiber configurations given in Fig. 4 was exposed to a damped sinusoidal acceleration - 13g at 0.8 Hz. This worst case loading is characteristic of an aerial plant scenario associated with sudden support pole removal.

Vibrational mode shapes, total swept areas, and maximum tensile stress histories are presented for all the optical fiber configurations examined. It is determined that the optical fiber configurations considered are sufficiently robust to withstand the rigors of the dynamic load imposed.

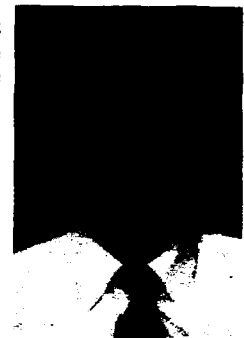
The optical fibers in splice tray organizers type B and C respond vigorously to this low frequency excitation as witnessed by the large swept area covered by the vibrating fiber. These large displacement excursions do not, however, produce high tensile stress in a single fiber loop. But, when many fiber loops are present, large displacement excursions can give more opportunity for the fibers to become tangled and intertwined.

It should also be noted that some fiber samples were subjected to more than 10,000 cycles at 27g during the vibration tests and that no failures or visible damage occurred.

## REFERENCES

1. P. B. Grimado, "Dynamic Characteristics of Aerial Fiber Optic Cable", *Optical Engineering*, V. 30, No. 6, P. 808, June 1991.
2. \_\_\_\_\_, "Splice Organizer Assemblies for Optical Fibers", TR-TSY-000769, Issue 1, Bellcore, March 1988
3. K. Bathe, E. L. Wilson, "Numerical Methods in Finite Element Analysis", Prentice-Hall, 1976.
4. J. S. Przemieniecki, "Theory of Matrix Structural Analysis", McGraw-Hill, 1968.
5. ANSYS, Engineering Analysis System, Theoretical Manual.
6. M. G. Salvadori, M. L. Baron. "Numerical Methods in Engineering", Prentice-Hall, 1962.

**Philip B. Grimado** received the BS degree in civil engineering from the City University of New York and the MS and PH.D. degrees in applied mechanics from Columbia University, New York, in 1962 and 1968, respectively. He joined Bell Laboratories in 1968, where his responsibilities included vulnerability studies of antiballistic missile systems, fire protection studies involving fire-risk analyses, heat transfer calculations, development of standard fire testing methods for telephone company equipment and development of algorithms for optimum control of building environmental equipment. Since 1983, he has been with Bell Communications Research (Bellcore), engaged in outside plant activities concerned with fiber optic cable placement, damage assessment, and optical fiber stress analysis.



**Rolf A. Frantz** is a distinguished member of technical staff in the Fiber Distribution and Reliability Research District at Bellcore. He joined Bell Laboratories in 1972, directly after receiving his Ph.D. degree from Brown University. His major responsibilities were in the field of electrical insulating materials, an area in which he continued to work upon coming to Bellcore in 1983. Since 1988, his work has focused on optical fiber coatings, with extent of cure, aging, and coating durability as areas of particular interest.



## A NEW FIBER OPTIC CABLE ASSEMBLY FOR HDTV RECORDING OF OLYMPIC WINTER GAMES SKI RACES

Pierre GAILLARD \* Jacques LE COMTE \*\* - Michel de VECCHIS \*\*\*

\* ALCATEL CABLE - 148 Av Jean Jaurès - 69344 LYON - FRANCE  
\*\* ALCATEL CABLE SYSTEMES - 35 Rue Jean Jaurès - 95871 BEZONS FRANCE  
\*\*\* ALCATEL CABLE - 30 Rue des Chasses - 92111 CLICHY - FRANCE

### ABSTRACT :

This paper describes a new Fiber Optic Cable Assembly developed for the Olympic Winter Games Ski Races.

It has been developed using the technology of Fiber Optic Tactical Cables with some changes due to specific conditions. Characteristics and results of preliminary tests in Winter conditions are described.

### INTRODUCTION

The recording of the ski contests during the next Olympic Winter Games in Albertville has created the need to develop optical fiber cables which are used between an intermediate node point and the main digital video switchers located at the level of the arrival line. Videosignals are digitalized and transmitted over links which are about 2000 meters long.

### FUNCTIONAL REQUIREMENTS FOR CABLES

The optical cables must be quickly and easily deployable along ski runs under normal environmental conditions of mountains in winter (ice, snow, low temperature,...).

Connectorization must also be simple and reliable under the same conditions.

These conditions are by many aspects similar to those of military tactical links. Specificities are due to the fact that the cable is normally laying in ice or snow and consequently the operating temperature is in the low range. All the tests of winding, unwinding, connecting and disconnecting must also consider this low temperature range and the presence of ice, snow and humidity. There is no need of metal free cable and the outer sheath must withstand aggressions by ski edges.

### CABLE DESIGN

We have reported last year the design of tactical Fibre Optic Cable Assemblies for Military Applications (1). We have used the same basic principles and technologies to develop this new cable i.e. :

- to use a loose structure, in our case a four groove slotted core structure.

- to use multimode fibers which are sufficient considering the required transmission parameters and offer advantages for an easy connection.

- to use an hermaphroditic expanded beam interface connector, which is field proven for military tactical conditions, has been extensively studied in particular considering ergonomics aspects, satisfies the different requirements and is fitted to the cable structure.

The initial structure of the cable presented last year is shown in Figure 1. Its main characteristics are :

Nominal outer diameter	7 mm
Nominal weight	38kg/km
Nominal thickness of sheath	0.8 mm
Maximum tensile load	220 daN
(corresponding to an elongation $< 1,5\%$ )	
Crush resistance	40 daN/cm
Minimum bending radius	

Static	100 mm
Dynamic	150 mm

Temperature range - 40 to + 70 °C  
with less than 0.2 dB attenuation increase for 850 and 1300 nm multimode fibres.

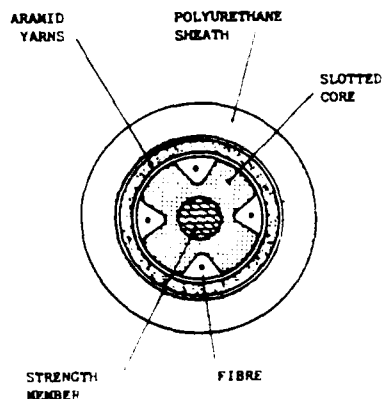


Figure 1

A new version of this cable with a reduced diameter of 6 mm has been developed. It enables to deliver lengths of 1000 m instead of 600 or 800 m on the standard size drums. Its main characteristics are :

Nominal outer diameter	6 mm
Nominal weight	30 kg/km
Nominal thickness of sheath	0.8 mm
Maximum tensile load	290 daN
Crush resistance	30 daN/cm
Minimum static bending radius	80 mm
Temperature range	-40to+70 °C

For the development of the new cable its was not necessary to keep the dielectric central strength member.

Consequently we have used a stainless steel rope which offers better flexibility and tensile performance. We have selected as basic structure the first version presented here. By using the steel rope, we have found experimentally that the tensile load is increased to 350 daN compared to 220 daN for the FRP strength member under the same conditions.

It must be noted that in the case of a lower required maximum tensile load, the version two should be used with the advantage of a lower weight and dimensions.

#### PRACTICAL RESULTS :

Several lengths of cable have been realized for preliminary tests and field experiments, incorporating four 50/125 Fibers.

The figure 2 shows the comparison between the different cables : this new cable is shown in the middle between the first version of the tactical cable (on the right) and the second version, reduced size of tactical cable (on the left). For these three cables a fire retardant sheath is used.

Considering the specific application, bandwidth of the fibres has been measured at 1300 and 1550 nm. These results are summarized in the following table.

	FIBER N°	BANDWIDTH FOR L = 2 km (in MHz)	
		AT 1300nm	AT 1550nm
Length N° 1	1	> 1000	604
	2	> 1000	553
	3	> 1000	575
	4	> 1000	545
Length N° 2	1	886	388
	2	> 1000	500
	3	> 1000	428
	4	887	360

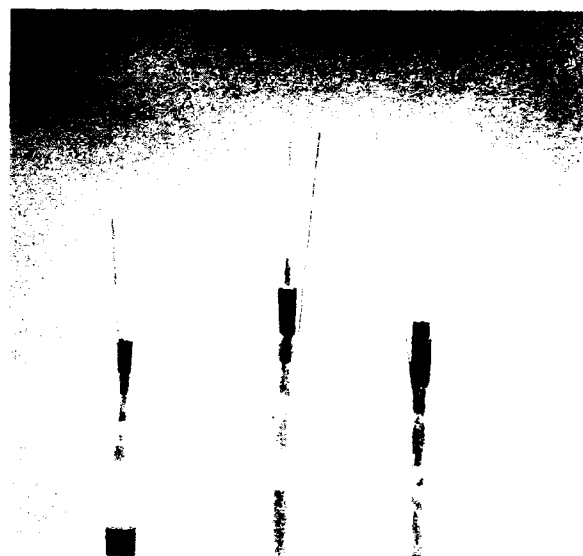


Figure 2

Thermal cycling according to IEC test 794-1-F1 have shown a stability similar to the case observed for tactical cable : less than 0.2 dB change between - 40 and + 70°C for multimode fibers at 850, 1300 and 1550 nm.

The lengths of cable have been equipped with hermaphroditic 4 channels connectors previously developed for tactical cables (1) (see figure 3).

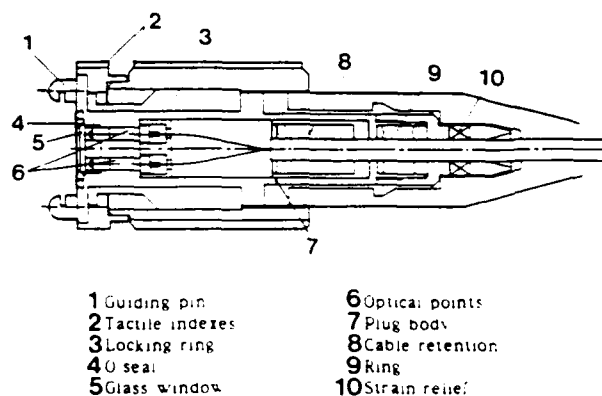


Figure 3

The table below summarizes the characteristics of the connector for multimode fibres.

TEST	RESULTS
Connections	4 channels
Insertion loss (0,85 and 1,3 $\mu$ m)	< 3 dB in the whole operating temperature range
Uniformity	+ - 0.2 dB
Operating temperature range	- 40°C < T < + 70°C
Storage temperature range	- 40°C < T < + 85°C
Mechanical endurance	1500 mating/unmating
Vibrations	5-300 Hz-amplitude 1.25 mm p-p
Mechanical shocks	30 g - 11 ms - 2.06 m/s
Shakes	1000 - 25 g - 6 ms
Water immersion	1 m depth (0.1 bar)
Tensile strength	220 daN

Figure 4 shows the connector

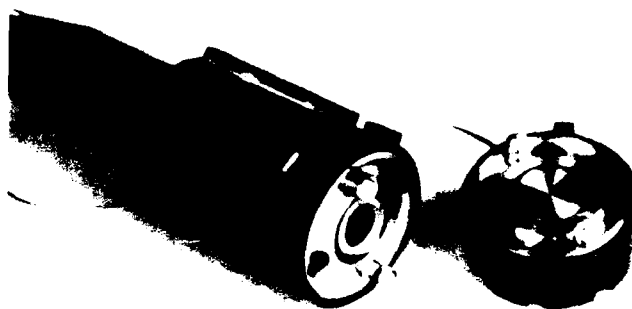


Figure 4

Preliminary experiments have been done by installing these lengths of cable in two French Winter Stations Val d'Isère and Méribel. Cables have been left during several months along ski runs at the surface or under snow depending of weather conditions. At the end of winter they have been recovered and tested in view of identifying any change on their characteristics. No significant change has been found which is very satisfactory.

As a consequence, similar cables are now in production for installation before the next Olympic Winter Games (February 1992 in Albertville) along the ski runs.

They will be used with terminal equipments that we have developed for the transmission of :

- Analog video signals having up to 11 MHz bandwidth (i.e. PAL/SECAM/D2MAC/TMAC...)

- Audio signals
- Data signals
- Digital video signals at 270 Mbits (D1 standard)

Different kinds of multiplex (both digital and optical) are used.

**CONCLUSION :** We have shown that it is possible to derive from military tactical optical cables other products corresponding to different applications. These field cables that can be used for a lot of applications offer attractive solutions due to their reduced size and weight.

It has been shown that several designs are available depending on the specific requirements. The availability of an easy-handled and reliable field connector, adapted to the cable, is a key issue for the development of such applications.

#### ACKNOWLEDGEMENTS

The authors thank SFP (Société Française de Production) for permission to publish the results of this work.

#### REFERENCE

- (1) JP. BONICEL - P. GAILLARD - M. de VECCHIS  
Tactical Fibre Optic Cable Assemblies  
I.W.C.S 1990 Proceedings pp 135-139.

#### BIOGRAPHY

P. GAILLARD - ALCATEL CABLE  
148 Av Jean Jaurès - 69344 LYON 6 FRANCE



Pierre GAILLARD was born in 1956. He received his engineer degree from the Ecole Catholique des Arts et Métiers in 1980. He joined LES CABLES DE LYON now ALCATEL CABLE in 1983 where he is in charge of cables definition and transmission characterisation.

J. LECOMTE - ALCATEL CABLE SYSTEMES  
35 Rue Jean Jaurès - 95871 BEZONS - FRANCE



LECOMTE was born in 1948. He is graduated from Ecole Speciale de Mécanique et d'Electricité, Paris. From 1972 to 1985 he has been engineer then Technical Manager of VISIODIS, an Alcatel Subsidiary involved in CATV Networks. In 1986, he joins CLTO another Alcatel Subsidiary as System Division Manager in charge of Fiber Optic Transmission Equipments. Since 1991 he is Technical Manager of ALCATEL CABLE SYSTEMES.

M. de VECCHIS - ALCATEL CABLE  
30 Rue des Chasses - 92111 CLICHY - FRANCE



Michel de VECCHIS was born in 1946. He is graduated from Ecole Nationale Supérieure des Télécommunications (1969). He joined LTT in 1970 where he worked on microwave components. He started to work on fiber optics in 1974 and has been Technical Director of the cable Division until the merging in 1986 of LTT cable activities with Les Cables de Lyon now Alcatel Cable. He is now Director of Technical International Marketing at Alcatel Cable Telecommunications Branch. He is involved in International Standardization of optical fibers and cables (Chairman of CECC WG 28 and Secretary of IEC SC 86 A).

# DESIGN OF AIR PRESSURIZED OPTICAL FIBER FILLED TUBE CABLE MINIMIZING THE PNEUMATIC RESISTANCE

K. S. RYOO      J. S. LEE      H. J. KANG

TAIHAN ELECTRIC WIRE CO., LTD. SEOUL KOREA

## ABSTRACT

Recently a unique hybrid cable design has been proposed by some cable makers to meet the air flow requirements of standard telecommunications air pressure systems and provided a product meeting the specifications of required optical cable.

We designed and developed hybrid optical fiber cable which exhibits good optical, mechanical and pneumatic resistance of less than  $0.9 \times 10^{-3} (\text{kg/cm}^2)^2 / (\text{g/min-m})$ . This hybrid optical cable also provides extra protection to the fiber by way of loose tube gel as well as longer Maintenance Section Length of cable maintenance.

## 1. INTRODUCTION

Adoption of filled tubes in air core cable provides extra protection to the fibers by way of the tube buffering gel, while still allowing dynamic pressurization and free air movement through the core.

In case we consider the cable inner side as a pipe, the meaning of pneumatic resistance is the frictional resistance to the air flow and the values of maintenance section length (MSL) can be changed according to this pneumatic resistance. Namely the less the pneumatic resistance, the longer the MSL and the economical effect would be increased due to the reduction of expense for operating and supervising the line fault equipment.

Furthermore when the gas leakage occurs from a defective point of cable sheath, easier detecting makes it possible to repair rapidly. Accordingly, air pressurized cable should be designed to minimize the pneumatic resistance. And in view of this design conception, we developed air pressurized cable exhibiting good optical,

mechanical, environmental properties, especially providing minimum pneumatic resistance.

## 2. CABLE DESIGN

The necessary conditions of air pressurized cable include small frictional resistance for minimizing disturbance to the air flow, simple and easy maintenance resulted from an extension of MSL, good optical, mechanical and environmental properties for external severe conditions, easy handling and so on.

To meet these several requirements, we designed and developed the air pressurized cable considering the following points.

- ① Pneumatic resistance must be minimized by expanding the effective cross section area of cable inside.
- ② Cable should fully endure the installation and operation condition.
- ③ Easy handling, small diameter and light weight.

We manufactured 20 fibers air pressurized optical fiber cable considering the conception of cable design mentioned above.

### 2.1 Optical Fiber Structure

Filled loose tube with 6~7 fibers are stranded around a central strength member. Fiber parameter and loose tube structure are shown in Table 1.

### 2.2 Cable Structure

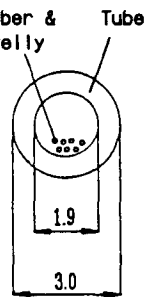
Newly designed air pressurized cable has a construction as Fig. 1. In order to increase air flow rate through the cable core, we adopted a air flow path, called air spacer made by polyester



film of 0.15mm thickness. This polyester tape in trapezoid shape was stranded around the central strength member with loose tube and we finally applied laminated aluminium polyethylene sheath over this stranded cable core.

Through the adoption of air spacer instead of air pipe, the effective cross section area of cable core was increased from 21mm<sup>2</sup> to 37mm<sup>2</sup> and the MSL was easily expanded because the pneumatic resistance decreased from  $2.55 \times 10^{-3}$  to  $0.9 \times 10^{-3}$  (kg/cm<sup>2</sup>)<sup>2</sup>/(g/min-m). Fig. 2 shows the conventional cable structure with air pipe.

Table 1. Fiber Parameters and Loose Tube Structure

Items	Parameters	Tube Structure
Fiber	Single Mode Matched Clad	
Attenuation Loss	Less than 0.4 dB/km at 1.3 $\mu$ m	
M F D	$9.8 \pm 0.5\mu$ m	
$\lambda c$	$1.1 \sim 1.28\mu$ m	
Cladding Diameter	$250 \pm 15\mu$ m	

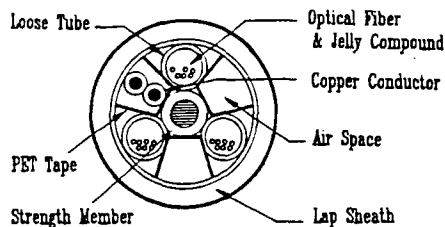


Fig 1 Newly Developed Type

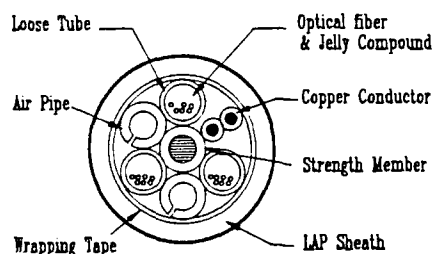


Fig 2. Conventional Type

Table 2 shows the cable parameters of conventional and newly designed cable.

Table 2. Cable Parameters

Items	Conventional	Newly
Fiber Number	20 - Fibers	20 - Fibers
Out Diameter	Nom. 13 mm	Nom. 13 mm
Cable Weight	Approx.150kg	Approx.140kg
Allowable Tensile Strength	260 kgf	260 kgf

### 3. Characteristics of Optical Fiber Cable

Newly designed cable and conventional one were tested for optical, mechanical, environmental and pneumatic resistance properties.

#### 3.1 Attenuation Loss in Cable Manufacturing

Fig.3 shows the attenuation loss of optical fiber cable measured in each manufacturing process. The attenuation loss change during each process are less than 0.02dB/km at 1.55 $\mu$ m. It means that this type of cable can be manufactured easily without attenuation change in cable manufacturing process.

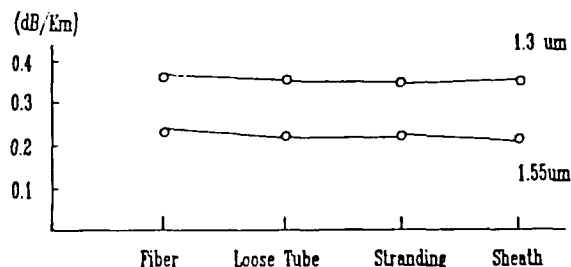


Fig.3 Attenuation of Manufacturing Process

#### 3.2 Pneumatic Resistance Property

The following equipment was prepared to evaluate the pneumatic resistance of cable and Fig.4 shows the test setup.

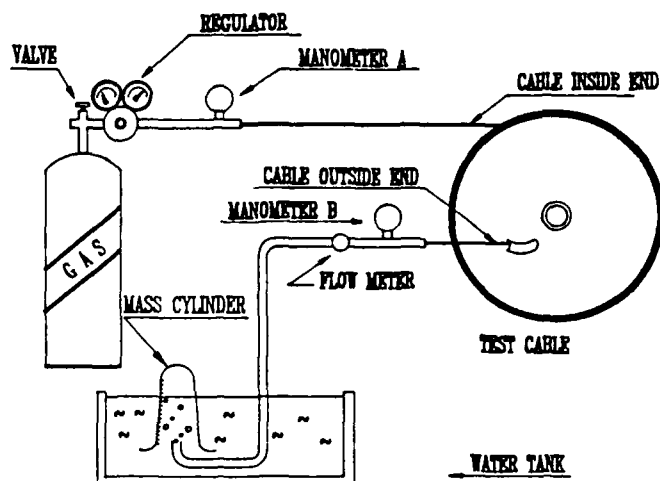


Fig.4 Test set-up of gas pneumatic resistance

- (1) Manometer A, B
- (2) Dried Air
- (3) Regulator
- (4) Flowmeter
- (5) Mass Cylinder

Dry air gas of 0.4 ~ 0.7 l/min was sufficiently injected to inner side of cable until reaching the point of air pressure equilibrium. We measured input pressure  $P_a$ , output pressure  $P_b$ , flow rate  $Q$  of air and also calculated pneumatic resistance "W" according to the following equation."

$$W = \frac{(P_a + P_o)^2 - (P_b + P_o)^2}{Q \cdot L \cdot \rho}$$

Where

W : Pneumatic Resistance ( $\text{kg/cm}^2$ )<sup>2</sup>/(g/min-m)  
 $P_a$ : Input Pressure of Air ( $\text{kg/cm}^2$ )  
 $P_b$ : Output Pressure of Air ( $\text{kg/cm}^2$ )  
 $P_o$ : Atmospheric Pressure ( $\text{kg/cm}^2$ )  
L : Cable Length (m)  
Q : Air Flow Rate (cc/min)  
 $\rho$  : Air Density (dry air =  $1.21 \times 10^{-3}$  g/cc)

As a result, we got improved pneumatic resistance of less than  $0.9 \times 10^{-3}$  ( $\text{kg/cm}^2$ )<sup>2</sup>/(g/min-m), being lower than about one third of that of conventional cable. Table 3 shows the properties for pneumatic resistance of newly designed cable and conventional cable.

Table 3. Pneumatic Resistance Properties

Items \ Type	Conventional Type	Newly Type
Pneumatic Resistance ( $\text{kg/cm}^2$ ) <sup>2</sup> /(g/min-m)	$2.55 \times 10^{-3}$	$0.9 \times 10^{-3}$
Effective Cross Section Area of Air	21 mm <sup>2</sup>	37 mm <sup>2</sup>

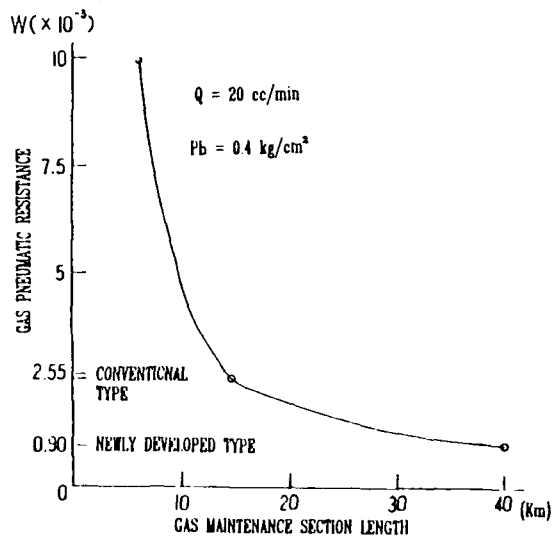


Fig. 5 Gas Pneumatic Resistance of Optical Cable

### 3.3 Relationship between Pneumatic Resistance and MSL

Fig 5. shows the relationship between pneumatic resistance and MSL.

If we use maintenance system which can detect in output pressure 0.4 kg/cm<sup>2</sup> and leakage flow rate 20 cc/min, maintenance section length MSL shall be about 40 km.

Therefore, newly designed cable makes it possible to carry out less expensive maintenance as a result from expanding MSL. And in the event of gas leakage caused by sheath damage, rapid settlements for longer distance can be made in case of the emergency alarm.

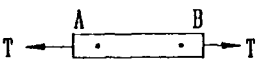
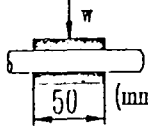
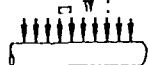
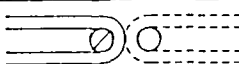
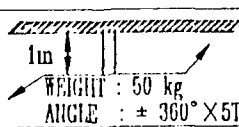
### 3.4 Mechanical and Environmental Properties

Newly developed cable was subject to the mechanical and environmental tests as shown in table 4.

Neither added loss nor break was observed in mechanical test. As a result of measuring loss owing to temperature, the added loss was observed to be less than 0.02 dB/km at 1.55 $\mu$ m between -40°C and +60°C.

As a result, it was verified that this cable has an good mechanical and environmental properties.

Table 4 Mechanical and Environmental Properties

ITEMS	CONDITION	TEST RESULT
TENSION	 <p>PULLING SPEED : 50mm/min TENSION : 260kg</p>	NO LOSS CHANGE (at 1.31 $\mu$ m and 1.55 $\mu$ m)
COMPRESSION	 <p>COMPRESSION PLATE : 50<math>\times</math>50 mm COMPRESSION LOAD : 200 kg</p>	DITO
IMPACT	 <p>WEIGHT : 1 kg HEIGHT : 1 m CYLINDER DIAMETER : 25 mm DROPPING TIMES : 10</p>	DITO
BENDING	 <p>MANDREL DIAMETER : 70 mm(5D) BENDING TIMES : 10</p>	DITO
TORSION	 <p>WEIGHT : 50 kg ANGLE : <math>\pm 360^\circ \times 5</math> TIMES</p>	DITO
TEMPERATURE CYCLE	+20 °C $\rightarrow$ -40 °C $\rightarrow$ +60 °C $\rightarrow$ 20 °C	NO LOSS CHANGE ( at 1.31 $\mu$ m) LESS THAN 0.02dB/km ( at 1.55 $\mu$ m)

### CONCLUSION

We have developed a new kind of hybrid cable applying tape spacer technique for the purpose of improving the pneumatic resistance properties. This cable consist of loose tube fibers, copper pair and polyester tape for air flow path. This cable exhibited good optical, mechanical, environmental characteristics, and excellent pneumatic resistance properties of less than  $0.9 \times 10^{-3} \text{ (kg/cm}^2\text{)}^2 \text{ / (g/min-m)}$  compared with conventional air pressurized cable. Now this type of cable has been in commercial service in some areas for one year.

### REFERENCES

1. Randy Smith, et al. A Unique Approach To Air Pressurized Optical Cable Employing Standards Fiber Tubes. 38th IWCS, 1989
2. S. Yonechi, et al. Proceeding of 29th IWCS, 1980
3. Sumitomo's Optical Fiber Cable Technology TR-83073, 1983



Ki-Sun Ryoo  
Taihan Electric Wire  
Co.,Ltd.  
785, Kwanyang-dong,  
Anyang-city Korea

K.S. Ryoo received his BS degree in mechanical engineering from Chosun University in 1983, and then joined Taihan Electric Wire Co., Ltd. He has been engaged in development of optical fiber cable. He is a member of CCITT sub-committee of Korea.



Jae-Sung Lee  
Taihan Electric Wire  
Co.,Ltd.  
785, Kwanyang-dong,  
Anyang-city Korea

J.S. Lee received his BS degree in electrical engineering from Chungbuk University in 1981, and then joined Taihan Electric Wire Co., Ltd. He has been engaged in development of optical fiber cable and accessory. He is a member of CCITT sub-committee of Korea.



Hee-Jeon Kang  
Taihan Electric Wire  
Co.,Ltd.  
785, Kwanyang-dong,  
Anyang-city Korea

H.J. Kang received his BS degree in electrical engineering from Hanyang University in 1978, and then joined Taihan Electric Wire Co., Ltd. He has been engaged in research and development of optical fiber cable. He is now manager of optical communication department. He is chairman of SG.6, CCITT sub-committee of Korea and a member of the Korean Institute of Communication Sciences.

# CHROMATIC DISPERSION DEPENDENCE FOR STRESS AND BENDING LOSS BY PHASE SHIFT METHOD

Y.T.KIM, K.I.JUN, Y.I.LEE

TAIHAN ELECTRIC WIRE CO.,LTD. SEOUL KOREA

## 1. ABSTRACT

This paper describes the dependence of chromatic dispersion for stress and bending loss in single mode fiber and show the relation between elongation by strain-optic coefficient and conventional method using the extension meter. Also through the relation between optical loss and elongation, maximum excess length that does not happen loss variation can be anticipated.

## 2. BACKGROUND

Recently in the world, it is increased to request about specification of 1.3 $\mu$ m and 1.55 $\mu$ m chromatic dispersion. Variation of chromatic dispersion is very important for operation of system and long-term reliability in optical fiber. Environmental stress give effect to fiber continuously and make changes of the index profile and length due to tensile stress and environmental temperature [2]. Also the increasing of bending loss decrease the life time in the optical fiber and effect chromatic dispersion and optical loss. It is necessary to find relation between stress and bending loss in zero dispersion wavelength.

Through the method to measure both variation of phase shift and optical power according to tensile stress, it can allow to get physical length of fiber with a few millimeter resolution and determine the excess length in loose tube [5]. This paper describe the effect of zero dispersion wavelength and optical power when stress and bending apply to fiber and obtain the relation between the elongation by using the strain-optic coefficient and conventional method.

## 3. THEORY AND EXPERIMENT

### 3.1 Chromatic Dispersion

The difference of group delay in adjacent wavelength is calculated as the prescribed FOTP-169. FOTP-169 prescribes the well-known and well-tried three-term sellmeier equation which was fitted to group delay data,  $\tau(\lambda)$ , using least mean-squares fitting technique [3] thus.

$$\tau(\lambda) = A\lambda^{-2} + B\lambda^{-3} + C \dots\dots\dots(1)$$

where A, B, C are constants. The chromatic dispersion  $D(\lambda)$  is obtained by differential fitting equation (1)

$$D(\lambda) = 2(A\lambda - B\lambda^{-2}) \dots\dots\dots(2)$$

and the zero dispersion wavelength  $\lambda_0$  is given by  $\lambda_0 = (B/A)^{1/2}$  and slope of zero dispersion at  $\lambda_0$  is

$$S_0 = 8A \dots\dots\dots(3)$$

### 3.2 Strain

The conventional strain in fiber is defined as the elongation  $\Delta L$  per unit length of fiber

$$E = \frac{\Delta L}{L} \dots\dots\dots(4)$$

Where E is strain, L is the test fiber length under strain and  $\Delta L$  is the elongation of the fiber.

To determine the strain of fiber, it should be need a accurate measurement of L and elongation  $\Delta L$ . Measurement of strain in long gauge length is performed by measuring the transit time delay  $\tau$  given by

$$\tau = \frac{N \cdot L}{C} \dots\dots\dots(5)$$

When C is speed of light, N is group index for fiber material and waveguide dispersion which varies between fiber core center refractive index and cladding refractive index. For fiber under load, transit time is changed

$$\Delta \tau = (N \cdot \Delta L + L \cdot \Delta N)/C \dots\dots\dots(6)$$

Elongation of the fiber creates an increase in transit time, However the stress reduce the group index and creating a decrease in transit time which is counter to the effect trying to measure. To compensate for the decrease in group index, correction factor should be used. Equation (6) is re-written :

$$\frac{\Delta \tau}{\Delta L} = \frac{N}{C} \left( 1 + \frac{L}{N} \cdot \frac{\Delta N}{\Delta L} \right) \dots\dots\dots(7)$$

Among equation (7),  $\Delta N / \Delta L$  is re-written by strain-optic coefficient where  $P_{ij}$  are the strain-optic tensor components and  $\nu$  is poisson ratio [1].

$$\frac{\Delta N}{\Delta L} = - \left( \frac{N^2}{2L} \right) [P_{12} - \nu (P_{11} + P_{12})] \dots\dots\dots(8)$$

the term in bracket represent the correction factor when taking into account the strain-optic effect. Using the strain-optic coefficients for pure silica, the numerical value for the term in bracket turns out to be 0.775, the equation may be re-written as following

$$\Delta L = \frac{\Delta \tau \cdot C}{N} (1.29) \dots\dots\dots(9)$$

A simplified schematic diagram of apparatus is shown in Fig. 1 Selection of wavelength is 1250 ~ 1350nm and 1500 ~ 1600nm and the repeatability of a measurement is 0.05nm in the wavelength of zero dispersion.

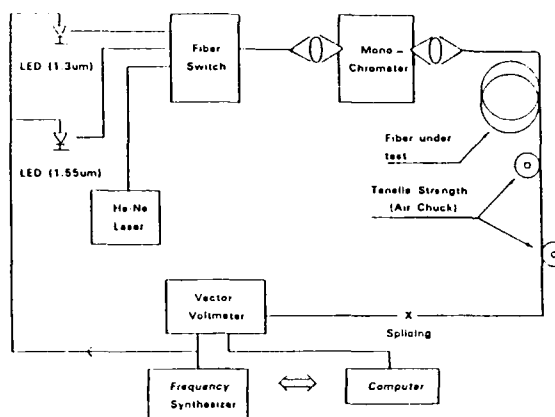


Fig. 1 Schematic diagram of measuring equipment

#### 4. RESULT

Three fiber were manufactured by Vapor Phase Axial Deposition (VAD) process and one fiber is MCVD process. Fiber A and B is conventional matched cladding fiber and fiber C is cutoff shifted fiber and fiber D is depressed cladding fiber.

Table : Type test fiber

Fiber	Type	Coating	MFD/Cutoff
A	Matched Cladding Fiber	Nylon	8.6
B	Matched Cladding Fiber	Acrylate	8.6
C	Matched Cladding Fiber	Acrylate	6.7
D	Depressed Cladding Fiber	Acrylate	7.5

Fig. 2 shows the variation of zero dispersion wavelength according to tensile stress. Maximum variation of zero dispersion wavelength is  $1.32\mu\text{m}$  in short fiber. But variation is decreased in long fiber. The reason is that tensile stress is effected to group delay very strongly and measuring deviation is increased in short fiber.

Fig. 3 shows the variation of zero dispersion wavelength that is winded with fiber in the different diameter of the mandrel. zero-dispersion wavelength is shifted  $0.7\text{nm}$  in  $15\text{mm}$  diameter and zero dispersion wavelength in cutoff shifted fiber does not change above the  $10\text{mm}$  diameter. Also slope of zero dispersion wavelength was not change. The group delay of fiber A, B and D are effected strongly in  $1.55\mu\text{m} \sim 1.6\mu\text{m}$  more than  $1.3\mu\text{m}$  in  $15\text{mm}$  diameter.

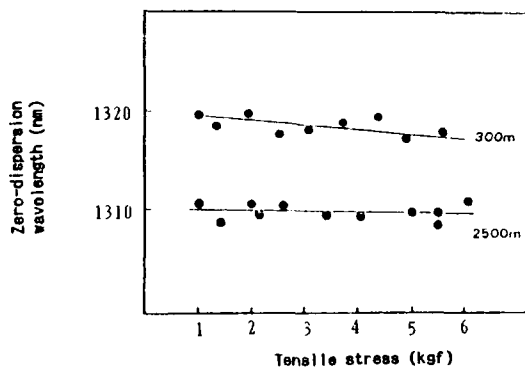


Fig. 2 Variation of zero-dispersion wavelength according to tensile stress and length (gauge length: 20m)

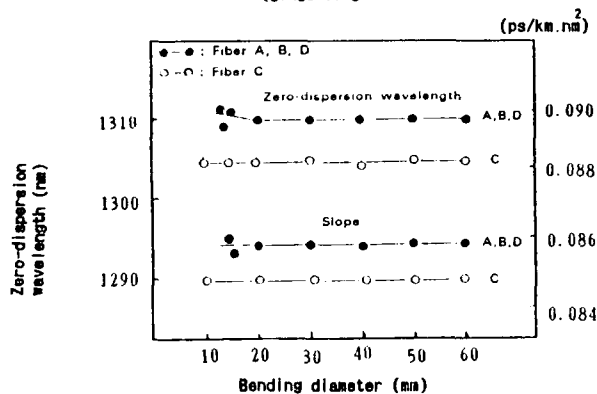


Fig. 3 Variation of zero-dispersion wavelength according to bending diameter (gauge length: 20m)

Fig. 4 shows variation of optical loss according to tensile stress. Optical loss is increased maximum  $0.09\text{dB}$  when elongation is  $25\text{mm}$ . It can be able to anticipate the maximum endurable excess length without increasing optical loss

Fig. 5 shows the comparison of elongation obtained between elongation meter in tensile stress system and phase shift method using strain-optic coefficient. If strain-optic coefficient is within  $0.775 \pm 0.02$ , the result is very similar compare to conventional method. The variation of zero-dispersion wavelength, optical power and elongation can be measured when tensile stress applied to fiber at the same time by using the phase shift method [4].

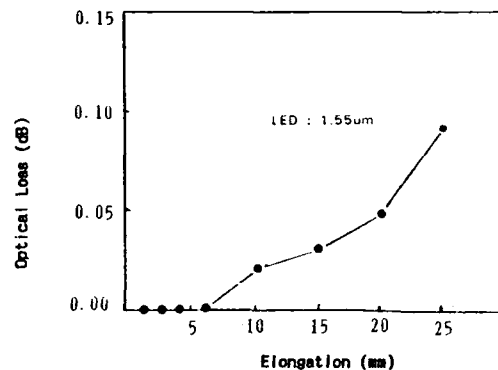


Fig. 4 Relation between the optical loss and elongation (gauge length: 60cm)

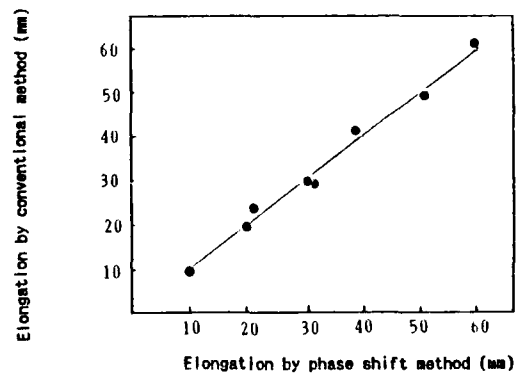


Fig. 5 Relation between elongation by conventional method and phase shift method (strain optic coefficient: 0.775)

## 5. CONCLUSION

Stress and bending loss dependence of chromatic dispersion for single mode fiber was investigated in  $1.3\mu\text{m}$  and  $1.55\mu\text{m}$  band. The effect of bending loss in the relative group delay is more sensitive  $1.55\mu\text{m} \sim 1.6\mu\text{m}$  than  $1.3\mu\text{m}$  when bending diameter is decreased. It is verified the cutoff shifted fiber wavelength has less variation than conventional fiber in zero dispersion wavelength and obtain the good result by the phase shift method using to strain-optic coefficient compare to conventional method.

## REFERENCES

- ① Axel Bertholds and René Dändliker "Determination of the Individual Strain-Optic Coefficient in Single-Mode Optical Fibers" Journal of Lightwave Technology, vol. 6 (1988)
- ② William H. Hatton and Masayuki Nishimura "Temperature Dependence of Chromatic Dispersion in Single Mode Fibers" Journal of Lightwave Technology, vol. LT-4, No. 10 (1986)
- ③ F. M. E. Sladen, H. S. Reichard and S. Uveges "Simple, fast and repeatable chromatic-dispersion measurement in laboratory, factory and field environments." DOD/ANSI/EIA Fiber Optic Standardization Conference (1987)
- ④ Arthur J. Barlow "Quadrature Phase Shift Technique for Measurement of Strain, Optical Power Transmission, and Length in Optical Fibers" Journal of Lightwave Technology, vol. 7 (1989)
- ⑤ W. Wenski B. Menze J. Schulte "Fiber strain during cable pulling : important factor in cable design" International Wire & Cable Symposium (1989)



Young-Taeg Kim  
Taihan Electric Wire  
Co., Ltd  
785, Kwanyang-dong,  
Anyang, Kyungki-do,  
430-060, KOREA

Y. T. Kim received his B.A degree from Pusan University in 1985. He joined Taihan Electric Wire Co., Ltd. and he has been engaged in measuring section of optical fiber. Now he is a engineer of the Quality Assurance Department.



Kun-Ik Jun  
Taihan Electric Wire  
Co., Ltd  
785, Kwanyang-dong,  
Anyang, Kyungki-do,  
430-060, KOREA

K. I. Jun received from Myungji Junior College in 1980. and joined Taihan Electric Wire Co., Ltd. He has been engaged in measuring and inspection of optical fiber. He is now a senior engineer of the Quality Assurance Department.



Yung-Ik Lee  
Taihan Electric Wire  
Co., Ltd  
785, Kwanyang-dong,  
Anyang, Kyungki-do,  
430-060, KOREA

Y. I. Lee received his M.S degree from Yonsei University in 1981. He joined Taihan Electric Wire Co., Ltd. and he has been engaged in measuring section of optical fiber. Now he is a Section Manager of the Quality Assurance Department.



# LONG LENGTH, HIGH SPEED AIR FEEDING OF OPTICAL UNITS BY PRESSURIZED AIR

Akira SANO Akio MOGI and Matsuhiko MIYAMOTO

FUJIKURA LTD.

1440 MUTSUZAKI SAKURA-SHI, CHIBA JAPAN

## ABSTRACT

Air carrying installation of optical units into pipes is promising as a flexible and casual installation strategy. This installation method does not need any civil engineering. The long distance and high speed installation is required. The parameters dominating air carrying performance are studied. As results, the surfaces of optical units and pipes are optimized to reduce friction constant. The installation of 1000m in length has been achieved. The long term stability of transmission loss installed optical units was confirmed for a pipe cable in test field.

## INTRODUCTION

Various types of optical cables had been implemented in the enlargement of optical fiber communication because of prominent features such as small size, light weight, low loss and high transmission capacity, etc. Air feeding installation method of optical fiber units is forming a unique and active category of optical cables. (1-6) This kind of cables are installed in two steps. In the first step, the cables comprising pipes are installed in a conventional manner. In the second step, optical units are carried into the said pipes by the force of pressurized air. Pipe cable and optical units are not usually installed at the same time. The second step installation can be delayed till optical fibers are demanded. And the second step installation does not need any civil engineer. Optical units can be easily installed from the ends of the pipe cable with a compact feeding apparatus. Moreover, the number of connecting points for pipe cables can be reduced, the fiber unit is less tensioned during installation, and the route is relatively easy to change. The removal of optical units is possible as well as air feeding. This technique have the advantages of flexibility and upgradability.

As for the carrying performance, the attainable carrying length and the feeding

speed are essential. The long distance air carrying performance is able to reduce the splice points and may broaden the application fields of this technique. Lately we have tried this technique that utilizes an air stream to install optical fiber cable. We have investigated the air carrying characteristics for various types of optical units and pipes. The key factors dominating the carrying performance has been found. The optical units and pipe surfaces have been optimized to reduce the friction constant as results.

## CONFIGURATION

The configuration of the PASS is given in Fig.1. The pressure feeding system comprises a pressure feeding device proper, a compressor, an air drier, an control unit and an optical fiber unit feeder. The optical fiber unit is forwarded by the pressure feeding device. The air is pressurized and dried by the compressor and the drier. The construction of the fiber unit is shown in Fig.2. As shown in this figure, the 6-fiber unit is coated with nylon followed by coating with polyethylene foam. The construction of the pipe to feed the optical fiber unit is shown in Fig.3.

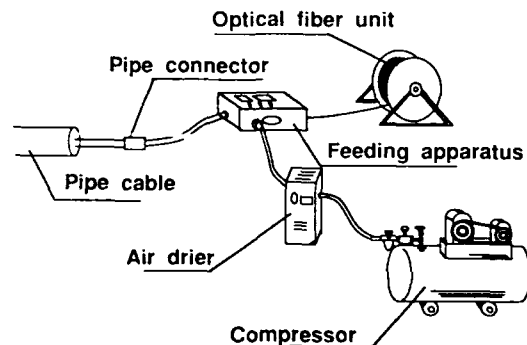


Fig. 1 System configuration

## ANALYSIS OF AIR CARRYING PERFORMANCE

The model of air feeding of fiber unit is shown in Fig.4. In the surface of the fiber unit placed in the polyethylene pipe, shear stress is produced by the viscosity of the air flowing through the pipe. The fiber unit is driven in the direction of the air stream when shear stress overcomes friction forces produced between the fiber unit and the inner wall of the pipe. Therefore, it is necessary to secure a sufficient flow rate of air driving the fiber unit and reduce the above-mentioned friction force in order to improve the pressure feed performance of the fiber unit. We have roughly estimated the attainable feeding length. The attainable air feeding length is determined by the force balance of the driving force and the resistant force of the unit when the unit goes through the pipe. The resistant force depends on the condition of the pipe. We assume the pipe wound in a drum for simplicity as shown in Figure 5.

The air flow in a pipe is theoretically given as a function of the position  $x$  from the inlet of the pipe, absolute pressures  $P_{in}$ ,  $P_{out}$  at the inlet and outlet of the pipe.

$$P(x) = \left( \frac{P_{in}^2 - P_{out}^2}{L} x + P_{in}^2 \right)^{\frac{1}{2}} \quad (1)$$

$$V(x) = \frac{V_0 P_0}{P(x)} \quad (2)$$

We confirmed the validity of this equation experimentally. The relation between the flow rate and the driving force is estimated experimentally as shown in Fig.6. The driving force operated on the 1 m long unit was measured by a load cell as a function of the flow rate. The measurement setup of driving force is shown in Fig.7. The inner diameter of the pipe is 6 mm and the outer diameter of the unit is about 2 mm. Optical fiber units with various surface roughness were evaluated. According to Fig.6, the driving force can be approximately represented by the 1.6-1.8 times power of flow rate regardless of the degree of the surface roughness. The surface roughness of the units increases the driving force apparently. The total driving force of the unit is calculated from Eq.(2) and the driving force constant estimated from Fig.6 as follows.

$$F_d = c \int_0^L V(t)^{1.6} dt \quad (3)$$

On the other hand, the resistant force  $F_b$  was supposed to be represented by the friction constant between unit and

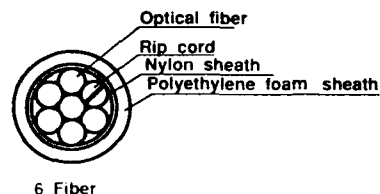


Fig. 2 Cross section structure of optical fiber unit

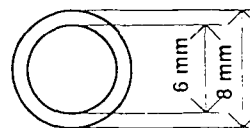


Fig. 3 Structure of feeding pipe

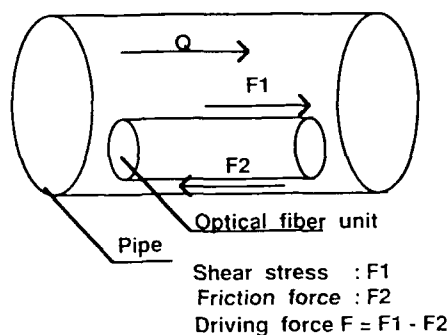


Fig. 4 Driving force of optical fiber unit

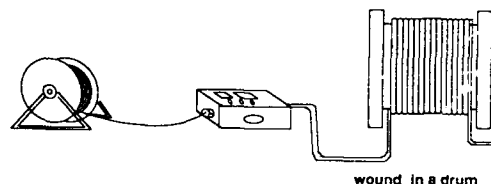


Fig. 5 Pressure feeding condition

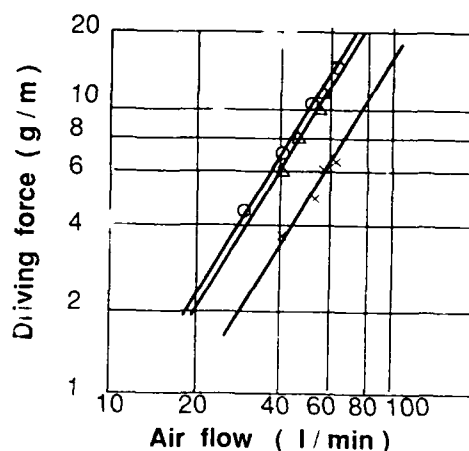


Fig. 6 Measured driving force

pipe. The integrated resistant force  $F_b$  along the unit in a pipe is given by

$$F_b(x) = F_0 \exp\left(\frac{\mu x}{2\pi R}\right) \quad (4)$$

where,  $R$  is the winding radius of the pipe in a drum. Fig.8 shows the curves of the driving force and the resistant force operated on the unit. The cross points of both curves show the balance condition. This condition means the maximum carrying length of the unit. The friction constants and the driving force coefficients are changed. The driving force coefficient is determined by the interaction between the unit surface and the air flow. The friction force increases exponentially. The reduction of the friction constant is considered to be more effective for the improvement of carrying length according to Fig.8. There is a trade-off of surface roughness of unit because the roughness increase not only the driving force but also the friction constant.

#### CARRYING PERFORMANCE AND FRIC. CONST.

Friction constants for various units and pipes were measured and the carrying performance were compared. The friction constant have been reduced by 1/4.

In general, the friction constant is determined by the following equation.

$$\mu = \frac{1}{\vartheta} \ln\left(\frac{F_d}{F_b}\right) \quad (5)$$

The dragging force of the unit with a back tension is measured as shown in Fig.9. The friction constant depends actually on the dragging speed, winding radius of a pipe, the length of samples and so on. The measurement condition was fixed and standardized. The two optical units and eight pipes with various inner surface conditions were evaluated. Results were plotted as a function of friction constant as shown in Fig.10. The air feeding performance of these combinations of unit and pipe was measured as follows. The pipes of 500 m in length are wound in drums with the same diameter. Feeding air pressure at the inlet was changed by the step of 1 kg/cm<sup>2</sup>. The minimum air pressure and feeding time for complete feeding was measured. Air pressure and carrying time are ranked in the same vertical axis. Minimum feeding air pressure is scaled in a vertical axis in the interval of 1 kg/cm<sup>2</sup>. Marks located in the same interval of the axis indicate the same minimum air pressure for complete feeding. Inside the interval, locations of marks indicate the feeding time. And the width of each interval corresponds to one hour. In other words, the ranking is lower, the better the carrying performance is in this fig-

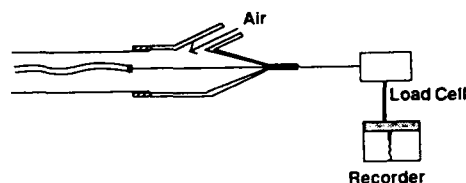


Fig. 7 Measurement setup for driving force

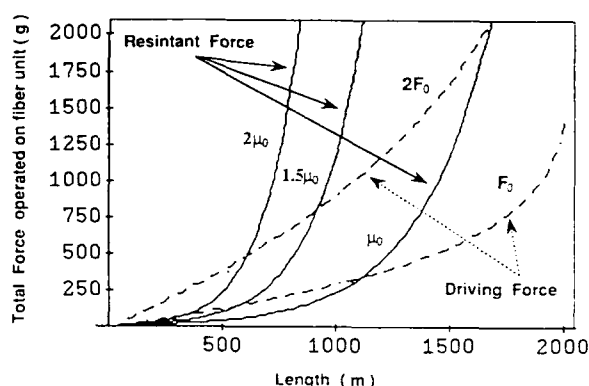


Fig. 8 The calculated driving force and resistant force

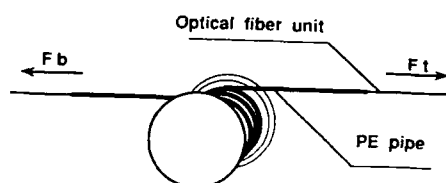


Fig. 9 Measurement setup of friction coefficient

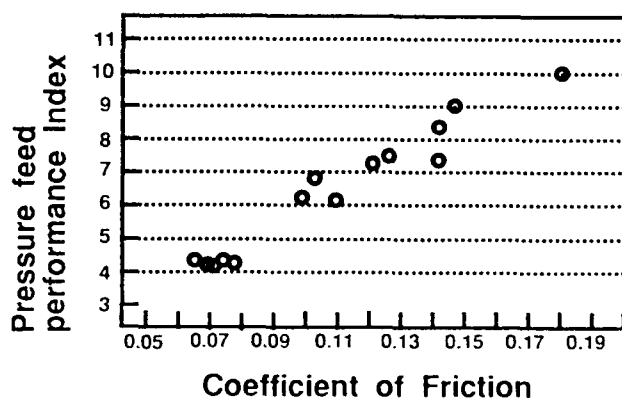


Fig.10 Air Carrying Characteristics

ure. It is noted that the order of ranking agrees well with the order of the friction constant. The feeding time less than 10 minutes has been achieved for lower friction constant combinations.

The friction constant between unit and pipe was reduced by harmonizing the surface roughness of optical units and the pipe and by the modification of the material. The combination of rough surface fiber unit and rough surface pipe indicates the large friction constant. The doping slipping agents into unit or pipe also reduced the friction constant. The friction constant was reduced to about 1/4 value relatively.

#### FIBER UNIT AND PIPE CHARACTERISTICS

The optical fiber units with optimized foamed polyethylene were tested. The transmission loss process variation is shown in Fig.11 for the 6-fiber unit coated with nylon and then with polyethylene foam. Measurements were taken using the OTDR method, at a wavelength of 1550 nm. There was not increase in transmission loss, i.e., this characteristics was stable.

The unit were subjected to 20 cycles of heat cycle test (24 hours per cycle) at temperature of -20 to +60 degree C to measure their transmission losses. Results are given in Fig.12. The increase in transmission losses was about 0.01 dB/km, this characteristic was stable.

Concerning the pipe material, we selected a high-density polyethylene-based material placing importance on the resistance to friction with the fiber unit, pressure feed performance at high temperatures (60-70 degs C), expected to be encountered in actual routes, and mechanical performance.

Table 1 shows the results of testing the polyethylene pipe for mechanical performance. Sufficient mechanical performance was shown for the pipe.

#### APPLICATION TO CABLES

An assembled pipe type cable were installed to investigate the applicability of the PASS method to cables. And long-term reliability was examined. Cable installation routes include straight, curved, ascending and descending sections. Total route length is 500 m. Fig.13 shows the construction of assembled four-pipe type cable. The subject unit for pressure feeding was the 6-fiber unit.

##### 1) Transmission loss after pressure feeding

There was no increase in transmission loss of singlemode fiber, i.e., this characteristics was stable. Moreover, in order to evaluate its long-term stability after pressure feeding, the fiber unit was

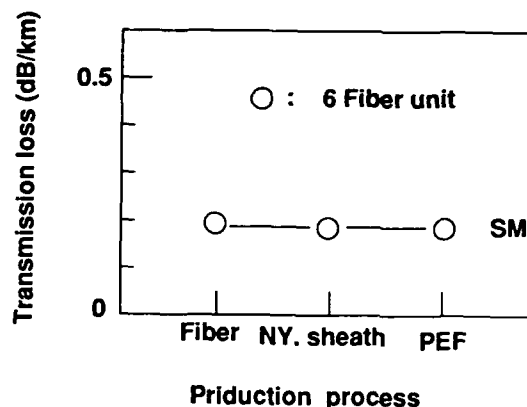


Fig.11 The change of transmission loss through the production process

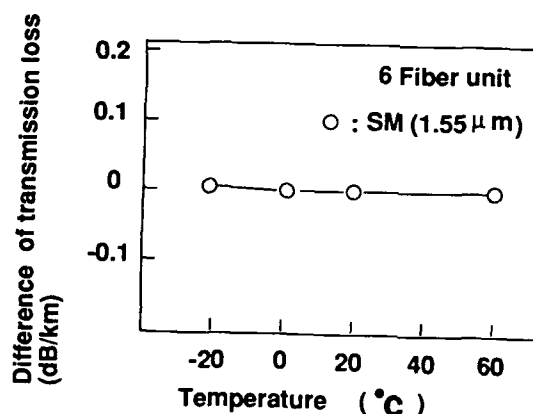


Fig.12 Temperature dependence of transmission loss

Table 1 Mechanical test of PE pipe

Item	Conditions	Result
Mechanical Test	Crush Plate width : 50 mm Weight : 20 kg	about 20 %
	Impact Height : 1 m Weight : 1 kg	30 - 40 %
Thermal Mechanical Test	Low temp. Impact Temperature : -20 °C Height : 2 m Weight : 1 kg	N. T.
	Low temp. Bend Temperature : -20 °C Mandrel diameter : 80 mm	N. T.
	High temp. Bend Temperature : 80 °C Mandrel diameter : 80 mm	N. T.

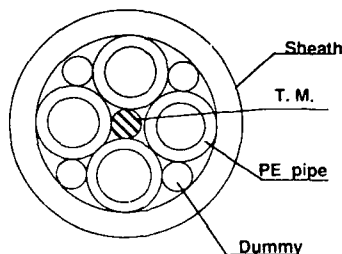
allowed to stand for one year to investigate the variation in transmission loss with time. Results are given in Fig.14. Measurements were taken after one month, after six months and after one year. There was no increase in transmission loss, i.e., this characteristics was stable.

## 2) Pressure feed performance

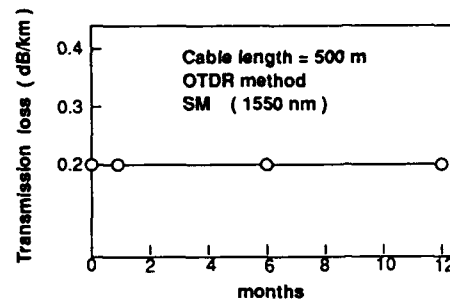
Initially pressure feed performance was evaluated applying an air pressure of 6 kg/cm<sup>2</sup>. Pressure feeding over the entire length was completed in about 30 minutes. And the route length of 1000 m was formed by joining two pipes at the end of the cable end. The air feeding through this joined pipe was tried and was achieved. Similar to the transmission loss, Prior to pressure feeding of the fiber unit, dry air was sufficiently blown through the pipe. Results are given in Table 2. No degradation in pressure feed performance was observed. Namely, pressure feeding after one year could be completed in the same period of time as that in the initial stages.

## 3) Mechanical performance

With the PASS method in which the fiber unit is pressure fed after cable installation, there is a possibility that external forces applied during installation may cause the pipe in the cable to be flattened or crushed. We evaluated its tension, bending, flexing, crushing, torsion, impact, vibration, etc., characteristics. For this evaluation, we investigated the ability of the pipe to pass a 4.0 mm steel ball through it and the flattening of the cable during testing as well as the flattening of the pipe after disassembly of the cable. Results are given in Table 3. It can be seen from the results that the pipe maintained the initial ability of passing the 4.0 mm steel ball. And that the pipe was not flattened when the cable was disassembled after the test.



**Fig.13** 4 pipe cable



**Fig.14** The long-term transmission loss change of installed optical fibers

**Table 2** The change of long-term pressure feed performance

Periods	Feed time (500 m)	Transmission loss after feed (dB/km at 1550 nm)
Initial	10 min.	0.21
1 month	10 min.	0.20
6 months	9 min.	0.20
12 months	9 min.	0.20

**Table 3** Mechanical test results of the four pipe cable

Item	Condition	Evaluation	Cable ellipticity (%)
Tensile Performance	Cable length = 100 m Tensile force = 210 kg	N. T	0.0
Repeated bending	Bending radius = 250 mm Angle = 180 deg. Number of cycle = 5	N. T	0.0
Flexing	Carrier pulley radius = 250 mm Angle = 135 deg. Tensile force = 210 kg Flexing section length = 1m	N. T	5.0
Crush	Weight = 100 kg / 50 mm Sample length = 1 m	N. T	2.2
Torsion	Tensile force = 25 kg Torsion angle = 90 Number of cycle = 3	N. T	0.0
Vibration	Span length = 1 m Frequency = 10 HZ Amplitude = 5 mm Number of cycle = one million	N. T	0.0
Impact	Impact area = 25 mm Weight = 1 kg Height = 1 m	N. T	2.0

## **CONCLUSION**

We investigated a method of installing optical fiber unit after completing cable installation. With this method, the coefficient of friction between pipe and fiber unit has been reduced to about 1/4 the ordinary value of friction coefficient. Its reduction is effective in improving the pressure feed performance. Using such pipes and units has made it possible to complete pressure feeding stably for 1000 m. Moreover, we have evaluated the degradation in pressure feed performance and the variation in transmission loss for the long term and have obtained stable results. Because of its prominent features, the pressurized air installation method is expected to expand its applications in the future to pipe composite cable, building room wiring cable etc.

## **REFERENCE**

- 1) S.A. Cassidy, M.H. Reeve: "A RADICALLY NEW APPROACH TO THE INSTALLATION OF OPTICAL FIBER USING THE VISCOUS FLOW OF AIR" IWCS Proceedings pp205-254, 1983
- 2) T. Matsumoto, H. Fudo, N. Fukae et al; "A Study of Installation method for Power and Telecommunication composite Network", National Convention of JIEE, Paper No.1177, 1988 in Japanese.
- 3) M. Wada, H. Fudo, S. Nishimura et al; "A Study of Pressure Feeding Characteristics of High fiber count ABF cables under various installation conditions", National Convention of JIEE, Paper No.207, 1989 in Japanese.
- 4) G. Katsuta, A. Toya et al; "Implementation of Optical fiber composite 66 kv CV cable utilizing Air Blown Fiber Installation", National Convention of JIEE, Paper No.1424, 1989 in Japanese.
- 5) Y. Harada; "Field Test Result of CBFC for Aerial Use", National Convention of JIEE, Paper No.C-5-8, 1991 in Japanese.
- 6) T. WADA, Y. KOIKE, T. SUZUKI, A. MOGI, M. SUEMATU; "Pressurized Air Carrying Fiber System", National Convention of JIEE, Paper No.208, 1990 in Japanese.

Akira Sano



Opto-Electronics  
Laboratory  
Fujikura Ltd.

1440 Mutsuzaki  
Sakura-shi, Chiba-ken  
285 Japan

Mr. SANO was born in 1960. He joined Fujikura Ltd. after his graduation from Kyoto University with a B.E. in 1984 and has been engaged in research and development of cable materials. He is an engineer of Telecommunication Cable Section and a member of IEICE of Japan.

Akio Mogi



Opto-Electronics  
Laboratory  
Fujikura Ltd.

1440 Mutsuzaki  
Sakura-shi, Ciba-ken  
285 Japan

Mr. Mogi was born in 1946. He joined Fujikura Ltd. after graduation from Haneda Institute High School in 1967 and has been engaged in research and development of the metallic cables and optical cables. He is now the senior engineer of telecommunication cable section and a member of IEICE of Japan.

Matsuhiro Miyamoto



Opto-Electronics  
Laboratory  
Fujikura Ltd.

1440 Mutsuzaki  
Sakura-shi, Chiba-ken  
285 Japan

Mr. Miyamoto was born in 1953. He received the B.S. degree from Nagoya Institute of Technology in 1976 and the M.S. degree from the Tokyo Institute of Technology in 1978. In 1978 he joined Fujikura Ltd. and has been engaged in research and development of optical fibers and cables. He is now the senior engineer of telecommunication cable section and a member of IEICE of Japan.

# Reducing Connecting Loss of Multiple Fiber Connectors by Expanding Mode Field Diameters

T.Ohmori

H.Hosoya

M.Akiyama

Opto-Electronics Laboratory, Fujikura Ltd.  
1440 Mutsuzaki, Sakura, Chiba, 285 Japan

## Abstract

In order to reduce connecting losses of multi-fiber connectors, it is necessary to align the optical axes of the single-mode fibers with an accuracy of the order of submicrons. Expanding the mode field diameter at the fiber splice makes it possible to reduce the splicing losses resulting from transverse offset of the fibers theoretically. We selected a method that heats the optical fibers of a fiber ribbon using a small gas burner to expand their mode field diameters. We obtained the optimal conditions by experiments. As a result, the average connecting losses of four-fiber connectors could be reduced from 0.25 dB to 0.19 dB.

## Introduction

Multiple optical fiber cables with high fiber counts up to 1,000 are introduced into subscriber loops in Japan. In installation of the cables, multi-fusion splice and multi-fiber connectors are used to splice the fiber ribbons. Although the splice loss of the fusion splice is lower, connectorized cable which has multi-fiber connectors at the ends are widely used because of shortening the installation time.

The factors that determine the splice loss of single-mode fibers involve transverse offset, tilt, difference of mode field diameters, inconsistency in refractive index, etc., [1]. Taking into account the existing fabricating and splicing techniques, transverse offset is the major cause of splice loss. Various methods of ex-

panding the mode field diameter of the fiber to decrease the contribution of this transverse offset have been reported [2], [3], [4], [5]. Examples of these methods are elongating the fiber in taper form [6], fabricating the fiber in inverted taper form [7], diffusing the dopant in the fiber with heating, etc..

This paper shows the results of investigation and experiments of expanding mode field diameter.

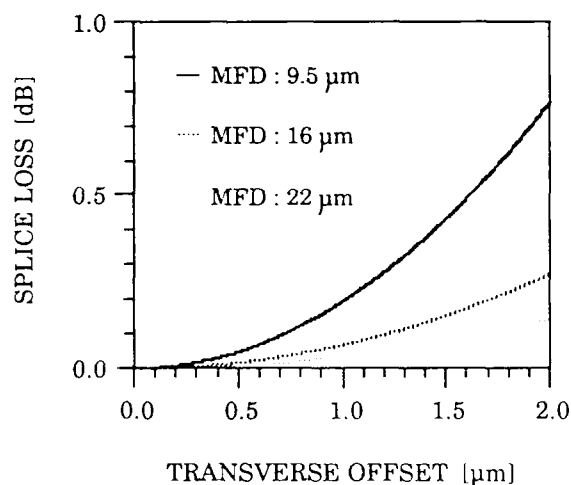
## Principle

To estimate the effect of expanding mode field diameter, the relation between transverse offset and splice losses is given in Fig. 1 with the mode field diameter as a parameter. As seen from this figure, the splice losses with a transverse offset of 1.0  $\mu\text{m}$  are 0.19, 0.07 and 0.04 dB for mode field diameters of 9.5, 16 and 22  $\mu\text{m}$ , respectively. Thus, expanding mode field diameter makes it possible to effectively reduce the contribution of transverse offset to splice losses.

To realize the expanded mode field diameter, the method that diffuse the dopant in the fiber with heating was investigated. This method permits to vary the refractive index distribution with the V value of each fiber virtually kept constant. Therefore, it is highly possible that the high-order mode will not take place and that radiative losses will not occur in the fundamental mode. The increase in losses resulting from the expanded mode field diameter should be negligible if this diameter is continuously expanded along the fiber axis and the expanded

portion is not bent. Moreover, it is possible to heat treatment any portion for the fiber and to maintain the outer diameter of the fiber unchanged, so such fibers, when attaching connectors to them, can be handled in the same manner as the ordinary ones.

Thus we selected a method that heats the fibers of a fiber ribbon using a small gas burner to cause thermal diffusion of germanium, a dopant in the core, in order to expand their mode field diameters.



**Figure 1** Splice loss versus transverse offset for various mode field diameters.

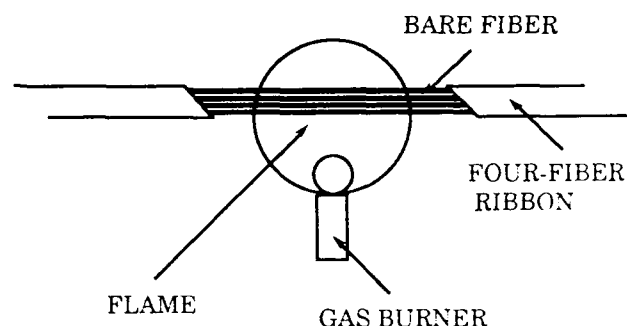
Wavelength : 1.31 μm

Angular misalignment : 0 degrees

### Method of Expanding Mode Field Diameter

Expanding the mode field diameter by thermal diffusion is possible by using an electric furnace, a small gas burner or the like. In this study, we expanded the mode field diameter using a gas burner. A schematic view of the heating system adopted by us is shown in Fig.2. The subject fiber ribbon was of four-fiber design. The UV jacket of this fiber ribbon was partly stripped off and the fibers were heated directly by gas burner. The heating temperature could be estimated to be around 1,600

degrees because the fibers just began to soften. To maintain the heating temperature constant, the flow rates of fuel gas and oxygen gas were finely controlled and the location of the small gas burner automatically controlled using a manipulator. Further, tension was controlled at lower than 10 gw to prevent the fibers being elongated. After heating, the fibers were cut each at the center of the heated portion and evaluated with a multi-fiber connector (MT connector) attached to them.



**Figure 2** A Schematic view of the heating system.

Firstly, the mode field diameter was investigated at a wavelength of 1.31 μm to confirm that this diameter was actually expanded. The results of measuring the mode field diameter for each heating time are given in Fig.3. From this figure, it can be found that the mode field diameter becomes larger with longer heating time. We succeeded in expanding the mode field diameter with good reproducibility by controlled in the range of  $16 \pm 1 \mu\text{m}$ .

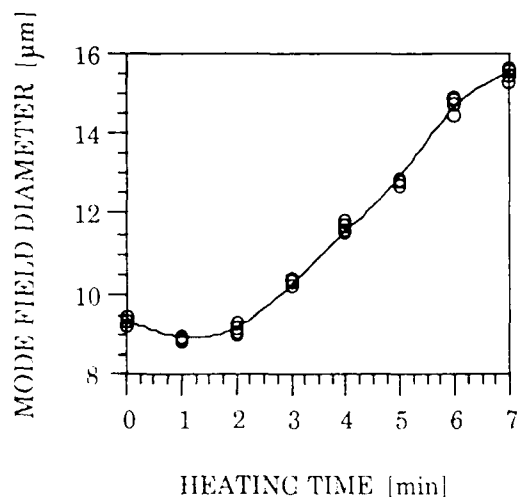
A near-field pattern (NFP) at 1.31 μm wavelength is shown in Fig.4. It can be seen from this figure that the high-order mode does not take place and axial symmetry is not disturbed significantly. The power distribution caused on the fiber endface when illuminated by a halogen lamp is shown in Photo.1 for reference.

Next, how the mode field diameter after heating of the fiber changes along the fiber axis was investigated. Results are given in Fig.5. The mode field diameter shows a smooth vari-

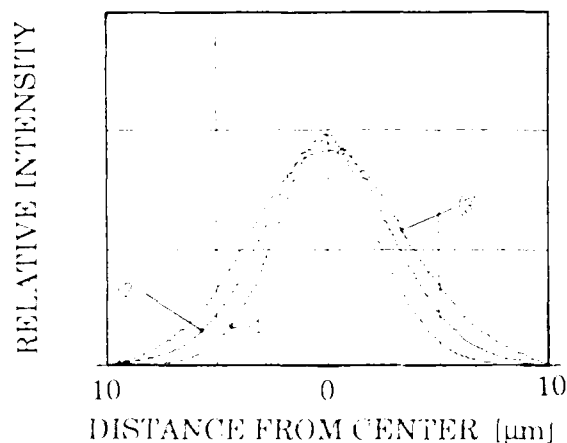


ation from 17 to 10  $\mu\text{m}$  over a length of 3 mm from the center of the heated portion. The differences in mode field diameter between the four fibers are as small as 1  $\mu\text{m}$ .

The optical fibers before and after heating were measured for refractive near-field pattern (RNFP). As a result, it was found that the refractive index difference after heating is smaller than that before heating. It can be grasped that germanium, a dopant in the core, is diffused with heating.

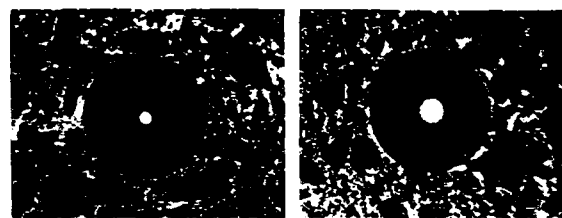


**Figure 3** Mode field diameter versus heating time.



**Figure 4** Near field pattern at 1.31  $\mu\text{m}$  wavelength.

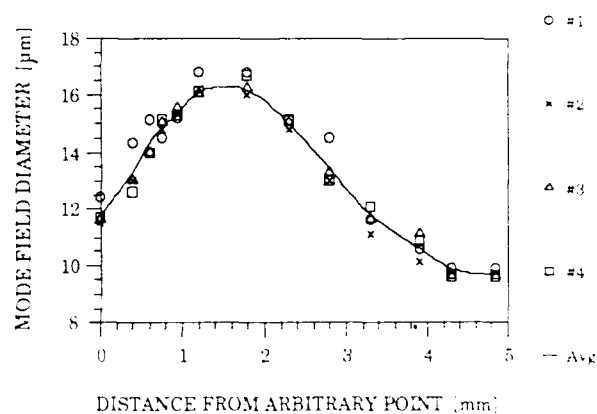
- (1) MFD : 9.4  $\mu\text{m}$
- (2) MFD : 12.2  $\mu\text{m}$
- (3) MFD : 15.1  $\mu\text{m}$



MFD : 9.5  $\mu\text{m}$

MFD : 20  $\mu\text{m}$

**Photograph 1** Power intensity.

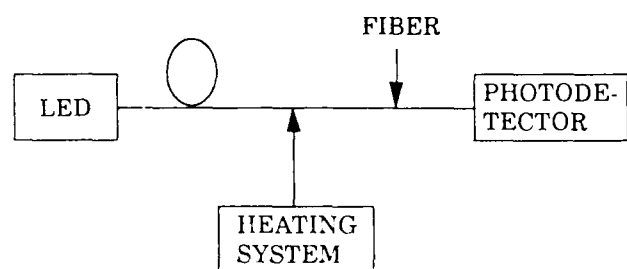


**Figure 5** Change of mode field diameter along the fiber axis.

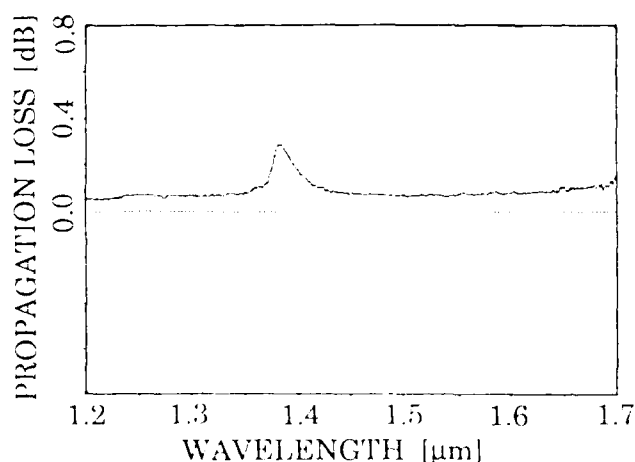
### Conditions for Expanding Mode Field Diameter

Theoretically it seems preferable that the mode field diameter be made as large as practicable. However, it was found that this actually results in greater propagation losses in the heated portion of the fiber. To confirm that the losses caused by heating or by expanding the mode field diameter vary, we performed an experiment using an experimental system shown in Fig.6. The heating system was the same as that shown in Fig.2. The wavelength dependency of the losses was measured for each heating time. The wavelength depend-

ency of the losses resulting from 10-minute heating is shown in Fig.7. In this graph, a peak value exists in the 1.38  $\mu\text{m}$  band. This loss is attributable to light absorption by OH radical. Further, a gentle increase in losses can be observed in the entire range of wavelengths.



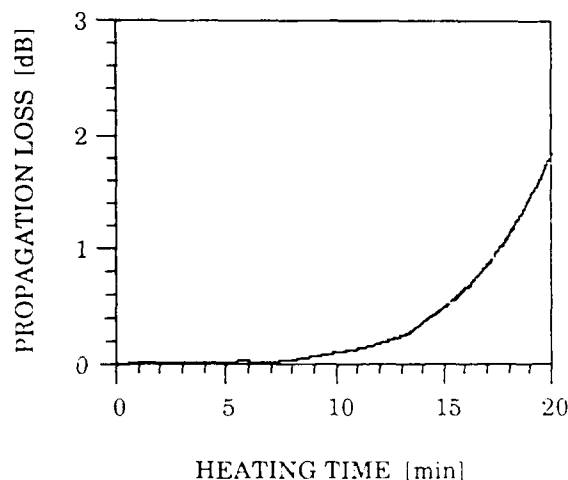
**Figure 6** Experimental system.



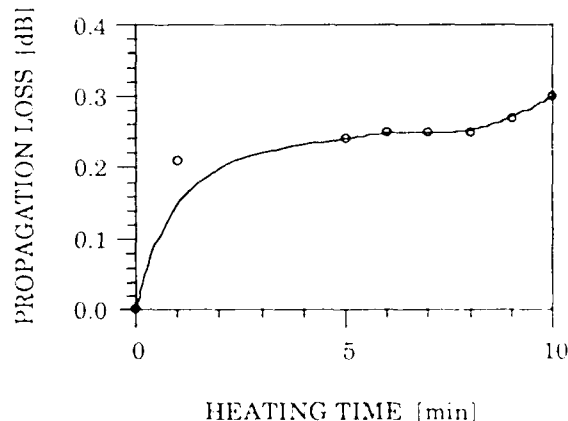
**Figure 7** Wavelength dependency of loss resulting from 10-minute heating.

The relation between heating time and loss is given in Figs.8 and 9 for wavelengths of 1.31 and 1.38  $\mu\text{m}$ , respectively. The light absorption by OH radical becomes greater with longer heating time and the amount of light absorbed by OH radical reaches saturation in a short time, but this virtually does not affect the loss at 1.31  $\mu\text{m}$ . Further, the increase in losses in the entire range of wavelengths, caused by short-time heating, is small. With longer heating time, the loss increases exponentially up to

a level that cannot be neglected, e.g., 10-minute heating increases the loss by 0.07 dB. Thus expanding the mode field diameter by increasing the heating time results in greater losses, so it is necessary to prevent this increase in losses.



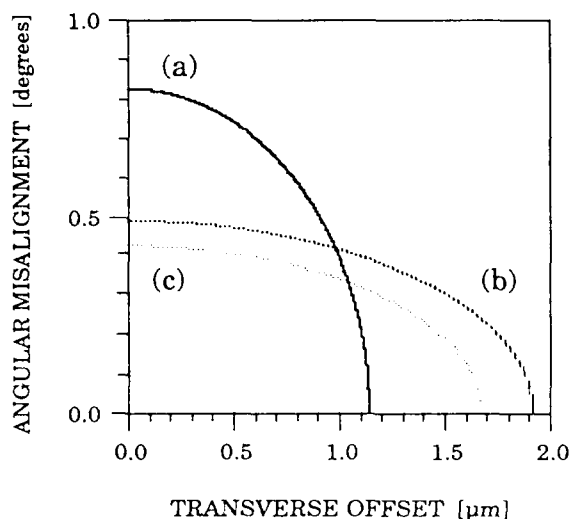
**Figure 8** Propagation loss at 1.31  $\mu\text{m}$  wavelength versus heating time.



**Figure 9** Propagation loss at 1.38  $\mu\text{m}$  wavelength versus heating time.

In addition, expanding the mode field diameter makes greater the contribution of angular misalignment to connecting losses. The relation between transverse offset and angular misalignment is shown in Fig.10 with the connecting losses as a parameter. Expanding the mode field diameter decreases losses by trans-

verse offset but increases losses by angular misalignment.



**Figure 10** Angular alignment versus transverse offset.

(a) MFD : 9.5 $\mu\text{m}$	Loss : 0.25 dB
(b) MFD : 16 $\mu\text{m}$	Loss : 0.25 dB
(c) MFD : 16 $\mu\text{m}$	Loss : 0.19 dB

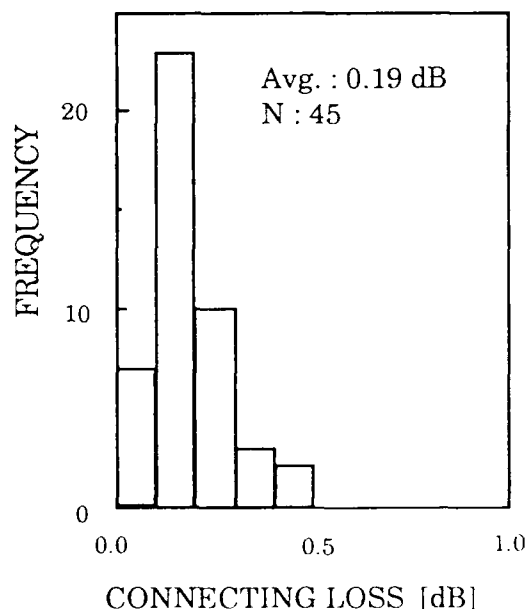
Therefore, it is important that the losses by heating and those by transverse offset and angular misalignment be controlled to attain a better trade-off between them. Taking into account these factors, we controlled the heating time at 7 minutes and expanded the mode field diameter to about 16  $\mu\text{m}$ .

### Connecting Characteristic of Multi-fiber Connectors With Expanded Mode Field Diameter

The method of fabricating a multi-fiber connector to be attached to a fiber ribbon of expanded mode field diameter will be described below. First, the fibers of a four-fiber ribbon were heated using the heating system shown in Fig.2. Controlling the heating time, the mode field diameter at the center of the heated portion of each fiber was expanded from 10 to 17  $\mu\text{m}$ . The fiber ribbon was then cut and a four-fiber MT connector was attached to it. Another four-fiber MT connector not subjected to heat

treatment was attached to the opposite side to the MT connector attached to the fiber ribbon of expanded mode field diameter.

Several four-fiber MT connectors with expanded mode field diameter were fabricated, connected at random and measured for connecting losses. Similarly ordinary four-fiber MT connectors on the opposite side to them were measured for connecting losses. A wavelength of 1.31  $\mu\text{m}$  and an index matching grease were used for this measurement. The average value of connecting losses was 0.25 dB for the ordinary four-fiber MT connectors and 0.19 dB for the four-fiber MT connectors with expanded mode field diameter. Thus the connecting losses of the four-fiber MT connectors could be reduced as shown by the graph of Fig.11.



**Figure 11** Loss histograms for four-fiber MT connectors with fibers expanded MFD.

Wavelength : 1.31  $\mu\text{m}$   
Using an index matching grease

Assuming that there is no angular misalignment, the average transverse offset can be determined to be about 1.1  $\mu\text{m}$  from the average value of connecting losses of the four-fiber MT connectors attached to the ordinary fiber rib-

bons and from Fig.1. For a mode field diameter of 16  $\mu\text{m}$ , the connecting loss with this value of transverse offset is about 0.09 dB. The loss of 0.19 dB obtained from the experiment is much greater than that value. It is considered as one of the reasons for this that the losses caused by tilt were too large to be neglected.

## Conclusion

By using a small gas burner, we could heat the multiple fibers of a single-mode fiber ribbon to expand the mode field diameters of all fibers equally and in short time. However, heating the fibers or expanding their mode field diameters increases losses. In order to prevent this increase in losses, the heating time was controlled and the mode field diameter was expanded. We succeeded in reducing the connecting losses of multi-fiber connectors by using the MT connectors with expanded mode field diameter. In addition to the reduction in splice losses, the MT connectors with increased mode field diameter will be able to find applications for other optical elements.

## Reference

- (1) D.Marcuse, "Loss Analysis of Single-Mode Fiber Splices," B.S.T.J., Vol.56, pp703-718, 1977.
- (2) Y.Kato, M.Miyauchi, "Splicing Technique for Active Transmission Lines," IEICE Japan, 2169, 1988.
- (3) M.Kihara, T.Nakashima, T.Haibara, M.Matsumoto, "A Fundamental Investigation for Splice Loss Reduction of Optical Fiber Connector," IEICE Japan, B-889, Spring 1991.
- (4) H.Hanafusa, M.Horiguchi, J.Noda, "Thermally-Diffused Expanded Core Fibers Fabricated by Heating with Microburners," IEICE Japan, C-276, Spring 1991.
- (5) K.Shiraishi, Y.Aizawa, and S.Kawakami, "Beam Expanding Fiber Using Thermal Diffusion of the Dopant," J.Lightwave Technol., Vol.8, No.8, August 1990.
- (6) K.Furuya, T.C.Chong, and Y.Suematsu, "Low loss splicing of single-mode fibers by tapered-butt-joint method," Trans. IECE Japan, Vol.E61, p.957, 1978.
- (7) N.Amitay, H.M.Presby, F.V.Dimarcello, and K.T.Nelson, "Optical fiber tapers - A novel approach to self-aligned beam expansion and single-mode hardware," J.Lightwave Technol., Vol. LT-5, p.70, 1987.

Teruhiko Ohmori

Fujikura Ltd.



Mr.Ohmori was born in 1966. He received the B.Sc. degree in physics from Aoyamagakuin University in 1990. He joined Fujikura Ltd. in 1990 and has been engaged in research and development of optical telecommunication cables and accessories. He is a member of the IEICE of Japan.

Hideyuki Hosoya

Fujikura Ltd.



Mr.Hosoya was born in 1959. He received the M.Sc. degree in physics from Yamagata University in 1983. He joined Fujikura Ltd. in 1983 and has been engaged in research and development of optical telecommunication cables and accessories. He is a member of IEICE of Japan.

Michio Akiyama

Fujikura Ltd.



Mr.Akiyama received the M.E. degree in Electrical Engineering from Yokohama National University in 1975 and joined Fujikura Ltd.. He has been engaged in the development of optical fiber, cable and accessory. He is now a chief of Fiber & Cable Accessory Section in Opto-Electronics Laboratory and a member of IEICE of Japan.

# **AN EVALUATION OF THE INTER-RELATIONSHIPS BETWEEN RHEOLOGICAL DATA OF FILLING COMPOUNDS AND FIBRE OPTIC CABLE PERFORMANCE**

G.Morland - Pirelli Cables\*  
D.Rees, G.White - Polytechnic of Wales\*\*

\*Pirelli-STC Cable Products Division, Newport, Gwent, UK.

\*\*Treforest, Mid Glamorgan, UK.

## **ABSTRACT**

The physical state of a filling compound is often described by means of cone penetration testing.

In this paper it is shown that an alternative approach was developed, based upon rheological analysis. Consideration of compound requirements both for processability and cable performance were determined, leading to a series of key rheological parameters being identified.

The results from rheological testing of filling compounds are compared to actual cable performance, and it is shown that critical material properties can be highlighted which would be missed by conventional analysis.

Based upon this knowledge a model is developed relating the yield stress of a filling compound to the optical performance of a slotted core cable.

## **1. INTRODUCTION**

As is widely recognised, the use of filling compounds in optical fibre cables, both in loose tube and slotted core application is a practical method for preventing water contact with the fibre, which is an essential requirement to maintain the physical properties of the fibre.<sup>(1)</sup> The performance of the compound and its interaction with the fibres and cable materials must be evaluated and take account of such issues as compatibility and compound drip/separation. In addition to this the rheological properties of the compound are also of paramount importance, both from the point of cable processing and cable performance.

The need to evaluate new filling compounds arose due to a requirement to change to higher performance materials in order to expand the potential market place. It was decided an essential part of this strategy was a change from 'hot', to 'cold' fill processing.

In undergoing a transition from hot fill processing with a polybutene/polythene mixture to a cold fill situation where one relies upon shear to break down particulate bonds and create molecular orientation enabling free flow, the use of a cone penetrometer was not considered suitable to provide

characterisation of such materials. In this paper an alternative approach was implemented where a controlled shear rate viscometer was used to produce rheological data on shear thinning compounds. It will be shown how this was related to both ease of cable processing and cable performance by enabling a map of the desired compound properties to be generated. This proved invaluable in reducing the number of development trials, quick screening of materials and maintaining quality control.

## **2. BACKGROUND**

The hot fill approach to filling compound injection which relies upon heat to create the desired blend before subsequent transfer has two fundamental associated problems:

(1). There is a risk of exposing the fibres to sudden thermal shock which may result in a deterioration in fibre strength. Furthermore the highly fluid state of the filling material will enhance the possibility of fibre cross over within the tube.

(2). The material viscosity is very temperature dependant in comparison to cold fill, resulting in leakage at elevated temperature and solidification at low temperature which invariably affect cable reliability and performance.

To overcome these problems, it was necessary to change to cold filling of fibre optic cables with the added benefit of increasing export capability.

To study a selection of hydrocarbon based cold fill compounds a viscometer was used to try to provide as much information about the flow behaviour of the material as possible. A compound has to be evaluated in this respect to cover two important areas:

(1). Processing - the viability of pumping at ambient temperature while closely maintaining excess levels and producing consistent material behaviour.

(2). In-cable performance - will a fibre or ribbon be able to move freely within the compound over the operational temperature or would attempted movement result in buckling/twisting due to resistance to motion.

This paper will demonstrate that rheological analysis is an excellent tool to critically evaluate the suitability of compounds

by providing more information than a cone penetration test, and information that allows discrimination between compounds to be more readily achieved.

### 3. METHODOLOGY

The analysis of a filling compound by means of a cone penetrometer will give a comparative measure of the physical state of the material. Typically just one reading would be attained, this in itself would not characterise the flow behaviour of the material as to whether it is newtonian or non-newtonian, neither would it give an indication of thixotropy or absolute values of viscosity.

In order to determine more about the material it would be necessary to vary the loading on the cone and measure the penetration achieved. Subsequently the load would have to be converted into a shearing stress and the penetration into a velocity gradient. When plotted, a curve similar to that of a flow curve can be generated.<sup>(2)</sup> Ultimately the determination of viscosity and other related parameters would not be an easily achievable task using this method.<sup>(3)</sup>

Alternatively, the viscometer is able to give a portrait of many rheological parameters of the material, which can also be measured as a function of temperature, such as flow behaviour, degree of thixotropy and yield stress.

The basis of measurements taken comes from flow curve generation where the material, from a position of rest, is exposed to linearly increasing shear rate. The corresponding material resistance to shear is recorded from which the shear stress is obtained. Plotting the two functions gives the flow curve, this can be used to model the behaviour of the material.

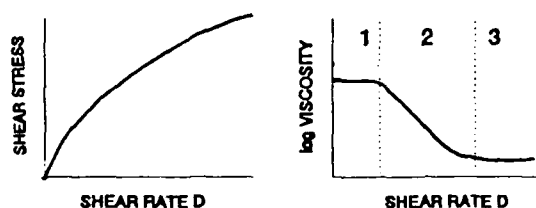


FIGURE 1. Pseudoplastic behaviour

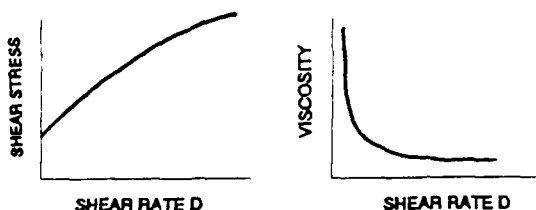


FIGURE 2. Viscoplastic behaviour

Figures 1 and 2<sup>(4)</sup> are two types of flow curve which appear similar but are significantly different when characterising the behaviour of a filling compound. Figure 1 shows a pseudoplastic material, it does in fact have three stages which

would be highlighted on a log-log viscosity plot of the viscosity curve. A newtonian region exists at low shear ( $< 10^{-3} s^{-1}$ ), a shear thinning region where there is molecular orientation and particulate bonding breaks down, and a newtonian region at high shear rate where the viscosity will remain relatively constant.

The curve shown does not however exhibit a yield stress value, that is the flow curve passes through the origin. An ideal filling compound will however show a yield stress as shown in figure 2, where the material is then no longer classified as pseudoplastic but instead viscoplastic.<sup>(5)</sup>

The subtle difference that occurs in the viscosity curve is that as shear rate tends to zero the viscosity will tend to infinity. This is seen from the equation for viscosity,  $\tau$  takes a constant value as  $\dot{\gamma}$  tends to zero.

$$\text{Hence: } \eta = \frac{\tau}{\dot{\gamma}} \rightarrow \infty \text{ as } \dot{\gamma} \rightarrow 0$$

Where  $\eta$  = Apparent viscosity  
 $\tau$  = Shear stress  
 $\dot{\gamma}$  = Shear rate

Typically one is interested in measuring the yield stress of a material as this will give an indication of the resistance that would be encountered by a fibre when trying to move through the compound. If it cannot move freely then buckling and breakage could occur.

It is difficult in generating a standard flow curve to obtain a precise value for yield stress due to the wide shear range covered which fails to focus on the critical low shear range. Normally separate testing would have to be done. However it is possible to apply a model to a smooth flow curve and from a good fit to get an indication of the yield stress.

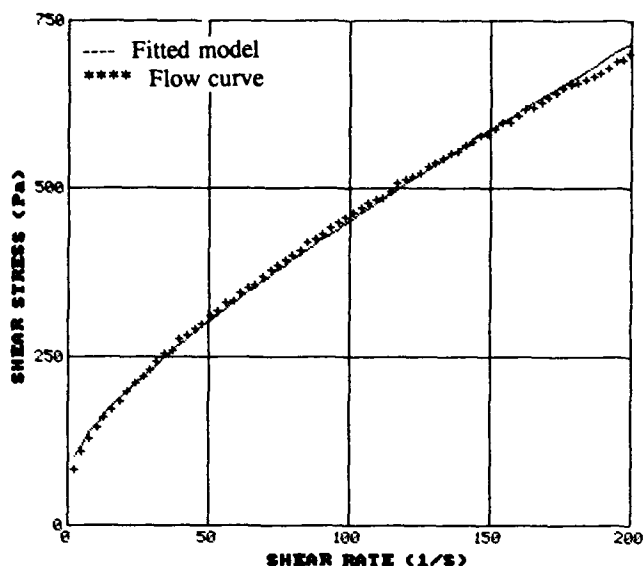
There are mathematical models available which can be used to estimate the yield stress for example Herschel Bulkley, Bingham and Casson.<sup>(6)</sup>

In attempting to fit a number of models to a flow curve of a filling compound it is shown in figure 3 that an ideal fit was found using the Casson model.

The Casson equation is given by:

$$\sqrt{\tau} - \sqrt{\tau_0} = \sqrt{\eta_a \cdot D} \quad (1)$$

Where:  $\tau$  = Shear stress  
 $\tau_0$  = Yield stress  
 $\eta_a$  = Apparent viscosity  
 $D$  = Shear rate



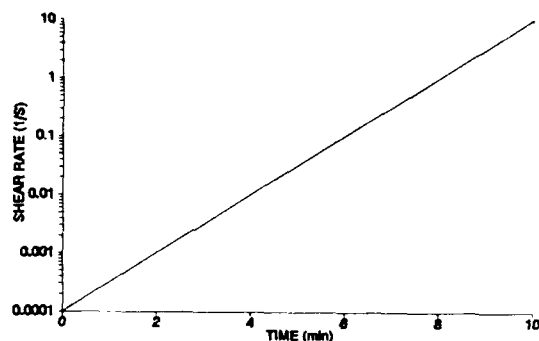
**FIGURE 3. Flow curve with fitted Casson model**

A correlation coefficient ( $R^2$ ) of 0.99 is given indicating an almost perfect fit in this particular case. The model gives a  $\tau_0$  value of 65Pa which can be interpreted as the true yield stress of the material.

This model was originally used to describe the behaviour of printing inks (based upon a system of mutually attractive particles suspended in a newtonian medium)<sup>(7)</sup>. It can be seen from these results that it provides a valid basis for a flow curve model. However with the range of compounds considered it was not possible to achieve a strong correlation each time as the majority did not show ideal behaviour, hence the yield stress was determined by using physical testing at low shear rate.

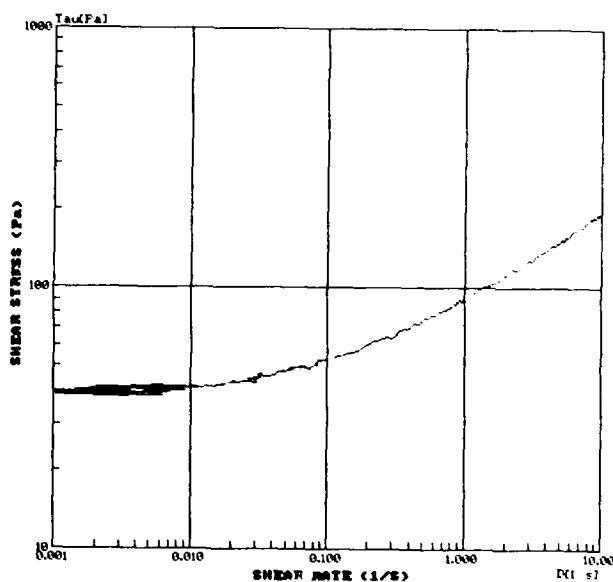
The determination of yield stress is open to personal interpretation, for example a static method such as the creep test using a controlled stress viscometer is limited by the fact that the yield stress measured is totally dependant upon the duration of the test, infact it has been argued that for infinitely long measurement times that no yield stress is observed.<sup>(8)</sup> In the dynamic test the yield value is determined by extrapolation of the flow curve and thus the lowest shear rate range covered will influence the recorded value. Thus in the case of a zero shear rate the flow curve would pass through the origin and no yield stress would be present.

To measure a quantity which would be classified for all purposes as the yield stress of a material a test sequence was devised which would measure the resistance to flow of the compound. The test is based upon a logarithmic increase in shear rate which allows resolution at the low shear rate region, as shown in figure 4.



**FIGURE 4. Shear sequence for yield stress determination**

It can be seen that initially the rate of increase is minimised thus highlighting the initial case of material flow. The generated flow curve is plotted on a log-log graph (figure 5) where the following effect is seen for a material exhibiting a yield stress.



**FIGURE 5. Flow curve for material exhibiting a yield stress**

Figure 5 shows that a constant stress response is being encountered at the lowest shear rate, defined as the yield stress. This can be thought of as the resistance to movement that the optical fibres would have to overcome. In a compound not exhibiting a yield stress the curve would continue on a downwards trend.

It is possible to make these measurements over an operational temperature range, which can become increasingly important for low temperature applications where the ability of fibres to move can be critical to the cable design.

During the analysis of filling compounds by means of rheological testing, two distinct requirements were looked for, the processability of the material at ambient temperature and

the performance of the material over the operational temperature range.

A selection of commercially available compounds were analysed including the hot fill material. Using these results and production trial experience key rheological parameters were identified to indicate performance.

#### 4. PERFORMANCE CHARACTERISTICS

##### 4.1 Processability

Ultimately the requirement is to be able to fill a loose tube or slotted core with compound at ambient temperature using commercially available equipment, taking into account the performance requirements of the filled component. This requires consideration of the following parameters.

##### 4.1.1 Shear thinning behaviour

A compound must for ambient application have a degree of fluidity such that it can fill an extruding tube or slotted core at a rate commensurate with the production speed. In the case of loose tube the material must be able to flow faster than the forming tube to achieve back pressure and complete tube filling.

If this degree of fluidity was representative of the material in the free standing state then one would have a problem associated with leakage of compound from the tube. Thus the ideal material should possess shear thinning behaviour, implying that the viscosity of the material will decrease as the degree of shear increases. The determination of this characteristic is relatively simple, a flow curve for the compound is produced and from this the relationship between viscosity and rate of shear is identified.

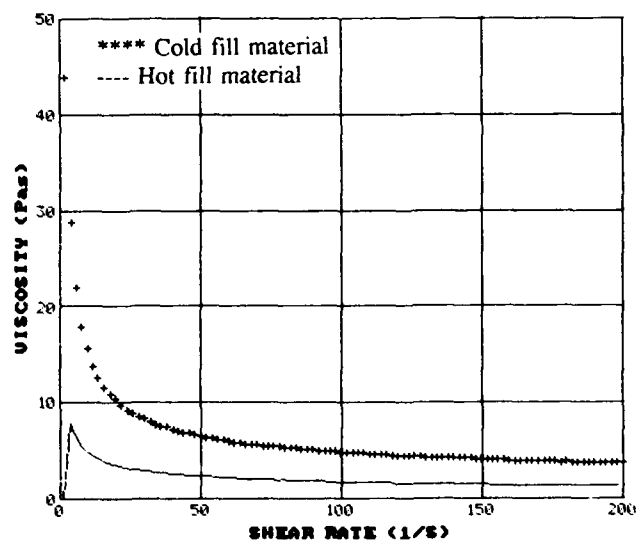


FIGURE 6. Viscosity curves comparison

Figure 6 shows viscosity curves for a hot and cold fill material, both measured at ambient temperature. The hot fill

material would at processing temperature give a flat newtonian response, however a comparison at ambient highlights the key differences between the two.

Most noticeable is the absence of shear thinning behaviour in the hot fill material, the viscosity remains fairly constant and will remain at this level after processing, this has implications on both the temperature performance of the material and optical performance of the loose tube.

In the former case the material is exhibiting a relatively low viscosity, thus when heat is applied a further reduction will make the compound fluid enough to start flowing. This accounts for the poor temperature performance of such materials and explains why leakage of the compound has been seen at 40°C.

The cold fill material gives a different response. Initially it is a gel like structure, it is on the application of shear converted into a mobile fluid which may be pumped at ambient temperature, the reason for this is the breakage of particulate bonds and the change in its molecular orientation.

The viscometer can be used to measure the degree of shear thinning of a compound, ideally one is looking for a material whose viscosity decreases most rapidly upon shear, decreasing the requirement of the pumping system and enabling a faster rate of flow. It has been found that in the production of loose tube that a base viscosity of 10 Pa.s should not be exceeded.

Of equal use in determining processability is analysis of the flow curve which can highlight effects not seen in the viscosity curve. Often a viscosity curve will not show initial material response, which can be a key factor in processing and performance. The following figures show examples of how a flow curve can be practically applied.

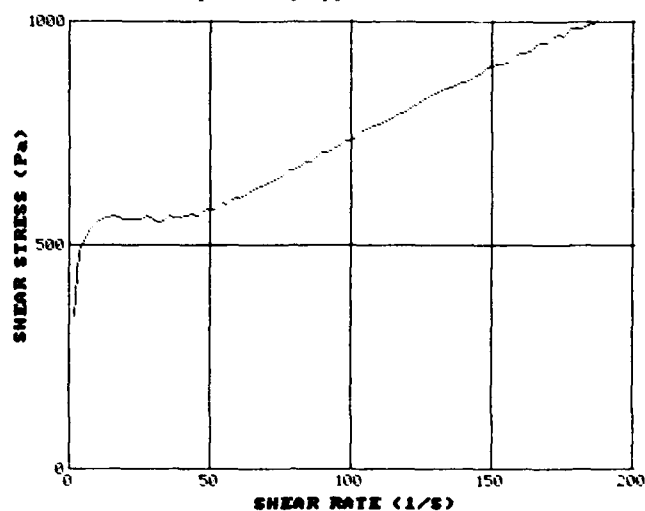


FIGURE 7. Flow curve comparison

Figure 7 shows the flow/viscosity curve for a compound used in a production trial. The initial impression given by the viscosity curve is that the material shows ideal shear thinning



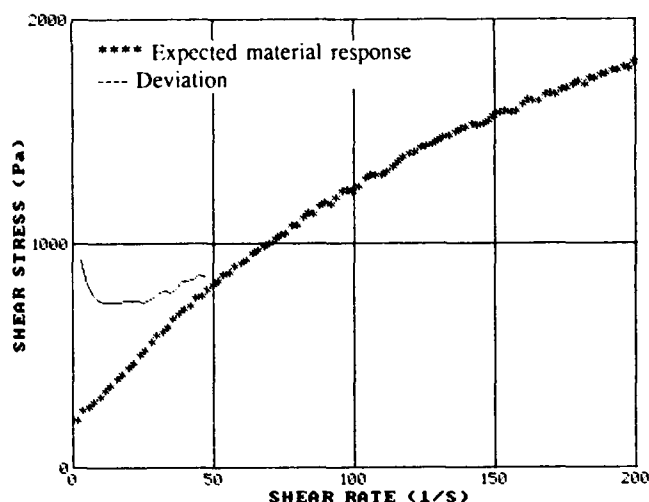
behaviour for processing, which was in fact correct. However it was virtually impossible to achieve an excess within the tube. This is believed to be as a result of the fibres being unable to move freely as tube shrinkage was occurring. Analysis of the flow curve shows that the material is exhibiting undesired behaviour with a distinct yield at 550Pa.

A similar example occurred in the case of a slotted cable incorporating a four fibre ribbon. The filling compound had been successfully used before and in this particular case the material had come within the specification of the cone penetration test. On production the cable, which relies upon excess ribbon to compensate for operational tension, showed excessive losses and point defects at 1550nm as shown in table 1.

COLOUR	loss at 1550nm dB/Km
RED	5.99
ORANGE	4.76
GREEN	1.46
BLUE	1.45

**TABLE 1.** Optical performance of four fibre ribbon at 1550nm

The optical losses experienced were associated with bunching of the ribbon and its inability to move freely within the compound. Rheological testing revealed that the material was not showing expected behaviour.



**FIGURE 8.** Comparison of flow curves

The material which caused the attenuation problems had a distinct yield point at about 1000Pa, by theory this can be attributed to the presence of a higher concentration of particles and larger particle size giving a stronger structure more resistant to flow.<sup>(9)</sup> It can be seen that once this peak is overcome that the material starts to behave as was originally expected, however such effects can only be of interest from a processing point of view.

Movement of fibre in service will be associated with low rates of shear which would not normally be seen using the cone penetrometer. This highlights the immense value of rheological testing both from an evaluation and quality control point of view.

#### 4.12 Thixotropy

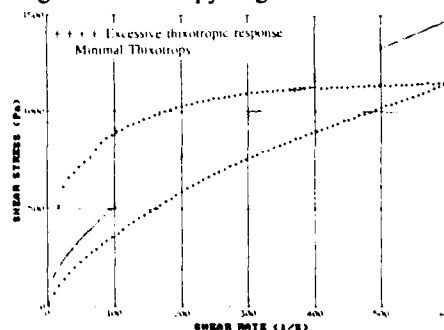
Production of a cable will inevitably involve shear working of a filling compound. In the case of a cold fill material this shear working is the sole mechanism by which a higher degree of fluidity is achieved. An important consideration is the time taken for the material to recover its original properties, defined as the thixotropy of the material. It is important to establish whether the material remains in the fluid state for a period of time after production or whether it should have rapid structure regeneration.

To answer this question an analysis was conducted on the output of a hot filling line (where the material will be fluid for considerable time) and a cold fill line where the material was known to show very little thixotropy.

For a sample of 500 loose tubes produced under hot fill and cold fill circumstances a count was taken of fibres showing defects at 1550nm. It was found that a far higher defect count existed in the hot fill process, approximately five times that of the cold fill. It is believed that the explanation for this lies in the state of the material just after the injection point. In the case of hot fill the material is highly fluid and offers little support to the fibres, the cold fill material with little thixotropy will help to lock the fibres together maintaining their positions, thus minimising the chance of defects.

A compound should be selected on the basis that it will allow the fibre to move freely if it requires to reposition to a state of equilibrium, and that this will still be the case if the temperature decreases. Given that this selection has been correctly made, to minimise the probability of defects occurring the compound should return to this state as soon as possible on the removal of a shearing stress. It is not necessary for the shear thinned structure to remain as a result of the original selection.

Hence the viscometer can be used to look at post injection behaviour of a sheared material to select one which shows a minimal degree of thixotropy. Figure 9 shows such a situation.



**FIGURE 9.** Thixotropic response comparison

The graph shows two flow curves that were produced by submitting the compounds to a linearly increasing degree of shear rate over a set period of time and then returned to rest under the same conditions. It can be seen that one of the compounds is not recovering its original structure in the set time period, thus exhibiting thixotropic behaviour. The other compound is not showing thixotropic behaviour as it is recovering its structure almost instantaneously. Thus in the case of the thixotropic compound the original structure will not be regained until after the tube is produced and as has been shown, maintaining fluidity can increase the likelihood of defects.

#### 4.2 Optical Performance of cable

The inter-relationship between cable performance and the physical properties of a filling compound is highly complex matter related to the movement of fibres in fluids. An attempt was made to create a simple model that related the movement of a ribbon in a horizontal slot to the yield stress of the compound.

A simple case was considered of two ribbons in a slot which restricts the movement of the ribbon, there is an overfeed of ribbon within the cable as it ultimately operates under tension.

The model is based upon the following assumptions:

1. The ribbon moves only in one direction
2. The redistribution of excess occurs in one movement
3. The effect of cable loading is not considered.

On the basis of a report<sup>(10)</sup>, it was assumed that losses due to macrobending would occur at a radius of curvature of 20mm, which in this case corresponds to a wavelength of 29.5mm.

For such a situation the relationship between wavelength and % overfeed is given by:

$$\lambda = 10\pi a x^{-1/2} \quad (2)^{(10)}$$

where  $a$  = amplitude of wave form  
 $x$  = percentage overfeed.

Substituting in (2) for a wavelength of 29.5mm yields an overfeed of 1.37%, which compares to a production average of 0.52%.

For a 1.37% excess to redistribute to an average 0.52% excess, a length of  $1.37/0.52 = 2.634m$  of ribbon is required.

The axial force associated with a bunched ribbon is given by:

$$F = 4 \cdot \pi^2 \cdot B \cdot \lambda^2 \quad (3)^{(10)}$$

Where  $B$  = Flexural rigidity of the ribbon

For the purpose of the model, in the case of a cable made up of two eight fibre ribbons in the slot acting as one unit, the flexural rigidity is given by  $16 \times 1.02Nmm^2 = 16.32Nmm^2$ .

This results in using equation 3 of

$$F = 4 \times 3.14^2 \times 16.32 \times 29.5^2 \\ = 0.74N$$

For the ribbon to move the material surrounding it must flow, for this to happen the yield stress of the material must be exceeded. Hence the axial force of the bunched ribbon must be sufficient to achieve this.

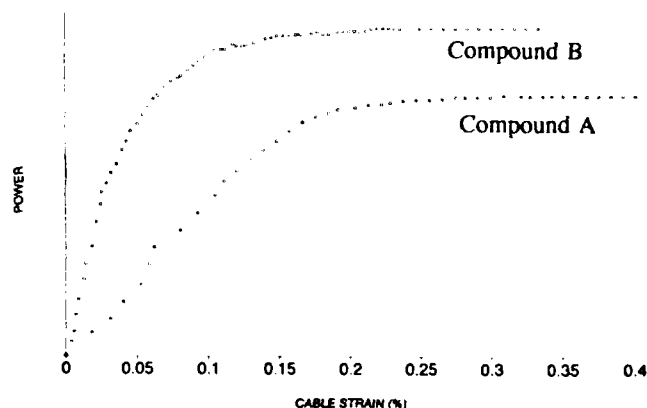
For this purpose the area of the ribbon is considered as the area of the two flat faces, which is  $10,500 \times 10^{-6}m^2$

Given that stress =  $\frac{\text{force}}{\text{area}}$

Then for ribbon movement to occur, the yield stress must be less than 70Pa.

In practice a yield stress of 90Pa has given successful results, however a value of 140Pa showed significant losses in the cable. The operation at a higher level is probably due to the effect of tensioning of the cable which the above analysis did not consider. The simplified model has however provided a valuable insight into the relationship between fibre movement and yield stress.

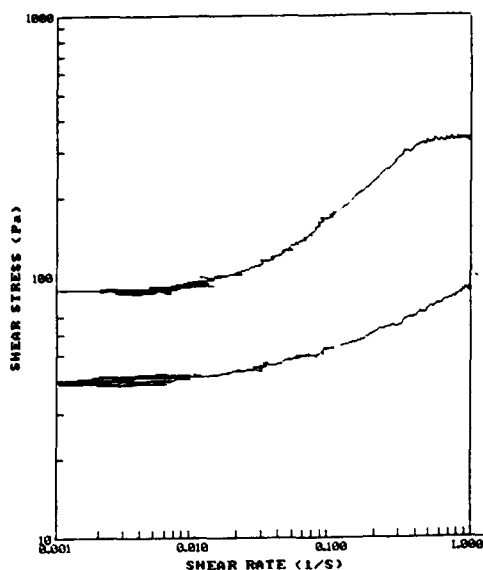
From the above it can be seen that the filling compound plays an important role on the performance of such a cable. To demonstrate this practically, trials were undertaken on two cables containing a ribbon within a slotted rod, each had a different filling compound. The cables were put under increasing load and the attenuation measured. As the load on the cable increased the attenuation levelled out as the excess was removed, the results showed that the loading level at which this occurred differed for the cables and this was related to the filling compounds used as shown in figure 10.



**FIGURE 10.** Optical performance of slotted cable as a function of load

For compound A the attenuation did not equilibrate until a cable strain of 0.3% was achieved, for compound B this occurred at 0.17%.

Cone penetration of the two materials gave values of 270dmm for compound A and 310dmm for compound B, a difference which does not indicate a major variation. Yield stress analysis gave values of 90Pa and 45Pa respectively as shown in figure 11.



**FIGURE 11. Yield stress measurement results for cable filling compounds**

It is interesting to note that a 50% decrease in yield stress leads to a approximately 50% reduction in load required for the operational performance of the cable to be reached. In terms of cone penetration of the compound the relationship is not so clearly defined, and this emphasises the importance of rheological analysis of filling compounds in conjunction with cable design.

## 5. CONCLUSION

The paper has shown for filling compound analysis the superior value of rheological testing over cone penetration. It has been shown that it is an essential tool for material selection both in terms of physical properties and processing. Initial results indicate the quantitative use of rheological analysis in predicting the performance of fibre within filled cable.

A simple model has shown that useful knowledge has been gained which has been beneficial to the development of cold fill cables.

## ACKNOWLEDGEMENT

The authors would like to express their thanks to the Teaching Company programme between Pirelli-STC Cable and the DTI/SERC for their support of this paper.

## REFERENCES

1. Hattori T., Akasaka N. Optimal design of jelly compound for optical cable. IWCS Proceedings 1988.
2. Sherman P. Industrial Rheology, p.84, London Academic Press, 1970.
3. Van Wazer J.R. Viscosity and flow measurement, p.290, Interscience publishers, 1963.
4. Schramm G. Introduction to Practical Viscometry, p.15, Haake, 1981.
5. Cheng D. C-H. Technicians training course in viscometry, Warren Spring Laboratory, 1990.
6. Schramm G. Introduction to Practical Viscometry, p.60, Haake, 1981.
7. Eirich F.R. Rheology, vol 4, p.239, London Academic Press, 1967.
8. Cheng D. C-H. Yield stress: A time dependant property. 1986.
9. Nielsen L.E. Polymer Rheology, p.167, Marcel Dekker, Inc. 1977.
10. Scanlan I.F, et al. Fibrespan ribbon bunching, analysis of the geometries, energies and forces involved, STC Technology Ltd, 1988.

Gavin Morland was born in Norwich, England in 1966. He attained a B.Eng (Hons) Degree in Materials Technology from Coventry (Lanchester) Polytechnic in 1989. He is presently working on a two year Teaching Company project leading to an M.Phil degree supported by Pirelli-STC Cable and the Polytechnic of Wales/DTI.



David Rees is the Associate Head of the Department of Electronics and Information Technology at the Polytechnic of Wales. He gained the degree of BSc in Electrical Engineering from the University College of Swansea in 1967, and a PhD in 1976. His industrial experience includes five years with British Steel and two years with Imperial Chemical Industries. Over the past ten years he has managed a SERC/DTI Teaching Company programme between the Polytechnic of Wales and STC. He is a fellow of the IEE and Chairman of the IEE Central Applications Professional group.



Dr. Graham White is a senior Lecturer in the Department of Mechanical and Manufacturing Engineering at the Polytechnic of Wales, specialising in engineering materials. He graduated from the Department of Metallurgy, University of Sheffield with the Degrees of B.Met(Hons), M.Met and PhD. He spent a year as a visiting scientist in the Department of Materials Science and Engineering, Massachusetts Institute of Technology on a Rotary Foundation Fellowship. He has extensive experience of industrial consultancy.



# EXTENDING THE LIFE OF POLYETHYLENE WIRE INSULATION

Joseph N. D'Amico  
Trevor N. Bowmer

Bellcore  
331 Newman Springs Road  
Red Bank, New Jersey 07701-7040  
U.S.A.

## ABSTRACT

The useful life of polyethylene insulation in open access aboveground closures can be substantially extended if its temperature is decreased during the "hot" hours of the day. Pedestal test facilities were constructed in New Jersey, and the following year, in Mesa, Arizona. Internal temperature reductions were achieved by convection cooling, internal venting, thermal insulation, and light/heat reflection. By utilizing a vented white metal pedestal cover we kept internal pedestal temperatures within 3 °F (2 °C) of the surrounding air and approximately 18 °F (10 °C) cooler than the unshielded standard green pedestals.

We anticipate that the remaining useful service life of the polyethylene insulated conductors in pedestals could be at least doubled under these conditions. More precise information on the slowing of thermal oxidative insulation aging will be available following the completion of the tests at Mesa.

Finally, many of the results reported herein can be applied to the fiber plant as well.

## INTRODUCTION

Widespread failures of polyethylene insulated conductor (PIC) insulations in the field<sup>1,2</sup> have led to improved stabilizer systems for insulations<sup>3</sup>. There remains, however, a very large number of open access telephone pedestals which contain PIC cable insulations considered to be "at risk" of premature failure. Not all minimally stabilized product will necessarily crack. That likelihood is dependent upon the actual stabilizer content, its dispersion, polymer stress, etc. as well as the climate (primarily the temperature) at the specific geographic location of the telephone pedestal.

It is apparent that if we could reduce the internal pedestal temperature during the hotter hours of the day, we could significantly extend the useful life of the PIC insulation.<sup>1</sup>

In this paper we describe several methods which may be employed to substantially lower the internal pedestal temperatures. Their efficacy and cost vary considerably. Some technologies will be more applicable to rehabilitating existing plant, while others are better suited to the new pedestal plant.

## EXPERIMENTAL

These experiments were conducted in two parts: First we conducted a trial at our Navesink (Red Bank, New Jersey) Laboratories. Standard 6 x 6 x 48 inch high green telephone pedestals<sup>†</sup> were installed on an unshaded grassy knoll to determine the effect that their color and design have on their internal temperatures. Those temperatures were measured as a function of color, venting, insulation, and plastic or metal covers. Standard and "semi-sealed" pedestals were compared as well as the affect of heavy copper cable loading.

Having analyzed the data from the Red Bank tests, we took our best and most feasible i. e., field installable, modifications and trialed them in a hot Southwest location (Mesa, Arizona). There we also included a metal pedestal painted beige, plastic pedestals, and a 10 inch green metal pedestal adapted for and containing fiber optic cables and equipment.

The temperatures of the pedestals were monitored near the top and the bottom of their terminal plates and in their bases. The shield temperatures of covered pedestals were also recorded. In all cases the results were compared to those obtained on the standard green pedestal in the same time period to eliminate any systematic errors.

The pedestals (non-fiber) in the Mesa Arizona field trial each contained an installed copper cable. By measuring the remaining thermal oxidative induction times (OIT) on both foamed/skin and solid conductor insulations we intend to accurately project the increased service life resulting from these pedestal modifications.

## Equipment Detail

### Pedestals:

At Navesink: We used PC 6/48A type standard steel pedestals manufactured to the requirements of Bellcore Technical Reference TR-TSY-000013 and painted green. Certain pedestals were repainted either white, silver - aluminum, or black. The pedestals were installed in the earth to their indicated "ground line". The effect of cable

<sup>†</sup> Telephone pedestals type PC 6/48A manufactured by Champion Metal Products, Strafford, MO.

loading was determined by installing six cables (containing a total of 600 conductor pairs) from the earth through the typical gravel base into the splice chamber of a reference pedestal. Two "semi-sealed" pedestals were also used, for a total of twelve ready access units.

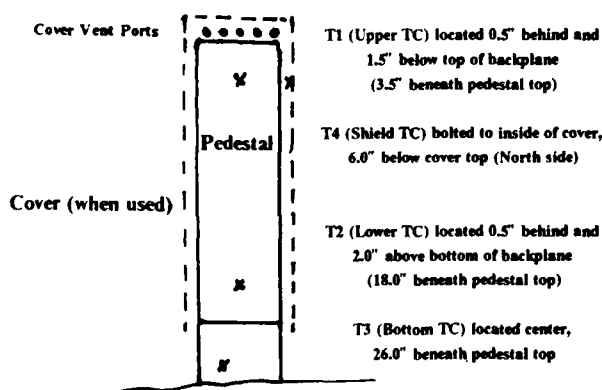
Some pedestals were vented by cutting slots (3/8 inch by 3 inches) in the doors (2 1/4 inches from the top and one inch from the bottom). The openings were shielded from the rain by metal awnings angled at 45°. Other pedestals were covered to protect them from the sun's rays. Commercial plastic (HDPE) flood covers were used. They provided about one inch of space around the pedestals and 2 1/4 inches above them. In some cases we replaced the air barrier with commercial fiberglass insulation. Some of the covers were painted white, others were left green as received.

Finally, some pedestals were shielded with vented covers. We modified the plastic flood covers which we've just described and had metal covers custom fabricated from (1/16 inch) aluminum to approximately the same dimensions. In both cases twenty 1/8 inch holes were evenly placed around the covers one inch below their tops to provide air circulation from their open bases around the pedestals to their tops. Some of these plastic and metal covers were painted white while others were left unpainted.

**At Mesa:** We installed PC6/48A metal pedestals in standard green, painted white or beige, and green with a white aluminum vented cover (as described above). We also installed two kinds of plastic pedestals (green), a flood cover type and a sealed dual chamber type. In addition we placed a standard 10 x 10 x 54 inch green metal pedestal that had been adapted for fiber optic service, for a total of 14 pedestals.

#### Thermocouples:

Up to three thermocouples were placed in each of the pedestals†. The two top-most sensors were located behind the splice plate, one near its top and the other near its bottom. The third thermocouple was positioned to measure the temperature in the pedestal near the ground level. In covered pedestals the third thermocouple was attached to the inner surface of the shield near its top and positioned to face North (Figure 1). The sole thermocouple in the pedestal containing fiber optic cables and equipment at Mesa was placed in the optical fiber connection tray located approximately eighteen inches below the pedestal top. Additional thermocouples sensed the outdoor air temperature and that within the insulated control equipment cabinet. There the thermocouples were connected via a switchboard to recorders.

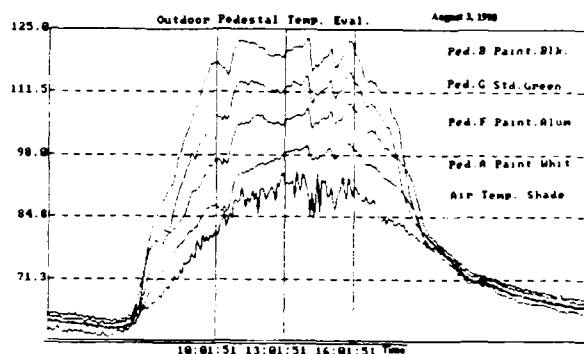


Thermocouple Placement In Pedestals

FIGURE 1

#### Recorders:

We used two types of recorders†. One unit printed the hourly temperature as sensed by up to forty thermocouples while the second type augmented it by selectively recording up to five signals for later computer analysis. (Figure 2) A third datalogger, similar to the second was also used during critical time periods.



A typical thermograph produced by the M-50 Datalogger  
(Numerical temperature data are provided every five minutes.)

FIGURE 2

#### Field Locations and Test Periods

The New Jersey pedestals were located in an unshaded grassy area at Bellcore's Navesink Laboratories. They faced East. The geographical coordinates of Bellcore's Navesink Facility in Red Bank (Lincroft) New Jersey are 40.4° North Latitude and 74.1° West Longitude. The test period began on August 2, 1990 and it continued into November of that year.

The Arizona test site is on an earthen area at the U S WEST Communications field service facility in Mesa, Arizona. Its geographical coordinates are 33.4° North Latitude and 111.8° West Longitude. There the test period began on June 5, 1991 and as of this date (August 1991), it still continues. (These pedestals also faced East.)

## RESULTS

#### New Jersey:

We analyzed the internal pedestal temperatures averaged over the six hours from 10 AM to 4 PM Eastern Daylight Savings Time. The solar heating of pedestals during ten clear sunny days in August (average temperature 80 to 90 °F), resulted in an internal temperature increase of 20 °F above ambient. By simply changing the pedestal's color to white, we reduced its internal temperature by 13 °F! (Figure 3 and Table 2)

† Ungrounded type K thermocouples with one sixteenth inch stainless steel sheath and type K washer thermocouples (for attachment to pedestal covers) manufactured by Omega Engineering, Inc., Stamford, CT.

‡ Model 3020T thermocouple datalogger with series 3000 forty channel multiplexer and model 50 datalogger, all manufactured by Electronic Controls Design, Inc., Milwaukee OR.

Painting a pedestal silver-aluminum had little affect since that color is basically a light neutral grey. Black, however, increased a pedestal's internal temperature rise by fifty percent when compared to the standard green. The color of an object is clearly closely associated with its ability to reflect or absorb solar energy. This phenomenon will be examined in depth below.

We covered pedestals to observe the affect of isolating them from the direct rays of the sun. We used commercial flood covers which have an open base and act as a bell jar over a pedestal to prevent water entry. The air within the covers (and the pedestals), unable to escape, was essentially trapped upon heating. The covers increased the temperature change within the pedestals by approximately fifty percent as compared to that in uncovered pedestals of the same color.

If those covers were insulated with fiber glass, there was a relatively slight reduction in the internal pedestal temperature increase. However, we also discovered that we had tightly sealed the pedestals from the environment. Moisture evolved from the bare earth within those pedestals could not escape when heated by the sun. Both the white and green covered pedestals developed so much condensation that they were internally completely covered with water droplets to the extent that the galvanized metal had begun to corrode on its edges.

We achieved the greatest temperature improvement by shielding a pedestal with a white vented aluminum cover. The internal pedestal temperature was reduced to 3 °F above ambient. The sun's rays were largely reflected by the white metal. With the cover vented both at its

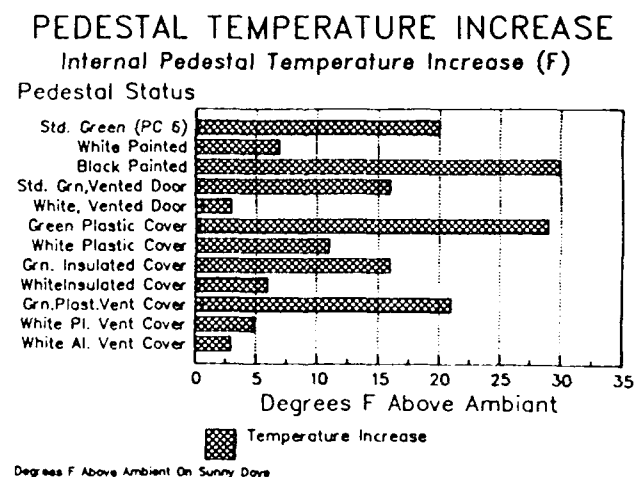


FIGURE 3

base and near its top, air heated between it and the pedestal quickly rose and escaped. The temperature measured on the side of the cover shaded from the sun was within a degree of ambient. White plastic, not having the thermal conductivity of aluminum, provided a temperature reduction to 5 °F above ambient. Unpainted aluminum, whose color is specularly that of a light grey, was poorer. The green vented covers, while worse than the white units, were 30% better than the unvented covers.

To increase venting, we cut slots in the pedestal doors with the thought that door replacement on existing field pedestals would be quick, easy and inexpensive. The temperature in the white pedestal rose only 3 °F above ambient, while little improvement was seen in the green pedestal. However, by venting the pedestal itself, we are exposing the wire works to substantially increased environmental contamination.

These comparative temperature measurements were made using unloaded pedestals. When six 100 pair cables were added to a standard green pedestal, they reduced its internal temperature by 4 °F. The temperature was measured in the splice area behind the backplane. Dimensions and temperatures are detailed in Table 3.

Table 4 compares the solar heating affect in New Jersey on a select group of pedestals during three consecutive months. From the relatively hot days of August (87 °F) through the cool days of October (75 °F), the temperature increase within the standard green pedestals remains at a constant 20 °F. During that time the noon solar altitude at 40° north latitude has changed from 66° to 39° with a resulting air mass increase to direct solar radiation reaching the earth's surface (i.e., optical path) of one atmosphere (from an air mass of 1.5 atmospheres to 2.5 atmospheres.)<sup>4,5</sup> This results in a decrease of the incident solar radiation on a horizontal plane at the earth's surface from approximately 2300 BTU/sq.ft./day to 1400 BTUs at the latitude of the test site.<sup>6</sup> The pedestals, however, being tall and narrow, during that time period present an increasingly effective heatable surface to the solar rays. The result is an extended peak heating season for the wires within the pedestal environment.

#### Arizona:

We determined the internal pedestal temperatures averaged both from ten AM to four PM (as we did for New Jersey) and from eight AM to six PM. The data shows that the temperature in Arizona rises rapidly to a broad peak before dropping in the evening. On sunny days in New Jersey, the temperature rises gradually to a peak in the early afternoon and then decreases gradually. While the internal pedestal temperatures follow the local ambient thermal profiles, the differences in pedestal temperatures in New Jersey and in Arizona were remarkably alike. At Mesa, painting a pedestal white reduced its internal temperature 14 °F as compared with the standard green metal pedestal while the use of a white vented metal cover resulted in a 17 °F drop. A light beige paint decreased the pedestal temperature 8 °F. A sealed green plastic pedestal exposed the wires to approximately the same temperatures as did the standard green metal pedestal. (All pedestals contained an installed copper cable.) Table 1 provides details.

#### PEDESTAL TEMPERATURE COMPARISON ARIZONA & NEW JERSEY

Internal Temperature Differences (°F) During Sunny Days  
As Compared To The Standard Green Metal Pedestal

Pedestal Status	At Mesa, Arizona*		
	A <sup>†</sup>	B <sup>‡</sup>	C <sup>‡</sup>
White Painted Metal	-14	-14	-13
Tan Painted Metal	-8	-8	---
White Al. Vented Cover	-17	-16	-17
White Plastic Vented Cover	---	---	-15
Green Plastic (C)	-0-	+1	---
Green Plastic (CS)**	-7	-7	---

\* Data from June and July, 1991  
\*\* This pedestal contained no internal obstructions or plates.

<sup>†</sup> Temperature differences are averaged, 8 AM to 6 PM.  
<sup>‡</sup> Temperature differences are averaged, 10 AM to 4 PM.

Table 1

The temperature of the large green pedestal containing fiber optic cable and apparatus was monitored in the fiber splice tray which is about 18 inches from the pedestal top. There the temperature was about two degrees higher than at the same location in the standard 6 inch pedestal.

## DISCUSSION

### Pedestal Color

Our test results show that the color of a pedestal has the greatest influence on its internal temperature. Several phenomena occur when solar radiation impinges upon an opaque object. Energy that is totally reflected from the object's top most surface is specularly reflected in the manner of a mirror with an angle of reflection equal to the angle of the incident radiation. The energy reflected would have the spectral distribution (or color) of its source and it may be defined as a surface's gloss.<sup>7</sup> Should that energy penetrate the top-most surface (as with most real, especially non-metallic or painted metallic objects), it would be scattered and/or partially (wavelength selectively) absorbed according to the nature of the substrate, wavelength of the radiation and any pigment particles present. The light reflected from the object may be considered as the result of two phenomena, non-selective scattering and wavelength selective absorption.<sup>8</sup> That energy which is not diffusely or specularly reflected (i.e., re-radiated) is absorbed by the object and heats it. The quantity of energy absorbed is dependent upon the absorptivity and the emissivity of the object. Most good absorbers are also good radiators. There are exceptions. Depending on its chemical and physical nature, a thin black oxide or sulfide coating on a bright metallic base material can result in the object's having a high energy absorptivity and a lower emissivity.<sup>9</sup> These conditions are not readily realized. We believe that the paint on the standard pedestal probably provides too thick a film to impart that property to it.

The solar radiation reaching the earth's surface is spectrally and quantitatively reduced by transiting the atmosphere. The principal mechanisms are Rayleigh scattering, Mie scattering, absorption by ozone and absorption by water vapor.<sup>10</sup> Ozone effectively absorbs most of the solar radiation in the ultraviolet region of the solar spectrum while water vapor has strong absorption bands in the infrared. The terrestrial solar spectrum for the direct component of sunlight is presented in Figure 4.<sup>11</sup> The result is a solar energy reaching the earth which is approximately 2/3 visual and 1/3 infrared radiation.<sup>12</sup>

The proportion in which the energy which impinges upon a telephone pedestal is reflected or absorbed is a function of its material and color; the latter, as previously described, being a property of its surface and near surface substrate. A white painted object utilizing a titanium oxide paint will reflect 88 to 95 percent of the incident solar radiation<sup>13</sup> while a medium green, such as specified by Bellcore's TR-TSY-000013 for pedestal terminal closures, will reflect only 20 percent of the incident visual light† and even less of the infrared. (Figure 5)

The beige pedestal trialed at Mesa had been painted a very light color, almost an off-white, yet it was only about half as effective as white in reducing the increase in pedestal temperature.

### Climatic Factors

We have examined principally the affects of direct solar heating on telephone pedestals. There are three other factors which we will mention briefly. Cloud cover has a marked influence on the solar energy which reaches the earth's surface. Clouds between the pedestals and the sun may block its direct radiation, while clouds elsewhere may scatter some of that energy and increase the diffuse radiation. Depending on the nature of the cloud cover and the solar altitude, as little as 10 to 20 percent of the solar energy may be transmitted to the ground.<sup>14</sup> In Table 2 we see that partly sunny days reduce pedestal solar heating 10 to 30 percent. Since we did not measure cloud cover, we did not present any data obtained on overcast or cloudy days. Air velocity, also, was not measured at the test site. Rain, as expected, has a large and rapid cooling affect on pedestal temperatures.

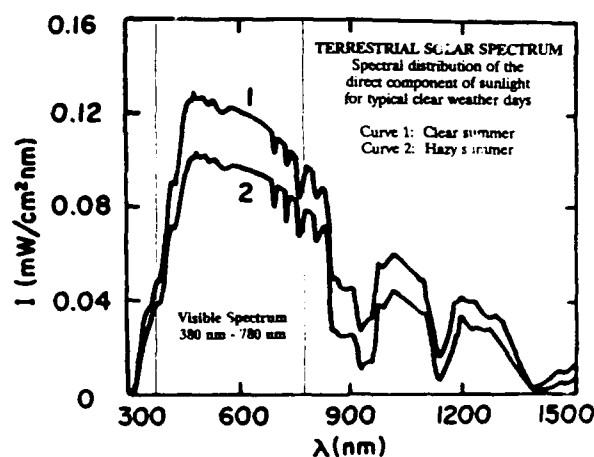
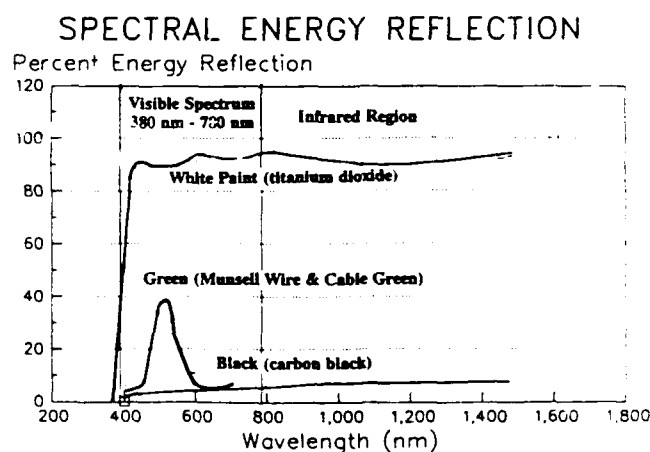


FIGURE 4



White & Black: Solar Energy Handbook  
Green: Measured Munsell Wire & Cable Centroid

FIGURE 5

† Munsell color standard green centroid (color designation 2.5G 5/12) measured by the writer using a sixteen point abridged color spectrophotometer

## Environmental Considerations

Any alteration of the traditional pedestal results in a change in the wire works environment. The standard open access closures provide a semi-sealed condition for the telephone plant. The substitution of a vented door subjects the wire works to complete contact with the external environment with some restriction to rain entry. At the other extreme, we found that the unvented insulated covers fitted tightly over the pedestals so as to effectively seal them from all but the earth beneath them. Moisture and water droplets collected on all surfaces. One can only speculate on the effects such a condition would have on the telephone system's electrical connections.

## Field History

In 1972 P. A. Link completed a nationwide survey on the status of PIC ((low density) polyethylene insulated conductor) insulations in pedestals.<sup>15</sup> His analysis divided the nation into "heat exposure" regions

as determined by the annual number of days plus the average temperature greater than 90 °F. Later work by T. N. Bowmer et al.<sup>1,16</sup> included temperature measurements within pedestals in New Jersey and Arizona. Their data which reported peak temperatures is comparable with that reported here.

## CONCLUSION

The remaining service life of PIC insulations can be extended by lowering the temperature of their pedestal environments. In outdoor pedestal test facilities both in New Jersey and Arizona we showed that the summer sunny day temperature within the standard green pedestal can be reduced by almost 10 °C (18 °F). This thermal reduction can be achieved by either painting the pedestal white and venting it (by replacing the door) or by covering it with a vented white metal shield. Although Arrhenius extrapolations to low temperatures are imprecise, a 10 °C reduction in closure temperature should at least double the remaining insulation service life. (Samples aged at the Mesa site are currently being tested to determine with greater precision the increased service life which pedestal temperature reduction will impart to PIC.) Since the change in pedestal color has the greatest affect, depending on use location, it may be necessary to balance the aesthetic rewards of the standard green and the cost of premature plant replacement.

## ACKNOWLEDGEMENTS

The authors thank Larry Green who fabricated specialized equipment at Belcore and Harlie Goss and William Thompson from Belcore's Quality Technology group in Phoenix for assisting with the installation and the monitoring of the equipment at the Mesa site. Especially they thank U S WEST Communications and specifically Felix Dees, Charles Frederick, Will Kerr and Bob Trevizo for their providing the site at Mesa and their assistance in installing and maintaining the equipment.

## PEDESTAL TEMPERATURE INCREASE

Internal Pedestal Temperature Increase (°F)  
Above Ambient During Sunny Days

Pedestal Variable	Pedestal Status	August Sunny Days <sup>†</sup>	Aug. Partially Sunny Days <sup>††</sup>
A. Color	Std. Green (PC 6)	20 ± 2 °F	18 ± 3 °F
	Std. Green (BSC6)	19 ± 1 °F	---
	White (PC 6)	7 ± 1 °F	---
	Silver-Aluminum (PC 6)	17 ± 1 °F	11 ± 6 °F
	Black (PC 6)	30 ± 1 °F	26 ± 4 °F
B. Cover (on PC 6)	Green Plastic	29 ± 2 °F	26 ± 4 °F
	White Plastic	11 ± 1 °F	8 ± 3 °F
C. Vented Shield (on PC 6)  (on BSC6)	White Aluminum	3 ± 1 °F	1 ± 1 °F
	Bare Aluminum	7 ± 1 °F	---
	White Plastic	5 ± 1 °F	---
	Green Plastic	21 ± 2 °F	---
	Green Plastic	19 ± 1 °F	---

<sup>†</sup> 10 days; Average daily temperature over six hour period (10 AM to 4 PM)  
80 to 90 °F, Mean: 87 ± 3 °F.  
<sup>††</sup> 2 days; Mean 83 ± 0 °F.

Pedestal Variable	Pedestal Status	Indicated Sunny Days <sup>†</sup>
D. Vented Door  (Unvented Control) (Vented Shield)	Std. Green (PC 6)	16 ± 1 °F
	White (PC 6)	3 ± 1 °F
	Std. Green (PC 6)	18 ± 1 °F
	White Aluminum over PC 6	3 ± 1 °F

<sup>†</sup> 4 days (Oct. 14,16,17; Nov. 3)  
Average daily temperature over six hour period (10 AM to 4 PM)  
71 to 79 °F, Mean: 75 ± 4 °F.

Pedestal Variable	Pedestal Status	Indicated Sunny Days <sup>†</sup>
E. Insulated Cover  (Uninsulated Control) (Vented Shield)	Green Plastic over PC 6	16 ± 2 °F
	White Plastic over PC 6	6 ± 2 °F
	Std. Green (PC 6)	20 ± 3 °F
	White Aluminum over PC 6	4 ± 1 °F

<sup>†</sup> 7 days (Aug. 29,30; Sept. 21; Oct. 3,5,14,17)  
Average daily temperature over six hour period (10 AM to 4 PM)  
72 to 85 °F, Mean: 77 ± 5 °F.

Table 2

## CABLE LOADING AFFECT

The Cable Loading Affect On Internal Pedestal Temperature During Sunny Days<sup>†</sup>

Std. Green Pedestal (PC 6)	Temperature Due To Solar Backplane	Increase Heating (°F) Location
	Upper	Lower
Without Cables	19 ± 3 °F	15 ± 2 °F
With Cables <sup>‡</sup>	15 ± 3 °F	10 ± 2 °F

<sup>†</sup> 5 September days  
Average daily temperature over six hour period (10 AM to 4 PM)  
73 to 87 °F, Mean: 80 ± 6 °F.

<sup>††</sup> Upper temperature measured in air 0.5" behind and 1.5" below top of backplane (3.5" beneath pedestal top)  
Lower temperature measured in air 0.5" behind and 2.0" above bottom of backplane (18.0" beneath pedestal top)  
Note: All pedestal comparisons use the upper pedestal temperature measurements unless otherwise indicated, since wires and splices are present in that area.

<sup>‡</sup> Cable loading consists of six 100 pair PIC cables extended from the earth through gravel into the splice area.

Table 3



## PEDESTAL TEMPERATURE INCREASE IN SUMMER AND FALL

Internal Pedestal Temperature Increase (°F) Above Ambient During Sunny Days<sup>†</sup>

Pedestal Status	August	September	October
Painted White	7 ± 1 °F (7) <sup>‡</sup>	8 ± 0 °F (2)	7 ± 1 °F (2)
White with Vented Door	---	---	3 ± 1 °F (3)
White Al. Vented Cover	3 ± 1 °F (9)	4 ± 2 °F (5)	3 ± 1 °F (5)
White Plastic Vented Cover	5 ± 1 °F (7)	7 °F (1)	7 ± 1 °F (4)
Std. Green (Control)	20 ± 2 °F (8)	19 ± 3 °F (5)	20 ± 3 °F (5)
Average Ambient Temperature	87 ± 3 °F (10)	80 ± 6 °F (5)	75 ± 3 °F (5)
Average Temperature Range	80 to 90 °F	73 to 87 °F	71 to 79 °F

<sup>†</sup> 10 days (August 2,3,4,12,17,18,26,27,29,30)

5 days (September 2,3,4,11,21)

5 days (October 3,5,14,16,17)

Average daily temperature over six hour period (10 AM to 4 PM)

<sup>‡</sup> () Indicates the number of days that data was available.

Table 4

## REFERENCES

1. Bowmer, T. N., "Cracking of Foam Skin Insulations In Pedestals", Proc. 37th. Int'l Wire and Cable Symposium (1988), pp 475-483
2. Bowmer, T. N. et al., "Stability of Polyethylene Insulations in the Field and Laboratory", Proc. 37th. Int'l Wire and Cable Symposium (1988), pp 490-499
3. Hitchcock, R. E., Private transmission based on Bellcore Quality Assurance industry wide survey of OIT (Oxidation Induction Time) test results.
4. Bush, G. E. and Richards, L. M. "Solar Energy and Technology Handbook", Part A, Ed. Dickinson, W. C. and Cheremisinoff, P. N., Dekker, New York, p. 48
5. Boer, K. W., Ibid, p. 77
6. Bush, G. E. and Richards, L. M., Ibid p. 54
7. Hunter, R. S., "The Measurement of Appearance", Hunter Associates Laboratory, Inc., Fairfax, VA, 1972, p. 7.1
8. Kubelka, P., "New Contributions to the Optics of Intensely Light Scattering Materials", Part I, J.O.S.A., Vol. 38, No. 5, May 1848, pp. 448-457, 1067
9. Lof, G. O., "Solar Energy and Technology Handbook", Part A, Ed. Dickinson, W. C. and Cheremisinoff, P. N., Dekker, New York, p. 226
10. Boer, K. W., "Solar Energy and Technology Handbook", Part A, Ed. Dickinson, W. C. and Cheremisinoff, P. N., Dekker, New York, p. 70
11. Ibid, p. 80
12. Patton, T. C., "Pigment Handbook", Vol. 3, J. Wiley, New York, p. 223, from Stefan 1879
13. Edlin, F., "Solar Energy Handbook", Ed. Kreider, J. F. and Kreith, F., McGraw-Hill, New York, Fig. 5.13, p. 5-18
14. Bahm, R. J., "Solar Energy and Technology Handbook", Part A, Ed. Dickinson, W. C. and Cheremisinoff, P. N., Dekker, New York, Fig. 5.2, p. 92
15. Howard, J. B., "Stabilization Problems with Low Density Polyethylene Insulations", 21th. Int'l Wire and Cable Symposium (1972), pp 329-341
16. Bowmer, T. N. et al., "Field Temperatures In Outside Plant", Proc. 39th. Int'l Wire and Cable Symposium (1990), pp 335-342



Joe D'Amico has worked on engineering and materials issues affecting all types of telecommunications and power cables in his 25 year career. He first worked with communications cable at Western Electric before joining General Cable Company in 1967. There as senior research physicist, he investigated the structure and composition of all types of telecommunications wire, cable and optical fiber as well as electrical power cables. Since 1985 he has worked at Bellcore, initially as a Quality Assurance Engineer and since 1989, as a member of the Polymer Chemistry and Engineering Research Group in Red Bank, New Jersey. Joe is a graduate of Seton Hall University. He received his MS degree from Fairleigh Dickinson University.



Trevor Bowmer is a member of the Polymer Chemistry and Engineering Research Group in Bellcore. He received his Ph.D. in chemistry from the University of Queensland, Australia, where he studied radiation chemistry of polymers. Joining Bell laboratories in 1980, he investigated radiation cured systems and lithographic materials. In 1984, he came to his present position where his interests include degradation mechanisms and characterization of polymeric materials used in telecommunications applications.

## Influence of the Quality of Plug-Jack Connect on the Transmission Characteristics

Ting-Chung Chang, Daw-Ming Fann, Po-Lung Yu,  
Chieh-Mei Hsiao, Kuang-Yi Chen

Telecommunication Laboratories  
P.O. Box 71, Chung-Li, Taiwan, 32099, R.O.C.

### Abstract

A modular telephone plug jack is a device to be placed on the customer side of the station protector and is an interface between customer wiring and terminal equipment. In order to meet the demand of reliability and functionality performance, the plug and jack contacts must be plated with hard gold.

In this paper, we dealt with some hard gold properties such as coating composition, hardness, porosity, contact resistance, corrosion resistance and hard-gold coating thickness. We also study the influence of hard-gold coating properties on the telephone transmission quality.

### Introduction

D.G.T. plan to achieve the target of ISDN in 2000. For the service of narrow band to provide are still dependent on tradition copper cable. For the reason that how to promote the existing OSP loop quality to meet the demand of 2B+D transmission is the major object of T.L., OSP laboratory. In modern telecommunication system, plug jack play a importance role in determining the system reliability. One of the key requirements of a telephone transmission is to establish and maintain an undisturbed flow of electric current applying with low contact resistance. Consequently the tendency of most metals to oxidize, tarnish, or corrode once exposure to environment has led to the nearly unanimous choose of gold as a plug jack contact material because of its excellent electrical properties and resistance to corrosion. There have been several papers which studying the corrosion behavior of hard gold contact in humid atmosphere containing low concentrations of  $\text{SO}_2$ ,  $\text{NO}_2$ , and  $\text{Cl}_2$  were reported (1,2,3). Some also dealt with the contact resistance affected by contact force or contact geometry (4). However investigator seldom pay attention to the relation between the contact material properties and the signal transmission frequency. The objective of the present work was to assess the influence of contact surface quality on the signal transmission in different frequency.

### Experimental

The test specimens are 10, 30, 50, 70, micro inches thickness of hard gold coating and tin coating plug jack. Their thickness are measured by X-Ray fluorescence method. The porosity of gold alloy coating layer were tested by the method of nitric acid vapor in according to ASTM B583-73 regulation, and it were examined by scanning electron microscope (SEM).

The far-end crosstalk loss (FEXT), near-end crosstalk (NEXT), and attenuation between two or four pairs transmission lines which were connected with plug jack were measured with ANRITSU ME325D automatic cable crosstalk measuring equipment in the range of 40 to 772 kHz. Figure 1 is the schematic diagram of the apparatus used for transmission properties measurement.

Contact resistance between plug and jack contact spring were measured using four-wire method, and the change in contact resistance ( $\Delta R$ ) for each contact pairs was also measured to evaluate the contact materials characteristics. Gold alloy composition was tested by dipping plug or jack contact spring in cyanide solution and was determined by applying the inductively coupled plasma atomic emission spectrometry (ICP-AES) method.

### Result and Discussion

#### A. Plug Jack Connector Contact Spring Characteristics

Gold alloy was electroplated onto the contact spring surface of plug jack connector because of the excellent electrical conductivity and inertness. The base material of plug and jack contact spring was phosphor bronze and its thickness was about 80 to 100 micro inches nickel plate layer as sublayer which acted as a barrier to prevent the migration of copper into the surface layer of gold alloy. Darko Rajhenbah had shown that alloying elements in gold alloy cobalt increase the coating layer hardness but > 0.5% cobalt has adverse influence on the increase of specific resistance and brittleness of gold coating layer (5). The amount of cobalt in gold alloy layer was

found out to be 0.3%. The result of porosity test in dependence of gold alloy layer thickness are shown in figure 2. From figure 2 it comes out that the number of pore per square centimeter decrease as the gold alloy layer thickness increase. Figure 3 is a example of jack contact spring after 30 minutes nitric acid vapor test. The corrosion products in the pores are found to be  $\text{Ni}(\text{NO}_3)_2 \cdot 6\text{H}_2\text{O}$  and  $\text{Cu}(\text{NO}_3)_2 \cdot 6\text{H}_2\text{O}$ . They are produced by nitric acid vapor which can penetrate into the gold alloy coating layer and interact with sublayer nickel and base material phosphor bronze.

#### B. The Transmission Properties of Plug Jack in Different Frequency

There are many connecting point from central office to resident; these including trunk cable (modular connector, for example AT&A 710, 3M 4000 D, Picabond mini connector), distribution jelly-filled cable (UY connector), cross cabinet, distribution joint boxes, terminal connector, inside wiring connector (plug jack). In this paper we focus on the influence of plug jack quality on the transmission properties (especially the crosstalk loss and insertion loss) of plug jack in different frequency.

Figure 4 to figure 6 illustrate the NEXT, FEXT, and attenuation of PE-PVC inside wiring cable connected by different hard gold alloy coating plug jack. The plots in fig. 4 and fig. 5 showed that the PE-PVC inside wiring cable connected with plug and jack, the NEXT, FEXT would worsen and the crosstalk loss increase rapidly with frequency according to following relation:

$A = k * f^{0.2}$  (when frequency is in the range of 10 to 300 kHz)

$A = k * f^{0.5}$  (when frequency is large than 300 kHz)

Where A is attenuation, k is a constant.

In spite of that the crosstalk loss value are still above the regulation value (6), which define the NEXT in the frequency of 40 kHz must be above 58.5 dB and the FEXT in 160 kHz must be above 55 dB.

We also measured the NEXT, FEXT and attenuation variation of plug jack after high humidity and temperature cycling test. Because gold is noble than tin, gold can establish a metallic interface between plug jack contact spring surface, but tin can not. So the NEXT, FEXT of gold alloy coated plug jack are no significant change and tin coated plug jack change more significant. The above results suggest that the connecting point of plug jack has negligible effect on crosstalk loss and attenuation.

Figure 7 showed the contact resistance change ( $\Delta R$ ) of plug jack after 72 hours salt fog test (7). From fig 7 it can be seen that there is marked increase in the contact resistance of tin coated and 10, 30, micro inches gold coating contact

spring. The increase of contact resistance value is influenced by the growth of insulating film on metal sublayer or the growth of film in the gold layer pores. From the SEM examination, there are many pores existing in 10, 30, micro inches gold coating layer and corrosion products can be found around the pores this is why contact resistance increase. On the other hand, the contact resistance degradation of tin coating contact spring is caused by surface corrosion which atmosphere is more reactive to surface finish than underplating materials.

#### Conclusion

(1) Result of morphological properties obtained from SEM and contact resistance showed that the plug jack contact spring hard gold coating layer needed a thickness above 50 micro inches.

(2) The plug jack connected to PE-PVC inside wiring cable the NEXT FEXT and attenuation would drop depend on the transmission frequency, but it still above regulation value.

(3) Overview, the transmission characteristic of subscribe loop was mainly dependent on the wire and cable itself. Plug jack connector had little effect on the crosstalk loss and attenuation of whole loop, the major consideration of connector quality was dropout and corrosion.

#### Reference

1. M. Antler, Plating, 53, 1431 (1966)
2. G.H. Koch, Material Performance, 35 (1988)
3. Kei-Ichi, IEEE Trans Components, Hybrids, Manuf. Technol., 4 (1973)
4. H. Irvin, IEEE Trans Components, Hybrids, Manuf. Technol., 393 (1988)
5. D. Rajhenban, 10th ICMC, (251) 1987.
6. ML 1021-2
7. ASTM B117-73

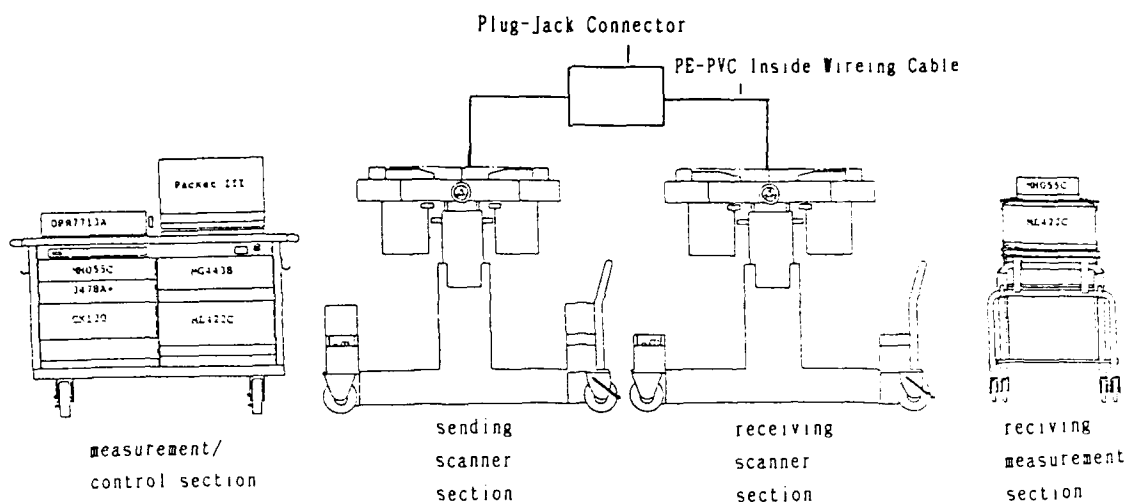


Figure 1. The Schematic Diagram Apparatus Used for Crosstalk loss and Attenuation

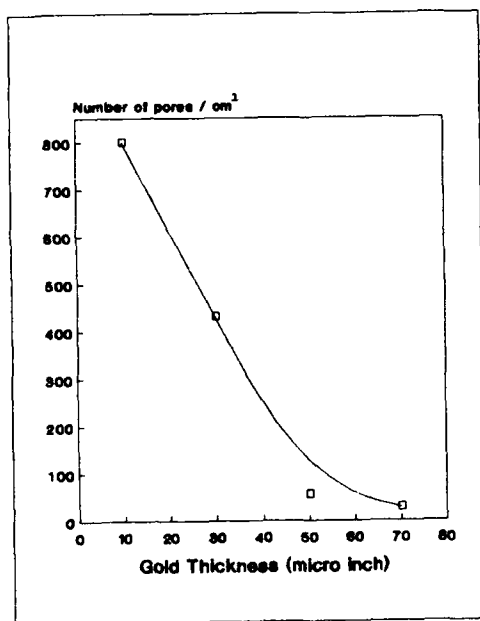


Figure 2. Relation Between the Number of Pores and Gold Coating Layer Thickness

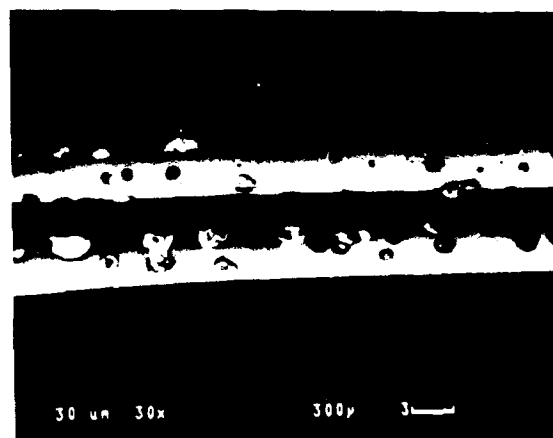


Figure 3. SEM Photomicrograph of 30 Micro Inches Gold Coating Jack Contact Spring After Nitric Acid Vapor Test

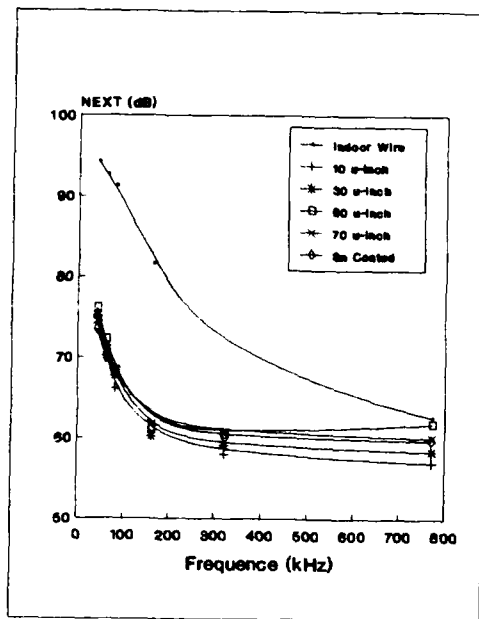


Figure 4. The NEXT of Plug Jack Conector in Different Frequency

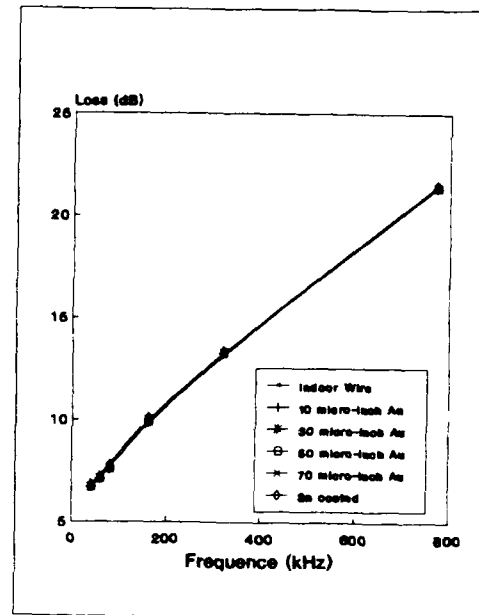


Figure 6. The Attenuation of Plug Jack Conector in Different Frequency

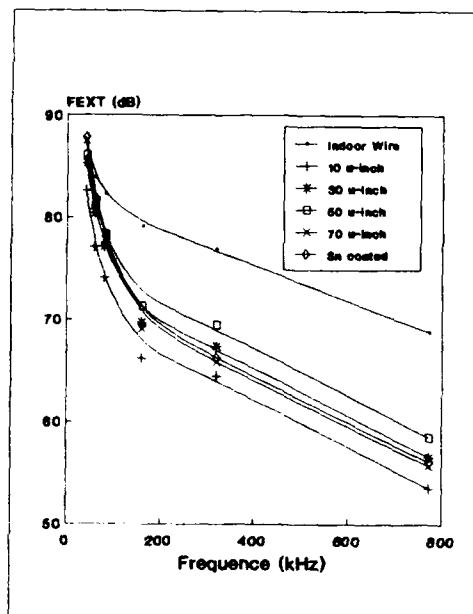


Figure 5. The FEXT of Plug Jack Conector in Different Frequency

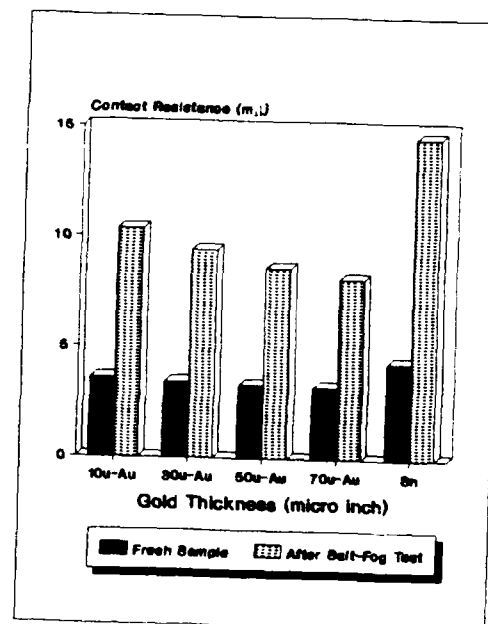


Figure 7. The Contact Resistance Change After Salt-Fog Test



Ting-Chung Chang  
Telecommunication Lab.  
P.O. Box 71  
Chung-Li, Taiwan, 32099  
R.O.C.

Ting-chung Chang received his M.S. degree in Applied Chemistry in 1984 from Tsing Hua University and then directly joined Telecommunication Laboratories. He is now a research scientist and a member of outside plant laboratory in T.L.



Daw-Ming Fann  
Telecommunication Lab.  
P.O. Box 71  
Chung-Li, Taiwan, 32099  
R.O.C.

Daw-Ming Fann received his M.S. in Chemical Engineering from National Taiwan Institute of Technology. He joined T.L. in 1982 and presently worked as a project leader in O.S.P. lab. of T.L.



Po-Lung Yu  
Telecommunication Lab.  
P.O. Box 71  
Chung-Li, Taiwan, 32099  
R.O.C.

Po-Lung Yu received his M.S. degree in Chemistry in 1972 from National Taiwan University. He joined Telecommunication Laboratory in 1983 and now was a research scientist in O.S.P. lab. of T.L.



Chieh-Mei Hsiao  
Telecommunication Lab.  
P.O. Box 71  
Chung-Li, Taiwan, 32099  
R.O.C.

Chieh-Mei Hsiao received his M.S. degree in Chemical Engineering from Tsing Hua University. She joined Telecommunication Laboratories in 1981 and presently worked as a research scientist in O.S.P. Lab. of T.L.



Kuang-Yi Chen  
Telecommunication Lab.  
P.O. Box 71  
Chung-Li, Taiwan, 32099  
R.O.C.

Kuang-Yi Chen was born in 1953 and received his Ph. D. degree in Electro-Optics from National Central University in 1990.

He has been engaged in research and development of optical fiber fabrication and communication technologies since 1977. He is currently the director of outside plant technology laboratory of T.L.

## FIBER OPTIC / COPPER CONDUCTORS COMPOSITE CABLE FOR SUBMARINE SENSORS SYSTEM

JP. BONICEL - PF. GIRAUD - P. GAILLARD - A. DE FILIPPIS

ALCATEL CABLE - LYON - FRANCE

### ABSTRACT

This paper describes a new optical fiber and copper conductors composite cable developed to be used with submarine sensors in an immersed detection network.

It is composed of an optical core containing 62.5/125 fibres, self resistant to hydraulic pressure, devoted to data transmission; this optical unit is surrounded by a layer of screened or unscreened copper conductors ensuring the power feeding and monitoring of the network. The cable outer protection is realized with a single or double layer armour. Specific anchoring devices have also been developed and are presented.

Various mechanical and environmental tests results performed on an optical unit qualification length and on a 3,500 metres long completed cable are presented.

### INTRODUCTION

Higher bit rates, longer distances, insensibility to electromagnetic perturbations have made the transmission media move to optical fibres for more and more various applications.

In particular the development of more and more complex sensors networks has created the need to develop composite cables including copper conductors and optical fibres; in this domain this paper presents a study conducted to answer a specific need for a cable intended to be used in a submarine sensors network.

This cable has been specially designed to present good mechanical properties, as it is intended to be laid on the sea bed at depths down to 1,000 metres.

### BASIC REQUIREMENTS

The basic requirements were as follows :

Functional requirements :

- four optical fibres with characteristics as shown in table 1 for data transmission;
- eight 2.5 sq.mm copper wires (300 V nominal voltage rating) and four 1.5 sq.mm screened copper wires (250 V nominal voltage rating) for power feeding and control;

- minimum breaking strength : 5,000 daN;
- operating hydrostatic pressure : 10 MPa;
- lifetime in sea immersion : 10 years;
- operating temperature range : 0°C/+30°C in water, 10°C/+50°C in air;
- storage temperature range : -20°C/+70°C (in air)

item	specified value
fibre type	62.5/125/250
numerical aperture	0.275
attenuation (dB/km)	
850 nm	3.7 max
1300 nm	1.5 max
bandwidth (MHz.km)	
850 nm	200 min
1300 nm	200 min

Table 1. Optical fibre characteristics

Additional requirements :

- good crush resistance
- suitable protection against hydrogen effects
- anti teredo protection
- cable core components shall be self resistant to the operating hydrostatic pressure so as to prevent possible failure (mechanical damage, corrosion...) of the outer protection.
- predicted lifetime in sea immersion : 20 years;
- development of specific anchoring devices operating under hydrostatic pressure

### CABLE STRUCTURE

The cable structure has been designed as follows in order to face the above mentioned requirements :

#### Optical core

- choice of a loose type structure with a suitable fibre over-length to guarantee a low strain rate on the fibres and therefore a high lifetime;
- choice of a hard thermoplastic slotted core, 6.3 mm diameter, to obtain good crush properties, with four slots containing one optical fibre each. The slots are filled with a suitable

ble silicone-based jelly to protect the fibres and ensure optical core longitudinal watertightness; the central strength member is made of a 7x0.6 mm steel rope.

- the optical core protection is realized with a 0.8 mm thick inner polyamid sheath, a single layer of 0.8 mm diameter steel wires armour to achieve a good tensile and hydrostatic pressure resistance, and a 1.2 mm outer lead alloy sheath (12.5 mm O.D.) for radial water and hydrogen tightness.

A cross section drawing of the optical core is given in fig 1.

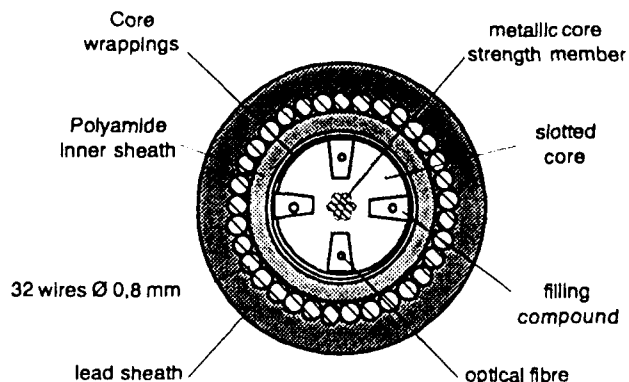


Figure 1. Cable core cross section

#### Electrical part

The electrical part is made of eight polyethylene insulated, stranded copper conductors of 2.5 sq.mm cross section, and four polyethylene insulated, copper braid screened and outer polyamid sheathed stranded copper conductors of 1.5 sq.mm cross section. These 12 conductors, having the same overall diameter of 4 mm, are helically stranded in one layer around the optical unit; the spaces between the conductors are filled with a suitable petroleum based jelly to ensure the cable core longitudinal watertightness.

#### Outer protection

The outer protection is made of :

- an inner low density polyethylene sheath, thickness 1.8 mm;
- an anti teredo protection, made of two 0.2 mm thick copper tapes helically applied, and a crepe paper bedding;
- a single or double layer armouring made of 2.2 mm (inner layer) or 2.4 mm (outer layer) diameter galvanized steel wires flooded with a bitumen compound;
- an outer HdPe sheath, thickness 2.5 mm.

A cross section drawing of the cable is given in fig 2 and a photograph is shown in figure 3.

The cable outer diameter is 41.3 mm and its nominal weight is 4,700 kg/km in air or 3,280 kg/km in water (double layer armouring) and 3,250 kg/km in air or 1,930 kg/km in water (single layer armouring).

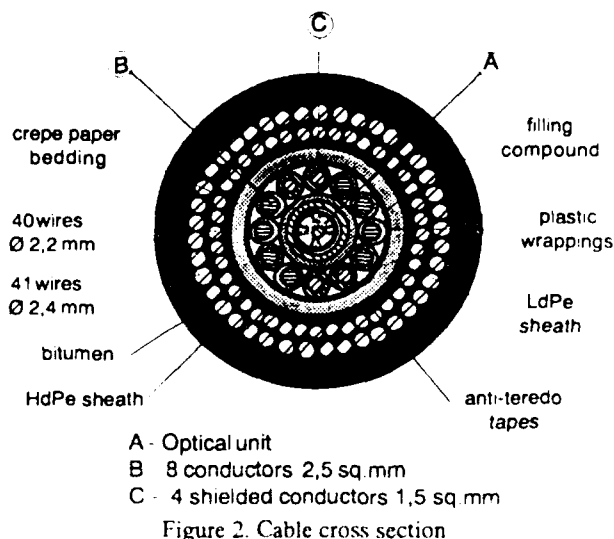


Figure 2. Cable cross section

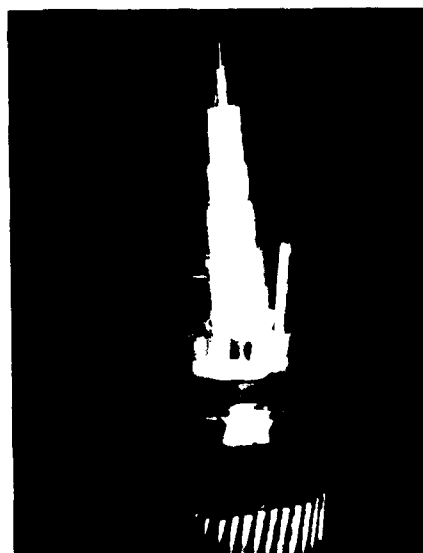


Figure 3. Photo of the completed cable

#### END FITTINGS AND SPECIAL HARDWARE

Specific anchorings and cable end fitting were also designed to be delivered with the cable length. These equipments are :

- an anchoring device, designed to transmit longitudinal efforts between the cable armour and either an anchoring point on land or an immersed part of the system. It is made of bronze (immersed) or stainless steel (land) and uses the principle of armour steel wires conical clamping, together with a thermosetting resin injection.
- a watertight and pressure resistant join, designed to ensure the transition between the cable core and immersed housings (electronics, cable core splitting...). It is made of bronze and the watertightness is realized using a special resin injection.

A general drawing showing the equipped cable end is shown in figure 4.



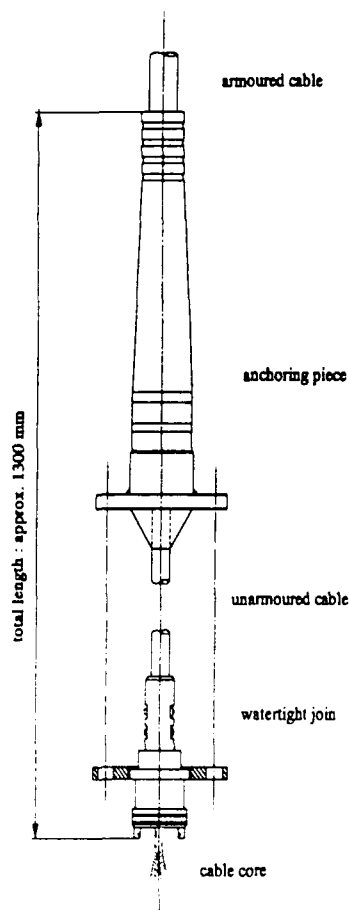


Figure 4. Cable end equipment

In addition, due to the cable length to be delivered (3,500 m) and its outer diameter, a special shipping drum has been designed and realized; its overall dimensions are 3,000 mm (flange diameter) and 2,910 mm (width) for a total weight of 17,400 kg (including the cable length). This special drum also includes a special housing to store the equipped cable end during transportation.

### **CABLE MANUFACTURING, TESTING AND QUALIFICATION**

#### **Optical core**

A prototype length of the optical core, approximately 600 m long, has been realized and tested in order to qualify its design. The tests realized and the obtained results are listed in table 2. Obtained results are in compliance with or exceed the specification.

The tensile test has been realized on a 200 m long part of the prototype optical core; during the test optical fibres were monitored either in loss change at 850 nm or in length variation. The test has been performed up to a maximum load of 5,000 N corresponding to a cable elongation of 0.15%; attenuation control showed variations within the measurement accuracy and slight evolution noted in fibre elongation is due to filling compound shearing. Obtained curves are shown in figure 5.

item	obtained result
transmission (initial)	compliant (850 and 1300 nm attenuation and bandwidth; no change from uncabled values)
tensile test	no measurable loss increase for 5,000 N/0.15% at 850 nm. fibre elongation less than 0.03% at 5,000 N.
pressure test	no measurable added loss at 15 MPa loss increase starts at approximately 30 MPa no residual added loss after 50 MPa
transmission (after mechanical testing)	compliant (850 and 1300 nm attenuation and bandwidth; no change from initial values)

(1 MPa = 10 N/cm<sup>2</sup> = 1 bar)

Table 2. Optical core qualification tests.

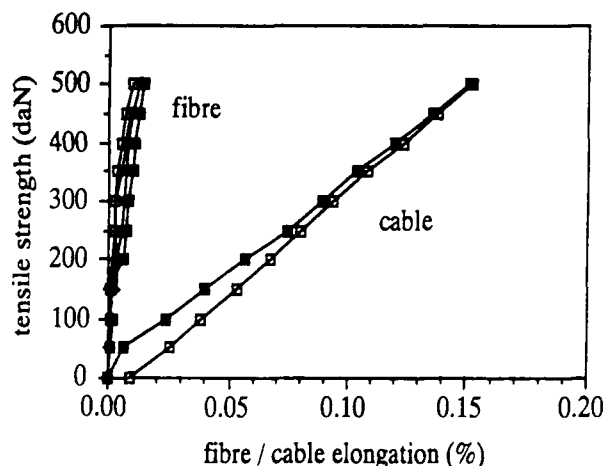


Figure 5. Optical core tensile test

The hydrostatic pressure test has been realized on a 50 m long sample taken from the optical core prototype length; the length submitted to the pressure was about 40 m and the fibres were looped for 1300 nm transmission loss control during the test. After the verification of the compliance with the specification (pressure maintained at 15 MPa for one hour), the pressure has been increased up to 50 MPa; loss increase has been found to start at about 30 MPa and no residual loss increase has been noted after pressure release. Attenuation curves vs pressure are given in figure 6.

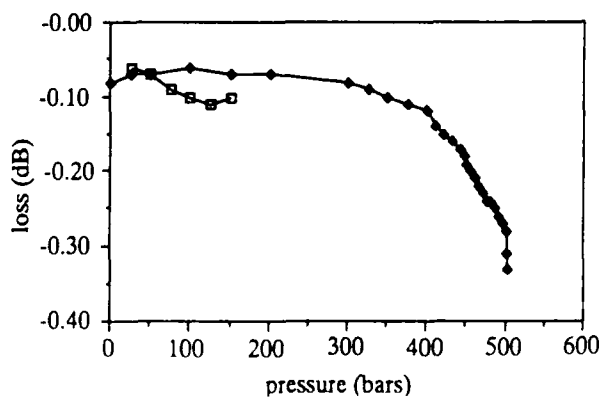


Figure 6. Optical core pressure test

A prototype of the watertight joint has been also successfully submitted to a hydrostatic pressure test up to 10 MPa.

#### Completed cable

The optical unit being qualified, the industrial length has been manufactured according to the above described specification. The total cable length realized was 3,600 m in one single length, including an extra length of 100 m for mechanical testing; the outer steel wires armouring has been realized with a double layer for the most important part of the cable (2,800 m, corresponding to the cable part laying on the seabed) and with a single layer for the remaining part so as to lighten the cable (700 m, corresponding to the immersed cable end). The transition between the two types of armouring has been realized by replacing the steel wires of the outer layer by glass reinforced plastic fillers so as to keep the outer diameter as regular as possible for outer sheathing.

This manufacturing has been successfully submitted to the standard quality control procedures applied to either dimensional or electrical or optical parameters at various manufacturing steps, including on the completed cable optical and dielectric tests after cable end fitting. In addition a tensile test using a set of anchoring equipment has been realized.

Obtained results are in compliance with the specified values; the tensile test, which is not a standard final test, has been realized on the single layer armoured 100 m extra length to qualify the completed cable and the anchoring equipment. The cable length effectively under test was 90 metres; the maximum tensile load applied was 50,000 N as specified, leading to a cable elongation of about 0.19%. For this value the measured fibre elongation was 0.05% with no residual effect after load removal; the calculated nominal breaking strength of the two layers armoured part is about 100,000 N. Photos showing the cable under tensile test, the equipped cable end and the cable length being shipped on its special drum are shown in figures 7, 8 and 9.

The cable laying has been realized from a special boat during summer 1991; no failure has been reported, confirming the obtained results and the correct design of the cable.

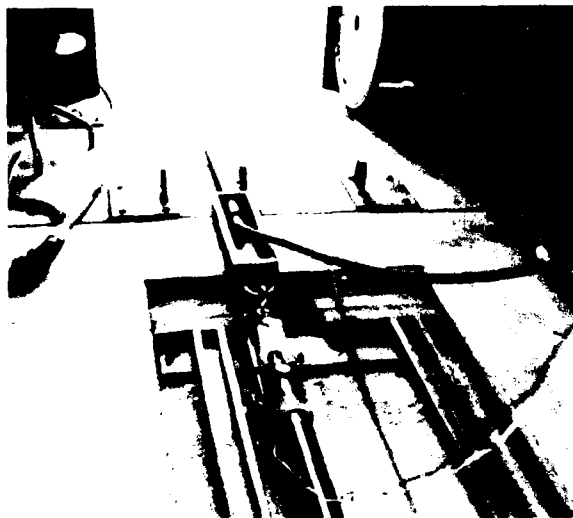


Figure 7. Cable under tensile test



Figure 8. Equipped cable end

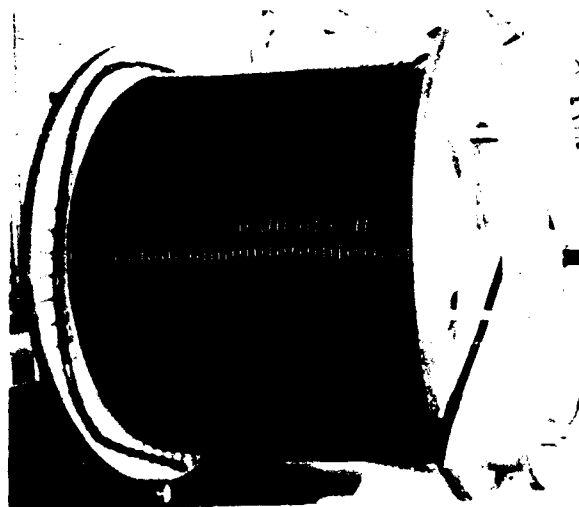


Figure 9. Cable on shipping reel

## **CONCLUSION**

The development of this composite cable has lead to the definition of a tensile and pressure resistant optical core surrounded by an electrical part with a submarine type outer protection. Such a product may be used as it is or with some adaptations (fibre count, number or type or section of the electrical conductors...) to take place of transmission media in various types of submarine sensors or transmission networks; but to be able to guarantee a 20 years lifetime, it is necessary to be very careful on the cable design (no strain on the fibres, no hydrogen hazards...), the qualification, manufacturing and quality assurance procedures.

## **BIOGRAPHY**

### **JP. BONICEL - ALCATEL CABLE**

148 Av. Jean Jaurès 69007 LYON - FRANCE



Jean Pierre BONICEL was born in 1952. He received his engineer degree from the Institut des Sciences de l'Ingénieur de MONTPELLIER (ISIM) in 1976. He joined Les Câbles de Lyon, now ALCATEL CABLE, in 1977 where he was in charge of material and mechanical problems for telecommunication cables. Now he is the head of telecommunication cables laboratory.

### **P. GAILLARD - ALCATEL CABLE**

148 Av. Jean Jaurès 69007 LYON - FRANCE



Pierre GAILLARD was born in 1956. He received his engineer degree from the Ecole Catholique des Arts et Métiers de LYON (ECAM) in 1980. He joined Les Câbles de Lyon, now ALCATEL CABLE, in 1983 where he is in charge of telecommunication cables definition and transmission characterisation.

### **A. DE FILIPPIS - ALCATEL CABLE**

148 Av. Jean Jaurès 69007 LYON - FRANCE



Alain DE FILIPPIS was born in 1952. He received his general certificate graduation in 1971. He joined Les Câbles de Lyon, now ALCATEL CABLE, in 1973 where he is in charge of copper and optical cables testing and transmission measurements.

### **P. GIRAUD - ALCATEL CABLE**

148 Av. Jean Jaurès 69007 LYON - FRANCE



Pierre GIRAUD was born in 1930. He received his engineer degree from the Ecole Catholique des Arts et Métiers de LYON (ECAM) in 1952 and from the Ecole Nationale Supérieure du Pétrole et des Moteurs (ENSPM) in 1955. He joined Les Câbles de Lyon, now ALCATEL CABLE, in 1961 where he is in charge of special cables for undersea power and data transmission cables.

# A STUDY ON HIGH SPEED TELEPHONE WIRE EXTRUSION LINE

Y. S. KIM

JUNE Y. HAH

TAIHAN ELECTRIC WIRE CO., LTD.  
785, KWANYANG-DONG, ANYANG CITY, KYUNGKI-DO, S-KOREA

## ABSTRACT

At present time wire and cable manufacturers want to speed up the telephone wire insulation up to 2400 m/min. or higher line speed while obtaining an absolutely regular smooth surface and good quality. Insulations with good mechanical properties, excellent surface quality, no insulation defect and high centricity factor can be obtained by using optimized extrusion equipments. In case of foam-skin insulations, the extrusion becomes more difficult at such line speed. There are numerous parameters which influence the quality and especially the capacitance.

This paper summarizes the key requirements for modern telephone wire extrusion line with high speed extrusion properties

## INTRODUCTION

Korea Telecoms has put foam-skin insulated local telephone cables to a good use to meet the ever increasing demand for diversified telecommunication services in place of the conventional paper insulated cables since 1988.

The foam-skin insulated cable is to improve mechanical strength and transmission characteristics such as cross-talk characteristics.

It has been rather difficult to maintain the good centricity and extremely low variation in capacitance of  $\pm 1.5$  pF/m at the process of high speed extrusion. The problems rising from high speed extrusion vary according to type of insulations.

- (1) Foam-Skin Insulation
  - (a) Insulation defect

- (b) Unstability of capacitance control
- (c) Rough surface
- (d) Open cell in foam structure
- (e) Wire elongation

- (2) Solid Insulation
  - (a) Poor output
  - (b) Insulation defect
  - (c) Rough surface
  - (d) Higher variation of insulation diameter
  - (e) Wire elongation

To meet the needs of the wire and cable industry for keeping melt flow homogeneity and constant melt flow temperature, the wire and cable manufacturers and extruder makers should be familiar with the change of characteristics for every type of material under a wide range of production conditions. They must be able to predict the melt flow, temperature profiles and output under the given conditions and materials, and determine the screw geometries that will provide optimum results.

In short, a superficial knowledge of the extrusion process is not enough. The cable manufacturers and extruder makers must have a deeper knowledge of what actually takes place from the moment the granule enter the barrel until the melt is forced through the die.

Wire and cable manufacturers came to demand more excellent characteristics in terms of high performance materials changes in heating and cooling system, screw geometry, and die design.

At present time insulations with approx. 0.12 mm wall thickness must be produced at a line speed of 2400 m/min. while obtaining an absolutely regular smooth surface and low capacitance variation.

In case of foam-skin insulation the extrusion is more difficult than solid insulation. Major problem was to avoid elongated conductor, rough surface of insulation, deterioration of cell structure, higher head pressure, continuously changing of the pressure, increase of capacitance variation, and many insulation faults, etc.. However, we solve technical problems encountered at high speed extrusion line for foam-skin insulated telephone wire.

Essentially, the extruder is the key element in any wire and cable extrusion line. As a result of our continued research for solving difficult technical problems, we would like to mention that cable manufacturers must keep in mind the following facts to achieve above-mentioned requirements at a high speed insulation over 2400 m/min..

Table-1 shows the basic factors.

# 1. Experiment

## 1) Material

The quality of high density polyethylene compound is influenced by molecular weight distribution

(MWD) and melt flow rates (MFR).

The molecular weight distribution has been a point of concern in relation to production quality and a topic of intense research. Extrusion for wire coating of communication cables needs such a high shear rate and good foam structure that samples of insulation materials which were considered to have particular MWD and Melt Flow Rates were prepared.

Table 2 shows the sample materials used in various experiments include 6 kinds of high-density polyethylene compounds.

Being all ethylene-hexene copolymer, they were evaluated for basic properties in accordance with REA PE 200 specification. The properties of the HDPE compounds are given in Table 2. The results in Table 2 show that all compounds conform to the REA PE 200 specification requirements.

The Melt Flow Rates (MFR) of the all compounds was similar but the MFRs of the sample A and B compound was lower than that of other compounds.

TABLE 1.

ITEM	FACTOR	PHENOMENA	RESULT
Extruder	<ul style="list-style-type: none"> <li>⊙ Design of feeding zone</li> <li>⊙ Design of screw</li> <li>⊙ Temperature control zone</li> </ul>	<ul style="list-style-type: none"> <li>⊙ Poor output</li> <li>⊙ Poor mixing condition</li> </ul>	<ul style="list-style-type: none"> <li>(a) Decrease of line speed</li> <li>(b) Rough surface</li> <li>(c) Insulation defect</li> </ul>
Cross-Head Pressure	<ul style="list-style-type: none"> <li>⊙ Die design</li> <li>⊙ Connection of coextruder</li> <li>⊙ Materials</li> </ul>	<ul style="list-style-type: none"> <li>⊙ Die swelling</li> <li>⊙ Increase of pressure</li> <li>⊙ Poor foam structure</li> </ul>	<ul style="list-style-type: none"> <li>(a) Insulation defect</li> <li>(b) Increase of capacitance variation</li> <li>(c) Wire draw down</li> <li>(d) Open-cell construction</li> </ul>
Material	<ul style="list-style-type: none"> <li>⊙ Stability of dielectric constant</li> <li>⊙ MI and MWD</li> <li>⊙ Color master batch</li> </ul>	<ul style="list-style-type: none"> <li>⊙ Increase of pressure</li> </ul>	<ul style="list-style-type: none"> <li>(a) Rough surface</li> <li>(b) Increase of capacitance variation</li> <li>(c) Poor mechanical properties of insulations</li> </ul>
Cooling Method	<ul style="list-style-type: none"> <li>⊙ Design of cooling trough</li> <li>⊙ Using of warm water and reservoir</li> </ul>	<ul style="list-style-type: none"> <li>⊙ Bad condition of cooling</li> </ul>	<ul style="list-style-type: none"> <li>(a) Bad surface</li> <li>(b) Poor mechanical properties of insulations</li> <li>(c) High variation of insulation diameter</li> </ul>
Production Conditions	<ul style="list-style-type: none"> <li>⊙ Select of die size</li> <li>⊙ Balance of output according to kind of raw material and extruder temperature profile</li> </ul>	<ul style="list-style-type: none"> <li>⊙ Die droll</li> <li>⊙ Poor foam structure</li> </ul>	<ul style="list-style-type: none"> <li>(a) Increase of capacitance and diameter variation</li> <li>(b) Lower concentricity</li> <li>(c) Poor mechanical properties of insulations</li> <li>(d) Open cell construction</li> </ul>

## 2) Extrusion Test

Extrusion tests were conducted on the production line. The extrusion line consists of a wire-drawing machine, annealer, pre-heater, extruder, water trough and automatic dual take-up.

The extension speed of this line was limited up to 2,400 m/min. since the maximum speed of wire drawing machine is 2,400 m/min..

This extrusion line can monitor and/or control the extrusion temperature, line speed, cross head pressure, coaxial capacitance, overall diameter of insulated conductor and spark failure, in addition to record coaxial capacitance, overall diameter and crosshead pressure.

Ultra-high speed extrusion was one of the goals of this experiment, in which Foam-Skin insulated cables with 0.4 mm conductors which were considered most difficult to manufacture are used.

The extrusion test parameters, such as the fluctuation range of coaxial capacitance and overall diameter, spark failure and surface appearance of insulated conductors are shown in Table 3. and Table 4.. Crosshead pressure, conductor diameters, tensile elongation and foam structure were also checked. The photos show the surface appearance of insulated conductors and foam structure.

## 2. Results and Discussion

### 1) The Relation Between Material properties and Extrusion Condition

Average molecular weight is a basic structural property. In our experiment, Mw and Mn for all HDPE compounds were proved to be favorable. Mw/Mn ratio is also an important factor that has effect on the properties and processing of polymer. Usually, we consider that the wider the MWD is, the better the extrusion. But the above thinking was found not correct.

The MWD data and Mw/Mn ratio did not indicate the reason for the differences in extrusion performance between the compounds or for the variations in insulation surface smoothness. For example, sample F with Mw/Mn value of 13.8 has wider MWD than other samples, and its extrusion is the worst.

Additionally, we also consider that the higher the flow ratio is, the better processing property. But neither the data in Table 3 nor the extrusion tests proved this idea. There is no strict corresponding relationship among the Melt Flow Rates.

Above test results indicate that the extrusion do not relate to MFR and MWD only.

As a result, we should evaluate the extrusion condition and select the optimum grade for insulation material according to extruder conditions.

### 2) The relationship of tooling and extrusion property

Foam insulation is produced by mixing a foaming agent with the polyethylene compound. Heat breaks up the chemical and creates bubble elements in the polymer.

The elements are created continuously along the extruder screw. Their number depends on the thermal condition of the polymer in the extruder. After the extrusion die, the pressurized elements expand into bubbles (cell).

Cell construction is very sensitive to temperature. The cell size depends on the time elapsing between the die and the first cooling device and on the viscosity of the polymer leaving the die.

Unsatisfactory temperature control and die design leads to overfoaming (poor cell construction) and the dielectric advantages of the cells are lost. Thus, the temperature control and die design must be very accurate.

Cross head pressure heavily depends on extrusion speed. For safe operation, it is important to hold down the crosshead pressure. By raising extrusion speed, the crosshead pressure rises as well. Especially some samples, which easily goes over the safety range of 700 kg/cm<sup>2</sup>, were found unfavourable. When head pressure is high, the results show the following:

- Rough surface and/or Insulation defect
- Increase of capacitance variation
- Open cell construction

- Wire elongation

Both pressure drop and shear rate in the extrusion tool should be minimized. The pressure drop depends on a die lip diameter and the shear rate under the function of the same tool dimension.

Both factors have an effect in the same direction on the process and therefore require the maximum permissible diameter.

The strong dependence of pressure drop and shear rate on the die lip diameter requires that die wear be avoided by inserting a diamond.

A die has been designed to keep shear rates at acceptable level of head pressure.

The die lip diameter is nearly same or slightly bigger than that of the insulation.

This reduces the shear rate to quite small values; the dielectric properties of polyethylene are not lost and the extrusion flow remains stable.

Some additional advantages are also gained;

- The centricity of the insulated wire is good due to optimum die diameter.
- Low pressures decrease friction in the extruder and make thereby over foaming easier to avoid.
- Low pressures increase the extruder output
- Low pressures decrease spark fault and wire elongation

Meanwhile, having a smaller or larger taper angle than optimum design enables dies to have a high head pressure. It was found that these problems were closely related to the optimum die angle.

In our experiment, 7° taper angle was proved better. These facts were noted and their influence on crosshead pressure was checked.

The results are shown in Table 4.

### 3. Conclusion

For the remedy, improvement on manufacturing facilities and optimum conditions has been considered. These problems affect safe and stabilized operation as well as cable quality.

Our experienced summary of the result is as follows.

- (a) We modified feeding zone design of screw and number of temperature control zone in order to increase output and improve mixing condition.
- (b) We found the most suitable material flow on extrusion head by using die design with 7° taper angle and slightly bigger than insulation diameter for controlling appropriate head pressure.
- (c) By modifying cooling trough, we can improve surface of insulation, deviation of insulation diameter and mechanical properties of insulations. Especially, we found that head pressure of (b) was greatly affected by die design, and not only excessive head pressure (over 700 kgf/cm<sup>2</sup>) but also lower head pressure (≈ 500 kgf/cm<sup>2</sup>) affected quality of insulations.
- (d) We reached the conclusion that the MWD data and Mw/Mn ratios have nothing to do with the differences in extrusion performance between the compounds and with the variations in insulation surface smoothness.

As the result, it was found that to the screw geometry, die and extrusion tooling design and extrusion conditions with suitable grade for insulation material. The optimum design of extruder and equipment was established.

### Reference

- 1) P.C. Francis, "Evaluation of Competitive HDPE Telephone Insulation Compounds", Technical Report No. 1216, 1990.
- 2) Zhang Yi Xi, 39th IWCS Proceedings, 1990.
- 3) Y. Morita, T. Takai, S. Yamaguchi, K. Nishida, 33th IWCS Proceedings, 1984.

Table 2. Characteristics of Insulation compounds

PROPERTY	SAMPLE	A	B	C	D	E	F	REA SPEC. (PE-200)
Melt Flow Rate (M.I.)	g/10min	0.58	0.55	0.80	0.75	0.76	0.78	0.20~2.0
Flow Ratio	MI <sub>10</sub> /MI	14.8	14.9	13.8	15.0	17.2	15.2	
	MI <sub>21.5</sub> /MI	79	107.7	104	120.1	84	85.2	
Density (Nominal)	g/cm <sup>3</sup>	0.945	0.943	0.947	0.946	0.948	0.948	0.941~0.959
Mw	×10 <sup>4</sup>	14.1	10.5	13.8	13.7	12.3	13.2	
Mn	×10 <sup>4</sup>	0.76	1.4	0.95	1.6	0.97	0.96	
Mw/Mn	-	18.5	7.5	14.6	8.6	12.7	13.8	
Melting Temp.	°C	132	132	131	134	132	134	

Table 3. The Extrusion Test Parameters and Properties of Insulation

PARAMETER	SAMPLE	A	B	C	D	E	F
Conductor Dia.	mm	0.4	0.4	0.4	0.4	0.4	0.4
Line speed	m/min.	2200	2300	2300	2300	2300	2300
Ext. Temp.	Main	°C	161~188	163~197	163~189	162~195	163~196
	Aux.		203~250	194~250	200~255	205~258	194~245
X-Head Pressure	Main	kg/cm <sup>2</sup>	440	423	550	490	405
	Aux.		585	560	700	700	590
Capacitance	pF/m	< ±1.5	< ±1.5	< ±2.0	< ±1.5	< ±1.0	< ±1.5
Spark Voltage	kV	1.2	1.2	1.2	1.2	1.2	1.2
Spark failure	No/Bo.	0	1~2	> 50	> 20	0	> 30
Foam Construction	-	Good	Good	Bad	good	good	Bad
Surface Roughness	-	Matt/Smooth	Matt/Smooth	Matt/Rough	Matt/Rough	Smooth	Rough
Thermal Oxidative Stability Test.	※(1)	> 90 Days	> 60 Days	-	< 120 Days	< 63 Days	< 48 Days

※(1) Tests are made in accordance with BELL Standard Testing Methods designated. (110 ° × 45 Days minimum)

Table 4. The Extrusion Test Parameters for facilities

ITEM		Die Angle			Shape of X-Head		Type of Screw		
PARAMETER		6 °	7 °	8 °	I	II	II	I	
Conductor Dia.	mm	0.4	0.4	0.4	0.4	0.4	0.4	0.4	
Ext. Temp.	Main	°C	163~188	161~185	163~184	163~183	163~182	163~186	163~191
	Aux.		185~250	195~245	210~255	200~250	194~249	180~250	180~250
X-Head Pressure	Main	kg/cm <sup>2</sup>	660	535	705	605	430	575	450
	Aux.		930	720	900	765	560	710	590
Line Speed	m/min.	2200	2200	2200	2200	2200	2200	2200	2200
Spark Voltage	kV	1.2	1.2	1.2	1.2	1.2	1.2	1.2	1.2
Spark Failure	No./Bo	35~40	5~10	15~20	> 20	< 5	10~15	< 5	> 20
Surface Roughness	-	Matt/Rough	Smooth	Rough	Matt/Rough	Smooth			
Coaxial Capacitance	pF/m	±1.5	±1.0	±2.0	±2.0	±1.5	±1.5	±1.0	±2.0
Die Hole Size	mm	0.67	0.65	0.66	0.67	0.67	0.65	0.67	0.67
Foam Construction	-	Bad	Good	Bad	Bad	Good	Good	Good	Bad

(REMARK) Insulation Overall Diameter ;  $\phi 0.64$  mm



Fig. 1 MWD Data of Testing Materials

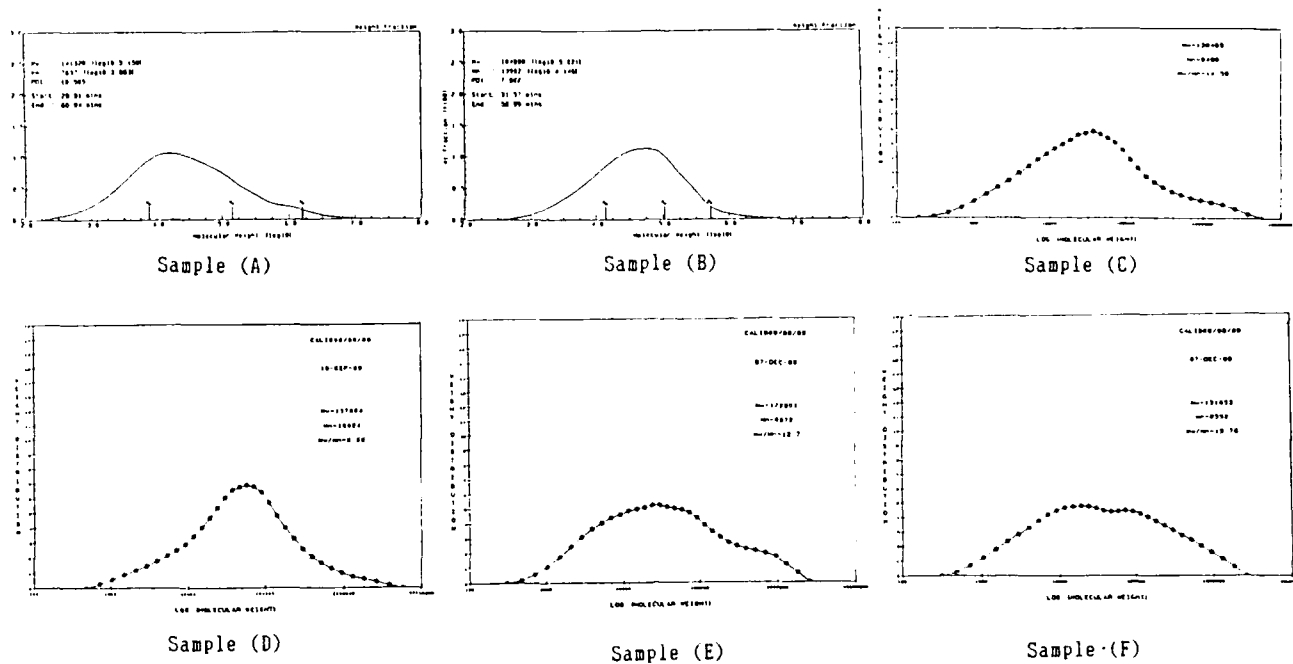
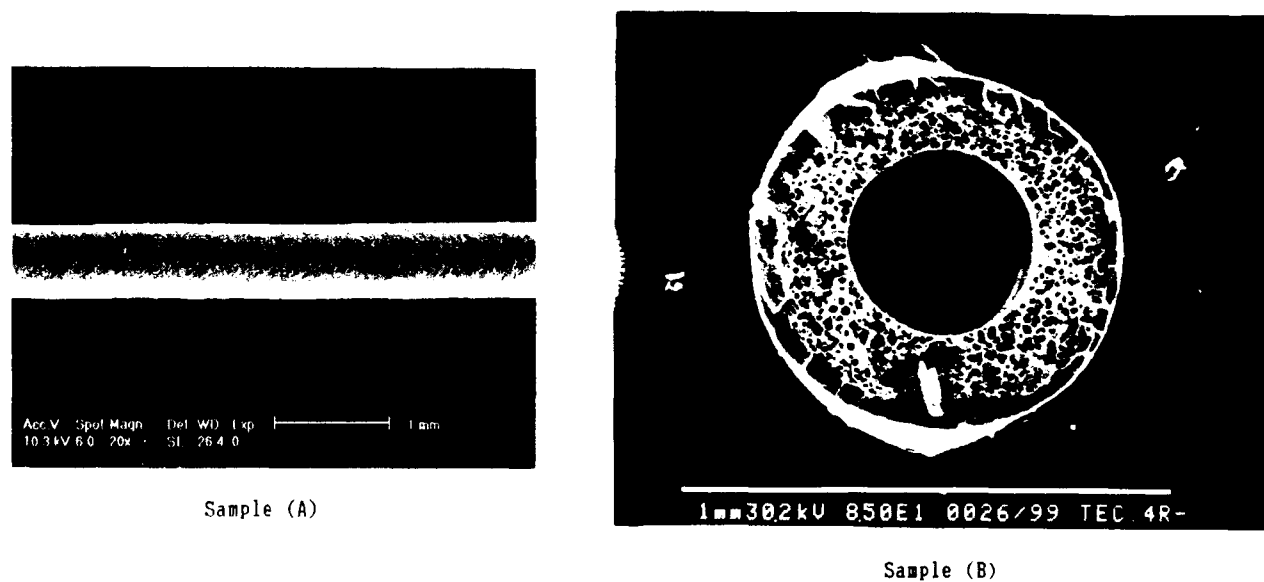


Photo. 1 The Surface Appearance of Insulated Conductors & Foam Structure

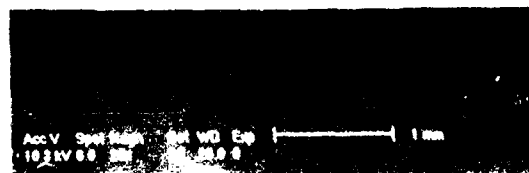
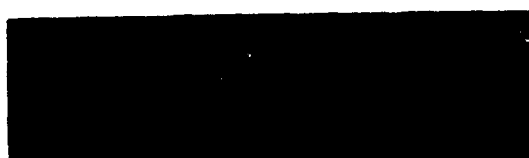




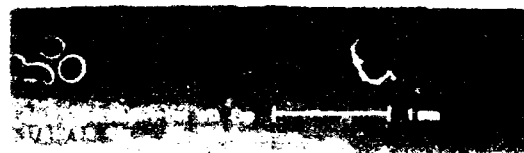
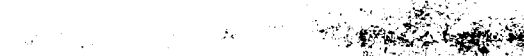
Sample (C)



Sample (D)



Sample (E)



Sample (F)



Yoon Seok Kim  
Taishan Electric Wire Co., Ltd.  
750, Kwanyang 1-dong, Anyang  
City, Kyungki-do, Korea

Y. S. Kim received his B. E. degree in metallurgical engineering from Sungkyunkwan University in 1983. He joined Taishan Electric Wire Co., Ltd. and he has been engaged in Communication cable Production and Technical Department. He is now a engineer of the communication cable engineering section.



June Young Bah  
Taishan Electric Wire Co., Ltd.  
750, Kwanyang 1-dong, Anyang  
City, Kyungki-do, Korea

June Y. Bah received his B. E. degree in electrical engineering from Hanyang University in 1978. And then joined Taishan Electric Wire Co., Ltd. and worked in the development of CATV coaxial cable and four shielded twisted pairs. He is now deputy general manager of the communication cable Engineering Department.

## **BLOWN FIBRE JUNCTION NETWORK FIELD TRIAL** **(13.6 km SPLICELESS LINK)**

N J MEDLEN, P L J FROST, P D JENKINS

BT Laboratories, Access Network Division  
Martlesham Heath, Ipswich, Suffolk, IP5 7RE, ENGLAND  
Tel: +44 473 643008

### **ABSTRACT**

Currently, to provide optical links in its Junction Network, BT installs subducted cables in lengths of less than 2 km which are then joined together. This technique requires three main operations; installation of subduct, installation of cable followed by jointing.

Potentially a more attractive approach is to use the Blown Fibre installation technique. This involves only two principle operations: installation of tubing and blowing in the fibre. This method also enables a faster provision of service, ease of route configuration and de-skilling of field operations.

This paper describes a field trial that used Blown Fibre to provide a spliceless inter office link over a distance of 13.6 km. The route runs between the two towns of Gloucester and Painswick which are situated in the southwest of England. This link is now the longest unspliced fibre optic transmission path within BT's underground network.

### **1. INTRODUCTION**

The Blown Fibre (BF) installation technique<sup>[1-6]</sup> is based on an interconnecting network of 6 mm bore tubes laid underground, into which composite 2mm diameter fibre units are installed using compressed air.

One of the primary advantages offered by the Blown Fibre cabling technique is the ability to install spliceless links. Historically the maximum unspliced length of Blown Fibre that had been installed was approximately 6 km. Improvements in fibre manufacturing processes have increased the availability of 25 km fibre lengths which in turn has significantly increased the opportunity for exploiting longer spliceless links. To investigate the installation issues associated with this technique a 13.6 km route between Gloucester and Painswick Exchanges was identified for a field trial.

The primary issues that were examined by this trial were as follows:

- (i) Could Blown Fibre be cost effectively used to supply long links?
- (ii) Could our existing installation techniques be used to install long distances?

(iii) Could Blown Fibre fibre unit be supplied in continuous 14.5 km lengths?

(iv) What could we learn from the trial?

### **2. TUBING INSTALLATION**

A subduct installation contractor was used to provision the external route with standard BF external seven tube bundle. At the exchanges internal two tube bundle was used to complete the route from the cable chambers to the equipment racks. No special handling was required for either of these installations.

### **3. PLAN OF FIBRE UNIT INSTALLATION**

Planning limits guarantee BF fibre unit installs 0.6 km in a standard blowing operation however in practice installations in the order of 0.9 km are possible. To achieve the installation of this 13.6 km continuous length a combination of *three range extending techniques*<sup>[7]</sup> was required. These techniques are outlined below:

#### **3.1 Centre Point Blowing**

The Centre Point Blowing method doubles the distance that can be installed with one set of equipment. The equipment is set up in the middle of the route and the fibre unit is blown from the pan storage container into the first direction. The pan is a plastic annular container approximately 0.5 m in diameter into which the fibre unit has been loaded in a rosetted format. The loading is such that it enables the fibre unit to be pulled from a stationary pan without tangles or lifted turns. Having completed the blowing in the first direction the remaining fibre unit is turned out into a second pan thereby presenting the other end of the fibre unit for blowing in the opposite direction (see figure 1). Due to the length of this fibre unit it was loaded into specialised pans such that both fibre unit ends could be presented without turning out the pan (see section 4 for full details).

Figure 1: Centre Point Blowing Technique

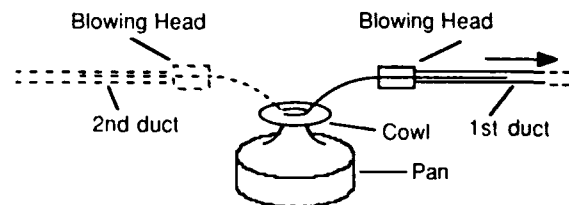


Figure 2: Tandem Blowing Technique

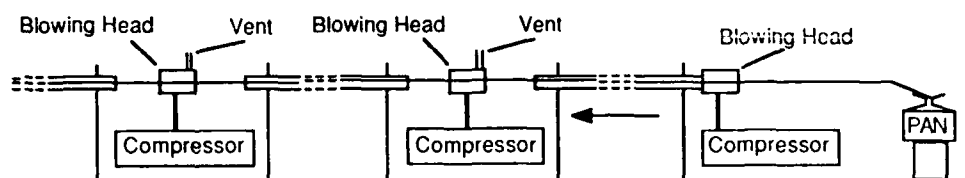


Figure 3: Pan and ELF Technique

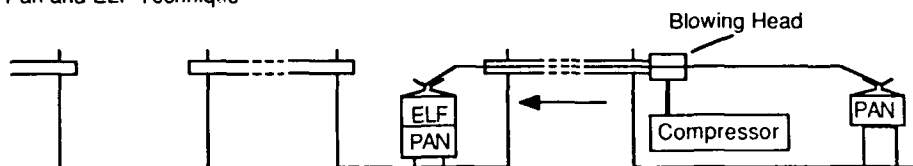


Figure 4: Standard Operation

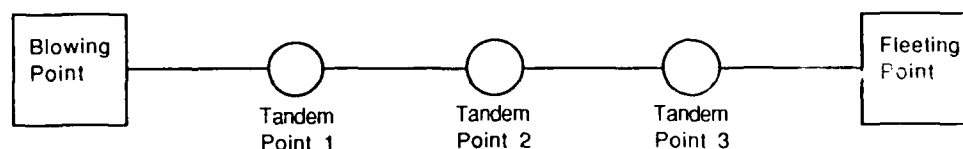
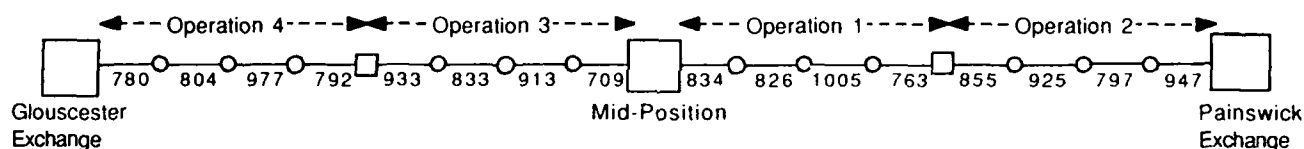


Figure 5: Gloucester to Painswick Blowing Plan Overview



Distance between blowing heads given in metres.

### 3.2 Tandem Blowing

The Tandem Blowing method uses blowing heads in series to increase the installation length (see figure 2). Potentially there is no limit to the installation distance other than the length of the available fibre unit.

### 3.3 Pan and ELF Blowing

The Pan and ELF Blowing technique uses an End Loop Fleeter (ELF) at the end of an installation length to collect the fibre unit into a pan. An excess length of fibre unit; sufficient to complete the link, is blown through the route and collected using the ELF (see figure 3). The pannal fibre unit is then turned out to present the front end of fibre unit which allows the fibre unit to be installed into the next section of the route.

These three techniques were combined to form the "standard operation" for this installation. Each standard operation spanned approximately 3.5 km and consisted of four blowing heads in series with an ELF at the end to collect the excess fibre (see block diagram in figure 4).

The Gloucester to Painswick route was divided into four of these operations as shown in figure 5. The fibre installation started at the mid-position from where it was blown to the collection points at the end of operations 1 and 3 before being reintroduced and blown through to the exchanges at Gloucester and Painswick.

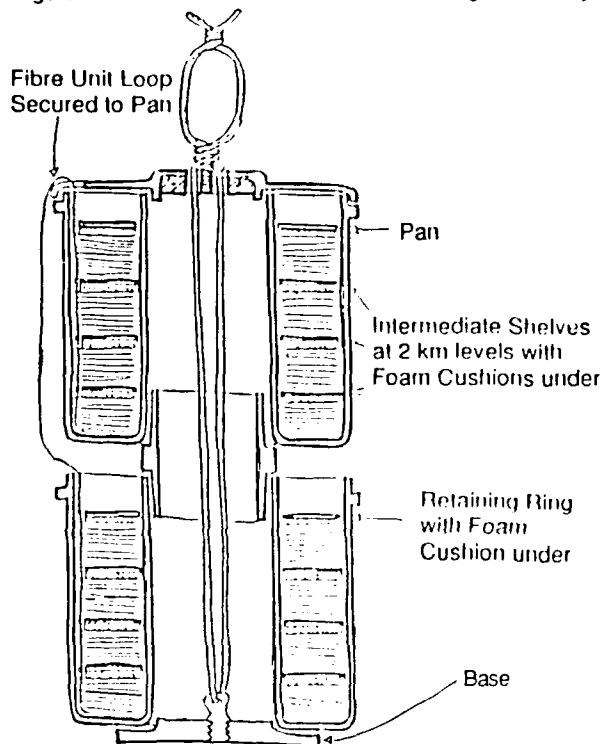
## 4. SPECIALISED STORAGE ASSEMBLY

The prototype storage system devised to handle the 13.6 km length of fibre unit was based on the existing Pan and ELF technique. Figure 6 shows a schematic section of the fully assembled system. In addition to the detail shown in the schematic two threaded rods were bolted through the lips of the pans to prevent the pans from parting company during transit.

The assembly incorporated two important features. The first was the spacer rings depicted in figure 6. These spacers prevented the weight of fibre unit compressing the layers towards the bottom of the pan. The second feature was that the fibre unit was loaded in such a way as to present both ends; one at the top of each pan. This meant that when the

pan's were split the fibre unit could be blown in both directions from the centre position without needing to turn out the fibre unit as is necessary in conventional centre point blowing. Figure 7 shows a pictorial representation of tandem blowing from the centre point once the storage system has been split.

Figure 6: Schematic Section of Loaded Storage Assembly.



## 5. FIBRE UNIT INSTALLATION

The requirement for the route was to supply eight singlemode optical fibres between Gloucester and Painswick exchanges. At the time of the installation only four fibre unit was available therefore it was necessary to install two units. Both these units were supplied by Optical Fibres plc and were successfully installed as far as the exchange rack side ducts using the operations described in section 3. The installation speed was typically 35 metres per minute and did not slow to negotiate the 1 in 5 gradients encountered during operation 2. Figure 8 shows the gradient profile of the route. It can be seen from the profile that the maximum installation heights was in the order of 200 m.

Once in the side duct the fibre unit was then routed onto the shelf through a short length of small bore tube. On the shelf a breakout unit was used to introduce the fibres into metre long capillary tubes. Thus terminated, all eight fibres were tested using an Optical Time Domain Reflectometer (O.T.D.R.). The tests were carried out from both the Gloucester and Painswick ends and gave an average loss of 0.33dB/km at 1300nm and 0.22dB/km at 1550nm. Figure 9 shows a typical trace.

A route provisioned using standard fibre cable, would typically show an attenuation of 0.51 dB/km at 1300 nm. It can therefore be seen from this trial that the use of Blown Fibre offers a potential power budget saving of 35% over a 13.6 km route by the removal of intermediate splices. Clearly this may in the future enable the use of longer repeater spacings or more cost effective transmission equipment.

Figure 7: Tandem Blowing from Centre Point.

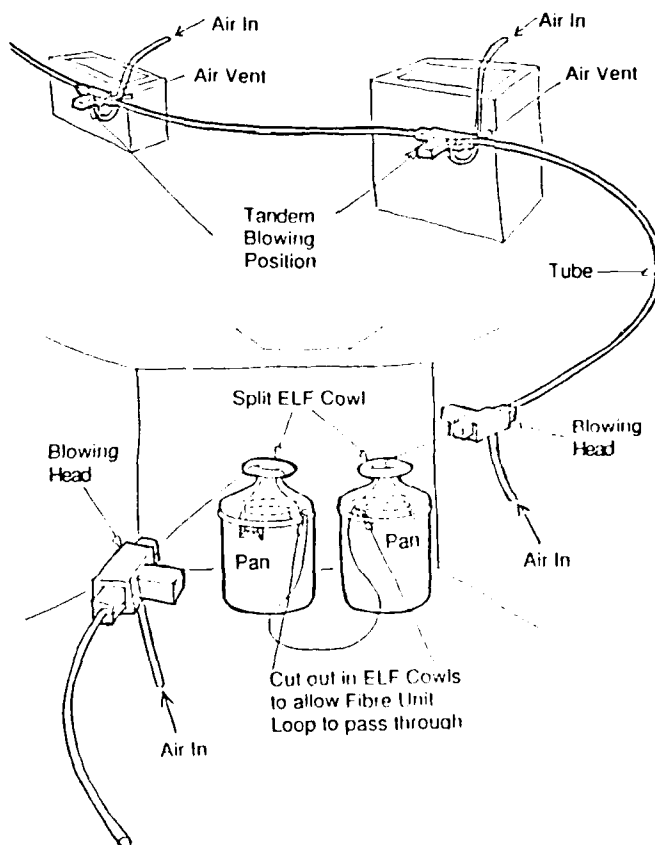


Figure 8: Gloucester to Painswick Route Gradient Profile

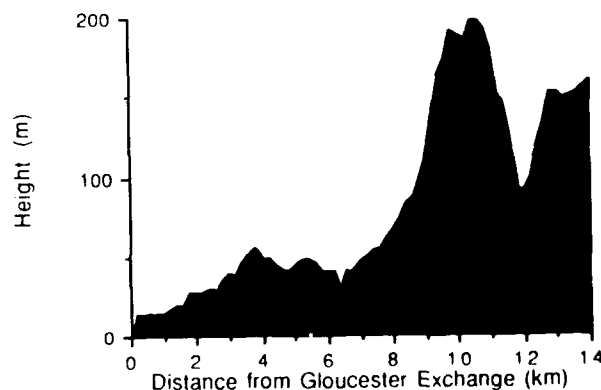
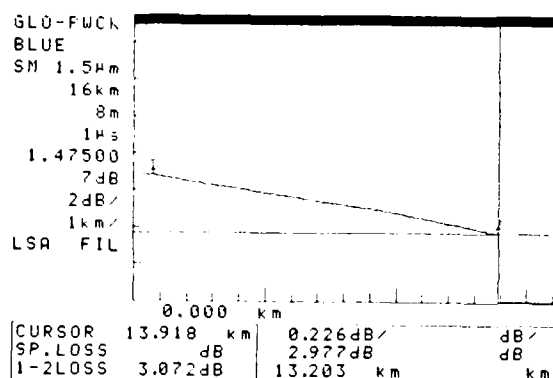
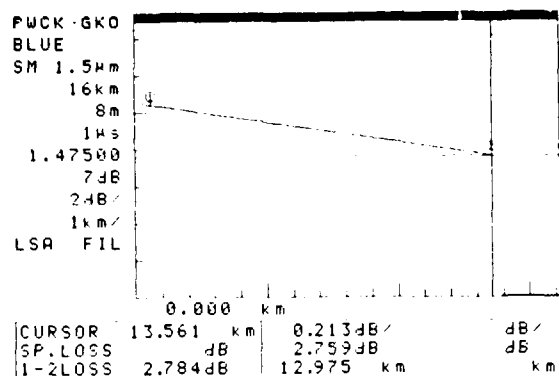


Figure 9: O.T.D.R. Traces of Blue coloured Fibre



## 6. COST EFFECTIVENESS

A comparative cost analysis showed that the cost of supplying an eight fibre, 14 km link using Blown Fibre was 5.1 % cheaper than using subducted conventional eight fibre cable. In addition having used Blown Fibre the cost of supplying a further eight fibres at a later date would be 31% of the cost of similarly increasing the link fibre count if subducted cable had been used. This would be achieved by Blowing Fibre units into two of the five unoccupied tubes whereas the cable option would require the installation of another route of subduct.

It is interesting to take the cost analysis one step further and consider the case of a planner making the decision between provisioning the link with eight or sixteen fibres. For the purpose of this comparison a notional unit has been introduced such that the total cost to supply the link using subducted conventional eight fibre cable is 100 units. The follow table gives the cost, expressed in notional units, of supplying the route with both eight and sixteen fibres using Blown Fibre and cable.

	8 fibres	16 fibres
8 fibre cable	100	200
16 fibre cable	-	115.2
Blown Fibre (4 fibre)	94.9	126.3

This table demonstrates the 5.1% saving that Blown fibre offers the eight fibre provision scenario and shows that if sixteen fibres are required on day one then sixteen fibre cable is the most cost effective option. However when the second eight fibres are supplied as spare for future use, as was the case for four of the fibres in this trial, then the costing becomes more involved. To demonstrate this, the cost of the planner making the wrong fibre count choice (ie Provision 8 fibres and require 16 fibres) is considered.

	Provisioned	Required	Cost of Error
1. Fibre cable	8	16	84.8
2. Fibre cable	16	8	20.3
3. Blown Fibre	8	16	11.1

The cost of error figures are defined for each case as follows:

1. The additional cost incurred from installing two eight fibre cables instead of one sixteen fibre cable.
2. The additional cost of provisioning sixteen fibre cable instead of using Blown Fibre to supply an eight fibre link.
3. The additional cost of supplying sixteen fibres using Blown Fibre instead of a sixteen fibre cable.

These figures show that the additional capital cost of providing eight spare fibres in a sixteen fibre cable is 20.3 notional units. However with the annual percentage rate (APR) for businesses in excess of 20 % it takes less than three years for the cumulative cost of provisioning the spare fibres to rise past the cost of using Blown Fibre to supply eight fibres now and another eight fibres when they are required.

The following three points can be summarised from this cost study.

1. It is cheaper to supply an eight fibre link using Blown Fibre than using subducted conventional eight fibre cable.
2. If sixteen fibres are required on day one or within two years of provision then the cheapest option is to use conventional sixteen fibre cable.
3. If eight fibres are required now and the second eight fibres are not required in the first two years then it is cheaper to use Blown Fibre to install eight fibre now and another eight fibre when required than to install a conventional sixteen fibre cable on day one.

All these costs are based on using two four fibre units to supply eight fibre counts therefore the use of eight fibre Blown Fibre units will offer the possibility of further savings.

## 7. CONCLUSIONS

1. Two 14.5km continuous lengths of four fibre Blown Fibre unit were successfully installed into a 13.6km route between Gloucester and Painswick. The installation used a combination of the three existing BF range extending techniques: centre point blowing, tandem blowing and Pan and ELF blowing. During the installation the fibre unit negotiated gradients in the order of 1 in 5 without a reduction in installation speed. This link is now the longest unspliced fibre optic transmission path within the BT underground network.
2. The cost of supplying a 14km, eight fibre link using currently available Blown Fibre technology is 5.1 % less than the cost of using contract labour to install subducted conventional eight fibre cable. In addition the cost of increasing the routes fibre count at a future date is approximately 31 % cheaper than the cost of using conventional cable. This is realised by blowing fibre units into unoccupied tubes whereas the cable option requires the installation of another route of subduct.
3. If a link requires sixteen fibres on day one or within two years of provision then the cheapest option is subducted conventional sixteen fibre cable. However if eight fibres are left unused for two years or more it is cheaper to use Blown Fibre to install two eight fibre links as they are required.
4. The total link attenuation was 4.46dB at 1300nm and 3.05dB at 1500nm giving attenuation per kilometre values of 0.33 dB/km and 0.22dB/km respectively. This represents a potential power budget saving of 35% compared with using standard fibre cable which typically has an attenuation of 0.51 dB/km at 1300 nm.
5. The prototype storage assembly devised to handle the 13.6 km length of fibre unit was based on the existing fibre Pan storage system. This prototype pan storage assembly incorporated special loading to allow access to both fibre unit ends and spacer rings to prevent the weight of the fibre unit compressing the lower layers. Both these features proved valuable for ease of installation.

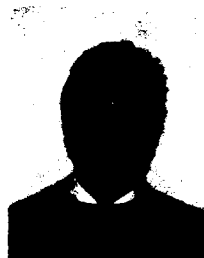
## 8. REFERENCES

1. Reeve M H and Cassidy S A: 'Installation of optical fibre units using viscous drag of air', ECOC Geneva (1983).
2. Cassidy S A and Reeve M H: 'A radically new approach to the installation of optical fibre using the viscous flow of air', BT Tech J, 2, No 1 (January 1984).
3. Cassidy S A and Hornung S: 'A fibre unit for blown fibre cable', IEE colloquium on Implementation and Reliability of Optical Fibre Cablelinks, London, Digest 1984/73 pp 5/1 (June 1984).
4. Cassidy S A et al: 'Optical characterisation of a trial link using blown fibre cable' IOOC, ECOC, Venice (1985).

5. Reeve M H et al: 'Design and implementation of an optical link using the blown fibre cable', BT Tech J, 3, No 4 (October 1985).
6. Hornung S, Cassidy S A, Yennadhiou and Reeve M H: 'The blown fibre cable', IEEE J Sel Area in Comms, SAC-4, No 5, (August 1986).
7. Freeman R A, Jenkins P D, Stockton D J and Wiltshire B: 'Advances in blown fibre installation methods', BT Tech J, 5, No 4, (July 1987).



Nicholas J Medlen joined BT Laboratories in 1987 after completing a BSc. Honours degree in Applied Physics. For the past four years he has been working in the Access Networks Division primarily addressing optical fibre plant and cabling issues.



Peter Frost joined BT Laboratories in 1973 as a trainee technician apprentice. In 1984 he joined an optical measurements group concerned with singlemode and multimode connectors. In 1988, he became responsible for the design of optical plant components for use in BT's local loop field trial. He holds a number of patents associated with optical plant and is now working on future component design.



Peter D Jenkins joined BT Laboratories in 1958 as a trainee technical apprentice. In 1960 he joined the Submarine Systems Division of BTL where he introduced many innovations to both analogue and optical cable technology. Since 1988 he has been responsible for the technical development of optical plant component and installation practices. He holds many patents for products in current use and development for BT.

## In situ characterization and reliability study of coatings on optical fibers

Yih-chyuan Lin, Jye-Meei Hsiao, Daw-Ming Fann,  
Shiow-Ing Wang, Kuang-Yi Chen

Telecommunication Laboratories  
P.O. Box 71, Chung-Li, Taiwan, R.O.C.

### Abstract

Methods to characterize in situ the coating on optical fibers were established and the long term stability of coatings in filling compounds was evaluated using these in situ methods for two fibers COR and UFO. TGA analysis show that COR coating has a thermodegradation activation energy of  $145 \pm 2$  KJ/mole and UFO is  $155 \pm 4$  KJ/mole. COR contains more weights of volatile components, an indication of under-cure. The in-situ DMTA results shown as measurable damping signals and dynamic modulus are as clear as to be distinguishable between COR from UFO. Shifts of damping signals due to aging in jelly filling compounds were observed, and a total loss of mechanical properties can occur when UFO fiber was aged in JF jelly at  $100^\circ\text{C}$ . The FT-IR applied by ATR or reflection technique presents spectra as good as regular spectra. The spectra indicate all fibers coatings are urethane based acrylates, and the absorption of jelly compounds by coating can be monitored. Jelly compounds tends to be absorbed more by UFO than COR. Results of absorption of jelly compounds can have drastic effect on alternating the mechanical performance of coating.

### Introduction

Polymeric coatings is necessarily adopted as the protection material for optical fibers in preserving optical fiber strength.<sup>(1)</sup> They protect the glass surface from moisture attack and prevents flaws from propagating.<sup>(2)</sup> In a typical optical cable, the coated fibers are submerged in water-proof filling compounds<sup>(3)</sup> or surrounded by water-blocking swelling materials<sup>(4)</sup>. A potential interaction between fiber coatings and water-blocking materials that may lead to the changes of chemical, physical, and mechanical properties on coatings always exists. Subsequently, a transmission loss can be induced. Though coating performance is claimed to be well-behaved in general, their long term stability still in doubt mostly by users due to lack of standard evaluating methods and unknown effects exerting by the diverse filling compounds and swelling materials from different sources used in the manufacturing. In addition, characterization of coating

properties is usually done on simulated films.<sup>(5)</sup> This leads to additional questions of how close will be between simulated coating films and coatings on real fibers because the processing conditions may not be exactly the same. As a result, to obtain direct and realistic information on coating performance, in-situ tests of the properties of coatings is practically needed. The established in-situ methods then can be used on on-line quality assurance for manufacture and on long term reliability evaluation for users.

The evaluation of coating reliability first comes to its thermal stability under various environments. For this purpose, the thermal analysis of thermogravimetry (TGA) is a standard, practical method and is often performed to measure the material stability in predicting aging and resistance to environmental exposure for polymeric materials such as optical fiber coatings. Furthermore, in order to obtain useful information that suggests the correlated end-use mechanical and structural performance, dynamical mechanical analysis (DMTA) is necessary to perform to uncover structural information such as glass transition temperatures or extent of crosslinkage or degree of degradation. Finally, the chemical and physical changes of coating due to environmental aging such as the absorption of jelly filling compounds by coatings can be detected by an infrared spectrometer through ATR techniques. All measurements are directly conducted on real optical fibers without special sample preparation. Such in-situ characterization offers the least sample perturbation and is much more realistic with the advantage of simplicity and straightforwardness.

### Experimental

#### Material

Two different commercial available, uncolored optical fibers were obtained and directly used in all measurements and aging experiments. They are designated as COR and UFO. All fibers have a total diameter of ca. 250  $\mu\text{m}$  with primary and secondary coatings coated on the bare fiber (125  $\mu\text{m}$  in diameter).



## Aging

Numbers of fix length of fibers were immersed in filling compounds JC and JF for COR and UFO respectively. They were aged at 50°C, 70°C, and 100°C, and removed for analysis at selected times. All fibers removed from filling compounds for analysis were first rubbed with a commercial "Filled Cable Cleaner" to remove surfacial residual jelly filling compounds.

## Thermogravimetry Analysis (TGA)

Sample of fibers were cut into lengths of 1-3 mm and directly used as the specimen for TGA analysis. The analysis was performed in a Perkin-Elmer TGA-2 system under nitrogen atmosphere using a sample weight of ca. 5 mg. Temperature was scanned from 50° to 650°C with heating rates (B) of 5°, 10° and 20° per minute. Various conversion were used in conjunction with different heating rates to calculate thermodegradation activation energy. It was done in a data station using a decomposition kinetics software based on Doyle, Ozawa, Flynn, and Wall proposed approximation<sup>(6)</sup>. Using various heating rates and assuming isofractional conversion, the approximation solution can be formulated as:

$$-d(\log B)/d(T)^{-1} \approx 0.457(E_a/R),$$

where B is the heating rate, T is the temperature, and  $E_a$  is the activation energy.

## Dynamic mechanical analysis (DMTA)

DMTA was conducted in a Polymer Laboratory PL-DMTA using a dual cantilever measuring fixture. The sample was scanned from -60°C to 90°C in a heating rate of 3°/min and a frequency of 1 Hz. Each sample was composed of 40 fibers (35 mm in length) arranging in parallel and was mounted on the fixture using a torque screw driver at 10 cN-m of torque. The sample geometry constant was calculated from: free length=7 mm, sample width=10 mm, and sample thickness=.25 mm. The mounted sample was shown in Fig.1.

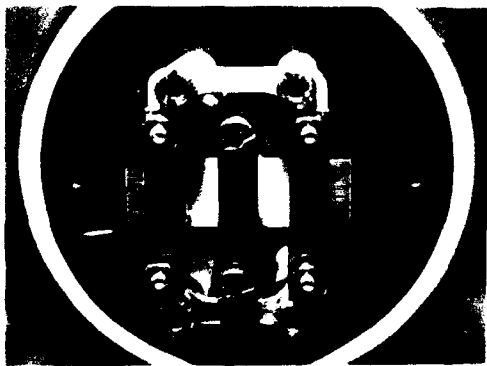


Fig.1 Sample mounting for DMTA measurement

## Infrared Spectrum analysis (IR)

Using the attenuated total reflectance (ATR) technique, the surfacial change of coatings was monitored by a Bruker IFS-85 FT-IR. Each sample was composed of 48 fibers with a length of 40 mm.

## Results and Discussion

### Thermogravimetry analysis

Thermogravimetric curves (TG) and the corresponding DTG curves of two tested optical fibers (UFO and COR) are shown in Fig. 2. The coatings on both fibers have similar temperatures on the onset and endpoint of decomposition when under nitrogen atmosphere. This is consistent with the fact that both fibers's coatings are urethane acrylate (see the IR spectra in Fig. 11-a and 113-a), and their degradation are govern by the same decomposition temperatures that controls the degradation of polyurethane acrylate. However, the individual decomposition process is quite characteristic to be easily distinguished from each other. As shown by the TG-DTG curves between 200 and 480°C, UFO exhibits two stages of decompositions corresponding to the differential TG peaks (DTG) peaks at 313° and 416°C while COR only gives a major weight-loss-change at 402°C. Also, When comparing at the same decomposition temperatures, UFO gives up less volatile components than COR at the low conversion region. The less conversion shown by UFO indicates that UFO is more stable than COR. In addition, the profiles of degradation curves for the same sample origins are all reproducible regardless the variation of sample batches, weights (from 4mg to 10 mg), and heating rates (5 to 20°/min). The indifference of sample weight and batches on the degradation profiles is a prove that measuring conditions (sample weights) are well-fitted into the range without causing perturbations. It may be due to the samples, which are pieces of cut fibers at 1-3 mm length, is unified in the shape through all measuring circumstances. This is apparent an advantage by directly taking the fibers as the sample specimens (i.e. in situ test) for measurement.

The characteristic dissimilar degradation curves shown on COR and UFO can be resulting from the difference of material origins or the discrepancy of curing process implemented on COR and UFO. The distinguishable difference shown by Fig. 2 implies that TGA is possible used as a qualitative method to identify the origin of fiber or the degree of cure. Fig. 3 and Fig. 4 are the thermogravimetric degradation (TG) curves and differential TG (DTG) of COR

and UFO fibers at various heating rates. All figures display a shift of degradation curves to higher temperatures for higher heating rates. The degradation activation energy ( $E_a$ ) at a particular conversion can be derived by plotting  $\log B$  vs.  $T^{-1}$  of various heating rates. The calculated results are shown in Fig. 5 as a plot of  $E_a$  versus conversion for COR and UFO. Fig. 5 indicates that the  $E_a$  values for UFO converge to a value of  $155 \pm 4$  KJ/mole after 6% of conversion, while for COR the converged value appears only after 10% of conversion at  $145 \pm 2$  KJ/mole. Both values are consistent with reported thermo-decomposition values for polyurethane ( $E_a \approx 141.9$ -- $160.9$  KJ/mole<sup>(7)</sup>). For low conversions, the value is lower than acceptable polymer decomposition values. It may be contributed from the evaporation of low molecular-weight compounds such as additives, or from the decomposition of uncured monomers. The comparison of long term stability between UFO and COR can be perceived by comparing the activation energies in Fig. 5. COR exhibits not only activation energies lower than UFO at high conversion region, but also at lower conversion regions. The higher  $E_a$  implies more stable in the long term. So coatings on UFO is likely durable than that on COR. Moreover, the more conversion required for COR to reach the converged decomposition energy implies that more percentage of easy decomposition materials occupy in the COR coatings. It may shorten the lifetimes of coatings when these materials are taken into account since they correspond to lower decomposition energies. As a result, if the low activation energy degradation dominate or have a significant effect on the overall degradation process, the stability of COR coatings may be doubtful.

#### Dynamical mechanical analysis (DMTA)

Fig. 6 and Fig. 8 represent the in-situ DMTA results of fiber COR and UFO respectively. Both show a recognizable damping signal (peak of  $\tan \delta$ ) but in different temperature region. The damping signal is an indication of the secondary phase transition of coating such as the glass transition and the different residing temperatures for COR and UFO implies they are different in molecular structure with different mechanical properties. The curve of storage modulus is shown as an uncommon profile that different from a regular DMTA curve. Actually, this is a characteristic indication of fiber structure, which is a glass fiber wrapped with a large portion of polymeric coating. At low temperatures where below the coating's  $T_g$ , the coating is quite hard and the mechanical response is mostly contributed by the part of polymeric coating. When the temperature increases, the coating gradually becomes softer and the storage modulus gradually decreases to a

minimum where the mechanical response from glass fiber becomes significant, and, all of a sudden, the modulus rises to a higher saturated value that corresponds to a pure glass fiber modulus. Therefore, one can observe the  $T_g$  of coating only at low temperature region where damping signal is the response of coating. At high temperature, the damping signal is dominated by the glass fiber.

Fig. 7 shows the DMTA results of COR fiber aged in JC jelly filling compound for one week at 50°C (Fig. 7-a), 70°C (Fig. 7-b), and 100°C (Fig. 7-c). The jelly immersed aging apparently results to a shift of damping signal from -31°C to -42°C. This is due to the absorption of jelly compound by the coating (see following IR study) and such action can cause a structural change of coating that may alter its mechanical performance to give unexpected results of overall fiber performance. High temperature aging such at 100°C as in Fig. 7-c shows a much pronounced aging effect that may have completely softened the coating as evidenced by the flat storage modulus profile and the appearance of a second damping signal at 35°C. The flat  $E'$  curve means the mechanical response is coming from the glass fiber through the temperature scan since only glass fiber give near no changes of mechanical response. Fig. 9 and Fig 10 show the DMTA results of UFO fiber aged in JF jelly filling compound for 1 week and 4 week at 50°C (Fig. 9-a and Fig. 10-a) and 70°C (Fig. 9-b and 10-b). The results of aging at 100°C was not able to obtain since the UFO coating have already degraded to tear off by itself under such condition. However, the aging effect shown on Fig. 9-a,b and Fig. 10-a results to no apparent shift of damping signal (-22°C) regardless the absorption of jelly compound. Yet Fig. 10-b shows a shift of damping signal to -40°C. Table 1 and 2 summarize the temperatures of damping signals and peaks of loss modulus ( $E''$ ) for COR and UFO fibers. As shown by the results, the absorption of jelly compounds by coating may alter coating performance and cause its mechanical performance become more temperature-dependent. Such effects exerted by jelly compounds and promoted by temperature are necessary to notice when the reliability of coating performance is a matter of concern.

#### Infrared Spectrum analysis (IR)

Using the Attenuated Total Reflection (ATR) technique, the infrared spectrum of coating can be directly measured without further sample preparation. Fig. 11-a is the IR spectrum of COR and is shown as an urethan acrylate. Fig. 11-b is the IR of jelly filling compound JC and is shown as a typical hydrocarbons (1377, 1457, and 2920  $\text{cm}^{-1}$ ) compounded with silica (broad peak at 1103  $\text{cm}^{-1}$ ). Fig. 12 shows the IR spectra of

COR coating aged in jelly JC for 8 weeks at 50°C (Fig.12-a), 70°C (Fig.12-b), and 100°C (Fig. 12-c). The IR of aged samples show a clear intensity increase on the C-H stretching at 2923 and 2858  $\text{cm}^{-1}$  and a moderate increase at 1376  $\text{cm}^{-1}$ . This is an indication that the jelly compound has been absorbed by the coating. The degree of absorption increases as the aging temperature increases. This is shown by Fig.12-c where the 1377 peak is much sharper to dominate its neighbor peak while, in Fig.12-a, it shows as a doublet with its neighbor peak. The effects is much more pronounced in UFO fiber aged in JF filling compound. As show in Fig.13-a (UFO fiber IR), Fig. 13-b (JF jelly), Fig. 14-a (UFO aged in JF at 50°C), Fig. 14-b (UFO aged in JF at 70°C), and Fig. 14-c (UFO aged in JF at 100°C), the intensity at 2923, 2954  $\text{cm}^{-1}$  and 1457  $\text{cm}^{-1}$  increase as the aging temperature increase. Fig. 14-c shows a tremendous absorption of jelly compound and one can observe by eyes that the coating is almost torn down already. By comparing Fig. 12 and Fig. 14, UFO coating apparently is more susceptible to JF jelly than COR to JC jelly. The infrared spectra give the evidence that the jelly can be absorbed by coating and DMTA results show it may have drastic effect to alter the mechanical performance. Quantitative correlation between the degree of absorption and DMTA results is necessary and is currently undergoing to elucidate the effects of jelly on the coating of optical fiber.

Table 1. Temperatures of tan delta and E" for COR fiber

aging time	temp.	tan delta	E"
-----	blank	-31°C	-30°, 29°C
8 weeks	50°C	-42°C	-42°, 37°C
8 weeks	70°C	-39°C	-39°, 33°C
8 weeks	100°C	-31°C	-31°, 40°C
-----			
1 week	50°C	-42°C	-44°, 28°C
1 week	70°C	-42°C	-41°, 31°C
1 week	100°C	-42°C	-43°, 35°C
-----			

Table 2. Temperatures of tan delta and E" for UFO fiber

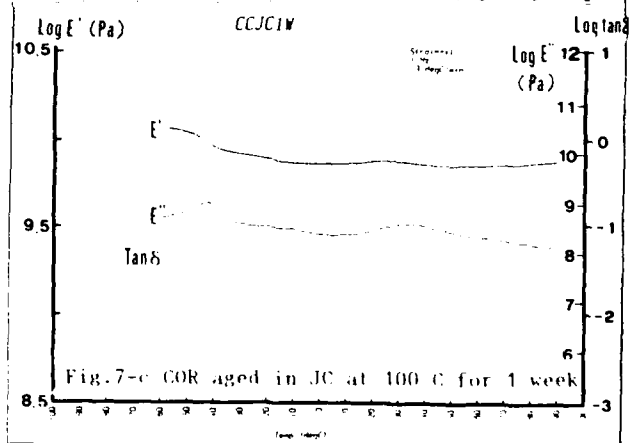
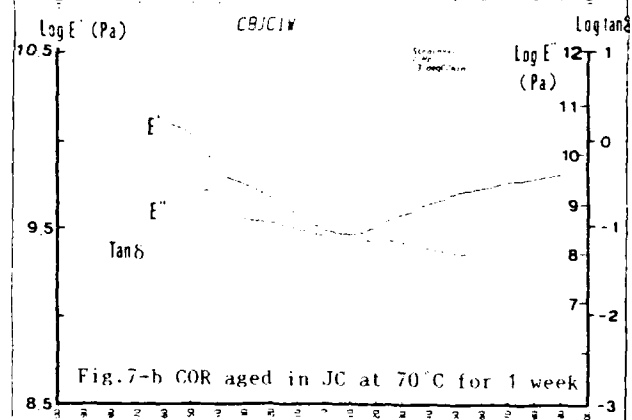
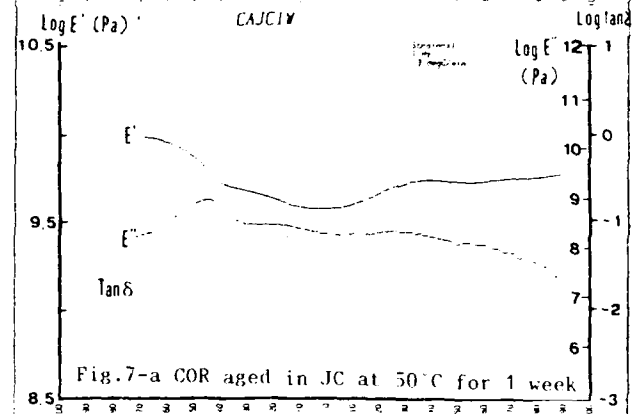
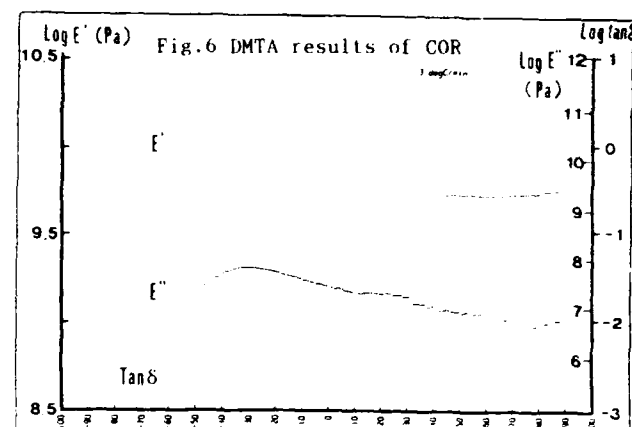
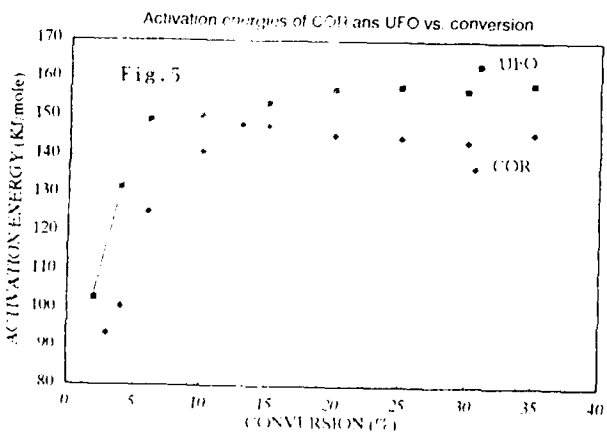
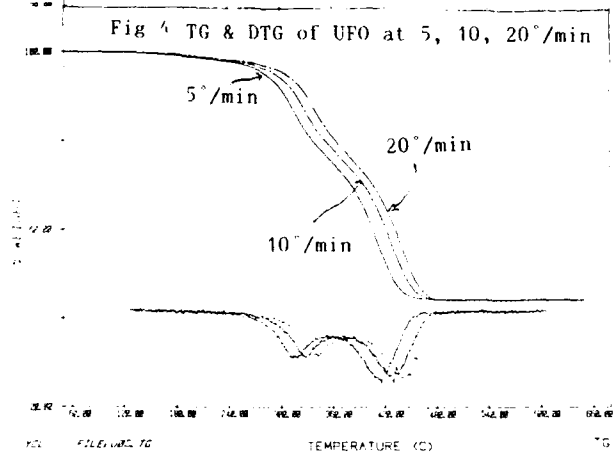
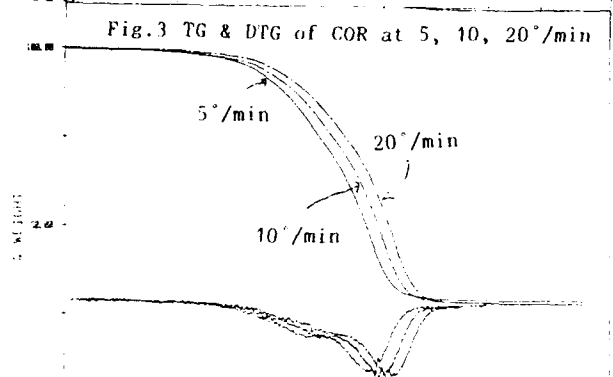
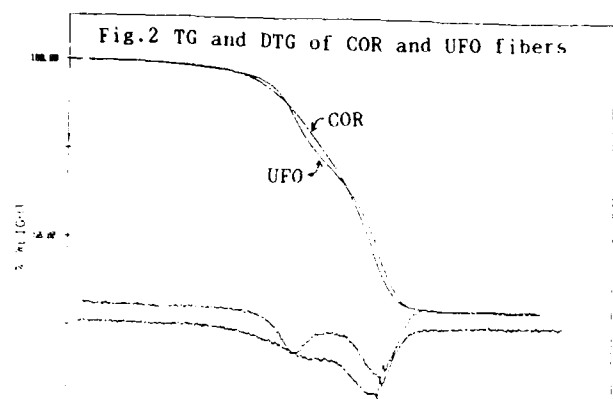
aging time	temp.	tan delta	E"
-----	blank	-21°C	-23°, 20°C
4 weeks	50°C	-22°C	-21°C
4 weeks	70°C	-40°C	-12°C
-----			
1 week	50°C	-20°C	-20°C
1 week	70°C	-22°C	-22°C
-----			

## Conclusion

In situ testing techniques for coatings on optical fibers were successfully developed by overcoming some sample handling problems, which were traditionally considered difficult. The in-situ methods offer rapid, inexpensive measurement, and the least sample preparative perturbation since the fibers were directly used in the analysis. Unlike general coating characterization of using simulated film samples, in-situ analysis of coating give the most realistic measurement on end-product properties. The simplicity and straightforwardness grant the advantage to use these methods in studying the long term stability of fiber coatings. As a result, the environmental degradations of coating caused by heat, interaction with filling compounds were examined by in-situ TGA, DMTA, and ATR-IR. The results show that jelly compound can be absorbed by coating and cause a change of mechanical performance. The effect can not be overlooked since the long term stability of coating on fibers is a major concern for the overall protection of optical fiber.

## Reference

- (1) Toler, J; Kar, G. ANTEC '88, 373 (1988)
- (2) Schuef, C.L.; Narasimham, P.L.; Oh, S.M. J. of Radiation Curing, April, 11 (1982)
- (3) Mitchell, D.M.; Sabia, R. IWCS, 29, (1980)
- (4) Kukita, S.; Nakai, T.; Hayashi A.; Koga, H. J. Lightwave Technol. 7(4), 710 (1989)
- (5) Simoff, D.A.; Chan, M.G.; Chapin, J.T.; Overton, B.J. Poly. Eng. and Sci. 29(17), 1177 (1989)
- (6) (a) Doyle, C.D. J. Appl. Poly. Sci., 6, 639, (1962)  
(b) Ozawa, T. Bull. Chem. Soc. Japan, 38, 1881, (1965)  
(c) Flynn, J.H.; Wall, L.A. Polym. Letters, 4, 323, (1966)
- (7) Gaboriaud, F; Vantelon, J.P. J. Polym. Sci. Chem. Ed., 19, 139, (1981); 20, 2063 (1982)



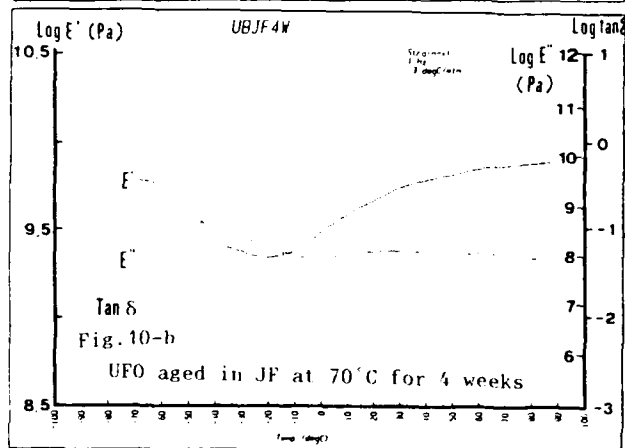
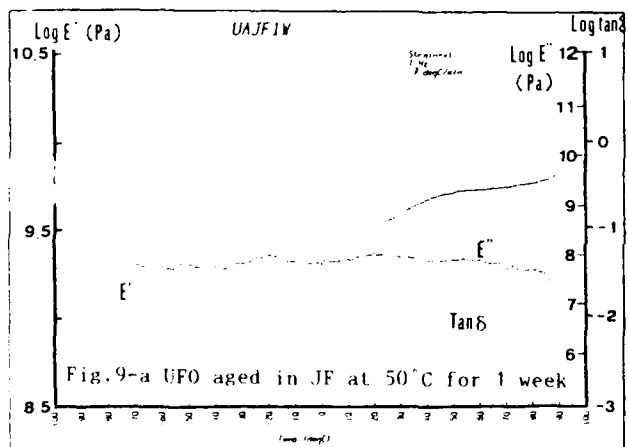
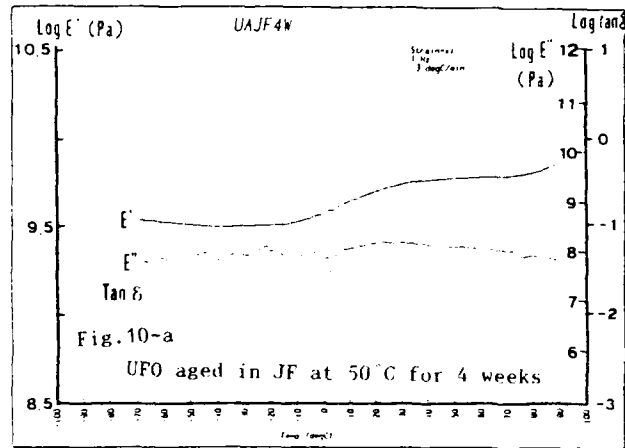
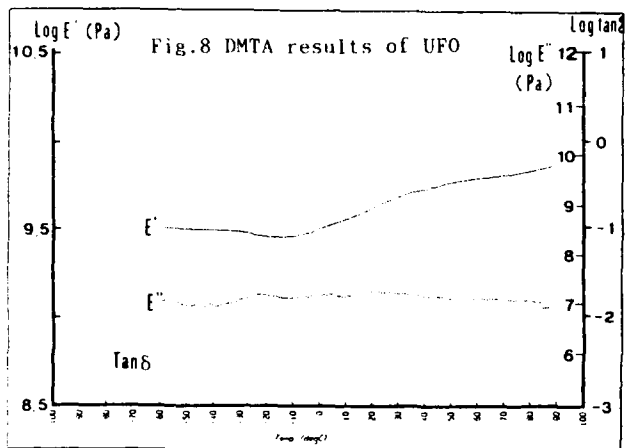


Fig.11-a IR spectrum of COR

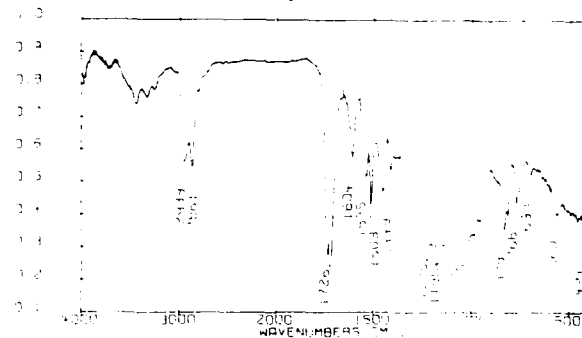


Fig.11-b IR spectrum of JC

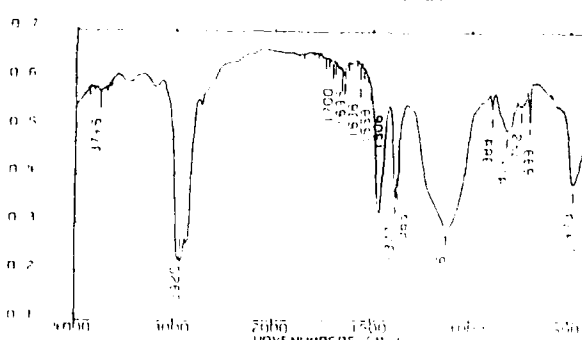


Fig.12-a IR of COR aged in JC at 50°C for 8 weeks

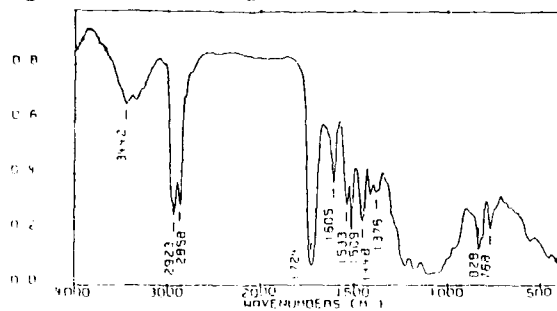


Fig.12-b IR of COR aged in JC at 70°C for 8 weeks

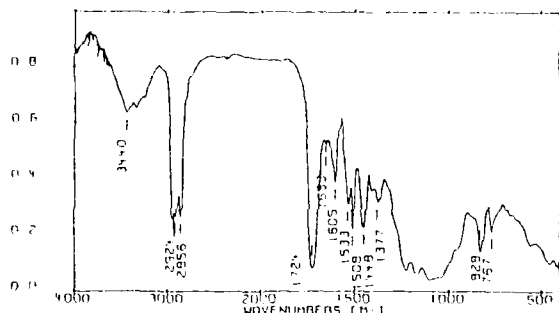


Fig.12-c IR of COR aged in JC at 100°C for 8 weeks

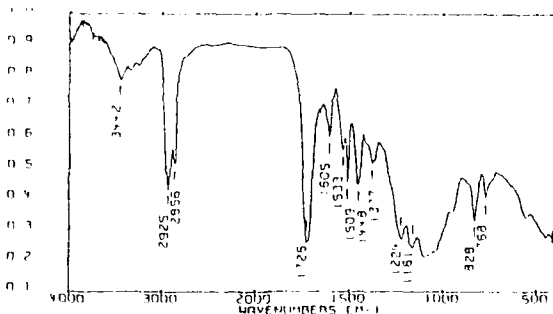


Fig.13-b IR spectrum of JF

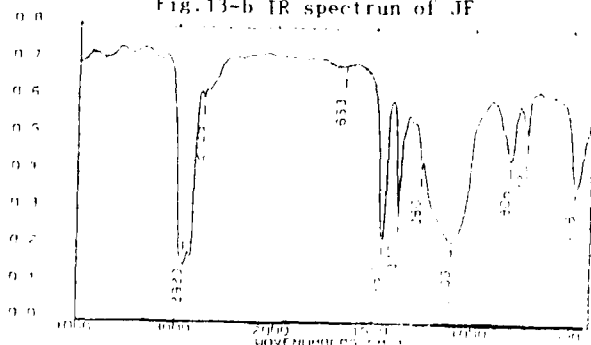


Fig.13-a IR spectrum of UFO

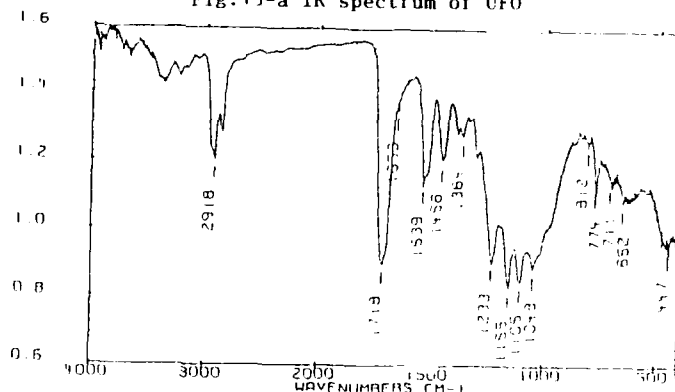


Fig.14-a IR of UFO aged in JF at 50°C for 4 weeks

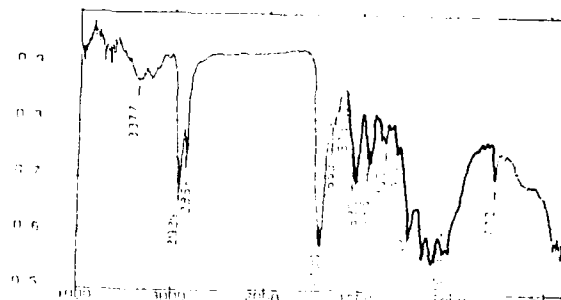


Fig.14-b IR of UFO aged in JF at 70°C for 4 weeks

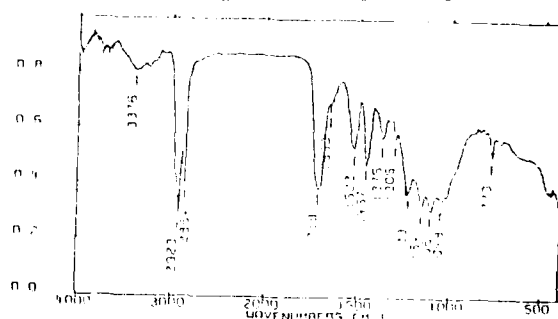
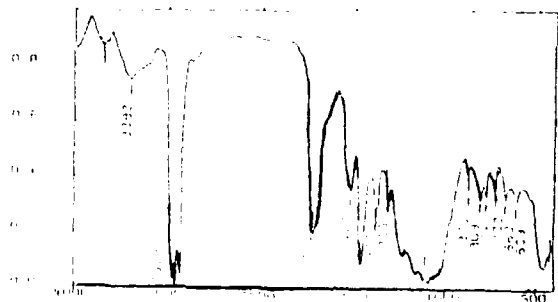


Fig.14-b IR of UFO aged in JF at 70°C for 4 weeks



## **Wear-Corrosion of Galvanized Steel and Stainless Steel Armor Wires in Submarine Cable**

J.H.Wang, Y.T.Horng, D.M.Fann, Kuang-Yi Chen

Telecommunication Laboratories  
P.O.Box 71, Chung-Li, Taiwan, R.O.C.

### **ABSTRACT**

The combination of corrosion and mechanical wear process, so called wear-corrosion, can promote the degradation of the armor metals of buried submarine cable. A laboratory technique to study the wear-corrosion is presented in this work. In addition to the electrochemical measurements, the measurements of coefficient of friction during the wear-corrosion process are also carried out. The results show that although the coefficient of friction and mechanical wear loss of stainless steel are higher at cathodic potentials than at the open circuit potential, cathodic protection is still beneficial because it stops the high corrosion rate promoted by the mechanical wear process.

### **INTRODUCTION**

Wear unavoidably occurs between the contacting and relatively moving bodies. The coefficient of friction can be changed by the corrosion products on the wear surface. On the other hand, the corrosion behavior of materials also be influenced by the wear process. This combination of electrochemical corrosion and mechanical wear process, so called wear-corrosion, can assist the degradation of the relatively moving bodies in a corrosive environment [1,2].

The galvanized steel and stainless steel are usually used as the armor wires in submarine cable. The corrosion behavior of these metals have been well known, however, the wear-corrosion properties emphasizing the interaction between corrosion and wear are not clearly understood until now. Wear-corrosion of stainless steel has been reported [3,4]. While a fundamental examination of the changes in friction coefficient and corrosion behavior during the wear-corrosion process of stainless steel has not been reported. It has been

shown [5,6] that the friction coefficient strongly depends on the corrosion condition of metals and plays an important role in wear-corrosion process.

In this paper, a laboratory technique simulating the wear process between the armor wires and sea sand is presented. The wear-corrosion characteristics is evaluated by measurements of friction coefficients, ac impedances and anodic polarization curves. The object of this study is to investigate the wear-corrosion properties of armor wires of submarine cable in 3% NaCl solution. A suggestion of minimizing the wear-corrosion rate of armor metals by potential control method has been provided in this work.

### **EXPERIMENTAL**

In this study, the galvanized steel, 304 and 316 stainless steels were prepared as the cylindrical specimens (20 mm in diameter x 20mm in length). The metallic coating thickness of galvanized steel was 100  $\mu$ m and the basal metal of galvanized steel was a carbon steel. The cylindrical specimen, rolling at a constant speed of 100 rpm, was abraded by a ceramic plate under a load of 0.2 kgf. Each specimen was abraded by the ceramic plate for two hours in 3% NaCl either under potentiostatic control or at their open circuit potentials. The mass loss rate was determined by weight and expressed in minigrams per hour (mg/hr).

In order to estimate the wear-corrosion properties, friction coefficient, ac impedance and anodic polarization curve of specimen were measured during the wear-corrosion process. The ac impedance measurements were made at the natural potential ( $E_{corr}$ ) with a 10 mV a.c. signal over the frequency range from 10 kHz to 5 MHz. The reference electrode is a saturated calomel electrode (SCE).

## RESULTS AND DISCUSSIONS

A summary of the results of mass loss rate are shown in Table 1. The mass loss rate of specimens are measured in three different conditions, namely, wear-corrosion condition, mechanical wear condition and natural corrosion condition. The wear-corrosion rate is determined by the mass loss of specimen at the open circuit potential during the wear process. The mechanical wear rate is measured at the cathodic potential, namely, -500 mV vs.  $E_{corr}$ . At such a cathodic potential, the electro-chemical corrosion is stopped and the wear is purely mechanical. The natural corrosion rate is determined by the mass loss of specimen in the natural corrosion condition without the mechanical wear. There are no obvious mass loss being measured for 304 and 316 stainless steels during the immersion time of two hours.

The wear-corrosion rates of galvanized steel, 304 and 316 stainless steels are 2.26, 0.88 and 0.58 (mg/hr), respectively, as shown in Table 1. The wear-corrosion rate of specimen increases in the order:

316 SS < 304 SS < galvanized steel

Under the cathodic protection, the mechanical wear rates of galvanized steel, 304 and 316 stainless steel are 1.10, 0.36 and 0.25 (mg/hr), respectively. The mechanical wear rate of specimen increases in the same order as the wear-corrosion rate does. It should be emphasized that the wear-corrosion rate (A) of each specimen is higher than the summation of mechanical wear rate (B) and natural corrosion rate (C) in Table 1. If neither the corrosion rate nor friction coefficient of specimen are changed by the wear process in a corrosive environment, the wear-corrosion rate of specimen is expected to be simply equal to the summation of mechanical wear rate and natural corrosion rate. The difference between (A) and (B+C) represents additional mass loss rate caused by wear-corrosion and can be thought to be an index of wear-corrosion property of materials. A wear-corrosion factor, namely,  $F$ , is defined in this study as  $(A-B-C)/A$ . The higher the value  $F$  of material, the higher tendency for the material being changed in corrosion behavior or friction coefficient during wear-corrosion process. The  $F$  values of galvanized steel, 304 and 316 stainless steel are 0.42, 0.59 and 0.57, respectively, and increase in the order:

galvanized steel < 304 SS < 316 SS

This result shows that the wear-corrosion property of galvanized steel is different from that of stainless steel, besides, the corrosion behavior or friction coefficient of stainless steel would change more significant than that of galvanized steel during the wear-corrosion process.

Measurements of friction coefficient and wear-corrosion rate of stainless steel and galvanized steel at different potential are presented in Fig. 2 and 3, respectively. The Fig. 2 shows that the friction coefficients and wear-corrosion rate of 304 and 316 stainless steel nearly keep at a constant value in the cathodic potential region, namely more negative than 700 mV(SCE). In the anodic potential region, although the friction coefficient of stainless steel dramatically decreases with the increasing potential, the wear-corrosion rate of stainless steel still increases with the potential. This result indicates that the oxide film of stainless steel increases in thickness with the anodic potential and provides a lubricity on the abraded surface, therefore, results in a decrease in the friction coefficient with an increasing potential when in the anodic potential range. In the cathodic potential ranges -700 to -1000 mV(SCE), the wear is merely mechanical and therefore the value of friction coefficient of stainless steel is the highest and independent of potential. Since the friction coefficient of stainless steel under the mechanical wear condition is higher than that under the wear-corrosion condition, it is thus concluded that the additional mass loss,  $A-(B+C)$ , of stainless steel in Table 1 is caused by the increase in corrosion rate, not the increase in friction coefficient. Based on the same reason, the increasing wear-corrosion rate of stainless steel with potential in the anodic potential region, as shown in Fig. 2, should be primarily caused by a significant increase in the corrosion rate.

For galvanized steel, a sharp increase in either the friction coefficient or the wear-corrosion rate with the anodic potentials is observed in Fig. 3. This result indicates that the friction coefficient of galvanized steel is promoted to a higher value by the corrosion product which is more and more thick with the increasing anodic potentials. As a result, the increase in wear-corrosion rate of galvanized steel would come from the increase in friction coefficient or corrosion rate.

The wear effect on ac impedance of specimens are shown in Fig. 4. It is observed that the ac impedance of each specimen is lower under wear-corrosion



condition than natural corrosion condition. For 304 and 316 stainless steel, the ac impedance is significantly decreased by the wear. Consequently, the corrosion rate of stainless steel would be markedly promoted by wear. Similar decrease in ac impedance is also present for galvanized steel but with a less tendency in comparison with the stainless steels. This result is consistent with that F value (wear-corrosion factor) of stainless steel is higher than that of the galvanized steel as shown in Table 1. To furthermore investigate the wear effect on corrosion behavior of stainless steel, measurements of polarization curve is also carried out in addition to the ac impedance measurements. The results are shown in Figs.5 and 6. Apparently, typical corrosion behavior of stainless steel has been markedly changed by wear. Besides the anodic current density is significantly increased, there are no pit initiation potential( $E_{np}$ ) and no passive region could be found in the anodic polarization curve of stainless steel during wear-corrosion process.

For galvanized steel, an obvious decrease in ac impedance is presented because of the wear effect, as shown in Fig.4. The polarization curves of galvanized steel with and without wear effect are shown in Fig.7. The anodic current is increased by the wear effect and the corrosion rate of galvanized steel is higher during the wear-corrosion than during the natural corrosion, which results are consistent with the results in Fig.4. It can conclude that the increasing wear-corrosion rate with potential, as shown in Fig.3, is corresponding to the increase in both the friction coefficient and corrosion rate. This result indicates that if the galvanized steel is anodically polarized by electrically coupling with another noble metal in a corroding solution, the wear-corrosion rate of galvanized steel would be dramatically promoted.

In regard of the fact that the wear-corrosion rate of armor metals is markedly dependent of potential, the galvanic coupling effect is important in the design of armor wires of submarine cable. The wear-corrosion rate of 316 stainless steel is the least, as shown in Table 1, whereas which is almost twice the mechanical wear rate under cathodic protection. Base on these results, electrically coupling 316 SS armor wires to the galvanized steel armor wires would be expected to decrease the wear-corrosion rate of 316 SS to a half value. On the other hand, the galvanized steel armor wires, work as a sacrificial anode, should be prevented from abrading with the sea sand. The above discussion

has described that the cathodic protection is beneficial to suppress the wear-corrosion rate of stainless steel armor wires in sodium chloride solution. However, the wear-corrosion properties of armor metals in natural sea water may be different from that in sodium chloride solution because that some calcium carbonate and magnesium carbonate would deposit on the cathodic protection area when in the natural sea water and therefore change the wear-corrosion behavior of the metal. Further study concerning the wear-corrosion characteristic of armor metals when in natural sea water is still going on in this work.

## CONCLUSIONS

- (1) The wear-corrosion rate of armor metals in this study increases in the order:  
  
316 SS < 304 SS < galvanized steel  
  
The wear-corrosion rate of stainless steel can be reduced to a half value by cathodic protection.
- (2) The wear-corrosion rate of galvanized steel markedly increase with the anodic potential, which is because of the significant increase in friction coefficient and corrosion rate.
- (3) Base on the changes in friction coefficient and corrosion rate, the electrochemical corrosion reaction is the primary rate controlling factor for 304 and 316 stainless steels during the wear-corrosion process.

## REFERENCES

1. J. Calling, "Principles of Tribology", p.106 (1978).
2. R.B. Waterhouse, "Tribology", (1970) 158-162.
3. H. Abd-EL-Kader and S.M. ElRaghy, Corrosion Science, Vol.26, No.8, pp.647-653 (1986).
4. C. Aller, A. Ball and B.E. Protheroe, Wear, 74 (1981-1982) 287-305.
5. E. Broszeit, F.J. Hess and E. Wagner, Wear, 30(1974) 311-319.
6. E. Wagner and Broszeit, Wear, 55 (1979) 235-244.

Table 1. Mass loss rate(mg/hr) of armor metals

conditions metals	(A) wear-corrosion	(B) mechanical wear	(C) natural corrosion
galvanized steel	2.26	1.10	0.22
304 ss	0.88	0.36	-
316 ss	0.58	0.25	-

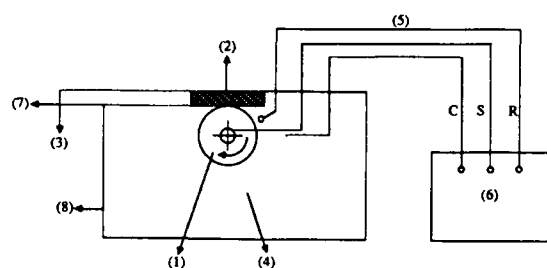


Fig.1 Schematic arrangement of the wear-corrosion tests:(1)cylindrical specimen (2)plate ceramic (3)load (4)counter electrode (5)reference electrode (6)potentiostat (7)load cell for force measurement (8)test chamber

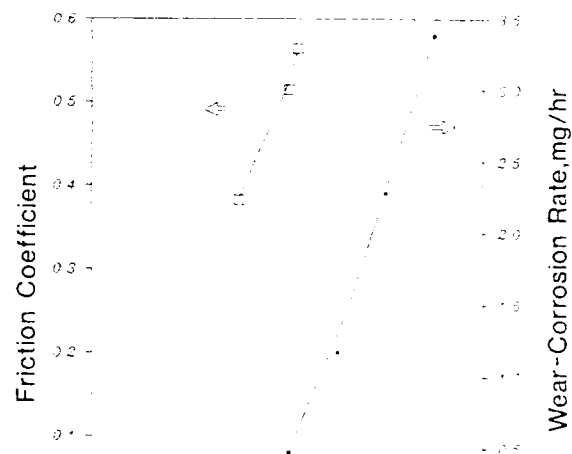


Fig.3 Dependence of friction coefficient and wear-corrosion rate with potential for the galvanized steel.

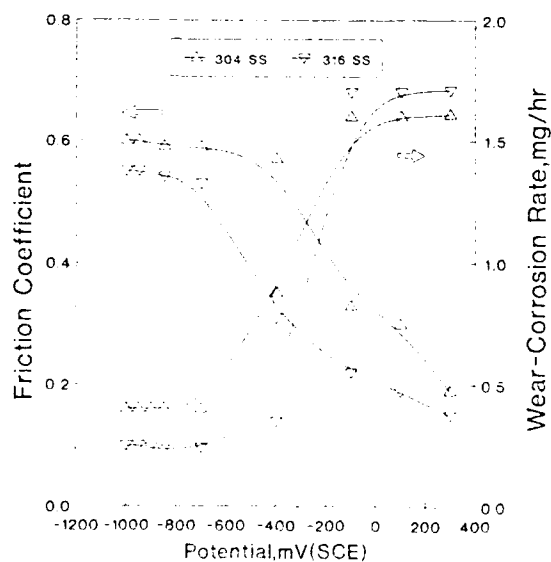


Fig.2 Dependence of friction coefficient and wear-corrosion rate with potential for 304 and 316 SS

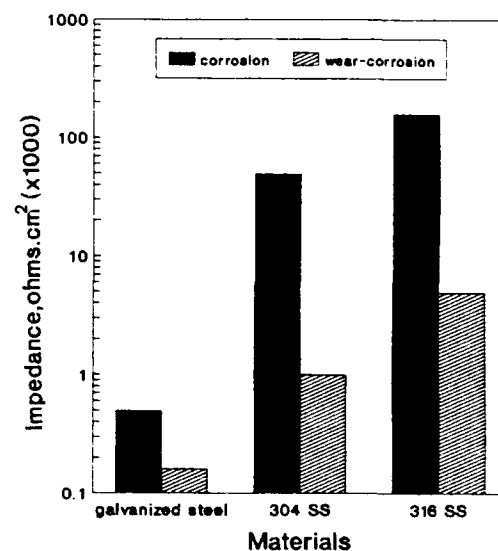


Fig.4 Wear effect on ac impedance.

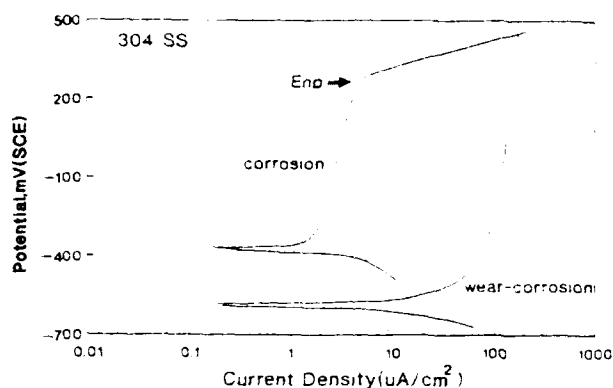


Fig.5 Wear effect on anodic polarization curve of 304 stainless steel.



Jyh-Hwa Wang  
Outside Plant Lab.  
Telecommunication Labs.  
P.O.Box 71, Chung-Li  
Taiwan, R.O.C.

Jyh-Hwa Wang received his M.S. degree in Materials Science from National Cherkung University in 1981. From 1983 to 1988, he worked in Materials Research Labs. In 1988, he joined T.L. and has been engaged in Outside Plant technology.

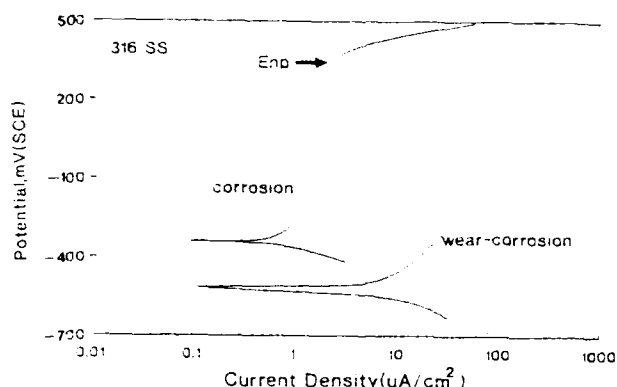


Fig.6 Wear effect on anodic polarization curve of 316 stainless steel.



Yaw-Tzong Horng  
Outside Plant Lab.  
Telecommunication Labs.  
P.O.Box 71, Chung-Li  
Taiwan, R.O.C.

Yaw-Tzong Horng received his M.S. degree in Electrochemistry in 1983 from National Taiwan Normal University. He joined T.L. in 1983 and has been engaged in Outside Plant technology. He is also a member of the Corrosion Engineering Association of the Republic of China.

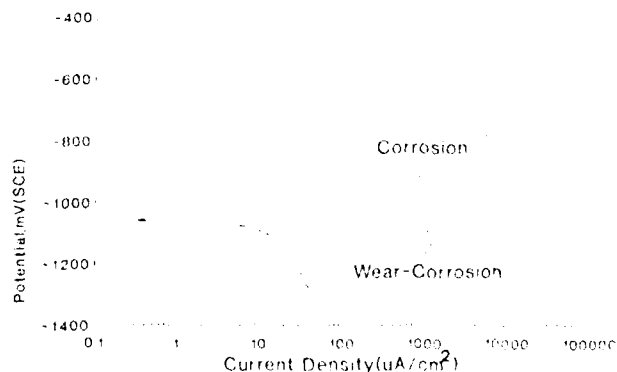


Fig.7 Wear effect on anodic polarization curve of galvanized steel.



Daw-Ming Fann  
Outside Plant Lab.  
Telecommunication Labs.  
P.O.Box 71, Chung-Li  
Taiwan, R.O.C.

Daw-Ming Fann received his M.S. degree in Chemical Engineering from National Taiwan Institute of Technology. He joined T.L. in 1982 and presently worked as a project leader in OSP Lab. of T.L.



Kuang-yi Chen  
Telecommunication Labs.  
P.O.Box 71,  
Chung-Li, Taiwan 32099

Kuang-yi Chen was born in 1953 and received his Ph.D. degree in Electro-optics from National Central University in 1990. He has been engaged in research and development of optical fiber fabrication and communication technologies since 1977. He is currently the director of outside plant technology laboratory of Telecommunication Laboratories.

## ANALYSIS OF TORSIONAL FIBER FAILURES

L. A. Reith, J. P. Varachi, Jr. and H. H. Yuce

Bellcore  
445 South Street, Morristown, NJ 07962

### ABSTRACT

*Tensile stress is the most common type of stress to arise in long fiber lengths, both during and after cable installation. Thus, tensile failures have been well characterized. As fiber is deployed in the loop network, however, failures at splice points are now becoming a noticeable source of failures. Torsional breaks at splice points are one new type of failure mode recently observed, thus warranting further investigation.*

*We derive an expression to describe the experimentally observed onset of crack branching in optical fibers fractured in torsion. In this relation, a crack correction factor is introduced to account for the different stress distribution which arises from torsional loading. The new correction factor is calculated from an fractographic analysis of low-stress, torsional fiber breaks using a scanning electron microscope.*

### 1. INTRODUCTION

The deployment of fiber into the local loop will require increased numbers of splice/termination points compared with feeder portions of the network. Although the amount of fiber at splice/termination points constitute only ~0.2 % of the deployed fiber, post-mortem analyses show that the majority of problems occur at these points<sup>1</sup> and thus, investigation into splice failures is of great interest. Recent studies have shown that mechanical, fiber-optic splices can be vulnerable to torsional breaks<sup>2</sup>.

Fracture surfaces of brittle materials, such as glasses and ceramics, exhibit several characteristic features. The flat smooth area around the fracture origin is referred to as the mirror, and is surrounded by a region which appears slightly roughened due to microbranching. This roughened area, known as the mist, is in turn bounded by a region of multiple fracture planes known as hackle. Beyond the hackle, the fracture surface is characterized by macroscopic crack branching. A typical fracture surface of a glass is illustrated in Fig. 1, where the mirror, mist, hackle, and crack branching regions are illustrated. In order for the four regions to be observed, the fracture stress must be small enough for these features to be included within the cross-section of the test specimen.

Although fractographic analysis has been used successfully to study tensile and flexural breaks in fibers<sup>3,4</sup>, no such analyses have considered torsional stresses. The purpose of this study was to derive an expression to describe the experimentally observed onset of crack branching in optical fibers fractured in torsion. In this relation, a correction factor is introduced to account for the different stress distribution.

The new correction factor is calculated from a fractographic analysis of low-stress, torsional fiber breaks using a scanning electron microscope (SEM). We will describe the experimental apparatus used to create the low-stress fiber breaks, as well as describing the calculation and giving values for the new correction factor.

### 2. ANALYSIS

Since it was established that the stress intensity approach can accurately predict the mirror-mist branching boundaries<sup>5,6</sup>, we assume that this criterion can also be utilized to experimentally generate the boundary correction factors associated with a given stress intensity expression. This would be the experimental equivalent of what Smith et. al.<sup>7</sup> and Newman and Raju<sup>8</sup> have done numerically to determine the correction factors for semi-circular surface cracks subjected to tension and flexure.

Kirchner and Kirchner<sup>11</sup> obtained the stress intensity factor,  $K_I$ , expressions at various points on the boundaries by incorporating the Smith et. al., analysis<sup>9</sup> for both tension (Eq. 1) and flexure (Eq. 2). They used the stress distribution for tension and flexure, through the rod specimen, to estimate the stress intensity factor along the branching boundaries for each particular loading:

$$K_I = \frac{2}{\sqrt{\pi}} \sigma_f \sqrt{r} Y(\theta)_{\text{Tension}} \quad (1)$$

$$K_I = \frac{2}{\sqrt{\pi}} \sigma_f \sqrt{r} Y(\theta)_{\text{Flexure}} \quad (2)$$

where  $\sigma_f$  is the fracture stress at the tensile surface,  $r$  is the radius measured from the fracture origin to the boundaries of the various fracture surface features, in particular mirror-mist or crack-branching boundary and  $2/\pi^{1/2}$  is a constant applicable to a two-dimensional solution.  $Y(\theta)_{\text{Tension}}$  is a

boundary correction factor which accounts for a tensile stress field and  $Y(\theta)_{\text{Flexure}}$  is another boundary correction factor which accounts for the variable stress field in the interior of the specimen when subjected to bending.  $\theta$  is the angle measured between a line drawn through the fracture origin perpendicular to the surface of the specimen and a line drawn from the origin to a particular point on the mirror-mist boundary.  $Y(\theta)_{\text{Tension}}$  and  $Y(\theta)_{\text{Flexure}}$  also account for crack shape proximity to the surface and size of the crack relative to the specimen size. Kirchner and Kirchner<sup>11</sup> utilized the above expressions, Eqs 1 and 2, at all the points along the mirror-mist and the mist-hackle branching boundaries in order to calculate  $K_I$  values along these boundaries. The stress intensity factor along the mirror-mist and mist-hackle branching boundaries were called  $K_m$  and  $K_h$  respectively. Or, in other words, Kirchner and Kirchner set  $K_I = K_m$  at the mirror-mist boundaries and  $K_I = K_h$  at the crack-branching boundaries in Equations 1 and 2 and then calculated their values along the periphery of the respective boundaries. The values for all the points on each particular boundary were estimated to be  $K_m = 2.33$  and  $K_h = 2.55 \text{ MPa m}^{1/2}$  respectively.

The stress intensity expression for torsion for glass fiber with a surface flaw can be given as:

$$K_I = \frac{2}{\sqrt{\pi}} \sigma_f \sqrt{r} Y(\theta)_{\text{Torsion}} \quad (3)$$

The boundary correction factor which accounts for the variable stress field in the interior of the specimen when subjected to torsional loading,  $Y(\theta)_{\text{Torsion}}$ , can be determined experimentally by fracturing specimens in torsion and then measuring the mirror-mist radius as a function of  $\theta$ , and by knowing the values for  $K_m$ ,  $\sigma_f$ .

$$Y(\theta)_{\text{Torsion}} = \frac{1}{2} \frac{K_m}{\sigma_f} \sqrt{\frac{\pi}{r_m(\theta)}} \quad (4)$$

As was the case for the tensile and flexural boundary correction factors ( $Y(\theta)_{\text{Tension}}$ ,  $Y(\theta)_{\text{Flexure}}$ ),  $Y(\theta)_{\text{Torsion}}$  also accounts for the effects of stress distribution, crack geometry, the presence of a free surface, and the angular dependence of the stress intensity factor.

### 3. EXPERIMENTAL PROCEDURE

To carry out experiments with fibers under torsional loading conditions, commercially available optical fibers with a 125  $\mu\text{m}$  OD were used. These had a protective acrylate coating with a 250  $\mu\text{m}$  OD.

The experimental set-up used to create low-stress fiber breaks consists of an automated rotational stage mounted on rigid support posts at a height of approximately 30 cm. The fiber was clamped and centered at the top of the apparatus using a clamping fixture attached to the rotational stage. The other end of the fiber was clamped to a fixed weight of 26 gm. to provide constant, uniform tension and prevent the fiber from buckling. The weight was allowed free vertical motion as the rotational stage turned, in order to maintain constant tension. However, the weight was sandwiched between two plates to prevent it from twisting.

The fibers were clamped by first chemically stripping off a short length of the acrylate coating from each end. The bare fiber was then epoxied into a 0.4 mm I.D./ 1 mm O.D. glass capillary tube using EPOTEK-353D thermal curing epoxy. The capillary tubes were gently clamped into brass tubes with set-screws. The brass tubes were in turn mounted on the rotational stage and attached to the weight.

In all cases the rotational stage was set for a rate of 40 sec/rev. This corresponds to a strain rate of approximately 0.25 - 0.35 %/min, depending on the gauge length of the fiber. Gauge lengths ranged from 16.5 - 24 cm. All measurements were taken at room temperature.

Before any fibers were subjected to torsional breaks, the shear modulus of the fiber was first measured, to ensure that the torsional stress would be measured accurately. We used the expression

$$T = \pi^2 G r^4 (\phi/L) \quad (5)$$

where  $T$  is the torque,  $G$  is the shear modulus,  $r$  is the fiber radius,  $\phi$  is the fractional twist, and  $L$  is the length of the fiber. The length of the fiber was measured between the epoxy attachment points before mounting. The computer's internal clock was used to keep track of total turns of the rotational stage once the computer started the motor stepping sequence.

In order to measure the shear modulus, a torque gauge was clamped to the bottom of the fiber instead of the weight. The gauge itself was allowed to rotate with the fiber, while the gauge center shaft was loosely inserted into a fixed chuck. As with the weight, the gauge was thus allowed free motion in the vertical direction but the center shaft was prevented from rotating. Thus, the torque could be measured as a function of twist per unit length. The torque gauge ranged from 0.003 to 0.03 oz-in (0.22 - 2.22 gm-cm) in 0.001 oz-in steps and was read manually.

Data were taken for a set of 10 fibers, and the shear modulus estimated by doing a least-squares fit to find the slope of the  $T$  vs.  $\phi/L$  curves. This resulted in a shear modulus of  $G = 30.2 \text{ GPa}$  with  $\pm 3\%$  standard deviation. This compared well with a value of  $31.3 \text{ GPa}$ , estimated using a Young's modulus,  $E = 72.9 \text{ GPa}$ , and Poisson ratio,  $\nu = 0.165$ , where  $G = E/(2(1+\nu))$ . One data set was also measured first with and then without the acrylate coating, and the coating was found to have a negligible effect on the shear modulus.

Low stress breaks were obtained by clamping the coated fibers in the glass capillary tubes as described above and then stripping the coating from a short center section. This usually was done mechanically. A hand-held cleaving tool with a graphite blade was used to nick the stripped section and create a large surface flaw. The fiber was then mounted in the apparatus, and twisted to the breaking point.

### 4. RESULTS

Optical fiber specimens were fractured while subjected to torsional loading and the fracture surfaces were examined and analyzed. Then these surfaces were photographed in the scanning electron microscope, and their respective mirror-mist radii were measured at selected angular intervals. The measured mirror-mist radii for various fracture stresses are given in Table 1.

Table 1 - Measured mirror radii and their respective angles for various fracture stresses

Angle (degrees)	Fracture Stress (MPa)				
	238	278	309	419	490
	$r_m$ ( $\mu m$ )	$r_m$ ( $\mu m$ )	$r_m$ ( $\mu m$ )	$r_m$ ( $\mu m$ )	$r_m$ ( $\mu m$ )
0	92	76	61	39	31
15	95	78	63	38	32
30	99	83	64	36	27
45	93	77	61	34	21
60	81	68	60	31	19
75	59	51	44	28	--

Figs. 2 and 3 illustrate a typical fracture surface for a optical fiber fractured in torsion. The three regions can clearly be seen in Fig. 2; a mirror region surrounds the fracture origin, followed by a mist region which is followed by hackle. It should be emphasized that in torsion, the mist region is limited to a very small area near the surface and the hackle consists of long parallel curve lines known as "twist hackle". The fracture origins are clearly evident in both Fig. 2 and 3.

The measurement of the mirror-mist radii (fracture mirror boundaries) was found to be a very difficult task. The fiber samples tended to fracture into a large number of fragments; this is increasingly true at the higher fracture stresses. Therefore, only two cases of relatively high fracture stresses were examined, 419 and 490 MPa, although many more tests were done to obtain higher fracture stresses. For these specimens it was not possible to measure the mirror-mist radius at every angle due to excessive shattering. For lower fracture stresses, the amount of fragmentation was less, but still had a great influence in obtaining mirror-mist radii measurements at higher angles.

The mirror-mist boundaries,  $r_m$ , obtained from fractographic analysis of low-stress torsional fiber breaks and  $K_m$  value<sup>11</sup> were utilized to compute a single boundary correction factor,  $Y(\theta)_{Torsion}$ , for the stress intensity factor expression determined for fibers with a surface flaw subjected to torsional loading (See Figure 4).

$Y(\theta)_{Torsion}$  values thus determined ranged from 0.839 at  $\theta = 0^\circ$  and decreased slightly until  $\theta = 30^\circ$  where they gradually increase toward the surface. Ideally the values of  $Y(\theta)_{Torsion}$  should increase gradually from 0 degrees to 90 degrees at the surface<sup>10</sup>. But as is obvious, this does not occur, perhaps due to several factors involved in the experimentation. One explanation could be that the mirror-mist boundaries elongate toward the neutral axis or the back surface between the same angles. Another reason could be due to the experimental mirror-mist radius measurements and/or as the result of decreasing stress field beneath the surface.

## CONCLUSIONS

An experimental technique was utilized to determine the value of a correction factor for a surface flaw in a fiber subjected to torsional loading. The torsional correction factor,  $Y(\theta)_{Torsion}$ , is deduced through a series of torsion experiments.  $Y(\theta)_{Torsion}$  values were calculated for each of the five fiber specimens fractured in torsion, and then a single set of average  $Y(\theta)_{Torsion}$  values were determined. Mirror-mist boundaries were in a shape of a semi-ellipse. These boundaries were small near the surface but increased in size across the surface. Between the angles of  $15^\circ$  to  $45^\circ$ , mirror-mist boundaries were elongated toward the neutral axis and/or back surface. As a result of extensive glass shattering the experimental boundaries were measured only at limited locations. This analysis did not take into account the affect of varying  $r_m/d$ .

## REFERENCES

1. J. P. Kilmer et. al., *Proc of SPIE 1366*; 85-91 (1990).
2. S. M. Leopold et. al., *Proc of NFOEC '91*, 2, 260 (1991).
3. J. J. Mecholsky et. al., *Ceramic Bull*, 56, No. 11; 1067 (1977).
4. J. J. Mecholsky et. al., *J. Amer. Ceram. Soc.*, 57, No. 10; 440 (1974).
5. J.W. Johnson and D.G. Holloway, *Phil. Mag.*, 14; 731 (1966).
6. J.J. Mecholsky et. al., *J. Mater. Sci.* 11; 1310-1319 (1976).
7. H.P. Kirchner and J.C. Conway, Jr., *J. Amer. Ceram. Soc.*, 70, No 6; 413 (1987).
8. H.P. Kirchner and J.C. Conway, Jr., *J. Amer. Ceram. Soc.*, 70, No 6; 419 (1986).
9. F.W. Smith et. al., *J. App. Mech.*, 34, No 4; 953 (1967).
10. S.C. Newman, Jr., I.S. Raju, *NASA Technical Paper # 1578*, Langley Research Center, (1979).
11. H.P. Kirchner and J.W. Kirchner, *J. Amer. Ceram. Soc.*, 62, No 3-4; 198 (1979).

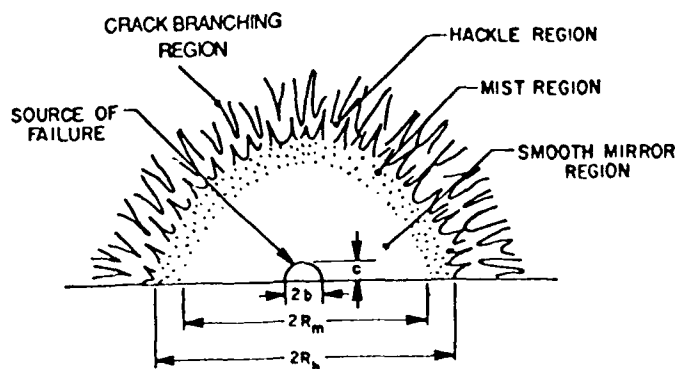


Figure 1 - A typical glass fracture surface



Figure 2 - Fracture Surface of a Optical Fiber Subjected to Torsional Loading

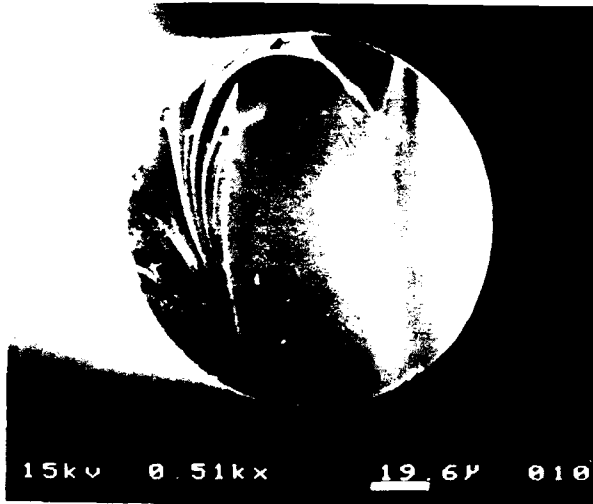


Figure 3 - Fracture Surface of a Optical Fiber Subjected to Torsional Loading

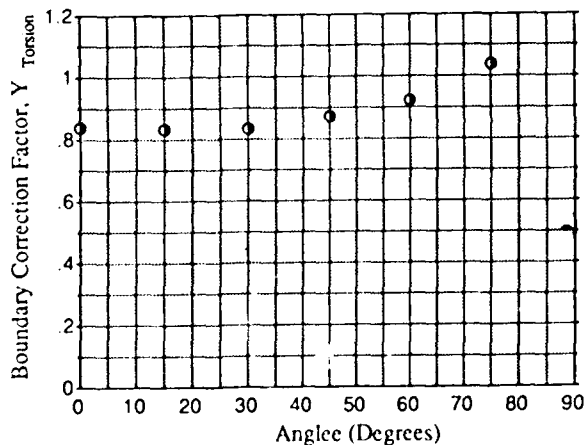


Figure 4 - The torsional correction Factor  $Y(\theta)_{Torsion}$  for a fiber with a surface flaw.



**Leslie A. Reith** received a B.A. degree from New York University in 1975, the M.Phil. degree from the City University of New York in 1979, and the Ph.D. degree from The University of Texas at Austin in 1981, all in physics. In 1981 she joined AT&T Bell Laboratories as a Member of Technical Staff. In 1984 she subsequently joined Bellcore, where she is presently a member of the Fiber Distribution and Reliability Research group in Morristown, N.J. Her recent research interests at Bellcore include reliability issues related to optical splices.

**John P. Varachi, Jr., P.E.**, received the BSME degree from Fairleigh Dickinson University, Rutherford, N.J. in 1976 and the MSME degree from Polytechnic Institute of New York, Brooklyn, N.Y. in 1978. He is currently District Manager, "Fiber Distribution and Reliability Research" at Bellcore. From 1969 through 1983 he was engaged in exploratory development at Bell Laboratories in mechanical design and analysis for telephone central office and outside plant apparatus. He also performed physical design and systems engineering for copper and optical fiber based digital loop electronic systems for outside plant and customer premises applications.

**Hakan H. Yuce** is a member of the Technical staff in the Fiber Distribution and Reliability Research District at Bellcore. He leads a research program dealing with long-term mechanical reliability of optical fibers and interconnections. Hakan provides technical input and support to organizations responsible for generic requirements and responds to clients' immediate needs related to consultation on reliability and field failures. He also plays an active role in the standards arena under EIA/TIA working committees 6.6.7, fiber coatings and 6.6.8, fiber reliability. Hakan has a B.S. degree in Mechanical Engineering from Technical University of Istanbul [1977], an M.S. in Mechanical Engineering from M.I.T. [1982] and a Ph.D degree in Mechanical Engineering and Material Science from Stanford University [1987].



## MOBILE OPTICAL CABLE ASSEMBLY ON TRANSPORTABLE RACK

Heinz W. Brückner, Georg Franken, Daljit S. Parmar

Kroschu-Kabelwerke, Kromberg & Schubert GmbH u. Co  
Wiegenkamp 21, 4292 Rhede, Germany

### Abstract

The mobile optical cable assembly, presented here, has been designed to install less time consuming high performance temporary connections in fiber-optic systems outside plant. The assembly consists of a non metallic heavy duty cable, terminated on both ends with suitable connectors. It is spooled on a cable reel which is mounted on a transportable rack or a caddy. The whole system operates over a wide range of temperature, resistant to hard environment, high tensile and radial stresses. The assembly is so light in weight that it can be handled by a single person.

### Introduction

With the increasing application of optical fiber cables and optical systems, the need to install temporary optical connections outside plant has gained much importance.

The initial work was undertaken to provide a mobile optical cable assembly at the request of the German Post Office (FTZ, Darmstadt). The aim was to connect the ship "Communica", while in dockyard to provide it with telecommunication facilities - a temporary connection with the help of multi or singlemode fiber cable.

To meet the environmental requirements, a heavy duty cable was developed containing 2 - 10 multimode or singlemode fibers with both cable ends terminated into suitable connectorized pigtails.

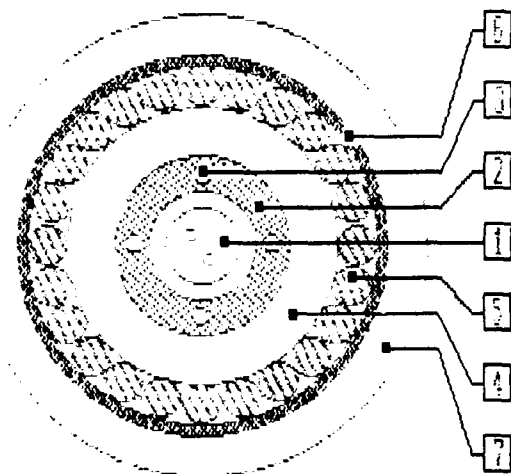
The cable described in this paper, is spooled on a metallic reel with both ends free to enable them to be plugged into existing equipment in operation.

The cable reel is mounted on a specially designed transportable rack whereby the unwinding or rewinding of the cable can be easily done. The cable reel size can be selected to intake cable lengths of upto 500 meters. An easy to handle and less time consuming temporary optical connection, i.e. a fiber optic extension system, has been successfully provided. This systems finds application in connecting measurement equipment in laboratory or field tests or where ever transmitting of optical signals is needed.

### Description of Cable

The materials of construction and the dimensioning of the individual cable components have been carefully selected to design the cable to operate under severe environmental conditions. The fibers are well packed in a loose tube so that very low to practically no attenuation change in the fiber transmission characteri-

stics, even under high tensile stress, is caused.



- 1.) Nylon loose tube filled with gel and optical fibers
- 2.) Reinforcing elements - Aramid-Rovings
- 3.) FRP Reinforcing elements
- 4.) PVC Innerjacket
- 5.) Special Aramid Cord Elements
- 6.) Core Wrapping
- 7.) Special Polyurethane Outer Jacket

Figure 1: Cable Design

The basic element of this heavy duty cable (Fig. 1) is a stable loose tube made out of Nylon 12 filled with a thixotropic gel. The tube is designed to intake two or more single or multimode fibers. This gel holds the fibers in place during the cable is pulled, bent or due to the thermal expansion of the cable.

This thixotropic gel is non drippable and avoids the entry of moisture into the tube.

The loose tube is strengthened with Aramid yarn in the radial as well as longitudinal direction. Some thin FRP-Elements of the size 0.35 mm integrated in the Aramid yarn, are equally distributed along the circumference of the loose

tube to avoid influence of temperature cycle on the fibers.

A PVC-inner jacket covers these strength members. To increase the compressibility of the cable a second layer of special Aramid-cord elements are wound around the inner jacket and finally a special Polyurethane outer jacket is extruded on the cable core to make the cable crush resistant. The outer jacket material is suitable against the influence of various oils, chemicals and sea water.

### Test And Measurements

#### Cable characteristics

Number of fibers	: 2 multimode graded index 50/125 $\mu$ m
Outer diameter	: 8 mm
Bending radius	: 150 mm
Weight	: 59 kg/km
Weight of assembly:	32 kg
Pulling force	: 2000 N
Lengths	: 250 m
Attenuation	: $2.5 \pm 0.2$ dB at 850nm $1.0 \pm 0.2$ dB at 1310 nm
Bandwidth	: $\geq 400$ MHz km at 850 and 1310 nm
Numerical aperture	: $0.21 \pm 0.1$

Table 1: Characteristics of tested cable

The cable (Characteristics of tested cable see Table 1), as described above, is about 8 mm in diameter and can withstand high tensile strength (Fig. 2) and radial pressure (Fig. 3) without causing any attenuation change. Series of tests were conducted to verify these results. The tests (Fig. 2) on the cable show as low as 0.1 dB/100 m attenuation change at 850 nm under a tensile strength of more than 2000 N where as the

attenuation change of less than 0.02 dB/100 m at 1310 nm wavelength was registered. An elongation of less than 0.2 % was measured at 2000 N.

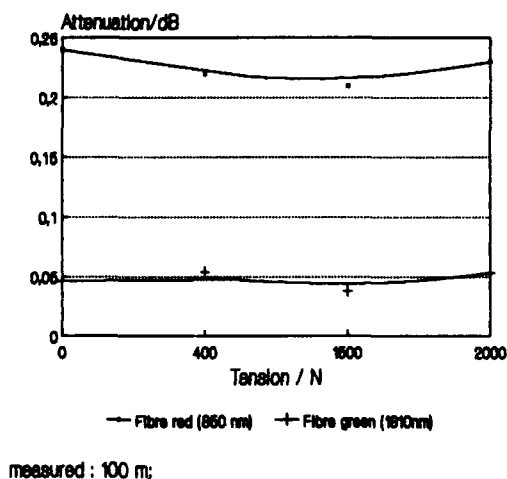


Figure 2: Effects of tensile strength on fiber attenuation

The radial pressure tests were conducted at 300 N/cm (Fig. 3). No attenuation change was measured.

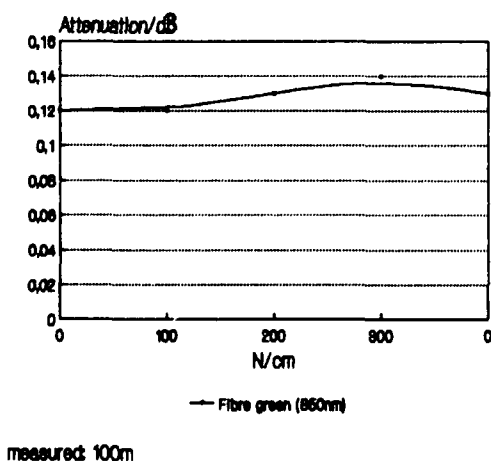


Figure 3: Effects of radial pressure on fiber attenuation

The thermal effects on the cable were measured between -40° C to +70° C. Even in this case, no attenuation change could be seen.

The cable passed the test of aging in oil and water at 7 days at 90° C.

### Optical Connectors

The cable assembly is preconnectorized on both ends with optical connectors to be plugged into the transmission equipment. These optical connectors, suitable for the respective application, are fabricated before completing the cable assembly. The standard optical connectors, e.g. F-SMA or ST-compatible connectors, are generally in use. Also in use is the German LSA-connector according to DIN 47256. In this case we fabricated the ST-compatible connectors.

The fabrication is done by feeding the fibers from the feeder cable within a breakout kit (Fig. 4) into a prefabricated fiberless pigtail cable. The individual fiber ends are then connectorized.

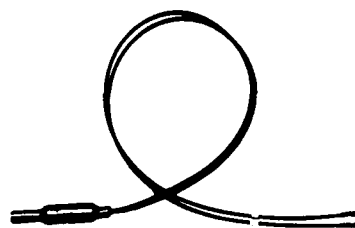


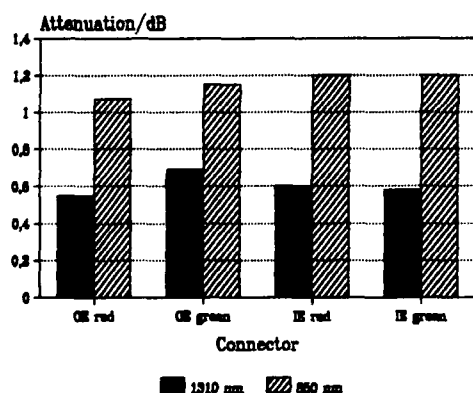
Figure 4: Fiber Breakout Kit, showing feeder cable and connectorized pigtails

The insertion loss of the assembly depends upon the quality of the optical connector and length of the cable and hence on the wavelength. For a ST-compa-

tible connector, the insertion loss was measured to be less than 0.7 dB at 1310 nm wavelength for 250 meter length of cable containing 50/125  $\mu$ m multimode gradient profile fiber. Measured at a wavelength of 850 nm, it increased by 0.6 dB (Fig. 5) which is a fiber dependent attenuation.

The tensile strength on this connectorized pigtail was measured to be more than 100 N. To avoid the entry of moisture and dust, the connectors are provided with dust covers.

The fiber breakout kits on both ends of the assembly are held in position with high strength yarn-mesh-pulling grip. This grip also helps in pulling the cable without causing any damage to the connectors, cabinet or the cable.



measured with 300 m dummy cord,  
ST-compatible connectors

Figure 5: Insertion loss of connectorized cable assembly

#### Assembly

The prefabricated cable as described above is wound on a metallic reel with the inner end guided kinkfree through the reelbase onto the outer of the flange.

About 10 meter length of the cable, with the prefabricated distribution cabinet and preconnectorized pigtails, are rolled together and suitably fixed on to the flange. The connectors are also safely kept in place into a rubber insulated spiral spring which is also affixed on to the flange.

The reel can be rotated with the help of a handle which is mounted on the flange. The reel is mounted on a transportable rack for cable lengths upto 500 meters where as for cable lengths upto 300 meters smaller reels can be used and mounted on caddies. The whole system is so light that it can be easily transported and put in operation by one person (see Table 2).

Cable Length	Reel Measurements		Assembly Weight
	Core Diameter	Core Width	
150 m	240 mm	170 mm	25 kg
300 m	320 mm	170 mm	35 kg
500 m	280 mm	500 mm	60 kg

Table 2: Available length and weight of cable assembly

#### Conclusions

The mobile optical cable assembly on transportable rack, presented above, has been successfully in operation to provide less time consuming temporary connections while transmitting optical signals outside plant. Because of its robust design it is suitable to be used in critical environments and it also finds application in laboratories, television studio and where ever an optical extension is needed. Due to its flexibility in the selection of various connector types, it can be used as an compatible optical extension cable.

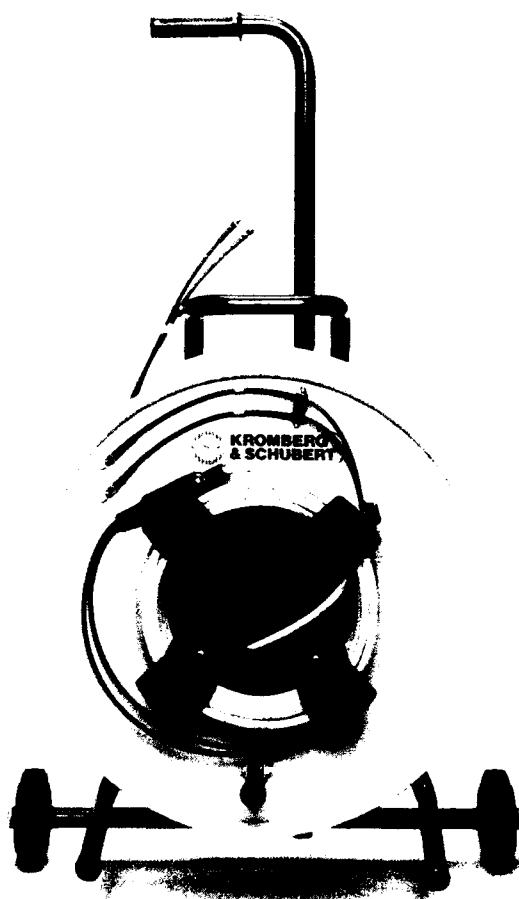


Figure 6: A Mobile Cable Assembly,  
suitable for 150 m

#### Acknowledgements

The authors wish their sincere appreciation to Mr. H. Reiner of FTZ, Bundespost Telecom, Darmstadt for initiating ideas at the initial stages. Thanks are also expressed to Mr. H. Dillge, Mr. K.H. Kremers and Mr. G. Mögenburg for constructive assistance in designing and testing of the system.



Heinz W. Brückner is head of the Product R&D Department of the Kroschu Kabelwerke. He studied Electrical Engineering at the Ruhr University of Bochum, Germany and received his Dipl.-Ing. Degree in the year 1977. He is specialized in the field of Opto-Electronics and cable systems for the automotive applications. Since 1986, he is member of the senior executive staff of the Kromberg & Schubert GmbH u. Co group.



Georg Franken studied Electrical Engineering at the Ruhr University of Bochum, Germany and received his Dipl.-Ing. Degree in the year 1989. He joined the R&D Department of Kroschu Kabelwerke in 1988 to work on his Dissertation. After successfully completing the project, he joined the Kroschu Kabelwerke as a Development Engineer where he is engaged in the development of fiber optics and fiber optic applications.



Daljit S. Parmar is head of Production of the Kroschu Kabelwerke. He received his B.Tech. in Chemical Engineering from the University of Madras, India in 1968 and M.Sc. in Process Engineering from the University of Bradford, UK in 1970. He holds a Ph.D. in Engineering Management from the Kennedy-Western University, California State Education. He has specialized in the field of Cable Technology and has more than 20 years of experience in the process development and production of a wide variety of wire and cables. Since 1986, he is member of the senior executive staff of the Kromberg & Schubert GmbH u. Co group.

## HOW IMPROVEMENT IN ARAMID PACKAGE STABILITY CAN LEAD TO HIGHER PRODUCTION SPEED OF OPTICAL FIBER CABLES.

Jack J. Bensink, Anton L. van den Bos

AKZO Fibers, Arnhem, Holland

### ABSTRACT

The development of Optical Fiber Cables (OFC) has now reached the stage where OFC producers start focusing on ways to optimize OFC production technologies. In this paper we look into ways to optimize the utilization of one important machine in the OFC production-line: the aramid stranding machine. In order to meet a growing demand from our customers for:

- heavier packages, to permit processing with longer running lengths and
- possibilities to operate at increased rotation speeds,

Akzo, as supplier of Twaron aramid, has investigated the processing limitations of different yarn bobbin make-ups on a specially designed laboratory stranding machine. All this has resulted in a deeper insight into the factors that influence the maximum rotation speed of a Twaron aramid package. In the future this knowledge will lead to more stable Twaron aramid yarn packages, suitable for higher rotation speeds!

### INTRODUCTION

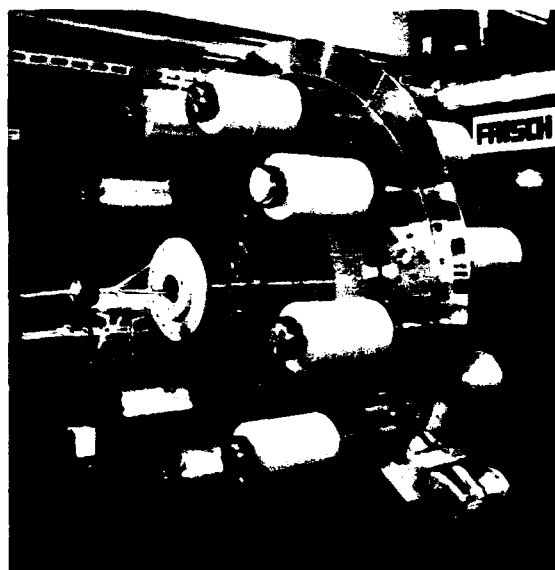
As is well-known, Twaron aramid is being used in different OFC cable designs (loose tube, slotted core, tight buffered) to protect the highly sensitive Optical Glass Fibers from linear, radial and flexural loads during production, installation and operation of the Optical Fiber Cable. Twaron aramid is specified for a lot of these cables because it combines the following properties:

- High tensile modulus
- Very low creep rate
- Low density
- High corrosion resistance
- Good dimensional stability
- High tensile strength

- Good dielectric behavior
- Good chemical stability
- Good fatigue resistance
- Good thermal insulating properties
- Excellent flame resistance and self extinguishing behavior
- Low smoke emission
- High flexibility

### THE STRANDING OF TWARON ARAMID

There are three ways to apply aramid in a cable: 1) longitudinally, by overhead or rolling take-off from a yarn bobbin in a creel; 2) longitudinally, by means of an aramid tape folded around the cable; 3) helically, by means of a stranding machine. The third method is generally preferred as it permits adjustment of the cable's flexibility and other properties as well as of the cable diameter, simply by changing the lay length. In almost all cases stranding machines are designed as the machine shown below:



#### Main characteristics:

- Rolling yarn take-off.
- Rotation speed: 150 - 250 rpm.
- Bobbin-bobbin distance: 70 cm.
- Yarn speed: 25 - 100 m/min.
- Max. bobbin weight: approx. 15 kg.
- Relatively high (regulated) yarn tension.

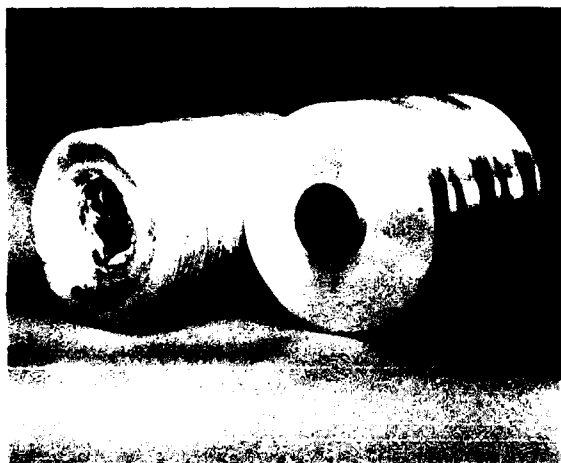
#### PACKAGE DEFORMATION

A well-known phenomenon in the textile world is the deformation of yarn bobbins due to centrifugal forces. Just as for other materials, under certain conditions (high rotation speeds, high yarn-bobbin weight) also Twaron aramid yarn bobbins may deform due to the centrifugal, acceleration and Coriolis forces acting on the package during the stranding process. From these forces the centrifugal forces have the greatest impact on the yarn package. The demolition process takes place very gradually, and is characterized by a slow outwardly directed movement of all yarn layers. Depending on the rotation speed this movement starts after 0,5 - 1 hour.

As long as the yarn layers stay within the tube length nothing will happen.

Problems may arise when the yarn layers start extending beyond the card bobbin and come into contact with machine parts, in which case yarn breakage may occur.

Under severe conditions, even the whole package may deform as is clear from the picture below, which shows a 10 kg Twaron aramid package tested at a rotation speed of 225 rpm! (running time: 1 hour, normal speed in practise: 100 rpm).



#### LABORATORY STRANDING MACHINE

In order to investigate the above-mentioned problem we have constructed a one-point laboratory stranding machine:



Technical specification of the laboratory stranding machine:

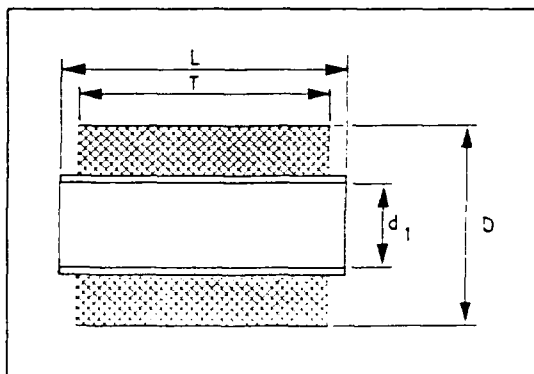
- Max. rotation speed: 400 rpm.
- Max. bobbin weight : 20 Kg.
- Bobbin-bobbin distance: 70 cm.
- Yarn speed: 5 - 500 m/min.
- Yarn tension: adjustable.

The specification is such that every practical situation can be simulated in a faithful way.

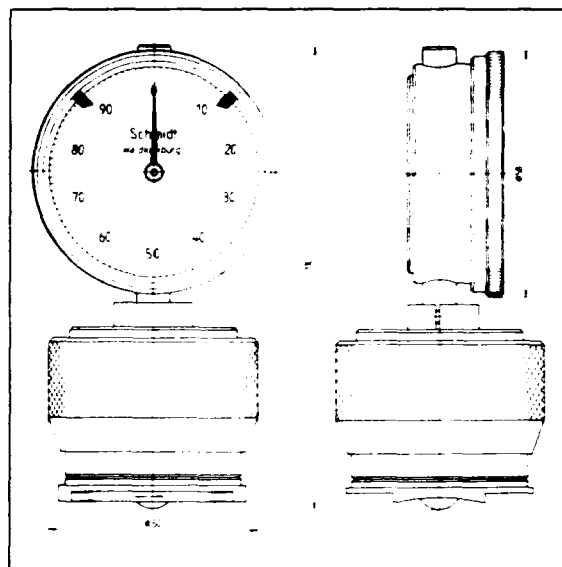
#### TESTING

Using standard moisture and finish contents Akzo tested yarn packages with the following counts: 1210, 1610, 2420, 3220, 4830, 6440 and 8050 dtex:

Weight:	Dimensions: (mm)			
(Kg)	Tube (Lxd1)		Tube (Lxd1)	
	216-Ø94		273-Ø77	
	T	D	T	D
4.0	190.5	Ø192	250	Ø167
4.5	190.5	Ø200	250	Ø175
5.0	190.5	Ø208	250	Ø182
5.5	190.5	Ø216	250	Ø189
6.0	190.5	Ø224	250	Ø196
6.5	190.5	Ø231	250	Ø202
7.0	190.5	Ø238	250	Ø208
7.5	190.5	Ø245	250	Ø214
8.0	190.5	Ø251	250	Ø220
8.5	190.5	Ø258	250	Ø226
9.0	190.5	Ø264	250	Ø231
9.5	--	--	250	Ø237
10.0	--	--	250	Ø242
10.5	--	--	250	Ø247
11.0	--	--	250	Ø252
11.5	--	--	250	Ø258
12.0	--	--	250	Ø262

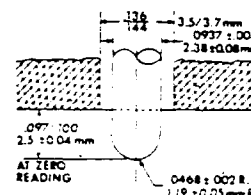


Also the standard winding ratios were observed (note: the winding ratio used for the 216-Ø94 bobbin is different from that used for the 273-Ø77 bobbin!). The main parameter that was varied, was the winding tension: viz. from standard to 1.5 X standard and 2.0 X standard. The winding tension has a direct effect on the package stability: very low tensions give a soft unstable package while, on the other hand, very high tensions may cause yarn damage and/or diabolic yarn packages. Because there is a direct relation between the winding tension and the (face) hardness of the yarn package, it is important that this hardness is measured in a standardized way. Before testing the packages on the stranding machine, we measured the hardness of the face and the shoulder by means of a Shore O hardness tester:



Shore O is a not officially standardized hardness unit, but it is often used in the textile world to measure the hardness of yarn packages. By hardness according to Shore is understood the resistance against the penetration by a body of a certain shape under a defined compressive force.

For Shore O the indentation body has the following dimensions:



The maximum spring force is 822 Grams.

On the stranding machine the above mentioned packages have been tested between 100 and 300 rpm, whilst the yarn speed was set at 40 m/min and the yarn tension at about 50 mN/tex. From our customers we know that for 4.5 kg packages the most common rotation speed is about 175 rpm, whilst for 10 kg packages the rotation speed is reduced to about 100 rpm and lower. The yarn speed of 40 m/min corresponds to values used in practise.



A package was qualified as unstable when the yarn layers extended beyond the card bobbin during processing. By means of a stroboscope this demolition process could be followed during rotation. Stable packages withstand the centrifugal, acceleration and Coriolis forces during the entire running time.

### TEST RESULTS

Through this extensive testing program we have found that the maximum rotation speed of a Twaron aramid package strongly depends on:

- 1) The package weight.
- 2) The hardness of the package face.
- 3) The inner tube dimensions.

The maximum rotation speed is hardly influenced by:

- 1) The hardness of the shoulder.
- 2) The yarn count.

In Enclosure I the recommended rotation speeds for the above-mentioned Twaron aramid yarn packages are given. These speeds are based on packages with a face hardness of more than 65 Shore O, the normal hardness of a Twaron aramid package. Lower Shore O face hardness values may seriously affect the package stability. Higher Shore O face hardness values only slightly enhance the stability. As these results also agree with experiences of our customers, we think that our laboratory machine reflects the practical situation.

### DISCUSSION

We have learned a great deal about the experiments we have carried out. Especially the higher maximum rotation speed of the 216 - Ø94 package compared with the 273 - Ø77 package was unexpected. Since the 273 - Ø77 package is more suitable for heavier weights, improving this package's stability in order to increase its maximum rotation speed now has first priority. Especially by optimizing the winding ratio in combination with other parameters (moisture content during winding, winding tension, etc.), we think we can further improve the maximum rotation speed of both the 273 - Ø77 package and the 216 - Ø94 package. Our goal is to improve the package stability in order to permit an increase of the maximum rotation speed by a factor 1.5.



Jack J. Bensink  
AKZO Fibers  
P.O. BOX 9300  
6800 SB ARNHEM  
HOLLAND

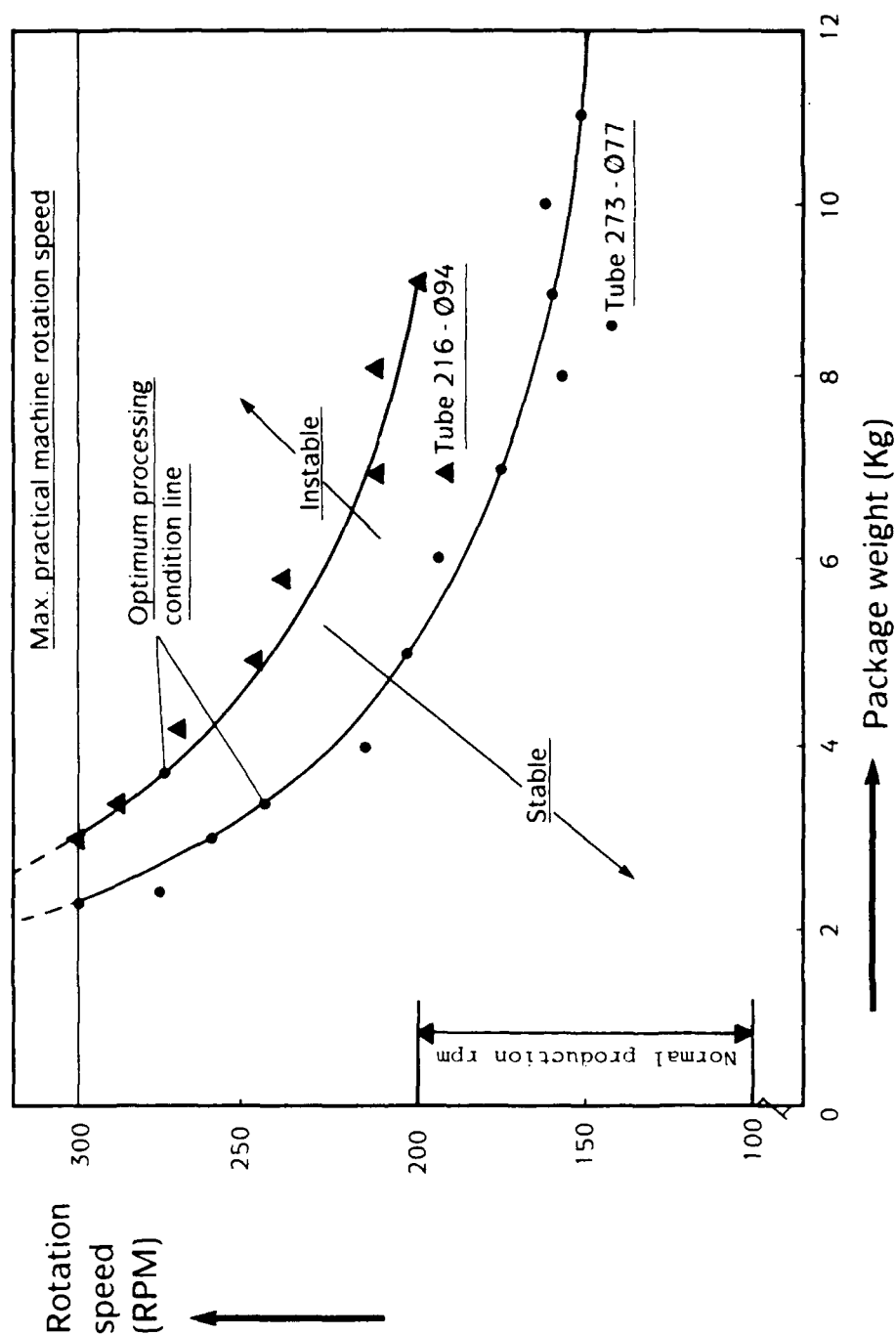
Jack J. Bensink was born in 1960 and received his B.E. degree in Mechanical Engineering at the Institute of Technology in Arnhem in 1985. From 1985 to 1990 he worked as a Processing Engineer at AKZO's Industrial Fibers Institute in Arnhem. Since June 1990 he is working as an OFC End-use Development Engineer.



Anton L. van den Bos  
AKZO Fibers  
P.O. BOX 9300  
6800 SB ARNHEM  
HOLLAND

Anton L. van den Bos was born in 1958. After his study at the University of Technology in Delft, Holland, he started working for AKZO Engineering. Since 1989 he has worked as a Technical Account Manager for the AKZO fibers division, where he is responsible for the technical service for Aramid fibers in the field of Optical Fiber Cables.

# Recommended rotation speeds for Twaron aramid yarn packages



ENCLOSURE 1

**DESIGN OF AN ARTICULATED REPAIR JOINT  
FOR A LIGHT WEIGHT, OPEN FIBRE OPTIC SUBMARINE CABLE.**

**Einar Betten, Morten Johansen**

**Alcatel Kabel, Norway.**

**ABSTRACT**

An articulated repair joint has been developed for contingency repairs of a light weight, "open" fibre optic submarine cable. The design goal was to reduce assembly time, simplify special tooling and improve handling capabilities compared to present repair joints.

The joint is designed with a breaking load of 200 kN, and can be handled over 1,5 m diameter sheaves under tension. Assembly time for jointing of a double armoured, 12 fibre cable is less than 12 hours. The joint has been qualified through an extensive test programme, fullscale trials and actual installations worldwide.

The complete joint kit is packed in a metal case (60X40X15 cm) and weighs less than 20kg. Its special tool kit is supplied in a similar case (60X40X25 cm), weighing less than 15kg. A patent claim has been filed for the design.

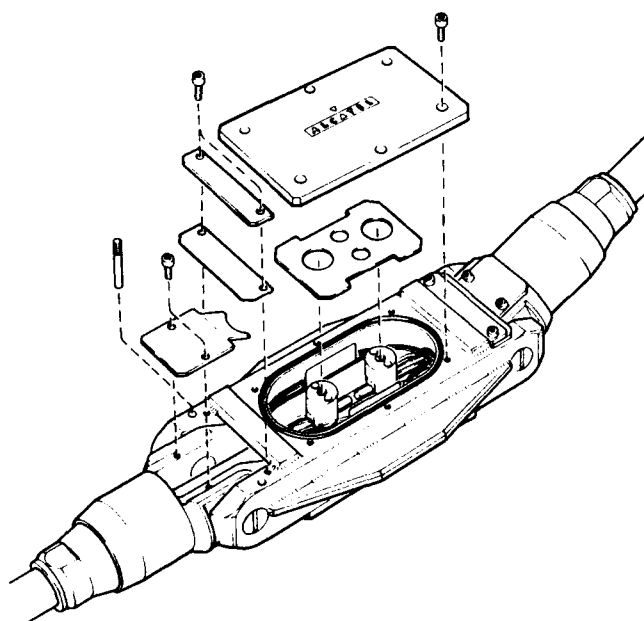


Figure 1.  
Expanded view of LOS Mk III Repair Joint.

**INTRODUCTION**

The Norwegian Telecom has a nationwide fibre optic system under construction requiring about 3000 km of submarine cable. For this system, Alcatel Kabel has developed a cable concept where the basic principle has been to produce a light weight cable which can be deployed by small cable ships. The project was named LOS, ( Long distance fibre Optical Submarine systems). It was soon realised that the "transoceanic" designs employing metal barriers around the cable core would make the cables too heavy. The target was to achieve the goal with an "open" design.

To complete the cable concept the Norwegian Telecom also required a repair joint which should withstand the same mechanical stresses as the cable. Important in this respect was that it should be able to handle the rated operating load of up to 200 kN, sustain the pressures at water depths down to 1300 m, and be capable of being handled over laying sheaves with diameters as small as 1.5 m. The joint should also accommodate up to 24 fibre splices and several different armour designs. As a further requirement it should be possible to complete jointing of a 12 fibre cable in less than 12 hours.

**JOINTING PHILOSOPHY**

Cable manufacturing, installation and operation incorporates several stages of regular and contingency jointing procedures.

**Element splicing**

During manufacturing of the cable up to the level of extrusion of inner sheath, each element in the cable can be spliced individually at random locations without diameter increase. Thus allowing production lengths of cable core to exceed delivery lengths of e.g. fibres.

**Core splicing**

Should production necessitate jointing of a cable with inner sheath extruded, a "core splice" is required. The splice requires

each element of the cable to be spliced over a short length, and without diameter increase. This splice is also required to sustain the same stresses as the cable core at this level.

#### Repair jointing

The third stage of splicing technique is applied for completed cables. Limitations in production facilities may require one or more planned joints.

The joint may also be used for repair of damage occurring during armouring, loading, installation and marine activities during the service life of the cable.

### DESIGN

#### Materials

The jointing enclosure consists of a seawater corrosion resistant stainless steel housing, with a cable armour termination unit at each end. The chosen high alloy steel does not require any corrosion protection coating, and thus simplifies the assembly procedure of the joint. However, as the enclosure is made from a more noble material than the cable armouring, the armour would corrode heavily should its outer protection be damaged. To avoid this galvanic corrosion, the cable armour is electrically insulated from the joint enclosure by a ceramic layer in the armour termination. The high alloy steel is also superior in tensile strength compared with standard used stainless steel.

#### Armour termination

The termination unit is locked to the cable armouring by threaded cones to avoid any slippage. Termination units for single, double and triple armoured cables have been designed. These terminations are also adapted to armour wires of various diameters, ranging from 2.6 mm and upwards. This is achieved by variation of the spacer cones in the termination unit.

The locking cones are pressed in with a hydraulic (hand operated) tool, ensuring the repeatability of the process through the amount of hydraulic pressure applied. The locking cones are made from a hardened carbon steel, and are therefore also insulated from metallic contact with the main body of the joint enclosure. As additional protection, the internals of the armour termination are protected by a zinc anode.

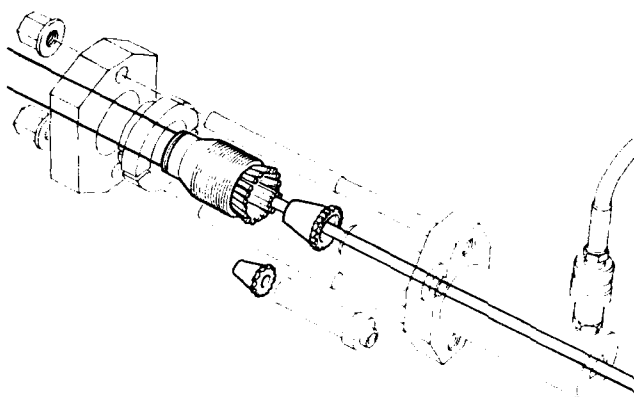


Figure 2.  
Assembly of armour termination unit.

#### Pivot mechanism

The termination units are connected to the splice housing by an articulated joint. The single axis hinge is supplemented with tilting fins on the joint housing. This allows a rectangular cross section design, which again is required for narrow passages through the cable machinery of a lay vessel. The articulated joint ensures that the minimum bending diameter of the joint complies to that of the cable, and allows the use of capstans down to 1.5 metres in diameter. The strength of the pivot is higher than the specified strength of the cable.

The single axis pivot simplifies the assembly procedure by allowing each cable termination to be completed separately before connection to the main housing. The pivot also improves interchangeability between the different armour terminations, should a requirement for jointing of different armoured cables arise.

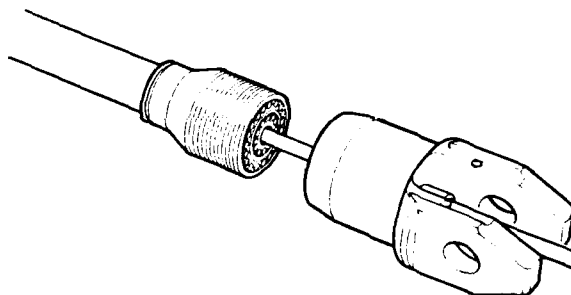


Figure 3.  
Assembly of pivot head on armour termination.

### Joint housing

The main housing has a compartment with a separate lid on each side to simplify the splicing and assembly procedure. The housing is designed to sustain the tensile load required for the cable. To avoid any attenuation increase in the optical fibres induced by excessive bending, the minimum bending radius of the fibres in the joint housing is larger than 30 mm. The size of a completed joint enclosure (housing connected to the termination units) is approx. 600 x 170 x 100 mm.

The tensile strength of the joint is determined by the cross-section of steel in the hinge area. Thus upgrading of the tensile strength of the joint is a matter of increasing the steel cross-sectional area in this region.

### Enclosure sealing

Sealing of the joint relies on two different methods. The armour termination will eventually be flooded, thus the main housing requires sealing between the cable inner sheath and the housing. Sealing on this level is achieved by a self energising rubber seal. The rubber tube is fitted over the entry tube of the joint housing and down onto the cable inner sheath.

The seal has been tested to 150 bars water pressure, and represent a permeation barrier equal to that of the inner sheath.

The lids of the joint housing are sealed with O-rings.

The joint housing is filled with silicone oil after the fibres have been spliced and coiled down. The silicone oil prevents grease from the cable being squeezed into the joint housing, and also protects the spliced fibres. There is no pressure difference between the cable internals and the joint housing.

## TESTING

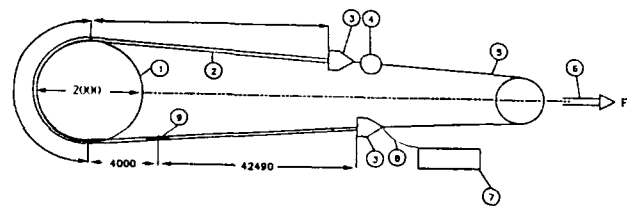
### Test programme

The repair joint has been developed so as to be able to sustain any anticipated strain during installation and recovery of a submarine fibre optical cable. A qualification programme defined by the Norwegian Telecom has been carried out to ensure that the repair joint meets the same requirements as the cable. The tests are similar to the test programme specified for the submarine optical cable. Completed joints have been tested with respect to :

- Temperature storage  
(-40°C to +70°C, 8 hrs. each)
- Temperature cycling  
(-10°C to + 40°C, 2 cycles, 12 hrs.)
- Straight Tensile Test  
(180 kN maximum tensile load)
- Dynamic Bend Tensile Strength  
(90 kN tensile load, 5x2x180° cycles, around 2m diameter sheave, ambient temperature 0°C to +5°C)
- Repeated Bending (Bend Fatigue)  
(±45° bending, 1m sheave diameter, 100 cycles)
- Hydrostatic pressure  
(150 bar for 24 hrs.)

The tests were carried out with satisfactory results. Neither additional loss, nor mechanical degradation were detected in the joint during any of the tests.

The tests demonstrate that the repair joint can be handled as an integral part of the cable, and that more than 90 % of the cable tensile strength is preserved in the joint.



Lengths in mm.

- |                 |                         |
|-----------------|-------------------------|
| 1. Cable sheave | 5. Wire                 |
| 2. Cable        | 6. Hydraulic cylinder   |
| 3. Pulling head | 7. Instrument container |
| 4. Load cell    | 8. Cable core           |
|                 | 9. Repair Joint         |

Figure 4.  
Dynamic bend tensile strength test setup.

### Trial installations

Trial installations have been carried out on two occasions. The first in 1988 by a cable vessel from the Norwegian Telecom. This installation was carried out in Byfjorden outside Bergen, Norway, in 500 metres of water. Two cable lengths were jointed together aboard the cable ship. Then the jointed cable was laid under normal procedures, over a 1.5 m capstan and a 1.5 m bow wheel. After the completed laying operation, the jointed cable was retrieved by the same machinery.

The second full-scale test was carried out in the Oslofjord, Norway in 1990, and incorporated a complete repair operation. A test cable laid at an earlier occasion was retrieved to the repair vessel, cut, jointed with the repair joint and repositioned on the seabed. The operation from when the diver first went into the water, to the completion of optical measurements after repositioning on the seabed, was executed in 14 hours. The jointing operation itself lasted less than 11 hours for the double armoured, 16 fibre cable.

The jointing work during the trial in 1990 was carried out in a specially equipped 12' jointing container placed aboard a "flatback" cable repair vessel. The container is fitted with lighting, heating, air filtering and airconditioning units. (The latter was not required in Norway in December.) The weight of the container is 2.0 metric tons.

#### SERVICE

Customer : Norwegian Telecom.  
Installation type : National network.  
Location : Trondheimsfjorden, Norway.  
Water-depth : 275 metres.  
Date of installation: April, 1989.

Customer : Trans Power, New Zealand  
Installation type : Power cable plant supervision, National network.  
Location : Cook strait, New Zealand.  
Water-depth : 230 metres.  
Date of installation: April, 1991.

Customer : Norwegian Telecom.  
Installation type : National network.  
Location : Sognefjorden, Norway.  
Water-depth : 130 metres.  
Date of installation: June, 1991.

Customer : Michigan Bell, U.S.A.  
Installation type : Bell network.  
Location : Lake Michigan, U.S.A.  
Water-depth : 30 metres.  
Date of installation: July, 1991.

#### CONCLUSIONS

Through testing and fullscale operations, the LOS Mk III repair joint has proved its ability to provide a contingency technique for repair of cable damages occurred during manufacture, installation or service life of a light weight, "open" fibre optic submarine cable. The joint preserves the inherent strength of the cable, can be handled as an integral part of the cable through the cable machinery of the lay vessel, is designed to simplify offshore assembly procedures and is assembled in less than 12 hours.

#### ACKNOWLEDGEMENT

The authors wishes to thank the Cables Division of the Norwegian Telecom for their active contribution in all stages of the development work.



Morten Johansen

Alcatel Kabel Norge AS  
Telecom Cables Division  
P.O.Box 130, Økern  
N-0509 Oslo 5, Norway

Morten Johansen (46) received his degree (Electronics) from Oslo College of Technology in 1973. He has for many years worked with development of silicon chip manufacturing technology, but joined STK (now Alcatel Kabel) in 1987. He is currently development manager with responsibility for fibre optic cables.



Einar Betten

Alcatel Kabel Norge AS  
Telecom Cables Division  
P.O.Box 130, Økern  
N-0509 Oslo 5, Norway

Einar Betten received his M.Sc. in Electrical Machines from the Norwegian Institute of Technology in 1984. He then joined up with the Offshore Division of Alcatel Kabel, working with installation of control cables for subsea oil-wells in the North Sea. In 1988 he started in the Telecom Cables Division, Fibre Optics, with responsibility for cable field splicing and installation techniques.

# TESTING OF SOME SINGLE MODE FIBRE CABLES AND RIBBONS BY THE $\alpha_{11_b}(\lambda)$ METHOD

T. Volotinen, L. Stensland\* and A. Björk

Ericsson Cables, Telecom Cables Division, P.O.Box 457, S-82401 Hudiksvall, Sweden,

\* Ericsson Cables and Networks, Research Center, S-17287 Sundbyberg, Sweden

## ABSTRACT

The  $\alpha_{11_b}(\lambda)$  method has been applied to single mode fibre cables' temperature and tensile performance tests using 30 m samples, and to fibre ribbon tests using 9 m samples. The fibre equivalent bend diameter and possible attenuation increase at 1550 nm (or at any wavelength) can be reliably estimated by the method. Cables and ribbons can be tested without generating the extreme conditions necessary for the LP01 mode attenuation increases. The bending of the fibres is more helpful and reliable information than attenuation values.

An SZ-stranded loose tube cable design was optimized. The bend diameter range for fibre movements inside a bad SZ-design in varying temperature was significantly larger than for helical cables. In the optimized slotted core SZ-design, a narrow bend diameter range was achieved together with a good tensile performance. The quality of fibre ribbons, whether any external micro and macro bends exist in the ribbon or not, can be determined with short samples using this method the method.

## INTRODUCTION

The development, testing and optimization of optical cables are expensive and time consuming tasks. With standard test methods based on direct fundamental mode attenuation measurements hardly any information of the fibre bending in cables can be obtained and very long cable samples, 1 - 2 km or more, must still be used. Attenuation increases can only be seen at extreme temperature or stress conditions, and the large variation of the bend sensitivity among the standard single mode fibres can cause confusion in conclusions.

The  $\alpha_{11_b}(\lambda)$  method has recently been developed to better adduce these problems and to solve them in single mode fibre cable tests [1, 2]. It is based on the LP11 mode bend attenuation (the  $\alpha_{11_b}$ ) measurements as a function of wavelength. The method can be applied to tests with short cable samples, down to 30 m in length, and to very short fibre samples, down to 2 m. The  $\alpha_{11_b}(\lambda)$  is measured using the LP01 mode output power as a reference (without

cutting the fibre) by a standard cut-back measurement instrument with modified software [1].

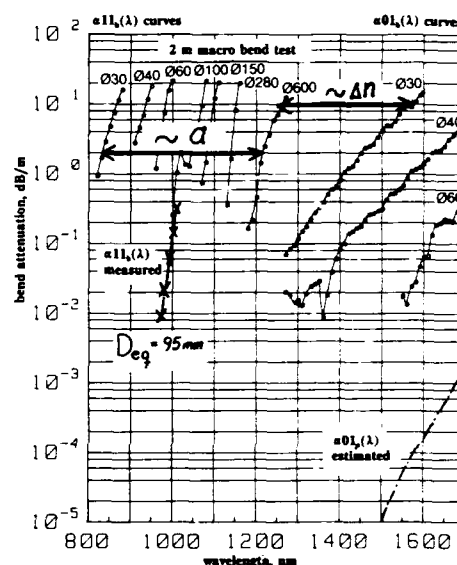


Fig. 1. The  $\alpha_{11_b}(\lambda)$  method. Fibre core radius  $a$  and ref.ind.diff.  $\Delta n$  are proportional to the differences shown in the plot [1].

In using the  $\alpha_{11_b}(\lambda)$  method, first the  $\alpha_{11_b}(\lambda)$  of a fibre in the test sample is measured, and an individual 2 m macro bend test for the fibre is performed on several bend diameters from 30 mm to 600 mm (Fig. 1). The equivalent bend diameter of the fibre in the test sample (the constant bend diameter that would cause the same total bend attenuation) is determined by using the 2 m test results as a reference bend diameter scale.

Furthermore, the structural parameters of the fibre refractive index profile (core radius and refractive index difference) are determined with the 2 m test by comparing the  $\alpha_{11_b}(\lambda)$  and  $\alpha_{01_b}(\lambda)$  curve series measured with the theoretical bend attenuation curves [1, 3]. Finally, the estimated attenuation increase of the LP01 mode at 1550 nm is calculated from the equivalent bend diameter and structural parameters using the theory [1, 3] (Fig. 1). The

macro bend attenuation of the LP01 mode on any bend diameter at any wavelength can thus be estimated, and even the fibre's micro bend sensitivity which is also dependent on the same structural parameters [1].

In this paper the  $\alpha_{11_b}(\lambda)$  method is applied to the optimization of an SZ-stranded loose tube cable design. The test results were compared to the corresponding helical design results partly presented in [1]. The methods reliability was additionally proved in short sample cable tests, and the method was also applied to 4-fibre ribbon tests in order to investigate macro and micro bends that can cause attenuation increases at extreme temperatures. A 9 m ribbon test based on the  $\alpha_{11_b}(\lambda)$  method was developed.

## THE CABLE EXPERIMENTS

The  $\alpha_{11_b}(\lambda)$  method was applied to two kinds of cable designs. The first design was a slotted core cable for duct installations (Fig. 2, [4]) with 6 secondary tubes (including 4 - 6 fibres each) placed in S-stranded slots, and the other was a similar design but slots and tubes were SZ-stranded. The single mode fibres in the cables were standard (CCITT G.652) fibres with a matched cladding refractive index profile.

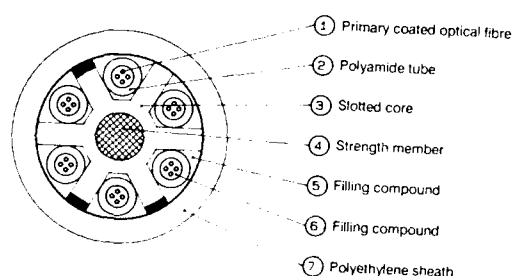


Fig. 2. The cable design investigated. [4]

Both cable types were investigated in several different samples with the intention to see the relationship between process parameters, fibre bending at room temperature and attenuation increases in extreme temperatures, as well as between the bending and tensile performance window. The helically stranded design was tested in 6 different samples with various excess lengths of fibres [1]. The SZ-stranded version was investigated in 8 different samples, 4 of them were also discussed in [1]. This design was examined by varying excess lengths, pitches and reverse lay lengths of stranding.

## The cable tests

The cable samples were investigated using the  $\alpha_{11_b}(\lambda)$  method, first in room temperature in 30 m sections turned on two different cable bend diameter, 120 cm and 65 cm.

After this the 65 cm coils were cycled in temperature test [1] from -40 to +70 °C 10 times. At least two fibres for two tubes in each cable were tested.

The same cables were investigated in tensile performance tests with straight 25 m sections using the method [1]. The  $\alpha_{11_b}(\lambda)$  measurements were done by a standard cut-back measurement instrument (FOA2000 made by Photon Kinetics Inc.) [1].

The results obtained by the  $\alpha_{11_b}(\lambda)$  method were compared to standard test results measured in long fibre or cable tests.

## THE RIBBON EXPERIMENTS

The intentions of the ribbon tests were to develop a repeatable and reliable test procedure with the  $\alpha_{11_b}(\lambda)$  method for short, 2 - 10 m ribbon samples. The test method was to show whether the fibres were well or badly placed in the ribbons. "Well" means that attenuation changes of the fibres at a temperature cycling test from -60 to +80 °C at 1550 nm do not exceed  $\pm 0.02$  dB/km, i.e., no micro or macro bends are generated in the fibres of the ribbons. "Bad" means larger attenuation increases.

Several ribbon lay-outs were tested with  $\alpha_{11_b}(\lambda)$  measurements, and a 9 m test lay-out was chosen. Both good and bad ribbons were found, and the results were compared with long fibre temperature cycling test results, and, for the good ribbons, to the cable test results as well.

## The 9 m ribbon test

For the 9 m ribbon test, the sample was turned 3.5 times (6.6 m) on a 600 mm diameter plate during the  $\alpha_{11_b}(\lambda)$  measurements of the sample (Fig. 3). About a 2 m section of the launching end of the fibres was separated from the ribbon coating and partly turned (45°) on a 600 mm bend diameter during these measurements [1]. The reference LP01 mode powers were measured with a mode blocking filter (1 turn on 20 mm) performed on the open fibre section. Other sections of the sample were kept as straight as possible during both measurements.

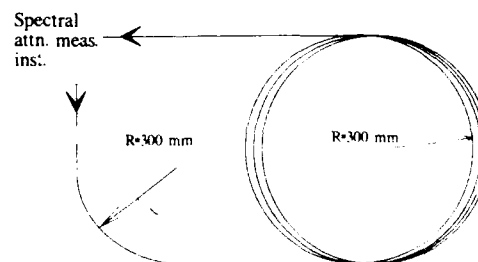


Fig. 3. The fibre lay-out of the 9 m ribbon test.

The 2 m reference macro bend tests were performed on 30 - 600 mm bend diameters as usual [1] for the samples



cut from the ribbon. For each bend diameter the actual bend length must be used in  $\alpha_{11_b}(\lambda)$  calculation. Because a fibre bending inside the primary coating can be changed in the colouring process or in the encapsulating process, original primary coated reference samples are recommended.

The  $\alpha_{11_b}(\lambda)$  curve of each fibre in the ribbon was compared to the corresponding 2  $\pi$  reference test curves. If the fibre was placed ideally in the ribbon, the  $\alpha_{11_b}(\lambda)$  of the ribbon would correspond to the  $\alpha_{11_b}(\lambda)$  curve in the 2 m test on a 600 mm bend diameter. Thus, the difference between these curves and their derivatives is proportional to the bends along the fibre. It can roughly be concluded that the larger the difference, the smaller macro bends exist along the fibre, and the lower the derivative of the ribbon  $\alpha_{11_b}(\lambda)$  curve, the more micro bends have been generated in the ribbon.

## FIBRE BENDING IN THE CABLE DESIGNS

### Equivalent bend diameter

The equivalent bend diameter for a fibre in a test sample is the constant bend diameter on which the whole fibre section should be curved to get the same total bend attenuation [1]. Such a parameter is necessary in order to describe fibre macro bending in cables by one discrete parameter. In most cases fibres are more or less randomly bent inside cables.

*Macro bend attenuation is exponentially dependent on the inverse bend diameter, i.e., the smallest existing bend diameter will give the largest contribution to the bend attenuation. Thus, it is convenient to use 'the equivalent bend diameter' in cable analysis. The equivalent bend diameter determined by the  $\alpha_{11_b}(\lambda)$  method is smaller than the mean bend diameter, but it is equivalent for the attenuation increases.*

For a fibre wound without micro bends on a mandrel, the equivalent bend diameter is the mandrel's diameter. A helically curved fibre also has a constant bend diameter equal to its equivalent bend diameter, which can be easily calculated from the helix parameters [5].

### Fibre bending in cables in varying tensile and temperature conditions

The bend radius of a curved fibre at every point and the fibre length to this point can be calculated only if the curve can be described mathematically. For fibres in real cables this can seldom be done with sufficient accuracy because of the characteristic structural variation of each design, various cable materials, and many variable process parameters. In addition, cables in factory tests are wound on drums, possibly with a varying tension.

Rough limits for the allowed bend diameter range for

fibres in the helix- and SZ-stranded cables investigated can be set by measuring the cables' actual construction parameters and using the simple helix equations [5] and the theory reverse lay stranding [6]. The optimum fibre position at room temperature is around the middle of the tube, and the limits for those bend diameter range without attenuation increases are the cases where the fibres lie along the inner (the largest bend diameter) or outer wall (the smallest bend diameter) of the stranded tubes. In the reverse sections of an SZ-cable there may exist a variation of about +20 - -80 % of the bend diameter in addition to the corresponding helical design may exist [6]. A slight buckling of the fibres down to almost 100 mm equivalent bend diameters can be allowed without causing attenuation increases [1].

The equivalent bend diameter in the cables studied decreases at low temperatures due to the axial compression of the cable, and increases at high temperatures. The temperature elongation of these cables is close to that of the plastic materials' used in them, and the elongation of the fibres can be estimated to be zero due to the low elongation coefficient of the glass.

Thus, by measuring the equivalent bend diameters and comparing them with the estimated allowed bend diameter range, the fibre position in the cable can be determined. When some samples of a design are first investigated in this way in temperature and tensile performance tests, the tensile and temperature performance of the cable can be estimated at room temperature by the  $\alpha_{11_b}(\lambda)$  method.

## RESULTS

The  $\alpha_{11_b}(\lambda)$  method's reliability was further studied in the cable and secondary coating tests (random bending) and macro bend tests of 20 different fibres (constant bend diameter). The equivalent bend diameter of a fibre in a sample can be estimated by a  $\pm 10$  % repeatability, and the corresponding macro bend attenuation of the LP01 mode can be estimated by a  $\pm 2$  % accuracy (Fig. 4). Only such  $\alpha_{11_b}(\lambda)$  measurements where macro bends dominated were used. The  $\alpha_{11_b}(\lambda)$  values can be measured by at least a  $\pm 5$  % repeatability (corresponds to a 5 nm repeatability at a wavelength scale), in most cases even by a  $\pm 1$  % repeatability.

The equivalent bend diameter range within which the fibres moves in an SZ-cable was seen to be dependent on the number of helical turns between the reverse points, the fibre excess length in the cable, and particularly on the cable core construction. The bend diameter range in the temperature test for the optimized slotted core cable was as narrow as for the good quality helically stranded slotted core cables (Fig. 5a, and [1]) simultaneously with a wide, 0.5 % tensile performance. The excess length variation shifts linearly the temperature bend diameter window of the cable on a bend diameter scale.

In the cables without a slotted core (Fig. 5b), the fibre

bend diameter changed at a very large window in the temperature test. The lower fibre excess length did not help, the bend diameter window was only shifted to larger bend diameters.

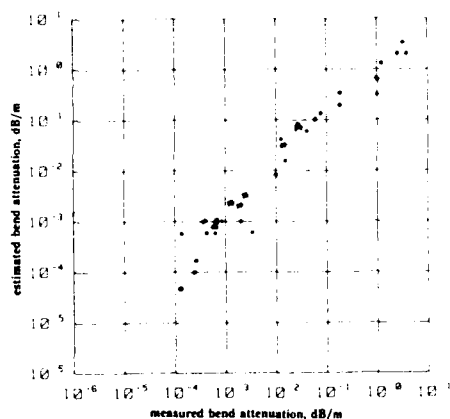


Fig. 4 The  $\alpha 01_p(1550 \text{ nm})$  estimated as a function of the measured attenuation increase,  $\alpha 01_b(1550 \text{ nm})$ . The \*-marked points are from cable tests and •-marked from fibre macro bend tests.

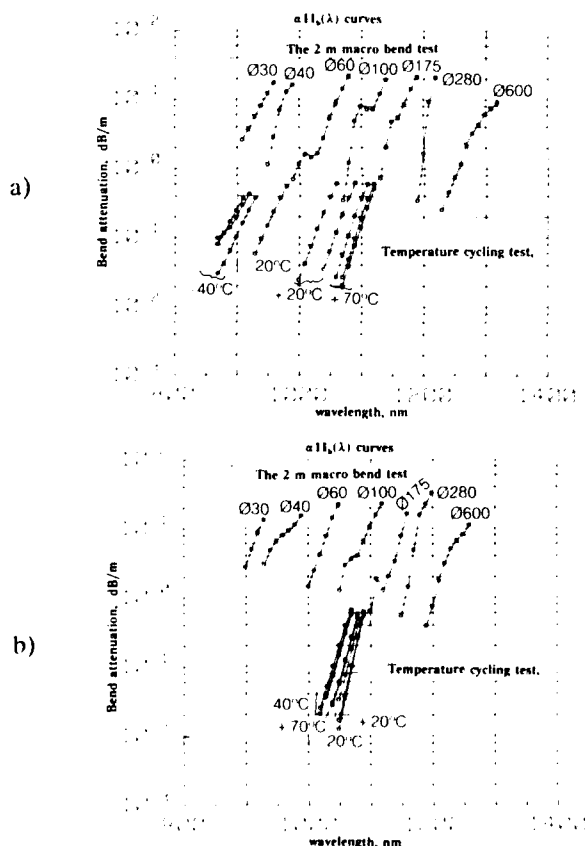


Fig. 5. Temperature test results for a) a 2.5-turn and b) for a 3.5-turn SZ-cable by the  $\alpha 11_b(\lambda)$  method.

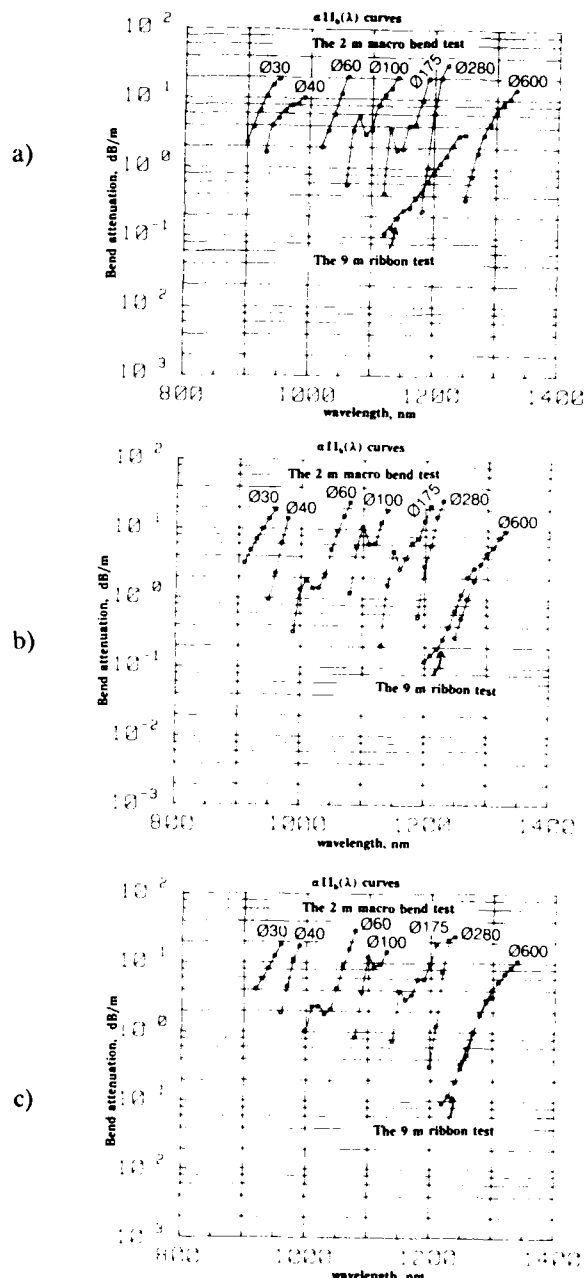


Fig. 6. The ribbon test results and their ref. tests for a fibre a) with micro bends, b) with macro bends, and c) without additional bends.

The 9 m ribbon test was proved to be reliable. A clear difference between well and badly situated fibres was seen. Both micro bends (Fig. 6a), additional macro bends (Fig. 6b), and ideally situated fibres (Fig. 6c) were found. The results correlated to the attenuation increases measured in

standard temperature cycling tests and in cable tests.

If necessary, the method's reliability can be improved by using a little longer fibre sample in the reference test to get at least 2 turns on a 600 mm bend diameter. The accuracy of the bend diameter determination can be improved by measuring several bend diameters between 280 mm and 600 mm in the reference test.

## SUMMARY

The cable tests: The fibre bending can be investigated in short cables by the  $\alpha_{11b}(\lambda)$  method without reaching extreme conditions for LP01 mode attenuation increases. An optimized SZ-stranded slotted core cable design was developed, and it has as narrow a bend diameter window of fibre moving in temperature variation as the good quality helical cables. For optimized loose tube cable designs, fibre bending, and temperature and tensile performance windows can be estimated from room temperature  $\alpha_{11b}(\lambda)$  measurements on 30 m samples, because the fibre excess length variation only shifts the fibre bend diameter window linearly.

The ribbon tests: The 9 m ribbon test method is a simple, informative and reliable test method for ribbons. Fibre bending, the equivalent bend diameter and whether there exist any micro bends in the ribbon can be estimated by the test. The sensitivity of the test can be improved, if necessary, by using longer ribbon samples. Very short ribbon samples, such as 2 m, can be used for rough determinations.

## ACKNOWLEDGEMENTS

The authors wish to thank their colleagues at Ericsson Cables for their help in the cable and ribbon tests and discussion of the results. The Nordic Industrial Fund and L M Ericsson's fund for the supply of electro-technical research are gratefully acknowledged for their support.

## REFERENCES

- 1 Volotinen, T., Influence of the Standard Single Mode Fibre Bends on Cable Properties Investigated by the  $\alpha_{11b}(\lambda)$  Method, Acta Polytechnica Scandinavica, Appl. Phys. Ser. No. 171, 1990 (Dissertation)
- 2 Volotinen, T. and Stensland, L., Method for single mode fibre bending studies in short fibres or cables. Proc. 37th IWCS. (1988), p. 710 - 721.
- 3 Marcuse, D., Curvature loss formula for optical fibres. J. Opt. Soc. Am. Vol. 66 (1976), No. 3, p. 216 - 220.
- 4 Larsson, A and Nygård-Skalman, K. Slotted Core Optical Fibre Cable. Ericsson Review. (1988), No. 3, p. 100 - 107.
- 5 Murata, H., Handbook of Optical Fibres and Cables, New York, Marcel Dekker, Inc., 1988.
- 6 Swieckicki, T.S., King, F.D. and Kapron, F.P., Unit Core Cable Structures for optical communication Systems. Proc. 27 th IWCS. (1978), p. 404 - 410.

## Authors



Dr. Tarja Volotinen is working as a technical specialist in the Optical Fibre Technology group at the Technical Department for development of cables at Ericsson Cables, Telecom Cables Division, Hudiksvall in Sweden. After her M.Sc. degree 1978, she worked with fiber optic measurement technology for Nokia Telecommunication Cables, in Helsinki, Finland. She joined Ericsson Cables in the autumn -86 responsible for optical fibre measurement technology until the autumn -88 and then she concentrated on her doctoral research [1] work until March 1991 when her Ph.D. thesis in Physics [1] was examined at the University of Helsinki.



Leif Stensland, is an expert on optical fibre technology at Ericsson Cables, and currently the chief of the Research Center of optical fibre network technology of Ericsson Cables and Networks in Sundbyberg, Stockholm, Sweden. He joined Ericsson Cables in 1982 as a manager of fibre and cable development, in particular for optical fibre preform process development. After his degree the licentiate of technology in Physics in 1971 from the Royal Institute of Technology in Stockholm, he led a group in fibre and integrated optics at the Institute of Optical Research in Stockholm until 1982.



Anders Björk is working as a development engineer at the optical cable product group at Ericsson Cables, technical department, at Hudiksvall. He joined Ericsson Cables in January 1989, and first did his technical work for his B.Sc. in computer science for the technical university of Gävle-Sandviken. At the moment he is type testing new cable designs and developing test methods.

## EVALUATION OF ANTIBALLISTIC SHEATHINGS FOR AERIAL FIBER CABLES

SUSANA CAMARA

CARLOS G. CORTINES

ALCATEL STANDARD ELECTRICA / MALIÑO - CANTABRIA - SPAIN

### ABSTRACT

We have performed a study of different sheathings used as an effective shooting protection. We verify that it is not enough to have barrier materials against pellets, but in addition, it is necessary that sheaths have the property of absorbing the collision energy, as collision could produce a decrease of signal transmission inside the cable without piercing the sheath.

In this paper we show all the materials that form the cables especially the sheathing, their technical properties, the shot tests and a report of designs for different applications attending to the distances and the kind of pellets.

### INTRODUCTION

The widespread development of Telecommunications and, above all, the advent of optical fiber, means that there are now a lot more users of these services and also that the requirements of the customary users in this sector have increased. One of the most interesting examples of this increase in requirements is that of Electricity Companies, who, on one hand, have been able to solve the technical problems which the use of metallic communication cables in electro-static and electro-magnetic atmospheres present. These problems are typical in electric supply systems. On the other hand limiting by law the frequencies of the use of microwaves, gratefully welcomed by the Electric sector, another problem has been solved.

The introduction of optical fiber has greatly increased the potenciality of communications and likewise the use of optical fiber.

In spite of optical fiber being a rather fragile raw material, the users expect cable manufacturers to supply them with high quality performances, not only as far as transmission is

concerned but also mechanical performances which resist installation plus a long lifetime in aggressive atmospheres. Although system designers plan their networks, in fixed installations, usually in ducts and buried, aerial installations are sometimes of absolute necessity. They are sometimes of absolute necessity for legal reasons or, as in the case of electricity companies, the cable runs through high voltage wires, in which case the cable cannot be buried.

A new parameter which must be taken into account when calculating and designing the route of aerial cables, as well as the usual one (sags, voltage, span length, etc.) is the ballistic resistance of the cable. As these cables have dielectric sheathing and their means of transmission is by optical fiber then ballistic resistance needs to be very high.

### ACTUAL SITUATION

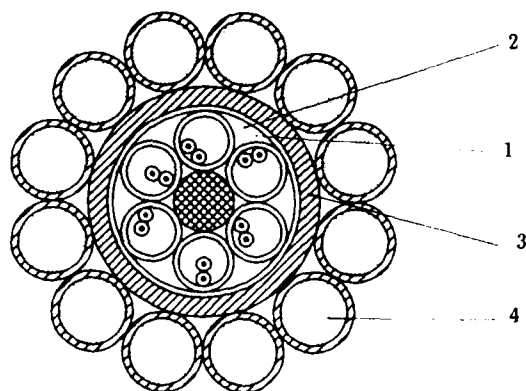
Electricity Companies have always been the greatest users of optical aerial cables. They use three types of aerial cables: OPGW, the self supporting type for very long length spans and lashed to the ground wire. Figures 1, 2 and 3 show the transversal sections of these cables.

The supply of energy and communication through the ground conductor of High Voltage aerial lines becomes simultaneous when the OPGW cable is used. This cable also provides not only a high quality telecommunication system but also high capacity transmission. However, the subject of this "Antiballistic Cables" paper is not about this cable due to its outer metallic composition.

The design of the self supporting cable is principally a study of a mechanic type adjusted to the maximum span of the line and to the geographical zone and atmospheric conditions in which it is located. Mechanic tension is achieved by means of aramid yarns placed between the jackets. Due to the mechanical characteristics, which these cables must boast of, it is necessary to pad them with a great amount of

high module yarns, which, undoubtedly, act as an antiballistic barrier, and which, up to the present have been used in order to provide them with this barrier.

FIGURE 1



OPGW CABLE

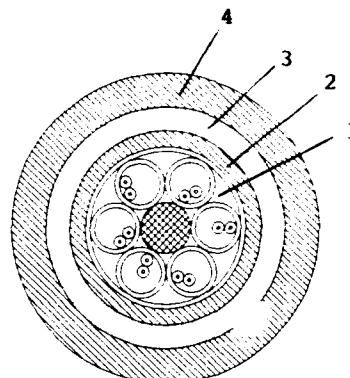
1. Optical Core
2. Filling Compound
3. Aluminium Tube
4. Allumoweld Wires

	Type I	Type II
Short-circuit current	17 kA	25 kA
Outer Diameter, mm	15	18
Weight, kg/km	680	891

However, our experiments have shown us that this protection alone, is not sufficient guarantee. If we wanted to guarantee that it was an antiballistic cable we would have to use so much yarn that it would make the cable financially unfeasible.

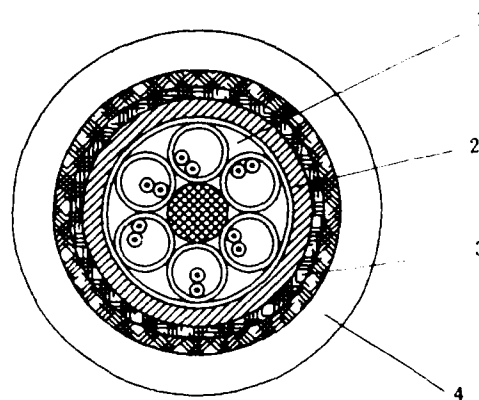
As regards structure the lashed cable is similar to the self supporting type, but owing to mechanical requirements, the amount of yarn used in the latter is lower than the amount used in the former.

FIGURE 2  
SELF SUPPORTING CABLE



1. Optical Core
2. Inner Jacket LLDPE
3. Aramide Yarns
4. Outer Jacket HDPE

FIGURE 3  
LASHED CABLE TO THE GROUND WIRE



1. Optical Core
2. Inner Jacket HDPE
3. Antiballistic Aramide Tapes
4. Outer Jacket HDPE

Outer Diameter: 16 mm  
Weight: 240 kg/km

## NEW CABLE

### 1. DESIGN

The solution that we have discovered consists in putting between the jackets aramide yarn woven tapes so that pellets cannot penetrate through them. This is achieved by a suitable selection, not only in the amount but also in the type of yarn woven, plus the type of weaving. This cable has basically, a structure similar to the conventional types as far as core and sheathings are concerned, even in self supporting cables the tapes do not rule out the use of aramide yarns as elements of resistance.

Figure 4 shows the new cable, in which the longitudinal layout of these tapes can be seen. This kind of layout can be carried out during the sheathing extrusion process, which not only makes its application easier but also brings down manufacturing costs.

In the design of these cables it is not only essential to build a barrier which stops pellets from penetrating into the inside core but also to stop the pellet from doing any damage even if it only hits the fiber. It is, therefore, necessary to place a buffer between the tapes and the optical core. The buffer will then receive the blast from the pellets, and in this way the optical core will be safe from any harm. As we shall see a variety of tests, with different types and amount of tapes, and also different materials for the inner and outer sheathing, have been carried out.

### 2. DESCRIPTION OF ARAMIDE YARN TAPES

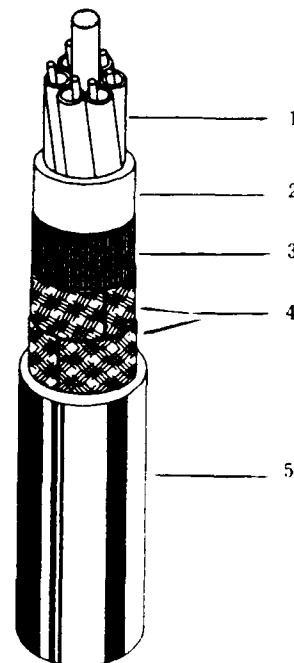
The tests were carried out using different types of aramide yarn woven tapes. From the results of these tests we chose a tape woven with 1260 dtex low modulus yarn, its thickness and weight were 0.6 mm and 0.045 g/cm<sup>2</sup> respectively. The width of the tape is adjusted according to the diameter of the cable it is to protect. We believe that a minimum distance of 15 meters will comply with the requirements of the clients for the type of munition used in bird hunting. With requirements in mind two tapes we applied as is shown in Figure 5 and the results obtained, as shown later.

### 3. TESTS

After tests were carried out on test pieces, the six prototype cables were selected and manufactured.

FIGURE 4

### ANTIBALLISTIC SELF SUPPORTING CABLES



1. Optical Core
2. Inner Jacket HDPE
3. Aramide Yarns
4. Antiballistic Aramide Tapes
5. Outer Jacket HDPE

Outer Diameter: 18 mm  
Weight: 285 kg/km

FIGURE 5

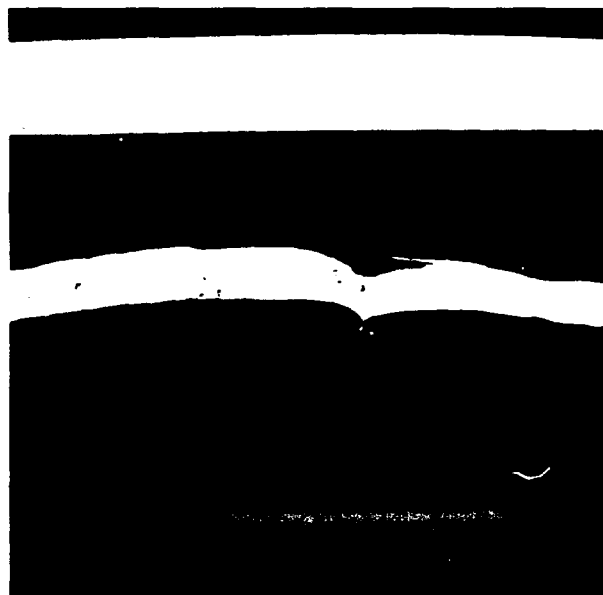


TABLE 1

RESULTS OBTAINED IN CABLES WITH THE FOLLOWING JACKETS: INNER JACKET LLDPE 0.8 mm  
OUTER JACKET HDPE 1.0 mm

SAMPLE No.	No. of TAPES	DISTANCE m	DIAMETER PELLET	HOLES IN OUT.JACKET	PELLETS STOPPED IN 1st TAPE	2nd TAPE	HOLES IN INN.JACKET	PELLETS IN OPTICAL CORE
1	1	25	5	17	6	-	4	1
2	1	25	6	19	8	-	2	-
3	1	20	5	14	4	-	6	2
4	1	20	6	16	4	-	7	1
5	2	20	5	17	8	4	1	-
6	2	20	6	20	6	6	0	-
7	2	15	5	13	4	4	2	2
8	2	15	6	19	7	4	3	3

TABLE 2

RESULTS OBTAINED IN CABLES WITH THE FOLLOWING JACKETS: INNER JACKET LLDPE 1.5 mm  
OUTER JACKET HDPE 1.0 mm

SAMPLE No.	No. of TAPES	DISTANCE m	DIAMETER PELLET	HOLES IN OUT.JACKET	PELLETS STOPPED IN 1st TAPE	2nd TAPE	HOLES IN INN.JACKET	PELLETS IN OPTICAL CORE
9	1	25	5	16	7	-	6	-
10	1	25	6	14	12	-	2	-
11	1	20	5	21	9	-	7	1
12	1	20	6	17	6	-	7	-
13	2	20	5	19	7	6	2	-
14	2	20	6	12	8	1	0	-
15	2	15	5	14	6	3	1	1
16	2	15	6	16	5	4	1	-

TABLE 3

RESULTS OBTAINED IN CABLES WITH THE FOLLOWING JACKETS: INNER JACKET HDPE 1.5 mm  
OUTER JACKET HDPE 1.0 mm

SAMPLE No.	No. of TAPES	DISTANCE m	DIAMETER PELLET	HOLES IN OUT.JACKET	PELLETS STOPPED IN 1st TAPE	2nd TAPE	HOLES IN INN.JACKET	PELLETS IN OPTICAL CORE
17	1	20	5	18	12	-	1	-
18	1	20	6	23	16	-	0	-
19	1	15	5	17	9	-	3	3
20	1	15	6	30	14	-	7	6
21	2	20	5	20	10	8	-	-
22	2	20	6	19	7	6	-	-
23	2	15	5	19	12	5	1	-
24	2	15	6	22	8	9	-	-

A 12 gauge shot gun (18.5 mm  $\phi$ ) was used to fire at the cables as this seemed to be the most harmful type of shot gun owned by the majority of hunters.

The following two shot gun loads were fired during the tests.

	Diameter mm	Weight of pellet, gr	Approx. No. of pellets in 10 gr
No. 5	3.00	0.204	50
No. 6	2.75	0.147	68

The results obtained are to be seen in Tables 1, 2 and 3.

### CONCLUSIONS

In view of the results obtained the effectiveness of the tapes was verified as well as the importance of choosing a suitable type of polyethylene for the inner sheathing. As can be seen, so as to avoid the spreading of the blast to the optical core, it becomes essential to use a PE of HD displaying substantial thickness (1.5 mm).

A double layer of adequately aramide woven tapes effectively protects aerial telecommunication cables against shot gun pellets fired by bird hunters. With the layout presented completely effective results, for distances of 15 m or over, have been achieved.

We believe that this is the most suitable solution for dielectric optical fibers since it does not make any great change in the design of the optical core. As we did not consider shorter distances to be of much interest, a study of them was not made.

These tapes cannot be thought of as possessing any tensile strength, therefore it is always necessary to include the usual pulling elements in the designs for these cables.



**SUSANA CAMARA** received her Master Degree in Chemistry from Oviedo University in 1984, where she specialized in Organic Chemistry.

She joined ALCATEL STANDARD ELECTRICA in 1987 working in the R & D Materials Department, where she is actually responsible for Material Developments of the Telecommunications Cable Division.

She is author of several papers, participating in different International Symposiums.



**CARLOS G. CORTINES** was born in 1944. In 1968 he graduated from Valladolid University with a Degree in Physics. He joined STANDARD ELECTRICA, S.A., today ALCATEL, and worked in the Engineering Department of the Telecommunication Cables Division. From 1982 he is the head of the Optical Fiber Development Group in ALCATEL STANDARD ELECTRICA, Cable Factory in Maliaño, Cantabria.



# FLAT CONDUCTOR CABLE SYSTEMS FOR TRANSMISSION OF AIRBAG SIGNALS WITHIN THE STEERING WHEEL OF CARS

F.Schauer

kabelmetal electro GmbH  
Special cables  
Sieboldstr. 10 8500 Nürnberg

## Abstract

To transmit the signals from the car to the steering wheel a special flatcable assembly was developed. To get a constant resistance and no shorttime interruption in every position of the steering wheel a flat cable formed like a clockspring is protected in a housing. Special constructions of cables were designed. The ends of the flat cable are connected to round cables as they are used in cars. The dimensions of the housings, the length and the thickness of the cable must be harmonized so, that the necessary revolutions of the steering wheel are assured.

## 1 Introduction

When the new generation of electronic equipment for the safety-system Airbag was put on the market a transmissionline between car and steering wheel was necessary which has constant resistance without any shorttime interruption in all positions of the steering wheel and in all cases of deceleration. Usual systems with slipring and carbon strip could not fulfill these conditions.

## 2 Description of the System

To create a transmission without a slipring, a flatcable was wound up to a clockspring and protected by a housing. As the flatcable has small cross sections which are not used in cars, the parts of the transmissionline which are not in

the housing, are made from vehicle cable with a cross section of 0.5 mm<sup>2</sup>. Picture 1 shows in front a flat-cable connected to the round-cable and wound up to a clockspring and behind a second one mounted into the housing.



Picture 1: flatcable  
clockspring

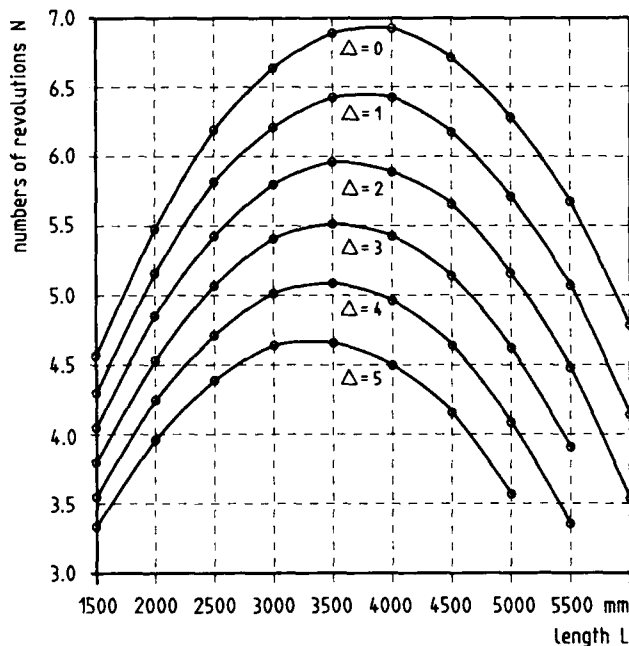
The system consists of 3 important parts: the flatcable, the housing and the outer connectors or lead wires with a point of contact between round- and flat-cable.

## 3 Housing

### 3.1 Revolution and Dimension

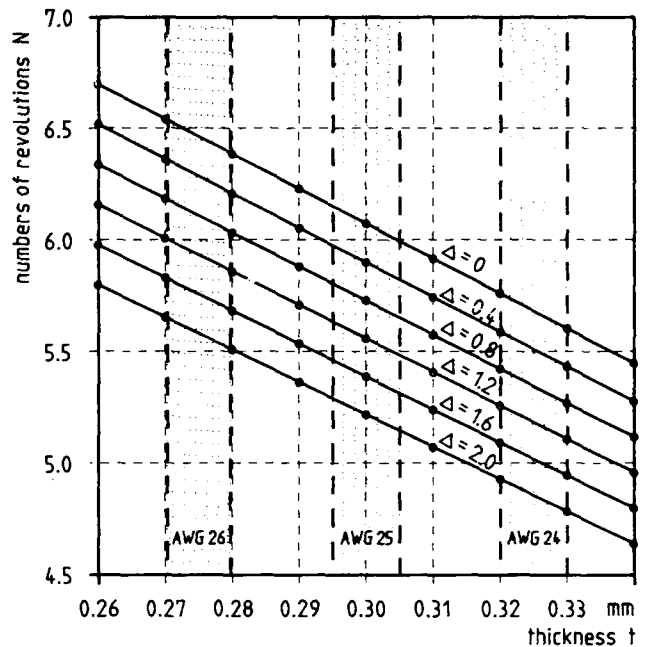
The revolutions, the system has to achieve, are different and depend

on the car. They reach from 3,3 up to 8. The dimensions of the housings are quite different too, because every car designer has his own ideas and influences the development and construction. So the outer diameter reaches from 70 up to nearly 150 mm, the inner diameter from 40 to 80mm. There is no chance for standardisation. So every car or car builder needs his own system. The number of revolutions depends on the volume, which is available to the flatcable clockspring. So it depends on the inner and the outer diameter  $D_i$ ,  $D_o$ , the thickness  $t$  and the length of the cable  $L$ . It is necessary to control the dimensions with a formula considering the geometric dependence. The result is shown in picture 2. In this case the thickness of the cable  $t$  and the outer diameter of the housing  $D_o$  are constant.



Picture 2:  $N = f(L)$   
Parameter:  $D_i + \Delta$

It is recognizable, that a cable that is too short or too long gives less revolutions. One can also see, that the smallest inner diameter gives the most revolutions. This dependence remains the same if we keep the inner diameter constant. By the same steps of the outer diameter the curves are laying closer together. A thicker cable needs more place. How the number of revolutions depends on the thickness of the cable is shown in picture 3.



Picture 3:  $N = f(t)$   
Parameter:  $D_i + \Delta$

In the picture the thicknesses of the available cables are marked. To get a high number of revolutions  $N$ , it is necessary to have a thin and long cable, a small inner diameter and a large outer diameter, but you hardly get all those things together.

### 3.2 Construction of Housing

It is the task of the housing to protect the flatcable from damaging and to guide the two points where the flatcable is connected to the outer cables, - or in another solution to a connector - while they move, that means during the revolutions. The flatcable must have the possibility of free movement. Solutions are known where the housing has layers of foils on both sides of the flatcable. These foils lower the noise of movement. There should be no noise when the steering wheel is moved and no rattle in the case of vibration. The torque should be less than 150 mNm and there should be no abbration between the rotating points. The following housing materials are available.

POM  
PA 6.6  
PA with PTFE  
PC  
PBTP

There should be a very small friction coefficient between the parts.

The normally used constructions have got a roll and a housing consisting of two parts. That makes two points which cause friction. In a new construction the roll and one housing element became one part, so that there is only one friction point left.

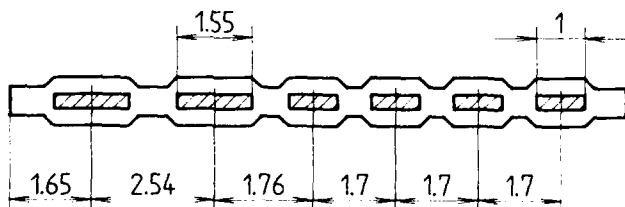
#### 4. Flatcable

##### 4.1 Materials

A flatcable with flat conductors is a very thin cable. The insulation of the cable needs a good abrasion strength and a smooth surface so that the windings of the cable could not stick together when the clockspring is moved. A foil of polyester is a good insulation material. Two foils covered with a special hotmelting adhesiv are laminated together and include the flat conductors. The adhesiv is a two component polyester compound which reaches its full hardness after about two days in normal atmosphere. This is necessary, because the steering wheel reaches temperatures about 90 to 100 °C if the car is standing in the sun. A normal thermoplastic adhesiv softens at these temperatures so that the foils delaminate and the cable becomes defect. If this happens, the clock-spring can't work any more because the insulation gets folds and the windings stick together.

##### 4.2 Construction of Cables

Normally three types of cables with two conductors are used for the transmissions of the signals for the airbag. Cross sections are AWG 24, 25, and 26. For horn and speed control connection three additional conductors are necessary. In that case a five conductor cable is used. Because the space is the same as for the two conductor cable, the conductors and the pitch are defined smaller. Picture 4 shows a cable with 6 cores.



Picture 4: 6 core cable

Instead of the normal pitch of 2.54 mm there is used a pitch of 1,7 mm. The 2 conductors of airbag keep the pitch of 2,54 mm and the 4 other conductors get the smaller pitch.

#### 4.3 Electrical Characteristic

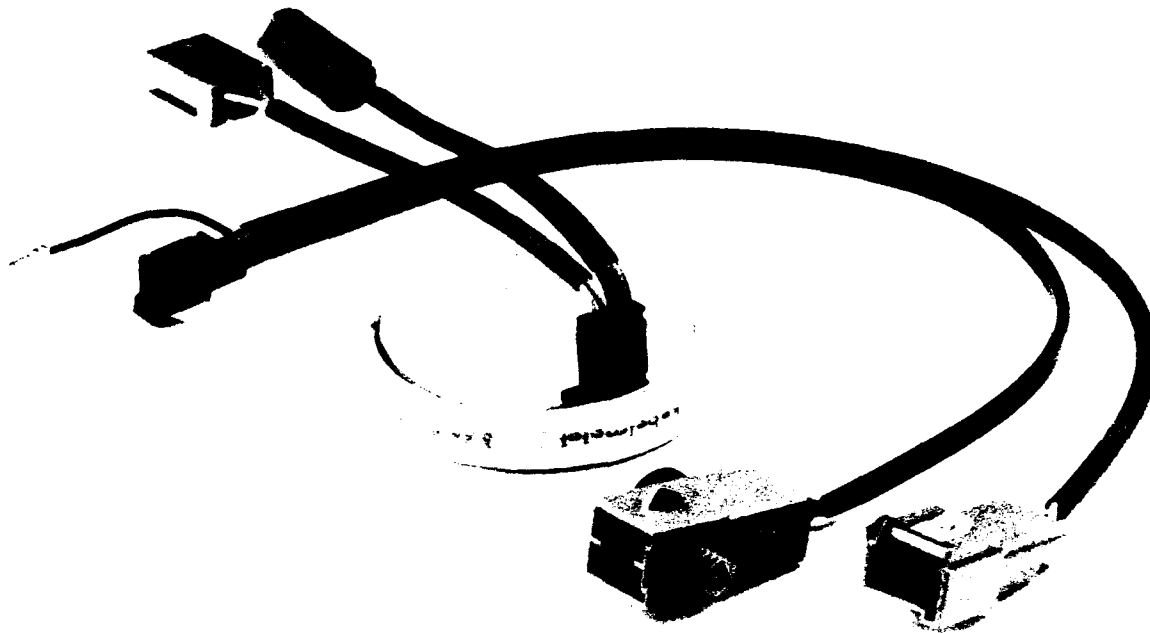
**4.3.1 Load Capacity:** Normally the cable is only used to transmit signals. For the heating element of the steering wheel a current of 8 amp should be transmitted. The question was which cross section of the flatcable would be necessary. In this case it is not possible to compare to the values which are given in standards because the heat conduction in the coil is unfavourable. The worse case is given, if the cable is wound up on block on the inner roll. For this case we have made measurements with the result, that the highest steady current can be around 3 amp, then the temperature rise is 80 K. For the three standart cross sections the maximum load is shown in picture 5. The values of flatcables which are laying straight are shown there, too.

cross section AWG	one cable straight amp	in the clocksp. amp
24	6,0	2,7
25	5,5	2,3
26	5,0	1,8

Picture 5 :load capacity

For the heating element or other equipments in the steering wheel with more than 35 W , or 3 amp, a sliding conduct must be used. If the current flows only on a period of 3 minutes, the value is aproximately twice.

**4.3.2 Temperatur Dependence of the Resistance:** For the electronic control system in the cars it would be desirable that the path of airbag has a constant resistance at all temperatures. Normally electrolytical copper is used. The resistance of the path rises up to 1,6 at 85 °C and falls down to 0,7 at min 40°C if the resistance at 20°C is 1,0. The values include the tolerances caused by the different lots of manufacturing .



Picture 6 : 5-conductor assembly

#### 5 Connection and Lead Wire

The first step was based on the idea, that the connection point is embedded in a moulded housing so that the connection point is protected. This technology is still used today for two conductor systems as they are shown in picture 1. For more conductor assemblies the soldered connection points between the flat and the round cables are together with the folded end of the flat cable and together with the pull - relief block of the stranded round wires embedded in a two-part housing which is closed by welding with ultrasonic. In picture 6 a five conductor assembly is shown.

The metallic connection may be manufactured by:

- welding
- soldering
- crimping

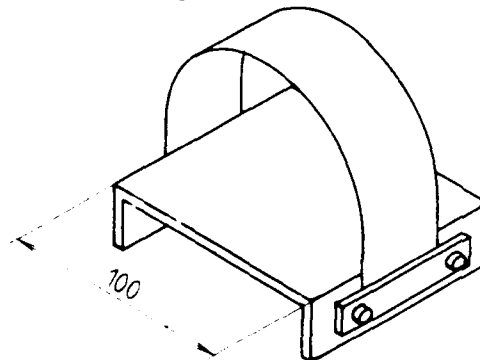
The crimping of flatcable with flatconductors is used in electronic equipments but not in cars. Further there is used an insulation displacement system so that the dimensions of the flatcable are not variable. But this is necessary for the definition of the clocksprings. Competent connector manufacturers and harness makers have made a lot of tests. The results are good but the resistance shows variations

in the lifespan of the contact. If a welded contact is used there might be problems if the conductor is smaller than AWG 25. A soldered contact provides the greatest number of possibilities for the dimensioning of conductor and pitch. We can look back to positive experiences using a reflow-soldering-system over more than five years.

#### 6 Tests and Specification

##### 6.1 Cable

A lot of tests were done, wherein the test of delaminating is a special test for the clockspring cable for airbag. The cable is fixed as shown in picture 7.



Picture 7: Delaminating test

For quality assurance a test for the delaminating temperature was defined. A little piece of the flatcable is fixed in a bend and stored in a heating-cabinet. A lot of specimens are stored at different temperatures. If the temperature is too high, the insulation delaminates or shrinks and delaminates. For the cables for airbag the delaminating point must be higher than 130°C. It may be done also a shrinking test in accordance to DIN 65109, but the delamination test is simulating better the application of clockspring for airbag.

## 6.2 Tests on Clocksprings

**6.2.1 Electrical Resistance:** As the whole system is controlled during the application, it is necessary to compare very exactly with the nominal value. Measurement is done with a four-point system. The resistance increases the lead wires and the connectors. If there is a permissible tolerance of 5 % or less in the requirements, every part must be measured and if required, selected.

**6.2.2 Torque:** The torque required to drive the interface assembly should not exceed the limits. There are different values from about 70 up to 150 mNm fixed for the clocksprings. If there will be done a 100 % final test, all defects in the mechanical parts, such as the housing or roll, or a fold in the flat cable, are found.

**6.2.3 Durability Test:** The most important test is the revolution durability test. The fixture of the clockspring should be similar to the "in car" mounting. There are made all together 1,4 mio cycles in the temperature reach from minus 30°C up to plus 80°C. One mechanical cycle comprises 2 revolutions clockwise and 2 revolutions counter clockwise and back to the center position. Then four times a movement of 12 degrees clockwise and counter clockwise close the cycle. The test will be continued in a dust cabinet. The assembly is placed in a cubical chamber in which fine powdered Portland cement is blown. Only assemblies with housings that will not let in the dust can stand this test.

## Nomenclature

AWG	American Wire Gauge
Di	Inner diameter of housing
Do	outer diameter of housing
L	length of flat cable
N	number of revolution
PA	Polyamid
PBTP	Polybuthylenthereftalat
PC	Polycarbonat
POM	Polyoximethylen, Polyacetal
t	thickness of flatcable

## Biography



Friedrich Schauer  
kabelmetal electro  
Sieboldstr. 10  
8500 Nürnberg  
Germany

Mr. Schauer was born in 1940. He joined kabelmetal electro after he received the degree Dipl. Ing. in electrotechnology in 1962 from the "Polytechnikum München". He has been engaged in the development of power cables, later special cables in particular flat cables. He is now head of the development department for special cable systems.

# A HIGH SPEED COATING PROCESS FOR OPTICAL FIBRE RIBBON

Jukka Kohtala, Juha Tanskanen

Nokia-Maillefer, Vantaa, Finland

Peter Fickling, Mats Eriksson

Ericsson Cables, Hudiksvall, Sweden

## Abstract

Ribbon is being made or proposed with designs having from 2 to 12 or more fibres. Many of the production units in use today are adaptations of existing fibre making plant which is cumbersome to use, does not attain especially high quality, and, for the sake of stability, cannot be run at speeds which give economical production. Coating is a very sensitive process; the fibres in the ribbon can easily develop unacceptable attenuation increases at low temperatures. Bubbles in the coating and bubble stripping have been a considerable problem. It was therefore decided that a method of manufacturing ribbon with good characteristics and with a production speed considerably higher than normal had to be developed. This paper presents an evaluation of this method with special emphasis on the heart of the process; a newly developed, high precision, acrylate coating applicator.

## Introduction

When optical fibre began replacing copper cable for the trunk telephone network it was mainly for the reason that a single fibre had the transmission capacity of several hundred copper conductors. The first fibre cables comprised very few, typically six, fibres but had comparatively, an enormous transmission capacity. However, as often happens when capacity becomes available, new niches were created and the demand soon absorbed all that extra capacity. Today optical fibre cables have become very widely used in subscriber networks to serve high speed, broadband telecommunication services, such as data, video and facsimile transmissions. This has led to a demand for cables with higher and higher fibre counts, often with 96 or more fibres. The spread of optical cable into the local area networks has generated

a further demand for cables with a high fibre count. Ribbon structures allow multifibre cables to be made compact and this is the main reason for their introduction. There are other advantages such as easier coupling for multiple testing of fibre bundles, quicker splicing especially in the field and simpler termination procedures. To realise these advantages a ribbon must fulfil strict geometrical and other requirements. Its production speed must also be high enough to yield an economical product and to meet the rapidly increasing market demand.

## Ribbon and cable design

A ribbon fibre structure is formed when 2 or more fibres are held together laterally either by taping or bonding the edges or encapsulating with a UV-curable resin. A view of an 4-fibre encapsulated ribbon is shown below in Fig. 1.

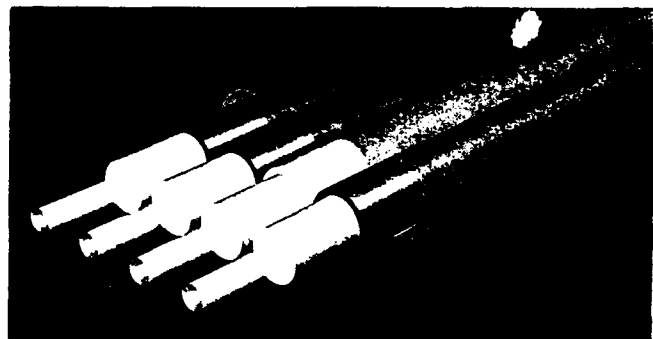


Fig. 1.

It is important that the whole ribbon matrix is free from gas bubbles especially between the fibres.

Fig. 2 depicts the cross section of an ideal encapsulated 4-fibre ribbon.

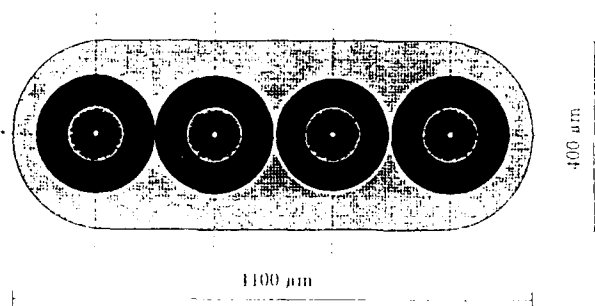


Fig. 2

Fig. 3 shows how compact a 96-fibre cable can be made. The ribbons are closely stacked in slots which surround a central strength member. This design, called a slotted core cable, has a diameter considerably less than a conventional type with a similar fibre count.

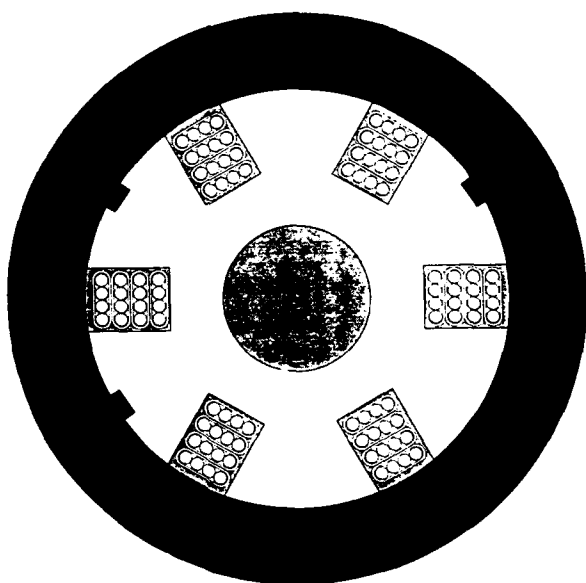


Fig. 3

Ribbons comprising 6 or more fibres are not generally used in cables. At this early stage of development the market abounds with different designs of ribbon and ribbon cables. This hinders any specific developmental work as does the absence of universally defined tolerances.

Prior to their incorporation into a ribbon, fibres are usually coloured with a UV-curable ink with special properties. (next section). The ribbon matrix can

consist of a soft inner enclosed by a hard outer, similar to a standard two-coat fibre, or a single matrix material with intermediate properties. The two-coat system can have separate applicators and UV-curing or be applied wet on wet.

### Coating Materials

Taping of fibres has been tried but has reliability problems, furthermore it is not easy to split nor does it leave a clean fibre after splitting; which is necessary when terminating fibre bundles.

Total encapsulation of the fibres is probably the commonest ribbon design today. With this type of structure, the interaction of the material used for the fibre outer coating, whether coloured or not, and the ribbon bonding acrylate is paramount in ensuring the desired break-out. Good break-out is the property whereby fibres can be peeled from the ribbon structure so cleanly that no trace of the outer ribbon material remains on any part of any fibre whilst leaving the colouring ink undamaged on each fibre. Normally, if one acrylate is applied over another, whether one of them is cured or not, there will be an excellent adhesion between the layers. To prevent this adhesion and achieve adequate break-out of the fibres, the coating materials have to be modified as do the coating techniques. The outer coating of the fibre, usually a UV-curable coloured ink, has to have its chemical structure altered so that adhesion to the ribbon acrylate does not occur. It is also vital that the colouring coat is adequately cured otherwise the outer matrix material will adhere to the surface of the fibre, even when using a modified ink. A particular difficulty with the modified material is the considerable slowing down of the cure rate compared with standard material. This exacerbates the curing problem.

Formally an outer silicon acrylate was used to produce good break-out and whilst it was effective, it had the undesirable property of leaving traces of itself on the fibres. It also needed overcoating with a harder more durable acrylate but this was not a problem if a wet on wet applicator was used.

An alternative approach to the break-out problem is to use standard fast cured inks and chemically modify the ribbon acrylate instead. Such materials are on the market and could give higher production speeds but hitherto we have not tested them.

Edge bonding is simpler than encapsulation. The sides of the fibres are bonded with a UV-curable acrylate (interstitial bonding) but no material is applied to the tops. They therefore lack the buffering protection which encapsulation engenders but produce smaller ribbons. Alignment is also more of a problem which can make multifibre (mass-splicing) terminations difficult. Break-out is less important so that standard fast curing colouring inks can be used in production.

## Equipment

The line configuration is shown in Fig.4.

It includes a multihead pay-off with facilities for up to 12 reels; the pay-off tension of each fibre being monitored to ensure perfect balance in the system. The fibres then pass, via a static discharger, into the UV-curable acrylate applicator, a double (wet on wet) coater of advanced design. The coater is preheated from beneath.

The remainder of the equipment, double UV-curing irradiators, capstan and take-up is a standard fibre drawing setup. There is provision for two different acrylates with a delivery pressure up to 4 bar and temperature up to 60°C.

## The Coating Process

The target for the project was to develop a high speed coating process for the manufacture of optical fibre ribbon with a matrix adhering to close geometrical tolerances and the optical properties of every fibre remaining unimpaired. The heart of the system is the *pressurized ribbon coating applicator* which was designed from the outset to run optimally with a coating speed of around 300 m/min. Using the various acrylate parameters it was possible to theoretically establish all the interactions between the internal fluid flows so that the angles and distances required for optimum performance and stability could be calculated with a considerable degree of accuracy. The first coater, built to this design, was subjected to intensive and painstaking experimental work aimed at perfecting the coating process. The applicator is shown in Fig.5.

The coater has four material inlets, allowing the use of either one or two different materials in a wet on wet process. The inner die system can be used for edge bonding only or, with a different pressure, for a buffer layer. When used for single material encapsulating the inner system ensures that the interstices are completely filled obviating the need for a bubble stripping device over the coater. The three die system was chosen to produce the best alignment with varying fibre diameters and to allow easy interchange to accommodate different ribbon designs or dimensions.

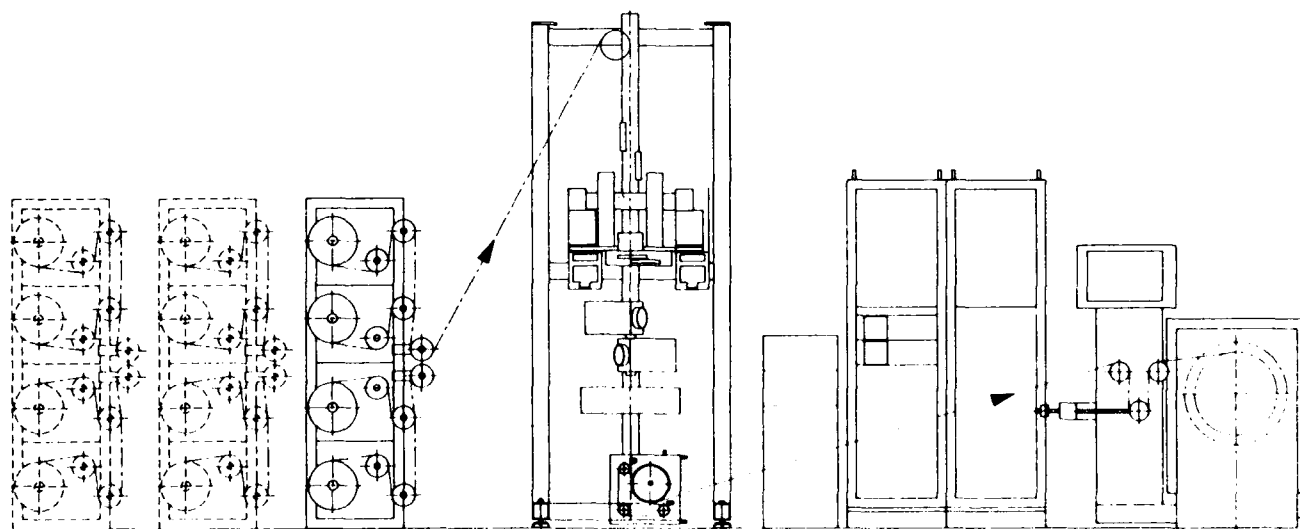


Fig. 4



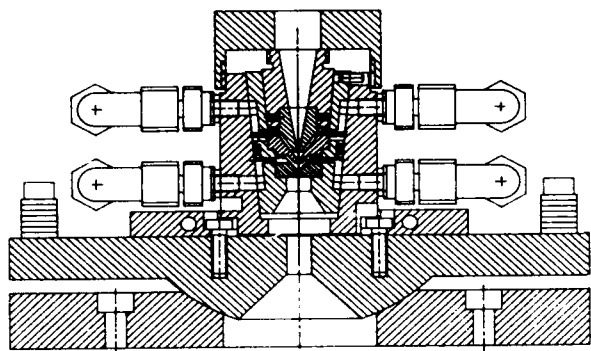


Fig. 5

In use the coater has achieved all that was expected of it. Alignment of the fibres, in both directions is good as is the ability to accept different coating materials and produce different ribbon designs to close tolerances. Reproducibility is well up to expectation. Cleaning is carried out without dismantling under normal production conditions. A remaining drawback is the degradation of the outer coating with speeds less than 200 m/min. but this is a limitation that has to be accepted. The coater has produced satisfactory results for edge bonded ribbons and, with alternative dies, a well aligned eight fibre ribbon was made. An example of a four fibre encapsulated ribbon produced with a line speed exceeding 300 m/min is shown in Fig. 6.

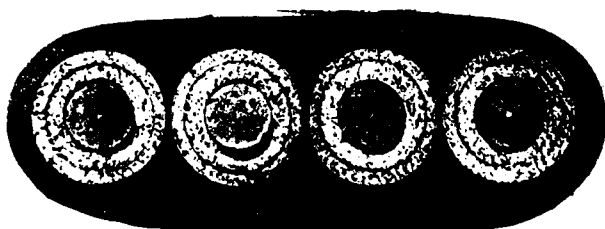


Fig. 6

## Test Results

All the tests results presented below relate to 4-fibre encapsulated ribbon with a double layer matrix of the same material. The fibres were standard single mode, coated with two acrylate layers and a UV-cured colouring ink. After colouring the nominal outer diameter was 250-260  $\mu\text{m}$  and the outer dimensions of the matrix 400 x 1100  $\mu\text{m}$ . Production speed was 200-300 m/min.

## Attenuation

Measurements were taken for each fibre before and

after making the ribbon. Subject to the limits of the measuring equipment, no increase in attenuation was detected. The results for the ribbon at 1300 nm and 1550 nm are presented in Fig. 7 and 8.

## Temperature Cycling

The ribbons were subjected to six complete cycles between -40 and +70°C and at the conclusion of the temperature cycling the temperature was taken down to the limit of the equipment, -83°C, and a measurement taken. The attenuation increase was maintained within the project target of 0.1 dB/km. It was also confirmed, by carefully examining the results, that the inner and edge fibres behaved similarly. See Fig. 9, 10 and 11.

## Microbending sensitivity

For this test a ribbon was passed twice between two pieces of p50 grade sandpaper. A reference measurement, without the upper sheet, was taken before and after loading. The load was increased in 2 kg steps producing the attenuation increases for inner and edge fibres shown in Fig. 12.

## Macrobending sensitivity

Measurements were taken with the ribbon describing a single 360° loop around different diameters of mandrel. The increase in attenuation for both the inner and edge fibres is shown in Fig. 13.

## Torsion sensitivity

If a ribbon is too sensitive to the effects of rotation it could produce unwelcome attenuation increases when incorporated into certain cable designs. This sensitivity was checked by taking the ribbon through a series of axial rotations and noting the attenuation for inner and edge fibres after each turn. See Fig. 14.

## DISTRIBUTION OF THE ATTENUATION

WAVELENGTH 1300 nm  
(total 650 measurements)

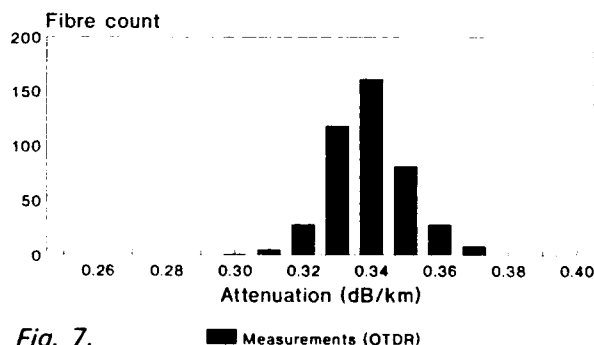


Fig. 7.

# DISTRIBUTION OF THE ATTENUATION WAVELENGTH 1550 nm (total 650 measurements)

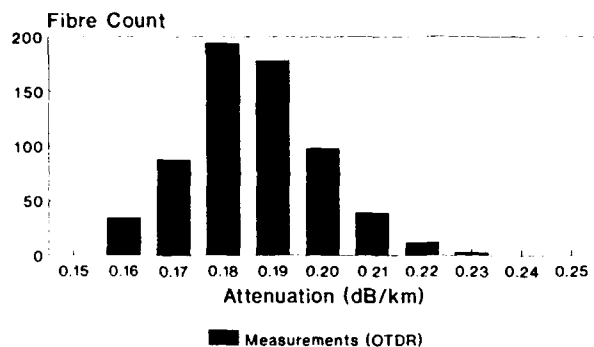


Fig. 8.

# TEMPERATURE CYCLING FIRST CYCLE

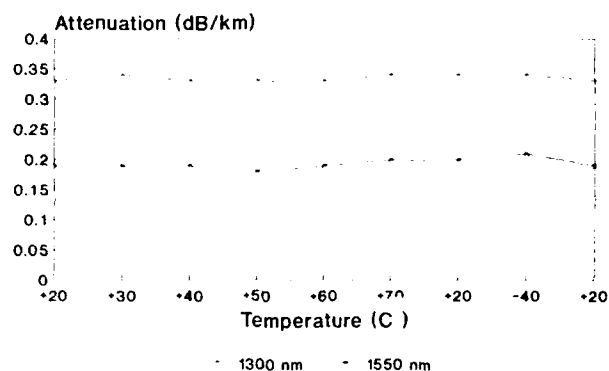


Fig. 9.

# MICROBENDING TESTS

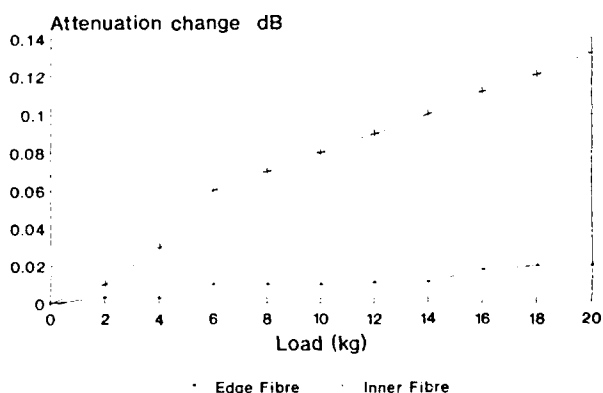


Fig. 12.

# TEMPERATURE CYCLING SECOND, THIRD AND FOURTH CYCLE

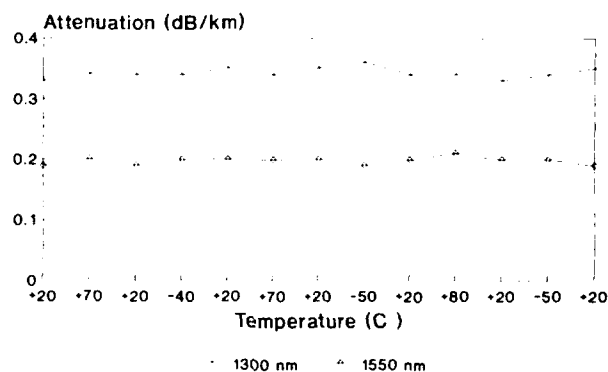


Fig. 10.

# MACROBENDING TESTS

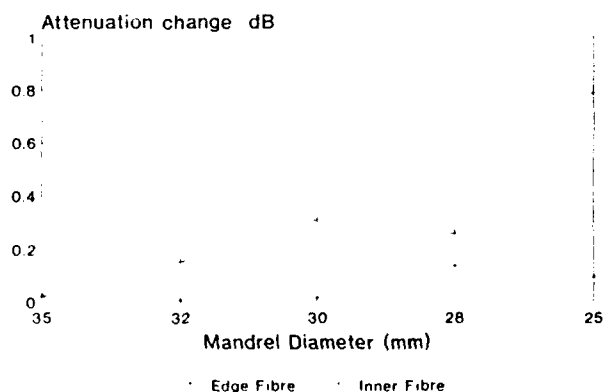


Fig. 13.

# TEMPERATURE CYCLING FIFTH AND SIXTH CYCLE

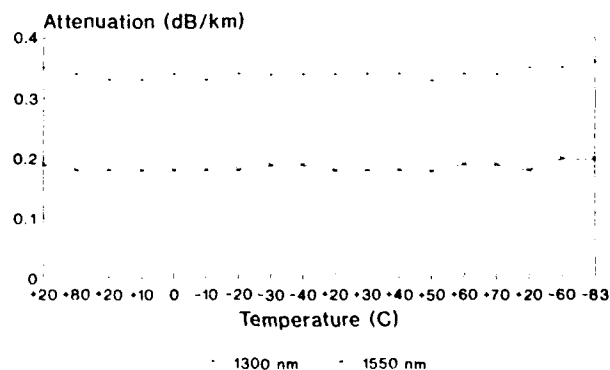


Fig. 11.

## TORSION TESTS

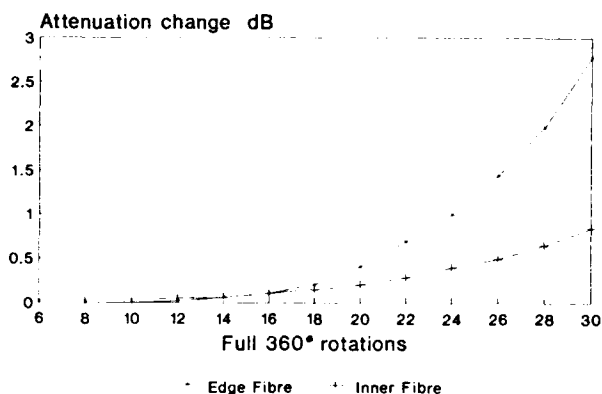


Fig. 14.

## Authors



**Peter Fickling** - received the HNC in elec. eng. from Aston Polytechnic, England in 1961. From 1961 to 1968 he worked as a power engineer on high voltage networks. In 1971 he received the BA degree in Geoscience from Cambridge University, England, the certificate in education in 1972 and the MA degree in 1976. After a period of language teaching from 1972 to 1977 he joined Ericsson Cables, Hudiksvall. In 1984 he moved to Ericssons Fiber Optic Center in Stockholm as a production engineer, returning to Hudiksvall in 1986. He is currently responsible for the development of fibre drawing and ribbon process techniques. He has been granted patents for coating applicators and more are pending.



**Mats Eriksson** - received the engineers certificate in machine technique from Polhemsskolan, Gävle, Sweden in 1977. He joined Ericsson Cables, Hudiksvall, the same year, but moved to Ericssons Fiber Optic Center in Stockholm in 1984. He returned to Hudiksvall in 1986 and is currently responsible for developing and testing fibre and ribbon line equipment. He has been granted patents for coating applicators and more are pending.



**Jukka Kohtala** - received the MSc degree in Physics from Turku University, Finland in 1983. After working for two years with Nokia Cables as a research engineer he joined Nokia-Maillefer in 1990. He is currently employed as product manager for the fibre optics department.



**Juha Tanskanen** - received the BSc degree in mechanical eng. from Wärtsilä Polytechnic, Finland in 1984 and the MSc degree in computer eng. from Tampere University, Finland in 1991. From 1984-1988 he worked as a designer for GWS-Perlos Connectors. He joined Nokia-Maillefer as a development engineer for the fibre optic group in April 1990.

## Conclusion

Extensive testing of the ribbons made using this advanced manufacturing process indicate that it can now be utilized to produce good quality ribbon at high speed. The applicator is versatile and can produce ribbon of different structures including both edge bonded and encapsulated designs with close tolerances.

Using the most recently developed ribbon matrix material it has been found that encapsulated ribbon, with one UV-curable ink and two layers of a single matrix material, has excellent temperature stability and good break-out properties. Different material is required for edge bonded structures.

Development so far is the first stage of a project to find more cost effective ribbon structures with better optical and mechanical properties.

## SELF-SUPPORTING OPTICAL FIBRE AERIAL CABLE WITH LARGE ALLOWABLE ELONGATION

F. Krahn, N. Lenge, G. Weckerle

ANT Nachrichtentechnik GmbH  
Bosch Telecom  
Backnang, Germany

### Abstract

Optical fibre aerial cables must withstand ice load, wind load and Karman vibrations without damage and without any increase in the fibre attenuation. If the cable has to be installed in wooded areas there is a risk of damage by falling trees. For minimizing this risk, a self-supporting optical fibre aerial cable has been developed with an allowable elongation of 1.5% which, together with a special suspension technique, withstands falling trees without damage and even without increase in attenuation, and returns automatically to its original position after removal of the fallen tree. This special suspension technique is based on the fact that at pole distances of about 50 m a roll-bearing is used at each pole, allowing bracing fields of about 1000 m or more.

### Introduction

Most optical fibre cables presently installed are either direct buried or in ducts. Although these practices are the most expensive ones, they are preferred to aerial installations, since the probability of damage to the aerial cable is higher and the sight of aerial cables between buildings is often disturbing. Nevertheless aerial cables can offer advantages with regard to installation convenience, costs and time, particularly in cases where support structures already exist, for example along railway tracks. On such routes, the overhead installation of the cable is the obviously best solution. All these installation advantages are counterbalanced by other factors which affect the cable usefulness. Aerial cables have to be designed to offer the optical fibres sufficient support to withstand the stress caused during installation, ice load and wind load as well as protection against other possible damages. In wooded areas there are two main factors which can damage an aerial cable. Firstly shot-guns which can lead to sudden fibre breaks or long-term failure due to moisture entrance. Secondly falling trees which can also cause sudden fibre breaks. These problems are very serious in the case of data transmission for passenger transportation.

This paper describes the basic requirements for the cable and the suspension technique. The concept has been applied to a self-supporting opti-

cal cable along a railway track of the Deutsche Bundesbahn near Karlsruhe. This concept can also be applied to other cable types.

### Required Cable Elongation

The required additional cable length  $x$ , needed in the case of a falling tree, can be calculated according to the following equation:

$$x = \sqrt{l^2 + h^2} + \sqrt{h^2 + (a-l)^2} - a - \frac{8f^2}{3a}$$

where:

- $a$  is the pole distance,
- $f$  the cable sag,
- $h$  the height of suspension,
- $l$  the distance measured from one of two poles where the tree falls (see fig.1)

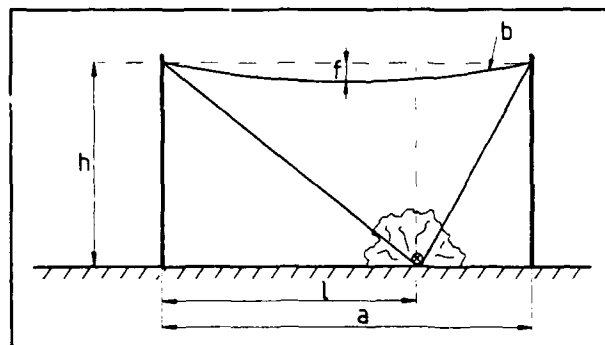


Fig.1: Geometrical conditions

Two extreme cases must be considered. In the first case, the tree falls in the middle between the two poles. In the second case, the tree falls in the direct vicinity of a pole.

Assuming a sag of 1% of the pole distance at a temperature of  $-5^{\circ}\text{C}$ , the additional cable length required for case 1 is as represented in figure 2, that for case 2 is as shown in figure 3.

Even in case 1 a cable elongation between 0.5% and 39% depending on the pole distance and height of suspension will occur. This is too much for an optical fibre cable.

For this reason, a special suspension technique is absolutely necessary. This problem is solved by a roll-suspension technique. This technique allows bracing fields of 1000 m or more to be realized. Throughout the poles between the two bracing poles the cable recline on suspension rolls as shown in fig. 4.

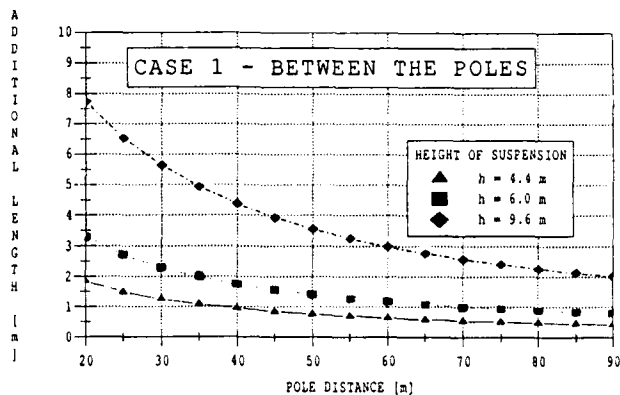


Fig. 2: Necessary additional cable length

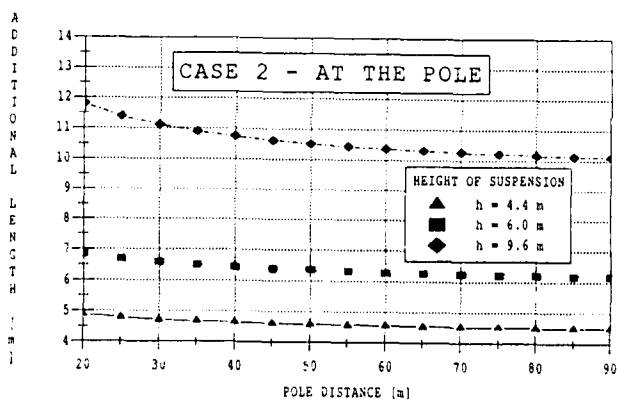


Fig. 3: Necessary additional cable length

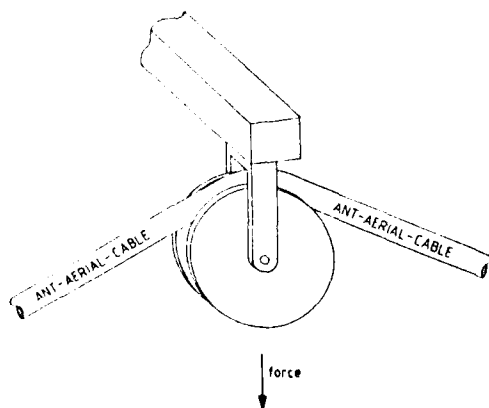


Fig. 4: Roll-suspension technique

In the case of a falling tree, two factors can contribute to the required additional cable length: the reduction of the sag between the individual poles within the bracing field and the cable elongation.

The part resulting from the reduction of the sag can be neglected. If we assume a bracing field of 1000 m with an average pole distance of  $a = 50$  m and a sag of 1% ( $f = 0.5$  m), this amounts to only:

$$\frac{8f^2}{3a} \cdot 19 = 0.25 \text{ m}$$

Thus, the total additional cable length must result from the cable elongation.

Using the described suspension technique, the cable elongation for example of 39% can be reduced to only 0.8%. Generally not the easiest, but the worst case must be considered. Thanks to this suspension technique, the cable elongation required in case 2 at the defined bracing fields and a suspension height of 9.6 m is only 1.0% to 1.2% as shown in fig. 5.

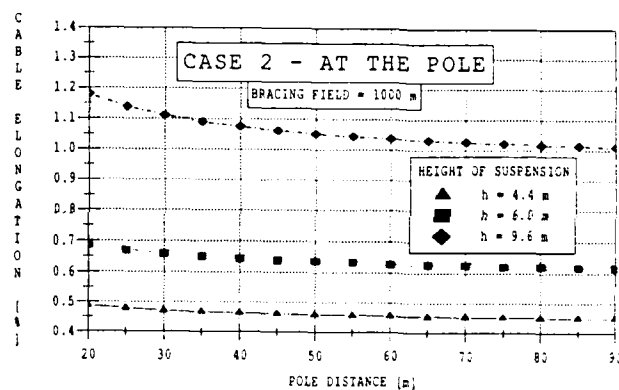


Fig. 5: Necessary cable elongation

A further great advantage of this suspension technique is the fact that there will be no vertical forces on the pole, neither during installation, nor in service or in the case of a crash. There are only forces in the direction of the pole. Of course, this does not apply to the bracing poles.

#### Cable Design

##### Core

As shown in fig. 6 the fibres are located in loose tubes which are stranded around a central member consisting of copper wires or polyethylene including glass yarns. The tube dimensions and the stranding pitch have been selected so that a cable elongation of up to 1.5% will be permissible. Up to this strain the fibre will be isolated from mechanical load. Furthermore the design ensures that the optical fibres are well protected against lateral forces.

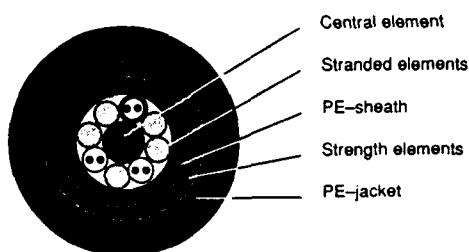


Fig. 6: Cable cross-section

#### Jacket and Strength Members

A low-density polyethylene inner sheath is applied over the cable core. Around this sheath the strength members are applied in two layers alternating in direction and preventing cable torsion. Over the last layer an adhesive compound is applied to bond the strength members to the surrounding jacket. This bond will improve the tension behaviour of the cable. Without such a bond jacket slippage or tearing could result. The outer diameter of the cable is 19 mm.

The strength members must have a Hooke's region of greater 2.0%, because a falling tree can cause cable bends with a minimum diameter of 800 mm. Thus, the strength members at the outer side of the cable bend are additionally stressed. The resulting elongation is about 1%, together with a worst-case cable elongation of 1% this leads to a total elongation of more than 2%.

The material used for the strength members is aramid. Aramid has the advantage of preventing a cable from being damaged by shot-guns firing from a distance of at least 20 m. Tests were carried out with caliber 12/70 and pellet sizes of 2.5 mm, 3.0 mm and 3.5 mm.

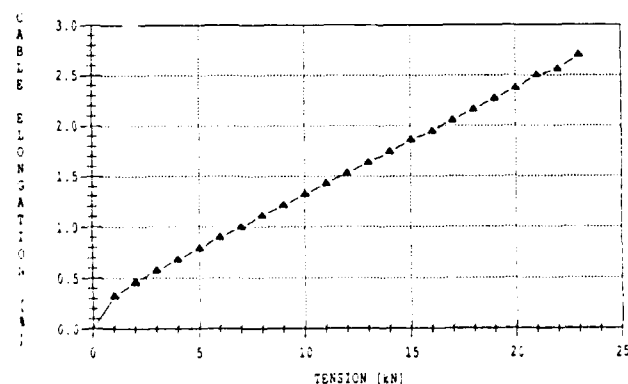


Fig. 7: Tensile performance

#### Results

The elongation and temperature behaviour of the cable is shown in fig. 7 and 8.

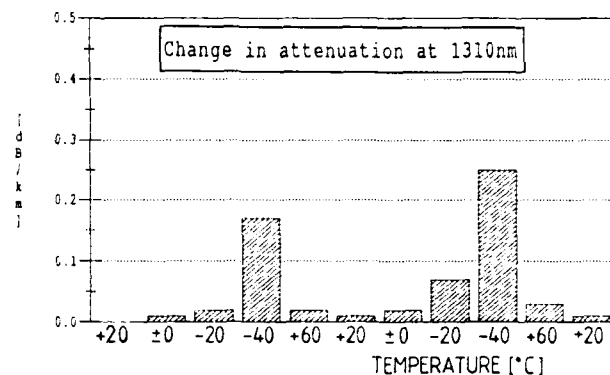


Fig. 8: Temperature behaviour

Further tests carried out are summarized in table 1.

Table 1

Tensile test (IEC 794-1-E1)	
Fibre strain at a cable elongation of 1.5%	0.0%
Attenuation change at a cable elongation of 1.5%	< 0.1 dB/100m
Breaking elongation (IEC 794-1-E1)	2.7%
Cable bending (IEC 794-1-E11)	
Attenuation change	< 0.1 dB
Result of shot damage down to a distance of 20 m	no damage of strength members
Crash test (IEC 794-1-E3) 3300N	< 0.1 dB
Impact test (IEC 794-1-E4)	
100 impacts, 0.5 Nm, 20°C	no fib. break
100 impacts, 0.5 Nm, -40°C	no fib. break
Repeated bending (IEC 794-1-E5) 10000 cycles	no fib. break
Vibration test (11 000 000 vibrations, frequency: 15 Hz, amplitude: + 6 mm)	no change in attenuation

#### Field Testing

The results of field testing are shown in fig. 9. The following parameters were measured from 05. Dez. 90 to 15. March 91: attenuation at 1310 nm, temperature, cable strength and wind velocity.

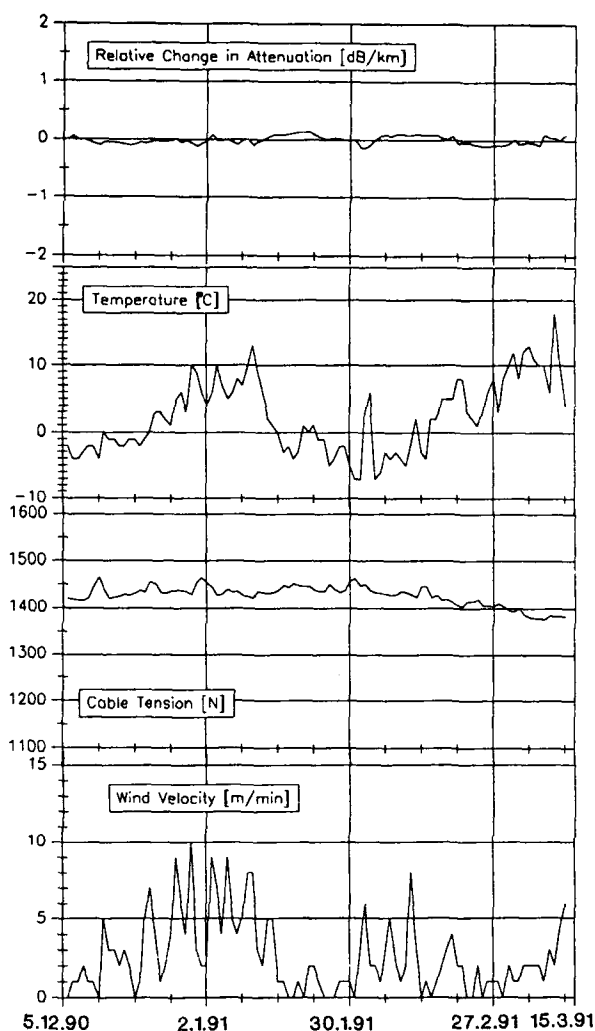


Fig. 9: Field testing results

### Conclusion

The field tests performed have shown that the described self-supporting optical fibre cable is appropriate for being installed along railway tracks. Neither climatic conditions such as temperature, ice or wind nor a falling tree can influence the optical behaviour in any way. The chosen roll-suspension technique permits an easy installation and avoids problems during service.

### Acknowledgements

The authors wish to express their thanks to Mr. Aichler from the Deutsche Bundesbahndirektion Stuttgart and to Mr. Weng from the Deutsche Bundesbahndirektion Karlsruhe for helpful technical discussions.

### References

1. Wenski W., Menze B., Schulte J. - Fibre strain during cable pulling: an important factor in cable design. IWCS, 1989, P 368 - 373
2. Buchwald R., Möcks L., Schmidt J. - Armaturen für Lichtwellenleiter-Luftkabel. Hauszeitschrift Firma Richard Bergner
3. Hoffren P., Karlsson J.O. - Selbsttragendes Glasfaserkabel für Anwendungen bei der Eisenbahn.
4. Rowland S.M. - The development of a metal-free, self-supporting optical cable for use on long span, high voltage overhead power lines. IWCS, 1987, P 449 - 456
5. Wong D., Lyons S. - Pre-stranded self supporting aerial cable design. IWCS, 1987, P 438 - 440
6. Grooten A., Bresser E.J., Berkens A.G.W.M. - Practical experience with metal-free self-supporting aerial optical fibre cable in high voltage networks. IWCS, 1987, P 426 - 437



Friedrich Krahn was born in 1939. He graduated from the University of Münster in 1970 with a Dr. rer. nat. in Physics. He then joined Felten & Guillaume Carlswerk AG and was first engaged in the field of innovation and diversification. In 1973 he was appointed head of the department for fibre optics research and development. In 1986 he joined ANT Telecommunications. He is now responsible for the optical fibre cable development within the Product Group Telecommunication Cable Systems.



Gregor Weckerle was born in 1962 in Offenburg, Germany. He studied electrical engineering at the FH Offenburg and graduated in 1989. He joined ANT Telecommunications in 1989. Since this time he has been engaged in the development and design of optical cables within the Product Group Telecommunication Cable System.



Norbert Lenge was born in 1956. After four years' work as research assistant at the Max-Planck-Institute in Stuttgart he graduated from the University of Stuttgart in 1984 with a Dr. rer. nat. in Physics. He joined ANT Telecommunications and was first engaged in the field of polymer cross-linking. Since 1987 has been responsible for progress engineering and construction of optical telecommunications cables within the Product Group Telecommunication Cable Systems.



# THE DEVELOPMENT AND TESTING OF AN EPOXILESS FIBER OPTIC CONNECTING SYSTEM

Nicholas A. Lee

3M Fiber Optics Laboratory, St. Paul, Minnesota

## Abstract

This paper describes the development and testing of a hot melt adhesive based fiber optic connecting system. This system offers several distinct advantages over previous epoxy based systems in the areas of installation time and ease of use. Critical developmental parameters, as well as the testing used to track those parameters, will be discussed. Additional system-level testing, performed both before and after product release will also be presented.

## Introduction

As early as 1987, 3M researchers foresaw the need for a fast, easily field installable, multimode fiber optic connector for use in the indoor local area network (LAN) environment. Perception of this need was based on several key characteristics of the fiber optic LAN environment, including high interconnection density, diverse installer expertise, and increased sensitivity to installed cost. A connectorization system which offered fast, user friendly installation would provide an excellent match to all of these characteristics.

Preliminary examinations indicated that the largest impediment to ease of use was the epoxy adhesive used to affix the connector to the cable. The time and effort required to meter, mix, dispense, apply, and cure the epoxy was prohibitive. Therefore, a program was launched to develop a high performance hot melt adhesive to replace epoxy in field installable multimode connectors.

## Adhesive Development

### Hot Melt Advantages<sup>1</sup>

Hot melt adhesives provide clear advantages over epoxy adhesives for use in field terminating fiber optic connectors. These advantages include:

1. Unlimited Shelf Life. Because a hot melt adhesive is a stable, chemically inactive thermoplastic, its characteristics are stable over time.
2. No Mixing. A hot melt adhesive is a single component system.

3. Unlimited Pot Life. A hot melt adhesive is activated for use (melted) by raising its temperature to a predefined level. Should the adhesive cool, it can be reactivated by raising its temperature again.
4. Short Cure Time. "Cure" is actually a misnomer when discussing a hot melt adhesive. The adhesive regains its solid characteristics as soon as it returns to room temperature. Thus, "curing" is just "cooling."
5. Connector Preloading. Since a hot melt adhesive can be melted then cooled to its solid state several times without affecting its physical properties, it can be injected as a liquid into a fiber optic connector and allowed to cool within the connector. The connector can then be packaged and stored, awaiting the time when it can be installed by simply heating the entire connector to the appropriate temperature and inserting the optical fiber through the re-liquified adhesive.

### Critical Parameters<sup>1</sup>

Although the aforementioned advantages are true for all hot melt adhesives, not all hot melt adhesives can be successfully used to terminate fiber optic connectors. Several key parameters must be specifically tailored in order to ensure success. These include:

1. Bare Fiber Adhesion. The adhesive must bond the optical fiber securely to the connector to ensure that the fiber does not slide relative to the connector, thereby degrading the optical performance.
2. Adhesive Hardness. In its solid state, the adhesive must be quite hard. High hardness enables the adhesive to wear away cleanly, while supporting the optical fiber during the connector polishing process.
3. Adhesive Viscosity. At its installation temperature, the adhesive's viscosity must be low enough to permit easy insertion of the optical fiber into the connector.
4. Cable Retention. The adhesive must bond the connector firmly to the fiber optic cable.
5. Temperature Cycling Range. The adhesive must

provide stable optical performance over a pre-determined temperature range.

**Table 1** lists each of these five parameters along with initial requirements and results achieved. In each case, the final adhesive formulation met or surpassed the initial requirements. In the case of Cable Retention, the specified requirement was achieved without the need to crimp the connector to the cable. Thus, the connectorization process was simplified even further.

**Hot Melt System Parameters**

Parameter	Requirement	Results Achieved
Bare Fiber Adhesion	>1000 psi. Shear	>1400 psi. Shear
Adhesive Hardness	>65 Shore D	68 Shore D @ 22° C.
Adhesive Viscosity	<5000 cp @ 200° C.	1250 cp @ 200° C.
Cable Retention	20 lb. (as per EIA FOTP-6)	20 lb. (as per EIA FOTP-6)
Temperature Cycling Range	-40° to 60° C.	-40° to 60° C.

**Table 1**

#### Developmental Testing

Each of the five parameters listed in **Table 1** was tested repeatedly over the course of the development effort. Of the five, Bare Fiber Adhesion and Temperature Cycling Range proved most challenging to achieve. These two tests will be discussed in detail.

#### Bare Fiber Adhesion

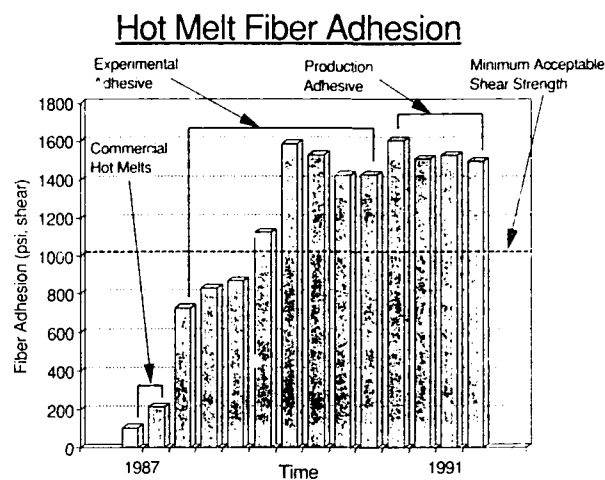
In order for a fiber optic connector to provide stable performance, it must maintain a rigid grasp on the optical fiber it contains. Any pistoning of the fiber within the connector will result in fluctuating power transmission and may even damage or destroy the optical interface. Thus, it is critically important that any means used to secure the fiber to the connector be able to resist the shear forces that fiber pistoning applies.

As indicated in **Table 1**, one requirement for the hot melt adhesive was the ability to resist shear stress up to at least 1000 psi. Initial testing using commercially available hot melt adhesives failed to reach even 250 psi. **Figure 1** shows a chronological listing of selected shear stress tests performed over the course of the hot melt program. By carefully adjusting the formulation of the adhesive to lower its surface energy, thus insuring uniform wetting of the fiber surface, shear stress resistance of over 1400 psi has been obtained.

#### Temperature Cycling Range

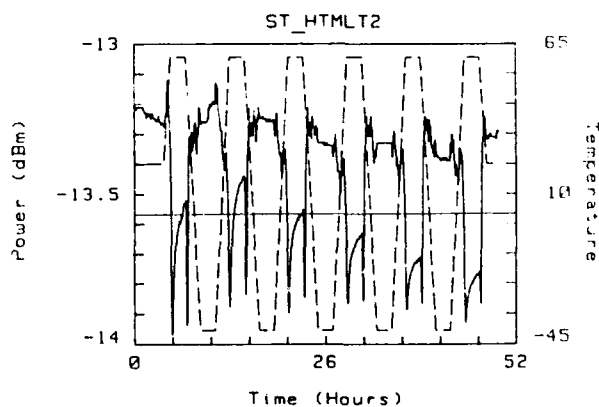
Since the various components of a fiber optic connector have differing coefficients of thermal expansion (CTE), stress will be induced in the connector and the fiber it contains as the connector's temperature changes. Thus, some variation in optical power transmission is bound to occur during temperature excursions. Careful tailoring of the

properties of the hot melt adhesive bonding the fiber to the connector can minimize this variation.



**Figure 1**

**Figure 2** illustrates a typical temperature cycling test performed using a preliminary hot melt formulation in a mated pair of multimode, keyed bayonet style connectors. The dashed, saw-tooth line represents the temperature profile the sample is experiencing. The horizontal line represents the optical loss level the sample must stay above to pass the test, and the jagged line across the center of the chart represents the change in optical loss experienced by the sample during the test. Clearly, the connectors under test were unable to provide the desired stability.



**Figure 2**

**Figure 3** illustrates a typical temperature cycling test performed using the final custom hot melt formulation. There are two noteworthy changes between this test and the test illustrated by **Figure 2**. First, the test measures relative optical power (dB) rather than absolute optical power (dBm). This simply reflects a change in the data logging

software. Second, the temperature profile has been altered slightly in order to conform with Bellcore TR-NWT-000326 requirements<sup>3</sup>. Again, the dashed, saw-tooth line represents the temperature profile the sample is experiencing, the horizontal line represents the optical loss level the sample must stay above to pass the test, and the jagged line across the center of the chart represents the change in optical loss experienced by the sample during the test. The connectors under test exhibit excellent stability, indicating that the hot melt formulation has been successfully tailored to minimize optical power fluctuation during temperature cycling.

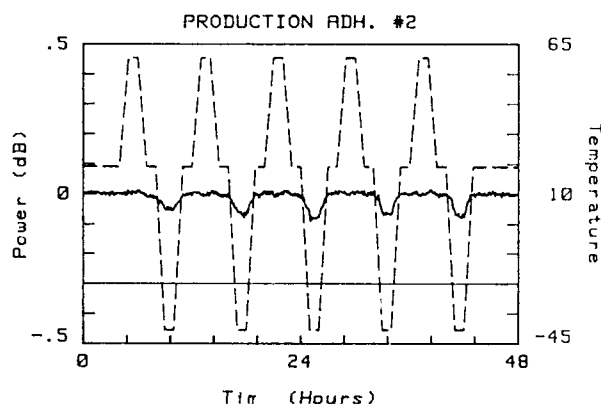


Figure 3

#### Pre-release Testing

Although the critical parameters outlined in the development program had been satisfied, a wide variety of additional testing was required before the hot melt connector system could be released commercially. Table 2 lists these tests as well as the standards on which they were based.

Test	Reference
Environmental Tests-	
Initial Insertion Loss,	EIA RS 455 FOTP 171
High Humidity Aging,	EIA RS 455 FOTP 5
Thermal Shock,	EIA RS 455 FOTP 3
Temperature Cycling.	Bellcore Profile <sup>3</sup> , 10 Cycles, -40°C to 60°C
Physical Integrity Tests-	
Cyclic Flex,	EIA RS 455 FOTP 1
Twist,	EIA RS 455 FOTP 36
Mating Durability,	EIA RS 455 FOTP 21
Cable Retention,	EIA RS 455 FOTP 6
Impact.	EIA RS 455 FOTP 2

Table 2

A detailed explanation of all the pre-release testing listed in Table 2 is available from 3M as a technical report.<sup>2</sup> In brief, the hot melt connector system passed all of the tests listed in Table 2

and was released commercially in the fall of 1990.

#### Extended Testing

After commercial release of the hot melt connector system, additional testing was performed to address specific customer needs and provide additional data on performance of the system under extreme conditions. An example of this testing is a high temperature unmate/remate test performed in March, 1991.

The purpose of this test was to characterize the performance of the hot melt connector when it was remated after extended exposure to elevated temperature in the unmated condition. The test was performed by first subjecting the mated connector to two cycles of -40 degrees C to 60 degrees C temperature cycling to establish a performance baseline, next unmating the connector at room temperature, reheating the unmated connector to high temperature (60 degrees C), holding the connector at that temperature for 90 minutes, and finally remating the connector. Any pistoning of the fiber within the connector during any part of the test would have been evident as a significant increase in optical loss.

Figure 4 illustrates the unmate/remate test described above. The point of interest in this figure is the return of the optical power value to within 0.02 dB of its original value after the connector was remated. This indicates that the fiber remained rigidly fixed within the connector during the test and did not undergo catastrophic pistoning. Tests of this nature serve to reinforce more conventional test results and promote a sense of confidence in the hot melt connector system.

#### Hot Melt Connector Reconnection at 60 Deg. C.

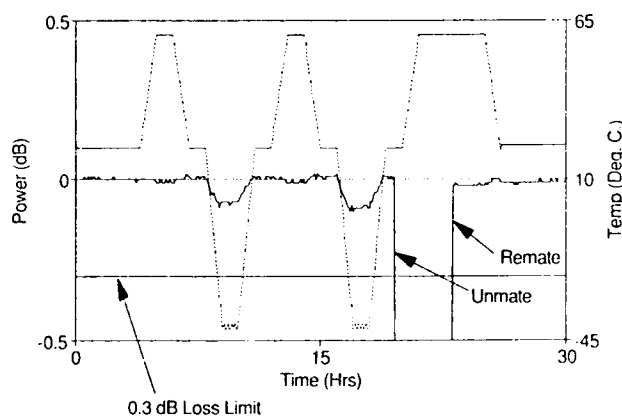


Figure 4

#### Conclusions

A fast, user friendly fiber optic connecting system has been developed based on replacing the epoxy adhesive customarily used to affix the fiber into the connector with a specially formulated hot melt adhesive. Using this system can reduce the time required to install fiber optic connectors, thereby

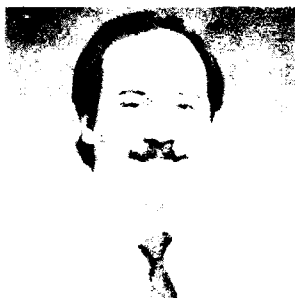
significantly reducing the installed cost. Extensive testing has been conducted which thoroughly demonstrates that the hot melt connecting system is effective, reliable, and well suited for use in LAN applications.

#### Acknowledgments

The author wishes to acknowledge the contributions made by Jim Toonen in developing and fine-tuning the hot melt formulation and Heidi Carlson in performing connector preloading, assembly, and testing.

#### References

- <sup>1</sup> N. A. Lee, "A Fast, Epoxiless Bonding System for Fiber Optic Connectors," SPIE Proceedings, Vol. 1365, 1990, pp.139-143.
- <sup>2</sup> "6100 Hot Melt Connector," 3M Telecom Systems Group, Technical Report #80-6105-8051-8, November 1990.
- <sup>3</sup> "Generic Requirements for Optical Fiber Connectors and Connectorized Jumper Cables," Bell Communications Research, Technical Reference #TR-NWT-000326, Issue 2, March 1991.



Nicholas Lee received a BS in mechanical engineering from the University of Minnesota in 1981, followed by a MS in mechanical engineering from the University of California in 1983. Prior to joining 3M in 1985, he was a member of technical staff at AT&T Bell Laboratories and Bellcore. He is currently a Senior Engineer in the 3M Fiber Optics Laboratory, working on advanced fiber optic connector designs and installation techniques.

Nicholas A. Lee  
3M  
Bldg.260-5B-08, 3M Center  
St. Paul, MN 55144-1000

**AN IMPROVED MEASUREMENT TECHNIQUE**  
**FOR DETERMINATION OF ALL PROPAGATION PARAMETERS**  
**IN BALANCED CABLES**

Jean-Yves GOBLOT

Karine GAUTIER

ACOME BP 45  
50140 – MORTAIN  
FRANCE

**ABSTRACT**

Through recent improvements in network analyzers, it is now easier to measure very precisely the input impedance on balanced cables terminated with an open or a short circuit. The computer, using these data, enables us to easily calculate the secondary parameters: characteristic impedance and propagation constant.

This technique has been utilized to calculate these parameters in both shielded and unshielded cables made of pairs or quads. The results are discussed comparing the calculations with measured results in the frequency range of 50 kHz to 20 MHz.

A comparison is made with those obtained through the use of other well known techniques. Finally, the influence of cable length on this measurement has been studied with the results reported in this paper.

**I. INTRODUCTION**

Today there is an increasing use of balanced cables for Local Area Networks (LAN's) operating in the frequency range of 1 MHz to 16 MHz. It is important to measure precisely, over a wide frequency range, the performance of the cable for:

- A. All propagation parameters
- B. Cross talk, both near and far end
- C. Susceptibility to Electromagnetic Interference

Our work has focused on the determination of the secondary constants of balanced cables, based on the measurement of their open and short circuit input impedance. While this technique is well known for the measurement of characteristic impedance (1), our effort was to determine the components of the propagation constant; attenuation and phase constant. Using the processing capability of a PC, we are able to break down these two components into the primary linear cable parameters, R, L, C, and G.

The purpose of this presentation is to compare the results achieved through direct measurement and with those from our calculations in determining both primary and secondary constants for balanced cables. We also compared our technique with recognized procedures for evaluating telecom cables up to 1 MHz. The last point developed relates to the influence of cable length on measurements and the correlation to cable structure.

**II. DESCRIPTION OF THE SET-UP**

The equipment used in our analysis consisted of a network analyzer manufactured by Hewlett-Packard, Model HP 4195.

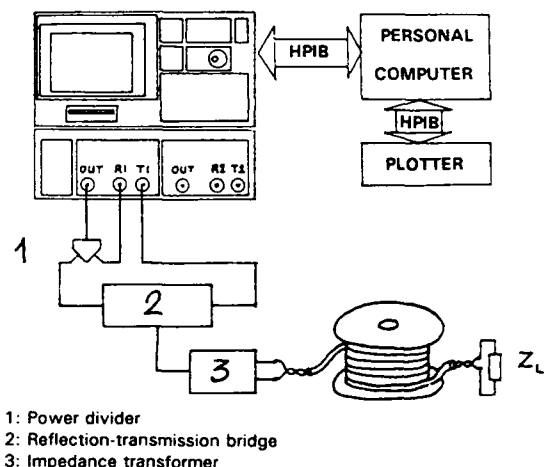


Figure 1 : Set-up description

This equipment has a direct read-out of the magnitude and phase of an impedance load connected to the associated transmission-reflection bridge. The complete measurement technique is schematically represented in Figure 1. It is completely automated through the computer which is equipped with a plotter for a print-out of the results.

The frequency range of the set-up is fixed by the band width of the connected equipment, e.g., from 50 kHz – 100 MHz however only the range 50 kHz – 20 MHz was explored for this paper.

The calibration procedure was conducted on the assembled test set-up including the balanced/unbalanced transformer utilizing three different measurements; open circuit, short circuit, and an impedance load matching the characteristic impedance of the transformer. The resultant information is then stored in the computer memory and can be used repeatedly without deviation in the validity of the calibration.

For the measurement of propagation parameters on a twisted pair, we connect the pair to the transformer and measure first the complex input impedance  $Z_{sc}$  when the other end is loaded with a short circuit and then its complex input impedance  $Z_{oc}$  when the other end is an open circuit.

These test results are then stored in the computer memory.

### III. CALCULATIONS USING $Z_{sc}$ AND $Z_{oc}$

All primary and secondary cable constants are calculated from the two complex impedances,  $Z_{sc}$  and  $Z_{oc}$ . These calculation procedures are well known (2) but have been repeated here for clarification of our work.

#### A. Propagation Parameters

One of the objectives of this technology is to determine the characteristic impedance  $Z_0$  and the propagation constant  $\gamma$  of the pair. This is done by calculation using the well known relations:

$$Z_0^* = \sqrt{Z_{sc}^* \cdot Z_{oc}^*}$$

$$\text{and } \tan h(\gamma \ell) = \sqrt{\frac{Z_{sc}^*}{Z_{oc}^*}}$$

where  $\ell$  represents the length of the cable under measurement.  $\gamma$  is complex, i.e.,  $\gamma = \alpha + j\beta$ .

with  $\alpha =$  real part of  $\gamma$  representing the attenuation of the pair.

$\beta =$  imaginary part of  $\gamma$  representing its phase constant.

$j =$  the complex operator for which  $j^2 = -1$ .

thus,

$$\alpha = \frac{1}{\ell} \cdot R_e \left[ \tan h^{-1} \left[ \sqrt{\frac{Z_{sc}^*}{Z_{oc}^*}} \right] \right]$$

in NEPERS/meter

$$\beta = \frac{1}{\ell} \cdot I_m \left[ \tan h^{-1} \left[ \sqrt{\frac{Z_{sc}^*}{Z_{oc}^*}} \right] \right]$$

in RADIANS/meter

Where  $R_e$  designates "Real part of" and  $I_m$  designates "Imaginary part of".

The propagation velocity  $v$  is also determined from the relation:

$$v = \omega / \beta$$

where  $\omega = 2 \pi f$  is the angular frequency (radians per second) for the frequency  $f$ .

\*: WHERE  $Z_0^*$  IS DEFINED AS THE COMPLEX IMPEDANCE:  $|Z_0|_e^{j\theta}$

#### B. Primary Parameters of a Pair

A pair is characterized by its linear primary parameters which are:

$R =$  Resistance (loop value)  
 $L =$  Inductance  
 $C =$  Capacitance  
 $G =$  Conductance

We can easily calculate the primary parameters knowing the secondary parameters  $Z_0$  and  $\gamma$ . These parameters are associated through the relations:

$$Z_0 = \sqrt{(R + jL\omega) / (G + jC\omega)}$$

$$\text{and } \gamma = \sqrt{\frac{R + jL\omega}{G + jC\omega}}$$

The extraction of  $R$ ,  $L$ ,  $G$ , and  $C$  from these equations gives, finally:

$$R = R_e(Z_0 \cdot \gamma)$$

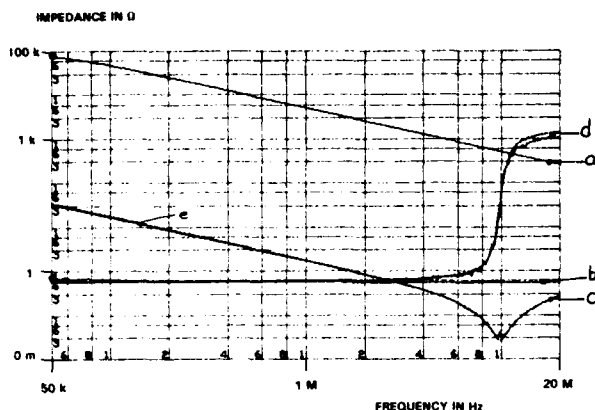
$$L = \frac{1}{\omega} I_m(Z_0 \cdot \gamma)$$

$$G = R_e \left[ \frac{\gamma}{Z_0} \right]$$

$$C = \frac{1}{\omega} I_m \left[ \frac{\gamma}{Z_0} \right]$$

### IV. DYNAMIC RANGE OF THIS MEASUREMENT TECHNIQUE

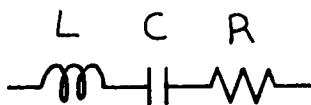
After the calibration performed as described in chapter II, we have measured several capacitors and obtained the results present in Figure 2.



**Figure 2:** Capacitor measurements  
a-b: magnitude and phase for  $C_1 = 32 \text{ pF}$   
c-d:  $C_2$   
e: calculated magnitude of impedance for  $C_2$ :  
Nominal Value of  $C_2 = 100 \text{ nF}$   
Actual Values of  $C_2$  are:  
 $C = 90.4 \text{ nF}$ ;  $L = 2.83 \text{ nH}$ ;  $R = 25.7 \text{ m}\Omega$

For  $C = 32 \text{ pF}$ , we have measured an input impedance at  $50 \text{ kHz}$  of  $100 \text{ k}\Omega$  which is in very good agreement with the calculated value. For higher values of capacitors, we are able to observe the resonance at high frequencies when the impedance due to the capacitive contribution is very small and the inductive contribution predominates.

This behavior is in complete accordance with the calculated curve obtained with the series equivalent circuit for capacitors given the following scheme:



An example illustrated by *Figure 2*, assuming a capacitor of  $100 \text{ nF}$ : Curve c is the measured curve and curve e is calculated with  $C = 90.4 \text{ nF}$ ;  $L = 2.83 \text{ nH}$ ; and  $R = 25.7 \text{ m}\Omega$ . There is a very close correlation over the entire frequency range.

In conclusion, we can measure input impedance from a value as low as  $50 \text{ m}\Omega$  up to  $50 \text{ k}\Omega$ .

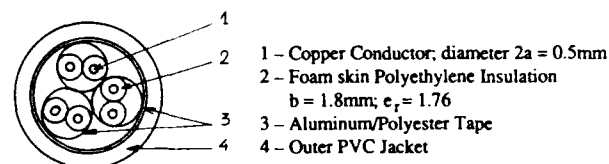
## V. COMPARISON OF MEASURED DATA AND THEORETICAL CALCULATION

A large number of balanced cables including individually shielded pairs & quads, overall shielded and unshielded cores, have been measured using the technique described in this paper.

All of the results are plotted for the frequency range  $50 \text{ kHz}$  to  $20 \text{ MHz}$  and compared with calculated values. These calculations are based on the precise determination of the primary parameters,  $R$ ,  $L$ ,  $C$ , and  $G$ . They take into account the proximity effect inside the pair itself as well as the influence of other conductors near the pair which may act as a shield.

The most difficult task is to determine the radius of this shield which is assumed to be cylindrical. The comparison between calculated and measured data permits us the precise evaluation of this parameter for a given structure.

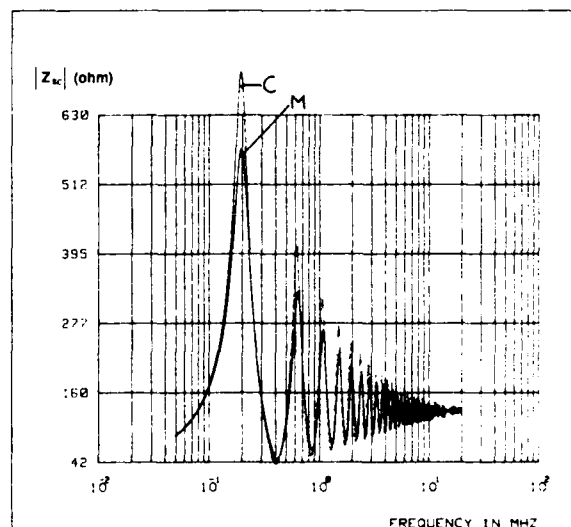
As a first example, we focused our attention on cable #1 represented schematically in *Figure 3*:



**Figure 3** Cable 1 structure

The length of the sample was  $250 \text{ m}$ .

As the shield is very close to the pair, we have taken for its diameter  $2a_2 = 3.4 \text{ mm}$ . That means that it is equivalent to a tube with a smaller diameter than the outer diameter of the pair.



**Figure 4** : Short-circuit input impedance on cable 1

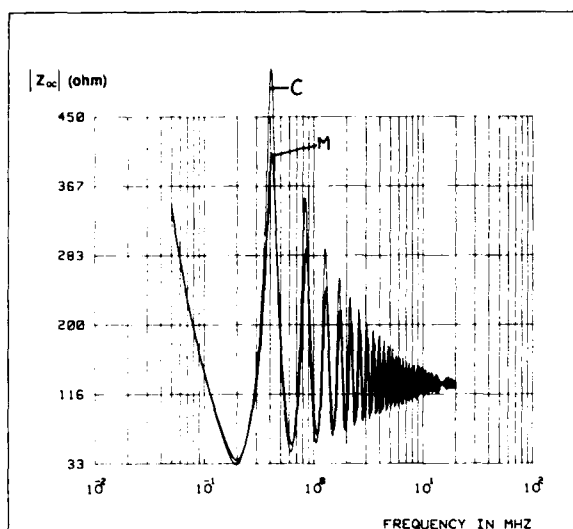


Figure 5 : Open-circuit input impedance on cable 1

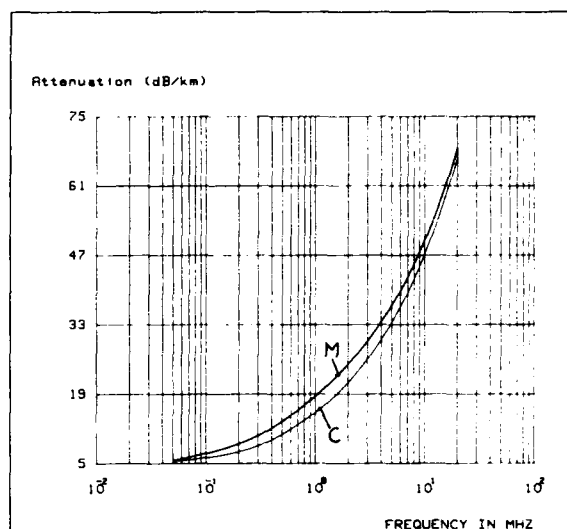


Figure 7 : Cable 1 attenuation

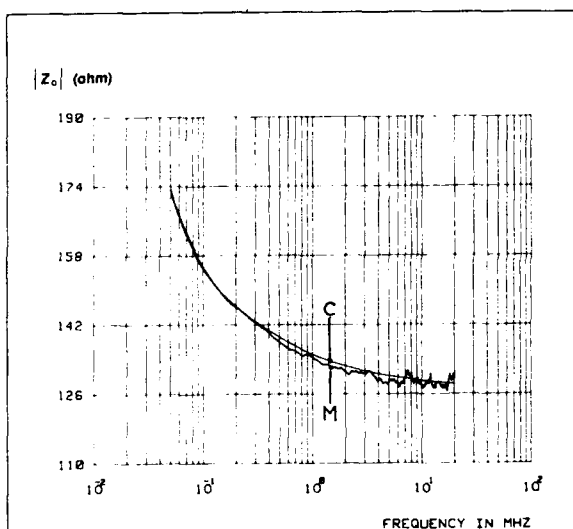


Figure 6 : Cable 1 characteristic impedance

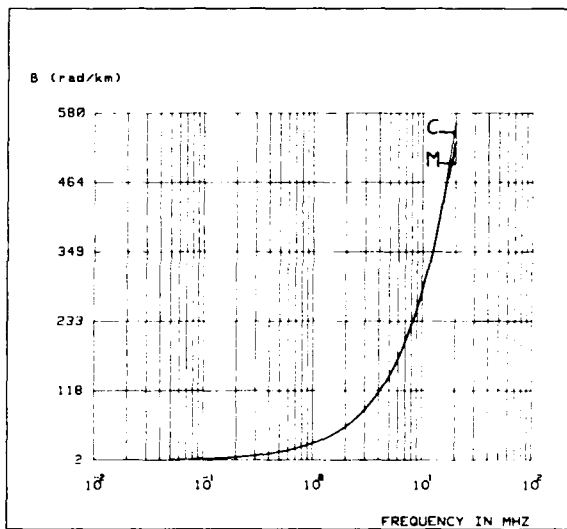


Figure 8 : Cable 1 propagation phase constant



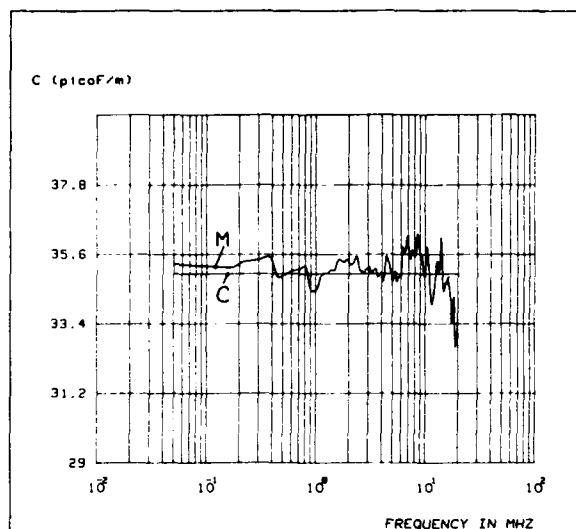


Figure 9 : Cable 1 capacitance

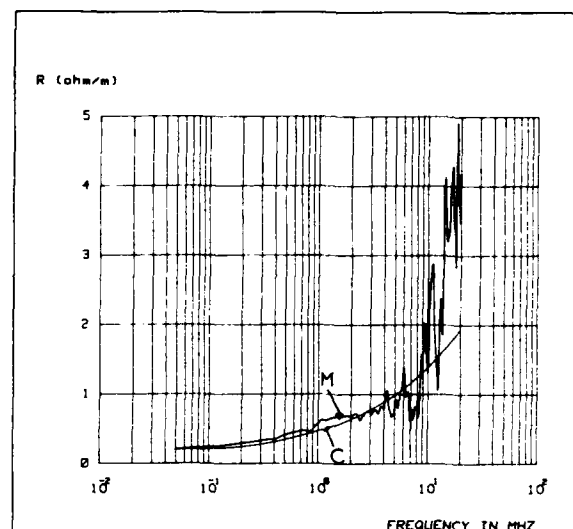


Figure 11 : Cable 1 resistance

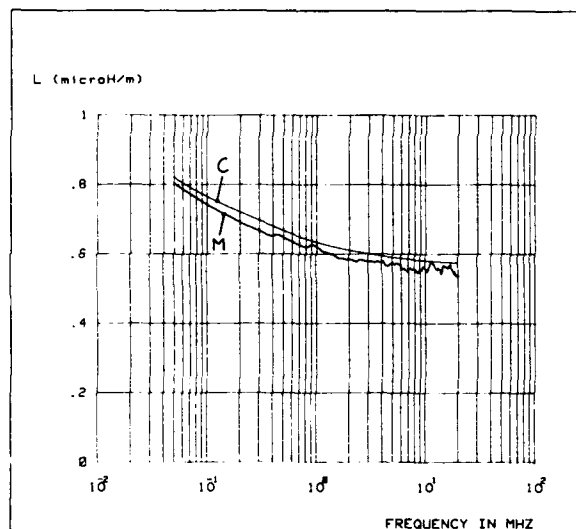


Figure 10 : Cable 1 inductance

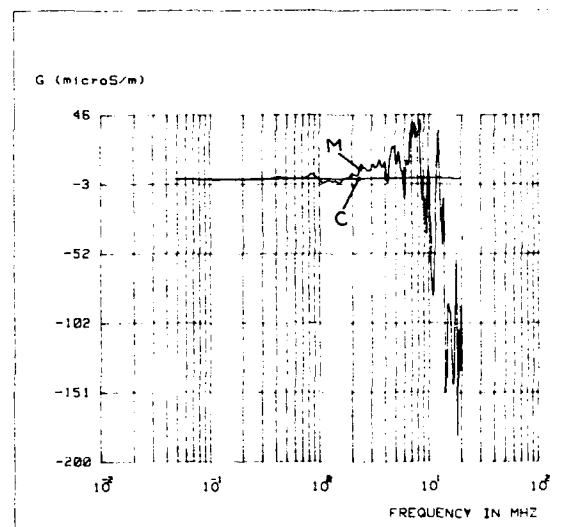


Figure 12 : Cable 1 conductance

Figures 4 to 12 show the comparison between measured data (curve M) and calculated data (curve C) for input impedance for short circuit  $Z_{sc}$ , input impedance for open circuit  $Z_{oc}$ , characteristic impedance  $Z_0$ , propagation  $\beta$ , attenuation  $\alpha$ , capacitance C, inductance L, resistance R and conductance G.

The agreement between curves M and C for  $\beta$  and  $Z_0$  is excellent.

The small difference for capacitance and inductance (1% on C value and 2% on L value) could be explained by small variations in the diameter of insulated elements.

The main difference is in the attenuation, especially above 100 kHz where our calculation is less than the measured result by about 3 dB/km up to 20 MHz. This point is not clearly understood today, it could be due to the shield which is very close to the pair in this particular structure. As a consequence, the predicted maxima and minima for  $Z_{oc}$  and  $Z_{sc}$  differ slightly from the measured values, but their position is determined with great accuracy.

Another important point to notice is the small oscillations around the mean value of  $Z_0$ . When the cable structure is well defined as in the case of cable #1, these oscillations are mainly due to the imprecision in the phase measurement on  $Z_{oc}$  and  $Z_{sc}$  around  $0^\circ$  and the great number of phase rotations when we go further in frequency. It looks like noise. If  $\theta_{sc}$ ,  $\theta_{oc}$  represent the angle of  $Z_{sc}$  and  $Z_{oc}$  respectively, then the angle of  $Z_0$  ( $\theta_0$ ) is defined as:

$$\theta_0 = 1/2 (\theta_{sc} + \theta_{oc})$$

so it is the sum of two components which oscillates around  $0^\circ$  with a large imprecision which is doubled for  $Z_0$ . In order to avoid this phenomenon,  $Z_0$  angle could be smoothed. This work will be done in the future.

A second cable (cable #2) without shield (Figure 13) was retained for this study and compared with this theory.

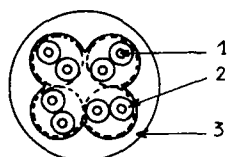


Figure 13 : Cable 2 structure

- 1 - Copper conductor, diameter  $2a = 0.6\text{mm}$
- 2 - PE insulation; diameter  $b = 0.96\text{mm}$
- 3 - PVC jacket

For the purpose of this paper, only  $Z_0$ ,  $\alpha$  and  $\beta$  have been drawn on Figures 14 to 16 and compared with theory.

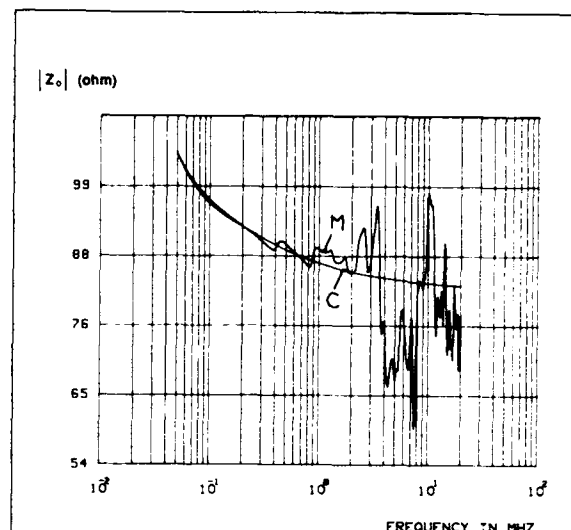


Figure 14 : Cable 2 characteristic impedance

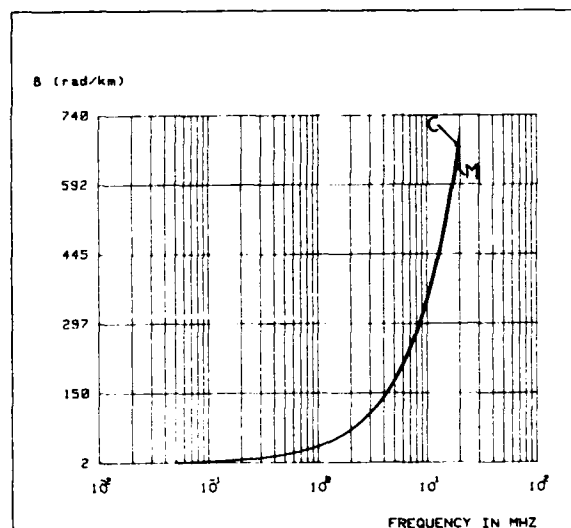


Figure 15: Cable 2 propagation phase constant

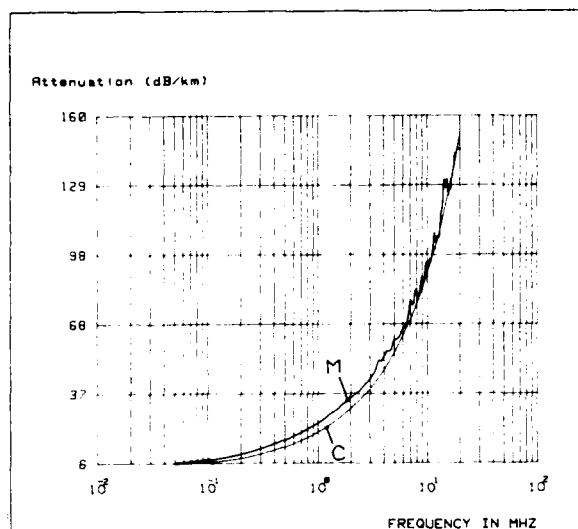


Figure 16 : Cable 2 attenuation

The phase constant is also very well predicted assuming a relative permittivity  $\epsilon_r = 2.6$ . The jacket was pressure extruded and a small quantity of PVC fills the space around the pair, modifying the dielectric environment and explains the higher value of  $\epsilon_r$  found. For PE ( $\epsilon_r = 2.34$ ).

The attenuation curve (Figure 15) is calculated in the case of an unshielded cable. It takes into account the radiated losses. We assume that they act as a resistance and this contribution is proportional to the frequency. The proportionality constant is then adjusted by trial and error and we have to determine in the future the correlation between this parameter and the cable structure which is not known today.

$Z_0$  curve is somewhat more difficult to interpret: cable #1 has been designed for telecommunication at voice frequency and not for high frequency transmission. The predicted behavior is quite good, but very strong variations modify the measured curve at high frequencies.

As no special care has been exercised for the production of the twisted pairs, these variations could be correlated to imprecision and imperfections occurring during the fabrication. This technique is therefore valuable to the cable manufacturer because it may be used to monitor the production and to spot opportunities to improve product quality.

A third cable (cable #3) is also studied here. It is made with 2 quads as illustrated on Figure 17 and has an overall shield.

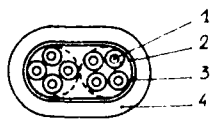


Figure 17 Cable 3 structure

1. Copper conductor; radius  $2a = 0.6\text{mm}$
2. Foam skin PE insulation diameter  $b = 1.2\text{mm}$ ;  $\epsilon_r = 1.72$
3. Aluminum / Polyester shield
4. Halogen free jacket

$Z_0$ ,  $\alpha$  and  $\beta$  curves are plotted on Figures 18 to 20.  $\beta$  matches the calculation as closely as for cable #1 and #2. The measured impedance shows little variations around its average value. These could be attributed to lack of homogeneity encountered in the quad fabrication process. For attenuation a difference of about 3 dB/km is also observed between 1 MHz and 20 MHz, starting about 50 kHz.

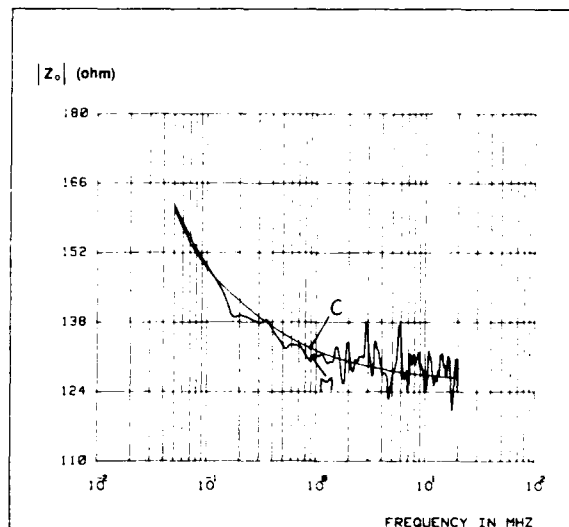


Figure 18 : Cable 3 characteristic impedance

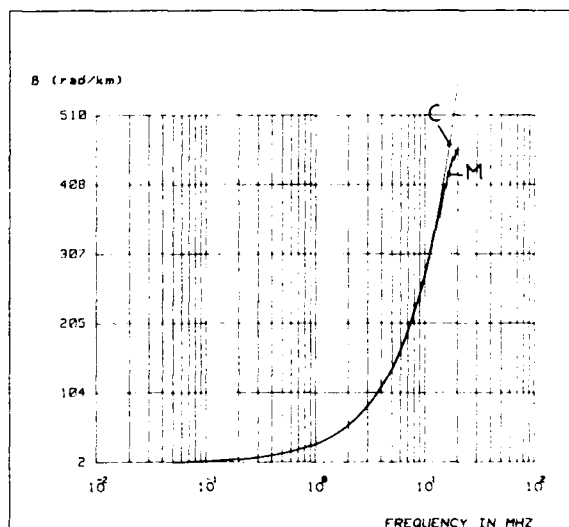


Figure 19: Cable 3 propagation phase constant

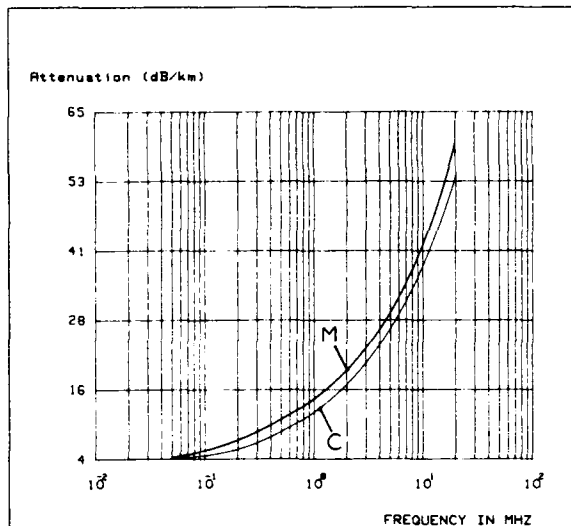


Figure 20 : Cable 3 attenuation

In conclusion, this measurement technique provides very reliable results on the primary and secondary parameters of shielded or unshielded pairs or quads. This behavior is well predicted by calculation except for attenuation of shielded cable where we have to analyze more thoroughly the effect of the physical structure of these cables in order to explain the difference observed here.

## VI. INFLUENCE OF LENGTH

This study has taken into account the influence of the length of the same cable (#1) on the results given by the  $Z_{oc}$  and  $Z_{sc}$  technique. The lengths used for this purpose vary from 10m to 1000m and for clarity, we present here only  $Z_0$  and  $\alpha$  on Figures 21 & 22. There are no differences in the attenuation curves of the entire frequency range except for the curve #4 (length  $l = 1000m$ ) where the dynamic range of our set-up is insufficient for precise measurement above 1 MHz.

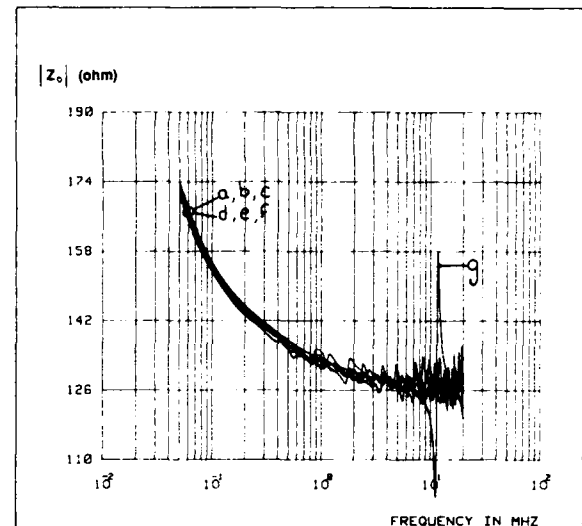


Figure 21 : Influence of the cable 1 length or  $Z_0$   
 $a = 1000$  m ;  $b = 500$  m ;  $c = 250$  m ;  $d = 125$  m  
 $e = 94$  m ;  $f = 62$  m ;  $g = 10$  m

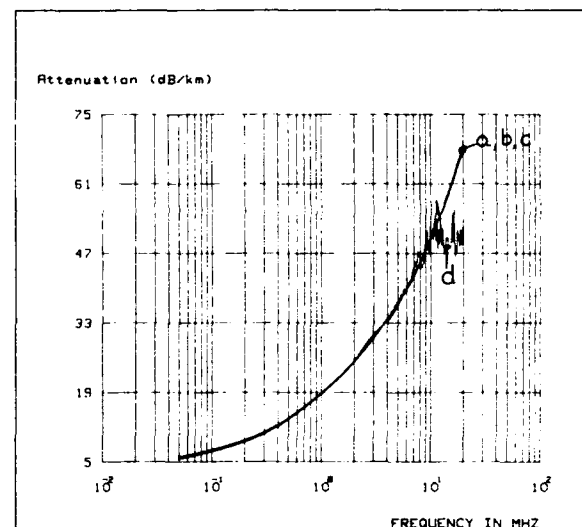


Figure 22 : Influence of cable 1 length on attenuation  
 $a = 10$  m ;  $b = 94$  m ;  $c = 500$  m ;  $d = 1000$  m

In case of  $Z_0$ , all the curves have the identical average value. Only small oscillations appear and they start at lower frequencies as the length increases. As seen earlier, they are mainly due to imprecisions in the phase measurement of  $Z_{sc}$  and  $Z_{oc}$ .

In conclusion, for a well defined structure,  $Z_0$  and  $\gamma$  obtained with the  $Z_{sc}$ ,  $Z_{oc}$  technique are independent of cable length.

## VII. COMPARISON WITH OTHER MEASUREMENT TECHNIQUES

Capacitance is an important parameter specified at 800 Hz on telecom cables. We can see in *Table 1* that this value is in complete agreement with the average value obtained by our new method and also with the calculated one.

**TABLE I**  
**CAPACITANCE C**

	Measured by a Cap Bridge @ 800 Hz	$Z_{sc}, Z_{oc}$ Technique
CABLE #1	35.3 pF/m	35.0 pF/m
CABLE #2	35.0 pF/m	35.3 pF/m
CABLE #3	70.8 pF/m	68.0 pF/m

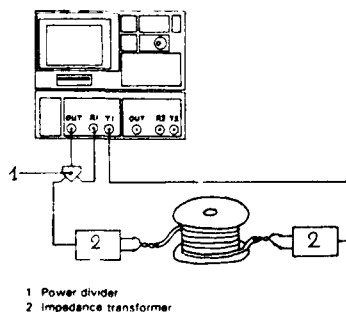
**TABLE II**

**CHARACTERISTIC IMPEDANCE,  $Z_0$  FOR CABLE #1**

FREQUENCY	50 kHz	100 kHz	500 kHz	1 MHz
R, L, C, G BRIDGE ON A CABLE LENGTH OF 10m	173 $\Omega$	155 $\Omega$	137 $\Omega$	133 $\Omega$
$Z_{sc}, Z_{oc}$ TECHNIQUE ON A CABLE LENGTH OF 10m	173 $\Omega$	156 $\Omega$	137 $\Omega$	133 $\Omega$
$Z_{sc}, Z_{oc}$ TECHNIQUE ON A CABLE LENGTH OF 250m	172 $\Omega$	154 $\Omega$	137 $\Omega$	135 $\Omega$

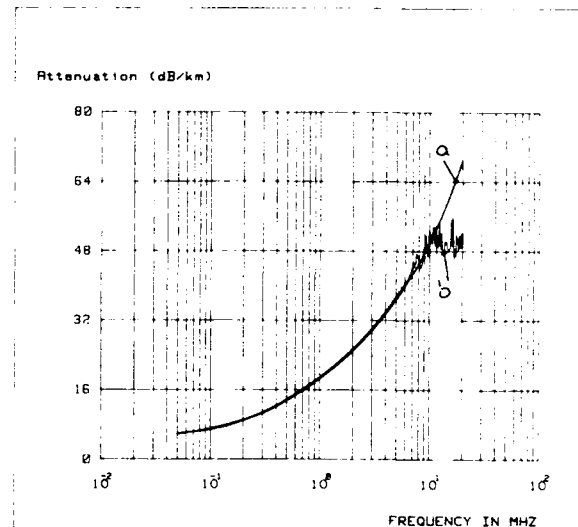
Until recently, we have measured characteristic impedance with R, L, G, and C bridges on very short lengths (typically about 10m) and for frequencies below 1 MHz. We have also reported in *Table I* the two different values of  $Z_0$  for the cable #1 for several frequencies in the range 50 kHz – 1 MHz, that are similar within 1%.

The last comparison made is relative to the attenuation. It is normally measured by the insertion loss technique meaning that the cable is put between two impedance matching transformers as represented in *Figure 23*.



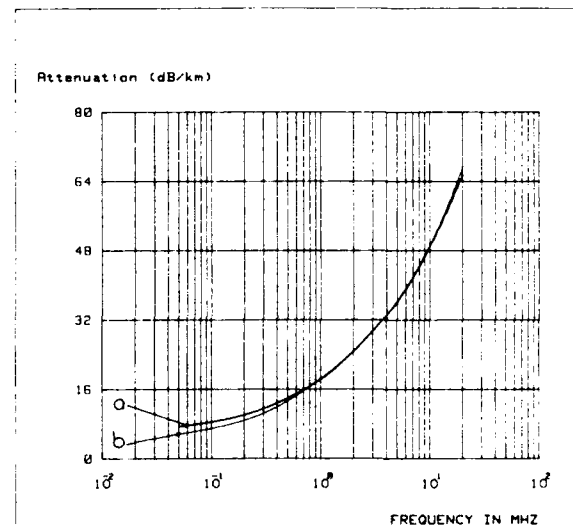
**Figure 23** Insertion technique description for attenuation measurement

We can see from *Figure 24* that for a length of 1000m, the curve obtained with this technique is the same as measured by the  $Z_{sc}, Z_{oc}$  technique. Above 10 MHz the measurement is in error because it is outside the dynamic range of the network analyzer.



**Figure 24** : Comparison between attenuation measured by the insertion technique (curve a) and by  $Z_{sc}-Z_{oc}$  technique (curve b) ; cable 1 length = 1000 m

If we look to the next figure (*Figure 24bis*) for the same cable with a length of 62 m, the two curves differ slightly in the range 50 kHz – 1 MHz.



**Figure 24bis** : Comparison between attenuation measured by the insertion technique (curve a) and by  $Z_{sc}-Z_{oc}$  technique (curve b) ; cable 1 length = 62 m

This length is very small compared with the wavelength of a 100 kHz signal ( $\lambda = 2250$  m for a propagation velocity of 75% of light) and we have to take care of the practical configuration of the set-up in this case. An equivalent circuit could be represented as in Figure 25.

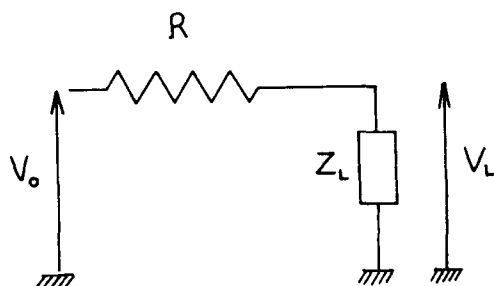


Figure 25 : Low frequency equivalent circuit

$R$  is the resistance of one conductor on the length  $l$  of cable and  $Z_L$  is the impedance of the transformer. With this simple scheme, the attenuation:

$$\alpha = 20 \log \frac{V_L}{V_o}$$

is then written as:

$$\alpha = 20 \log \frac{Z_L}{Z_L + R} \text{ (dB)}$$

The calculation has been done for cable #1 at 10 kHz for several lengths from 62 m to 1000 m. Table III summarizes the results and Figure 26 shows the influence of the length on the attenuation measurement made with the insertion loss technique (the expected value on this cable at 10 kHz calculated in the case of an infinite length is 3.81 dB/km).

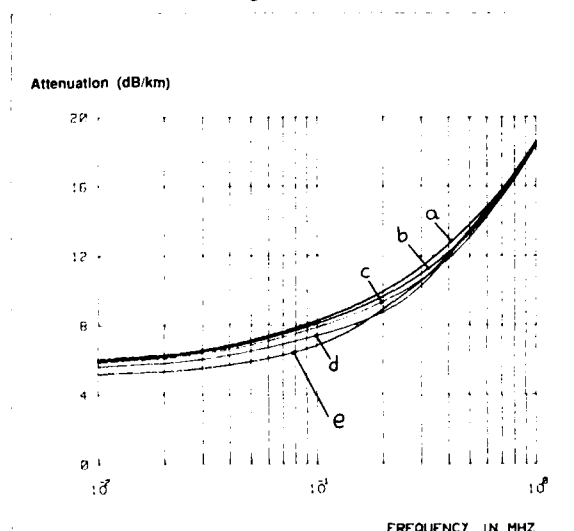


Figure 26 : Influence of cable 1 length on attenuation measured by insertion technique  
a = 62 m ; b = 94 m ; c = 125 m ; d = 250 m  
e = 500 m

They are in complete accord with the prediction which means:

- A.  $\alpha$  for low frequency is determined by the continuous equivalent circuit.
- B. For frequencies above 1 MHz, if the length of cable is always greater than  $\lambda/10$ , the results given by the insertion loss technique and the  $Z_{sc}$ ,  $Z_{oc}$  technique are the same.
- C. Between 10 kHz and 1 MHz, the length influences the attenuation of the cable measured by the insertion loss technique.

TABLE III

TRANSFORMER IMPEDANCE  $Z_L = 124\Omega$

LENGTH (m)	CONTINUOUS RESISTANCE IN $\Omega$ OF ONE CDR (RADIUS) = 0.25 mm	$ \alpha^1 $ (dB)	MEASURED ATTENUATION @ 10 kHz FOR THE LENGTH $l$ (dB)
62	5.43	0.372	0.371
94	8.23	0.558	0.555
125	10.90	0.734	0.735
250	21.90	1.410	1.410
500	43.80	2.630	2.600
1000	87.50	4.640	4.600

$$|\alpha^1| = 20 \log \left[ \frac{Z_L}{Z_L + R} \right]$$

## CONCLUSION

We have demonstrated that measurements of input impedance on twisted pairs or quads terminated respectively with a short or an open circuit are now very easy to obtain and produce precise values.

The two parameters,  $Z_{sc}$  and  $Z_{oc}$  are sufficient to characterize totally all of the propagation parameters of the balanced pair and yield by calculation with great accuracy the secondary constants  $Z_o$  and  $\gamma$  as well as primary constants,  $R$ ,  $L$ ,  $C$ , and  $G$ . The time needed for this operation is very short and proves that the technique described in this paper is suitable for production cable testing. We are now working on the complete integration of this technique in an automated set-up which can address multiple pairs or quads.

This will be designed for measurements in the frequency range up to 20 MHz. A further step in our research laboratory is to evaluate this technique for frequencies as high as 125 MHz needed for a CDDI network using copper cables.

## **REFERENCES**

- (1.) H. W. FRIESEN "An improved characteristic impedance measurement technique" 39th International Wire & Cable Symposium, November 1990, pp 608-617.
- (2.) P. M. PRACHE; H. JANNES; M. TROUBLE; G. CLAVAUD "Cours de lignes a grande distance" EYROLLES.

## **BIOGRAPHIES**



Jean-Yves GOBLOT was awarded his PH.D. from INSA de RENNES in FRANCE in 1984. His first position was as a researcher in organic chemistry of conductive materials for "Centre National d Etudes des Telecommunications". He joined ACOME in 1986 and is now responsible for the development of new electrical measurement techniques on copper cable and also for research in the area of plastic optical fibers.



Karine GAUTIER who is a technician in physics measurement techniques graduated from IUT de CAEN in FRANCE. She joined ACOME in 1989 where she is presently working on electrical measurements.

# AN ASSESSMENT OF MEASUREMENT ERROR ASSOCIATED WITH CLIP-ON POWER METERS ON PRIMARY COATED FIBRE

D A Ferguson, S M James, D Drouet, S M Dennis

BT Labs, Martlesham Heath, Ipswich, Suffolk, IP5 7RE, UK

## 1. ABSTRACT

Clip-on Optical Power Meters<sup>1</sup> have been developed for use in BT's Local Loop Optical Fibre Trial<sup>2</sup> (LLOFT). These devices, which clip-on to primary coated single-mode fibre, offer an alternative to conventional *end-on* power measurements by measuring the signal which escapes from a small bend enforced in the fibre. This measurement technique provides non-intrusive live fibre maintenance, allowing the optical loss of the fibre network to be monitored without disruption to customer services.

The accuracy of these devices is compromised by the variability of certain fibre characteristics. Although this fibre dependent error can be eliminated by calibrating the fibre network during installation, it is important that it is reliably quantified so that the feasibility of clip-on maintenance of uncalibrated fibre networks can be assessed.

In this poster clip-on power meter measurements of coloured and uncoloured fibres are used to analyse errors due to bend loss performance and diversity of primary coatings. Further measurements are carried out using a clip-on test-bed, providing a more accurate assessment of the error due to primary coating variability.

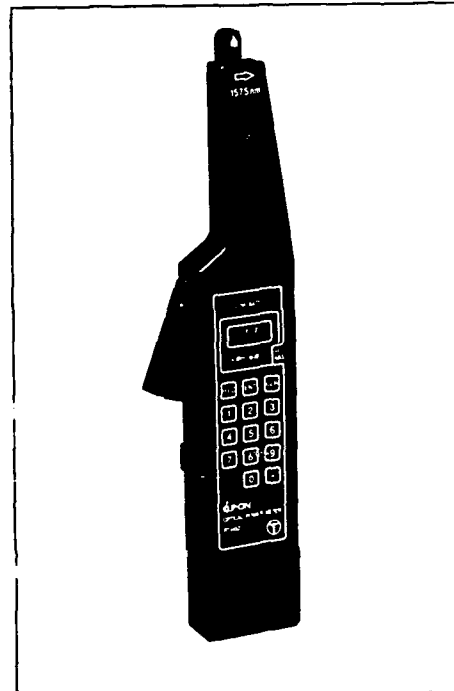


Figure 1. Clip-on optical power meter

## 2. CLIP-ON OPTICAL POWER METER

- Hand held Optical Power Meter (figure 1).
- Clips on to fibre to measure optical power extracted from small bend.
- two types: intrusive and non-intrusive (figure 2).
- Non-intrusive head has small insertion loss - allows measurements on live fibre without disruption to customer.
- Intrusive head has high insertion loss - not suitable for use on fibre carrying traffic, but is insensitive to fibre bend loss variation.
- can be used on optical networks such as the passive optical networks in BT's LLOFT trial in the UK<sup>2</sup> for point to point loss measurements, fibre splitter performance verification and fibre fault diagnosis.

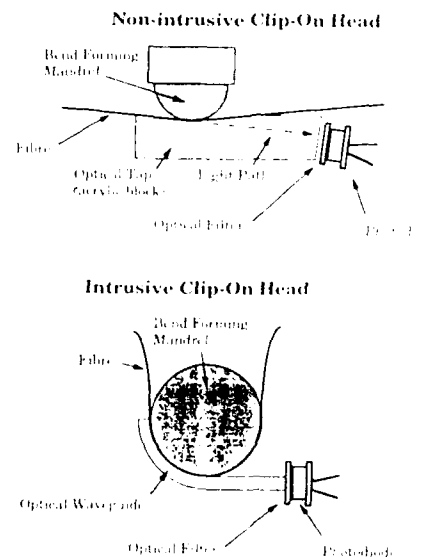


Figure 2. Clip on Power Meter Optical Heads



	Intrusive power meter	Non-intrusive power meter
Dynamic range	0 dBm to -45 dBm	0 dBm to -45 dBm
Operating wavelength	1300 nm, 1520 nm	1575 nm
Insertion loss	> 20 dB	≤ 2 dB
Device accuracy*	± 0.2 dB	± 0.2 dB

\* on calibrated fibre

Table 1. Clip-On Power Meter Performance

### 3. CLIP-ON MEASUREMENT ACCURACY

Although repeated measurements at one position on a fibre (table 1) are reproducible to within  $\pm 0.2$  dB of the average value ( $1\sigma$ ), an additional fibre related error ( $\pm 2$ dB) is introduced when measuring different fibres. For the purposes of the LLOFT trial this error is compensated by calibrating each fibre with a calibration number  $k$ .

$$k = P_0 - P_g$$

where  $P_0$  = fibre throughput power  
 $P_g$  = Power detected by waveguide

$k$  combines the collection efficiency of the waveguide with the measurement uncertainty due to bend loss and primary coating variations to provide the true throughput power.

This approach is suitable for the LLOFT trial, since the fibre count is relatively low and well controlled, however future PONs are unlikely to contain calibrated fibre since this practice would be expensive.

### 4. ANALYSIS OF FIBRE VARIATION

It is important to understand impact on clip-on measurement accuracy of variation in the fibre bend performance and primary coating in order to assess the feasibility of clip-on power meters as a fibre maintenance tool.

#### 4.1 Bend Loss

- Varies from fibre to fibre depending on fibre wavelength cut-off ( $\lambda_c$ ) and Mode Field Diameter (MFD) values. The maximum and minimum values of these parameters define the specification box as shown in fig 3. The  $\lambda_c$  and MFD values of all fibres used in this work are also indicated in this diagram.

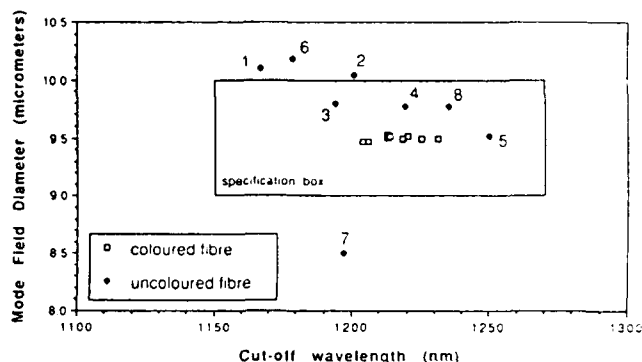


Fig 3. Mode Field Diameter and Cut-off Wavelengths of fibre samples

#### 4.1.1. Measurements

Five uncoloured fibres (labelled #1 - #5) which are distributed across the extent of the fibre specification box have been calibrated for both intrusive and non-intrusive clip-on measurements (figure 4)

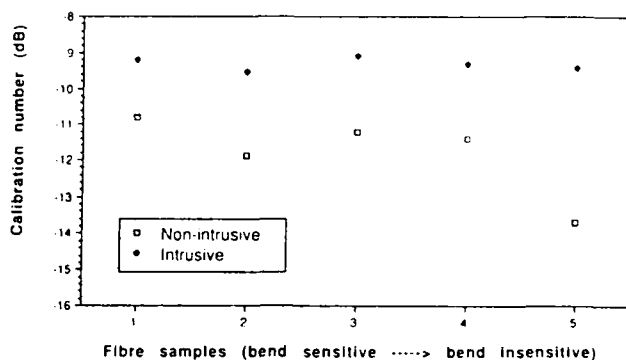


Figure 4. Intrusive and non-intrusive calibration numbers

The range in calibration numbers for each measurement is shown in table 2.

Clip-on power meter	Calibration number range
Intrusive	$\pm 0.25$ dB
Non-intrusive	$\pm 1.50$ dB

Table 2

#### 4.1.2 Conclusion

The influence of fibre bend loss performance on the range of calibration numbers is small for intrusive measurements, but significantly large for non-intrusive measurements.

#### 4.2 Primary coating variations

It is reasonable to anticipate that clip-on measurements may also depend on the nature of the fibre's primary coating, especially if the fibre is coloured. We have used an intrusive clip-on power meter, which we have already shown to be relatively independent of fibre bend loss variation, to assess the range in calibration numbers that can be expected as a result of variations in the primary coating.

##### 4.2.1 Power Meter Measurements

Eight clear and eight coloured fibres (UV cured inks) have been calibrated using an intrusive clip-on power meter. The results are shown in figure 5.

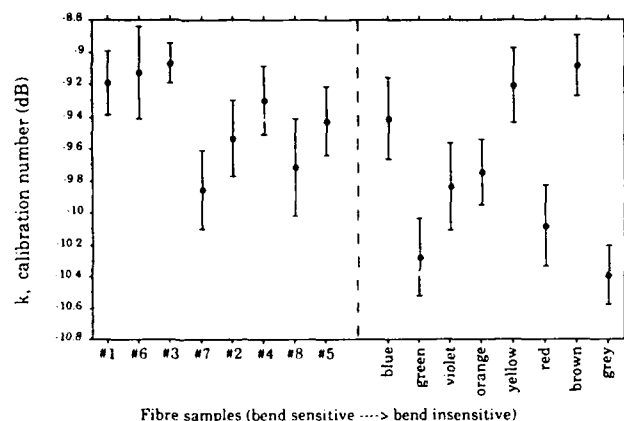


Fig 5. Intrusive power meter fibre measurements.

- Average of 100 measurements at one point on each fibre.
- Error bars =  $\pm 1$  standard deviation

##### 4.2.1.1 Analysis

Measurements on the samples of uncoloured fibres (fig 5) show that there is little correlation between bend loss performance and calibration number since:

- fibres #1, #3 and #6 have almost identical calibration numbers despite having quite different bend loss performances.
- fibre pairs #3 and #7, and #4 and #8 have quite different calibration numbers despite similarities in their bend loss performances.

This evidence is further supported by measurements on coloured fibre (fig 5). Despite having similar bend loss performances, indicated by their position in the specification box (fig 3), the range of calibration numbers for these fibres is almost twice that of the uncoloured fibre samples (table 3).

Fibre type	max cal number	min cal number	difference
clear	9.8 dB	9.1 dB	0.7 dB
coloured	10.4 dB	9.1 dB	1.3 dB

Table 3

##### 4.2.1.2 Conclusion

Since the measurement errors due to bend loss and primary coating performances are independent of each other, the total measurement error due to fibre variability is the sum of the two contributions (table 5).

Power meter	bend loss error	coating error	total error
Intrusive	$\pm 0.25$ dB	$\pm 0.65$ dB	$\pm 0.90$ dB
Non-intrusive	$\pm 1.5$ dB	$\pm 0.65$ dB	$\pm 2.15$ dB

Table 5. Breakdown of error due to fibre variability

#### 4.2.2 Clip-On Test-bed Measurements

In order to quantify the coating performance error more accurately under more controlled conditions a new clip-on test-bed was designed to incorporate improvements to the fibre handling mechanism (figure 6).

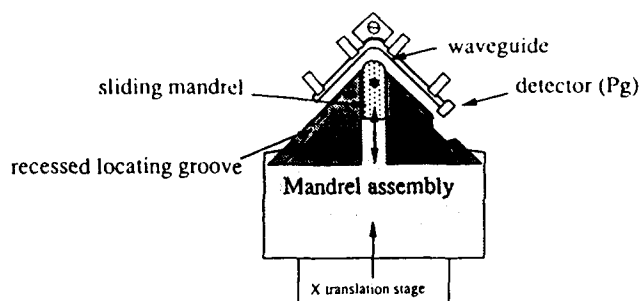


Figure 6. Clip-on Testbed

- Simulates conditions during an intrusive clip-on power measurement.
- Improvements to measurement accuracy by:

- Recessed locating grooves fix height of fibre with respect to the waveguide.
- Accurate control of gap between mandrel and waveguide.

##### 4.2.2.1 Measurement

- A convenient figure of merit describing coating performance variation is the ratio

$$R = \frac{P_g}{P_o - P_i}$$

where  $P_i$  = fibre throughput power before clip-on  
 $P_o$  = fibre throughput power after clip-on  
 $P_g$  = power measured by waveguide

This ratio shall be referred to throughout as the *R-value*.

- Measurement procedure
  - load fibre into mandrel assembly
  - push sliding mandrel forward and secure
  - move mandrel assembly forward on translation stage to establish 220  $\mu$ m gap between mandrel and waveguide.
  - Measure  $P_o$  and  $P_g$  after three minutes.
  - Disengage mandrel assembly, unload fibre and measure  $P_i$

This device was used to measure the R-value of the samples of clear and coloured fibre used previously. In addition, fibre coloured using heat cured inks were also measured for comparison of colouring processes.

The bend loss performance of the fibre samples are shown in figure 7.

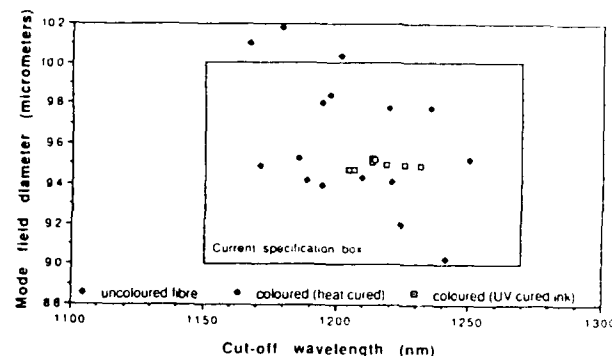


Figure 7. Bend loss performance of coloured fibre

##### 4.2.2.2 Results

Fig 8 shows the R-values for each set of fibres tested, and table 6 compares the R-values of fibres with the same colour from both sets of coloured fibres.

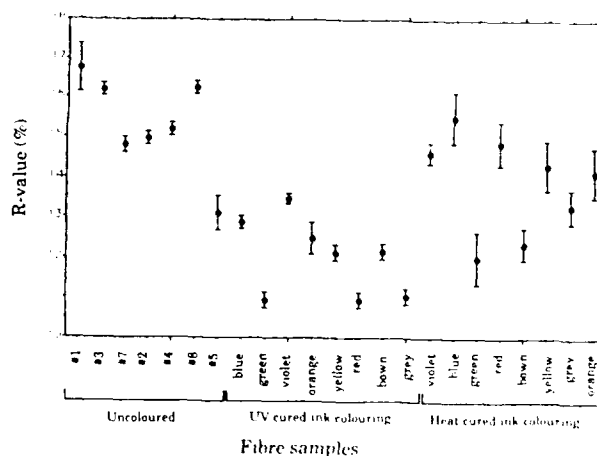


Figure 8. R-values for coloured and uncoloured fibres

colour	UV cured ink	Heat cured ink	full range
red	10.96 %	14.87 %	3.91 %
orange	12.48	14.15	1.67
yellow	12.13	14.31	2.18
green	10.96	12.00	1.04
blue	12.90	15.51	2.61
violet	13.47	14.59	1.12
brown	12.15	12.36	0.21
grey	11.05	13.30	2.25

Table 6

#### 4.2.2.3 Conclusions

- Comparison of measurements on the uncoloured fibre samples using the intrusive power meter and the clip-on test-bed shows that the error in measurement of the coating performance has been improved by a factor of 2.
- Measurements of the uncoloured fibres using the clip-on test-bed demonstrate a small bend loss performance despite the R-value being normalised to the bend loss of the fibre. This indicates that the collection efficiency of the waveguide may not be independent of the fibre bend performance.
- There is no clear relationship between R-values for fibres of the same colour but different ink type *per se*. Since the inks used are chemically quite different this is not unexpected.
- Range of R-values  
Care must be taken when comparing the range of R-values from one fibre set with another since it has been shown that there is a residual bend loss dependence associated with the measurement. However comparison of R-values of the uncoloured fibre set with the heat cured coloured fibre set is valid since these fibres occupy similar sized regions of the specification box. Our results show that the range in R-values is almost twice as large for coloured fibre than for uncoloured.
- Clearly many more measurements on a larger sample of fibres are required before more specific performance trends can be described.

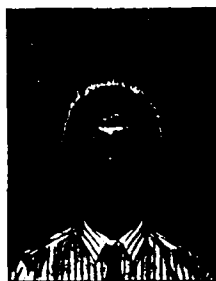
## 5. GENERAL CONCLUSIONS

We have shown that clip-on optical power meters may be used to measure the throughput power of calibrated, coloured or uncoloured primary coated fibre to within an accuracy of  $\pm 0.2$  dB.

Measurements on uncalibrated fibre have a worst case measurement uncertainty of  $\pm 2.15$  dB (non-intrusive measurement). Operationally this level of accuracy may be sufficient for clip-on power meters to be used as maintenance tools, since the majority of faults that occur on fibre have high losses, eg fibre breaks. However more accurate clip-on power measurements are required in order to characterise the optical loss performance of fibre networks. We have shown that fibre calibration allows this level of accuracy to be achieved however it is clear that the diversity of fibre bend performance and primary coating structures may hinder the characterisation of uncalibrated fibre networks using clip-on technology.

## References

- 1 S M James *et al.*, "Clip-ON" - a possible measurement technique for future optical networks. IWCS Nov 1989
- 2 T R Rowbotham, Plans for a British Trial of Fibre to the Home, IEE Conference on Telecommunications, April 1989.



David Ferguson joined BT Labs in 1986 after graduating from Heriot-Watt University, Edinburgh, with a degree in Physics. He presently works in the Access Operations and Maintenance Section on the development of novel optical test equipment for optical fibre networks maintenance.



Simon James joined BT as a trainee technician in 1977. He graduated from Brunel University, London, in 1987 with a degree in Electrical Engineering and moved to BT Labs, engaged in optical test equipment development. He currently leads a group involved in Operations & Maintenance activities for new local network technologies.



Dominik Drouet joined BT Labs in 1979 as a Trainee Technician Apprentice. Following this he joined the Visual Telecommunications Division, working on Still Picture TV systems. In 1987 he moved to the Operations & Maintenance Section where he is now involved in the development of fibre test methods and instruments employing 'clip-on' technology. He has a BTEC Higher National Diploma in Electronics and Communications Engineering.



Simon Dennis joined BT Labs in 1986 as a Trainee Technician Apprentice. In 1989 he joined the Access Networks division where he works on the development of optical test equipment in the Access Operations and Maintenance Section. He has a BTEC Higher National Certificate in Electronics and Telecommunications Engineering.

# THE EFFECT OF PROOF TESTING ON THE MINIMUM STRENGTH OF OPTICAL FIBER

G. S. Glaesemann

Corning Incorporated  
Corning, New York

## Abstract

Flaw growth during the unloading portion of a simulated proof test cycle was measured. Using unloading rates of 400 kpsi/s (2800 MPa/s), failures during unloading were measured as low as 37% of the 400 kpsi (2800 MPa) proof stress. These results, when juxtaposed with well-known proof test theory, demonstrate that the final strength after proof testing is determined solely by the unloading rate. Both theory and experimental results contrast with the common industry practice of relying on the dwell time to establish truncated strength distribution. Unloading rates greater than 10,000 kpsi/s (70,000 MPa/s) are suggested to minimize crack growth during unloading.

## Introduction

Proof testing of glass, ceramic and composite materials is routinely used as a means for limiting the size of the largest flaw. In the case of glass optical fiber, special machines have been created to proof 100% of the fiber length to a predetermined tensile stress. Flaws with strengths below the proof stress are eliminated while those that pass are limited in size. Proofing of glass articles such as optical fiber is complicated by the fact that pre-existing surface flaws exposed to moisture grow subcritically when stressed sufficiently. Thus, in addition to the failure of weak flaws, proofing can stimulate the growth and subsequent failure of flaws that would pass the proof stress if proofing were conducted under inert conditions.

The purpose of this research was to experimentally investigate the consequence of crack growth during proofing. In particular, the effect of the unloading rate during proof testing examined. First a review of published literature on the fundamentals of proof testing of fatigue-susceptible materials is presented.

## Background

Figure 1 schematically illustrates the stress time history of fiber as it passes through the proof test cycle. First the fiber is loaded to the proof stress,  $\sigma_p$ , at a stress rate given by  $\dot{\sigma}_1$  followed a dwell time,  $t_d$ , at a constant stress equal to the proof stress. Finally the fiber is unloaded from the proof stress to essentially zero stress at rate  $\dot{\sigma}_u$ . For the purposes

of this study, the loading and unloading rates are assumed to be constant and the stress is defined as that actually experienced by the glass in the glass/polymer composite. Assuming a fatigue environment during proof testing, flaw growth can occur during all of the three stages sketched in Figure 1.

## Failure During Proofing

Strength degradation for a given applied stress history can be expressed by the well-known damage equation for subcritical crack growth in brittle materials,<sup>1</sup>

$$S_f^{n-2} - S_i^{n-2} = -\frac{1}{B} \int \sigma(t)^n dt \quad (1)$$

where  $\sigma$  is the stress applied to the fiber whether it be a dynamic, static, or cyclic loading with time,  $S_i$  is the initial strength at the beginning of the test,  $t = 0$ , and  $S_f$  is the final strength for the stress history. The constants  $n$  and  $B$  are crack growth parameters. Equation (1) has been applied to the various components of proof testing.<sup>1</sup>

**Failure during loading:** Failure during the loading portion of the proof stress is similar to failures during dynamic fatigue testing where fibers are loaded at constant stressing rate until failure. For dynamic loading, the stress during loading,  $\sigma(t)$  in Eq. (1), is given by  $\dot{\sigma}_1 t$  and the upper limit of integration is  $t = \sigma_p / \dot{\sigma}_1$ . Integrating Eq. (1) for this condition gives the equation for the final strength,  $S_f = \sigma_f$ .

$$\sigma_f^{n-2} = S_i^{n-2} - \frac{\sigma_p^{n+1}}{B(n+1)\dot{\sigma}_1} \quad (2)$$

Curve a in Figure 2 gives a schematic representation of strength degradation to failure during the loading portion of the proof test cycle. Note from Eq. (1), that strength degradation is reduced by increasing the loading rate.

**Failure during dwell time:** In this case the fiber passes the loading portion but fails at the proof stress,  $S_f = \sigma_p$ , as shown by curve b in Figure 2. The upper limit of integration in Eq. (1) is  $t = \sigma_p / \dot{\sigma}_1 + t_d$ , where failure occurs at  $t_d$  into the dwell time. Completing the integration yields,

$$\sigma_p^{n-2} = S_i^{n-2} - \frac{1}{B} \left[ \frac{\sigma_p^{n+1}}{(n+1)\dot{\sigma}_1} + \sigma_p^n t_d \right] \quad (3)$$

Thus, a flaw with an initial strength greater than the proof stress grows and subsequently fails during the dwell time. Note that it is impossible for flaws to grow during the dwell time to a final strength below the proof stress, and that the

minimum final strength is exactly equal to the proof stress. Even though this statement seems elementary, it becomes obvious that the dwell time plays virtually no role in establishing the minimum strength. From Eq. (3) the final strength,  $S_f = \sigma_p$ , is independent of when in the dwell time,  $t_*$ , failure occurred. The dwell time does, however, contribute to crack growth during the proofing process in that the longer the time  $t_*$ , the greater the initial strength,  $S_i$ , will have to be for failure to occur during the dwell period.

**Failure during unloading:** Unloading cannot be ignored in proof testing since it is another opportunity for flaw growth. The upper limit of integration of Eq. (1) is now  $t = \sigma_p/\dot{\sigma}_l + t_d + (\sigma_p - \sigma_*)/\dot{\sigma}_u$  where  $\sigma_*$  is the stress at failure during unloading as shown schematically by curve c in Figure 2. The failing strength during unloading is then,

$$\sigma_*^{n+2} - \frac{\sigma_p^{n+1}}{B(n+1)\dot{\sigma}_u} = S_i^{n+2} - \frac{1}{B} \left[ \frac{\sigma_p^{n+1}}{(n+1)\dot{\sigma}_l} + \sigma_p^n t_d + \frac{\sigma_p^{n+1}}{(n+1)\dot{\sigma}_u} \right] \quad (4)$$

The strength at failure during proofing then is a culmination of crack growth during loading, dwell, and unloading.

#### Passing the proof test

Flaws that pass the proof stress have a final strength that is affected by all three components of the proof test cycle. The stress cycle now occurs over a total time of  $t = \sigma_p/\dot{\sigma}_l + t_d + \sigma_p/\dot{\sigma}_u$ . Integration of Eq. (1) over the entire proof-test cycle yields the final strength of those fibers that survive the test:

$$S_f^{n+2} = S_i^{n+2} - \frac{1}{B} \left[ \frac{\sigma_p^{n+1}}{(n+1)\dot{\sigma}_l} + \sigma_p^n t_d + \frac{\sigma_p^{n+1}}{(n+1)\dot{\sigma}_u} \right] \quad (5)$$

The schematic representation of strength degradation for flaws that pass the proof test cycle in Eq. (5) is shown by curve d in Figure 2. The most significant observation is that according to Eq. (5), the flaws can grow during unloading from the proof stress and still pass the proof test cycle. Therefore, it is important to reflect on current industry practices for establishing proof test requirements where only dwell time is considered.

Let us continue to focus on the effect of unloading during proofing. If the unloading rate is infinitely fast, the last term on the right side of Eq. (5) is zero, thereby leaving the proof stress during dwell time as the potential opportunity for crack growth during proofing. In this particular case, however, the final strength cannot be less than the proof stress since the flaw can only grow to near the proof stress during dwell with no further means to continue growth after the dwell. Thus, unloading is the only means for the final strength to be less than the proof stress. That is, for proofing in a fatigue environment, the final strength is determined primarily by the amount of crack growth during unloading. The faster the unloading rate, the stronger the fiber will be; similarly, the slower the unloading rate is, the weaker the fiber will be. The only influence the dwell time has on crack growth during unloading is that growth during this period has the potential of increasing the probability of growth during unloading.

Fuller et. al.<sup>1</sup> have discussed the effect of unloading more rigorously than the above treatment. For flaws that pass the

proof test cycle, the flaw with an initial strength such that it just passes the proof stress consequently will have the minimum final strength,  $S_{fmin}$ . This is shown schematically in Figure 3.  $S_{fmin}$  is significant since it is the strength of the largest flaw that survives proofing poses the greatest concern from a reliability point of view. The initial strength of this flaw that just passes the proof test will be denoted by  $S_i^*$ . Similarly, there is a flaw with an initial strength infinitesimally lower than  $S_i^*$  that just fails during unloading. The breaking stress of this flaw therefore is the minimum strength of all flaws that break during unloading and will be denoted by  $\sigma_{*min}$ .

Setting  $S_i = S_i^*$  in Eqs. (4) and (5) and combining the two equations yields the following relationship between the minimum strength after proof testing,  $S_{fmin}$ , and the minimum strength during proofing,  $\sigma_{*min}$ .

$$S_{fmin}^{n+2} = \sigma_{*min}^{n+2} \left[ 1 - \frac{1}{B(n+1)} \left( \frac{\sigma_{*min}^1}{\dot{\sigma}_u} \right) \right] \quad (6)$$

Fuller et al.<sup>1</sup> simplified Eq. (6) by noting that the flaw corresponding to initial strength  $S_i^*$  will come infinitesimally close to touching the unloading portion of the stress curve in Figure 3. The slope of the strength degradation curve,  $dS/dt$ , at its closest point to the unloading portion of the stress curve will be nearly equal to the unloading rate,  $\dot{\sigma}_u$  or  $dS/dt = -\dot{\sigma}_u$ . The following relation for the minimum unloading strength was derived by Fuller et. al.<sup>1</sup>.

$$\sigma_{*min} = [B(n-2)\dot{\sigma}_u]^{1/3} \quad (7)$$

Substitution of Eq. (7) into Eq. (6) yields a simple relation between  $S_{fmin}$  (the minimum strength after proofing),  $\sigma_{*min}$  (minimum strength of the specimen failing during unloading), and  $n$  (crack growth parameter).

$$S_{fmin} = \sigma_{*min} \left( \frac{3}{n+1} \right)^{1/2} \quad (8)$$

or

$$S_{fmin} = [B(n-2)\dot{\sigma}_u]^{1/3} \left( \frac{3}{n+1} \right)^{1/2} \quad (9)$$

From Equation (9), the minimum strength after proofing is determined only by the unloading rate and crack growth parameters. That is to say, the largest flaw surviving proofing does not depend on the dwell time or the loading rate, but is a function of unloading rate only. The higher the unloading rate is, the greater the minimum strength after proofing will be.

Fuller et. al.<sup>1</sup> note that to avoid failure during unloading, one must choose an unloading rate high enough to yield  $\sigma_{*min}$  in Eq. (7) greater than the proof stress,  $\sigma_p$ . To perform this calculation, however, the crack growth parameters  $n$  and  $B$  and the flaw size of interest must be known apriori. In the case of optical fiber, the parameter  $B$  for flaws large enough to just pass a 50 kpsi (350 MPa) proof test is extremely difficult to measure since such flaws are rare. However, given actual data for unloading failures, one can make several qualitative deductions about minimum strength after proofing.

### Experimental Apparatus and Procedure

A simple method for measuring the strength distribution of long fiber lengths was recently developed.<sup>2</sup> The approach taken was to stress the fiber in a continuous fashion such that the small flaws survive, but the large flaws fail. A schematic of the test apparatus is shown in Figure 4 and consists of a proof testing machine and a remote pulley assembly. The pulley assembly consists of a pulley mounted on a load cell, both of which are attached to a pneumatic slide. A complete description of the equipment may be found in reference 2.

The proof tester acts only as a fiber payout machine. Fiber is payed out under low load from the proof tester around the remote pulley assembly and back to the proof tester. A total of 20 meters of fiber is contained between capstans A and B. After the fiber is payed out, the proof tester stops, the pulley assembly moves on the slide, and the fiber is loaded to a predetermined load level. As soon as the maximum load is reached, the pulley unloads the fiber by returning to its original position. The load is carefully monitored during the entire load pulse event. If the fiber passes the load pulse without failing, another 20 meter length is indexed into the gauge length and the load pulse is repeated. Thus, each 20 meter length essentially is subjected to a proof test cycle of loading and unloading (but no dwell), with the maximum preset load being the proof stress.

One hundred kilometers of an unproof-tested 125  $\mu\text{m}$  titania-doped silica-clad developmental fiber was tested in the above manner with a preset maximum fiber stress of 400 kpsi (2800 MPa). The loading and unloading rates were maintained at 400 kpsi/s (2800 MPa/s) and all testing was performed in an ambient environment (20 C, 60% RH).

The typical load pulse is shown in Figure 5 for fiber passing the test. In addition to expected fiber failures during the loading portion of the pulse, 13 unloading failures were recorded. Figures 6a and 6b show examples of failure during loading and unloading, respectively. Unloading strengths,  $\sigma_u$ , ranged from 147 to 384 kpsi (1030 to 2690 MPa) and are summarized in Table I.

### Discussion

It is clear from the data in Table I that flaws in optical fiber can grow during the unloading portion of the proof test cycle in addition to growth during the loading portion and dwell time. Also, unloading failures occur below the proof stress level since the applied stress is always less than the proof stress during unloading. From Eqs. (8) and (9), these results strongly suggest that flaws just passing the proof test cycle have post proof strengths less than the proof stress.

The lowest unloading strength,  $\sigma_u$ , in the 100 kilometers of fiber tested was found to be 147 kpsi (1030 MPa) or 37% of the 400 kpsi (2800 MPa) proof stress. The minimum unloading strength,  $\sigma_{u\min}$  in Eq. (7), for a 400 kpsi/s (2800 MPa) unloading rate, is probably less than 37% of  $\sigma_p$  due to the relatively small sample size. Fuller et. al.<sup>1</sup> have stated that to avoid unloading failures one should choose an unloading rate according to Eq. (7) such that  $\sigma_{u\min} \geq \sigma_p$ . For our test results, we assume  $\sigma_{u\min}$  for  $\sigma_u = 400$  kpsi/s (2800 MPa/s), as 147 kpsi (1030 MPa) and calculate B, for an n of

30, to be 280 kpsi<sup>2</sup>s (13,700 MPa<sup>2</sup>s). Equation (7) is plotted in logarithmic form in Figure 7 where  $\ln \sigma_{u\min}$  is plotted versus  $\ln \sigma_u$  for n = 30 and B = 280 kpsi<sup>2</sup>s (13,700 MPa<sup>2</sup>s). Assuming actual strength degradation during unloading to follow the 1/3 power dependence in Eq. (7) suggests that an unloading rate greater than 7500 kpsi/s (52,500 MPa/s) is needed to avoid unloading failures during our simulated proof test.

From Eq. (8), the minimum strength after proofing,  $S_{\min}$ , is always less than  $\sigma_{u\min}$  by a factor of 0.9 for typical fiber n values of 20 to 30; and therefore, assuming 147 kpsi (1030 MPa) to be close to  $\sigma_{u\min}$  yields  $S_{\min}$  to be  $147 \times 0.9 = 132$  kpsi (930 MPa). Thus, for the simulation of proof testing in this report, the minimum strength of fiber surviving the proof-test cycle is approximately 33% of the 400 kpsi (2800 MPa) proof stress. Fortunately, most modern-day fiber proof testing machines operate at much higher unloading rates and according to Eq. (9), it is unlikely that such low post-proof strengths exist. However, this study highlights the need to focus on the unloading portion of present day proof testers in determining the minimum strength after proofing.

In the particular case where the unloading rate is just fast enough to avoid unloading failures,  $\sigma_{u\min}$  is infinitesimally less than the proof stress,  $\sigma_{u\min} = \sigma_p$ , and therefore,  $S_{\min} = 0.9 \sigma_p$ . Even though unloading failures are avoided in this case, strength degradation still occurs during unloading resulting in a truncation strength,  $S_{\min}$ , slightly less than  $\sigma_p$ . As the unloading rate is increased beyond the rate too fast for unloading failures the truncation strength,  $S_{\min}$ , increases from  $0.9 \sigma_p$  and in the limit approaches the proof stress level at infinite unloading rates. Thus, for two fibers with identical pre-proof strength distributions, the one with the higher unloading rate, i.e., higher machine speed, will have the higher truncated strength.

### Implications

Of a more practical nature is the understanding we can draw from these experiments about proof testing in the fiber manufacturing industry. Loading, dwell, and unloading components all contribute to crack growth during proofing. However, proof testing standards today rely solely on the dwell time to account for crack growth during proofing. The proof-test theory review and data presented in this study demonstrate that the unloading portion of the proof test is responsible for establishing the truncated strength after proofing, and that the faster the unloading rate is, the higher the truncated strength will be. Proper proof testing, therefore, requires the knowledge, the control and proper account of the unloading portion of the proof test cycle. Even though more data are needed, it is estimated that an unloading rate greater than 10,000 kpsi/s (70,000 MPa/s) is required to minimize unloading failures and strength degradation below the proof stress level during unloading of the fiber.



## References

1. E.R. Fuller, Jr., S.M. Wiederhorn, J.E. Ritter, Jr., P.B. Oates, "Proof Testing of Ceramics, Part 2: Theory," J. Mater. Sci., 15, 2282-2295 (1980).
2. G.S. Glaesemann and D.J. Walter, "Method of Obtaining Long-length Strength Distributions for Reliability Prediction," Opt. Eng., 30 (6), 746-748 (1991).

Table 1. Stress at Failure Data During Unloading at 400 kpsi/s from a Maximum Load of 400 kpsi. Data ranked from strongest to weakest.

kpsi	MPa
383	2680
358	2500
347	2430
368	2580
337	2360
331	2320
268	1880
263	1840
189	1320
189	1320
189	1320
157	1100
147	1030

Figure 1.  
Schematic of Stress/Time History for Proof Testing

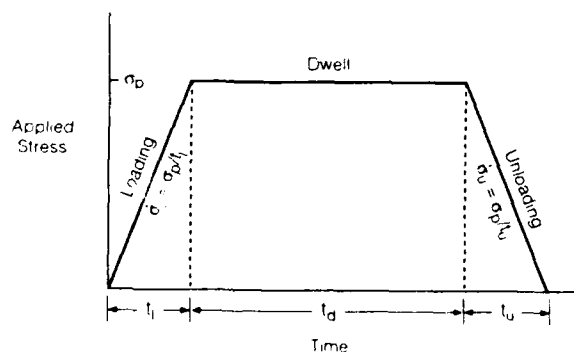


Figure 2.

## Schematic Diagram of Strength Degradation during Proof Testing

Curve labeled  $\sigma$  gives the applied stress as a function of time.  
Reference 1.

- (a) Loading failure
- (b) Dwell failure
- (c) Unloading failure
- (d) Passing the proof test, for flaws with different initial strengths,  $S_i$

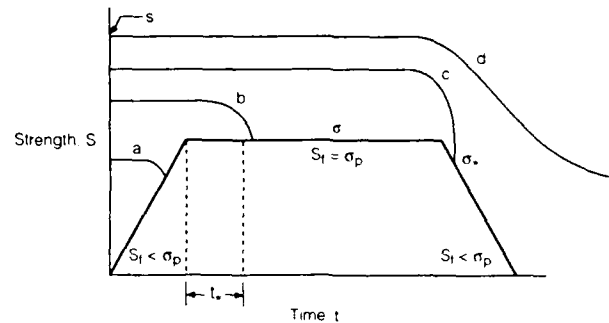


Figure 3.

## Definition of Critical Initial Strength, $S_i^*$ , Minimum Failure Stress $\sigma_{*min}$ , and Minimum Strength, $S_{*min}$ , After the Proof Test

Specimens with initial strengths greater than  $S_i^*$  will survive, while those with strengths less than  $S_i^*$  will fail.

Reference 1.

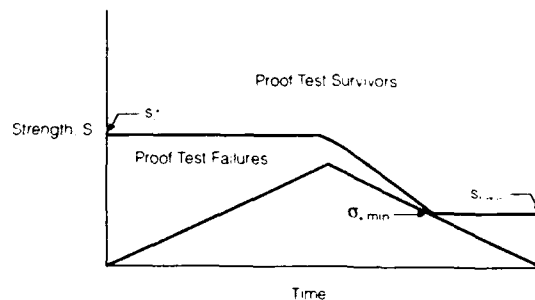
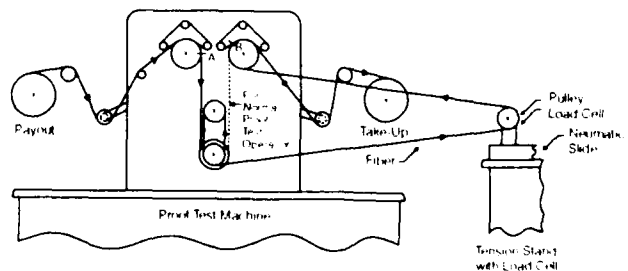
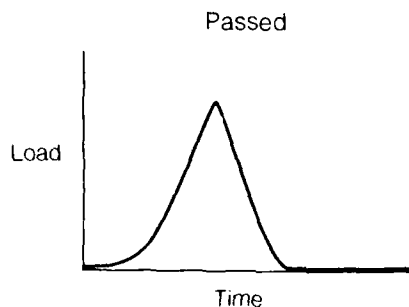


Figure 4.

## Schematic of Continuous Fiber Strength Test Apparatus

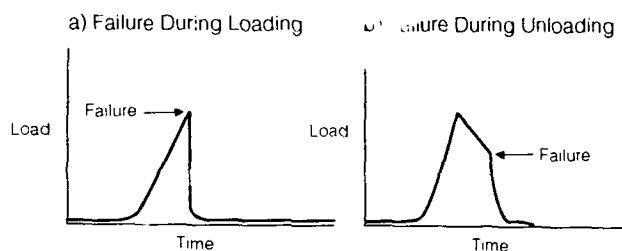


**Figure 5.**  
**Loading Cycle**

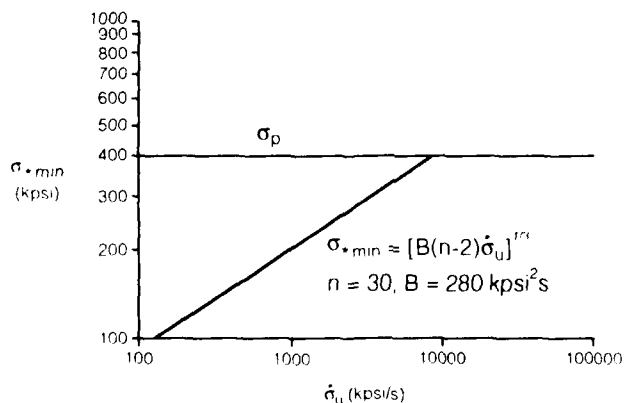


G. Scott Glaesemann, SP-DV-01-8 Corning Inc., Corning, N.Y. 14831. Glaesemann is a senior development engineer responsible for the optical waveguide strength laboratory at Corning. He has been employed by Corning for five years at the Sullivan Park research and development facility. Glaesemann received his master's degree and Ph. D. in mechanical engineering from the University of Massachusetts and a B. S. in mechanical engineering from North Dakota State University. He is a member of the American Ceramic Society.

**Figure 6.**  
**Failure During Loading Cycle**



**Figure 7.**  
**Failure Stress During Unloading as a Function of Unloading Rate**



## DEEP WATER DEPLOYMENT OF ARMoured OPTICAL CABLE

David I. Curtis, John N. Russell, Peter Worthington

STC Submarine Systems, Southampton, U.K.

### ABSTRACT

The North Pacific Cable system (NPC) runs from Miura, Japan to Pacific City, USA with a branch to Alaska (Figure 1). Approximately 9500 km of cable was supplied for the system (by STC, UK and NEC, Japan) making it the longest optical cable system in the Pacific. It is also the highest capacity trans-Pacific cable, with a capacity equivalent to 85,000 telephone circuits. The system was installed in the latter part of 1990 and early 1991, and commercial service began on 1 May 1991.

As the cable route had to cross the subsea mountain range known as the Emperor Seamount range (ESM), the choices of cable design had to be closely considered against the terrain variations. A relatively benign route could have been identified with a 1000 km detour, but calculations showed that with suitable cable design modifications a direct crossing of the ESM range was possible. The task was to lay a cable in deep water (>4 km) in an area of steep slopes and high sea bed currents. Light armoured (C65) cable was chosen to give the required protection.

A special transition cable for use between the normal lightweight deep water cable and the armoured cable was developed. This had increased torsional stiffness to resist the twist generated by the armoured cable, and a special grooved outer sheath to provide extra grip in the ship cable laying machinery. Performance of the cables in deep water was checked theoretically and two sea trials were carried out to demonstrate the viability of the approach.

### INTRODUCTION

The normal unarmoured (lightweight) cable used in the deep water segments of submarine systems cannot be laid in areas where there are strong sea bed currents. Such currents cause relative movement between the cable and sea bed, leading to abrasion of the polyethylene jacket and eventual high voltage breakdown of the cable insulation. To provide sufficient weight for stability on the sea bed, light armour (C65) cable was selected for the ESM crossing. This cable is normally used for the buried segments of systems in depths of less than 1 km.

In addition to providing stability on the sea bed, the steel wire armouring greatly increases the resistance of the cable to abrasion and scouring caused by movement of the sea bed material over the cable in the presence of high currents.

Initial estimates of twist and torque that would be generated by the C65 in depths of 4 km were made, and two major problem areas were identified:-

- Cable tension at the transition from C65 to lightweight cable would exceed the safe level for grip in the tyres of the ship's laying engine.
- The torque generated by the armoured cable could cause excessive twist in the adjacent lightweight cable, leading to potential loop throwing problems either on the sea bed or on the ship.

To overcome these problems a special transition cable was developed, designated Lightweight Screened Grooved cable (LWSG). This was based on the normal deep water lightweight screened (LWS) cable with an additional high density polyethylene outer sheath to increase the torsional stiffness of the cable. A shallow spiral groove was cut into this outer sheath to provide the extra required grip in the tyres of the linear cable engine to be used for cable laying.

Tests had shown that this type of grooving was particularly effective in increasing the grip with wet cable. Using a single wheel pair test arrangement, measured tension at onset of slip was typically doubled from about 5 kN to 10 kN per wheel pair.

In view of the high predicted laying tensions, 2% proof tested fibre was used for the Emperor Seamount cables instead of the normal value of 1.6% used for NL deep water cable.

Figure 2 shows the construction of the three cables (LWS, LWSG and C65 light armour).

The physical characteristics are summarised in Table 1.

**TABLE 1**  
**CHARACTERISTICS OF CABLE USED IN THE NPC SYSTEM**

	NL LWS	NL LWSG	NL C65
O/D (mm)	31.8	37.8	43.0
Weight in air (kg/m)	1.57	1.87	3.69
Weight in water (kg/m)	0.75	0.71	2.20
UTS (kN)	165	170	310
EA (MN)	20.0	20.2	50
GJ (Nm <sup>2</sup> )	37	70	100
Torque per kN (Nm)	0.0	0.0	2.0
H (deg. knots)	50	45	75

Note: EA = Tensile stiffness

GJ = Torsional stiffness

**CABLE STABILITY IN EMPEROR SEAMOUNT CROSSING**

**The Emperor Seamount**

Seamounts are subsea mountains similar in profile to oceanic islands of volcanic origin, often rising several kilometres above the ocean floor. They are characterised by circular or elliptic bases with steep slopes. Seamounts are often grouped in chains forming subsea ridges, which can be very long. The Emperor Seamount chain forms an almost continuous north-south feature that can be traced from the Hawaiian ridge in the south to the Aleutian trench in the north. Steep slopes present problems with cable laying as control of slack is greatly impaired and cable suspensions can be left on the sea bed. Any such suspensions could lead to premature failure from high stress abrasion and fatigue at the support points between suspensions.

For the Emperor Seamount crossing a col between two seamounts (Jimmu and Suiko) was selected, and a route along the lower contours of Suiko was chosen to minimise slopes and also avoid the centre of the valley of the col where currents would be highest. Even so, sea bed slopes of 10° were unavoidable with the selected route (see Figure 3).

A survey of the NPC route was carried out in 1988 by Cable and Wireless (Marine) and during this survey the Emperor Seamount crossing was studied in great detail. A current meter was placed close to the sea bed in a depth of 4 km for a period of 20 days. Maximum sea bed currents of 0.46 m/sec were observed in this period, with predicted 10 year maxima of 0.7 m/sec.

At these levels of current, lightweight cables are not stable and will suffer damage from relative movement between cable and sea bed. (In most deep

water areas in the Pacific, sea bed currents are less than 0.1 m/sec and LW cable is completely stable in service.) In addition, high currents acting during laying will cause a light cable to be moved off line during descent, resulting in the final position on the sea bed being significantly displaced from the surveyed route.

Hence use of the heavier C65 armoured cable to provide stability in service also ensures that the cable can be laid accurately on the required course.

Considerable work had been commissioned previously by STC to study the stability of cables in the presence of sea bed currents (Ref. 1), and this was used to confirm the suitability of C65 for the ESM crossing. The results are summarised in the next section.

**Cable Stability in Sea Bed Currents**

If cable on the sea bed is subjected to a transverse current, the maximum current at which it is stable is given by:-

$$V_c = \left\{ \frac{w}{0.5 \rho d (C_L + C_D/\mu)} \right\}^{1/2} \quad \dots (1)$$

Where: W = Cable weight in water

d = Cable diameter

C<sub>L</sub> = Lift coefficient) Both ~ 1 for cable  
at typical sea bed

C<sub>D</sub> = Drag coefficient) velocities.

= Friction coefficient between cable  
and sea bed

This is the critical velocity acting at the cable mean height above the sea bed (d/2), and is the velocity at which cable movement will start to occur.

For comparison between cables the critical velocity at a greater height (1.0 m) is used, which is a more convenient height for measurement.

Assuming a logarithmic profile, the current at 1.0 metre is related to the current at the cable by:-

$$V_{1.0} = V_{(d/2)} \frac{\{\ln(1.0) - \ln(Z_0)\}}{\{\ln(d/2) - \ln(Z_0)\}} \quad \dots (2)$$

Where: Z<sub>0</sub> = Sea bed roughness figure

Taking a worst case figure for Z<sub>0</sub> of 10<sup>-4</sup> metre (i.e. a smooth sea bed), the critical current for stability can now be evaluated using (1) and (2). This is shown in Figure 4 for NL LWS cable and NL C65 armoured cable.

It can be seen that LWS cable is not stable at the predicted maximum currents in the ESM crossing, whereas C65 armoured cable is stable at currents of up to 1.0 m/sec.

Experimental work by the Hydraulics Research Station using cable samples in tanks, has shown that this theoretical approach is conservative in predicting cable stability.

#### TENSION, TORSION AND TWIST IN SERVICE

The C65 armoured cable and LWSG transition cables were designed to provide the required degree of protection for the Emperor Seamount crossing, and to have sufficient strength and grip in the cable laying equipment to allow safe deployment in deep water.

In order to determine the torsional performance of the cables in service, theoretical analysis of torque, twist and tension in service was carried out.

Excessive twist can lead to premature failure of cable under high tension, as it causes unequal load sharing in a torsionally balanced strength member.

Twist can also cause problems in deployment where the cable is under low tension (in the ship's tank or on the sea bed) resulting in loop throwing and kink formation in the cable.

The theoretical analysis of the twist in the LWSG transition cable and C65 armoured cables showed that deployment in 4 km was possible without exceeding safe levels of twist.

Land based tests at higher than predicted levels of twist and tension were carried out on the cable and joints.

Two sea trials were also undertaken in order to check the measured performance of the cable and compare with theoretical predictions.

#### Theoretical Model for Laying a Deep Water Transition

The general relationship between twist, torque and tension for a cable is (Ref. 2).

$$\phi = \frac{1}{GJ} \{ M - KT \} \quad \dots (3)$$

Where:  $\phi$  = Twist per unit length

$GJ$  = Torsional stiffness

$M$  = Externally applied torque

$K$  = Torque generated per unit tension

$T$  = Cable tension

(The negative sign for the internally generated torque  $KT$  indicates that twist is in a direction to unlay the helix of the armouring.)

In the case of LWS or LW cables which are torsionally balanced,  $K = 0$  and (3) becomes:-

$$\phi = \frac{M}{GJ}$$

For armoured cable, the internally generated torque causes the cable to twist during deployment. In steady state laying of armoured cable there is no externally applied torque to the cable (if any such torque is present initially it will decay exponentially to zero as laying proceeds). Hence, under these conditions, with cable tension at the ship of  $T_s$ , the twist at the ship is:-

$$\phi_s = \frac{-KT_s}{GJ}$$

As the cable sinks to the sea bed tension falls to zero, and the twist in the cable at the sea bed is also zero. Under steady conditions, therefore, with zero sea bed tension, armoured cable is laid on the sea bed with no twist.

The cable is, however, twisting during the descent from ship to sea bed. Hence, when a transition is made to another cable type, this cable is subjected to the twisting of the armoured cable as the transition descends.

Twisting of the transition cable will now result in an external torque in the cable. This torque is held by friction at the sea bed and on the ship. That is, there are no free ends to allow twist to occur and thus reduce the torque present in the transition cable.

The magnitude of the torque and twist can be calculated by solving the basic equations (Eq. 3) for the two types of cable.

Figure 5 shows schematically a transition at an intermediate stage between ship and sea bed.

For steady laying of a single cable type at constant speed the cable between ship and sea bed is a straight line at an angle to the horizontal of:-

$$\alpha = \cos^{-1} \left\{ \left( 1 + 0.25 \left( \frac{H}{V} \right)^4 \right)^{1/2} - 0.5 \left( \frac{H}{V} \right)^2 \right\} \quad \dots (4)$$

$$\approx H/V \text{ for small } H/V$$

Where:  $H$  = Cable hydrodynamic constant

$V$  = Ship laying speed

For two cable types in suspension, a simple model is to assume that both cables remain straight lines with angles given by (4) for each cable type. (This is not completely correct as the cables adjacent to the transition would be smooth curves in order to satisfy equilibrium conditions at the transition.)

Referring to Figure 5, the equations relating to twist, tension and torque for the two cables are:-

$$\text{Cable No. 1 (Sea Bed } M = \overline{GJ}_1 \phi_o + K_1 T_o \quad \dots (5)$$

$$\text{(Transition } M = \overline{GJ}_1 \phi_1 + K_1 T_1 \quad \dots (6)$$

$$\text{Cable No. 2 (Transition } M = \overline{GJ}_2 \phi_2 + K_2 T_2 \quad \dots (7)$$

$$\text{(Ship } M = \overline{GJ}_2 \phi_3 + K_2 T_3 \quad \dots (8)$$

The cable tensions can be related to the lengths of cable in suspension. For straight line cable configuration, the cable tension in depth  $h$  is  $w$  ( $w$  = cable unit weight in water) independent of the cable angle.

Hence we have:-

$$\text{Cable No. 1 ( } T_o = 0 \quad \text{at Sea bed}$$

$$( T_1 = w_1 h_1 \quad \text{at Transition}$$

$$\text{Cable No. 2 ( } T_2 = T_1 \quad \text{at Transition}$$

$$( T_3 = w_1 h_1 + w_2 (h - h_1) \quad \text{at Ship}$$

Where  $h$  = depth,  $h_1$  = depth between transition and sea bed.

Initially there is a total amount of twist in the cable in suspension given by:-

$$\Phi_{I_1} = \frac{-K T_3 L_I}{\overline{GJ}_1} \quad \dots (9)$$

Where:  $L_I = \frac{h}{\sin \alpha_1}$  = Initial length of cable No. 1 in suspension

As laying of the transition proceeds, some twist will be laid on the sea bed (since  $\phi \neq 0$  if  $M \neq 0$ ). However, as there are no free ends, the total amount of twist in suspension and on the sea bed must remain constant and equal to  $\Phi_{I_1}$ .

The total twist laid on the sea bed is:-

$$\Phi_o = \int \phi_o \cdot dL$$

where the integral is over the length of cable laid on the sea bed from the time the transition leaves the ship.

Hence the twist remaining in suspension in cables 1 and 2 at an intermediate time shown in Figure 5 is:-

$$\Phi_{I_{1+2}} = \Phi_{I_1} - \Phi_o \quad \dots (10)$$

From this a new value for the twist per unit length in the cable at the sea bed can be determined using Equations (5) to (8) to give:-

$$\phi_o = \frac{\left\{ \Phi_{I_{1+2}} + \frac{K_1 T_1 L_1}{2 \overline{GJ}_1} + \frac{K_2 (T_2 + T_3) L_2}{2 \overline{GJ}_2} \right\}}{\left( L_1 + L_2 \cdot \frac{\overline{GJ}_1}{\overline{GJ}_2} \right)} \quad \dots (11)$$

Having determined  $\phi_o$ , the other values of twist and the external torque,  $M$ , can be determined using Equations (5) to (8).

#### Estimated Twist and Tension for Emperor Seamount Cables

For the Emperor Seamount crossing, the first transition is from LWSG (deep water) to armoured cable, followed by a transition from armoured cable to LWSG.

Of these, the most severe case in terms of tensile and torsional stress is the transition from armour to LWSG, as the transition cable has to support the weight of the armoured cable during laying.

Figure 6 shows the calculated twist and tension in the LWSG cable as a function of length of cable paid out after the transition. This is plotted for 4 different laying speeds (2, 3, 4 and 5 knots).

It can be seen that the laying speed does not greatly influence the peak twist that occurs, which is approximately 0.075 turns/m in each case (1 twist in 13 metres). However, increasing laying speed increases the length over which the twist occurs. Hence a low laying speed is preferable to reduce risk of twist-induced problems.

At low laying speeds, however, the cable angle increases and becomes closer to the vertical.

Cable tension can then be significantly affected by wave induced motion of the ship. This dynamic tension component is given by:-

$$T = \pm \left( \overline{EA} \cdot m \right)^{1/2} \cdot v_g \quad \dots (12)$$

Where:  $\overline{EA}$  = Cable tensile stiffness

$m$  = Mass/unit length

and  $\pm v_g$  is the peak vertical velocity of the ship at the point of cable suspension (i.e. stern or bow).

Figure 6 shows that the expected laying tension in steady conditions with no ship motion is about 85 kN with C65 cable in suspension, falling to 28 kN when the transition to LWSG is at the sea bed.

If a low laying speed were used so that cable angle was close to the vertical, the dynamic tension component with C65 cable in suspension in 4 km depth will be approximately  $\pm 40$  kN in adverse weather conditions (with  $V_g = \pm 3$  m/sec. assumed).

This increases the peak tension to over 120 kN, which exceeds the maximum safe tension for deployment of the LWSG cable.

By using a laying speed of 3 knots, the cable angle for the C65 is reduced to about  $30^\circ$  which results in worst case dynamic loading of only  $\pm 20$  kN, and maximum laying tensions of 105 kN in the LWSG cable. This corresponds to a cable strain of about 0.6% which is a safe figure for 2% proof tested fibre.

A laying speed of 3 knots was therefore selected to enable safe laying in adverse weather conditions, but without subjecting excessive lengths of cable to the highest level of twist in deployment.

#### SEA TRIALS

Two sea trials were carried out in order to check the performance of the cables in deployment and to establish procedures for subsequent use on the system lay.

A short trial was carried out in May 1989 using 6 km of C65 armoured cable and 14 km of LWSG transition cable. This trial demonstrated the feasibility of deployment of the cables in 4 km depth but was too short to accurately simulate tensile and torsional loadings that would occur on system laying.

A full-scale sea trial was carried out in September 1989. A schematic of the cable used in the sea trial is shown in Figure 7, together with the system configuration to be used for the Emperor Seamount crossing.

The trial used 10 km of C65 armour, which was sufficient to establish steady laying conditions in a depth of 4 km. A length 17.4 km of LWSG (the same length as in the system) was deployed between the transition and the trial repeater housing.

As a further precaution against twist, the cable was paid out through a carousel ( $360^\circ$  turn) installed between ship tank and cable engine. This was designed to prevent twist that may be present outboard from reaching the cable in the tank. Loop throwing can be caused by twist applied to cable at low tension in the region between tank and cable engine.

#### Sea Trial Results

The trial was laid at a steady pay-out speed of 3 knots, which was estimated as optimum for system deployment.

During the trial the following parameters were continuously monitored:-

- Tension
- Twist
- Optical length (strain)
- Optical attenuation

Figure 8 shows the results of the tension and twist measurements made during the pay-out of the transition from C65 to LWSG.

The twist in the LWSG showed a steady increase to a peak of about 0.065 turns/m after paying out 6 km, followed by a steady reduction as pay-out continued. By the time the repeater was launched (17.4 km pay-out), there was no significant twist in the LWSG cable. The measured peak twist was somewhat less than the theoretical figure (0.075 turns/m) and the twist decayed more rapidly than expected as pay-out continued.

This may be accounted for by an increase in torsional stiffness of the LWSG as the high density polyethylene sheath is cooled in deep water. It is also possible that the armouring is generating less torque than expected because of hysteresis and friction. The calculated figure for torque is based on torque developed when tension is applied to the cable. In this case, torque is developed as tension is removed from the cable as the transition sinks to the sea bed.

The measured tension during the transition was as expected, falling from a maximum of 90 kN with all armour cable in suspension to 30 kN when the transition reached the sea bed.

The optical monitors on the trial showed no change in loss, and the measured residual strain in cable on the sea bed was less than 0.01%. The trial had demonstrated the viability of the proposed Emperor Seamount crossing, and the system installation could therefore proceed as planned.

#### SLACK CONTROL

The route survey showed that the selected route through the Emperor Seamount crossing required direction changes to follow the optimum (minimum slope, minimum currents) route. From the recommendations of the survey it was decided to lay a relatively high degree of slack on the sea bed to compensate for inevitable inaccuracy caused by slope, sea bed currents, direction changes and transitions of different cable types. Target figures of 7% slack in the C65 and 5% in the LWSG cable were selected, compared to typically 1% - 2% slack normally used for deep water cable.

This is the target slack on the sea bed. The ship required different targets for deployed slack in order to compensate as far as possible for the sea bed slopes and cable transitions.

#### Slack Compensation for Sloping Sea Bed

The extra slack that must be laid to compensate for a sea bed slope of  $\beta$  is:-

$$\Delta s = \frac{\sin(\alpha_s + \beta)}{(\sin \alpha_s + \sin \beta)} - 1 \quad \dots (13)$$

Where:  $\alpha_s$  = Cable angle at ship given by Eq. 4

This expression is negative for positive  $\beta$  (laying up a slope) and positive for negative  $\beta$  (down a slope).

Typical slack compensation for a 10° slope for LWSG cable at 3 knots is  $\pm 2.5\%$ .

#### Slack Compensation at a Cable Transition

As the steady state laying angles of the cables each side of the transition are different, compensation is required for the change in geometry. The required extra slack is given by:-

$$\Delta s = \frac{\sin \alpha_1 - \sin \alpha_2 + \sin(\alpha_2 - \alpha_1)}{\sin \alpha_2 - \sin(\alpha_2 - \alpha_1)} \quad \dots (14)$$

Where:  $\alpha_1$  = Laying angle of cable No. 1 prior to transition

$\alpha_2$  = Laying angle of cable No. 2 after the transition

and  $\alpha_1, \alpha_2$  are given by Eq. 4

For example, a transition from LWSG to C65 at 3 knots requires an additional 5% slack to be laid for the period of descent of the transition from ship to sea bed. Figure 9 shows the calculated slack that was required to be laid by the ship in order to meet the target figures on the sea bed calculated for a constant laying speed of 3 knots.

#### Computer Modelling

As a further check on the correct slack requirements a computer model was developed to determine cable profiles in suspension during deployment of transitions, joints or repeaters. Results of this finite difference model agreed well with the results given using the simple straight line approximation.

#### SYSTEM LAY

The Emperor Seamount crossing was laid as part of the main deep water lay of the NPC system by cable and wireless using the cable ship "Cable Venture". This was one of the longest deep water cable operations that has been undertaken, and was carried out in November and December 1989.

The Emperor Seamount cable deployment proceeded as planned. Maximum tension in the LWSG transition cable was less than 100 kN. Cable twist was estimated by observers positioned at the stern of the ship. Maximum twist in the LWSG cable was estimated at approximately 1 turn in 12 metres, falling rapidly to zero as pay-out continued. No twist was observed inboard in cable under low tension. Cable and transition handling procedures, which had been well rehearsed prior to the lay, were carried out without difficulty.

#### CONCLUSIONS

The design task of achieving a suitable cable for the complex ESM crossing was successfully proven first through sea trials and then the system lay. This enabled significant savings in system length and cost compared to more benign options for the route.

#### REFERENCES

1. "Stability of Submarine Cables"  
Hydraulics Research Station Report Ex 918  
March 1980.
2. "Submarine Cable Mechanics and Recommended Laying Procedures"  
C.E. Roden, Bell Telephone Laboratories  
December 1964

#### BIOGRAPHIES

John N. Russell was born in 1954 in Birmingham, England. He graduated in applied physics from University College, London, in 1975. In the same year he joined STC Transmission Products Division at Basildon. Later he moved to the new Optical Fibre Unit which was being set up at Harlow, where he worked on measurements, installation and cable design for land line systems. In 1982 Mr. Russell moved to STC Submarine Systems in Southampton where he is working on the design of submarine cable as head of the cable design section.

Peter Worthington is a development engineer with STC Submarine Systems which he joined in 1974. He received a BSc in Electronics and Electrical Engineering from the University of Birmingham in 1971. Since 1977 he has been involved in the development of optical cables for submarine systems.

David I. Curtis was born in 1954 in Nottingham, England. He graduated in mathematics from the University of East Anglia, Norwich, in 1980. He worked as a development engineer in the coaxial cable industry before joining STC Submarine Systems in 1987, where he is involved in cable design and deployment issues.



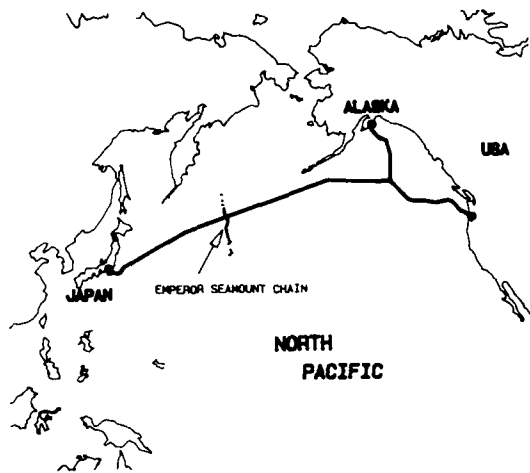
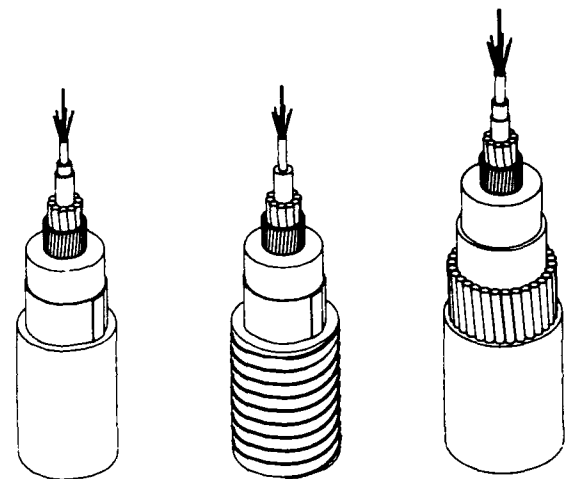


FIG. 1  
NORTH PACIFIC CABLE SYSTEM



LIGHTWEIGHT SCREENED      LIGHTWEIGHT SCREENED GROOVED      C65 ARMoured CABLE

FIG. 2  
STC CABLE TYPES

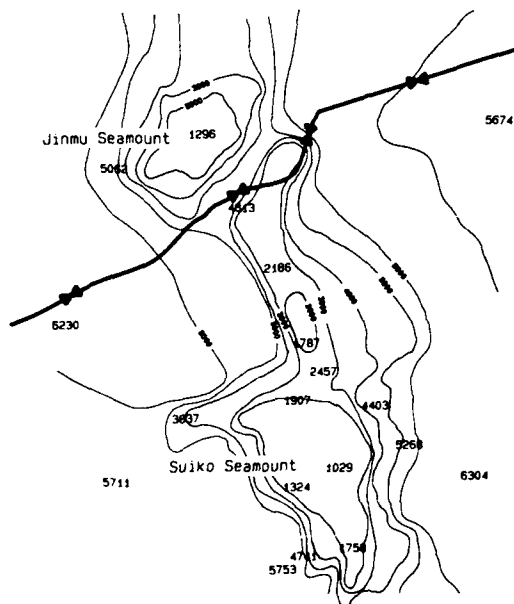


FIG. 3  
EMPEROR SEAMOUNTS CROSSING

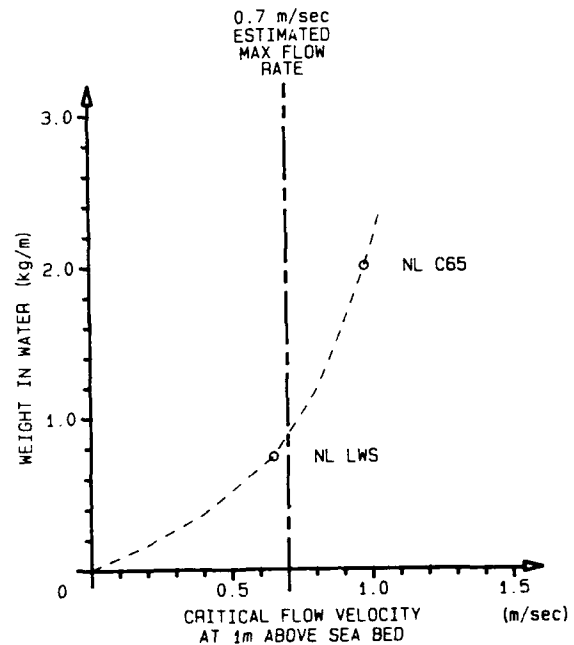


FIG. 4  
CABLE STABILITY IN SEABED CURRENT

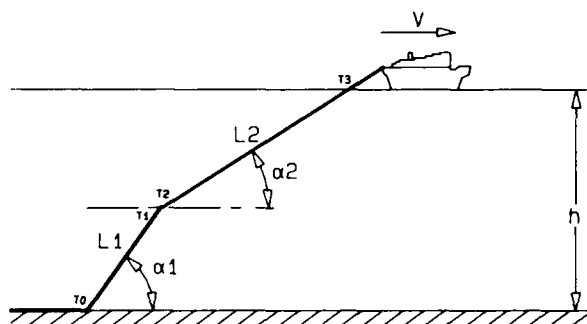


FIG.5.

LAYING A TRANSITION FROM ARMoured  
TO LIGHTWEIGHT CABLE

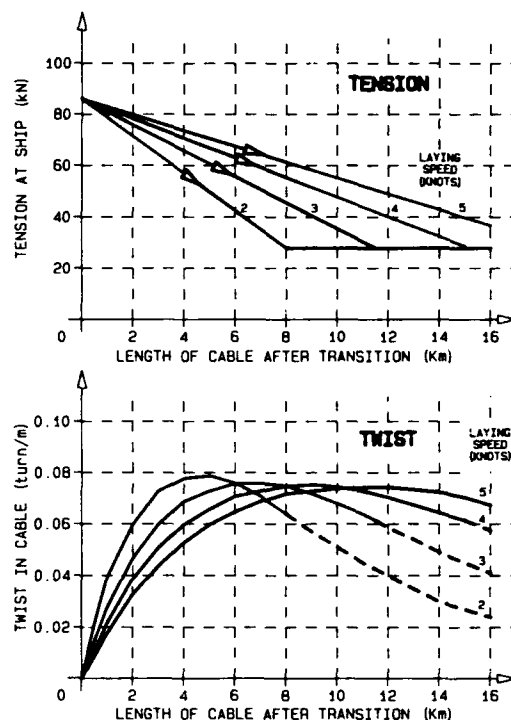


FIG.6

THEORETICAL TENSION AND TWIST IN LSWG CABLE

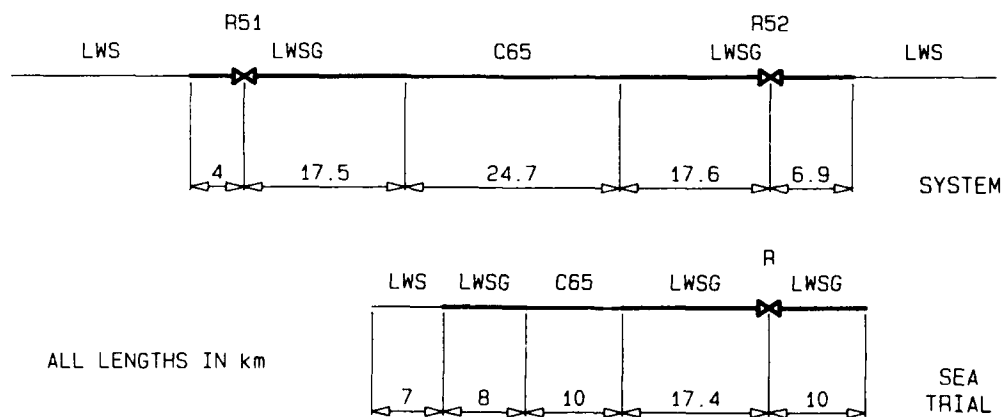


FIG.7.

SLD OF SYSTEM AND 2nd SEA TRIAL

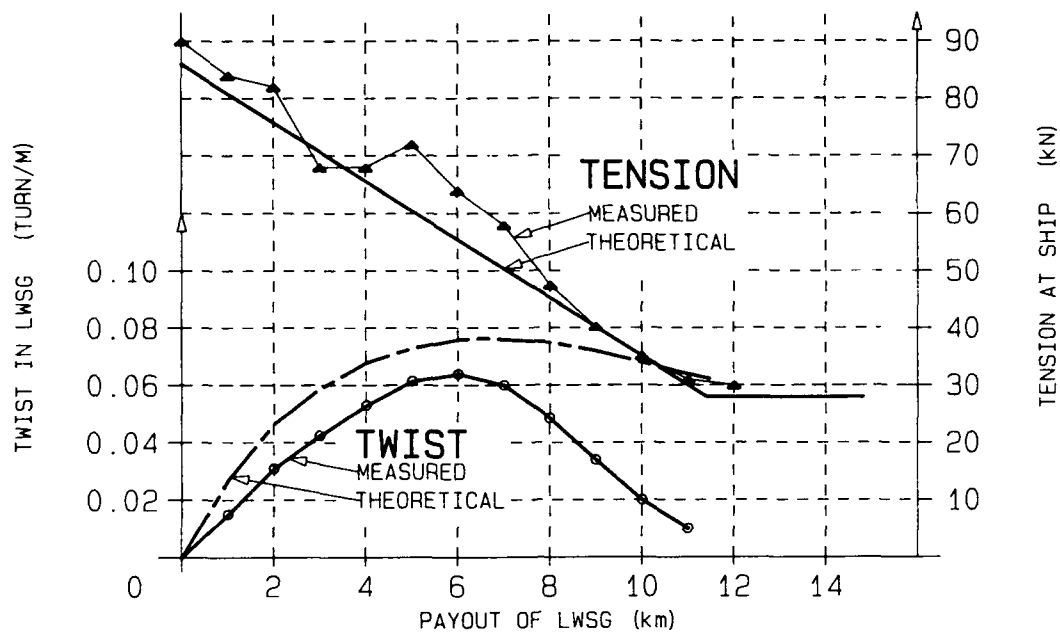


FIG.8 SEA TRIAL RESULTS

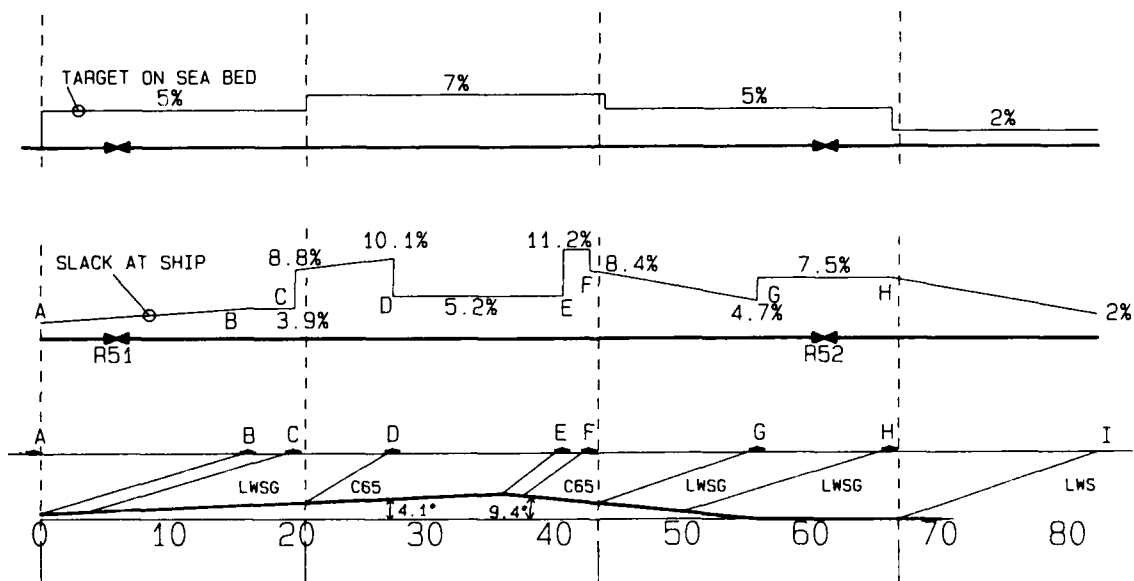


FIG.9 SLACK PROFILE

## THE IMPACT OF SUBMARINE NETWORKS ON THE DEVELOPMENT OF FIBER OPTIC TECHNOLOGIES

R. JOCTEUR\* - R. BOIRAT\*\* - M. de VECCHIS\*\*\*

\*ALCATEL CABLE - 170 Avenue Jean Jaurès - 69344 LYON - FRANCE

\*\*ALCATEL CIT Centre de Villardereaux - 91625 LA VILLE DU BOIS - FRANCE

\*\*\*ALCATEL CABLE - 30, Rue des Chasses - 92111 CLICHY - FRANCE

### ABSTRACT

This paper reviews advanced fiber optic submarine systems and the impact on related evolution of fiber optic technology itself. Forecast of the future submarine systems is presented in both cases of unrepeated and repeated (regenerators and amplifiers) applications. Examples are given concerning expected performances : distance - bit rate etc... and technologies used. Consequences on relevant evolution of fiber optics design and characteristics are discussed. Possible consequences on other applications in the broadband terrestrial network are analysed.

### 1 - INTRODUCTION

The submarine systems market is pushing the development of transmission systems, new technologies and products in the field of fiber optic for the following reasons :

- worldwide sales are rapidly increasing : already installed or contracted 1982-1991 systems sales - 5.5 B US \$. Forthcoming projects up to 1995/1996 - 9 B US \$.
- More than 60 % of the world market is open market : that is favorable to a strong economical and technical competition.
- The technical solutions are various for different applications : local, regional, international and transcontinental links corresponding to a large range of lengths.

- The upgradability is generally required as soon as the initial investment is decided.

The objective of this presentation is to review the necessary R and D program to satisfy the needs identified in these forthcoming projects, in the area of fiber optic technology, developments on fiber design and manufacturing methods. Other applications in the broadband transmission and distribution terrestrial network, such as in landline trunk systems, digital subscriber line or analogic videocommunications systems take benefit of the progresses achieved. So the drawbacks of this fast evolution : increase of R and D expenses, development cost depreciation, risk of early obsolescence, multiplicity of research projects, are lessened by the appearance of new applications or new needs (fig. No 1).

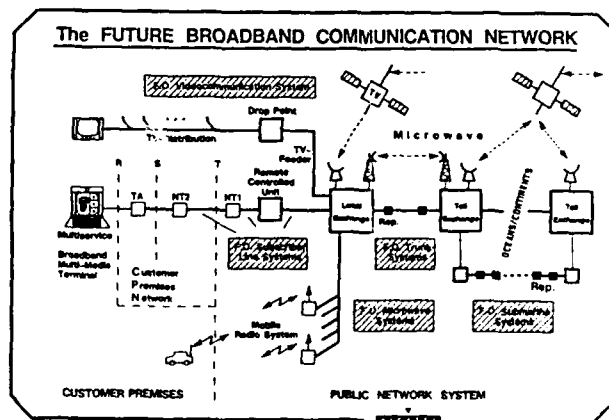


Figure 1

## II - TECHNOLOGIES FOR SUBMARINE SYSTEMS

### II-1 Today

Conventional technology applied today to submarine systems is based on intensity modulation and direct detection :

- on the transmitter side information is impressed on the light of the laser source through its injection current,

- at the receiver the light is detected by a photodiode which turns photons to electrons, that is modulated light into electrical signal.

Such technology allows following typical features :

- for repeaterless systems

140 Mbit/s - 200 km - 40 dB power budget,

560 Mbit/s - 170 km - 34 dB power budget.

- for very long systems, with regenerative repeaters

560 Mbit/s - 120 km span - 24 dB power budget.

These characteristics enable to implement very interesting systems such as, for instance

- DIEPPE-BRIGHTON - 150 km - installed with 140 Mbit/s stream without repeater, which will be shortly upgraded at 560 Mbit/s without changing the cable,

- ALMERIA-MELILLA - 200 km - installed in 1990 - 140 Mbit/s upgradable to 560 Mbit/s without repeater,

- TAT 9 transatlantic system - around 6,000 km - at 560 Mbit/s - to be installed by the end of 1991.

### II-2 Tomorrow 1992-1994

But new research results, especially with optical amplification at 1.5  $\mu\text{m}$ , give very attractive possibilities to increase power budget, therefore to increase distance and/or bit-rate, also to simplify repeaters.

An optical amplifier is made of an erbium doped fiber pumped with a powerful laser at 1.48 or 0.98  $\mu\text{m}$ , with suitable couplers to mix input signal and pump light and to launch output light in the line fiber. This type of amplifier offers for our purpose better characteristics than the semiconductor one does, in term of overall gain, saturation power, sensitivity to light polarization, noise, linearity, etc...

*In unrepeated link field*, use of optical amplifiers is planned by end of 1992 or 1993 to increase distance between terminals, as booster and preamplifier respectively at transmitter and receiver sides. Gains of 10 (booster) to 16 dB (both booster and preamplifier) are expected on power budget leading to an increase of length of 50 to 80 km.

Instead of preamplifier we can put doped fiber in the cable just far enough from the receiver and pump it remotely from the terminal. The so-called repeater has no active components and therefore is passive. This offers more gain than with preamplifier. 30 km extra gain on the distance is possible. For instance, putting the doped fiber around 45 km before the receiver, distance of 320 km between terminals at 622 Mbit/s seems realistically achievable.

Of course, increasing the product bit-rate  $\times$  distance increases problems with propagation. At first we can, or must, use dispersion shifted fiber in order to decrease chromatic dispersion effect. We must also decrease spectrum width of modulated light. This seems possible with very promising three sections lasers which offer very narrow spectrum (2 MHz for instance) and reduced chirping effect if they are made with multi quantum well structure. In any case use of external modulator can avoid the chirping of the laser and this will be probably mandatory for very high bit-rates.

Thus components and devices become more sophisticated with hard specifications, difficult to get. An interesting solution to relax requirements on spectral and dispersion characteristics is to make use of Forward Error Correcting code, naturally at the cost of electronics and small increase of line rate.

We have implemented a Reed Solomon code which is cyclical, of high efficiency and suitable to frame structure of data. For instance, with a redundancy close to 20 %, this code is able to correct 8 consecutive errors in 100 adjacent bits, in fact 64 over 800 with multiplexing. Thus bit error ratio can jump from  $10^{-3}$  to  $10^{-4}$  by using FEC code.

In practice such a code works best for a not corrected bit error ratio lower than  $5 \cdot 10^{-5}$  and guarantees error free transmission. In addition, sensitivity is improved by about 5 dB that increases length by 25 km.

*Thus, using all these possibilities, booster, remote preamplifier, FEC code, external modulation, 300 km between active terminals could be reasonably achieved at 2.5 Gbit/s by 1995.*

### 11-3 Later on - 1995/2000

Obviously the technology of optical amplification can also be used *in repeatered systems field* in so far as reliability of components can be achieved. In this case optical signal which carries information is no longer regenerated but only amplified without changing its optical form. This simplifies repeater by avoiding fast electronics for amplification clock recovery, decision, reshaping, ... and sophisticated optoelectronic components.

As a consequence optical amplifier is transparent to the bit-rate, what is an interesting feature for designing systems.

However, about propagation aspect, we have to consider the total length of the system, for instance 5 to 10,000 km for transoceanic links. With such lengths propagation difficulties arise not only from the well-known chromatic dispersion effect - some of the frequencies of the signal spectrum go faster than others and the signal spreads out after propagating along the fiber - but also from non-linear effects, mainly Kerr self phase modulation - the refractive index of the fiber changes with light intensity, leading also to an alteration of the signal form.

An ideal solution is to compensate for one effect by the other and to use an optical signal with well defined shape and intensity which will propagate without distortion along the fiber. Such a signal, which corresponds to "solitary" solution of equation of propagation is named "soliton", which owns noteworthy properties of stability and preservation.

For instance, one could think that the attenuation of the fiber would make disappear the optimal conditions of soliton propagation because the intensity of the optical pulse decreases when it propagates. Fortunately Soliton accepts some variation of its intensity, as it accepts light fluctuation of fiber parameters, ..., providing that the corresponding distance of these changes is less than a typical length, its Soliton period.

It is therefore possible to amplify optical signal from time to time with optical amplifiers in order to compensate for the attenuation of the fiber.

However optical amplifiers produce noise and this noise combines with solitons leading to random jitter of these pulses. Thus propagation of very high bit rate solitons along very long distance is limited, for example around  $10 \text{ Gbit/s} \times 10,000 \text{ km}$ . All these considerations, maximum accepted attenuation between amplifiers, too large jitter, too high bit error ratio, give a trade off for the gain around 10 dB, not so high than technology allows, as much as economy would like to get.

Any how it is possible to design very long systems with high bit rate using in-line optical amplifiers. Not close to limits in jitter, in distortion, in error rate, the shape of the signal may not be of soliton form, that simplifies source, modulation and electronics. But in all cases non linear effects, jitter due to noise, ..., have to be considered and amplifier gain will be limited.

*This is what is done to design the next generation of transoceanic systems, with no regenerative repeaters, only optical amplifiers, probably at 5 Gbit/s, with 40 to 50 km span, possibly installed by the end of 1995.*

#### II-4 Past 2000

This generation just above mentioned is "soliton-like", that means non linear effects are taken into account but pure soliton may not be used. No doubt the following generation will apply Soliton technology with probably several multiplexed very high bit-rate channels on the same fiber.

May be at this time fluoride glasses will be developed, with their very attractive promise of extremely low attenuation : 0.02 dB/km. This would divide the number of repeaters by a factor of ten, as well as increase distance between terminals by the same factor !

Naturally plenty of work has to be done, especially with propagation (what will be chromatic dispersion, what will be non linear effects ?), also because the wavelength is not 1.5  $\mu\text{m}$  but 2.5, because sources and detectors are not truly available, etc... without forgetting work on fiber and cable.

But progress is running faster and faster. We can dream and wager for a field experiment by 2010. The stake is so huge that we should win.

### III - RELEVANT FIBER OPTIC TECHNOLOGY EVOLUTION

Germanium doped standard fiber optic for submarine systems operating at 1.55  $\mu\text{m}$  up to 1 Gbit/s, the standard fiber optimized at 1.3  $\mu\text{m}$  can be used with no penalty on the power budget. The span length or the maximal distance of the system is limited by the fiber attenuation. The attenuation decrease is achieved by means of the process mastership and production equipments quality. To reduce the splices number, long lengths are produced despite the high level of proof test which is applied on all the fibers. Typically, the average length of standard fibers manufactured by MCVD process from 45 km capacity preform, is 15 km after 1.5 % proof test. The mean attenuation is 0.197 dB/km as shown on the repartition curve (fig. No 2) related to the link PALERMO-PALMA-ESTEPONA.

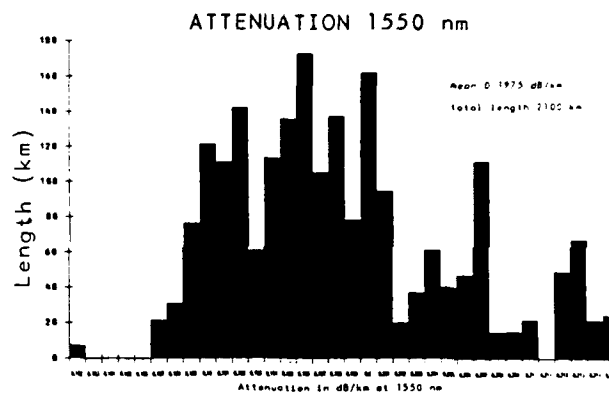


Figure 2

#### III-1 Pure silica core fiber

A 10 % additional decrease of the attenuation, equivalent to a cost reduction of 3 to 4 % on a 3x560 Mbit/s systems 3000 km long link, can be achieved by an appropriate selection of dopants in the core and the cladding. The MCVD process allows to deposit pure silica core layers in a substrate tube of fused or synthetic silica, which is fluorine doped. An index difference  $\Delta n =$

$-5.10^{-3}$  can be obtained by using an atmospheric pressure plasma torch through which is projected a mixture of silicon and fluorine halogenides. The average attenuation is less than 0.18 dB/km.

The Spanish domestic link as mentioned § II.1 uses pure silica core fiber. The regeneration span of the 560 Mbit/s system reaches 135 km, instead of 120 km with standard fiber..

We must point out the great flexibility and versatility of the MCVD process for making complex index profiles, deposition of various dopants and reproducibility of fiber optogeometrical characteristics. The plasma technology is particularly adapted to the fluorine doped synthetic silica tubes of which the use is a condition to reduce the core dopant level and by this way to reduce the Rayleigh diffusion.

#### III-2 Dispersion shifted fiber

The bit rate increase is a key parameter of the cost reduction in submarine systems. The increase to 5 Gbit/s of the future transoceanic system with optical amplifiers needs long and expensive developments and in particular those of dispersion shifted fiber and rare earth doped fiber.

Lightguide dispersion shifted fiber is optimized for operation in the 1550 nm wavelength region. This product is especially intended for use in very high bit rate optically amplified systems over transoceanic systems up to 5 Gbit/sec over 10,000 km. For use in such transmission systems, special requirements are needed :

- low intrinsic attenuation
- low chromatic dispersion
- low polarization mode dispersion.

Specific developments on fiber design and manufacturing process are in progress to optimize the transmission characteristics.

- Low intrinsic attenuation

The combination of MCVD performant process and fiber design contributes to decrease the intrinsic attenuation in the 1550 nm wavelength region. The process versatility, the selection of dopants nature and contents, and the index profile configuration allow to achieve the lowest intrinsic attenuation.

- Low chromatic dispersion

Optogeometrical properties and process reproducibility are the key parameters to control with accuracy :

- waveguide dispersion
- zero dispersion wavelength
- adjustment of zero dispersion wavelength with operating wavelength
- dispersion slope.

- Low polarization mode dispersion

Small core ovality and small stress assymetry generate a low polarization mode dispersion over long distances.

The forecast concerning dispersion shifted fibers seems presently to be moving from "moderate" to "strong" requirements for the next generation of submarine systems operating at 5 Gbit/s with fibers amplifiers.

Very significant progresses have been made in the fabrication of such fibers in order to achieve simultaneously minimal losses (0.21 dB/km), minimal dispersion (0.05 ps/nm.km at the system wavelength), and low polarization dispersion ( $< 0.20 \text{ ps/km}^{1/2}$ ). Trapezoidal index profile fiber configuration has been optimized.

### III-3 Erbium doped fiber

The Erbium doped fiber will be used in lumped repeaters, booster amplifiers and preamplifiers. The doping concentration is close to 100 ppm, the fiber length is 10 to 100 meters and the amplifier gain is depending on concentration and length. The optimization of this product is going on. Generally the core composition is an aluminium and germanium codoped silica. For preform making, MCVD process can be used; Erbium introducing method is made up from a gaseous phase or liquid phase. Specific measurements methods must be developed for high value of index difference and Erbium radial distribution control.

Another future use of Erbium doped fiber could be as distributed amplifier for soliton transmission. Long lengths of Erbium doped dispersion shifted fiber could be needed with very low attenuation and low polarization dispersion. The doping concentration should be decreased to less than 1 ppm. Some explorations started on such fiber.

At least, to improve lifetime of Erbium doped fiber, particularly when stored in lumped amplifiers, a carbon hermetic coating will be applied on the fiber.

### III-4 Fiber based passive components

Different technologies are under investigation or industrially developed to produce passive components. Integrated optic on glass or silicon and fiber fusion technique are currently used for making couplers, multiplexers, splitters, etc... In the optical amplifier some passive components are needed with specific and strong requirements.



Technologies and performances characterization, qualification, quality insurance and manufacturing tests are performed to select the best and the most reliable component for a given function. Fusion technique using all types of fibers as described in the previous paragraph is particularly performant, reliable and harsh environment resistant, and could be qualified as component in submerged amplifiers.

Fiber based passive components could be used in the future analogic broadband distribution network, in the booster amplifier and in the cable plant as coupler and splitter, taking benefit of the submarine qualification.

### CONCLUSION

The weight of the submarine systems in the future broadband communication network is considered as heavy. The trends of the technology have been shown to improve cost and performances of the submarine systems repeated or not, in several steps up to the end of century. The direct impact on optoelectronic components and fiber optics development program has been pointed out and the case of fiber optics has been especially examined. In the field of fiber technology, more and more technological developments are required to improve processes, to specify new special design and to reach the absolute quality; the main axes of development have been reviewed.

### ACKNOWLEDGEMENTS

The authors would like to thank D.A.I. and C.N.E.T. from FRANCE TELECOM for their support and the fruitful cooperation on this work and the corresponding research projects.

### BIOGRAPHY

**R. BOIRAT - ALCATEL CIT**  
Centre de Villarceaux - 91625 LA VILLE DU BOIS  
CEDEX - FRANCE



Robert BOIRAT is a graduate of the Ecole d'Ingénieurs des Arts et Métiers (Cluny, Paris) and of the Ecole Supérieure d'Electricité (Malakoff). He joined the CGE Group, named now Alcatel Alsthom, in 1952 and initially was involved in RADAR then in automatization equipment. In 1972 he joined Central Research Centre of the Group, in Marcoussis, working in optical communication field. He became head of Research Centre for Optical Communication at Alcatel-CIT in 1980, involved in advanced photonics such as coherent techniques, optical amplification or photonic switching. He is also responsible for transmission research programme in Alcatel Group.

**R. JOCTEUR - ALCATEL CABLE**  
170, Av. Jean Jaurès - 69344 LYON - FRANCE



Robert JOCTEUR was born in 1933 in Lyon, France. He graduated from the University of Lyon with an MS in mathematics and physics, then joined Les Câbles de Lyon now Alcatel Cable to undertake research into copper telecommunication cables. In 1974, he started working on optical fiber cable technology, and in 1983 took over responsibility for the development of submarine optical fibers. Mr. Jocteur is at present Technical Director of the Telecommunication Department in Alcatel Cable.

**M. de VECCHIS - ALCATEL CABLE**  
30, Rue des Chasses - 92111 CLICHY - FRANCE



Michel de VECCHIS was born in 1946. He is graduated from Ecole Nationale Supérieure des Télécommunications (1969). He joined LTT in 1970 where he worked on microwave components. He started to work on fiber optics in 1974 and has been Technical Director of the cable Division until the merging in 1986 of LTT cable activities with Les Câbles de Lyon now Alcatel Cable. He is now Director of Technical International Marketing at Alcatel Cable Telecommunications Branch. He is involved in International Standardization of optical fibers and cables (Chairman of CECC WG 28 and Secretary of IEC SC 86 A).

# The First Commercial Introduction of Multi-fiber Optical Submarine Cable

Masao OHBA \*, Sakae OHSHIRO \* , Osamu KAWATA\*\*, and Takuya UENOYA \*

\* NTT Network Systems Development Center, Tokyo, 100, Japan

\*\* NTT General Planning Headquarters, Tokyo, 100, Japan

## Abstract

An innovative multi-fiber optical submarine cable containing up to 48 optical fibers has been developed for application to trunk optical cable networks. This new type of cable provides a major advance in construction efficiency for optical submarine transmission spans. This cable was commercially introduced in 1991. This paper introduces multi-fiber optical submarine cable technologies, and presents the first commercial test results.

## 1. Introduction

Since Japan is a nation of islands, submarine telecommunication cables have played very important roles in the construction of telecommunication networks. Optical submarine cables have been deployed primarily for trunk transmission lines since 1983 in Japan. From the initial stage of introduction, NTT's conventional optical submarine cables have been accommodated a maximum of 12 optical fibers. More than 3,000 km of cables have been introduced to date.

Because of environmental extremes which affect operation the necessity for long-term reliability, especially mechanical stability for submarine environments, there is much more demanding placed on submarine cables than on terrestrial cables. However, increase of cable diameter due to the multiplication of fibers in the cable reduces mechanical performance. Moreover, it causes some difficulty in cable handling or mismatching at cable installation facilities. The new cable maintains the same size and weight as conventional optical

submarine cables. There is no parallel to this multi-fiber optical submarine cable which is capable of being submerged to several thousands of meters.

This paper describes the necessity of multiplying the fiber count in an optical submarine cable and the basic concepts behind 48-fiber optical submarine cable design and cable characteristics, cable jointing techniques. The first commercial test results are also provided showing excellent transmission characteristics. These also show that the new cable has sufficient practical performance to play a part in the construction of the fiber optic submarine network.

## 2. Significance of Fiber Multiplication for Fiber Optic Submarine Transmission Lines

The introduction of optical fibers into telecommunication transmission lines brought drastic cost reductions in the construction of large-capacity transmission line facilities due to extended repeater spans. When optical fibers were first introduced, repeater spans were extended over several tens of kilometers. However, there are some current systems which have more than a hundred kilometers of repeater spans <sup>(1)</sup>. Moreover, in the research stages, many experimental results concerning very long-span transmissions accompanied by improvement in both coherent transmission and optical amplifier techniques are reported. For example, a 364-km repeaterless transmission that employs 2.5 Gb/s CPFSK heterodyne detection method and EDF amplifier as a post-amplifier <sup>(2)</sup>, and a 2,200-km long-distance transmission using 25 in-line EDF amplifiers have been reported <sup>(3)</sup>. These reports will have greater

impact on optical submarine transmission lines especially for domestic use due to the use of extended repeaterless sections necessary to bridge longer distance.

Some general advantages of repeaterless systems over repeated systems are mentioned, such as cost effectiveness as submarine repeaters and electrical power supply equipments is not necessary, increased reliability free from trouble caused by holding up power feed. Especially, the greatest advantage is easy upgradability to more advanced transmission systems which are compatible with terrestrial transmission equipment, as a matter of course, these equipment have no restriction in the number of transmission systems to be set up. This means that repeaterless systems are basically the same as terrestrial systems.

Though submarine transmission lines need no underground facility and enable the construction of long-span routes over short periods of time compared with terrestrial routes, however, there are several problems with transmission route design because of much smaller number of optical fibers in a submarine cable than in a terrestrial cable. For example, exchange of multiplexing between the submarine section and terrestrial section at the cable landing points makes networks complicated, and plural installations over the same submarine section leads cost increase. Therefore, arrangements for transmission line facilities to enable to coordinate submarine sections with terrestrial sections have become indispensable.

To design submarine cables with the same maximum number of optical fibers as terrestrial cables confers to make networks simpler and to reduce construction and maintenance costs of transmission lines. Accompanied by extensions in repeaterless spans, fiber optic submarine transmissions will be more widely deployed not only for conventional usage such as channel crossing or linking the mainland with isolated islands, but also for linking large coastal cities (Inter city Trunk Line) and allowing trunk loops to be made to link many islands and so on <sup>(4)</sup>.

Thus 48-fiber optical submarine cable has been developed in order to satisfy present and future demand for multiplying optical fibers in submarine transmission lines (Fig.1).

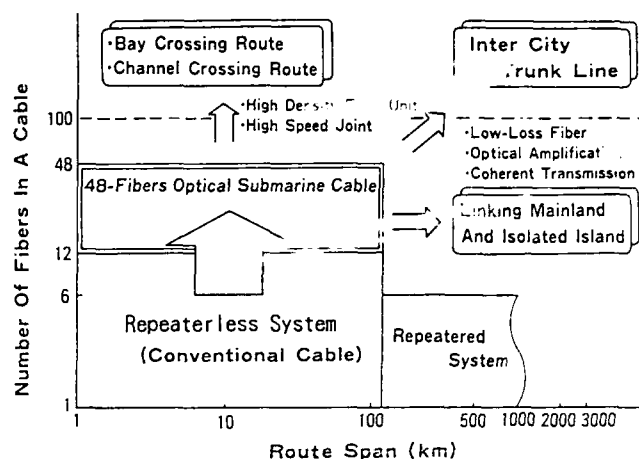


Fig.1 Expansion of application areas for optical submarine cable by progress of technologies

### 3. Cable Design

#### 3.1 Basic Concepts

Figure 2 shows a cross section of NTT's conventional optical submarine cable <sup>(5)</sup>. Most current optical fiber cables employed around the world are based on the following structure, namely an optical unit is accommodated in the center of the cable core, a pressure-resistant and tensile-member composite shell encloses the optical unit. This cable shell not only protects the optical unit against mechanical pressure but also functions as a hermetic layer shutting out external moisture and the adverse effects of hydrogen which would cause optical loss increases. The basic cable structure is formed by sheathing polyethylene around this shell. Many required conditions need to be satisfied in the design of optical submarine cables as illustrated in Fig.3. Conventional cables are manufactured to satisfy these requirements.

Problems caused by drastically increasing the number of fibers in submarine cables primarily originate in the increase of the outer diameter of the optical unit. Similar increases of cable cross sectional structures with the aim of accommodating more fibers causes losses in cable long span productivity and more difficult during construction.

There are some trials to design making cable shell structures simple such as open type cables using hermetic optical fibers <sup>(6)</sup> . However, some problems remain regarding the pressure-resistivity of such kind of cables.

The 48-fiber optical submarine cable was designed to best suit repeaterless submarine sections under several thousand of meters of water, making full use of proven conventional cable techniques to be earlier practice. Cross sections of the new optical cable are shown in Fig.5. To increase fiber density, the following techniques have principally been applied <sup>(7)</sup>.

- (1) Up to 48 fibers are accommodated in an optical unit which consists of four twined 12-fiber optical subunits.
- (2) In order to expand the inner diameter of the pressure-resistant shell, the inner pipe of the conventional cable has been removed. Instead of this, a complex pressure-resistant layer consisting of single-layer steel strands covered with copper tubing has been deployed.

This new cable has attained a fiber density four times higher than a conventional one, maintaining both *outer diameter and weight*. The main features of the new cable compared against conventional cable are shown in Table 1.

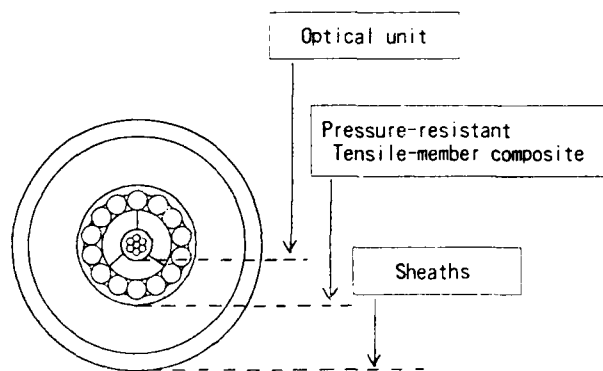


Fig.2 Structure of conventional cable

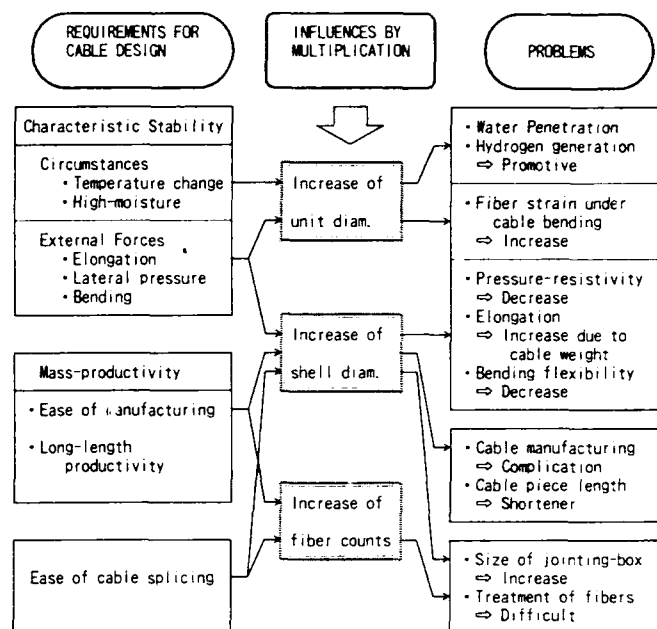


Fig.3 Relationship between requirements for cable design and problem due to multiplication of optical fiber

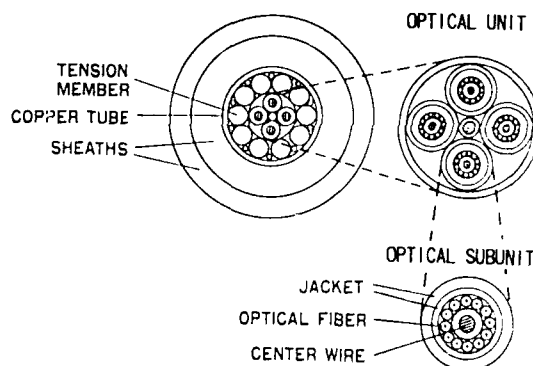


Fig.4 Structures of 48-fiber optical submarine cable

Table 1 Main features of multi-fiber cable and conventional cable

Items	Multi-fiber Cable	Conventional Cable
Maximum number of optical fibers	48	12
Outer diameter ( mm )	22.5	22.5
Weight ( in air ) (kg/m) ( in water )	1.2 0.45	1.2 0.45
Breaking tension ( tons )	10	10

### 3.2 Optical Unit Structure

The optical unit consists of optical subunits which is formed of single optical fibers arranged around a center wire and coated with three layers of UV curable resin. This subunit is similar to the optical unit in a conventional cable and has proven long-term reliability in the field. It has superior characteristics such as stability against temperature changes, repressed water penetration, lower hydrogen generation, and ease of manufacture<sup>(8)</sup>.

In order to accommodate more fibers in a limited space, the diameter of the coated fiber has been reduced from  $400\mu\text{m}$  to  $250\mu\text{m}$  which is the same as that for terrestrial use. Figure 5 shows the relationship between the number of fibers in a subunit, the number of stranded subunits and the total fibers accommodated. As a result, four 12-fiber subunits for the optical unit has been employed.

The optical unit structure which consists of stranded optical subunits has no resemblance to any submarine cables in use around the world. Combined subunits are also coated with UV curable resin to enable suppressed water penetration.

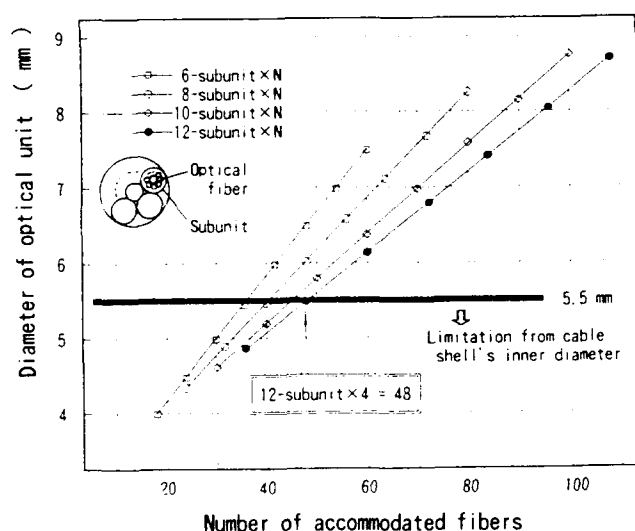


Fig.5 Relationship between number of fibers in a subunit and the number of subunits and total accommodated fibers

### 3.3 Cable Shell Structure

In order to protect the optical unit inside, the cable shell must not be crushed by lateral force or elonged by tension. In conventional cable, sufficient thicked iron pipe enclosing the optical unit and steel strands around the pipe function act as the pressure-resistant layer and the tensile-member, respectively. To accommodate thicker optical units, the shell for multi-fiber cable has had its inner diameter expanded by removing the iron pipe (Fig.6).

The maximum lateral pressure exerted on the submarine cable is  $10\text{ kgf/mm}$ , from cable installation equipment on a cable ship. The cable shell was designed to resist lateral force by pushing forces between the steel wires which also function as tensile-member and surrounding copper tube. Figure 7 shows the relationship between the number of steel wires and the strain on the shell pipe under assumed lateral pressure. As can be seen, the number of wires is limited to less than 10 to prevent shell deformation.

On the other hand, a cable breaking tension of over 10 tons is required, however, excessive wire diameters cause greater weight which should be avoided. The designed region decided by these restrictions is the hatched area in Fig.8. As a result, the maximum inner diameter of the cable shell is 5.5 mm.

To make copper tubing fit the periphery of the circularly arranged steel wires, small diameters of steel wire fill up the gaps between the main wires and tubing.

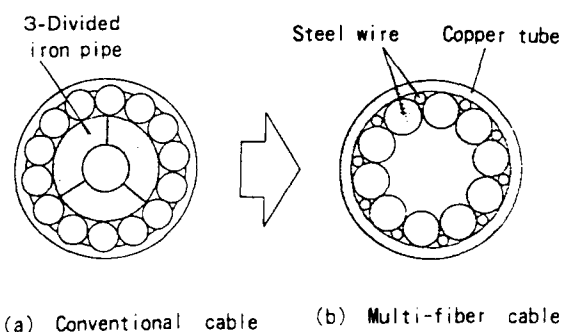


Fig.6 Structure of pressure-resistant function

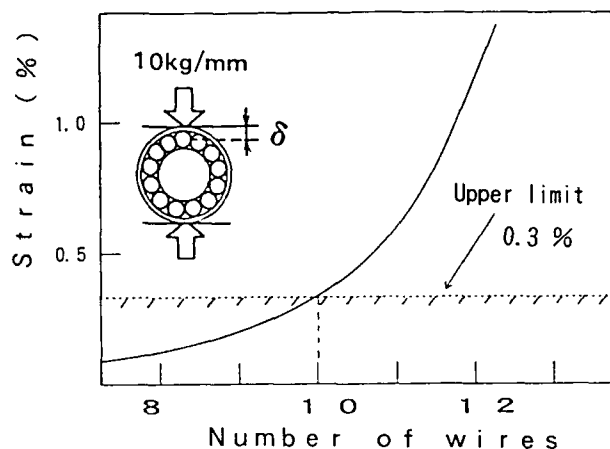


Fig. 7 Relationship between pipe strain due to lateral force and number of wires

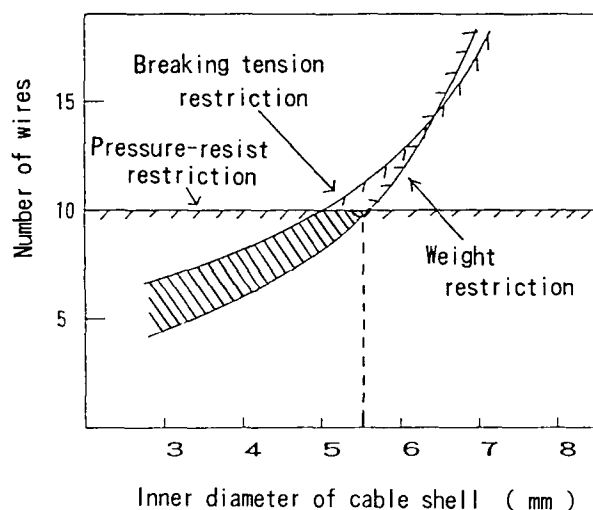


Fig. 8 Relationship between Restrictions in Cable Shell Design and Inner Diameter of Cable Shell

### 3.4 Cable Jackets and Armor Structures

The structures of polyethylene sheaths and steel armor are the same as for conventional cable. Table 2 lists varieties of optical submarine cables. These cables are used according to sea depths or conditions of the sea bottom.

Table 2. Varieties of Cables

Items		Structure	Application
Armorless Type	Light-weight Cable	LDPE + HDPE (O.D. : 22.5 mm)	Mid-deep sea areas
	Buriable Cable	LDPE + HDPE (Thickened) (O.D. : 29 mm)	Shallow sea areas Cable burying section
	High-reinforced Cable	LDPE + HDPE + Steel tape + HDPE (O.D. : 31 mm)	Mid-deep sea areas Protection from abrasive damage or shark bite
Armored Cable		Normal cable + single or double steel armor layer (armor diameter: 5 mm, 7 mm)	Shallow sea areas Buried or non-buried

### 3.5 Characteristics

Table 3 shows test results for the new cable under the same test conditions as for conventional cable. Every result is equal to conventional ones. Tension-elongation characteristics for armorless cable are plotted in Fig. 9, which suggest this cable has sufficient mechanical characteristics for deep sea use. The maximum water depth for the new cable, calculated from the fatigue theory, considering normal processes of cable laying and recovery including 10 hours of holding time for repairs, is 2,000 m even when 1 % strain proof tested fibers are used<sup>(9)</sup>. The increase in strain on fibers while cables are bent, is originated in the increase of radius for fiber layers of optical unit, and that greatly influences the maximum depth of cable installation at sea.

The capacity to withstand a maximum water depth of 2,000 m is sufficient for domestic use. However, as a matter of course, this cable can be used at deeper depths, if 2 % strain proof tested fibers are employed.

Table 3. Test results of manufactured cable

Items	Test conditions	Results
Temperature change	+ 5°C ~ + 30 °C	Optical loss change : Within $\pm 0.001$ dB/km
Lateral pressure	10 kg/mm : 1 hour	No loss increase
Water pressure	800 kg/cm <sup>2</sup> : 0.5 hour	No loss increase
Water penetration	Water : 100 kg/cm <sup>2</sup> pressure : 550 kg/cm <sup>2</sup>	24 m / 1290 min. 80 m / 290 min.
Bending	Radius : 0.4 m 1/2 turn	Loss change: 0.003 dB Max (recovery after release)

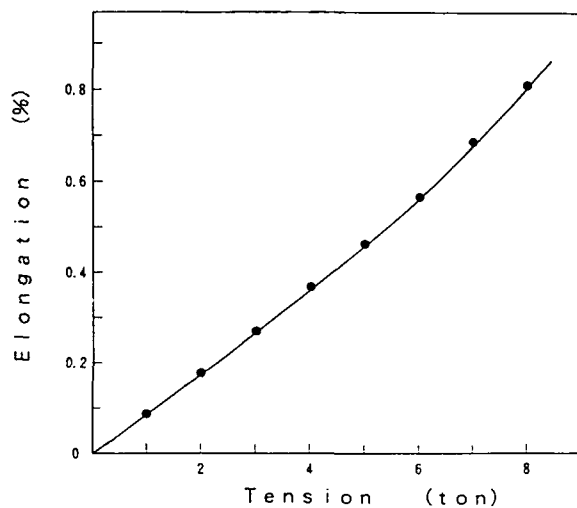


Fig.9 Tension-elongation characteristics

#### 4. Cable Jointing and Multi-fiber Treatment Techniques

Accompanied by the multiplication of cables, cable jointing equipment (joint-box) has also been altered.

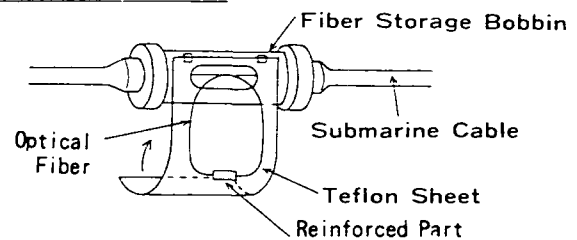
The main functions of the joint-box are to connect tensile-members of each cable and to position and store spare optical fibers. To joint tensile-members, conventional techniques are available, because conventional collective wire chucking method is not influenced by changes in the number or diameter of steel wires<sup>(10)</sup>. Therefore, the fundamental structure primarily determined by the first function above is similar to a conventional joint-box.

On the other hand, new techniques of fiber storage have been employed in order to maintain both joint-

box outer diameter and length of the main straight part as much as possible, against increases in the number of stored fibers. With the conventional method, spare fibers were wound around the fiber storage bobbin. When handling a small number of fibers, the conventional method is best way to house fibers in compact spaces. However, an increase in the number of fibers and a reduction in coated fiber diameter cause an increase in optical loss after stored due to fiber cross over on the bobbin and other difficulties in the handling or ordered arrangements of fibers. For the multi-fiber cable, spare fibers are arranged in six piled trays each eight fibers coiled into small loops (Fig.10). This method has been adapted from the terrestrial fiber treatment technique.

Against the increase in fiber counts, it is also essential to splice fibers efficiently, as the time for cable jointing is limited when cable repairs are conducted on a cable ship. As a result, the mass-fusion splicing method which had proven efficiency in terrestrial ribbon-fiber splicing has been applied to submarine cable<sup>(11)</sup>. In order to adopt mass-fusion splicing to single fibers of the new submarine cable, a method has been employed to position four fibers vertically in line and bind them together with adhesive (Fig.11). The spliced part of the four fibers are reinforced as a group. This also contributes to efficient fiber storage because it saves space.

#### Conventional Method



#### New Method

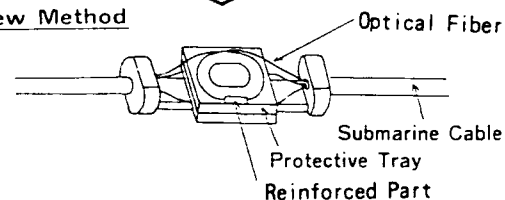


Fig.10 Fiber storage method in joint-box

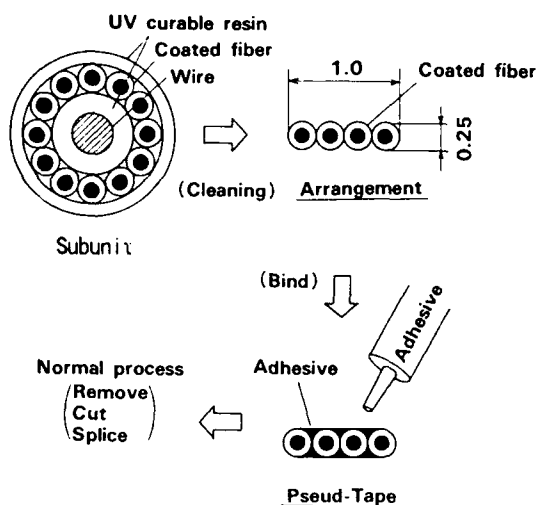


Fig.11 Mass-fusion splicing process for temporary arranged optical fiber

## 5. Commercial Introduction

### 5.1 Outline

A new multi-fiber optical submarine cable was introduced on Kyusyu into the section between Kumamoto (Hondo city) and Nagasaki, in March 1991 for the first time (Fig.12). The repeater span for this section is 78 km including 27 km of submarine section. The transmission system is the F-600M System conforming to SDH with a transmission speed of 600 Mb/s<sup>(1,2)</sup>.

The cable employs twenty-four 1.5  $\mu\text{m}$  dispersion-shifted optical fibers which have proven their high transmission performance in the field and realize maximum repeater span of 120 km for current system.

Commercial tests have been carried out in this section to evaluate the new cable's performance by investigating its transmission characteristics through processes from cable manufacture to construction.

### 5.2 Commercial Test Results

#### 5.2.1 Cable Manufacturing

The optical unit for the introduced cable consists of two subunits each accommodating twelve 1.5  $\mu\text{m}$  dispersion-shifted optical fibers, and two dummy subunits. Thinner optical fiber can be spliced by high-strain proof method within the optical subunit as well as for conventional cable. Consequently, 27.3

km of cable is manufactured in single cable piece. The cable is armored with steel wires with diameters of 7 mm.

Optical loss changes for twenty-four fibers were measured through the cable manufacturing stages from subunit to polyethelene sheathing. Measurement results are shown in Fig.13. The value of loss change is 0.0018 dB/km on average, 0.005 dB/km at maximum. These values permit practical use.

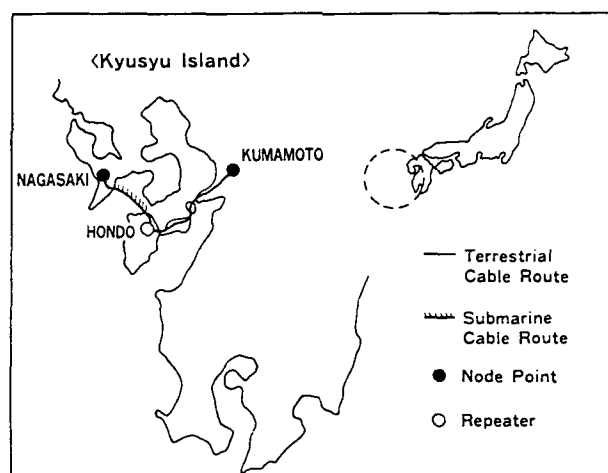


Fig.12 First introduction route

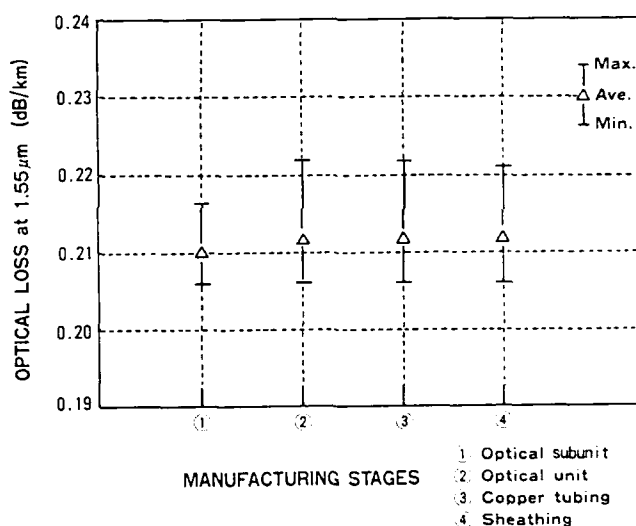


Fig.13 Loss changes during cable manufacturing



### 5.2.2 Cable Installation

The cable was installed by cable ship and buried all section by plow type cable burying machine at the same time. The maximum water depth and burying depth were 72 m and 110 cm, respectively. Cable installation was carried out over 8 hours.

Figure 14 shows loss changes and cable tension during cable installation. Two sets of loop-returned optical fibers (54 km for each loop) were measured at wavelengths of  $1.55\ \mu\text{m}$  and  $1.65\ \mu\text{m}$ . Each measurement result shows insignificant loss changes.

From these results, no occurrence of significant loss changes was verified in the commercial test. This means the new cable has sufficient performance to maintain excellent transmission characteristics for the optical fibers accommodated.

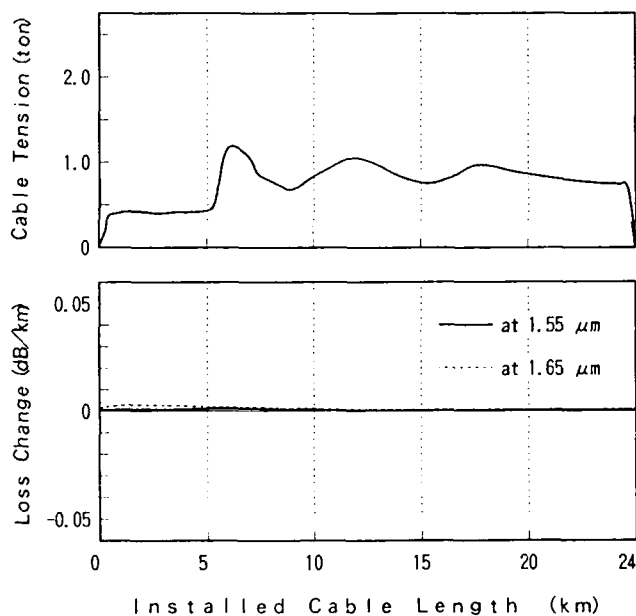


Fig.14 Loss changes during cable installation

### 6. Future Prospects

The object of development behind the 48 fiber optical submarine cable is the construction of an efficient transmission line for submarine sections. As a result, the construction cost of cable per

optical fiber has been remarkably reduced in comparison to the plural installation of conventional cable. However, as shown in Fig.15, conventional cable has economical advantages over the new cable with fiber counts of less than 12. Further, conventional cable is designed most suitable for repeatered systems which need a maximum of six fibers. Therefore, the two types of cables will be selected according to the number of optical fibers for transmission lines, for the time being.

As present terrestrial trunk cables have fiber counts of 100 and more than this in the near future, submarine cables hope to rival these counts. To attain about 100-fibers in a submarine cable, a basic change in the structure of the cable is necessary. In addition, once a submarine cable is damaged, higher counts of fiber in a cable brings larger trouble in telecommunication because whole transmission lines in the cable are out of services while the cable is repaired. Consequently greater advances in submarine cable construction technology are also necessary to prevent high-counts fiber submarine cables from troubles due to external factors.

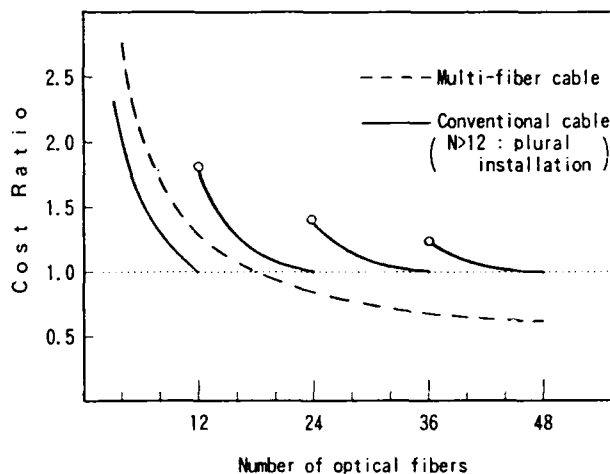


Fig.15 Construction cost per fiber counts for multi-fiber cable and conventional cable

## 7. Conclusion

This paper has described multi-fiber optical submarine cable technologies, and it has detailed excellent results for the first commercial introduction of the new cable. The 48-fiber optical submarine cable will be deployed over several repeaterless optical submarine transmission routes around the country in the near future. The role of this new type cable will become increasingly important as it is more widely deployed.

## Acknowledgements

The authors are grateful to Mr. K. Sato for his valuable advice and engineers in NTT Submarine Cable Engineering Center for their supports for commercial tests in cable constructing.

## References

- (1) K. Uema, et al., "Commercial introduction results of 1.55  $\mu$ m dispersion-shifted fiber submarine cable" 37th IWCS, 1988.
- (2) T. Sugie, et al., "A 2.5 Gb/s, 364 km CPFSK Repeaterless Transmission Experiment Employing an Er-doped Fiber Amplifier and SBS Suppression Optical Link" Topical Meeting on Optical Amplifier, 1990.
- (3) S. Saito, et al., "An Over 2,200 km Coherent Transmission Experiment at 2.5 Gbit/s using Erbium-doped-fiber Amplifiers" OFC'90, 1990.
- (4) O. Kawata, "Objective Areas of Optical Submarine Systems and Prospects of Future Technology" International Seminar on Optical Fiber Submarine Cable Systems, 1990.
- (5) K. Ishihara, et al., "Design and Characteristics of Submarine Optical Fiber Cable" Review of the E.C.L. vol.33 No.6, 1985.
- (6) N. Yoshizawa, et al., "A One-hundred fiber Submarine Cable Composed of Hermetically Coated Fiber Ribbons Inserted into Slots" 38th IWCS, 1989.
- (7) N. Yoshizawa, et al., "Design and Sea Trial Results of a 48-fiber Submarine Optical Fiber Cable (in Japanese)" The Transactions of the Institute of Electronics, Information and Communication Engineers, vol. J74-B-I No.6, 1991.
- (8) N. Yoshizawa, et al., "Design and Characteristics of Optical Fiber Unit for Submarine Cable" Journal of Lightwave Technology, vol. LT-3, No.1, 1985.
- (9) Y. Miyajima, et al., "Fiber Strength Assurance for Deep Submarine Optical Fiber Cable Using the Proof-testing Method" Journal of Lightwave Technology, vol. LT-3, No.2, 1985.
- (10) K. Ishihara, et al., "Submarine Optical Cable Splicing" Review of the E.C.L. vol.33 No.6, 1985.
- (11) Y. Kato, et al., "Single-Mode Optical Fiber Ribbon Splicer" 36th IWCS, 1987.
- (12) K. Maki, "Synchronous Digital Transmission Systems with NNI" NTT Review, vol.1 No.3 1989.



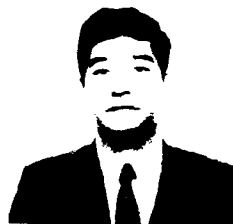
Masao Ohba

NTT Network Systems  
Development Center

Tokyo, Japan

Masao Ohba received his B.E. degree in electrical engineering from Nagoya University in 1986. He joined NTT in 1986. He is an engineer in the Telecommunications Cable Systems & Outside Plant Group in NTT Network Systems Development Center.

He is a member of the Institute of Electronics, Information and Communication Engineers of Japan.



Osamu Kawata

NTT General Planning  
Headquarters

Tokyo, Japan

Osamu Kawata received his B.E. and M.E. degrees in electrical engineering from Tokyo Institute of Technology in 1974 and 1976. He joined NTT in 1976. He is a Manager of Engineering Strategy Technology Research Department.

He is a member of the Institute of Electronics, Information and Communication Engineers of Japan.



Sakae Ohshiro

NTT Telecommunications  
Development Center

Tokyo, Japan

Sakae Ohshiro received his B.E. degree in electrical engineering from Ryukyu University in 1988. He joined NTT in 1988. He is an engineer in the Telecommunications Cable Systems & Outside Plant Group in NTT Network Systems Development Center.

He is a member of the Institute of Electronics, Information and Communication Engineers of Japan.



Takuya Uenoya

NTT Network Systems  
Development Center

Tokyo, Japan

Takuya Uenoya received his B.E. and M.E. degrees in electrical engineering from Waseda University in 1971 and 1973. He joined NTT in 1973. Since 1989, he has been a General Manager in the Telecommunications Cable Systems & Outside Plant Group in NTT Network Systems Development Center.

He is a member of the Institute of Electronics, Information and Communication Engineers of Japan.

OPTICAL SUBMARINE CABLES WITHOUT SUBMERGED REPEATERS  
FOR THE ITALIAN 565 Mbit/s COASTAL HOPPING NETWORK ("FESTOON PROJECT")

A.Bolza, F.Magnani, E.Occhini

Pirelli Cavi S.p.A., Milan, Italy

Abstract

The paper gives in the first part a description of the dispersion shifted optical fibers used in the Italian 565 Mbit/s coastal hopping network and of the general characteristics of the transmission system adopted. A reference is also made to the experiments in progress with optical amplifiers. These devices can be envisaged either to increase the unrepeated cable lengths of future links or to allow an increase in the transmission capacity of an already installed link.

The second part is devoted to the design and manufacture of the submarine cables, including the discussion of the physical characteristics required during laying and recovery and the tests performed.

Successively, in the third part, the laying procedures are described, together with the cable ship used and her facilities. Near the shore, where the risk of damage caused by trawlers or anchors is higher, the cable is reinforced and designed to be buried in the sea bottom.

1. Introduction

In the mid Eighties the Italian Post Office (ASST) decided to realize a nationwide long distance optical network involving 6500 km of land cables and 1350 km of submarine cables. Shortly afterwards, however, the rapid increase in traffic and the need to enhance the Italian telecommunications infrastructure in the European context required a further strengthening of the long distance network. This led to the development of a 565 Mbit/s coastal hopping submarine system without submerged repeaters, commonly known as "Progetto Festoni" (Festoon Project). The first phase of this project, which involved the installation of approximately 1800 km of optical cables along Italy's western coast, was implemented between late 1989 and early 1991.

2. The Italian Coastal Hopping Network

The Italian 565 Mbit/s coastal hopping network consists of a system of submarine links all along the Italian coast, the first phase of which connects the nodes of the land network from Genoa to Palermo in the Tyrrhenian Sea (see Fig.1). The average length of the links is about 146 km with a maximum of 182 km (see Table 1). The system operates at the same bit rate of the ASST land network and, as requested by the customer, does

not employ submerged repeaters.

Taking into account the environmental conditions of this project the use of submarine cables had



Fig.1 - Italian Coastal Hopping Network

many advantages over land cables, the most important being:

- a very significant reduction in installation time resulting from the intrinsic speed advantages of submarine laying compared with land installation, particularly in densely populated areas;
- the elimination of the problems related to the attainment of rights of way, which can cause major delays in land projects or even make them impossible;
- the possibility of exploiting, as a back-up to the land network, a completely independent system having the same transmission characteristics so that the submarine and the

land links constitute a completely integrated network.

LINK		LAND PART	SUBMARINE PART	TOTAL LENGTH
GENOVA	PISA	14.5	14.6	29.1
PISA	GRUGLIANO	11.5	14.6	26.1
GRUGLIANO	PIVITAVECCHIA	26.5	14.6	41.1
PIVITAVECCHIA	PIEMONTE	16.5	14.6	31.1
PIEMONTE	PIEMONTE	14.5	14.6	29.1
PIEMONTE	NAPOLI	11.5	14.6	26.1
NAPOLI	SALERNO	11.5	14.6	26.1
SALERNO	SALEA	11.5	14.6	26.1
SALEA	LAMEZIA	11.5	14.6	26.1
LAMEZIA	MESSINA	11.5	14.6	26.1
MESSINA	ALAGATA	11.5	14.6	26.1
ALAGATA	SALERNO	11.5	14.6	26.1
TOTAL		140.5	140.6	281.1

TAB. 1 - Actual Length of the Links (km)

Of course this ambitious project involved the use of very sophisticated equipment and cables to reach the performances required for the transmission of 565 Mbit/s over lengths of almost 200 km without submerged repeaters. On the other hand, a significant reduction of the submarine lengths in order to use more standard equipment and cables, would have made the solution much less attractive both from an economical and a technical point of view.

### 3. Optical Fiber Characteristics

The main characteristics of the 565 Mbit/s transmission system are indicated in Table 2. Since unrepeatable links having lengths of the order of 200 km with an overall dispersion  $\leq 600$  ps/nm were required, the only possible choice was to use Dispersion Shifted (D.S.) fibers. As is well known, D.S. fibers have a special distribution of the core refractive index in order to locate the point of zero dispersion in the proximity of the wavelength corresponding to the so called third window (1550 nm), where the attenuation of silica based fibers reaches its minimum.

This choice implied a slight increase in attenuation compared to conventional single mode fibers, so that it was necessary for the longest links to establish a selection procedure in order to maintain the attenuation  $\leq 0.2$  dB/km.

In Table 3 the relevant characteristics of the optical fibers used in the project are collected. In Figs. 2 and 3 a typical refractive index distribution and the corresponding behaviour of the fiber dispersion are indicated.

At this point, comparing Tables 2 and 3, it is easy to verify that in these conditions maximum lengths of the order of 200 km without signal

regeneration are actually feasible. As already mentioned the longest link of the project has a length of 182 km.

OPTICAL SOURCE:	LASER InGaAsP DFB;
PHOTO DETECTOR:	APD InGaAs;
WAVELENGTH:	1535 - 1575 nm;
SPECTRAL WIDTH OF OPTICAL SOURCE AT HALF AMPLITUDE:	0.2 nm;
TYPICAL OUTPUT POWER OF THE OPTICAL SOURCE:	$> -3.8$ dBm;
TYPICAL POWER AT S POINT:	$> -1.4$ dBm;
TYPICAL SENSITIVITY OF THE RECEIVER FOR BER = $10^{-10}$ :	$< -41.9$ dBm;
TYPICAL SENSITIVITY AT POINT R FOR BER = $10^{-10}$ :	$< -40.1$ dBm;
EQUIPMENT MARGIN:	1 dB;
AVAILABLE ATTENUATION BETWEEN POINTS S AND R:	40.5 dB;
MAXIMUM DISPERSION BETWEEN POINTS S AND R:	600 ps/nm;

TAB. 2 - Electro-Optical Characteristics of the System

<u>OPTICAL CHARACTERISTICS</u>	
FIBER TYPE:	SINGLE MODE, DISPERSION SHIFTED;
OPERATING WAVELENGTH RANGE:	1535 - 1575 nm;
ATTENUATION FOR CONNECTION LENGTH $\leq 160$ km:	$\leq 0.22$ dB/km at 1535-1575 nm;
ATTENUATION FOR CONNECTION LENGTH $\geq 160$ km:	$\leq 0.20$ dB/km at 1535-1575 nm;
TOTAL DISPERSION:	$\leq 3$ psec/(nm km) at 1535-1575 nm;
CUT-OFF WAVELENGTH:	1270 $\pm$ 150 nm;
REFRACTIVE INDEX DIFFERENCE:	0.9% (NOMINAL).
<u>DIMENSIONAL CHARACTERISTICS</u>	
MODE FIELD DIAMETER:	8.1 $\pm$ 0.7 $\mu$ m;
DIAMETER OVER THE CLADDING:	125 $\pm$ 2 $\mu$ m;
MODE FIELD ELLIPTICITY:	$\leq 10\%$ ;
CLADDING ELLIPTICITY:	$\leq 2\%$ ;
ECCENTRICITY BETWEEN MODE FIELD AND CLADDING:	$\leq 1 \mu$ m.
<u>MECHANICAL CHARACTERISTICS</u>	
MINIMUM BENDING RADIUS:	40 mm;
"SCREEN TEST":	1.5%.

TAB. 3 - Summary of the Fiber Characteristics

Finally, from the point of view of mechanical characteristics, the screening test applied to all fibers corresponds to a 1.5% deformation.

### 4. Future Upgrading of the Transmission System using Optical Amplifiers

An explicit requirement of the project was the possibility to upgrade its capacity from 565

Mbit/s to 2.4 Gbit/s without replacing the cables already installed.

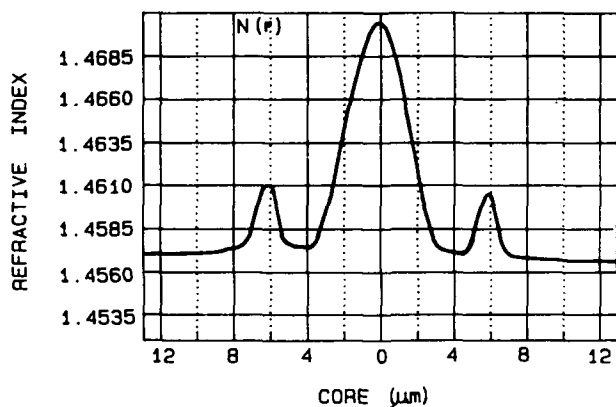


Fig. 2 - Refractive Index Profile of a Single Mode D.S. Fiber

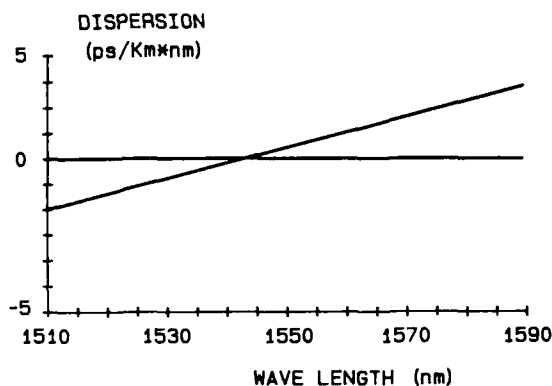


Fig. 3 - Dispersion of a Single Mode D.S. Fiber.  
Wave length at dispersion zero = 1541 nm  
Dispersion at 1550 nm = 0.55 ps/km.nm  
Dispersion at 1530 nm = -0.69 ps/km.nm  
Dispersion at 1570 nm = 1.75 ps/km.nm

In principle optical fiber characteristics allow this increase in transmission bit rates but receiver sensitivity becomes the critical point. In fact the increase in transmission capacity implies a reduction in receiver sensitivity, thus making the power budget insufficient for the longest links of the project.

To solve this problem, the use of optical amplifiers<sup>1,2</sup> has been considered (Fig. 4) both as power amplifiers at point S (sending point) and as preamplifiers at point R (receiving point). This compensates for the above mentioned reduction in sensitivity of the receivers and the exploitation of the system at 2.4 Gbit/s can therefore be obtained by simply changing the terminal equipment.

A simplified scheme of the optical amplifier is presented in Fig. 5. This optical amplifier involves the use of a silica based active fiber, similar to the transmission fibers but doped with

Erbium.

As is well known, Erbium atoms are excited by a suitable radiation coming from a pump laser and injected in the active fiber by means of a dichroic

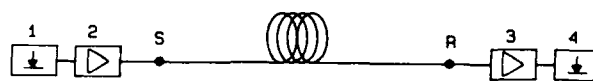


Fig. 4 - Transmission Line with Optical Amplifiers at Both Ends.  
1-Emitter; 2-Optical Amplifier;  
3-Optical Preamplifier; 4-Receiver.

coupler. The collisions between the photons emitted by the transmitter and the excited atoms cause the emission of other photons having wavelength equal to that of the incident photons therefore producing the amplification of the transmitted signal. The wavelength at which this amplification takes place is between 1530 nm and 1560 nm.

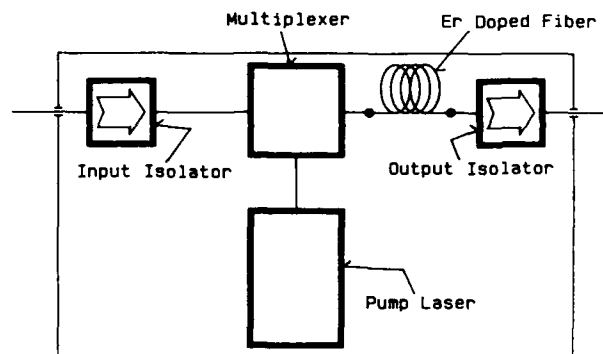


Fig. 5 - Simplified Scheme of an Optical Amplifier

It is worth noting that these amplifiers can be very easily connected to the transmission fibres with negligible insertion losses, as in conventional fiber splicing.

The possibility of coupling in this way a power of 15 dBm with the transmission fiber has already been demonstrated.

Furthermore, experiments performed with this type of optical amplifiers have also demonstrated the possibility of transmitting 11 Gbit/sec over 260 km of D.S. fibers. This result implies that, with the same fibers and direct transmission, it is possible in principle to transmit 2.4 Gbit/s over distances of the order of 1000 km before the dispersion of the fiber becomes a limiting factor. Of course, in order to transmit over such a distance, the use of many optical amplifiers is

necessary to compensate the fiber attenuation, but the above quoted figure gives an idea of the margin of the actual transmission system from the point of view of D.S. fiber dispersion. A field trial with optical amplifiers is now in progress on the actual system, using a pair of fibers of the two contiguous links Pomezia-Formia and Formia-Napoli which have been connected together, thus obtaining a total transmission length of 248 km. The most important characteristics of this link are described in Table 4.

. BIT RATE	565 Mbit/sec
. POWER AT "S" POINT	13 DBm
. SENSITIVITY AT POINT R for BER = $10^{-10}$	- 44 dBm
. AVAILABLE ATTENUATION BETWEEN POINTS S AND R	56 dB
. SYSTEM MARGIN	1 dB

TAB.4 - Electro-Optical Characteristics of the Link with Optical Amplifiers

#### 5. Submarine Cables

The submarine cables which have been adopted for the project are of the grooved core type (see Figs. 6 and 7), with 6 grooves and 2 fibers in each groove for a total of 12 transmitting fibers.

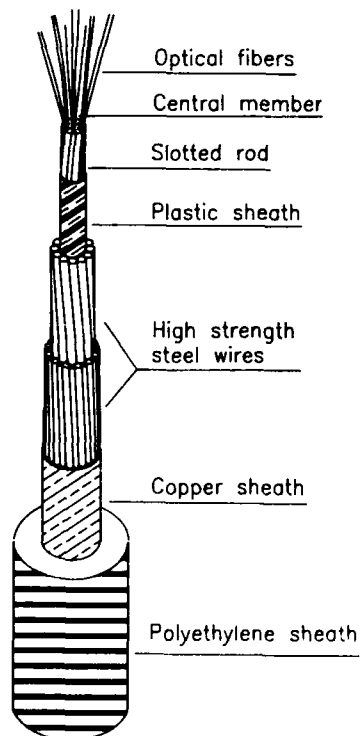


Fig. 6 - Light Weight Submarine Cable

The core and in particular the shape of the

grooves have been designed in order to obtain a complete mechanical decoupling of the optical fibers from the mechanical stresses applied to the cable between well defined limits which will be discussed later. This decoupling is essentially

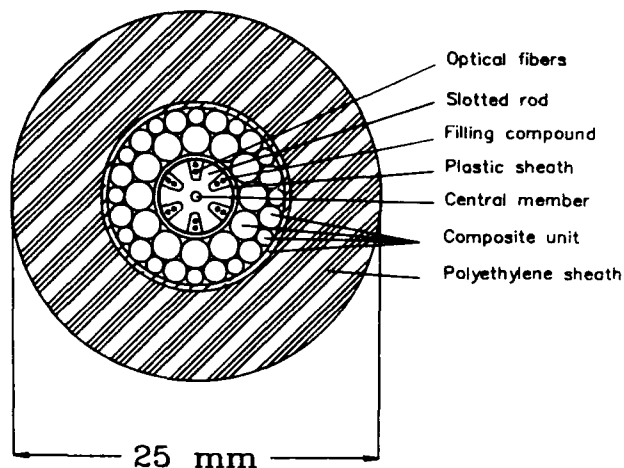


Fig.7 - Light Weight Submarine Cable

obtained by an elastic elongation of the central member applied during the deposition of the fibres in the cable core. When the stress causing the elongation is removed after the deposition of the fibres they take their precalculated positions in the grooves.

The core is surrounded by a plastic jacket and by a mechanical resistant structure made with two layers of high strength steel wires designed to withstand both the pulling tensions during laying and recovering operations and the external water pressure.

Over the mechanical resistant structure a continuous longitudinally welded copper sheath is applied to prevent the radial penetration of water.

The void spaces inside the copper sheath, are filled with suitable sealing compounds designed to:

- prevent longitudinal water penetration;
- absorb irreversibly the  $H_2$  molecules which can be released by the materials present in the structure<sup>4</sup>.

Over the copper sheath a polyethylene jacket is extruded and successively external armours are applied as necessary.

The external armours are designed to protect the cable near the shores against transversal stresses caused by ship anchors, trawlers, etc.

In Figs. 8,9,10 the different types of external armours used in the project are illustrated; they are chosen as a function of sea depths following the criteria illustrated in Table 5. For depths greater than 1600 m a Light Weight deep sea cable without external armour has been envisaged.

The mechanical characteristics of the cables with and without external armours are recorded in the same Table 5. The relevant deformations have been

theoretically calculated and verified by means of suitable experiments.

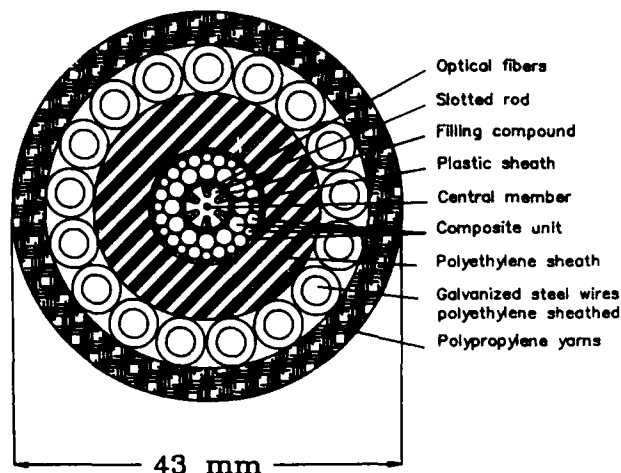


Fig. 8 - Light Weight Armoured Cable

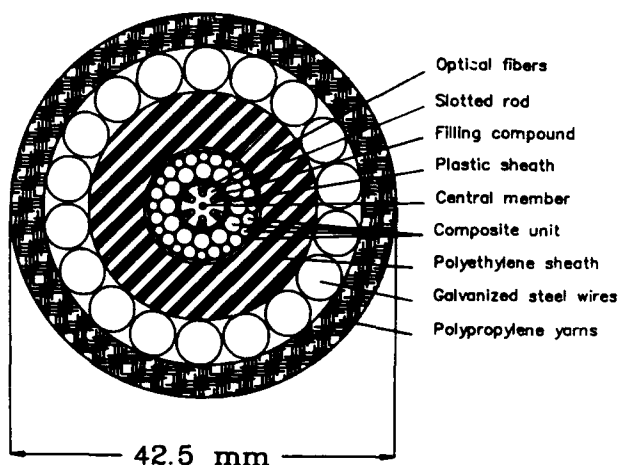


Fig. 9 - Single Armoured Cable

The stress-strain characteristic of the Light Weight deep sea cable, obtained by applying a mechanical tension to the cable through a freely rotating pulling head, is represented in Fig. 11 together with the corresponding deformations of the optical fibers. It is easy to verify that up to a tension force of 3000 kg, corresponding to a cable deformation of about 0.23%, the fibers are not submitted to any stress. On the other hand the maximum mechanical tension which can be anticipated in the case of a difficult recovery is conventionally given by the equation:

$$T_2 = 2.5 \, wd$$

where

$T$  = mechanical tension  
 $w$  = unit weight of the cable in water  
 $d$  = sea depth.

For the depth  $d = 3000 \, \text{m}$  tension  $T_2$  reaches the value of 4750 kg with a deformation of the cable of 0.42%. Observing Table 5, it is easy to note

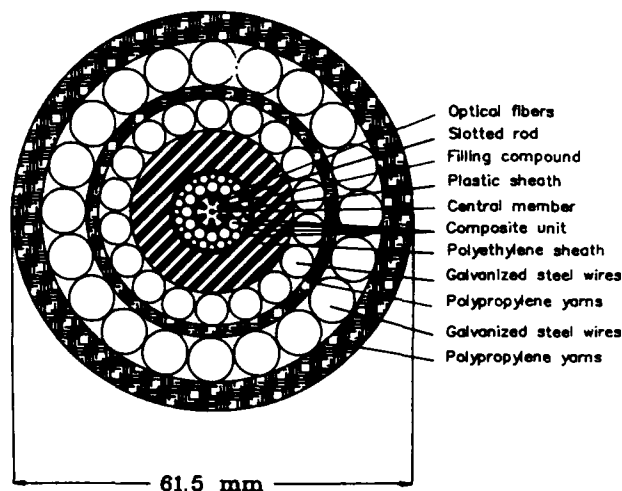


Fig. 10 - Double Armoured Cable

CABLE TYPE	DA	SA	LWA	LW
LAYING MAXIMUM DEPTH $d_0$ : [m]	100	800	1600	3000
UNITARY WEIGHT IN WATER $w$ : [kg/m]	8.1	3.0	1.4	0.636
PULLING FORCE AT $T_0 = wd_0$ : [kg]	810	2400	2240	1900
DEFORMATION AT $T_0$ : $\epsilon_0$ [%]	0.01	0.11	0.14	0.14
PULLING FORCE AT $T_1 = 1.6 \, wd_0$ : [kg]	1300	3840	3580	3040
DEFORMATION AT $T_1$ : $\epsilon_1$ [%]	0.03	0.17	0.22	0.22
PULLING FORCE AT $T_2 = 2.5 \, wd_0$ : [kg]	2030	6000	5600	4750
DEFORMATION AT $T_2$ : $\epsilon_2$ [%]	0.07	0.29	0.33	0.42
CABLE ROTATIONS AT $T_2$ : [TURNS/100 m]	1	11	21	28

TAB. 5 - Different Types of Submarine Cables Used for the Coastal Hopping Network and their Mechanical Characteristics.

$T = wd$  : is the pulling force on board the ship required to lay a cable having unit weight in water  $w$  at the depth  $d$  with no residual force on the sea bottom;

DA: Double Armour cable;

SA: Single Armour cable;

LWA: Light Weight Armour cable;

LW: Light Weight cable.

that this is the highest deformation reached by the different cable types used in the project. Under these conditions the optical fibers are submitted to a deformation of 0.1%, to be compared with the screening value of 1.5% to which the fibers are submitted during the mechanical screening test.



In order to simulate the situations which happen during the actual laying and recovery of the cable, tension tests with the Light Weight cable

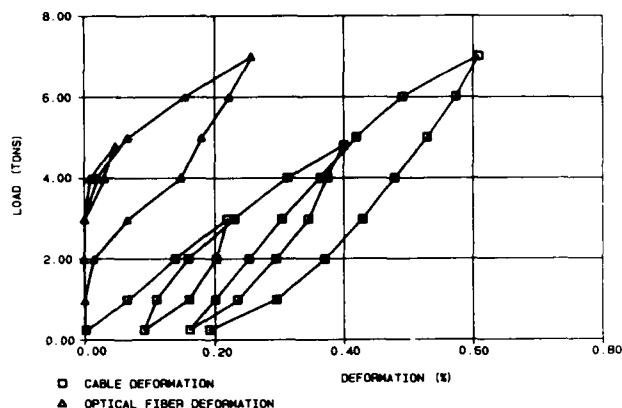


Fig. 11 - Mechanical Characteristics of the Light Weight Cable Obtained with a Freely Rotating Pulling Head

passing back and forward on a pulley having a 3 m diameter have been executed under tension  $T_2 = 4750$  kg. The attenuation of the optical fibers returned completely to the original values after the unloading of the cable.

Similar tests were made at  $T_1 = 1.6$  wd = 3040 kg with the tension force applied for a time span extended to 48 h, in order to represent the actual situation during a repair at sea. In this case no variations of attenuation during the test were observed. This result is in good agreement with Fig. 11 which shows that in correspondence with this mechanical tension the optical fibers are still practically unstressed.

The mechanical performances discussed above have been considered more than satisfactory with respect to the requirements of the project under consideration. Additional cable designs have been also developed for more exacting situations and have been used in other recent projects.

The mechanical specifications of the cable included also an hydrostatic pressure withstanding test at 400 bar for 96 h and a longitudinal water tightness test at 200 bar for 7 days. Both these tests have been successfully passed.

The experience gained laying the twelve links of the first part of the project (see Table 1) fully confirmed the results obtained in the above tests. Finally it may be interesting to recall that the void spaces inside the mechanical resistant structure have been filled with a special sealing compound which can chemically absorb the amount of  $H_2$  released by the structure components. The use of this compound allows to reach safely a high level of filling of the cable without the necessity to take into account the presence of  $H_2$  during the cable life, with the correlated well known negative effects on the attenuation of the fibers. In fact, without this absorption, the  $H_2$  relative pressure should have been, roughly speaking, in the inverse proportion to the volume of voids present in the structure, making a

satisfactory filling very risky.

## 6. Installation of the Submarine Cables

Prior to the laying of the cables a detailed marine survey was carried out for each link in order to define all the parameters needed to design a proper installation.

The data collected were mainly bathimetric and side scan sonar records in the offshore portion, while in the landing areas, where improved cable protection was envisaged, additional sub-bottom data were collected.

Regarding the choice of the cable routes, the difference between the features of a coastal hopping and a conventional submarine connection must be taken into account.

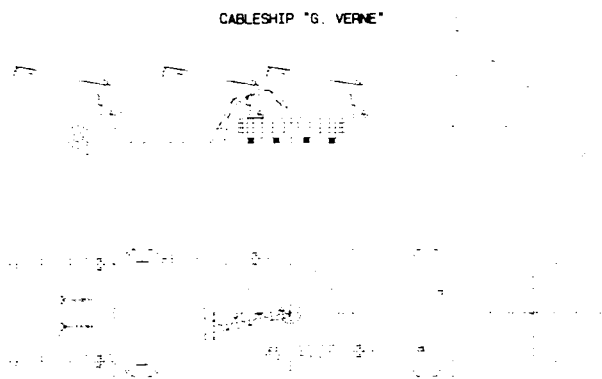


Fig. 12 - Cables ship "Giulio Verne"

In fact the characteristic of a coastal hopping route is to start heading offshore as a conventional lay, to turn roughly parallel to shore as soon as the environment allows it and then, after a relatively short length, to head back toward shore. Taking into account the uneven morphology of the Italian coasts and of the sea bottom in the areas involved, the selected routes were carefully defined with the introduction of several turning points in order to follow the most suitable bottom profile.

The cables ship "Giulio Verne" (Fig. 12)<sup>5</sup> was used for the laying operations. The main characteristics of the ship are summarised in Table 6. The high manoeuvrability of this ship is ideally suited for the type of cable routes involved.

The computation of the ship speed and position, needed to control the proper cable quantity to be paid-out, was performed with a radio positioning system using up to nine shore stations. This solution, which implies a rather sophisticated shore network and on-board data logging and computing, was required because of the complexity of the cable routes which made conventional and simpler methods not acceptable.

As regards the potential damages due to fishing activities or other hazards, an accurate analysis of the risks involved was carried out.

The solution adopted was to embed the cables up to 35 m of water depth, which was shown to be the

most risky area. Two different embedding machines were used according to the soil conditions: a self-propelled trenching machine for harder soil (Fig. 13) and a jetting machine for sandy/muddy soil (Fig. 14).

BUILT IN	1984
LENGTH	128.27 m
BREADTH	30.48 m
DRAFT (OPERATING 4 THRUSTERS)	8.50 m
DRAFT (OPERATING ONLY STERN THRUSTERS)	5.50 m
DEADWEIGHT	15.000 t
CABLE CAPACITY	9.500 t
MAXIMUM SPEED	10 kn
PROPULSION	4 x 1700 hp

TAB. 6 - Main Features of the Cables ship Giulio Verne

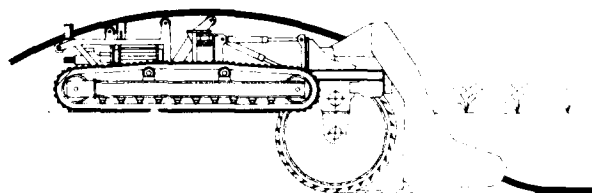


Fig. 13 - Trenching and Embedding Machine

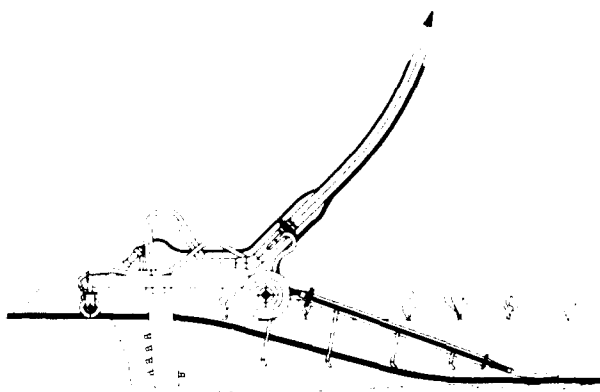


Fig. 14 - Jetting Machine

Extending the protection to a greater water depth would have significantly increased the relevant costs and was not justified by the risk analysis carried out in connection with this project. It should however be noted that embedding techniques are already available for depths up to 900 m and can be considered in cases of real need.

## 7. Conclusions

The many aspects related to the realization of a large 565 Mbit/s coastal hopping submarine cable system with maximum unrepeated lengths of the order of 200 km have been reviewed.

A complete integration among the different components of the system (terminal equipment, optical fibers, submarine cables, laying techniques, cable protection) was proved to be essential in order to bring to a successful completion the first major coastal hopping network in the world.

Field tests using optical amplifiers are in progress and are expected to demonstrate the possibility of increasing the transmission capacity of the above network from 565 Mbit/s to 2.4 Gbit/s.

## 8. Bibliography

- [1] Present Status of Erbium Doped Fiber Amplifier and Laser.  
A.Righetti.  
O.E.C. 1990 Conference, Tokyo, July 1990.
- [2] High Power Erbium Doped Fiber Amplifiers Operating in the Saturated Regime.  
R.I.Laming, J.E.Townsend, D.N.Payne, F.Meli, G.Grasso, E.J.Tarbox.  
IEEE Photonics Technology Letters, Vol.3, No.3, March 1991.
- [3] An 11 GBit/sec, 260 km Transmission Experiment Using a Directly-Modulated 1536 nm DFB Laser with two Er-Doped Fiber Amplifiers and Clock Recovery.  
A.Righetti, F.Fontana, G.Del Rosso, G.Grasso, M.Z.Iqbal, J.L.Gimlett, R.D.Standley, J.Young, N.K.Cheung, E.J.Tarbox.  
ECOC 1989.
- [4] Overcoming the Hydrogen Problem in Optical Cables.  
P.Anelli, G.Grasso, E.Modone, B.Sordo, F.Esposto.  
International Wire and Cable Symposium, Cherry Hill, November 1985.
- [5] "Giulio Verne": the Italian Innovative Cable Ship.  
G.Bazzi, G.Monti, F.Magnani, F.Corbellini.  
Conference on Electrical Power Supply Industry (CEPSI), Singapore, November 1990.



ALDO BOLZA  
Pirelli Cavi SpA  
Milan, Italy

Aldo Bolza received his Dr. Ing. degree from the University of Naples in 1967. He joined Pirelli in 1968 and has since held several engineering and management positions in Italy, the U.K. and Canada.

He was responsible for Pirelli's submarine cable activities from 1989 to 1991 and is currently Director of R&D of Pirelli Cavi S.p.A.

He is a Fellow of the IEE and a Senior Member of the IEEE.



FRANCESCO MAGNANI  
Pirelli Cavi SpA  
Milan, Italy

Francesco Magnani received his Dr. Ing. degree from the Politecnico of Milan in 1969. He joined the R&D Department of Pirelli Cavi in 1971. He was involved in different development projects of telecommunication and power cables and accessories. He is now responsible for system engineering for turn key projects, including cables, equipment, accessories and installation.



ELIO OCCHINI  
Pirelli Cavi SpA  
Milan, Italy

Elio Occhini was born in Viareggio (Italy) in 1928.

In 1952 he obtained his electrical engineering degree from the Polytechnic Institute of Milan. In 1953 he joined the Research Laboratories of Pirelli Cavi, in 1972 was appointed R & D Manager and from 1979 to the end of 1990 he held the position of Chief Engineer.

From January 1991 he is Senior Technical Consultant to Pirelli Cavi SpA.

He is a member of the A.E.I. (Italy), a Fellow of the I.E.E.E. (USA), a member of OSA and a Fellow of the I.E.E. (UK).

Dr. Occhini is author and co-author of many papers published in Italy, the UK and the USA.

# Design and Test Result of OS-560M Optical Submarine Cable, Repeater Housing and Coupling

Y. Noguchi, I. Marugome, N. Norimatsu, Y. Yamazaki, H. Yamamoto

KOKUSAI DENSHIN DENWA CO., LTD. (KDD)  
2-3-2 Nishi-shinjuku, Shinjuku-ku, Tokyo 163, JAPAN

## Abstract

This paper describes the design and test results of OS-560M optical submarine cable, repeater housing and cable coupling used in the fourth Transpacific Cable (TPC-4) which is now under construction toward the ready for service (RFS) date of October, 1992.

The OS-560M optical submarine cable have adopted highly purified silica core with fluorine-doped cladding optical fiber because of its low attenuation property. The average attenuation characteristic of the cabled fiber is 0.180 dB/km at 1.55  $\mu\text{m}$ .

In order to accomodate six(6) regenerative circuits in the repeater housing, repeater pressure housing and cable coupling is redesigned from those of the OS-280M. Design evaluation tests such as temperature test, tensile test, water pressure test have been extensively conducted and concluded in good performance. At the final stage of its development, it has been confirmed that modified repeater housing and cable coupling have its conformability to the laying facilities of the cable ship through the handling test on board cable ship.

span length for the OS-560M system can be extended to about twice that of the OS-280M system. The optical parameters are optimized taking into account various stresses in the cable manufacturing, cable handling, laying and 25 years life time. Through the various evaluation tests such as water pressure test, tensile test, temperature test, etc., it has been confirmed that the characteristics of the OS-560M optical fiber submarine cable are stable for the 25 years design life.

With regard to the repeater, repeater pressure housing is redesigned in order to accomodate six(6) regenerative circuits in the housing. Cable coupling is also redesigned to accomodate the fiber splices between cable and repeater in it. Various evaluation tests using prototype repeater housing and cable couplings were conducted including the handling test on board ship. The results obtained from these evaluation tests were good in performance.

This paper describes the design and test results of the OS-560M cable, which is currently entering into commercial production, as well as the newly developed repeater housing and cable coupling.

## Introduction

The OS-560M optical fiber submarine cable system<sup>[1],[2]</sup>, designed to operate at a wavelength of 1.55  $\mu\text{m}$ , has been developed as a successor of the OS-280M system, used in the third Transpacific Cable system (TPC-3) which operates at a wavelength of 1.3  $\mu\text{m}$ <sup>[3],[4]</sup>. The OS-560M system is currently entering into commercial production, and is applied to TPC-4 which will be ready for service in October 1992. The mechanical / electrical design of the optical submarine cable used in the OS-560M system is the same as that of the OS-280M system, which has already proven itself in TPC-3 and the other cable systems<sup>[5]</sup>. Regarding the optical design, the OS-560M system chooses 1.55  $\mu\text{m}$  wavelength and uses optical fiber<sup>[6]</sup> of a highly purified silica core with fluorine-doped cladding in order to make use of low attenuation property of silica based fiber at maximum. The attenuation property of a highly purified silica core fiber at 1.55  $\mu\text{m}$  wavelength is roughly half that of a germanium-doped core optical fiber at 1.3  $\mu\text{m}$  wavelength. As a result, the repeater

## Cable Design

Table 1 shows the mechanical / electrical design parameters of the OS-560M lightweight optical fiber submarine cable. These design parameters are the same as that for the OS-280M LW Cable. Optical fibers in the cable are screened with 2% elongation and all the splicing points in the cable are screened with 2.5%. So that, the optical fibers in a cable can withstand the tension during the recovery from a depth of up to 8,000 meters.

The OS-560M cable is designed to withstand water pressure of up to 850kgf/cm<sup>2</sup>, which would allow the cable to be laid across the Japan Trench. (TPC-3 crossed the Japan Trench at 8,190 meters.) Figure 1 shows the cross-sectional view of the OS-560M optical submarine cable. The cable consists of an optical fiber unit with six(6) optical fibers, a water pressure resistance layer composed of a three devided steel pipe, high-tensile steel strands, a copper tube, and a layer of polyethylene insulation with an external polyethylene jacket. The OS-560M optical submarine

cable uses highly purified silica core with fluorine-doped cladding optical fibers of which zero chromatic dispersion wavelength is around  $1.3\ \mu\text{m}$ . This optical fiber is designed for a  $1.55\ \mu\text{m}$  wavelength transmission where the transmission loss of silica based fiber is minimized. The major fiber parameters are optimized<sup>[7]</sup> in order to take advantage of the low-loss characteristics and to minimize the transmission loss change due to the microbending resulting from cable manufacturing, cable handling, etc., and to keep stable characteristics during 25 years. [ Note : This optical fiber is based on the recommendation in CCITT SGVX G.654. ]

The optical fiber unit contains six(6) color coated optical fibers in order to identify each other. The stranding pitch has been changed from 200mm in case of the OS-280M cable to 300mm in order to speed up the production of the optical fiber unit. These modification might affect on the curing of the unit forming material (UV-curable resin) surrounding the optical fibers in the optical fiber unit manufacturing process, and there might be a possibility that excessive microbending losses are induced by heating during the cable manufacturing process. Therefore, we conducted various evaluation tests such as heat cycle test, long term stability test, and as a result it was confirmed modified optical fiber unit has a good performance.

In addition, while the repeater span length of the OS-280M system was 50 to 70km, the repeater span length of the OS-560M system can be extended to more than 120km. Maximum unit cable length is set as 75km taking into account technical point of views such as existing cable manufacturing facilities, manufacturing efficiency, maximum repeater span length, etc., and economical point of view.

Items		Objectives
Water Pressure		more than 850 kgf/cm <sup>2</sup>
Breaking Strength		more than 10 ton
Lateral Pressure		more than 100 kgf/cm
Cable Modulus		more than 20 km
Cable Elongation		less than 0.7 % at 7 ton
Cable Torque		less than 1.3 kgf.m at 7 ton
Minimum Bending Radius		1 m
Weight	in Air	less than 1.0 ton/km
	in Water	less than 0.5 ton/km
D.C. Resistance		less than 0.7 $\Omega$ /km at 3° C
Insulation Resistance		more than $2 \times 10^6$ M $\Omega$ .km
Withstand Voltage Characteristic		more than $\pm 35$ kV D.C. for 5 min

Table 1. Cable Design Parameter  
(Deep Water Cable)

Items	Objectives
Optical Attenuation ( $1.53 \sim 1.57\ \mu\text{m}$ )	less than 0.21 dB/km
Chromatic Dispersion ( $1.53 \sim 1.57\ \mu\text{m}$ )	less than 21 ps/km/nm
Mode Field Diameter	$10.5 \pm 1.0\ \mu\text{m}$
Cut-off Wavelength *1	$1.35 \sim 1.60\ \mu\text{m}$

\*1: This is defined for a 2m length of fiber

Table 2. Optical Fiber Parameter  
( $1.55\ \mu\text{m}$  Wavelength)

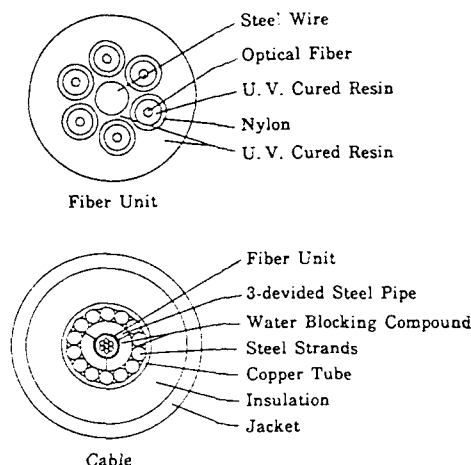


Figure 1. Lightweight Cable Structure

## Optical Characteristics of Mass Produced Cable

### Optical Fiber

Over the 20,000km optical fiber has been manufactured in a mass production base. Average value of optical attenuation and dispersion at  $1.55\ \mu\text{m}$  are 0.177 dB/km, 18.8 ps/km·nm, respectively. Average unit length screened with 2% elongation is 15.4km.

### Cable

The optical fibers are stranded into the fiber unit and cabled through the assembling process of three divided steel pipe, tensile steel strands, copper tube and the extrusion process of insulation / external jacket layers. Figures 2 and 3 show both the optical loss change during cable manufacturing process and the optical loss distribution of cabled fibers of roughly 3,700 km cable. The average loss increased during the manufacturing processes (from the optical fiber unit process to the insulation / external jacket process) is 0.003 dB/km. Average optical loss after the cabling

is 0.180 dB/km at 1.55  $\mu\text{m}$ , a minimum value is 0.170 dB/km and a maximum is 0.189 dB/km. Furthermore, average chromatic dispersion is 19.8 ps/km/nm (at 1.57  $\mu\text{m}$ ) and average splicing loss is 0.044 dB (at 1.55  $\mu\text{m}$ ).

This means 150km of repeater spacing will be possible.

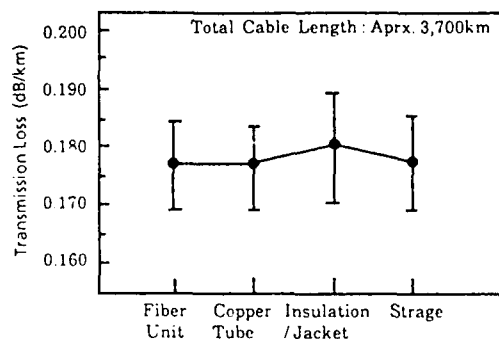


Figure 2. Transmission Loss Characteristic during Cable Manufacturing

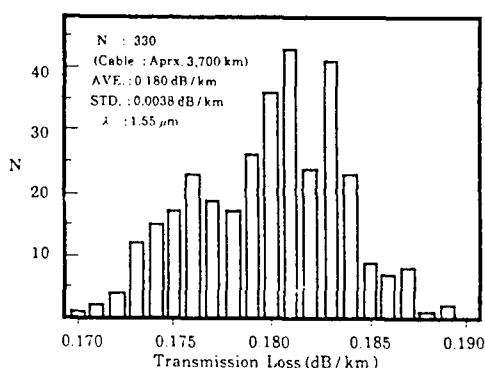


Figure 3. Distribution of Cabled Fiber Loss

### Cable Evaluation Test Results

Following evaluation tests on the mechanical stresses that the cable will be suffered during the laying and recovery processes were conducted using an ocean simulator<sup>8)</sup>, and other testing facilities.

#### Temperature Test (Figure 4)

A temperature characteristic between -20 °C and 50 °C was evaluated by looping the six optical fibers of each 500m length cable sample to form a loss measurement length of 3km, and it was confirmed that there was a tendency towards reduced transmission loss at lower temperature and increased transmission loss at higher temperature, the variation was still within  $\pm 0.004$  dB/km from the loss at 15 °C.

#### Water Pressure Test (Figure 5)

With a reference transmission loss at water temperature of 3 °C and cable tension of 0.5 tons, transmission loss change was evaluated with water pressure up to 800 kgf/cm<sup>2</sup> by looping six optical fibers of each 200m length cable sample to form a loss measurement length of 1.2km. It was varied by 0.001 dB/km or less, which was within the limits of measurement error.

#### Tensile Test (Figure 6)

With a reference transmission loss at water temperature of 3 °C and cable tension of 0.5 tons, transmission loss change was evaluated with tension up to 6 tons by looping six optical fibers of each 200m length cable sample to form a loss measurement length of 1.2km. It was varied by  $\pm 0.001$  dB/km or less, which was within the limits of measurement error.

#### Tensile Test with Bending

One of 144 meter length of test sample cable was wound on a sheave with a radius of curvature of 1.5 meters and the other end was stretched at  $6 \pm 1$  tons of tension for five hours. The transmission loss varied by  $\pm 0.001$  dB/km or less, which was within the limits of measurement error. In addition, after testing, the portion of the cable which was in contact with the sheave was opened up and checked on the mechanical deformation. As a result, no definite abnormalities were found.

#### Combined Test of Water Pressure and Tension

With a reference transmission loss at water temperature of 3 °C and water pressure of 0 kgf/cm<sup>2</sup> and cable tension of 0.5 tons, transmission loss change was evaluated by looping six optical fibers of each 200m length cable sample to form a loss measurement length of 1.2km when the cable was left for twelve hours under 800 kgf/cm<sup>2</sup> of water pressure and 5 tons of tension. It was varied by 0.002 dB/km or less, which was within the limits of measurement error.

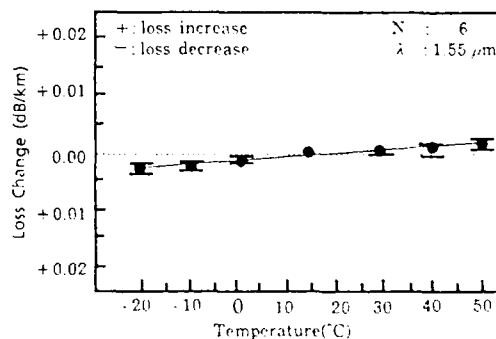


Figure 4. Temperature Characteristic

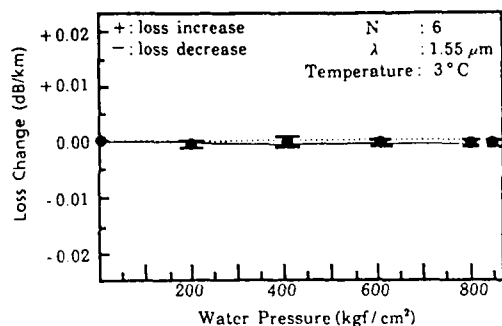


Fig. 5 Water Pressure Characteristic

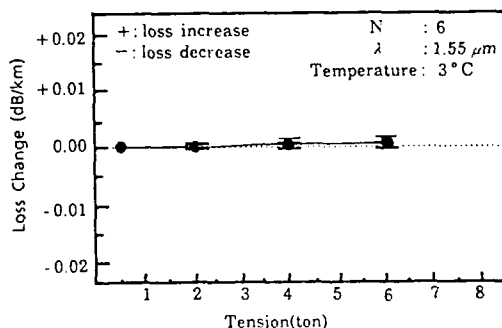


Fig. 6 Cable Tension Characteristic

### Repeater Housing

#### Design Parameters

Table 3 shows the mechanical design parameters of the OS-560M repeater housing. The cable and repeater should be able to be laid, recovered and buried using existing cable ship, cable laying facilities, and submarine cable plow. Cable-handling experiments on the cable ship in order to estimate the physical shocks on the repeaters during laying and recovery operations has been conducted. As a result, it has been confirmed that repeater is required to withstand the shock of 100G, and shock absorption / heat dispersion device are required to absorb the physical shock and disperse the heat from the internal repeater circuit. Repeater housing mechanical structure is fixed taking into account the design parameters tabled in Table 3 and the following points.

- (1) Housing method of the repeater circuit
- (2) Position of the joint chamber (housing of the fiber splicing points between repeater and cable)
- (3) Interface structure between the repeater and the cable

Items	Objectives
<b>(i) Fundamental Requirement</b>	
Maximum Sea Depth	8,000 m
System Design Life	more than 25 years
Handling Capability	to be laid / recovered using existing cable ship laying facilities up to 8,000m
<b>(ii) Pressure Housing</b>	
Airtightness	less than 20% RH(Relative Humidity) during 25 years
Water Pressure	more than 800 kgf/cm <sup>2</sup>
Shock	more than 100 G
Vibration	No damage on vibration frequency 10~500 Hz
High Voltage Resistivity	more than $\pm 15$ kV
Heat Dispersion	more than 6°C of temperature difference between surface of Housing and surface of insulation surrounding repeater circuit
<b>(iii) Feedthrough</b>	
Airtightness	less than $5 \times 10^{-6}$ atm-cc/sec (Helium gas of 800 kgf/cm <sup>2</sup> , 60min)
Water Pressure	more than 800 kgf/cm <sup>2</sup>
Shock	more than 100 G
Vibration	No damage on vibration frequency 10~500 Hz
Transmission Loss Change	less than 0.1 dB

Table 3. Mechanical Design Parameter of Repeater Housing

#### Mechanical Design

Figure 7 shows the mechanical structure of the repeater housing.

##### (1) Repeater housing

In order to mount six(6) regenerative circuits(3 subsystems), the outer diameter of the housing increases by 70mm to 321mm from that of the OS-280M system and the length is shortened. The joint chamber is placed inside of the coupling, and the distance between the gimbal pins at both ends is shortened by 240mm to 1,360mm. As a result of these changes, the weight of the repeater in air is now roughly 470 kg.

##### (2) Repeater and cable interface

As shown in Figure 7, by physically connecting the joint chamber surface plate in the coupling with the chip at the tip of the tail cable (copper pipe jacketed by polyethylene) of the repeater, the power feeding line is constituted, and the fibers from the repeater are guided through the tail cable into the joint chamber. The chip, made of beryllium copper alloy, is soldered to the tail cable. The airtight integrity of the connection between the chip and the joint chamber is maintained by a metal O-ring.

##### (3) Shock-absorbing / heat-dispersing structure

In addition to making changes in the dimensions of the repeater housing and in the requirements for

withstanding shocks, the resonating frequency needed to prevent the amplification of shocks to the repeater circuit is re-examined, assuming that metal absorbers would be used to absorb shocks and disperse heat.

Regarding the heat dispersion characteristics, a target is set at 6 °C or less for the temperature difference between the outer surface of the repeater housing and the surface of the insulation surrounding the repeater circuit.

#### (4) Optical fiber feedthrough

Highly purified silica core fibers with the polyimide-jacket are used for the optical feedthrough to keep airtight structure based on the OS-280M technology of which the airtightness is obtained by the soldering technique.

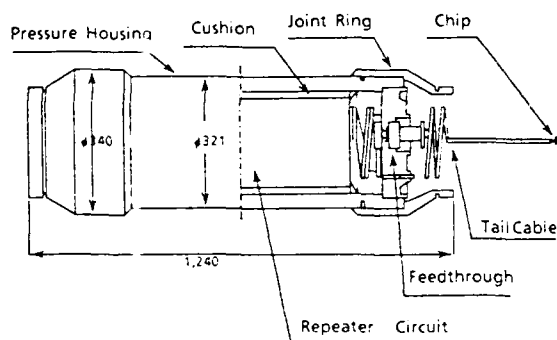


Figure 7. Schematic Assembly Diagram of Repeater Housing

#### Evaluation Test Results

Prototype repeater housing was tested from various aspects. Followings are the test results.

##### (1) Shock test

It was confirmed that there was no change in the optical and electronic characteristics of the repeater circuit before and after applying shocks of at least 100G acceleration for a duration of at least 0.7ms five times in both the axial and radial directions.

##### (2) Heat dispersion characteristics

The temperature difference between the surface of the repeater housing and the surface of the repeater circuit was 5 °C or less. In addition, the variation of the temperature on the surface of the repeater circuit was within 1 °C.

##### (3) Optical fiber feedthrough characteristics

Table 4 shows the evaluation test results of optical fiber feedthrough. It shows that the optical feedthrough is stable.

Items	Test Results
Temperature Test (-10 ~ 60°C)	No change in Transmission Loss
Vibration Test (10 ~ 500 Hz)	No damage
Shock Test (100 G)	No damage
Airtightness (Helium gas of 800 kgf/cm <sup>2</sup> , 60min.)	less than $5 \times 10^{-6}$ atm-cc/sec
Loss Change (before and after the above test programs)	less than 0.1 dB

Table 4. Feedthrough Evaluation Results

### Cable Coupling

#### Design Parameters

Table 5 shows the design parameters for the cable coupling. Joint chamber, which accommodates splicing points of the fibers from repeater and cable, is provided in the cable coupling, and it is based on the OS-280M cable joint box (JB)<sup>19)</sup>, which has already proven itself in terms of housing the fiber splicing points and mechanical characteristics. The following points are also taken into account in the cable coupling mechanical design.

- (1) Reduction of costs by using a structure similar to the JB and using common jointing equipment and techniques.
- (2) Proven techniques regarding characteristics for airtight integrity and resistance of water ingress.

Items	Objectives
Maximum Sea Depth	8,000 m
System Design Life	more than 25 years to be laid/recovered using existing cable ship-laying facilities up to 8,000m
Handling	more than 800 kgf/cm <sup>2</sup>
Water Pressure	more than 100 G
Shock	No damage on vibration frequency 10~500 Hz
Vibration	more than ±15 kV
High Voltage Resistivity	more than 6 °C of temperature difference between surface of Housing and surface of insulation surrounding repeater circuit
Heat Dispersion	less than $5 \times 10^{-6}$ atm-cc/sec (Helium gas of 800 kgf/cm <sup>2</sup> , 60min)
Airtightness	Transmission Loss Variation (Splice Loss) (before being accommodated and after)
Transmission Loss Variation (Splice Loss) (before being accommodated and after)	less than 0.25 dB less than 0.1 dB

Table 5. Mechanical Design Parameter of Cable Coupling



### Mechanical Structure

Figure 8 shows the mechanical structure of the cable coupling.

#### (1) Joint chamber structure

Splicing points of the fibers from repeater and cable are fixed in place on the metal cylinder. The fibers with excess length are wound around the cylinder while maintaining a radius of curvature of at least 30mm.

The power feeding line is composed continuously by the chip, joint chamber cover, water pressure housing, anchor disk, and safety pipe. As for insulation, polyethylene is molded around the outside of the joint chamber assembly, and continues with the tail cable of the repeater and cable.

#### (2) Cable anchoring structure

As for the OS-280M cable anchoring structure, the high-tensile steel wires and three-devided steel pipe of the cable are wedged in another places by their respective metal cones. For the OS-560M cable anchoring structure, both the wires and the steel pipe are wedged in the same place with a single cone, which allowed us to shorten the length of the cable coupling by 50mm.

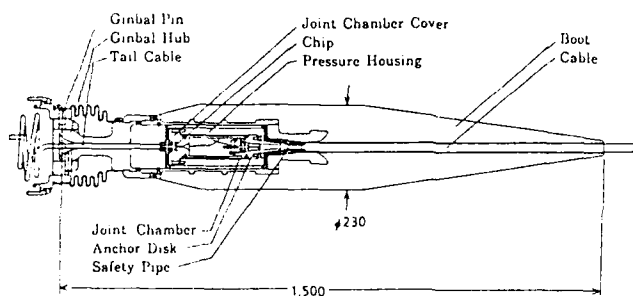


Figure 8. Schematic Assembly Diagram of Cable Coupling

### Evaluation Test Results

#### Cable Anchoring

All thirty test samples were evaluated in terms of the breaking strength after the temperature cycle testing and sea-water immersion testing, and it was confirmed that initial breaking strength of ten (10) tons or more was maintained. It was also confirmed that the cable anchoring structure did not cause any transmission loss change.

#### Long-Term Water Pressure Resistance Testing

Long-term (1 year) water pressure resistance test was conducted, placing a joint chamber is a cable coupling with its molded insulation in water pressure

testing equipment under 850kgf/cm<sup>2</sup> of pressure. There has still been no change in the structure of the equipment and no transmission loss change.

#### Cable Coupling

A repeater housing, a prototype couplings, and a cables were connected and wound on a sheave with a diameter of three meters and evaluated mechanical characteristics using long cable tensile test equipment. The test results show that all requirements have been met. The optical loss change during the tests was within the limits of measurement error.

Stand-alone test on the coupling for temperature, vibration resistance, shock resistance, and voltage resistance characteristics were also conducted. The test results show that all requirements have been met.

#### Handling Tests aboard the Cable Ship

Prototype repeater housing that contained an shock detector (frequency characteristics : DC to 1kHz, detectable in each of 3 principle planes), cable couplings and cables were jointed and then shipboard handling tests were conducted. Figure 9 shows the configuration of the test system. [ Note ; Transmission loss change was also monitored continuously ]

#### (1) Shock measurement

While the repeater was passing through the cable-laying facilities at speeds from 0.5 to 2.0 knots, the shocks on the repeater were converted to optical signals and measured in real time. Test results indicated that, as before, the greatest shock (vector sum of each axis; x, y, z) occurred when the repeater entered the DO/HB; a reading of 61.5G was obtained when laying the cable at 2.0 knots. The repeater slipping from the DC/E were also examined due to its increased weight; the maximum shock measured in that instance was 70.2G.

Figure 10 shows the results of a Fourier transformation on the maximum shock waveform in order to analyze the frequency characteristics of the shocks. As can be seen in the figure, many of the frequency components were from 200Hz to 700Hz.

On the basis of the above results, the resonance frequency were set at 1kHz for the shock-absorbing / heat-dispersing structure of the repeater.

#### (2) Optical transmission loss change measurement

The optical transmission loss change was measured to be 0.003dB or less, which was within the limits of measurement error.

#### (3) Conditions while passing through the cable-laying equipment

It was confirmed that there were no hindrances when passing through the cable-laying facilities, such as the DO/HB and the DC/E.

#### (4) Connection with the cable

After testing, the repeater housing and coupling were opened up, but found no physical deformation.

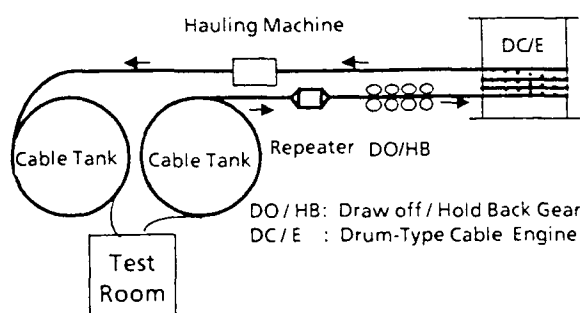


Figure 9. System Configuration of Handling Test on Board Cable Ship

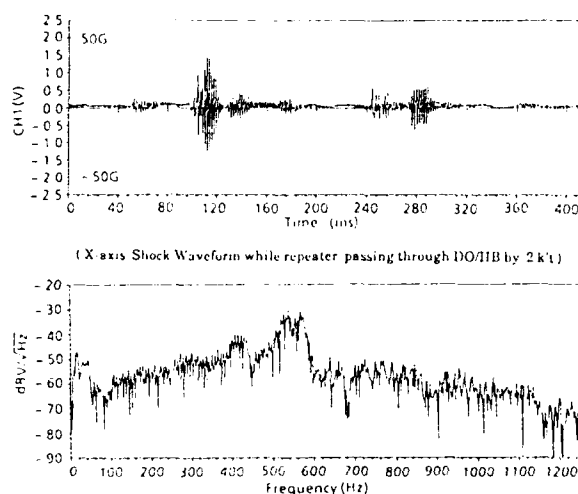


Figure 10. Fourier Transformation Result of Shock Waveform

#### Conclusion

This paper described the design and evaluation test results of the OS-560M optical fiber submarine cable, repeater housing, and cable coupling. Highly purified silica core fiber with fluorine-doped cladding optical fiber is adopted for the OS-560M optical submarine cable, in order to take advantage of the low loss transmission characteristics at 1.55  $\mu\text{m}$  wavelength. Various evaluation tests show good performance. The OS-560M optical submarine cable with an average transmission loss of 0.180 dB/km (1.55  $\mu\text{m}$ ) is currently being commercially produced in maximum unit lengths of 75 kilometers.

Two new design elements concerning the repeater housing and the coupling are also implemented :

- (1) the repeater housing is expanded along its diameter and shortened along its length; and
- (2) the joint chamber is housed in the coupling.

Evaluation test of the repeater housing and cable coupling shows that in all respects the requirements have been met the requirements.

These results show that the OS-560M optical fiber submarine cable and its associated mechanical devices can be commercially applicable.

#### Acknowledgements

The authors would like to thank Dr. K. Nosaka, executive vice president of KDD; Dr. Y. Niino, director of the Submarine Cable Systems Department, Network Development Headquarters, in KDD, and Mr. H. Wakabayashi, the group leader of the Lightwave Communications Systems Group in the KDD Research and Development Laboratories.

They also wish to acknowledge NTT or their cooperation and wish to thank Fujikura Co. Ltd., Sumitomo Industries Ltd., Furukawa Electric Co. Ltd., Fujitsu Ltd., NEC Co., and Ocean Cable Co. Ltd., for their manufacturing of optical fiber units, cables, cable couplings, repeater housings.

#### Reference

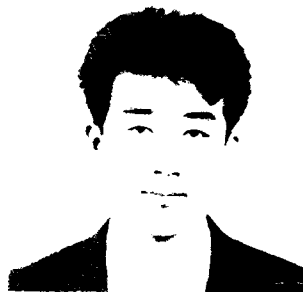
- [1] E. Nazuka, et al., "The OS-560M Optical Submarine Cable System", IEICE of Japan, OCS91-60, March, 1991
- [2] M. Chvoba, et al., "The OS-560M Optical Submarine Repeater", IEICE of Japan, OCS91-61, March, 1991
- [3] Y. Niino, "The OS-280M Optical-Fiber Submarine Cable Systems", IEEE, J. of Lightwave Tech, LT-2, No. 6 Dec. 1984
- [4] Y. Yamazaki, et al., "Fiber Seal Design of OS-280M Optical Fiber Submarine Repeater", Suboptics '86, 219-224 (1986)
- [5] Y. Yamazaki, et al., "The OS-280M Optical Fiber Submarine Cable", Suboptics '86, 123-128(1986)
- [6] S. Tanaka, et al., "Pure silica core matched cladding single mode fiber for submarine cable, Suboptics '86, 137-142(1986)
- [7] Y. Namihira, et al., "Design and Evaluation of 1.55  $\mu\text{m}$  Wavelength Region Loss-Minimized Optical Fiber Submarine Cable", IEICE of Japan, OCS88-18, 55-60, June, 1988
- [8] K. Furusawa, et al., "Long Length Tension and High Water Pressure Test Facility for Optical Fiber Submarine Cables", IEICE of Japan, CS83-150, 61- 68(1983)
- [9] K. Kobayashi, et al., "Jointing of OS-280M Optical Fiber Submarine Cable", Suboptics '86, 253-258 (1986)



Mr. Yasushi Noguchi was born in Kumamoto, Japan on April 5, 1956. He received the B. S. degree in Electrical Engineering from Oita University in 1980, respectively. He joined Kokusai Denshin Denwa Co., Ltd. in 1980. He has been engaged in the development and construction of optical fiber submarine cable system in KDD Head office since 1990.



Mr. Yoshihiko Yamazaki received the B.S. degree in 1974 and the M. S. degree in 1976 in Electrical Engineering from Tohoku University, Japan. He joined KDD Research and Development Labs. in 1976, and has been engaged in research and development of optical fiber submarine cable system. He was transferred to KDD Head Office in 1983, and has been engaged in the development and construction of optical fiber submarine cable system.



Mr. Ikuro Marugome was born in Nagasaki, Japan on November 26, 1963. He graduated the course of the Electrical Engineering of Sasebo College of Technology in 1984. He joined Kokusai Denshin Denwa Co., Ltd. in 1984. He has been engaged in the development and construction of optical fiber submarine cable system in KDD Head office since 1988.



Mr. Hitoshi Yamamoto received the B. S. degree in 1971 and the M. S. degree in 1973 in Communication Engineering from Osaka University, Japan. He joined KDD Research and Development Labs. in 1973, and has been engaged in research and development of optical fiber submarine cable system since 1977. He was transferred to KDD Head Office in 1983, and has been responsible for the development and construction of optical fiber cable, repeaters and terminal equipment.



Mr. Naoki Norimatsu was born in Fukuoka, Japan on December 27, 1960. He received the B. S. degree in 1981 and M. S. degree in Electrical Engineering from Kyushu University in 1983, respectively. He joined Kokusai Denshin Denwa Co., Ltd. in 1985. He has been engaged in the development and construction of optical fiber submarine cable system in KDD Head office since 1989.

G. Berthelsen, J.S. Andreassen, T. Birkeland, G. Lang, K. Nyaas

## Abstract

The basis for the cable was the qualified open design developed for the Norwegian Telecom, into which a lot of effort has been put to ensure a very low internal hydrogen pressure. The results from these cables have been reported by the Norwegian Telecom.

In the following the background work and the tests carried out during the project leading up to the selection of the fibre to be used, as well as experience with this fibre in a commercial submarine cable will be described.

The Cook Strait is particularly known for its strong tidal currents. Due to these heavy currents it was necessary to make the fibreoptic cables unusually heavy to be safely installed and remain stationary on the seabed. Therefore the cable was given an armouring consisting of multilayer steel wires and steel tapes. The cable cross-section is shown in Fig. 1.

### Fibre types

- A standard SM fibre from vendor A (SMH-A)
- A standard SM fibre from vendor C (SMH-C)
- A dispersion shifted fibre from vendor B (DSH-B)
- A dispersion shifted fibre from vendor C (DSH-C)



## Hydrogen

To investigate the resistance to hydrogen permeation at accelerated conditions a pressure chamber had previously been built. In this chamber a pressure of 20 atmospheres and a temperature of 85 °C was imposed on the fibres. Inside the chamber about 1 km of fibre was placed in a loose coil in a tray of outer diameter 230 mm.

Spectral attenuation measurements were carried out before the fibres were placed in the pressure chamber. At regular intervals the pressure and temperature were taken back to ambient, whereafter the fibres were taken out of the chamber and new spectral measurements were made. All measurements were carried out within 2 hours after the fibres had been taken out of the chamber.

The reversible excess loss was measured as the height of the 1244 nm peak referred to the baseline of the spectral curve in this region. The results for a period of 371 days are shown in Fig. 2

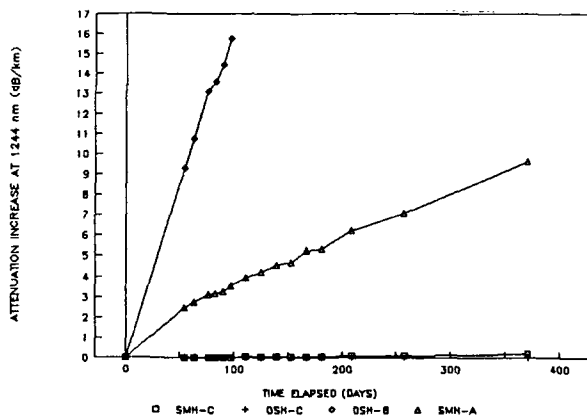


Fig. 2

These accelerated results have subsequently been transposed to operational conditions of 25 years, and ambient temperature and partial pressure of hydrogen using the following equation:

$$\frac{C(t)}{C(\infty)} = 1 - e^{-\left[\frac{(t-\tau_i)}{\tau_f}\right]}$$

where  $C(t)$  is the time dependant concentration of hydrogen,  
 $C(\infty)$  is the equilibrium concentration,  
 $t$  is the elapsed time,  
 $\tau_i$  is the initil lag time,  
 $\tau_f$  is a characteristic time constant.

Using this equation the excess loss due to hydrogen in dB/km/atm. at 1550 nm after 25 years and at 4 and 10 °C are:

Fibre type	4 °C	10 °C
SMH-A	$3.0 \times 10^{-4}$	$6.4 \times 10^{-4}$
SMH-C	$6.1 \times 10^{-6}$	$1.3 \times 10^{-5}$
DSH-B	$1.9 \times 10^{-3}$	$4.1 \times 10^{-3}$
DSH-C	$< 1.0 \times 10^{-7}$	$< 1.0 \times 10^{-6}$

The measured values for DSH-C are so low that an extrapolation is difficult, and the figures are thus given for the smallest measurement which can honestly be extrapolated.

For comparison the saturation value for the fibre itself (which a non-hermetic fibre would attain) is 0.78 dB/km/atm.

## Mechanical properties

The cable the fibres are to be used in is designed for non-hermetic fibres with the fibres placed in slots with an excess length of about 0.4 %. Thus in this case the claimed better fatigue performance of hermetic fibres are not utilised, and the requirement is only that the hermetic fibres are at least as good as non-hermetic fibres in terms of n-value.

To ascertain this, a limited number of tensile tests were carried on short samples (about 5 m) at pulling rates across four decades, eg. 0.011, 0.11, 1.1 and 11 %/min. The results are shown below including the breaking strengths associated with the given n-values. Because of the statistical uncertainties with the limited data, the figures are given as ranges rather than absolute figures.

Fibre type	n-value	Breaking strength (N)
SMH-A	40-500	32-36
SMH-C	60-500	28-32
DSH-B	200-11000	52-54
DSH-C	60-800	27-32

Similar tests with non-hermetic standard fibres from vendor C and a much larger sample size shows n-values in the range 17 to 18.

## Splicing

In 1989/1990 hermetic fibre were offered in lengths of 10 to 15 km, thus in a 43 km long cable with 12 fibres there will be a significant number of factory splices. These factory fibre splices are required to have a low loss and a high strength. A comprehensive programme was carried out to evaluate the splicability of each fibre type, and the results are shown below. Splice loss is given as the average of OTDR measurements in both directions, and strength as the breaking strength at a pulling rate of 2 %/min on a 50 cm sample including the splice.

The sample size is several hundred for each fibre type.

The tests were carried out over a period of 6 months and some improvements on the splicing parameters are included in the results. Splices with visual defects are not included, and only splices which were accepted on loss were strength tested.

Fibre type	Splice loss (dB/km)	
	mean	max
SMH-A	0.02	0.06
SMH-C	0.03	0.07

DSH-B	0.10	0.15
DSH-C	0.03	0.10

Fibre type	Breaking strain (%)	
	min	mean
SMH-A	1.2	1.8
SMH-C	1.0	1.5

DSH-B	1.0	1.6
DSH-C	1.2	1.7

## Bending performance

Microbend tests were carried out to evaluate whether the hermetic coating would have any effect on the cabling performance of the fibres. The microbend results are based on a sandpaper test using 100 grit paper and measuring loss increase.

The results are shown in Fig. 3.

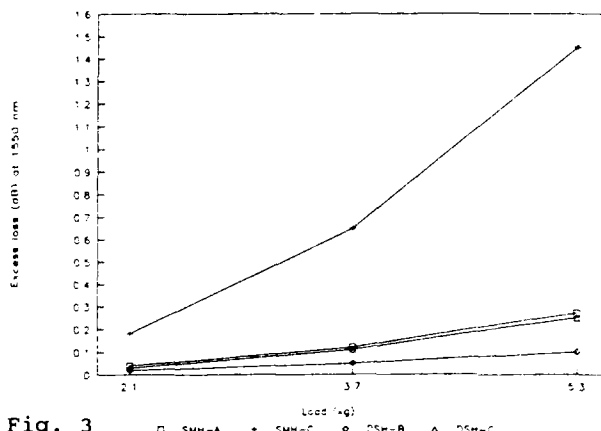


Fig. 3

## Other tests

Several other tests were also performed, but they did not differentiate the fibre types. These were tests like macrobend, ageing in filling compound, temperature cycling, temperature cycling in filling compound, temperature cycling of cable core.

## Type testing of cable

The customer required a comprehensive type test programme to be carried out and approved before manufacturing of the main cables could commence. This programme included both optical, mechanical, environmental and repair splice tests, but only those relevant to the hermetic fibres are described here.

## Tensile test

A 50 m long sample of a complete cable was mounted in a tensile test bench and the attenuation in the fibres as well as the strain in the fibres and the cable was monitored as the tension was changed.

The cable was strained to 0.5 % to investigate the behaviour of the armour at extreme loads, and at this strain the excess length of the fibres was used up such that the fibres also saw strain. The results are shown in Fig. 4

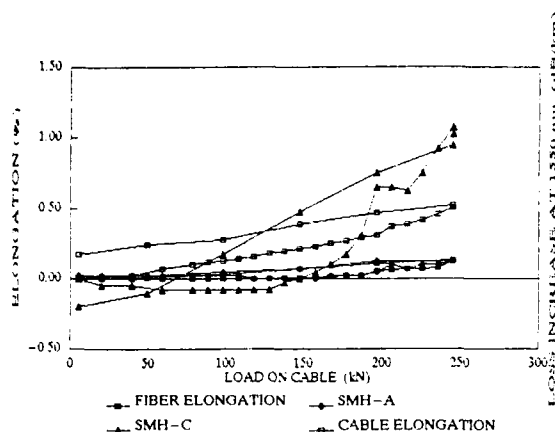


Fig. 4

It can be seen that the SMH-A fibre attenuation follows the fibre strain curve, while the SMH-C increases dramatically.

#### Hydrogen level

A 35 m length of complete cable was placed in a chamber in water where the temperature can be varied to perform accelerated hydrogen generation tests. All 12 non-hermetic fibres in a sample cable were loop spliced together, and spectral attenuation measurements were carried out at different temperatures over a period of 4 months.

Based on these measurements the hydrogen pressure was determined to be approximately 0.8 atm. at a water temperature of 10 °C.

#### Choice of fibre

The fibre to be used in the Cook Strait cable was then selected on the basis of the data above. As there were many parameters involved a scheme was used where all parameters were rated from 1 to 10 based on performance and perceived importance for this project. The results were grouped and turned out as shown below

	SMH-A	SMH-C	DSH-B	DSH-C
Hydrogen	6	9	2	10
Fatigue	6	5	10	5
Splicing	10	7	4	10
Cabling	7	1	10	10
Commercial	10	2	4	6
Customer	10	10	5	5
Total	49	34	35	46

It should be noted that all the results have been viewed from the point of view of a user of fibres in cable manufacturing. Thus no effort has been put into explaining differences between the fibre types because of inherent factors as matched/depressed cladding, higher/lower MFD, higher/lower concentricity errors, etc.

It should also be noted that all factors are evaluated as they appeared in May 1990.

There are clearly two groups where in the lower, the SMH-C and the DSH-B fall out because of poorer general performance, and specifically on cabling and on hydrogen respectively.

The tests show that the DSH-C fibre is technically better than the SMH-A fibre. However, when the commercial element (price and delivery time) and the fact that the customer has specified a standard fibre was taken into account, the SMH-A fibre was selected.

#### Manufacturing experience

Neither during manufacturing, loading, transport nor installation had special measures to be imposed because the cable contained hermetic fibres. The cable was at all stages handled as it would have been with "normal" fibres.

#### Attenuation

The requirement from the customer was that the attenuation of the fibres should be less than 0.27 dB/km at 1550 nm in cable. The attenuation of the fibres were measured after every process with an OTDR, and the results at 1550 nm are shown below.

Production stage	dB/km	
	mean	max
Incoming inspection	0.22	0.23
Stranding	0.22	0.23
Inner sheath	0.22	0.23
Armouring	0.22	0.23
Installation	0.22	0.24

A repair splice had to be performed during the marine operation, which accounts for the slight increase in the "after installation" figure with respect to the other processes.

## Splicing

The internal requirement defined from the results from the qualification tests was a factory splice loss  $\leq 0.1$  dB/splice, and a proof test level of 1.2 %. The proof test of the fresh fibre was 1.0 %. The fibres were spliced in the stranding machine from individual lengths of 11 km.

A total of 86 factory splices were made during manufacturing with a mean splice loss of 0.05 dB. The maximum value was 0.10 dB.

It should however be noted that splice tests carried out during incoming inspection on the fibres revealed that it was difficult to use the splicing parameters arrived at during qualification and achieve the same low losses on the delivery fibres. The splice parameters therefore had to be defined again.

In hindsight it could also be commented that the internal requirement on factory splice loss is more stringent than it need be to satisfy the specification on average fibre attenuation, and this might have been relaxed, rather than to spend the considerable effort of establishing a new set of splicing parameters. However, at the time it was decided to keep to the specified value.

## Hydrogen

As part of the incoming inspection a sample testing on the hydrogen resistance performance was carried out.

This test showed that the results achieved for the fibres received for the real manufacturing were different from those achieved for the qualification fibres. Looking at the values transposed to 25 years and 10 °C they were as follows in dB/km/atm at 1550 nm:

SMH-A qualification  $6.4 \times 10^{-4}$

SMH-A manufacturing  $7.0 \times 10^{-5}$

## Installation

The two 43 km lengths of fibre optic cables were successfully installed together with three high voltage cables in the Cook Strait by the c/s Skagerrak during the first quarter of 1991.

## Conclusions

It has been shown that hermetic fibres are now state of the art. They can be handled in any existing cable designed for "normal" fibres without any special consideration.

The inclusion of the right hermetic fibres will eliminate any hydrogen problem, even in the designs with the highest published hydrogen levels (close to 10 atm).

Two 43 km lengths of an "open" design cable with hermetic fibres, an unusually heavy armour and a traditional outer protection has been designed, manufactured and installed. The internal hydrogen pressure is about 0.8 atm, but the projected impact on attenuation is  $\ll 0.0001$  dB/km at 1550 nm after 25 years.

## Accnknowledgements

The authors wish to thank Trans Power New Zealand Ltd. for their positive attitude during the whole project, and for their kind approval of this paper.





Gunnar Berthelsen

Alcatel Kabel Norge AS  
Telecom Cables Division  
P.O.Box 130, Økern  
N-0509 Oslo 5, Norway

Gunnar Berthelsen (44) received a B.Sc (Electronics) from Heriot Watt University, Edinburgh in 1971, and joined STK, Oslo as a cable design engineer the same year. He started work with fibre optic systems in 1977. He is currently Technical Manager with responsibility for fibre optics in Alcatel Kabel.



Bjørn Broen

Alcatel Kabel Norge AS  
Telecom Cables Division  
P.O.Box 130, Økern  
N-0509 Oslo 5, Norway

Bjørn Broen (33) received his degree (Automation) from Bergen College of Technology in 1982, and joined STK (now Alcatel Kabel) in 1985 where he worked with marine installation. He is currently working with environmental testing of fibre optic cables.



Jon Steinar Andreassen

Alcatel Kabel Norge AS  
Telecom Cables Division  
P.O.Box 130, Økern  
N-0509 Oslo 5, Norway

Jon Steinar Andreassen (30) received a B.Sc (Physical Electronics) from the Norwegian Institute of Technology in 1986 and has been with STK (now Alcatel Kabel) since the same year, where he works with research and development of fibre optic cables, with special emphasis on topics related to mechanical lifetime of fibres.



Geraldine Lang

Alcatel Kabel Norge AS  
Telecom Cables Division  
P.O.Box 130, Økern  
N-0509 Oslo 5, Norway

Geraldine Lang (25) received her B.Eng (Electrical and Electronic Engineering) from Strathclyde University, Glasgow in 1987 and joined STK (now Alcatel Kabel), the same year, where she works with research and development into fibre optic cables. She is particularly concerned about fibre testing, including hydrogen testing.



Tom Birkeland

Alcatel Kabel Norge AS  
Telecom Cables Division  
P.O.Box 130, Økern  
N-0509 Oslo 5, Norway

Tom Birkeland (32) received a B.Sc (Electro-chemistry) from the Norwegian Institute of Technology in 1983, and joined the Metallurgy laboratory at STK (now Alcatel Kabel) in 1986 where he worked with corrosion protection of submarine cables. He is currently working on research and development of submarine fibre optic cables.



Kaj Nyaas

Alcatel Kabel Norge AS  
Telecom Cables Division  
P.O.Box 130, Økern  
N-0509 Oslo 5, Norway

Kaj Nyaas (45) has a background as a telephone exchange installer at STK, but has been working with development of splicing technology for fibres in the Communication Cable Division of STK (now Alcatel Kabel) since 1983.

## STRUCTURE AND HIGH VOLTAGE DC BEHAVIOUR OF SUBMARINE CABLE MOULDINGS

J. Bishop\*, I. Doble\*, H.K.C. Chan\*\*, L.A. Dissado\*\*, S.V. Wolfe\*\*,  
A.E. Davies†

\* STC Submarine Systems, Southampton, UK,

\*\* BNR Europe, Harlow, UK, † University of Southampton, UK

### ABSTRACT

Submarine cable systems are required to have a very high reliability over a twenty five year lifetime. This means that all manufacturing processes and production screening tests are designed to a very high standard.

This paper concentrates on one specific component of a submarine system - the high voltage polyethylene cable insulation and mouldings. Relationships between insulation and moulding structure and DC high voltage breakdown performance are demonstrated, and factors giving rise to DC ageing effects are discussed. It is concluded that space charge effects are the prime cause of ageing and it is shown how a new method for measuring space charge, the pressure wave propagation technique, could become an extremely efficient production tool for screening mouldings to ensure high reliability.

### 1. INTRODUCTION

Submarine cable systems are designed with a high reliability factor, particularly in view of the difficulty, cost and timescales of repair operations. All system components including cable, are engineered in this way; the properties of the optical fibres, for example, are very well understood, so that parameters such as proof test levels can be defined to provide high reliability fibre at minimum cost. Submarine systems are currently DC powered to a maximum voltage of 10 kV and are designed for a 25 year lifetime. In consequence, stringent proof tests are applied to submarine cable polyethylene insulation and mouldings, and an insulation thickness is employed which gives a large safety factor compared with the theoretical and actual breakdown strength of the material.

With the advent of optical amplifier systems, system voltages could be even higher than at present. This paper describes the results of a programme of work aimed at understanding DC breakdown

and ageing behaviour of DC insulation in order to achieve high reliability at minimised cost.

Traditionally, DC insulation behaviour is poorly understood compared with AC insulation. In DC insulation there are no fatigue related ageing mechanisms such as water treeing<sup>(1)</sup>, and no direct means of predicting lifetime from simple short term tests as in AC<sup>(2)</sup>. However, the measured breakdown strength still remains considerably below that of the theoretical value, and high reliability is often achieved by over-specification and over engineering.

It is becoming increasingly accepted that DC ageing, if it occurs, is associated with space charge effects<sup>(3)</sup>. Previously, this has been almost impossible to quantify, but recent developments in analytical techniques have enabled direct measurements of space charge magnitudes and spatial distribution to be made<sup>(4)</sup>.

Discontinuities such as mouldings or joints in bulk insulation are generally considered to be potentially the weakest link. This programme has therefore concentrated on the relationship between physical and morphological aspects of the insulation in moulded joints and DC breakdown and ageing behaviour, together with preliminary findings of space charge measurements.

The work is reported in three sections:

- (i) Assessment of bulk breakdown behaviour and ageing.
- (ii) Relationship between breakdown behaviour and polymer structure.
- (iii) Space charge determination as a measure of DC ageing.

### 2. DC BREAKDOWN BEHAVIOUR IN BULK POLYETHYLENE MOULDINGS

In AC insulation, a relationship exists between measured electrical breakdown

strength and the rate of voltage increase during the test procedure. This relationship can be used to yield information relating to the ageing behaviour of the insulation<sup>(5)</sup>. No similar relationships have been reported for DC insulation, and the work in this section investigates:

- (i) whether there is an effect of ramp rate on breakdown strength,
- (ii) whether ageing occurs in DC insulation by a different mechanism than AC.

Laboratory-produced test plaques have been used to examine specific materials parameters, but all ageing measurements have been carried out on actual submarine cable mouldings manufactured on production equipment, in order to reproduce full details of production mouldings. The typical insulation thickness in production mouldings is ~6 mm.

All measurements have been carried out using negative polarity, as previous breakdown strength measurements on cable have indicated this to be the most severe condition.

## 2.1 Effect of Ramp Rate

To investigate the effect of ramp rate, breakdown strength measurements were carried out on sets of 15 compression moulded samples at four ramp rates from 30 kV min<sup>-1</sup> to 120 kV min<sup>-1</sup> on 250 µm plaques manufactured from submarine cable grade polyethylene. Figure 1 is a schematic diagram of a test plaque, and test results are shown in Table 1. It can be seen that there is no significant effect of ramp rate, with the Weibull characteristic breakdown strength typically in the region 430 kV mm<sup>-1</sup> to 470 kV mm<sup>-1</sup>.

Ramp Rate kV min <sup>-1</sup>	Weibull Characteristic Breakdown Strength, kV mm <sup>-1</sup>
30	426
60	442
90	470
120	458

Table 1

Weibull Characteristic Breakdown Strength as a Function of Ramp Rate for Compression Moulded Samples

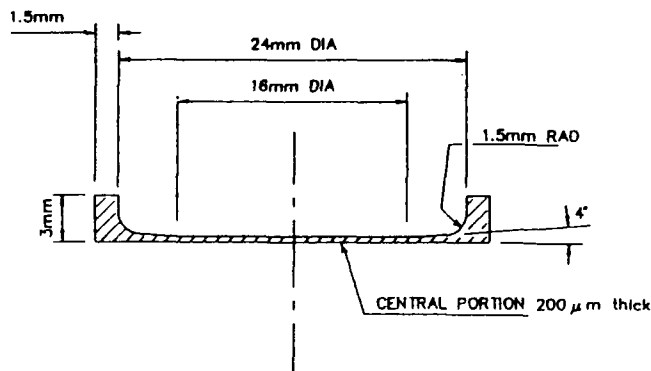


FIGURE 1. Schematic diagram of test plaque

## 2.2 Ageing Effects

A number of factors could give rise to ageing phenomena in DC insulation, from macroscopic effects such as contaminants to microscopic effects such as morphological features. This section of the programme concentrates on the effect of inclusions.

Two sets of test samples were prepared using standard production equipment. Figure 2 shows a schematic diagram of a typical moulding. The first sample set was prepared under a typical clean production environment, and the second set was prepared by introducing a low level of metallic and organic particles into the moulding.

Each sample set was divided into two groups. The first group was tested by ramping to failure at a rate of 60 kV min<sup>-1</sup>. The second set was subjected to a static voltage of 100 kV, which was significantly lower than the measured ramp breakdown voltage. Samples were aged at this static voltage for a maximum of 76 days, and the time to breakdown was noted for any samples which failed. Results are shown in Table 2.

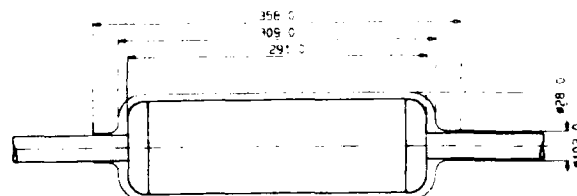


FIGURE 2. Schematic diagram of typical moulding. Dimensions in mm

Sample	Ramp Breakdown Strength, kV	Time to Failure at 100 kV (days)
Clean	> 350	> 76 (no breakdown)
Containing inclusions	> 300	< 7 (~ 50% failure rate)

Table 2

Comparison Between Ramp Breakdown and Ageing Breakdown Data in Full Mouldings

The results indicate that in these samples, little change is seen in the bulk breakdown behaviour measured by ramping to failure (although there is a marked difference between the breakdown strength measured here and that measured on laboratory plaques). However, there is a very clear ageing effect in contaminated samples - breakdown can occur in times as short as a few days at 100 kV compared with times in excess of 76 days with no breakdown observed in standard samples.

3. RELATIONSHIP BETWEEN STRUCTURE AND BREAKDOWN IN SUBMARINE CABLE MOULDINGS

3.1 Structure and Morphology of Mouldings

Submarine cable mouldings are manufactured by an injection moulding technique using a single point injection and two vent ports. The major difference between this technique and a conventional injection moulding process is that this is essentially an injection weld - the ends of the mould cavity are actually polyethylene, which melts and bonds to the injectate during the moulding. One end of the cavity is cable polyethylene, and the other end is a premoulded polyethylene sleeve.

Series of 'short shot' mouldings combined with microscopic analysis of moulded sections has permitted modelling of the detailed polyethylene flow behaviour inside the mould cavity. Figures 3-5 show a typical 'short shot' moulding using coloured injectate. This has enabled the shape and nature of the injection weld region to be established. The injection process leads to two circumferential



FIGURE 3. Short shot moulding showing injection and vent positions



FIGURE 4. Short shot moulding viewed from vent position



FIGURE 5. Short shot moulding viewed end-on

amalgamations at the cable end and the premoulded sleeve, and also a longitudinal amalgamation where the two melt fronts meet. Figure 6 shows a schematic diagram of the mould filling process.

Figure 7 shows a cross section taken from the cable end of the moulding along the vent position. There are several key features to be noted here; (a) is the amalgamation boundary itself, where the injected polyethylene welds to the parent cable polyethylene. In the injected polyethylene itself, flow lines are evident, (b). A second boundary, (c) is evident in the parent cable beyond the amalgamation boundary (a). This is the melt boundary, showing the position to which the parent polyethylene melts back during the moulding process. The region between (a) and (c) is therefore completely molten during the moulding process. The parent polyethylene beyond (c) has been subjected to a thermal gradient associated with the mould cooling regime.

The thermal gradient can be measured by differential scanning calorimetry (DSC), (Figure 8) and results in a local density change away from the melt boundary, (Figure 9).

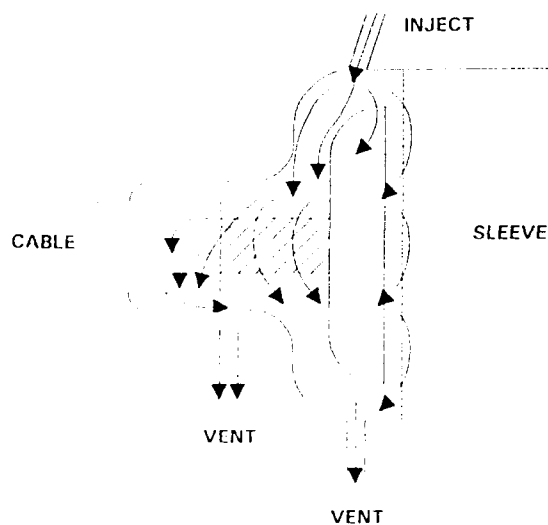


FIGURE 6. Schematic diagram of mould filling process

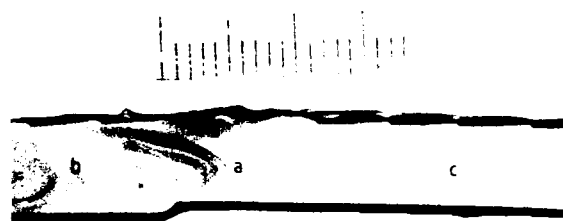


FIGURE 7. Cross section of cable end of moulding

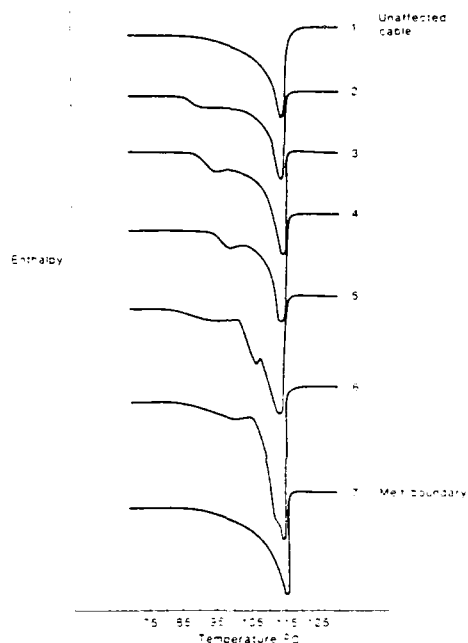


FIGURE 8. DSC traces of polyethylene across a thermal gradient (1.5 mm intervals)

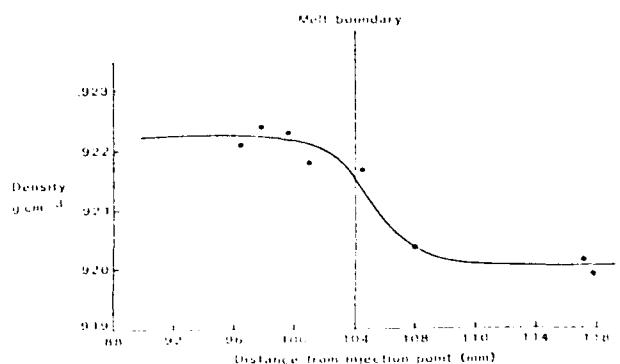


FIGURE 9. Density changes across to melt boundary

If the thermal gradient is too steep, then high localised stresses will be produced due to the local density changes, and the amalgamation boundary approaches the melt boundary, (Figure 10). This leads to mechanical and electrical weaknesses in the moulding, and even local voiding, as seen in Figure 10, and therefore thermal gradients are kept as shallow as possible within the constraints of the moulding process.

When samples have been contaminated, the most often observed contamination site is the amalgamation boundary, (Figure 11). This is to be expected, as any contamination present either within a mould cavity, on cut surfaces of the insulation or at the injectate front, will be swept ahead of the injectate during the mould filling process and be trapped at the amalgamation boundary.

Similar features are observed at the other end of the mould cavity, where the polyethylene injectate bonds to the premoulded sleeve.



FIGURE 10. Moulding showing small cavity due to proximity of melt and amalgamation boundaries

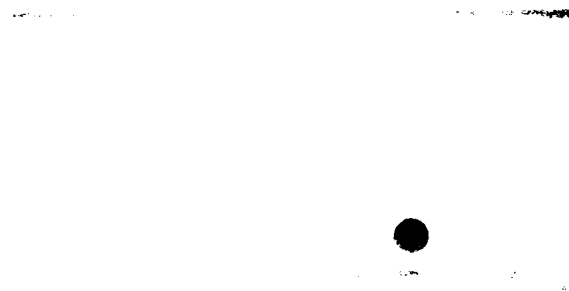


FIGURE 11. Moulding showing large scale and small scale contaminants on amalgamation boundary

### 3.2 Breakdown Effects in Moulding

This work concentrates on correlations between observed structure, breakdown events and measured breakdown strengths in submarine cable mouldings manufactured on production equipment.

In controlled experiments samples with a high concentration of inclusions which break down at low voltages, typically < 100 kV, generally exhibit a 'wormhole' breakdown track closely associated with an amalgamation boundary, (Figure 12). In these cases it is often possible to observe remnant inclusions in the vicinity of the breakdown track. It is likely that an inclusion layer on the amalgamation boundary forms a low resistance path, and breakdown probably occurs by thermal runaway. In some cases a heat affected zone is visible around the breakdown path, (Figure 13).

FIGURE 12. 'Wormhole' breakdown on amalgamation boundary (transverse section)

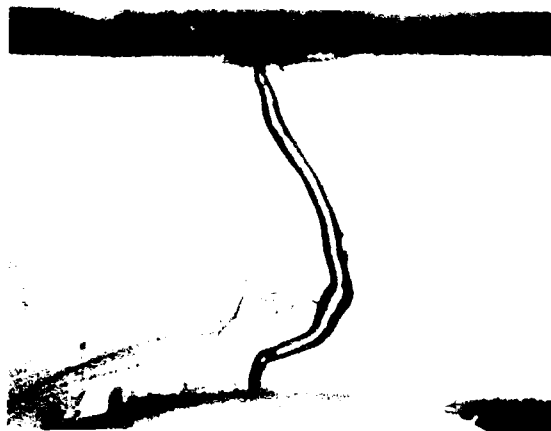


FIGURE 13. 'Wormhole' breakdown showing heat-affected zone

This type of breakdown is also possible when there are only low levels of inclusions, if they are orientated in such a way as to form a continuous path. When this occurs, a low resistance path still forms at the amalgamation boundary, and breakdown still occurs at relatively low voltages.

If inclusions are randomly distributed in a moulding, however, they do not necessarily appear to contribute to the breakdown event.

The amalgamation boundary itself is not always the weakest link. Breakdown sometimes occurs along local sites of high mechanical stresses. Figure 14 shows a breakdown site in a moulding where there was high mechanical stress and where inclusions had been concentrated.

When mouldings have been produced using steep temperature gradients so that the melt and amalgamation boundaries are very close, low voltage breakdowns may occur in this region of high stress due to voids or cavities being produced, as discussed in the previous section. Figure 15 shows the breakdown track in a sample which failed at <100 kV. A cavity at the breakdown inception site is clearly visible.



FIGURE 14. Breakdown associated with mechanical stress

In some breakdown events where limited ageing has occurred, breakdown is clearly independent of the flow patterns in the moulding. Figure 16 shows a breakdown which has occurred at 235 kV, caused by an electrical tree. The sample had previously undergone ageing for nine days at 100 kV. The tree has initiated at the outside surface of the insulation, and has progressed through the material independently of the flow patterns. Once the tree has approached the central conductor, electron injection has occurred and thermal runaway finally takes place through the 'branch' of lowest resistance. Similar tree breakdowns also occur at very high voltages during ramp tests.



FIGURE 15. Breakdown due to proximity of melt and amalgamation boundaries



FIGURE 16. Electrical tree breakdown, independent of flow lines

#### 4. SPACE CHARGE MEASUREMENTS

Space charge can now be measured directly in bulk polymers by means of a pressure wave propagation technique, originally developed by Lewiner. A laser is used to produce an intense, rapid pressure wave which propagates through a sample. As the pressure wave sweeps through the sample, the atomic structure is compressed, and two effects are observed:

- (i) displacement of charge,
- (ii) variation of relative permittivity

By monitoring the current as the pressure wave traverses the sample it is therefore possible to observe an image of the charge distribution in the sample. Figure 17 shows a schematic diagram of the process.

A preliminary study using this technique has investigated whether space charge can develop in submarine cable mouldings.

Samples were cut from amalgamation boundaries and injected polyethylene in uncontaminated samples. These were then subjected to 9 kV DC, and probed for space charge using the pressure wave propagation technique. In all samples there was a gradual increase in space charge with time up to a maximum level, which was reached within 21 days. All samples attained the same level of space charge within that time.

When a higher voltage of 30 kV was applied to the samples, the same maximum level of space charge was reached, but within a much shorter time period (typically one day).

Figure 18 shows a typical pressure wave propagation trace.

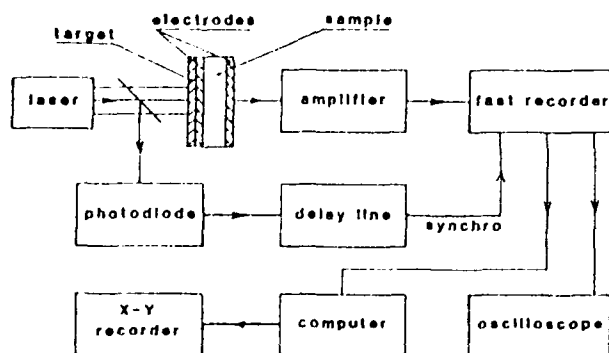


FIGURE 17. Schematic diagram of pressure wave propagation technique

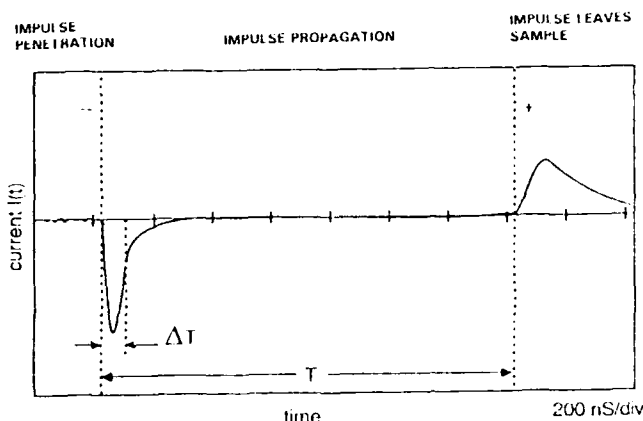


FIGURE 18. Typical pressure wave propagation trace

#### 5. DISCUSSION

Work described in sections 3 and 4 shows how the reliability of mouldings can be increased by controlling the structure, and explains many features of structure and contamination related breakdown.

Examples of short term ramp breakdowns were shown, as well as breakdowns occurring at static voltages after a finite ageing period. Although differences in the type of breakdown are evident between low and high voltages ('wormhole' to tree breakdown), no obvious visual differences could be seen between short term and ageing breakdown.

Work described in section 2.1 showed that there was no dependence of breakdown voltage upon ramp rate. This implies that the probability of breakdown under constant stress is independent of time, so that the insulation will either break down on the timescale of a ramp experiment at the applied voltage  $V$ , or survive indefinitely at that voltage.

Results in section 2.2 for samples containing inclusions show that this is clearly not the case, and that time dependent processes do occur. There are a number of time dependent processes which may occur in DC insulation, all of which involve space charge build-up. These can include mechanisms such as local currents (due to the polymer's inhomogeneous semicrystalline structure) and partial discharges in voids. In both of these cases, local damage is caused in the insulation the effect of which is actually minimised by space charge build-up. These processes are therefore unlikely to be responsible for the observed constant stress failures.



A third mechanism which is more likely to be responsible is hetero-charge build-up. Hetero-charge clouds are formed when charges from the bulk of the insulation are attracted towards the counter electrodes, which causes an increase in the local field in this region. Under DC stresses, the hetero-charge may continue to increase over a period of time. This continues to increase the field at the electrodes until breakdown takes place by the easiest mechanism such as charge injection from the counter electrode giving thermal runaway, or rupture of a mechanically weak path. The origin of the charge carriers may be various, from dissociable contaminants or electrode injection for example. This mechanism will therefore exploit any weaknesses or combination of weaknesses present in the material, such as regions of high localized mechanical stress, contaminants, high conductivity etc, particularly where any of these elements create an orientated plane in the insulation.

If ageing and breakdown is likely to occur by this mechanism, then measurement of space charge under a constant DC voltage would be likely to show the space charge magnitude increasing with time (until breakdown finally occurs). This is clearly different from normal samples which appear to reach a ceiling level in space charge irrespective of time or voltage.

Although further work is necessary, these initial findings suggest that space charge measurement is a technique which can be used as a screening test to detect the potential for ageing in mouldings.

## 6. CONCLUSIONS

As submarine cable systems are designed for high reliability, manufacturing processes and screening techniques have been developed to a very high standard to eliminate defects and inhomogeneities detrimental to short and long term performance. This has been achieved by an understanding of the factors giving rise to electrical weaknesses and thereby controlling moulding processes accordingly.

This work has given further insight into ageing processes in DC insulation, and has indicated how a new analytical tool could be used as very efficient alternative screening process. It has been shown that ageing processes appear to be associated with unlimited space charge build-up, and the pressure wave propagation technique is an invaluable new method for direct

detection of this, as this work has demonstrated that ageing processes in DC insulation cannot be detected by the accelerated technique used in AC insulation.

Although further work is required to establish in detail how the pressure wave propagation technique could be used as a rapid method to identify mouldings susceptible to DC ageing processes, it is envisaged that this technique will become an important screening test in submarine systems manufacture.

## REFERENCES

- 1 M.T. Shaw and S.H. Shaw, 'Water Treeing in Solid Dielectrics', IEEE Trans EI-19, 419-452, 1984.
- 2 J.C. Fothergill and L.A. Dissado, Chapt. 6, 'Electrical Degradation and Breakdown in Polymeric Insulation' in Recent Advances in the Morphology of Polymeric Cable Insulation, Ed. G.C. Stevens, P. Peregrinus Press, U.K., 1988.
- 3 J. Lewiner, 'Evolution of Experimental Techniques for the Study of Electrical Properties of Insulating Materials', IEEE Trans EI-21, 351-360, 1986.
- 4 T. Ditchi, C. Alquie and J. Lewiner, 'Electrical Properties of Electrode/Polyethylene/Electrode Structures', IEEE Trans EI-24, 403-408, 1989.
- 5 L.A. Dissado, J.C. Fothergill, S.V. Wolfe and R.M. Hill, 'Weibull Statistics in Dielectric Breakdown: Theoretical Basis, Applications and Implications', IEEE Trans EI-19, 227-233, 1984.

## ACKNOWLEDGEMENTS

The authors would like to thank M.J. Parry and C. Duggan for their help and advice on preparing this paper.



Jim Bishop  
STC Submarine Systems  
West Bay Road  
Western Docks  
Southampton  
SO9 4YE  
UK

Jim Bishop was born in London, England in 1965. He obtained a BSc in Chemistry with Polymer Science in 1989.

After spending a year developing fire retardant fillers for polymers he joined STC Submarine Systems in 1990 to concentrate on High Voltage Reliability in collaboration with Southampton University.



Ian Doble  
STC Submarine Systems  
West Bay Road  
Western Docks  
Southampton  
SO9 4YE  
UK

Ian Doble joined STC Submarine Systems in 1987 where he is now Principal Engineer. He received a BSc in Physics from Southampton University in 1982.

As well as being responsible for many aspects of cable development, he established close links to Southampton University, Department of Electrical Engineering by setting up a High Voltage Reliability research programme with them.



Howard K.C. Chan  
BNR Europe Ltd  
London Road  
Harlow  
Essex  
CM17 9NA  
UK

Howard Chan gained a BSc in Chemistry from the University of Hull, studied polymer science and technology at the National College of Rubber Technology and is now a Senior Principal Research Engineer of BNR Europe Ltd. He has worked on many R & D activities for telecommunications including the following: polymer films, coatings and encapsulation; electromechanical relays and switches; sub-sea optical cable and joints. His expertise is in the areas of reliability, testing and failure analysis.



Len A. Dissado  
BNR Europe Ltd  
London Road  
Harlow  
Essex  
CM17 9NA  
UK

Len Dissado was born in St. Helens, England. He gained his PhD from University College, London University and was awarded a Research Fellowship at the Australian National University. After a period with the Atomic Energy Authority at Harwell, and a further period at ANU, he joined the Dielectrics Group at Chelsea College, London University in 1977. He has been working as consultant with STC Technology (now BNR Europe Ltd) since 1980, specializing in the area of dielectrics and DC insulation.



Sue V. Wolfe  
BNR Europe Ltd  
London Road  
Harlow  
Essex  
CM17 9NA  
UK

Sue Wolfe was born in London, England. She joined STC in 1970 to work on cable materials and cable development. She gained her BSc from Thames Polytechnic in 1976, and her PhD from Queen Mary College, University of London in 1982. After a period as Head of Department in the London School of Polymer Technology at the Polytechnic of North London she returned to STC Technology (now BNR Europe Ltd) in 1989 where she has continued to work in optical fibre cables, particularly in the area of high voltage reliability.

# HYDROGEN SOURCES FOR SIGNAL ATTENUATION IN SUBMARINE OPTICAL FIBER CABLES AND THE EFFECT OF CABLE DESIGN

George Schick, Karen A. Tellefsen, Aaron J. Johnson, Casey J. Wiczorek, and Robert M. Kanen

Bell Communications Research  
Morristown, NJ

## ABSTRACT

Research and field experience showed that molecular hydrogen entering into submarine optical fiber cables cause signal attenuation in the fibers. The results of our laboratory and field studies, reported in this paper, indicate that hydrogen formed by corrosion of the armor wires, by stray dc current pick-up, and by hydrogen-producing bacteria in the surrounding environment cannot be kept out of the fibers by overlapped, corrugated steel shield. However, hermetically sealed lead and copper tubes can stop hydrogen permeation into the fibers. The level of signal attenuation is directly proportional to the partial pressure of hydrogen inside the cable. In the laboratory we have measured hydrogen indicators ( $H_{ind}$ ) between 2.3 and 6.2 dB/km. In the field, because of the high over-all pressure in deep waters,  $H_{ind}$  in excess of 20 dB/km was measured.

Based on a mathematical model of diffusion through a metal tube, taking into account the high over-all pressure in deep water, and considering long term reliability we propose a generic requirement and an accompanying test to eliminate hydrogen caused signal attenuation in the future.

## Introduction

It is well documented in the literature that hydrogen diffusion into optical fiber cables can cause signal attenuation.<sup>(1-3)</sup> Among the several possible hydrogen sources, break-down of organic materials in the cable by heat<sup>(4)</sup> and by microorganisms<sup>(5)</sup>, corrosion of metallic components (e.g. aluminum, steel) inside the cable,<sup>(6,7)</sup> corrosion of the galvanized steel armor wire,<sup>(8-10)</sup> and the effect of anaerobic hydrogen-producing bacteria in the environment<sup>(10)</sup> have been investigated.

Our early laboratory experiments established that the most likely hydrogen sources for submarine optical fiber cables are corrosion of the armor wires, hydrogen-producing bacteria, and the combination of these two sources.<sup>(10)</sup> Because the signal attenuation by hydrogen diffusion into the fiber has been reported almost exclusively in submarine cables, the work by Anderson et.al.<sup>(11,12)</sup>, correlating the attenuation with the partial pressure of hydrogen and thus with the depth of water at the location of the cable, is particularly important. We should not lose sight of the fact that submarine optical fiber cables can be part of the Local Exchange Plant as well as the Inter Exchange Plant.

Many designs of optical fiber cables have an overlapped, corrugated-steel inner armor, which is probably not an effective barrier to hydrogen which can diffuse easily into the cable at the overlap of the tube. Additionally, attenuation measurements of optical fiber cables with hermetically sealed lead barriers installed at water crossings have shown little or no hydrogen-caused darkening, even though these cables have uncoated galvanized-steel armor wires that are likely to produce abundant hydrogen.<sup>(12)(13)</sup> Hydrogen diffuses through solid lead slowly, if at all<sup>(14)</sup>, so it is likely that the lead acts as a barrier

against ingress of hydrogen into the cable. Hermetically sealed tubes of other metals may also prevent hydrogen from getting into the cable. Therefore, it would be useful to determine the rate at which hydrogen diffuses into the inner parts of cables of different designs to predict the time needed for the cables to show hydrogen-caused darkening, and how well different cable designs prevent hydrogen from entering the cable interior. A mathematical model of hydrogen diffusing through a sealed metal tube in a cable sheath may give insight into this problem.

Some designs of underwater cables use plastic-coated armor wires and/or stainless-steel armor wires to prevent the formation of corrosion-generated hydrogen at the cable. This may reduce the probability that the cable will suffer hydrogen-caused signal attenuation, but it may still be possible for hydrogen to enter the cable under some conditions. Although stainless steel corrodes more slowly than galvanized steel, enough hydrogen may be generated cathodically to cause fiber darkening. Plastic coverings on armor wire prevent hydrogen generation only if the covering remains on the armor; it is possible for the plastic covering to be damaged during cable installation or dredging, which will expose the armor to corrosive conditions. An experiment in which a piece of cable with damaged plastic jackets on the armor wires is exposed to salt water may show whether hydrogen-caused fiber darkening is possible under such conditions.

## Purpose of the Experiments

Our laboratory and field studies are conducted as part of a program intended to formulate generic requirements and accompanying tests intended to ensure resistance to hydrogen-caused signal attenuation in submarine optical fiber cables.

This will be especially important if telecommunications signals are transmitted at 1550 nm, since hydrogen-caused attenuation is greater at 1550 nm than at 1300 nm, the transmission wavelength currently used. Also, the 1300 nm transmission window may extend from 1275 nm to 1330 nm; hydrogen-caused attenuation is high at 1275 nm.

## Experimental Methods

### Laboratory experiments

A widely used type of cable was exposed to conditions that imitate real-plant environments to establish whether or not this cable structure can provide a barrier to hydrogen diffusion. The cables were exposed to these environments for 94 to 147 days. During this time, signal attenuation in the 1100-1600 nm wavelength range and partial pressure of hydrogen inside and outside of the cable were measured.

The hydrogen permeation experiment was done by sealing a short sample of cable into a tube, and sealing one end of the cable into a gas sampling apparatus, taking care that only the inner portion of the cable is open to the sampling apparatus. The cable may be exposed to a hydrogen atmosphere by passing hydrogen gas through the tube, and the amount of hydrogen that diffuses into the cable can be measured by sampling small portions of gas from the sampling apparatus and analyzing it for hydrogen content.

## Field experiments

Electrochemical tests were conducted to ascertain the corrosion status of the armor wires on attenuated submarine optical fiber cables in various telephone plant locations, and bottom sediments were collected and analyzed for hydrogen-producing bacteria at the same locations.

## Materials and Laboratory Test Procedures

### Signal attenuation tests

The optical fiber cable used in these experiments is of 1.02 cm (0.4 in) OD. It has corrugated, overlapped, plastic-coated steel shield under a polyethylene outer jacket. The 12 color-coded fibers are located in a plastic center tube.

Four 50-meter sections were cut from this cable and coiled in two layers on the outer surface of a rigid PVC cylinder (Fig. 1) that has 1.27 cm (0.5 in) OD holes 2.54 cm (1 in.) apart on its entire surface. For three of the cable samples, 0.23 cm (0.091 in.) OD galvanized steel wire was placed between the interstices of both the first and second layers of the cable, and coils of the same wire were placed inside the three PVC cylinders (Fig. 1). The cable samples and associated galvanized steel wires, and one cable sample without exposed metal were placed in 30-liter-capacity glass test chambers (Fig. 1). These test chambers have rigid PVC covers secured to their tops. Gas tightness of the test chambers was ensured with VITON seals. The cable ends and the galvanized steel wire ends were brought above the cover plate inside epoxy resin filled glass tubes. Other associated equipment: heaters, a platinum auxiliary electrode, a salt bridge for a calomel reference electrode, pressure gauges, valves for gas sparging, gas blanketing, water inlet, gas-sampling ports, and pressure regulator were also attached to or incorporated into glass tubes connecting the insides of the test chambers with the outside. All of these glass tubes were passed through stainless-steel feed-throughs that were threaded into the PVC tops (Fig. 2). The design of the cable end and fiber holders, enabled us to sample the gas and measure the over-all pressure in the head space and in the spaces at the two cable ends, where hydrogen can be present only by migration through the cable (Fig. 2). The last 1.5 m (5 ft) of fibers at both cable ends were used to concatenate the 12 fibers to form a 600-meter-long fiber, and to splice the two ends of this long fiber to the signal attenuation measuring equipment.

The signal attenuation in the fibers was monitored between 1100 nm and 1600 nm with equipment similar to that described in the Electronic Industries Association Standard EIA-455-78. The gas samples for all of the tests were analyzed for hydrogen content with a Gow-Mac isothermal 580-type gas chromatograph with a 2.5m-long, 3mm-diameter molecular sieve 5A column and thermal conductivity detector. Argon carrier gas (99.998%) was used at a flow rate of 30 cm<sup>3</sup>/min. The column, detector and injector temperatures were set to 50, 135 and 135°C respectively, and the detector current was 40mA. The detector signal was recorded and processed on a Spectra Physics integrator.

The experiments were conducted in two different environments: (a) 3.5% (by weight) NaCl solution, and (b) a culturing solution (Table I) inoculated with a hydrogen-producing bacteria (*Clostridium acetobutylicum*, ATCC\* 824).

The NaCl solution was used to ascertain whether corrosion of the galvanized steel (an extensively used material of the armor wire on submarine cables) can generate hydrogen in sufficiently large quantity so that its diffusion into the fiber can cause signal attenuation. A further use of the NaCl solution was the simulation of dc stray current pick-up, using a potentiostat with a platinum auxiliary electrode (stray current source), producing hydrogen evolution at the surface of the galvanized steel wire.

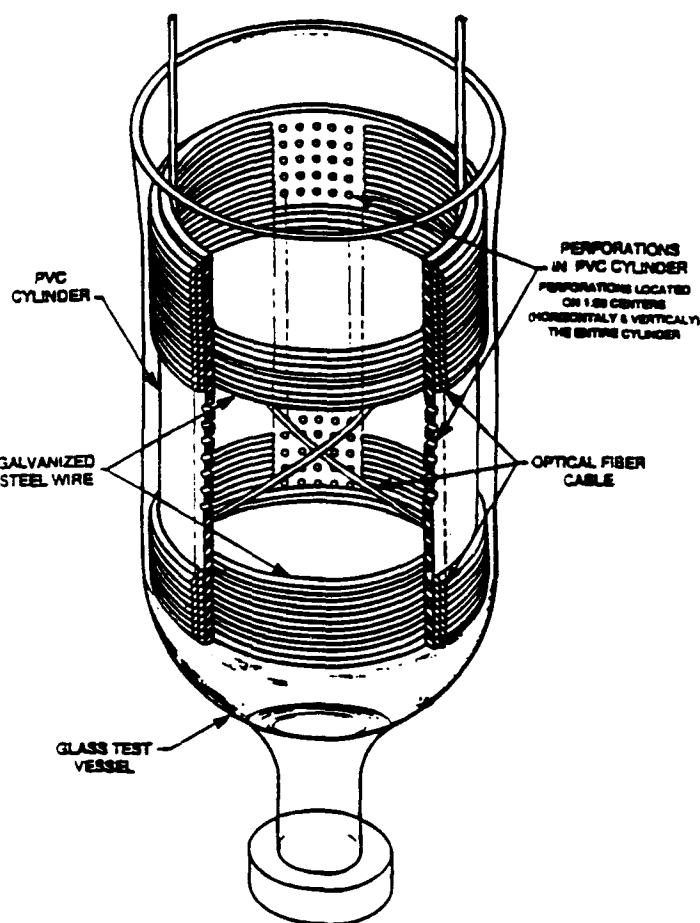
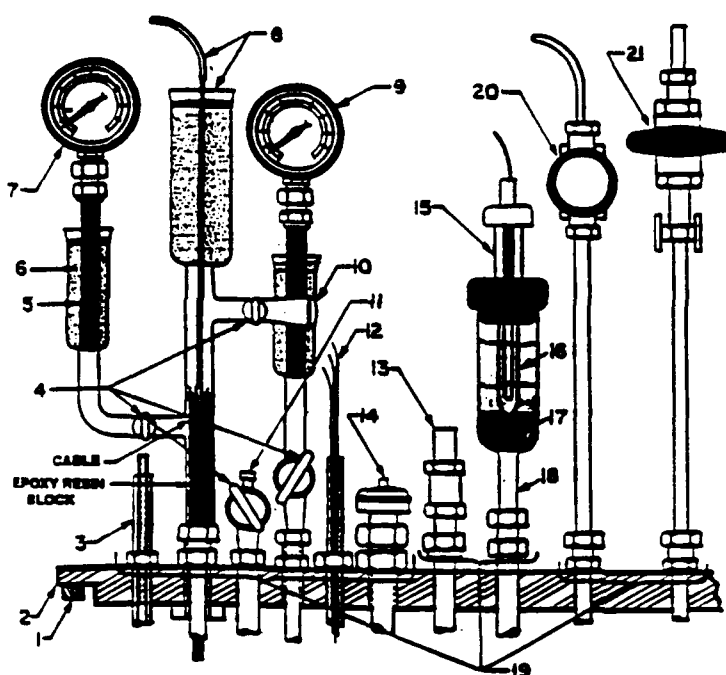


Figure 1. Illustration of the cable sample on PVC cylinder and the attached galvanized steel wire inside the glass test chamber.

The inoculated culturing solution was used to evaluate the signal-attenuating effect of the hydrogen-producing bacteria alone. This test represents a condition where the armor wires are insulated and corrosion cannot contribute to the evolution of hydrogen. In another test chamber the hydrogen was generated both microbiologically and by corrosion. The culturing solution is sufficiently corrosive to generate enough hydrogen for signal attenuation.<sup>(10)</sup> We used the hydrogen-producing bacteria alone in these tests, because our previous studies in mixtures of hydrogen-producing and sulfate-reducing bacteria indicated the rate of hydrogen consumption by SRB could only temporarily reduce the signal-attenuating effect of the hydrogen-producing bacteria.<sup>(10)</sup>

The heater units in the test chambers were adjusted so that the outer surface temperatures of the liquid-containing test chambers were  $32 \pm 2^\circ\text{C}$ . In three of the test chambers, two containing only cable and galvanized-steel wire and one containing only cable, the hydrogen was generated by corrosion, microbiological fermentation of dextrose, and the combination of corrosion and fermentation. In the fourth test chamber, the rest potential of the galvanized-steel wire, measured against a saturated calomel reference electrode, was established in two days; then, the galvanized steel, the calomel reference electrode and a platinum auxiliary electrode were connected to a potentiostat, and a potential more cathodic than the rest potential was imposed upon the galvanized steel (working electrode). This experimental set-up represented dc current pick-up by the galvanized steel wire from a

\* ATCC = American Type Culture Collection  
1203 Parklawn Drive, Rockville, MD 20852



#### LEGEND:

1. VITON SEAL
2. PVC COVER
3. PLATINUM AUXILIARY ELECTRODE
4. VACUUM STOPCOCK
5. COPPER TUBE
6. EPOXY RESIN
7. PRESSURE GAUGE (FOR INSIDE THE CABLE)
8. CABLE AND FIBERS, HOLDER
9. PRESSURE GAUGE (FOR HEAD SPACE)
10. GAS SAMPLING PORT (FOR INSIDE THE CABLE)
11. GAS SAMPLING PORT (FOR HEAD SPACE)
12. GALVANIZED STEEL WIRES
13. CHECK VALVE
14. HEATER
15. CALOMEL REFERENCE ELECTRODE
16. KCl SOLUTION
17. AGAR WITH NaCl SOLUTION
18. SALT BRIDGE
19. STAINLESS STEEL FEED-THROUGH WITH ZYTEL FERRULE (SHOWN WITHIN BRACKETS)
20. NEEDLE VALVE FOR GAS INLET
21. BALL VALVE FOR LIQUID INLET.

Figure 2. A segment of the PVC cover of the glass test chamber with the cable end holder, heater, salt bridge and calomel reference electrode, pressure gauge, gas sampling port, gas inlet and liquid inlet valves and Pt electrode.

TABLE I

#### Culturing Solution for *Clostridium Acetobutylicum*

5 gram	Bacto-peptone
5 gram	Bacto-trytone
5 gram	Yeast extract
10 gram	Glucose
0.005 gram	Hemin
0.2 ml	0.5% solution of vitamin K <sub>1</sub> in 95% ethanol
20 ml	Salts solution
1000 ml	Deionized water

The solution pH was adjusted to  $7.3 \pm 0.2$  and degassed with  $N_2$ .

After transferring the culturing solution into the test chambers and further purging with  $N_2$ , 1 millimole of  $Na_2S$  was added as reducing agent.

Salts Solution contains per 1 liter of deionized water

0.23 gram	$CaCl_2 \cdot 2H_2O$
0.48 gram	$MgSO_4 \cdot 7H_2O$
1.0 gram	$K_2 HPO_4$
10.0 gram	$NaHCO_3$
2.0 gram	NaCl

stray current source (here the platinum electrode); field-installed cable with bare armor wire may pick up stray currents from a foreign plant's cathodic protection or dc transit lines. The set potential difference and the current flow was monitored. Hydrogen was generated at the galvanized steel wire.

The signal attenuation was measured against two unexposed reference fibers in all the test chambers at 54 different wavelengths between 1100 nm and 1600 nm. >From these data the hydrogen indicator,  $H_{ind}$ , defined by Anderson et al.<sup>(11)</sup> as signal attenuation at 1240 nm less that at 1310 nm, was calculated and plotted as the function of time.

Gases were sampled in each test chamber from the head space (outside the cable) and the two cable ends (inside the cable) using a 0.5 ml gas-tight syringe with a valve. The chromatograph was calibrated each day that gas analyses were made with duplicate samples of 0.250 ml of 99.9% hydrogen and 0.500 ml of room air (about 21% oxygen and 78% nitrogen). Data for the partial pressure of hydrogen ( $p(H_2)$ ) were also plotted as a function of time.

The over-all pressure of the gas in the head spaces and at the two cable ends were also measured to be taken into account at the calculation of the  $p(H_2)$  values.

#### Hydrogen permeation test

Four different types of cable were exposed to hydrogen in this work:

1. An optical fiber cable designed for underwater installation with an overlapped corrugated steel tube and plastic coated stainless steel armor wires.
2. A lead-sheathed cable with copper wires and pulp insulation.
3. A coaxial cable with a hermetically sealed copper tube.
4. An optical fiber cable designed for underwater installation with an inner lead sheath and galvanized steel armor wires.

The armor wires, jute and tar coverings, and outer plastic jackets were removed from both ends of the optical fiber cable samples, leaving 5 to 10 cm of the inner metal tube exposed. Likewise, the polyethylene outer layer of the coaxial cable was removed to expose the inner copper tube.

The pieces of cable were sealed with epoxy resin in either a glass hydrogen exposure vessel, or a 4-inch OD, rigid, polyvinyl chloride

pipe, with brass fittings for hydrogen inlet and exhaust, shown in Fig. 3. A glass gas sampling cap (see Fig. 3) was sealed on one end of the cable sample so that only the inner metal tube of the cables was open to gas sampling space. The gas-sampling caps were made with vacuum stopcocks and septum ports to allow removal of gas for analysis with a syringe. The other end of the cable samples was completely sealed in epoxy resin. The length of cable exposed to hydrogen ranged from 75 to 90 cm.

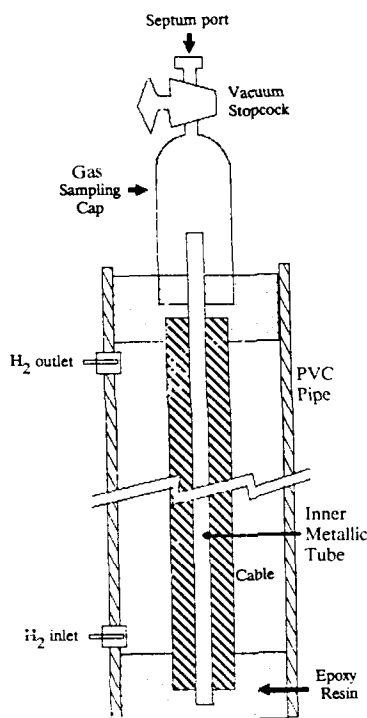


Figure 3. 4 inch O.D. PVC pipe apparatus for hydrogen exposure of cables.

Hydrogen gas, 99.9% pure, was passed through the gas exposure tubes at a flowrate of about 5 to 10 cm<sup>3</sup>/min, so that the cable samples were exposed to a hydrogen pressure of about 1 atm.

In a separate experiment, not involving the direct introduction of hydrogen, a piece of the optical cable with the overlapped barrier had three strands of the nylon jute outer covering removed and the plastic coating on the exposed stainless steel armor wire was partially removed with a rasp to simulate severe damage to cables that may occur during installation or dredging. This piece of cable was sealed in a 4-inch OD, rigid, polyvinyl chloride pipe and a gas sampling cap with epoxy resin as described above for the hydrogen exposure experiments. A single hole was drilled in the pipe to allow it to be filled with a 3.5% by weight NaCl solution. After filling the pipe, the fill hole was sealed with a rubber stopper. A 25 cm length of the cable was exposed to the salt solution. The purpose of this experiment was to determine whether stainless-steel armor wires with damaged plastic coating in a corrosive environment could produce enough hydrogen to cause fiber darkening.

Periodically, 0.5 ml samples of gas were taken from the gas sampling caps for hydrogen analysis.

#### Field Tests

##### Potential survey

The potentials of the galvanized-steel armor wires were measured against a Cu/CuSO<sub>4</sub> reference electrode in freshwater and against an

Ag/AgCl reference electrode in salt water as a function of distance from the water's edge at the cable crossing. One end of a 2500-foot lead wire on a reel was connected to the cable armor in a manhole 20 to 80 feet from the water's edge. The other end of the wire was connected to the negative terminal of a recording voltmeter of 2.5 megohm input resistance. The positive terminal of the recording voltmeter was connected to the reference electrode through a submersible adapter with a 200-foot lead. The recording voltmeter, the wire reel and the reference electrode were placed on a boat, and by slowly moving over the cable, continuous potential measurements were recorded.

#### Bottom Sediment Sample Collection and Analysis

The bottom sediment samples were collected at 35 to 65 feet depth either by divers or by a Jacobson dredge,\* and transferred from the dredge into glass containers with plastic-lined screw-cap tops. The containers were filled to the brim to maintain their anaerobic condition, and stored away from light. The test samples were prepared in a glove box under N<sub>2</sub> atmosphere. We designed the glass sample holders to maintain anaerobic conditions and to minimize the entrapment of N<sub>2</sub> gas in them. The test samples were prepared in three different ways: (1) small (0.5g to 1.0g) sediment sample in cooked meat with glucose nutrient to establish the presence or absence of hydrogen-producing bacteria, (2) a 5.08 cm (2 inch) galvanized steel wire surrounded with the sediment sample to ascertain the hydrogen-generating contribution of armor-wire corrosion, and (3) sediment sample alone to see if hydrogen can be generated without artificial additives. Gas samples were collected from the test specimen holders in 0.5 ml syringes, and analyzed in a Gow-Mac isothermal 580-type gas chromatograph.

#### Results and Discussion

The most important result of the experiments in this study is that hydrogen generated by corrosion, stray current pick-up, or microbiological fermentation of hydrocarbons can diffuse into the fibers in the cables with overlapped steel shields. The partial pressures of hydrogen inside the cable are high enough to cause significant levels of signal attenuation.

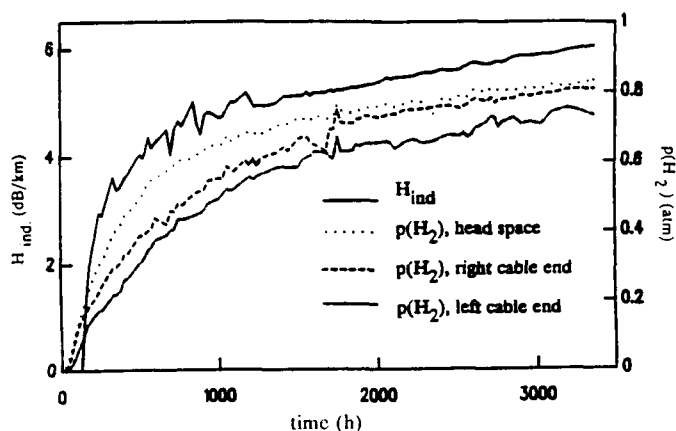
A. The effect of corrosion of galvanized steel wire in 3.5% NaCl solution.

Figure 4 indicates that the partial pressure of hydrogen ( $p(H_2)$ ) generated by corrosion of galvanized steel wires gradually increases with time and levels off at 0.86 atm. in the head space and at an average of 0.81 atm in the cable. The average  $p(H_2)$  of the cable was determined by adding the  $p(H_2)$  values measured in the right and left ends of the cable and dividing by two. The corresponding hydrogen indicator ( $H_{ind}$ ) is 6.2 dB/km. Because the  $H_{ind}$  and  $p(H_2)$  vs. time curves look very similar, regardless of the source of the hydrogen, instead of repeating the curves the equilibrium values of the above data are listed in Table II. The attenuation increase observed as a result of corroding galvanized steel wire is in good agreement with the results of Hardwick et al.<sup>(9)</sup> measured on galvanized-steel armored optical fiber cable.

B. The effect of stray direct-current pick-up by galvanized steel wire in 3.5% NaCl solution.

In the experiment where the current pick-up shifted the potential of the galvanized steel wire by 60mV in the negative direction, and the current varied between 70mA and 115mA (corresponding current densities are 6.1μA/cm<sup>2</sup> and 10μA/cm<sup>2</sup>), the  $p(H_2)$  in the head space reached 0.85 atm. and in the cable an average of 0.76 atm. The corresponding  $H_{ind}$  reached 4.8 dB/km (Table II).

\* Two galvanized steel lead weighted half-cylinders, connected through a hinge on one side and kept open by either spring loading or a mechanical latch. When the dredge contacts the bottom the mechanism that kept open the half-cylinders releases and the dredge scoops up the bottom sediment.



**Figure 4.** Hydrogen indicator  $H_{ind}$  and hydrogen partial pressure [ $p(H_2)$ ] curves vs. time for an optical fiber cable exposed to 3.5 percent sodium chloride solution and corroding galvanized steel wire.

**TABLE II**

**Hydrogen Indicator and Partial Pressure of Hydrogen Data of the Laboratory Experiments**

Experimental Conditions	$pH_2$ In Head Space (atm.)	AVG. $pH_2$ In Cable (atm.)	$H_{ind}$ (dB/km)
Cable and Galvanized Steel Wire in 3.5% NaCl Solution	0.86	0.81	6.2
Cable and Galvanized Steel Wire in 3.5% NaCl solution. Stray DC Current Shifted the potential of Wire by -30mV	0.54	0.55	3.8
Cable and Galvanized Steel Wire in 3.5% NaCl Solution. Stray DC Current Shifted the potential of Wire by -60mV	0.85	0.76	4.8
Cable and Galvanized Steel Wire in 3.5% NaCl Solution. Stray DC Current Shifted the potential of Wire by -90mV	0.78	0.76	5.4
Cable in Inoculated Hydrogen-Producing Bacteria Culturing Solution	0.35	0.21	2.3
Cable and Galvanized Steel Wire in Inoculated Hydrogen-Producing Bacteria Culturing Solution	0.86	0.51	5.9

In a separate experiment, the current pick-up (16mA - 28.5 mA), corresponding current densities  $1.4\mu A/cm^2$  -  $2.5\mu A/cm^2$  shifted the potential of the galvanized steel wire by 30 mV in the negative direction. The corresponding  $H_{ind}$  gradually increased and reached a plateau of 3.8 dB/km (Table II). As expected, the level of  $p(H_2)$  and the resulting  $H_{ind}$  are dependent on the magnitude of picked-up stray dc current density.

C. The effect of hydrogen-producing bacteria alone on the signal attenuation of optical fiber cable.

In the test chamber where the cable sample, without any metal, was exposed to an inoculated hydrogen-producing bacteria culturing solution, the  $p(H_2)$  in the head space reached 0.35 atmosphere over night and maintained this level throughout the experiment. The average  $p(H_2)$  in the cable reached 0.21 atm. The corresponding  $H_{ind}$  gradually increased and reached a plateau of 2.3 dB/km (Table II). The experiments conducted in inoculated hydrogen-producing bacteria solution show that the hydrogen-producing bacteria alone can generate sufficient hydrogen to cause appreciable signal attenuation.

D. The combined effect of corrosion and hydrogen-producing bacteria on the signal attenuation in optical fibers.

In the test chamber where the cable sample and galvanized steel wire together were exposed to the inoculated culturing solution of hydrogen-producing bacteria,  $p(H_2)$  in the head space gradually increased and reached 0.86 atm., and in the cable the average  $p(H_2)$  flattened out at 0.51 atm. The corresponding  $H_{ind}$  also gradually increased and leveled off at 5.9 dB/km (Table II). As expected, the combination of bacteria and galvanized steel corrosion generated more hydrogen and caused more than twice the  $H_{ind}$  than the bacteria alone.

E. Potential Surveys of Submarine Optical Fiber Cables

The locations where the potential surveys were conducted and bottom sediment samples were collected are characterized in Table III, and are designated by the same letters as used by Anderson et al.<sup>(11)</sup>

We conducted potential surveys at two fresh water crossings (K and F). The potential survey data from location K indicate very little loss of zinc. This means that even relatively low rate of corrosion can generate enough hydrogen to cause signal attenuation in optical fiber cables. The data from location F show the presence of a long galvanic cell where the armor wire potential at the west shore is -1.1 volt (anode) and at the east shore it is -0.55 volt (cathode). The latest 1240 nm OTDR measurements at this location showed 27.3 dB/km attenuation at the east shore, and 22.8 dB/km at the west shore. The higher attenuation is at the cathodic (hydrogen producing) end of the galvanic cell. The magnitude of the attenuation can be explained by the fact that the water is 200 feet deep, representing more than 7 atm. pressure over the cable.

We conducted potential surveys at six salt water locations using an Ag/AgCl reference electrode. The surveys at locations B and W show armor wires with very little loss of zinc. The corrosion at location E is more advanced than at B and W. A large galvanic cell exist between armor wires closer than 0.3 km to the shore (anode) and the armor more distant from the shore (cathode). This galvanic cell and 120 feet of water depth are the causes of the high  $H_{ind}$  (Table III). The cables at locations S, A and O are buried 4 to 8 feet deep in the bottom sediment. Their potentials are uniform from shore to shore, most likely because the cables are surrounded by salt water saturated mud (Table III). The potential data indicate that at location S the armor is completely covered by zinc, at location A the zinc is partially corroded away, and at location O most of the zinc is gone (Table IV). These differences in potential do not necessarily mean widely different rates of corrosion, but rather a variation of zinc coating thickness on the armor wires.

F. Bottom Sediment Analysis for Hydrogen

The bottom sediment samples from each locations were kept in the sample holders for 24 to 144 hours before sampling for  $H_2$  gas. The results of the hydrogen analyses are listed in Table V.

The bottom sediments of all locations, both fresh and salt waters, contain active hydrogen-producing bacteria at the cable crossings. The reason why the bottom sediments alone generated only trace to small amounts of hydrogen is that the sediment samples contained only small amounts of material from which the bacteria can produce hydrogen. However, the main sources of the hydrogen-producing bacteria are: medical waste, sewage (both human and animal), food and some

TABLE III

Characterization of the Locations of  
Potential Survey and Bottom Sediment Collection

Location Code	Water type	Depth (feet)	Cable inst. date	Armor type	1300nm loss (dB/km)	1240nm loss (dB/km)	$H_{ind}$ (dB/km)
K	fresh	20	mid-1980's	double galv. steel	0.41	1.52	1.02
F	fresh	200	1986	double galv. steel	NA	NA	25.0
Y	fresh	13	1986	double galv. steel	0.52	2.58	1.97
Z				double galv. steel	0.61	2.35	1.64
E	salt	120	mid-1980's	double galv. steel	0.82	12.75	11.84
W	salt	40	mid-1980's	double galv. steel	0.69	7.82	7.04
B	salt	60	1985	double galv. steel	0.63	5.16	4.44
A	salt	25	mid-1980's	double galv. steel	0.90	4.97	3.98
S	salt	35	mid-1980's	double galv. steel	0.73	8.62	7.79
O	salt	35	mid-1980's	double galv. steel	1.08	7.94	6.76

TABLE IV

Potential Survey Data of Galvanized Steel Armor  
Wires on Three Submarine Optical Fiber Cables  
at Salt Water Crossings

Location	Depth (Feet)	Hind. (dB/km)	Potential vs. Ag/AgCl (volt)		
			Average	Maximum	Minimum
A	25	3.98	-0.778	-0.775	-0.781
S	35	7.79	-0.949	-0.946	-0.953
O	35	6.76	-0.649	-0.646	-0.652

soils.<sup>(15)</sup> Therefore we cannot exclude the possibility that materials for hydrogen production were not present in the past or will not be present in the future in large quantities, causing substantial hydrogen production at current and future cable crossings.

The data obtained from the sediment samples with galvanized steel (Table V) support our statement that armor-wire corrosion, indicated by potential surveys, is a strong contributor of hydrogen that causes signal attenuation in the submarine optical fiber cables. In fact, if we compare the hydrogen-analysis data of the bottom sediments with and without galvanized steel (Table V), the corrosion of the galvanized-steel armor wire appears to be the main contributor of hydrogen.

### Hydrogen Permeation through Cables

Figure 5 shows the partial pressure of hydrogen,  $p(H_2)$ , measured in the gas sampling cap, vs time for the optical fiber cable with the overlapped corrugated steel tube exposed to 1 atm  $H_2$ . The  $p(H_2)$  for this cable increased to 0.1 atm in less than 500 hours (about 3 weeks). The initial slope of the  $p(H_2)$  vs time data is  $3.5 \times 10^{-4}$  atm/hour, giving a linear penetration rate of  $1.8 \times 10^{-3}$  atm  $cm^3/cm$ /hour. This shows that the overlapped barrier allows penetration of a significant amount of hydrogen through the barrier into the cable core where the optical fibers are located, which will cause darkening of the fiber. It has been determined that 0.1 atm of hydrogen is enough to cause problems for telecommunications signals.<sup>(16)</sup> This hydrogen penetration most likely occurs at the overlap of the tube. The  $p(H_2)$ , measured in the gas-sampling cap, vs time for the lead-sheathed cable, the copper-sheathed cable, and the lead-sheathed optical cable is shown in Fig. 6. None of these types of cables showed more than 0.001 atm of  $H_2$  in over 2000 hours, demonstrating that a hermetically sealed metal tube prevents large amounts of hydrogen from diffusing into the optical fibers. The  $p(H_2)$ , measured in the gas-sampling cap vs time for the optical fiber cable with the overlapped corrugated steel tube and damaged plastic coating on the stainless steel armor wires exposed to 3.5% NaCl is shown in Fig. 7. A  $p(H_2)$  of 0.04 atm. of hydrogen was attained in about 1600 hours. The slope of  $p(H_2)$  vs time is  $3.2 \times 10^{-5}$  atm/hour or a linear permeation rate of  $2.3 \times 10^{-5}$  atm  $cm^3/cm$ /hour. While this is better than the same type of cable exposed to 1 atm of hydrogen, it still shows that a significant level of hydrogen-caused darkening may occur within a year or two. Note that this experiment simulated a cable with severely damaged plastic coating over the armor wire, and many cables installed at water crossings may not be as badly damaged.

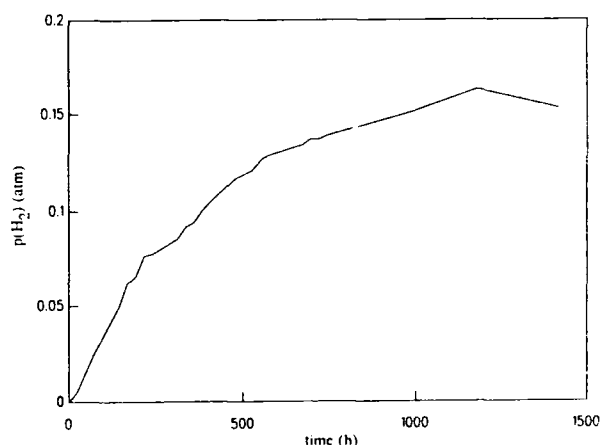


Figure 5. Inside  $p(H_2)$  vs time for an optical cable with an overlapped barrier exposed to 1 atm  $H_2$ .

### Mathematical Model of Hydrogen Diffusion into a Sealed Metal Tube

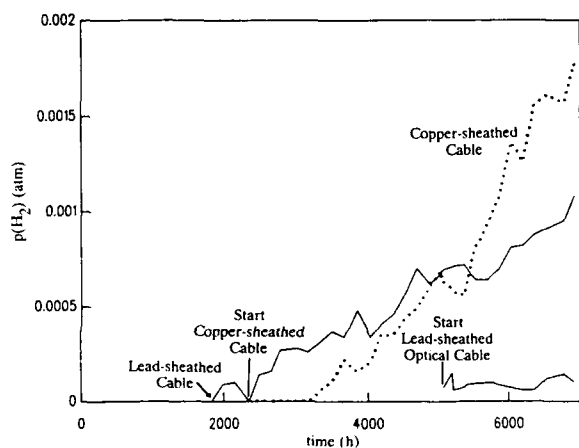
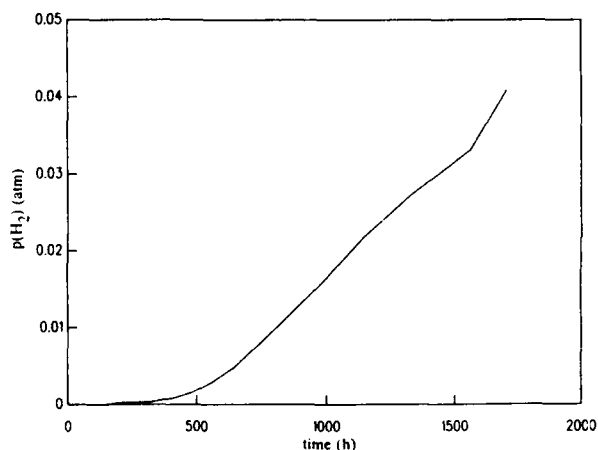
The inner metallic barrier of a submarine optical cable may be modeled as a hollow tube exposed to hydrogen on the outside, and the time required for a particular  $p(H_2)$  to be attained inside the tube is given by the following equation:



TABLE V

## Hydrogen Analysis results in Bottom Sediment Samples

Location	Type of Water	Sediment Sample in Nutrient		Sediment Sample with Galv. Steel		Sediment Sample Alone	
		Avg. Weight of Sample (g)	Percent H <sub>2</sub> in Sample Holder	Avg. Weight of Sample (g)	Percent H <sub>2</sub> in Sample Holder	Avg. Weight of Sample (g)	Percent H <sub>2</sub> in Sample Holder
K	Fresh	0.97	32.7 - 100.0	2.80	20.6 - 100.0	2.99	trace - 0.6
F	Fresh	0.92	26.3 - 75.0	3.50	18.7 - 86.7	3.68	trace
Y and Z	Fresh	0.54	11.3 - 50.9	2.42	0.6 - 1.48	3.42	trace
E	Salt	0.95	8.4 - 79.9	2.66	7.5 - 71.5	3.33	trace - .04
W	Salt	0.61	24.4 - 64.8	2.91	18.0 - 85.7	3.38	trace
B	Salt	0.54	28.8 - 80.1	2.70	12.0 - 90.1	2.99	trace - 0.1

Figure 6. Inside  $p(H_2)$  vs time for cables with sealed metal barriers exposed to 1 atm  $H_2$ .Figure 7. Inside  $p(H_2)$  vs time for an optical cable with an overlapped barrier and stainless steel armor wires with damaged plastic coating exposed to 3.5% NaCl solution.

$$t = \frac{-2dV \left( \frac{p(H_2)_{out}}{p(H_2)_{in}} \right)^*}{A P_H} \left( \left( \frac{p(H_2)_{in}}{p(H_2)_{out}} \right)^* + \ln \left[ 1 - \left( \frac{p(H_2)_{in}}{p(H_2)_{out}} \right)^* \right] \right)$$

where  $p(H_2)_{out}$  is the partial pressure of hydrogen outside the tube,  $p(H_2)_{in}$  is the partial pressure of hydrogen inside the tube,  $d$  is the wall thickness of the tube,  $V$  is the volume inside the tube,  $A$  is the area of the outer surface of the tube,  $P_H$  is the permeation coefficient of hydrogen through the tube material. The details of the derivation of this equation is given in the Appendix. Permeation coefficients, calculated from data given in Smithells<sup>[14]</sup>, and the results of calculations of the time required for hydrogen diffusion into iron, copper and aluminum tubes 1 cm in diameter with 0.5 mm wall thickness are given in the following table.

Hydrogen Diffusion in Metal Tubes*				
Metal	Permeation coefficient **	Outer $p(H_2)$ atm	Inner $p(H_2)$ atm	Time required years
Iron	$5.6 \times 10^{-9}$	1	0.1	0.1
		1	0.9	2.8
		8	1	0.32
		8	7	7.1
Copper	$3.7 \times 10^{-14}$	8	0.01	380
Aluminum	$3.5 \times 10^{-18}$	8	0.01	4,100,000

\* For a metal tube with a 1 cm diameter and a 0.5 mm wall thickness.

\*\* atm cm<sup>3</sup>/(mm cm<sup>2</sup>s)/atm<sup>2</sup> at 298°C

Note that it was assumed that the metal tubes were empty for these calculations. The metal tubes inside real optical cables contain several components, including fiber, with different hydrogen solubilities.

The hydrogen permeation coefficient of iron is considerably higher than that for copper or aluminum, and the model predicts a significant  $p(H_2)$  inside the tube within a year. The hydrogen permeation coefficient of steel is close to that of iron, hence it seems likely that a hermetically sealed steel tube would not prevent hydrogen-caused darkening of optical fibers for a reasonably long time. The time required for hydrogen to penetrate the tube increases with wall thickness. Copper has a smaller hydrogen permeation coefficient and a few hundred years are required to attain significant levels of hydrogen, even when exposed to an external  $p(H_2)$  of 8 atm. Such a high  $p(H_2)$  may be found when the cable is installed 220 ft or more underwater, because the upper limit for  $p(H_2)$  in atmospheres is given

by the depth of the cable divided by 32 ft plus 1 atm. Some cables are installed at water crossings at depths of over 200 ft<sup>[11]</sup>. Hydrogen has an extremely low solubility in solid lead, if it is soluble at all, so an inner lead sheath is a better barrier to hydrogen permeation than a copper tube.

#### Long-Term Reliability Considerations for Optical Fiber Cables

The pressure of hydrogen inside an optical cable follows approximately the empirical equation:

$$p(H_2)_{in} = p(H_2)_{out} (1 - \exp(-t/\tau)) \quad (1)$$

where  $p(H_2)_{in}$  is the pressure of hydrogen inside the cable,  $p(H_2)_{out}$  is the pressure of hydrogen outside the cable,  $t$  is time and  $\tau$  is an empirical time constant. This relation also approximately describes cables with sealed metal tubes, however,  $\tau$  will increase with  $p(H_2)^{1/2}$ .

To ensure the long-term reliability of optical cables and the prevention of excessive hydrogen-caused darkening of the fibers, the pressure inside the cable should remain below an upper limit,  $p(H_2)_{in,max}$ , over the designed life of the cable,  $t_{life}$ . The highest possible  $p(H_2)_{out}$  a cable can be exposed (in atmospheres) is given by  $(1 + 1/32 \text{ ft})$ , where 1 is the depth in feet of the cable underwater. From these values, a minimum value for  $\tau$  can be calculated.

$$\tau_{min} = \frac{t_{life}}{\ln \left( 1 - \frac{p(H_2)_{in,max}}{1 + 1/32 \text{ ft}} \right)} \quad (2)$$

A maximum permeation,  $P_{H,max}$ , coefficient for hydrogen in a cable inner barrier material may be calculated from the following equation:

$$P_{H,max} = \frac{-2 d V \left\{ p(H_2)_{out} \right\}^2}{A t_{life}} \left( \left( \frac{p(H_2)_{in,max}}{p(H_2)_{out}} \right)^2 + \ln \left( 1 - \frac{p(H_2)_{in,max}}{p(H_2)_{out}} \right) \right) \quad (3)$$

where  $d$  is the wall thickness of the inner tube of the cable,  $V$  is the volume inside the tube, and  $A$  is the area of the outer surface of the tube.

The following table gives minimum value of  $\tau$ , expected  $p(H_2)$  inside a cable with a sealed metal tube after 40 days of exposure to 1 atm of  $H_2$ , a proposed test procedure, for different cable life times and installation depths for  $p(H_2)_{max} = 0.1 \text{ atm}$ . It also gives the maximum permeation coefficient for a metal tube 1 cm in diameter and a wall thickness of 5 mils.

$t_{life}$ years	depth feet	$p(H_2)_{out}$ atm	$\tau_{min}$ years	$p(H_2)_{in}$ atm*	$P_{H,max}$ **
25	32	2	480	0.0003	$3 \times 10^{-12}$
	224	8	2000	0.00015	$1.5 \times 10^{-12}$
10	32	2	190	0.00008	$8 \times 10^{-12}$
	224	8	800	0.0004	$4 \times 10^{-12}$

\* exposed for 40 days to 1 atm  $H_2$  at 25°C

\*\* for a metal tube 1 cm in diameter with a wall thickness of 5 mils, in  $\text{atm cm}^3/(\text{mm cm}^2 \text{ s atm}^2)$  at 25°C

Although it is possible to measure  $p(H_2)$  as low as those given in the above table with gas chromatography, the hydrogen indicator,  $H_{ind}$ , cannot be measured for  $p(H_2)$  less than 0.015 atm for a kilometer of fiber, because it is unreliable to measure attenuations less than 0.1 dB.

Iron and steel have permeation coefficients of about  $6 \times 10^{-9} \text{ atm cm}^3/(\text{mm cm}^2 \text{ s atm}^2)$  at 25°C<sup>[12]</sup>. Since this is about 1000 times greater than the  $P_{H,max}$  values given in the table above, steel would not be an acceptable material for a hydrogen-resistant inner barrier 1 cm

in diameter with a 5 mil wall thickness. For copper, the  $P_H$  is  $4 \times 10^{-4} \text{ atm cm}^3/(\text{mm cm}^2 \text{ s atm}^2)$  at 25°C<sup>[14]</sup>, and it would be a suitable material for a hydrogen-resistant barrier.

#### Possible Future Generic Requirements for Underwater Optical Fiber Cables

It is possible for hydrogen to be produced by sources other than the corrosion of cable components, such as bacterial action, and it is possible for the plastic coverings on cable armor wire to be damaged during or after cable installation, allowing corrosion of the armor. Therefore, a generic requirement intended to ensure that a cable is resistant to hydrogen ingress via diffusion is preferable to one intended to ensure that the outer components of the cable do not produce hydrogen when exposed to a corrosive environment. A test procedure for this requirement may be based on the diffusion of hydrogen into a cable. The  $p(H_2)$  inside the inner barrier would be measured after a specified time of exposure to 1 atm of hydrogen for a one-meter piece of optical cable sealed in a PVC pipe or other appropriate enclosure. Since the  $p(H_2)$  inside the optical cable with the overlapped tube started to level off after about 1000 hours, or 40 days, and optical cables at water crossings often show attenuation about a month after installation<sup>[1]</sup>, 40 days would be a reasonable exposure time for this test procedure. In order for a type of cable to meet the generic requirement for resistance to hydrogen-caused fiber darkening, the  $p(H_2)$  inside the cable would be less than a specific upper limit. This upper limit for  $p(H_2)$  inside the cable has not yet been determined, but would be based on information concerning the maximum lengths of cable installed underwater, the maximum depth of water where cables are installed, the ranges of transmission frequencies used, and the maximum amount of signal attenuation allowed for hydrogen-caused darkening. For a cable installed up to 224 feet underwater, with an expected life of 25 years, and a  $p(H_2)_{in,max}$  of 0.1 atm, then the  $p(H_2)$  inside the cable after 40 days of exposure to 1 atm  $H_2$  should be less than 0.00015 atm.

#### Conclusions

- Submarine optical fiber cable armor (galvanized steel) corrosion and/or stray dc current pick up by the armor can generate hydrogen that can cause signal attenuation.
- Plastic-coating on armor wire prevents the generation of  $H_2$ , by corrosion and stray current pick up, if the coating isn't violated and remains intact. If the plastic coating is severely damaged, enough  $H_2$  may be generated by corrosion or stray current pick-up to cause signal attenuation in the optical fibers, even if stainless-steel armor wire is used.
- Hydrogen-producing bacteria may generate substantial amounts of hydrogen at water crossings that can cause signal attenuation. This phenomenon is independent of the armor wires.
- Overlapped metal barriers do not prevent  $H_2$  from diffusing into the cable and causing signal attenuation in the optical fibers.
- Hermetically sealed lead or copper tubes do prevent  $H_2$  from diffusing into the cable. Iron and steel are not good materials for hydrogen-resistant barriers for cables because they are too permeable to hydrogen.
- A generic requirement for resistance of submarine optical fiber cables to hydrogen-caused signal attenuation can be based on exposure time cable samples to hydrogen.

#### REFERENCES

- [1] S. R. Nagel "Reliability Issues in Optical Fibers," in Reliability Considerations in Fiber Optic Applications, D. K. Paul ed., Proc. SPIE 717, 8 (1987)

- [2] B. Wiltshire and M. H. Reeve, *J. Lightwave Technology*, 6 (2), 179 (1988)
- [3] J. Stone, *Lightwave Technology*, LT-5 (5), 712 (1987)
- [4] I. Plitz and P. Warren, "Evaluation of Hydrogen Generation from Optical Fiber Cable," *Proceedings of the 36th International Wire and Cable Symposium*, p 616, (1987)
- [5] S. Kukita, T. Nakai, A. Hayashi, and H. Koga, "Design and Performance of Nonmetallic Waterproof Optical Fiber Cable Using Water-Absorbent Polymer," *J. Lightwave Technology*, 7 (4), 740 (1989)
- [6] D. L. Philen and C. H. Gartside III, "Prevention of Hydrogen Gas Induced Loss in Optical Fibers by Proper Lightguide Cable Design" *Proceedings of the 33rd International Wire and Cable Symposium*, p.415, (1984)
- [7] K. Amano and Y. Iwamoto, "Optical Fiber Submarine Cable Systems," *J. Lightwave Technology*, 8(4) p. 595 (1990).
- [8] S. R. Barnes, N. Pitt, and J. N. Russell, "The Effect of Hydrogen on Submarine Optical Cables," *Electrical Communications* 59 (4) 429 (1983).
- [9] N. E. Hardwick III, L. C. Hotchkiss, J. J. Blee, and D. L. Philen, "Corrosion-Resistant Armor to Prevent  $H_2$  - Induced Loss in Underwater (Wire-Armored) Fiber Optic Cable," *Proceedings of the 38th International Wire and Cable Symposium*, p. 689, (1989).
- [10] G. Schick, K. A. Tellefsen, A. J. Johnson and C. J. Wiczorek, "Hydrogen Sources for Signal Attenuation in Optical Fibers," *Proceedings of the 39th International Wire and Cable Symposium*, p. 244 (1990).
- [11] W. T. Anderson, A. J. Johnson, J. P. Kilmer, and R. M. Kanen, "Hydrogen Gas Effects on Installed Submarine Single-Mode Fiber Cables," *Proceedings of the 37th International Wire and Cable Symposium*, p. 188 (1988)
- [12] W. T. Anderson, A. J. Johnson, and A. DeVito, "Field Measurements of the Effects of Hydrogen Gas on Installed Submarine Single-Mode Fiber Cables," *Proceedings of the 38th International Wire and Cable Symposium*, p. 611 (1989)
- [13] N. H. Skovgaard, A. Baungaard and K. Bundgaard Jensen, "Performance of Low-Loss Submarine Cables", *Proceedings of the 37th International Wire and Cable Symposium*, p. 23 (1990).
- [14] C. J. Smithells, *Metals Reference Book - Vol. 2*, Butterworth, (1955).
- [15] L. V. Holdeman, E. P. Cato, and W. E. C. Moore: "Anaerobic Laboratory Manual" 4th ed. Virginia Polytechnic Institute and State University, Blacksburg, VA 24061, Nov. 1977.
- [16] K. W. Plessner and S. J. Stannard-Powell, "Attenuation/Time Relation for OH Formation in Optical Fibers Exposed to  $H_2$ " *Electr. Lett.* 20(6) (1984) 250-254.

## Appendix A

The pressure of hydrogen inside a sealed metal tube inside a cable sheath depends on the amount of hydrogen that diffuses through the sheath from outside. The cylindrical tube can be approximated by a thin planar sheet of material containing a volume, because the wall thickness of the tube is small with respect to its radius. The rate of change of hydrogen pressure inside a sealed thin sheet of material of area A containing a volume V is given by the following equation:

$$\frac{dp(H_2)_{in}}{dt} = J \times \frac{A}{V} \quad (A.1)$$

where the flux,  $J$ , is the quantity of hydrogen passing through a unit area per unit time. The flux of hydrogen through a material is given by the equation:

$$J = -D_H \frac{dc_H}{dx} \quad (A.2)$$

where is  $D_H$  is the diffusion coefficient for hydrogen in the material,  $c_H$  is the concentration of hydrogen in the material and  $\frac{dc_H}{dx}$  is the concentration gradient in the x direction, that is through the thickness of the sheet. [7] If the hydrogen is diffusing through a thin sheet of material with different pressures of hydrogen on either side, then one may assume that a steady state condition is attained, where the flux is constant within the sheet, and the following approximation may be used:

$$J = D_H \frac{(c_{H_{out}} - c_{H_{in}})}{d} \quad (A.3)$$

where  $c_{H_{out}}$  and  $c_{H_{in}}$  are the concentrations of hydrogen in the material at the outer and inner boundaries of the material, respectively, and  $d$  is the thickness of the material through which the hydrogen is diffusing. Note that an initiation time is needed for a near steady state condition to be attained of about  $\frac{d^2}{6 D_H}$  [9]. This time is generally short with respect to the time needed for a significant pressure of hydrogen to be attained inside the cable sheath, since it does not depend on the solubility of hydrogen in the tube material as does the hydrogen pressure inside the tube, as will be discussed below.

Hydrogen is dissolved in metals, such as iron or copper, as atomic hydrogen. The solubility of hydrogen depends on the square root of the pressure of hydrogen in the gas phase, as given by the equation below.

$$c_H = K_s^{1/2} \left( p(H_2) \right)^{1/2} \quad (A.4)$$

where  $K_s^{1/2}$  is the solubility constant of hydrogen in the metal. Substituting equation A.4 into equation A.3 gives:

$$J = \frac{D_H K_s^{1/2}}{d} \left( \left( p(H_2)_{out} \right)^{1/2} - \left( p(H_2)_{in} \right)^{1/2} \right) \quad (A.5)$$

The permeation coefficient,  $P_H$ , of hydrogen for metallic materials can be defined as follows:

$$P_H = D_H K_s^{1/2} \quad (A.6)$$

Substituting equation A.5 into equation A.1. gives:

$$\frac{dp(H_2)_{in}}{dt} = \frac{P_H A}{d V} \left( p(H_2)_{out} \right)^{1/2} \left( 1 - \left( \frac{p(H_2)_{in}}{p(H_2)_{out}} \right)^{1/2} \right) \quad (A.7)$$

Solving this differential equation gives:

$$t = \frac{-2 d V \left( p(H_2)_{out} \right)^{1/2}}{A P_H} \left( \left( \frac{p(H_2)_{in}}{p(H_2)_{out}} \right)^{1/2} + \ln \left( 1 - \left( \frac{p(H_2)_{in}}{p(H_2)_{out}} \right)^{1/2} \right) \right) \quad (A.8)$$

## AUTHORS



**George Schick** received a Dipl. Eng. degree in Electrochemistry and Electrometallurgy from the Ecole Nationale Supérieure d'Electrochimie et d'Electrometallurgie de Grenoble, France in 1958, the MS degree in Metallurgy from Massachusetts Institute of Technology in 1961, and the Ph.D. in Metallurgy and Materials Science from New York University in 1972. He worked at Bell Telephone Laboratories from 1961 to 1983 in the area of corrosion. In 1984 he joined Bell Communications Research where he is working on corrosion control and on the effects of the environment on optical fibers. Dr. Schick is a member of the National Association of Corrosion Engineers and the American Society for Testing and Materials.



**Karen A. Tellefsen** received the B.S. degree in Chemistry from Stevens Institute of Technology in 1977 and the Ph.D. degree in Physical Chemistry from the University of Ottawa, Ontario in 1988. She worked for Energetics Science, Inc. between completing her B.S. degree and beginning her Ph.D. program, where she worked on the development of an electrochemical hydrazine vapor detector. She joined Bell Communications Research in 1988, where she is working on corrosion control and on the effects of the environment on optical fibers. Dr. Tellefsen is a member of the National Association of Corrosion Engineers, the Electrochemical Society and the American Chemical Society.



**Aaron J. Johnson** received the B.S. degree in Electrical Engineering and Economics from Carnegie-Mellon University in 1980 and the M.S. degree in Electrical Engineering from Georgia Institute of Technology in 1981. He worked for IIT Research Institute from 1982 to 1984, where he was engaged in electromagnetic compatibility analysis. Since 1984, he has been with Bell Communications Research where he has been developing novel optical fiber measurements and writing generic requirements for optical fibers and optical fiber cables. Mr. Johnson is a member of the Optical Society of America.



**Casey J. Wiczorek** is a member of the Optical Cable Group in Bellecore, Morristown, NJ. He joined Western Electric in 1967 and worked on various cable designs and manufacturing processes. He is currently responsible for the development of generic requirements and test procedures for optical cables. He holds a B.S. degree in Mechanical Engineering from Fairleigh Dickinson University and did graduate work at Stevens Institute of Technology.



**Robert M. Kanen** came to work for Bell Communications Research in 1986. He attended Champlain College and Worcester Polytechnic Institute. During the twenty years before working at Bellecore, he was employed by ITT-Federal Electric, HRB-Singer, Singer Co., R.H. Wagner Co., as well as four years of Naval Electronics.

# HYDROGEN EFFECTS IN OPTICAL FIBER CABLES: A NEW APPROACH BY DIRECT PRESSURE MEASUREMENT

B. MISSOUT

A. GOURONNEC

CABLES PIRELLI  
Saint-Maurice FRANCE

FRANCE TELECOM  
CNET Lannion FRANCE

## ABSTRACT

A new method of estimating the maximum fiber attenuation in an optical fiber cable due to hydrogen effects is proposed. The method is based on the direct measurement of hydrogen partial pressure evolution in significant lengths of optical cable under severe but realistic environmental conditions.

The method has been applied to a range of cable designs used in France Telecom's terrestrial network and the results obtained have been compared with those obtained in the field.

Consideration has also been given to the use of more hermetic cable structures and these are compared with existing cables types in terms of their vulnerability to hydrogen effects.

## INTRODUCTION

According to France Telecom's field experience existing methods for estimating the long term effects of hydrogen on fiber attenuation tend to over estimate the asymptotic partial pressure reached.

Thus, a method was needed to approach, as close as possible, the hydrogen partial pressure evolution: both on significant lengths of cable, and in climatic conditions no more constraining than maximum operating conditions.

The method proceeds on three steps:

- evaluation of leakage coefficient, of the outer sheath alone,
- direct measurement of hydrogen partial pressure inside a complete cable, versus time,
- using a mathematical modeling determination of the maximum reachable pressure and associated time.

The maximum allowable partial pressure is deduced from maximum acceptable losses in accordance with known experimental laws.

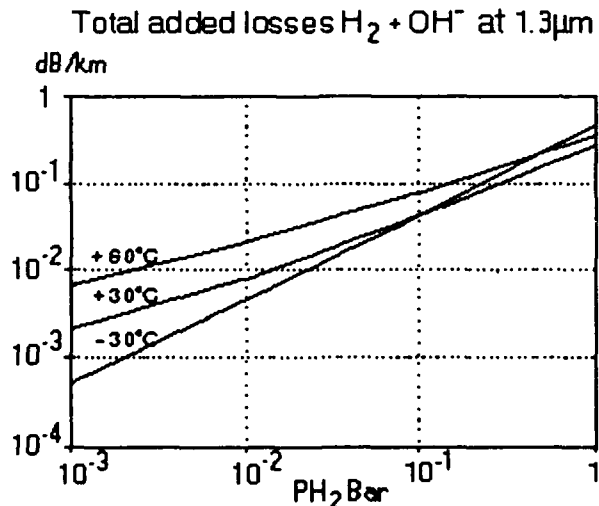
## REVIEW OF HYDROGEN EFFECTS ON FIBERS<sup>(1)</sup>

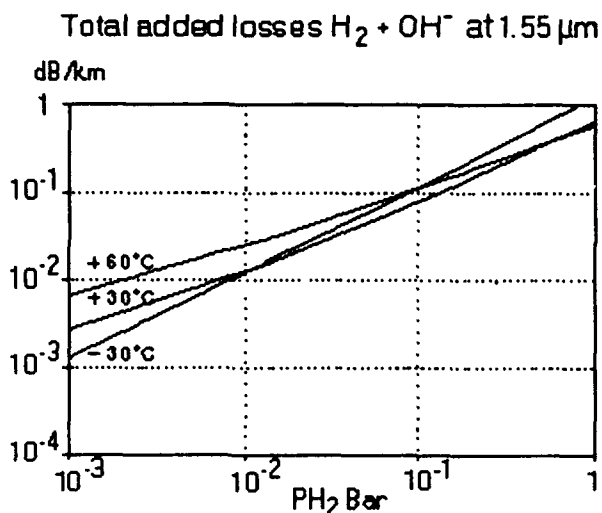
Hydrogen has mainly two types of effects on optical fibers:

- the direct, reversible physical effect of H<sub>2</sub>;
- the irreversible chemical reduction by H<sub>2</sub> of the doping oxides.

The lower the initial attenuation of the fibers, the more critical is the attenuation increase. Hence the effect of H<sub>2</sub> will be considered only in the low attenuation single-mode fibers used in long distance transmission at wavelengths of 1.3 or 1.55 microns.

The curves below present the maximum cumulative attenuation increased (H<sub>2</sub> + OH) after 25 years of exposure under stable pressure and temperature conditions.

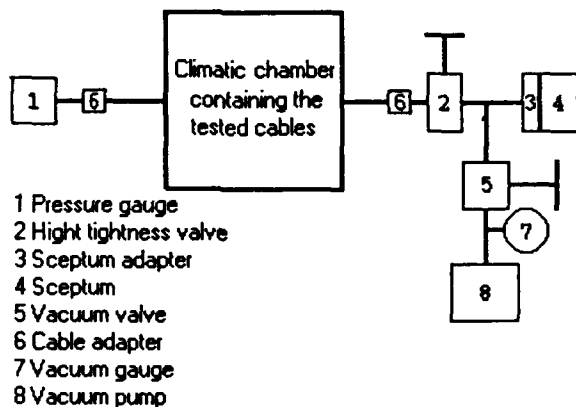




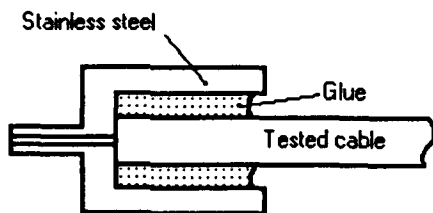
## PRESENTATION OF MEASUREMENT METHOD

### Measurement Apparatus

The figures below show the apparatus used and a detailed view of glued adapters.



Measurement apparatus



Cable adapter

### Remarks

- The adapters must be glued very carefully with two-component polyurethane glue, on a primer coat on the polyethylene sheath (EVA dissolved in hot xylene).
- An eight-positions apparatus has been constructed, so that eight cables could be tested simultaneously.

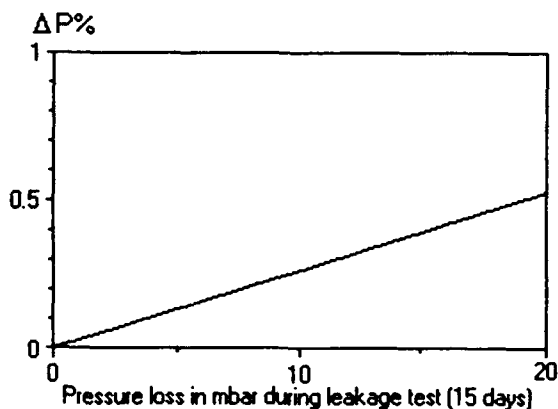
### Control of apparatus gas-tightness

To check the gas-tightness of the setup, an unwelded stainless steel tube was coated with a polyethylene sheath to simulate a perfectly gas-tight cable sheath. The setup described was used to measure the leakage on 20 cm samples, placed in a climatic chamber held at 20°C and filled with one bar of air plus one bar of hydrogen.

The maximum decrease in pressure observed with transducer (1) over a 15-day interval was 2 mbar. This leakage is due to the hydrogen permeation through the glue of the cable adapters (6), and to the leakage of valve (2) and at the apparatus couplings.

The figure below gives the curve of the relative error induced on the  $H_2$  pressure measurement by the apparatus leakage, calculated from the leakage test, for:

- leakage test  $PH_2 = 1$  bar,  $V_0 = 20$  cm<sup>3</sup>
- cable measurements  $PH_2 = 10$  mbar,  $V_0 = 500$  cm<sup>3</sup> (for 100 m of cable)



$\Delta P\% = H_2$  Relative pressure error due to leakage during measurement time of 90 days

The value found, which is less than 0.2 %, is very much smaller than the accuracy of the chromatographic process used, and can therefore be neglected.

## Permeation Measurements

### Sheath Permeation

The central cores of the cables are first withdrawn, leaving hollow tubes of sheath six to ten meters long. Adapters (6) are mounted on these tubes, which are then placed in a climatic chamber, where they are held at constant temperature.

As in the previous case, the pressure decrease is checked. This decrease corresponds to the hydrogen permeation through the sheath tube wall. The results are given in section: Measurements.

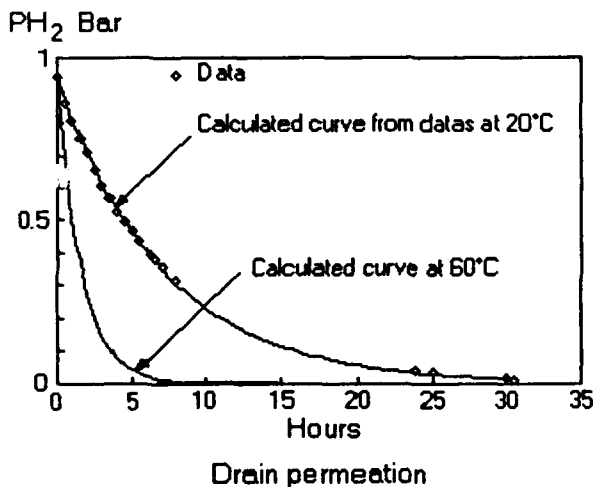
### Drain Permeation

For jelly-filled cables, the measurement method proposed is based on the possibility of collecting representative samples of the internal cable atmosphere, at the cable end. To do this, tubes, small enough to not disturb the internal gas equilibrium, are inserted in the core during the cable construction. These tubes are used as drains (see the sectional drawings of the cables).

To validate this procedure and choose the best type of drain, the permeation rates of various tubes were measured, using the same technique as for measuring the sheath permeation.

The curves presented below represent, for the tube retained (2.9 mm o.d., 0.25 mm wall thickness, polypropylene):

- the measured decrease in H<sub>2</sub> pressure as a function of time at 20°C;
- the H<sub>2</sub> pressure decrease at 60°C, calculated from the results at 20°C.



The curves obtained show that the permeation time of the hydrogen through the drain wall is short enough to be neglected.

## Measurements on Cables

### Sampling of Gases

Two drains are inserted in each cable, so that the total volume sampled (6 samples of 2 cm<sup>3</sup>) would be less than one percent of the total internal gaseous cable volume.

After the climatic chamber is stabilized at 20°C, the gas is sampled as follows for analysis:

- the part of the apparatus between valve (2) and sceptor (4) is evacuated using vacuum pump (8), valve (5) is then turned off.
- valve (2) is turned on and, when the pressure inside the cable, read at (1), stabilizes after 10 or 20 seconds, valve (2) is turned off again.
- the two samples are then taken successively through sceptor (4) using a syringe equipped with a valve.

### Analysis by Gas Phase Chromatography

The gas samples concentrations are controlled by gas phase chromatography. The vector gas used is argon, so that the measurement can be referred to the oxygen and nitrogen in the air sample.

The apparatus was calibrated with a standard (air + H<sub>2</sub>) gas mixture to determine the precision of the measurements.

- The measurement precision is  $\pm 5\%$  for an H<sub>2</sub> partial pressure of 0.2 mbar, i.e.  $\pm 0.01$  mbar.
- For lower values, the amplifying calculations in the apparatus are used. These values at the limit of the background noise should be considered only as a search for traces, the smallest detectable being of the order of 0.01 mbar.

## Mathematical Modeling

### Basic Formulas<sup>(2)(3)</sup>

#### Generation of H<sub>2</sub> for Aluminum

The experimental law is as follow:

$$V_2 = h \cdot V_1 \cdot \sqrt{\frac{2}{t_1}} \cdot e^{\frac{E}{R} \left( \frac{1}{T_1} - \frac{1}{T_2} \right)} \quad (\text{moles/cm}^2 \cdot 10^{-7})$$

$h$  = relative humidity (60 % = 0.6; 100 % = 1);

$V_1$  = quantity of hydrogen generated in the time interval  $t_1$  at temperature  $T_1$  (°K);

$V_2$  = quantity of hydrogen generated in the time interval  $t_2$  at temperature  $T_2$  ( $^{\circ}\text{K}$ );

$\frac{E}{R} = 5200 \text{ } ^{\circ}\text{K}^{-1}$  (for aluminum) at constant temperature and 100 % relative humidity;

$$V = b \cdot \sqrt{t}$$

"b" = generation coefficient of  $\text{H}_2$  in  $\text{cm}^3/\text{day}^{1/2} \cdot \text{m}$  of cable

#### Generation of $\text{H}_2$ for Metals Other than Aluminum

The experimental law is as follow:

$$V_2 = h \cdot V_1 \cdot \frac{t_2}{t_1} \cdot e^{\frac{E}{R} \left( \frac{1}{T_1} - \frac{1}{T_2} \right)} \quad (\text{moles}/\text{cm}^2 \cdot 10^{-7})$$

$\frac{E}{R} = 5400 \text{ } ^{\circ}\text{K}^{-1}$  (for steel) at constant temperature and 100 % relative humidity;

$$V = b \cdot t$$

"b" = generation coefficient of  $\text{H}_2$  in  $\text{cm}^3/\text{day} \cdot \text{m}$  of cable

Variation of  $\text{H}_2$  Partial Pressure in the Cables (the hydrogen pressure outside the cable is zero)

$$dP = \frac{P_0}{V_0} \cdot (-dV_p + dV_g)$$

$V_0$  = total internal gaseous cable volume, in  $\text{cm}^3/\text{m}$  of sheath

$$P = P_a + P_{\text{H}_2} \quad \text{and} \quad P_0 = P_a + P_{\text{H}_2} \text{ initial};$$

$V_p$  = permeated volume

$V_g$  = generated volume.

#### Permeation Alone

$$P_{\text{H}_2} = P_a + (P_0 - P_a) e^{-A t}$$

$$A = a \frac{P_0}{V_0}$$

"a" = leakage coefficient  $\text{cm}^3/\text{bar} \cdot \text{day} \cdot \text{m}$  of cable

$$a_{T_1} = a_{T_2} \cdot e^{\frac{E}{R} \left( \frac{1}{T_2} - \frac{1}{T_1} \right)}$$

$$\frac{E}{R} = 3000 \text{ } ^{\circ}\text{K}^{-1} \text{ (for polyethylen)}$$

"a" = leakage coefficient, in  $\text{cm}^3/\text{bar} \cdot \text{day} \cdot \text{m}$  of cable

#### Permeation Plus Generation For aluminum (initial $P_{\text{H}_2} = 0$ )

An approximate solution to the first order is done by a series decomposition

$$P \approx B \cdot e^{-A \cdot t} \cdot \left( 1 + \frac{A \cdot t}{3} \right) \cdot \sqrt{t} \quad B = b \frac{P_0}{V_0}$$

$$t \text{ to reach } P_{\text{max}} \approx \frac{0.69}{A} \quad P_{\text{max}} = \frac{B}{2 \cdot A \sqrt{t}} \approx \frac{0.6 \cdot B}{\sqrt{A}}$$

#### Permeation Plus Generation For metals other than aluminum (initial $P_{\text{H}_2} = 0$ )

$$P = \frac{B}{A} (1 - e^{-A \cdot t})$$

$$P_{\text{max}} = \frac{B}{A}$$

#### Generation Alone (no permeation of sheath) For aluminum:

$$P = \frac{P_0}{V_0} \cdot V_i (1 - e^{-\frac{b}{V_i} \cdot \sqrt{t}})$$

$V_i = \Sigma$  of the volumes of water initially contained in the air and all the internal cable materials, for an initial relative humidity of 100 % (i.e  $h = 1$ ).

#### Generation Alone (no permeation of sheath) For metals other than aluminum:

$$P = \frac{P_0}{V_0} \cdot V_i (1 - e^{-\frac{b}{V_i} \cdot t})$$

#### Practical Implementation of the Measurement Method

The proposed apparatus was used according to the following experimental procedure to determine the maximum pressure of  $\text{H}_2$  reachable in a given type of cable:

- A test cable is manufactured, and fitted with drains if it is a jelly-filled cable.
- Sampling of sheath.
- The sheath leakage is measured, and the sheath permeation coefficient "a" is determined from the theoretical modeling.
- The variation in the partial pressure of hydrogen is measured.
- If the stabilisation in hydrogen partial pressure is not fully reached, the generation coefficient of  $\text{H}_2$ , "b", is determined, and  $P_{\text{max}}$  and  $t_{\text{max}}$  are calculated from "a", "b" and from the theoretical modeling.

**Note:** In practice, the coefficient and "b" is determined to provide the best adjustment between measured values and corresponding theoretical curves.

This method, using practical measurements, integrates all the effects related to hydrogen generation, such as the electrolytic phenomena, the protection of the metals by the filling jellies, etc. Such approach is applicable to all cases proposed, as long as the pressure readings reach a high enough level to guarantee measurement accuracy, which in our case is  $P_{\text{H}_2} > 0.1 \text{ mbar}$ .



## MEASUREMENTS

The method described has been applied to several test batches, and this paper reports the results obtained with one such representative batch.

**Cables Tested** (see sectional drawings. below)

Three categories of cables of five types were tested.

- metal free cables:

type 1

- cables with aluminum sheath:

type 2: jelly filling and polylaminated sheath

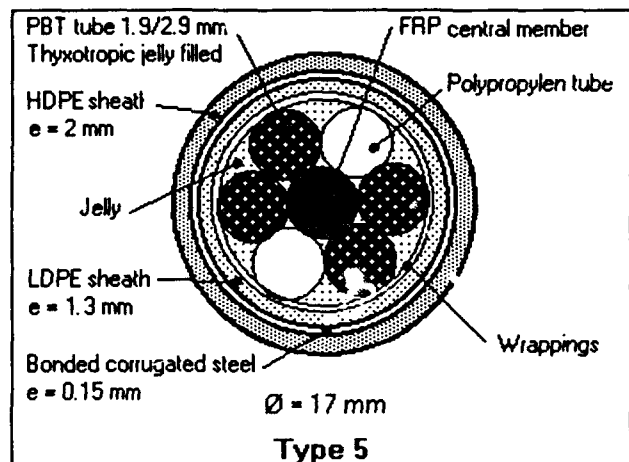
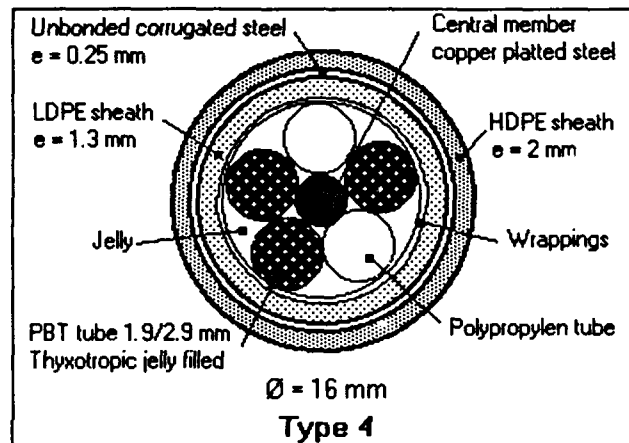
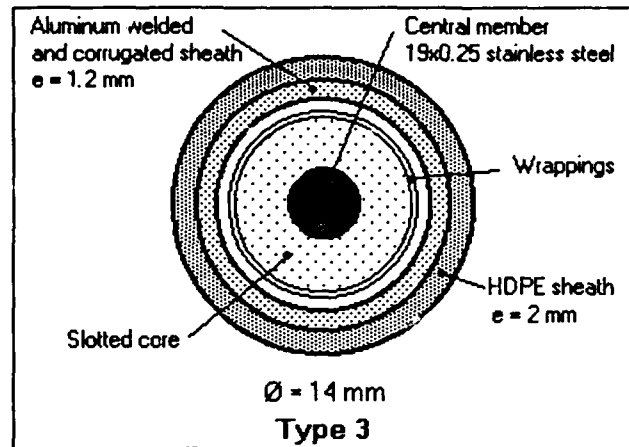
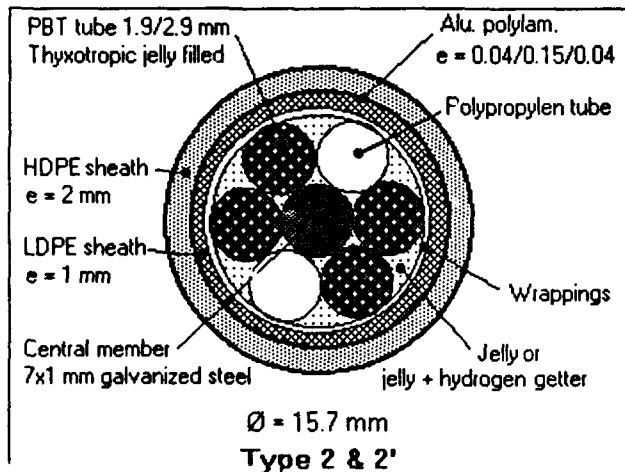
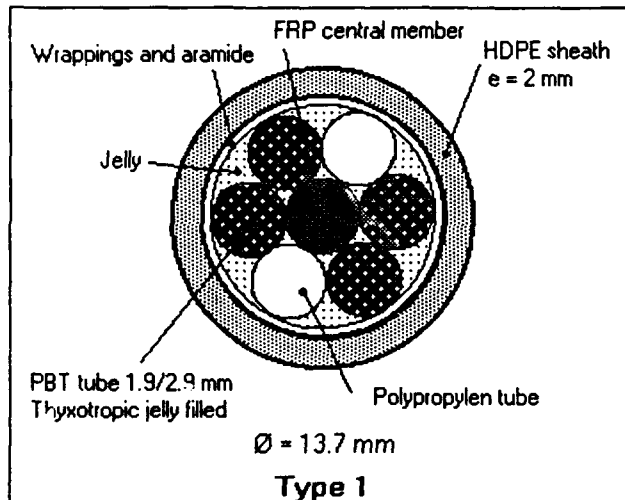
type 2': jelly filling including hydrogen getter and polylaminated sheath

type 3: welded aluminum sheath

- cables with steel sheath:

type 4: uncoated corrugated steel

type 5: coated corrugated steel bonded to the sheath



### Test Conditions

To simulate the more severe conditions in the field:

- the cable samples represented in figures 1 to 3 were placed in a climatic chamber describing the following cycles: 66 hours at 60°C and 99 % relative humidity, then 6 hours at 30°C (the temperature is lowered to - 30°C in order to ease the circulation of gases

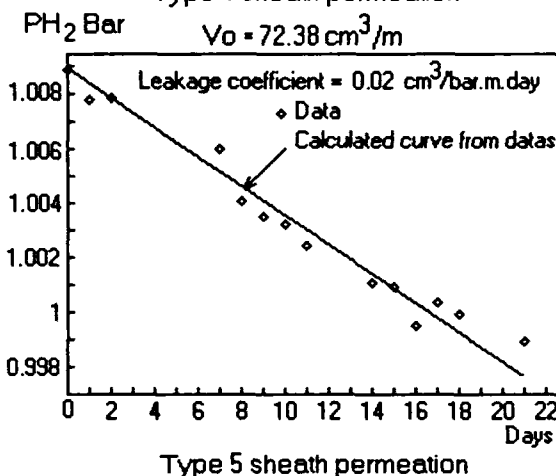
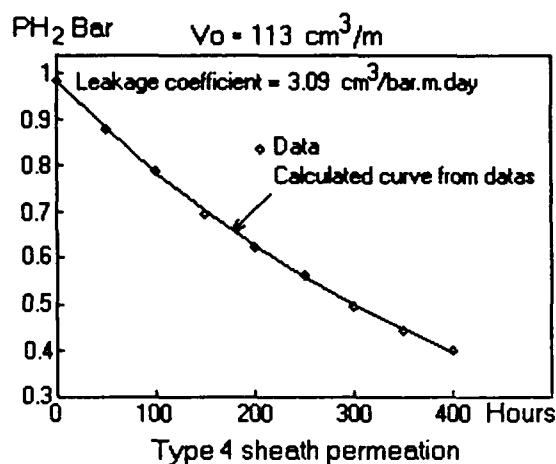
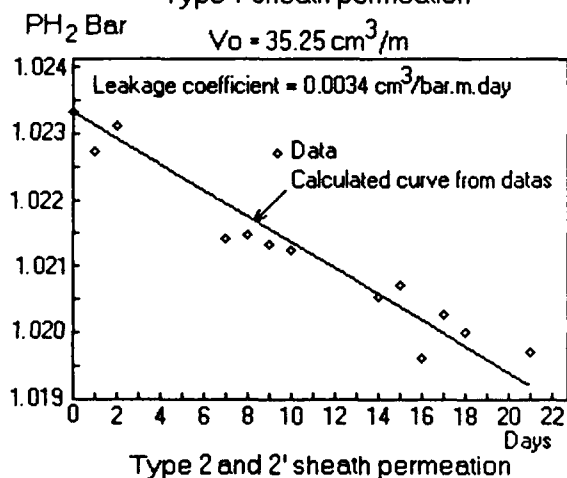
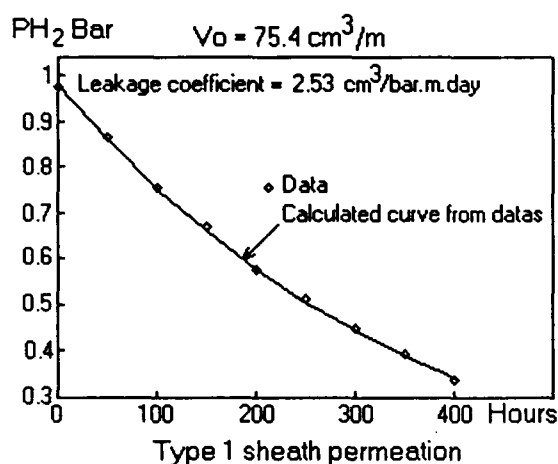
mechanically, and the six-hour duration is the needed time for cables to reach this temperature).

- the cable samples types 4 and 5 were placed directly in a tank of water, held at 60°C.

### Measurements on Cable Sheath

The method of measurement described above was used to measure the decrease in pressure as a function of time, after hydrogen pressurization of the sheath under test.

For each type of sheath construction two samples were measured. The figures below plot the measurement data and the matched theoretical curve, the corresponding leakage coefficient is then calculated.



### Preliminary Analysis of Sheath Permeation Results

- The leakage through the welded aluminum sheath may be considered null, so that the corresponding curve is not given.
- For those sheaths where the wall subjected to the permeation is clearly defined geometrically, as in the case of types 1 and 4, it is possible to calculate the permeation coefficient. The value obtained of  $2.10^{-8} \text{ cm}^3/\text{cm.bar.s}$  at 20°C is within the range of values given in the literature <sup>(3)</sup>.
- Among the different measurements carried out on types 2 and 5, results here reported are the lowest; maximum values are ten times greater. Such a large range underlines the dependance on the bonding quality of overlap and also the effect of tape coating thickness.
- The discrepancy observed between the two types 2 and 5 can be explained by difficulty to get a good bonding of the overlap on corrugated tapes.

## Measurements on the Cables

Measurements were then made on sample cables about 200 m long, using the method described above. The table of measurements below gives the H<sub>2</sub> partial pressure readings in millibar (two dosages per sampling).

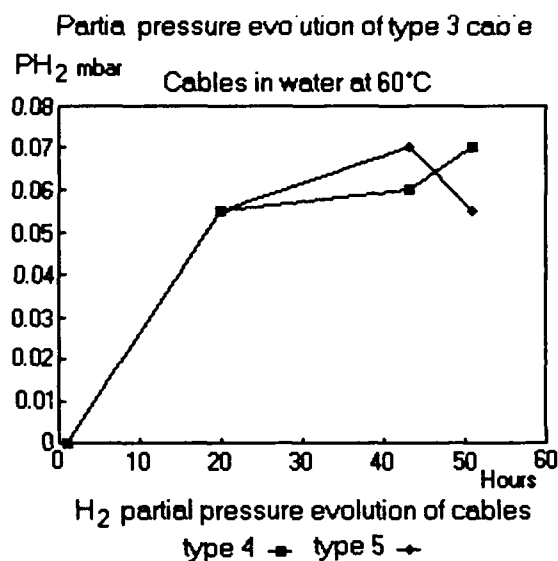
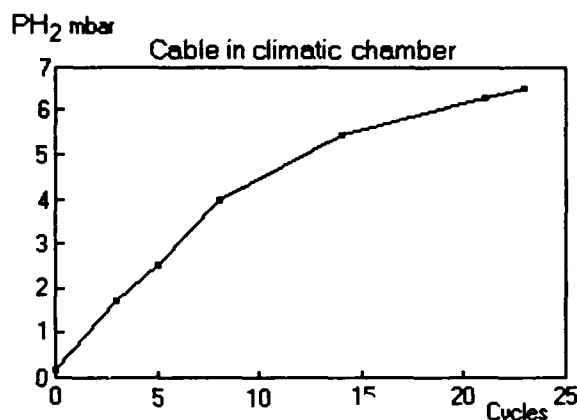
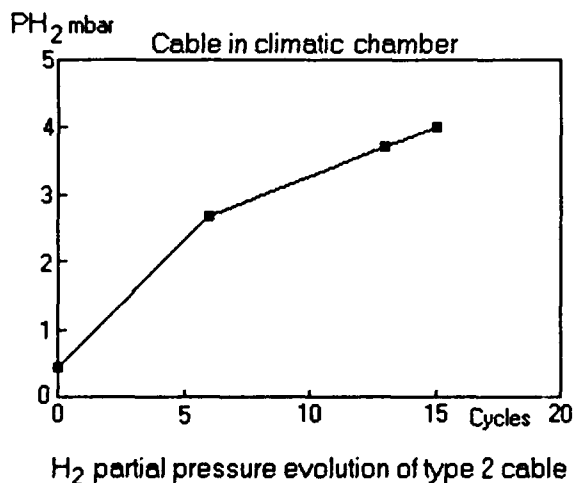
As during gas sampling the climatic chamber temperature is stabilised at 20°C, the cables internal total pressure have been checked to verify that the air permeation at 60°C is small enough to not disturb gases proportions in the sample.

	Nb de cycles							Cycle
	0	3	5	8	14	21	23	
Type 1				0,00 0,00	0,00 0,00	0,00 0,00	0,00 0,00	1
Type 2				0,43 0,43	2,66 2,68	3,69 3,74	4,01 3,99	1
Type 2'				0,00 0,00	0,00 0,00	0,01 0,00	0,00 0,00	1
Type 3	0,15 0,16	1,74 1,69	2,63 2,41	3,97 3,99	5,45 5,42	6,30 6,29	6,51 6,49	1
Type 4				0,00 0,00	0,05 0,06	0,06 0,06	0,07 0,07	2
Type 5				0,00 0,00	0,05 0,06	0,07 0,07	0,06 0,05	2

Cycle 1: Cables in climatic chamber: 1 cycle is 72 hours (66 hours at 60°C and 99 % relative humidity, then 6 hours at - 30°C).

Cycle 2: Cables immersed in water at 60°, one cycle = 72 hours.

The curves corresponding to types 2, 3, 4 and 5 are given below.



## Preliminary Analysis of Results

-The measurements on type 1 cables reveals no trace of hydrogen. Comparison with the values found on type 4 (similar leakage rate), demonstrates that:

- at the level of the detection used, the presence of traces of H<sub>2</sub> seems only related to metal presence;
  - as a consequence, the hydrogen generation at these temperatures (maximum 60°C) from unmetallic materials, is at least of the second order compared with water decomposition by a metal.
- The measurements on type 2' cable show the effectiveness of the hydrogen getter.

## MEASUREMENT RESULTS PROCESSING

### Example of Determination of Practical Coefficients

The proposed method is applied as an example to type 2 cable.

Even in a filled cable, the inner volume is never empty of gas, and the actual value of internal gaseous volume,  $V_o$ , is not precisely known (to improve accuracy of measurements, if needed, it would be directly measured).

So to proceed the calculations we have considered, in the possible range, two values  $\beta$  expressed in ratio of total internal gaseous volume of the cable. For tested cables  $V_o$  includes also the two drains internal volume. The use of an estimate range for  $\beta$  is generally convenient. But for some cases where more accuracy is

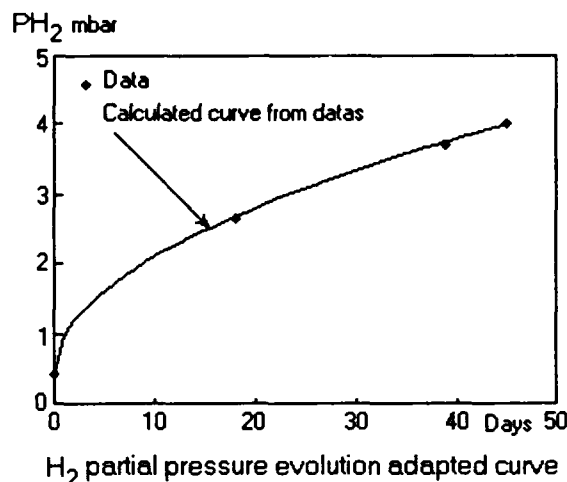
$\beta$	$V_o$ cm <sup>3</sup>	T °C	"a" 10 <sup>-3</sup>	"b" 10 <sup>-3</sup>	Pmax mbar	t Pmax years
0.3	32.6	20	3	2.5	4.1	30
		60	13.2	17.2	13.4	4.6
0.5	48.3	20	3	3	5	45
		60	13.2	25.6	16.4	7

"a" = leakage coefficient of sheath previously measured

"b" values at 20°C are calculated from those at 60°C

requested, the present measurement method allows also to determine actual value of  $V_o$  on a given cable. To this purpose, a known amount of H<sub>2</sub> is injected at a known pressure, in the cable, then the pressure evolution is observed and  $V_o$  is given by calculation. Accuracy may also be improved by extending measurements up to 90 days.

Measurements points at 60°C and corresponding curves adjustments are given below.



## Conclusions on Structures Tested

### Preliminary Remarks

The more stringent situation concerns single mode fibers at 1.55  $\mu$ m.

Assuming a maximum attenuation increase of 0.01 dB/km, according to experimental data, the maximum partial pressure of H<sub>2</sub> is then 10 mbar for a mean temperature of 20°C.

The different cables structures are evaluated on basis of such a limit of 10 mbar.

### Type 1 Cables

These structures are totally permeable to hydrogen. The lack of any detection of traces, even at as low a level as 0.01 mbar, shows that by comparison with type 4 cables the generation of H<sub>2</sub> from unmetallic materials is at least of the second order compared to water decomposition by metals.

These structures therefore present no utilization risk under normal conditions of use.

### Type 4 and 5 Cables

Such structures, either bare or bonded steel corrugated tape, can be considered as slightly closed.

The measurements, show only H<sub>2</sub> traces, at the limit sensitivity of chromatography detector.

Assuming as confident the measured values and with a large over-estimation the maximum, expected value will never exceed a few tenths of a mbar.

These structures therefore present no utilization risk under normal conditions of use.

### Type 2 Cables

The measurements and mathematical simulations show that, in the general case of use at a mean temperature of 20°C, the partial pressure of H<sub>2</sub> will reach only 5 mbar within thirty to forty years.

For continuous use at temperatures greater than 20°C, the limit of 10 mbar can be exceeded, so this type of structure is **unadvisable**.

But, if this type of cable should have to be used, it is recommended to carryout previously a serie of practical measurements to quantify the H<sub>2</sub> risk on the actual structure.

The results obtained on the type 2' structure demonstrate the effectiveness of the hydrogen getter.

#### Notice

For cables type 1, 2, 4 and 5 having permeable sheath, the permeation rate also depends on the partial pressure of H<sub>2</sub> outside the cable. This external pressure is normally null; but if it is not, the simulations presented should be revised in consideration of the hydrogen pressure existing outside the cable. This situation may exist in cases of:

- use of metal duct, or external metallic armouring of the cables (decomposition of the water by the metal(s));
- soils containing organic materials or geothermal sources releasing sulfated hydrogen, which is then transformed into hydrogen by the metals included in the cable.

#### Type 3 Cables

The maximum partial pressure reached in this case is an inverse function of the existing actual internal gaseous volume V<sub>0</sub>, and a direct function of the quantity of water stored in the manufacturing process. The maximum reachable partial pressure versus time can be quantified from the total water amount and measured V<sub>0</sub>.

Then for filled cables, this structure is dangerous, particularly in case of water penetration, which could in certain cases accelerate the phenomenon. For unfilled cables, the hydrogen can flow longitudinally and then may escape through the plastic splicing closures.

The case of welded steel sheath is similar with lower hydrogen generation.

#### Comparison to Operational Experience in France Telecom Networks

At the beginning of the 80s, multimode fibers cables with welded aluminum sheath were used, and no attenuation increase has been detected. Probably due that these cables are unfilled, and so the hydrogen

evolved was able to circulate and to escape through the plastic splicing closures.

Sheaths with aluminum tube have no longer been in use for more than seven years. For example, for exchange to exchange and long-distance intercity links, the cables used are either metal-free (type 1) and installed in plastic ducts, or with corrugated bonded steel tape (type 5) in case of direct burial.

On a general survey of several years, no attenuation increase assignable to H<sub>2</sub> presence has been reported, which is in accordance with the results presented here.

## CONCLUSIONS

#### Cable Evaluation

The main conclusions, in correlation with actual observations in the field, are the following:

- At temperatures corresponding to practical cable use, the generation of H<sub>2</sub> by the non metallic materials is at least of the second order compared to water decomposition by metals (no trace of hydrogen found in metal-free cables).
- The hydrogen getter is effective.
- The effect of galvanized steel strength members seems not decisive: the high generation values from the literature are in fact not confirmed probably due to corrosion protective effect of jelly. However the use of such strength members is not recommended.
- The values of the coefficients "a" and "b" determined by this measurement method fall within the ranges given in the literature.
- The cable structures can be classified, into three categories of risk (for cables without any hydrogen getter) depending on the type of sheath (see table below).

Sheath	no risk	doubt	risk
plastic	x**		
bare or bonded steel	x**		
alu polylam		x*	
welded or extruded			x

\* For normal operating conditions

\*\* According to operating temperature

This classification refers to common terrestrial cable construction. It is obvious that various steps may be taken to limit or even eliminate the risks associated with the use of some of the above components.

### Validity of the Method

The results obtained show that, by direct measurements on cable lengths under environmental conditions similar to those encountered in service it is possible to estimate within a reasonable time (three to six months):

- the maximum pressure of hydrogen;
- the corresponding times, and thereby to precise the risks of attenuation increase.

This method may also help to design the suitable cable structure versus practical environmental conditions.

For some cases where more accuracy is requested, it is advisable to measure previously the actual internal gaseous volume of the cable.

### Extension of the Method

The method presented could be applied to other cases such as:

- partial pressure measurement of other gases such as water vapor, by adapting the vector gas and chromatography;
- hydrogen partial pressure evolution in submarine cables, by measurement at atmospheric pressure and then transposition of results at operating pressure.



**Bernard MISSOUT**

**CABLES PIRELLI**  
Direction R&D  
1, rue des Usines, Saint-Maurice  
94227 Charenton le Pont Cedex  
FRANCE

Bernard MISSOUT, born in 1948, graduated from the Ecole Nationale Supérieure des Arts et Métiers in 1971, joined in 1989, the Research and Development Management of Cables Pirelli where he is presently in charge of studies and development about optical fiber cables, at the Telecommunications Department.

### ACKNOWLEDGEMENTS

The authors wish to thank J. Javaudin and P. Very, both from Cables Pirelli, respectively for measurements and general assistance; P. Anelli, from Cavi Pirelli, for theoretical and technical assistance; O. Fournier and J.P. Louboutin, both from France Telecom CNET Lannion, for their helpful discussions and suggestions.

### REFERENCES

- (1) Kiofumi Mochizuki et al: Influence of Hydrogen on Optical Fiber Loss in Submarine Cable, Undersea Lightwave Communications (IEEE Press)
- (2) D. W. Van Krevelen: Properties of Polymers Elsevier second completely revised edition
- (3) J. Brandrup and E. H. Immergut: Polymer Handbook Wiley-Interscience Publications



**Alain GOURONNEC**

**FRANCE TELECOM**  
CNET Lannion A ELR/CSD  
BP 40 22301 Lannion cedex  
FRANCE

Alain GOURONNEC graduated from the "Conservatoire National des Arts et Metiers" has been first engaged in drawing and cabling studies for optical fibers and cables, since 1986 he is in charge, as group manager, of copper and optical fiber cables in the "Cables et Support en Distribution" CNET department.

# EXAMINATION OF THE STRENGTH CHARACTERISTICS, HYDROGEN PERMEATION AND ELECTRICAL RESISTIVITY OF THE CARBON COATING OF A NUMBER OF 'HERMETIC' OPTICAL FIBRES

E S R Sikora, J V Wright, S J Pycock and M J Yates

BT LABORATORIES, MARTLESHAM HEATH, IPSWICH, UK

## 1. ABSTRACT

Carbon coatings have been applied to optical fibres by a number of manufacturers in an effort to decrease stress corrosion through reduced water permeation to the surface of the silica and to reduce the rate of hydrogen diffusion into the fibre core. If they are to have wide appeal standard testing techniques will be needed. In this report we have examined the strength, hydrogen permeation and electrical characteristics of a number of hermetic optical fibres.

## 2. INTRODUCTION

A number of techniques such as sputtering, evaporation, ionization and glow discharge, can be used to deposit carbon films, [1], giving different carbon structures and transport properties.

Relatively few papers have been published detailing the strength, fatigue and hydrogen susceptibility of carbon coated fibre, [2,3,4,5,6]. The resistance to stress corrosion as described by the stress corrosion susceptibility constant ( $N$ ) has been substantially improved. Values of  $N$  between 70 and 180 have been obtained for dynamic fatigue in water at 90°C and 25°C respectively [2,3] and 200 in air at 23°C [3] compared to between 20 and 30 for non-hermetic fibre at 25°C. The larger  $N$  values for the hermetic fibre indicate that the diffusion of water through the hermetic coating is negligible when compared to non-hermetic fibre. Fibre manufacturers have monitored the hydrogen permeation through their carbon coatings by measuring the resultant attenuation at different temperatures and hydrogen pressures; from 50°C to 125°C at 11 atmospheres [4], 50°C to 155°C at 140 atmospheres [5], and 100°C at 1 atmosphere [6]. These tests have shown that carbon coated fibres offer a significant reduction in loss due to hydrogen compared to non-hermetic fibres.

This report examines the strength and fatigue characteristics, the loss due to hydrogen and the electrical resistivity of the carbon coating of eight fibres supplied by three different manufacturers. The carbon coatings examined were between 200Å and 1000Å thick. The coatings were applied on-line after the pulling furnace.

## 3. DESCRIPTION OF 'HERMETIC' CARBON COATING

The structure of thin films of carbon is unlike that of amorphous silicon in that the carbon has two preferred bond types. The two bond types can give rise to areas in the film where each carbon atom is bonded to four other carbon atoms in a tetrahedral, diamond like, structure and other areas where each carbon atom is bonded to three other carbon atoms in a planar aromatic, graphite like structure. The proportion of each type of bond structure, the stresses in the bonds, and the level of impurities are determined largely by the method of deposition. For example: sputtering and evaporation can be used whereby single carbon atoms or small clusters strike the substrate with low energies (no acceleration of particles) and hydrogen is excluded from the carbon supporting material: ionised carbon and hydrocarbon is formed by the extraction of carbon ions or hydrocarbon molecule ions from an ionization device and deposited onto a biased substrate: reactive deposition in a glow discharge of hydrocarbons and hydrogen gas.

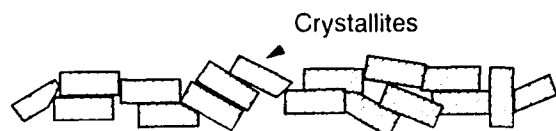
The deposition method for the commercial samples examined is not known by us but it is believed that the carbon coating is applied by pyrolysis of a hydrocarbon such as methane. A carrier gas, possibly nitrogen or helium, can be used to increase the gas pressure in the pyrolysis chamber to atmospheric. Heating of the hydrocarbon to between 1500°C and 1800°C, by the fibre emerging from the pulling furnace, results in carbon atoms being deposited on the fibre surface. Most of the deposition is thought to take place in the region of maximum temperature. The gas mixture can be preheated to give an effective increase in the deposition rate.

Pyrolysis is not a single step process [7] whereby all the hydrogen atoms are removed leaving carbon atoms free to attach themselves to the fibre. It involves the formation of an entire series of molecular species of progressively decreasing hydrogen fraction. Two competing mechanisms: a) the rate of pyrolysis, b) the rate of diffusion through a relatively viscous conduction zone next to the fibre, control the formation of the carbon coatings. Tests have shown [8,9,10,11] that the carbon coatings examined mainly consist of disordered graphitic crystallites whose textured C-axes are

perpendicular to the longitudinal axis of the fibre. A typical microstructure of pyrolytic graphite is shown in Fig (1).

FIG.(1)

### Schematic of Pyrolytic Carbon Coating



Three material characteristics effectively control the coating density; the crystallite size, the crystallite orientation (the angle the C-axis makes with the fibre) and the crystallite perfection. The deposition temperature of the coating, the concentration of hydrocarbon gas [12,13] and the pulling rate will to a great extent control these characteristics. In general the smaller the crystallite and the more random the orientation, the greater the probability of microvoids forming during cooling of the coating resulting in a coating density less than that of a single crystal. A decrease in crystallite perfection away from that of graphite or an increase in the interlayer spacing will also decrease the density.

Hydrogen is likely to diffuse through microvoids formed at the crystallite boundaries during cooling [14] and by hydrogen ion transfer between unsatisfied carbon valencies [15]. Thus smaller, randomly orientated crystallites may allow hydrogen to diffuse through at a faster rate.

The electrical resistivity is also a function of the crystallite size, orientation and perfection, [16]. Due to the resistivity along the C-axis being much larger than that in the basal plane the resistivity along the fibres will largely be controlled by the number and mobility of the charge carriers along the basal planes of the crystallites. Coatings made up of small crystallites are thought to have an energy gap between the valence and conduction bands,[16]. The energy gap reduces with increasing crystallite size. The carbon atoms at the crystallite boundaries act as electron traps causing the coatings to be p-type material in which the electrical resistance is mainly due to excess carriers (holes) in the valence band. Two scattering processes will control the mobility of the charge carriers; scattering due to lattice vibrations and scattering occurring at the crystallite interfaces and lattice imperfections. Thus the larger the crystallite size and the better the orientation the closer will the resistivity approach that of a single graphite crystal,  $0.39 \times 10^{-4} \Omega \text{ cm}$  [7] compared to about  $60 \times 10^{-4} \Omega \text{ cm}$  for amorphous carbon [17].

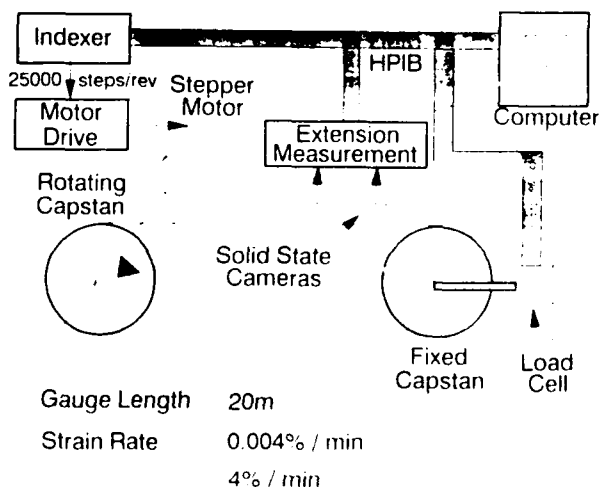
### 4. FACTORS AFFECTING THE STRENGTH AND FATIGUE OF CARBON COATED FIBRES

The initial strength of a fibre is governed by the size of the largest surface crack. The deposition process and the stresses at the carbon/silica interface will tend to induce cracks at the silica interface the size of which is likely to depend on the energy with which the carbon impacts the silica surface during deposition and the level of radial stress acting on the silica due to the cooling of the coating after deposition. The thicker the coating and the higher its modulus (radial and circumferential) the larger will be the radial stress. Low adhesion between the carbon and the silica will also tend to induce surface cracks in the silica if relative motion takes place.

The elastic moduli, tensile and shear strengths of the carbon will depend on the crystallite size, the orientation and perfection, the temperature and the type of bond between any crystallites so that values for the strength characteristics of graphite materials found in the literature not obtained directly from the coatings can only be used as rough guides.

Long term strength will depend on the rate of water permeation through the carbon coating. If the coating is not cracked and is pinhole free the rate of water permeation will be negligible as the coatings are almost impervious to hydrogen. If on the other hand the coating is damaged through corrosion or by mechanical handling such that cracks are induced in the coating or there are pinholes in the coating, hydrogen and water may permeate through at a faster rate. This may not lead to a high hydrogen induced loss if the cracks/pinholes are sufficiently far apart but may cause stress corrosion of the silica at the crack site.

Figure 2. SCHEMATIC OF DYNAMIC FATIGUE TEST EQUIPMENT





## 5. EXPERIMENTAL WORK

The fibres used for the dynamic fatigue tests, hydrogen permeation tests and resistance measurements are given in Table (1).

TABLE 1. FIBRES EXAMINED TO DATE

FIBRE ID	COATING THICKNESS in $\mu$	HISTORY
A	850	hydrogen tested
E	850	NOT hydrogen tested
F	220	NOT hydrogen tested
B	400	hydrogen tested
C	800	hydrogen tested
D	800	hydrogen tested
G	800	NOT hydrogen tested
H	650	NOT hydrogen tested

### 5.1 STRENGTH AND FATIGUE

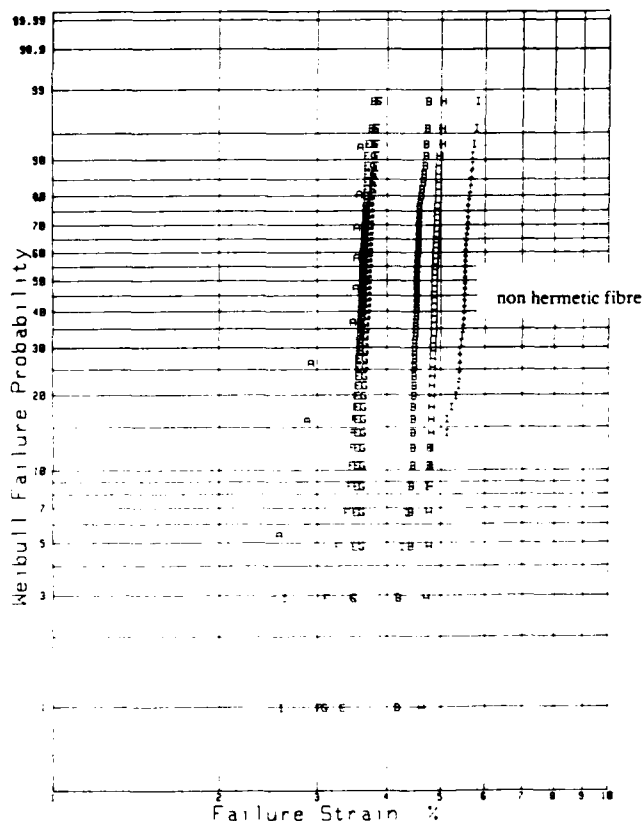
The hermetic fibres were subjected to dynamic fatigue tests using a 20m gauge length to obtain the initial tensile strength of the fibre and an estimation of the stress corrosion susceptibility constant N. Unlike non-hermetic fibre where the N value is generally independent of the initial size of the cracks, with hermetic fibre the N value will largely depend on the the size and position of cracks/pinholes in the carbon coating necessitating the N value to be obtained from long gauge length tests.

A schematic of the 20m gauge length tensile test equipment is shown in Fig(2). The fibre is wound round two capstans, one fixed and the other rotating. A load cell is attached to the fixed capstan while the rotating capstan is driven by a stepper motor. The strain is measured independently using two fixed CCD cameras monitoring the position of two targets attached to the fibre. The ambient temperature during testing is  $\approx 20^\circ\text{C}$ .

Three strain rates are used, 0.00011%/sec, 0.00029%/sec and 0.064%/sec giving failure times of approximately 8hrs, 4hrs and 1min respectively. Figure (3) is a Weibull plot of the failure strains, at 0.064%/sec, for fibres A,B,E,F,G, and H. The weakest fibre is A and the strongest fibre is H. The Weibull slope (m value) of all the fibres tested at 0.064%/sec, except fibre A, are nearly vertical indicating a narrow crack distribution. The mean failure strains and the number used to estimate the N and m values at the different strain rates are given in Table (2), any results not part of the main population have been excluded. The thinner coatings (B,H) tend to have the highest mean failure strain, except for the thinnest (F). Table (3) shows how the m value varies with the strain rate. As the strain rate is reduced the m value decreases for all fibres. Two fibres A and G also show a decrease in m value even though the mean failure strains have increased slightly.

Of the fibres which showed a reduction in the failure strain (E,F,B) the decrease between 0.064%/sec and 0.00029%/sec was  $\approx 0.3\%$ . Fibres F and B decrease by  $\approx 0.6\%$  between 0.00029%/sec and 0.00011%/sec. Fibre H on the other hand decreases by 0.52% and 0.1% between the fastest and middle strain rate and the middle and slowest strain rate respectively.

Figure 3. CUMULATIVE FAILURE PROBABILITY AT A STRAIN RATE OF 0.064%/sec



Although caution needs to be used interpreting the N values, as the m values are not constant for any fibre and the fact that relatively few results have been used to estimate N, the trends are clear. A and G have the largest N value, Table (4), while the others are lower than expected. The N value for B and F reflects an increase in crack growth per unit time unlike fibre H which has a reduction in crack growth per unit time as the strain rate is decreased. Fibre E seems to be inconsistent with A and G in that it has a low N value and a relatively thick coating.

## 5.2 LOSS DUE TO HYDROGEN

The spectral attenuation of fibres A,B,C and D has been measured with respect to time with the fibres immersed in a hydrogen atmosphere at 60°C and 54 atmospheres. Two other fibres F and H are at present on test. The temperature of 60°C was chosen to increase the rate of diffusion through the coating whilst at the same time minimising any microbending losses due to changes in the mechanical characteristics of the polymer coatings. Fifty four atmospheres is simply the upper limit of the pressure vessel. A more detailed description of the experiment is given in [18].

TABLE 2. EFFECT OF STRAIN RATE ON MEAN FAILURE STRAIN

FIBRE ID	MEAN FAILURE STRAIN (%) FOR A STRAIN RATE OF (%/sec)					
	0.00011 %/sec	No used	0.00029 %/sec	No used	0.064 %/sec	No used
A	3.55	4			3.53	9
E			3.3	3	3.6	49
F	3	4	3.5	3	3.7	46
B	3.7	6	4.3	9	4.6	47
G	3.8	6			3.7	50
H	4.2	4	4.3	3	4.82	50

The hydrogen induced attenuation at 1.24 $\mu$ m for fibres A, B and C at 60°C and 54 atmospheres of hydrogen is shown in Fig(4), as a function of time. Compared to non-hermetic fibres the increase in optical loss for the three fibres is negligible. Notwithstanding this there are significant differences between the fibres. The loss of fibre A is much greater than that of fibres B and C. Note that the loss of B

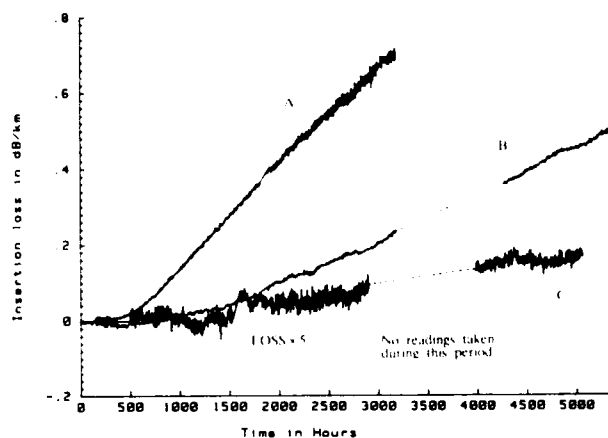
TABLE 3. WEIBULL SLOPES (m) AT DIFFERENT STRAIN RATES

FIBRE ID	WEIBULL SLOPE (m) FOR A STRAIN RATE OF (%/sec)		
	0.00011 %/sec	0.00029 %/sec	0.064 %/sec
A	14		43
E		16	61
F	5	17	32
B	6	20	56
G	16		63
H	8	32	76

TABLE 4. N VALUES

FIBRE ID	N VALUE	MEAN FAILURE STRAIN (%) FOR A STRAIN RATE OF (%/sec) USED IN CALCULATION OF N		
		0.00011 %/sec	0.00029 %/sec	0.064 %/sec
A	>>200	3.55		3.53
E	55		3.3	3.64
F	100		3.5	3.7
F	40	2.8	3.5	3.7
B	35	3.66	4.3	4.58
B	76		4.3	4.58
G	>>200	3.82		3.73
H	46	4.2		4.82

Figure 4. ATTENUATION DUE TO INTERSTITIAL HYDROGEN AT 1.24 $\mu$ m FOR FIBRES A, B AND C



and C has been multiplied by a factor of 5 to clarify the differences between the traces. The rate of increase of attenuation of fibre D, Fig(5), on the other hand was similar to a non-hermetic fibre. The carbon coating of fibre D was therefore not hermetic to hydrogen for a considerable portion of its length. Damage to the coating during handling was ruled out after tests designed to simulate rough handling, carried out on a length of fibre pulled from the same preform, failed to induce an increase in loss. A visual examination of fibre D showed that the adhesion of the

carbon coating to the silica was relatively weak compared to the other three fibres. On its own it is improbable that this would give rise to the measured loss. On the other hand if poor adhesion between the carbon coating and the silica made the formation of very small cracks more probable hydrogen could easily diffuse through the coating and between the coating and the silica.

### 5.3 RESISTANCE MEASUREMENTS

Electrical resistance measurements were undertaken to determine whether they could be used to differentiate between carbon coatings that have a high rate of hydrogen permeation and those which have a low rate.

Twelve volts was chosen as the standard applied voltage as a balance between too low a current measurement and too high an applied voltage affecting the resistance of the coating. All the results were obtained using fibre lengths whose polymer coatings had been stripped off to ensure good repeatability.

To enable the resistivity of the coatings to be calculated the thickness of each coating was measured by transmission electron microscopy, [8,9,10,11]. The accuracy of the present thickness measurements is of the order of  $\pm 20\%$ . This obviously affects the accuracy to which the resistivity can be calculated. Although the resistivity can only be quoted to  $\pm 20\%$  the maximum variation in the resistance measurements is of the order of  $\pm 2\%$ .

FIG.(5) Attenuation due to Hydrogen at 1.24 $\mu$ m for fibre D

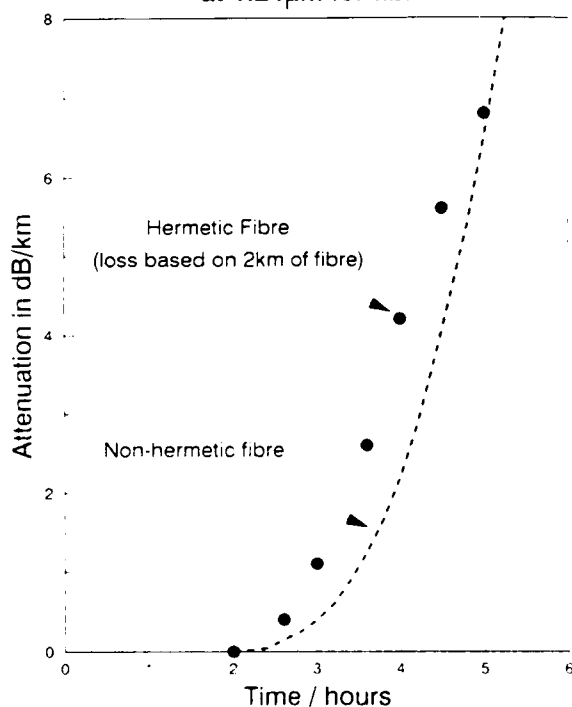


TABLE 5. RESISTIVITY 20°C at 50% RH

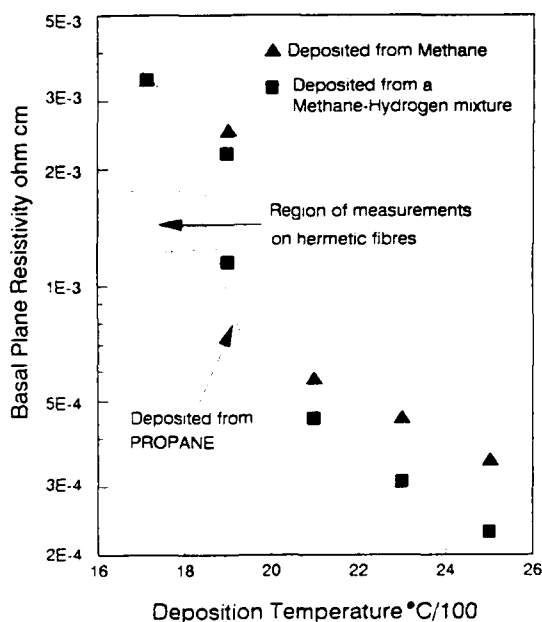
FIBRE ID	RESISTIVITY $\Omega\text{cm}/1\text{E-4}$	
	MEAN VALUE	$\pm 95\%$ CONFIDENCE LIMITS (variation in resistance)
A	14.7	0.42
B	11.6	0.25
C	16	0.38
D	$\approx 40$	
E	14.4	0.03
F	11.5	0.99
G	15.8	0.07
H	26.5	0.92

To determine whether the resistivity values were affected by fluctuations in resistance at the joint between the metal conductor, (joined to each end of the carbon coated fibre using 'silver dag'), and the carbon coated fibre the resistance was measured as a function of length. The slope of the regression line through the four points along each length of fibre, between 10mm and 300mm was then converted to resistivity. As end effects were small the rest of the measurements were taken on single lengths of fibre between 250 and 300mm long.

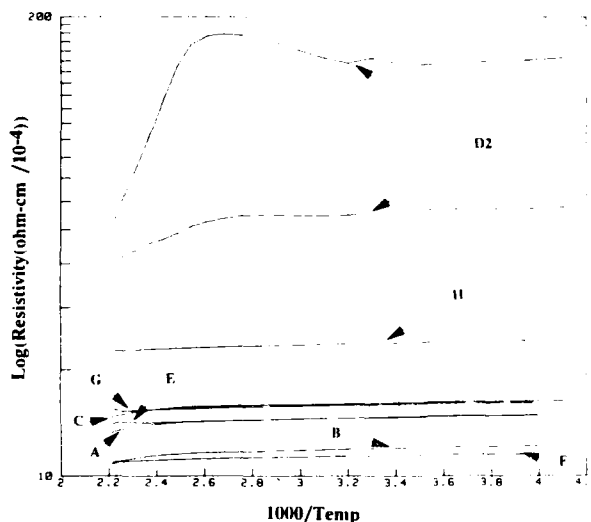
Table (5), shows the resistivities of the fibres tested. Fibres A, B, C, E and F have a similar resistivity while the initial sample from the fibre that had a higher attenuation due to hydrogen, fibre D, has a much higher resistivity. Fibre H has a resistivity higher than fibres C and G but lower than that of D. The results are typical of pyrolytic graphite [16,18,19] as shown in Fig(6) where the resistivity of different pyrolytic graphites are plotted against deposition temperature.

To determine whether the resistivity along fibre D was constant it was cut into three lengths D1, D2, D3 and the resistance at each end of the three lengths was measured. The resistivity of D1 was found to be similar to the fibres which had a good hydrogen performance. The resistivity along fibre D was therefore similar to fibres A, B and C for approximately 2.5km after which it increased to over  $100 \times 10^{-4} \Omega \text{ cms}$  over a short length of fibre, and reaching values of  $\approx 190 \times 10^{-4} \Omega \text{ cms}$  towards the end of the fibre length.

**FIG.(6) Variation of Electrical Resistivity with Deposition Temperature.**



**Fig (7) Variation of Resistivity with inverse Temperature.**



Fibre D1 was then immersed in hydrogen at 60°C, 10atm, for a period of 425hrs. No change was found in the attenuation at 1240nm before and after the test indicating that the high hydrogen permeation for fibre D shown in Fig(5) was due to hydrogen diffusing into the fibre only over approximately half of the fibre, (lengths D2 and D3).

As the change of resistivity with temperature depends on the electronic structure of the carbon coatings which is strongly dependent on the deposition conditions plotting resistivity against temperature can therefore give an indication whether the coating structures are similar.

Figure (7) is an Arrhenius plot of the resistivity of the fibres. It clearly shows a distinct difference between the group of fibres A, B, C, E, F, G and fibres H and D2. The confidence limits are not drawn for clarity. An idea of the uncertainty of the measurements is given in Table(5). Between -30°C and  $\approx 100^\circ\text{C}$  the resistivity for each of the fibres decreases by about 4%. Above  $\approx 100^\circ\text{C}$  the resistivity starts to change more rapidly, generally decreasing with temperature. Fibres E and G which show a slight increase are expected to behave similarly to fibre D2 where a slight increase is followed by a rapid decrease in resistivity as the temperature is increased. This behaviour is consistent with that of pyrolytic graphite [16] where the resistivity is controlled by the number and mobility of excess charge carriers, holes. Up to about 100°C there seems to be insufficient energy for the formation of significant numbers of intrinsic carriers (electron/hole pairs) so there is little change in the resistivity. As the temperature is increased still further the number of intrinsic carriers increases significantly so reducing the resistivity.

Four measurements of resistivity with temperature were taken for fibre D2, two from each end. As expected the resistivity is much larger with a distinct difference between the two ends, the end closest to length D1 having a

substantially smaller resistivity than the other end. Three interesting features are noticeable; the average slope below about 90°C are similar to those of the other fibres, the plots are noisier insofar as there are a number of excursions from the mean slope, and that the decrease in resistivity at temperatures above  $\approx 100^\circ\text{C}$  is significantly greater than that for the other fibres.

#### 5.4 SEM and TEM EXAMINATION

The coatings were also examined using SEM and TEM techniques to provide a physical interpretation of the resistivity measurements. A scanning electron microscope (SEM) examination of fibres B and D using an X-ray technique (EDX) provided relative thicknesses of the carbon coatings. No features such as defects/cracks were observed, at a magnification of 20,000, on lengths of fibre D examined. The surface of the coatings on fibres B and D were smooth at the same magnification, [21]. If defects existed they would have to be smaller than about 100nm.

The six fibres were also examined by transmission electron microscopy (TEM), [8,9,10,11]. Thin sections from each

**TABLE 6. INTERPLANAR SPACINGS MEASURED FROM THE ELECTRON DIFFRACTION PATTERN TAKEN FROM THE FIBRE COATINGS**

FIBRE ID	MEASURED INTERPLANAR SPACINGS ( $\text{\AA}$ )			
	{0002}	{1010}	{0004}	{1120}
Graphite single crystal for comparison	3.35	2.13	1.67	1.23
Graphite small crystallites for comparison	3.71	2.13	1.87	1.23
A	3.52	2.05	1.77	1.18
B	3.61	2.12		1.19
C	3.64	2.1	1.83	1.19

**TABLE 7. CRYSTALLITE PARAMETERS**

FIBRE ID	COATING PARAMETERS		
	Crystallite Dimension C-axis ( $\text{\AA}$ )	Inter-planar distance $\text{\AA} \pm 10\%$	Average Orientation of C-axis wrt fibre radius (degrees)
Reference [7]	10	3.7	
A	<15		$\pm 25$
B	<20		$\pm 25$
C	<15	3.7	$\pm 25$
F	<20	3.6	$\pm 18$
H	<20	3.7	$\pm 40$

fibre were prepared by mechanical polishing and ion beam milling enabling the coatings to be examined along the longitudinal direction of the fibres. Improvements to the preparation of fibres F and H allowed a greater length of coating to be examined in a direction tangential to the radius. The diameters of the diffraction ring patterns, Table (6), suggest the coatings to be largely made up of disordered graphitic crystallites rather than a single crystal or an amorphous structure. The 0002 and the 0004 reflections are intense in only two opposing directions over an angular range given in Table (7). The 1010 and 1120 are intense over the same angular range but are perpendicular to 0002. This implies a strong texturing of the crystallites such that their C-axes are, on average, orientated radially to the fibre. One of the fibres, H, has very weak texturing, and the 0002 and 1010 arcs can just be discerned. TEM micrographs of fibre H suggest the carbon surface has a slight ripple. The estimation, where possible, of the crystallite size in the C-direction, the average orientation and the interplanar distance, Table (7), agree well with the resistivity measurements carried out here and also those reported in the literature.

## 6. DISCUSSION

The initial strength, the lifetime and the hydrogen performance of the fibres are controlled by the microstructure and thickness of the coatings. In general the results suggest that the thicker the coating the lower the initial strength. It might be expected that the larger and the better orientated the crystallites are the lower the hydrogen diffusion for a given thickness.

The initial tensile strength, the N value and the variation in the crack distribution has been estimated from dynamic fatigue results obtained from 20m gauge length samples in tension. In general it has been found that the thicker the coating the smaller the mean failure strain tends to be with the exception of fibre F which has the thinnest coating and a low mean failure strain.

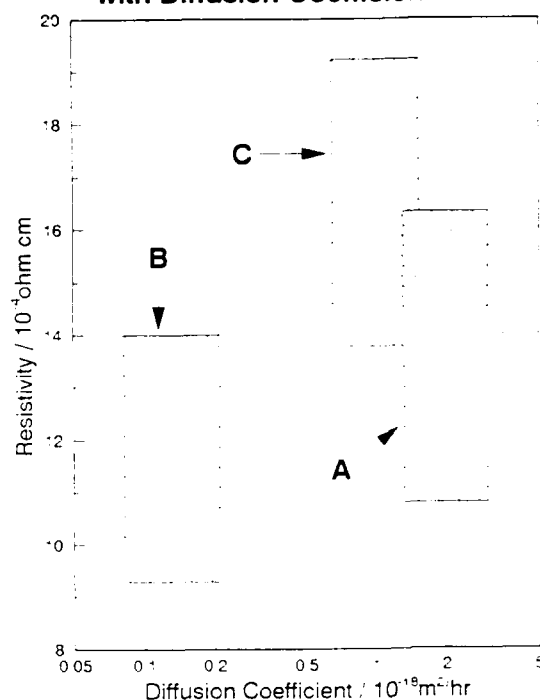
The crack distribution as described by the m value becomes wider as the strain rate is decreased. This is unlikely to be due to a real change in the crack distribution on the surface of the fibre before the tests, but due to a variation in the rate of crack growth during the tests. Increased testing times, lower strain rates, will tend to allow small variations in the chemical processes at the crack tip to affect the failure strain. As the reduction in m value also occurs with fibres A and G whose mean failure strains at 0.00011%/sec are slightly greater than those at 0.064%/sec it is probable that crack blunting is also taking place. The effects of crack blunting can also be seen in the results for fibre H when comparing the mean failure strains for strain rates of 0.00029%/sec and 0.00011%/sec.

The N values of all the fibres tested are larger than those obtained from non-hermetic fibre. The N value for the fibres with the thinner coatings, B, F and H, are noticeably smaller than for fibres A and G the two fibres with the thickest coatings. It is possible that cracks, which may occur during the tests, in the thinner coatings offer a more direct route for water to reach the silica surface than cracks in the thicker coatings. The exception to this is fibre E which also has an N value of 55 and a coating thickness of about 850Å.

From the present hydrogen results three of the four fibres (A,B,C) would be suitable for use in cable systems where

hydrogen may be a problem. From the electrical resistivity results and TEM analysis (crystallite orientation  $\pm 18^\circ$ ) it is expected that fibre F will also have a good hydrogen performance. Fibre H with its higher electrical resistivity and weaker texturing (crystallite orientation  $\pm 40^\circ$ ) is expected to have a worse hydrogen performance than the other fibres tested except for fibre D2. The higher electrical resistivity may tentatively be ascribed to the weaker texturing, that is the larger angular spread of the C-axis to the fibre radius. It is suspected that a processing fault during the application of the carbon coating on fibre D increased its hydrogen permeation for part of its length.

FIG.(8) Variation of Electrical Resistivity with Diffusion Coefficient at 60°C



There is no correlation between the N value and the hydrogen diffusion coefficient through the coatings using the present fatigue testing techniques. A probable explanation is that the hydrogen attenuation was measured on fibre wound under a low tension onto a fibre drum while the N value was obtained from fibre under a high tensile strain.

Electrical resistivity and TEM measurements indicate that the coatings are made up of small graphitic crystallites whose C-axes have an average orientation between  $\pm 16^\circ$  and  $\pm 40^\circ$  to the fibre radius. There is also evidence from the literature, [14,15] to suggest that hydrogen may diffuse through pyrolytic carbon coatings at microvoids and crystallite boundaries. The diffusion coefficient may therefore be affected by the size and orientation of the crystallites. Coating thickness is another factor which will affect the rate of hydrogen diffusion. The diffusion coefficient for hydrogen through the carbon is given by [22]:

$$D_c = \frac{t^2}{6\tau} \quad (1)$$

Where t is the coating thickness and  $\tau$  is the time for hydrogen to start diffusing into the silica, assuming a linear concentration gradient in the carbon coating. The relationship between the hydrogen diffusion through the carbon coating and the electrical resistivity is shown in Fig(8) where the diffusion coefficient calculated for the three fibres, using the lag times from Fig(4), is plotted against the electrical resistivity values given in Table(5). There does seem to be a clear correlation between the diffusion coefficients and the electrical resistivity of fibres B and C.

Fibre A was expected to have a higher resistivity given its greater hydrogen permeation. It is unlikely that its resistivity was incorrectly measured as a number of measurements were made on different lengths of fibre. It may be that the crystallite interfaces are trapping fewer electrons due to contamination by other atoms such as hydrogen, leading to more intrinsic carriers and a lower resistivity. Such contamination might not affect the rate of hydrogen permeation through the coating. Further work is required to determine the reasons for the low resistivity of fibre A. It may be that the different manufacturing processes may give slightly different correlations between the resistivity and the diffusion coefficient.

Fibre D would not be suitable for use in cable systems as its diffusion coefficient varies from  $\approx 0.3 \times 10^{-18} \text{ m}^2/\text{hr}$ , which is similar to fibres A and B, to  $\approx 4 \times 10^{-11} \text{ m}^2/\text{hr}$ , the value for ordinary silica fibres. The reason for the high resistivity and high hydrogen diffusion is not clear at present. The thickness of the coating, as far as it has been measured, is the same as fibre C. The microstructure of fibres C, D1 and D2 was, using TEM techniques, found to be similar. If the coating thickness and the microstructure of the two fibres is similar the difference in the resistivity and the hydrogen coefficient could be due to cracks smaller than the resolution of the SEM, about 100nm, and too far apart to be easily seen using the TEM. It is possible that poor adhesion between the carbon coating and the silica would allow hydrogen to diffuse along the fibre so reducing the number of cracks needed in the carbon.

The hydrogen diffusion measurements on fibre D indicate a need for on-line monitoring of the carbon deposition process. The electrical resistance of any length of carbon coating will be a function of two variables, the thickness and the microstructure, so that it would be difficult to control the process using resistance as the only measured variable in the feedback loop. Data on the coating thickness or the microstructure would have to be obtained on-line by a different technique if electrical resistance is to be used for the on-line quality control of the carbon coatings.

The present strength results indicate that the stress corrosion behaviour cannot be inferred from the hydrogen performance of the fibre without further information on the mechanical stability of the coatings.

## 7. CONCLUSIONS

- Fibres with thinner coatings tend to have higher initial strengths.
- The strength distribution becomes wider as the strain rate is reduced.
- The N value of fibres A and G is  $> 200$  while that of the other fibres is between 35 and 100 depending on the strain rates used in the calculations.

- Significant crack blunting can occur as demonstrated by fibres A, B and H.
- Although the hydrogen permeation rate through the carbon coatings of fibres (A, B and C) made by three different manufactures has been shown to vary significantly they would be suitable for use in current cable systems.
- The hydrogen diffusion coefficient of a fibre (D) assumed to be hermetic has been shown to vary by approximately seven orders of magnitude between the two ends of the fibre.
- Measurements of electrical resistivity of fibre D were used to determine which lengths had a hydrogen diffusion coefficient similar to the other three fibres.
- Electrical resistivity and TEM measurements suggest that the carbon coatings probably consist of graphite crystallites with their basal planes roughly parallel to the surface of the silica.
- A correlation between the electrical resistivity and the hydrogen diffusion coefficient has been demonstrated.
- On-line quality control of the coating deposition process using electrical resistance techniques would necessitate separating the effects of thickness and microstructure.
- Further work is required to determine the limits, to which the resistivity can be used to assess the hydrogen performance, and the most suitable technique to assess the strength and the long term fatigue characteristics of the fibres.

## 8. ACKNOWLEDGEMENTS

The authors would like to thank A Webster for the preparation of the TEM samples.

## 9. REFERENCES

- [1] ELECTRICAL TRANSPORT AND ELECTRONIC PROPERTIES OF AMORPHOUS CARBON FILMS. Th. Frauenheim, U. Stephan, K. Bewilogua, F. Jungnickel, P. Blaudeck, E. Fromm. Thin Solid Films, VOL. 182, pages 63-78, 1989.
- [2] RECENT DEVELOPMENT IN HERMETICALLY COATED OPTICAL FIBRE. K. E. Lu, G. S. Glaesemann, R. V. Vandewoestine, G. Kar, J. of Lightwave Technology, VOL. 6, No. 2, February 1988.
- [3] MECHANICAL RELIABILITY OF HERMETIC CARBON COATED OPTICAL FIBRE. J. T. Krause, C. R. Kurkjian, F. V. Di Marcello, R. G. Huff. paper 2.8, EFOC/LAN (Amsterdam) 1988.

- [4] AMORPHOUS CARBON AS AN EFFECTIVE HERMETIC BARRIER AGAINST  $H_2O$  AND  $H_2$  FOR OPTICAL FIBRES. K. E. Lu, G. S. Glaesemann, M. T. Lee, D. R. Powers. paper 19B3-4 IOOC (Japan) 1989.
- [5] HYDROGEN PERMEATION IN OPTICAL FIBRES WITH HERMETIC CARBON COATINGS P. J. Lemaire, K. S. Kranz, K. L. Walker, R. G. Huff, F. V. Dimarcello. Electronics Letters Vol. 24, No. 21, 13 October 1988.
- [6] CHARACTERISTICS OF CARBON COATED OPTICAL FIBRE. M. Ooe, Y. Ishiguro, K. Kobayashi, K. Nagayama, I. Ogasawara, G. Tanaka, M. Watanabe. paper 19B3-3 IOOC (Japan) 1989.
- [7] PYROLYTIC FILM RESISTORS: CARBON AND BOROCARBON. R. O. Grisdale, A. C. Pfister, W. van Roosbroeck. BSTJ, page 271, April 1951.
- [8] INTERNAL COMMUNICATION. M. Yates. BT Laboratories, 7 October 1990.
- [9] INTERNAL COMMUNICATION. M. Hockly. *ibid*, 8 November 1990.
- [10] INTERNAL COMMUNICATION. M. Yates. *ibid*, 3 December 1990.
- [11] INTERNAL COMMUNICATION. M. Yates. *ibid*, 7 August 1991.
- [12] DEPOSITION, STRUCTURE, AND PROPERTIES OF PYROLYTIC CARBON, J. C. Bokros. Chemistry and Physics of Carbon Vol. 5, Marcell Dekker 1973.
- [13] VARIATION IN THE CRYSTALLINITY OF CARBONS DEPOSITED IN FLUIDIZED BEDS. J. C. Bokros. Carbon Vol. 3, pages 201-211, 1965.
- [14] SEMICONDUCTIVITY AND DIAMAGNETISM OF POLYCRYSTALLINE GRAPHITE AND CONDENSED RING SYSTEMS. S. Mrozowski. Physical Review Vol. 85, No. 4, February 1952.
- [15] HYDROGEN DIFFUSION AND SOLUBILITY IN PYROLYTIC CARBON. R. A. Causey, T. S. Elleman, K. Verghese. Carbon Vol. 17, page 323-328, 1979.
- [16] ELECTRICAL PROPERTIES OF PYROLYTIC GRAPHITE. C. A. Klein. Reviews of Modern Physics Vol. 34, No. 1, January 1962.
- [17] KAYE & LABY, Table of physical and chemical constants
- [18] EXAMINATION OF THE HYDROGEN PERMEATION AND THE ELECTRICAL RESISTIVITY OF FOUR 'HERMETIC' OPTICAL FIBRES. E.S.R. Sikora, J. V. Wright, S. J. Pycok, M. J. Yates. EFOC/LAN (London) 1991
- [19] PYROLYTIC GRAPHITES: THEIR DESCRIPTION AS SEMIMETALLIC MOLECULAR SOLIDS. C. A. Klein. J. of Applied Physics Vol. 33, NO. 11, November 1962.
- [20] DEFECT STRUCTURE AND PROPERTIES OF PYROLYTIC CARBON. L. C. Blackman, G. Saunders, A. R. Ubbelohode, F.R.S. Proc. Roy. Soc. (London), A264, pages 19-40, 1961.
- [21] INTERNAL COMMUNICATION. D. R. Wood. BT Laboratories, 10 May 1990.
- [22] INTERNAL COMMUNICATION. B. Wakefield. *ibid*, 9 May 1990.
- [23] THE MATHEMATICS OF DIFFUSION. J. Crank.



# Stress-induced and stress-free ageing of optical fibres in water

W. Griffioen, W. Ahn, A.T. De Boer, G. Segers

PTT Research, Box 421, 2260 AK Leidschendam, The Netherlands

## Abstract

We observed anomalies ('knees') in the fatigue behaviour of optical fibres in water with double-mandrel experiments. With two-point-bending experiments on fibres, that were stored in water, stress-free ageing is observed. Inert-strength measurements and STM photographs of aged fibres indicate that 'pits' are formed in the silica surface. To understand the mechanism for this the residual stress of the silica surface is measured. A model is presented which partially explains the 'knees' in relation with stress-free ageing.

## Introduction

Recently the rate at which metal-free fibre-optic cables are installed has increased drastically. This is done to save costs and also to fully exploit the benefits of the dielectric optical fibre, such as the insensitiveness for lightning and the absence of hydrogen formation due to corrosion of metal parts. The use of metal-free cables brings with it the risk of the fibres being surrounded by water. Especially in the 'wet' Netherlands situation where the HDPE (High-Density Poly-Ethylene) ducts are full of water this will surely be the case. The notorious 'knees', found in the static-fatigue behaviour of optical fibres placed in water, are a reason to doubt if existing lifetime-estimations of the fibres are realistic.<sup>1</sup> It was not clear whether these 'knees' were due to a change in the ('power-law') stress-induced crack growth at a certain stress-level or due to a time effect, e.g. from the coating, superposed on mentioned crack-growth<sup>1</sup>. To separate these effects, both long-running (double-mandrel) static-fatigue experiments in water and (two-point-bending) dynamic-fatigue experiments after ageing of the fibres in water were done.<sup>2,3</sup> To check if 'pits' are formed during stress-free ageing in water, also inert strengths were measured before and after ageing. STM-photographs are made after this ageing too. In a model stress-free aging, determined from two-point-bending experiments, is used to explain the 'knees', measured with double-mandrel experiments. In this model stress-free 'pit'-formation is not yet incorporated. There is no theory yet

which explains the latter effects. To check if the fibres are really stress-free, the fibres' residual surface-stress is measured. (Residual-) stress-induced crack growth is investigated as a possible cause for the formation of 'pits'.

## Double-Mandrel

Double-mandrel static-fatigue experiments were performed on uv-acrylate-coated fibres in water of 30, 40 and 50°C and a pH-value of roughly 7. In Figure 1 a Weibull-plot of times to fracture from fibres stored in water of 30°C is shown as an example.

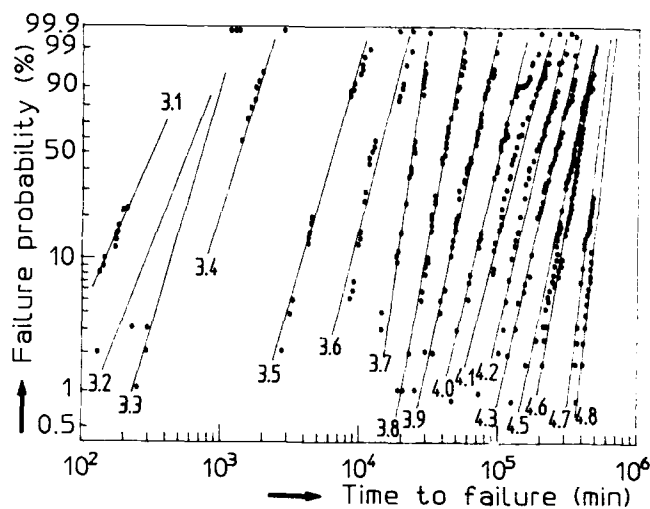


Figure 1: Weibull-plot of double-mandrel times to fracture  $t_f$  of fibres stored in water of 30°C. The numbers indicate the mandrel diameter  $d_m$  in mm

In Figure 2 the median time to fracture  $t_f$  is given as a function of mandrel diameter  $d_m$ . 'Knees', at which the corrosion susceptibility  $n$  drops from a value above 20 down to 6 - 8, can be clearly recognized<sup>1</sup>.

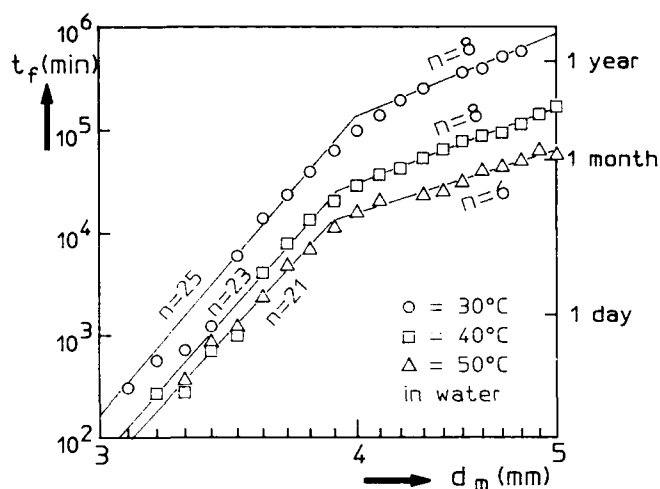


Figure 2: Median double-mandrel time to fracture  $t_f$  as a function of mandrel diameter  $d_m$

## Two-point-bending

Two-point-bending dynamic-fatigue experiments were performed on the same kind of fibres, after stress-free ageing in water. The fibres were stored on loosely wound 20-cm spools, immersed in a tank filled with deionized water with a pH-value of roughly 7. The fibres were tested at ambient conditions, within half an hour after leaving the water. In Figure 3 a Weibull-plot of two-point-bending strains  $\epsilon_d$  is given at different plate-speeds  $v$  (1  $\mu\text{m/s}$  - 1 mm/s) for fibres at ambient conditions and after ageing in water of 50°C. It is clear that not only the fracture strain decreases dramatically after ageing in water, but that also the Weibull-parameter  $m$  drops (from 75 to 25).

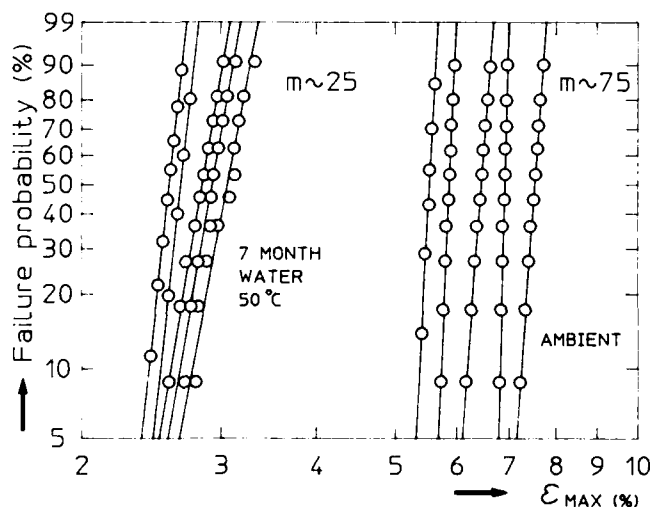


Figure 3: Weibull-plot of two-point-bending strains  $\epsilon_d$  at different plate-speeds for fibres at ambient condition and after 7 months in water of 50°C

In Figure 4 the median strains at fracture  $\epsilon_d$  as a function of plate speed  $v$  are given for fibres that were stored at ambient conditions and subsequently in water of 60°C for 1 up to 7 months. A dramatic decrease in fibre strength is observed while the magnitude of  $n$  (slope in Figure 4) remains almost constant.

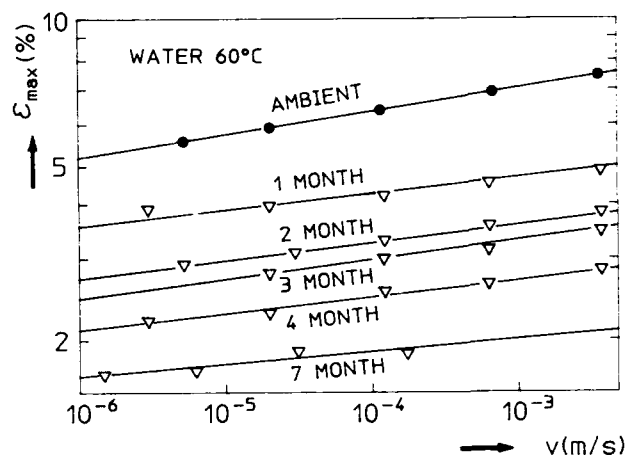


Figure 4: Median strain at fracture  $\epsilon_d$  in two-point bending experiments as a function of plate speed  $v$

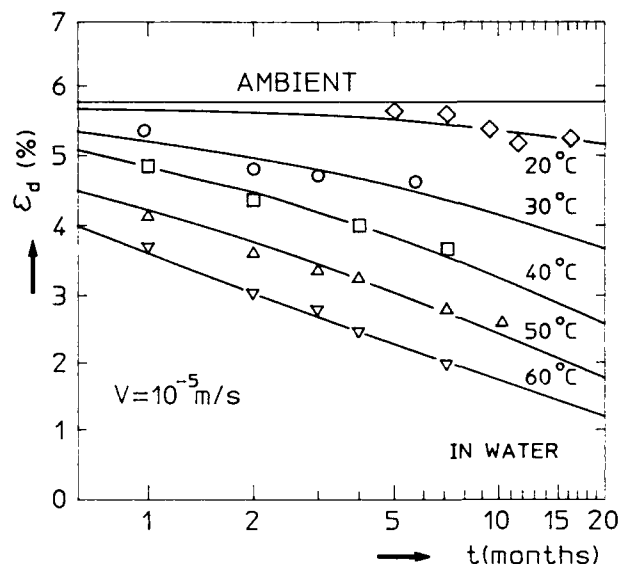


Figure 5: Median strain at fracture  $\epsilon_d$  in two-point bending experiments ( $v$  is  $10^{-5}$  m/s) as a function of storage time  $t$  in water

In Figure 5 the median strains  $\epsilon_d$  at fracture at a plate speed of  $10^{-5}$  m/s are given as a function of the storage time  $t$  in water of 20 up to 60°C. The curves show a continuous decrease of fracture strains with time. The strength as a function of time is fitted by an 'S-curve' on a logarithmic scale (it is however not clear whether the strengths relax to zero or to a residual level):

$$\epsilon_d = \frac{\epsilon_d(0)}{1 + (t/t_0)^\eta} \equiv f(t) \cdot \epsilon_d(0) \quad (1)$$

Here  $\epsilon_d(0)$  is the strain at fracture before ageing in water and  $t_0$  and  $\eta$  are fitting parameters. In Figure 5 fits are drawn with a  $\eta$ -value of 0.6 and  $t_0$ -values of 1000, 50, 15, 5.5 and 2.3 months for 20, 30, 40, 50 and 60°C respectively.

To check if 'pits' are formed during stress-free ageing in water, also inert strengths were measured before and after ageing. This was performed with two-point bending on fibres in vacuum for 1 week.<sup>3</sup> The results are shown in Figure 6. The accuracy of these measurements decreases with strength since also the  $m$ -values decrease (down to 20 at 60°C) and the number of detected fractures decreases (down to 3 per set of plates at 60°C). A decrease in 'vacuum-strengths', which are really the inert values since the strengths are independent of fracturing speed, is clearly present. Hence it is concluded that 'pits' are formed. This is also supported by the fact that the  $m$ -values decreased (also seen in measurements at ambient condition: Figure 3), which is only possible when the initial flaw distribution has been changed.

From Figure 5 and 6, using formulas for two-point-bending strengths and a  $n$ -value of 20,  $B$ -values (scale-factor for speed of crack growth) of  $10^{-6}$ ,  $10^{-5}$  and  $10^{-4}$  GPa<sup>2</sup>s are obtained for aged fibres in 40, 50 and 60°C respectively.<sup>3</sup> These  $B$ -values should, according to stress-induced crack-growth theory, be the same as the value of  $10^{-8}$  GPa<sup>2</sup>s for unaged fibres.<sup>3</sup> The increase of the  $B$ -value might be caused by a change of 'chemical environment' (not probable because this would result in a decrease in the speed of crack growth). It might also indicate that the ('power-law') stress-induced crack-growth theory cannot be used from the start, especially not for unaged, pristine fibres.

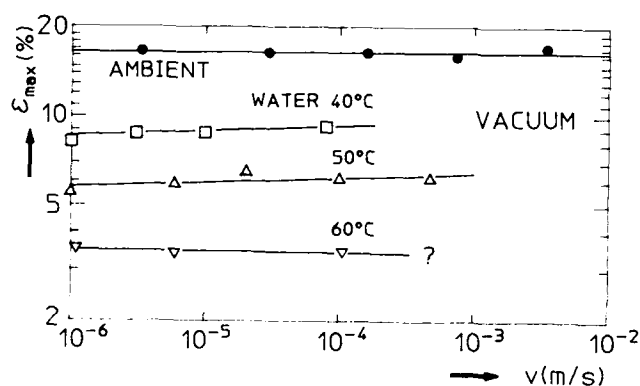


Figure 6: Inert strengths of fibres, measured with two-point bending in vacuum, from ambient condition and after ageing in water of 40, 50 and 60°C during 7 months

## STM-photographs

Another proof for 'pit-formation' during stress-free ageing of the fibres is found with the help of Scanning Tunneling Microscopy (STM). 'Nanoscopic' photographs are made from the silica surface of the fibres with a commercial available STM-nanoscoop.<sup>9</sup> In Figure 7 a), b) and c) the surfaces are shown of an unaged fibre and of the same fibre, aged in wa-

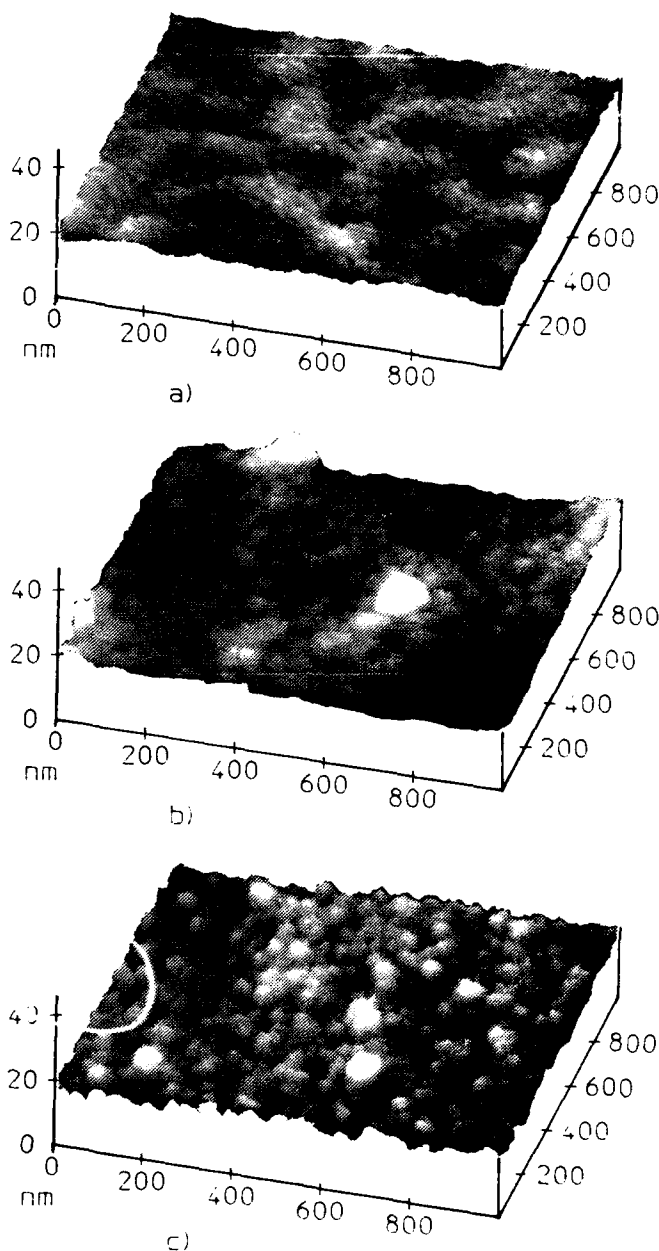


Figure 7: STM-photograph of the fibre's surface, a) unaged and after ageing in water of b) 40 and c) 60°C during 7 months

ter of 40 and 60°C during 7 months, respectively. It is clear that the surface roughness has increased due to the stress-free ageing. This behaviour is also found by Robinson and Yuce.<sup>6</sup> The large particles in Figure 7 b) are probably due to the gold plating or due to dust particles. From linear scans over 1 µm, maximum flaw-sizes on a nanoscopic scale are estimated. Large-scale undulations are not considered since they do not contribute significantly to stress concentrations. In this way effective crack depths of 2, 3 and 6 nm are found for the surfaces of figure 7 a), b) and c) respectively. This correspond to a maximum fibre strain of 20, 16 and 11% respectively.<sup>3</sup> These values show the same decrease as for the measurements of the inert strengths. The measured inert strengths are however lower since the effective test length with two-point bending is larger than 1 µm.<sup>4</sup> Moreover in the experiments a two-dimensional surface is stressed while the crack depths are obtained from a one-dimensional scan.

### Surface strain

In order to check if the fibres were really stress-free during the ageing in water the stress profiles of the fibres are measured. This is done because after pulling the fibre from the preform a thermally- (difference in expansion coefficient) or mechanically- (difference in viscosity; effect depends on pulling force) induced stress may be expected at the surface of the fibre. The stress profiles of the fibres are measured with an equipment which uses the photoelastic effect.<sup>5</sup> In Figure 8 the measured axial and radial stresses  $\sigma(r)$  of the tested, unaged, fibre are shown as a function of the distance  $r$  to the core (ageing of the fibres did not affect the stress profile). It is clear that at the surface of the fibre a residual axial tensile-stress of roughly 22 MPa is present (extrapolated since the measuring accuracy drops close to the sur-

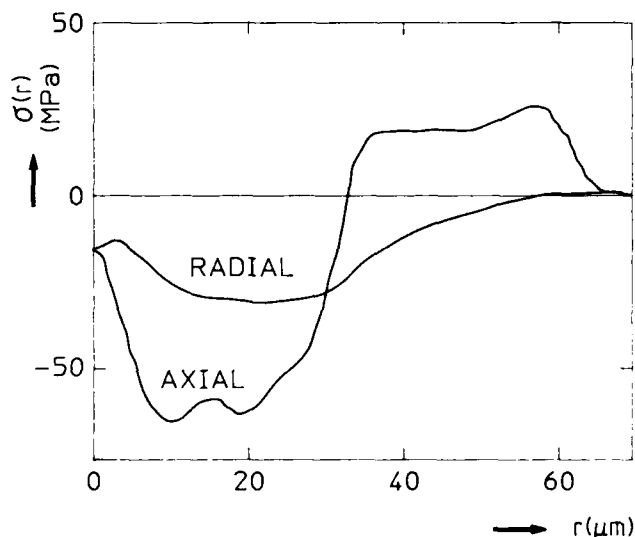


Figure 8: Residual axial and radial stress  $\sigma(r)$  of the tested, unaged, fibre as a function of the distance  $r$  to the core

face). This stress is even lower than the surface tensile-stress of 45 MPa, due to the loosely winding of the fibres on the spools. The total tensile stress at the surface of 67 MPa is much lower than the stress of roughly 5 GPa at which the fibres are fractured.

## Discussion

### Time-dependent $B$ -value

From crack-growth theory it can be derived that, for an applied stress  $\sigma$  sufficiently below the inert strength  $\sigma_i$ , the time to fracture  $t_f$  is given by:<sup>3</sup>

$$\sigma_i^{n-2} = \int_0^{t_f} \frac{\sigma^n}{B} dt \quad (2)$$

Here  $B$  is a factor, inversely proportional to the speed of crack growth. A cause for the strength decrease after ageing in water might be a stress-independent time effect, e.g. loosening of the 'chemically near' primary coating (after aging in water the primary coating spontaneously slides down just by handling the fibres)<sup>1</sup>. Changes in the chemical environment of the fibres and even the filling of the cracks with water can also be responsible for a stress-independent time effect.

In an attempt to relate the 'knees' from the mandrel experiments with stress-free ageing, a model is introduced in which  $n$  has a fixed value and  $B$  is a function of time. Using equation 1 and the relation between fracture strain  $\epsilon_d$  and plate speed  $v$  for two-point bending, the time dependence of  $B$  follows from the time behaviour of  $\epsilon_d$ :<sup>3</sup>

$$B(t) = \frac{C d_f E_0^n \epsilon_d(0)^{n-1}}{v(n-1) \sigma_i^{n-2}} \left[ f(t) \left\{ 1 + \frac{1}{2} \alpha \epsilon_d(0) \cdot f(t) \right\} \right]^{n-1} \quad (3)$$

Here  $C$  is a constant (1.198),  $d_f$  the diameter of the uncoated fibre,  $E_0$  the Young's modulus and  $\alpha$  a constant for nonlinearity in elastic behaviour of the silica glass. The (maximum) static stress  $\sigma$  in a fibre wound around a mandrel is:<sup>3</sup>

$$\sigma = E_0 \left[ 1 + \frac{1}{2} \alpha \frac{d_f}{d_m} \right] \frac{d_f}{d_m} \quad (4)$$

Solving equation 2 numerically, using equations 1, 3 and 4, the time to fracture  $t_f$  is found as a function of mandrel diameter  $d_m$ , stress-free ageing incorporated. Next  $t_f$  is corrected for differences between test lengths for double mandrel (1 mm) and two-point bending (20 µm), using Weibull statistics with a Weibull parameter of 100.<sup>2,4</sup> Figure 9 is constructed using the results obtained by the two-point-bending measurements after aging in water and the fits of Figure 5. 'Knees', like those in Figure 2, are clearly present. Differences with Figure 2 can partially be explained by the fact that the two-point bending measurements were performed on fibres being in ambient condition for half an hour.

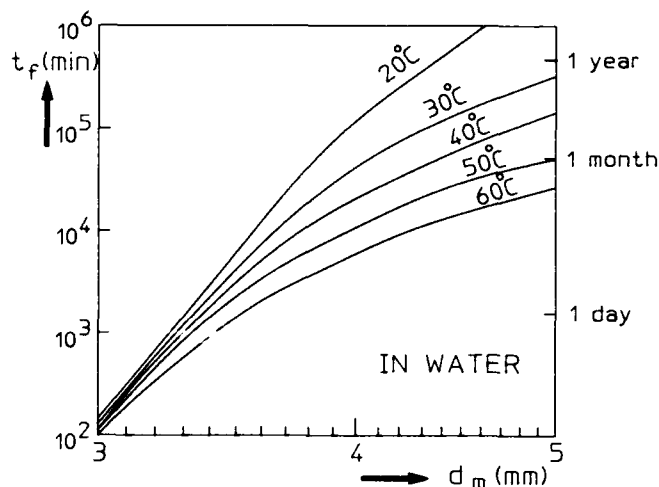


Figure 9: Calculated median time to fracture  $t_f$  as a function of mandrel diameter  $d_m$  derived from two-point bending experiments after storage of the fibres in water

The presented model only takes into account that the crack growth of an aged fibre is higher due to a change in 'chemical environment'. 'Pit' formation in stress-free condition is however also present, as is clear from the measurements. The mechanism of this phenomenon is however not clear. It is also not clear how this behaviour can be fitted and translated into 'knees'. France et al. developed a model by assuming that, over the first half of the lifetime, strength degradation is caused by zero-stress ageing ('pit-formation') and, over the last half, by fatigue.<sup>7</sup> It is believed that in the double-mandrel experiments a combination of both stress-free 'pit' formation and increase in speed of crack growth is present.

#### 'Pit-formation'

From inert-strength measurements and STM-photography it is concluded that cracks have grown or 'pits' are formed. The question is what is the mechanism for this is. For a fibre surface under a static tension  $\sigma_a$  the cracks should, when stress-induced corrosion is the mechanism, grow according to crack-growth theory:<sup>1</sup>

$$\frac{\sigma_{ia}}{\sigma_i} = \left[ 1 - \frac{\sigma_a^n t_a}{B \sigma_i^{n-2}} \right]^{\frac{1}{n-2}} \quad (5)$$

In this equation  $t_a$  is the ageing-time and  $\sigma_{ia}$  is the inert strength after ageing. Since the  $n$ -values are usually high ( $\geq 6$ ) the inert strength  $\sigma_{ia}$  remains almost constant during a certain time, and then drops suddenly when  $\sigma_a^n t_a$  approaches  $B \sigma_i^{n-2}$ . For instance, when the inert strength after 7 months ageing has dropped with a factor of 2, the fibres will fracture after additional ageing, shorter by a factor of  $2^{n-2}$  (equation 5), which takes about 2 weeks and 1 minute for an  $n$ -value of 6 and 20 respectively. This behaviour is not shown by the experiments. Moreover comparable crack growth would

result in a fracture time of less than 1 second for e.g. the 40°C, 5-mm mandrel- experiment (applied stress of 1.8 GPa, much higher than the 67 MPa 'stress-free' condition) when results of figure 6 are used. This comparison is based on an equal product  $\sigma^n t$ , which is a measure for ageing.<sup>3</sup> The double-mandrel results, given in Figure 2, show much larger fracturing times. Hence it is concluded that 'pit-formation' is not caused by ('power-law') stress-induced crack growth.

Differential stress-free etching of the silica surface by the warm water is a possible mechanism for the formation of 'pits'. This may be affected by inhomogeneities in and/or loosening of the primary coating. It is not yet clear what the magnitude of this effect is, and how it depends on environmental conditions. Another possibility is crack nucleation on a pristine silica surface.<sup>8</sup> This is energetic favourable, only when a stress is present on the surface (is the 'stress-free' 67 MPa sufficient for this?) and when material is removed by a corrosive agent (water). The final surface distortions are expected to be smaller than 1 nm and afterwards the mechanism will switch to stress-induced crack growth. At this moment it is in study if our measurements are in agreement with this theory.

## Conclusions

We observed anomalies ('knees') in the fatigue behaviour of optical fibres in water with double-mandrel experiments. With two-point-bending experiments on fibres, which were stored in water, stress-free ageing is observed. Inert-strength measurements and STM photographs prove that in the latter case 'pits' are formed. These 'pits' are shown not to be caused by ('power-law') stress-induced crack growth resulting from a small residual stress on the silica surface. The true mechanism is still unclear. In an attempt to relate the 'knees' with stress-free ageing a model is presented in which a stress-independent time effect, e.g. a primary coating effect, influences the scale factor for the speed of stress-induced crack growth. The model explains the 'knees' but does not yet incorporate stress-free 'pit' formation.

## References

1. C.R. Kurkjian, J.T. Krause, M.J. Matthewson, *Strength and fatigue of silica optical fibers*, J. Lightwave Technol., 7 (1989) 1360.
2. P.C.P. Bouten, H.H.M. Wagemans, *Double mandrel: a modified technique for studying static fatigue on optical fibres*, Electron. Lett., 20 (1984) 280.
3. W. Griffioen, G. Segers, E. Van Loenen, *Two-point bending apparatus, fracturing optical fibres at different speeds in one run; measurements in standard and vacuum environment*, Proc. 39th Int. Wire and Cable Symp. (1990) 368.

4. M.J. Matthewson, C.R. Kurkjian, S.T. Gulati, *Strength measurements of optical fibres by bending*, J. Am. Ceram. Soc., 69 (1986) 815.
5. P.K. Bachmann, W. Hermann, D.U. Wiechert, *Stress in optical waveguides. 2: Fibers*, Applied Optics, vol. 26, no. 7 (1987) 1175.
6. R.S. Robinson, H.H. Yuce, *Scanning tunneling microscopy of optical fiber corrosion: Surface roughness contribution to zero-stress aging*, J. Am. Ceram. Soc., 74 [4] (1991) 814.
7. P.W. France, W.J. Duncan, D.J. Smith, K.J. Beales, *Strength and fatigue of multicomponent optical glass fibres*, J. Mater. Sci., 18 (1983) 785.
8. P.C.P. Bouten, *Lifetime of pristine optical fibres*, Thesis, Eindhoven, The Netherlands, 1987.
9. Nanoscope II, Digital Instruments, Inc., 6780 Cortona Drive, Santa Barbara, CA 93117, USA.

## Biographies



Willem Griffioen was born in Oegstgeest, The Netherlands, on October 8, 1955. He received the M.S. degree in physics and mathematics from Leiden University, Leiden, The Netherlands, in 1980. He worked at Leiden University from 1980 to 1984, where he investigated macroscopic quantum properties of liquid and solid  $^3\text{He}$ .

$^4\text{He}$ -mixtures at ultra-low temperatures and in high magnetic fields. In 1984 he joined PTT Research, Box 421, 2260 AK Leidschendam, The Netherlands. His work includes research and development of fibre-optic cables, installation techniques and reliability of optical fibres. At this moment he works at Ericsson Cables AB, Box 457, 824 01 Hudiksvall, Sweden in the scope of a half-year-exchange project.

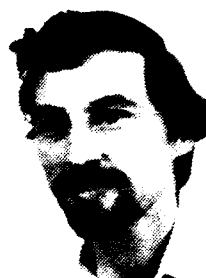


Willy Ahn was born in Bodjonegoro, East Java, Indonesia, on October 4, 1937. He followed a study in physics at the Delft Polytechnic High school, Delft, The Netherlands. He worked at the little reactor of Delft Polytechnic High school from 1963 to 1967, where he worked on a molecule model of cyclohexane with

cold neutrons. In 1967 he joined PTT Research, Box 421, 2260 AK Leidschendam, The Netherlands. He started working with thin-film methods for high frequencies. Recently he worked on optical- and mechanical-characterization of optical fibres.



André de Boer was born in Utrecht, The Netherlands, on July 19, 1964. He studied astronomy at Utrecht University, The Netherlands. After 6 years he switched his study to physics with specialisms biophysics and environmental science. This study is nearly completed with a M.S. degree. From 1990 he simultaneously joined PTT Research, Box 421, 2260 AK Leidschendam, The Netherlands, where he is involved in mechanical reliability of optical fibres and cables.



Gerrit Segers was born in Lisse, The Netherlands, on August 9, 1954. He completed his study with a B.S. degree in electronic engineering in 1975. After his military services he joined a company where he worked at the service department of nautical apparatus. From 1980 to 1986 he worked at the Christiaan Huygens Laboratory at Noordwijk, The Netherlands, where he was involved in the engineering of electronics of radar-systems. In 1987 he joined PTT Research, Box 421, 2260 AK Leidschendam, The Netherlands, where he is involved in engineering in both analog and digital electronics.

# FATIGUE BEHAVIOR OF COATED OPTICAL FIBERS IN WATER

SHUJI OKAGAWA and KEIGO MAEDA

THE FURUKAWA ELECTRIC CO., LTD.

## Abstract

The dynamic fatigue properties of optical fibers with different water absorption and acidity in a primary coating, and also carbon coated fiber were measured in 40-80 °C water. By analysing experimental results with the exponential law model, fatigue behavior of coated fibers was quantitatively evaluated in terms of the frequency factor and the activation energy for crack growth reaction, instead of  $n$  value on the power law. And static fatigue,  $n$  value, and lifetime of coated fibers in water have been estimated by this model.

## I. Introduction

In water fatigue rate of coated optical fibers is accelerated, and to prevent water from reaching the glass surface, optical fiber cable has been usually filled with jelly compounds or water blocking materials. In this cable design the fatigue parameter, " $n$  value" based on the power law, plays a central role on the mechanical reliability assurance. However, with increasing the demands to use optical fibers in wider areas, e.g., undersea, aerial, subscriber system, etc., there has been the possibility that optical fibers are subjected to aqueous environment. In such a case, mechanical lifetime can not be predicted by the power law because in a high stress/short time region of the static fatigue data, fatigue parameter  $n$  is an order of 20 as same as the value in the normal non-aqueous condition, while in a lower stress/longer time region the value is known to fall down to less than 10[1]. Some authors have called this strange phenomenon "fatigue knee"[2]. And from the standpoint of optical fiber industry, it is necessary to develop a model, which interprets these whole phenomena and enable the lifetime prediction in an actual low stress/long time region by extrapolation of the experimental results in a high stress/short time region.

With the exponential law model we have already

reported the preliminary results, in which "fatigue knee" was expressed as a curved form rather than an intersection of two lines[3]. In this paper we will discuss the fatigue behavior in water for different optical fibers, which have different water absorption and acidity in a primary coating and have a thin carbon coating on silica fiber.

## II. Question on the power law model

Crack growth velocity  $v$  is expressed by the empirical power law as shown in Equation (1), and this simple law has been widely applied to optical fiber strength assurance.

$$v = A_1 K_1^n \quad (1)$$

$$K_1 = \sigma Y \sqrt{c} \quad (2)$$

where  $K_1$  is the stress intensity factor,  $n$  is the fatigue parameter,  $\sigma$  is the applied stress,  $Y$  is a geometric constant ( $\approx \sqrt{\pi}$  [4]),  $c$  is the crack size, and  $A_1$  is constant.

In Eq.(2), the fracture occurs when  $K_1$ , which contains two parameters  $\sigma$  and  $c$ , reaches the critical stress intensity factor  $K_{1c}$  ( $=8.1 \times 10^{-3}$  GPa  $\sqrt{m}$ [2]) and fracture strength is definitely determined by crack size. Eqs. (1) and (2) imply that no crack growth occurs in the case of  $\sigma = 0$ . However, in water strength is degraded by zero-stress aging. This means that application of Eq. (1) to fatigue behavior in water is not adequate.

## III. Application of the exponential law model

Based on the chemical reaction kinetics, there has been several attempts to express the crack growth velocity as an exponential form given by Eq.(3)[1],[5].

$$\nu = A \exp \left( -\frac{E}{RT} + \frac{n'}{RT} \frac{K_1}{K_{10}} \right) \quad (3)$$

where  $E$  is the activation energy,  $R$  is the gas constant,  $T$  is the absolute temperature, and  $A$  and  $n'$  are constants.

In this model, Eq.(3) leads to crack growth even if  $\sigma = 0$  and contains more physical meanings compared to the power law.

#### IV. Experimental Procedure

The optical fibers with a diameter of 125  $\mu\text{m}$  were usually coated with a soft UV curable urethane acrylate as a primary layer and with a hard UV curable urethane acrylate as a secondary layer to 250  $\mu\text{m}$ . Furthermore, in order to clarify the coating effect on the fatigue behavior, we used the optical fibers coated with different UV curable primary coatings controlled to change their water absorption and acidity, and also the optical fiber with a thin layer of amorphous carbon between fiber surface and primary layer. This carbon coating was about 500Å in thickness. These properties of fiber coatings are summarized in Table I.

Table I  
Coating structures of tested fibers

No.	Carbon layer	Primary layer		
		Material	Water (%) absorption	pH
1	none	a	1.3	5.0
2	~ 500Å	a	1.3	5.0
3	none	b	0.9	5.3
4	none	c	1.8	4.4

Secondary layer was the same for all fibers.

No.3 fiber mainly consists of polycarbonate urethane acrylate prepolymer to reduce its water absorption, and No.4 fiber contains oligoester acrylate as a monomer to make an atmosphere around the glass more acid. Water absorption was determined according to JIS K7209 using the method B. And acidity was measured with a distilled water of 10 ml containing a cured primary coating resin of 0.2 g. On the evaluation of fatigue behaviour the dynamic fatigue tests were conducted in 40, 60, and 80 °C water by tensile testing at strain rates rang-

ing from  $6 \times 10^{-2}$  GPa/sec to  $2 \times 10^{-1}$  GPa/sec. A minimum of ten specimens with a gage length of 30 cm in water were tested at each strain rate.

#### V. Experimental Results

The dynamic fatigue behavior on this exponential model is given by Eq.(4)[4]. Parameters  $\alpha$ ,  $\beta$ , and  $\gamma$  are determined by a trivariate regression of Eq.(4):

$$\ln(\sigma d / \dot{\sigma}) = \alpha + \beta / T - \gamma \sigma d / T \quad (4)$$

$$\alpha = \ln(2 K_{10} / S i \cdot Y \cdot A) \quad (5)$$

$$\beta = E / R \quad (6)$$

$$\gamma = n' / R S i \quad (7)$$

where  $\sigma d$  is the fracture strength,  $\dot{\sigma}$  is the stressing rate, and  $S i$  is the inert strength. Figures 1 to 4 show dynamic fatigue properties in terms of this model for No.1 coated fiber to No.4, respectively. The solid lines in these figures represent the regression lines corresponding to Eq.(4). Three parameters ( $\alpha$ ,  $\beta$ , and  $\gamma$ ) obtained by regression analysis are listed in Table II. From the figures these calculation results well coincide with experimental data, except for No.2 carbon coated fiber in Fig.2, where the regression lines declined a little compared to the experimental data. This means that behavior of carbon coated fiber would not be thoroughly expressed by a model based on the crack growth reaction in spite of the exponential or the power law and it will be necessary to develop another model for carbon coated fiber in further study. With this in mind, the exponential law model is also applied to carbon coated fiber in this paper because the model is expected to provide a more accurate and safer practical lifetime prediction for carbon coated fiber than the power law model and fits, of course, the data of standard non-carbon coated fibers well.

As for the coating effect on dynamic fatigue in water, it should be noted that carbon coated fiber (No.2 specimen) showed little strength reduction even at 80 °C and maintained more than 5 GPa in strength. On the other hand, Three non-carbon coated fibers (No.1, 3 and 4 specimens) exhibited about 20% strength reduction at 80 °C compared with those in the normal condition. Further details of the coating effects are discussed in the next section with three parameters in Table II.



Table II  
Fatigue parameters obtained by the regression analysis of the exponential law model

No.	$\alpha$ (ln sec)	$\beta$ (K)	$\gamma$ (K/GPa)
1	-17.4	$1.47 \times 10^4$	$1.72 \times 10^3$
2	-6.3	$2.80 \times 10^4$	$4.68 \times 10^3$
3	-12.7	$1.23 \times 10^4$	$1.62 \times 10^3$
4	-12.4	$1.25 \times 10^4$	$1.61 \times 10^3$

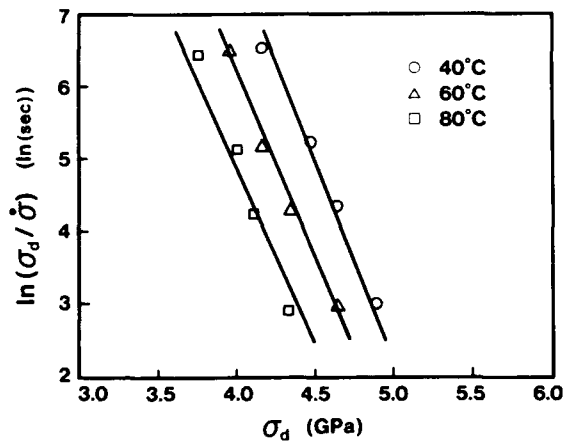


Figure 1. Dynamic fatigue of No. 1 fiber in water.

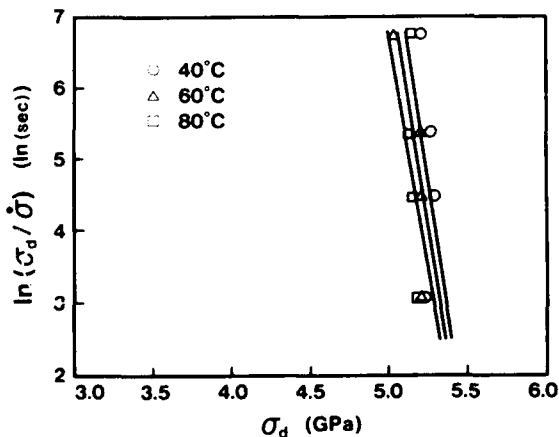


Figure 2. Dynamic fatigue of No. 2 fiber in water.

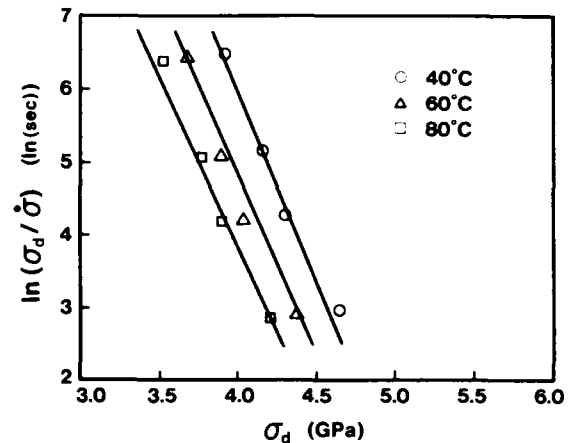


Figure 3. Dynamic fatigue of No. 3 fiber in water.

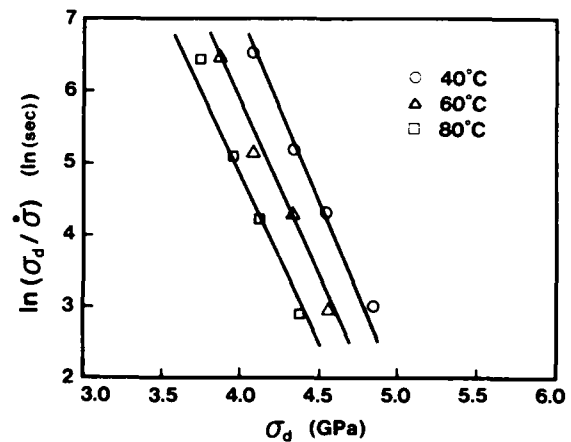


Figure 4. Dynamic fatigue of No. 4 fiber in water.

## VI. Discussion

### (1) Physical and chemical meanings of parameters $\alpha$ , $\beta$ , and $\gamma$

Three parameters are represented by physical and chemical parameters as shown in Eqs.(5) to (7). That is,  $\alpha$  contains  $S_i$  and  $A$  which relates to the frequency factor.  $\beta$  refers to  $E$ , and  $\gamma$  is expressed by the ratio of  $n'$ , which relates to the activation volume  $V_i$  to  $S_i$ .

$n'$  and  $E$  for different glass compositions are described in ref.[4], where  $n'$  shows almost the same value as  $E$ , such a way that  $n' / E = 0.73 \sim 1.23$ . So assuming  $n' = E$  in this paper,

Eq.(8) easily means the inert strength.

$$S_i = \beta / \gamma \quad (8)$$

$S_i$  in Eq.(8) corresponds to  $\sigma_d$  in Eq.(4) at  $T \rightarrow 0$ . Usually it is difficult to obtain the inert strength because tensile test at a very high stress rate must be conducted under a liquid nitrogen atmosphere. Assumption of  $n' = E$  still leads to  $E = S_i V$  since  $n' = S_i V$  [6].

Parameters  $A$ ,  $E$ , and  $S_i$  determined by this method are summarized in Table III, where  $K_{IC}$  is assumed to be  $8.1 \times 10^{-2} \text{ GPa}\sqrt{\text{m}}$  for all four fibers including No.2 carbon coated fiber in calculating the constant  $A$ .

Table III

Fatigue constants of the crack growth reaction estimated by the exponential law model

No.	$A$ (m/sec)	$E$ (kJ/mol)	$S_i$ (GPa)
1	$1.93 \times 10^{-6}$	$1.23 \times 10^2$	8.56
2	$6.35 \times 10^{-6}$	$2.33 \times 10^2$	5.99
3	$2.40 \times 10^{-6}$	$1.03 \times 10^2$	7.60
4	$1.73 \times 10^{-6}$	$1.04 \times 10^2$	7.79

The inert strength of three non-carbon coated fibers (No.1, 3, and 4) has reached around 8 GPa, while that of carbon coated fiber (No.2 sample) was about 6 GPa. This means that inert strength of No.2 fiber seems to be mainly determined by a thin carbon layer on glass surface. Actually strength of carbon coated fiber has been improved by optimizing the qualities of a carbon layer such as surface roughness and thickness, and has been the same as that of usual silica optical fibers [7].

The constant  $A$  is proportional to frequency factor, which is a measure of the effective collision between water molecules and a crack to lead to the crack growth reaction. And smaller constant  $A$  means higher fatigue resistance. With respect to this constant  $A$ , that of carbon coated fiber is far smaller than those of the others. It is reasonable to assume that a carbon layer prevents water reaching fiber surface and there is no appreciable interaction between carbon layer itself and water. Next, concerning the protection by UV resin coatings against water, No.3 fiber with a lower water absorption and No.4 fiber with a more acid primary coating show smaller values of

constant  $A$  and assume to have reduced water attacking, compared with No.1 fiber. But dynamic fatigue results of these three fibers were almost in the same manner as shown in Figs.1, 3, and 4.

This seems to attribute differences in the activation energy  $E$ , which means a barrier against the crack growth reaction, and higher  $E$  implies higher fatigue resistance. The activation energy of No.1 fiber is about 20 kJ/mol larger than that of No.3 or No.4 fiber, and their smaller constants  $A$  appear to be compensated by this larger  $E$ . After all, the effects of water absorption and acidity in a primary layer on the activation energy was not remarkable in the range of this experiments. On the other hand, carbon coated fiber (No.2 specimen) exhibits twice or more larger  $E$  compared with the others. It is clear that the carbon layer hardly reacts with water and has fatigue resistance superior to normal non-carbon coated optical fibers.

Assuming  $n' = E$  in this paper, the activation energy has more distinguish effect on fatigue behavior of coated fibers than constant  $A$ , because it affects both the slope ( $\gamma / T$ ) and the intercept ( $\beta / T$ ) of the dynamic fatigue plot derived from Eq.(1).

## (2) Predicted static fatigue behavior of coated optical fibers

Now we apply this model to static fatigue behavior. That is, by using these  $\alpha$ ,  $\beta$ , and  $\gamma$  the time-to-failure  $t_s$  is given by Eq.(9):

$$t_s = \frac{T}{\sigma s^\gamma \gamma} \left( \frac{T}{\gamma} + \sigma s \right) \times \exp \left( \alpha + \beta / T - \gamma \sigma s / T \right) \quad (9)$$

where  $\sigma s$  is the applied stress. The time-to-failure of tested fibers at any temperature and any applied stress can be predicted by Eq.(9), using  $\alpha$ ,  $\beta$ , and  $\gamma$  in Table II. Figs.5 and 6 illustrate the calculation results of the static fatigue in 40, 60, and 80 °C water for No.1 fiber as a representative of three non-carbon coated fibers and No.2 carbon coated fiber, respectively. In both cases, with decreasing applied stress  $\sigma s$ , the slope ( $n$  value) of  $\log t_s$  vs.  $\log \sigma s$  plot also decreases. On this model the "fatigue knee" is expressed as a curved form rather than an intersection of two lines on the power law model. Comparing the time-to-failure scale in Fig.5 with that in Fig.6, it should be noted that mechanical reliability of optical fibers has been improved dramatically by introducing a carbon layer on glass surface.

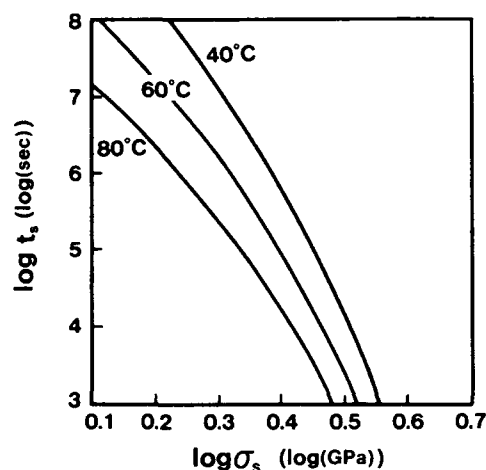


Figure 5. Predicted static fatigue of No. 1 fiber in water.

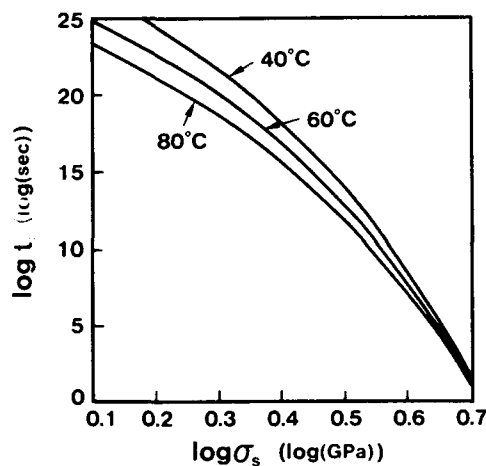


Figure 6. Predicted static fatigue of No. 2 fiber in water.

(3) Fatigue parameter "n" expressed by exponential law model

By differentiating natural log of Eq.(9) with respect to  $\ln \sigma_s$ , the fatigue parameter  $n$  is given by Eq.(10):

$$n = - \frac{\partial \ln t_s}{\partial \ln \sigma_s} = \gamma \sigma_s / T - (T / \gamma \sigma_s + 1)^{-1} + 2 \quad (10)$$

The dependence of  $n$  on applied stress is demonstrated in Figs.7 and 8 for No.1 standard

non-carbon coated fiber and No.2 carbon coated fiber, respectively.  $n$  value decreases linearly with decreasing  $\sigma_s$ . As can be seen from Eq.(10), the dependence of  $n$  on  $\gamma$  is also in a similar manner as that on  $\sigma_s$  and carbon coated fiber with larger  $\gamma$  leads to larger  $n$  value as shown in Fig.8. In addition, with increasing temperature,  $n$  value decreases slightly. As a result,  $n$  value seems to be not a physical constant from which fatigue behavior in water can be totally interpreted and the lifetime prediction based on  $n$  value is not appropriate.

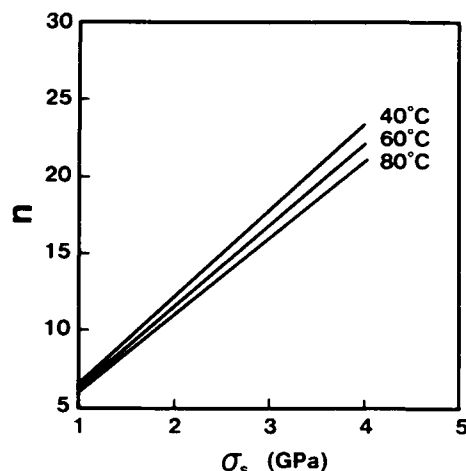


Figure 7. The dependence of  $n$  on applied stress for No. 1 fiber in water.

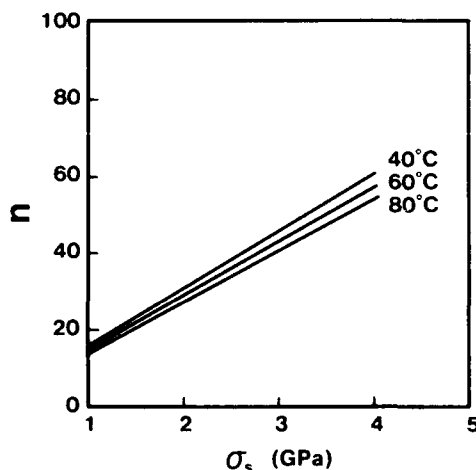


Figure 8. The dependence of  $n$  on applied stress for No. 2 fiber in water.

#### (4) Lifetime prediction by exponential law model

When a proof test with a test stress of  $\sigma_p$  is made on optical fibers, flaws corresponding to less inert strength than  $\sigma_p$  are eliminated. And the minimum time-to-failure  $t_{min}$  has been defined as the time that the survival largest flaws having an inert strength of  $\sigma_p$  lead to a failure due to static fatigue[8]. Applying this principle to exponential model,  $t_{min}$  is given in Eq.(11), by substituting  $\sigma_p$  into  $S_i$  in Eq.(9) and assuming  $n' = E$ .

$$t_{min} = \frac{2K_{sc}^2}{\sigma_p^2 Y^2 A} \frac{RT}{E} \left( \frac{\sigma_s}{\sigma_p} + \frac{RT}{E} \right) \times \exp \left[ \frac{E}{RT} \left( 1 - \frac{\sigma_s}{\sigma_p} \right) \right] \quad (11)$$

Fig.9 represents a lifetime diagram in the constant  $A$  vs. the activation energy  $E$  plots, which satisfy a minimum time-to-failure of 20 years in 25°C water after a proof test with a strain of 1 percent. From Fig.9, in order to meet the requirement standard fibers must be used under a condition in which the ratio of allowable service stress to proof stress is less than 30 percent. On the other hand, carbon coated fiber is allowed to use up to 70 percent in the ratio and expected to apply wide areas where high long-term reliability is needed.

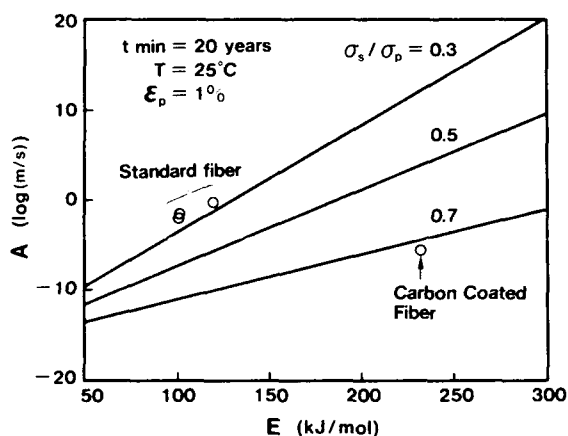


Figure 9. A lifetime diagram for coated fibers in water based on the minimum time-to-failure.

#### VII. Conclusions

Based on the chemical reaction kinetics, in which crack growth velocity is expressed in an exponential form, fatigue behavior of coated optical fibers in water has been studied and the key points to be clarified are summarized as follows:

- (1) The dynamic fatigue test results of the standard coated fibers in water were well expressed by the exponential law model. With respect of coating effects on the fatigue behavior, carbon coated fiber exhibiting a higher fatigue resistance provided a lower frequency factor and a higher activation energy. But in order to fully understand the behavior of carbon coated fiber, it will be necessary to develop another model that would not be based on the crack growth reaction.
- (2) In static fatigue predicted by this model with dynamic fatigue test results, the slope ( $n$  value) of  $\log t_s$  vs.  $\log \sigma_s$  plot decreased with decreasing the applied stress. The "fatigue knee" was expressed as a curved form rather than an intersection of two lines on the power law.
- (3) By this model, the fatigue parameter " $n$ " was given as a function of applied stress, temperature, and only parameter  $\gamma$ .  $n$  value decreased linearly with decreasing applied stress and  $\gamma$ . Further, with increasing temperature,  $n$  value decreased slightly. This suggests that fatigue parameter " $n$ " would not be a physical constant from which fatigue behavior in water can be totally interpreted and the lifetime prediction based on  $n$  value leads to an over-estimation.
- (4) In lifetime prediction by applying the minimum time-to-failure principle to this model, it is assumed that in water standard fibers must be used under a condition where the ratio of allowable service stress to proof stress is less than 30 percent, while carbon coated fiber is allowed to use up to 70 percent in the ratio.

# References

- [1] J. T. Krause et al., Adv. Ceram. Mater., 3(2), p.118-121, 1988, etc.
- [2] C. R. Kurkjian et al., J. Lightwave Technol., vol.7, no.9, p.1360-1370, 1989.
- [3] S. Okagawa et al., IECE Jpn. National Conference Record, C-564, 1989, in Japanese.
- [4] J. E. Ritter et al., J. Mater. Sci., 19, p.4087-4092, 1984.
- [5] S. M. Wiederhorn et al., J. Amer. Ceram. Soc., 53, p.543-548, 1970.
- [6] P.C.P. Bouten, in Proc. 13th ECOC, p.223-224, 1987.
- [7] N. Yoshizawa et al., J. Lightwave Technol., vol. 9, no.4, p.417-421, 1991.
- [8] D. Kalish et al., in Proc. Int. Wire Cable Symp., p.331-341, 1978.



Shuji OKAGAWA

The Furukawa Electric Co., Ltd.  
No.6, Yawata-Kaigandori,  
Ichihara, Chiba, 290,  
JAPAN

Mr. Okagawa graduated from Osaka University in 1981 with a M. Sc. in chemistry. Then he joined The Furukawa Electric Co., Ltd., Chiba, Japan, and has been engaged in research and development of plastic materials and manufacturing methods for optical fiber cable.

He is now a senior research engineer of Optical Fiber Transmission Section, Opto-Technology Laboratory, The Furukawa Electric Co., Ltd.



Keigo MAEDA

The Furukawa Electric Co., Ltd.  
No.6, Yawata-Kaigandori,  
Ichihara, Chiba, 290,  
JAPAN

Mr. Maeda graduated from Kyoto University in 1981 with a B. Sc. in industrial chemistry. Then he joined The Furukawa Electric Co., Ltd., Chiba, Japan, and has been engaged in research and development of plastic materials and manufacturing methods for optical fiber cable.

He is now a production engineer of Optical Fiber, Fiber Optics & Telecommunications Division at The Furukawa Electric Co., Ltd.

## MECHANICAL BEHAVIOR OF HERMETICALLY COATED OPTICAL FIBER

H. H. Yuce and J. P. Varachi, Jr  
Bellcore  
445 South Street  
Morristown, NJ 07962

P. L. Key  
Bellcore  
331 Newman Springs Road  
Red Bank, NJ 07701

### SUMMARY

The mechanical behavior of a commercially available hermetic fiber, which has an amorphous carbon film between the glass surface and the polymer coating, has been compared to the behavior of a conventional polymer coated fiber. We found that the strength of the hermetic fiber is somewhat lower than the non-hermetic fiber and that the strength distribution is broader. Atomic force microscopy (AFM) was used to show that the surface of the hermetic fiber is rougher than the surface of the non-hermetic fiber, thereby explaining the strength difference. However, the stress corrosion resistance of the hermetic fiber was so much greater than for the non-hermetic fiber that the initial strength advantage of non-hermetic fiber is negated for long term reliability considerations.

In general, the hermetic fiber held up well after low stress aging in water at temperatures up to 60°C. There was, however, a decrease in stress corrosion resistance when the testing or aging was carried out above 60°C.

### INTRODUCTION

The current successful use of silica-based optical fibers in communications systems has resulted from two parallel developments in glass fiber technology: a large reduction in optical attenuation in appropriate bandwidths and a significant improvement in fiber mechanical properties. The reduction in attenuation was achieved primarily by removing impurities that caused absorption of optical energy in silica. The improvement in mechanical behavior has resulted from reductions in the size of flaws, such as surface abrasions and microcracks present in all glass fibers, by minimizing damage to the fiber during drawing, and by application of protective polymeric coatings immediately after drawing.

The initial strength of a fiber is determined by the size of the largest flaw present; the long term strength is controlled by the slow growth of flaws in the fiber in the presence of stress and/or a corroding species in the environment. This latter process is known as fatigue (static and dynamic) in the literature on glass and as stress corrosion in other fields.

Current fibers have a strength of almost 800,000 psi in short lengths<sup>1</sup>, which corresponds to a flaw depth of about 0.03  $\mu\text{m}$  and a stress level approaching the theoretical maximum value based upon simultaneous fracture of all atomic bonds in the fiber cross section. The depth of such a flaw is about 0.02% of the diameter of the glass fiber or only about 200 times the silicon-oxygen bond length!

Further reductions in the initial flaw size and corresponding increases in initial strength seem unlikely, so industry has begun to focus on increasing long term strength by developing coatings that prevent chemical species in the environment from contacting the glass surface. Several materials have been tried including metals such as aluminum,<sup>2,3</sup> indium,<sup>4</sup> and tin,<sup>5</sup> and compounds such as silicon oxynitride and silicon carbide, and carbon.<sup>6</sup> In most of the early work with such coatings, significant improvement in stress corrosion resistance was obtained but at the expense of decreases in initial strength, increases in microbending losses, and decreases in draw speed due to slow deposition rates. However, higher strength hermetic fibers having a thin amorphous carbon layer between the glass and the conventional polymeric coating<sup>7,9</sup> have recently been developed. Such fibers hold considerable promise for applications requiring long term reliability or for service in harsh environments.

### EXPERIMENTAL

For our experiments, we obtained several kilometers each of a hermetic and a non-hermetic coated fiber from a major manufacturer of optical fibers. Both fibers contained a nominal 125  $\mu\text{m}$  diameter fused silica strand coated with a UV-cured urethane acrylate coating to an overall diameter of 250  $\mu\text{m}$ . However, before the polymer coating was applied to the hermetic fiber, an amorphous carbon coating about 300-500 Å thick was applied by a chemical vapor deposition process.

The principal objective of our program was to determine the effectiveness of the hermetic coating in preventing moisture from causing accelerated crack growth. We conducted dynamic fatigue experiments on the two fibers in the as-received condition in water at temperatures of 23, 40, 60, 80, and 85°C. In addition to testing as-received fibers, we tested fibers that we had aged in water at temperatures

of 40, 60, 80, and 85°C. For aging, long lengths of each fiber were loosely wound on 12 inch diameter glass spools which were then immersed into a glass tank filled with deionized water buffered at pH 7 and held at the aging temperature with a recirculating heater. The ends of the individual fiber strands remained outside the tank to prevent water from entering. Aged fibers were removed from the aging tanks for dynamic fatigue testing after periods of 1, 7, 30, 84, and 182 days.

The dynamic fatigue tests were carried out using a two-point bending apparatus<sup>10</sup> consisting of two parallel platens, one fixed and one driven by a computer controlled servo motor, between which a fiber loop is bent until it breaks. A piezoelectric transducer attached to the fixed platen detects the fiber break and signals the computer to stop the motion of the moving platen. The stress at failure is calculated from the platen separation at failure, the fiber dimensions, and the elastic modulus of the glass. Bending tests were conducted at a range of stress rates (8.7, 0.87, 0.087, and 0.0087 ksi/sec) so that the dynamic fatigue behavior of the fibers could be characterized. For each condition of temperature and stress rate, we tested 31 unaged samples for dynamic fatigue. After aging, dynamic fatigue tests of 21 samples from each aging condition and each stress rate were conducted in water at 23°C.

In addition to the dynamic bending tests, the as-received fibers were tested in a static bending test. This test uses two parallel aluminum plates with 30 machined mating grooves. Individual fiber loops are placed into each groove between the two plates which are separated by a spacer with a thickness chosen such that a specified stress is placed upon the fiber loops. A series of such tests were made with spacers producing stresses ranging from 450 ksi to 520 ksi. Each bending fixture with its 30 specimens was immersed in a glass tank filled with deionized water buffered at pH 7 and maintained at a constant temperature of 40, 60, 80, or 85 °C using a recirculating heater. Fiber breaks were detected by a piezoelectric transducer mounted on the side of the tank and recorded by a computer so that the time history of fiber breaks could be analyzed.

An atomic force microscope (AFM) was used to examine the surfaces of the as-received and aged fibers. The polymer coating on the fiber was removed before the examination by dipping the fiber into hot (200°C) H<sub>2</sub>SO<sub>4</sub> and rinsing in deionized water.

## RESULTS AND DISCUSSION

The dynamic bending strengths of the hermetic and the non-hermetic fibers plotted as a straight line on Weibull coordinate axes (Figure 1). This indicates that the failure distribution can be approximated by a Weibull cumulative probability distribution of the form:

$$F = 1 - 2 - \left( \frac{\sigma}{\sigma_{50}} \right)^m$$

where  $F$  is the cumulative probability of failure at a stress less than or equal to  $\sigma$  and  $\sigma_{50}$  is the median strength. The

parameter  $m$  is the slope of the curve on Weibull axes and provides a measure of the breadth of the strength distribution, with large values of  $m$  associated with narrow distributions. The relative breadth of the strength distribution can be calculated from this equation as:

$$\frac{\sigma_{90} - \sigma_{10}}{\sigma_{50}} \approx \left( 3.32^{\frac{1}{m}} - 0.152^{\frac{1}{m}} \right)$$

where  $\sigma_{90}$ ,  $\sigma_{50}$ , and  $\sigma_{10}$  are the 90th, 50th and 10th percentile strength values respectively.

As shown in Figure 1, the strength data fit a Weibull distribution very well. The median strengths, Weibull distribution parameters  $m$ , and the breadths of the strength distributions,  $(\sigma_{90} - \sigma_{10})$  for the unaged fibers are summarized in Table 1 and for the fibers aged in water for 1 month in Table 2. In general, the unaged hermetic fiber is about 100 ksi weaker than the unaged non-hermetic fiber and it exhibits a slightly wider distribution of strength. In both cases there is a relatively small decrease in strength as the testing temperature is increased. The hermetic fiber aged for 1 month (and tested at 23°C) shows a similarly small decrease in strength with aging temperature. However, the aged non-hermetic fiber showed a large decrease in strength with increases in aging temperature with the strength decreasing below that of the hermetic fiber at an aging temperature between 60 and 80°C. The breadth of the aged non-hermetic fiber strength distribution is still somewhat smaller than that of the hermetic fiber.

These strength results are consistent with the surface roughness of the hermetic and non-hermetic fiber as measured with the atomic force microscope. Surface profiles from the unaged fibers are shown in Figure 2; note that the vertical scale is twice as sensitive for the non-hermetic fiber. The surface of the hermetic fiber is rougher than that of the non-hermetic fiber, consistent with the lower initial strength of the hermetic fiber. However, as shown in Figure 3, the surface of the aged, non-hermetic fiber is rougher than that of the aged hermetic fiber, which again is consistent with the strength results. These qualitative observations on the relative surface roughnesses can be put on a more quantitative basis by considering the maximum value of roughness height obtained from the AFM:

Fiber	Roughness Height (nm)
Unaged, non-hermetic	1.8
Aged, non-hermetic	16.1
Unaged, hermetic	5.2
Aged, hermetic	10.9

The bending dynamic fatigue results for the unaged fibers are shown in Figure 4 where the median strength values for each fiber are plotted as a function of stress rate. If it is assumed that the rate of growth of flaws in the presence of stress depends upon the stress intensity factor at the tip of the flaws raised to a power  $n$ , then it can be shown<sup>11</sup> that the failure stress is related to the rate of stressing  $\dot{\sigma}$  by

$$\sigma = B \dot{\sigma}^{\frac{1}{(n_d + 1)}}$$

In the above equations,  $B$  and  $n_d$  are constants. The parameter  $n_d$  is known as the dynamic crack growth exponent or stress corrosion susceptibility constant; the larger the value of  $n_d$ , the more resistant is the fiber to crack growth. Values of  $n_d$  were obtained by fitting the above equation to the stress versus stress rate data; the values of  $n_d$  for the unaged fibers are:

Test Temperature °C	Hermetic	$n_d$ Non-hermetic
23	255	21.0
40	245	20.7
60	180	19.5
80	135	17.8
85	120	16.5

Both fibers showed a significant increase in stress corrosion susceptibility as measured by decreasing values of  $n_d$  with increasing temperatures. A similar trend was noted by Duncan et al.<sup>12</sup> who explained the decrease using a reaction rate model for corrosive attack of glass by water. The decrease in  $n_d$  for the hermetic coating is particularly large although the absolute value still is much greater than that of the non-hermetic fiber.

The values of  $n_d$  and the median bending strength for the hermetic fiber after aging for periods up to 182 days in water at temperatures of 40, 60, 80 and 85°C are listed in Tables 3 and 4 respectively. The median strengths showed small decreases with increasing aging temperature and increasing aging time. Unlike the results for different test temperatures, the values of  $n_d$  for the aged fiber showed significant decreases only for aging temperatures of 80°C and above. Comparison of the effect of aging temperature and testing temperature on  $n_d$  indicates that stress accelerates the process producing the decrease in  $n_d$ . This suggests that the relatively large changes in  $n_d$  observed in the short time tests at elevated testing temperatures may result from stress enhanced diffusion of moisture through the hermetic coating.

The bending static fatigue results for unaged hermetic and non-hermetic fibers are shown in Figure 5. If it is assumed that the initial strength of the fiber fits a Weibull distribution and if the power law dependence for crack growth rate is assumed, it can be shown<sup>13</sup> that the median time-to-failure,  $t_f$ , at constant stress,  $\sigma$ , is given by:

$$t_f = C \sigma^{-n_s}$$

where  $C$  is a parameter independent of both  $\sigma$  and  $t_f$  and  $n_s$  is the static crack growth exponent. The values of  $n_s$  and  $n_d$  theoretically should be the same but differences are usually observed which arise from the differences in static and dynamic testing procedures. Values of  $n_s$  were obtained by fitting this equation to the time-to-failure versus applied stress data, which should plot as a straight line on log-log coordinates. As seen in Figure 5, the data

for the non-hermetic fiber can best be fit by two straight lines. This so-called knee or transition in the static fatigue data has been observed by several workers<sup>14</sup>. The values of  $n_s$  obtained from these data are:

Test Temperature °C	Hermetic	$n_s$ Non-hermetic
40	-	12.3, 22.5
60	235	10.4, 20.3
80	210	8.7, 19.0
85	195	7.9, 18.9

In this table, the two values of  $n_s$  listed for the non-hermetic fiber are for the low stress and high stress regions respectively. Note the  $n_s$  decreases with test temperature as was observed for  $n_d$ .

As noted above the hermetic fiber has a much larger value of  $n$  and a somewhat smaller value of strength than the non-hermetic fiber. The former decreases the rate of crack growth; the latter increases it. The net effect of simultaneous variations in strength and  $n$  on crack growth can be estimated by considering a more general form of the equation for time-to-failure in static fatigue<sup>15</sup> than that used above:

$$t_f = \frac{A \left( \frac{K_o}{K_c} \right)^n S^{(n-2)}}{(n-2) \sigma^n}$$

where  $K_o$ ,  $K_c$ ,  $A$  are constants for a given glass and are independent of  $n$ ,  $S$  is the strength,  $\sigma$  is the applied stress and  $n$  is the crack growth exponent. The ratio of the time to failure at a stress,  $\sigma$  for two fibers of differing strengths,  $S$ , and  $n$  is given by:

$$\frac{t_1}{t_2} = \left( \frac{K_o}{K_c} \right)^{(n_1 - n_2)} \left( \frac{n_2 - 2}{n_1 - 2} \right) \frac{\sigma^{(n_2 - n_1)} S_1^{(n_1 - 2)}}{S_2^{(n_2 - 2)}}$$

Letting subscript 1 refer to a hermetic fiber and subscript 2 refer to a non-hermetic fiber, the following parameters are considered:

Parameter	Hermetic	Non-hermetic
$n$	200	20
$S$ , ksi	600	700
$\sigma$ , ksi	50	50

Using values of  $K_o = 0.371 \text{ ksi(in)}^{\frac{1}{2}}$ ,  $K_c = 0.72 \text{ ksi(in)}^{\frac{1}{2}}$ <sup>15</sup>, the ratio of  $t_{\text{hermetic}}$  to  $t_{\text{non-hermetic}}$  is  $\approx 10^{140}$ ! Clearly, the large value of  $n$  for hermetic fibers far outweighs the relatively small decrease in their strength relative to non-hermetic fibers.

## CONCLUSIONS

The mechanical behavior of a commercially available hermetic fiber, which has an amorphous carbon film between the glass surface and the polymer coating, has



been compared to the behavior of a conventional polymer coated fiber. This comparison indicated:

1. The bending strength data for both fibers could be fit well by a Weibull distribution. The Weibull slope parameter,  $m$ , of the hermetic fiber was somewhat smaller than that of the non-hermetic fiber indicating that the hermetic fiber had a slightly broader distribution.
2. The median strength of the unaged hermetic fiber was about 100 ksi less than that of the non-hermetic fiber. However, the hermetic fiber is much less susceptible to strength losses following aging in water at temperatures up to 60°C than the non-hermetic coated fiber.
3. The atomic force microscope was used to show that the height of fiber surface roughness correlated with strength, low strengths being associated with rougher surfaces.
4. The hermetic fiber has a significantly larger crack growth exponent,  $n$ , as determined by both dynamic and static fatigue than the non-hermetic fiber. Aging in water caused decreases in the value of  $n$  for both fibers but the value of  $n$  for the hermetic fiber remained significantly above that for even the unaged non-hermetic fiber.
5. For a given value of applied stress, the large value of  $n$  for the hermetic fiber results in much slower crack growth than with a non-hermetic fiber even though the strength of the hermetic fiber is somewhat lower than the non-hermetic fiber. Thus, hermetic fibers should have higher mechanical reliability for a given application than non-hermetic fibers.

## REFERENCES

1. C. R. Kurkjian and D. Innis; "Understanding mechanical properties of lightguides: a commentary"; **Optical Engineering**; 30(6) 681-689 (1991).
2. D. A. Pinnow et al; "Reductions in static fatigue of silica fibers by hermetic jacketing"; **Applied Physics Letter**; 34(1) 17-19 (1979).
3. K. Inada and T. Shiota; "Metal Coated Fibers"; **Optical Fiber Characterization and Standards**; Proc SPIE 584; 99-106 (1985).
4. M. Sato et al; "Mechanical and Transmission Properties of High Strength Indium Coated Optical Fiber"; **Proceedings 30th International Wire and Cable Symposium**; 45-50 (1981).
5. V. A. Bogatyrev et al; "High-strength hermetically sealed optical fibers"; **Soviet Technical Physics Letters**; 14(5) 343-344 (1988).
6. R. Chauduri and P. C. Schultz; "Hermetic Coating on Optical Fibers"; **Reliability Considerations in Fiber Optic Applications**; Proc SPIE 717; 27-32 (1986).
7. R. G. Huff and F. V. DiMarcello; "Hermetically coated optical fibers for adverse environments"; **Optical Devices in Adverse Environments**; Proc SPIE 867; 40-45 (1987).
8. K. E. Lu et al; "Hermetically Coated Optical Fibers"; **Proceedings 36th International Wire and Cable Symposium**, 241-244 (1987).
9. N. Yoshizawa and Y. Katsuyama; "High-Strength Carbon Coated Optical Fibre"; **Electronic Letters**; 25(21) 1429-1431 (1989).
10. H. H. Yuce et al; "Mechanical Properties of Optical Fibers in Bending"; **Proc Seventh Intl Conf on Integrated Optics**; 2; 44 (1989).
11. A. G. Evans; "Slow Crack Growth in Brittle Materials Under Dynamic Loading Conditions"; **International Journal of Fracture Mechanics**; 10 251-259 (1974).
12. W. J. Duncan et al; "The Effect of Environment on the Strength of Optical Fiber"; **Strength of Inorganic Glass**; C. R. Kurkjian (ed); Plenum Press, New York, 309-328 (1985).
13. F. P. Kapron and H. H. Yuce, "Theory and measurement for predicting stressed fiber lifetimes"; **Optical Engineering**; 30(6) 700-708 (1991).
14. H. C. Chandan and D. Kalish; "Temperature dependence of static fatigue of optical fibers coated with a UV-curable polyurethane acrylate"; **Journal American Ceramic Society**; 65(3) 171-173 (1982).
15. P. L. Key et al; "Mechanical Reliability of Optical Fibers"; **Journal of Non-Crystalline Solids**; 38 & 39 463-468 (1980).

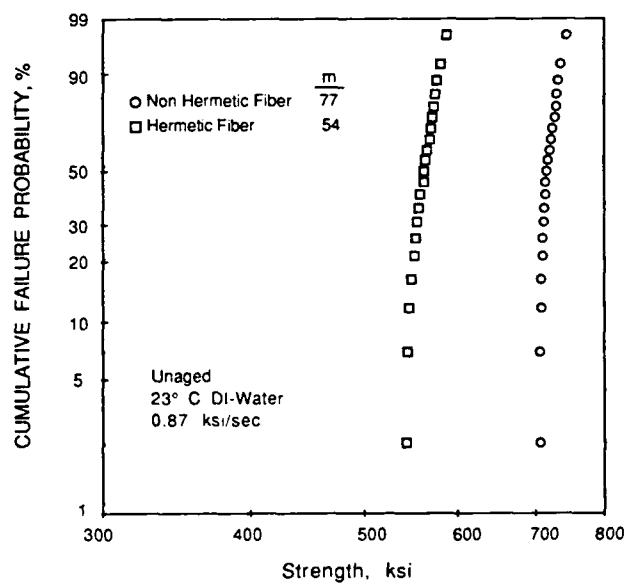


Figure 1 - Bending Strength Distribution for Unaged Fibers

**Table 1 - Dynamic Bending Strength of Unaged Fibers (1)**

Test Temperature °C	Hermetic			Non-Hermetic		
	$\sigma_{50}$ ksi	$m$	$\sigma_{90} - \sigma_{10}$ ksi	$\sigma_{50}$ ksi	$m$	$\sigma_{90} - \sigma_{10}$ ksi
23	618	54	35	729	77	29
40	616	57	33	726	72	31
60	606	48	39	721	66	34
80	597	40	46	702	61	35
85	591	31	58	688	53	40

(1) All fibers tested at 0.87 ksi/sec.

**Table 2 - Dynamic Bending Strength of Fibers Aged 1 Month (1)**

Aging Temperature °C	Hermetic			Non-Hermetic		
	$\sigma_{50}$ ksi	$m$	$\sigma_{90} - \sigma_{10}$ ksi	$\sigma_{50}$ ksi	$m$	$\sigma_{90} - \sigma_{10}$ ksi
40	610	53	35	707	51	36
60	606	46	40	668	52	39
80	603	48	38	526	49	33
85	595	36	51	460	42	34

(1) All fibers tested in 23°C water at 0.87 ksi/sec.

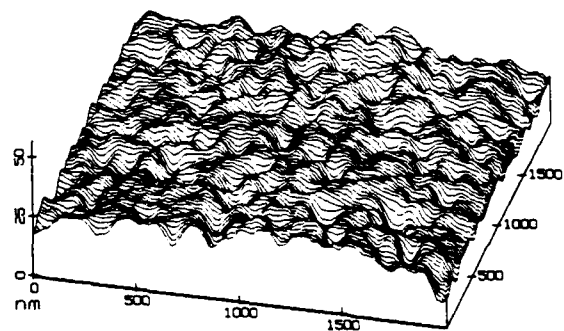
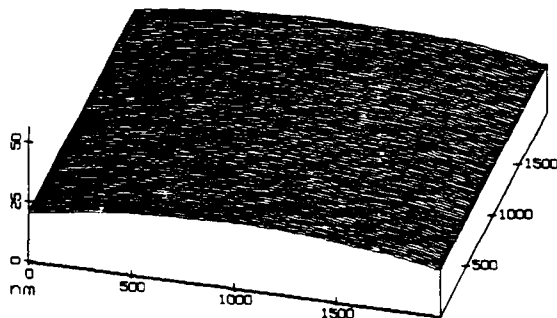
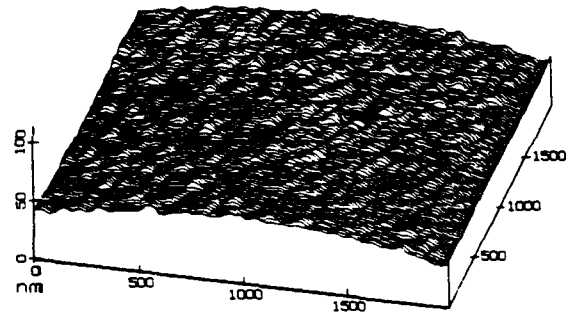
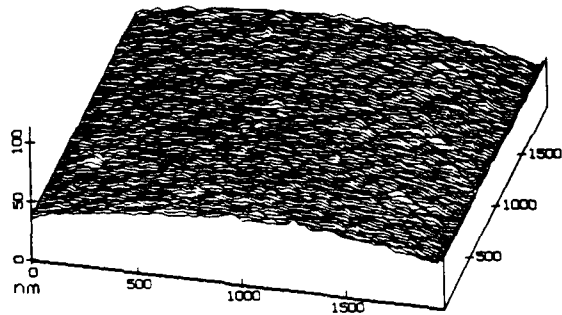


Figure 2 - Surface roughness of unaged fibers measured by atomic force microscopy.

Upper figure is hermetic fiber;  
lower figure is non-hermetic fiber.

Figure 3 - Surface roughness of aged fibers measured by atomic force microscopy.

Fibers aged for 85 days in 85°C water.

Upper figure is hermetic fiber;  
lower figure is non-hermetic fiber.

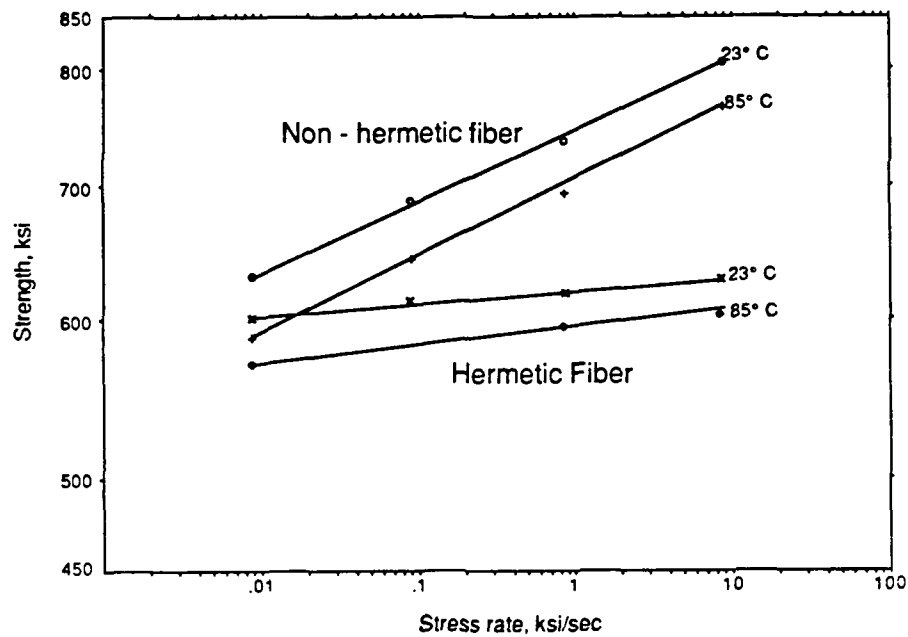


Figure 4- Dynamic Fatigue Strength in Bending of Unaged Fibers

Table 3 -  $n_d$  for Aged Hermetic Fibers (1)

Aging Time (days)	Aging Temperature (°C)			
	40	60	80	85
1	225	220	195	190
7	210	200	195	175
30	215	210	175	140
85	215	200	160	130
182	210	200	145	115

(1) All samples tested in 23°C water.

Table 4 - Median Dynamic Strength (ksi) for Aged Hermetic Fibers (1)

Aging Time (days)	Aging Temperature (°C)			
	40	60	80	85
1	618	616	611	605
7	615	616	609	606
30	610	606	603	595
85	606	597	591	586
182	615	616	609	586

(1) All samples tested in 23°C water at 0.87 ksi/sec.

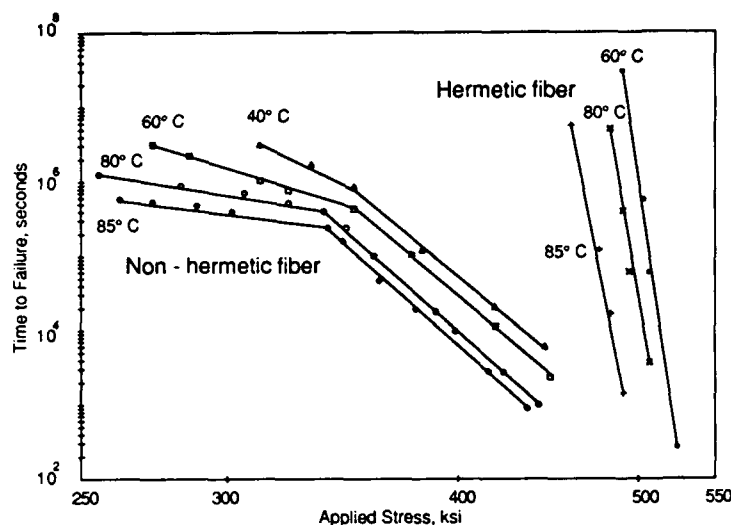


Figure 5 - Static Fatigue in Bending of Unaged Fibers



**John P. Varachi, Jr., P.E.**, received the BSME degree from Fairleigh Dickinson University, Rutherford, N.J. in 1976 and the MSME degree from Polytechnic Institute of New York, Brooklyn, N.Y. in 1978. He is currently District Manager, Fiber Distribution and Reliability Research at Bellcore. From 1969 through 1983 he was engaged in exploratory development at Bell Laboratories in mechanical design and analysis for telephone central office and outside plant apparatus. He also performed physical design and systems engineering for copper and optical fiber-based digital loop electronic systems for outside plant and customer premises applications.



**Hakan H. Yuce** is a Member of Technical Staff in the Fiber Distribution and Reliability Research District at Bellcore. He leads a research program dealing with long-term mechanical reliability of optical fibers and interconnects. Yuce provides technical input and support to organizations responsible for generic requirements and responds to client's immediate needs related to consultation on reliability and field failures. He also plays an active role in the standards arena under EIA/TIA working committees 6.6.7, fiber coatings and 6.6.8, fiber reliability. Hakan has a B.S. degree in Mechanical Engineering from Technical University of Istanbul [1977], an M.S. in Mechanical Engineering from M.I.T. [1982] and a PhD degree in Mechanical Engineering and Materials Science from Stanford University [1987].



**Leland Key** is District Manager of Metallurgical Science and Engineering Research at Bellcore in Red Bank, New Jersey. After receiving a PhD in Materials Science from the University of California at Berkeley, Mr. Key joined Bell Labs where he conducted research on the mechanical behavior of materials. In 1983, he joined Bellcore where he is responsible for metals research.

## LONG-TERM RELIABILITY OF 900 $\mu\text{m}$ BUFFERED FIBERS

J. J. Farro, R. A. Frantz, J. P. Kilmer, C. J. Wieczorek, and H. H. Yuce

Bellcore

445 South Street, Morristown, NJ 07962

### ABSTRACT

The majority of optical fibers used in telecommunications applications are coated to a diameter of 250  $\mu\text{m}$  with a UV-cured urethane acrylate protective coating. For applications where more handling and craft activity are expected, it is desirable to apply an additional buffer coating (or coatings) to increase the outer diameter to 900  $\mu\text{m}$ . As these fibers are increasingly deployed in the loop plant and on customer premises, they are likely to be exposed to a wide variety of harsh environments. The effects of high humidity and temperature and of several common chemicals on the mechanical and optical properties of 900  $\mu\text{m}$  buffered fibers are the subject of this paper. We show that the effects of these environments on the characteristics of the fibers vary according to the type of buffer coating material.

### 1. INTRODUCTION

As fiber penetrates further into the loop or distribution portion of the network, its deployment will be marked by distinct differences from that of the interoffice and feeder portions of the network. There will be an increase in the number of cable sheath openings and increased craft activity at these sheath openings. Post mortem analyses performed by Bellcore show that the majority of problems occur, not along the continuous spans of cable runs that constitute approximately 98% of the deployed fiber, but rather at the sheath openings and splice or terminating points which constitute the remaining 2% [1]. We know that the composite structure of an optical cable protects the fibers from outside plant (OSP) environments, but when this protective sheath is penetrated and the fibers in the cable are exposed, significant adverse effects on fiber reliability can be expected. Consequently, we concentrate our efforts on the behavior of optical fibers at these sheath openings in the OSP.

One question that is central to this issue concerns the use of 900  $\mu\text{m}$  outside diameter (OD) "buffered fiber" versus 250  $\mu\text{m}$  OD "protective coated" fiber. Bellcore's Generic Requirements permit the use of 900  $\mu\text{m}$  fiber in indoor applications [2] and buried service drop cable [3]; however, it is not recommended for general purpose distribution cables [4]. The question arises as to whether buffered fiber should be recommended for OSP applications such as in the "last mile". On the one hand, it might be expected that the buffered fiber would be preferred for loop applications, since increased handling is expected and 900  $\mu\text{m}$  buffered fiber appears to be better suited, in general, for craft activity. With its larger OD, it feels

more rugged to craft personnel than "delicate" 250  $\mu\text{m}$  fiber -- possibly because the 900  $\mu\text{m}$  OD is comparable to a 24 gauge wire. On the other hand, the larger OD is a negative factor for higher fiber count cables. For fiber counts above 72, the OD of cables using 900  $\mu\text{m}$  fiber becomes prohibitively large. There is some sentiment that for inside plant (ISP) applications, 900  $\mu\text{m}$  fiber is warranted, since the construction of ISP cables is not as rugged as OSP cable and the extra protection of 900  $\mu\text{m}$  buffering is necessary.

To address these concerns, a reliability study of 900  $\mu\text{m}$  buffered fibers for OSP use was initiated, the first results of which are reported in this paper. Parameters such as fiber strength, coating strippability, and buffer coating degradation were tracked and correlated after commercially available products were exposed to accelerated aging environments. Ultimately, the handleability or robustness that is actually needed for loop applications will be quantified and used to assess the reliability issues affecting both 250  $\mu\text{m}$  and 900  $\mu\text{m}$  fiber in OSP applications.

### 2. TYPES OF 900 $\mu\text{m}$ FIBERS

900  $\mu\text{m}$  buffer coated fiber can be manufactured in either "tight buffered" or "loose buffered" constructions. These represent the different strippability requirements that may be applicable to buffer coating depending upon the performance desired. A "tight buffered" 900  $\mu\text{m}$  jacket is tightly coupled to the underlying coating layers. The product is typically manufactured by extruding a thermoplastic elastomer (e.g., Hytrel<sup>®</sup>), polyvinylchloride (PVC), or nylon jacket over a 250 to 500  $\mu\text{m}$  diameter acrylate-coated fiber supplied by a fiber manufacturer. When this coating is mechanically stripped, it generally exposes the 125  $\mu\text{m}$ -diameter glass in a single stripping operation. This is an advantage because it requires one less stripping operation than the "separately strippable" buffer coating described below. Tight buffered fiber is also often preferred by connector/cable assembly manufacturers, since the tight buffering gives the manufacturer something tangible to attach to in order to provide strain relief at the connector, thus reducing coating shrinkback or "pistoning"; consequently, telephone company personnel may encounter this type of product when they make their own pigtailed by cutting jumper cords in half. However, tight buffered fiber is generally perceived to be very hard to strip and often requires users to "nibble" away at it in 0.5-inch lengths. This increases the risk of damaging the fiber surface, both through the repeated cutting operations and through scraping off the cut lengths over the exposed glass.

In contrast, a "loose buffered" or "separately strippable" construction is characterized by a loose coupling between the buffer coating and the underlying coating layers. Mechanical

The segment of the loop network referred to as the "last mile" extends from the Remote Feeder Termination (remote terminal) to a Service Access Point (pedestal) near the house where the service cable is connected and extended to the subscriber premises.

stripping of the 900  $\mu\text{m}$  coating exposes the 250  $\mu\text{m}$  protective coating, which can then be stripped in a conventional way with a second stripping operation and/or tool. This product is often perceived to be more craft friendly, even though it requires two stripping operations, because the 900  $\mu\text{m}$  buffering is removed easily. Sometimes lengths as long as a few inches can be removed in a single stripping operation because the buffer coating is not mechanically bound to the 250  $\mu\text{m}$  protective coating.

One fiber manufacturer provides a 500  $\mu\text{m}$  acrylate coating to reduce the microbending-induced loss due to the 900  $\mu\text{m}$  jacketing process. One of our test fibers (fiber C) used this 500  $\mu\text{m}$  fiber in its construction.

### 3. MECHANICAL PROPERTIES OF OPTICAL FIBERS

Desirable mechanical properties of optical fibers include high strength, small strength variability, high fatigue resistance and high aging resistance. With improvements in preform quality and drawing environment, long-length, high-strength optical fibers are being produced routinely [5]. Such fibers, with strengths in the range of 5.5 GPa (800,000 psi) in short gage lengths (less than 1 meter), are usually characterized by a narrow, unimodal strength distribution. The common UV-cured polymer coatings provide adequate fatigue resistance, as described by a fatigue parameter in the range of 20-30, in a benign environment.

However, since aging in adverse environments can severely degrade fiber strength and modify its fatigue resistance [6-11], the long-term reliability of optical fibers may be affected. Some chemical species, especially water, are known to have very detrimental effects on the mechanical behavior of optical fibers. This effect is manifested in different ways depending on the stress state of the optical fiber sample under investigation: (1) *time delayed failure mechanisms* such as static or dynamic fatigue, and (2) *zero-stress aging*. Static fatigue is the time-dependent failure of glass, in a given environment, under a constant stress that is less than the instantaneous fracture strength. Dynamic fatigue is the time-dependent failure of glass, in a given environment, under a constant stressing rate resulting in a fracture strength that is less than the strength in an inert environment.

The topic of fiber aging under low or zero stress is still a controversial issue. The effect of low- or zero-stress aging on optical fibers is of considerable importance in cables or in splice cases because fibers can encounter a high humidity or chemical environment that can degrade their strength. These aged fibers may be stressed later during routine maintenance or other repair work. The effect of aging on the mechanical reliability of optical fiber is therefore an important consideration in any system design.

### 4. EXPERIMENTAL PROCEDURE

The objective of this study was to determine the long-term mechanical reliability of 900  $\mu\text{m}$  buffered optical fibers in anticipated telecommunication service environments. Accordingly, we obtained several kilometers of commercially available fibers from four different suppliers; the fibers were designated A through D. Each fiber had a nominal glass diameter of  $125 \pm 2 \mu\text{m}$  coated with primary/secondary coatings (UV-curable urethane acrylates, or silicones) to  $250 \pm$

15  $\mu\text{m}$  or  $500 \pm 15 \mu\text{m}$ , followed by an extruded hard buffer (Hytrel, PVC or nylon) to  $900 \pm 15 \mu\text{m}$ . Sample A used in our testing is composed of a conventional 250  $\mu\text{m}$  fiber jacketed to 900  $\mu\text{m}$  with PVC. Sample B is composed of a conventional 250  $\mu\text{m}$  fiber covered by a 400  $\mu\text{m}$  silicone-based soft layer and jacketed to 900  $\mu\text{m}$  with nylon. Sample C is composed of the new 500  $\mu\text{m}$  acrylate coated fiber jacketed to 900  $\mu\text{m}$  with Hytrel. Sample D is similar to sample A except it is made by a different manufacturer. While 50/125 multimode has been reported to be more sensitive to microbending loss [12], single-mode fiber was used exclusively for this study since it is more widely deployed in telecommunication applications. We also tested a fiber consisting of a nominal 125  $\mu\text{m}$  diameter fused silica strand coated with a UV-cured urethane acrylate coating to an overall diameter of 250  $\mu\text{m}$ . Designated as fiber E, it is the same as fiber A but without the PVC jacket.

The mechanical properties of the five fibers were determined as received and after aging in various environments as given in Table 1.

Table 1 - Exposure Environments

1. Household cleaning solution at room temperature, 23° C [aqueous ammonia solution, ~3.5% ammonia by weight]
2. Bleach at room temperature, 23° C [aqueous solution of 5.25% sodium hypochlorite]
3. Gasoline at room temperature, 23° C [regular, unleaded]
4. WD-40 at room temperature, 23° C [household spray lubricant]
5. High temperature and humidity, 85 °C, 94 % RH

The center sections of 2m long samples from each of the five fibers were loosely placed into open containers containing household cleaning liquid, bleach, gasoline and WD-40 and also into an environmental chamber where the temperature and humidity were kept constant ( $85 \pm 1^\circ \text{C}$  and  $94 \pm 4 \% \text{RH}$ ). The ends of the samples remained outside the containers. At intervals of 1 day, 1 week, 1 month, and 6 months, a minimum of 31 samples from each supplier were removed from the aging solution and tested. Strength testing was carried out by tension (strain rate: 10%/min, gage length: 0.5 m) with a screw-driven universal tensile testing machine in a laboratory ambient environment of 23° C and relative humidity of 50%. Samples were gripped on 0.1 m diameter capstans covered with a soft elastomeric sleeve. Masking tape was used to secure the ends of the fiber to the capstans.

In addition, the stripping force required to remove the coating was measured using a commercial stripping tool mounted in a screw driven universal tensile testing machine. The gage length of the stripping test samples was 1.5 cm and the stripping rate was 2.5 cm/min. The stripping force was measured for fibers in the as-received condition and after exposure to the environments given in Table 1 at intervals of 1 day, 1 week, 1 month and 6 months. Also, samples of each fiber were examined in detail both as received and after each of the aging periods. Physical, mechanical, and chemical changes in the buffer coatings were recorded.

Finally, attenuation measurements were made on two of the buffered fibers (fibers B and C) in an 85° C and 95% relative humidity environment at a wavelength of 1550 nm. Approximately one kilometer long fibers were wound loosely about glass mandrels 0.3 m in diameter, and these fibers were placed in an environmental chamber and fusion spliced to the fibers leading to the test equipment. Consisting of a 1550 nm laser source, wide-area detector, optical switch, lock-in amplifier and a computer controller, the equipment was located in a nearby laboratory which was linked to the environmental chamber by a short length of optical cable. Baseline readings were obtained, after which the chamber was heated to 85° C for seven days with uncontrolled humidity. Heat was applied to the fibers before the humidity was raised to determine the effects of high heat on the fiber alone. After the seventh day, humidity was increased, and measurements were taken daily to determine the attenuation change of the buffered fibers.

## 5. RESULTS AND DISCUSSION

### Stress-Free Aging

The median strengths of the fibers both initially and after stress-free aging are plotted in Figures 1 through 5. Fiber B appears to be designed to meet the "separately strippable" construction described above; this created serious experimental difficulties in measuring the fiber strength, so no values are plotted for this fiber. Cleaning liquid (Figure 1) had the largest effect on the strength, followed by bleach (Figure 2) and high humidity and temperature (Figure 5). The strength reductions experienced by fibers A, C, and D are comparable after six months of aging in cleaning liquid and bleach; this agrees with earlier studies on 250  $\mu$ m coated fibers [11-12]. The rate of decrease in strength during aging in the high humidity and temperature environment is dependent upon the buffer coating [13-15]; this is particularly evident in comparing the behavior of fibers C and D in Figure 5.

The model of Michalske and Freiman [16] for stress corrosion in glass is based on an interaction between chemical species in the environment and strained bonds at the crack tip resulting in scission of the Si-O bonds. The model places two requirements on stress corrosion agents. First, the molecule must have both an electron and a proton donor site. Second, the molecule must be small enough to rapidly diffuse to the crack tip. Water and ammonia were shown by Michalske to meet this requirement. Household bleach consists of a solution of sodium hypochlorite. It is suggested that

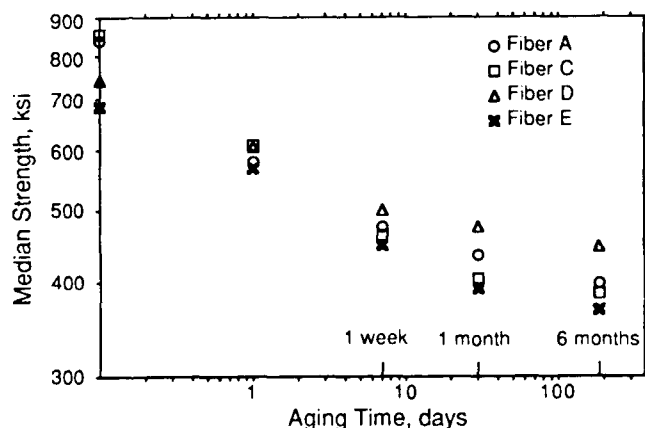


Figure 1 - Effect of Stress-Free Aging in Cleaning Liquid on Fiber Strength

hypochlorous acid meets the Michalske requirements and is the stress corroding agent responsible for the effect observed on the strength. Relatively small effects were observed for aging in gasoline and WD-40. This is consistent with the Michalske model since these two chemicals contain primarily larger molecules.

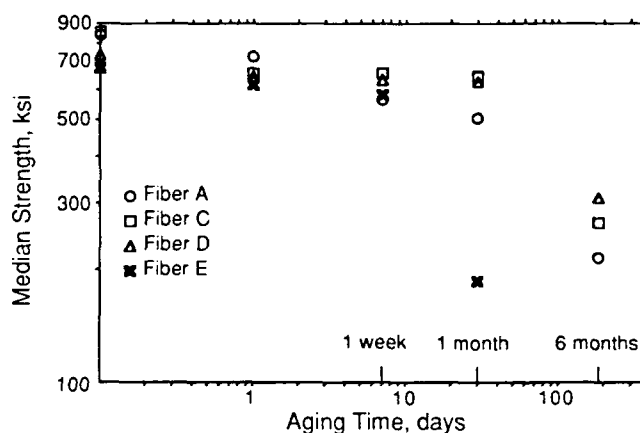


Figure 2 - Effect of Stress-Free Aging in Bleach on Fiber Strength

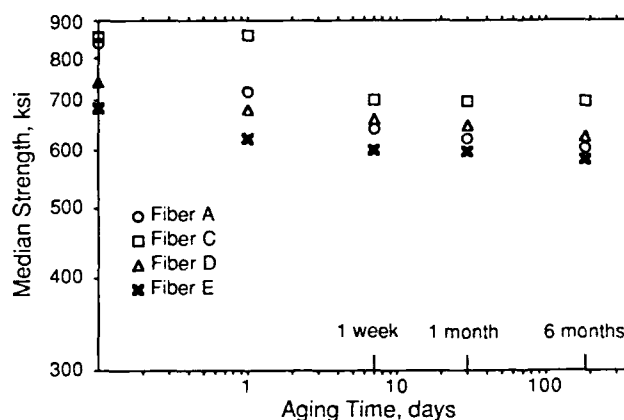


Figure 3 - Effect of Stress-Free Aging in Gasoline on Fiber Strength

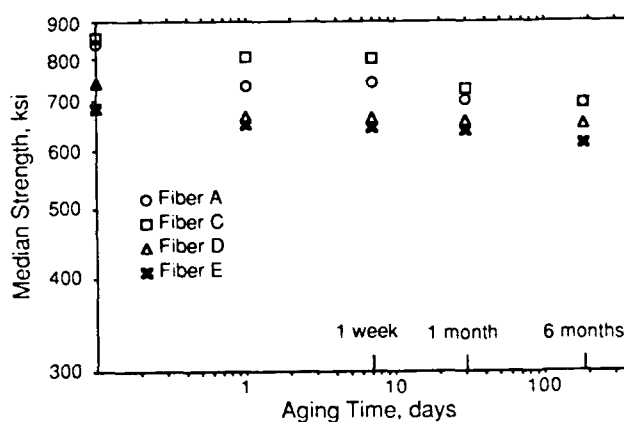


Figure 4 - Effect of Stress-Free Aging WD 40 Liquid on Fiber Strength

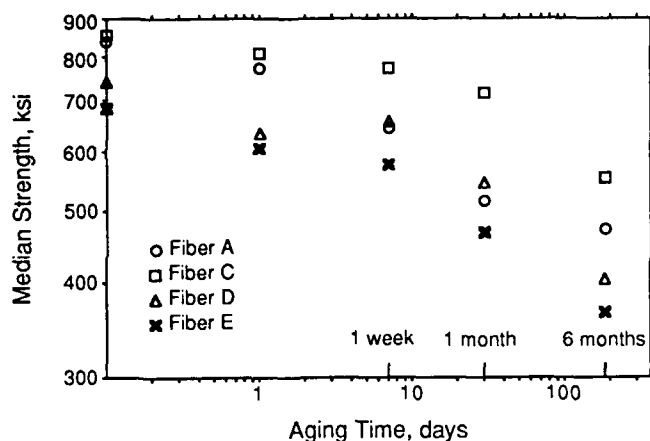


Figure 5 - Effect of Stress-Free Aging in 85° C & 94% RH on Fiber Strength

Figures 6 and 7 contrast the failure stress distributions for fibers A and E, both unaged and after 24 hours in each of three aging conditions. These fibers differ only in the PVC buffer coating that was applied to fiber A. Note that in all cases fiber A has a higher median strength, although only marginally so after aging in cleaning liquid. In this latter case, the strength distribution is particularly broad for fiber A due a number of lower-strength test samples, which suggests that this PVC buffer coating may be particularly susceptible to penetration by the cleaning liquid, resulting in a direct attack on the glass surface comparable to that seen for unbuffered fiber E.

#### Strip Force

The aging environments used here had varying deleterious effects on the strip force for these buffer coatings. Figures 8 through 12 compare the strip force measurements for aged samples with those for the as-received fibers. The strip force for fiber B represents the force required to strip only the buffer coating in this loose buffered construction. The most significant changes occurred for the PVC buffered fibers (A and D) that were aged in gasoline, where the strip force decreased by over 85% for both samples after six months (Figure 10). The high humidity and temperature environment (Figure 12) and, to a lesser degree, the cleaning liquid (Figure 8) also lowered the mean strip force for these two PVC-buffered fibers. Since the initial strip force for fiber D exceeds the maximum 3 lb force currently specified in the Bellcore Generic Requirement [2], these decreases actually bring it into conformance with the requirement.

The nylon (fiber B) and Hytrel (fiber C) buffer coatings seemed better able to withstand the harsh aging environments. However, the strip force for fiber B actually increased during aging in the bleach solution (Figure 9). When aged in WD-40, fiber C also experienced a substantial increase in strip force (Figure 11), with the result that it exceeded the Bellcore Generic Requirement of 3 lb force.

#### Buffer Coating Degradation

During extended aging, the fluids in which the fiber samples were immersed can function as solvents for the buffer coating materials. This can cause leaching or extraction of material and also chemical reactions that discolor or otherwise degrade the buffer coatings. Several examples of such degradation were found in the present tests.

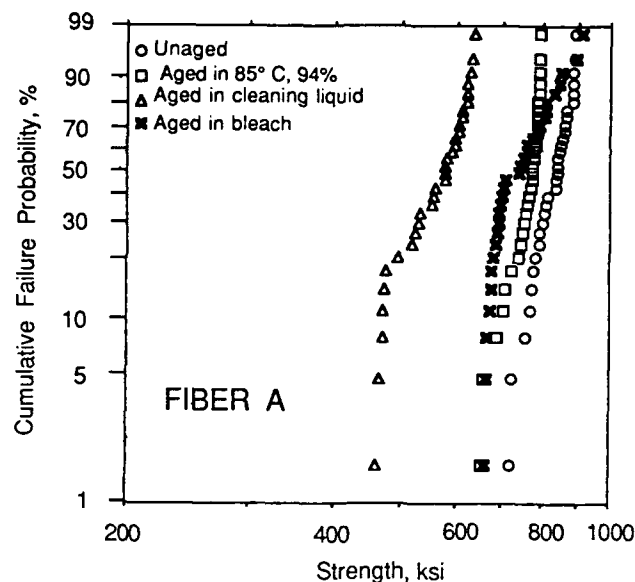


Figure 6 - Effect of Stress-Free Aging in Various Environments on Fiber Strength after 1 Day Aging

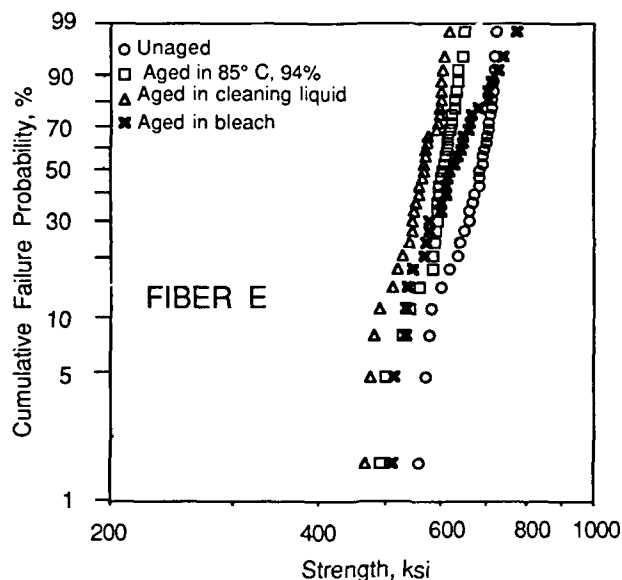


Figure 7 - Effect of Stress-Free Aging in Various Environments on Fiber Strength after 1 Day Aging

Extraction of material can cause both weight loss and volume loss of the buffer coating. This was most pronounced with fibers A and D (PVC buffer coatings) after aging in gasoline. Weight losses of 5 to 10% were measured after 6 months of aging, while the OD of these fibers decreased by 5-8% in the same time interval. Fiber C (Hytrel buffer coating) showed a decrease of about 4% in OD, but actually gained weight (about 8%) during the 6-month gasoline immersion. Fiber B (nylon buffer coating) was relatively unaffected by the gasoline immersion, but did show about a 3% decrease and a 5% weight loss after six months of aging in the high humidity and temperature environment.



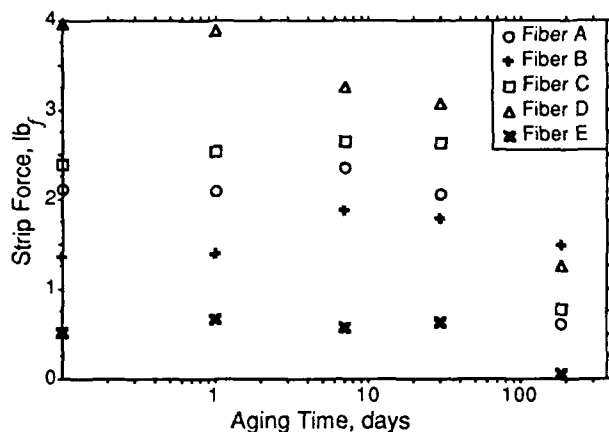


Figure 8 - Effect of Stress-Free Aging in Cleaning Liquid on Strip force

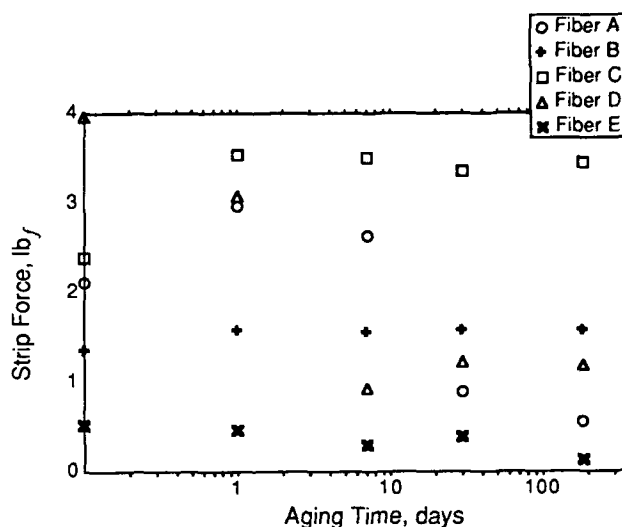


Figure 11 - Effect of Stress-Free Aging in WD 40 on Strip Force

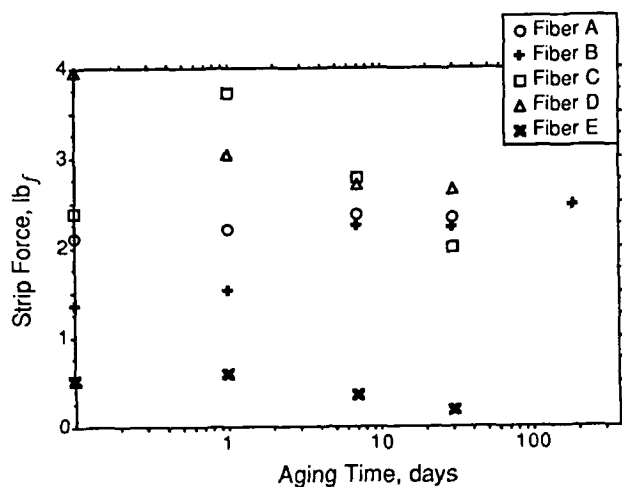


Figure 9 - Effect of Stress-Free Aging in Bleach on Strip Force

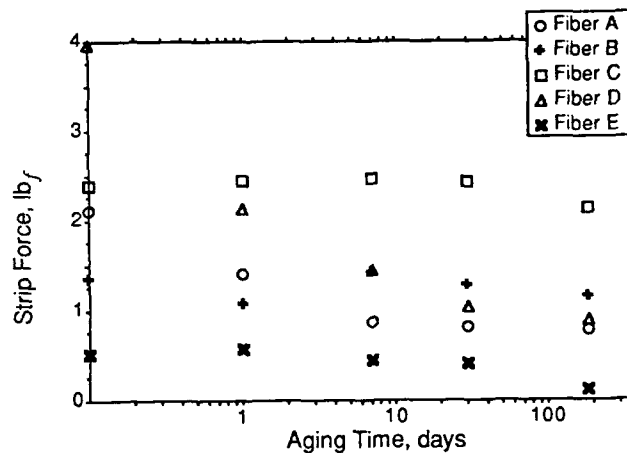


Figure 12 - Effect of Stress-Free Aging in 85° C, 94% RH on Strip Force

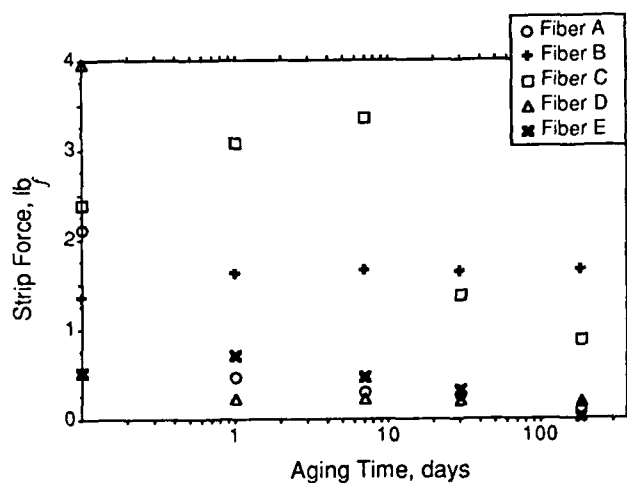


Figure 10 - Effect of Stress-Free Aging in Gasoline on Strip Force

Fourier Transform Infrared (FTIR) spectroscopic analysis of several aged samples showed a significant loss of plasticizer from both PVC buffer coatings after aging in gasoline. This is consistent with the losses of weight and volume observed. These observations are also consistent with the significant decrease in strip force noted above. The extraction of plasticizer by gasoline leaves these buffer coatings as stiff tubes. Molecular crosslinking limits the circumferential shrinkage of the buffer coating on the protective coating and, depending upon the adhesion between the coatings, may draw the inner coating away from the glass. The result is that the entire coating structure easily strips off.

Pronounced color changes were also observed in the PVC and nylon buffer coatings. After six months of aging, the PVC coatings (A and D) showed slight yellowing from exposure to cleaning liquid, gasoline, and WD-40. Both coatings developed a chocolate brown color from exposure to bleach.

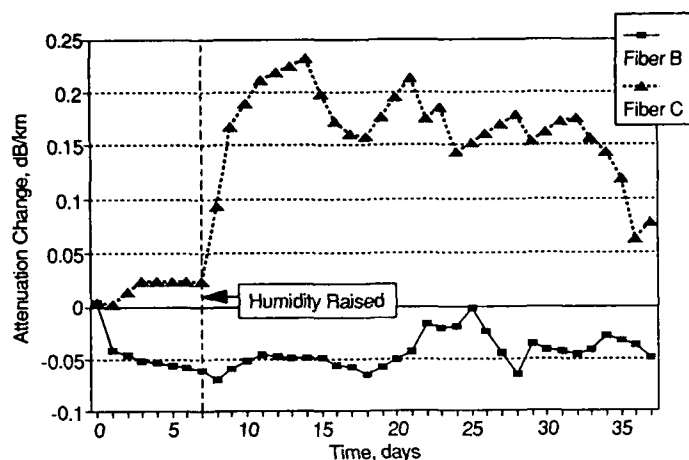


Figure 13 - Attenuation Change during 85° C, 94% RH Aging

The nylon coating (B), which started out a bright yellow color, showed little or no discoloration from exposure to gasoline or WD-40; however, both the bleach and the cleaning liquid effectively bleached the coating to a very pale yellow, almost cream, color. Finally, the Hytrel coating (C) yellowed only after six months aging in gasoline; however, after six months in the bleach it lost its integrity nearly completely so that it crumbled off the fiber when touched.

#### Attenuation

As can easily be seen in Figure 13, the humidity had a relatively strong effect on the transmission characteristics of the fiber with the Hytrel buffer coating (Fiber C). Microbending was induced by the distortion of the buffer material under the high heat/high humidity conditions. The effect on the nylon-buffered fiber (Fiber B) was minimal. This may be due to the soft silicone layer between the fiber and the nylon coating acting as a "cushion" to reduce any microbending effects caused by a change in the dimensions of the buffer coating. The microbending loss in buffered fibers has not been detected in the field because the short deployment lengths have not impacted the loss budget of the system.

## 6. CONCLUSIONS

The mechanical behavior of aged and unaged 900  $\mu\text{m}$  buffered silica fibers has been studied both in a humid environment and in various common chemicals as a function of time. The buffer coating material has a strong effect on the mechanical and aging behaviors of these fibers. In addition to reductions in strength and strip force, the environments studied here caused embrittlement, weight loss, shrinkage, and discoloration of the coatings. Nonetheless, comparison to a typical non-buffered fiber shows that the buffer coatings do provide additional protection against loss of strength and eventual failure. Initially, the high humidity environment caused an increase in attenuation in the fiber with Hytrel buffer coating; however, the microbending-induced loss dissipated as the coating to glass interface reached a stable condition.

## REFERENCES

1. J. Kilmer et. al., *Proc of SPIE 1366*, 85-91 (1990).
2. "Generic Requirements For Interbuilding Optical Fiber Cable," Bellcore TR-NWT-000409; Issue 2 (September 1990).
3. "Generic Requirements For Optical And Optical/Metallic Buried Service Cable," Bellcore TR-TSY-000843, Issue 1 (January 1989).
4. "Generic Requirements For Optical Distribution Cable," Bellcore TR-TSY-000944, Issue 1 (July 1990).
5. F.V. DiMarcello, C.R. Kurkjian and J.C. Williams, "Fiber Drawing and Strength Properties," in *Optical Fiber Communications*, Vol. 1, T. Li, Ed., 179-248, Academic Press, Orlando, FL (1985).
6. T.T. Wang and H.M. Zupko, *J. Mater. Sci.* **13**, 2241-2248 (1978).
7. J.T. Krause and C.J. Shute, *Adv. Ceram. Mater.* **3**, 118-121 (1988).
8. M.J. Matthewson and C.J. Kurkjian, *J. Amer. Ceram. Soc.* **71**, 171-183 (1988).
9. C.J. Kurkjian, J.T. Krause and M.J. Matthewson, *J. Lightwave Tech.* **7**, 1360-1370 (1989).
10. H.C. Chandan and S.C. Perry, *J. Amer. Ceram. Soc.* **68**, C90-C91 (1985).
11. H.H. Yuce, A.D. Hasse and P.L. Key, *Proc. SPIE 992*, 211-217 (1989).
12. J. Kar et. al., *Proc of IWCS '87*, 288-232 (1987).
13. D. Roberts, E. Cuellar and L. Middleman, *Proc. SPIE 842*, 32-40 (1988).
14. T. Wei and B.J. Skutnik, *J. Non-Cryst. Solids* **102**, 100-105 (1988).
15. H.H. Yuce et. al., *Proc. IWCS '88*, **37**, 732-737 (1988).
16. T. A. Michalske and S. W. Freiman, *J. Amer. Ceram. Soc.* **66**(4), 284-287 (1983).



**Jerry J. Farro** is a member of the Optical Cables and Distribution Terminals/Closures group in Bellcore, Morristown, NJ. He joined Bellcore in 1989 and is currently responsible for the development of generic requirements and test procedures for optical fiber. He holds a B.S. degree in Electrical Engineering from Rensselaer Polytechnic Institute and has an M.S. from the Georgia Institute of Technology.



**Rolf A. Frantz** is a Distinguished Member of Technical Staff in the Fiber Distribution and Reliability District at Bellcore. He holds BS and MS degrees from Cornell University and a PhD in Engineering mechanics from Brown University. He joined Bell Laboratories, where his major responsibilities were in the field of electrical insulation, an area in which he continued to work upon joining Bellcore in 1983. Since 1988, he has focused on optical fiber coatings, particularly extent of cure, aging, and coating durability.



**Dr. Joyce Kilmer** received his Ph.D. in Electrical Engineering from the University of Florida and joined Bellcore as a Member Technical Staff of the Optical Cables District in the Fiber Optic Technology Division in 1984. In 1988, he was temporarily reassigned to Fiber Optic Systems District to study the effects of reflections on fiber optic system performance. In 1989, he was promoted to District Manager of the Optical Connector, Splicing and Closures District. In 1990, he was reassigned to District Manager of the Optical Cables and Distribution Terminals/Closures District. In this capacity he is responsible for writing generic requirements, performing product and post-mortem analyses, and developing long term reliability testing of optical fiber, optical fiber cable, and distribution terminals for Fiber-in-the-Loop (FITL).



**Casey J. Wiecezorek** is a member of the Optical Cable Group in Bellcore, Morristown, NJ. He joined Western Electric in 1967 and worked on various cable designs and manufacturing processes. He is currently responsible for the development of generic requirements and test procedures for optical cables. He holds a B. S. degree in Mechanical Engineering from Fairleigh Dickinson University and did graduate work at Stevens Institute of Technology.



**Hakan H. Yuce** is a member of the Technical staff in the Fiber Distribution and Reliability Research District at Bellcore. He leads a research program dealing with long-term mechanical reliability of optical fibers and interconnections. Hakan provides technical input and support to organizations responsible for generic requirements and responds to clients' immediate needs related to consultation on reliability and field failures. He also plays an active role in the standards arena under EIA/TIA working committees 6.6.7, fiber coatings and 6.6.8, fiber reliability. Hakan has a B.S. degree in Mechanical Engineering from Technical University of Istanbul [1977], an M.S. in Mechanical Engineering from M.I.T. [1982] and a Ph.D degree in Mechanical Engineering and Material Science from Stanford University [1987].

## EFFECTS OF THE ENVIRONMENT ON AN UNPROTECTED REEL OF OPTICAL FIBER CABLE

H. H. Yuce, C. Wieczorek, A. DeVito, J. P. Varachi, Jr., and J. P. Kilmer

Bellcore  
445 South Street, Morristown, NJ 07962

### ABSTRACT

*Although optical fibers have moved rapidly from the laboratory to widespread deployment, there have been relatively few field failures reported, and most of these have been due to external causes such as dig-ups. Initial concerns about fiber breakage due to the brittle nature of glass have, fortunately, not materialized. In this paper, we examine one of the few field cases involving fiber breaks that resulted from aging of optical fibers under extreme environmental conditions for more than four years. An abnormally high incidence of fiber breakage in this cable was reported by the craft during normal installation after aging. Although there have not been many such failures reported, mechanical failures are still considered a possible cause of reliability problems and continue to receive considerable attention. In this study, we show how atomic force microscopy (AFM) can be a helpful method to analyze the cause of fiber failures. Such information can be very useful in determining responsibility for repair or replacement.*

### 1. INTRODUCTION

Optical fibers are being deployed rapidly into the telephone plant; by the end of 1990, there were almost 10 million fiber-km installed. The average age of installed fiber optic cables is about 8 years for multimode fibers (12 years maximum) and 4 years for single mode fibers (8 years maximum). Considering the rapidity with which this technology moved from the laboratory to the field and the large amount of installed cable with significant exposure, there have been relatively few failures of fiber optic cables.<sup>1</sup> This trend, if continued, bodes well for the long term reliability of this technology.

Desirable mechanical properties of optical fiber are high strength, small strength variability, high fatigue resistance and high aging resistance. With improvements in preform quality and drawing environment, long-length, high-strength optical fibers are being produced routinely.<sup>2</sup> Such fibers, with strengths in the range of  $\sim 10^4$  psi in short gage lengths, are usually characterized by narrow, unimodal strength distributions with large Weibull slope parameters ( $m \sim 50$ -100). The commonly used UV-cured polymer coatings provide adequate fatigue resistance, as described by a fatigue parameter of  $\sim 25$ , in a benign environment. However, since

aging in adverse environments can severely degrade fiber strength and modify the fatigue resistance of optical fibers<sup>3,4</sup>, long-term reliability of optical fibers is no longer assured. Some chemical species, especially water, are known to have detrimental effects on the mechanical properties of optical fibers. This is manifested in different ways depending on the stress state of the optical fiber: (1) time delayed failure mechanisms such as static or dynamic fatigue, and (2) zero-stress aging.

Static fatigue is the time-dependent failure of glass, in a given environment, under a constant stress that is less than the instantaneous fracture strength. This delayed fracture is a function of the coating, applied stress, temperature, and chemical species, particularly the presence of water. The stress-assisted hydrolysis of the silicon-oxygen network of the glass<sup>5</sup> results in the growth over time of microscopic surface flaws into larger critical cracks. The development of the flaws is influenced by the surrounding environment. The surface reactivity in a given environment determines the fiber's ultimate strength, because of its effect on crack tip growth. Dynamic fatigue is a time-dependent failure of glass, in a given environment and under a constant stress rate resulting in a fracture strength that is less than the strength in an inert environment. The loss of strength in high-strength glass fibers in the absence of stress in some corrosive environments such as water is called zero-stress aging.

The underlying mechanism of glass failure under static fatigue conditions has been well documented<sup>6,7</sup>. But, the reasons for loss of strength of glass fibers under zero-stress aging is still a controversial issue. Proposed mechanisms involve absorption of water molecules on the surface, promoting crack growth during subsequent strength testing<sup>12</sup>, or corrosive reactions leading to surface flaws which can act as nuclei for cracks<sup>8</sup>. The surface reactivity of silica-based glasses in different environments determines the ultimate strength of these materials because of the effect on crack tip growth. The effect of low or no stress aging of optical fibers is of considerable importance in cables or in splice cases because fibers can encounter high humidity and high temperatures (e.g. pedestals) or other chemical species such as water (e.g. manholes) which can degrade the strength. These aged fibers may then be subsequently stressed during routine maintenance or other repair work. The effect of zero-stress aging on the mechanical reliability of optical fibers is therefore an important consideration in any cable installation.

Atomic force microscopy (AFM)<sup>13</sup> has been shown to be a useful technique for the examination of surfaces from the Angstrom to the micrometer scale. AFM is a useful method for measuring the surface roughness because this high resolution allows the quantitative measurement of real-space surface roughness. We have examined the mechanical characteristics and surface roughness of field aged fibers by using AFM and show that the loss of strength of the fibers is related to changes in surface roughness on the nanometer scale.

## 2. FAILURE ANALYSIS

### 2.1 Background

It was reported to Bellcore that a reel of cable had been stored outside for approximately 4 years without thermal wrap protection. When a portion of it was planned to be installed, some changes to the cable jacket and fibers were noticed. The original identification markings were orange on the outermost cable layer on the reel, but faded to a very pale yellow. In working with these fibers, an abnormally high incidence of fiber breakage occurred under normal handling. The cause for these breaks was not obvious, and the reel was sent to Bellcore for analysis.

### 2.2 Test Samples

The cable was shipped on a sturdy wooden reel secured to a wooden pallet. The cable construction consisted of buffer tubes stranded around a dielectric central member. Placed around the buffer tubes was a layer of aramid yarn which in turn was protected by a polyethylene jacket.

The fiber samples were selected from different cable layers to determine the degree of aging based on the amount of exposure to the environment (e.g. solar effects, etc.). In this study, we identify the fiber samples by the relative position with respect to the outer most layer on the reel. We denote the outer most layer as Layer-1 and each successive layer as Layer-2, 3, etc.

## 2.3 Experiments

### 2.3.1 Cable Jacket Material Analysis

Bellcore conducted outer cable jacket yield strength and ultimate elongation tests on samples taken from the cable jacket. These tests were conducted to evaluate any changes that may have taken place as a result of exposure to the environment. The test was conducted in accordance with the test procedure specified in TR-TSY-000020, *Generic Requirements for Optical Fiber and Optical Fiber Cable, Issue 4, March 1989*. Samples were taken from both Layer-1 and Layer-3 of the reel. The results of the tests indicated that there was no significant difference in the minimum yield strength and minimum elongation between the jacket samples taken from Layer-1 and Layer-3. The test produced an average yield strength of 1282 psi and an average elongation of 700% for Layer-1 samples and an average yield strength of 1316 psi and an average elongation of 700% for Layer-3 samples. This met the requirements specified in TR-20, Issue 2, which was in effect at the time of the cable manufacture.

Clearly, these results indicate that exposure of this cable to the environment did not adversely affect the cable jacket material.

### 2.3.2 Fiber Analysis

A successful failure analysis requires an understanding of possible failure mechanisms. In the case of optical fibers, this requires an understanding of the mechanical behavior of glass. The principal tools required for our analysis of field and laboratory aged fibers are summarized below.

#### 2.3.2.1 Experimental Procedures

**Tensile Strength** - The dynamic tensile strengths of the laboratory aged and field aged fibers are measured with a screw-driven universal tensile testing machine in a laboratory environment of 23° C and relative humidity of 50%. Tensile strength is determined at a strain rate of 5%/min with a gage length of 20 in. Thirty-one samples were taken from each representative layer to determine the median strength and strength distribution.

#### Two-point Bending Strength and Dynamic Fatigue Behavior

A computer controlled, two-point bending apparatus<sup>14</sup> was also used to determine the strength and dynamic fatigue behavior of the fibers. The test apparatus consists of two parallel platens, one fixed and one moving, between which a fiber loop is bent until it breaks as shown in Figure 1. The moving platen is driven by a computer controlled stepper motor; the rate of closure can be varied so that the maximum stress in the fiber loop changes at a constant rate. Fiber failure is sensed by an acoustic transducer which signals the computer to stop the moving platen and record the platen separation at failure. The stress at failure is calculated from the platen separation, the elastic modulus of the glass, and the dimensions of the fiber. Because the effective gage length is very small<sup>14</sup>, the probability of measuring a fiber sample containing a large flaw is very small, so the test results tend to be uniform and unimodal. Bending tests were conducted at a range of stress rates (9, 0.9, 0.09, and 0.009 ksi/sec) so that the dynamic fatigue behavior of the fibers could be characterized. The experiments were conducted in a laboratory environment of 23° C and relative humidity of 50%. For each case and stress rate 21 samples were tested.

**Stripping Test** - The force required to strip the coating is measured using a commercial stripping tool mounted on a screw-driven universal tensile testing machine. The gage length of the stripped section was 1.2 inches and the test was conducted at the rate of 20 in/min. The experiments were conducted in a laboratory environment of 23° C and relative humidity of 50%. We tested 51 samples from each layer (1-4) of the cable.

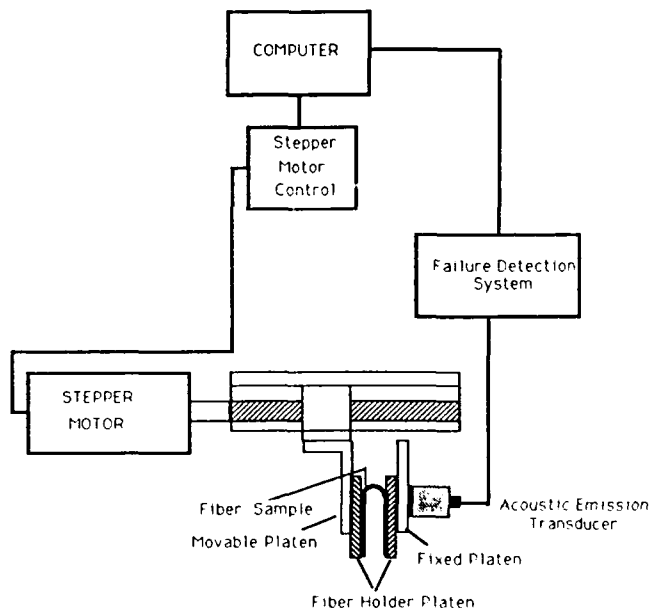


Figure 1 - Schematic of Two-Point Bending Fiber Strength Testing Apparatus

**Surface Roughness Measurements** - A commercially available AFM was used to examine the surfaces of the aged and unaged fibers at magnifications up to one million times. The AFM allowed us to make direct observations of any surface imperfection caused by aging. The AFM has a very sharp tip, a few atoms wide at the end, attached to a micro-cantilever arm (Figure 2) that is on the order of 100-200 microns long. The tip is brought into contact with a sample and is scanned across the surface, usually in a raster pattern. The deflection of the cantilever is monitored as the tip is scanned. The deflection signal is used in a feedback loop similar to the way the tunneling current is used in an STM. In our unit, the scanning is accomplished with a piezoelectric tube scanner. The data can be acquired by measuring the cantilever deflection signal as the tip is scanned, or by adjusting height of the sample using feedback to maintain a constant cantilever deflection signal. In our AFM, the deflection signal is produced by focusing the output of a laser diode to a spot on the back side of the cantilever and measuring the reflected light from this spot with a photodiode. The polymer coating on the fiber was removed before AFM examination by dipping the fiber briefly in hot (200° C) sulfuric acid and rinsing in distilled water. In order to insure representative results, a number of samples from each layer were used. Each sample was also examined with at least two different AFM tips, minimizing the possibility of misinterpreting tip-induced artifacts in the images.

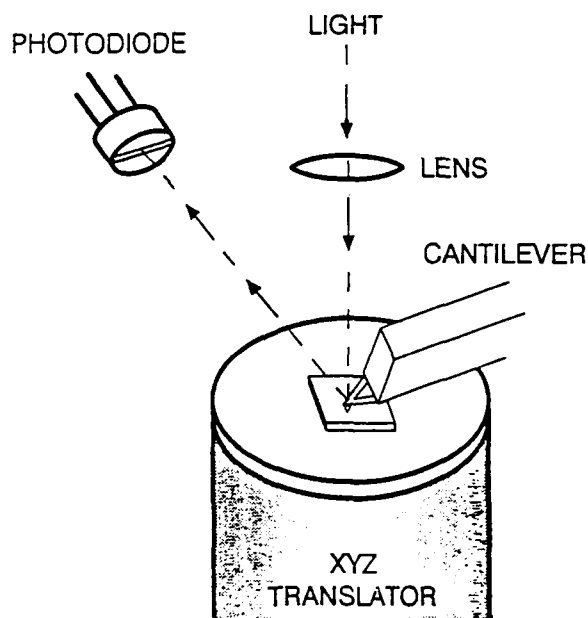


Figure 2 - Schematic of the Atomic Force Microscope

## 2.3.2.2 Results and Discussions

### Dynamic Strength

The strength data for tension and two-point bending plotted in Figures 3 and 4 show a good fit to a Weibull distribution of the form:

$$F = 1 - e^{-(\sigma/\sigma_0)^m}$$

In this equation F is the cumulative probability of failure at a stress less than or equal to  $\sigma$ ;  $\sigma_0$  and m are empirical distribution parameters. The values of the Weibull exponent  $m_d$  and the median strength for both tension and two-point bending tests are obtained from the appropriate Weibull relationship where  $F=0.5$  and are summarized in Table 1. As observed in Figures 3 and 4 and Table 1, fiber strength decreased towards the outer cable layer. The differential decrease in strength of the fibers appears to be correlated to the severity of environmental exposure. As shown in an earlier study<sup>15</sup>, the outer layers of cable on the reel were probably exposed to higher temperatures than the lower layers which obviously influenced the trends of strength reduction shown in Figures 3 and 4. Since the gage length of tensile strength tests is ~500 times greater than 2 point bending tests (25 cm versus less than 0.05 cm), tensile strength results were lower than the two-point bending strength results. But still, in comparing strength distributions of samples of different gage lengths, Figure 3 (tension) and Figure 4 (two-point bending) show that similar strength reductions are present.

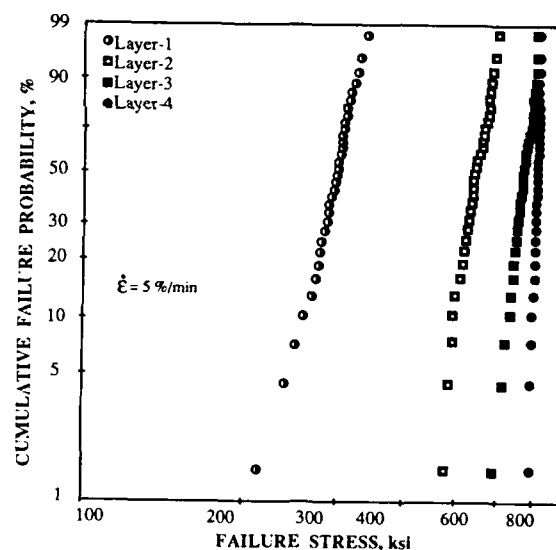


Figure 3 - Weibull Strength (Tension) Distribution

Table 1 - Summary of Strength Tests

LOCATION OF FIBERS IN THE CABLE	MEDIAN TENSILE STRENGTH, ksi	$m_d$	MEDIAN TWO-POINT BENDING STRENGTH, ksi	$m_d$
Layer-1	289	9	326	14
Layer-2	515	11	551	23
Layer-3	631	20	682	37
Layer-4	675	32	707	54

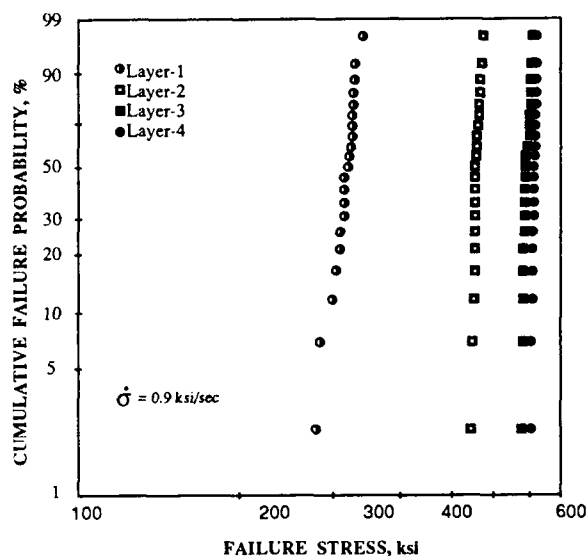


Figure 4 - Two-Point Bending Weibull Strength Distribution

#### Dynamic (Two-point Bending) Fatigue

Table 2 summarizes dynamic fatigue (two-point bending) results for fiber samples, taken from different layers of the cable. If it is assumed that the rate of growth of flaws in the presence of stress depends upon the stress intensity factor at the tip of the flaws raised to a power  $n$ , then it can be shown<sup>16</sup> that the failure stress is related to the rate of stressing  $\dot{\sigma}$  by:

$$\sigma = B \dot{\sigma}^{\frac{1}{n_d + 1}}$$

where  $n_d$  is the crack growth exponent associated with the power law dependence of the crack growth rate and  $B$  is an experimental parameter. The effects of aging conditions on the values of  $n_d$  are well documented.<sup>16,21</sup> In this study, we observed an increase in  $n_d$  associated with excessive aging conditions (Layers-1, 2). This result also suggests<sup>9</sup> that the fiber samples taken from the outermost layers (Layers-1, 2) of cable aged more than inner cable layers (Layers-4, 5...etc).

Table 2 - Summary of Dynamic Fatigue [Two-Point Bending] Tests

LOCATION OF FIBERS IN THE CABLE	FATIGUE PARAMETER $n_d$
Layer-1	23.0
Layer-2	21.7
Layer-3	20.9
Layer-4	21.2

#### Coating Behavior

The coating stripping test was performed on fiber samples from each layer of the cable. The results for strip force is shown in Table 3. We again observed some sign of degradation in coating adhesion with respect to fiber location which we also attribute to the effect of temperature. Coating strip force for outer layer aged fibers showed higher variation in distribution and lower values than lower layer samples.

#### Glass Behavior

A series of AFM images of aged fibers, at various layers on the cable reel, are shown in Figures 5-8. Figure 5 shows a typical roughness observed on the surface fibers aged inside Layer-1 of the cable. The surface of aged fibers in Layer-1 can be characterized as having developed pits ~10-65 nm<sup>1</sup> across with an amplitude of ~10-60 nm. In contrast, the surface of the fiber at Layer-4 (Figure 8) showed a corrugation amplitude of ~0.1-1 nm with features 0.2-1.5 nm across. Figures 6 and 7 show surface profiles of the fibers aged in Layer-2 and Layer-3 of cable. The degree of surface roughness of the aged fibers is consistent with the strength results<sup>22,24</sup>. The roughness of the fibers increased with increasing exposure to the hostile environment, with the most dramatic roughening occurring in the fiber samples that aged inside Layer-1 (outermost layer). Images of fibers aged inside Layer-4, Layer-5... etc. were similar. The relative surface roughness can be put on a more quantitative basis, as given in Table 4, by measuring the maximum value of flaw depth obtained from the AFM.

Table 3 - Summary of Coating Strip Force

LOCATION OF FIBERS IN THE CABLE	MEDIAN STRIP FORCE, LB <sub>f</sub>	MIN. STRIP FORCE, LB <sub>f</sub>	MAX. STRIP FORCE, LB <sub>f</sub>
Layer-1	0.62	0.12	1.02
Layer-2	0.84	0.38	1.16
Layer-3	0.81	0.65	1.09
Layer-4	0.90	0.71	1.20

<sup>1</sup> 1 nm = 10<sup>-7</sup> cm = 3.94x10<sup>-8</sup> inches.

**Table 4 - Summary of Maximum Value of Surface Roughness Height Obtained from the AFM Measurements**

LOCATION OF FIBERS IN THE CABLE	ROUGHNESS HEIGHT nm
Layer-1	59.5
Layer-2	13.2
Layer-3	2.6
Layer-4	1.1

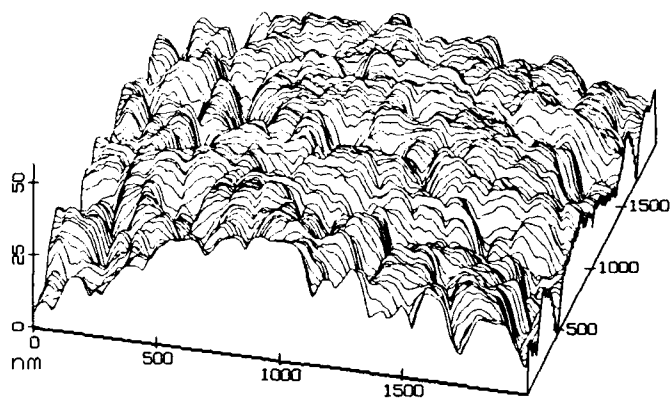


Figure 5 - A typical AFM Image Observed on the Surface Fibers Aged Inside Layer-1

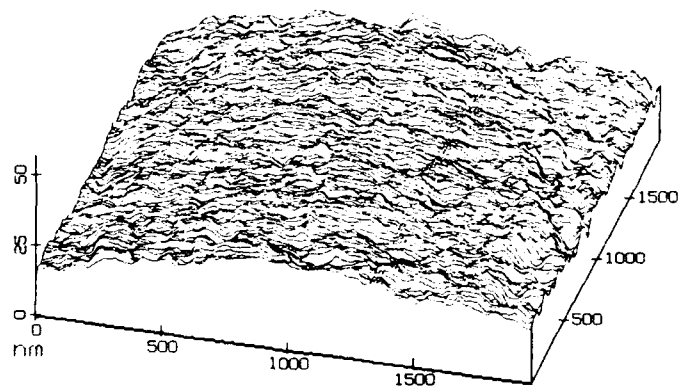


Figure 6 - A typical AFM Image Observed on the Surface Fibers Aged Inside Layer-2

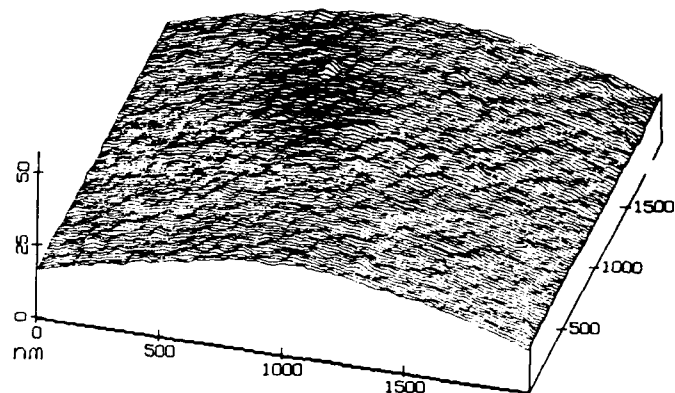


Figure 7 - A typical AFM Image Observed on the Surface Fibers Aged Inside Layer-3

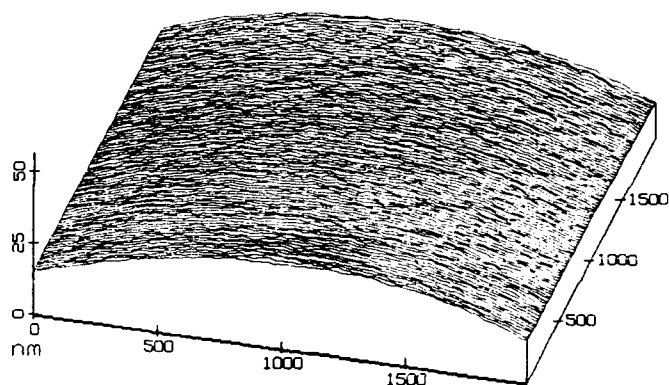


Figure 8 - A typical AFM Image Observed on the Surface Fibers Aged Inside Layer-4

### 3. CONCLUSIONS

Although no significant changes to the outer cable jacket were observed, significant changes in fiber strength, fatigue resistance, coating adhesion and surface roughness were observed on the fiber samples removed from first or outermost layer of the cable. The results obtained from the fiber analysis agree with the results of earlier studies<sup>22,24</sup> showing that the fibers in the cable were exposed to extreme environmental conditions for long periods of time. The fiber surface roughness decreased in amplitude, both vertically and laterally, for each layer removed from the outermost cable layer, consistent with earlier predictions<sup>22,24</sup>. The strength degradation was a direct result of the absence of a thermal wrap protection on the cable reel, since outer layers were exposed to greater temperature rise<sup>15</sup>. This thermal wrap material is designed to limit solar heating of the cable to within 10° C of the ambient temperature. Bellcore recommends that all cables stored on reels outdoors be wrapped with a thermal wrap material meeting the requirements of TR-TSY-000020, *Generic Requirements for Optical Fiber and Optical Fiber Cable*.



## REFERENCES

1. J. Kilmer et. al., *Proc of SPIE 1366*, 85-91 (1990).
2. F.V. DiMarcello et al., *Optical Fiber Communications*, I, T. Li, Ed., Academic Press, Orlando, FL 179(1985).
3. T.T. Wang, H.M. Zupko, *J. Mater. Sci.* **13**, 2241(1978).
4. J.T. Krause, C.J. Shute, *Adv. Ceram. Mater.* **3**, 118(1988).
5. M.J. Matthewson, C.J. Kurkjian, *J. Amer. Ceram. Soc.* **71**, 171 (1988).
6. C.J. Kurkjian et al., *J. Lightwave Tech.* **7**, 1360(1989).
7. H.C. Chandan, S.C. Perry, *J. Amer. Ceram. Soc.* **68**, C90(1985).
8. H.H. Yuce et al., *Proc. SPIE 992*, 211 (1988).
9. H.H. Yuce et. al., *Proc. SPIE 1174*, 279 (1989).
10. S. M. Wiederhorn, *J. Non-Cryst. Solids* **19** 169(1975).
11. T. A. Michalske, S. W. Freimen, *J. Am. Ceram. Soc.*, **66** [4] 284(1983).
12. B.K. Tariyal, D. Kalish, Glass Div., Fall Mtg. Am. Ceram. Soc., Paper 8-CG-77F (1977).
13. H. H. Yuce, et.al., *Proc. Seventh Int. Conf. on Integrated Optics* **2** 44(1989).
14. M. J. Matthewson and C. R. Kurkjian, *J. Am. Ceram. Soc.*, **69** [11] 815(1986).
15. T.M. Bowmer, *Proc. 39th IWCS*, 335(1990).
16. A. G. Evans, *Int J of Fract Mech.* **10**, 251(1974).
17. D. Roberts, et. al., *Proc. SPIE 842*, 32(1988).
18. W.J. Duncan, et. al., *Strength of Inorganic Glass*, C.R. Kurkjian, Ed., Plenum Press, New York 309(1985).
19. S. Sakaguchi and T. Kimura, *J. Amer. Ceram. Soc.* **64**, 259(1981).
20. J. E. Ritter, et al., *J. Amer. Ceram. Soc.* **71**, 988-992 (1988).
21. R.D. Maurer, in *Strength of Inorganic Glass*, C. R. Kurkjian, Ed., Plenum Press, New York, 291 (1985).
22. H.H. Yuce et. al., OFC '90 Postdeadline Paper, Paper PD14 (1990).
23. R.S. Robinson and H.H. Yuce, *J. Am. Ceram. Soc.*, **74** [4] 814(1991).
24. H. H. Yuce et. al., to be published in *Trans of Am. Ceram. Soc.*, 1990 *Glass Fall Meeting*, Orlando, FL., (November, 1990).



**Hakan H. Yuce** is a member of the Technical staff in the Fiber Distribution and Reliability Research District at Bellcore. He leads a research program dealing with long-term mechanical reliability of optical fibers and interconnections. Hakan provides technical input and support to organizations responsible for generic requirements and responds to clients' immediate needs related to consultation on reliability and field failures. He also plays an active role in the standards arena under EIA/TIA working committees 6.6.7, fiber coatings and 6.6.8, fiber reliability. Hakan has a B.S. degree in Mechanical Engineering from Technical University of Istanbul [1977], an M.S. in Mechanical Engineering from M.I.T. [1982] and a Ph.D degree in Mechanical Engineering and Material Science from Stanford University [1987].



**Casey J. Wieczorek** is a member of the Optical Cable Group in Bellcore, Morristown, NJ. He joined Western Electric in 1967 and worked on various cable designs and manufacturing processes. He is currently responsible for the development of generic requirements and test procedures for optical cables. He holds a B. S. degree in Mechanical Engineering from Fairleigh Dickinson University and did graduate work at Stevens Institute of Technology.

**Anthony DeVito** joined Bellcore's Optical Cable District, as a Member of Technical Staff, July of 1988. He is currently involved in post-mortem analysis and writing generic requirements for optical fiber cables. Prior to joining Bellcore he worked as a member of the Transmission Product Evaluation Staff at Bell South Services in Birmingham, Alabama. His responsibilities included the technical analysis of fiber optic splicing equipment, test sets and optical cables. He has 18 years experience with the Bell Operating Companies in the area of Outside Plant Construction, Construction Methods, and Fiber Cable Installation and Testing.



**John P. Varachi, Jr., P.E.**, received the BSME degree from Fairleigh Dickinson University, Rutherford, N.J. in 1976 and the MSME degree from Polytechnic Institute of New York, Brooklyn, N.Y. in 1978. He is currently District Manager, "Fiber Distribution and Reliability Research" at Bellcore. From 1969 through 1983 he was engaged in exploratory development at Bell Laboratories in mechanical design and analysis for telephone central office and outside plant apparatus. He also performed physical design and systems engineering for copper and optical fiber based digital loop electronic systems for outside plant and customer premises applications.



**Dr. Joyce Kilmer** received his Ph.D. in Electrical Engineering from the University of Florida and joined Bellcore as a Member Technical Staff of the Optical Cables District in the Fiber Optic Technology Division in 1984. In 1988, he was temporarily reassigned to Fiber Optic Systems District to study the effects of reflections on fiber optic system performance. In 1989, he was promoted to District Manager of the Optical Connector, Splicing and Closures District. In 1990, he was reassigned to District Manager of the Optical Cables and Distribution Terminals/Closures District. In this capacity he is responsible for writing generic requirements, performing product and post-mortem analyses, and developing long term reliability testing of optical fiber, optical fiber cable, and distribution terminals for Fiber-in-the-Loop (FITL).

## SINGLE-FIBER CABLE ASSEMBLIES FOR TACTICAL APPLICATIONS

B. V. Darden, K. Katherisan, and B. G. LeFevre  
AT&T Bell Laboratories, Norcross, GA 30071

J. B. Fluevog  
AT&T Network Cable Systems, Norcross, GA 30071

V. E. Kalomiris  
U. S. Army CECOM, Ft. Monmouth, NJ 07703

### ABSTRACT

Single-fiber cable assemblies with a small hermaphroditic connector have been designed for use in tactical fiber-optic communications systems and robotic vehicle applications. The assemblies are intended for use wherever bi-directional transmission is required and are designed to operate while meeting environmental and mechanical conditions typically encountered in tactical applications. Both multimode and single-mode versions were developed with 2.5 and 4.0 mm diameter cables. A completed assembly consists of a 1-km all-dielectric cable with a tightly-buffered radiation-hardened fiber terminated with hermaphroditic ST® connectors. Prototype samples measured at 1300 nm show an average insertion loss of less than 1.5 and 1.0 dB for multimode and single-mode respectively and a loss change of less than 1.0 (MM) and 0.5 (SM) when subjected to thermal cycling, temperature/humidity cycling, high and low storage temperature extremes and low-pressure altitude exposure.

### 1.0 INTRODUCTION

For many tactical fiber optic communications systems and tethered or robotic applications, bi-directional transmission over a single optical fiber is required. AT&T has developed a class of single-fiber (simplex) cable assemblies for both multimode and single-mode applications under design criteria similar to that of the two-fiber Tactical Fiber Optic Cable Assembly (TFOCA) previously developed for the U. S. Army CECOM (1). Several features of the successful TFOCA units have been incorporated into the simplex designs with two important distinctions: The cables are smaller (2.0 and 4.0 mm vs. 6.0); the connector employs ST® technology rather than biconic. These and other features of the cable assemblies, along with performance testing results, will be described in this paper.

### 2.0 BACKGROUND

Successful deployment of tactical communications systems requires high reliability, consistent

performance and expedient field repair. Fiber optic technology has been developed to these standards and has been widely accepted because of significant advantages such as elimination of electromagnetic interference and pulse susceptibility, elimination of problems associated with multi-ground circuits, and high resistance to radiation effects.

The single-fiber cable assemblies developed in this work are appropriate for many tactical applications including radar remoting, radio remoting, and various robotic systems. They meet the critical requirements of ease of deployment, field cleanability, durability, consistent performance, and cost competitiveness.

### 3.0 CABLE ASSEMBLY DESIGN

The cable assemblies consist of 1-km of multimode or single-mode all-dielectric cable (each at 2.5 or 4.0 mm diameter) terminated with small hermaphroditic ST® (HST) connectors. Each cable contains a single tightly-buffered radiation hard fiber. The multimode units are operational at 850 or 1300 nm and the single-mode at 1300 or 1550. They are designed for an operating temperature range of -46° to 71°C and storage temperature extremes of -57° to 85°C.

The design and performance of the cable and connector components will be discussed in the following sections before presenting the results from complete assembly samples.

#### 3.1 SINGLE-FIBER CABLES

The cross-sectional view of the four cable designs are given in Figure 1. The fibers have dual acrylate coatings and are tightly buffered with a 0.9 mm O.D. polyester elastomer. Both the coating and the buffer are mechanically strippable, a feature which facilitates repair and connector termination. Aramid yarns are stranded over the buffered fiber and function as the tensile-load carrying members. Appropriate amounts of yarn are used to attain 270 and 1350 N ratings for the 2.5 and 4.0 mm cables, respectively. A flame-retardant polyurethane outer jacket is extruded over the outer jacket. The average weights for the cables are less than 5.6 kg/km for the 2.5 mm cables and less than 12.8 for the 4.0 mm. The cables exhibit less than 2.0%

elongation at 270 and 1350 N.

Cable samples of the above type have been subjected to a series of environmental and mechanical tests to determine field worthiness as discussed in a previous publication (2). The samples passed the performance criteria detailed in reference (3). Selected performance values are given below.

The attenuation rate for multimode cables was less than 3.5 dB/km at 850 nm and less than 1.25 dB/km at 1300 nm. The two primary environmental tests are temperature and accelerated aging. The cables were evaluated for the extended temperature cycling range of -55° to 85°C (5 cycles) and accelerated aging conditions of 110°C for 10 days. Multimode cables showed less than 0.5 dB increase in attenuation at 850 and 1300 nm and single-mode cables less than 0.3 at 1300 and 1550 nm. Other environmental tests included ice crush and radiant heat. Mechanical tests included operating tensile load (180 and 300 N), cold bend, impact, knot, compression, cyclic flexing, twist bend, and corner bend. The cables showed less than 0.5 dB attenuation increase for the knot and corner bend tests and less than 0.2 dB for the remaining tests.

### 3.2 CONNECTOR

The simplex HST connector is shown in Figure 2. It is 8.6 cm long by 1.4 cm in diameter and weighs less than 30 grams with dust cover. It is a true hermaphroditic unit, hence any cable end can be mated with any other or with a companion bulkhead receptacle. It employs ST® connector technology whereas the duplex TFOCA units employ biconic components. The key alignment components are a ceramic ferrule on which is mounted a close-fitting bifurcated sleeve so that two similarly equipped ferrules can be mated. The sleeve acts as an alignment mechanism and provides the hermaphroditic feature.

Other design features of the HST connector are: Cable retention hardware not requiring adhesives, waterproofing seals, modified coupling threads for strength and easy engagement, a corrosion-resistant finish, materials selected for strength and EMI shielding effectiveness, and a configuration for easy field cleaning. Samples have been tested to the requirements of field ruggedness per CECOM contract No. DAAB07-85-C-K556 as detailed in previous publications (4, 5). Selected performance values are summarized here.

The connection loss of SM HST units averaged 0.44 dB with a standard deviation of 0.27 dB. For MM the average and sigma were 0.50 and 0.30. During thermal cycling (-46° to 71°C), high temperature exposure (85°C), low temperature exposure (-55°C), thermal shock (-57° to 71°C), water immersion, humidity, dust, and mud (cleanability), the maximum loss change was 0.25 dB. The connector/cable interface was tested by twisting (1000), flexing (3000) and tension (cable

retention and strength of mated pair to 1335 N) with loss increases of less than 0.2 dB. Other mechanical tests include shock, shock drop, vibration and mating durability (1000 times). Again the maximum loss increases were less than 0.2 dB.

### 3.3 CABLE ASSEMBLY PERFORMANCE

Four samples each of the 1-km MM and SM cable assemblies with 2.5 and 4.0 mm diameter cables were tested for insertion loss and environmental performance to the requirements and in the sequence shown below. All measurements were made at 1300 nm using either a laser or LED source.

**TABLE 1 - CABLE ASSEMBLY TEST CONDITIONS**

Test	Conditions
Insertion Loss	Concatenation (FOTP 171)
Thermal Cycle	-46° to 71°C, 5 cycles
Humidity	65° to 30° to 20°C at 94% RH, 5 Cycles
Storage Temp	-57° and 85°C, 240 hrs. ea.
Altitude	10,000 ft. operating 40,000 ft. non-operating

**TABLE 2. TEST SEQUENCE**

Test	Assembly Type			
	MM		SM	
	2.5	4.0	2.5	4.0
Insertion Loss	4	4	4	4
Temperature Cycle	4	4	4	4
Humidity	2	-	2	2
Storage Temp	2	2	2	2
Altitude	2	-	2	2

#### Insertion Loss:

Insertion loss measurements from the samples of Table 1 gave mean and sigma values of 1.56 and 0.56 for the 8 MM cable assemblies and 0.85 and 0.38 for SM. No

distinction was made between the two different cable sizes when randomly selecting samples for the eight-cable concatenation measurements. In addition to these values concatenation measurements were made on a separate group of 6 MM and 14 SM 4.0 mm deliverable cable assemblies under the CECOM contract. Those averages were 1.23 and 0.78 dB respectively with sigma values of 0.34 and 0.33. See Figures 3 and 4.

#### Environmental Tests:

The results of the thermal cycle tests are given in figures 5 and 6. In each case the curves represent the average values for the samples tested. For the MM case two of the original samples (one each of the 2.5 and 4.0) were excluded from the data because of two sources of error. In one sample a fiber break inside a connector ferrule was traced to an incorrect fiber stripping and insertion procedure. In another the sample showed an early large decrease in attenuation (improvement) due to incomplete seating of the test lead adaptor cables at the start of the test. The average change was less than 1.0 dB for MM and 0.5 for SM. The results of the humidity test are shown in figures 7 and 8. The average change was less than 0.6 dB for MM and 0.2 for SM. The results for the storage temperature and altitude tests are not shown in graph form; however, the loss changes were less than 0.5 dB for both MM and SM.

#### 4.0 CONCLUSIONS

The simplex cable assemblies described herein meet the requirements for tactical applications as prescribed by U. S. Army CECOM. The assemblies are light-weight, rugged, easy to deploy, and readily maintained.

#### 5.0 ACKNOWLEDGEMENTS

The authors acknowledge the help of I.L. Pennington, R. L. Sweatt, I. Rapaport, G. A. Sandels and J. A. Edmondson for sample preparation and testing.

#### REFERENCES

1. B. V. Darden, K. Kathiresan, B. G. LeFevre, J. B. Fluevog and V. E. Kalomiris, "Single and Multimode Tactical Cable Assemblies," Proceedings of 38th International Wire and Cable Symposium, pp 648-657, Atlanta, November 1989.
2. K. Kathiresan, L. C. Hotchkiss, S. P. Gentry, J. F. Fluevog and V. E. Kalomiris, "Single-Fiber Tactical Cables For Single-Mode and Multimode Systems," Proceedings of 37th International Wire and Cable Symposium, pp 608-617, Reno, Nevada, November 1988.
3. "Single-Fiber Optical Cable Assemblies (SFOCA)," U. S. Army CECOM Contract No. DAAB07-85-C-K556.
4. B. V. Darden, B. G. LeFevre, and V. E. Kalomiris, "Hermaphroditic Small Tactical Connector for Single-Fiber Applications," SPIE International Symposium and Exhibition on Optical Engineering and Photonics, Orlando, Florida, April 1991.
5. B. V. Darden, B. G. LeFevre, and V. E. Kalomiris, "Hermaphroditic Small Tactical Connector for Single-Fiber Applications," 1991 IEEE Communications Theory Workshop, Rhodes, Greece, July 5, 1991.

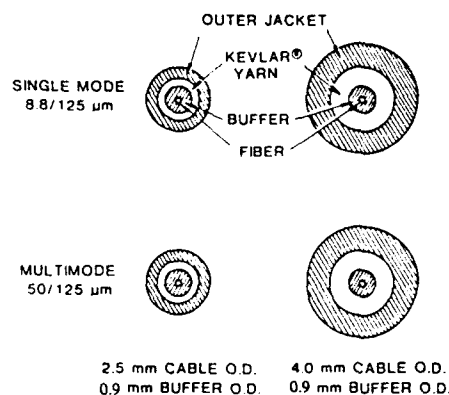


Figure 1. Single-Fiber Optical Cable Designs

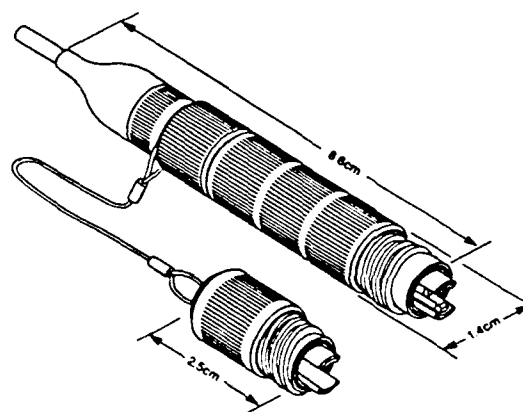


Figure 2. Hermaphroditic Simplex Connector

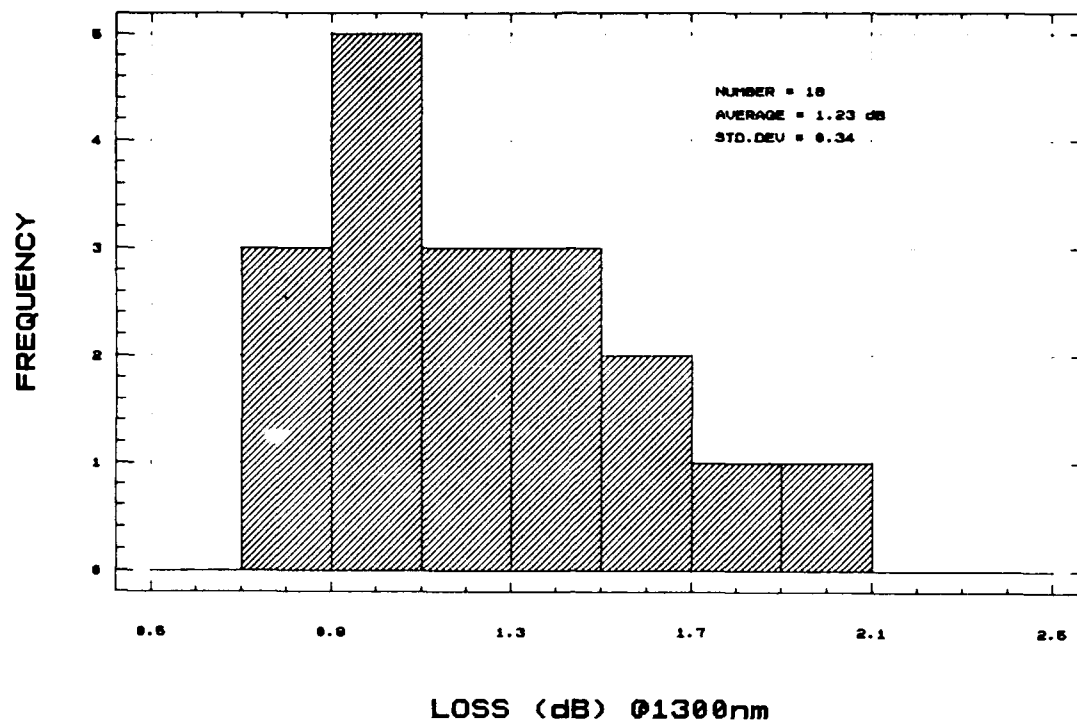


Figure 3. Multimode Insertion Loss, 4.0 mm Deliverables

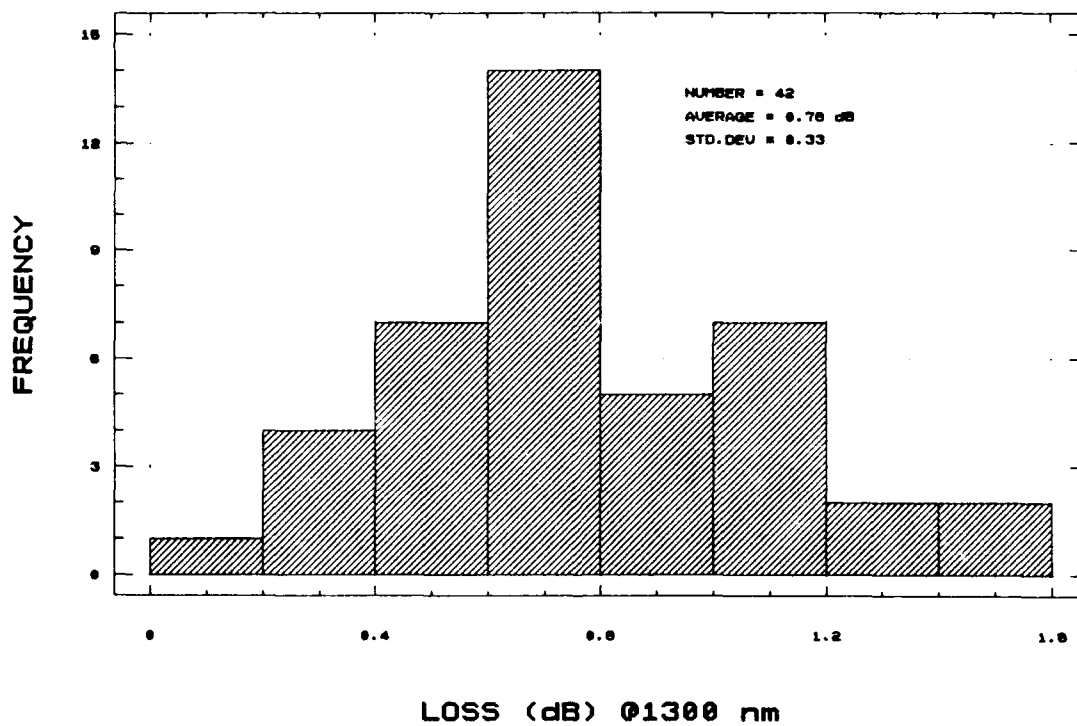


Figure 4. Single-Mode Insertion Loss, 4.0 mm Deliverables

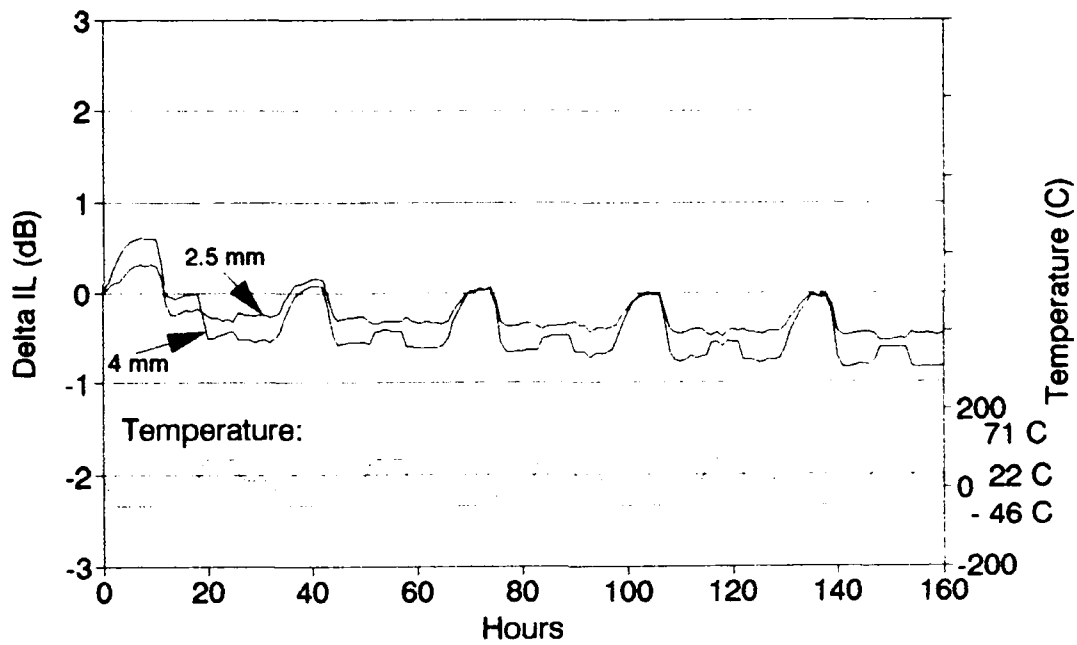


Figure 5. Multimode Thermal Cycle Results

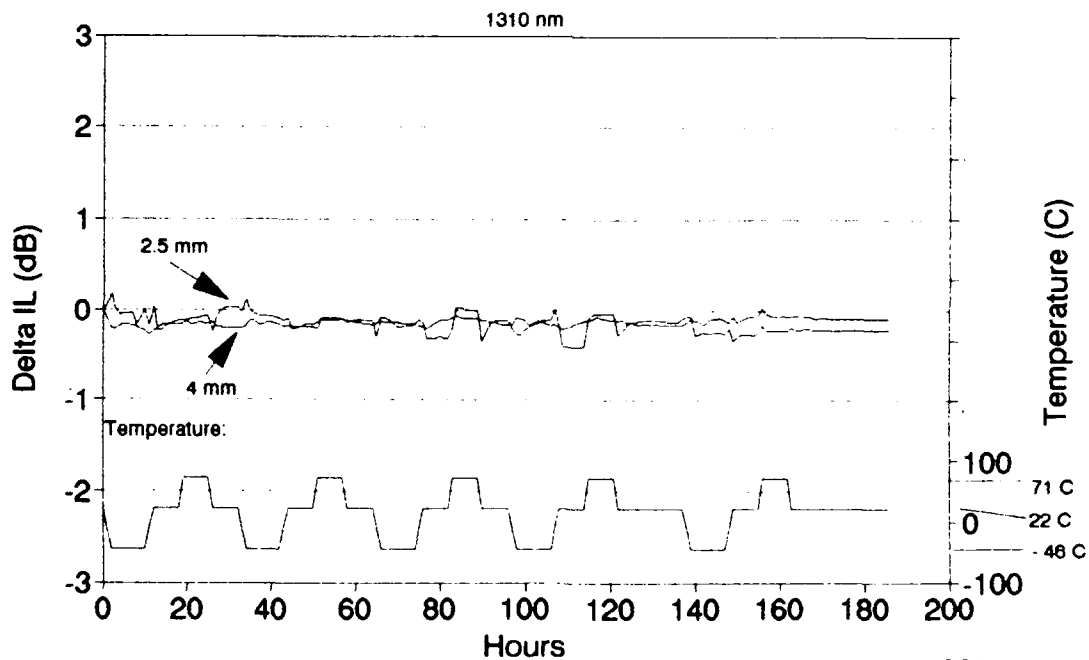


Figure 6. Single-Mode Thermal Cycle Results

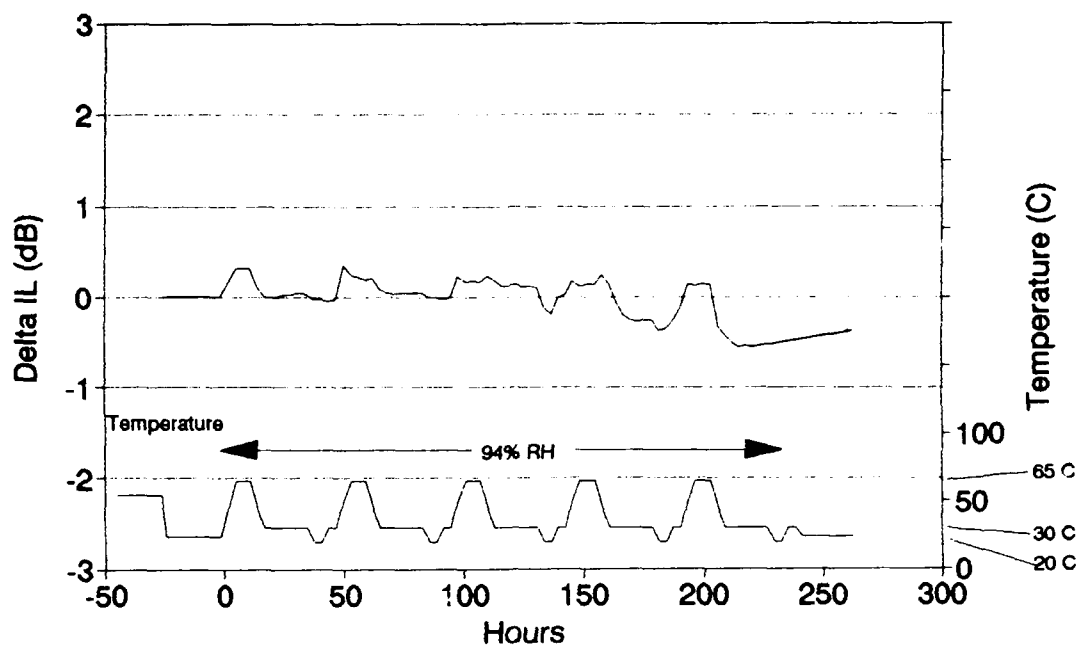


Figure 7. Multimode Humidity Results

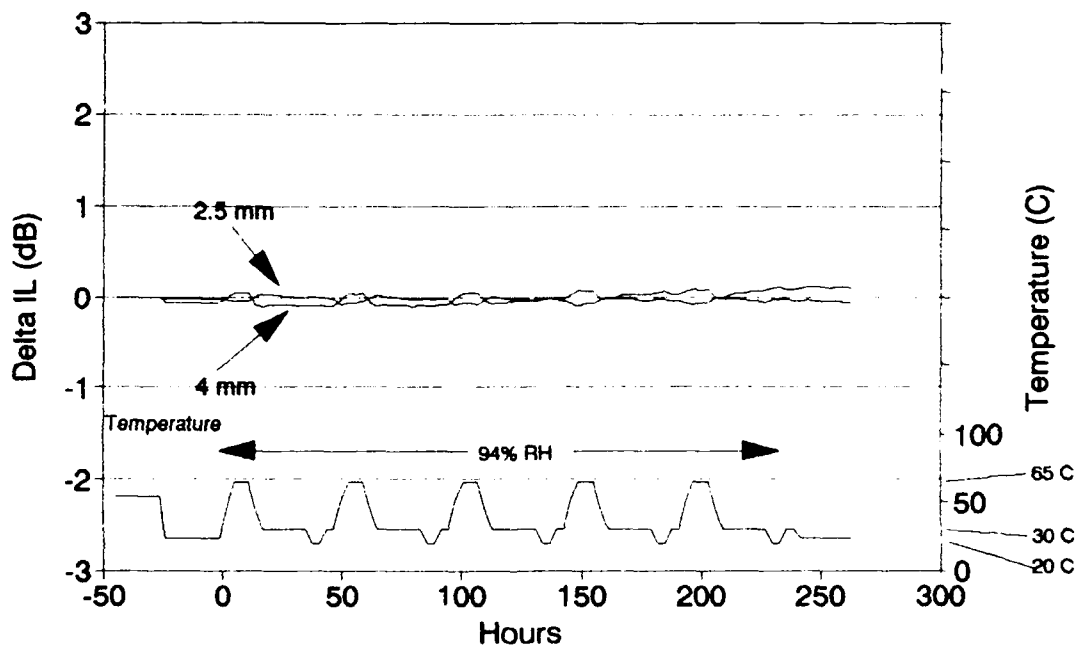


Figure 8. Single-Mode Humidity Results



**B. V. DARDEN** is a member of Technical Staff at AT&T Bell Laboratories, Norcross, Georgia. He received a B. S. degree in Engineering from North Carolina State University in 1951, and held engineering positions with Western Electric until 1960 when he joined AT&T Bell Laboratories. He is currently a member of the Connector System Development Group.



**KRIS KATHIRESAN** is a Member of Technical Staff in the Lightguide Technology Department at AT&T Bell Laboratories in Norcross, Georgia. He is responsible for the design and development of specialty cables, including military applications.

Dr. Kathiresan joined AT&T Bell Laboratories in 1985. He has a B. E. Hons in Mechanical Engineering from University of Madras, India, an M. E. in Aerospace Engineering from Indian Institute of Science, India, and a Ph. D. in Engineering Science and Mechanics from Georgia Institute of Technology, Atlanta, Georgia.

Dr. Kathiresan is a Senior Member of American Institute of Aeronautics and Astronautics and a Member of American Society of Mechanical Engineers. He is a registered Professional Engineer (Mechanical) in States of Georgia and Florida.



**BRUCE G. LeFEVRE** is a Member of Technical Staff at AT&T Bell Laboratories, Norcross, Georgia. He received his B. S. (Colorado School of Mines) and Ph. D. (University of Florida) in Physical Metallurgy. He joined AT&T Bell Laboratories in 1976 after ten years on the faculty of Georgia Institute of Technology. He has been involved in the study of metals and alloys used in the manufacture of cables and connectors, and is currently working with fiber-optic connectors and cable assemblies.



**JILL B. FLUEVOG** is a Development Engineer in the Lightguide Cable Engineering Department at AT&T Network Systems, Norcross, Georgia. She joined AT&T in 1985 after receiving a Bachelors Degree in Chemical Engineering from Georgia Institute of Technology. She is responsible for the development of lightguide cable products and processes for military applications. Ms. Fluevog is a member of American Institute of Chemical Engineers, Institute of Electrical and Electronics Engineers and Society of Plastic Engineers.



**VASILIOS E. KALOMIRIS** is Chief Scientific Advisor for Local Area Division at CECOM's Center for Command Control and Communications. Previously he was the branch chief for Local Area Networks and Fiber Optics. He joined the U. S. Army CECOM eleven years ago. Prior to joining CECOM he was employed by ITT-EOPD as a Project Engineer responsible for the design and development of various fiber optic cable systems. One of his projects was the design and development of the first air-layable fiber optic cable. He also worked for General Cable Corporation R&D as a Optic Research Engineer involved with the design, development and manufacture of a prototype super conductive power cable with flexible core. Vasilios holds three patents in fiber optic connector design.

Education: Vasilios has a B. A. in Mathematics, B. S. in Electrical Engineering, and M. S. in Electrical Engineering, all from New York University, and an M. B. A. from Fairleigh Dickinson University. He is a member of AFCEA, IEEE and the Technical Chamber of Greece (Society of Professional Engineers). He received the 3rd Annual Engineering Excellence Award for 1986 from CECOM, served for three years as chairman of the Tri-Service Group on fibers, cables and connectors, currently is chairing the point to point systems group.

## SINGLE FIBER TACTICAL CABLES WITH MULTIPLE FIBER DESIGNS

J. B. Fluevog and W. H. Ficke, AT&T Network Cable Systems, Norcross, Georgia 30071, U.S.A.

W. S. Liu and K. Kathiresan, AT&T Bell Laboratories, Norcross, Georgia 30071, U.S.A.

### ABSTRACT

The design and development of three all-dielectric single fiber cables for use in tactical fiber optic communication systems have been completed. These cables were developed to meet the stringent optical, mechanical, and environmental requirements typical of tactical applications. The development effort was guided by the detailed performance criteria given in the Military Specification, DOD-C-85045C, "General Specification for Fiber Optics Cables (Metric)". The cable designs include dispersion shifted single-mode, 62.5/125  $\mu\text{m}$  radiation hardened multimode, and 100/140  $\mu\text{m}$  multimode fiber versions. The cable construction is similar to the single fiber single-mode and 50/125  $\mu\text{m}$  radiation hardened multimode tactical cables previously developed for the U.S. Army. The cables have undergone extensive environmental and mechanical testing per the military specification. Environmental tests include temperature cycling, humidity cycling, and accelerated aging. Mechanical tests include twist bend, cyclic flexing, impact, cold bend, operating tensile load, etc. The results of the optical, environmental, and mechanical performance tests are presented in this paper.

### INTRODUCTION

The design and development of single fiber optical cables for use in tactical fiber optic applications have been completed. This development effort was guided by the detailed performance criteria given in the Military Specification, DOD-C-85045C, "General Specification for Fiber Optics Cables (Metric)". The cable size is designed to be 2.5 mm in diameter for a compact and lightweight construction with a tensile rating of 270 Newtons. These cables can be used in radar remoting, robotic vehicle control/communication, and other general tactical communication system applications. The cables can be deployed either from backpack, a ground vehicle, or from a helicopter.

The cable design utilizes three fiber types. The three different fiber types are a single-mode and two sizes of multimode fibers. The single-mode cable uses a 7.0  $\mu\text{m}$  mode-field diameter dispersion shifted single-mode fiber. The multimode cable uses either a 62.5/125  $\mu\text{m}$  radiation hardened multimode fiber or a 100/140  $\mu\text{m}$  multimode fiber.

For all applications, the fibers are proof tested to 690 MPa (100 ksi). The dispersion shifted single-mode cables are optimized for operation at the 1550 nm wavelength, and the multimode cables can be operated at the 850 nm and the 1300 nm wavelength. The cables can be used in either one- or two-way transmission. The cable design should be selected based on the type of application.

The operating temperature range of these cables is  $-46^{\circ}\text{C}$  to  $71^{\circ}\text{C}$ . The design criteria for these single fiber cables are similar to those used for the single and two fiber single-mode and 50/125  $\mu\text{m}$  radiation hardened multimode tactical cables previously developed for the U.S. Army CECOM.<sup>[1]</sup> [2] [3] In the following, the design, development and performance test results for the three single fiber tactical cables described above are presented.

### CABLE DESIGN

The cross section of the cable design is given in Figure 1. The cable design is all-dielectric in construction and uses either the single-mode or multimode fiber described above. The fiber is coated with a dual acrylate coating which is mechanically strippable. The fiber is then tight-buffered to 900  $\mu\text{m}$  (.035 inch) diameter with a blue-colored polyester elastomer. The buffering material is also mechanically strippable in order to facilitate repair and connector

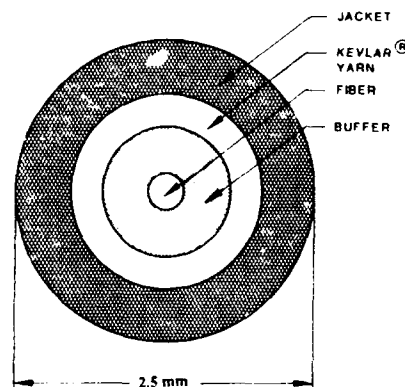


Figure 1. Cross Section of Single Fiber Optical Cable

termination in the field. The buffering material was chosen to minimize microbending losses induced by exposure of the cable to temperature extremes of  $-46^{\circ}\text{C}$  and  $71^{\circ}\text{C}$  and to meet the stringent mechanical performance requirements. Aramid yarns, which are the main tensile-load-carrying members, are stranded over the buffered fiber. Appropriate amounts of aramid yarns are used for the cable to attain the 270 N tensile rating. A flame-retardant polyurethane outer jacket is then extruded over the aramid yarn.

## PERFORMANCE

The cables were subjected to all the required optical, environmental and mechanical performance tests. The fibers were also subjected to a battery of optical, mechanical and dimensional requirements before they were used in the cables. In the following cable performance evaluation, three cable samples for each design were used for the

environmental tests. Similarly, for all of the mechanical tests, the results correspond to triplication of tests.

Before subjecting the cables to environmental and mechanical tests, an attenuation test was conducted on the finished cables. Typically the cables were manufactured in 1-km lengths. The attenuation results for the dispersion shifted single-mode cables at 1310 nm and 1550 nm, and 62.5/125  $\mu\text{m}$  radiation hardened and 100/140  $\mu\text{m}$  multimode cables at 850 nm and 1300 nm are given in Figures 2, 3, and 4, respectively. The requirement for the dispersion shifted single-mode cables is that the attenuation be  $\leq 0.5$  dB/km at 1310 nm and  $\leq 0.35$  dB/km at 1550 nm. Requirements for 62.5/125  $\mu\text{m}$  radiation hardened multimode cables are  $\leq 4.0$  dB/km at 850 nm and  $\leq 1.5$  dB/km at 1300 nm. Corresponding requirements for 100/140  $\mu\text{m}$  multimode cables are  $\leq 6.0$  dB/km at 850 nm and  $\leq 3.0$  dB/km at 1300 nm. As shown in the figures, the three cable designs meet the attenuation requirements.

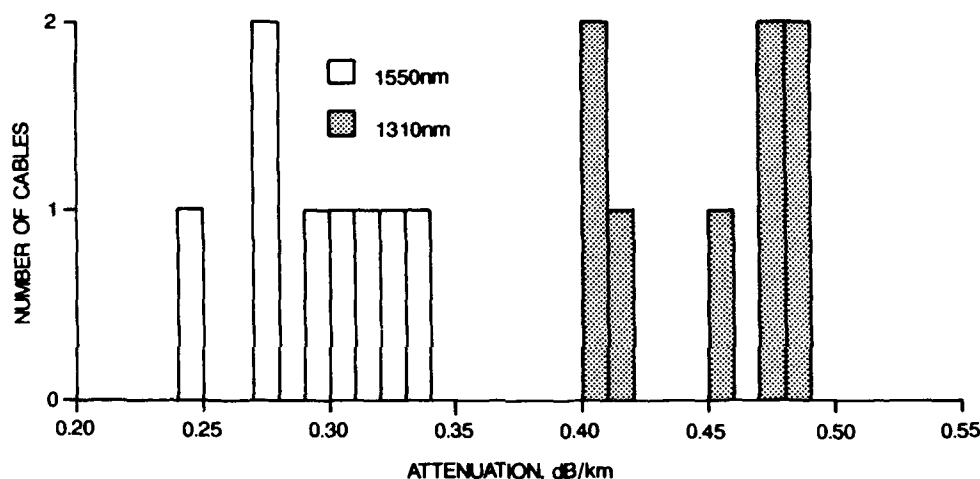


Figure 2. Dispersion Shifted Single-Mode Single Fiber Cable Attenuation

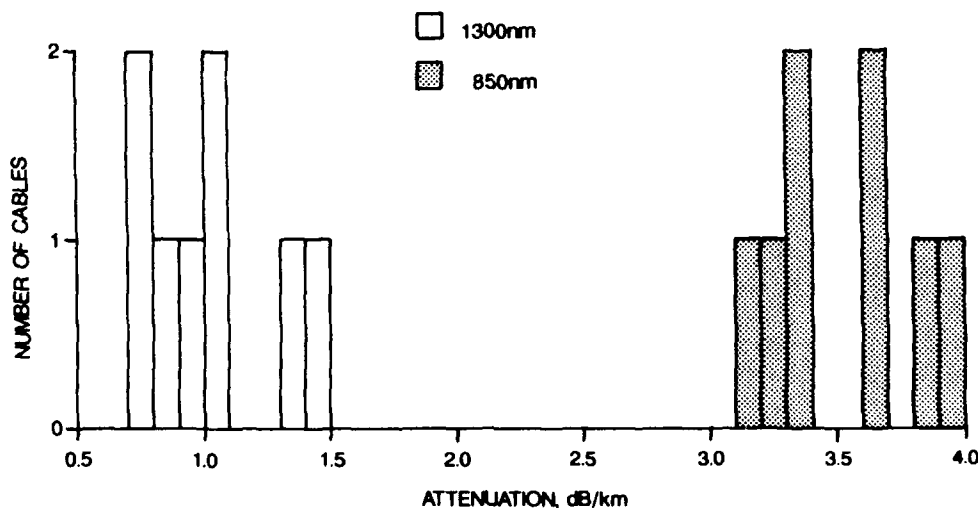


Figure 3. Radiation Hardened Multimode 62.5/125  $\mu\text{m}$  Single Fiber Cable Attenuation

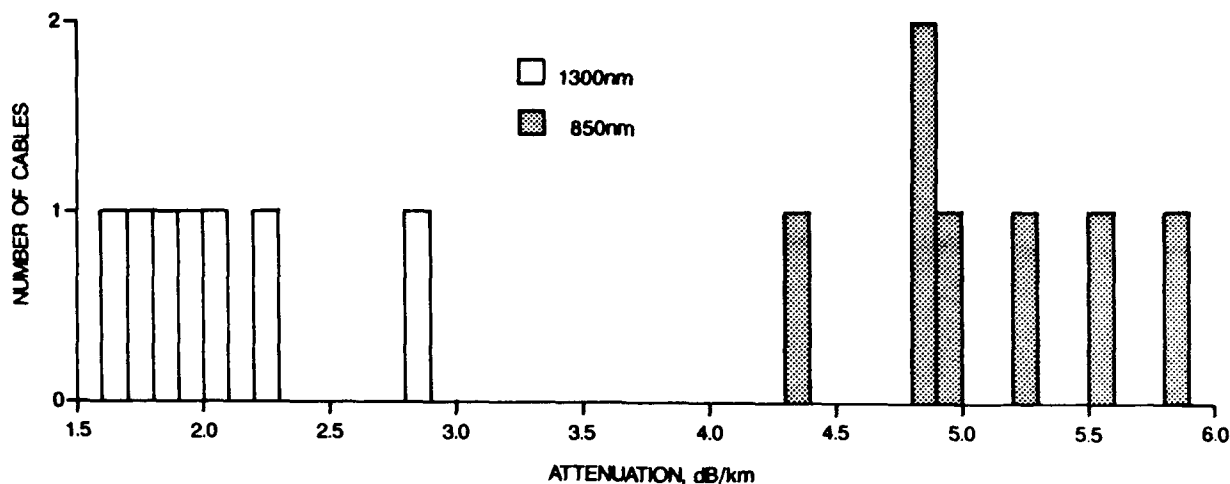


Figure 4. Multimode 100/140  $\mu$ m Single Fiber Cable Attenuation

The three primary environmental tests are temperature cycling, humidity cycling, and accelerated aging. The temperature cycle used for the cable evaluation is presented in Figure 5. The results of temperature cycling for all three cable designs are presented in Figures 6 through 8. The requirement of maximum increase in attenuation for the dispersion shifted single-mode fiber cables is 0.3 dB/km at 1310 nm and 1550 nm. For 62.5/125  $\mu$ m radiation hardened multimode fiber cables, the maximum increase in attenuation is 0.5 dB/km at 850 nm and 1300 nm. For 100/140  $\mu$ m multimode fiber cables, the maximum increase in attenuation is 1.5 dB/km at 850 nm and 1300 nm. The results are given for five temperature cycles for the temperature range of -46°C and 71°C. All cable designs pass the requirements showing excellent performance.

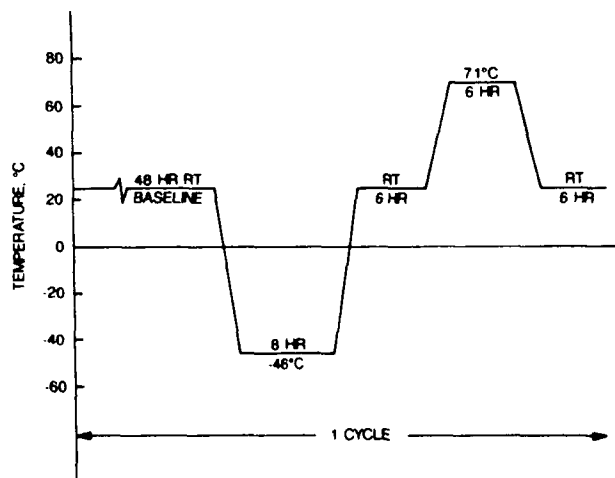


Figure 5 Temperature Cycle for Single Fiber Cables

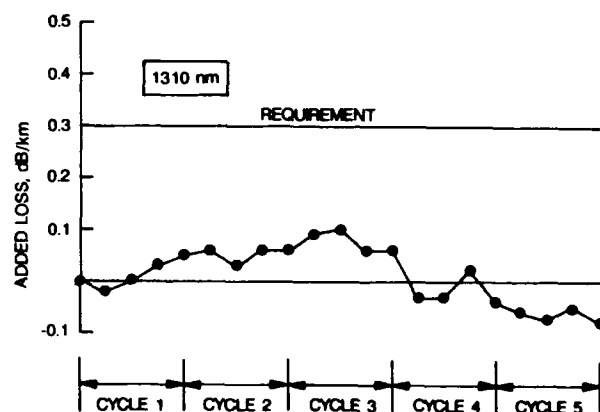


Figure 6 Temperature Cycling Test Results for Dispersion Shifted Single-Mode Fiber Cable

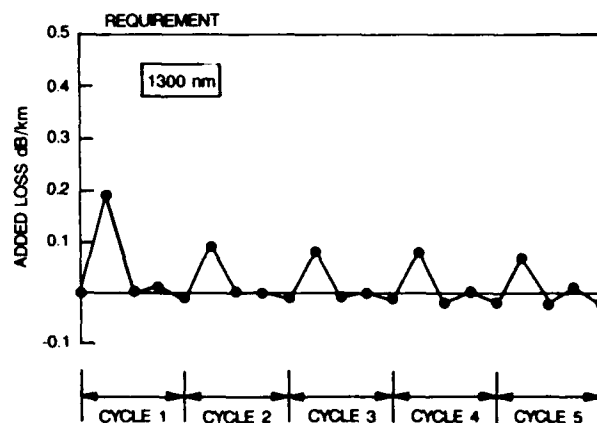


Figure 7 Temperature Cycling Test Results for 62.5/125  $\mu$ m Radiation Hardened Multimode Fiber Cable

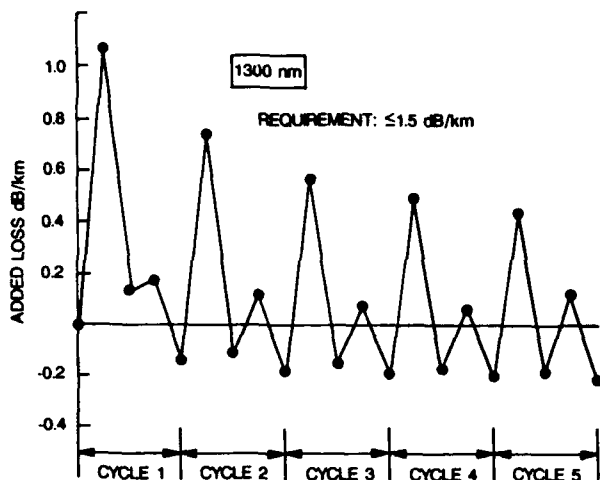


Figure 8 Temperature Cycling Test Results for 100/140  $\mu\text{m}$  Multimode Fiber Cable

The humidity cycle used for the cable evaluation is presented in Figure 9. In the humidity cycle, the cables are subjected to a constant relative humidity of  $94 \pm 4\%$  and cycled between the temperatures of  $20^\circ\text{C}$  and  $65^\circ\text{C}$ . The maximum increase in attenuation requirements for the humidity cycle are the same as those for the temperature cycling test. The results for five humidity cycles are presented in Figures 10, 11, and 12 for the dispersion shifted single-mode fiber, the 62.5/125  $\mu\text{m}$  radiation hardened multimode fiber, and the 100/140  $\mu\text{m}$  multimode fiber, respectively. All the cable designs pass the humidity cycle maximum attenuation increase requirements.

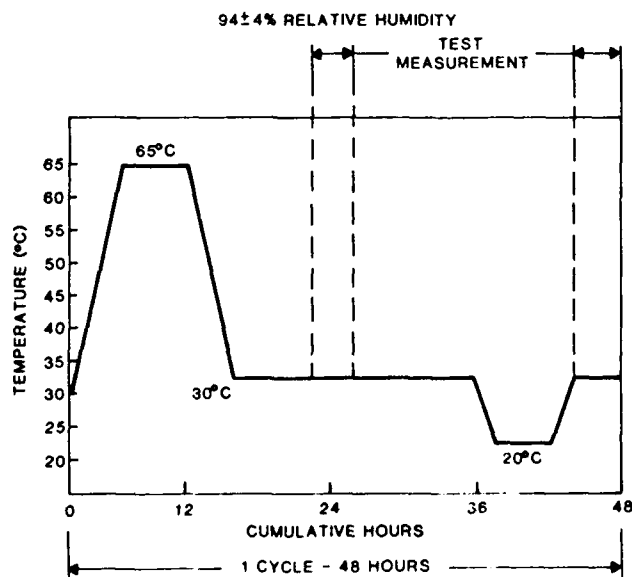


Figure 9 Humidity Cycle for Single Fiber Cables

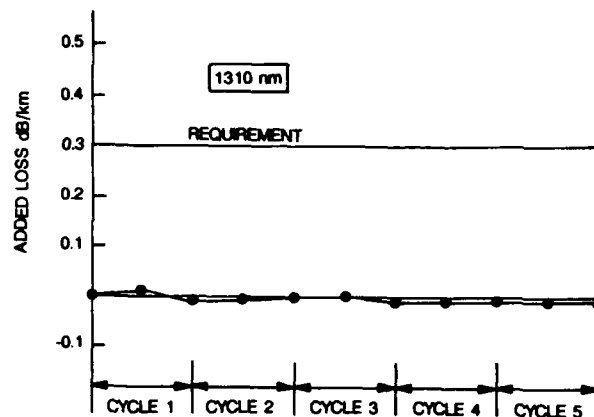


Figure 10 Humidity Cycling Results for Dispersion Shifted Single-Mode Fiber Cable

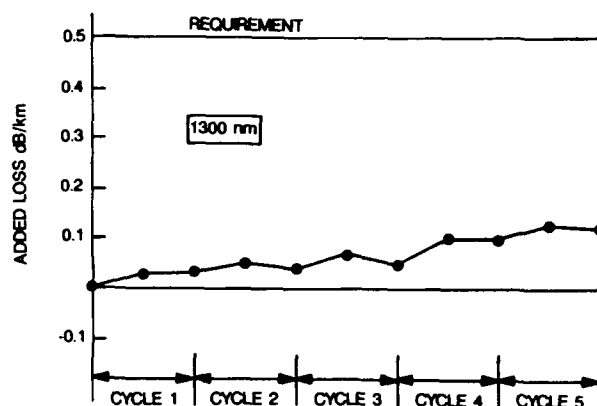


Figure 11 Humidity Cycling Results for 62.5/125  $\mu\text{m}$  Radiation Hardened Multimode Fiber Cable

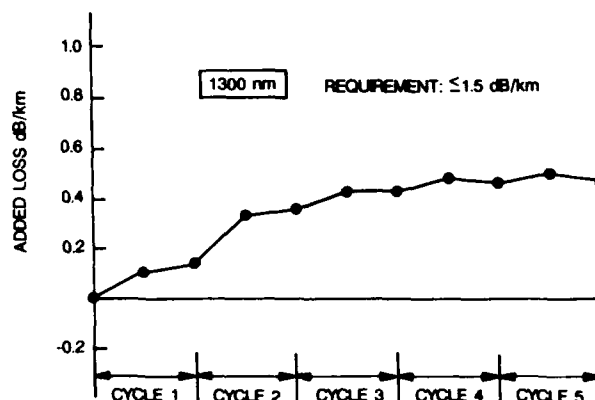


Figure 12 Humidity Cycling Results for 100/140  $\mu\text{m}$  Multimode Fiber Cable

The accelerated aging test consists of subjecting the cables to a temperature of 110°C for 10 days. This test temperature and duration simulates the mechanical response of the cable materials to an exposure of 85°C for the design life of 20 years. This simulation criteria was arrived at using the viscoelastic mechanical properties equivalence principle described in Reference 4. The results for the accelerated aging tests are presented in Figures 13 through 15. The added loss requirements for accelerated aging tests are also the same as those for the temperature cycling test. These results show excellent performance of the cables in the accelerated aging test.

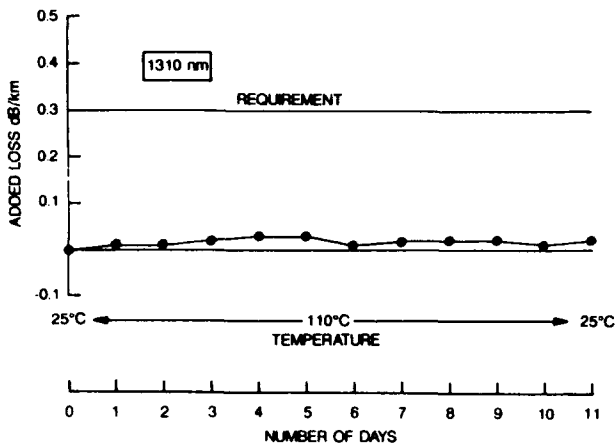


Figure 13 Accelerated Aging Test Results for Dispersion Shifted Single-Mode Fiber Cable

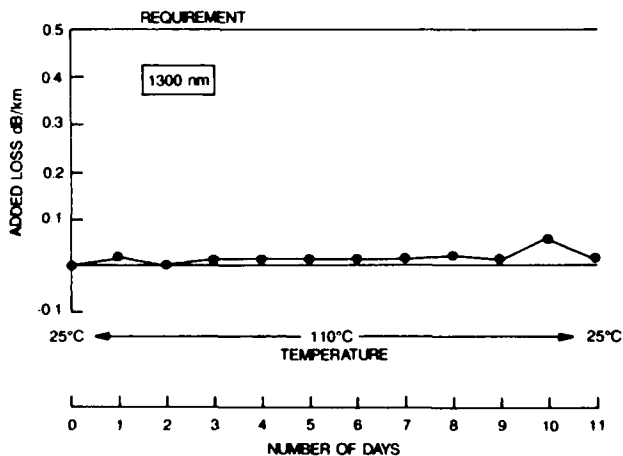


Figure 14 Accelerated Aging Test Results for 62.5/125  $\mu\text{m}$  Radiation Hardened Multimode Fiber Cable

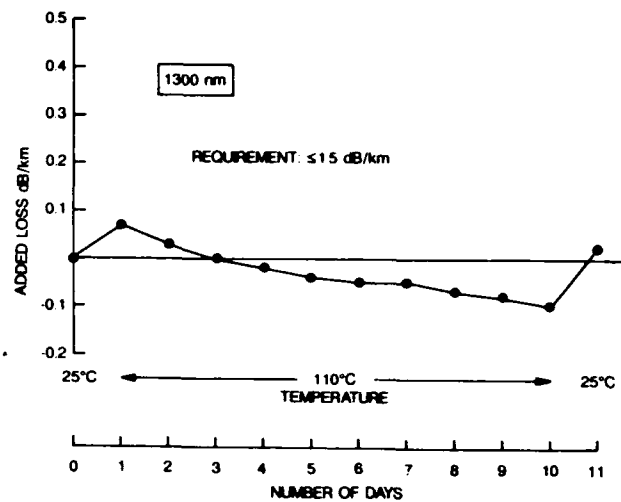


Figure 15 Accelerated Aging Test Results for 100/140  $\mu\text{m}$  Multimode Fiber Cable

The cables were also subjected to the required mechanical tests. These tests and the results of the mechanical tests are summarized in Tables I and II. Table I presents the results for the dispersion shifted single-mode fiber cable at the 1310 nm wavelength. Table II presents the results for both the 62.5/125  $\mu\text{m}$  radiation hardened and 100/140  $\mu\text{m}$  multimode cable designs at the 1300 nm wavelength. As can be seen from the tables, the three cable designs either meet or surpass the mechanical requirements. The knot test is not required for small diameter cables, but for thoroughness in evaluation, the test was performed and the results are included in the tables for information.

The twist bend test specified in the military specification uses the test procedure DOD-STD-1678, Method 2060, "Cable Twist-Bend". In this procedure a test mass of 10 kg is specified for all cables less than 6.4 mm in diameter. The 10 kg requirement of DOD-STD-1678 is very stringent for smaller diameter cables. Most industry procedures for similar tests specify masses which vary proportionally to the cable diameter. Thus, the mass was reduced to 2 kg and the number of cycles for the cables was reduced from the 2000 cycles. EIA/TIA-455-91, "Fiber Optic Cable Twist-Bend Test," does provide masses based on cable sizes, and the cables will be tested using this procedure in the future.

The weight requirement for cable was a maximum of 6.0 kg/km. The nominal diameter and weight results for the cable are 2.52 mm and 5.7 kg/km, respectively.

**TABLE I MECHANICAL TEST RESULTS FOR DISPERSION SHIFTED SINGLE-MODE FIBER CABLE**

NO	TEST DESCRIPTION	REQUIREMENTS	RESULTS mean/max
1	Mass	FED-STD-228, 8311 $\leq 6$ kg/km	5.7 kg/km
2	Twist Bend 25° C	DOD-STD-1678, 2060 Mandrel Dia. = 12.5 mm 2 kg, 1000 cycles Added Loss, $\Delta \leq 0.2$ dB	0.00/0.01 dB
	Twist Bend 71° C	DOD-STD-1678, 2060 Mandrel Dia. = 12.5 mm 2 kg, 500 cycles Added Loss, $\Delta \leq 0.2$ dB	0.00/0.01 dB
	Twist Bend -46° C	DOD-STD-1678, 2060 Mandrel Dia. = 12.5 mm 2 kg, 1000 cycles Added Loss, $\Delta \leq 0.2$ dB	0.00/0.00 dB
3	Cyclic Flexing 25° C	DOD-STD-1678, 2010 Mandrel Dia. = 12.5 mm 2 kg, 2000 cycles $\Delta \leq 0.2$ dB	0.00/0.00 dB
	Cyclic Flexing 71° C	DOD-STD-1678, 2010 Mandrel Dia. = 12.5 mm 2 kg, 2000 cycles $\Delta \leq 0.2$ dB	0.01/0.02 dB
	Cyclic Flexing -46° C	DOD-STD-1678, 2010 Mandrel Dia. = 12.5 mm 2 kg, 2000 cycles $\Delta \leq 0.2$ dB	0.00/0.00 dB
4	Impact 25° C	DOD-STD-1678, 2030 0.5 kg, 100 cycles 15 cm, $\Delta \leq 0.2$ dB	0.00/0.03 dB
	Impact 71° C	DOD-STD-1678, 2030 0.5 kg, 50 cycles 15 cm, $\Delta \leq 0.2$ dB	0.00/0.00 dB
	Impact -46° C	DOD-STD-1678, 2030 0.5 kg, 50 cycles 15 cm, $\Delta \leq 0.2$ dB	0.00/0.00 dB
5	Cold Bend	DOD-STD-1678, 2020 Mandrel Dia. = 12.5 mm, -46° C, 5 kg, 3 Turn $\Delta \leq 0.2$ dB	0.00/0.01 dB
6	Freezing Water Immersion	DOD-STD-1678, 4050 -10° C, 24 Hrs; -2° C, 1 Hr $\Delta \leq 0.2$ dB	0.00/0.00 dB
7	Knot	DOD-C-85045, 300N (66lbf), Mandrel Dia. = 12.5 mm $\Delta \leq 0.5$ dB	0.29/0.34 dB
8	Compression	DOD-STD-1678, 2040 10.1 cm Dia., 450N (100lbf) $\Delta \leq 0.2$ dB	0.00/0.00 dB
9	Tensile Strength	EIA-455-33A 270N(60 lbf), Elongation $\leq 2.0\%$ $\Delta \leq 0.2$ dB	$\leq 0.5\%$ 0.01/0.01 dB
10	Operating Tensile Loading	EIA-455-33A 180N(40 lbf), 24 Hrs. $\Delta \leq 0.2$ dB	0.00/0.02 dB
11	Flammability	DOD-STD-1678, 5010 60 Angle Test, Flame travel distance $\leq 10$ cm Extinguish $\leq 30$ sec.	3.73/4.14 cm <1 sec.

TABLE II

MECHANICAL TEST RESULTS FOR 62.5/125  $\mu\text{m}$  RADIATION HARDENED  
AND 100/140  $\mu\text{m}$  MULTIMODE FIBER CABLES

NO	TEST DESCRIPTION	REQUIREMENTS	RESULTS mean/max	
			62.5/125 FIBER	100/140 FIBER
1	Mass	FED-STD-228, 8311 $\leq 6 \text{ kg/km}$	5.8 kg/km	5.7 kg/km
2	Twist Bend 25° C	DOD-STD-1678, 2060 Mandrel Dia. = 12.5 mm 2 kg, 1000 cycles Added Loss, $\Delta \leq 0.5 \text{ dB}$	0.00/0.04 dB	0.04/0.07 dB
	Twist Bend 71° C	DOD-STD-1678, 2060 Mandrel Dia. = 12.5 mm 2 kg, 500 cycles Added Loss, $\Delta \leq 0.5 \text{ dB}$	0.00/0.00 dB	0.00/0.05 dB
	Twist Bend -46° C	DOD-STD-1678, 2060 Mandrel Dia. = 12.5 mm 2 kg, 1000 cycles Added Loss, $\Delta \leq 0.5 \text{ dB}$	0.00/0.00 dB	0.00/0.00 dB
3	Cyclic Flexing 25° C	DOD-STD-1678, 2010 Mandrel Dia. = 12.5 mm 2 kg, 2000 cycles $\Delta \leq 0.5 \text{ dB}$	0.00/0.01 dB	0.00/0.01 dB
	Cyclic Flexing 71° C	DOD-STD-1678, 2010 Mandrel Dia. = 12.5 mm 2 kg, 2000 cycles $\Delta \leq 0.5 \text{ dB}$	0.01/0.03 dB	0.00/0.02 dB
	Cyclic Flexing -46° C	DOD-STD-1678, 2010 Mandrel Dia. = 12.5 mm 2 kg, 2000 cycles $\Delta \leq 0.5 \text{ dB}$	0.00/0.00 dB	0.01/0.02 dB
4	Impact 25° C	DOD-STD-1678, 2030 0.5 kg, 100 cycles 15 cm, $\Delta \leq 0.5 \text{ dB}$	0.00/0.01 dB	0.00/0.01 dB
	Impact 71° C	DOD-STD-1678, 2030 0.5 kg, 50 cycles 15 cm, $\Delta \leq 0.5 \text{ dB}$	0.00/0.01 dB	0.00/0.01 dB
	Impact -46° C	DOD-STD-1678, 2030 0.5 kg, 50 cycles 15 cm, $\Delta \leq 0.5 \text{ dB}$	0.00/0.00 dB	0.00/0.01 dB
5	Cold Bend -46° C	DOD-STD-1678, 2020 Mandrel Dia. = 12.5 mm 5 kg, 3 Turns $\Delta \leq 0.5 \text{ dB}$	0.00/0.00 dB	0.00/0.00 dB
6	Freezing Water Immersion	DOD-STD-1678, 4050 -10° C, 24 Hrs; -2° C, 1 Hr $\Delta \leq 0.5 \text{ dB}$	0.02/0.07 dB	0.01/0.01 dB
7	Knot	DOD-C-85045 300N (66 lbf) Mandrel Dia. = 12.5 mm $\Delta \leq 0.5 \text{ dB}$	0.34/0.46 dB	0.06/0.08 dB
8	Compression	DOD-STD-1678, 2040 10.1 cm Dia. 450N (100 lbf) $\Delta \leq 0.5 \text{ dB}$	0.00/0.01 dB	0.02/0.02 dB
9	Tensile Strength	EIA-455-33A 270N (60 lbf) Elongation $\leq 2.0\%$ $\Delta \leq 0.5 \text{ dB}$	$\leq 0.5\%$ 0.00/0.04 dB	$\leq 0.5\%$ 0.00/0.00 dB
10	Operating Tensile Loading	EIA-455-33A 180N (40 lbf), 24 Hrs $\Delta \leq 0.5 \text{ dB}$	0.11/0.13 dB	0.33/0.37 dB
11	Flammability	DOD-STD-1678, 5010 60 Angle Test Flame travel distance $\leq 10 \text{ cm}$ Extinguish $\leq 30 \text{ sec.}$	4.14/4.26 cm <1 sec.	3.40/3.61 cm <1 sec.



## CONCLUSIONS

The single fiber tactical cables described herein meet and surpass all the optical, environmental and mechanical requirements imposed by the Military Specification, DOD-C-85045C, "General Specification for Fiber Optics Cables (Metric)". Cables with different fiber types have been developed for use in varied tactical applications. The technology utilized in the design and development of these cables is similar to that of their single and two fiber single-mode and multimode predecessors, enhancing field serviceability, compatibility and maintainability.

## ACKNOWLEDGEMENT

A project of this nature requires support from many organizations. The authors gratefully acknowledge the extensive contributions of several members of AT&T Network Cable Systems and AT&T Bell Laboratories.

## REFERENCES

1. "Single Fiber Optical Cable Assemblies (SFOCA)", U. S. Army CECOM Contract No. DAAB07-85-C-K556.
2. "Tactical Fiber-Optic Cable Assemblies (TFOCA)", U. S. Army CECOM Contract No. DAAB07-84-C-K551.
3. "Single-Mode Fiber Optic Communication Systems (SIMFOCS)", U. S. Army CECOM Contract No. DAAB07-85-C-K565.
4. K. Kathiresan, et al., "Selection and Test Criteria for Polymeric Materials for Tactical Fiber-Optic Cables", Proceedings of the 1988 Annual Technical Conference (ANTEC) of the Society of Plastic Engineers, Atlanta, Georgia, April, 1988.



Jill B. Fluevog is a Member of Technical Staff in the Fiber Optic Cable Engineering Department at AT&T Network Cable Systems, Norcross, Georgia. She joined AT&T in 1985 after receiving a Bachelors Degree in Chemical Engineering from Georgia Institute of Technology. She is responsible for the development of fiber optic cable products and processes for military applications. Ms. Fluevog is a member of American Institute of Chemical Engineers, Institute of Electrical and Electronics Engineers, Society of Automotive Engineers, and Society of Plastic Engineers.



William H. Ficke is the Supervisor of the Lightguide Qualification Laboratory in the Fiber Optic Cable Engineering Department at AT&T Network Cable Systems, Norcross, Georgia. He is responsible for the mechanical and environmental qualification and developmental testing for C outside Plant, Premises, Specialty, and Military Fiber Optic Cables. He joined AT&T in the Copper Cable Development Engineering Department in 1972. He has an AAS degree in Aeronautical Engineering from New York State University.



Wing S. Liu joined AT&T Bell Laboratories in Norcross, Georgia in 1986 as a Member of Technical Staff in the Fiber Optic Media Department. He is responsible for the mathematical modeling, design and development of fiber optic building cables and specialty cables, including those for military applications. Prior to his current assignment, he was working on analytical modeling and design of fiber optic splicing. He received his BSME, degree from Polytechnic Institute of New York in 1984, and MSME degree from Massachusetts Institute of Technology in 1986 specializing in Robotics.



Kris Kathiresan is a Member of Technical Staff in the Fiber Optic Technology Department at AT&T Bell Laboratories in Norcross, Georgia. He is responsible for design and development of specialty fiber optic cables, including military applications. Dr. Kathiresan joined AT&T Bell Laboratories in 1985. He has a B. E. Hons degree in Mechanical Engineering from University of Madras, India, an M. E. in Aerospace Engineering from Indian Institute of Science, India, and a Ph. D. in Engineering Science and Mechanics from Georgia Institute of Technology, Atlanta, Georgia. Dr. Kathiresan is a Senior Member of American Institute of Aeronautics and Astronautics and a Member of American Society of Mechanical Engineers. He is a registered Professional Engineer (Mechanical) in States of Georgia and Florida.

## A FAMILY OF NON-HALOGEN THERMOPLASTIC FIBER-OPTIC CABLES FOR SHIPBOARD APPLICATION

K. Kathiresan, J. B. Fluevog, S. P. Gentry, C. J. Arroyo, and L. R. Sherrets  
AT&T Bell Laboratories and AT&T Network Cable Systems, Norcross, Georgia

### ABSTRACT

The overwhelming advantages of fiber-optic technology for shipboard application are many and are well known. In addition to weight and space savings, it also offers immunity from electromagnetic interference, accommodation of future technological growth, etc. Application of fiber-optic technology for shipboard systems poses a very challenging and difficult task of the development of transmission cables. Fiber-optic cables for shipboard application are one of the most complex and demanding to design and manufacture. The stringent design specification is primarily derived from the considerations of safety of personnel aboard ship, and the operation, reliability and survivability of the shipboard systems. Shipboard fiber-optic cables with a low/no-halogen thermoplastic jacket material have been developed. Cable designs with different fiber counts were manufactured and evaluated using the existing specification. This paper presents the cable designs and performance results.

### INTRODUCTION

Fiber-optic technology, the transmission medium of choice for commercial telecommunications, is now becoming a medium of choice in military applications. Fiber-optics is currently being used and/or experimented with in several military and specialty applications, such as in tactical, aircraft, fiber-optic guided missiles and other weapon systems, control systems, computers and telecommunications. The U. S. Navy is also working very intensely to efficiently integrate fiber optics in both shipboard systems, and ship-to-shore and shore facilities. With regard to shipboard systems, the U.S. Navy has recognized the overwhelming advantages fiber optic systems can provide to enhance a ship's operational capability. It should be noted that fiber optics affords the opportunity:

- to remove tens of thousands of pounds from a ship's weight and reduce cable space requirements by providing cables that are lightweight and have small diameters

(volume), yet increase the information carrying capability compared to present copper cable systems, thereby enhancing the ship's operational capability. It is estimated that as much as 90% weight and space reduction of transmission media can be achieved by replacing copper cables with fiber-optic cables.

- to integrate all ship's systems and sub-systems, i.e., control (machinery), sensors, alarms, weapons, surveillance, telecommunications, administration, video, etc., into a single survivable network aboard a ship.
- to be assured that this network is capable of sustaining technological and capacity growth, and that the components are designed to last for the life of the ship.
- to implement a cable plant that provides immunity against electromagnetic pulse (EMP), electromagnetic interference (EMI), and radio frequency interference (RFI) and that requires no sheath grounding.
- to install a cable plant that is more secure and has crosstalk better than -100 dB (eg. TEMPEST).
- to achieve cost effectiveness when compared to copper-based systems and to enhance the overall reliability, survivability, and capability of a new class of warships.

In order to achieve all of the above advantages, fiber-optic cables for shipboard application are being developed. The design, development and manufacture of shipboard cables are demanding and difficult, because of the stringent performance requirements. This stringent design specification, MIL-C-0085045D (NAVY), is primarily derived from the considerations of safety of personnel aboard ship, and the operation, reliability, and survivability of the shipboard systems.

The above specification requires that the cables have low toxicity, contain low or no-halogen, generate low smoke and acid gas, be flame retardant, operate under extreme operating and storage temperature ranges, withstand stringent mechanical requirements and very high water pressure, survive hostile fluids at high temperature, and meet other demanding criteria. All the above requirements, individually

and in most combinations thereof, can be met with appropriate material selection and cable design features. Meeting all of the requirements simultaneously without any exceptions may be very difficult and/or may result in expensive cables. For example, meeting the high temperature fluid exposure requirement may call for radiation crosslinking or continuous vulcanization of jacketing materials. There are some thermoplastic materials available which will meet the fluid requirements, but are too stiff for shipboard applications. These aspects make the design, development, and manufacture of shipboard cables most difficult and challenging. The design, development, and performance evaluation of one-, four-, and eight-fiber cables with either radiation-hardened 62.5/125  $\mu\text{m}$  multimode or single-mode fibers for shipboard applications have been completed and are presented below.

### CABLE DESIGNS

The development of one-, four-, and eight-fiber shipboard cables has been completed. The building block for the four- and eight-fiber cables is a single fiber cable. This single-fiber cable is commonly known in the U. S. military as the Optical Fiber Cable Component (OFCC). The cross section of the 2.0-mm outer diameter OFCC is given in Figure 1. The OFCC uses either a radiation-hardened 62.5/125  $\mu\text{m}$  multimode or the 8.8  $\mu\text{m}$  mode-field diameter depressed-clad single-mode fiber. The fiber is tight buffered to a diameter of 900  $\mu\text{m}$  with a polyester elastomer material. The OFCC contains this buffered fiber as the core, surrounded by

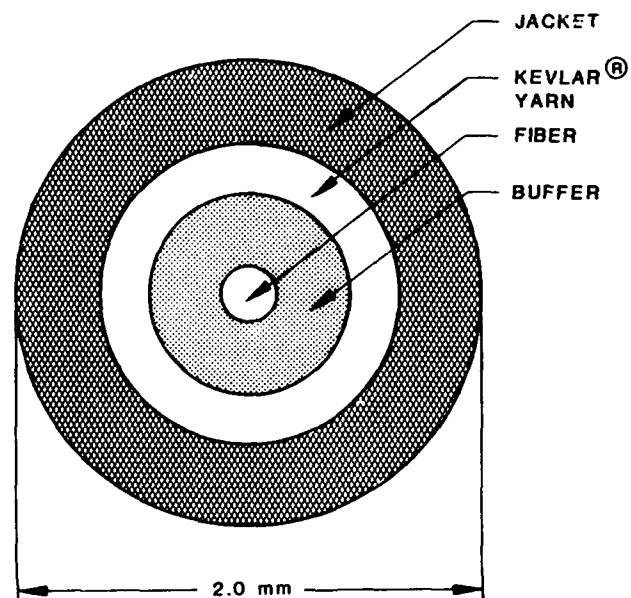


Figure 1. Cross Section of Optical Fiber Cable Component (OFCC)

Kevlar® yarn strength members and a low-halogen outer jacket.

An isometric view of the four-fiber cable is presented in Figure 2. The cable consists of a central waterblocking yarn with four single fiber cables stranded over it along with waterblocking yarns. Over the OFCC units, two layers of Kevlar® yarn strength members are stranded with opposite lay directions along with waterblocking members. A low-halogen outer jacket is then extruded over the Kevlar® yarn strength members. The components and the cable were designed such that the cable is very flexible, compact, and meets the waterblocking requirement more than adequately. The outer diameter of the four-fiber cable is 8.0 mm.

An isometric view of the eight-fiber cable is presented in Figure 3. As can be seen in the figure, the eight-fiber cable design and construction are very similar to those of the four-fiber cable except for the fiber count. The outer diameter of the eight-fiber cable is 11.25 mm.

### PERFORMANCE RESULTS

The shipboard cable performance evaluation consists of optical, chemical, environmental and mechanical tests. Optical properties along with numerous other dimensional and mechanical requirements are checked at the fiber stage, and fibers which meet all the specifications are then used for cabling. The fibers used were proof tested to 690 MPa. The wavelength of operation for the multimode cables is 1300 nm, though they may also be operated at 850 nm. Similarly, the wavelength of operation for the single-mode cables is 1310 nm and may also be operated at 1550 nm. The following test results correspond to the primary wavelength of operation at 1300 nm region. The general and optical properties of the cables are given in Table I.

The chemical tests consist of acid gas generation, halogen content, toxicity index, and fire and smoke properties. The requirements of these tests and the results are presented in Table II. The one-, four-, and eight-fiber cables meet the acid gas generation, halogen content, and toxicity index requirements with good margin. The halogen content results correspond to the total content of the four halogens, namely fluorine, chlorine, bromine and iodine.

Table III shows the fire and smoke properties of the cables. The fire and smoke properties are also a part of the chemical properties. The cables pass the IEEE-383 flame test. While the IEEE-383 test is not required by the specification, the cables were tested and the results are reported for information. The specification requires the UL-910 plenum cable fire test,

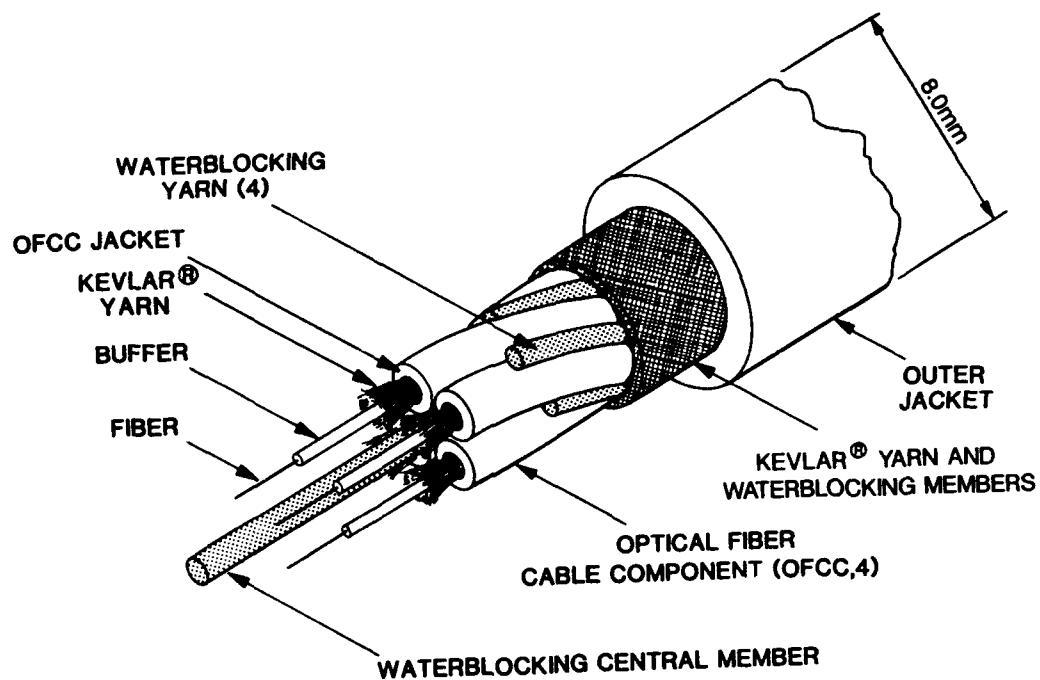


Figure 2. Isometric View of 4-OFCC Shipboard Cable

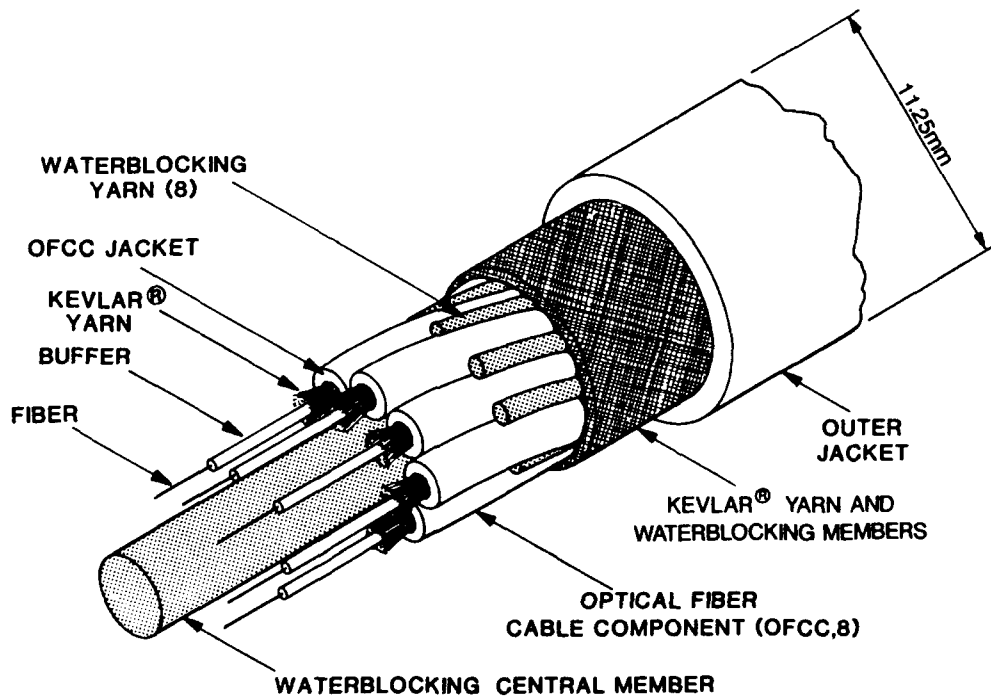


Figure 3. Isometric View of 8-OFCC Shipboard Cable

**TABLE I. GENERAL AND OPTICAL PROPERTIES OF SHIPBOARD CABLES**

PARAMETER	CABLE DETAIL
Cable Designs	1, 4, and 8 OFCCs
Fiber Types	62.5/125 $\mu$ m Rad-Hard Multimode and Single-mode
Specification	MIL-C-0085045D (NAVY)
Jacket Material	Thermoplastic
Primary Wavelength of Operation	1300 nm for Multimode 1310 nm for Single-mode
Cabled Fiber Maximum Attenuation	2.0 dB/km for Multimode 1.0 dB/km for Single-mode

with two modifications to the requirements. The first modified requirement is that the flame spread time product value for the cable for the first ten minutes of the test using the ASTM-E-84 procedure shall be less than or equal to 27.5 m-min. The standard UL-910 requirement is that the flame spread should be less than or equal to 1.52 m for the total test duration of 20 minutes. The second modified requirement is that the cable should meet the standard UL-910 smoke requirements (average optical density  $\leq 0.15$  and maximum optical density  $\leq 0.5$ ) or the cable's specific optical density under flaming combustion ( $D_m$ ) using ASTM-E-662 procedure should be  $\leq 225$ . The above modified requirements are applicable for four- and eight-fiber cables only. The single-fiber cable (OFCC) is not required to meet any of the above requirements, except the ASTM-D-662 specific optical density under flaming combustion requirement. The table shows that all the cables meet the specified fire and smoke requirements.

**TABLE II. CHEMICAL PROPERTIES OF SHIPBOARD CABLES**

TEST	REQUIREMENT	CABLE PERFORMANCE		
		1-OFCC-MM and 1-OFCC-SM	4-OFCC-MM and 4-OFCC-SM	8-OFCC-MM and 8-OFCC-SM
Acid Gas Generation	MIL-C-0085045D (NAVY) < 2.0%	0.02%	0.19%	0.16%
Halogen Content	MIL-C-0085045D (NAVY) < 0.2%	0.01%	0.04%	0.03%
Toxicity Index	NES 713 < 5.0	3.36	3.02	2.16
Fungus Resistance	MIL-STD-810, Method 508 Grade I	Grade I	Grade I	Grade I

MM - Multimode ; SM - Single-mode

**TABLE III. FIRE AND SMOKE PROPERTIES OF SHIPBOARD CABLES**

TEST	REQUIREMENT	CABLE PERFORMANCE		
		1-OFCC-MM and 1-OFCC-SM	4-OFCC-MM and 4-OFCC-SM	8-OFCC-MM and 8-OFCC-SM
Flame Propagation and Smoke Generation	IEEE-383 Flame Spread < 2.4 m (Not a Requirement)	2.2 m	1.3 m	1.3 m
	UL 910			
	Average Optical Density < 0.15	0.02*	0.11	0.09
	Maximum Optical Density < 0.5	0.25*	0.5	0.44
	Flame Spread - Time Product for First 10 Minutes < 27.5 m-min	40.5 m-min*	12.8 m-min	10.9 m-min
Specific Optical Density Under Flaming Combustion	ASTM-E-662 $D_m$ < 225	58	50	170

\* - Not a Requirement for 1-OFCC-MM or 1-OFCC-SM Cables

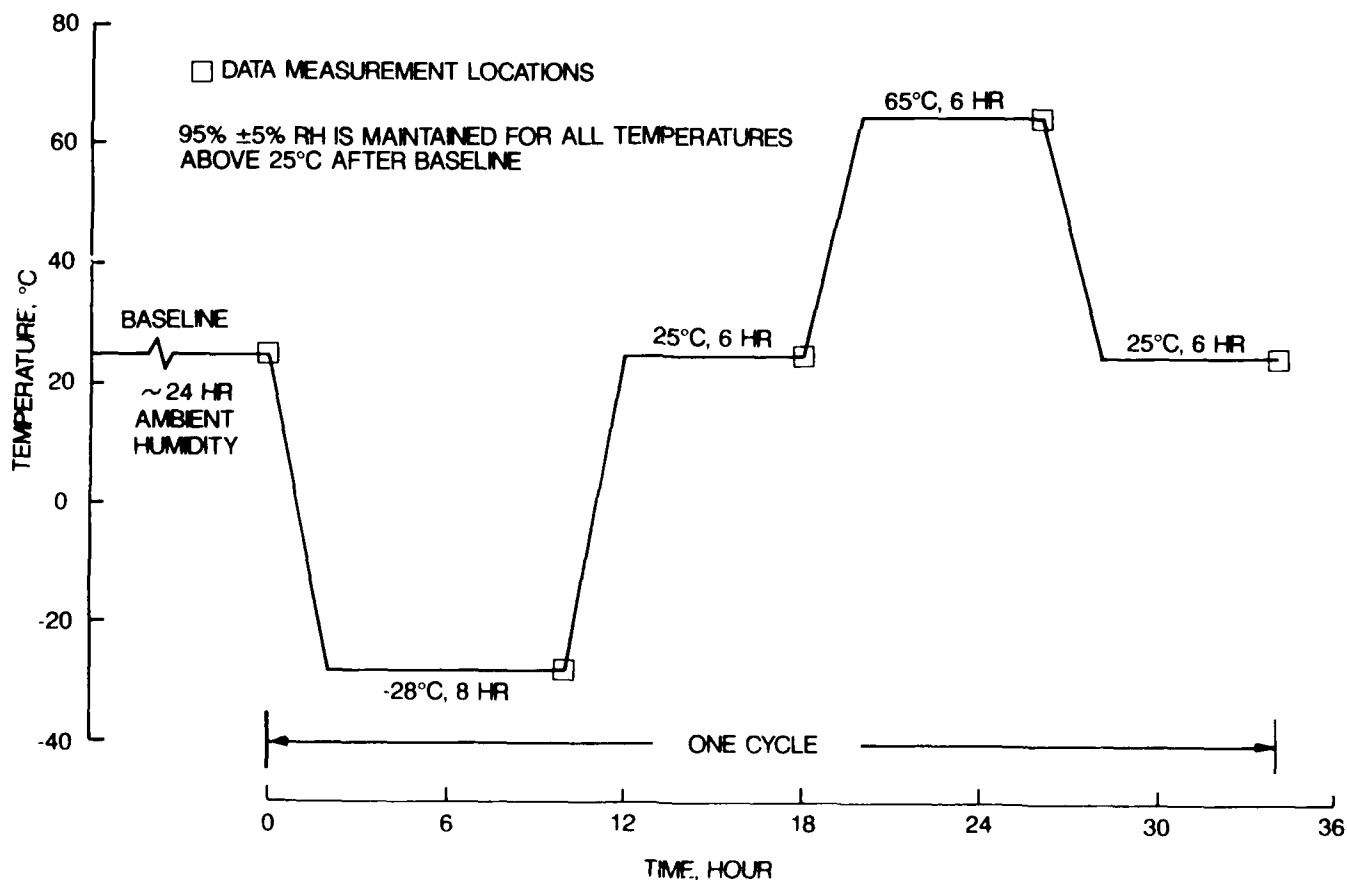
Three of the most important environmental tests for shipboard applications are thermal shock, temperature cycling at high humidity, and accelerated aging. The cable same set of samples was subjected to each of the above three tests. The results of thermal shock test are given in Table IV. After the thermal shock test, the samples were then exposed to the temperature-humidity test. The temperature-humidity cycle is presented in Figure 4. The results of the temperature-humidity cycling performance for the one-, four-, and eight-fiber cables are given in Figures 5 through 7, respectively. Each figure includes results for both the multimode and single-mode versions of the cable. The samples were then subjected to the accelerated aging test. In the accelerated aging test, the cables were subjected to a constant temperature of 100°C for 240 hours. The results of the accelerated aging

performance for the one-, four-, and eight-fiber cables are given in Figures 8 through 10, respectively, and each figure includes results for both the multimode and single-mode versions of the cable. The cables meet and surpass the requirements for the three environmental tests showing excellent performance.

The cables were then subjected to a long list of environmental and mechanical tests. The remaining environmental tests include thermal shock, gas flame, weathering, fluid immersion, water absorption, salt spray, jacket self-adhesion or blocking, vibration, and shock. The mechanical tests include tensile loading, dynamic bend, cyclic flexing, torsion, flexure, twist bending, crush, radial compression, impact, corner bend, dripping, hydrostatic pressure, waterblocking, cable jacket tear strength, cable abrasion resistance, cable

**TABLE IV. THERMAL SHOCK TEST RESULTS FOR SHIPBOARD CABLES**

TEST	REQUIREMENT	CABLE PERFORMANCE					
		1-OFCC-MM	1-OFCC-SM	4-OFCC-MM	4-OFCC-SM	8-OFCC-MM	8-OFCC-SM
Thermal Shock	EIA-455-160, Added Loss < 0.5 dB/km for Multimode < 0.3 dB/km for Single-mode	0.00 dB/km	0.02 dB/km	0.15 dB/km	0.06 dB/km	0.25 dB/km	0.03 dB/km



**Figure 4. Temperature-Humidity Cycle for Shipboard Cables**

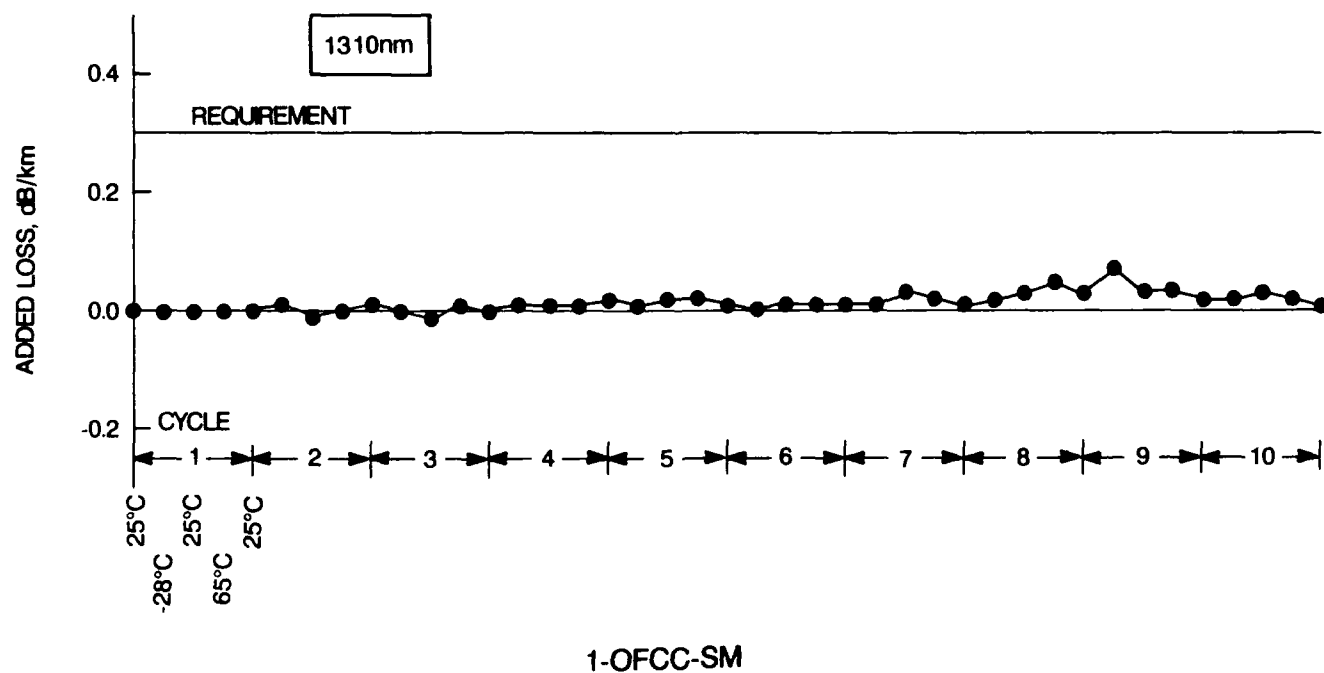
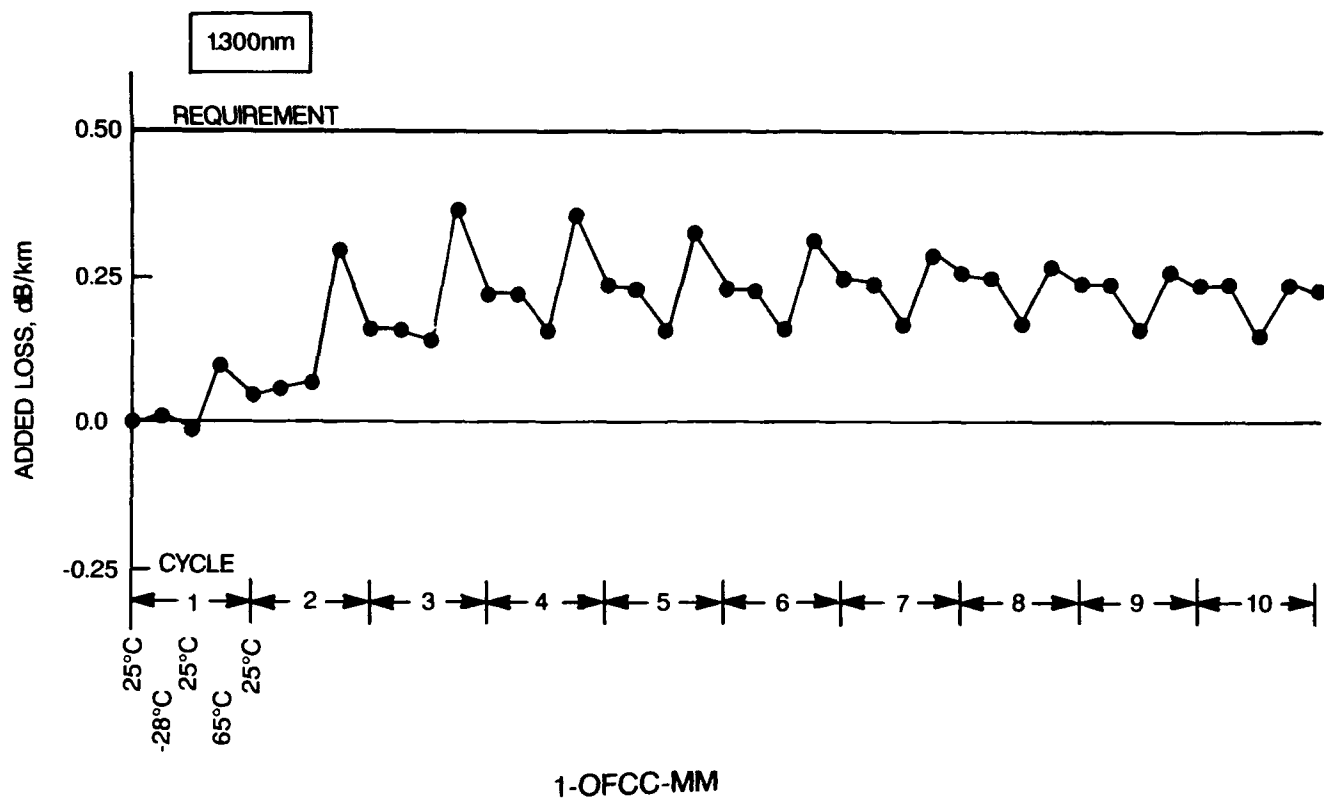


Figure 5. Temperature-Humidity Test Results for 1-OFCC Cables



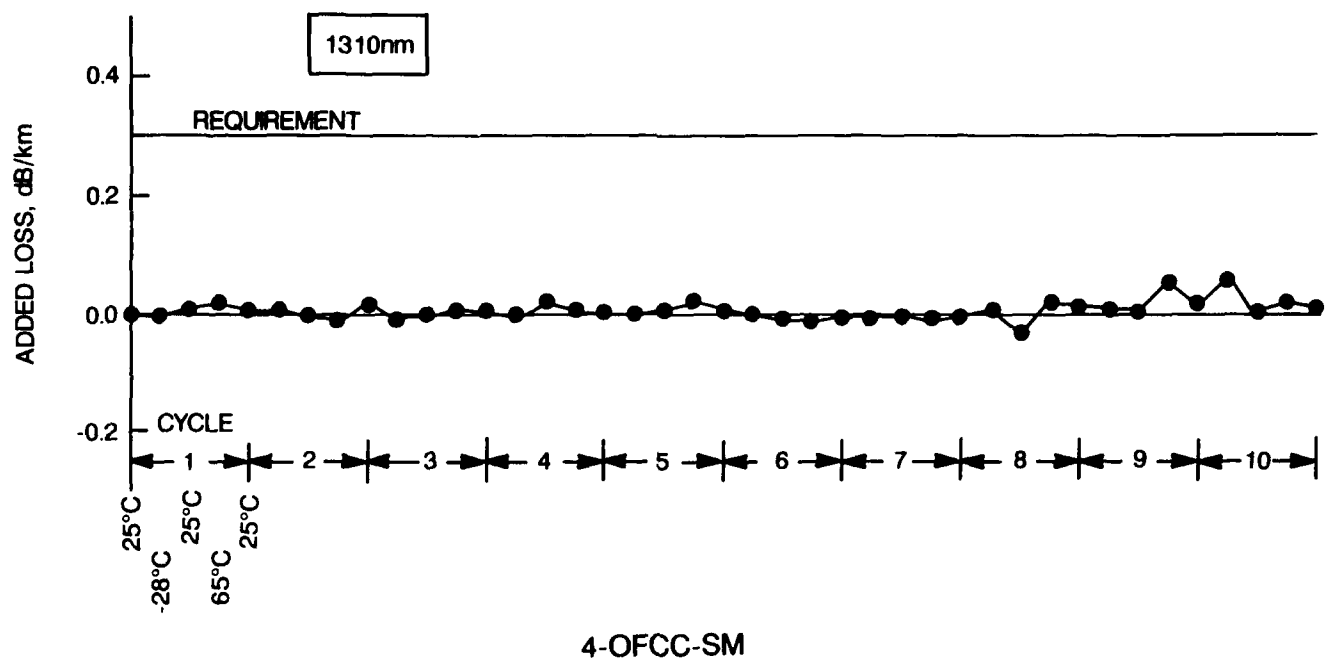
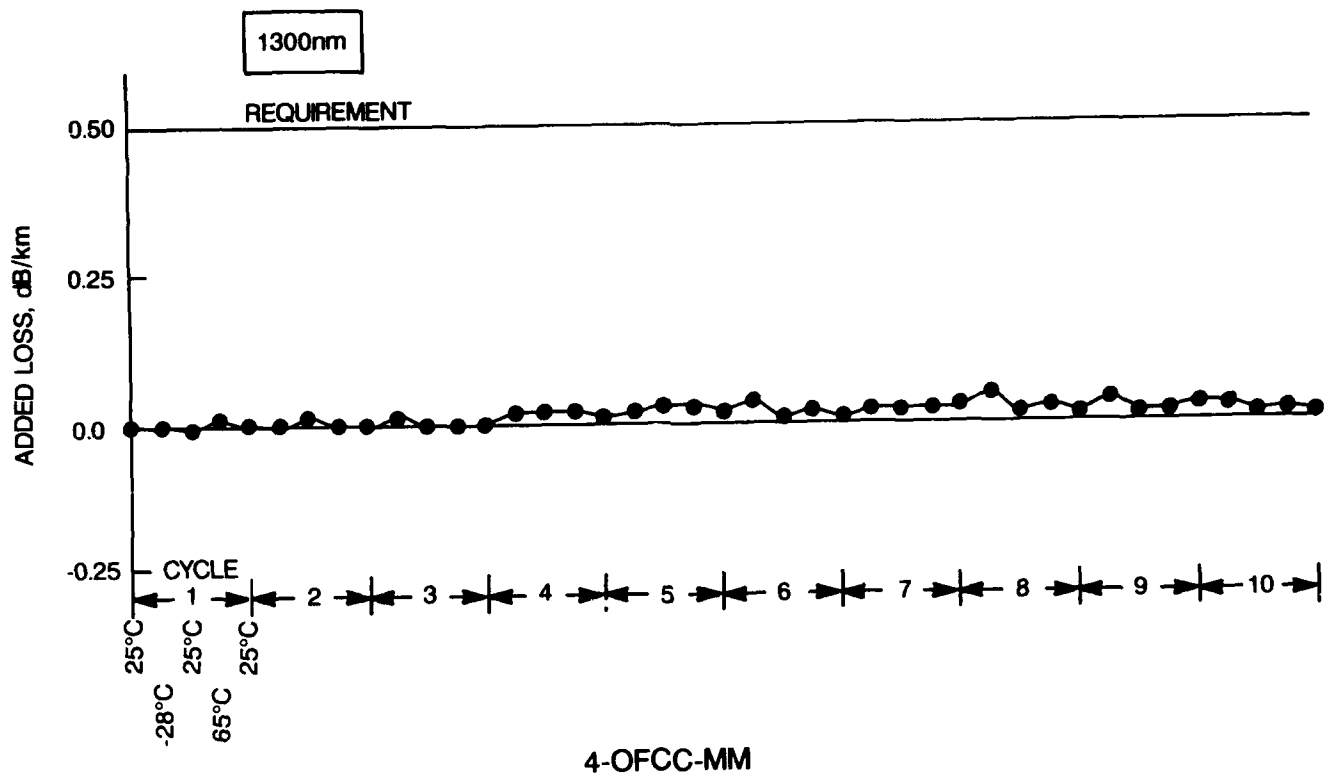


Figure 6. Temperature-Humidity Test Results for 4-OFCC Cables

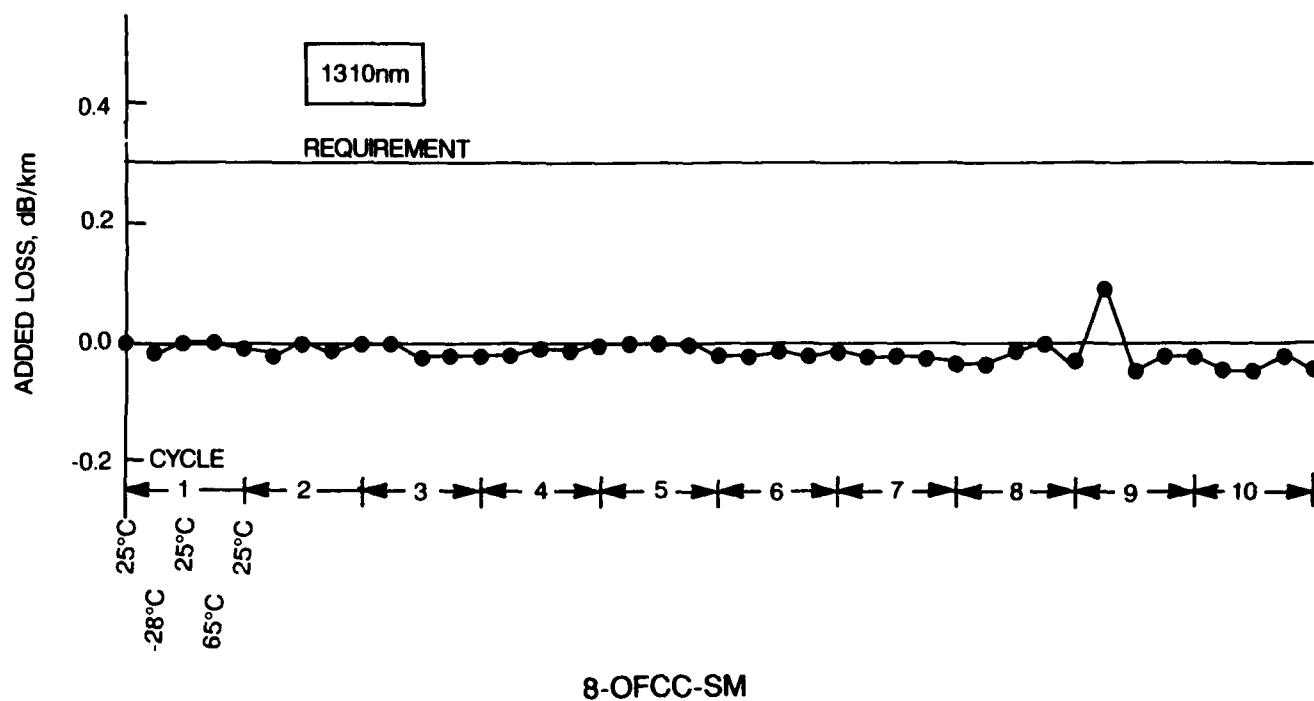
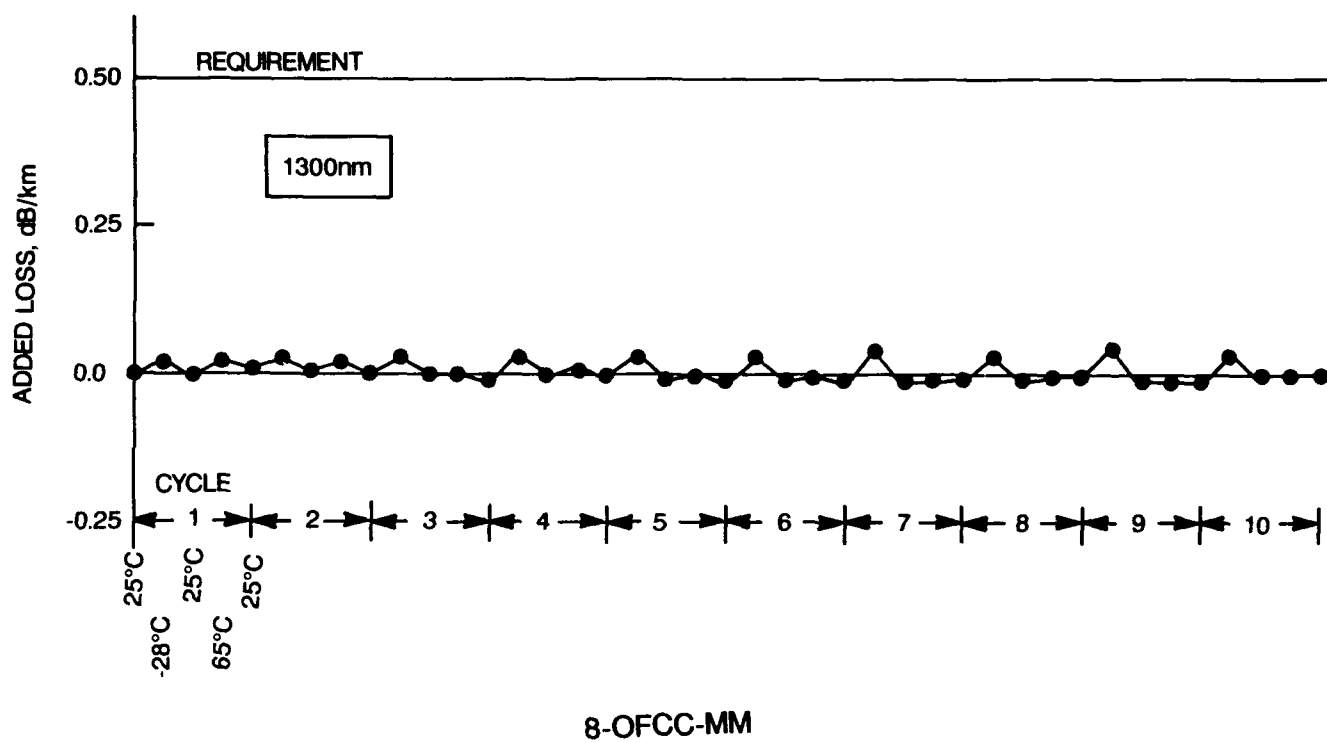


Figure 7. Temperature-Humidity Test Results for 8-OFCC Cables

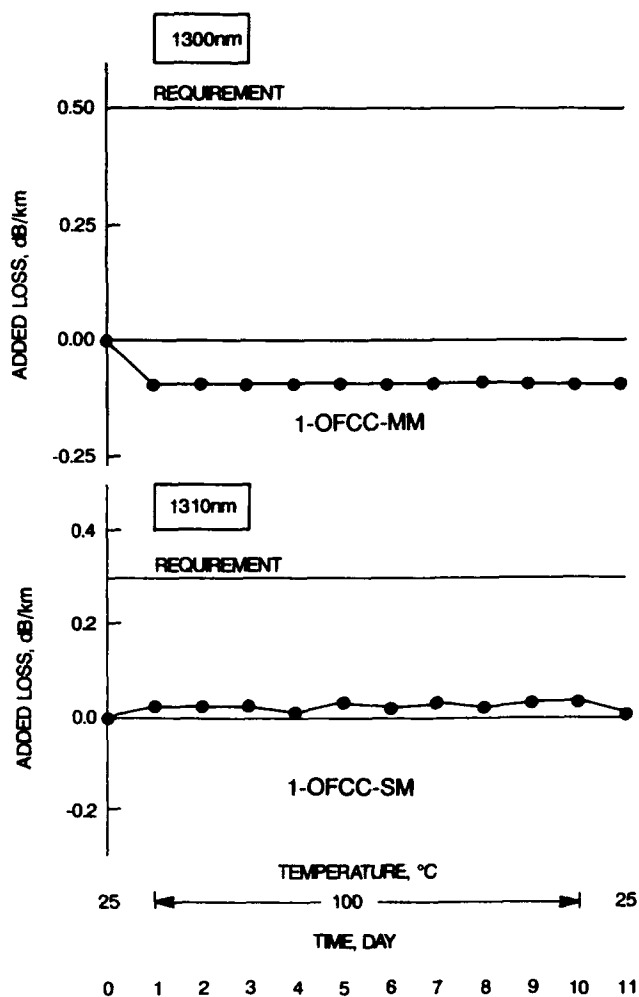


Figure 8. Accelerated Aging Test Results for 1-OFCC Cables

shrinkage, cable element removability, and durability of identification markings. The 7.0 MPa hydrostatic pressure test is intended for qualifying the cable for submarine applications. For brevity, the results for the remaining environmental and mechanical tests are not reported and are available upon request from the authors. The remaining environmental and mechanical performance of the cables either meets or surpasses the specification requirements in terms of test loading, number of cycles, and/or attenuation change.

### CONCLUSIONS

The design, development, and performance evaluation of fiber-optic cables with one-, four-, and eight-fibers for shipboard systems have been completed. The cables either meet or surpass the requirements specified in the MIL-C-0085045D (NAVY) specification.

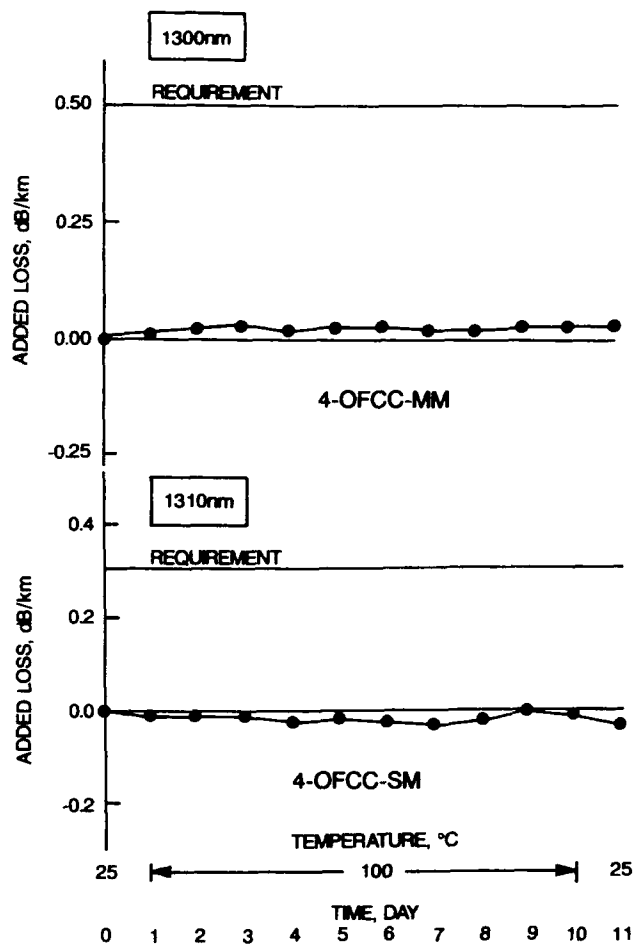


Figure 9. Accelerated Aging Test Results for 4-OFCC Cables

### ACKNOWLEDGEMENTS

The authors gratefully acknowledge the support and contributions of several members of AT&T Bell Laboratories and AT&T Network Cable Systems.

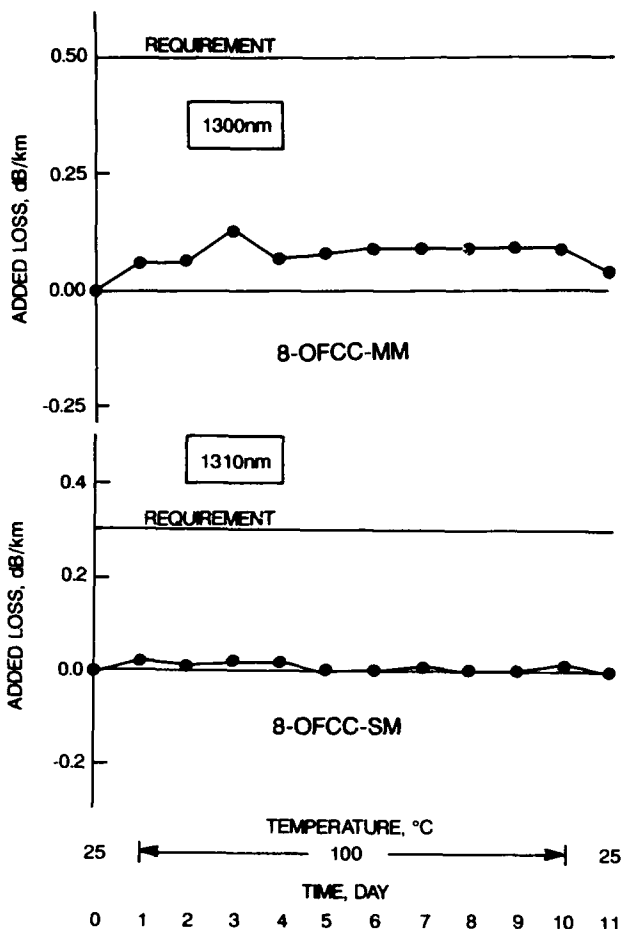


Figure 10. Accelerated Aging Test Results for 8-OFCC Cables

Kris Kathiresan is a Member of Technical Staff in the Fiber-Optic Media Department at AT&T Bell Laboratories in Norcross, Georgia. He is responsible for the design and development of specialty cables, including military applications. Dr. Kathiresan joined AT&T Bell Laboratories in 1985. He has a B. E. Hons in Mechanical Engineering from University of Madras, India, an M. E. in Aerospace Engineering from Indian Institute of Science, India, and a Ph. D. in Engineering Science and Mechanics from Georgia Institute of Technology, Atlanta, Georgia. Dr. Kathiresan is a Senior Member of American Institute of Aeronautics and Astronautics and a Member of American Society of Mechanical Engineers. He is a registered Professional Engineer (Mechanical) in the States of Georgia and Florida.

\* \* \* \* \*

Jill B. Fluevog is a Member of Technical Staff in the Fiber-Optic Cable Engineering Department at AT&T Network Cable Systems, Norcross, Georgia. She joined AT&T in 1985 after receiving a Bachelors Degree in Chemical Engineering from Georgia Institute of Technology. She is responsible for the development of fiber-optic cable products and processes for military applications. Ms. Fluevog is a member of American Institute of Chemical Engineers, Institute of Electrical and Electronics Engineers and Society of Plastic Engineers.

\* \* \* \* \*

Sherrie P. Gentry joined AT&T Bell Laboratories, Norcross, Georgia in 1982 and is a Member of Technical Staff in the Fiber-Optic Media Department. Her current responsibilities in the Fiber-Optic Measurement and Computing Support Group include environmental testing of fibers and cables and fiber characterization and diagnostic measurements. She received a Bachelors in Electrical Engineering Technology from Southern Technical Institute.

\* \* \* \* \*

C. John Arroyo joined AT&T Bell Laboratories in Whippany, New Jersey in 1969, and has worked in research and development of copper and fiber-optic cables at Norcross, Georgia, since 1978. As a member of Technical Staff, his responsibilities include fiber-optic cable development concepts, sheath design, standardization of lightning tests, and cable specification. John received the Design News Journal "Excellence in Design Award" in 1981 for a "Helical-Wrap Peel Strength Test". He co-authored the "Outstanding Technical Paper" at the 30th IWCS, November, 1981, and received the "Fiber-Optics Award" from AT&T International in July, 1990, for his contribution in fiber-optics technology. John has co-authored seven technical papers and received seventeen patents related to cable design.

\* \* \* \* \*

Larry R. Sherrets is a Senior Product Manager (Federal Market) in the Optical Fiber and Cable Department at AT&T Network Cable Systems, Norcross, Georgia. He joined AT&T at the Omaha Works in 1969. He attended the University of Nebraska (Engineering/Psychology). He currently is responsible for planning, development, and marketing of Fiber Optic Products for Military Applications for the U. S. Government.

\* \* \* \* \*

# FIBER OPTICS ASSEMBLY AS LIGHT SIGNAL CONCENTRATOR IN INDOOR DIFFUSE INFRARED COMMUNICATIONS SYSTEM

Chris J. Georgopoulos\* and George N. Bakalidis\*\*

\*University of Patras, Greece

\*\*University of Thrace, Greece

## Summary

Small infrared antennas in a wireless optical system have the dual task of uniformly radiating and 360 - degrees receiving of incoming optical signals. Conventional hemispherical antenna fixtures present problems associated with the flexibility of the antenna, the shadows due to obstacles and the large number of p-i-n detectors that are required. In this paper fiberoptic assemblies are presented that could replace the conventional IR antennas. For maximum efficiency, the bundle of optical fibers can be used to form an assembly in combination with the so called detector-immersion-lens technique. This results in a reduced number of photodetector diodes, and in some amplification since the maximum concentration achievable in diffuse radiation with an immersed absorber in a dielectric medium of index of refraction  $n$ , is approximately  $n$ .

## Introduction

Today, local area networks (LANs) for communications are characterized by fast evolution resulting in multiple problems in interconnecting terminals and peripherals due to the large number of cables, either they are copper wires or fiber optics<sup>1</sup>.

An alternative technique for confined spaces is the use of infrared (IR) diffuse light channel<sup>2,3</sup>. Using, for example, IR wireless terminals in the form of a network for in-house communication (e.g., in laboratories, offices, classrooms, etc.), presents many advantages including cost reduction during the installation and elimination of Electromagnetic Interference (EMI).

In a system like the above, data, voice and other information are coded and modulated into a carrier frequency that rides on an infrared diffuse-light channel from terminal's or ceiling transponder's IR light-emitting diode (LED) array forming the transmitter to a receiver's p-i-n diode array on a terminal. In such a system (Fig.1) radiation transmitted by the LEDs of the transmitter at 900nm are diffusely scattered from the surrounding walls, ceiling, and other objects in the room, thus filling the whole space with optical signal carrier. Reception is nondirectional, i.e., the photodiodes (actually p-i-n arrays) receive the incoming radiation from a wide field of view (FOV).

In the IR diffuse light communication channel a difficulty is encountered not only in uniformly dis-

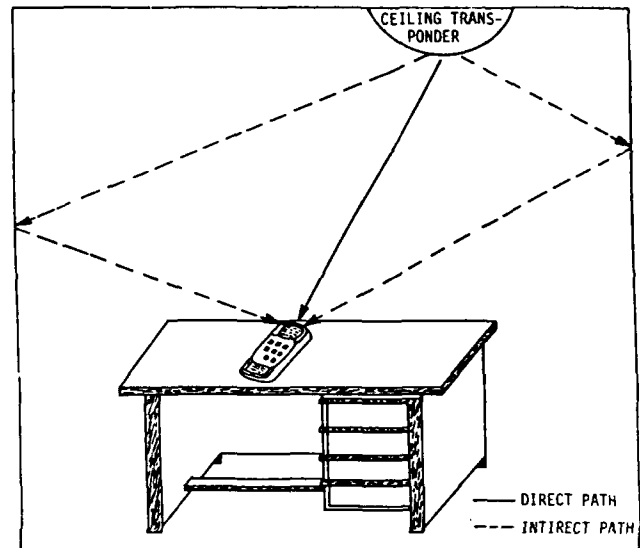


Figure 1: Typical free-space IR optical link in indoor applications.

tributing the optical power in the room, but also in collecting and directing to detectors light signals coming from omnidirectional sources. One way is to use a large number of LEDs and p-i-n diodes on a hemispherical or spherical antenna. However, such a solution is costly because a large number of detectors must be used to avoid IR signal shadows due to obstacles in a room. Another problem is the high capacitance of parallel connected detectors that degrades the performance of receiver (lower operating frequency).

In this paper, a different solution is proposed in which optical cable assemblies are considered. Such assemblies are flexible and can feed the photodetectors from different directions and through various optical obstacles. For maximum efficiency, the bundle of optical fibers can be used in combination with the detector - immersion-lens technique.

## Present State of the Art of IR Antennas for Indoor Applications.

### Problem Areas

The problems in designing an IR radiating/receiving antenna ("fixture") are due to the following

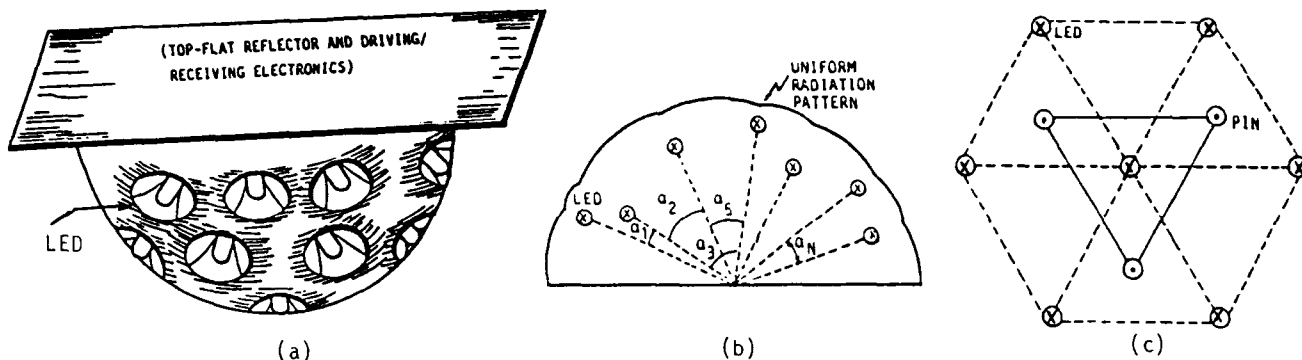


Figure 2: Conventional hemispherical IR antenna configurations: a) Sketch of LED assembly with individual reflectors and top-flat reflector. b) LED uniform radiation distribution pattern. c) Mixed LED and p-i-n diode arrangement.

reasons : 1) Infrared radiation is not visible; therefore, special equipment and test setups are required to establish its level at various points or zones in an indoor installation. 2) A relatively large number of small IR sources have to be mounted in such a way that an optimized illuminating fixture is formed. 3) The same fixture usually must incorporate not only the IR sources, but also the IR detectors. 4) Driving/receiving and other electronic control circuitry may have to be included in the same fixture. 5) Fixtures for ceiling mounting would be different than corresponding fixtures used in each IR telset or in other terminals<sup>4</sup>.

#### Conventional IR Radiating Configurations.

To meet the requirement of uniformly distributing IR energy in a room with somewhat symmetrical dimensions, a hemispherical fixture can be used (Fig.2a). On this fixture the LEDs can be arranged to form among them (groups of three) triangles whose each side presents an "opening" approximately equal to the angle (-3dB) of their radiated power. All angles (Fig.2b) are equal, i.e.,  $\alpha_1 = \alpha_2 = \dots = \alpha_N$ , so that the total radiation is approximately uniform to all directions. On the other hand, the photodiodes (p-i-n) can be placed at the center of every other triangle formed by the LEDs on the same hemispherical base (Fig.2c). This is possible because transmitting and receiving in the up-and down-link (to and from center transponder unit) takes place at different times and there will be no crosstalk. Here too, it is very desirable that the sensitivity angles (-3 dB) be equal to those of LEDs for uniformity purposes. It is also to be noted that in certain cases a spherical structure could be used. These IR antenna fixtures, however, are expensive since a large number of LEDs and p-i-n detectors have to be mounted on the external surface on the hemisphere (or sphere). Especially, as mentioned previously, the large number of detectors that are needed in order to avoid IR signal shadows, results in degraded detection performance.

#### Fiber Cone Assembly for IR Signal Guiding

A fiber bundle designed in the form of a cone (Fig.3), where the entrance diameter is larger than the exit diameter transmits and reduces the image

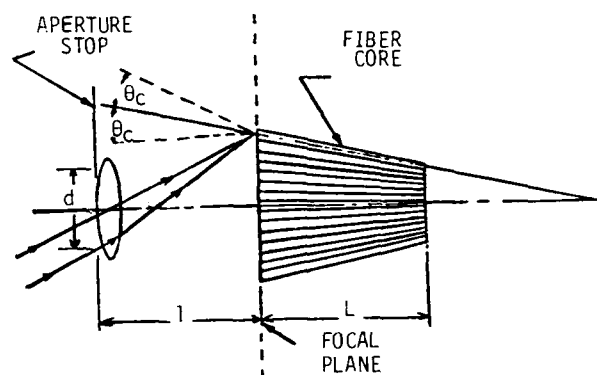


Figure 3: Fiber optic cone with focusing external lens.

size and conveys it from one plane to another<sup>5</sup>. The gain  $G$  of this structure is given by the relationship:

$$G = \left( \frac{d_1}{d_2} \right)^2 \tau = \frac{1 - \cos \theta_e}{1 - \cos \theta_i} \tau \quad (1)$$

where:  $d_1, d_2$  = the entrance and exit diameters of the cone  
 $\tau$  = the transmission efficiency of the bundle  
 $\theta_i, \theta_e$  = the incident and exit angles of the ray.

For the critical angle in a fiber we have:

$$\sin \theta_c = \frac{1}{N_0} \left( N_1^2 - N_2^2 \right)^{1/2} \quad (2)$$

where:  $N_1, N_2, N_0$  = the indices of refraction of the core, coating, and surrounding medium, respectively

For the case a fiber cone the critical angle will be as follows:

$$\theta_c = \sin^{-1} \frac{N_0}{N_1} \left[ 1 - \left( \frac{N_2}{N_1} \right)^2 \right]^{1/2} \cdot \left( \frac{d_2}{d_1} \right) \quad (3)$$

The surface of a conventional lens is curved and all rays reaching the lens are bent to form

an image focused on one or more detectors. For a fiber cone, no such ordered phase relationship exists and an image must be formed at the cone entrance by an external lens (Fig.3).

#### Combined fiberoptic and Detector-Immersion-Lens Assembly.

The incorporation of a lens in front of the fiber cone (Fig.3) creates a problem since light sources (LED) have to be used in the same assembly. An alternative configuration is shown in Fig.4. It can be made in hemispherical (spherical is also possible) form where fiberoptic pieces have been placed vertically to an immersion-lens combination and surrounded by a plastic material.

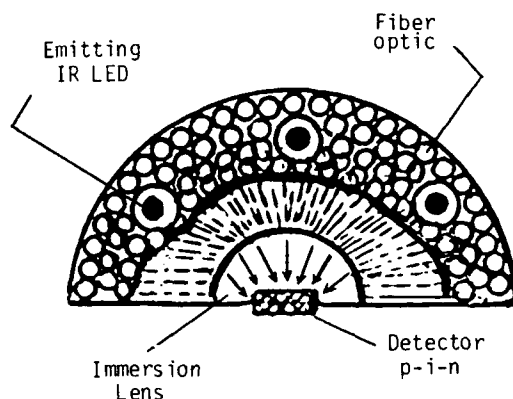


Figure 4 : Fiberoptic assembly in combination detector-immersion-lens.

In comparison to the fiber cone the hemispherical scheme for ceiling mounting or the spherical scheme as a terminal mounted antenna have the following two major advantages:

- 1) The LEDs can easily be accommodated on the surface of the antenna or they can be inserted in small wells with or without small reflectors with their edge flashed to the external surface of the hemisphere.
- 2) Using an immersion lens, a gain equal to the square of index of refraction  $n$  can be achieved as explained below.

The possibility of using reflectors or immersion lenses to enhance the output of detectors of diffuse (homogeneous and isotropic) radiation encountered in scatter communication systems (room with diffuse IR light) is of very high interest. According to the theory, reflectors can yield no optical gain, whereas immersion lenses can provide gain equal to  $n^2$ , where  $n$  is the index of refraction of the immersion medium<sup>6,7</sup>. The immersion lens in the proposed assembly is shown separately in Fig.5. The geometrical-optics reasoning shows that the hemisphere will exhibit  $n^2$  optical gain (neglecting Fresnel losses)<sup>7</sup> provided that the size  $L$  of the detector is small compared with  $R_s/n$ , where  $L$  and  $R_s$  are of the same dimensions. Considering, for example, a plastic lens with  $n = 1.33$ , the gain

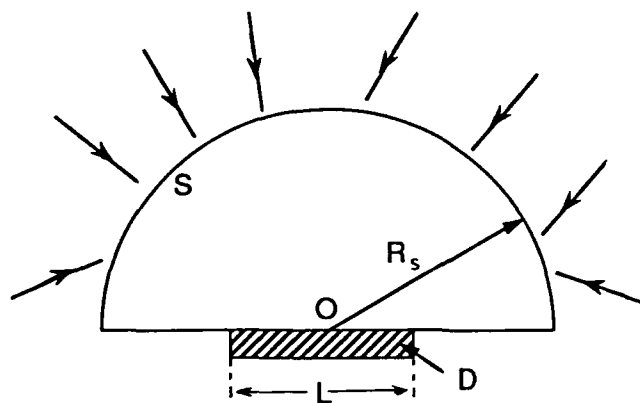


Figure 5: Practical detector-immersion lens combination.

would be  $n^2 = (1.33)^2 \approx 1.77$  (Theoretical).

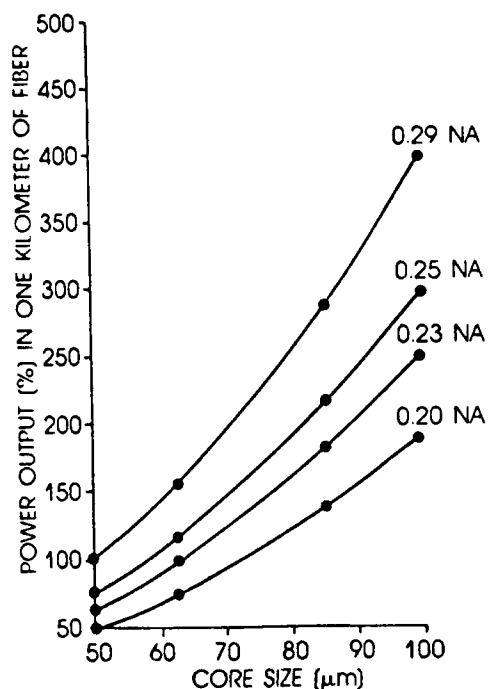
#### Fiberoptic Properties Affecting IR Antenna Assembly

Single-mode or fiber bundles have been used in the past in visible and near-IR related technologies, e.g., in spectroscopy. Recently, this technology has gained popularity in the IR region. Quartz or silica fibers are used in visible, while fluoride and now chalcogenide fibers are used in the IR region. Special fiberprobe assemblies can be used with transmission and attenuated, specular, and diffuse reflectance heads for various sampling requirements. High-sensitivity detectors are recommended for use with these accessories.

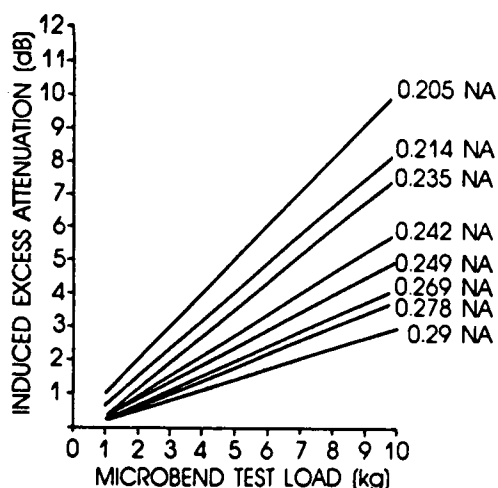
As in all fiberoptic applications, in order to achieve optimum IR antenna assembly performance, when fibers are used, certain major parameters should be taken into account when selecting the correct fiberoptic type. In general, step-index fiber could be selected for low data rate applications, graded-index for medium to high data rates, and single-mode for very high data rates<sup>8</sup>. On the other hand, step-index fiber presents lower sensitivity to microbending losses and it has nearly twice the amount of light-coupling efficiency of graded-index fibers.

As an illustrative example here, we consider the effect of core size and numerical aperture (NA) on the power throughput of graded-index optical fibers (Fig.6a)<sup>9</sup>. The output powers are shown as a percentage, relative to the output of a reference fiber, with 50- $\mu\text{m}$  core and 0.29 NA. According to the above reference, throughput measurements were made with wavelength at 850nm, using fibers with 4 dB/km attenuation. Core size has a very high impact on total power transmission for available fibers with typical numerical aperture and attenuation ranges. For instance, for an NA of 0.20, loss rating of 4 dB/km, and transmission wavelength of 850 nm, power output increases from 48% for a 50 $\mu\text{m}$  core fiber to over 190% for a 100 $\mu\text{m}$  core fiber. These percentages are relative to the power output of a reference fiber with a 50- $\mu\text{m}$  core and 0.29 NA.

As a second example, we consider the effects of NA on microbending losses. Microbending will occur in an IR-antenna assembly because it is very desirable to guide diffuse IR light from various points to a single point. As shown in Fig. 6b, higher NA has the advantage of higher resistance to microbending losses.



(a)



(b)

Figure 6 :a)Effect of core size and NA on the power throughput of graded-index optical fibers  
b)The microbend sensitivity of optical fibers. According to Ref. 9, the measurements were made on 100/140-μm coated, radiation-hard, step-index fibers.

## Conclusion

In this paper, the case of fiberoptic IR antenna assemblies for indoor communications has been discussed. Of all schemes that were studied, the hemispherical (or spherical) assembly with fiber optics in combination with detector-immersion-lens offers the maximum efficiency.

## References

- [1] C.J. Georgopoulos, "Alternative Communications Techniques in the Office of the Future," in Proc. HETELCON'83, Athens, Greece, August 25-30, 1983.
- [2] F.R. Gfeller and U. Bapst, "Wireless In-House Data Communication via Diffuse Infrared Radiation," Proc. IEEE, Vol. 67, No.11, Nov.1979, pp. 1474-1486.
- [3] C.J. Georgopoulos, "PABX-Infrared Network Interfaces," Proc. Fiber Optics and Communications Local Area Networks (FOC/LAN), Atlantic City, N.J., October 10-14, 1983, pp.295-299.
- [4] C.J. Georgopoulos and J.J. Korasis, "Modeling and Analyzing Small IR Antennas for Indoor Microbroadcasting Systems," in Proc. of AMSE '84 : Modeling and Simulation Conference, Athens, Greece, June 27-29, 1984, pp. 17-29.
- [5] R.Y. Wong and M.R. Jafarpour, "Optical System with Fiber Optical Elements," Optical Engineering, Vol. 20, No.1, Jan/Feb. 1981, pp.95-97.
- [6] M.E. Marhic, et al., "Reflectors and Immersion Lenses for Detectors of Diffuse Radiation," J. Opt. Soc. Am., Vol. 72, No.3, March 1982, pp. 352-355.
- [7] R.E. Jones, Jr., "Collection Properties of Generalized Light Concentrators," J. Opt. Soc. Am., Vol. 67, No.11, Nov. 1977, pp.1594-1598.
- [8] C.J. Georgopoulos, Fiber Optics and Optical Isolators, Gainesville, Virginia:DWCI, 1982.
- [9] M. Aslani and C. DeLuca, "Practical Considerations in Selecting Optical Fibers," Laser Focus/Electro-Optics, August 1984, p.110.

Authors' biographies  
(see next page)





Dr. Chris J. Georgopoulos has been educated in both Greece and USA and possesses the following degrees : BA, BS (EE), MS (EE) and Ph.D (EE). From 1963 to 1972 he worked in USA (Wang Labs, Sylvania, and Raytheon Co.) and in 1972 he joined the Technical Research Staff of the University of Patras where he worked on a number of research projects till 1976.

In 1977 Dr. Georgopoulos was elected full professor of the Chair of Electronics and Director of the Electronics Laboratory in the School of Engineering of University of Thrace, Xanthi, Greece. From March 1978 to August 1979 he was the Dean of Engineering School of University of Thrace. From 1985 to 1989 he was the Electronics Division Chairman and Director of the Electronics and Digital Systems Labs of University of Thrace. During 1986-87 he was Visiting Professor in the Electrical Engineering Dept. of University of Lowell, MA (USA). In October 1989 Dr. Georgopoulos joined the Electrical Engineering Dept. of University of Patras as full Professor.

Professor Georgopoulos has received five patents covering his inventions and several awards for his innovative and cost reduction ideas; has written some 40 technical reports on research, design and development projects; has published and presented more than 60 technical papers, and has authored a series of text books in the field of electronics and digital systems (in Greek language). He is also the author of four books of worldwide circulation : a) Fiber - Optics and Optical Isolators (DWCI:VA, USA, 1982), b) Interface Fundamentals in Microprocessor- Controlled Systems (D. Reidel Publishing Co., Dordrecht, Holland, 1985), c) Interference Control in Cable and Device Interfaces (ICT, VA, USA, 1988), d) Microwave Edge Series (ITC, USA, 1990).

Professor Georgopoulos is heading the Optoelectronics and EMC Research Group and his research and development interests include fiber optics and IR communications mobile communications, sensors and EMC studies for system interfaces. He has been a consultant in the above areas in Europe and USA.

Dr. Georgopoulos is a Professional Engineer in the State of Massachusetts, a member of Technical Chamber of Greece, a senior member of IEEE, a member of IEEE Optical Communications Committee, a member of the E.A.M.E.C. (European African, and Middle East Committee) of the IEEE Communications Society, and a member of the IEC TC 84/WG 17 (IR Standardization Group).



Mr. George Bakalidis received his BS degree in Physics in 1988 from University of Ioannina, Greece. Currently he is a Research Associate in the Electrical Engineering Dept. of University of Thrace, Greece. His research interests include fiber optic special assemblies and infrared communications for indoor applications.

# External Photoelastic Polarization Modulation For Optical Fiber Data Transmission

Hijiri Nimura\*, Akira Fujisaki\*, and Hiroyuki Fudou\*\*

\*The Furukawa Electric Co.,Ltd/\*\*Kansai Electric Power Co.,Ltd

## Abstract

We report the data transmission with external photoelastic polarization modulation (EPPM) method. In the experiment, the data transmission system by EPPM is estimated to have minimum received optical level of -24dBm and the terminals up to 25, when transmission signal is 1200bit/s FDM data. This method enables data transmission using a simple tap and optical fiber remain unbroken.

## 1. Introduction

Today, an intensity modulation scheme is widely used to modulate light in optical communication system. In this report, we proposed a new modulation method, which called EPPM method.<sup>1)</sup> The proposed method does not modulate the intensity of light directly, it modulates polarization state of the light by applying an intentional vibration into fiber. With this method, a voice communication has been demonstrated and put into practical use. In this report, we described the experiment results of a high quality FDM data transmission using the EPPM method.

## 2. Basics of the EPPM method and experimental set-up

The EPPM method utilizes a photoelastic effect introduced into the optical fiber with lateral stress by piezo-electric device. This effect causes phase difference between x and y-axis components of polarization of a light signal in the fiber. This phase difference is converted into intensity modulated signal by polarizer positioned in front of the receiver. As shown in Fig.1, a transducer ( piezo-electric device ) applies a lateral stress into the optical fiber only by clipping on it. Since a certain relation exists between the drive voltage of the transducer and phase differences in optical fiber, phase differences are modulated with vibration frequencies of transducer. This technique enables the data transmission without cutting an optical fiber so that the data terminal equipments can be easily multiplied.

Fig.2 shows the schematic diagram of a data transmission system using the proposed EPPM technique, which consists of one central control equipment and N data terminal equipments. In the system, frequency division multiplexing (FDM) with N carrier frequencies is used. Each carrier is modulated by the information signal with frequency shift keying (FSK) format at 1200bit/s. The central control equipment identifies the each data transmitted from N data terminals.

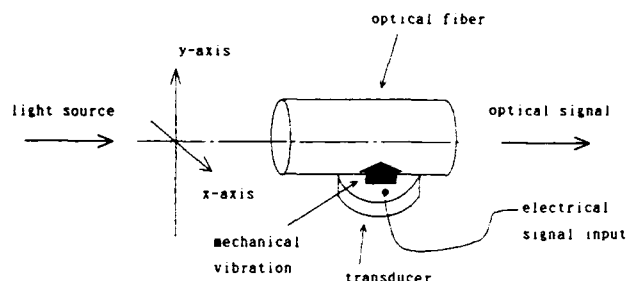


Fig.1 A transducer ( piezo-electric device ) applies a lateral stress into the optical fiber only by clipping on it.

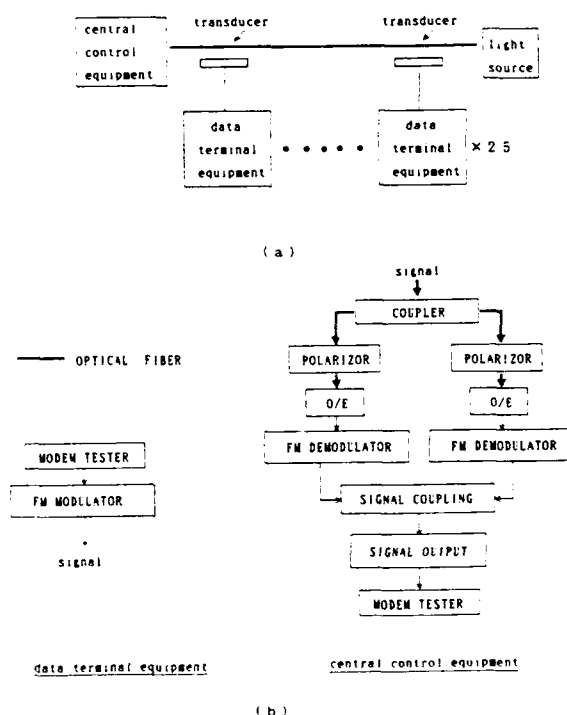


Fig.2(a) The schematic diagram of a data transmission system using the EPPM technique, which consists of one central control equipment and N data terminal equipments. (b) The scheme of terminal equipment and central equipment.

### 3. Experiment

In this experiment, the carrier frequency is ranged from 1.00MHz to 2MHz corresponding to the mechanical resonance frequency range of the transducer. In the data terminal equipments, an electrical signal with FSK format is converted to a mechanical vibration which is converted to a optical signal by the EPPM method. In the central control equipment, transmitted optical signals are detected by a photo diode resulting in a electrical signal. Especially in receiver end, polarization diversity scheme is used to compensate the influences of polarization fluctuation caused by vibrations due to dancing, temperature change in installed optical fiber.

#### 4. Minimum receiving optical level and S/N ratio

In the data transmission of experiment, a 1.00MHz electrical carrier was modulated by FSK signals with speed of 1200bit/s and deviation of 9kHz. Piezo-electric device is a disk with 1cm radius, and converts electrical signals into polarization modulated optical signals.

Fig.3 shows the experimental results of BER measurement using random signals. A minimum receiving optical level of -24dBm was obtained at  $BER = 10^{-6}$ , this bit error rate (BER) realize a high quality data transmission.<sup>21</sup>

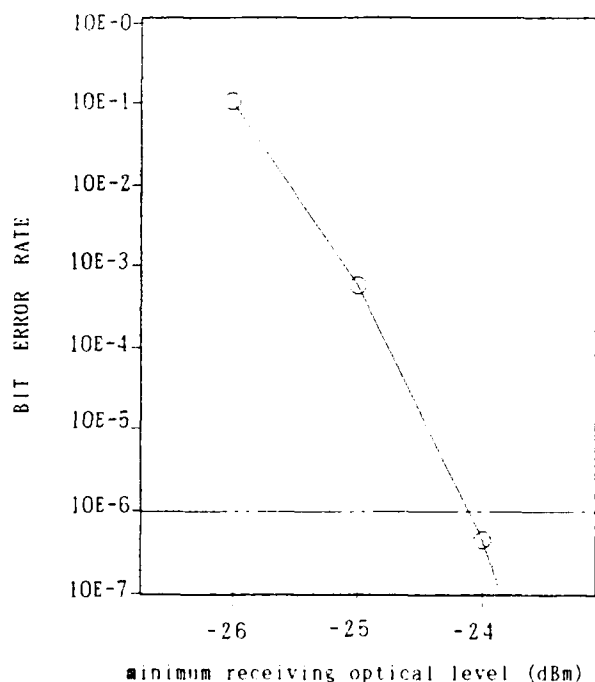


Fig.3 The experimental results of BER measurement using random signals.

### 5. FDM Performance Evaluation

In the system using EPPM method, the carrier frequency was restricted by the performance of the piezo-electric device.

In actual operation, influences of harmonics on desired signal could be considered. Therefore, a frequency range of 1.0MHz to 2.0MHz was chosen in the experiment. The maximum number of terminal equipment would depend on the spacing of the carrier frequencies. The frequency spacing in FDM is mainly determined by bandwidth of the narrow-band filter ( ceramic filter ) in the demodulation circuit on the received equipment. Fig.4 shows the frequency characteristics of the ceramic filter with bandwidth of 30kHz. As shown in Fig.4, essential 3dB-bandwidth is 20kHz.

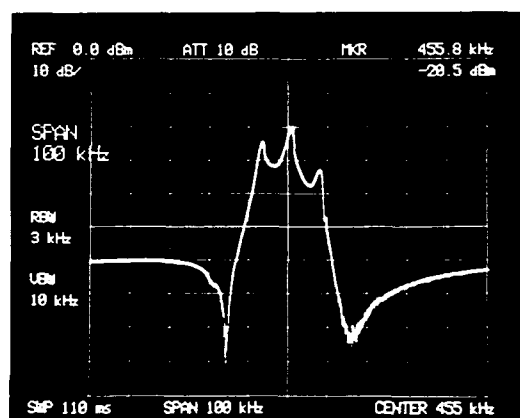


Fig.4 The frequency characteristic of ceramic filter with bandwidth of 30kHz.

It is important to consider the frequency variations of the electric circuit as a margin. Frequency variations of the oscillator circuit and of the other electric circuit can be considered to the cause of frequency fluctuations detecting signal. The frequency variations of the oscillator circuit is the range of  $\pm 1$ kHz for the setting frequency. The frequency variations of the other electric circuit is less than  $\pm 2$ kHz by both the transmitter and receiver side. As a result, a total margin of approximately 10kHz for each side is considered to be sufficient. The difference between the resonance frequency of the piezo-electric device and the carrier frequency, as the frequency fluctuates, will cause the decrease of S/N ratio.

The degradation of S/N is 2dB near 1.0MHz if the frequency deviates 10kHz. At 1.5MHz and higher frequencies, the frequency band that cause the degradation of S/N of 2dB is larger than 50kHz. Fig.5 shows the frequency characteristics of a 1.00MHz piezo-electric device when a signal is applied to SM optical fiber. The frequency band that cause the

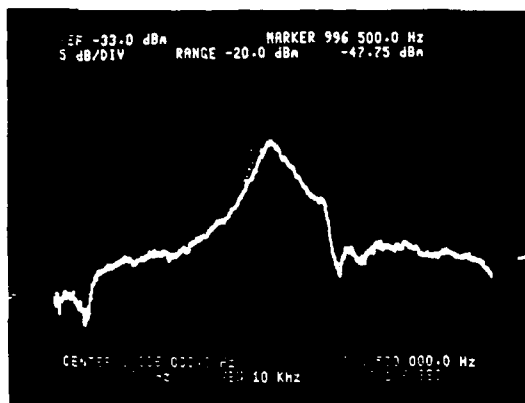


Fig.5 The frequency characteristic of 1.00MHz piezo-electric device when a signal is applied to SM optical fiber.

degradation of S/N of 2dB is 20kHz. These results show that the degradation of S/N can be ignored for the frequency fluctuations less than  $\pm 3$ kHz applied to the piezo-electric device.

Since the 3dB-bandwidth of the ceramic filter is 20kHz, a minimum frequency multiplex spacing of 20kHz is possible. According to the experimental results, a system margin of 20kHz is enough, resulting a minimum frequency multiplexing spacing of 10kHz.

Considering to the condition of bit error generation, the minimum possible carrier frequency spacing was confirmed. The signal was a FSK signal with a speed of 1200bit/s and deviation of 9kHz. The carrier with higher frequency was modulated by signals of '0' and '1' in proportion of 1:1 and the other one was modulated with a random FSK signal. The tests are performed at 1.00MHz - 1.01MHz for lowest frequencies ( Fig.6 ) and at 1.96MHz - 2.00MHz for highest frequencies ( Fig.7 ). And the polarization states of the optical fiber was varied by a retarder at the photo-detection level of -21dBm.

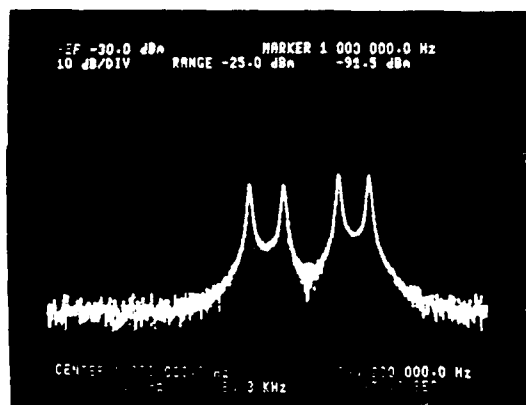


Fig.6 The frequency characteristic of 1.00MHz and 1.01MHz FSK signals.

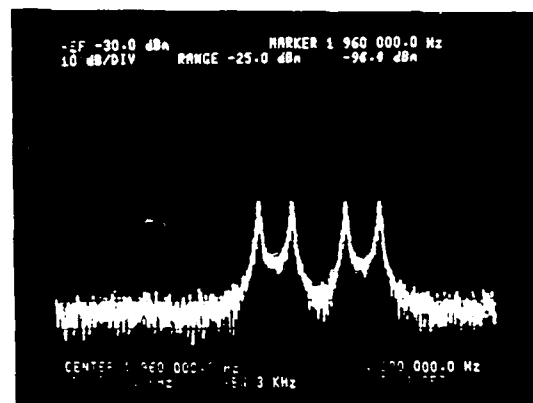


Fig.7 The frequency characteristic of 1.96MHz and 2.00MHz FSK signals.

Cross talk was not detected and the condition of bit error generation was no problem for the receiving optical level of -21dBm with intentional polarization fluctuation. The experimental results suggest that FDM data transmission with data terminals up to 25 between 1.00MHz and 2.00MHz in spacing 10kHz will be possible at a receiving optical level of -21dBm.

## 6. Verification of FDM

Section 4 and 5 verified data transmission with a minimum receiving optical level of -21dBm and in carrier frequency spacing of 10kHz. The results of verification tests conducted in the frequency range of 1.00MHz and 1.01MHz were described here.

The same communication method as described in sections 4 and 5 was used. The BER was measured with the carrier frequency on 1.00MHz signal.

Fig.8 shows the comparison between the BER of 1.00MHz signal with FDM and that of single 1.00MHz signal.

## 7. Concluding

The test results confirm that a data transmission systems with data terminals up to 25 and minimum receiving optical level of -21dBm will be possible using the FPM system for 1200bit/s FDM-FSK signal.

The FPM method is effective on up link, from data terminal equipments to central control equipment. To complete a duplex transmission, a down link is also necessary, which can be achieved by either local detection method or the use of coupler. The local detection enable the data transmission without cutting an optical fiber. Using the optical coupler in down

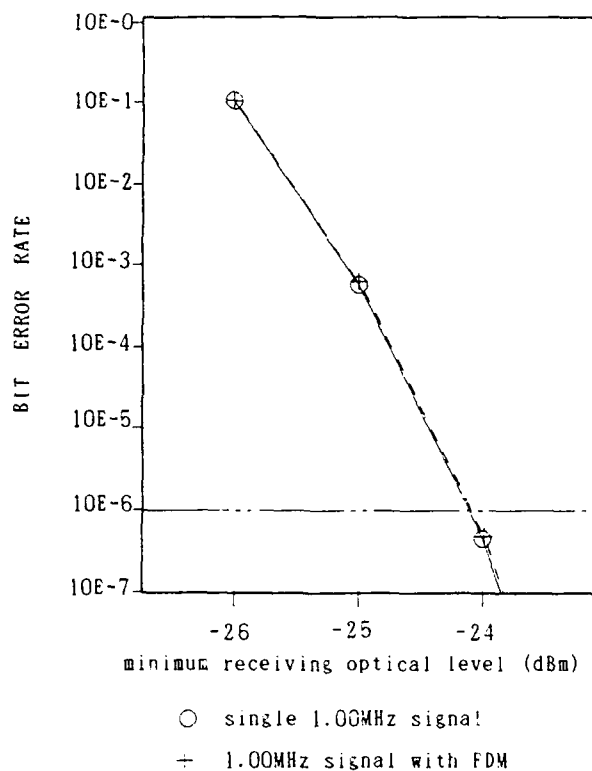


Fig.8 The comparison between the BER of 1.00 MHz signal with FDM and that of single 1.00MHz signal.

link, a wideband signal distribution allowing a value added service of picture transmission, data transmission, and telephone can be achieved.

#### References

- 1)A.Fujisaki,"OPTICAL TALK SET AND OPTICAL CABLE IDENTIFIER USING MOLARIZED-MODDULATION-WAVE-EXTERNAL-MODULATION METHOD",39th IWCS,1990, pp418-423
- 2)Joseph C.Palais,"FIBER OPTIC COMMUNICATIONS", Prentice-Hall Inc.
- 3)T.Takahashi,"COMMUNICATION SYSTEM AND TRANSMISSION METHOD",in Japanese, Electronics Communicationns Assosiation,pp455



HIJIRI NIMURA

The Furukawa  
Electric Co.,Ltd

Mr.Nimura received B.S.degree in physical engineering from Touhoku University in 1989 and joined The Furukawa Electric Co.,Ltd.

He has been engaged in optical fiber transmission research section.



AKIRA FUJISAKI

The Furukawa  
Electric Co.,Ltd

Mr.Fujisaki received B.S.degree in electrical engineering from Waseda University in 1987 and joined The Furukawa Electric Co.,Ltd.

He has been engaged in optical fiber transmission research section.



HIROYUKI FUDOU

The Kansai  
Electric Power  
Co.Inc.

Mr .Fudou graduated Sumoto Industrial high school in 1966 and joined The Kansai Electric Power Co.Inc.

He has been in charge of department of planning power distribution.

# MEASUREMENTS OF LOW HYDROGEN LEVELS IN INSTALLED OPEN FIBEROPTIC SUBMARINE CABLES.

S. Hopland

Norwegian Telecom  
Cables Division  
Oslo, NORWAY

## ABSTRACT

In this paper we present new data on the time dependence of hydrogen induced loss in installed open submarine fiberoptic cables with various types of armouring. Generally, the time dependence of hydrogen induced losses in cables shows individual patterns. Heavy armoured cables have higher levels than light armoured cables due to increased amounts of armour. Measurements made on cables stored on land have shown that initial hydrogen will present in installed cables for many years. LA cables installed up to 4.5 years have generally very low hydrogen levels with no signs of any delayed hydrogen induced loss increase due to water penetration through the outer high density polyethylene jacket. Measurements on buried cables have not shown increased hydrogen induced loss. Local damages on outer jackets are few and contribute very little on total hydrogen induced loss.

## 1. INTRODUCTION

In the last years several reports have been published on hydrogen evolution in fiberoptic underwater armoured cables with no hermetic barrier to protect the fibers from hydrogen ingress<sup>1-4</sup>. In these reports, there is a general agreement that hydrogen evolves from corrosion of the armour wires. However, only few investigations have been made of actual hydrogen levels in installed cables; and the measured hydrogen levels have varied several orders of magnitude. Some reports have measured large hydrogen levels in installed cables; predicting a strong dependence on sea depth of the hydrogen level. Another report<sup>5</sup> predicts that cable burial will generally increase the hydrogen level significantly after a relatively short time.

In a previous paper we reported very low hydrogen levels in light armoured cables up to 2.5 years after installation, with no signs of any depth dependence on hydrogen level. A few measurements made on the time dependence of the hydrogen level indicated a small increase with time on some of the cables.

In this report we present new data on the time dependence of the hydrogen induced loss in installed cables with various types of armouring. Data are also given on buried cables, installed trial cables and cables stored on land. The measurements cover the time period from cable production up to 4.5 years after installation.

## 2. CABLE CONSTRUCTIONS AND MARINE ENVIRONMENT

Norwegian Telecom uses submarine cables from two different cable manufacturers. The cable construction consist of a metal free cable core which may be of the slotted core or the loose tube design. The cable core is surrounded by a jacket of polyethylene, and then follows an armour consisting of galvanized steel wires. A rubber asphalt or bitumen filling compound is used around the steel wires to prevent longitudinal water intrusion and corrosion. Finally, an outer jacket of high density polyethylene is used to give extra protection against water corrosion. The cable construction for the light armoured cable (LA) is shown in Fig. 1. For the heavy armoured cable (HA), an extra layer of armour is applied to provide extra tensile strength.

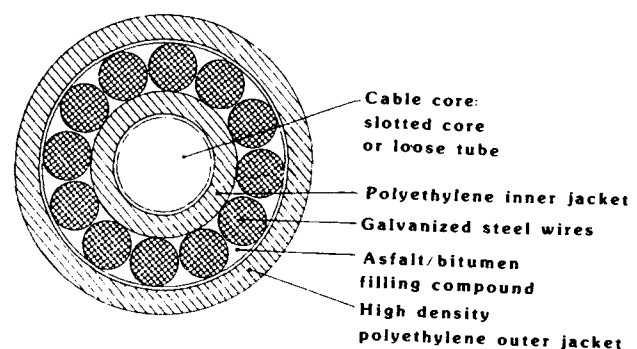


Figure 1: Submarine light armoured (LA) cable construction.

Norwegian Telecom uses submarine cables to build parts of the trunk and regional network along the coastline. The cables are laid with high precision along optimal routes between landing points. The routes and the landing points are chosen to avoid fishing activities and according to the bottom topography. In the Norwegian fjords, a cable route will typically follow steep, rocky bottom near the landing points, while the middle part of the route may be flat with clay and/or sand. The cables are usually laid directly on the sea bottom, but in some areas where fishing activities (trawlers) cannot be avoided, the cable is buried. The burial depth is determined according to the sea bottom conditions, but will usually be no less than 60 cm. LA cable is used in areas with no risk of fishing activities, while HA cable is used in areas with light fishing activities or on routes where the cable is buried.

### 3. PREVIOUS MEASUREMENTS

Previous measurements showed very low hydrogen induced losses on installed LA cables 2.5 years after installation<sup>1</sup>. The hydrogen induced loss in the same cables, measured on small leftover lengths stored dry on land, had decreased to nearly zero level in this time scale. We also showed that hydrogen induced loss was present in each cable shortly after production due to initial corrosion of the armour wires.

This implies that if initial hydrogen is the only hydrogen generated in a cable, the hydrogen level in cables will generally go through some time cyclis and eventually drop off to zero. Increased temperature will increase the hydrogen level and shorten the time constants in the cyclis.

However, for installed cables, it seems reasonable to assume that, in addition to initial hydrogen, delayed corrosion may occur after some time due to possible water penetration through the outer high density polyethylene jacket.

### 4. NEW MEASUREMENTS

Measurements have been made on time dependences of hydrogen levels in installed cables, cables stored on land and installed trial cables with various types of armouring. We have also measured hydrogen levels in areas where cables are buried and in areas with damages on the outer jackets.

#### 4.1 Measured cables

Totally, we have measured 35-40 different cables repeatedly, both light armoured and heavy armoured. The cables have been cables stored on land, installed cables and deployed trial cables. The length of the installed cables varies between 4 km and 20 km and the maximum installation depths varies between 20 m and 1000 m. The deployed trial cables and the cables stored on land have been mainly short lengths. All of the cables have been

of the construction type showed in Fig. 1, except for one cable having a different outer protection consisting of asphalt/polypropylene yarn.

#### 4.2 OTDR and spectral measurements

The peak wavelength of hydrogen induced loss have been found to be 1244 nm<sup>1,6</sup>, and by using two different OTDR-modules at 1238 nm and 1241 nm, we are able to detect 50 % and 70 % of the loss increase at 1244 nm, respectively. For each cable a minimum of 3 fibers were measured every time, and average loss values were used to calculate the hydrogen induced loss at 1244 nm and the hydrogen induced loss variations with time. The time interval between measurements have varied according to the expected variations of hydrogen level. The OTDR-modules at 1238 nm and 1241 nm was also used to map out variations in hydrogen level along the length of each individual cable.

On the short cable lengths, fibers were looped and spectral loss curves were made in addition to OTDR-measurements. OTDR-measurements at 1310 nm and 1550 nm were made each time for control purposes.

### 5. MEASUREMENTS RESULTS

#### 5.1 Cables not deployed in sea

If cable lengths for some reason are not deployed in the sea, they are stored dry on land. Earlier measurements made on LA cables indicated that the initial hydrogen level goes through some cyclis and return to nearly zero level after a time period of less than 2.5 years when stored at an average temperature of approximately + 10 °C<sup>1</sup>. Since then, we have regularly measured one HA and one LA cable length stored dry on land. For the HA cable, the storage temperature have followed air temperature except for the first 20 days after production (armouring) when the cable was stored in the factory at room temperature. The LA cable was stored the first 3 months in the cable ship at approximately + 20 °C. The results are shown in Fig. 2.

We register that the HA cable reaches a first maximum level in approximately 2 months. After that, hydrogen induced loss have passed through two minima and one maximum. The variations in hydrogen induced loss through the year may be explained by air temperature variations. The average temperature in the whole storage period was + 7.1 °C. For the LA cable, the behaviour of the hydrogen induced loss is similar to the HA cable; only showing generally lower induced loss.

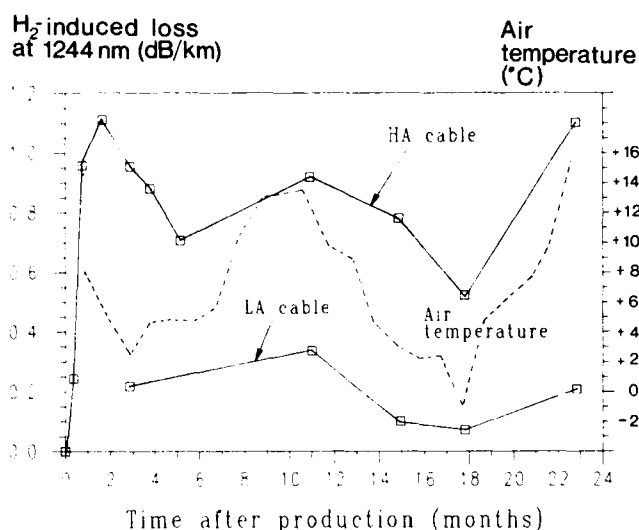


Figure 2: H<sub>2</sub>-induced loss in cables stored on land.

For the HA cable, we can not register any clear tendency for hydrogen induced loss to decrease during the storage period. For the LA cable, there is a slight tendency for the induced loss to decrease during the storage period, which is in agreement with our earlier measurements made on leftover lengths stored on land.

These results implies that for installed cables, at temperatures 3-5 °C, initial hydrogen will be present in the cables for several years.

## 5.2 Cables before installation

Time may pass between the production and the actual installation of fiberoptic submarine cables; varying from a few days up to one month. Therefore, cables may be temporarily stored in the factory or in the cable ship. We have measured the hydrogen level in 3 cables shortly after production (armouring) at a storage temperature of + 20-25 °C. The results are shown in Fig. 3.

We register that LA and HA cables reach a first plateau of hydrogen induced loss within 20-30 days after armouring. Consequently, the thermal history of a cable before installation will affect the time dependence of hydrogen level after installation. Examples of this effect are shown in chapter 5.3.

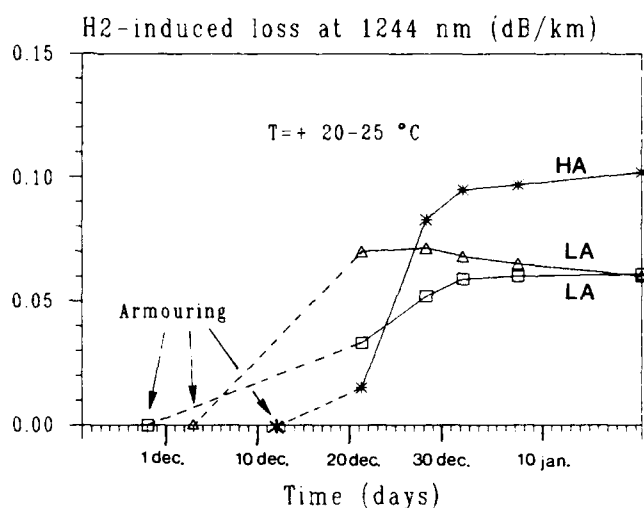


Figure 3: H<sub>2</sub>-induced loss in cables before installation.

## 5.3 Installed cables

### 5.3.1 Cables in the first phase after installation

During 1989, Norwegian Telecom installed several submarine cables of LA and HA type. We have selected a number of cables of each type and measured them regularly since installation. In some of the cables, the time delay between production and installation were minimal; only a few days. The rest of the cables were stored in the factory or in the cable ship for 10-30 days at + 20-25 °C before they were installed.

In Fig. 4 and Fig. 5 is shown the hydrogen induced loss for LA and HA cables, respectively, up to 25 months after installation, for cables installed shortly after production. The results show that the hydrogen induced loss in LA cables reach a first maximum level or plateau 4-9 months after installation. After that, one cable has passed through a second maximum, other cables seem to be on their way to a second maximum, and one cable have reached only one plateau so far. In fact, each cable has its own individual pattern. For the HA cables, the time before a first plateau is reached is 12-25 months or longer.

Clearly, the hydrogen induced loss in the HA cables are on average higher than in the LA cables in accordance with the greater amount of armour in HA cables. Also, the time constants for the HA cables are longer than for the LA cables, which one would expect due to longer diffusion distances for hydrogen in HA cables.



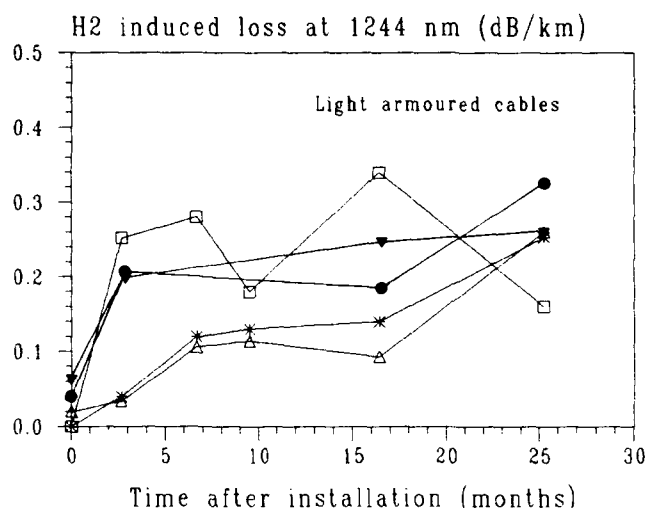


Figure 4: H<sub>2</sub>-induced loss in "fresh" LA cables after installation.

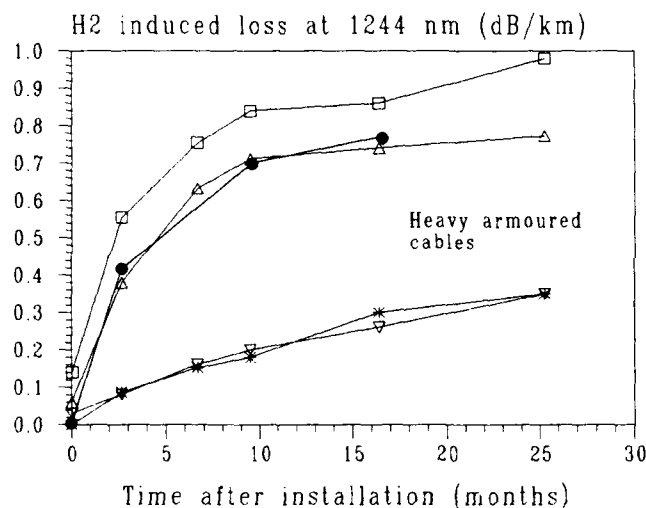


Figure 5: H<sub>2</sub>-induced loss in "fresh" HA cables after installation.

In Fig. 6 are shown the hydrogen induced losses in LA and HA cables up to 17 months after installation for cables that were stored for 10-30 days at + 20° C in the cable ship before they were installed. Hence, at the installation time, each cable have passed through a part of its initial hydrogen course. For many cables, we can register that temperature lowers the hydrogen level in the first few months. After that, each cable follows its own individual pattern.

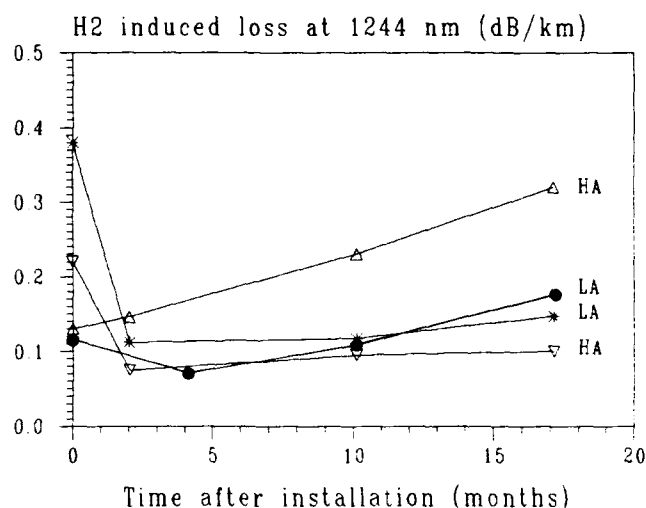


Figure 6: H<sub>2</sub>-induced loss in "matured" LA and HA cables after installation.

### 5.3.2 Cables at longer times after installation

We have also made regular measurements on LA cables beeing installed for up to 50 months. The results are shown in Fig. 7. We register only small changes in hydrogen induced loss with time. We can also here see different patterns for induced loss developement in the cables. There is no evident trend for any general loss increase which could indicate any delayed hydrogen reaction due to water penetration through the outer high density polyethylene jacket.

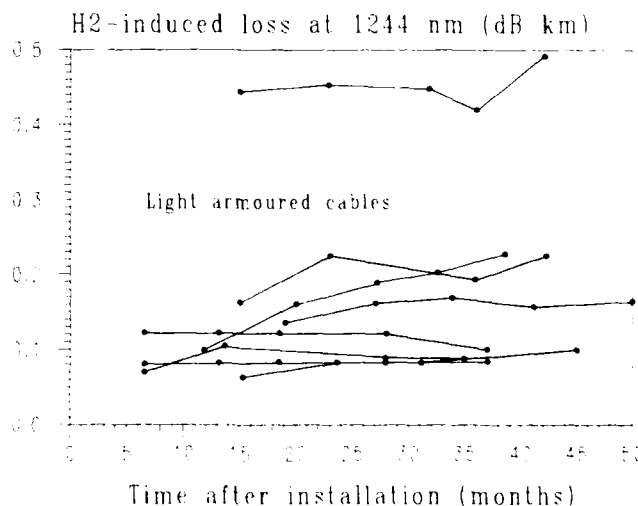


Figure 7: H<sub>2</sub>-induced loss in LA cables at longer times after installation.

### 5.3.3 Cable with outer protection of asphalt/polypropylene yarn

Norwegian Telecom have installed one 7 km long cable at a maximum depth of 400-500 m with an outer protection of asphalt/polypropylene yarn. Up to 2 years after installation, this cable showed a uniform low level of hydrogen induced loss along its length<sup>1</sup>. After that, the hydrogen induced loss in this cable has increased steadily. In particular, the hydrogen induced loss near the beach joints (part 1 and part 4), have increased more than the middle part of the cable (part 2 and part 3); laying mainly on flat bottom. In Fig. 8 the development of hydrogen induced loss for the different parts of this cable is shown. The reason for this development may be that the "shore ends" of the cable are more exposed to sea movements which gradually wash out the asphalt/polypropylene protection layer and cause increased corrosion. The deeper middle part of the cable, mainly laying on flat bottom, may have moved into the soft clay bottom, or the sea movements are less pronounced; hereby resulting in less corrosion.

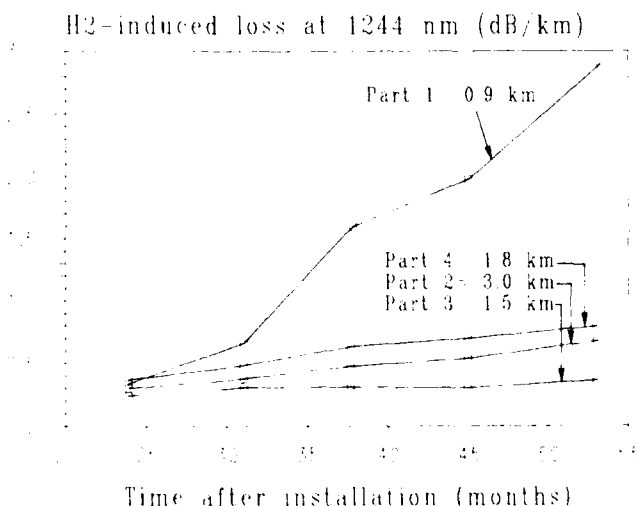


Figure 8: H<sub>2</sub>-induced loss in different parts of a cable with outer protection of asphalt/polypropylene yarn.

### 5.3.4 Trial cables

To find out more about possible delayed reactions caused by sea water, two short LA cable lengths were deployed in sea water at approximate depths of 50-100 m. These cable lengths were leftover lengths from early installations, and had been stored on land for 2-3 years. In these cables, the hydrogen induced losses at 1244 nm were found to be zero. One cable was the LA construction showed in Fig. 1, while the other cable had asphalt/polypropylene yarn as outer protection. Fig. 9 shows the deve-

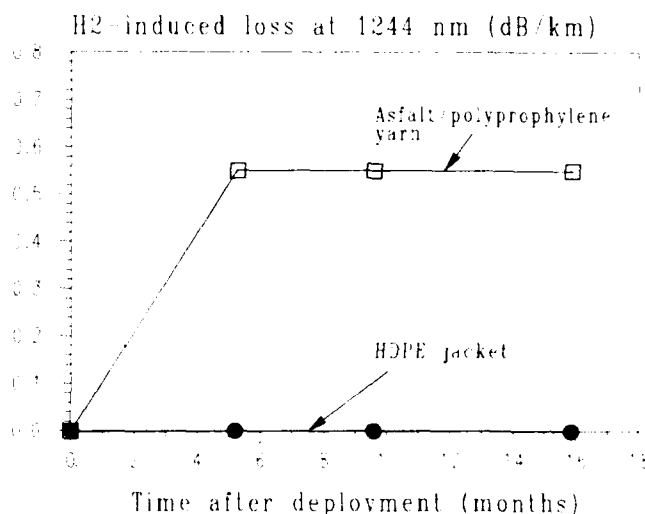


Figure 9: H<sub>2</sub>-induced loss in trial cables after deployment.

lopement of hydrogen induced losses up to 16 months for the two cables. There is no signs of any hydrogen in the standard construction, while the asphalt/polypropylene yarn cable shows a relatively low constant hydrogen level. These results are in agreement with the observations on our installed cables.

### 5.3.5 Buried cables

In a few cases we have partly buried installed cables to protect them against fishing activities. The hardness of bottom materials can be expressed by their so called shear strength, and the bottom materials in the areas of our buried cables can be characterized as relatively soft. The burial depth for the cables has been approximately 60 cm. We have studied the distribution of hydrogen induced loss along the buried/unburied parts of our cables. Table 1 summarizes the results.

Cables	Total length (km)	Buried length (km)	Shear strength (kN/m <sup>2</sup> )	Time after burial (months)	Atten. 1241 nm unburied (dB/km)	Atten. 1241 nm buried (dB/km)
Cable 1(HA)	12	4.2	sand	16	0.94	0.94
Cable 2(LA)	3.8	2.4	10-20	8	0.71	0.64
Cable 3(LA)	10	4.5	10-20	8	0.53	0.56

Table 1: H<sub>2</sub>-induced loss in buried cables.

Since we have observed that most cables have initially some small variations in hydrogen induced loss along the length, it is not possible to reveal any increased hydrogen induced loss in the buried parts of any of the cables.

### 5.3.6 Characteristics of outer jacket damages

In our earlier work<sup>1</sup> we found that in a few cases where the outer high density polyethylene jacket had been damaged, an increased hydrogen evolution was found in a small area near the damage where water penetration along the armour wires had resulted in increased corrosion. A local damage can be characterized by the cable length affected by increased hydrogen induced loss and the magnitude of induced loss in this cable length. These two parameters may be a function of time. Such damages are easily located on the 1238 nm and 1241 nm OTDR traces, while they are not visible on the 1310 nm OTDR traces. We have investigated all the measured cables, a total length of approximately 325 km with a total installation time of approximately 72 years, and we have found a small number of damages. A summary is shown in table 2.

Damage	Cable	Cause of jacket damage	Depth (m)
D1	Cable A	Retrival/new installation of cable	50
D2			50
D3	Cable B	Installation of cable	200
D4	Trial cable	Installation of cable	1000

Table 2: Summary of observed cable jacket damages.

The time dependence of cable length affected by increased hydrogen induced loss and magnitude of hydrogen induced loss, respectively, are shown in Fig. 10 and Fig. 11.

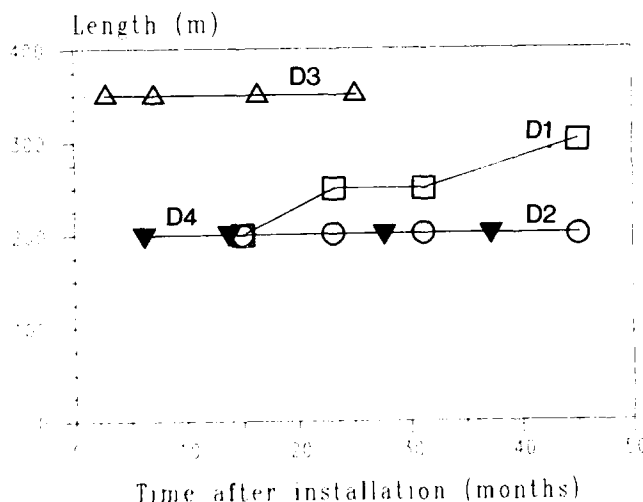


Figure 10: Cable length affected by increased H<sub>2</sub>-induced loss in cables with jacket damage.

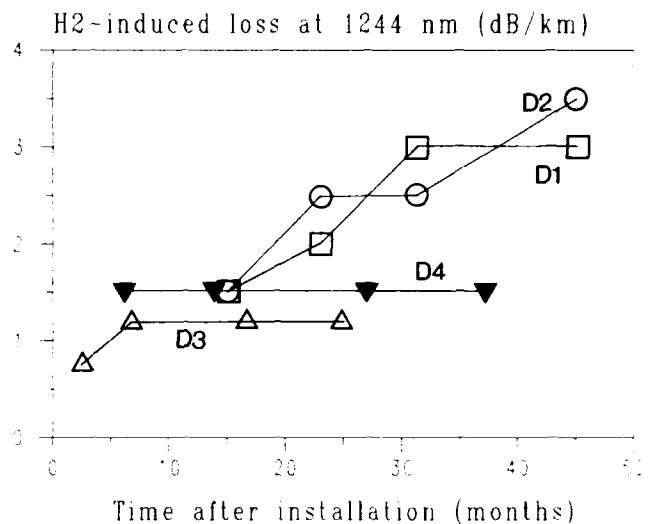


Figure 11: H<sub>2</sub>-induced loss in areas with cable jacket damage.

The cable length affected by increased hydrogen induced loss have stabilized shortly after the occurrence of a damage, and a typical length is 200-350 meters.

For cable B and trial cable, the hydrogen induced loss stabilizes after few months at a level of 1-2 dB/km. For cable A, the hydrogen induced loss at 1244 nm have increased somewhat since our measurements started, and is presently 3-4 dB/km. We register that cable A is installed in a heavy polluted marine environment (chemical waste), while this is not the case with cable B and trial cable.

Clearly, increased local hydrogen level due to a typical jacket damage will not affect the cable's total hydrogen level much. For example, on a 10 km cable length, damage D3 will increase the hydrogen induced loss at 1244 nm by 0.04 dB/km.

All the damages were found on cables installed several years ago. Since then, our installation/-retrival methods have improved and this should contribute to lower the frequency of cable jacket damages even further.

### 5.3.7 Depth dependence

We have previously found no depth dependence of the hydrogen induced loss<sup>1</sup>. Our new measurements have confirmed this observation; no evidence of any depth dependence is found. On the contrary, we have observed that, on the cable with outer protection of asphalt/polypropylene yarn, the hydrogen induced loss on the shallow parts of the cable has become greater than on the deeper middle part of the cable.

#### 5.4 Attenuation increases at 1310 nm and 1550 nm

The attenuation increases in our installed HA cables at 1310 nm and 1550 nm were found to be approximately 0.01 dB/km and 0.035 dB/km, respectively, for levels of hydrogen induced loss at 1244 nm of 0.7-0.8 dB/km. In the LA cables, the attenuation increases at 1310 nm and 1550 nm were only marginal.

#### 6. CONCLUSION

We have presented substantial new data on the time dependence of hydrogen induced loss in open LA and HA fiberoptic submarine cables. Measurements on cables stored on land have shown that initial hydrogen will be present in installed cables for many years. Measurements on installed cables have indicated that cables have individual time dependences of hydrogen induced loss. Hydrogen induced loss is generally higher and time constants are longer in HA cables than in LA cables due to the greater amounts of armour and longer diffusion distances. The thermal prehistory of cables will affect the time dependence of hydrogen induced loss in the first phase after installation. Measurements made on "dry" installed trial cables have shown no evidence of any delayed hydrogen induced loss due to water penetration through the outer high density polyethylene jacket up to 1.5 years. LA cables installed up to 4.5 years have shown generally very low hydrogen induced loss with no evident signs of any delayed hydrogen induced loss increase. In a part of a cable with outer protection of asphalt/polypropylene yarn, the hydrogen induced loss have increased substantially, probably as a result of outwashing of the outer protection. Measurements made on buried cables have not shown any increased hydrogen induced loss in the buried parts compared with the unburied parts. The frequency of outer jacket damages on installed cables are very low, and the hydrogen induced loss increase on a 10 km cable length due to a typical jacket damage is small. We have found that hydrogen levels of 0.7-0.8 dB/km at 1244 nm corresponds to induced losses at 1310 nm and 1550 nm, of approximately 0.01 dB/km and 0.035 dB/km, respectively. Finally, there are no signs of any depth dependence of the hydrogen induced loss in our cables.

#### 7. ACKNOWLEDGEMENT

The author would like to thank I. Gangsø, P. Berglund, J. Fladberg and E. Marhaug at Norwegian Telecom, Cables Division, for helpful assistance in collecting the field data. Thanks also to our cable manufacturers for continuous valuable discussions on the subject.

#### 8. REFERENCES

1. S. Hopland: "Investigation of total and distributed hydrogen levels in installed fiberoptic submarine cables": IWCS 1989, pp. 684-688.
2. N. Hardwick et al.: "Corrosion-resistant armour to prevent H<sub>2</sub>-induced loss in underwater (wire-armoured) fiber optic optical cable": IWCS 1989, pp. 689-695.
3. G. Shick et al.: "Hydrogen sources for signal attenuation in optical fibers": IWCS 1990, pp. 244-254.
4. W. T. Anderson et al.: "Field measurements of the effects of hydrogen gas on installed submarine single-mode fiber cables": IWCS 1989, pp. 675-683.
5. N. Skovgaard et al.: "Performance of low-loss submarine cables": IWCS 1990, pp. 23-26.
6. J. Stone: "Interactions of hydrogen and deuterium with silica optical fibers: A review": Journal of Lightwave Technology, Vol. LT-5, No. 5, May 1987.



Svend Hopland

Norwegian Telecom  
Cables Division  
Munch's gate 5B  
N-0130 Oslo 1, NORWAY

Svend Hopland graduated from the Norwegian Institute of Technology in 1985 with a Ph. D. on optical fibers. In 1986 he joined Norwegian Telecom, Cables Division. He is presently a senior engineer on fiberoptic cables.

## O. F. RIBBON CABLE SYSTEM TECHNOLOGY: THE ITALIAN EXPERIENCE

F. ESPOSTO, F.MONTALTI, F.NANNI

SIP-DG Via di Valcannuta 250 Rome ITALY

### Summary

In order to foster the introduction of the optical fibre in the subscriber loop, different approaches were made to reduce the cost of cables, materials and installation.

The ribbon cable system technology, which appears to be a promising solution, has been introduced in the Italian Telecommunication Network at the end of 1990 with several field trials.

This paper describes the Cable System used in Italy as well as the first results from the field involving cable installation, splicing performances and overall link measurements.

The results obtained helped in making a first comparison between the ribbon technology and the "traditional" single fibre technology.

### 1. Introduction

The introduction of the optical fibre in the subscriber loop is one of the aspects of a general process of digitalization of the loop network that is already in progress with the provision of 300.000 POTS by means of 2 Mbit/s DLCs.

The use of the optical fibre will allow to overcome the technical limits of the metallic cables, to optimize the utilization of the network infrastructures in the congested metropolitan areas and to pave the way to the future synchronous technologies and wide band services.

The first experiments in Italy with the optical fibre in the subscriber loop were carried out in the year 1988 with several business subscribers in the metropolitan areas of Milan, Turin and Rome. The cables and components used were the same installed in the trunk and long distance network.

In the subscriber network, with the average length not very long (1.5 - 2 km typically), no problem occurs with the transmission performances of the link.

In this situation, considering the volume of fibres, cables and components that are involved, it is of the outmost importance to investigate all the areas of possible cost saving and pursue the objective of a total cost reduction in every part of the link. In this way it is possible to take advantage of multiple splicing techniques, mass production of components, development of new installation procedures.

In general a synergy between plant components and installation techniques must be reached that

guarantees both technical performances and cost objectives.

The right answer is a "Cable System" technology" where the integration of cables, splicing techniques, materials and installation is performed. Such an approach optimize all the network components in terms of cost and performances in order to guarantee the economy of the optical link, the reliability and the consistency to the specification.

The SIP (Italian Telecommunication Operating Company) decided to take advantage of the optical fibre ribbon technology already used in some other Countries as a basis for the trials in the subscriber loop in Italy.

### 2. The Cable System

The "Cable System" consists on an integrated system of modular elements (cables, mechanical connectors, fan-outs, optical terminations, closures, cabinets, MDF) whose components are assembled as much as possible in the factory.

All the elements meet the goal of high quality and performances and their use lead to the reduction of components cost, to more simple installation procedures and to the possibility in the future of an automatic monitoring and management of the network with a reduction of maintenance costs and with an increase of availability of the local network.

The key components of the "Cable System", namely the fibre ribbon, the mechanical splice and the fan-out, are being described in the following paragraphs.

#### 2.1 Fibres and Cables

The configuration of the subscriber network requires to hold fibre cables in due consideration with straightforward fibre groups identification and separation capabilities and ease of fibre handling. The fibre ribbon represents up to date a very good solution for these problems and, in addition, it allows the design of high fibre count cables with quite small outer diameter for conduit installation.

The solution of 4 fibre ribbon (Fig. 1) has been adopted and cables of 4, 8, 20, 100 and 400 fibres have been provided by the Italian cable Manufactures following the SIP specifications.

The fibre used is Single Mode Reduced (SMR) optimized for 1300 nm and with good performances at 1550 nm because of its good behaviour towards

both to micro and macrobending.

The 100 fibre cable (Fig. 2) has a loose slotted core design with 5 grooves where the ribbons, organized in groups of 5, are positioned.

The 400 fibre cable (Fig. 3) is built up stranding four 100 fibre units together with one dummy unit around a central member.

The cables core is metal free, jelly filled with PU and PE inner and outer sheaths with a double layer of aramidic yarns as pulling element. An heat welded corrugated tape made by 0.15 mm thick stainless steel acts as humidity barrier and rodent protection.

The reduced dimensions of both cables (outer diameter around 20 mm for 100 fibres and 40 mm for 400 fibres) allow an easy installation inside the existing ducts and this performance is very useful in the local network especially in the congested metropolitan areas.

The structure of the 20, 8 and 4 fibre cables is the same; the 4 and 8 fibre cable are also manufactured with flame retardant LSOH sheath instead of PU and PE in order to meet the strict Italian law requirements for indoor cables.

For this reason the 100 fibre termination cable, inside the central office between the pot-head joint and the main distribution frame, has the same kind of sheaths.

The optical characteristics of the fibres and the mechanical characteristics of the cables are shown in table 1 and 2.

## 2.2 Multiple jointing techniques

Considering the high number of splices in the subscriber loop, one of the principal problems concerns the ease and speed of jointing, also bearing a relatively high connection loss.

This has led to the development of simultaneous multiple fibre splicing techniques either by fusion or by mechanical connectors with considerable reduction in jointing times.

### 2.2.1 Fusion mass splicing

The procedure for splicing the fibre ribbons is quite similar to the one used for the single fibre.

The ribbon coating is removed by means of a suitable stripping device and the 4 fibres are cutted at the same time with a cleaving tool.

Automatic splicing equipments assure optical and environmental performances similar to the single fibre ones.

### 2.2.2 Mechanical splicing

The MT mechanical joint developed by NTT is based on the alignment of two plastic moulded ferrules by means of two guide pins and a clamp spring (Fig. 4). This product is used to preconnectorize in the factory one end of the cable; in such a way the field installation is simplified, being reduced to a mere manual operation, while the quality of the termination is largely increased.

As alternatives the mechanical joints Array Splice (AS) of ATT and Silicon Multifibre Connectors (SMC) of Siemens have been tested, both

based on the alignment of silicon grooved chips.

These three techniques, quite similar in performances, are currently under evaluation in term of cost and availability of production facilities in Italy.

## 2.3 Connectors

The main characteristics to be considered in choosing an optical connectors are: low insertion loss, high values of return loss, high reliability, miniaturization and low cost.

SIP decided to choose the SC type connector (Fig. 5) among the components tested. It consists in a zirconia cylindrical ferrule polished in a convex way in order to assure the physical contact between the fibres, inserted in a outer plastic moulded housing. It is going to be manufactured in Italy and is installed since June 1991 in the Italian network.

## 2.4 Fan-out

At both ends of the local loop, in the main distribution frame and in the subscriber premise, the transition between the fibre ribbon terminated with mechanical joints and the single fibre patch-cords terminated with the SC connector plugs is assured by the fan-out (Fig. 6).

This element consists in a lengths of ribbon jacketed with a protection sheath and terminated with a mechanical joint at one end and four SC connector plugs at the other.

The fan-out is factory assembled and installed when the system is put into operation; its use allows a reduction of cost of the cable termination and makes the installation easier. In table 3 the optical performances of multiple joints, connectors and fan-outs are shown.

## 3. Installation components

Taking into account the peculiar characteristics of the subscriber network in terms of flexibility and future implementations, a complete new line of materials for the splicing and termination of the fibre ribbon were developed.

Efforts were made to reduce as much as possible the number of products in order to benefit of cost reduction by large scale production.

The Cable System components are the following:

- main distribution frame in mechanical European standard technique for the termination with fan-outs of 400 fibres (Fig. 7);
- splice closures for 400 fibres and 100 fibres: both can be used for the line as well as the pot-head joints. The closures allow the branching of up to five cables from the principal one (i.e. 100 fibre cable in and 5x20 fibre cables out);
- mid span branching closure: allows the extraction of up to 40 fibres from an already installed 100 fibre cable without service interruption;
- distribution cabinet for underground installation: allows the distribution of five 4 fibre cables from a 20 fibres cable;

- distribution cabinet for indoor installation with the same characteristics as above;
- subscriber termination for one or two fan-outs.

All the above components are reenterable, can accommodate both mechanical and fusion splices, and are designed to match the preterminated cable ends.

#### 4. Field Trials

The Cable System technology has been field tested in several experiments in Italy during 1990 in Rome, Turin, Padua and Naples with a number of business subscribers.

An example of a subscriber link configuration with the details of the components used is shown in fig. 8.

Taking into account safety considerations it was decided to have a complete underground network.

The installation of the cable inside tortuous and congested duct systems together with the constraint of pulling the cable in only one direction because of the preterminated end, limited the cable length size, in particular for the 400 fibre cable (about 500 m). Cables were installed with pulling winches and occasionally by hand.

A total of about 1500 km of fibre has been deployed. The 400 fibre and 100 fibre cables account respectively for the 36.4 and the 55.1 % of the overall fibre.

As far as installation typologies are concerned most of the cable (63.4 %) has been installed inside ducts and only 14.3 % in trenches.

The cables up to 100 fibres have been laid inside 50 mm diameter plastic ducts (three of them equipped a 125 mm duct) while the 400 fibre cable inside 125 mm diameter ducts.

The use of cable lengths with one factory preterminated and requires the combination of mechanical and fusion splices alternating along the link.

The ribbon technology allows a considerable reduction in jointing times; in particular with the mechanical splice, the jointing procedure reaches the maximum of simplicity.

A total of about 1154 multiple splices have been made (615 by MT connectors and 539 by fusion).

For what concerns the fusion splices losses, an average value of 0.06 dB with a standard deviation of 0.04 dB was attained (Fig. 9).

The automatic splicing equipment proved to work in a satisfactory manner. The correlation between the actually measured loss of fusion multiple splices and the loss estimated by the splicing equipment is fairly good with a correlation factor greater than 0.8. In fact only 3% of the splices had to be redone after the final bidirectional measurement.

The average loss value of the mechanical splice was 0.52 dB with standard deviation 0.29 (Fig. 10).

Both the values are consistent with the provisional SIP specification for the plant acceptance tests (maximum values of 0.2 dB and 1.2 dB for the fusion and the mechanical splices respectively).

After the final acceptance test all the links have been put into operation and are successfully carrying normal traffic.

#### 5. Conclusions

The experience gained with the implementation of several plants with the ribbon "Cable System" technology allows to draw some preliminary conclusions.

The advantages of the ribbon "Cable System" compared to the traditional technology come out from the high packaging density of the fibres, the ease of ribbon handling, the preassembly of components in the factory, the use of multiple interconnection techniques.

All these factors guarantee a high quality and contribute to the reduction of the installation costs also shifting labour man power cost to cables and components. Other areas of cost saving are envisaged in the feasibility of automatic optical measuring techniques of the cables in the factory and of the overall installed link.

In a future perspective, the ribbon "Cable System" will allow also the flexible access to the network, the possibility of an automatic reconfiguration of the link and the surveillance of the network from the Central Office.

On the other hand the use of preassembled cables ends of precise length both on line and in the central office need a very accurate planning of the outside plant configuration.

One item of the utmost importance is the development of new techniques of installation on the last part of the subscriber network where the common practice of pulling only one cable inside a sub-duct becomes antieconomic as the number of subscriber grows. New subscriber cables with smaller outer diameter as well as multi-hole preformed plastic ducts are under development and will be tested in the field.

Computer aided measurement techniques for the final acceptance test as well as a monitoring technique for the plant surveillance from the Central Office will be implemented in the near future in order to exploit the benefits of the Cable System.

Considering the satisfactory results of the first trials and in order to clarify points that need further study and to define with better accuracy the installation costs, it was decided to implement the introduction in the subscriber network of the Cable System to provide high frequency services to large and medium size business subscribers in the major cities in Italy.

A total of 13.000 km of fibre will be deployed in the subscriber loop in 1991 and an implementation is foreseen for 1992.

MECHANICAL CHARACTERISTICS OF CABLES

NUMBER OF FIBRES	4-8	20	100	400
Outer diameter (mm)	13	16	19.5	40
Weight (kg/km)	180	270	370	1300
Max pulling strenght (kg)	60	300	350	450
Minimum bend radius (mm)	170	300	300	400
Factory lenght (m)	2000	3000	3000	500

TABLE 1

OPTICAL FIBRE CHARACTERISTICS

	1300 nm	1550 nm
MFD (um)	9.4	10.5
Cladding diameter (um)	125	125
Primary coating diam. (um)	250	250
Attenuation (dB/km)	<0.44	<0.28
Chromatic dispersion (ps/nm km)	<3.4	<18
Cut off wavelenght (nm)	<1280	<1280

TABLE 2

COMPONENTS OPTICAL PERFORMANCES

	INSERTION LOSS (dB)		RETURN LOSS (dB) (directivity)
	average value	std deviation	minimum value
Mass fusion splice	0.06	0.04	60
Array splice	0.30	0.19	40
SMC connector	0.36	0.19	40
MT connector	0.52	0.29	35
SC connector	0.1	0.05	35
Fan-out	0.62	0.34	35

TABLE 3

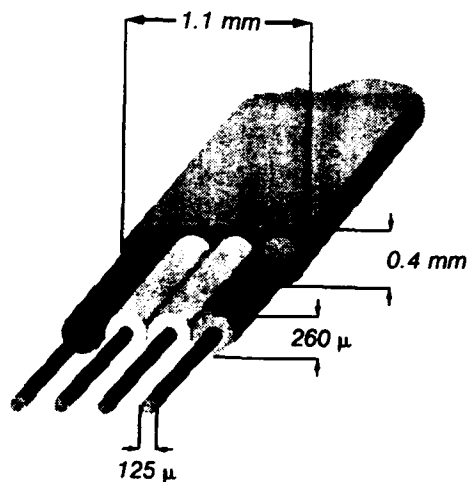


Fig. 1 - Four fibre ribbon

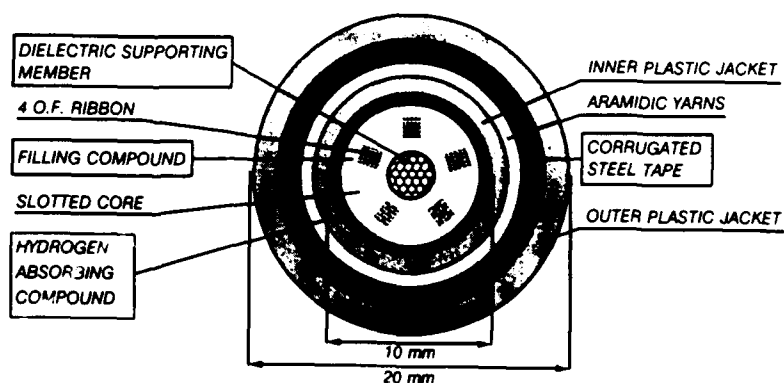


Fig. 2 - 100 fibres cable



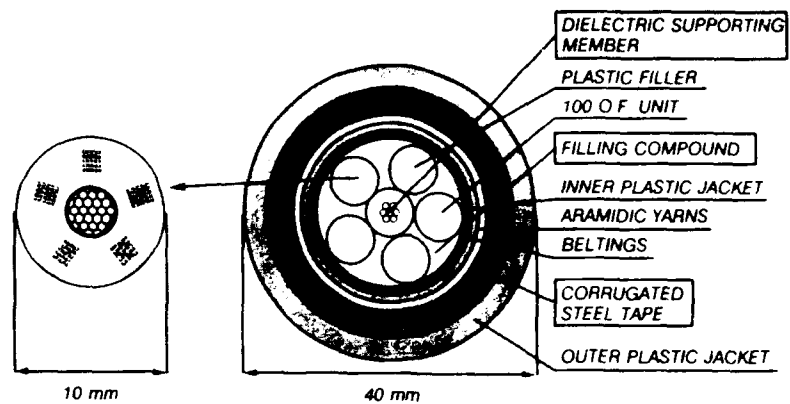


Fig. 3 - 400 fibres cable

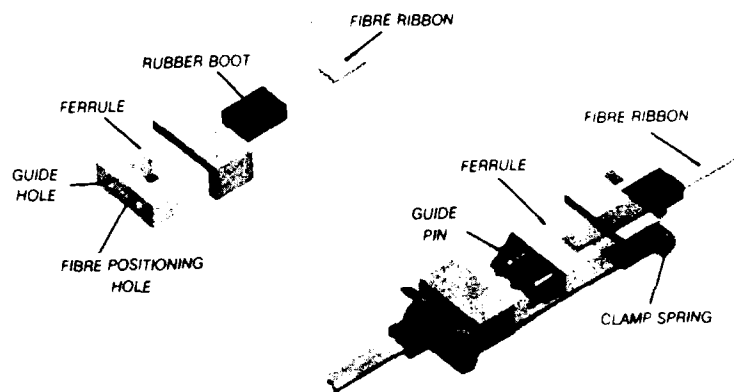


Fig. 4 - MT connector

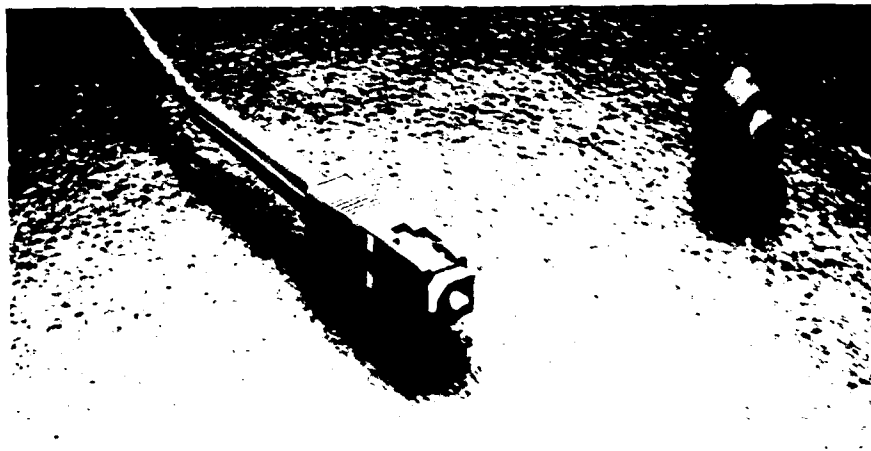


Fig. 5 - SC connector

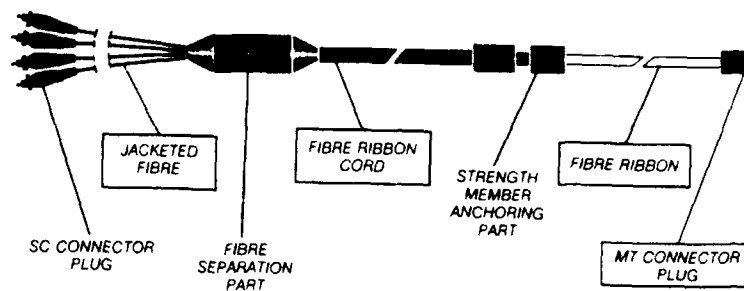


Fig. 6 - Fan-out

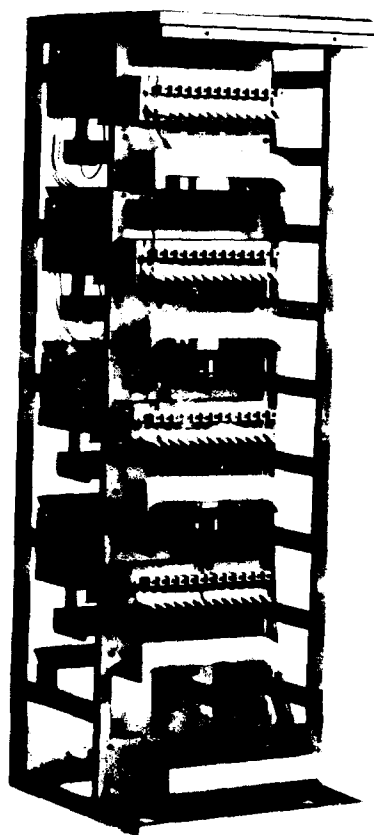


Fig. 7 - 400 o.f. Main Distribution Frame

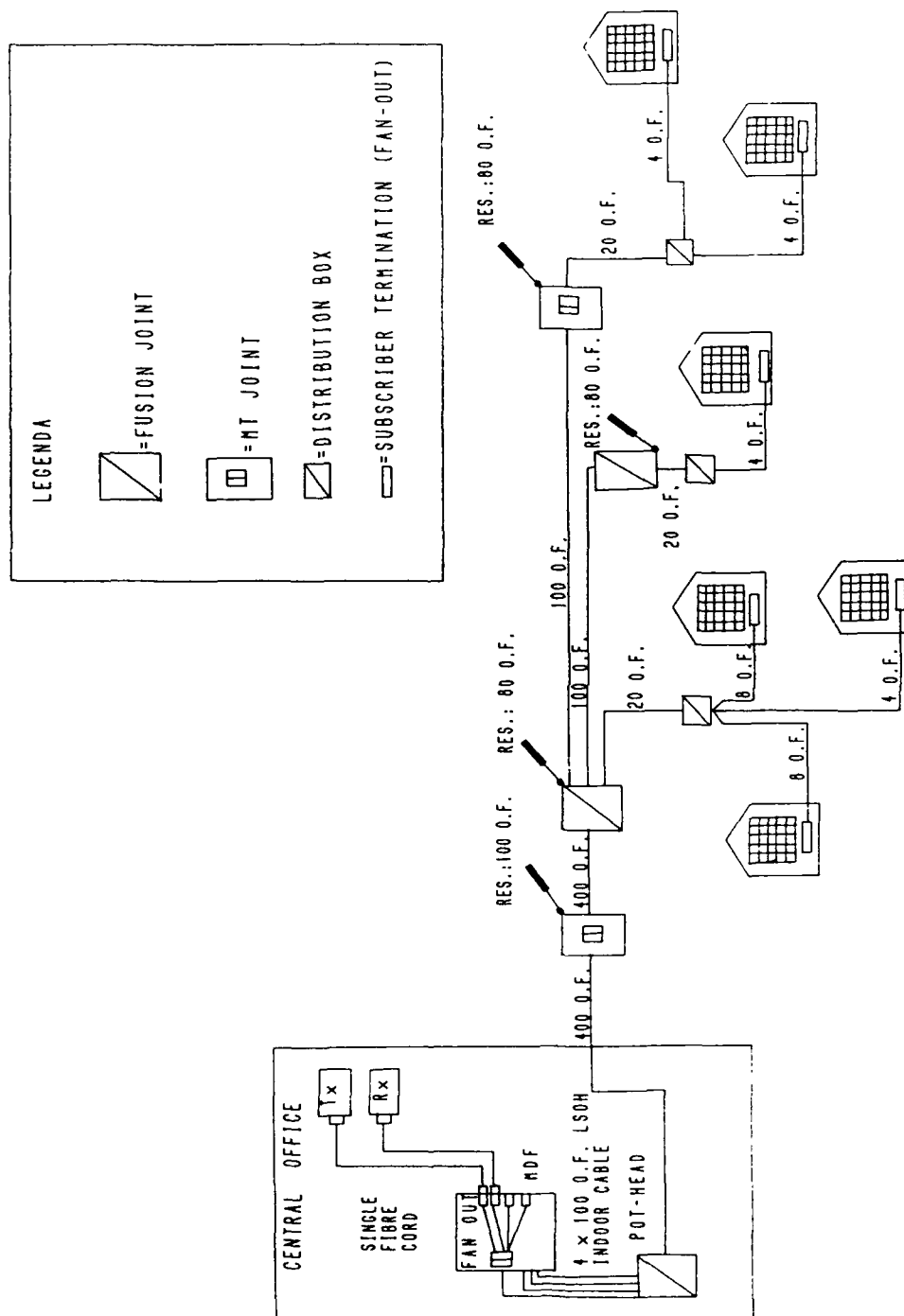


FIG. 8: EXAMPLE OF SUBSCRIBER LINK CONFIGURATION

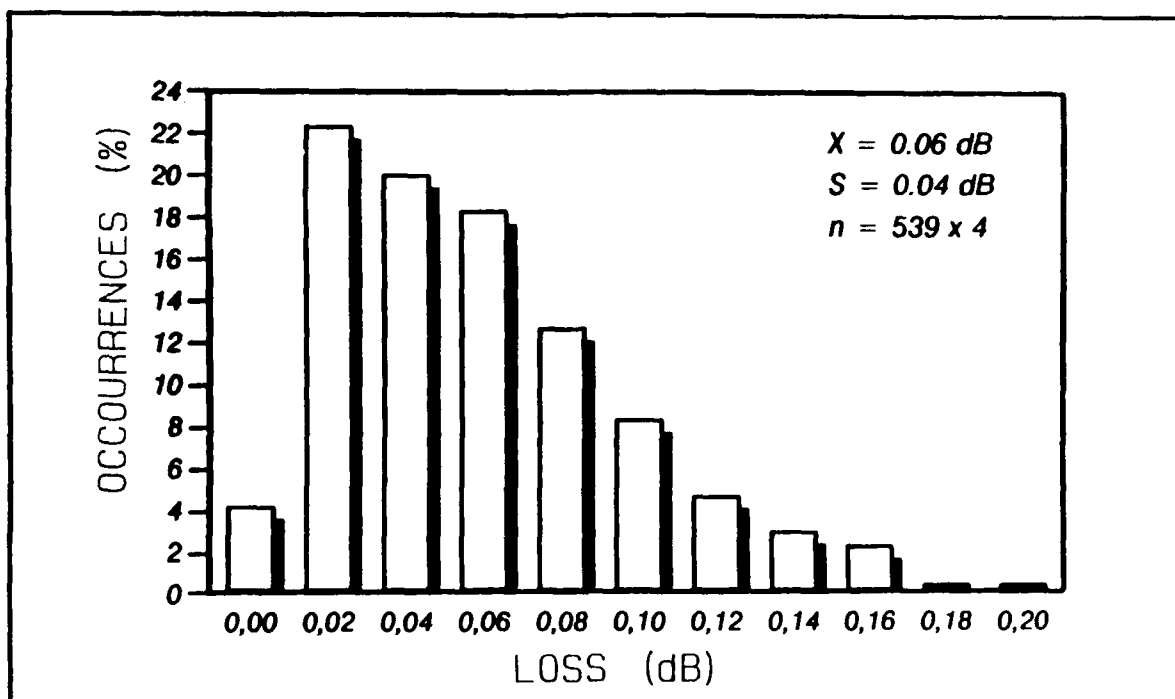


Fig. 9 - Fusion splice loss histogram

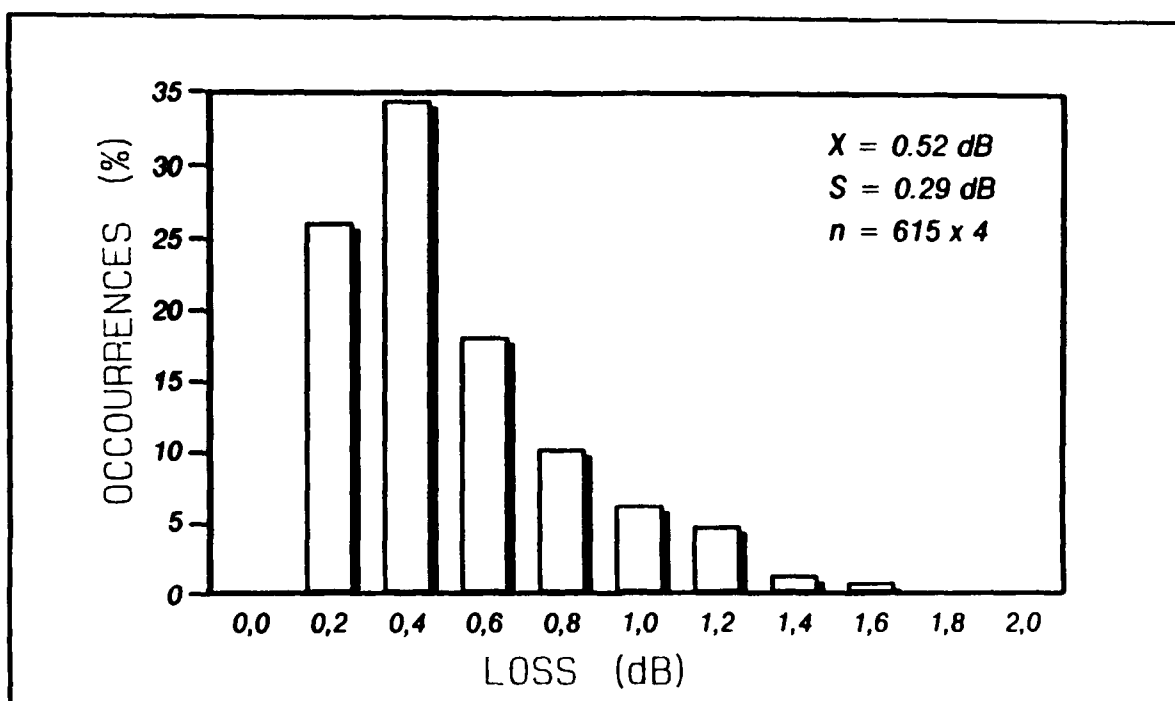


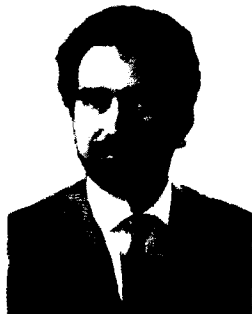
Fig. 10 - MT splice loss histogram



Feliciano Esposto was born in Arcevia (Ancona), Italy, in 1948. He received his doctorate in Physics from the University of Torino in 1976. In 1969 he joined CSELT, where he did research on optics and optical communications, particularly holography and optical fibre characterization. Since 1980 he is with SIP Headquarters, the Italian Telecommunication Operating Company, which like CSELT belongs to the STET group, where is manager of the "Outside Plant Technologies" Section in the Engineering of Transmission Division. His involved in the activities of the Standardization International Bodies, namely CCITT, IEC, CECC and ETSI. He is co-author of many papers and lectures at Superior School "Guglielmo Reiss Romoli".



Fabrizio Nanni was born in Rome, Italy, in 1960. He received his doctorate in Physics from the University of Rome. During his studies from 1986 he has collaborated with a laboratory of research on optical communications: Fondazione "U. Bordonni" in Rome working on photoconductivity ultrafast phenomena, semiconductor lasers and ultrafast photodiodes characterization. In 1988 he joined SIP (Italian Telecommunication Operating Company) Headquarters where he has been engaged in the study and development of optical fibres, copper cables as well as optical cables specification and characterization both in laboratory and in field. Moreover his present responsibilities include CCITT Comm. XV, ETSI-TM1, CECC WG28 and COST218 activities.



Francesco Montalti was born in Florence, Italy, in 1953. He received his doctorate in Physics from the University of Rome in 1976. In 1979 he joined Face Standard Research Centre where he did research on optical fibres, optical components and thin film technologies. In 1985 he joined SIP (Italian Telecommunication Operating Company) Headquarters where after being involved in the optical and metallic cables specifications, is now in charge of the Cable Group in the "Outside Plant Technologies" section. His responsibilities include the activities of CCITT Comm. IV, IEC TC86B, CECC WG26. He lectures at Superior School "Guglielmo Reiss Romoli".

# A radically new, ultra-high-speed method for the installation of cables in ducts

W. Griffioen  
G.J. Prins

PTT Research, P.O. Box 421, 2260 AK Leidschendam, The Netherlands

## Abstract

A radically new, ultra-high-speed method for the installation of cables in ducts is described. A high-speed moving cable will slide on its own, equally distributed, inertia without suffering exponential force build-up in curves. Centrifugal forces are compensated for any curvature of the duct by a proper cable tension. Some ways to supply this tension and to accelerate the cable before installation are described. Theory says that 10 km of fibre-optic or other cable can be installed in one shot of 2 minutes. This theory is checked by scale-model straight- and looped-trajectory field trials. Here 1536 m of cable is installed in 2 minutes and 5 right-angled curves and 6 loops are passed in 7 seconds respectively. For understanding, friction coefficients between cable and duct are measured at high speeds.

## Introduction

The use of fibre-optic cables for telecommunication has caused an enormous increase in practical cable lengths. This is caused by the lower cable weight which allows for larger lengths on one single reel. In addition, as the attenuation of the fibre itself is very low, splices are the dominant loss contributors and should be avoided as much as possible. In the past short pieces of telecommunication cable were buried directly into the ground. Nowadays in many countries fibre-optic cables are installed in pre-installed ducts. A commonly used technique for installing cables in ducts is pulling with a winch rope. When the cable is under tension, the cable will be pulled against the duct-wall in curves and undulations in the trajectory, causing friction. The pulling force will then increase exponentially with length due to the fact that the friction is proportional to the tension in the cable<sup>1</sup>. This so called "capstan effect" limits the cable length that can be installed in one single pull. The "capstan effect" can be avoided by distributing the pulling force along the length of the cable. Cable blowing is a well-known technique to achieve this.<sup>2,3</sup>

In this paper a radically new approach, the "high-speed technique", is presented where the pulling force is also distributed along the length of the cable.<sup>4</sup> First the cable and the reel are accelerated to a very high (rotational) speed. Some ways to perform this are described. The cable then decelerates until standstill, sliding in the duct, driven by its own inertia. The inertia "force" is equally distributed over the length of the cable. Due to high (apparent) centrifugal forces that appear in curves the deceleration will be high and the cable stops soon. These centrifugal forces can be compensated by applying a proper tensile force to the cable. In that case the compensation holds for any curve, no matter what its radius of curvature is. The tensile force in the cable is obtained by applying a high enough force at the cable head, by means of a winch rope or a shuttle. The feeding of the cable is controlled such that the transversal force at the cable, measured in a curve at the injection side, is kept zero.

In a field trial a lightweight cable, stored in "figure-eight's", is installed in a duct with the use of an air-powered shuttle. The experimental setup is kept simple, avoiding high power engines, as it is not meant to reach maximum performance, but to check the theory. This experiment is performed to prove the theory for the "sliding inertia". In another experiment 100 m of cable, stored on a reel now, is installed in a duct in which 5 right-angled curves and 6 complete loops are present. This experiment is performed to prove theory for the centrifugal-force compensation by means of a proper cable tension. For better understanding also measurements of the friction coefficient between cable and duct are performed at high speeds (appendix).

## Theory

The theory of force build-up in cables which are pulled in ducts is developed long ago.<sup>1</sup> In this theory reaction forces exercised by the duct on the cable in different directions due to the cable mass and due to the cable tension in curves are taken into account. Forces due to a change in speed (acceleration) of the cable are low in conventional installation

(speed of order 1 m/s) and are hence not considered in the above mentioned (static) theory. This is also true for the centripetal reaction forces of the duct, necessary to lead the cable through curves. In the present paper an installation technique is described in which the speeds are ultra-high (order 100 m/s). This means that the installation of the cable must be treated dynamically, taking into account all above mentioned terms.

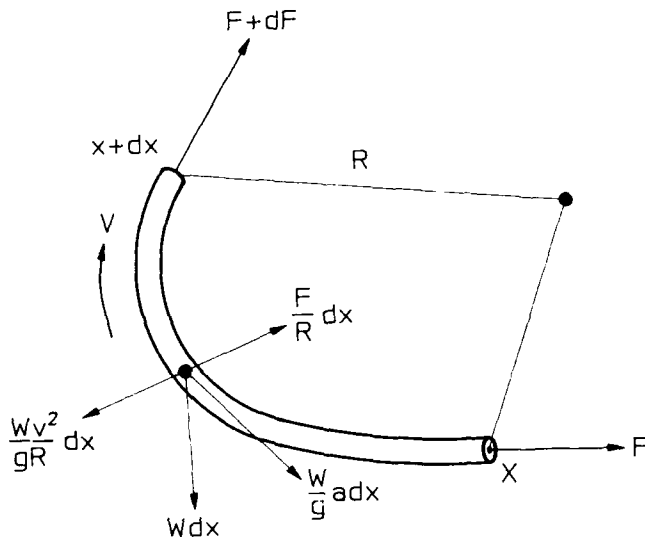


Figure 1: Forces acting on a cable moving in a duct

In figure 1 all forces acting on a piece of cable  $dx$ , moving with a uniform (longitudinal) speed  $v$ , are shown. For reasons of clarity not the reaction forces of the duct on the cable, but the (apparent) forces of the cable itself are given. Forces due to cable stiffness and buckling or to slopes in the ducts can also be treated, but are not considered in this paper.<sup>3,5</sup> The duct reacts with a normal force which compensates the resultant of the gravity force  $Wdx$ , the centrifugal force  $Wv^2 dx / (gR)$  and the transversal component of the cable tension  $Fdx/R$ , with  $W$  the cable-weight per unit of length,  $g$  the acceleration of gravity,  $v$  the speed of the cable and  $R$  the radius of curvature of the duct. The friction force acting on the cable follows by multiplying this normal force with the friction coefficient  $f$  between cable and duct. The increase  $dF$  of a pulling force  $F$  over a length  $dx$  for this dynamic situation is obtained by adding the "inertia force"  $Wadx/g$  of the cable, with  $a$  for the acceleration of the cable, to the mentioned friction force:

$$dF = \left[ \frac{W}{g} a + \frac{f}{R} \sqrt{(WR)^2 + (F - Wv^2/g)^2} \right] dx \quad (1)$$

In this formula it is assumed that the curve in the duct is in a horizontal plane. In practice ducts can be curved in all directions, but this does not change the force build-up very much.<sup>3</sup> For zero  $a$  and  $v$  the basic formula for the static force build-up is obtained.<sup>1</sup>

Consider the situation that  $a = -fg$  and  $F = Wv^2/g$ . From equation 1 hence follows that  $dF = 0$  which means that there is no force build-up in the cable anymore. The first condition means that the cable just slides by its own inertia. The second condition means that a proper tensile force is applied to the cable in order to compensate for the centrifugal force of the moving cable. Both centrifugal force and transversal component of the cable tension are inversely proportional to  $R$ , which means that these effects compensate each other for every curvature once the compensation criterion is reached. In this case every curve can be followed by a high-speed moving cable without transversal forces acting on the cable which disturb the curve.

Interlude: An example in which nature itself controls the proper tensile force, to compensate for the centrifugal force, is a high-speed running piece of cable in a closed loop (figure 2). In that case every shape of the cycling cable can be obtained. In figure 2 an artificially applied perturbation is shown, which is maintained for a relatively long time ( $> 100$  cycles), in a cable that runs with 50 m/s. This may be an unexpected result since one expects a nice round loop as is the case with a lasso. The difference can be explained by the fact that the "knot" connecting the rope, held by the cowboy, with the loop is "resetting" the path every turn. It is now clear that a moving cable under proper tension can pass a stationary perturbation without transversal forces acting on that cable to disturb the perturbation. This can be compared with a tensed, stationary, string in which a perturbation travels with speed  $v = \sqrt{FW/g}$ , set by nature, which is the same relation between speed and tension.<sup>6</sup> Another example, in which nature controls the proper tension, is a rope following a launched harpoon which is accelerated from a resting pile (this is not true when using a reel to store the rope).

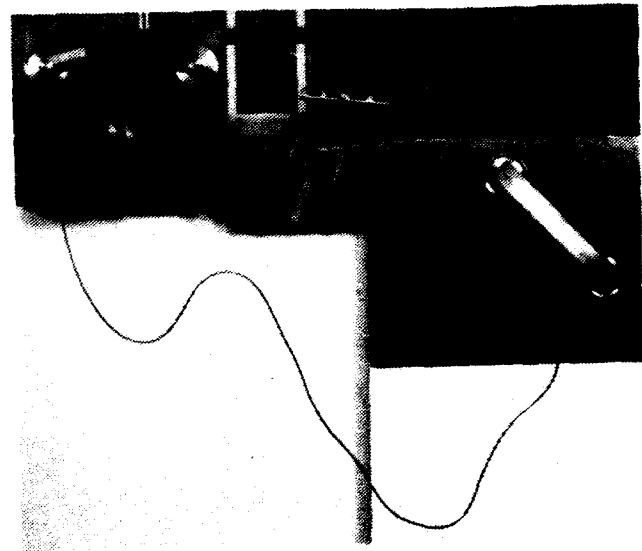


Figure 2: High-speed (50 m/s) running loop of cable with artificially applied perturbation

When the above mentioned criteria of sliding and zero transverse force are fulfilled a situation is obtained in which a cable slides in the duct, decelerating, while the force along the cable remains constant. The length  $\ell$  over which the cable slides in this condition is obtained with  $a = -fg$  and by using the boundary condition that the speed of the cable drops from  $v_0$  at the start to zero at the end:

$$\ell = \frac{1}{2} \frac{v_0^2}{fg} \quad (2)$$

When the transversal component of the cable tension does not exactly compensate the centrifugal force of the moving cable,  $dF = 0$  is obtained from equation 1 when  $a = -fg \cdot \sqrt{1 + (F_0/WR)^2}$  with  $F_0 = F - Wv^2/g$ . In this case a more general formula for the sliding installation length is found:

$$\ell = \frac{1}{2} \frac{v_0^2}{fg} / \sqrt{1 + (F_0/WR)^2} \quad (3)$$

The force  $F_0$  is the effective cable tension which is measured indirectly by measuring the transversal force of a cable moving through a curve. In figure 3 an experimental setup is shown which is used to measure  $F_0$  at the injection side of the duct. The measured transversal force  $F_t$  is equal to  $2\sin(\alpha/2) \cdot F_0$ .

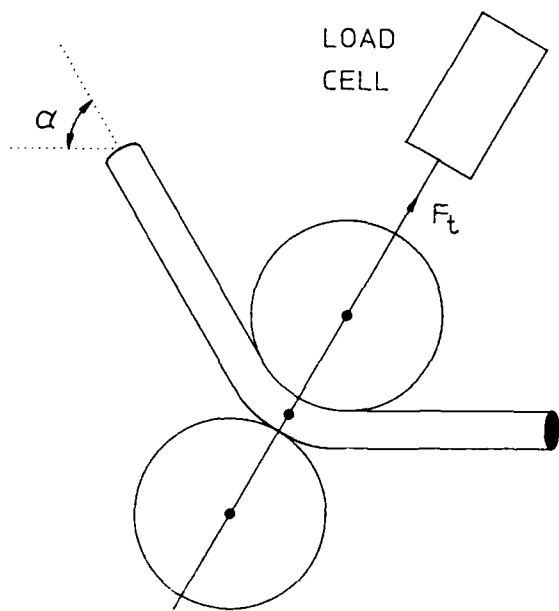


Figure 3: Experimental setup for measuring effective cable tension  $F_0$

When the deceleration of the cable is controlled by keeping the effective cable tension  $F_0$  at the injection side of the duct as small as possible, and when the applied force at the cable-head is equal to  $Wv^2/g$  (plus the mentioned small  $F_0$ ) the cable slides over a length  $\ell$ , according to formula 3. When the

pulling force at the cable head is much higher than  $Wv^2/g$  the cable tension decreases to the latter value along the cable from the head until the injection side. In this case the deceleration of the cable is less than in the situation that  $F_0$  is kept small all along the cable. The heat production, caused by the friction between cable and duct, will however be larger. Care should be taken that this heat production is not too high. For this reason it may be necessary to control the pulling force at the cable-head too in cases of extremely high installation speeds (the heat-production per unit of time and length can be reduced down to  $fWv$ , which is left due to the cable mass). When the pulling force at the cable head is much lower than  $Wv^2/g$  the cable decelerates soon until the situation  $F = Wv^2/g$  is reached at the cable head. When the pulling force at the cable head is zero, e.g. when the cable reaches the end of the duct, the cable stops soon.

A general solution of equation 1 may be obtained by substituting:

$$z = \frac{F_0}{WR} \quad c = \frac{a}{fg} \quad u = \frac{\sqrt{1+z^2}-1}{z} \quad (4)$$

After integration the next equation is obtained:

$$\frac{f}{R} x = \left[ \operatorname{arcsinh} z - \frac{2c}{\sqrt{1-c^2}} \operatorname{arctan} \left[ \frac{(1-c)u}{\sqrt{1-c^2}} \right] \right]_{z=z_0}^{z=x} \quad (5)$$

Note that for  $a$  and  $v$  equal to zero and with  $x = R\theta$ , with  $\theta$  the angle along which the duct is curved, again the force build-up formula in curves for the static situation is obtained. Equation 5 holds for  $c < 1$ . The second part of the right-hand side of equation 5 is equal to  $u$  when  $c = 1$  and goes to infinity for  $c = -1$ . For  $c > 1$  equation 5 can be re-written by using  $i \cdot \operatorname{arctan}(ix) = -\operatorname{arctanh}(x)$  with  $i$  defined as  $\sqrt{-1}$ .

It is assumed that the cable on the reel is accelerated until the maximum speed  $v_0$  before the cable is installed (how will be discussed later). This means that the pulling force  $F$  on the cable is not able to accelerate cable and reel in the first part of the trajectory any further. The acceleration  $a$  will hence be equal to zero. This situation is maintained until an installation length  $x_0$ , which is obtained by solving equation 5 for  $c = 0$ :

$$x_0 = \frac{R}{f} \left[ \operatorname{arcsinh} \left\{ \frac{F_0}{WR} \right\} \right]_{F_0=F_0(0)}^{F_0=F-Wv_0^2/g} \quad (6)$$

Next the installed length, speed and acceleration of the cable can be obtained iteratively with equation 5. A numerical example, with  $W = 1N/m$ ,  $R = 30m$  (corresponding to undulations of  $2^\circ/m$ ),  $f = 0.15$  - this is lower than for traditional pulling because with the described technique the peaks in friction, occurring when the cable starts moving from standstill, do not appear -,  $F = 2000N$  (cable-head) is given in figure 4.<sup>3</sup> The starting speed used is  $v_0 = 100m/s$  and it is assumed that  $F_0(0)$  is kept zero.



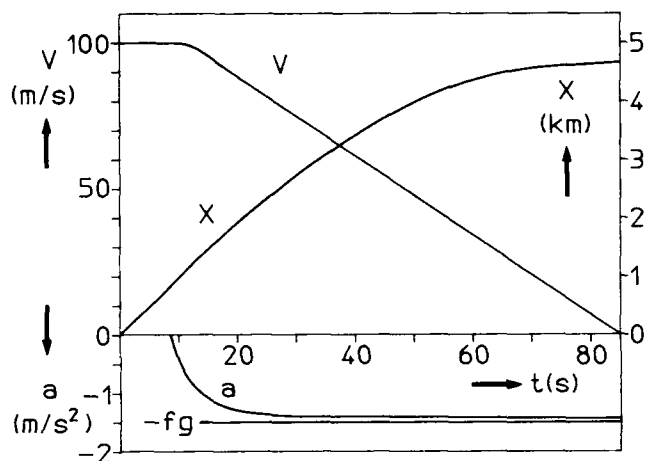


Figure 4: Numerical example of cable installed-length  $x$ , speed  $v$  and acceleration  $a$  as a function of time  $t$

## Practice

Until now it was just assumed that cable installation started with a very high speed. This is not easy to achieve. A lot of energy is necessary to accelerate a long cable on a reel to a very high speed. If this energy must be applied in a very short time, a lot of power is needed. It is preferable to accelerate the complete cable reel first before starting the installation of the cable in the duct. The development of a mechanism that grips the cable from the high-speed running reel is one possibility. A more clever and safer method is shown in figure 5.<sup>4</sup> A cable is inserted in a duct first and attached to a pulling source (an air-powered shuttle in figure 5). The cable is however de-coupled from the pulling source for rotation about its axis. The reel, cable loop and controlling-, guiding- and protection-means will all together start with rotating until the desired speed is obtained. In that case the cable piece inside the duct will rotate around its axis. Then all rotating (light-weight) parts, except the cable reel, will be braked in a very short time. From that moment on the cable runs into the duct with very high speed while the rotation around its own axis has stopped. Now the sliding situation is reached in which the speed of the reel is controlled by the  $F_0$ -sensor.

Another possibility is to accelerate a cable reel in the first part of the installation very quickly. This can be performed by using high-power engines or by using energy stored in a flywheel in combination with a high-capacity clutch. It is also possible to avoid the need to accelerate the whole cable length in the first time. A cable can also be accelerated bit by bit, e.g. when the cable is stored in a heap or in "figure-eight's".

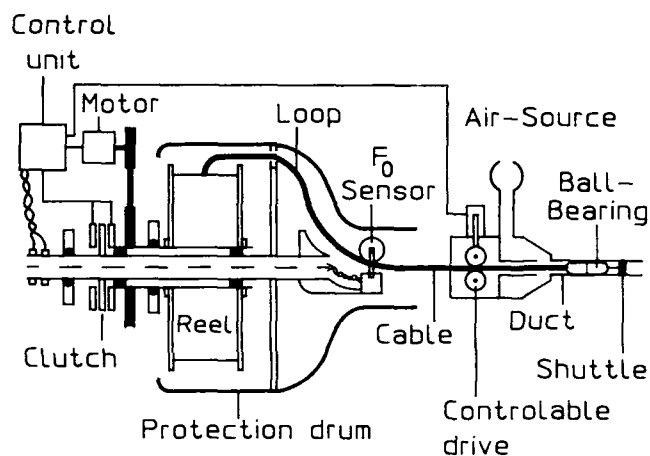


Figure 5: Mechanism to accelerate the reel before installation

Another practical point is the pulling-source, necessary to supply the cable tension which is needed to compensate the effect of the centripetal force. One method is the use of an air-powered shuttle. In this case the cable is also surrounded by a high-speed airflow. This is very useful to avoid a reversed "cable-blowing effect". For low-diameter ducts, however, the speed of the airflow forms the limit for the high-speed technique (about 2 and 4 km of trunk fibre-optic cable in ducts with inner diameter of 26 and 40 mm respectively). Another technique is the use of a low-friction pulling rope with a high-speed winch. With this technique it is also recommended to blow the cable in addition. In order to exploit fully the benefits of the high-speed technique extra study is needed, e.g. the development of a light-weight pulling-rope with wheels. But then the possibilities are almost unlimited. The weight of the cable is not of importance anymore. The only parameter that counts is the ratio between maximum pulling force and weight per unit of cable-length. This sets the maximum speed at which the centrifugal force can be compensated by the transversal component of the cable tension. For trunk fibre-optic cables with e.g. a weight of  $1\text{N/m}$  and a maximum pulling force of  $2000\text{N}$  it is possible to install 10 km in one shot, taking only 2 minutes.

## Experiments

### Straight trajectory

Most of the experimental setups which are described in the preceding chapter need powerful or difficult to develop equipment. For this reason a simple scale model is build in order to prove the theory. The experiments are performed with light-weight ( $W = 0.12\text{N/m}$ ,  $\Phi = 3\text{mm}$ ) PVC-jacketed single-

fibre cables. To accelerate a reel with a few kilometers of this cable in a very short time would still need a lot of power. For this reason the cable is stored in "figure-eights" in a special container as is shown in figure 6. An air-powered shuttle is used to supply the pulling force. In order to eliminate for a pressure build-up in front of the shuttle this space is evacuated before the start. A device as is shown in figure 3 is used to measure the effective cable tension  $F_0$  just before entering the pressurized space. The speed of the pick-up wheel is controlled in such a way that  $F_0$  is maintained as small as possible. The effect of the pressure rise when the cable enters the duct is overcome by forcing an airflow with high speed through a narrow tube first and bleeding a part of this flow after this tube. The experiment is performed in a rather straight (one 270°-curve) trajectory of 2 km of HDPE ducts with an inner diameter of 26 mm. Only a very small amount of paraffin oil is present in the duct for lubrication.

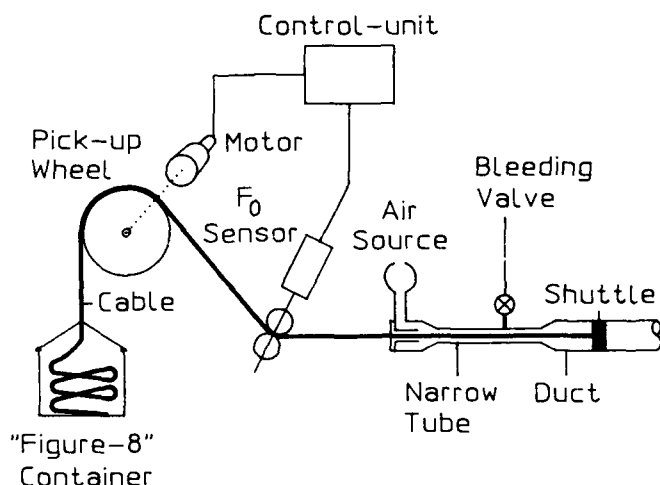


Figure 6: Schematic of the straight-trajectory field trial

In figure 7 the speed of the cable is given as a function of time. In this figure also the transversal force  $F_t$ , which is a measure for the effective cable-tension  $F_0$  is shown. After about 60 s  $F_t$  shows a peak (pick-up of an irregular loop) resulting in a sudden decrease in speed. The speed however recovers afterwards. Maybe this indicates that the pulling force is still effective here. This is possible because the trajectory is rather straight. The decrease of speed in the first part of the trajectory can be explained by a higher friction coefficient between cable and duct at high speeds as may be expected for lubricated ducts (see appendix). Finally a length of 1536 m was installed in only 2 minutes with a maximum speed of 34 m/s. It was quite impossible to install this length by normal pulling and hence the "sliding on inertia" effect is proved by this experiment.

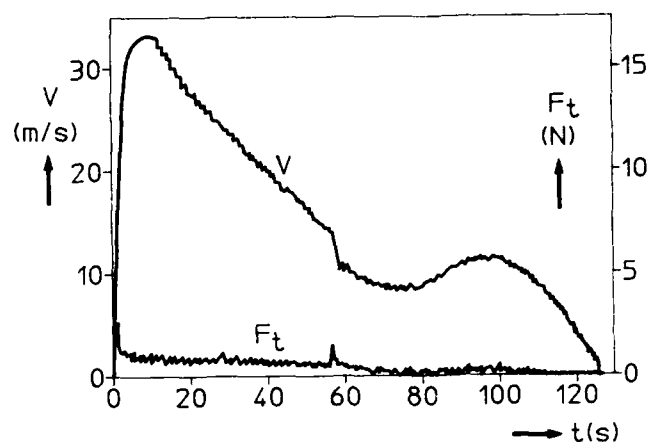


Figure 7: Speed  $v$  and effective cable tension  $F_0$  as a function of time  $t$  in the straight-trajectory field trial

### Looped trajectory

The effect of compensating the centrifugal-force by a proper cable tension is proved in a shorter (85 m) trajectory in which 5 right-angled curves and 6 loops of 360° (last 40 m) are present. Now a special "dry-lubricated" HDPE duct with an inner diameter of 12 mm is used. The shorter cable length gives the possibility to install from a cable reel, which is driven by a controlled motor to give a small effective cable-tension  $F_0$ . Because this trajectory is extremely curved the effective cable-tension  $F_0$  inside the duct must be kept very small (formula 3). Therefore another "sensor/drive" unit (no. 2) is placed inside the pressurized space as can be seen in figure 8.

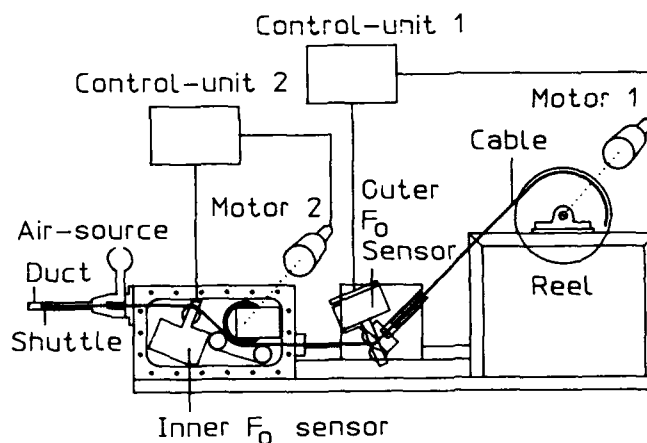


Figure 8: Schematic of the looped-trajectory field trial

In figure 9 the speed as a function of time is shown. In the first 3.5 s the cable is in the part (45 m) in which only 5 right-angled curves are present. In that case the force at the shuttle is capable to pull (as in the old pulling-technique) the cable along the duct. Hence the speed remains at it's maximum of 15.5 m/s, as can be seen in figure 9. Then, when entering the loops, the pulling effect of the force at the shuttle is not sufficient anymore to pass all the curves. Now the sliding-on-inertia condition is reached which causes the decrease in speed, shown in figure 9. This decrease in speed corresponds to a deceleration of  $1.4 \text{ m/s}^2$  which gives an effective friction coefficient of 0.14. When the end of the duct is reached the cable speed has dropped to 9.5 m/s. It was not easy to increase the maximum speed and the installation length with this experimental setup. This is due to the limited power (1 kW) of the motors which makes controlling very difficult. The trajectory was however such that traditional pulling of a cable was far from possible.

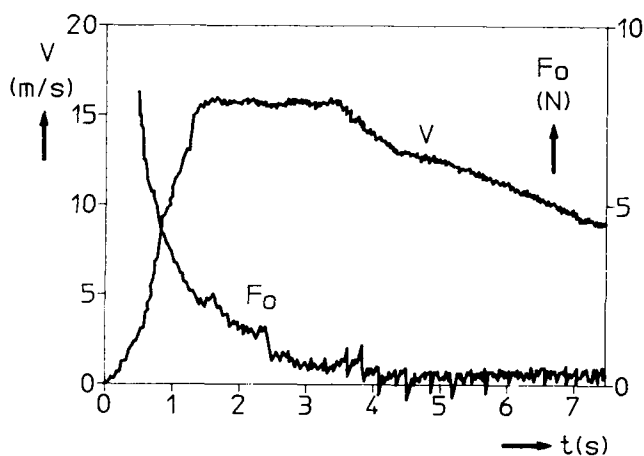


Figure 9: Speed  $v$  and effective cable tension  $F_0$  as a function of time  $t$  in the looped-trajectory field trial

## Conclusions

With the described ultra-high-speed method for the installation of cables in ducts much longer lengths can be installed than with existing techniques. A length of 10 km of fibre-optic trunk cable can be installed, according to theory, in one "shot" taking only 2 minutes. Since the "capstan-effect" is avoided this result will also be obtained in curved duct-trajectories. The mass of the cables is not of importance for the functioning of the described installation-method. Hence any cable (e.g. copper telecommunication- or power-cables) with the same maximum-pulling-force to weight ratio as for a fibre-optic trunk cable can be installed with the same performance. The theory is proved by scale-model field trials

in straight- and looped-trajectories. Here 1536 m of cable is installed in 2 minutes and 5 right-angled curves and 6 loops are passed in 7 seconds respectively. With the described technique a lot is possible and much money can be saved, but also a lot of development is still necessary. The friction coefficients between cable and duct are measured. The fact that lubrication causes an increase in friction at high speed explains some deviating results. The friction remains constant when a "dry-lubricated" duct is used.

## Acknowledgements

The authors wish to express their thanks to C.L. de Jong, K.F. Betke, P. Lardee and G. Bal for the construction of the experimental setups, B. Friderich, G. Segers and H. van Wijngaarden for their valuable support on laboratory measurements and J.C. Veenis and his crew members for arranging the field experiments.

## References

1. Buller, "Pulling tension during cable installation in ducts or pipes", General Electric Review, pp.21-23, august 1949.
2. S.A. Cassidy and M.H. Reeve, "A radically new approach to the installation of optical fibre using the viscous flow of air", Proc. IWCS (1983) 250.
3. W. Griffioen, "The installation of conventional fibre optic cables in conduits using the viscous flow of air", J. Lightwave Technol., vol.7, no.2 (1989) 297.
4. W. Griffioen, G.J. Prins, Patent Pending.
5. W. Griffioen, H.A.L.M. De Graaf, "Blowing optical cables in the Netherlands", Proc. EFOC/LAN (1991) 83.
6. Silicore<sup>TM</sup> from DURALINE corporation, box 1445, Middlesboro, KY 40965, United Kingdom.
7. H.M. Kemp, "Procedure for the experimental determination of friction coefficient between a cable and duct", Proc. IWCS (1987) 557.
8. S. Timoshenko, J.N. Goodier, "Theory of elasticity", McGraw-Hill, New York, 1951.

## Appendix

### Friction-coefficient

Measurements of friction coefficients between cable and duct are performed with equipment as shown in figure 10. The duct which has to be tested is cut into two halves along its length. One part is attached to the rim of a bicycle-wheel, in a rim-similar way and with a smooth joint. A sample of cable is placed along 90° of this "duct-rim". A weight is attached at one side of the cable while the other side of the cable is attached to a load cell (see figure 10). When the wheel is rotating with a certain speed  $v$  (at the rim) the friction coefficient between the cable and duct for this speed follows from  $F_1$  and  $F_2$ . Care has been taken that the weight is low and the measuring time is short to avoid heating of cable and duct, especially at high speeds, as much as possible. Large amounts of lubricant cannot be tested at high speeds of the wheel because a lot of it is swept away then.

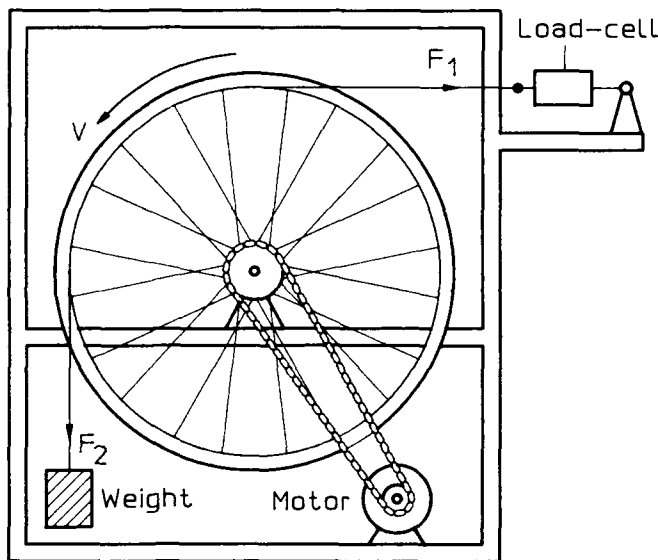


Figure 10: Experimental setup to measure the friction coefficient between cable and duct for different speeds

The cable which is used in the test is the same PVC-jacketed single-fibre cable as is used in the field trials. Two kind of ducts, both with inner and outer diameters of 12 and 16 mm respectively, are used. The first one is made out of pure HDPE and is tested dry, with paraffin oil and with water (in the latter case a cable with HDPE-jacket was used). The second duct also consists of HDPE, but has a solid "lubrication" inner-layer.<sup>6</sup> This duct is only tested dry. The experimental results are given in figure 11.

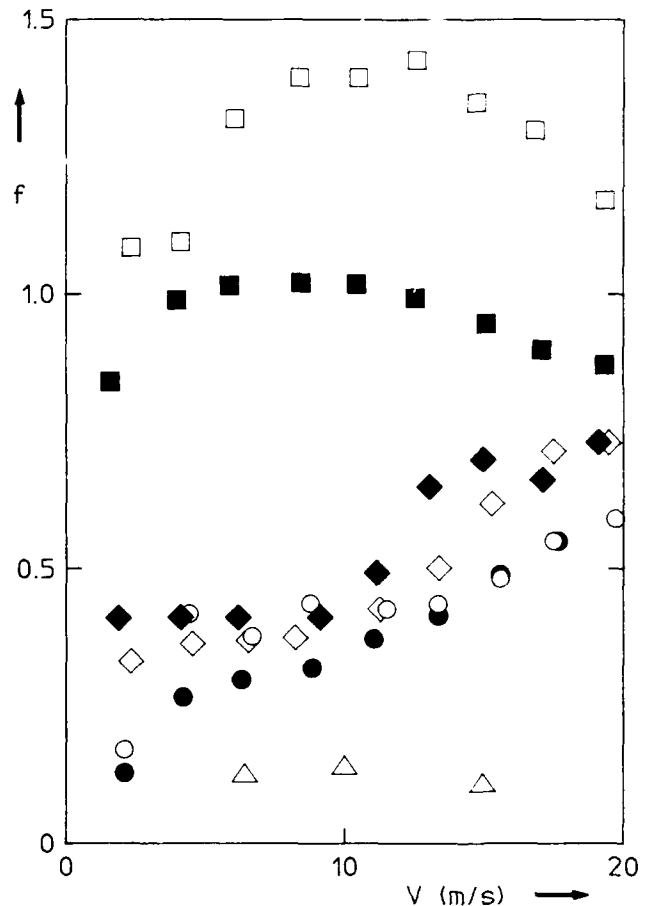


Figure 11: Friction coefficient between cable and duct as a function of speed for a PVC-jacketed cable with dry- (rhombi) and lubricated- (squares=paraffin oil and triangles=water) HDPE ducts and also for "dry-lubricated" HDPE ducts (circles). Weights of 40 and 100 grams are used, indicated by open and solid symbols respectively

From figure 11 it is clear that lubrication with paraffin oil causes an increase in friction, contrary to the situation at lower speeds.<sup>7</sup> This can be explained by a speed-dependent lubricant-viscosity friction. Since this friction does not depend on the force at which the cable is pushed against the duct-wall its effect is higher for lower weights, as can be seen in figure 11. The friction coefficient for dry ducts is much lower, but still increases with speed. Also when using "dry-lubricated" ducts the friction coefficient, which is lower now, increases with speed. This increase with speed can probably be explained by heating of cable and duct. This is supported by the fact that cooling with a slight amount of water results in low friction coefficients at all speeds. Moreover the looped-trajectory field trial, in which the tension in the cable is much smaller (and hence the heat production is less), indicates that the friction coefficient between cable and "dry-lubricated" duct is only 0.14.

## Biographies



Willem Griffioen was born in Oegstgeest, The Netherlands, on October 8, 1955. He received his M.S. degree in physics and mathematics from Leiden University, Leiden, The Netherlands, in 1980. He worked at Leiden University from 1980 to 1984, where he investigated macroscopic quantum properties of liquid and solid  $^3\text{He}/^4\text{He}$ -mixtures at ultra-low temperatures and in high magnetic fields. In 1984 he joined PTT Research, Box 421, 2260 AK Leidschendam, The Netherlands. His work includes research and development of fibre optic cables, installation techniques and reliability of optical fibres. At this moment he works at Ericsson Cables AB, Box 457, 824 01 Hudiksvall, Sweden in the scope of a half-year-exchange project.



Geert Jan Prins was born in Sidderburen, The Netherlands, on January 13, 1938. He received his B.S. degree in 1965 at Rotterdam, and the B.S. degree in measuring- and control-technique in 1973 at Dordrecht, both in The Netherlands. From 1961 he worked at the Waterloopkundig Laboratorium and at TNO at Delft, a.o. on the development of ship-manoeuving simulators. From 1973 he was the head of the consultant department of a sub-contractor company for soil working at Halfweg, The Netherlands. In 1981 he joined PTT Research, Box 421, 2260 AK Leidschendam, The Netherlands. His work includes the development of automatic processing of postal letters and parcels, control-systems and installation techniques.

# ENVIRONMENTAL CHALLENGES FACING THE INSTALLATION OF THE SECOND PERTH TO ADELAIDE OPTICAL FIBRE CABLE ROUTE

Giulio Consiglio  
Les Kiss

John Groom  
Peter Latoszynski

Edwin Johansen

Telecom Australia - Melbourne, AUSTRALIA

## ABSTRACT

The second 2500 kilometre Perth to Adelaide optical fibre cable route was required to provide extra capacity between the West and East coasts of Australia and to provide necessary route diversity for Telecom Australia's high capacity broadband network. Environmental factors had a significant impact on the installation techniques applied to this project. In particular, rock sawing was required on 550 km of the route, and a 43 km section crossed an environmentally sensitive prawn trawling region characterised by difficult installation conditions. Furthermore, approximately 800 km of the route is the natural habitat of the Western Australian Christmas Tree, a plant that has a record of causing significant cable damage by its parasitic root system. The Southern Hairy Nosed Wombat also posed a threat because of its deep burrows and ability to damage cables.

Some of the considerations and solutions to these unique environmental challenges are presented in detail in this paper.

## INTRODUCTION

A nationwide, high capacity, single mode optical fibre cable network has been installed in Australia over the past six years [1][2]. This network has been developed to link all major capital cities within Australia and includes plans for full route diversity between all major cities.

As part of this strategy, a second major intercapital trunk link using single mode optical fibre cable is being installed between Perth and Adelaide. The route selected for this second link meant facing some unique challenges from Australian flora and fauna not previously encountered on optical fibre cable installations.

## ROUTE SELECTION

To combine with installation of Regional projects in Western Australia, and to achieve an overall cost benefit to Telecom, the link followed a route from Perth due South to near Bunbury (Figure 1), and then due East rejoining the Eyre Highway about 200 km East of Esperance. The general route of the cable follows the Eyre Highway then breaks away and proceeds across Spencer Gulf and on to Adelaide.

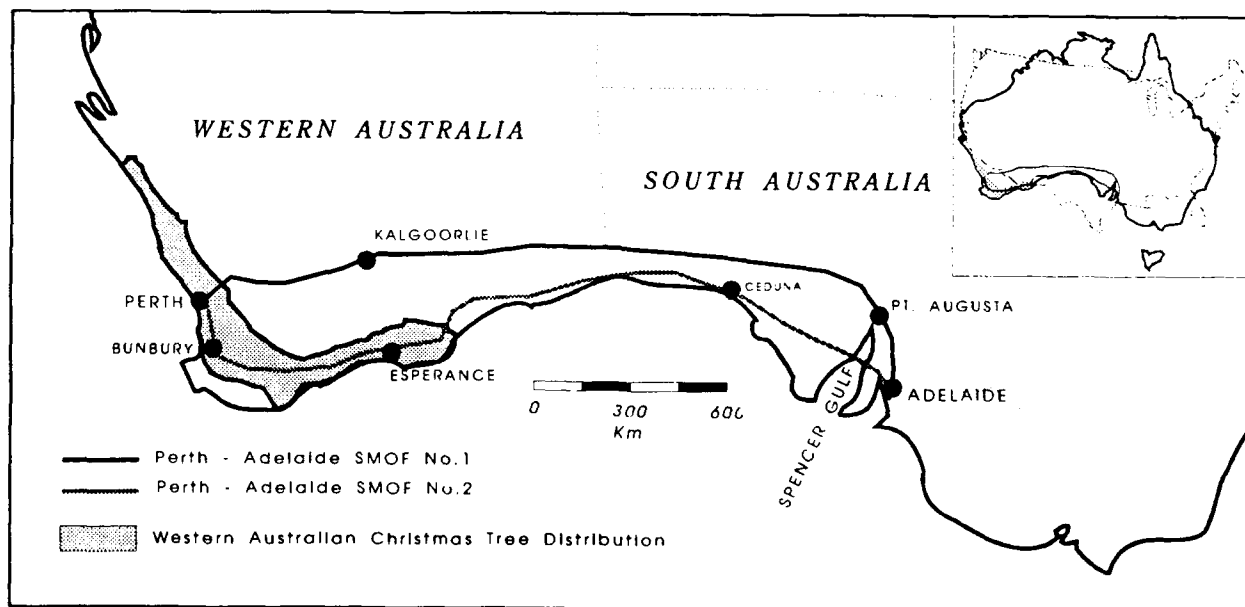


FIGURE 1 PERTH TO ADELAIDE OPTICAL FIBRE CABLE ROUTES

This route provided a physically diverse route from the first Perth to Adelaide single mode optical fibre cable which was installed directly East from Perth and followed the more northerly route along the Australian National Railways Reserve.

#### ENVIRONMENTALLY RESPONSIBLE INSTALLATION TECHNIQUES

The first Perth to Adelaide optical fibre route follows a northerly route traversing the Nullarbor Plain and other terrain with approximately 20% unrippable rock. The installation methods and network performance have been previously described [3]. It is noted that a significant clean up cost was incurred through the necessary use of blasting and cross-ripping techniques, although the use of rocksaws was also effectively deployed.

Since that time the Nullarbor Plain has been declared a National Park and has been nominated for World Heritage listing, consequently the general obligations to environmental issues have been increased. Further, the expected level of unrippable rock was much greater for the second route and was estimated to be in excess of 500 km. It was therefore necessary to further investigate route preparation techniques for this installation in an attempt to improve both the route preparation rate and cost. To ensure against the excessive generation and exposure of large boulders during the ripping process, only two techniques could be generally considered; these were rocksawing and the use of an impact ripper. Negotiations with National Parks and Wildlife staff, however, excluded the use of the impact ripper in the National Park on the basis of its sheer size and bulk (in excess of 100 tonnes). Furthermore, this technology had not been sufficiently proven for Telecom Australia to adopt its use on this critically timed project.

Accordingly, following on from developments in rocksaw design gained on the first Perth to Adelaide project, a number of Telecom Australia rocksaws, together with two commercially available rocksaws modified to Telecom Australia's requirements were purchased.

Currently a total of seven rocksaws are strategically employed on this installation and to date, have proven to be both technically and environmentally satisfactory.

#### CHRISTMAS TREE ROOT ATTACK

##### Background

The second Perth - Adelaide optical fibre route traverses regions of Western Australia that are the natural habitat of the Western Australia Christmas Tree, a plant that has a record of causing significant damage to buried small size copper conductor cables through attack by its parasitic root system. The roots are capable of penetrating the nylon jacket and polyethylene sheath leading to ingress of water and, on

occasions, severing of individual conductors or the cable. Consequently, the possibility of similar attack on the second Perth - Adelaide cable was of concern.

##### Plant Characteristics

The Western Australia Christmas Tree is a member of the mistletoe family and is a small multi-trunked tree up to 10 metres high and is classed as the largest of the root parasites in the world.

The plant is endemic to Western Australia and its distribution is confined to a narrow band of less than 150 kilometres in width through the South-West region of the state. The terrain in these areas is predominantly low lying coastal plains consisting of sandy soils.

Lateral roots are the plant's prime source of moisture and nutrients, which are obtained from host plant roots. The mechanism by which this is achieved occurs in a number of stages culminating in a rounded fleshy body which encircles the host root. Within this body a horn like structure develops which provide the means of slicing into the host root hence directing nutrient paths into its own vascular system.

The maximum depth to which Christmas Tree roots will venture in search of these roots is unknown. Field observations indicate that in some instance the roots have penetrated the soil to depths of approximately one metre, similar to the depth of buried optical fibre cable.

##### Root Interaction with Telecommunications Cables

Due to their non-specificity in selecting a host, the roots of the Christmas Tree have been known to attack telecommunications cables. Records of penetration and complete severing of cables date back to the early 1970s and the level of faults in the region have been significant.

The more severe attacks, where complete severing of the cable has occurred, have been associated with two pair lead-in cable which has an outer diameter of 8 mm. Attack on larger cables, up to 11 mm in diameter, have been less frequent and resulted in only minor penetration of the sheath.

There has been no report of cables greater than 11 mm in diameter being affected. Similarly, cables installed in 20 mm diameter unplasticised PVC (UPVC) pipe have been found to be unaffected by these roots.

The optical fibre cable planned to traverse regions inhabited by the Christmas Tree had an outer diameter ranging from just under 11 mm to 13 mm. The sheath and jacket materials were also identical to conventional metallic cable which had previously been attacked. Consequently, due to the importance and increased capacity of optical fibre cables, cable protection options had to be considered and implemented.

### Cable Protection Options

The investigation into the characteristics of the Christmas Tree root system has not provided a comprehensive solution to the problem of root attack. However, a number of options to minimise the risk of optical fibre cable damage were available.

The option of removal of the trees along the route was considered environmentally unacceptable, and in fact this is a protected species.

Avoidance of root prone areas was not practical particularly as government environmental clearance allowed installation of cable along a very narrow corridor of the route.

Use of UPVC conduit (20 mm diameter) has been proven to be resistant to root attack due to a combination of its hardness and dimensions (diameter and thickness). This solution, however, proved to be uneconomical and would severely retard installation productivity.

Using flexible high density polyethylene (HDPE) split pipe and ploughing it directly into the ground with a modified plough tractor was also considered. There is, however, the possibility of the fine roots entering the pipe via the slit and eventually attacking the cable inside. The overall cost factor also made this option unacceptable.

The maximum depth of root penetration is presently unknown, however, it is generally considered that root activity predominantly occurs within the top 30 cm of the soil, only occasionally venturing to depths of up to 1 metre. Laying the cable at maximum plough depth (up to 1.6 metres) may not completely isolate the cable from the roots but is expected to minimise the risk of attack. The cost of preparing the route for burial at this depth, however, is prohibitive.

Examination of the characteristics of the root system suggested that there may be a limit on the size of the host root which could be attacked. Extensive statistical analysis combined with experience from field staff indicated that cables with a minimum diameter of 16 mm would minimise the risk of damage. This increased diameter could easily be achieved on existing cable designs by extruding an extra layer of polyethylene sheath without seriously imposing on the flexibility of the cable. This solution proved to be the most practical and economical and allowed conventional installation techniques to be used.

### SOUTHERN HAIRY NOSED WOMBAT

Approximately 250 kilometres of the optical fibre cable route traversed the natural habitat of the Southern Hairy-nosed wombat in the Nullarbor National Park in South Australia. Although wombats are powerful, stocky, burrowing marsupials, there was little information on damage caused to telecommunications cables by wombats. However, investigations indicated that they had

the ability to damage optical fibre cable unless it was armoured.

Due to the substantial cost penalty of using armoured cable and because the evidence of damage to telecommunications cable was minimal it was decided to install standard, all-dielectric cable along this part of the route. The area is currently under surveillance for wombat activity near the immediate cable route.

### SPENCER GULF CROSSING

#### Background

Part of the second Perth to Adelaide project route is 43 kilometres across the Spencer Gulf in South Australia (Figure 2). The route was selected to provide the most direct link from Adelaide to Ceduna where a satellite earth station was to be connected to the intercapital optical network. Use of the crossing reduced the total project length by approximately 200 kilometres and maintained the appropriate separation from the first Perth to Adelaide project. Analysis showed that three cable crossings, separated by approximately 1 kilometre, would ensure full system availability on the route should one of the cables be damaged.

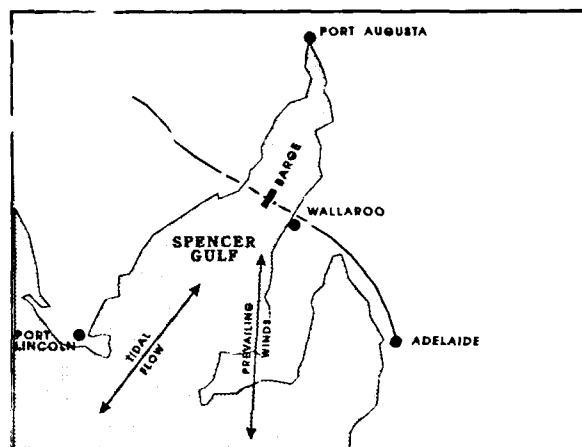


FIGURE 2 SPENCER GULF ROUTE

#### Submarine Cable Design

Primarily based on cost, a miniature design of submarine cable was selected for the project. The 16 fibre cable consisted of a single loose tube containing the fibres, surrounded by 14 galvanised high tensile steel wires and a high density polyethylene outer sheath. The outer diameter of the cable is 11.8 mm and its short term tensile rating is 16 kN. Additional tensile strength was provided where required by the use of add-on protection consisting of steel wire rope contained within a polyethylene housing. The additional tensile strength provided by the add-on protector is 110 kN for short term load application [4].



As the cable contains galvanised armouring, but does not feature a moisture barrier, considerable attention was given to the possibility of hydrogen induced attenuation increase. The cable used has an extremely effective corrosion protection system (flooding compound) around the armouring wires, which results in a low rate of hydrogen generation. The absence of a moisture (and gas) barrier is also beneficial in permitting any hydrogen generated to permeate out of the cable structure. A trial installation of 15 kilometres length, in up to 25 metres of sea-water, over a period of six months has shown no measurable increase in attenuation at 1240 nm (a main hydrogen peak wavelength). The attenuation of the cable at 1300, 1240 and 1550 nm will be monitored closely over time to confirm satisfactory operation.

#### Environmental Hazards

Very soon after adopting the concept of a submarine cable crossing of the Spencer Gulf, it was quite clear that considerable effort would be required to nominate and quantify both the cable security hazards and the environmental hazards associated with the cable installation. It was well known that marine activities in the area were associated with heavy shipping, intensive prawn trawling and recreational boating.

Discussions with marine experts revealed that anchors from large cargo vessels would, in rough seas, penetrate 3 to 4 metres into sand or clay. No means of cable burial could economically eliminate this hazard. Declaration of a no-anchor zone and the installation of separated cables with redundant capacity would ensure network reliability. Recreational vessel anchor penetration was found to be less than 40 cm.

Investigations of the impact of prawn trawling nets on the sea bottom revealed that even intensive trawling over a period of a day was unlikely to reduce cable burial depth by more than 100 mm. However, longer term loss of cover would be allowed for with a conservative burial depth.

#### Sea Bottom Survey

The sea bottom survey of the three cable routes showed a generally flat, featureless sea bottom with sand-grass beds existing near both shores. Typically, there was 0 to 0.4 metres of sand over several layers of rock.

On the eastern region several diamond cut core samples were taken revealing the rock thickness to be in the order of 0.6 metres thick over a layer of sand.

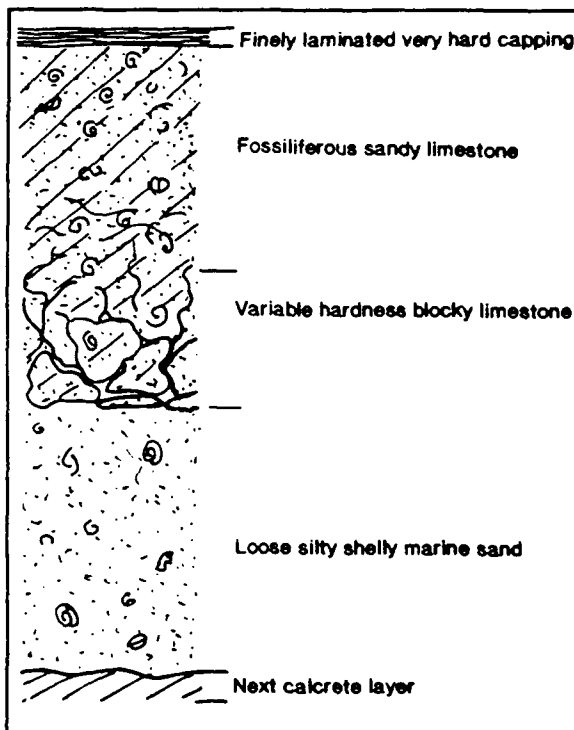
The core samples revealed the following (Figure 3):

- (a) a finely laminated, very hard capping of 10 to 40 mm thick.
- (b) a massive limestone mid-region 250 to 400 mm thick.

- (c) a fractured and friable limestone lower region of 150 to 250 mm thick.

The compressive strength of the core samples was consistent with the rock nature generally ranging from 90 Mpa down to about 3 Mpa. The highest test value achieved was over 120 Mpa.

On the western region the rock was not as thick or hard and generally existed as thin fractured blocks.



**FIGURE 3 TYPICAL SECTION THROUGH CALCRETE SEQUENCE**

#### Installation Aspects

The hardness and extent of the rock within the burial zone for the three 43 kilometre submarine crossings clearly indicated that very reliable, heavy-duty equipment would be required to securely bury the cables within a reasonable time frame.

The total length of the difficult installation conditions meant that the project duration would be in the order of months. During such a lengthy period winds exceeding 100 km/hour and sea swell and chop of up to 4 metres could be expected. The marine vessels used must cope with such conditions without cable damage and preferably without the need to cut the cable in order for the installation vessel to seek shelter. In addition, the ability to accurately maintain a course while operating in rough weather was required.

An extensive region of shallow water at the western landfall suggested that a shallow draft barge would offer significant advantages in installation in this region.

With a maximum water depth of only 30 metres it was recognised that a marinised version of a hydraulically powered land rocksaw would most economically provide the reliability and power required for the cable burial.

Telecom Australia's contractor arranged the use of equipment which fulfilled these requirements. A purpose built cable laying barge was the prime installation vessel and was used in a configuration in which the barge was winched sideways across the gulf. This allowed the barge to face into the prevailing northerly and southerly winds and sea currents. In addition, a four anchor mooring anchor system used in conjunction with two 400 HP thruster motors permitted continuation of installation in high winds and heavy seas.

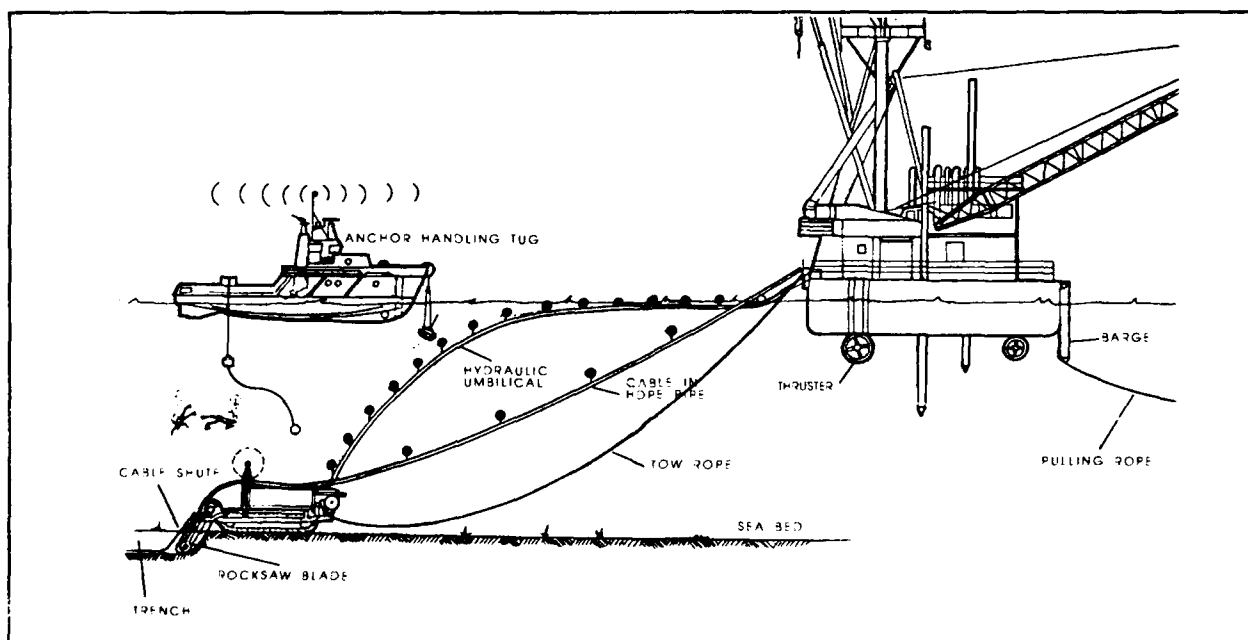
A marinised and modified land tractor of American origin was the cable burial equipment for the marine part of the installation. The diesel engine and hydraulic pump were mounted on the deck of the barge and provided hydraulic power to the tractor's hydraulic motors for powering the rock cutting chain and tracks, via a number of 70 metre long hydraulic hoses. The marine rocksaw has a number of features which proved to be very useful in achieving a successful installation as follows:

- \* 800 horsepower available for rocksawing
- \* Very heavy duty rock cutting chain 450 mm wide.
- \* Capability to rocksaw to a depth of 2 metres.
- \* Capability of laying cable to a depth of 1.8 metres via a cable laying chute attached to the rear of the rock cutting blade.
- \* Ability to self track which is useful in shallow water.
- \* Suitability for being towed when out of sight in deep water and directional control from self tracking would be difficult to achieve.

Figure 4 illustrates the installation method.

#### The Installation Achieved and Environmental Impact

Diver inspections were conducted at four sites on the route primarily to assess the environmental impact of the installation. As part of this process small excavations were made to determine cable burial depth and to determine the nature of the damage to the various sub-bottom layers. It was noted by the divers that the rocksaw had produced a very uniform trench approximately 450 mm wide and from 1.7 to 1.9 metres deep through rock and sediment. Assessment of the installation clearly indicated negligible impact on the environment.



**FIGURE 4 SUBMARINE CABLE INSTALLATION METHOD**

## Cable Security Achieved

At a cable burial depth of 1.8 metres, most often through at least one layer and usually through more layers of calcrete, the cable is considered to be extremely well protected from the hazards associated with prawn trawling and recreational boating. Although a no anchoring zone has been declared in this region, large vessels' anchors may be used here in emergency situations. There appears to be a high probability that in such a situation no part of the anchor would find its way to the bottom of the backfilled, relatively narrow trench to cause cable damage.

## CONCLUSION

A range of unique environmental challenges were presented with the installation of the second Perth to Adelaide optical fibre cable route. Solutions were successfully developed to establish a secure installation with minimal impact on the environment.

## ACKNOWLEDGEMENTS

The permission of the Deputy Managing Director, Telecom Australia to publish this paper is acknowledged.

## REFERENCES

- [1] E.Johansen, B.M.Faulks, B.T.deBoer - "Installation, Evaluation and Future Design of Optical Fibre Long-Haul Routes in Australia", Proceedings of the 35th International Wire and Cable Symposium, Reno, Nevada, November 1986.
- [2] L.Kiss "Performance of Optical Fibre Cables and Operations and Maintenance Procedures in the Australian Telecommunications Network", Proceedings of the 37th International Wire and Cable Symposium, Reno, Nevada, November 1988.
- [3] P.Hulbert, M.McKiterick, R.Schuster - "Developments and Experience in the Installation of the Perth to Adelaide Optical Fibre Route", Proceedings of the 38th International Wire and Cable Symposium, Atlanta, Georgia, November 1989.
- [4] W.Giebel - "On the Crest of a New Wave in Optical Submarine Cable Technology", Proceedings of the 38th International Wire and Cable Symposium, Atlanta, Georgia, November 1989.

## AUTHORS

### Giulio Consiglio

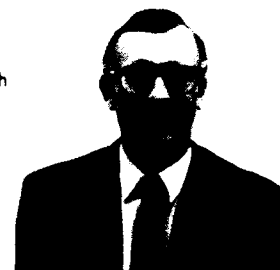
Optical Cable Networks Branch  
Telecom Network Engineering  
10/518 Little Bourke Street  
Melbourne, VIC 3000  
AUSTRALIA



Giulio Consiglio joined Telecom Australia in 1982 after graduating from the Royal Melbourne Institute of Technology in Electrical Engineering. Since then he has been closely involved with optical fibre cable design, development, specifications and test procedures. Currently, he has national responsibility for the coordination and provisioning of Telecom Australia's optical fibre cable requirements.

### John Groom

Optical Cable Networks Branch  
Telecom Network Engineering  
10/518 Little Bourke Street  
Melbourne, VIC 3000  
AUSTRALIA



John Groom joined Telecom Australia in 1972 after graduating in Electrical Engineering. Since then his responsibilities have included metallic cable design, development and introduction of new safety equipment and practices into external plant operations, and optical cable design. Currently he has responsibility for Telecom Australia's major submarine optical fibre cable installations.

### Dr. Edwin Johansen

Transmission Resources  
and Standards Branch  
Telecom Network Engineering  
12/518 Little Bourke Street  
Melbourne, VIC 3000  
AUSTRALIA



Ed Johansen received the BE degree in 1970 and PhD in 1978 from the University of Western Australia. In 1974 he joined the Research Laboratories of Telecom Australia and has worked on aspects of optical fibre technology and systems since 1978. From 1987 to 1991 he had full responsibility for all external plant aspects of optical fibre technology within Telecom Australia. Currently his responsibilities include resource and standards issues of transmission technology.

Les Kiss

Optical Cable Networks Branch  
Telecom Network Engineering  
10/518 Little Bourke Street  
Melbourne, VIC 3000  
AUSTRALIA



Les Kiss joined Telecom Australia in 1971 after graduating in Mechanical Engineering at Melbourne University. He has had extensive experience in the external plant area, in particular in cable design and specifications and in the installation of cable plant. He currently has national responsibility for Telecom Australia's installation plant and practices for optical fibre cables in the inter-exchange network.

Peter Latoszynski

Telecommunication Science  
and Technology Branch  
Telecom Research Laboratories  
770 Blackburn Road  
Clayton, VIC 3168  
AUSTRALIA



Peter Latoszynski is an Applied Science Graduate of Footscray Institute of Technology (1975) and also gained post graduate qualifications in Analytical Chemistry from the Royal Melbourne Institute of Technology in 1980. Peter joined the Telecom Australia Research Laboratories in 1972 and has held a variety of technical positions prior to specializing in polymer technology. He is currently Principal Polymer Chemist responsible for network materials stabilisation, new cable materials and electro-active polymers.

# Optical Fiber Cable Transfer Splicing Machine

Y. TAMAKI , H. KATAYOSE , H. YOKOSUKA

Opto-Electronics Laboratory Fujikura Ltd.  
1440, Mutsuzaki, Sakura-shi, Chiba, 285, Japan

## Abstract

As optical fiber cable networks expand, the need for techniques to maintain optical lines has grown. Methods of replacing existing optical fiber lines with new fiber cables have become essential. As multiconductor optical fiber cables replace conventional ones, multiconductor connectors are being widely used to enhance the efficiency of installation. Towards this end, we have developed a fiber transfer splicing machine that exchanges optical fiber cables faster and more reliably.

## 1. Introduction

Now that optical fiber cables are being widely used in cable networks the number of fibers in optical fiber cables is increasing steadily. A 1000-fiber cables consisting of 4-fiber or 8-fiber ribbons has already been developed and is being widely used in Japan. In order to splice or measure a large fiber count cable, a fiber ribbon connector is being widely used both in the field and in buildings.

As optical fiber cable networks expand, maintenance techniques have become increasingly important for ensuring smooth operation. Reliable methods of replacing faulty optical fiber cables are greatly needed.

We have developed a fiber transfer splicing machine that makes it possible to replace optical fiber lines by switching the connectors at both ends of the fiber line. This transfer splicing machine is intended primarily for use in manholes. The device is compact, lightweight and portable. It switches 4-fiber and 8-fiber single mode multifiber optical connectors (MT connectors) by firstly removing the retaining clip in an MT connection.

Two such transfer splicing equipment are used simultaneously to transfer both ends of a cable. The line is replaced in less than 20ms on average with a connection loss fluctuation of below 0.5dB. The synchronous error between the two devices is less than 1ms.

The transfer splicing machine also allows for a manual or automatic return to the original connection should any problem arise during or after the switching operation. When returning a cable to its original connection, the switching time is again less than 20ms on average with a connection loss fluctuation of less than 0.5dB.

## 2. System

### 2.1 System configuration

Figure 1 shows the optical fiber cable transfer splicing system configuration.

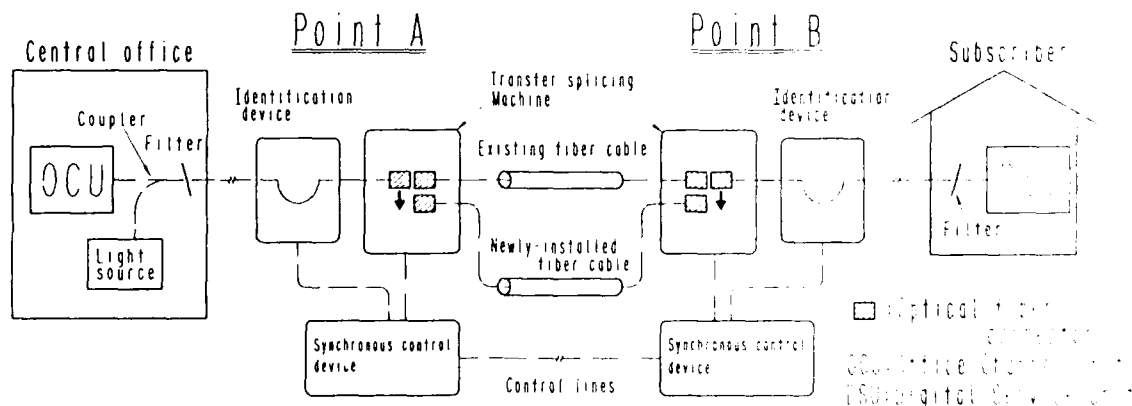


Fig.1 System configuration

This system[1] consists of a pair each of fiber transfer splicing machines, synchronous control devices, and fiber identification devices[2]. The functions of these components are listed in Table 1.

Table 1 Functions of system components

System Components	Functions
Fiber transfer splicing machine	Automatically transfers optical connectors
Synchronous control device	<ul style="list-style-type: none"> <li>Controls the transfer operation of the transfer splicing machine</li> <li>Detects the conductor identification signal light</li> <li>Point-to-point talk function</li> <li>Data communication function</li> <li>Displays the contents of transfer splicing and the results of measurements</li> </ul>
Fiber identification device	<ul style="list-style-type: none"> <li>Detects the conductor identification signal light</li> <li>Verifies the tape fiber line number</li> </ul>

During transfer splicing, conductors are identified by injecting an identification signal light of 1.55 $\mu$ m modulated to 270Hz from the central office, then bending an optical fiber at the transfer point with the synchronous control device, and there after checking for the presence of the conductor identification signal light through the bending light injected at the time the fiber is bent.

To transfer optical fiber cables, the MT connector on the existing cable side which is used at the optical fiber cable splicing point must be set on the fiber transfer splicing machine. Another MT connector on the new cable side must also be set on the same transfer machine. These two connectors are then used to transfer the cables.

The transfer splicing procedure and the results of measurements are shown on the display of the synchronous control device.

In addition, the state of work at the two transfer splicing points is transmitted in data communication between the two points via the control device and output on the display of the control device.

The talk function of the control device can also be used at the two working points for checking the progress of work at the other point.

inject the conductor identification signal light from the central office, and identify the conductors at the two transfer splicing points by using the synchronous control device and the fiber identification device. As for the new cable to be laid, inject the identification signal light into the cable from the transfer splicing point on one side and verify the injected identification signal light at the other work point, then identify the conductors. At this time, the line number of the tape fiber must also be identified.

After verifying the same conductors of the new and existing cable at both work points, set the optical connectors at the splicing points onto the fiber transfer splicing machines.

Ensure synchronization between the two work points, and simultaneously switch the two splicing points.

Transfer other optical fiber conductors in the same manner. After transferring all optical fibers in the cable, replace the splicing section back into the mechanical closure. This completes the transfer splicing process.

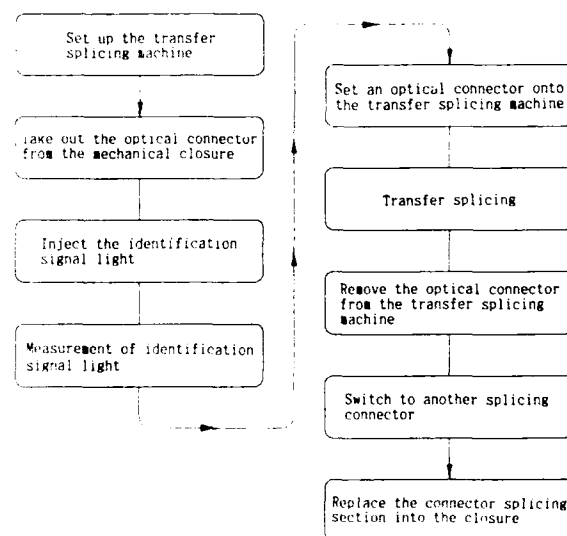


Fig.2 Transfer splicing process

## 2.2 Procedure for transfer splicing

Transfer splicing is based on the procedure shown in Fig.2. These are as follows.

First, set the transfer splicing machine at two work points.

Then, obtain the splicing point of the existing fiber cable to be transferred from the mechanical closure. Then,

## 3. Design

### 3.1 Basic design

The fiber transfer splicing machine quickly and reliably switches the existing MT connector of the existing line to the new MT connector at the splicing point of an optical fiber cable.

Since the existing line has a transmission signal passing through it, the transfer operation must be highly reliable. In addition, the transfer time must be as short as possible because the hit time of the transmission signal must be minimized.

Additionally, this machine must be carried to transfer splicing points and operated in a limited space. Therefore, it must be compact and light.

### 3.2 Optical fiber connector

The mechanically transferable multifiber connector (MT connector)[3] as shown in Fig.3 is used at the splicing point of the optical fiber cable to be transferred.

The MT connector consists of a pair of plastic ferrules produced by transfer molding, two alignment pins, and a clamp spring. In the plastic ferrule, two alignment holes are made with 4 or 8 optical fibers arranged between them.

The two alignment pins can move freely in the axial direction inside the alignment holes in the ferrule. The alignment holes are axially through.

The alignment pin is approximately 3mm longer than the ferrule length. If the alignment pins are fully inserted in one ferrule at splicing, the pins can still be inserted into the other ferrule by an additional 3mm to ensure reliable splicing.

When splicing is completed, the alignment pins are inserted into the alignment holes in the opposite ferrule, and a clamp spring is mounted on the ferrules to splice fibers with pressure applied on the splicing ends. On the splicing ends, an index-matching gel is applied to reduce return and connecting losses.

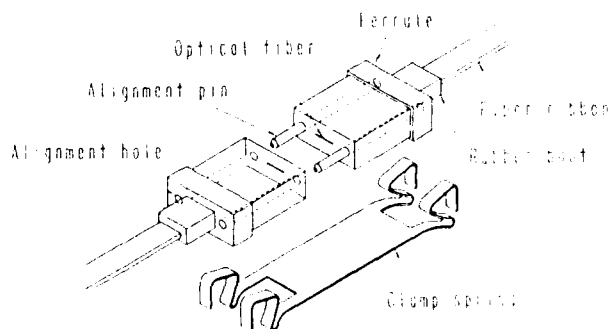


Fig. 3 MT connector structure

### 3.3 Procedure for connector transfer splicing

Figure 4 shows the procedure for transferring the MT connectors. In the even of a malfunction, the MT connector is returned to the original position by reversing the procedure shown in Fig.4. Briefly the steps are as follows:

- 1) Set a connector for the existing cable and a connector for the new cable onto the fiber transfer splicing machine.
- 2) Remove the clamp spring. Simultaneously, apply pressure using the transfer splicing machine.
- 3) Slowly move the alignment pins into the plug on one side.
  - 1) Move the alignment pins quickly.
- 5) Move the connector plug to the position of the new plug.
- 6) Insert the alignment pins into the connector.
- 7) Remove the plug on the existing cable side.
- 8) Mount the clamp spring. Simultaneously release the pressure from the transfer machine.

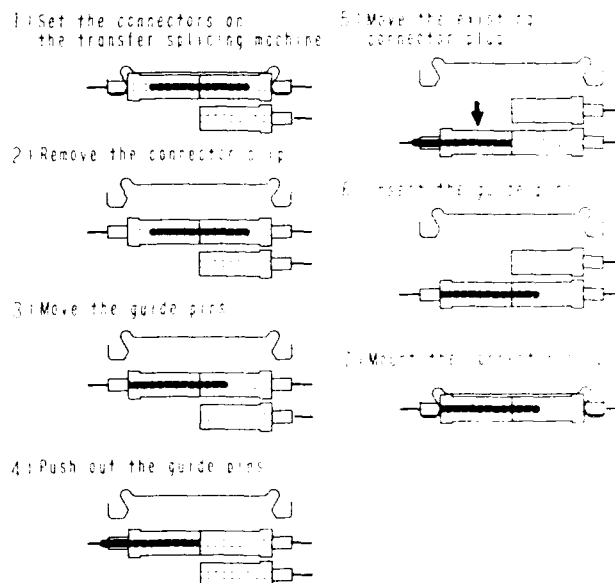


Fig. 4 Connector transfer splicing process

### 3.4 Transfer mechanism

The transfer machine is divided into two main sections, the transfer operation section and the clamp spring removal/fitting section[1][5].

The transfer operation section consists of a base on which the existing connector and new connector are set, a mechanism to

vertically move the connector that is to be transferred, and a mechanism to open/close the base.

To minimize the transfer time, connector are set onto the transfer machine in layers and are positioned so as to terminate movement by the shortest possible stroke.

To prevent the connector ends from rubbing against each other and becoming damaged when the connector is moved, the connector base is designed to open when the connector moves and close as soon as the connector stops.

When the connector base closes or opens, mechanical pressure is applied to or released from the connector. That is, when the clamp spring is removed in the transfer process in the last section, the setting base closes and mechanical pressure substituting for the clamp spring acts on the connector to ensure stability. When the clamp spring is mounted, the setting base opens to release the mechanical pressure.

To move the alignment pins in the connector, movement is divided into two stages to decrease the transfer time. During the initial process, the alignment pins slowly move inside the connector and stop when 3mm is left in the connector plug. Then, a 3mm stroke is administered at high speed to complete the transfer operations.

At this point, it has been proven that the stability of the connectors can be maintained if the alignment pins are inserted 2mm or more into the connector plug on one side. Therefore, the transfer time can be reduced by moving the pins at a high speed only through the unstable area.

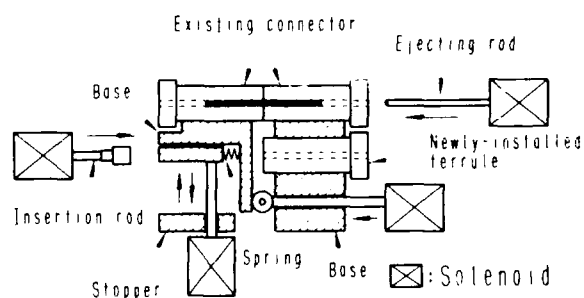


Fig. 5 Transfer mechanism

The clamp spring removal/fitting section consists of a claw to open/close the clamp spring, a drive mechanism for the claw, and another drive mechanism to move the claw vertically. The clamp spring is opened or closed by inserting the opening/closing claw downward into four loading bent slits in the spring and moving the claw.

The vertical drive mechanism incorporates a mechanism to accommodate variations in the vertical dimension of the clamp spring to ensure that the spring can be mounted at the specified position. In addition, this mechanism prevents the connector from being subjected to excessive force.

The spring opens and closes concurrently with the connector setting so as to minimize changes in the pressure on the connector end.

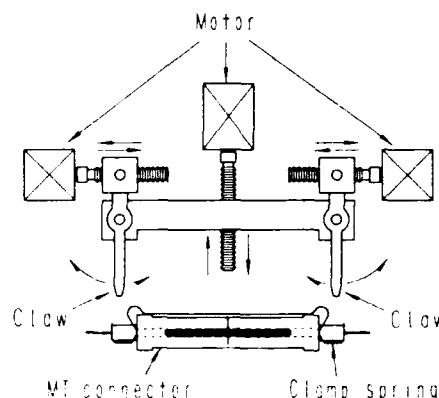


Fig. 6 Clamp spring removal and fitting mechanism

## 1.Characteristics

### 1.1 Transfer time

We used the measurement system shown in Fig.7 to transfer the MT connectors and measure the transfer time. The transfer time is measured starting when the light is off and ends when the level fluctuation is 0.5dB relative to the level achieved after transfer.

The measurement results indicated that the transfer time is 20ms on average. Fig.8 shows the transfer waveform. We then set the operating temperature to 0°C and 10°C and measured the transfer time in the same manner. There was little difference in the transfer time. Table 2 lists the results of these measurements.

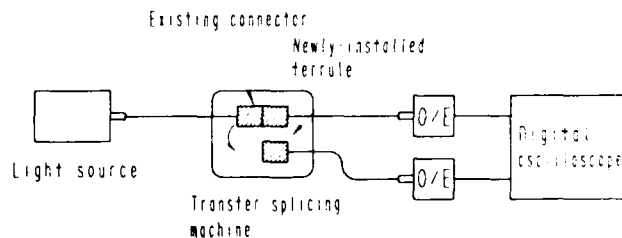


Fig. 7 Measurement system for transfer time



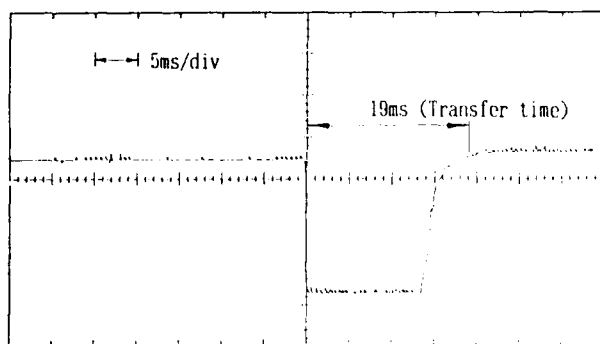


Fig. 8 Optical transfer waveform

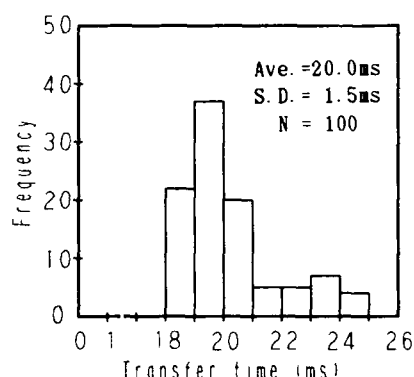


Fig. 9 Transfer time

Table 2 Relationship between operating temperature and transfer time

Operating temperature	Transfer time
0 °C	21 ms
25 °	20 °
40 °	20 °

## 1.2 Connection losses

### 1) Splicing loss

To verify the connecting loss characteristics of the MT connector during transfer splicing with the transfer machine, we compared the characteristics of manual splicing and splicing with the transfer machine.

The MT connector used for measurements of the normal level. As shown in Fig.10, the measurement results indicate that the difference in the loss characteristics between manual and mechanical splicing is very low. Thus, using a transfer machine did not result in greater connecting losses.

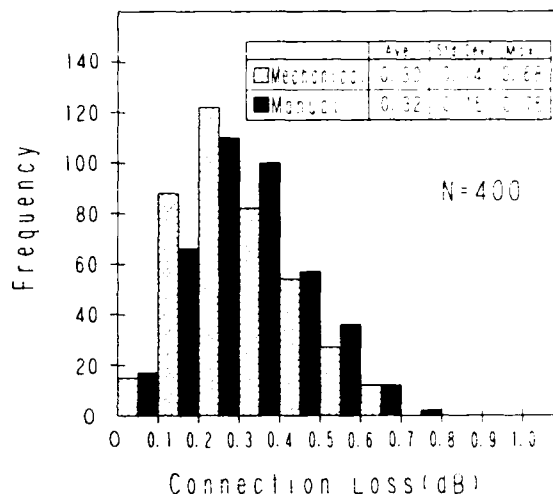


Fig. 10 Connection loss

### 2) Fluctuations in connecting losses

We measured variations in the connecting losses that occur when loading or unloading the clamp spring.

The measurement covered both the clamp spring removal process and fitting process. The MT connector used for this measurement was the same as that used for evaluation in the previous section.

The measurement provided stable results from both the removal and fitting processes, with losses varying 0.5dB or less.

## 5. Conclusions

We produced a prototype fiber transfer splicing machine and used it in the transfer splicing of an optical fiber line. With this prototype, we achieved an average transfer splicing time of 20ms and a loss variation during transfer splicing of less than 0.5dB. This fiber transfer splicing machine will be useful for transfer splicing work in the future subscriber optical line network.

We intend to continue field experiments to verify the characteristics of the equipment and carry out reliability tests of durability, environmental characteristics, and others to realize the future use and enhance operability and reliability.

## References

- [1] I. Watanabe, M. Shimizu and H. Kobayashi  
"Optical Fiber Cable Transfer Splicing  
System", IWCS, 1989, pp. 191-197.
- [2] M. Shimizu et al., "Identification  
Method for Optical Fiber Transmission  
Operation Lines with Local-Light  
Injection and Detection Coupling  
System", IWCS, 1990, pp. 735-741.
- [3] S. Nagasawa et al., "Mechanically  
Transferable Multifiber Connectors",  
IOOC'89, paper 21C2-1, 1989.
- [4] H. Kobayashi et al., "Design and  
Performance of Optical Multifiber  
Connector Transfer Splicing Mechanism",  
IECE(B-1), Vol. J74-B-1 NO.5, pp. 408-416  
, 1991.
- [5] H. Kobayashi et al., "Clamp Spring  
Removal and Fitting Method for Optical  
Multifiber Connector with Index  
Matching Material", IECE(B-1), Vol. J74-  
B-1 NO.6, pp. 185-194, 1991.



Hiroichi Katayose

Opto-Electronics  
Laboratory  
FUJIKURA LTD.

1440, Mutsuzaki,  
Sakura-shi, Chiba, 285  
Japan

Hiroichi Katayose received the B.S.  
degree in Electronic Engineering in  
Nagaoka Technological University in 1983.  
He has been engaged in research and  
development of telecommunication cables  
and accessories.

Mr. Katayose is a member of the  
Institute of Electronics and  
Communication Engineers of Japan.



Yasuhiro Tamaki

Opto-Electronics  
Laboratory  
FUJIKURA LTD.

1440, Mutsuzaki,  
Sakura-shi, Chiba, 285  
Japan

Yasuhiro Tamaki was born in 1955. He  
received the B.E. degree in mechanical  
engineering in 1977 from Saitama  
University.

He joined Fujikura Ltd. in 1982 and  
has been engaged in research and  
development of telecommunication cables  
and accessories.

Mr. Tamaki is a member of the  
Institute of Electronics and  
Communication Engineers of Japan.



Hiroshi Yokosuka

Opto-Electronics  
Laboratory  
FUJIKURA LTD.

1440, Mutsuzaki,  
Sakura-shi, Chiba, 285  
Japan

Hiroshi Yokosuka graduated in mechanical  
engineering from Tokyo Metropolitan  
Technical Junior College in 1967.

He has been engaged in development of  
telecommunication cables and accessories.  
He is now a Manager of the Fiber and  
Cable Accessory Department in Opto-  
Electronics Laboratory of Fujikura Ltd.

Mr. Yokosuka is a member of the Institute  
of Electronics, Information and  
Communication Engineers of Japan.

A NEW SERIES OF CABLE ACCESSORIES FOR  
OPTICAL FIBER SUBSCRIBER LOOP NETWORKS AND PREMISES WIRING SYSTEMS

Roberto BIAZZI, Stefano CRICO

SIRTI SpA - Via Vida, 19  
20127 Milano, Italy

**ABSTRACT**

The commercial subscriber and intra-building wiring systems available today are not sufficiently modular and flexible such as to guarantee a complete transparency to all the services and to meet the stringent requirements of the future applications. For this reason SIRTI, the major installation company in Italy, taking into account all its experience of sixty years of installation of telecommunication and power networks in Italy, has developed a fiber optic solution based on optical cables, components and accessories. This proposal is capable at the same time to implement a premises network system according to EIA/TIA "Commercial Building Wiring Standard" architecture as well as a fiber optic solution for subscriber loop networks.

This paper describes the problems related to the choice and development of this line of accessories and components which can be suitable for different types of environments and can be adopted to meet the different needs of the users.

**INTRODUCTION**

Over the last few years an increasing importance has been attached to telecommunication systems not only in public environment but also inside private organizations (offices, banks, business areas, campuses, research and development centers, airports, railways,...).

The techniques developed so far for the implementation of fiber optic networks have been designed as suitable especially for long-haul networks. The needed integration of the existing fiber optic trunk and junction networks with the new optical subscriber loops

and with the foregoing local area networks inside private organizations requires the development of an "ad hoc" solution. These two realities are both related to the connection of the subscriber, seen from a public operator point of view as well as from the private network environment. Consequently they have a lot of common problems and possible solutions may find their way on the substrate of the same communication system.

In the design phase of the system and the accessories a detailed analysis of the ambient is required. The goal of the preliminary study driven within SIRTI has been the definition of the different needs of a local network in comparison with long-distance network requirements, taking into account the main installation techniques, using both copper and optical fibers as a physical layer.

As an example, a very generic scheme of a network is shown in figure 1.

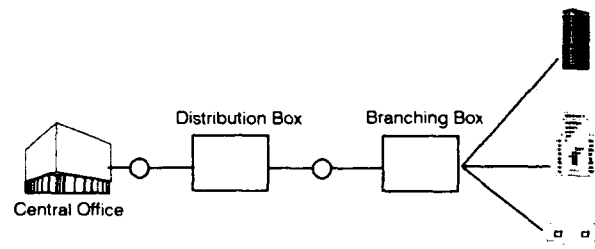


Figure 1  
Scheme of a generic network

Compared to a geographical or metropolitan area network a premises wiring system intended to cover a limited area shows the following characteristics, regardless if the network is within a public environment (Central Office to Branching Box and eventually TLC outlet) or a private one (Internal Building Wiring) :

- . reduced area (1-2 km);
- . no regeneration need;
- . large number of users per area unit;
- . multiple sectional points;
- . frequent reconfiguration need;
- . strong technological impact;
- . heterogeneous traffic.

A suitable complete premises wiring system (accessories, components and cables) capable to meet the characteristics mentioned above shall have the following features:

- . Modularity and easy configurability: different cabling system elements need to be modular so to allow easy network configuration. The TLC infrastructure shall be designed on a planning base able to consider the network lifetime (15-20 years).
- . Cheap installation, maintenance and reconfigurability: in consequence of users' change of position or network expansion the cabling system needs to be easily and rapidly reconfigured. The cost of a premises wiring system installation shall be compared to the end of life cost. The end of life cost is strongly influenced by the maintenance cost and by interruption of the users working activity due to reconfiguration interventions.
- . TLC systems independence: TLC infrastructure shall be designed during the building plan apart from network applications.
- . In accordance with LAN (Local Area Network) standard: this feature allows to support the most common local applications.
- . Multifunctionality: a premises wiring system shall be able to support heterogeneous traffic (voice, video and data) avoiding superimposed networks.

However, as much as possible the same standardized modules suitable for

different uses with the purpose of reducing costs and increasing modularity and interchangeability will be kept as the winning principles of the overall system.

### SUBSCRIBER LOOP NETWORKS

Although most of the attention of the development activity has been devoted to the aspects covered by the EIA/TIA "Commercial Building Wiring Standard"<sup>1</sup> architecture, some specific designs have been identified which are more likely devoted to a public environment. These solutions take into account the problems related to the traditional telephone network installation practices in view of the development of high-speed data communication, MAN (Metropolitan Area Network) standards and value-added services such as the integration of voice, data and video signals.

#### Compact fan-out

Coming into a more detailed description of the new accessories designed for this purpose, a starting point has been to consider a compact fan-out structure as the basic component to provide a transition from multifiber units to individual fiber connectors. This component, in fact, allows a high density fiber termination to be implemented in a short time in Main Distribution Frames (within the Central Offices, for instance) as well as at Distribution Cabinets (in the street) or at Branching Boxes (at the Customers Premises). The termination of the feeder cable using fan-out, in fact, allows network flexibility at individual fiber level (any individual feeder fiber can be cross-connected to any secondary distribution fiber). More generally fan-out may be used any time it is necessary to have access to individual fibers.

Due to the higher fiber counts of cables, it seems that also in this case the use of fan-out can give a lower cost in network implementation because of overall time saving during installation.

The fan-out shall both be factory and field installable. Factory installation has to be preferred, whenever possible, for lower cost and better performance. Furthermore, fan-out technique would

allow an overall time and cost saving on network implementation. Once the cable side has been properly terminated via mass splice or multifiber connector, fan-outs can be fitted to interface cable fibers to the equipment any time there are requirements for further subscriber activations. This can be done with very simple tooling and with no active control of performance. In addition, initial investment to implement the network can be limited.

The compact and fully integrated fan-out (Patented) has been built in such a way that both the single-way and the multi-way connectors are incorporated in the structure. It is clear that in this scenario the possibility to have a fan-out connector which realizes a direct transition from a multi-fiber to a single-fiber unit is very interesting in some environments where the saving of space is of primary importance. Of course also the design of the compact fan-out connectors can be such as to suit the needs of cabling and of the accessories which are used in the specific application.

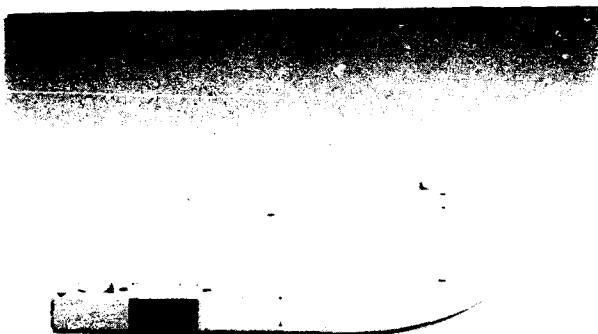


Figure 2  
Compact fan-out  
(Patented)

The device design has been based on the attempt to reduce as much as possible the dimensions of the fan-out. Some constraints had to be considered in this effort, as the eventual need to arrange the extra lengths of fiber and the minimum distance between the single and multi-way connectors to allow the

polishing of the plugs themselves. This has been the reason why the envisaged solution considers the need to have an extra length of fiber to allow an easier polishing and mounting of the single and multi-fiber units. This leads to the realization of a box containing a drum of fixed diameter (at least eight centimeters) around which the fibers are arranged, with the single and multi-fiber units placed at an angle of 90° between each other. A picture of the fan-out is shown in figure 2.

#### Main distribution frame

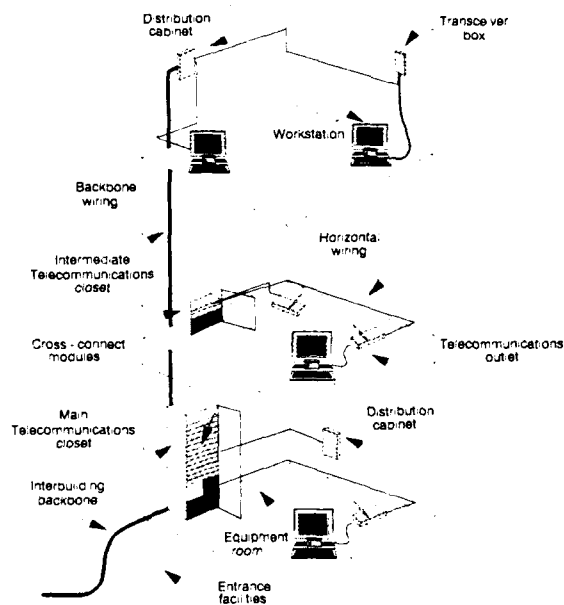
Main Distribution Frames (MDF's) shall allow individual access to cable fibers and their cross-connection to the equipment. Up to now cable termination at MDF's has been carried out by splicing single preconnectorized fiber cords to cable fibers. This procedure is very time consuming due to the always higher fiber counts of cables. Because of this it is not suitable for high density fiber termination. The fan-out technology, on the contrary, appears to be a very suitable terminating procedure at MDF's. Of course it is more attractive as far as it combines small size, robustness, suitability to high density termination through the use of connectors which can easily be packaged together.

The Main Distribution Frame developed is based on the use of the external N3 frame (to host modules of 19 inches or 600 centimeters). The frame is designed to contain and fix a number of compact fan-outs which allow the connection among the ribbon fibers of the external cables and the fibers of the cables internal to the Central Offices. The connection is made possible also by jumpers which allow to separate the subscriber distribution from the topographic structure of the network, to make an easier re-routing of the network itself. The full capability of the Frame is of 400 fibers both entering and exiting with a total number of 100 fan-out in slots of 25 units. The single fiber cables as well as the feeder cables can enter in the Frame from the top or the bottom.

#### FIBER OPTIC BUILDING WIRING SYSTEM

The need to meet the end user requirements and to satisfy the over

mentioned features requires a premises wiring system architecture according to a widely used and acknowledged standard. The reference standard is the recently approved EIA/TIA n°568 "Commercial Building Wiring Standard"<sup>1</sup>. The network architecture included in EIA/TIA 568 standard is described in figure 3.



- Figure 3 -  
EIA/TIA 568 wiring architecture

According to this standard the functional areas in which a building cabling system is organized are:

- . Horizontal Wiring: "it is the portion of the TLC wiring system that extends from the work area TLC outlets to the TLC closet".

- . Backbone Wiring: "the function of the backbone wiring is to provide interconnections between TLC closet, equipments rooms and entrance facilities in the TLC wiring system structure".
- . Work Area: "the work area components extend from the TLC outlet end of the Horizontal Wiring system to the station equipment. The station equipment can be any of a number of devices included but not limited to telephones, data terminals and computers".
- . TLC Closet: "it is an area within a building set aside for exclusive purpose of housing equipment associated with the TLC wiring system".
- . Equipment Room: "it is defined as an area within a building where TLC system are housed".
- . Entrance facilities: "it consists of the TLC service entrance to the building".

Accessories, components and cables described in the following sections are capable to cover each functional area and to satisfy the related requirements.

Over the last few years fiber optic has become a strategical media not only in a public environment but also in local area network and in building installations.

The features offered by fiber optic such as heterogeneous traffic integration capability, high bandwidth, low attenuation, EMI immunity, intrinsic over-voltage protection, reduced in weight and in size cables and lower number of cables needed makes this media suitable to implement an innovative premises wiring system able to satisfy the stringent over mentioned requirements and to be in accordance with technological progress. Besides the use of fiber optic is in agreement with LAN standard and with EIA/TIA 568 standard. The fiber optic penetration process in premises environment will be developed in two phases: a short term phase in which existing copper systems will be integrated by fibers and a medium term phase in which end users will be interconnected by fibers directly (Fiber-To-The-Desk). This evolutionary process will lead to

premises networks exclusively based on fiber optic.

#### Fiber optic

According to main LAN standards such as IEEE 802.3 CSMA/CD, IEEE 802.4 Token Passing, IEEE 802.5 Token Ring, ANSI X3T9.5 FDDI and cabling standard EIA/TIA 568, the suggested fiber optic type is graded-index multimode 62.5/125 micron. This is a compromise choice based on attenuation and bandwidth performances.

Besides, in comparison with 50/125 micron fiber and in the wavelength operation range (850 nm and 1300 nm), 62.5/125 micron fiber shows better performances in term of macrobending loss (Table 1) and optical power source coupling.

Diameter (mm)	850 nm		1300 nm	
	50/125 $\mu$ m	62.5/125 $\mu$ m	50/125 $\mu$ m	62.5/125 $\mu$ m
25	0.20	0.03	0.40	0.08
20	0.35	0.07	0.51	0.14
15	0.77	0.15	1.28	0.34
10	1.66	0.25	2.80	0.59

\* shift compared to reference level

\*\* 10 pops

- Table 1 -

Macrobending loss in multimode fibers

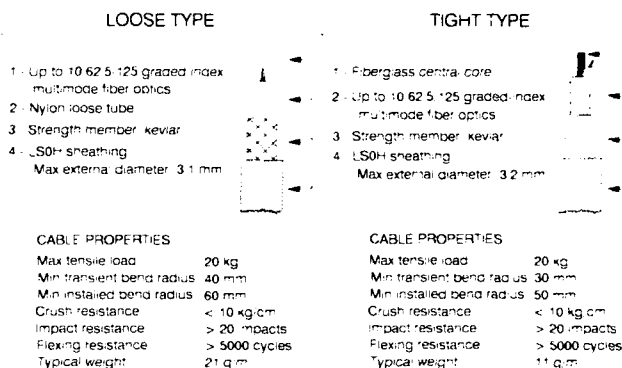
This result is particularly interesting in premises applications in which the installation infrastructures present frequent reduced radius bends (2-3 cm).

#### Fiber optic cables

The stringent requirements in terms of building installation infrastructure, people safety and equipment integrity in the case of fire require an appropriate premises optical cable design. Cable structure shall be reduced in size (external diameter) and in weight but, at the same time, able to guarantee good capacity (number of fibers) and good mechanical performances (min bend radius, max

tensile load, crush, impact and flexing resistance). The safety requirements to be met in the event of fire force installation companies to use LS0H (Low-Smoke-Zero-Halogen) sheathed cables capable to guarantee not only flame resistance and fire retarding but also low-smoke non toxic emission and very low-smoke gas generation<sup>2</sup>.

As an example two premises optical cables are presented, the former is of the loose coating fiber type and the latter of the tight coating fiber type (Figure 4).



- Figure 4 -

Fiber optic premises cables

These can be used both in Horizontal and in Backbone Wiring. In Horizontal Wiring each cable is 4 fibers organized so that each TLC outlet is equipped with two ports, one for LAN application and the second for generic transmission (data, voice or video). In Backbone Wiring, cables are used in their maximum configuration (ten or twelve fibers respectively); if more fibers are required cables can be organized in bundle structures.

Besides optical fiber premises wiring system includes single fiber cables (TLC outlet) and twin optical fiber cords (Cross-connect module, TLC Closet, Work Area and TLC Outlet).

#### Optical connectors

A premises cabling system shall offer the maximum level of flexibility in optical connector choice. Accessories shall be able to house each type of

commercial connector (ST, SC, EC, FC, Biconic, SMA, FDDI,...) to ensure the maximum compatibility with already existing systems. However, in the design of the accessories, the SC connector technology has been applied with a large use of single-way and multi-way components. In fact, because of his characteristics, SC connector appears to be a very suitable choice to meet the premises wiring requirements offering the following features:

- . its shape is rectangular, giving four advantages compared to other connectors: lower loss fluctuation during coupling and uncoupling cycles, easier insertion operation, high compression strength and high compactness;
- . push-pull coupling mechanism allows quick axial operation by incorporating self-locking and unlocking feature. End user is just used to handle push-pull components (electric plugs);
- . low cost, handleness and lightness are achieved combining the use of zirconia ferrules and plastic-molded housing;
- . good optical performances (less than 0.5 dB insertion loss with multimode fibers).

Besides, the use of SC connectors in public environment forecasts a large production with consequent cost reduction in advantage for premises application.

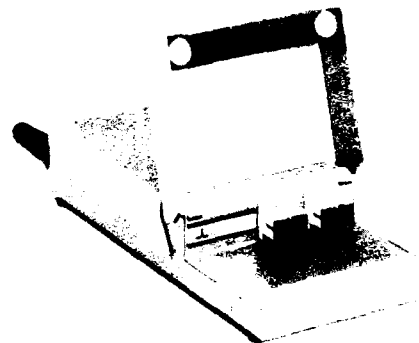
#### User ending

Each fiber in Horizontal Wiring multi-fiber cables shall be connectorized and accommodated in TLC outlets. The transition between multi-fiber cables and single fiber cables shall be realized through two methods. The first method, suitable for network configuration with fixed outlets, is realized through fusion splices (each splice loss less than 0.1 dB). This approach doesn't allow reconfiguration and shall be used preferably in wall outlets. The second method allows, through the use of on purpose designed optical components (fan-outs and mechanical multiple splices), to realize a flexible user network with reconfiguration capability; in this

case the TLC outlets can be moved with no expert installation staff needed. Factory fan-outs assembly allows to obtain a low-cost, low optical loss component. The installation phase is easy and consists only in the interconnection between the two parts of mechanical splice, one on user side and the other on Horizontal Wiring cable end.

#### TLC Outlet

TLC outlet is the accessory that implements the double function to protect the above described user ending and to implement the physical network user interface. TLC outlet shall be designed to make the installation phase simple, to allow an easy use and to be able to house different types of optical connectors. In figure 5 an example of TLC outlet is presented.



- Figure 5 -  
TLC outlet

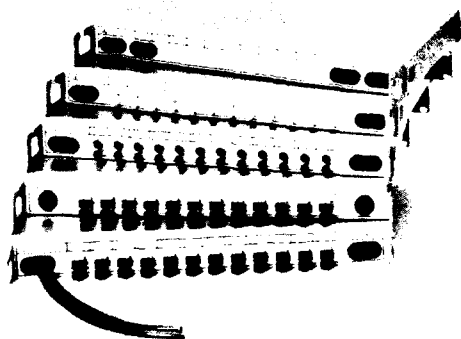
This TLC outlet offers two optical ports protected by a frontal door against external potential dangerous factors (accidental crash, dust,...). Presented TLC outlet can be floor, desk or wall mounted.

#### Cross-connect module

Cross-connect module is used to house fiber endings (Horizontal Wiring and



Backbone Wiring) in a centralized manner and to allow an easy network configuration using optical patch-cords. The use of cross-connect modules represents a potential high flexibility point in a cabling system. A good planning design phase to size the correct number of modules to be housed in TLC Closet is required not only to satisfy the current needs but also to guarantee future network expansion capability. Module is also equipped with splice organizers used to protect fusion splices implemented between horizontal or backbone fibers and connectorized (all commercial fiber optic connectors shall be supported) semi-jumper single fiber cable. Cross-connect module dimensions shall be in accordance with standard dimensions (19-inches). In figure 6 an example of fiber optic cross-connect modules is shown.



- Figure 6 -  
Cross-connect modules

This module is capable to house up to 24 fiber optic connectors in a 1U 19-in. rack. Optical cables entrance and configuration labels are accommodated on the frontal panel. Cross-connect structure is completely removable from the rack module to make installation and maintenance operation easier. The same module can be used to splice fiber together allowing up to fifty fusion splices protection capacity.

## CONCLUSIONS

In this paper the problems related to the design of accessories and components suitable both for subscriber loop networks and standard premises wiring systems have been debated. A complete line of fiber optic accessories and components (Distribution Frames and Racks, Termination and splicing modules, outlets, single-way and multi-way optical connectors, fan-out and cables) developed by SIRT I have been presented.

## REFERENCES

1. EIA/TIA Commercial Building Wiring Standard
2. R.Biazzi, U.Morganti - Use of high safety cables for inside application-EFOC/LAN 1991



Roberto Biazzi  
SIRTI SpA - via Vida, 19 - 20127  
Milano - ITALY

R. Biazzi was born in Monza, Italy, in 1961. He graduated in Electronic Engineering and specialized in Telecommunication Networks at Politecnico of Milano. He joined Cables and Optical Technologies Department of Sirti in 1988 where he was involved in the research and development activity related to fiber optic local area networks application. At present he is responsible for Advanced Fiber Optic Networks group devoted to study and develop fiber optic premises wiring systems and fiber optic application for private customers.



Stefano Crico  
SIRTI SpA - via Vida 19 - 20127  
Milano - ITALY

S. Crico was born in Milano in 1959. He received his University degree in Nuclear Engineering from the Politecnico of Milano in 1984. He passed 1 year between 1982 and 1983 for an EURATOM stage at the "Laue-Langevin" Institute in Grenoble (FRANCE). In 1985 he joined FIAR in the Defence Group, Electro-Optics Department, where he was manager of the IR sensors engineering. In 1988 he joined SIRTI, cables and optical technology department, where he was involved in passive optical component design and in manufacturing and characterization techniques for almost two years. During this period he has been involved in standardization activity as a member of CECC and EIA working groups on connectors. In 1990 he got the responsibility of the marketing of Optical Components and Accessories within SIRTI. He is author of 5 papers.

# CABLE TRANSFER AND SUPERVISORY SYSTEM FOR TRUNK OPTICAL FIBER CABLES

Hiroatsu MATSUMOTO \*, Yutaka YOKOO \*\*, Kiminori SATO \*, and Takuya UENOYA \*

\* NTT Network Systems Development Center, Tokyo, 100, Japan

\*\* NTT Telecommunications Software Headquarters, Kanagawa, 210, Japan

## 1. Abstract

NTT has developed a new operation, administration, and maintenance system called FITAS (Fiber Transfer and Test System) for application to trunk optical cable networks. The system provides a major advance in construction and maintenance efficiency, namely it enables operation and maintenance work on optical fiber cable networks--cable transfer, fault location, supervision of transmission characteristics--without in any way interrupting services over the network.

The system was deployed commercially in 1990 and has been operating satisfactorily. The basic concept and measured results showing the system's full capabilities are presented.

## 2. Introduction

NTT has been deploying trunk optical fiber cable networks based on single-mode fiber cables since 1983.

Dispersion-shifted fiber cable has been in use since 1988. <sup>(1)</sup> These networks, offering through-put capacity up to several Gbit/s, have been deployed nationwide. As optical fiber cable networks have become more extensive, operation tasks such as fault location, supervision of transmission characteristics, and cable transfer have become correspondingly more complicated. Nevertheless, construction and maintenance work concerning optical fiber cables have been carried out manually at NTT since they were first introduced. Especially in the case of long trunk lines, repeater stations are often located very far from towns. This makes it very difficult to locate faults in an optical fiber cable in a short time. The time element can be extremely important in an emergency. This has led to demand for a high-performance operation system which will not disrupt the service provided over the cables.

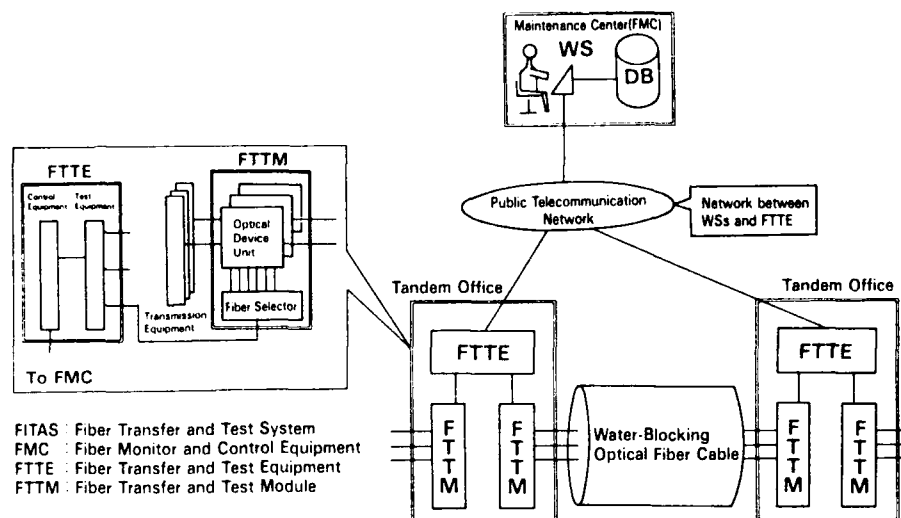
Recently, a number of reports have appeared that propose operation, administration, and maintenance (OA&M) systems for application to optical fiber cable networks. <sup>(2) (3) (4) (5)</sup> In order to fully exploit the extensive optical network that has been deployed throughout Japan, NTT have developed an OA&M system capable of performing automatic cable transfer and supervision of optical fiber cables which meets the demands of the new fiber cable environment. The system is capable of automatic supervision of transmission characteristics, fault location and cable transfer from a remote maintenance center.

## 3. System Configuration

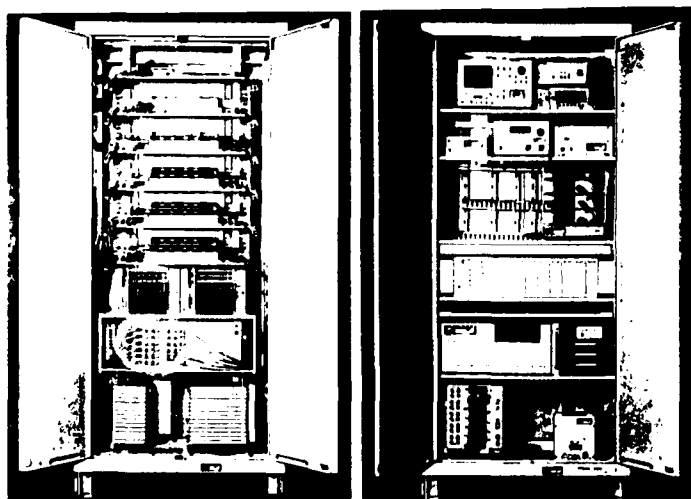
A schematic configuration of the system is shown in Fig.1. It consists of three key elements: a Fiber Transfer and Test Module (FTTM) (picture 1), a Fiber Transfer and Test Equipment (FTTE)(picture 2), and a Fiber Monitor and Control equipment (FMC). The FTTEs are controlled by the FMC, and the FTTMs are controlled by an FTTE. Main specifications for the system are summarized in Table 1.

### 3.1 Fiber Transfer and Test Module (FTTM)

The FTTM is installed in buildings such as telephone offices or tandem offices. Each FTTM consists of fiber selectors and optical device units. A fiber selector connects the test equipment in the FTTE and the optical device unit. It is composed of connectors and a movable mechanism with three axes, and mechanical optical switching equipment. As the name indicates, the fiber selector selects the optical fiber to be measured or transferred according to the commands issued by the FMC in the maintenance center. The optical device unit accommodates WDM couplers, filters, and multifiber mechanical switches. Figure 2 shows a schematic overview of the optical device



**Fig.1 Cable Transfer and Supervisory System for Optical Fiber Cable**



picture 1 FTTM

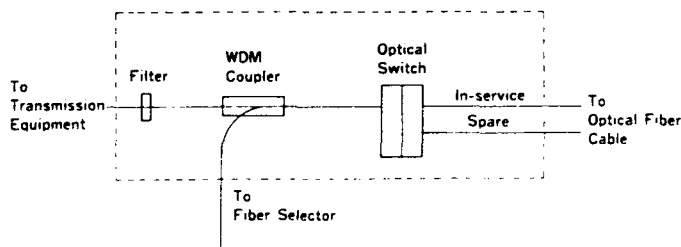
picture 2 FTTE

**Table 1 Main System Specifications**

Items		Contents
Optical device unit		8 fibers/unit maximum 300 fibers/FTTM
Test frame (FTTE)		maximum 10 FTTM controllable
Work station (FMC)		maximum 20 FTTE controllable
Transfer function	Transfer time	<10msec.
	Transfer unit	2 fibers/4 fibers
	Transmission medium	1.55 $\mu$ m DS fiber      SM fiber
	Monitor wavelength	1.31 $\mu$ m      1.55 $\mu$ m
Test function	Line length	80km      40km
	Measurement items	<ul style="list-style-type: none"> <li>Transmission characteristic (optical attenuation/splice loss)</li> <li>after cable construction</li> <li>before/after cable transfer</li> <li>periodical monitoring</li> <li>Fault location</li> </ul>

unit. A bit-rate-free transfer switch, incorporating high-speed multifiber mechanical switches, has been introduced into optical cable networks for the first time. It enables optical fiber cable transfer in units of 2 fibers at the same time. Furthermore, optical fiber cable transfer can be realized within such a very short time that the services over the network are never interrupted.

The monitor light from the test equipment is injected into an in-service fiber line through the WDM coupler. The communication light and the monitor light propagate simultaneously in an optical fiber. The optimum wavelength separation filter allows the communication light to be transmitted and interrupts the wavelength of the monitor light. It is set in



**Fig.2 Optical Device Unit**

front of the transmission equipment, so the monitor light does not influence the communication light. Therefore, this system can carry out various tests and operations with no degradation in the transmitting quality of the communication light.

This optical device unit is capable of supporting both dispersion-shifted fiber and conventional single-mode fiber cables. If the communication light wavelength is  $1.31\ \mu\text{m}$ , the monitor wavelength will be  $1.55\ \mu\text{m}$ . On the other hand, if the communication wavelength is  $1.55\ \mu\text{m}$ , then the monitor wavelength will be  $1.31\ \mu\text{m}$ . The optical characteristics of the optical device unit are established by taking both the dynamic range of measurement capability and an estimate of the communication line into consideration. Then, the possible line lengths of the monitoring operation are 80 Km in the case of dispersion-shifted fiber cable and 40 Km in the case of conventional single-mode fiber cable. The number of optical device units housed in the FTTM frame is in proportion to the number of optical fibers which are accommodated in it. An FTTM frame can accommodate up to a maximum of 300 fibers.

### 3.2 Fiber Transfer and Test Equipment (FTTE)

The FTTE is also installed in buildings such as telephone offices or tandem offices. It accommodates control equipment and test equipment, including an optical power meter, a light source, and an OTDR (Optical Time Domain Reflectometer). The FTTE can control the FTTM with commands from the FMC and it carries out attenuation measurements and other tests.

Also, it can return the test results to the FMC. The FTTE can control up to a maximum of 10 FTTMs.

### 3.3 Fiber Monitor and Control Equipment (FMC)

The FMC is usually located in a transmission maintenance center. It is a workstation which can control several FTTEs inside its maintenance area. The FMC can control up to a maximum of 20 FTTEs. The FMC, which is composed of a personal computer and a data base sends optical line tests and fiber transfer commands to the FTTE. It can also administrate fiber information for up to a maximum of 10,000 fibers. On the other hand, there is a portable workstation which can be easily carried by a field engineer.

## 4. System Functions

The key functions performed by the system are as follows.

### (1) Remote cable transfer:

Fiber transfer between the FTTMs can be carried out in units of 2 fibers by simultaneously transferring the connectors in the optical device units. Moreover, cable transfer is performed remotely from the FMC, and takes the same amount of time regardless of the bit-rate.

### (2) Automatic test:

Transmission characteristics of optical loss and splice loss, and other tests needed in optical line construction are automatically measured. Measured data are analyzed and stored in a data base.

### (3) Periodical monitor:

The system can periodically check for loss increase in an optical fiber and detects cable joint flooding. It immediately alerts the maintenance center when optical line faults occur or are likely to occur because of optical loss increase. These in-service optical fiber characteristics are automatically measured without disturbing the transmission system.

### (4) Remote fault location:

Faults along the optical fiber cable are pinpointed and remotely processed through the FMC. When an optical line fault occurs, the system distinguishes it instantly and displays it on a remote centralized work station.

Advantages of the system resulting from the above functions are currently available. First of all, the system substantially reduces the amount of optical fiber cable construction and maintenance work required and permits the easy integration and concentration of facilities management work. Secondly, it provides early detection of both faults and the degradation of transmission characteristics. Finally, the system contributes to higher quality telecommunication services by drastically shortening the time it takes to make repairs and implement cable transfer.

## 5. Commercial Results

The cable transfer and supervisory system for optical fiber cables were first introduced in Japan into 3 routes (Urawa-Kumagaya, Tokyo-Nagoya, Osaka-Hiroshima). Cable transfer was executed at 5 points on these 3 routes by invoking the system's transfer capability.

### 5.1 Optical Device Unit

Measured transmission characteristic results for the optical device units are summarized in Table 2. As shown in the table, insertion loss over both transmission signal and test paths by unifying switches, couplers, and filters is very low. On the other hand, the crosstalk is sufficiently high so that the monitor light does not influence the communication light.

Cable transfer is carried out by the multifiber mechanical switches, based on the optical cable transfer system developed by NTL.<sup>(6)</sup> The transfer waveforms of the multifiber mechanical switch in the optical device unit are shown in Fig.3. The entire switching sequence, including response and transfer time, takes less than 10 ms. Detailed temporal distributions of the response and transfer times for the switch are shown in Fig.4. The mean response time was 3.46 ms and the maximum response time was 4.60 ms. On the other hand, the mean transfer time was 2.07 ms and the maximum transfer time was 4.25 ms.

Table 2 Measured Results of Optical Device Units

Items	Average (dB)	Standard Deviation	Maximum (dB)	Minimum (dB)
Insertion loss (Main path) at 1.55 $\mu$ m	0.94	0.13	1.11	0.56
Insertion loss (Test path) at 1.31 $\mu$ m	3.12	1.10	5.80	1.13
Crosstalk (Test path) at 1.55/1.31 $\mu$ m	-69.81			

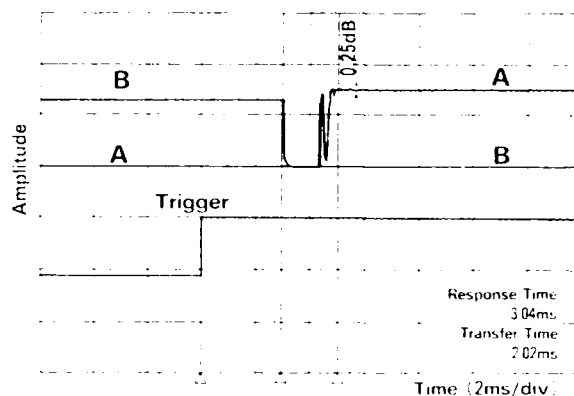


Fig.3 Transfer Waveforms of Multifiber Mechanical Switch

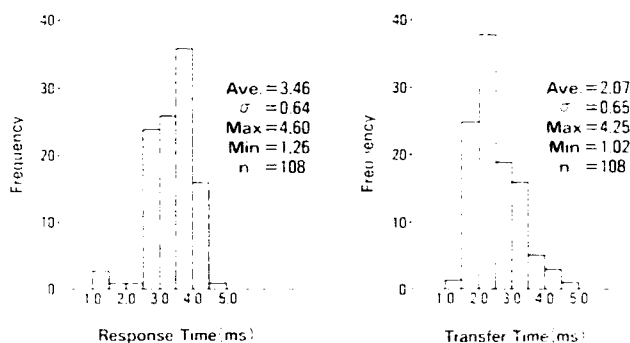


Fig.4 Distribution of Transfer and Response Time of Multifiber Mechanical Switch

### 5.2 Fiber Selector

Figure 5 shows the loss fluctuation of the fiber selector which was examined in a repeated switching test (up to 5000times). It can be seen that the loss fluctuation is less than 0.2 dB and that the fiber selector remains stable after repeated switching.

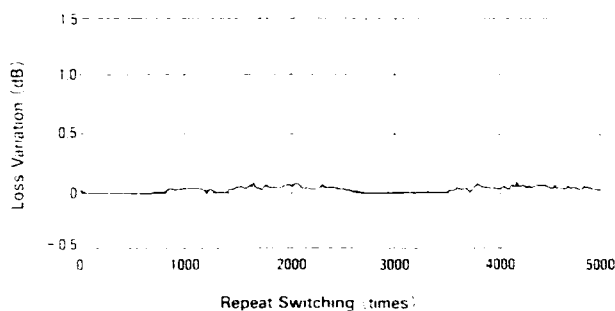


Fig.5 Loss Variation of Fiber Selector due to Repeated Switching

### 5.3 System Evaluation Results

Overall performance for the mechanical and optical characteristics of the system have been evaluated including performance on repeat switching, the heat cycle, and vibration tests before system introduction. Results are summarized in Table 3. The loss variation and the transfer time variation of the optical device unit are less than 0.1 dB and 1.0 ms respectively. These results show very stable characteristics, which ensure the system's long-term reliability.

Table 3 System Evaluation Results

Items	Test condition	Results
Optical device unit	Repeat switching >500times	Loss variation <0.1dB
	High temperature +60 C	
	Low temperature -10 C	
	Heat cycle 0~+40 C	Transfer time variation <1.0msec.
	Impact 100G, 6msec.	
	Vibration 10~45Hz/1min. 0.5mm p-p	
Fiber selector	Repeat switching 30000times	Loss variation <0.2dB
	Heat cycle 0~+40 C	
	Vibration 10~45Hz/1min. 0.5mm p-p	

### 5.4 Operating Results

Automatic measurement and data processing for optical pulse echo tests, and the various other tests needed in optical line construction can be carried out more quickly by exploiting the limits of system. Figure 6(a) shows a comparison between the testing procedures when the optical line was completed, before and after the introduction of the system. By adopting the functions of the system, the total cable construction testing time and the operating time have been cut by 40% and 90%, respectively.

Fiber transfer during cable removal work can also be carried out more quickly. The system can transfer 2 fibers at the same time. Fiber transfer between the FTTMs can be carried out in less than 0.01 second by simultaneously transferring the connectors which are accommodated in the optical device units. As a result, it is possible to reduce the time needed for cable removal. Figure 6(b) shows a comparison

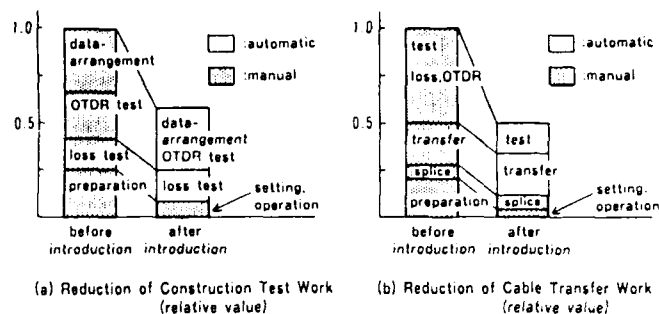


Fig.6 Effect of System

between the cable transferring procedures, at the time of cable removal before and after the introduction of the system. The total cable transfer time and the operating time have been cut by 50% and 85%, respectively.

### 6. Conclusions

- (1) A cable transfer and supervisory system termed Fiber Transfer and Test System (FITAS) for application to trunk optical cable networks has been developed.
- (2) FITAS was put into commercial service by NTT in 1990.
- (3) Results collected after deploying the system demonstrate FITAS works as designed: it provides bit-rate-free and highly reliable cable transfer and supervises optical fiber cable transmission characteristics without interrupting services.
- (4) Deploying FITAS will reduce cable construction work and maintenance operations, and bring facilities management together in a centralized location.

The central features of FITAS -- a highly reliable transmission circuit, preventative maintenance on optical cables, and the reduction of time taken in repair or replacement of cables -- will all contribute to the improved quality of service offered by NTT. NTT is now introducing the FITAS system into every new trunk optical cable routes.

#### Acknowledgements

The authors are grateful to Mr. O. Kawata, Mr. A. Sekiguchi and Mr. I. Nakamura for their valuable advice.

#### References

- (1) K. Uema, et al., "Commercial introduction results of 1.55  $\mu$ m dispersion-shifted fiber submarine cable" 37th IWCS, 1988.
- (2) F. A. Huszarik, et al., "Installation and testing of multiservice fiber links in the subscriber loop: a case study" 37th IWCS, 1988.
- (3) Y. Koyamada, et al., "Basic concept of fiber optic subscriber loop operation system" ICC'90, 1990.
- (4) T. Uenoya, et al., "Operation, administration and maintenance systems of the optical fiber loop" GLOBECOM'90, 1990.
- (5) H. Takasugi, et al., "Design and evaluation of automatic optical fiber operation support system" 39th IWCS, 1990.
- (6) I. Watanabe, et al., "Optical fiber cable transfer splicing system using optical fiber connectors" 38th IWCS, 1989.



Hiroatsu Matsumoto

NTT Network Systems  
Development Center  
Tokyo, Japan

Hiroatsu Matsumoto received his B.S. and M.S. degrees in physics from Tokyo University in 1985 and 1987. He joined NTT in 1987. He is an engineer in the Telecommunications Cable Systems & Outside Plant Group in NTT Network Systems Development Center.

He is a member of the Institute of Electronics, Information and Communication Engineers of Japan.



Yutaka Yokoo

NTT Telecommunications  
Software Headquarters  
Kanagawa, Japan

Yutaka Yokoo received his B.E. degree in electrical engineering from Shinsyu University in 1979. He joined NTT in 1979. He is a senior engineer in the Optical Fiber Loop Maintenance Operations System Project in NTT Telecommunication Software Headquarters.

He is a member of the Institute of Electronics, Information and Communication Engineers of Japan.



Kiminori Sato

NTT Network Systems  
Development Center  
Tokyo, Japan

Kiminori Sato received his B.E. degree in electrical engineering from Kyoto University in 1979.

He joined NTT in 1979. He is a senior engineer in the Telecommunications Cable Systems & Outside Plant Group in NTT Network Systems Development Center.

He is a member of the Institute of Electrical and Electronics Engineers, and the Institute of Electronics, Information and Communication Engineers of Japan.



Takuya Uenoya

NTT Network Systems  
Development Center  
Tokyo, Japan

Takuya Uenoya received his B.E. and M.E. degrees in electrical engineering from Waseda University in 1971 and 1973. He joined NTT in 1973. Since 1989, he has been a General Manager in the Telecommunications Cable Systems & Outside Plant Group in NTT Network Systems Development Center.

He is a member of the Institute of Electronics, Information and Communication Engineers of Japan.



## A Real-Time Configuration Management System for Line Facilities in Optical Fiber Networks

Katsuya YAMASHITA, Fumio OHTSUKI, Mitsuhiro TATEDA and  
Yahei KOYAMADA

NTT Telecommunication Field Systems R&D Center  
Tokai-mura, Ibaraki-ken, 319-11, Japan

### ABSTRACT

Automated database updating is achieved in a configuration management system for optical fiber transmission lines by developing two new hardware components. The first is an optical connector with an EEPROM module in which the identifying codes of the optical fibers are recorded. The second is a small bidirectional optical data transmitter, which allows the ID codes of the optical fibers to be automatically and remotely read from an operation center. Whenever the fiber connections are changed, the data transmitter automatically detects the changes by reading the ID codes of each connected pair. The data changes are transmitted to the operation center, and the line configurations database is updated automatically and in real-time. With this technique, errors caused by manual database modification are greatly reduced, resulting in more reliable and speedy communication services.

### 1. INTRODUCTION

Properly assigning transmission media to subscribers is very important in supplying speedy and reliable communication services. In a conventional management system<sup>1</sup>, extensive manpower is necessary to update the configuration database. This database contains the current line. Because data modifications are entered manually through keyboards, errors inevitably occur and are accumulated in the long term, resulting in reliability<sup>2</sup> limitations. Furthermore, as long as the management system requires manual database modifications, real-time configuration management, which reflects current configurations at any time, is impossible because of working delays in manual modification. In particular, it is difficult to obtain correct and sufficient line operation information about object cables under fields where construction is occurring. Therefore, it is necessary for several workers with arrangement sheets to be separately stationed at offices, several related fields, or subscriber premises.

Accumulated errors and lack of real-time capability also influence centralized automation of optical transmission media operations<sup>3</sup>. This involves the configuration management system, a media test/surveillance system<sup>4</sup> and a media switching system<sup>5</sup>.

In order to solve these problems, a new configuration management system is proposed. This system has real-time and automated data updating capability, and bidirectional data communication capability.

### 2. SYSTEM FABRICATION

Key components of this system are memories built into each line facility, a bidirectional transmitter with microprocessors and a single optical fiber line for data transmission. A system block diagram is shown in Figure 1. Line facility data are recorded in the memories, which are installed in each facility component. The data for the semiconductor memories is initially written according to identification codes by component (cable) manufacturers or network vendors. The semiconductor memories are built into or attached to optical connectors. The transmitter with microprocessors is called a local controller (LCTR). The LCTR is installed near the facility components that will be managed, and is optically concatenated to adjacent LCTRs. Therefore, it can recognize configuration changes in real-time by successive or on-and-off reading of memory data in each facility component. A workstation (WS) set up at a control center office is directly connected to the nearest LCTR, and communicates with other LCTRs through the single fiber line. Data of facility components is transmitted to the workstation, which automatically updates the management database in real-time when data changes are detected.

The LCTR has functions other than those mentioned above. It has a multi-channel A-D converter which can be connected with various sensors. This allows automated and remote sensing capability. The workstation can sense such things as water penetration, temperature, and oxygen density. This function contributes to highly reliable network lines and safer field construction. The LCTR also has an additional electrical serial data interface. Therefore, instead of carrying thick arrangement or line information sheets, line workers can directly access the center database through other computers attached to the interface. For example, when dropping a fiber to a new subscriber premise from an aerial closure, correct fiber identification is very important. Although optical fiber identifiers<sup>6,7</sup> have

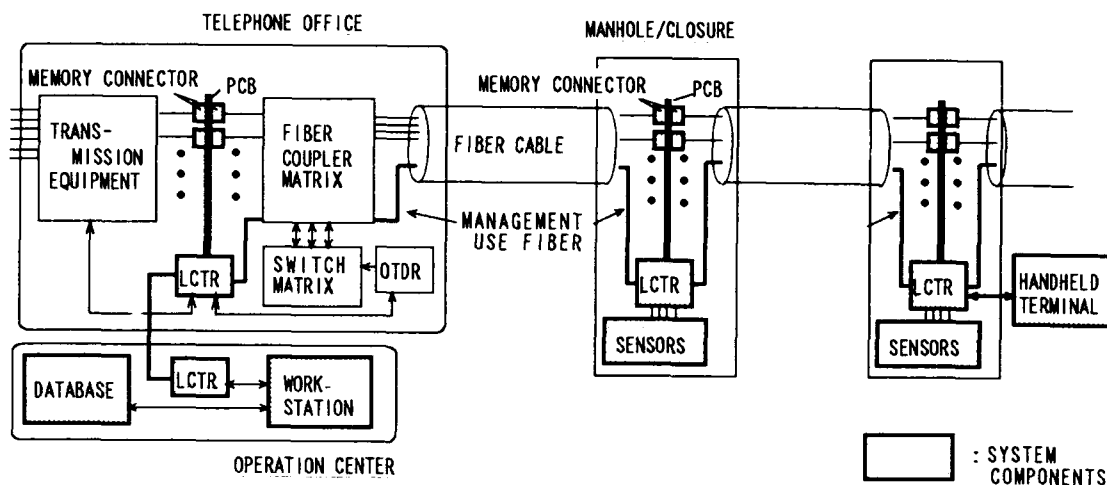


Fig.1 A block diagram of a real-time configuration management system for line facilities of optical fiber networks

been utilized, they are not efficient or safe because it is necessary to bend each fiber to identify the target fiber. In the new system, it is possible to efficiently and accurately select an appropriate idle fiber by asking the workstation the current service conditions of all fibers. Thus, more reliable database and bidirectional data communication allows more efficient field construction.

### 3. LOCAL CONTROLLER

#### 3.1 BASIC CONSTRUCTION AND FUNCTIONS

Local controllers (LCTR) are installed in fiber terminated modules (FTM) at central offices as well as fiber access closures in outside fields where high resistance is required against significant changes in temperature and humidity. LCTRs should be small and have few components. Block diagram of an LCTR is shown in Fig.2. A laser diode or LED is used as a transmitter as well as a detector. By using a fiber coupler in front of the laser diode, bidirectional repetition can be achieved. The number of active optical devices can be reduced to one fourth of that is conventional optical data repeaters, which require two laser diodes and two photo-detectors. A single-chip micro-controller with two channel serial communication interfaces is also included in the LCTR. One of the interfaces is used for half duplex optical communication at a transfer rate of 125 kb/s. The other is a 9600 bps RS-232C interface for an external terminal. The microprocessor controls optical signal bidirectional repetition and response upon interruption from the external terminal. The microprocessor also has a four channel A-D converter which can be connected to various sensors for environmental sensing. When transmitting data for configuration management or on-and-off environmental sensing, the rate is significantly less than 1 Mb/s.

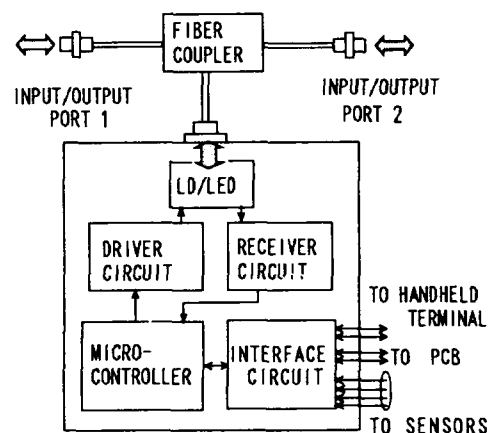


Fig.2 A block diagram of a local controller

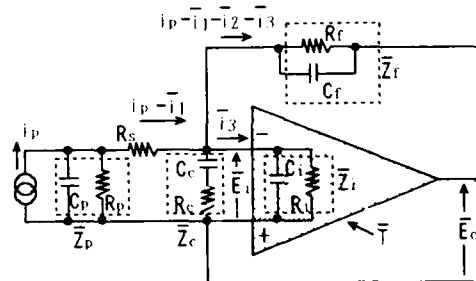


Fig.3 An equivalent circuit of an O-E converter with a transimpedance amplifier

### 3.2 Bandwidth of transmitters as detectors

An O-E converter model is shown in Fig.3. The bandwidth of the laser diode O-E converter is calculated as follows. The transimpedance of this model is given by

$$\bar{S}(\omega) = -(U - jV)/(U^2 + V^2) \quad (3.1)$$

$$\begin{aligned} U &= a_f + a_i(a_f + a_p + a_i + a_c) - b_i(b_f + b_p + b_i + b_c) \\ V &= b_f + a_i(b_f + b_p + b_i + b_c) + b_i(a_f + a_p + a_i + a_c) \\ a_f &= 1/R_f, \quad b_f = \omega C_f, \quad a_p = 1/R_p, \quad b_p = \omega C_p \\ a_i &= 1/R_i, \quad b_i = \omega C_i \\ a_c &= \omega^2 C_i^2 R_c / (1 - \omega^2 C_i^2 R_c^2) \\ b_c &= \omega C_c / (1 + \omega^2 C_i^2 R_c^2) \\ a_i &= \cos \phi \text{ABS}(\bar{T}), \quad b_i = -\sin \phi / \text{ABS}(\bar{T}) \end{aligned}$$

where,  $\phi$  and  $\bar{T}$  are the internal phase shift and the open-loop transfer function of the amplifier. Responses for a narrow band amplifier (gain-bandwidth = 4.5 MHz) and an ideal wide band amplifier (gain-bandwidth is infinite) are shown in Fig.4, where junction capacitances of the diodes are 10 pF (laser diode) and 200 pF (LED). Greater amplifier bandwidth results in greater O-E converter bandwidth. With an ideal amplifier, the O-E converter bandwidth is determined by  $1/(2\pi C_p R_s)$ , where  $R_s$  is the diode equivalent series resistance.

For actual O-E converters, there is another bandwidth limitation, which is determined by the optical power level and noise level. Total noise current is given by

$$i_{n,\text{total}} = (i_{en}^2 + i_{in}^2 + i_{ft}^2 + i_{pt}^2)^{1/2} \quad (3.2)$$

where the amplifier input noise voltage component  $i_{en}^2$ , input noise current component  $i_{in}^2$ , feedback resistance thermal noise component  $i_{ft}^2$ , and laser diode parallel resistance thermal noise component  $i_{pt}^2$  are given by

$$\begin{aligned} i_{en} &= e_n |\bar{T}| (1 + |\bar{T}| \beta) / R_f \\ &\approx e_n B^{1/2} (1 + C_p / C_f) / R_f \\ i_{in} &= i_n B^{1/2} \\ i_{ft} &= (4k_B B T_a / R_f)^{1/2} \\ i_{pt} &= (4k_B B T_a / R_p)^{1/2} \end{aligned}$$

$\beta$  is the feedback rate,  $k_B$  is the Boltzman constant,  $T_a$  is the air temperature, and  $B$  is the amplifier bandwidth. Equivalent optical noise power in dBm is given by

$$P_n \approx 10 \log_{10} [10^{-3} \cdot h\nu / (\eta q) \cdot i_{n,\text{total}}] \quad (3.3)$$

where  $h$  is the Planck constant,  $\eta$  is the quantum efficiency,  $\nu$  is the light frequency, and  $q$  is the electron charge. Relationship between the required bandwidth and the allowable optical noise level is a function of diode junction capacitance as shown in Fig.5. An allowable noise level of -39 dBm at a line loss of 0 dB is calculated when the LED is a transmitter/detector, and when the launched power into the coupler is -20 dBm, the losses of the two

couplers are 8 dB, the noise margin is 11 dB, and  $C_p$  is 200 pF. An LED bandwidth of 1.2 MHz is shown in Figure 5. For a line loss of 10 dB, the estimated bandwidth becomes 300 kHz because the allowable noise level decreases to -49 dBm. In the same way, a 200 MHz bandwidth for an InGaAsP/InP laser diode with a line loss of 0 dB is calculated, where  $C_p = 10$  pF, transmission power is 0 dBm. When the line loss is 10 dB, the estimated bandwidth becomes about 40 MHz for the laser diode. Although the bandwidth is restricted by the noise limitation mentioned above, when the laser diode is a transmitter and a detector, it allow a sufficient bandwidth for our proposed management system. The data transfer clock rate is only 125 kb/s in the prototype LCTR of our proposed management system, so that both of the LED and the LD are available. Thus, laser diodes will become indispensable in improving LCTR functions for multi-channel telephone communication among LCTRs in line construction.

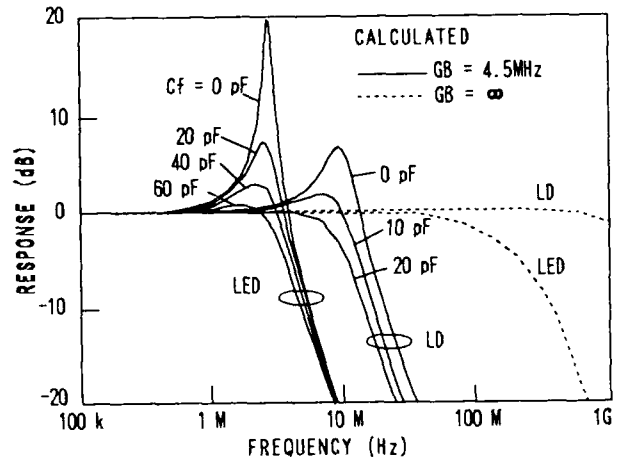


Fig.4 A relationship between amplifier bandwidth and transimpedance frequency response dependence of an O-E converter with an LED or LD as a detector ( $C_c=0$ ,  $R_c=\text{infinite}$ ,  $R_p=10$  M ohms,  $C_p=200$  pF (LED), 10 pF (LD),  $R_i=100$  T ohms,  $C_i=2$  pF,  $R_s=10$  ohms)

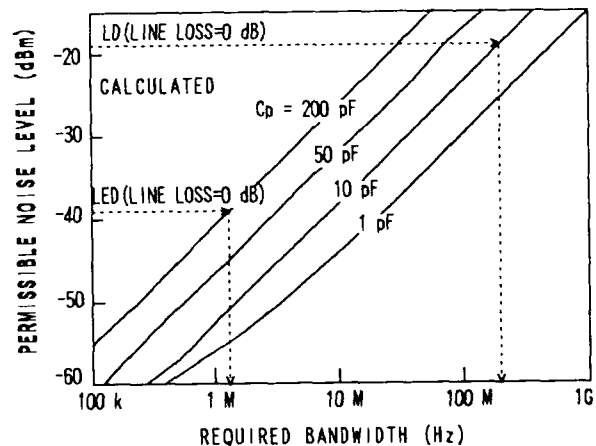


Fig.5 The relationship between required bandwidth, noise power and junction capacitance

## 4. MEMORY CONNECTORS

### 4.1 Connector construction

The memory connector consists of a conventional optical ferrule, an EEPROM (Electrically Erasable Programmable Read Only Memory) installed in the connector housing, and electrodes. Two types of memory connectors are fabricated. One is an SC<sup>10</sup> single fiber connector with a push-pull contact for fiber terminated modules (FTM). The other is an MT<sup>11</sup> multi fiber connector for connections in fiber closures. These connectors are shown in Fig.6. A 4 kbit serial data EEPROM is used because it does not require power to maintain data and because it has fewer electrodes than the parallel type. The EEPROM module package is a single-inline (SIP) type with a size of 8 x 6.2 x 2.2 mm, which is common for SC and MT memory connectors. The memory modules are connected to the SC-2 connectors (SC connectors without housing) and to the MT connectors.

### 4.2 Printed circuit board

Forty MT memory connectors and a memory chip select interface can be installed on a single-sided 114x65 mm printed circuit board (PCB), as shown in Fig.7(a). Ten PCBs can be set up in a standard aerial fiber closure. Eighty fibers are included in

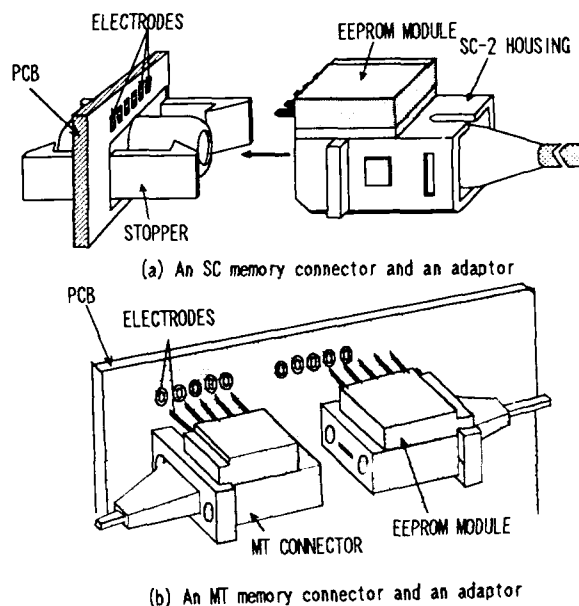


Fig.6 Memory connector fabrications

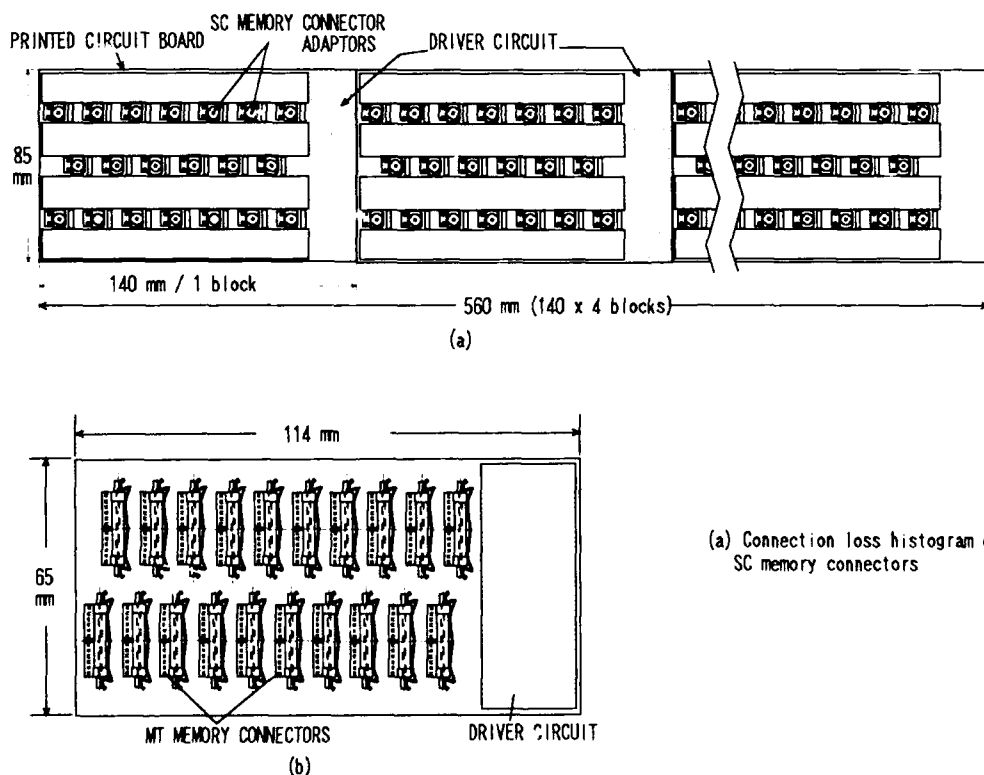


Fig.7 Printed circuit boards for memory connectors

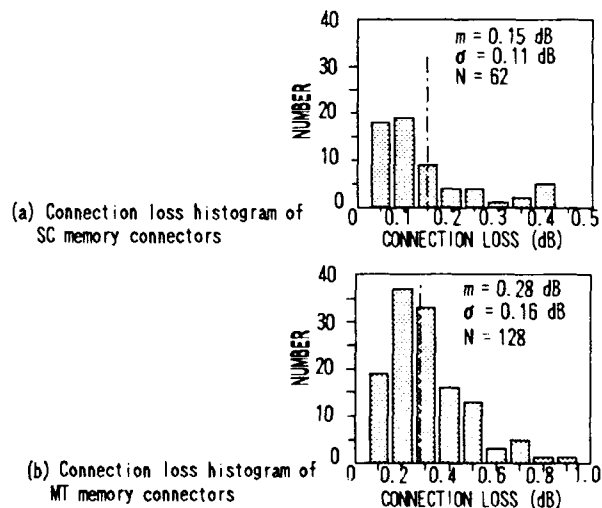


Fig.8 Connection loss histograms of memory connectors after attaching on PCBs

one PCB when a 4-fiber MT connector is used. When using a double sided PCB, twice the number of connectors can be loaded. Eighty SC memory connectors per side can be connected on a 85 x 560 mm PCB as shown in Fig.7(b). Single SC PCBs correspond to single MT PCBs, and each PCB includes eighty fibers.

#### 4.3 Memory information

Individual connector information up to 512 ASCII characters is written at the cable manufacturers or in the field, as shown in Table 1. This information is read by the LCTR from the PCB, on which connectors are optically joined to other connectors and electronically connected to the PCB pattern, as shown in Fig.7. The LCTR knows the assignments of the PCB connector ports and the connector ID codes of the connectors on the PCB. The LCTRs send the assignment data to a workstation in the operation center. When connector changes occur on the PCB, the assignment table changes and the workstation automatically detects changes and updates the configuration database.

Table 1. Individual information of memory connectors

Item	code example
line code	A107U
connector code	EEPROM00232
connector type	SM_MTM_V1
fiber type	SM1550ND
date of manufacture	F02_19910616
cable name	F910412_a1
unit number	F910412_0
fiber number	F910412_07
initial loss	0.27dB910616
fiber length	477.5meter
mode field dia.	9.73um
eccentricity	0.61um
customer	SPECIAL ***
memory date	19910616

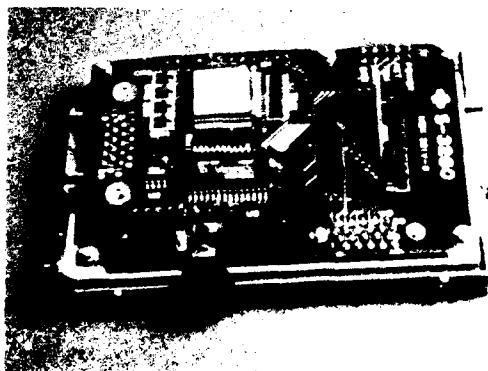


Fig.9 A local controller (LCTR)

#### 4.4 Performance

After attaching the memory modules to the PCB, connection loss histograms were obtained, as shown in Fig.8. The initial mean value of the loss for the SC connectors was 0.16 dB, so that a -0.01 dB loss change was generated on average. The electrode insertion direction is the same as the optical connector insertion direction for the connectors, so that loss changes become very small. However, the initial mean loss was 0.26 dB for the MT connectors with a 0.02 dB loss increase. The electrode axis and the optical axis of MT connectors are perpendicular to each other. Therefore, optical connections are affected more than those of SC memory connectors by low electrode compliance.

The area occupied by an SC memory connector on a connector matrix board is 39% smaller than that of an SC connector and 20 % greater than of an SC-2 connector. With MT memory connectors, the area is about 10 % greater than that of a conventional MT connector. These memory connectors may be small enough for use with FTM or fiber closures.

#### 5. SYSTEM EXPERIMENT

A prototype system is configured. Eight LCTRs are concatenated through a single line of single mode fibers. The first LCTR is electronically connected with a parallel interface to a workstation, and is optically connected with the second LCTR. The LCTR is shown in Fig.9. It has four functions:

- 1) read/write connector information,
- 2) sensing water penetration, temperature and so on by using a 4-ch A-D converter,
- 3) terminal interface, and
- 4) LCTR-to-WS or LCTR-to-LCTR bidirectional data transmission.

LCTR hardware specifications are summarized in Table 2.

Table 2. Prototype LCTR specifications

Items	spec.
micro controller	8 bit with SCI, ADC, timer, 12 kByte ROM, 512 Byte EEPROM
data transfer rate	125 kb/s
signal code	NRZ
laser output power	-2 dBm
allowable line loss	15.5 dB min
analog data interface	4 ch. 0 to 5V
memory connector I/O	256 connectors max
terminal I/O	RS-232C, 9600 bps
power	5 V x 1.0 A
size	90 x 60 x 20 mm

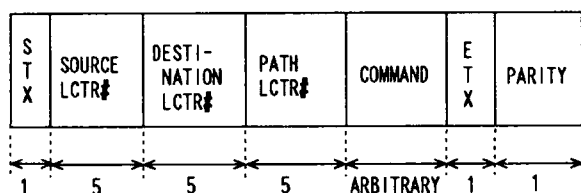


Fig.10 A data format for LCTR communications

A single laser diode is used as a transmitter and a detector for the LCTR, so that the signal is half duplex asynchronous NRZ. The bandwidth of the LCTR head amplifier is about 200 kHz. The communication data format is shown in Fig.10. The effective data transfer rate decreases when the repeater (LCTR) number increases because of a data regeneration when using software. For example, the rate for a 512 Byte data transfer is 15 kb/s between the workstation and the first LCTR, and becomes about 5 kb/s between the workstation and the 8th LCTR.

The UNIX workstation operates as a control center, which can simultaneously execute several kinds of tasks. These tasks are:

- 1) real-time line configuration surveillance and automated database updating,
- 2) database applications,
- 3) environmental sensing inside or around fiber closures or FTMs,
- 4) transfer of fiber identification data or service status data to the field, and
- 5) communication with terminals connected to LCTRs.

A demonstrated window is developed with HP-UX 7.05, X11R3 and OSF-Motif, as shown in Fig.11.

## 6. CONCLUSION

In order to improve database reliability in network configuration management, a novel system with memory connectors and local controllers was developed and demonstrated. This system provides real-time database updating, which contributes to more speedy and reliable line operation and construction. additional functions, such as environmental sensing and fiber identification, also contribute to safer and more efficient line construction. In the future, developed hardware reliability will be able to be evaluated and effective data transfer rates will be increased so that LCTR networks can be improved.

## ACKNOWLEDGMENT

The authors wish to thank Dr. Koushi Ishihara, Dr. Yoshikazu Yamamoto for their useful suggestions, comments and encouragement throughout this work.

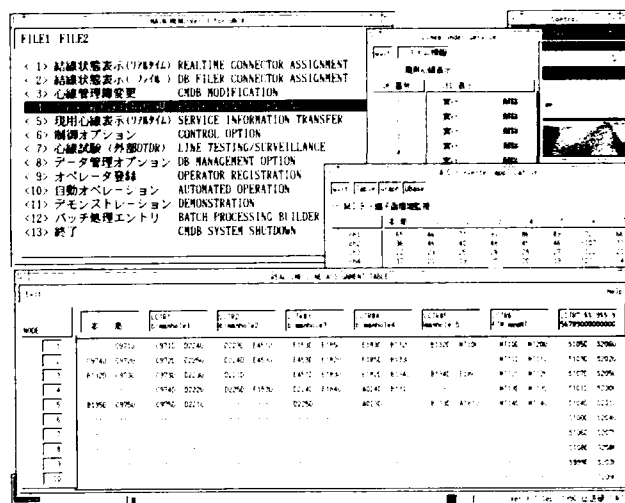


Fig.11 A demonstration example of a workstation CRT

## REFERENCES

1. NTT Shisetsu, Vol.35, No.2, pp.34-43, 1984. (in Japanese)
2. R. Barstow, "Centel Bashes Database Errors," Telephony, Jan. 28, pp.36-39, 1991.
3. Y. Koyamada et al., "Basic Concepts of Fiber Optic Subscriber Loop Operation Systems," IEEE ICC'90, 341.1.1.- 341.1.5.
4. H. Takasugi, N. Tomita, T. Lenoya, I. Nakamura and Y. Yokoo, "Design and Evaluation of Automatic Optical Fiber Operation Support System," 39th IWCS Proc., pp.623-629, 1990.
5. T. Katagiri, Y. Koyamada, M. Tachikura and Y. Katsuyama, "Nonblocking 100 x100 Optomechanical Matrix Switch," 40th IWCS Proc. to be published.
6. E. Maekawa, K. Yamashita et al., "Measuring Equipment for Optical Subscriber Lines," Rev. of E.C.L., Vol.34, pp.669-675, 1986.
7. S. M. James, "NonIntrusive Optical Fiber Identification Using a High-Efficiency Macro-bending Clip on Optical Component," Electron. Lett., Vol.24, No.19, pp.1221-1222(1988).
8. M. Enomoto et al., "Half Duplex Optical Communication System by Using an LED as Source and Detector Device," IEICE Japan J71-B, 8, pp.955-962, 1988. (in Japanese)
9. J. J. Geddes et al., "Semiconductor Junction Transceiver for Fiber Optic Communication," Electron. Lett., Vol.14, No.7, pp.214-216, 1978.
10. E. Sugita, K. Isawa and T. Shintaku, "Design of High-Performance Push-Pull Coupling Optical Fiber Connectors," IEICE Japan, Vol.470-C, No.10, pp.1405-1414, 1987. (in Japanese)
11. S. Nagasawa, H. Furukawa, M. Makita and H. Murata, "Mechanically Transferable Single-Mode Multifiber Connectors," Proc. IOOC '89, pp.48-49, 1989.



Katsuya Yamashita

NTT Telecommunication Field  
Systems R&D Center

Tokai-mura, Ibaraki-ken,  
319-11, Japan

Katsuya Yamashita received B.S.E.E. degree from Kumamoto University, Kumamoto, Japan in 1975. After joining the Electrical Communications Laboratories, he worked on research and development of submarine optical fiber cables and optical fiber measuring equipment. He is now Senior Research Engineer, Supervisor, in Telecommunication Field R&D Center, responsible for optical fiber network media management. He is a member of the IEICE Japan.



Mitsuhiro Tateda

NTT Telecommunication Field  
Systems R&D Center

Tokai-mura, Ibaraki-ken,  
319-11, Japan

Mitsuhiro Tateda received B.S. and M.S. degree in physical engineering from the University of Tokyo in 1972, 1974, respectively. And he received Dr. of Science degree from the University of Tokyo in 1982. After joining the Electrical Communications Laboratories, he was engaged in research on transmission characteristics of optical fibers, optical integrated circuits, optical fiber measuring techniques and computer vision. He is now Senior Research Engineer, Supervisor, in Telecommunication Field R&D Center, responsible for research on low loss optical fiber and superconductor. He is a member of the Optical Society of America, IEEE, the Optical Society of Japan and the IEICE Japan.



Fumio Ohtsuki

NTT Telecommunication Field  
Systems R&D Center

Tokai-mura, Ibaraki-ken,  
319-11, Japan

Fumio Ohtsuki graduated from Mito Technical High School 1967. After joining the Electrical Communications Laboratories, he was engaged in research on protection of telecommunication lines against lightning surge, electromagnetic compatibility. He is now Senior Research Engineer in Telecommunication Field R&D Center, responsible for optical fiber network media management. He is a member of the IEICE Japan.



Yahei Koyamada

NTT Telecommunication Field  
Systems R&D Center

Tokai-mura, Ibaraki-ken,  
319-11, Japan

Yahei Koyamada received B.S., M.S., and Ph.D. degree from Osaka University, Osaka, Japan in 1970, 1972, 1978, respectively. After joining the Electrical Communications Laboratories, he was engaged in research on surface acoustic wave devices, subscriber optical fiber cables and optical fiber measuring techniques. He is now Senior Research Engineer, Supervisor, in Telecommunication Field R&D Center, responsible for research and development of test and surveillance systems for optical fiber network media using optical time domain reflectometry. He is a member of the IEICE Japan.

## HIGH POTENTIALITIES IN FIBER PREFORM MANUFACTURING USING VERY LARGE AND PRECISELY BORED SILICA INGOTS

D.PAVY\* - M.MOISAN\* - I.HARDY\* - P.GROSSO\* C.LE SERGENT\*\* - D. TREGOAT\*\*

\* CNET-LAB/OCM 22300 LANNION (France)

\*\* Alcatel Alsthom Recherche 91460 MARCOUSSIS (France)

### ABSTRACT

Preform technologies based on the direct use of very large and precisely bored silica ingots have very attractive potentialities to reduce optical fibre cost and to improve fibre geometry. We have developed a promising fabrication process which consists of only two steps : deposition and collapsing, avoiding the overcladding operation. Results on preforms made from either commercially available or special precision machined tubes, are presented.

### INTRODUCTION

The application of optical fibers in the subscriber network requires a drastic cost reduction of each optical components. Regarding fibers it has to be kept in mind that the reduction of the direct cost has to be achieved without compromising on connection cost affecting parameters such as geometrical properties. New preform technologies or hybrid processes using overcladding techniques are presently investigated by a few laboratories<sup>1 2</sup>. An alternative and attractive new approach is the direct deposition inside very thick substrate tubes. It allows the fabrication of high capacity preforms in only two steps namely deposition and collapsing. However, heat transfer becomes difficult as tube thickness rises, and current burner technologies are no longer appropriate for thickness over 5 mm.

We present here a new process which implements SPCVD (Surface Plasma Chemical Vapor Deposition) for the deposition inside 20-25 mm thick tubes and RF furnace heating for the collapsing. Experiments have been carried out both with commercially available tubes and with special precision tubes made from drilled and grinded plasma torch cheap silica blanks.

### POTENTIALITIES OF VERY THICK SUBSTRATE TUBE

#### b/a ratio requirement

Regarding the deposition process, the preform capacity is obviously related to the maximal deposited thickness and to the admissible optical cladding to core b/a ratio. Figure 1 shows the optical power distribution calculated at various wavelengths from the propagation theory<sup>3</sup> applied to a matched-clad single-mode fibre (MCSM). The poor quality of quartz substrate tubes implies the b/a ratio of conventional fibre to reach a value of about 6, although the major part of the optical signal propagates in a very small central region of the fiber. The additional 1.385  $\mu$ m loss estimated on MCSM fibre is plotted on Figure 2 versus b/a for low and high OH content substrate tubes. The contribution of the OH absorption appears to be negligible at b/a larger than 2.5 and 4.2 respectively.

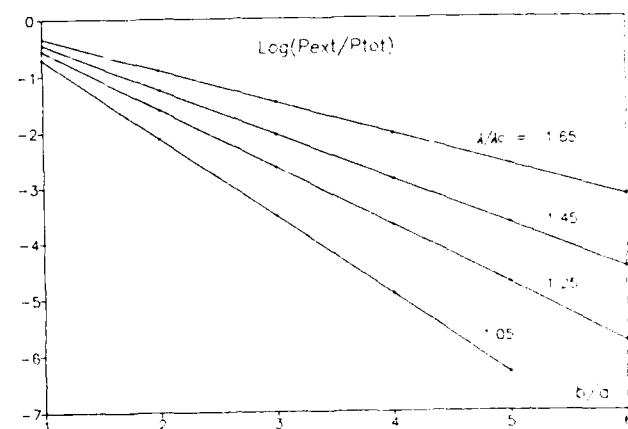
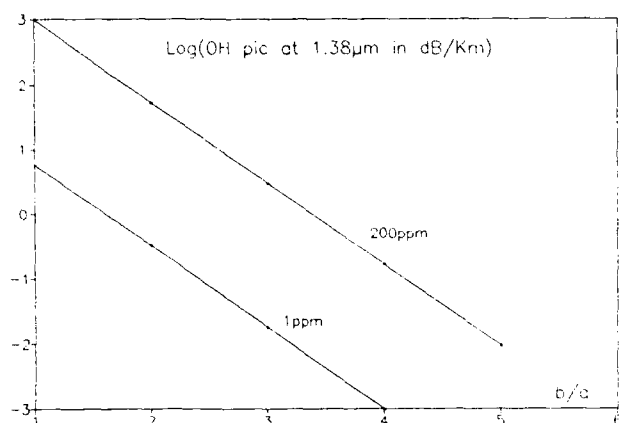


FIGURE 1 Calculated optical power distribution in a MCSM fiber for different wavelength/cut-off wavelength ratios (evanescent field approximation).





**FIGURE 2** Additional OH loss at 1.385  $\mu\text{m}$  versus b/a ratio in a MCSM fibre for low and high OH cladding tube and  $L_c = 1.25 \mu\text{m}$ .

#### Considerations on the inside deposition

For a given b/a ratio, a higher csa (cross sectional area) of the substrate tube requires a higher deposition thickness. Table 1 illustrates the role of high csa tubes and reduced b/a ratios on the deposition rate, compared with a conventional tube (ie:ODxID=30x25mm). For a 3 mm thickness deposition, a 10mm walled tube (ie:45x25mm) yields a 100km/m preform capacity for b/a = 6. For a 17.5mm thick tube (ie:60x25mm) and a b/a ratio of 4, the same 3 mm deposition thickness provides a 200 km/m preform and therefore a two fold fabrication rate. Using the same tube size, a further increase by a factor of two can be achieved with a 1.5mm deposit thickness if a b/a value of only 3 can be accepted.

#### Considerations on the collapsing

Previous studies on the viscous flow theory of collapsing have given a simple formulation of the collapsing velocity  $V_r$  for an homogeneously composed and heated tube<sup>4</sup> :

$$V_r = dR_i/dt$$

$$V_r = [\Delta P + \sigma (R_e^{-1} + R_i^{-1})] / [2\eta R_i (R_e^{-2} - R_i^{-2})]$$

where  $R_i, R_e$  = outer and inner radius

$\Delta P$  = inner/outer pressure difference

$\sigma$  = surface tension

$\eta$  = viscosity

Then collapsing time can be written by :

$$T_c = R_i/V_r$$

Another collapsing velocity  $V_m$ , which is closer to the real fabrication rate is the collapsed mass per unit of time. It could be expressed by :

$$V_m = \text{const}2.csa.(T_c)^{-1}$$

As shown in Table 1, in case of  $\Delta P=0$ , the collapsing velocity  $V_m$  increases as well as the collapsing time with the thickness of the substrate tube. For example, a 10mm thickness (ie:45x25mm) yields a collapsing rate 1.9 times higher than a 2.5mm thickness (ie:30x25mm) and a 20mm tube (ie:60x25mm) allows an additional increase of 1.6 time. Moreover, as demonstrated by Geyling an ellipticity can grow during collapsing if the pressure difference  $\Delta P$  is larger than a critical value and this critical  $\Delta P$  rises as the walls become thicker<sup>5</sup>. A thick tube would therefore collapse in a more stable way than a thin one and applying a small pressure difference would give a further enhancement of the collapsing rate with no significant damage on geometry.

Tube Thickness (mm)	b/a	Deposition Thickness (mm)	Preform Capacity (Km/m)	Deposition Time (u.a)	Deposition Rate (u.a)	Collapsing Time (u.a)	Collapsing Rate (u.a)
2.5	6	0.65	22	1.0	1.0	1.0	1.0
10.0	6	3.00	100	4.6	1.0	2.4	1.9
17.5	4	3.00	200	4.6	2.0	3.0	3.0
17.5	3	1.5	200	2.3	4.0	3.3	2.8

**TABLE 1** Thickness tube influence on deposition and collapsing rates.

## POTENTIALITIES OF PRECISELY MACHINED TUBES

High purity low cost silica is required to make up the cladding substrate tube of low b/a preforms. So a suitable way could be based on a mass production technology such as plasma torch which has already led to the manufacture of optical quality silica ingots<sup>6</sup>. The ability of large ingots to be drilled and grinded allows the suppression of the pulling operation. It also provides a good geometrical accuracy compared to specification of commercially stretched tubes. A good concentricity between the core and the outer cladding of the final fiber could therefore be expected which is a basic parameter for low cost connections<sup>7</sup>.

## EXPERIMENTAL

### SPCVD Deposition

The principles of SPCVD have already been published<sup>8, 9</sup>. The new equipment designed for deposition inside bored ingots is shown on figure 3. The large c.s.a. deposition tube is supported by two short lengths of conventional silica tube welded to its both ends. Then it is placed into a furnace at about 1200° C and a microwave plasma column is sustained by a propagating 2.45 GHz surface wave which is launched through the tube by using a Surfaguide exciting structure<sup>10</sup>.

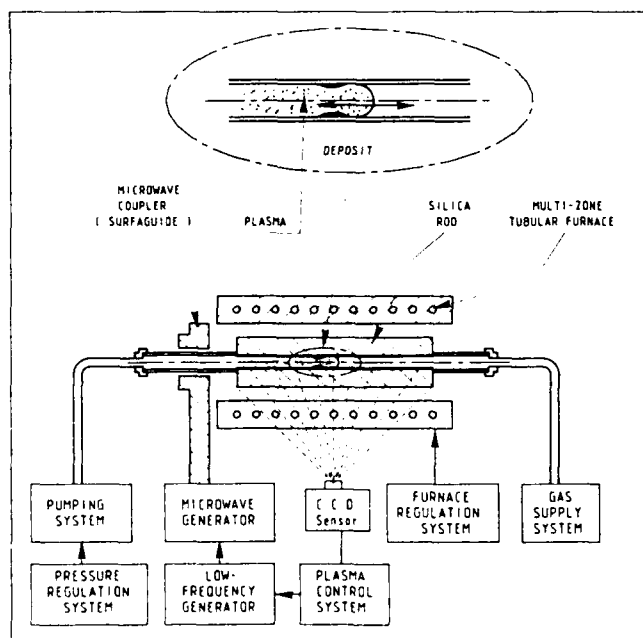


FIGURE 3 : The SPCVD set-up

Reactants are fed under a 5 to 20 mb pressure and heterogeneous reactions (chloride oxidation and oxide deposition) take place near the gas flow-plasma boundary. Doped silica layers are built up therefore just by modulating the microwave power. For given experimental conditions the plasma column length and consequently the useful deposition length decrease as the dielectric silica tube thickness rises. An interesting point in using both thick tubes and SPCVD is that for thickness beyond 12 mm, this decrease becomes very slight.

### Furnace collapsing

The experimental set up developed for the collapsing of tubes with large cross sections is schematically shown in figure 4. The preform ends are held by the mandrels of a glass working lathe. The heads of which can be synchronously moved in a fully controlled way. A stationary hot zone of about 2000° C is created by a graphite induction furnace operating at 10 to 30 KHz. While rotating the tube is traversed to and fro through the furnace at a moderate speed of 10 to 20 mm/mn. The number of required passes is related to several parameters : silica quality, inner diameter, internal pressure and wall thickness. For example a natural silica bored ingot with a 15 mm thickness and a 20 mm inner diameter can be fully collapsed in 4 passes. The resulting rate is about 10 g/mn and can reach 25 g/mn by applying a negative pressure difference of 10 to 20 mb inside the tube.

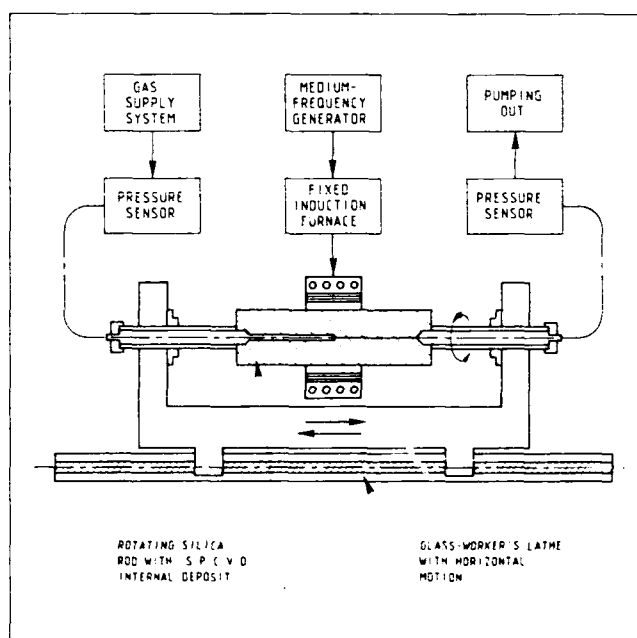


FIGURE 4 : The furnace collapsing set-up

## RESULTS

Matched-clad single-mode fibres have been prepared from natural and synthetic silica tubes. The thickness was 12.5 mm and the inner diameter 25 mm (ie : 50 x 25 mm). Typical operating conditions have been a 0.7 g/mn deposition rate over a 500 mm length a 4 passes collapse over a 400 mm length without any pressure difference. Other operating parameters are listed in the Table 2.

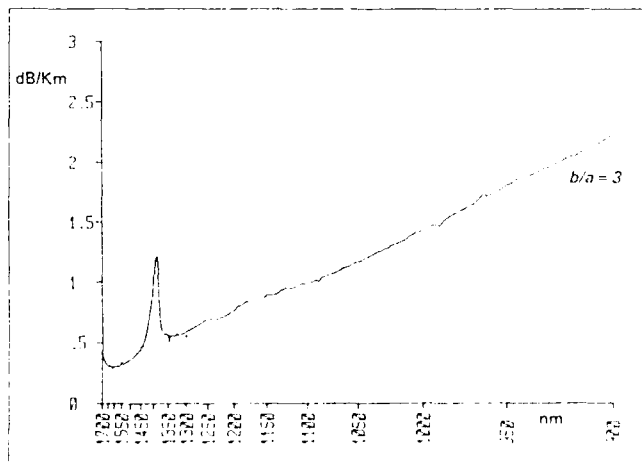
It has to be mentioned that the higher collapsing rate is achieved with natural instead of synthetic silica, which suggests that the key parameter is IR absorption and not viscosity. It has also to be pointed out that the amount of silica vaporized during the collapsing stage does not exceed 0.25 % instead of 10 to 20 % in current burner conditions.

Preform capacities are about 50 km (ie : 125 km/m) and typical attenuation results are presented in figure 5 for stretched tubes. As shown in figure 6, performances of fibres made from machined tubes are slightly damaged for b/a value of 3. The surface preparation of machined tubes, prior to deposition, is more critical because of the great sensitivity of the plasma process to initial substrate defects.

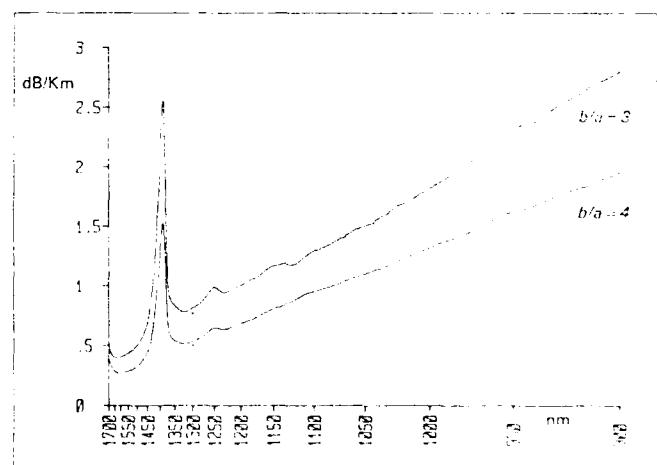
Tube quality	Natural	Synthetic	Synthetic
b/a	5	4	3
deposition thickness(mm)	2.7	1.7	1.0
deposition time* (H)	7.5	5.5	4.0
collapsing time* (H)	3.5	4.0	4.0
collapsing rate (g/mn)	9.7	8.0	8.0

\* including preparation time of about 2H for deposition and 1H for collapsing.

**TABLE 2** Operating deposition and collapsing parameters.



**FIGURE 5 :** Spectral attenuation of MCSM fibre (synthetic commercial silica stretched tube, OD x ID = 50 x 25 mm).



**FIGURE 6 :** Spectral attenuation of MCSM fibre (synthetic commercial silica machined tube, OD x ID = 50 x 25 mm).

## SUMMARY

A new preform fabrication technology based on the direct use of very thick substrate tubes has been successfully developed in order to produce single-mode fibers with high fabrication rate. SPCVD deposition and subsequent RF furnace collapsing have been demonstrated both using commercially available tubes and 17.5-25 mm thick precision silica ingots. Preform capacities of 125 km/m have been obtained and 200-300 km/m has been shown to be feasible. The loss level achieved is about 0.25 dB/km at 1.55  $\mu$ m. Experimentally collapsing rates are about five times higher than with thin wall tubes and the silica burnt-off has been practically suppressed. This technique which offers additional potentialities regarding geometry improvement should lead to a significant increase of cost effectiveness in the areas of fiber production and connection.

# REFERENCES

- [1] J.B. Mac CHESNEY, D.W. JOHNSON, D.A. FLEMMING, F.W. WALZ : Elect. Lett., 23, 19, (1987), pp1005-1007
- [2] P. GEITNER, H. HAGEMAN, H. LYDTIN, J. WARNIER: J. Lightwave Technology, LT-6, 10, (1988) pp1451-1454
- [3] L.B. JEUNHOMME : Single Mode Fiber Optics, New-York Dekker (1983)
- [4] J. KIRCHHOF : Physica Status Solidi (a), 60, (1980), k127
- [5] F.T. GEYLING, K.L. WALKER, R. CSENSITS J. Applied Mechanics, 50, (1983), pp303-310
- [6] P. ALDEBERT, M. FAURE, V. NEUMANN, P. RIPOCHE, B. WURIER : Conf. Proc. 10th ECOC, Stuttgart, (1984), pp300-301
- [7] G. LE NOANE : Conf. Proc. 9th JNOG, Lannion, (1988), pp98-99
- [8] D. PAVY, M. MOISAN, S. SAADA, P. CHOLLET, P. LEPRINCE, J. MARREC : Conf. Proc. 12th ECOC, Barcelona, (1986), pp19-22
- [9] J. GOUDEAU, M. CORNEBOIS, J.G. FITOUSSI, D. PAVY, M. MOISAN, S. SAADA, P. CHOLLET : Conf. Proc. 9th JNOG, Lannion (1988), pp104-105
- [10] M. MOISAN, C. FERREIRA, Y. HAJLAOUI, D. HENRY, J. HUBERT, PANTEL, A. RICARD, Z. ZAKRZEWSKI : Rev. Phys. Appl., 17, (1982) pp707-727



Dominique PAVY  
CNET/LAB/OCM  
22300 LANNION  
FRANCE

Dominique PAVY received his ceramist engineer diploma from ENSCI in 1976 and his Ingenieur Docteur diploma from University of Orleans in 1979. He joined CNET in 1981 where he is in charge of studies a new preform fabrication processes in Department of Optical Cables and Fibres of CNET.



Monique MOISAN  
CNET/LAB/OCM  
22300 LANNION  
FRANCE

Monique MOISAN received her Doctor degree from the University of Rennes (France) in 1971. She joined CNET in 1983 where she is in charge of studies a new preform fabrication processes in Department of Optical Cables and Fibres of CNET.



Isabelle HARDY  
CNET/LAB/OCM  
22300 LANNION  
FRANCE

Isabelle HARDY received her engineer diploma from INSA in 1981 and her Docteur III<sup>e</sup> cycle diploma from University of Toulouse in 1984. She joined CNET in 1986 where she is in charge of studies a new preform fabrication processes in Department of Optical Cables and Fibres of CNET.



Philippe GROSSO  
C.N.E.T/LAB/OCM

22300 LANNION  
FRANCE

Philippe GROSSO received his optic engineer diploma from CNAM in 1978. He joined CNET in 1983 where he is in charge of drawing fibre studies in Department of Optical Cables and Fibres of CNET.

Christian LE SERGENT

Alcatel-Alsthom  
Recherche

91460 MARCOUSSIS

Christian LE SERGENT studied chemistry at Orsay University and received a licence ès Science in 1961. Then he joined Laboratories of Marcoussis where he is at present head of the glass and process group in the Optics and Electrochemistry Department of AAR.



Denis TREGOAT  
Alcatel Alsthom  
Recherche

91460 MARCOUSSIS

Denis TREGOAT received the Doctor degree from University of Rennes in 1985. He joined Laboratories of Marcoussis in 1985 and is research engineer on CVD processes, in the Optics and Electrochemistry Department of AAR

# A Profiling System for Large Optical Fiber Preforms

T. Abiru, M. Nakayama, R. Yamauchi

Fujikura Ltd.

1440 Mutsuzaki, Sakura-shi, Chiba-ken, 285 JAPAN

## Abstract

We have investigated a profiling system for large optical fiber preforms. The system is consisted of a refractive index measurement equipment and fiber characteristics estimation programs. The measurement setup can measure the refractive index profile up to 100 mm diameter preforms. And the system also measures the core eccentricities of preforms.

Our estimation program calculates all the fiber characteristics predictable from a refractive index profile. The results are useful to control and to stabilize the characteristics of the optical fibers.

## 1 Introduction

As the demand for a huge amount of optical fibers in telecommunications grows, the pressure for low-cost and high-productivity fiber manufacturing is increasing, too. Optical fiber preforms have increased their size to satisfy those requirements. The total length of fibers, which drawn from one preform, has become far over a hundred kilometers. While the enlargement of preform size improves the productivity, risk of losing many kilometers of fibers is also increasing of a single preform fails. If we can estimate the transmission and dimension characteristics of the fibers in the preform manufacturing stage, most of the risk can be avoided. So, an excellent preform analysis system is of great importance.

Two-step VAD process is one of the solutions to reduce the production cost for manufacturing optical fibers.[1] In the first step, a primary preform is made. The primary preform's cladding to core diameter ratio,  $D/d$ , is about 4. This ratio is enough to prevent water penetration to the core region from the outer part of the cladding.

However, in order to make a fiber of 125  $\mu\text{m}$  diameter, it is necessary to have a  $D/d$  of about 13 for conventional single mode fibers. In the second step, the rest of cladding part is deposited.

For the two-step VAD process, the size enlargement of the preforms also improve productivity. The sizes of some preforms have already been over 80 mm in diameter. But there is no commercially available refractive index profiling equipment which can measure such a large preform so far. For the time being, the maximum preform diameter seems around 100 mm as far as an operator handles the preform by hand.

We adopted the dynamic spatial filtering method[2] to measure the refractive index of optical fiber preforms. In terms of dimensional properties, we also have designed the equipment to measure the core eccentricity.

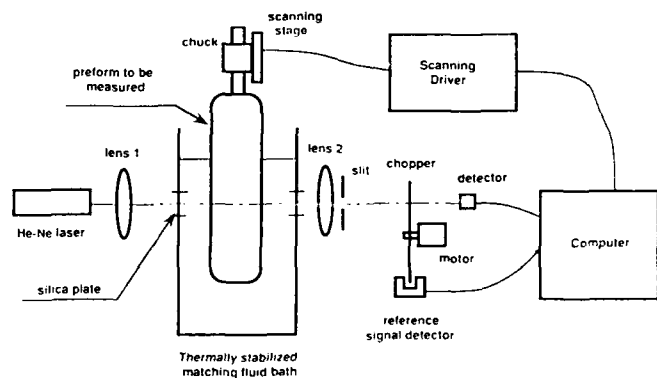


Fig 1. Schematic diagram of the refractive index measurement setup

## 2 Experiments and the results

### 2.1 Measurement setup

Figure 1 shows the schematic diagram of the

measurement setup. A preform to be measured is clamped vertically, and is immersed in a thermally stabilized index matching fluid bath. The preform and the bath are not fixed to each other. This structure is flexible to measure various diameters of preforms in sequence. This setup has a slit to mask higher order diffraction spots generated by the periodical refractive variations in a VAD optical fiber preform.[3]

## 2.2 Measurements and estimations

Figure 2 is an example of a deflected angle distribution. The abscissa is a distance from the preform center, and the ordinate is a deflected angle in degree. An eccentricity will be estimated from this curve. Eccentricity is a distance between the core and the cladding centers. A center position is determined by finding a rotational symmetry center of the curve for either the core and the cladding.

From a result of numerical simulations, we found that the eccentricity estimation error is in order of the relative refractive index difference between the cladding and the matching fluid. So it is normally less than 0.1 %, then this estimation is accurate enough compared with that of eccentricity measurement for fibers.

After an Abel integration of a deflection angle distribution, a refractive index profile is obtained. Figure 3 is an example of a preform for the dispersion shifted single mode fiber.

The fiber characteristics, such as cutoff wavelength, mode field diameter(MFD), chromatic dispersion and constant curvature loss, are estimated by a vector analysis program which is written in FORTRAN. The estimation automatically follows the profile measurement. It takes about one minute to estimate all the characteristics for a conventional single mode fiber.

## 2.3 Evaluation of the system

A hundred pairs of preform and fiber samples were measured to evaluate this profiling system in our two-step VAD process

At the end of the first step, the profiling system estimates the optimal fiber diameter(OFD) for a primary preform measured. OFD is an imaginably diameter of the fiber which satisfies that the cutoff wavelength takes a target value, for instance, 1.20

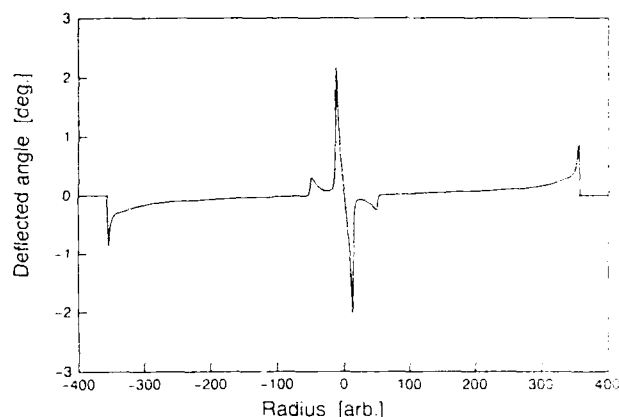


Fig 2. Deflected angle distribution of DSM

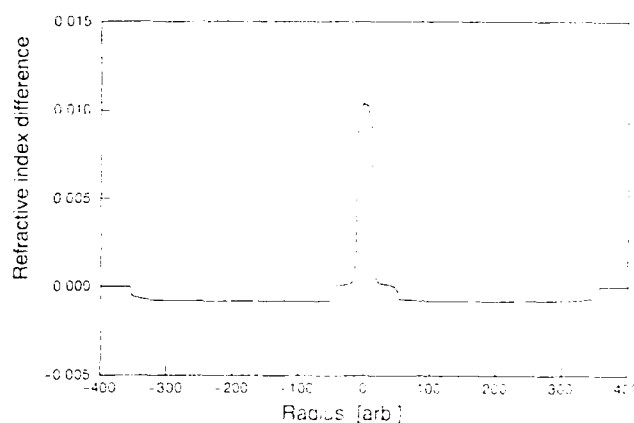


Fig 3. Refractive index profile of DSM

Table 1. Characteristic changes between processes

characteristics	Step-1	Step-2	Fiber
fiber diameter [μm]	35.0	125.0	125.4
cutoff wavelength [μm]	1.22	1.23	1.24
mode field diameter [μm]	9.51	9.52	9.51
chromatic dispersion [ps/km/nm]	-0.26	-0.25	-0.22
constant curvature loss [dB/m]	1.25	1.07	0.72
core eccentricity [μm]	--	0.32	0.2

$\mu\text{m}$ . In case of the two-step VAD process, OFD takes the values between 30 and 50  $\mu\text{m}$ . Of course, it depends on the fiber type.

The overcladding quantity is calculated from the ratio of an OFD to 125  $\mu\text{m}$ . And after the second step, the profiling system predicts the fiber characteristics of a completed preform, which should be drawn into 125  $\mu\text{m}$  in diameter. Table 1 shows an example of changes of the characteristics in each step. In Table 1, "Step-1" and "step-2" columns mean the estimated values just after the step 1 and step 2, respectively. "Fiber" column shows measured values at the fiber stage. Step-1's cutoff wavelength was fixed to 1.22  $\mu\text{m}$  which is the center value of the specification range. Step-2's estimated diameter was fixed to 125  $\mu\text{m}$  to predict the characteristics when it becomes a fiber.

Figure 4 shows the correlations between the estimated value (abscissa) and the measured one (ordinate). Figure 4a, 4b and 4c are the correlation of cutoff wavelength, MFD and eccentricity, respectively. They show good agreements. They are accurate enough to control the characteristics of the fibers. The standard deviations of each estimation error are shown in Table 2. Constant curvature loss is less accurate than other items because it is difficult to distinguish the macrobending loss from the microbending loss in the actual measurements.

### 3 Conclusion

We have investigated a profiling system with a

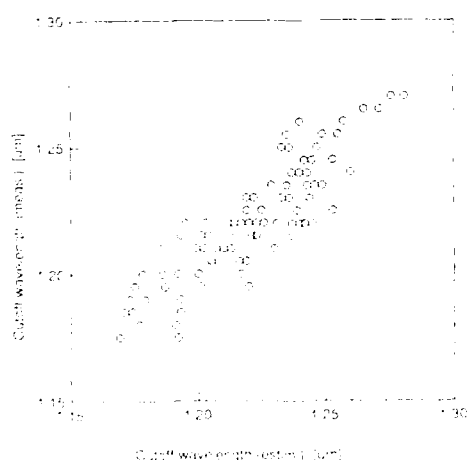


Fig 4a. Estimated Cutoff Wavelength

Table 2. Standard deviations of each characteristics' estimation error

characteristics		standard deviation
cutoff wavelength	[ $\mu\text{m}$ ]	0.012
Mode Field Diameter	[ $\mu\text{m}$ ]	0.05
chromatic dispersion	[ps/km/nm]	0.02
constant curvature loss	[dB/m]	3.2
core eccentricity	[ $\mu\text{m}$ ]	0.15

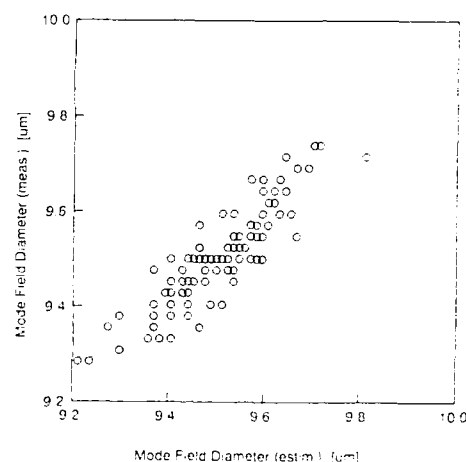


Fig 4b. Estimated Mode Field Diameter

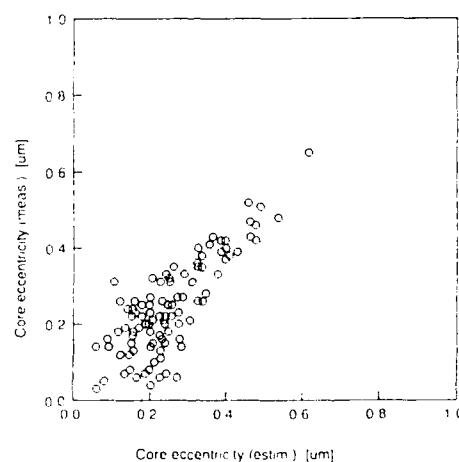


Fig 4c. Estimated Core Eccentricity



refractive index measurement equipment for large optical fiber preforms around 100 mm diameter. The system has proved to be effective to help our two-step VAD process.

We are now planning to improve the estimation accuracy and to reduce the measuring man-hours to cut production costs.

#### 4 References

- [1] "Fully Synthesized Single Mode Fiber Fabrication by Two-Step V.A.D. Process Using High Rate Cladding Deposition Burners", A.Wada et al., 11th ECOC '85
- [2] "Variation of refractive-index profiles in single-mode fiber preforms measured using an improved high-resolution spatial-filtering technique", I.Sasaki et al., 6th ECOC '80
- [3] "Refractive-index profile measurement of large preforms: a new technique", H.Kishi et al., 19th OFC '87



Tomio Abiru  
Fujikura Ltd.

Tomio Abiru is an engineer of Fiber process section, Opto-electronics Lab., Fujikura Ltd. He joined with Fujikura in 1983. Since then, he has been engaged in R&D of optical fibers. He received BE from the Chiba univ. in 1983. He is a member of the IEICE of Japan.



Masakazu Nakayama  
Fujikura Ltd.

Masakazu Nakayama is an engineer of Fiber process section, Opto-electronics Lab., Fujikura Ltd. He joined with Fujikura in 1986. He has been engaged in R&D of optical fibers since 1987. He received BEE from the Electric univ. in 1986. He is a member of the IEICE of Japan.



Ryozo Yamauchi  
Fujikura Ltd.

Ryozo Yamauchi is a manager of Fiber Section, Opto-electronics Lab., Fujikura Ltd. He joined with Fujikura in 1974. Since then, he has been engaged in R&D of optical fibers, cables, and optical components. He received Ph.D degree from the Nagoya university in 1984. He is a member of both the IEICE of Japan and the OSA.

# Relaxation of internal stress in fully-fluorine-doped single-mode fibers

Keigo Maeda, Shuji Okagawa and Hiroaki Ohnuma

THE FURUKAWA ELECTRIC CO., LTD.

## Abstract

The relaxation of internal stress in Fully-fluorine-doped single-mode fiber (called FF fibers) at elevated high temperatures was investigated. The internal stress of FF fibers, which was mainly governed by drawing conditions such as tension and temperature, affected the transmission characteristics. A model for relaxation was proposed, and internal stress change with time in the fibers could be evaluated from this model based on viscoelastic theory. The evaluation showed that no change in an internal stress would be found after 25 years at 25 °C.

## 1. Introduction

Fully-fluorine-doped single-mode fiber (called FF fiber), which has slightly fluorine doped core with deeply fluorine depressed cladding, is useful to realize the transmission losses of less than 0.20 dB/km at 1.55  $\mu$ m, and has been applied to submarine cables[1].

However, tensile internal residual stress in core part of such fiber is larger than that in germania doped fibers, because drawing tension is mainly applied for more viscous core part compared to cladding part. And the tensile internal stress in core part decreases refractive index difference between the core part and cladding part, and causes the changes in transmission

characteristics[2] such as loss and cutoff wavelength. By optimizing the drawing conditions, we have realized FF fibers with a transmission loss of less than 0.173 dB/km (average value) at 1.55  $\mu$ m.

On the next stage for practical use, the question has arisen, that is whether or not this internal stress changes in actual service time. In order to confirm the long term reliability of the cables utilizing FF fibers, evaluation on the change in an internal stress during actual service time was carried out in this paper.

## 2. Experiment

### (1) Samples

Fiber samples of 125  $\mu$ m in diameter were prepared by drawing from the preform rods which were synthesized in VAD based process. They had slightly fluorine doped core with deeply fluorine depressed cladding.

### (2) Measuring of internal stress

Tensile internal stress in core part was evaluated by measuring with a polarized microscope. Fig.1 is a schematic diagram showing the method of measuring the internal stress in FF fibers. First linearly polarized light from the polarizer passed through a sample turns elliptically polarized ray due to photoelastic effect of the sample. Next, the elliptically polarized ray passed

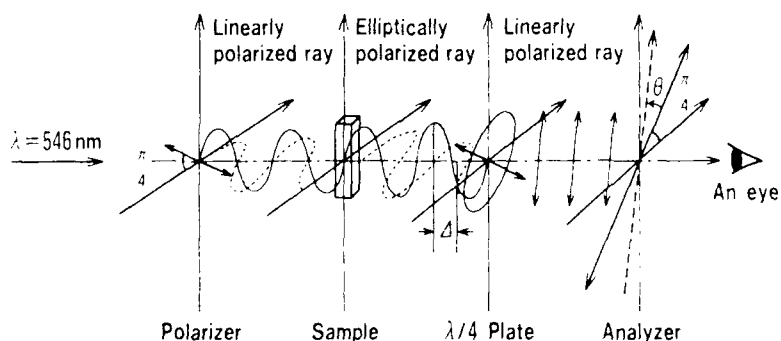


Fig.1 Schematic diagram of the stress measuring utilizing polarization microscope.

through the  $\lambda/4$ -plate turns again linearly polarized ray which plane of polarization is rotated to an angle  $\theta$  according to the shape of the ellipse. The angle  $\theta$  is determined by rotating analyzer to obtain the most dark visual field. Internal stress can be calculated from equations (1) and (2).

$$\frac{\theta}{180} \lambda = d \cdot \Delta n \quad \dots\dots (1)$$

where  $\lambda$  is wavelength(546nm) of measurement ray,  $d$  is thickness of the sample and  $\Delta n$  is difference of refractive index.

$$\Delta n = C \cdot \sigma \quad \dots\dots (2)$$

where  $C$  is photoelastic constant( $3.4 \times 10^{-5} \text{mm}^2/\text{kg}$ ) of silica glass and  $\sigma$  is stress.

### (3)Relaxation of internal stress

The urethane-acrylate fiber coatings were removed. And samples were held in a furnace. The temperature range of the experiment was  $400^\circ - 800^\circ\text{C}$ . All the operation were carried out in an air atmosphere.

## 3.Results and discussion

### (1).Drawing condition dependence of transmission characteristics in FF fibers

The tensile internal stress in core part reduced the refractive index difference between the core part and cladding part. Fig.2 shows the drawing tension dependence of cutoff wavelength and zero-dispersion wavelength. With increasing the drawing tension the cutoff wavelength sifted to shorter one and the zero-dispersion wavelength shifted to longer one.

Fig.3 shows the drawing tension dependence of transmission loss in FF fibers. A region of drawing tension to minimize transmission loss was found in the fabrication conditions for FF fibers. The difference of internal stress between core and cladding of FF-fiber increased with increasing drawing tension, which seemed to cause the transmission loss increase at  $1.55 \mu\text{m}$  for irregularity at the core and cladding interface. The other hand, the decrease of tension led to higher temperature drawing compared with that in the optimum condition, that might produce defect centers with optical absorption in infrared wavelength.

From the results, it was important to investigate long-term stability of internal stress in FF fibers.

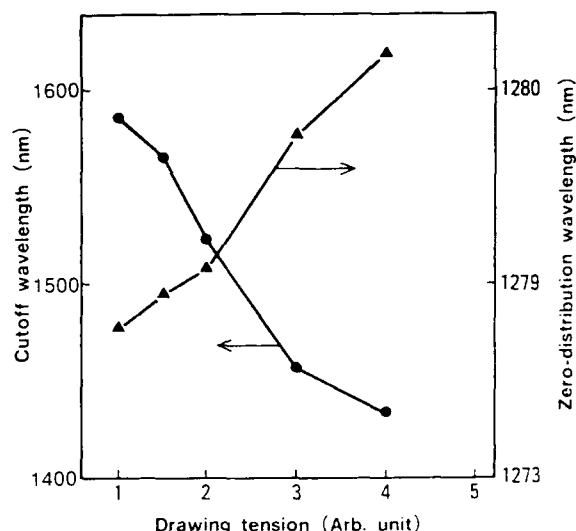


Fig.2 Drawing tension dependence of cutoff and zero-dispersion wavelength

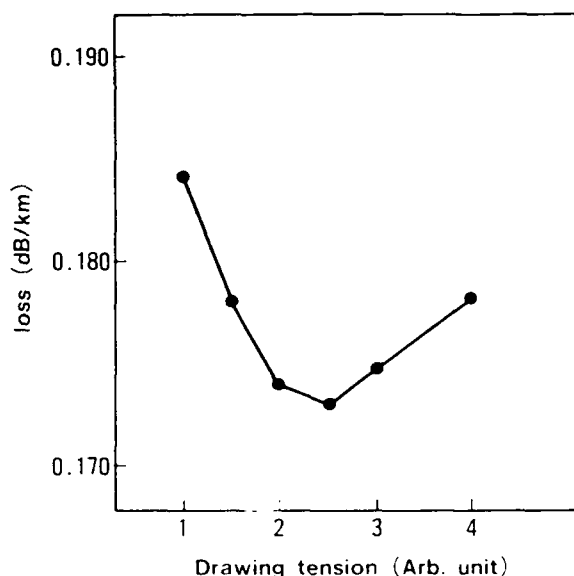


Fig. 3 Drawing tension dependence of transmission loss in FF-fibers

## (2) Relaxation of internal stress of FF fibers at elevated temperature

Fig.4 shows the internal stress changes in core part at different temperatures. Relaxation of internal stress was significantly observed in a higher temperature region (above 600°C).

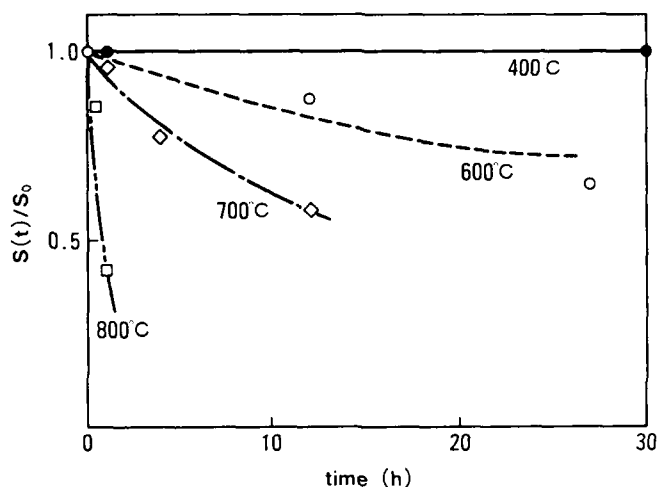


Fig.4  $S(t)/S_0$  vs. time

We assumed that internal stress  $S(t)$ , was given by Eq.(3) which was based on the Maxwell relaxation model:

$$S(t) = S_0 \exp(-t/\tau) \quad \dots \quad (3)$$

where  $S_0$  is the initial internal stress, and  $\tau$  is the time of relaxation. Plots of  $\ln(S(t)/S_0)$  at different temperatures versus time gave straight lines as shown in Fig.5. The slopes of each line refer to  $-1/\tau$ .

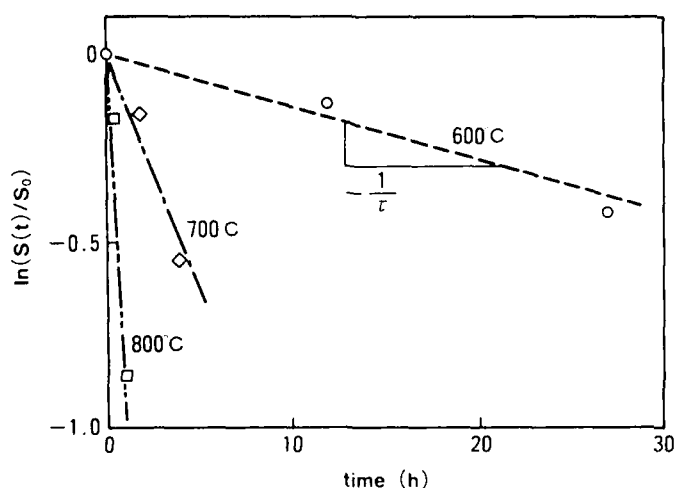


Fig.5  $\ln(S(t)/S_0)$  vs. time

Further the temperature dependence of  $\tau$  is usually expressed by an Arrhenian type relation as shown in Eq.(4):

$$\tau = \tau_0 \exp(\Delta H/RT) \quad \dots \quad (4)$$

where  $\tau_0$  is constant,  $\Delta H$  is the apparent activation energy,  $R$  is the gas constant (8.314 J/mole · K), and  $T$  is the temperature in Kelvin. An apparent activation energy  $\Delta H$  of 159 kJ/mole was obtained by plotting  $\ln \tau$  vs.  $1/T$  (Fig.6). By combining equations (3) and (4), the internal stress in FF fibers after time  $t$  at a given temperature could be calculated. The evaluation showed that the change in internal stress would be negligible after 25 years at 25°C as shown in Table I.

Table I Internal stress change after 25 years at different temperature

After 25 years	Temperature °C		
	3	25	100
$1-S(t)/S_0$ (%)	$0.0 \times 10^{-6}$	$1.1 \times 10^{-13}$	$4.4 \times 10^{-9}$

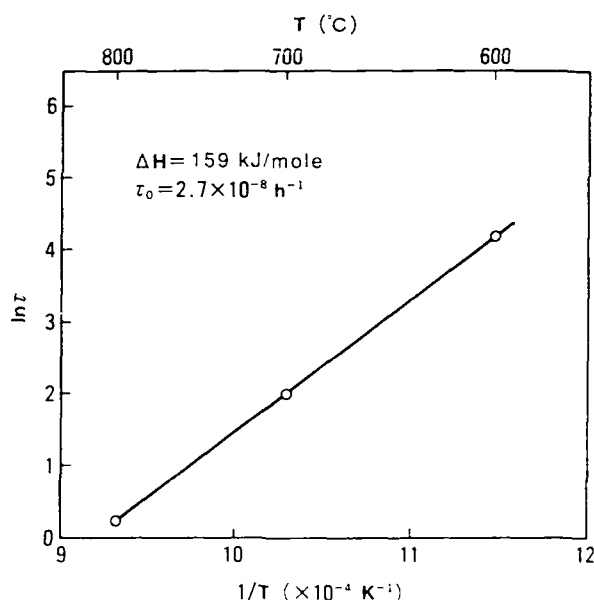


Fig.6 Determination of the apparent activation energy of internal stress relaxation by plotting  $\ln \tau$  vs.  $1/T$

Based on these results, thousands kilometers of FF fibers have been successfully applied to the submarine cables. Fig.7 shows the loss value distribution of FF fibers. The average transmission loss was reduced to 0.173 dB/km.

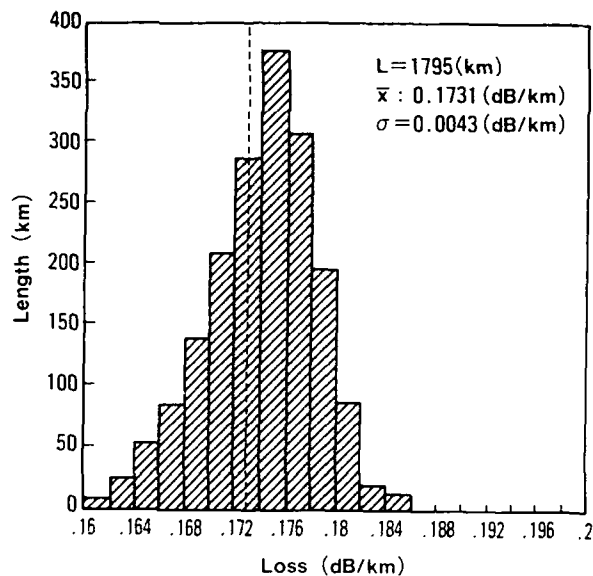


Fig.7 Loss distribution of FF-fibers

#### 4.Conclusion

The relaxation of internal stress in FF fibers at elevated high temperatures was investigated. A model for relaxation is proposed to determine the value of the apparent activation energy. The evaluation showed that no change of internal stress would be found after 25 years at 25 °C. And we have achieved the FF fibers with a transmission loss of 0.173 dB/km(average value) at a wavelength of 1.55  $\mu\text{m}$ .

#### <References>

- [1] Mikio Ogai et al., ECOC'87, Proc., pp.167.
- [2] Yoshinori Hibino et al., Appl.Phys.Lett.50(22),June 1987,pp.1565.



Keigo MAEDA

The Furukawa Electric  
Co.,Ltd.  
6 Yawata-Kaigandori,  
Ichihara, Chiba, 290  
Japan

Mr. Maeda graduated from Kyoto University in 1984 with a B.Sc. in industrial chemistry. Then he joined The Furukawa Electric Co.,Ltd., Chiba, Japan, and has been engaged in research and development of plastic materials and manufacturing methods for optical cable.

He is now a production engineer of Optical Fiber, Fiber Optics & Telecommunications Division at The Furukawa Electric Co., Ltd.



Hiroaki OHNUMA

The Furukawa Electric  
Co.,Ltd.  
6 Yawata-Kaigandori,  
Ichihara, Chiba, 290  
Japan

Mr. Ohnuma graduated from Tokyo University in 1984 with a B.Sc. in physics. Then he joined The Furukawa Electric Co.,Ltd., Chiba, Japan, and has been engaged in development of optical fibers and cables.

He is now a staff of quality assurance Dept., Fiber Optics & Telecommunication Division at The Furukawa Electric Co., Ltd.



Shuji OKAGAWA

The Furukawa Electric  
Co.,Ltd.  
6 Yawata-Kaigandori,  
Ichihara, Chiba, 290  
Japan

Mr. Okagawa graduated from Osaka University in 1981 with a M.Sc. in chemistry. Then he joined The Furukawa Electric Co.,Ltd., Chiba, Japan, and has been engaged in research and development of plastic materials and manufacturing methods for optical cable.

He is now a senior research engineer of Optical Fiber Transmission Section, Opto-Technology Laboratory, The Furukawa Electric Co., Ltd.

# Coating Stripping Force Measurement: A New and Quick Test Method for the Determination of the Degree of Curing for Optical Fibre Coating

H. Marsman, R. Wauben, G. Kuyt  
Philips Optical Fibre B.V.  
P.O. Box 218, 5600 MD Eindhoven  
The Netherlands

## Abstract

*An inquiry has been made into the suitability of various methods of determining coating cure, for use as an in-production process and quality inspection tool.*

*This paper describes the known methods : MEK extraction test, FTIR (Fourier Transform Infrared Spectroscopy), Coating Compressibility test and Coating Stripping Force measurement. A comparison between these measuring techniques is included. The stripping force measurement has turned out to be a reliable and quick method of determining the degree of curing of double-layer coating systems. Moreover, this technique is shown to be capable of measuring a severe coating overcure.*

## 1 Introduction

In general, optical fibres used for telecommunication purposes are primary-coated with two layers of UV-curable acrylates. These coatings are selected by their physical and chemical characteristics. For the coating to have its characteristic properties specified by the coating manufacturer, a good-quality coating cure has to be ensured. For the cable manufacturer the result will be smoothness of the cabling process and constant quality in conformity with the product type approval.

A search is being made for a method of determining the cure of the coating, which can be used as a process control tool by the fibre manufacturer. To be fit for use this method has to meet specific requirements. It is necessary to have a quick and simple method, and the test has to be performed by production staff in a production environment. Then the operator is able to control an essential drawing process parameter. Furthermore the test should require neither expensive equipment or too much analytical knowledge for correct interpretation of test results nor time-consuming sample preparation.

The following test methods are described in the next chapter:

- MEK extraction test
- FTIR (Fourier Transform Infrared Spectroscopy);
- Coating Compressibility test
- Coating Stripping Force measurement

## 2 Description of the test methods

### 2.1 MEK extraction test

MEK extraction is the oldest and most widely used method in fibre industry, and is therefore regarded as a reference test method for comparison. This means that the new test should give at least as much information as the MEK extraction test.

This test enables extraction of all the coating material which is not polymerised. The first step is to determine, by full curing, the amount of additives in the coating. This amount depends on the specific coating materials used for the inner and outer layers, and consists of mainly photoinitiator, inhibitor and similar additives. The method is described in detail in [1]. In case of less than full curing the monomer material that has not reacted is measured.

About 3 g of dried glass fibre is weighed accurately [Mv]. This 3 g is then extracted for 15 hours with MEK (methyl ethyl ketone) in a Soxhlet Extraction Apparatus. After drying its weight is determined [Me]. The coating is removed by burning in a furnace (1000 °C). The glass residue is weighed [Mg]. The loss of weight (in %) as a result of the extraction with MEK then is:

$$\Delta M = \frac{Mv - Me}{Mv - Mg} \cdot 100\%$$

A typical test result is given in figure 1.

The MEK extraction test itself takes about one day, which is too long for information to become available for process control in production. Furthermore, for process

control for a complete production plant a lot of equipment and a full-time operator are needed. Therefore, the MEK extraction test is unfit for process control.

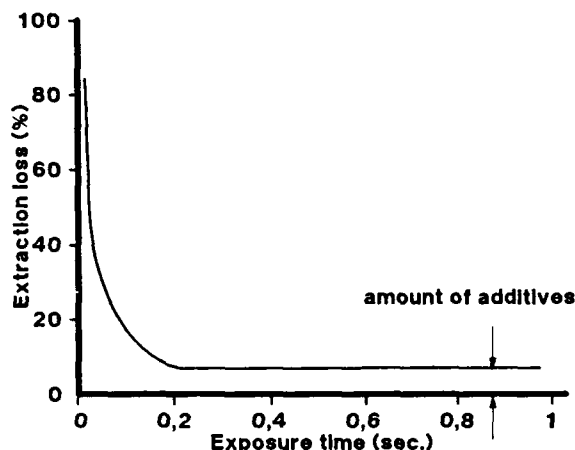


fig 1: Typical extraction loss as a function of exposure time

## 2.2 FTIR

The Fourier Transform Infrared Spectroscopy (FTIR) technique has been developed by DeSoto's Analytical and Computer Applications Research Department (ACAR). It has been designed primarily to compare different liquid coating batches [2]. FTIR measures the change in acrylate absorbance at  $810\text{ cm}^{-1}$ , which wavelength is characteristic of the reaction of functional groups like the double bond ( $\text{-C=C-}$ ) in the monomer. In the polymerisation reaction the double bond disappears and the absorbance at this specific wavelength changes. FTIR measures the concentration (in %) of monomers that have not reacted. The measurement signal for the liquid coating is set to 0% and that for a deliberately overcured coating to 100%. This technique is adapted for use with coated optical fibres using an array of 20 pieces (about 3 cm long) of fibre, secured at both ends using adhesive tape [3]. This array is then firmly clamped to the MIR (Multiple Internal Reflectance accessory). The spectrometer used is a Nicolet FT-IR series 500.

Results can be available within an hour. This test has a high repeatability on condition that sample preparation is performed with great care by skilled operators. The curve fitting and the mathematical procedures are performed by the attached computer system.

A disadvantage of the technique is that, owing to the wavelength used, FTIR only measures the cure of the outer surface (about  $3\text{ }\mu\text{m}$  thick) of the coating. Furthermore, the equipment requires a high capital investment.

## 2.3 Coating Compressibility Test

As the E-modulus of the coating depends on the degree of cure it is possible to relate this degree to the compressibility of the coating.

For this test six pieces of fibre, 5 cm long, are placed between two horizontally placed parallel plates. Pressure is exerted on one plate. See figure 2. The displacement of this plate, measured with a micrometer displacement gauge, is dependent of the hardness of the coating. The displacement of the upper plate is defined as the displacement at  $10^5\text{ Pa}$  and is expressed in a percentage of the full fibre diameter. Sample preparation is easy and results can be obtained within 15 minutes.

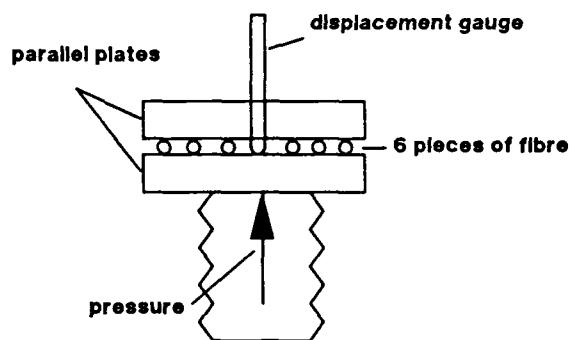


fig 2 : Test set-up for compressibility test

## 2.4 Coating stripping force measurement

The stripping force is a result of shrinkage owing to both polymerisation and temperature drop and to adhesion of the buffer coating to the glass. The coating cures at relatively high temperatures. When cooling to room temperature, the coating shrinks more than the glass. The degree of curing acts on the polymerisation shrinkage and therefore partly on the stripping force.

The coating is removed from the fibre with a stripping tool. The force required for this removal is measured with a tensile strength measuring device. The stripping force is defined as the mean value of several pieces of fibre. A proposal for standardisation has been submitted to the IEC [4]. The stripping speed was 100 mm/min. The tool was the Micro Electronics Microstrip MS1, with cutting blades .006 inch. A typical stripping force measurement result is shown in fig 3.

The results are available within five minutes after fibre-drawing. Equipment is easy to operate.



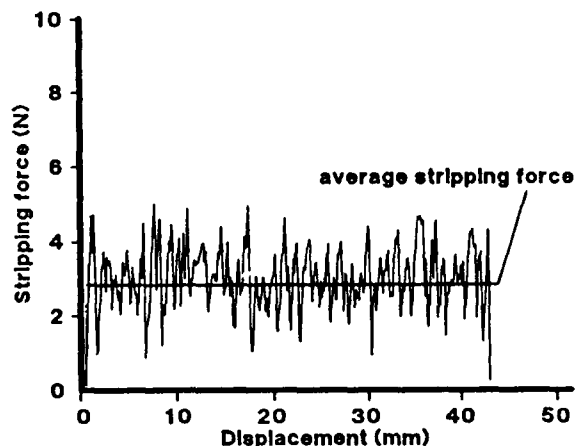


figure 3. Typical Stripping Force Measurement Result

### 3 Comparison between test methods

#### 3.1 Test fibre

The fibre used for comparison between the various test methods is drawn from one preform. This preform is drawn at different speeds with a different number of UV curing ovens. A few hundred metres are drawn under the same conditions for a large enough quantity of sample for each test to be available.

The exposure time is calculated by division of the length of the number of outer coating curing ovens used, by the drawing speed. The exposure of the inner coating is left out of consideration; in all cases one UV curing oven is used for this inner coating layer. The coatings used for this experiment are commercial UV-curable coatings.

#### 3.2 Results

The results are listed in Table 1 and figure 4.

Exposure time	Extraction	FTIR	Compressibility	Stripping force
(sec.)	(%)	(%)	(%)	(N)
1.00	7.60	98.9	16.5	3.40
0.80	6.70	100	16.3	3.22
0.50	7.70	98.2	15.7	2.88
0.40	6.40	95.5	15.7	2.84
0.30	6.40	95.4	16.5	2.78
0.20	7.80	87.7	15.7	2.52
0.17	11.0	80.9	15.5	1.80
0.13	18.3	76.7	23.1	1.50
0.07	26.4	62.1	37.8	0.66
0.05	38.4	51.9	-	0.34
0.03	43.6	49.6	-	0.32

Table 1. Results

#### 3.3 Discussion

In this inquiry the MEK extraction test has been used as the reference test. The results obtained with the fibres point to a constant extraction loss from 0.2 sec exposure time onwards, for our coating material and our application technique. This 0.2 sec point is therefore defined as the 100% cure point; addition of more UV-energy will result in an overcure of the coating material because all the monomer molecules are already linked. This means that the other tests should at least allow meaningful interpretation until this 100% cure point.

The compressibility test allows measurement of the cure only until 0.17 sec exposure time, again for our coating material and application technique. Therefore this test fails to meet our requirements. In the past this test has proved to be effective for one-layer coated optical fibre.

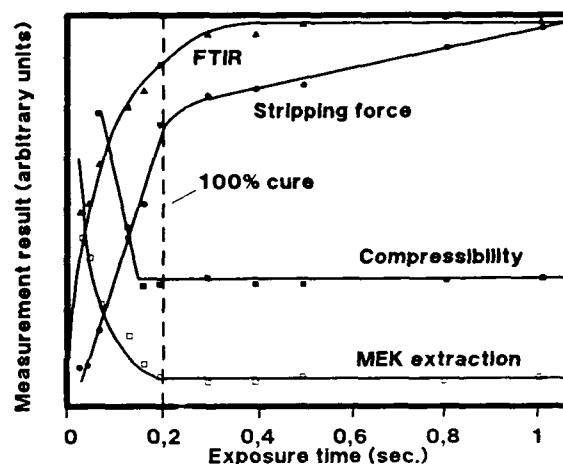


fig 4 : Comparison of measurement results

As can be seen in figure 4, both FTIR and stripping force measurement meet the requirements.

As stated before, FTIR only measures the cure of the outer coating surface. This is why this test is used as a surface-cure test instead of a bulk-cure test [1]. Surface-cure does not necessarily guarantee good bulk-cure; on the other hand good bulk-cure automatically guarantees adequate surface-cure. A change in curing conditions like UV-wavelengths of lamps influences surface-cure more than bulk-cure. Stripping force measurement however is by definition a bulk-cure test method.

For practical reasons the stripping force measurement is also preferable to the FTIR because it does not require expensive equipment. It is a quick test method and it does not need analytical knowledge for interpretation of the results. The fibre-drawing operators are able to do the test themselves and to rapidly obtain accurate information on the coating curing process.

Both FTIR and stripping force measurement allow determination of overcure. FTIR yields a continuous change

until about 30 % overcure (in our definition), but the stripping force measurement allows determination of a severe overcure of the coating caused by extremely high UV-doses or defective equipment.

#### 4 Conclusions

The MEK extraction test is a suitable technique of measuring coating cure, and is used as a reference test method for the determination of the 100% cure point. For process control it is unacceptable because the feedback time is too long .

Measurement of the compressibility is an unsuitable method of determining the cure of double-layer coating systems.

FTIR and Stripping force measurement can be used for control of the degree of coating cure.

Stripping force measurement is preferable because it is a cheap and quick test method, suitable for in-production process control.

Stripping force measurement also enables detection of severe coating overcure.

#### 5 References

- [1] Specification CW 1500A Draft 1 for Terms Definitions and Reference Test Methods for Single Mode Optical Fibres, British Telecom PLC London, Nov. 1990.
- [2] J.M.Julian and A.M.Millon: "Quality Control Testing of UV Curable Coatings Using FTIR" Journal of Coatings Technology Vol 60 No 765 Oct 1988.
- [3] E.F.L. D'Souza: "The measurement of cure in optical fibre coatings" Technical Report British Telecommunications PLC, London, 1990.
- [4] Committee Draft IEC 86A (secretariat) 111: Optical Fibre strippability; Test method for IEC 793-1: Generic Specification for Optical Fibres.



**Henk Marsman** was born in Glanerbrug, The Netherlands, in 1957. He received the B.S. degree in Chemistry in 1981. He started at Mobil Chemicals in Tiel and joined Philips Optical Fibre Eindhoven in 1984. His work mostly involves development of coating technology.



**Roland Wauben** was born in Hasselt, Belgium, in 1952. He received the B.S. degree in Chemistry in 1973. He started at Philips Research Laboratories in Eindhoven where he worked on photoconductivity of glasses. In 1983 he joined Philips Optical Fibre and is now manager of the process engineering department.



**Gerard Kuyt** was born in 1950 in The Hague, The Netherlands. He received the B.S. degree in Electro Technique. In 1973 he joined Philips Research Laboratories in Eindhoven in the optical communication system group. In 1981, he joined Philips Optical Fibre and is currently responsible for application activities.

# OPTICAL FIBER FAILURE PROBABILITY PREDICTIONS FROM LONG-LENGTH STRENGTH DISTRIBUTIONS

G. S. Glaesemann

Corning Incorporated  
Corning, New York

## Abstract

Strength data from a recently developed apparatus for measuring long-length fiber strength distributions are analyzed in terms of proof test theory for truncated distributions. Data are fitted using Weibull statistics and scaled for bending and tensile lengths ranging from 1 meter to 100 kilometers. Most tensile applications require strength data near the proof stress level. For failure probability levels less than  $1 \times 10^{-5}$ , most bending applications need be concerned with flaws near the proof stress level.

## Introduction

A schematic of a 1986 strength distribution of 16.5 kilometers of titania-doped silica-clad fiber proof tested to 50 kpsi (345 MPa) is shown in Figure 1.<sup>1</sup> Observe that after testing nearly 17 kilometers of fiber the distribution lacks flaws that are of the greatest reliability risk for most applications, namely those near the proof stress level. For the purposes of reliability prediction near the proof stress level much more fiber must be tested. Also, the amount of time required to manually create multi-kilometer strength distributions using common industry test methods makes the creation of such distributions costly.

The purpose of this paper is to present a recently developed technique for measuring the strength distribution near the proof stress level and to examine how one might use these data for making reliability predictions.

## Creating a Long-Length Strength

### Distribution

A new fiber strength testing method was recently developed for obtaining data on many kilometers of fiber in a more timely fashion.<sup>2</sup> It is believed that this test method will enable engineers to better assess the failure probability of flaws near the proof stress level. As shown in Figure 1, 95% of the flaws on 20 meter gauge lengths have strengths greater than 500 kpsi (3500 MPa), and therefore, do not present a reliability risk for long-length applications. The approach taken in the development of a long-length strength distribution was to avoid testing the strong flaws to failure. This was accomplished by loading fibers during tensile testing to a maximum load below the high strength region as shown schematically in Figure 2, where the maximum load during testing is set to break all flaws below 400 kpsi (2800

MPa) and pass those that are stronger.

A complete description of the operation of the equipment is given in reference 2 and only a brief description will be given here. The test apparatus is shown schematically in Figure 3 and consists of a proof testing machine for paying out fiber into the gauge length under low loads. The gauge length consists of 20 meters of fiber which starts at point A on the payout tractor, travels around a remote pulley assembly and back to point B on the take-up tractor. The pulley assembly consists of a pulley mounted on a load cell, both of which are attached to a pneumatic slide. Fiber is paid out under low load into the gauge length, after which the pulley assembly moves on the slide and the fiber is loaded to a predetermined maximum load level. As soon as the maximum load is reached, the pulley returns to its original position. The load is carefully monitored during the entire load pulse and if failure occurs, the breaking load is recorded. Typical load pulses are shown in Figure 4 for fiber that passes and fails the test. If the fiber passes the load pulse test, another 20 meter length is indexed into the gauge length and the load pulse is repeated. The loading and unloading rates are in the 200 to 400 kpsi/s (1400 to 2800 MPa/s) range and, therefore, the probability of subcritical crack growth during testing is high. Using the above apparatus, 386 kilometers of titania-doped silica-clad fiber<sup>4,5</sup> proofed to 50 kpsi (350 MPa) were tested to a maximum stress level of 350 kpsi (2450 MPa) in approximately 4 weeks. All testing was carried out under ambient conditions (20°C, 60% RH). The number of recorded failures below 350 kpsi (2450 MPa) was 106 out of a total 19,300 individual 20 meter tests. The failure probability, F, was assigned to each fiber failure using the median rank method.

$$F = \frac{(I-0.3)}{(J+0.4)} \quad (1)$$

where I is the fiber rank ranging from 1 for the weakest to 106 for the strongest fiber, and J is the total number of tests; namely, 19,300. The data are shown in Figure 5 as a Weibull plot of  $\ln \ln(1/(1-F))$  versus  $\ln \sigma_f$ , where  $\sigma_f$  is the fracture strength. The upper end of the strength distribution stops at the maximum stress level of 350 kpsi, as planned, and the lower end extends to a stress level slightly above the proof stress of 50 kpsi (350 MPa). The above data demonstrate the capability of obtaining multi-kilometer strength distributions in a relatively short period of time.

The theoretical shape for inert strength distributions of proof tested specimens is shown in Figure 6 from reference 3. The pre-proof distribution has a constant slope m. Flaws away

from the proof stress are unaffected by the proof stress and are shown to follow the pre-proof distribution. Those that grow subcritically during proofing have a post-proof slope of  $n-2$ , where  $n$  is the well known fatigue susceptibility parameter from the power law crack velocity model. Finally the distribution is truncated near the proof stress level as indicated by a vertical line. For fast unloading rates the truncation strength is no less than 90% of the proof stress.<sup>3</sup>

The distribution in Figure 5 differs from the theoretical distribution in that our testing demonstrates subcritical crack growth due to a fatigue environment. In the case where fatigue occurs during strength testing, the truncation strength level will be less than the proof stress, simply because flaws that just pass the proof stress will grow during subsequent strength testing and fail at a stress level below the proof stress. The flaws in the  $(n-2)$  slope region will, after crack growth during the strength test, end up with a slope  $n+1$ .<sup>6</sup> The data in Figure 5 are linear above the 125 kpsi (875 MPa) stress level with a slope,  $m$ , of approximately 2. Below 125 kpsi (875 MPa), the data indicate the transition to a higher slope region prior to truncation shown in Figure 6. However, too few flaws were obtained in this region to accurately determine where a slope of  $n+1$  begins, obviously, many more kilometers of data are needed.

#### Predictions from long-length strength distributions

Optical fibers in the field experience a variety of stress conditions over different fiber lengths. For example, in splice enclosures, relatively short lengths of fiber are subjected to bending; however, considering the number of splice enclosures involved, hundreds and even thousands of meters of fiber are under stress. In this common situation it is important to determine which flaws pose the greatest risk to mechanical reliability. For applications involving kilometers of fiber under low stress, it is common to treat the fiber as if it were no stronger than the proof stress level. However, as fiber comes closer to the home, it is expected to have greater mechanical reliability, thereby, requiring the knowledge and accountability of flaw distribution at and above the proof stress level. Since measured tensile strength distributions typically use lengths that do not match those deployed in service or model loading configurations such as bending, one must scale the distribution to the length and loading configuration appropriate for a given application.

Weibull's cumulative failure probability distribution has found wide applicability for describing the dependence of strength on size. The failure probability at an applied stress  $\sigma$  is given by,<sup>7,8</sup>

$$F = 1 - \exp \left[ - \int \left( \frac{\sigma}{\sigma_0} \right)^m \frac{dA}{A_0} \right] \quad (2)$$

where  $m$  is the Weibull slope,  $A$  is the surface area under stress  $\sigma$ , and  $A_0$  is the surface area corresponding to the characteristic strength  $\sigma_0$ .

#### Tensile Loading

For the case of uniaxial tensile loading, the stress at failure is distributed uniformly over the cross section,  $\sigma = \sigma_f$ , and  $dA = r dl d\theta$  where  $l$  is the fiber length,  $r$  is the fiber radius and  $\theta$  is the angle as shown in Figure 7. Substituting these values into Eq. (2) yields,

$$F = 1 - \exp \left[ - \int_0^{2\pi} \int_0^{l_t} \left( \frac{\sigma_f}{\sigma_0} \right)^m \frac{r dl d\theta}{A_0} \right] \quad (3)$$

where  $l_t$  is the total length in tension. Integration yields the probability of length  $l_t$  failing at stress  $\sigma_f$ ,

$$F = 1 - \exp \left[ - \left( \frac{\sigma_f}{\sigma_0} \right)^m \frac{2\pi r l_t}{A_0} \right] \quad (4)$$

Thus, Eq. (4) can be used to scale the data for gauge length of area  $A_0$  and characteristic strength  $\sigma_0$ , to lengths  $l_t$ . For  $l_t$  equal to the test length,  $A_0 = 2\pi r l_t$  and Eq. (4) simplifies to the more familiar Weibull form,

$$F = 1 - \exp \left[ - \left( \frac{\sigma_f}{\sigma_0} \right)^m \right] \quad (5)$$

The usefulness of this distribution is that it can be transformed into a linear format as,

$$\ln \ln \left( \frac{1}{1-F} \right) = m \ln \sigma_f - m \ln \sigma_0 \quad (6)$$

where  $m$  is the Weibull slope and  $-m \ln \sigma_0$  is the intercept.

Recall that data in Figure 5 are plotted in terms of  $\ln \ln(1-F)$  versus  $\ln \sigma_f$  according to Eq. (6); however, as previously observed, the data are not linear, but rather has a characteristic curvature associated with a truncated distribution.<sup>3</sup> Theoretical models for curved distributions are significantly more complex than Eq. (4), and the scaling of such distributions is justified. However, here we take a more pragmatic approach that simplifies scaling significantly, especially in the case of bending.

The distribution in Figure 5 is not extensive enough to attain the theoretical slope of  $n+1$ ; so, for discussion purposes, ranks 1 to 15 were fit to Eq. (6) yielding a slope of approximately 5. Similarly, ranks 15 through 106 were fit to Eq. (6) yielding a Weibull slope of 1.7. The composite distribution is shown in Figure 8. The Weibull parameter  $\sigma_0$ , for each portion of the distribution is also given in Figure 8. Using Eq. (4), where  $A_0$  is the total area for 20 meter test lengths and 62.5  $\mu\text{m}$  glass radius, the composite distribution is scaled to a range of new lengths  $l_t$  in Figure 9. Note again that these distributions are degraded following proof testing due to crack growth during strength testing. As expected, the failure probability for each strength level is increased as the in-service length increases. Also note that the shift is slightly greater for the region of the distribution with lower  $m$  value. Conversely, as the in-service length decreases, the probability of encountering a flaw near the truncation strength also decreases. However, for a typical failure probability

requirement of  $1 \times 10^{-5}$ , the predicted distribution shows that even applications using only 1 meter lengths in tension need be concerned with flaws below the 600 kpsi (4200 MPa) "high strength" region shown in Figure 1. For stressed lengths 100 kilometers and greater, Figure 9 shows that reliability designs should be focused primarily on flaws near the proof stress level. The data in Figure 9, when matched with a given application, will also help focus on the type of data needed for reliability determinations.

### Bending.

The surface tensile stress due to bending of fiber also is a reliability concern, since large stresses are easily generated. However, bending places a considerably smaller area under stress compared to uniaxial tension, due to the fact that only half of the fiber surface is under tensile loading (Figure 10), and the stress distribution over that surface is highly nonuniform. Therefore, it is important to determine what portion of the strength distribution is of concern for a given bend application.

The simplest bending situation is where the entire fiber length in bending experiences a constant bend radius. The Weibull scaling laws for the more complex case of 2-point bending have already been derived by Matthewson et. al.,<sup>9</sup> and therefore, the analysis here will follow their form and notation.

The surface tensile stresses generated by fiber bending are dependent entirely on the bend configuration. The stress,  $\sigma$ , is zero at the neutral axis,  $\theta=0$ , and reaches a maximum at  $\theta=\pi/2$ ; see Figure 7. The well known relationship between stress,  $\sigma$ , and the bend radius  $R$  is given by,

$$\sigma = \frac{r \sin \theta}{R} E \quad (7)$$

where  $r$  is the fiber radius and  $E$  is its Young's modulus. Young's modulus for optical glass fiber has been found to vary linearly with strain, according to  $E = E_0(1+3\epsilon)$ , for strength levels of concern in this study, where  $E_0$  is the zero strain modulus.<sup>10,11</sup> Thus, the maximum bend stress,  $\sigma_b$ , at  $\theta=\pi/2$  only occurs along a thin line along the fiber lengths and is given by,

$$\sigma_b = \frac{E r}{R} \quad (8a)$$

Therefore, the bend stress at any point on the tensile surface is simply,

$$\sigma = \sigma_b \sin \theta \quad (8b)$$

The Weibull cumulative failure probability distribution for the case of pure bending is obtained by substituting Eq. (8b) into Eq. (2), where  $dA = r d\theta d\theta$  yielding,

$$F = 1 - \exp \left[ - \int_0^\pi \int_0^{l_b} \left( \frac{\sigma_b \sin \theta}{\sigma_0} \right)^m \frac{r d\theta d\theta}{A_0} \right] \quad (9)$$

Integrating over length  $l_b$  reduces the above equation to,

$$F = 1 - \exp \left[ - \left( \frac{\sigma_b}{\sigma_0} \right)^m \frac{r l_b}{A_0} \int_0^\pi \sin^m \theta d\theta \right] \quad (10)$$

Following the derivation of Matthewson et. al.<sup>9</sup> we let,

$$G(m) = \frac{1}{2} \int_0^\pi \sin^m \theta d\theta = \int_0^{\pi/2} \sin^m \theta d\theta = \frac{\sqrt{\pi}}{2} \frac{\Gamma(\frac{m+1}{2})}{\Gamma(\frac{m+2}{2})} \quad (11)$$

where  $\Gamma(m)$  is the gamma function which is readily determined using polynomial approximations.<sup>12</sup> Substitution of Eq. (11) into Eq. (10) gives the cumulative failure probability distribution for bending in terms of maximum bending stress,  $\sigma_b$ , and the length under bending,  $l_b$ , for a fiber of radius  $r$ .

$$F = 1 - \exp \left[ - \left( \frac{\sigma_b}{\sigma_0} \right)^m \frac{2r l_b}{A_0} G(m) \right] \quad (12)$$

Thus, given  $\sigma_0$  and  $A_0$  from the composite 20 meter gauge length tensile distribution in Figure 8, one can calculate the failure probability for various lengths in bending. Figure 11 shows failure probability predictions for a range of bend lengths.

The predictions in Figure 11 show that, similar to the tensile distribution, the longer the bend length is, the greater the failure probability will be. However, the predicted distributions in bending show a lower failure probability for the same length and stress level than that given by tensile distributions in Figure 9. This is a consequence of the fact that bending places fewer flaws at risk than tension. The predicted distribution for 100 meter lengths in bending is shown in Figure 11 to fall on top of the original 20 meter tensile distribution. Thus, for the Weibull slopes in this data, loading 100 meters to a constant radius in bending is equivalent to loading 20 meters in tension. This will be discussed further in a later section.

In light of the bend predictions we now examine a common application that uses bending; namely, splice enclosures. The goal here is to determine that portion of the distribution which is most critical for making reliability predictions. As a worse case, we assume that in a splice enclosure 1 meter of fiber is placed in bending under a constant radius. The predicted distribution for this application is shown in Figure 11. For a failure probability requirement of  $1 \times 10^{-5}$ , flaws with strengths in the 150 kpsi (1050 MPa) range are expected to be encountered (note that post-proof strengths are somewhat greater than the fatigue strengths obtained in this study). For failure probabilities  $< 1 \times 10^{-5}$ , flaws with strengths near the proof stress level will be encountered even for 1 meter lengths in bending. When one accounts for all of the fiber in splice enclosures, such a low range of failure probabilities may not be unreasonable.

### Mean strengths in Bending and Tension.

The mean strength for a distribution of the form,

$$F = 1 - \exp\left[-\left(\frac{\sigma}{\sigma_0}\right)^m\right] \quad (13)$$

is given by,<sup>9</sup>

$$\bar{\sigma} = \sigma_0 \Gamma\left(1 + \frac{1}{m}\right) \quad (14)$$

Thus for the tensile distribution in Eq. (4) the mean strength is,

$$\bar{\sigma}_t = \sigma_0 \left(\frac{A_0}{2\pi r l_t}\right)^{\frac{1}{m}} \Gamma\left(1 + \frac{1}{m}\right) \quad (15)$$

and similarly the mean strength for a constant bend radius from Eq. (12) is,

$$\bar{\sigma}_b = \sigma_0 \left(\frac{A_0}{2r l_b G(m)}\right)^{\frac{1}{m}} \Gamma\left(1 + \frac{1}{m}\right) \quad (16)$$

The ratio of the mean strength for a fiber with a constant bend radius to mean tensile strength is then,

$$\frac{\bar{\sigma}_b}{\bar{\sigma}_t} = \left[\frac{\pi}{G(m)} \frac{l_t}{l_b}\right]^{\frac{1}{m}} \quad (17)$$

Thus, the mean strength in bending can be predicted given the mean tensile strength, the ratio of tensile to bend lengths and the Weibull slope parameter,  $m$ . This analysis is particularly useful since mean bend strength for a constant bend radius cannot easily be measured. Figure 12 is a plot of the ratio of mean strengths in Eq. (17) for a 20 meter tensile length and a range of bend lengths. As the Weibull slope,  $m$ , increases, i.e., variability in flaw size decreases, the difference in mean strengths decreases. For  $m$  values less than 15 the ratio of mean strengths is a strong function of the variability in flaw size.

An alternate expression for the failure probability in bending is obtained by substituting the value for  $\sigma_0$  in Eq. (15) into Eq. (12) giving,

$$F = 1 - \exp\left[-\left(\frac{\sigma_b}{\sigma_t}\right)^m \frac{1}{\frac{\pi}{G(m)} \frac{l_t}{l_b}} \Gamma^m\left(1 + \frac{1}{m}\right)\right] \quad (18)$$

Knowing the mean strength for a given tensile strength distribution and the unimodal Weibull slope, one can calculate the failure probability for a given bend stress and bend length.

### Equivalent tensile length.

It is difficult to determine the flaws that are of greatest reliability risk for bending applications, due to the complexity of the stress distribution over the fiber surface. Large flaws near the neutral axis are of lower risk than small flaws at  $\theta = \pi/2$ . It therefore is helpful to translate the bend

condition to an equivalent tensile condition.<sup>9</sup>

The equivalent tensile test length,  $l_{eq}$ , for a given bend length,  $l_b$ , is determined where the mean tensile strength equals the mean bend strength in Eq. (17),

$$l_{eq} = \frac{G(m)}{\pi} l_b \quad (19)$$

Equation 18 is plotted in Figures 13 and 14 for the equivalent tensile length as a function of bend length, for both long- and short-length applications, respectively. For an  $m$  value of approximately 15, the equivalent tensile length is nearly 1/10th the bend length. That is to say, a 1 kilometer length in bending is equivalent to testing 100 meters in tension. This analysis is helpful in determining the appropriate strength testing requirements for reliability prediction. For example, a bending application involving a total of 1000 kilometers requires tensile data for approximately 100 kilometers of fiber.

### Summary

Long-length strength distributions are necessary for making failure predictions at very low probabilities. In this paper, a 386 kilometer strength distribution was examined in light of theoretical distributions of proof tested fibers. This distribution showed the beginnings of the classical truncated distribution associated with proof testing; however, it lacked data near the proof stress level where Weibull slopes are believed to be on the order of  $n$ . The distribution was extended to strength levels near the proof stress level in a conservative fashion using conventional Weibull statistics. This composite distribution was then scaled to a variety of lengths for both bending and tensile applications.

Even though bending only stresses 10 to 20% of the fiber surface when compared to tension, bending applications need be concerned with flaws near the proof stress level, particularly for high reliability requirements. Such analyses are needed for reliability predictions and in determining strength testing requirements for various tensile and bending applications.

### References

1. K.E. Lu, G.S. Glaesemann, M.T. Lee, D.R. Powers, and J.S. Abbott, "Mechanical and Hydrogen Characteristics of Hermetically Coated Optical Fiber," *Opt. Quantum Electron.* 22, 227-237 (1990).
2. G.S. Glaesemann and D.J. Walter, "Method of Obtaining Long-length Strength Distributions for Reliability Prediction," *Opt. Eng.*, 30 (6), 746-748 (1991).
3. E.R. Fuller, Jr., S.M. Wiederhorn, J.E. Ritter, Jr., P.B. Oates, "Proof Testing of Ceramics, Part 2: Theory," *J. Mater. Sci.*, 15, 2282-2295 (1980).
4. G.S. Glaesemann and S.T. Gulati, "Dynamic Fatigue Data for Fatigue Resistant Fiber in Tension vs. Bending," in *1989 Technical Digest Series, Vol. 5, Proc Optical Fiber Communication Conference*, 48 (1989).

5. G.S. Glaesemann, M.L. Elder, and J.W. Adams, "Dependence of fatigue resistance on Titania doping of silica-clad optical fiber," presented at Optical Fiber Communication Conference, post-dead paper PD13-1 - PD13-4 (1990).

6. J.E. Ritter, Jr, N. Bandyopadhyay, and K. Jakus, "Statistical Reproducibility of the Dynamic and Static Fatigue Experiments," Amer. Ceram. Soc. Bul. 60 (8) 798 - 806 (1981).

7. W. Weibull, "Statistical Distribution Function of Wide Applicability," J. Appl. Mech., 18(3) 293-297 (1951).

8. W.D. Scott and A. Gaddipati, "Weibull Parameters and the Strength of Long Glass Fibers," in *Fracture Mechanics of Ceramics*, Vol. 3, edited by R.C. Bradt, D.P.H. Hasselman and F.F. Lange (Plenum Press, New York, 1978) pp. 125-42.

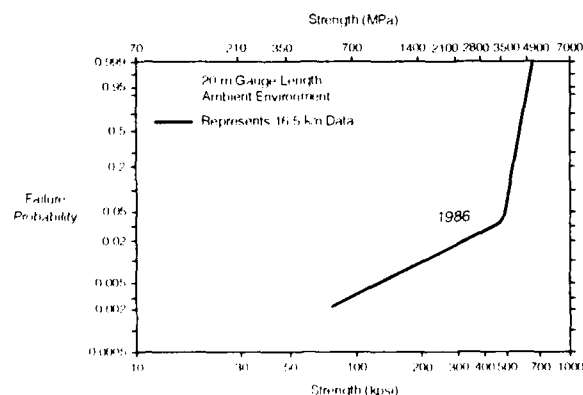
9. M.J. Matthewson, C.R. Kurkjian, and S.T. Gulati "Strength Measurement of Optical Fibers by Bending," J. Am. Ceram. Soc., 69 (11) 815-821 (1986).

10. G. S. Glaesemann, S. T. Gulati, and J. D. Helfinstine, "The Effect of Strain and Surface Composition on Young's Modulus of Optical Fibers", Optical Fiber Communication Conference, 1988 Technical Digest Series, Vol. 1 (Optical Society of America, Washington, DC 1988), p. 26.

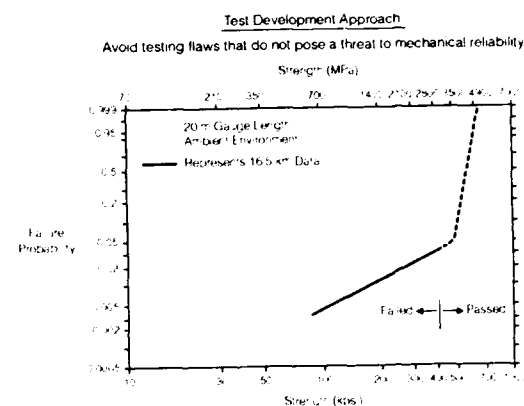
11. J.T. Krause, L.R. Testardi, and R.N. Thurston, "Deviations from Linearity in the Dependence of Elongation upon Force for Fibers of Simple Glass Formers and of Glass Optical Lightguides," Phys. Chem. Glasses 20(6) 135-139 (1979).

12. M. Abramowitz and I.A. Stegun, Handbook of Mathematical Functions. Dover, New York, 1964.

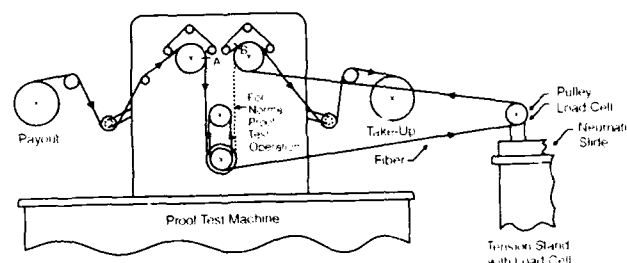
**Figure 1.**  
**Strength Distribution of Standard Silica-Clad Fiber**



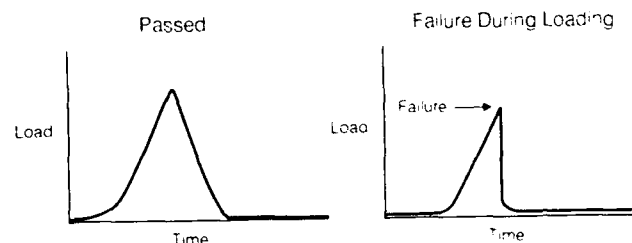
**Figure 2.**  
**If Every 20 m Specimen Stressed to Only 400 kpsi (2800 MPa)**



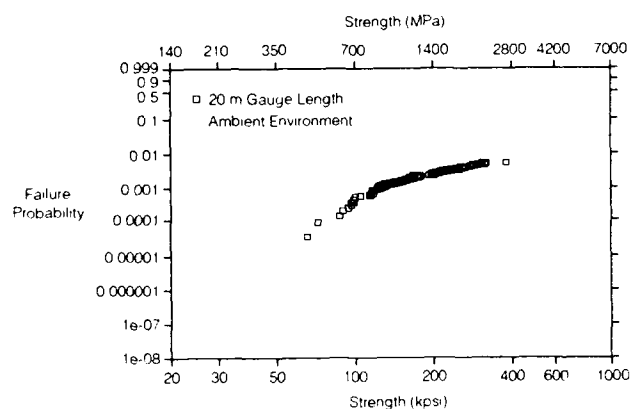
**Figure 3.**  
**Schematic of Continuous Fiber Strength Test Apparatus**



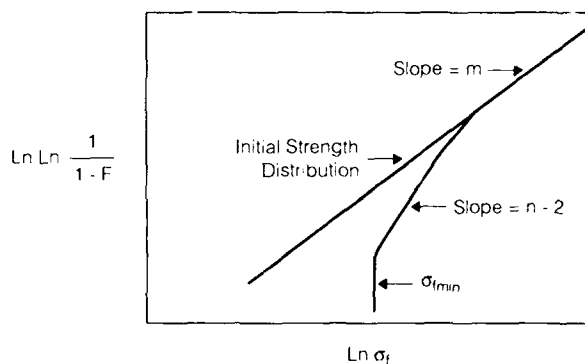
**Figure 4.**  
**Loading Cycle of 20 Meter Gauge Length**



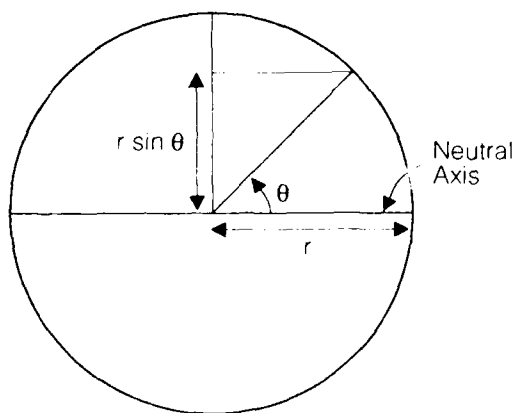
**Figure 5.**  
Strength Distribution of 386 Kilometers of  
Titania-Doped Silica-Clad Fiber



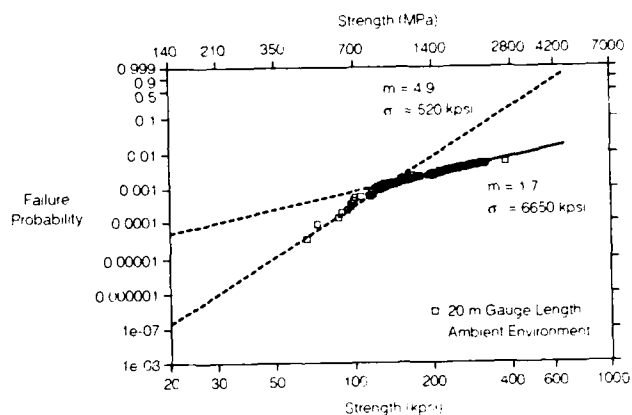
**Figure 6.**  
Theoretical Strength Distribution after Proof Testing  
Reference 3.



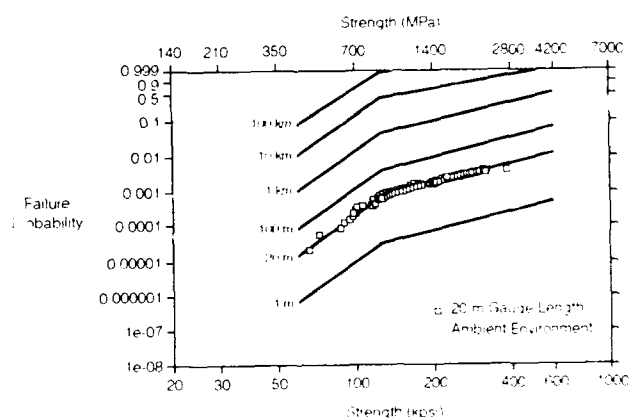
**Figure 7.**  
Cross-Section of Fiber



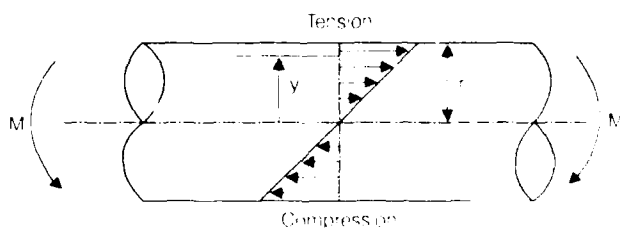
**Figure 8.**  
Composite Long-Length Strength Distribution



**Figure 9.**  
Failure Probability Predictions for Tension

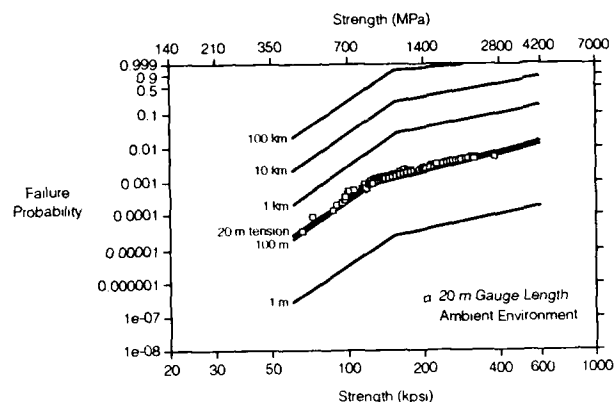


**Figure 10.**  
Fiber in Bending

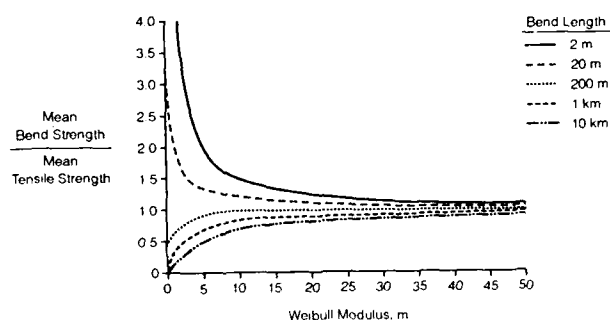




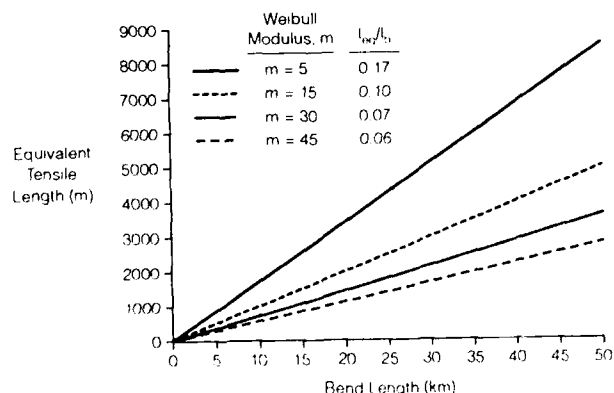
**Figure 11.**  
**Failure Probability Predictions for Bending**



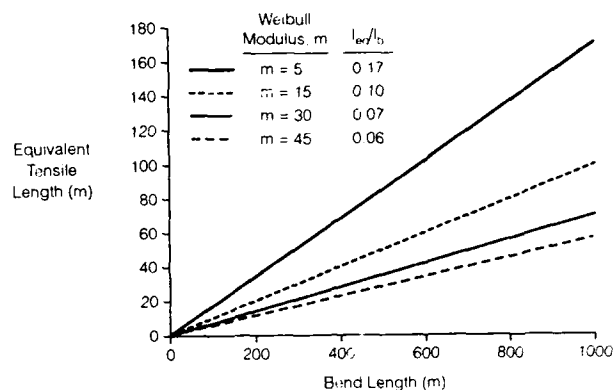
**Figure 12.**  
**Predicted Mean Bend Strength**  
**20 Meter Tensile Measurement**



**Figure 13.**  
**Equivalent Tensile Test Length for Bent Fiber**  
**Long-Lengths**



**Figure 14.**  
**Equivalent Tensile Test Length for Bent Fiber**  
**Short-Lengths**



G. Scott Glaesemann, SP-DV-01-8 Corning Inc., Corning, N.Y. 14831. Glaesemann is a senior development engineer responsible for the optical waveguide strength laboratory at Corning. He has been employed by Corning for five years at the Sullivan Park research and development facility. Glaesemann received his master's degree and Ph. D. in mechanical engineering from the University of Massachusetts and a B. S. in mechanical engineering from North Dakota State University. He is a member of the American Ceramic Society.

# LABORATORY TESTING AND FAILURE ANALYSIS OF FIBER INTERCONNECTIONS

T. (Mike) Wei

GTE Laboratories Incorporated, Waltham, MA 02254

and

Hakan H. Yuce

Bellcore, Morristown, NJ 07960

## SUMMARY

Standard laboratory tests under harsh environmental conditions are routinely carried out on splice and connector products so they can meet performance specifications and reliability requirements. However, degradation and even failures could still occur to fiber interconnections in the field. These field problems provided opportunities for a better understanding of factors which impact the reliability of fiber interconnections in practical uses. By analyzing field samples of splices and connectors, we have learned how they degraded or failed during installation or in a service environment. These field problems were attributed to poor product quality, deficiency in installation practices, or severe service environment. In cases of new failure mechanisms, continuing development of new test procedures will be needed to address these specific reliability concerns so future laboratory testing can better assure the reliability of the fiber network.

## INTRODUCTION

With the migration of optical fiber into the subscriber loop, both performance and reliability requirements of fiber components have to be reconsidered. On one hand, enhancements in performance and reliability of commercially available optical fibers have been actively pursued; on the other hand, concerns over reliability of splices and connectors are now being addressed. These concerns are heightened by the continuing introduction of new products into the marketplace and eventually the fiber network.

To assure that interconnection products meet performance and reliability requirements, several standard tests under harsh environments are routinely performed in the laboratory to simulate accelerated aging under service conditions.

Nevertheless, occasional performance degradation and even failures, such as discontinuity, increased insertion loss or increased reflection, could still appear during installation or service. Postmortem analyses were at times conducted to elucidate the causes of field problems. These recurring problems point out the urgent need for better knowledge of factors which affect the reliability of splices and connectors in practical applications.

In this study, various analytical techniques,<sup>1</sup> such as optical microscopy, scanning electron microscopy (SEM) and x-ray imaging, were used to evaluate failed splices and connectors. Analyzing field samples have offered us unique opportunities to learn how connectors and splices degraded or failed during installation or in a service environment. In most cases, breakdowns were directly linked to hardware or fiber failures, defects, or loss of fiber retention.<sup>2</sup> These problems can then be attributed to poor product quality, deficiency in outside plant practices, or severe service environment.<sup>3</sup>

Failure analyses of field samples, complementary to standard environmental and aging tests, have provided useful information about degradation and failure mechanisms in splices and connectors. These field problems may not otherwise be possible to reproduce in a laboratory. Understanding field failures will then contribute to the development of new test procedures, and further improvements in product designs or outside plant practices.

## INSTALLATION OF SPLICES AND CONNECTORS

Most interconnection products have to pass a series of optical, mechanical and environmental tests in the laboratory. These tests are based on standard fiber optic test procedures (FOTPs) issued by Telecommunications Industry Association (TIA). The majority of over twenty FOTPs for

splices and connectors involve measurements of optical performance under various environmental conditions. However, laboratory tests might not guarantee that all products survive a trouble-free service life, while new failure mechanisms are being discovered in field samples. Only with a good understanding of degradation and failure phenomena, can new test procedures be developed to detect them in laboratory testing.

Currently, field problems can happen to factory-built connectors, or field-installed splices and connectors, despite going through strict qualification processes. Aside from poor product quality, field problems of fiber interconnections usually originate from inadequate or improper assembly practices.

Whereas there are a wide variety of splice and connector products, three basic operations are common to most assembly practices:

(1) Fiber preparation: It includes coating stripping, fiber cleaning and cleaving/polishing operations, so two pieces of fiber can be joined and aligned.

(2) Fiber alignment: Both active or passive alignment techniques are used to assure low insertion loss and low reflection. The specific alignment method to be used depends on applications, interconnection designs, and cost and performance requirements.

(3) Fiber retention: Maintaining fiber alignment and mechanical integrity of a splice or connector over the service life is the key to its long-term reliability.

### SOLVING FIELD PROBLEMS

Most field problems are related to products of poor quality or deficiencies in assembly practices, in which several operations could potentially jeopardize reliability of the fiber link. For example, effects of environmental conditions on reliability are closely related to the design and materials properties of each product.

During assembly, although both stripping and cleaning operations will not influence the optical performance of splices and connectors, they inevitably degrade fiber strength and may affect the long-term reliability of fiber interconnections.<sup>4-6</sup> The cleave angle of fiber influences performance of fusion splices, and the finish of fiber ends impacts connector performance. In addition, field-installed splices and connectors could become more vulnerable if craftspeople are exposed to poorly maintained field tools, inadequate practices or training, and difficult working conditions.

Because of one or more of these factors, splices and connectors, despite passing a series of inspection and environmental tests, could occasionally fail during installation or service. Most field problems can be put into three categories:

(1) Discontinuity in a fiber link: An "open" line is most likely caused by fiber failure due to stress-induced fatigue.

(2) Increase in insertion loss: Increasing fiber separation in a mechanical splice or a connector can result in an intermittent or permanent increase in the insertion loss.

(3) Increase in reflection: Contamination, fiber fracture, and loss of fiber retention can cause an intermittent or permanent increase in reflection (decrease in the optical return loss) of a splice or connector.

### Analytical Techniques

Since different splice or connector products use different designs and materials, the failure mechanism of each product could be unique. A single analytical technique may not be able to provide an exact diagnosis. Sometimes, combining several analytical techniques allows the failure mechanism to be more clearly identified.

Several analytical techniques<sup>1</sup> have been used in determining the cause of failure and identifying the location and composition of each defect. Table 1 summarizes techniques used in analyzing field samples and their applications. These include optical microscopy,<sup>4</sup> SEM (with energy dispersive x-ray spectroscopy and backscattered electron imaging), and x-ray imaging.

Table 1.  
List of Analytical Techniques for Failure Analysis

Analytical Technique	Applications
<i>Optical Microscopy</i>	Fractographic analysis, defect locating
<i>Scanning Electron Microscopy</i>	Fractographic analysis, defect locating
<i>energy dispersive x-ray spect.</i>	Defect identification
<i>backscattered electron imaging</i>	Defect locating
<i>X-ray imaging</i>	Defect locating

### Examples of Failure Analyses

(1) During fusion splicing, a section of fiber was found impossible to splice. SEM techniques revealed the presence of an "air line" defect inside this section of fiber. Figure 1 shows the backscattered electron image of a cleaved fiber end. From the energy dispersive x-ray spectroscopy, contamination of aluminium was found near the defect site, which was located outside the fiber core. Such a defect was most likely formed from an air bubble inside the preform during fiber drawing.

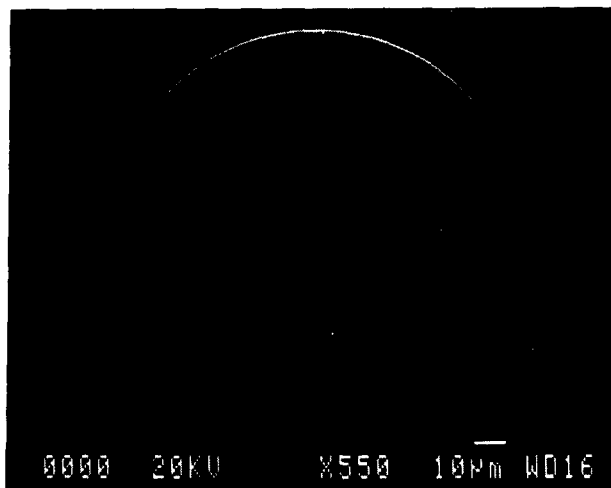


Figure 1. Backscattered electron image of the fiber endface, showing the "air line" defect.

(2) A high failure rate of connectors was experienced during installation. Figure 2 taken from x-ray imaging reveals that the fiber fractured near the entrance to the glass capillary. Fiber failures were most likely linked to damage suffered during fiber preparation.

(3) When mechanical splices failed prematurely, SEM and optical microscopy were used for fractographic analyses of fiber pieces inside the splice samples. Figure 3 presents an SEM micrograph of the fractured fiber removed from a splice sample. The shape of the fracture surface indicated that it was resulted from the presence of a high torsional stress. The stress was most likely introduced when the splice was placed inside the closure.

These and other field samples have served to demonstrate the benefits of failure analysis. That is, laboratory testing could not fully assure the reliability of splices and connectors without continuing development of new tests to address specific failure mechanisms.

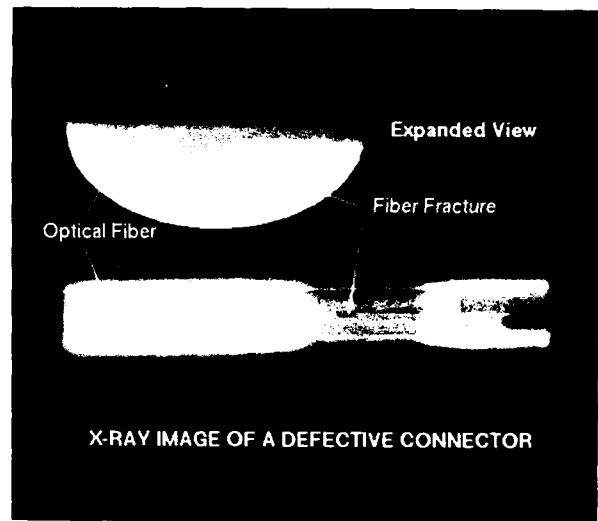


Figure 2. X-ray image of a failed connector. The break in the lighter color image of fiber indicates where the fiber fractured.

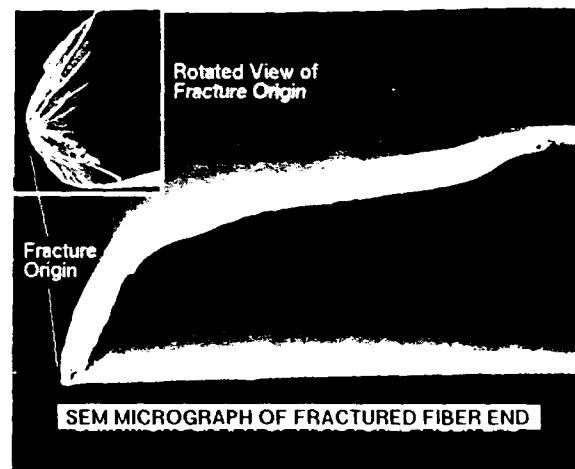


Figure 3. SEM micrograph of the fractured fiber removed from a mechanical splice, showing the presence of a high torsional stress.

### CONCLUSION

Various analytical techniques have been applied to failed field samples and provided useful information about failure mechanisms in splices and connectors. Such information, otherwise difficult to gather in laboratory testing, should constitute the basis for further improvements in product designs or installation practices. Continuing development of new laboratory tests to address specific reliability issues should then better assure the reliability of the fiber network.

### ACKNOWLEDGMENTS

The authors thank Daniel Cotter, Brian Devlin, William Koenigsberg and Donna Thomas for their technical assistance in analyzing field samples.

### REFERENCES

1. H.H. Yuce and T. Wei, "Application of analytical methods in fiber reliability studies," to be presented at SPIE OE/FIBERS '91, Boston, MA, paper #1580-65 (1991).
2. W.C. Young, "Introduction to reliability-related problems in optical fiber connectors," *Optical Engineering* **30**, 821 (1991).
3. T.N. Bowmer, R.J. Miner, and R.C. Coker, "Field temperatures in outside plant," *Proc. 39th IWCS*, p. 335 (1990).
4. W.R. Wagner, "Failure analysis of fiber optic connectors," *Advances in Ceramics* **22**, 389 (1988).
5. T. Wei, H.H. Yuce, C.H. Hasz, and P.L. Key, "Degradation of fiber strength during coating stripping," *Proc. 38th IWCS*, p. 199 (1989).
6. H.H. Yuce, P.L. Key, and T. Wei, "Mechanical reliability considerations for fusion splices in optical fibers," *Proc. 39th IWCS*, p. 400 (1990).

T. (Mike) Wei is a Research Supervisor in the Optical Fiber and Components Department of GTE Laboratories Incorporated, 40 Sylvan Road, Waltham, MA 02254, where he is responsible for fabrication, characterization, and reliability studies of optical fiber and components. Mike provides technical support and consultation services in fiber optic technology to telephone operating companies within GTE. He is an active participant of EIA/TIA working groups on fiber coatings and fiber reliability. He received a Ph.D. degree in physics from the University of Pennsylvania (1976), and has been involved in optical fiber research since 1978.

Hakan Yuce is a Member of the Technical Staff in the Fiber Distribution and Reliability Research District at Bellcore, 445 South Street, Morristown, NJ 07960. He leads a research program dealing with long-term mechanical reliability of optical fibers and interconnections. Hakan provides technical input and support to organizations responsible for generic requirements and responds to clients' immediate needs related to consultation on reliability and field failures. He also plays an active role in the standards arena under EIA/TIA working committees 6.6.7, fiber coatings, and 6.6.8, fiber reliability. Hakan has a B.S. degree in Mechanical Engineering from Technical University of Istanbul (1977), an M.S. in Mechanical Engineering from MIT (1982), and a Ph.D. degree in Mechanical Engineering and Material Science from Stanford University (1987).

# Computerized Acceptance Test on Field-installed Optical Fibre Cables; Applications and Results

Horst Middel, Gerhard Schweiger

Deutsche Bundespost Telekom, FTZ Darmstadt, Germany

## Summary:

The structure of the types of optical fiber cable used in the DBP T trunk network (FLN) is introduced in brief. The bridgeable repeater spacings are presented in relation to the fiber quality used and the number of splice joints. This is followed by a breakdown of the quantity of optical fiber cables currently installed in the DBP T network, with a look ahead to developments in the coming years. Following a basic description of the acceptance measurements conducted on already installed optical fiber cables, the method of computerized acceptance tests using a PC is described in detail. Subsequently the evaluation of the measured data is explained with reference to examples and the results of the evaluation are discussed. In conclusion, a brief outline is provided of the prospects for potential future developments.

## 1. Cable specifications and planning rules

From the very outset, DBP T has used optical fiber cables with bundle conductors which are laid up around a central element made from glass fiber-reinforced plastic. Depending on the cable type, the bundle conductors can contain 2, 4 or 10 fibers and are filled with a special filler. The cable core contains a further 2 to 4 copper wires for maintenance purposes and is filled with petroleum jelly for longitudinal water tightness.

The cable jacket comprises an aluminum composite layer sheath with glass and aramide yarns bonded on the inside for strain relief purposes. Figure 1 shows a typical basic structure of the optical fiber cables.

The fibers used are single mode fibers with an attenuation of max. 0.36 dB/km (trunk network) and 0.45 dB/km (local network) with 1310 nm and a maximum dispersion of 3.5 ps/nmkm (trunk network) and 5 ps/nmkm (local network).

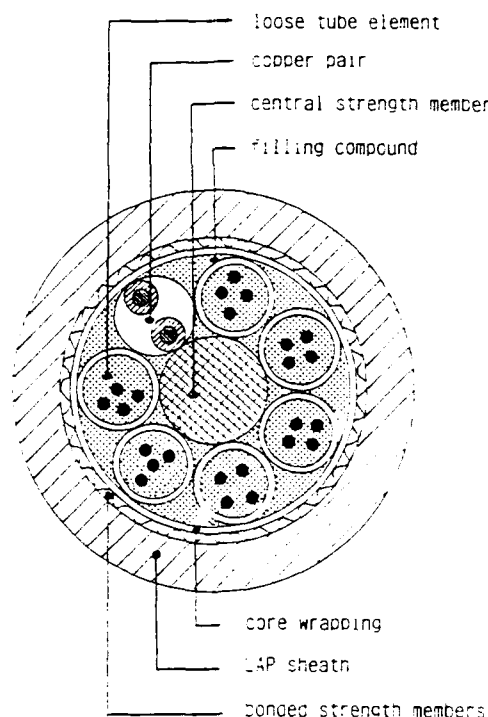


Figure 1: 24 fibre cable

Assuming a splice loss of 0.1 dB/km (trunk network) and 0.2 dB/km (local network) and a maintenance margin of 0.18 dB/km, repeater spacings of 36.4 km (trunk network) and 24 km (local network) can be bridged. The maximum system bit rate is currently 565 Mbit/s in the trunk network and 140 Mbit/s in the local network.

## 2. Optical fiber cables installed in the DBP T network

DBP T began laying the first test sections with

optical fiber cables in 1979/1980. From 1983 onwards optical fiber cables with graded index fibers were installed in the trunk network. Since 1985 new cable lines laid in the trunk network have consisted exclusively of optical fiber technology with single mode fibers. From 1986 to 1990 an optical fiber overlay network was established in 29 major German cities and this is being added to continuously.

Optical fiber technology has also been used almost exclusively in recent years for the local junction cables for digital operation between local exchanges installed. Finally, since 1990 and following German reunification, optical fiber cables only have been used from the very outset to develop the new trunk network in East German states. Figure 2 provides an overview of the quantities of optical fiber cable installed in the trunk and local networks since 1980 and 1986 respectively as well as the planned figures until 1993:

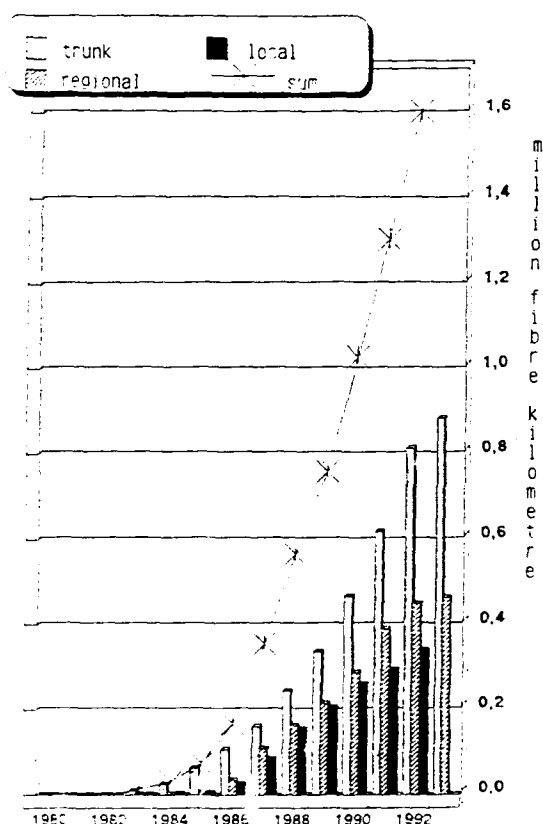


Figure 2: Optical fibres in the network of the Deutsche Bundespost TELEKOM

By the end of 1990, therefore, 46,700 km of cable with 756,000 km of fiber had been installed in the trunk network, and 15,000 km

of cable with 262,100 km of fiber utilized in the local network: in other words, already over 1 million km of fiber have been installed in the DBP T network. In 1991 alone some 1,800 km of cable with over 53,000 km of fiber will be laid in the new trunk network of the acceding East German states.

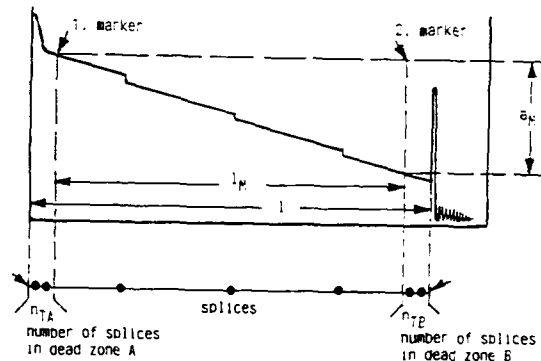
### 3. Regulations for acceptance tests

In principle, "acceptance tests" are conducted on all optical fiber cables once installed. This involves comparing the determined desired value (fiber attenuation plus splice loss) with the measured actual total loss value. All measurements are conducted with OTDR. The calculations allow for the areas of the dead zones at the beginning and end of the measuring path. Figure 3 shows the calculation of desired and actual attenuation values for a cable section again in detail:

desired value:

$$A_{des} = l \times \alpha + n \times a_s$$

actual value:



$$A_{act} = a_m + (1-l_m) \times \alpha + (n_{TA}+n_{TB}) \times a_s$$

- $l$  = total section length (km)
- $\alpha$  = attenuation coeff. = 0.36 dB/km
- $n$  = total number of splices
- $a_s$  = splice loss = 0.1 dB
- $l_m$  = measured length (km)
- $a_m$  = measured loss (dB)

Figure 3: Determination of the desired ( $A_{des}$ ) and the actual ( $A_{act}$ ) value of the section loss

If the actual value measured exceeds the predetermined desired value a "fault analysis" measurement must be conducted on the fiber concerned in order to detect the exact cause of the fault. This involves measuring each individual fiber attenuation coefficient and splice loss at both ends of the cable line and then calculating the arithmetical average.

A measurement of this kind can also be conducted as a "section analysis" on all the fibers making up a cable. This provides a large

number of data indicating the level and statistical distribution of the fiber attenuation and splice loss in installed optical fiber cables. However, these measurements are extremely time-consuming with the result that the decision was taken in 1988 to conduct such measurements on only 2 fibers in the cable in each case. The results were passed to the FTZ for statistical evaluation.

#### 4. Implementation of computerized acceptance tests

In 1988 as well, investigations were under way into possible "computerized" methods of performing acceptance tests. These were generally also to include section analysis for all the measured fibers. In addition to the total section loss (fiber attenuation plus splice loss) detailed information could consequently be obtained about the statistical distribution of fiber attenuation in the individual cable segments and of splice loss thanks to the large volume of measured data available.

In certain cases the data thus obtained permitted adjustment of existing planning data, that is worst case planning could be modified in favor of plans based on statistics.

"Computerized" measurements of this kind can already be implemented by several OTDR types with the aid of an integrated software program. However, this has the disadvantage that, under certain circumstances, splice loss is either measured at the wrong location or is not detected at all and consequently not included in the statistical evaluation since the splices are regarded as very good.

For this reason appropriate software was developed in 1989 for controlling the existing OTDR by PC. Computerized tests have been carried out on all trunk cables in a total of 10 agencies since the beginning of 1990. In 6 out of the 10 agencies, the measurements are conducted with both 1310 nm and 1550 nm.

Let us now take a closer look at how the computerized acceptance test is conducted with the aid of an example. Figure 4 shows the basic set-up of the measuring station.

A commercially available OTDR with pulse widths and total dynamics suitable for conducting measurements on long cable lengths is controlled by a personal computer (PC) via a GPIB interface. For practical reasons, the printer is best located in a central position in the office. The item being measured is connected to the OTDR with single mode PC connectors by means of a 10 m jumper cable

Before measuring begins, data including line number, total length, cable type, number of fibers, number of cable segments, length of measuring lead, cable manufacturer,

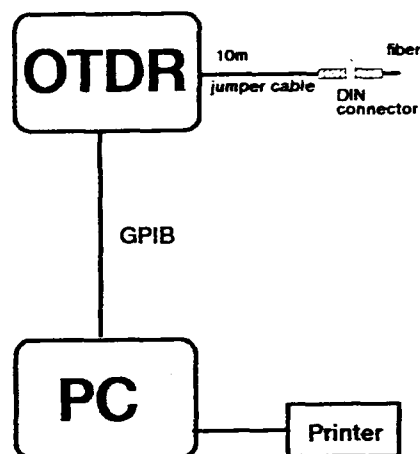


Figure 4: Test assembly for the automatic measurement

installation company and length of the individual cable segments is entered in the PC as shown in table 1.

#### Display of line data 24.07.1991

OPD:Stuttgart FA/DSt:FA 2/FKB  
 Name:Held  
 Type of line:ISFVK Line No.:030752  
 Sector No.:1 Sector:Stgt 10 -- Stgt 20  
 OTDR:Anritsu Serial No.:69753  
 Type:MW 910C/955C  
 Cable supplier:SEL/F  
 Cable type:A-DSF(L)(ZN)2Y.10x4E.0,38F...  
 Number of fibers:40  
 Number of splice joints:10  
 Length of sector (m): 13518.9  
 Length of measuring lead (m): 9.0

#### Length overview 24.07.1991

##### No. Cable segment length (m)

1	2.0
2	46.1
3	1911.8
4	1895.7
5	1882.3
6	1928.8
7	1808.5
8	1967.2
9	2045.2
10	29.3
11	2.0

Length of sector (m): 13518.9  
 Length of measuring lead (m): 9.0  
 Number of cable segments: 11  
 Desired value of section loss (dB): 5.867

Table 1: Input of the relevant section data



The computer then calculates the desired value and effects the OTDR settings necessary for section measurement and modified to suit the section's specific requirements (selection of distance range, selection of the pulse width in line with the section being measured, adjustment of the refractive index by measuring the end reflex).

Next the system determines the total loss of the section, followed by the actual value, allowing for the dead zones at the beginning and end of the cable section in the calculation as in manual measurement. Table 2 shows extracts from a typical result log:

#### Acceptance test

Type of line: ISFVk Line No.: 218105/001  
Sector: Koblenz11 -- Bad Ems4  
Date: 20.06.1990  
Desired value of section loss (dB): 6.713

#### Measurement of section loss with 1310 nm wavelength

Fiber No.	Input value A	Ref. index A	Measured length A	Measured value A
1	52.533	1.4797	14881.0	5.697
2	53.163	1.4790	14881.0	5.498
3	52.724	1.4790	14872.0	5.299
4	52.176	1.4799	14879.0	5.753

Fiber No.	Section loss A	Input value B	Ref. index B	Measured length B
1	6.253	52.600	1.4797	14881.0
2	6.051	50.514	1.4790	14881.0
3	5.858	53.720	1.4806	14872.0
4	6.310	50.581	1.4799	14879.0

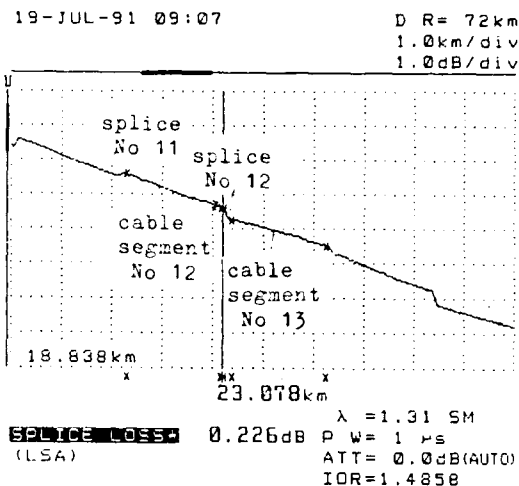
  

Fiber No.	Measured value B	Section loss B	Av. section loss	Actual > desired?
1	5.823	6.379	6.316	no
2	5.372	5.925	5.988	no
3	5.308	5.862	5.862	no
4	5.729	6.298	6.298	no

Table 2: Result of section loss measurement

This is followed by the section analysis during which the OTDR, under PC control, systematically measures each fiber attenuation coefficient and each splice loss of the fibers along the entire length of the cable. All the settings made here comply with those possible with manual measurement allowance made for the dead zone, optimum setting of markers for measuring the fiber attenuation coefficient (2 markers) and splice loss (5 markers), minimum length < 300 m for measuring the fiber attenuation coefficient, end reflex masking

etc. The operator monitors these settings, as shown in Figure 5 taking a single splice loss measurement as an example, and has an opportunity of accepting them as satisfactory after each setting or of intervening manually. This prevents incorrect measurements that could be made by an individual length being entered incorrectly, for example, (measurement of the splice loss at the wrong location).



Measurement of attenuation coefficient / cable segment No.				OTDR:
Line:	ISFVk 838678 2	Splice/cable segment No.	Splice loss (dB)	Fiber att. coeff. (dB)
Measuring location:	Darmstadt			
Sector length (m):	33562.4			
Measuring lead (m):	18.0			
Number of fibers:	12			
Number of splice join:				
Desired attenuation:				
OTDR setting?				0.143 0.496
Setting OK				0.238 0.327
Manual setting adjustment				0.128 0.419
				0.105 0.454
				0.837 0.458
				0.395 0.423
				0.265 0.283
Fiber No.:				
Measuring wavelength:				
Input value:				
Effective refractive index:	1.4858	9	0.262	0.400
Measuring length (m):	33114.0	10	0.224	0.421
Measured value (dB):	16.458	11	0.155	0.558
Section loss (dB):	16.811	12	0.225	
Breach of upper limit:	yes			

Figure 5: Control of cursor points

Figure 6 shows the practical layout of a typical measuring station in an exchange during the acceptance test on an optical fiber cable support rack.

All these measurements are now conducted on all the fibers in a cable and from both ends of the section. The PC then calculates the average splice loss and fiber attenuation coefficient values.

The results of these measurements are subsequently printed out in the office in log form. They are used to verify and document the cable's suitability for measurement qualification purposes. In addition, the results for each cable line are stored on floppy disk and sent to the FLZ twice a year.



Figure 6: Typical measuring station

Table 3 shows extracts from a typical log:

#### Acceptance test

Type of line: ISFVk Line No.: 218105/001  
 Sector: Koblenz11 -- Bad Ems4  
 Date: 20.06.1990  
 Desired value of section loss (dB): 6.713  
 Page No.: 3.0

#### Measurement of fiber attenuation coefficient and splice loss with 1310 nm wavelength

Fiber No.: 1

Cable segment No.	1	2	3
Attenuation coefficient A	-----	-----	0.345
Attenuation coefficient B	-----	-----	0.346
Av. attenuation coefficient	-----	-----	0.346

Splice No.	1	2	3
Splice loss A	-----	-----	0.024
Splice loss B	-----	-----	0.132
Av. splice loss	-----	-----	0.078

4	5	6	7
0.340	0.358	0.321	0.352
0.378	0.354	0.350	0.335
0.359	0.356	0.336	0.344

4	5	6	7
0.014	0.101	0.117	0.15
0.004	-0.008	0.192	0.183
0.009	0.046	0.154	0.162

Table 3: Results of fiber attenuation coefficient and splice loss measurement

Fiber No.: 2

Cable segment No.	1	2	3
Attenuation coefficient A	-----	-----	0.345
Attenuation coefficient B	-----	-----	0.330
Av. attenuation coefficient	-----	-----	0.338

Splice No.	1	2	3
Splice loss A	-----	-----	0.024
Splice loss B	-----	-----	0.116
Av. splice loss	-----	-----	0.070

4	5	6	7
0.345	0.338	0.347	0.330
0.335	0.351	0.345	0.337
0.340	0.344	0.346	0.344

4	5	6	7
0.052	0.040	0.187	-0.022
0.026	0.024	0.021	0.158
0.039	0.032	0.104	0.068

Fiber No.: 3

Cable segment No.	1	2	3
-------------------	---	---	---

Table 3 (cont'd)

#### 5. Evaluation of measured data

The section data are transferred to floppy disk and forwarded to the FTZ. Here the data are automatically read into a PC for subsequent further statistical processing. The evaluation program developed specially for this purpose now allows the data to be summarized according to the following criteria:

1. Regional or supra-regional trunk network
2. Installation of cables by DBP T or by third parties
3. Differentiation between cable types with 2, 4 or 10 bundle conductors
4. Differentiation between various cable suppliers
5. Arrangement of data according to geographical districts

All these options can also be combined with each other as desired.

As Table 4 shows, the average values and standard deviation are evaluated initially as follows:

- Fiber attenuation coefficient for the entire section (in dB/km)
- Fiber attenuation coefficient for individual lengths (in dB/km)

- Splice loss (in dB) and
- The resultant average joint spacing

#### Statistical evaluation of the measured results by criteria

23.07.1991 13:39:40

Type of measurement: A  
Line No.: 030  
OPD: all  
Installation: F  
Cable supplier: all  
Fibers/bundle conductor: 4

Attenuation coefficient of installed section in dB/km with		
	1310 nm	1550 nm
Number of values	1236	912
Average value (Av.)	0.396	0.249
Standard deviation (SD)	0.025	0.029
Av. + 3*SD	0.473	0.337
Minimum value	---	---
Maximum value	---	---
Attenuation coefficient of individual lengths in dB/km with		
	1310 nm	1550 nm
Number of values	17976	13270
Average value (Av.)	0.345	0.199
Standard deviation (SD)	0.013	0.011
Av. + 3*SD	0.385	0.231
Minimum value	0.300	0.165
Maximum value	0.600	0.568
Splice loss obtained in dB with		
	1310 nm	1550 nm
Number of values	17047	12538
Average value (Av.)	0.062	0.053
Standard deviation (SD)	0.048	0.041
Av. + 3*SD	0.206	0.177
Minimum value	0.000	0.000
Maximum value	0.452	0.512

Average joint spacing (km): 1.804

Table 4: Statistical evaluation of several sections

The evaluation also shows the underlying number of measured values assessed. In addition, the table header indicates the criteria forming the basis of the evaluation. In the example these are:

- Line numbers 030 ... (supra-regional trunk network)
- All geographical districts

- All cable suppliers
- Summary of cables with 4 bundle conductors
- Installation by third parties (F)

Furthermore, the statistical distribution of the values can be shown in predetermined limit ranges. The program prints out the following distributions, as shown in Table 5:

- Distribution of splice loss with 1310 nm
- Distribution of splice loss with 1550 nm
- Distribution of fiber attenuation coefficient with 1310 nm
- Distribution of fiber attenuation coefficient with 1550 nm

#### Distribution of splice loss with 1310 nm

Total	:	17074	100.0%
0.000 - 0.024 dB:		3498	20.5%
0.025 - 0.049 dB:		4870	28.6%
0.050 - 0.074 dB:		3591	21.1%
0.075 - 0.099 dB:		2064	12.1%
0.100 - 0.124 dB:		1331	7.8%
0.125 - 0.149 dB:		707	4.1%
0.150 - 0.174 dB:		438	2.6%
0.175 - 0.199 dB:		224	1.3%
0.200 - 0.224 dB:		134	0.8%
--> 0.025 dB:		190	1.1%

#### Distribution of splice loss with 1550 nm

Total	:	12538	100.0%
0.000 - 0.024 dB:		3214	25.6%
0.025 - 0.049 dB:		4006	32.0%
0.050 - 0.074 dB:		2568	20.5%
0.075 - 0.099 dB:		1298	10.4%
0.100 - 0.124 dB:		704	5.6%
0.125 - 0.149 dB:		356	2.8%
0.150 - 0.174 dB:		165	1.3%
0.175 - 0.199 dB:		97	0.8%
0.200 - 0.224 dB:		56	0.4%
--> 0.025 dB:		74	0.6%

#### Distribution of attenuation coefficient with 1310 nm

Total	:	17976	100.0%
0.300 - 0.309 dB/km:		8	0.0%
0.310 - 0.319 dB/km:		102	0.6%
0.320 - 0.329 dB/km:		1366	7.6%
0.330 - 0.339 dB/km:		4832	26.9%
0.340 - 0.349 dB/km:		5079	28.3%
0.350 - 0.359 dB/km:		4186	23.3%
0.360 - 0.369 dB/km:		1709	9.5%
0.370 - 0.379 dB/km:		463	2.6%
0.380 - 0.389 dB/km:		144	0.8%
--> 0.390 dB/km:		87	0.5%

Table 5: Distribution of fiber attenuation coefficient and splice loss

(continued next page)

# Distribution of attenuation coefficient with 1550 nm

Total	:	13270	100.0%
0.160 - 0.169 dB/km:		6	0.0%
0.170 - 0.179 dB/km:		65	0.5%
0.180 - 0.189 dB/km:		1297	9.8%
0.190 - 0.199 dB/km:		6746	50.8%
0.200 - 0.209 dB/km:		3521	26.5%
0.210 - 0.219 dB/km:		1149	8.7%
0.220 - 0.229 dB/km:		327	2.5%
0.230 - 0.239 dB/km:		84	0.6%
0.240 - 0.249 dB/km:		31	0.2%
--> 0.250 dB/km:		44	0.3%

Table 5 (cont'd)

As shown in Figure 7, the distributions can be output in graphic form either as composite or individual graphs for enhanced clarity:

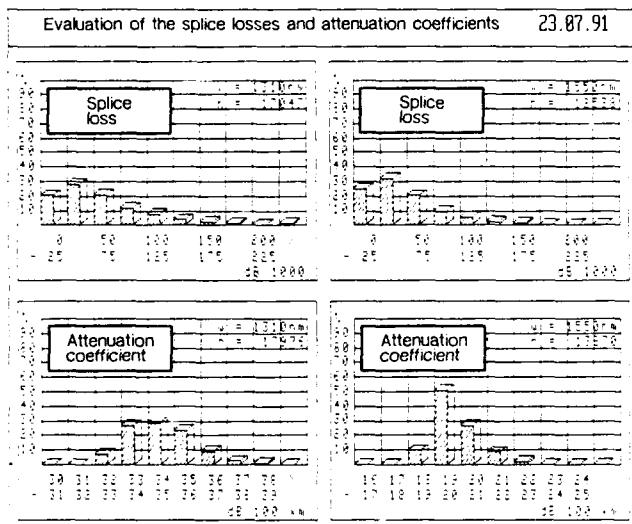


Figure 7: Graphical distribution of fiber attenuation coefficient and splice loss

This permits a comparison of relevant data which were summarized under different selection criteria in each case. Figure 8, for instance, compares Telekom-installed and company-installed sections of cable lines belonging to the regional trunk network with two fibers per bundle conductor.

In the same way the results of the fiber attenuation coefficient can be compared for the same type of cable produced by different manufacturers, for example.

## Evaluation of the splice losses

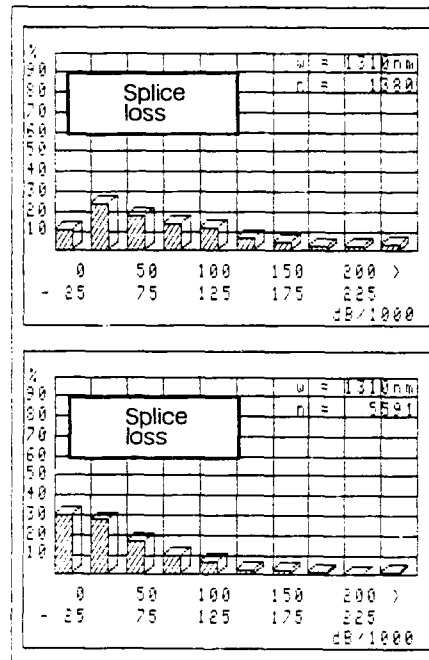


Figure 8: Comparison between e.g. company-installed and Telekom-installed sections

## 6. Discussion of results

Investigations such as these permit the following conclusions to be reached:

- Conclusions as to the overall configuration and general quality of the installed optical fiber cables in the various network areas
- Information on the quality of installation work, and
- Assessments of the delivery quality of the cables of different suppliers.

Table 6 shows the summarized results obtained on the basis of 356 optical fiber cable systems installed from 1990 to mid-1991.

## Statistical evaluation of the measured results by criteria

23.07.1991 11:29:35

Type of measurement: all  
Line No.: all  
OPD: all  
Installation: all  
Cable supplier: all  
Fibers/bundle conductor: all

Table 6: Total results from 356 cable sections

(continued next page)

Attenuation coefficient of installed section in dB/km with		
	1310 nm	1550 nm
Number of values	3678	2242
Average value (Av.)	0.417	0.275
Standard deviation (SD)	0.046	0.048
Av. + 3 * SD	0.556	0.420
Minimum value	---	---
Maximum value	---	---

Splice loss obtained in dB with		
	1310 nm	1550 nm
Number of values	37823	23396
Average value (Av.)	0.066	0.061
Standard deviation (SD)	0.056	0.058
Av. + 3 * SD	0.234	0.235
Minimum value	0.000	0.000
Maximum value	0.608	0.574

Attenuation coefficient of individual lengths in dB/km with		
	1310 nm	1550 nm
Number of values	40881	25186
Average value (Av.)	0.346	0.200
Standard deviation (SD)	0.016	0.015
Av. + 3 * SD	0.395	0.246
Minimum value	0.300	0.160
Maximum value	0.600	0.589

Average joint spacing (km): 1.652

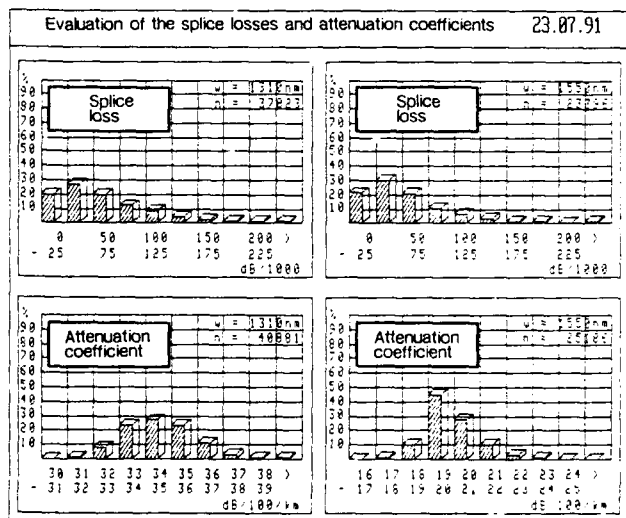


Table 6 (cont'd)

This evaluation is based on the data for a total of 3,678 measured fibers with 40,881 individual values for the fiber attenuation

coefficient and 37,823 values for measured splice loss.

Plans for cable lines in the trunk network are currently based on the following planning data (average values for installed cables):

- Fiber attenuation: less than 0.36 dB/km (with 1310 nm)
- Splice loss: less than 0.1 dB/km
- Distance between 2 splices: approx. 2 km

The following data are derived from the results of the depicted table:

- Measured average fiber attenuation: less than 0.345 dB/km
- Measured average splice loss: 0.07 dB, giving a value of 0.04 dB/km for the loss of one splice with an average splice spacing of 1.67 km.

If these empirical values are taken into account for planning purposes, a theoretical extension of the repeater spacing from 36,6 km to 40.6 km results for a 565 Mbit/s system.

This gain cannot be utilized, however, since the plesisynchronous 565 Mbit/s systems currently used are dispersion limited.

## 7. Future prospects

The computerized acceptance tests are scheduled for continuation at least until the end of 1992.

Critical appraisal will be made of any possible influences such as:

- The use of a new generation of thermal splicing tools with clearly improved splicing results
- The utilization of new cable types with central steel element and reduced diameter of the bundle conductors

Any conclusion will be drawn as regards possible modifications to planning data and changes to cable design.

As regards the future utilization of the installed optical fiber cables in the third window with 1550 nm, the data now available in statistical form will be a useful aid for operating the existing network with new services and future transmission facilities.



Horst Middel

Deutsche Bundespost  
Telekom

Am Kavalleriesand 3  
D 6100 Darmstadt  
Germany

Horst Middel received his diploma in telecommunication engineering in 1966 and joined the Deutsche Bundespost Telekom. Since 1974 he has been located in the Telecommunication Engineering Center (FTZ) in Darmstadt. He was engaged in the cable technique of copper and optical fibre cables and is now responsible for cable measurements.



Gerhard Schweiger

Deutsche Bundespost  
Telekom

Am Kavalleriesand 3  
D 6100 Darmstadt  
Germany

Gerhard Schweiger received his masters degree in electrical engineering from the Technical University in Munich 1957 and joined the Deutsche Bundespost Telekom in 1958. Since 1966 he has been located in the Technical Engineering Center (FTZ) in Darmstadt. He is currently Head of Division "Outside Plant".

## PLANNING FOR THE FUTURE: THE IMPORTANCE OF A STRUCTURED FIBER CABLING STRATEGY

Bryan Hatfield, Michael Coden, Brian Ramsey

CODENOLL TECHNOLOGY CORPORATION

This paper presents a migration strategy towards FDDI for fiber optic LAN wiring based on two basic concepts. The first concept, suggested by the Electronics Industries Association's (EIA) TR-41-8.1 working group, is the three tier wiring topology. This basic topology itself can be configured into ring, star or bus networks. The three-tier hub structure will virtually serve all network applications, including the very important case where a hierarchy of IEEE 802 LANs are interconnected by an FDDI backbone.

The second concept concerns the medium itself. In its current draft, EIA TR-41-8.1 does not recognize fiber as an option for the horizontal wiring. The strategy proposed here differs in this aspect and recommends fiber for both vertical and horizontal wiring.

The choice of fiber optic medium not only satisfies the current requirements of the IEEE 802 LANs operating in the range of 4 to 20 Mbps, but will equally well serve data speed requirements of 100 Mbps for FDDI and SMDS in the decades ahead. With current trends in the market, the cost of fiber has become compatible with shielded twisted pair. The initial incremental investment for fiber cable plant more than justifies itself, in terms of a simpler migration path to higher data rate services and applications without costly redesign and rewiring of office cable plant.

### INTRODUCTION

The increasingly rapid introduction of ever more powerful work stations and desktop computers, full screen graphics and high speed I/O peripherals has created a need to share and exchange information at ever increasing speeds. This need is reflected in the establishment of standards for local area networks (LANs).

The primary standards being implemented today are those of the IEEE 802 family - Carrier Sense Multiple Access with Collision Detect (CSMA/CD) or Ethernet (IEEE 802.3); Token Bus (IEEE 802.4) and Token Ring (IEEE 802.5). These standards define LANs which will operate at maximum data rates of 10, 20 and 16 Mbs respectively. Already it is perceived that these data rates will soon become limiting, if they are not already so, for many LAN applications. This explains then the very keen interest in the Fiber Distributed Data Interface (FDDI) standard currently under development by ANSI.

FDDI is a 100 Mbs data rate, token-ring LAN with an optical transmission rate of 125 Megabaud. It will accommodate as many as 500 nodes spaced up to 2 km apart. Typical applications which will utilize the high bandwidth available in FDDI include communication between main frames, as a backbone to interconnect lower-speed (eg. IEEE 802) LANs through file servers, bridges, gateways, and a means of linking workstations and high-end PCs especially in CAD/CAM/CAE, financial, advertising and other image processing environments.

Because of its very high speed, the FDDI standard has been written around optical fiber as the transmission media (F stands for Fiber). As the advantages of fiber optics over twisted pair or coaxial cable become increasingly evident -- higher bandwidth, smaller size and weight, immunity to EMI -- optical fiber is more and more seen as the ideal cabling for office building, campus and industrial environments. Recognizing this fact, all three IEEE 802 standards have either developed or are in the process of writing standards for fiber optic media. The inherent advantages of fiber notwithstanding, for the lower speed (IEEE 802) LANs where copper conductors can provide an adequate solution, there is a very spirited cost based competition between the various transmission media.

Given that the labor cost associated with installing a building cabling system often exceeds the cost of the materials and that a system once installed should be expected to have a 10-20 year useful operating life, it would seem that rather than allowing the cabling system to evolve with the supported LAN, it would be better to install a single cabling system which could support any LAN evolution. As it is evident that this evolution will almost certainly include higher data rates, fiber optics is the only media which can support this strategic approach.

The key to installing a fiber optic cabling system is to select a wiring topology and termination scheme that will accommodate any future choice of LAN protocol and to choose fiber and connector types for long term hardware compatibility. The cabling strategy described here addresses both of these major issues--wiring topology and optical fiber specification--and is applicable to all current and future LAN implementation scenarios.

## CABLE PLANT TOPOLOGY

The Electronic Industries Association (EIA) TR-41.8.1 Working Group has for some time been developing a Commercial and Industrial Building Wiring Standard. Although the work of this group is not yet complete, it does serve as a very good example of the recommended cable plant wiring topology.

Basically a three-level star wiring topology such as that illustrated in Figure 1 is suggested. The maximum distances shown in Figure 1 are those currently recommended by EIA TR-41.8 for optical fiber. That portion of the star wiring from the work area (wall outlet) to the wiring closet is referred to as the Horizontal Wiring from the fact that most of the wiring on this level will be in the horizontal plane of the building. The wiring from the Wiring Closet to the first Cross-Connect and between Cross-Connects is referred to as the Vertical Wiring or Building and Campus Backbones. These terms in all cases are meant to be descriptive. The Wiring Closet and Cross Connects are sometimes referred to as Hubs (Work Group, Building and Campus).

The objective of the star wiring topology, particularly the Backbone sections, is to enable installation of the wiring to proceed without prior detailed knowledge of the communications service which will be supplied. The limitation to three levels of hubs will adequately serve virtually all network applications while remaining simple to administer. On smaller sites a single cross-connect system may be desirable.

In many cases the user has requirements for both voice and data equipment at a work location. Although the focus here is on fiber optics for LAN applications, the considerations apply equally well to voice requirements and in many instances, particularly the horizontal wiring, cable or cables containing more than one transmission media (say, fiber optics and unshielded twisted pair) will be installed.

It should be noted that the wiring strategy being proposed here differs from the developing EIA standard in at least one important aspect. In its present (incomplete) state EIA - TR-41.8.1 does not recognize fiber optics as an option for the horizontal wiring. This is very short-sighted. As noted in EIA - TR-41.8.1 after construction of a building, the horizontal wiring is usually much less accessible than the vertical wiring. The time to make changes can be extremely high with attendant disruption to the occupants in the area and their work.

These factors make the choice of horizontal cable types and their layout very important. The strategic arguments for fiber optics apply equally well to the horizontal and vertical wiring. Consideration of a wide range of user applications must be given in order to reduce or eliminate the probability of requiring changes to the horizontal wiring in the face of unforeseen user requirements.

The functionality of a Hub, be it wiring closet or cross-connect, is illustrated in Figure 2. Generally speaking, all incoming and outgoing transmission lines, fiber optics or other, are terminated in patch panels. To minimize current costs, some users prefer to leave unused fibers un-terminated. Also present in the Hub will be signal distribution and regeneration equipment. This will be specific to the particular LAN protocol being implemented. Use of the star wiring and patch panels allows any desired LAN topology and protocol to be implemented now and changed to meet any future, presently unknown, requirements making changes only in the electronics and interconnections without changing the basic cable plant. Figures 3-5 illustrate this point, showing how the basic star wiring topology can be configured as a ring (Figure 3) passive or active star (Figure 4), or linear bus (Figure 5). Figure 6 illustrates the important case where the upper level of the star wiring is configured as a ring (FDDI) while the lower levels are configured for either rings (IEEE 802.5) or passive stars (IEEE 802.3).

One of the questions to be addressed when planning a fiber optic cable plant is just how many fibers to install. What makes this question so difficult is that once in place any cable plant, because of its installation expense, should have a 20-year life. Users thus need to consider the nature of their network requirements over this period. These should include compatibility with emerging standards, evolving capacity requirements, the need for multiple sub-nets, redundancy, etc. Also to be considered is the desirability of other services, such as color video at the workstation.

Multimode optical fiber has more than enough bandwidth to meet all of today's and most of tomorrow's LAN applications. Its use, rather than higher bandwidth single mode fiber, results in lower overall system costs. However, in looking to the future, some network planners, in anticipation of increasing bandwidth requirements, specify cables containing one or more single mode fibers, in addition to multimode fibers.

The point is that if a cable plant should contain enough fibers for both current and future requirements, the cost of increasing capacity becomes incremental - just terminate the fibers and install the appropriate electronics.

All of the IEEE 802 standards require a single duplex fiber optic cable to connect a node (one fiber for the transmit signal and one for the receive signal). FDDI, on the other hand, provides two wiring options. Stations may be attached to either a dual counter-rotating ring or through concentrators in lower cost single ring sub-networks. These 100 Mbs sub rings are connected to each other and to the main dual ring through concentrators. Which of the two implementations a user will choose depends upon a number of factors such as existing cable plant, reliability requirements, etc.



At the lowest or horizontal level of the three-layer wiring hierarchy, a single ring sub-network will usually best serve the user's requirement. Therefore, the two fiber cables initially installed for an IEEE 802 network will map directly into a single ring FDDI sub-network. It is only in the vertical wiring, and very likely only at the highest layer, that one might wish to make provision for a dual FDDI ring. This is demonstrated in Figure 7 which illustrates how, with proper planning, a fiber optic Ethernet (or IEEE 802.3) star topology segment can be easily migrated to a dual, counter rotating FDDI ring. At the time the Ethernet network is installed, a second duplex fiber optic cable is run from the Hub to every network station. The cost of installing this initially spare fiber cable is minimal if it is done at the same time as the primary installation. When it is time to upgrade the network to FDDI, the passive star coupler is simply disconnected and jumpers on the patch panel re-configure the cable plant into a ring. What were initially spare fiber optic cables now become the second of the dual counter-rotating rings. The major cost of this conversion lies not in the cable plant but rather in replacing the Ethernet Station Interface with the one appropriate to FDDI.

Unless one has the prescience to determine beforehand which nodes on some future FDDI network will be on the dual main ring and which will be on some single ring subnet, it is probably best to plan on running at least four fibers to each potential FDDI node on the horizontal wiring and certainly at least four fibers on the vertical or backbone wiring.

#### OPTICAL FIBER CHARACTERISTICS

The fiber optic cable properties currently specified in the various IEEE 802 and ANSI FDDI standards are summarized in Table I and Figure 8. It should be noted that while the media portion of all these standards are well established and stable, in many cases the standards themselves still have Draft status. This means that however unlikely, some important changes are still possible.

The discussion in this section is from the point of view of a user who wishes to install and use fiber now with an IEEE 802 type LAN with the provision that in the future some or all of the fiber optic cable plant would be upgraded to FDDI use. It was shown in the preceding section how star wiring allows for this topologically. The purpose of this section is to assure that the fiber installed now will have the proper characteristics for use in both IEEE 802 and FDDI LANs.

The first point to be kept in mind is that the IEEE 802 LANs have been specified for operation at a nominal optical wavelength of 850 nm while FDDI is intended to operate at 1300 nm. Any fiber intended for dual use must, therefore, exhibit the proper characteristics at both wavelengths. Most glass fiber sold today with core diameters of 50um, 62.5um, 85um and 100um operate

satisfactorily with both wavelengths. You should, however, check the manufacturers specifications.

All of the LAN standards define a 62.5/125 micron reference fiber for purposes of testing and verifying various fiber optic parameters. All of the standards, however, explicitly include the use of other multimode fiber sizes. This is both in recognition of a large installed base of fiber other than 62.5/125 and the expected continuation of the popularity of other fiber sizes in certain areas. In any event, all multi-mode fibers are included in the various standards with the understanding that use of fiber other than 62.5/125 may change some parameters, such as coupled optical power or optical fiber attenuation, which, in turn, might affect other parameters such as maximum achievable link length. The effect, if any, can be determined by relative simple arithmetic calculation.

The fiber dispersion characteristic is typically presented in the form of a modal bandwidth. For the purposes of specification, fiber bandwidth is approximated as an inverse linear function of length. That is, a 500 MHz-Km (FDDI) fiber will present approximately 250 MHz of bandwidth (four times the optical line rate of 125 M baud = 62.5 MHz) at the maximum FDDI distance of 2 km. It is not necessary that all fiber optic cable intended for use in FDDI LANs exhibit a 500 MHz-km modal bandwidth. If the known maximum node separation is  $L_{max} < 2\text{km}$ , then it is only necessary that

$$\text{Modal Bandwidth} > 250 L_{max} \text{ (MHz-km)}$$

The chromatic dispersion parameters provide a measure of the speed at which different colors (wavelengths) of light travel through a multimode optical fiber. Since all of the existing and developing fiber optic LAN standards employ wide spectral width LEDs as the optical source, chromatic dispersion will contribute, together with modal dispersion, to the overall system bandwidth. Chromatic dispersion has relatively little influence upon the performance of lower data rate IEEE 802 LANs, but becomes more important when upgrading a system to the higher data rates of FDDI if cable lengths are long.

The Appendix contains manufacturer's data on fiber optic cables. The cables in this data sheet will conform to the specifications of both the 850nm IEEE 802 standards and the 1300nm FDDI standard.

With the exception of IEEE 802.3, all of the IEEE 802 standards are deferring to FDDI as regards the fiber optic connector specification. The duplex connector specified by FDDI, however, is not yet in widespread use. It should be noted that the various standards define only those connectors which form part of the media dependent interface to the equipment being defined by the standard. Other connectors, particularly those at Hub patch panels and the wall panels, are user's choice. It is

necessary only that their normal optical loss, together with the fiber attenuation and other normal optical losses present in the transmission path (such as a passive star coupler) satisfy the total cable plant loss requirement specified in the standard. If the fiber optic cable plant is terminated at the wall outlet, as indicated in Figure 1, with connectors of the user's choice, then a change of LAN protocol will at most require a change in the short (1 to 3 meter) equipment to wall plate hook-up cable.

#### SUMMARY

This paper has presented a fiber optic LAN wiring strategy based upon two basic concepts. The first is the three-tier star wiring topology. From this basic topology

any desired LAN topology--ring, star or bus--can be derived. The three-tier structure provides adequate flexibility for most applications, including the very important case where a hierarchy of 802 LANs interconnected by an FDDI backbone is required.

The second premise concerns the media itself. The media portions of what can be expected to be, over the next ten years or so, the primary, standard LANs are today well enough defined to permit their installation with little fear that they will be changed. Moreover, with little effort, a single fiber optic media can be chosen which will not only satisfy the current requirements of IEEE 802 LANs operating at 4-20 Mbs, but will equally well serve the 100 Mbs requirements of FDDI in the years to come.

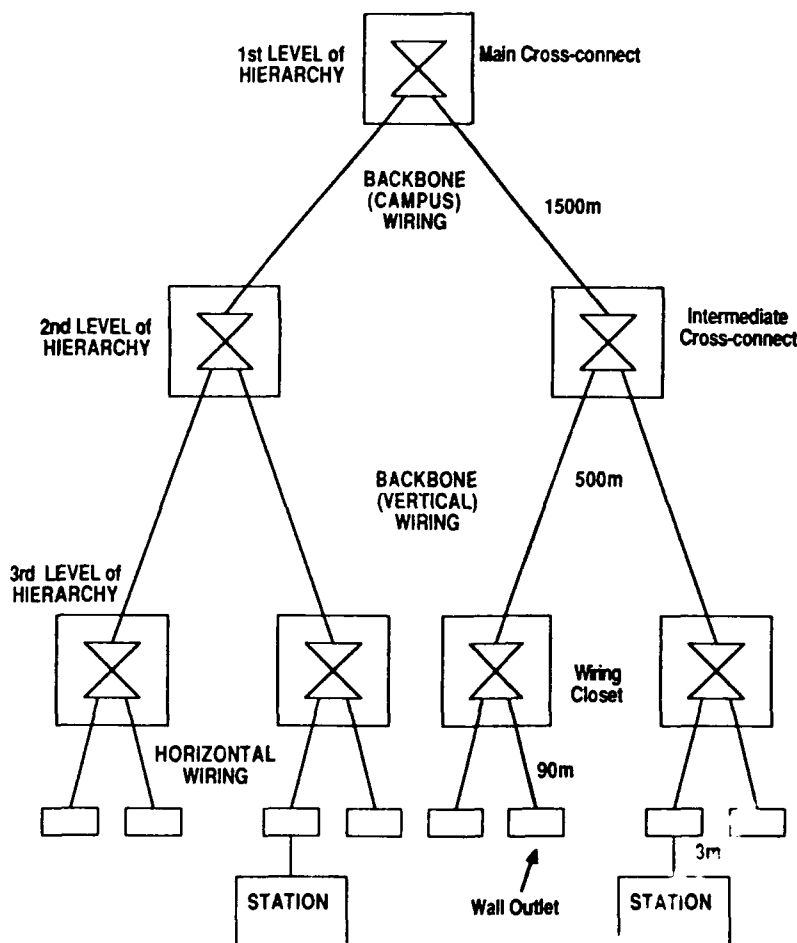
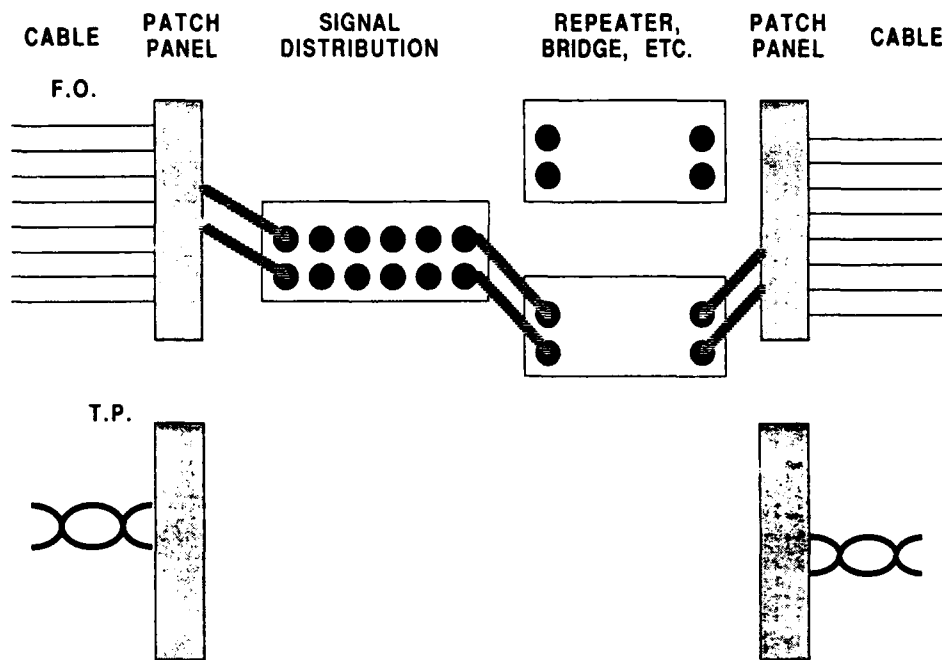
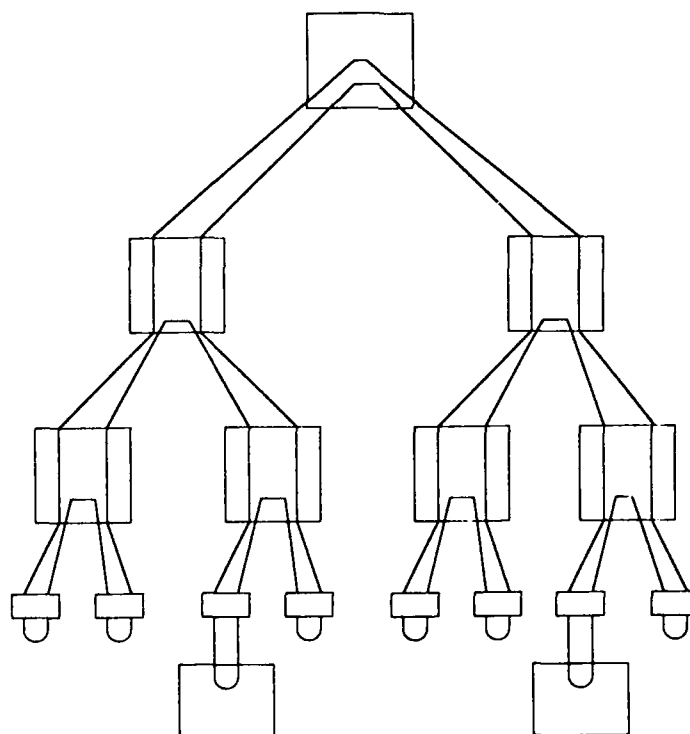


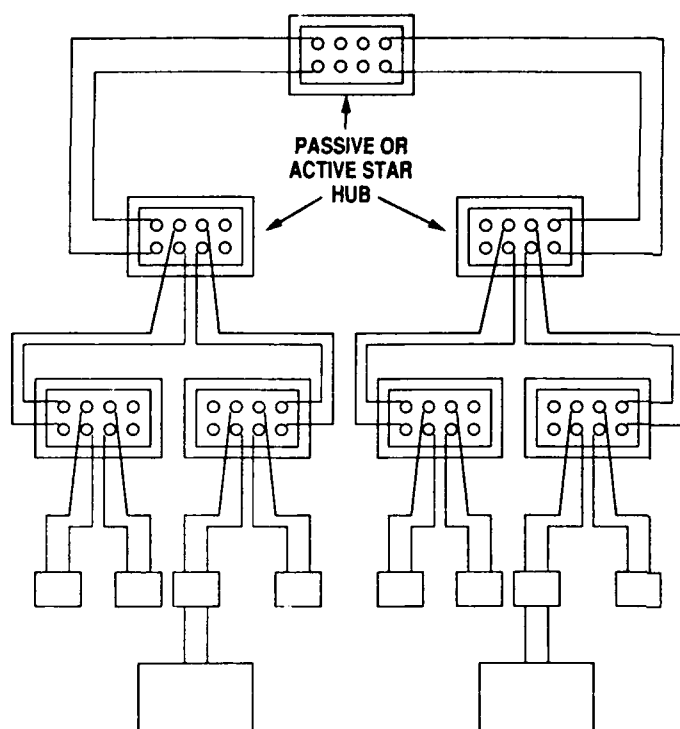
FIGURE 1. RECOMMENDED STAR WIRING TOPOLOGY



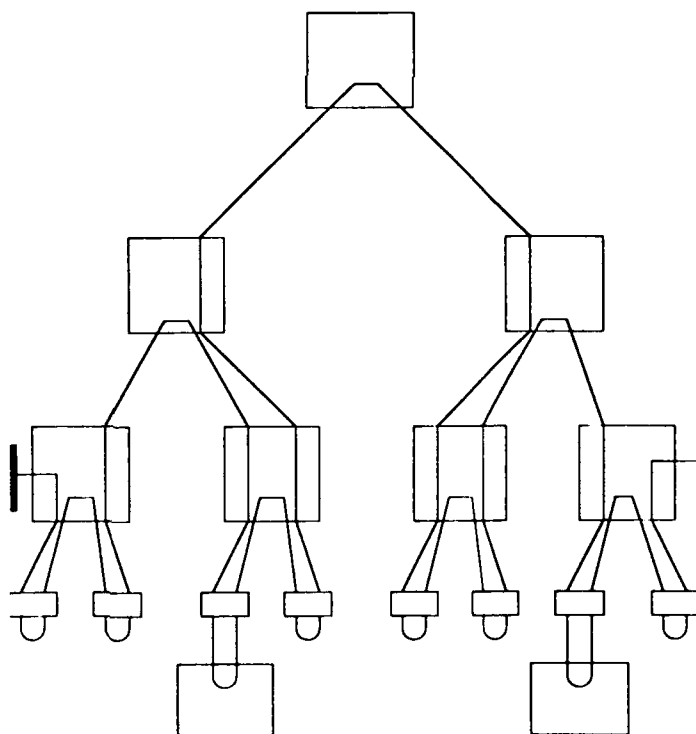
**FIGURE 2. HUB FUNCTIONALITY**



**FIGURE 3. RING TOPOLOGY IMPLEMENTED USING ALL PURPOSE PHYSICAL STAR WIRING**



**FIGURE 4. PASSIVE OR ACTIVE STAR TOPOLOGY IMPLEMENTED USING ALL PURPOSE PHYSICAL STAR WIRING**



**FIGURE 5. LINEAR BUS TOPOLOGY IMPLEMENTED USING ALL PURPOSE PHYSICAL STAR WIRING**

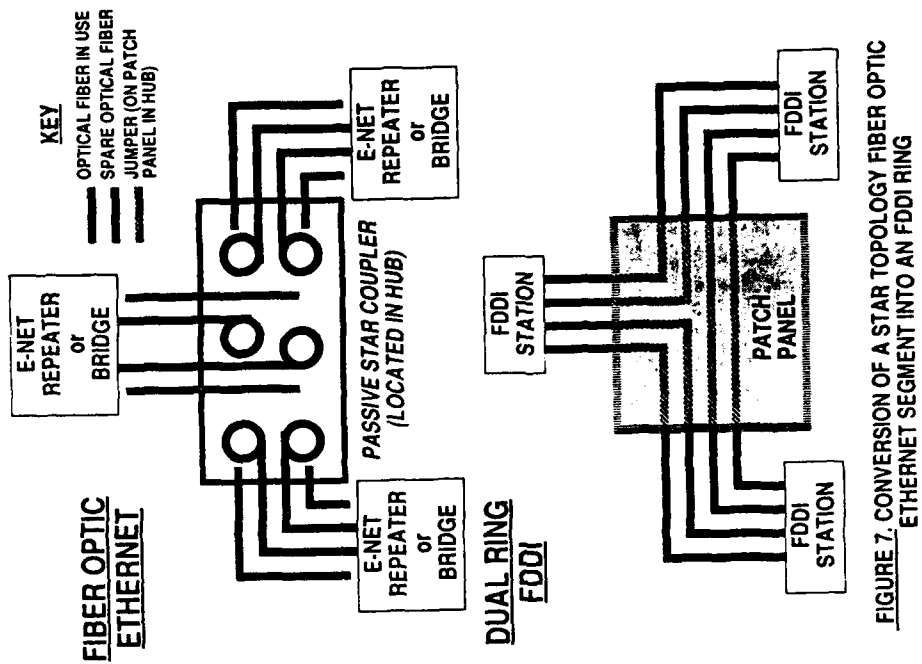


FIGURE 7. CONVERSION OF A STAR TOPOLOGY FIBER OPTIC ETHERNET SEGMENT INTO AN FDDI RING

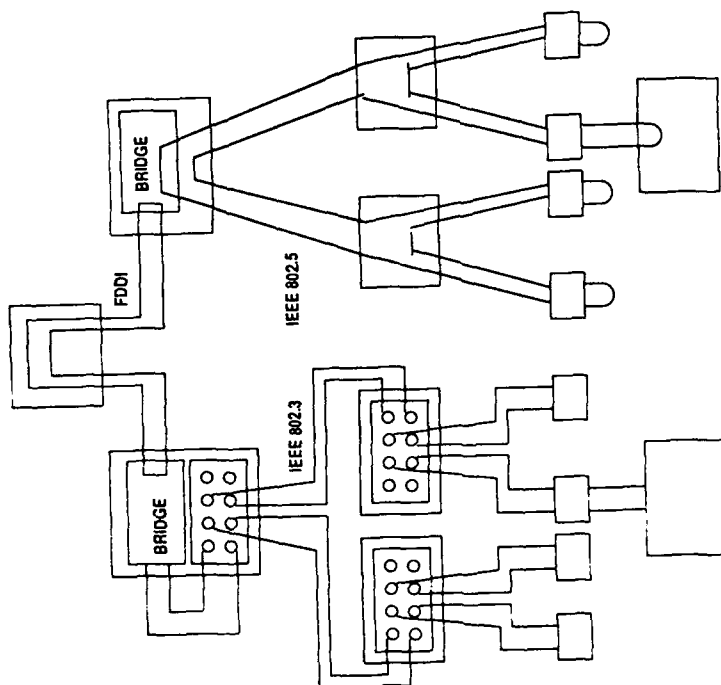


FIGURE 6. FDDI BACKBONE WITH IEEE 802.3 & 802.5 SUB-NETS IMPLEMENTED USING SAME ALL PURPOSE PHYSICAL STAR WIRING

TABLE I - Summary of Fiber Optic Cable Characteristics

	802.3 FOIRL	802.31 10BASE-P <sup>(1)</sup>	802.4	802.5 <sup>(1)</sup>	FDDI <sup>(1)</sup>
Optical Fiber (Core/Cladding-NA) Reference	62.5/125-.275	62.5/125-.275	62.5/125-.275	62.5/125	62.5/125-.275
Other Allowed	50/125 85/125 100/140	50/125-.23 85/125-.26 100/140-.275	50/125 85/125 100/140	50/125 100/140	50/125-.20 50/125-.22 85/125-.26 100/140-.29
Nominal Wavelength (nm)	850	850	850	850	1300
Maximum Attenuation Optical Fiber (dB/Km)		3.75		4.0	2.5
Total Cable Plant (dB)	8	FA-12 <sup>(2)</sup> FP-26 <sup>(3)</sup>	27	12	11
Minimum Modal Bandwidth (MHz - KM)	150	150		150	500
Chromatic Dispersion Slope (ps/nm <sup>2</sup> -km)				.093	See Fig 7
Zero Dispersion Wavelength(nm)				1365	See Fig 7
Maximum Fiber Length(km)	2.0	FA-2.0 <sup>(2)</sup> FP-0.5 <sup>(3)</sup>			2.0
No. Fibers Pairs per Attachment	1	1	1	1	1 or 2
Connectors Simplex (one fiber per connection)	SMA	ST			
Duplex (two fibers per connection)			FDDI	FDDI	FDDI

Notes: (1) These standards exist in draft form at the present time

(2) Active Star Network

(3) Passive Star Network; Loss = Star Coupler + 2x (Loss of Longest F.O. Link) + Connector Loss

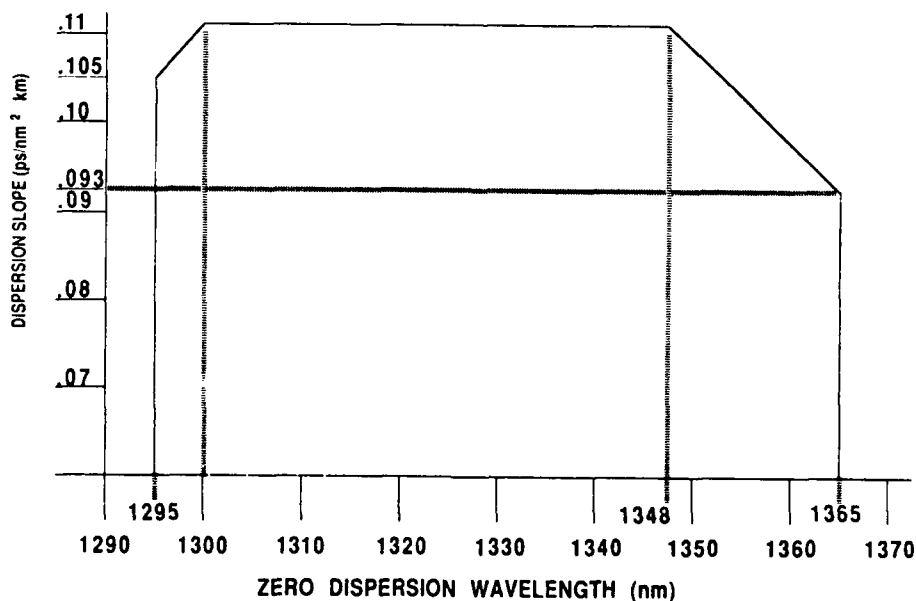


FIGURE 8. MINIMUM DISPERSION WAVELENGTH AND SLOPE LIMITS  
(FROM ANSI X3T9.5, FDDI PHYSICAL LAYER MEDIUM  
DEPENDENT SPECIFICATION, JULY 1, 1988).

#### BIOGRAPHIES

**Michael H. Coden** has been President and Chief Executive Officer of Codenoll Technology Corporation, a vertically integrated manufacturer of fiber optic components and data communications systems, since its incorporation in 1980. From 1977 to 1979, he was the Manager of Exxon Enterprises Optical Information Systems, a manufacturer of semiconductor laser and related products, and from 1975 to 1977 he was a Program Manager at Exxon Enterprises Inc. with responsibility for evaluating venture capital investments. Prior to 1975 Mr. Coden held management positions at Digital Equipment Corporation, Hewlett-Packard Company and Maher Terminals, Inc. Mr. Coden has a Bachelor's Degree in Electrical Engineering from the Massachusetts Institute of Technology, a Master's Degree in Business Administration from Columbia University, and a Master's Degree in Mathematics from the Courant Institute of Mathematical Sciences at New York University. He has taught computer science at Columbia University Graduate School of Business and semiconductor physics at Fairleigh-Dickinson University Electrical Engineering Department.

**Dr. W. Bryan Hatfield**, after a brave but unsuccessful bout with cancer, succumbed late this summer, 1991. He was an expert in the area of networking standards and an active member of the IEEE 802 networking committee, as well as ANSI X3T9.5, the FDDI standards-making body. He received his PhD in Physics from Stanford University and upon joining Codenoll Technology had 20 years of research and product development experience with Bell Laboratories, Singer and AM International. His specific experience includes plasma discharge and liquid crystal display technologies, thin film magnetic devices, magnetographic printing and advanced electronic packaging concepts. At Codenoll, he was Vice President-Standards and Reliability, concerned with the development of standards for local area networks and performance of Codenoll products and systems.

**Brian J. Ramsey** joined Codenoll Technology Corporation in November 1989. He is currently serving as Director of Marketing, with responsibility for marketing, product development, strategic relationships with technical partners and technical support.

Prior to joining Codenoll, Ramsey served as Regional Sales Manager of the New York region for Novell. As general manager of one of the initial NetWare Centers established in 1986, Ramsey was responsible for establishing the New York region for Novell.

Before joining Novell in November 1985, Ramsey served as Executive Vice President of Jersey Micro Systems, which was one of the early distributors of microcomputer networks such as Televideo, Novell, and Molecular. Previously Ramsey worked with McGraw-Hill Information Systems for 10 years, during which he held a number of positions in product management and sales. Mr. Ramsey earned a bachelor's degree from Bard College Annandale-on-Hudson, NY and has studied for his MBA at the University of Toledo and NYU.

CODENOLL TECHNOLOGY CORPORATION  
1086 North Broadway, Yonkers, NY 10701  
914/965-6300

# INSTALLED COST OF FIBER OPTIC CONNECTORS ON VARIOUS FIBER SIZES

John C. Huber

3M Company, Austin TX

## ABSTRACT

Recently optical fibers have become the transmission medium of choice for short distance telecommunications. Optical fibers are now being installed in homes and offices. These applications usually require connectors to be installed two-at-a-time. The installed cost of these connectors is a substantial barrier to rapid deployment of fiber in these applications. This paper describes a model to estimate the installed cost of connectors. It demonstrates the cost reductions achieved by fast curing adhesives and large size fibers. And it offers some suggestions for future work.

## ESTIMATED LINK COST

The number of factors and the range of costs for installing a fiber optic link have wide variances depending on the application and many other factors. In telephony applications and data communication backbone network communications, there have been almost ten years of experience which has reduced this uncertainty. Furthermore, in these applications, the cable and cable installation costs far outweigh any reasonable level of connector installation costs. So the variance in installed cost of connectors on these long links has not been a critical issue. However, as fiber penetrates closer to the home and the desktop, the connector installed costs become more significant. And much of the experience in other applications does not directly apply. For example in long links, it is commonplace to install dozens of connectors at one sitting; so expensive and bulky tools were not a big problem. Specialized crews could be fully employed in installing connectors; so a high level of skill and extensive training were not a big problem.

To be specific, the Fiber Distributed Data Interface (FDDI) link from the concentrator to the workstation has been selected for analysis. This link has two fibers which span 100 meters and include 12 mated ferrules in connectors, 8 of these are in the FDDI MIC connector as specified by the FDDI standard. See Figure 1. The estimates for costs are shown in Table 1. These reflect the experience of installing many thousands of connectors and are similar to two recent studies: Clavenna(1) and an unpublished survey performed for the Low Cost Fiber

PMD working group of the ANSI X3T9.3 committee(2). The survey included several manufacturers, several installers and several end-users and is felt to be the most comprehensive publicly reported.

## FDDI LINK LAYOUT

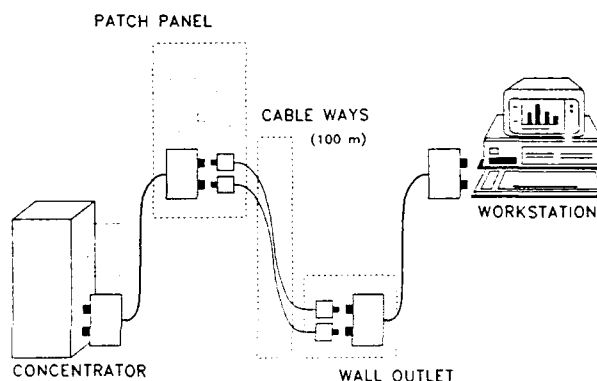


FIGURE 1

TOTAL COST OF FDDI WORKSTATION-TO-CONCENTRATOR CABLE LINK

ITEM	UNITS	QUANTITY	COST	TOTAL	%
CABLE	m	100	\$1.10	\$110.00	14
CABLE INSTALLATION	m	100	\$3.40	\$340.00	44
OUTLET CONNECTOR	ea ST	2	\$41.20	\$82.40	11
CLOSET CONNECTOR	ea ST	2	\$21.03	\$42.06	5
DUPLEX JUMPER	ea MIC	2	\$99.50	\$199.00	26
				<hr/> \$773.46	

TABLE 1

All the connectors taken together comprise 42% of the total cost of the link. Connector cost is dominated by the cost of installing the connector on the cable, whether done on site or in a specialized cable assembly facility. It is the cost of the labor to install the connector that dominates installed cost. Yet the technical literature does not contain much specific information to estimate this cost.

A computer-based model of connector installation was developed to make a systematic study of installed costs. The model is a simple spreadsheet and its parameters can be easily modified. In addition, the sequence of tasks can be easily rearranged to accommodate different installation practices. A printout of the spreadsheet is shown in Exhibit 1.



CALCULATION OF INSTALLED COST						
TYPE: EPOXY ADHESIVE; MANUAL POLISH; 62.5/125 GLASS FIBER; "SLOW" TIMES						
#	TASK NAME	TIME-RANGE		TIME	TIME	
		FAST	SLOW	TASK	ELAPSED	
0.00	0.00					
SETUP	START			0.00	0.0	- UNIT COSTS -
SETUP	PREPARE WORK SITE	3.0	6.0	6.00	6.0	CONNECTOR \$8.33
SETUP	PREP: HEAT OVEN	5.0	7.0	7.00	13.0	SUPPLIES \$0.54
SETUP	PREP: LAY OUT TOOLS	2.0	4.0	4.00	17.0	TOOL KIT \$1,150
SETUP	PREP: OPEN CABLE SHEATH	2.0	10.0	10.00	27.0	KIT LIFE 5,000
SETUP	PREP: MIX & LOAD EPOXY	3.0	6.0	6.00	33.0	LABOR/HR \$60.00
SETUP	PREP: SIMULTANEOUS TASKS			-7.00	26.0	
SETUP	PREPARATION COMPLETED				26.0	- TOTAL COSTS -
SETUP	TOTAL				26.0	SUPPLIES \$1.08
1	START			26.00	26.0	CONNECTOR \$16.66
1	PREPARE CONNECTOR	0.3	0.6	0.60	26.6	TOOL KIT \$0.46
1	PREP: FIBER	1.2	2.4	2.40	29.0	LABOR \$101.40
1	PREP: FILL CONN & CRIMP	2.0	4.0	4.00	33.0	-----
1	PREPARATION COMPLETED				33.0	TOTAL \$119.60
1	PAUSE FOR OVEN			0.00	33.0	
1	CURE: PUT IN OVEN	0.1	0.2	0.20	33.2	AVG COST \$59.80
1	CURE EPOXY	20.0	30.0	30.00	63.2	
1	COOL	2.0	4.0	4.00	67.2	
1	WAIT FOR POLISHING			0.0	67.2	
1	POL: CLEAVE & INSPECT	0.5	1.0	1.00	68.2	
1	POLISH: COARSE	1.0	2.0	2.00	70.2	
1	POL: CLEAN & INSPECT	0.3	0.6	0.60	70.8	
1	POLISH: FINE	2.0	4.0	4.00	74.8	
1	POL: CLEAN & INSPECT	0.3	0.5	0.50	75.3	
1	POL: FINAL CHECK	0.3	0.5	0.50	75.8	
1	POLISHING COMPLETED				75.8	
1	TOTAL			49.8		
2	START			33.00	33.0	
2	PREPARE CONNECTOR			0.60	33.6	
2	PREPARE FIBER			2.40	36.0	
2	PREP: FILL CONN & CRIMP			4.00	40.0	
2	PREPARATION COMPLETED				40.0	
2	PAUSE FOR OVEN			0.00	40.0	
2	CURE: PUT IN OVEN			0.20	40.2	
2	CURE EPOXY			30.00	70.2	
2	COOL			4.00	74.2	
2	WAIT FOR POLISHING			1.60	75.8	
2	POL: CLEAVE & INSPECT			1.00	76.8	
2	POLISH: COARSE			2.00	78.8	
2	POL: CLEAN & INSPECT			0.60	79.4	
2	POLISH: FINE			4.00	83.4	
2	POL: CLEAN & INSPECT			0.50	83.9	
2	POL: FINAL CHECK			0.50	84.4	
2	POLISHING COMPLETED				84.4	
2	TOTAL			51.4		
PACKUP	START			84.40	84.4	
PACKUP	PREP: COOL OFF OVEN	5.0	7.0	7.00	91.4	
PACKUP	PREP: PUT TOOLS IN KIT	2.0	4.0	4.00	95.4	
PACKUP	PREP: CLEAN WORK SITE	3.0	6.0	6.00	101.4	
PACKUP	PREPARATION COMPLETED				101.4	

EXHIBIT 1

In this model, there are two sets of variable parameters. One set applies to the specific connector installation practice and is the range of times to perform each task. These are entered in the columns named "TIME-RANGE, FAST, SLOW." The time entries are those for trained and experienced installers; they do not represent novices on one hand or champions on the other hand. The entries in the FAST column are the fastest times normally observed; these are not the fastest times by the fastest installers. Similarly, the entries in the SLOW column are the slowest times normally observed. A word of caution is necessary here, fast is not necessarily better than slow. Higher quality of work, better optical performance and fewer rejects are more often encountered by installers near the slow end of the range rather than the fast end. Remaking one connector can offset the entire difference between the fast-working and lower-paid installer and the slow-working and higher-paid installer for a job of four connectors.

The other set of parameters for the model are independent of the specific connector installation practice and are listed on the right side of the spreadsheet. These include the connector price, supplies, tool kit price, tool kit life and labor rate. Although one would normally expect that higher paid installers work faster and do better work, this is not an absolute rule.

As can be seen from Exhibit 1, the setup and packup times are substantial contributions to the total elapsed time for the job. To be realistic, these times must be included. They have a considerable impact when small numbers of connectors are being installed at a time; about 40% for two connector installations.

This spreadsheet can be run for the range of parameters and for any number of connectors. The results are shown in Figure 2. While there is a considerable range of costs, it is clear that the variability is larger for small numbers of connectors. And the FDDI installation is precisely this situation. Two connectors must be installed at each wall outlet adjacent to each workstation; % of the cost is labor. Near the concentrator in the communications closet, connectors will be installed twelve at a time or more; then labor is 67% of the cost.

INSTALLED COST OF CONNECTORS  
Epoxy adhesive; manual polish

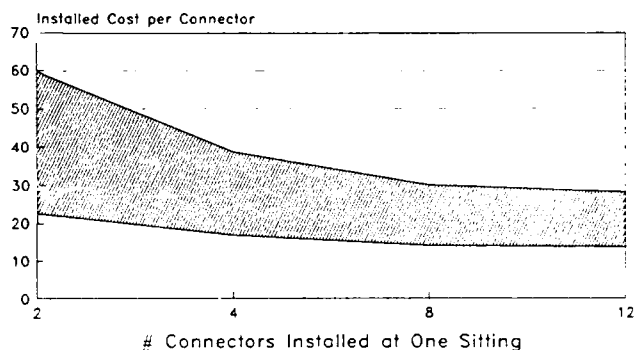


FIGURE 2

The results from the model can also be shown graphically as in Figure 3. It can be seen that the time to cure the epoxy in common connectors is the next largest contributor to the elapsed time.

# CONNECTOR INSTALLATION - 62.5/125 FIBER Epoxy Adhesive; Manual Polish

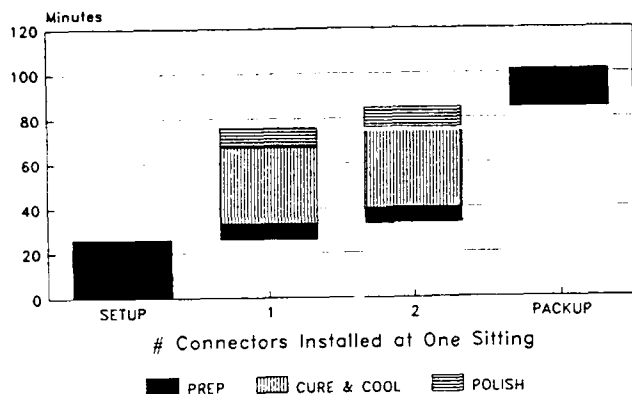


FIGURE 3

Fast acting adhesives have been introduced to reduce the time and cost of curing epoxy. Examples are ultraviolet light curing and hot melt adhesives. These adhesives typically cure in a few minutes.

When entered in the model, these adhesives dramatically reduce the installed cost of connectors. Most of the advantage is in labor saving. For two at a time, the labor drops to 49% of the cost. Total installed costs are 35-42% lower than epoxy. The results are shown in Exhibit 2 and Figure 4. Furthermore there is little compromise in using fast-curing adhesive connectors. The optical performance of hot melt adhesive connectors is equal to epoxy connectors.

CALCULATION OF INSTALLED COST									
HOT MELT ADHESIVE; MANUAL POLISH; 62.5/125 GLASS FIBER; "FAST" TIMES									
#	TASK NAME	TIME-RANGE		TIME	TIME				
		FAST	SLOW	TASK	ELAPSED				
SETUP	START			0.00	0.00	-- UNIT COSTS --			
SETUP	PREPARE WORK SITE	3.0	6.0	3.00	3.0	CONNECTOR	\$6.93		
SETUP	PREP: HEAT OVEN	5.0	7.0	5.00	8.0	SUPPLIES	\$0.30		
SETUP	PREP: LAY OUT TOOLS	2.0	4.0	2.00	10.0	TOOL KIT	\$1,150		
SETUP	PREP: OPEN CABLE SHEATH	2.0	10.0	2.00	12.0	KIT LIFE	5,000		
SETUP	PREP: MIX & LOAD EPOXY	na	na	0.00	12.0	LABOR/HR	\$30.00		
SETUP	PREP: SIMULTANEOUS TASKS			-4.00	8.0				
SETUP	PREPARATION COMPLETED				8.0				
SETUP	TOTAL			8.00	8.0	-- TOTAL COSTS --			
1	START			0.30	8.0	CONNECTOR	\$6.93		
1	PREP: PUT CONN IN OVEN	0.3	0.6	0.30	8.3	SUPPLIES	\$0.60		
1	PREPARE FIBER	1.2	2.4	1.17	9.5	CONNECTOR	\$13.86		
1	PREP: PAUSE FOR MELTING			0.00	9.5	TOOL KIT	\$0.46		
1	PREP: INSERT FIBER	0.3	0.5	0.25	9.7	LABOR	\$14.44		
1	PREPARATION COMPLETED				9.7	TOTAL			
1	COOL	3.0	4.0	3.00	12.7	AVG COST			
1	WAIT FOR POLISHING			0.00	12.7				
1	POL: CLEAVE & INSPECT	0.5	1.0	0.50	13.2				
1	POLISH: COARSE	0.5	1.0	0.50	13.7				
1	POL: CLEAN & INSPECT	0.2	0.3	0.17	13.9				
1	POLISH: FINE	1.3	1.7	1.33	15.2				
1	POL: CLEAN & INSPECT	0.3	0.7	0.33	15.6				
1	POL: FINAL CHECK	0.3	0.5	0.25	15.8				
1	POLISHING COMPLETED				15.8				
1	TOTAL			7.80	9.7				
2	START			9.72	9.7				
2	PREP: PUT CONN IN OVEN			0.30	10.0				
2	PREPARE FIBER			1.17	11.2				
2	PREP: PAUSE FOR MELTING			0.00	11.2				
2	PREP: INSERT FIBER			0.25	11.4				
2	PREPARATION COMPLETED				11.4				
2	COOL			3.00	14.4				
2	WAIT FOR PREV CONNECTOR			1.37	15.8				
2	POL: CLEAVE & INSPECT			0.50	16.3				
2	POLISH: COARSE			0.50	16.8				
2	POL: CLEAN & INSPECT			0.17	17.0				
2	POLISH: FINE			1.33	18.3				
2	POL: CLEAN & INSPECT			0.33	18.6				
2	POL: FINAL CHECK			0.25	18.9				
2	POLISHING COMPLETED				18.9				
2	TOTAL			9.17	18.9				
PACKUP	START			18.88	23.9				
PACKUP	PREP: COOL OFF OVEN	5.0	7.0	5.00	23.9				
PACKUP	PREP: PUT TOOLS IN KIT	2.0	4.0	2.00	25.9				
PACKUP	PREP: CLEAN WORK SITE	3.0	6.0	3.00	28.9				
PACKUP	PREPARATION COMPLETED				28.9				

EXHIBIT 2

CALCULATION OF INSTALLED COST						
CRIMP & CLEAVE TECS CONNECTOR; 200/230 TECS FIBER; "FAST" TIMES						
#	TASK NAME	TIME-RANGE	TIME	TIME		
		FAST	SLOW	TASK	ELAPSED	
SETUP	START			0.00	0.0	- UNIT COSTS -
SETUP	PREPARE WORK SITE	1.0	2.0	1.00	1.0	CONNECTOR \$15.00
SETUP	PREP: HEAT OVEN	na	na	0.00	1.0	SUPPLIES \$0.54
SETUP	PREP: LAY OUT TOOLS	1.0	2.0	1.00	2.0	TOOL KIT \$995
SETUP	PREP: OPEN CABLE SHEATH	2.0	4.0	2.00	4.0	KIT LIFE 5,000
SETUP	PREP: MIX & LOAD EPOXY	na	na	0.00	4.0	LABOR/HR \$30.00
SETUP	PREP: SIMULTANEOUS TASKS			0.00	4.0	
SETUP	PREPARATION COMPLETED				4.0	- TOTAL COSTS -
SETUP	TOTAL				4.0	SUPPLIES \$1.08
1	START			4.00	4.0	CONNECTOR \$30.00
1	PREPARE CONNECTOR	0.3	0.6	0.30	4.3	TOOL KIT \$0.40
1	PREPARE FIBER	1.2	2.4	1.17	5.5	LABOR \$5.72
1	PREP: FILL CONN & CRIMP	1.0	2.0	1.00	6.5	
1	PREPARATION COMPLETED				6.5	TOTAL \$37.19
1	PAUSE FOR OVEN			0.00	6.5	AVG COST \$18.60
1	CURE: PUT IN OVEN	na	na	0.00	6.5	
1	CURE EPOXY	na	na	0.00	6.5	
1	COOL	na	na	0.00	6.5	
1	WAIT FOR POLISHING	na	na	na	6.5	
1	POL: CLEAVE & INSPECT	na	na	0.00	6.5	
1	POLISH: COARSE	na	na	0.00	6.5	
1	POL: CLEAN & INSPECT	na	na	0.00	6.5	
1	POLISH: FINE	na	na	0.00	6.5	
1	POL: CLEAN & INSPECT	na	na	0.00	6.5	
1	POL: FINAL CHECK	0.3	0.5	0.25	6.7	
1	POLISHING COMPLETED				6.7	
1	TOTAL			2.7		
2	START			6.72	6.7	
2	PREPARE CONNECTOR			0.30	7.0	
2	PREPARE FIBER			1.17	8.2	
2	PREP: FILL CONN & CRIMP			1.00	9.2	
2	PREPARATION COMPLETED				9.2	
2	PAUSE FOR OVEN			0.00	9.2	
2	CURE: PUT IN OVEN			0.00	9.2	
2	CURE EPOXY			0.00	9.2	
2	COOL			0.00	9.2	
2	WAIT FOR POLISHING			na	9.2	
2	POL: CLEAVE & INSPECT			0.00	9.2	
2	POLISH: COARSE			0.00	9.2	
2	POL: CLEAN & INSPECT			0.00	9.2	
2	POLISH: FINE			0.00	9.2	
2	POL: CLEAN & INSPECT			0.00	9.2	
2	POL: FINAL CHECK			0.25	9.4	
2	POLISHING COMPLETED				9.4	
2	TOTAL			2.7		
PACKUP	START			9.43	9.4	
PACKUP	PREP: COOL OFF OVEN	na	na	0.00	9.4	
PACKUP	PREP: PUT TOOLS IN KIT	1.0	2.0	1.00	10.4	
PACKUP	PREP: CLEAN WORK SITE	1.0	2.0	1.00	11.4	
PACKUP	PREPARATION COMPLETED				11.4	

EXHIBIT 3

Recently there have been introductions of crimp and cleave connectors for 62.5/125 fiber. But concerns about higher insertion loss and lower durability have limited their acceptance.

### CONCLUSION

It has been shown that it is possible to estimate the installed cost of fiber optic connectors in a systematic way, using a simple spreadsheet model. The installed cost is greatly affected by labor costs. But installed costs of \$22.59 to \$59.80 for epoxy connectors when installed two at a time are a substantial barrier to fiber networks penetrating to the home and the desktop. Faster curing adhesives have reduced these costs by 35% to 42%. Larger fibers lend themselves to simple, crimp and cleave connectors, which leads to further reductions.

The model's results for epoxy connectors, hot melt connectors and crimp-and-cleave connectors are shown in Table 2.

### CONNECTOR INSTALLATION - 62.5/125 FIBER Hot Melt Adhesive; Manual Polish

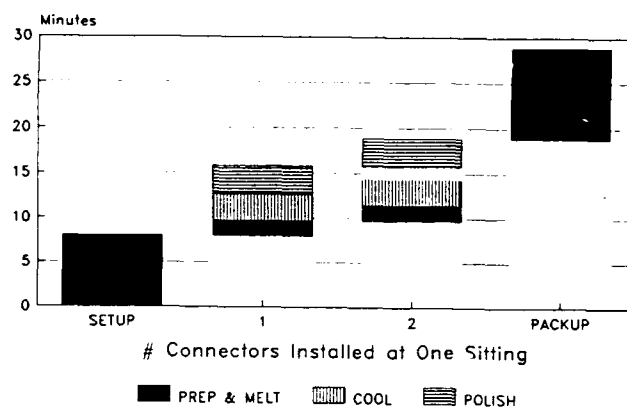


FIGURE 4

All of the above discussion has used the common 62.5/125 micron fiber. The degree of difficulty in installing connectors is directly related to the size of the fiber. Scratches from the abrasive polishing paper affect small core fibers much more than large core fibers. Small cladding and coating of fibers makes them harder to handle and take more time during installation. In general, large fiber sizes lead to lower installation costs.

Crimp and cleave installation practices for 200/230 micron fibers have been commonly used in factory automation and process control applications for over five years. They can be installed by an electrician using simple tools. There is no adhesive to cure and there is no polishing. Recent tests have demonstrated that this fiber has bandwidth adequate for FDDI applications.

The model can be used to estimate the installed cost of crimp and cleave connectors too. The results are shown in Exhibit 3. Installed costs are 21-53% lower than for epoxy connectors, when done two at a time.

# COMPARISON OF INSTALLED CONNECTOR COSTS

- # CONNECTORS INSTALLED AT ONE SITTING -

	2	4	8	12
--	---	---	---	----

## EPOXY

SLOW	\$59.80	\$38.75	\$30.07	\$28.28
FAST	\$22.59	\$16.90	\$14.18	\$13.77
DIFF	\$37.21	\$21.85	\$15.89	\$14.51

## HOT MELT

SLOW	\$34.87	\$25.37	\$20.75	\$19.20
FAST	\$14.60	\$12.11	\$10.99	\$10.61
DIFF	\$20.27	\$13.26	\$9.76	\$8.59

## CRIMP & CLEAVE

SLOW	\$28.30
FAST	\$17.77
DIFF	\$10.53

## % IMPROVEMENT - HOT MELT OVER EPOXY

SLOW	42	35	31	32
FAST	35	28	22	23

## % IMPROVEMENT - CRIMP & CLEAVE OVER EPOXY

SLOW	53
FAST	21

TABLE 2

The model described in this paper is not claimed to be absolute. As stated earlier, the installed cost of fiber optic connectors is subject to many variables. A particular person, using a particular connector, following particular instructions, conforming to particular work rules, and other factors may give substantially different results. The results from this model cannot be taken as exact; they are estimates. But it is believed that the results are accurate enough to be a guide for further product development.

## FUTURE WORK

It is clear from this analysis that more progress must be made to further reduce the installed cost of connectors. This is especially true for installing connectors two at a time, such as at the wall outlet for FDDI workstations. If fiber to the desktop is to be commonly available, the installation and maintenance must be done by people available on site, usually electricians. The more a fiber optic connector installation is like a common electrical connector installation, the faster fiber will be accepted. The ideal fiber optic connector would cost \$1.00 and be installed in one minute by an electrician using a \$10.00 tool than can hang from his belt. This would result in an installed cost of \$1.50 to \$2.00, depending on labor rate. Present connectors cost about ten times this much, when done two at a time.

A thorough analysis is needed to choose which path is most productive -- large core fiber, refinements of crimp and cleave connectors for small fibers and/or further decreases in adhesive curing and connector polishing time.

- 1 Clavenna, Scott, "Clearing Up the LAN Cable Confusion," p 1-9, FIBER DATACOMM Newsletter, July 1991, v4, #7, published by Information Gatekeepers, Inc, Boston MA
- 2 Fink, Robert L. and Trang Nguyen, presented to Low Cost Fiber PMD working group, ANSI X3T9.3 on July 17, 1991

Dr. Huber is Laboratory Manager for the Private Network Products Dept in the TelComm Products Division of 3M Company. He has been involved in telecommunications product development for 13 years, industrial communications for 8 years and fiber optics for 6 years. He has been involved with the development of 17 new products. He can be reached at 3M Company, PO Box 2963, Bldg A144-2N-01, Austin TX 78769

# FDDI FINDS FAT FIBER

Rudolph A. Montgelas

Ensign-Bickford Optics Company  
Avon, CT

## **Abstract**

Large-core, 200  $\mu\text{m}$  hard clad, step-index optical fiber is proposed for use in horizontal FDDI links of 100 meters or less. This fiber has sufficient bandwidth and attenuation properties for cable runs from the concentrator to the desktop. Fat fibers offer superior mechanical and optical coupling properties due to the polymer cladding and large core. Transceiver and connector manufacturers are already designing low-cost components to take advantage of the improved optical coupling offered by these fibers. Fiber optic systems using fat fibers are presently under consideration at the FDDI low-cost fiber ad hoc working group as a low-cost media alternative to 62.5/125 graded-index based systems.

## **Introduction**

One of the primary tasks a fiber optics system designer faces is to select the most cost-effective and reliable system components available on the market. There is a myriad of fiber, connector and transceiver devices available today. Each component provides distinct performance advantages depending on the application. Emerging industry standards such as ISDN, SONET and FDDI can help the designer target the appropriate hardware. Restrictions imposed by these standards can also prevent an economical implementation. Recently, a large core, step-index "Fat Fiber" has emerged which could offer the designer an effective alternative when selecting system components.

Traditionally, the majority of communication cables installed in buildings have been twisted-pair telephone cables and shielded coaxial CATV cables. These cables restrict the bandwidth of communication equipment connected to the network. Ethernet represented a significant improvement by providing a 10 Mbps broadband transmission scheme. Today, computer systems are more powerful. CPU processing speeds have increased and memory sizes have expanded, placing severe demands on a network to provide reliable, fault-tolerant data transmission. Fiber optic cables, with their large signal carrying capacity, low signal loss and RFI/EMI immunity, offer superior performance at a reasonable cost.

## **FDDI Standards**

Fiber optic cables are now routinely used for the connection of computer systems and peripheral devices in office buildings, campus environments and factory floors. Fiber networks allow users to share high data rate resources such as file servers, CAD mainframes, and CD-ROM databases. Consequently, this shared resource enhances computer workstation capacity and reduces system costs. The Fiber Distributed Data Interface (FDDI), sponsored by the American National Standards Institute (ANSI), was initiated to address a need for an interoperability standard of fiber optic network, hardware and communication protocols. It describes the requirements for interoperability at data rates of 100 Mbit/s using a dual token ring archi-

ture. The dual ring allows defective link nodes to be bypassed by an optical switch in the event of a component failure.

Figure 1 shows a simplified sketch of the topology for an FDDI network. Concentrator stations are connected with a counter-rotating fiber optic backbone. The backbone will allow thousands of nodes to be connected in series. Each node on the ring may be located up to two kilometers away from the next node. The application environment at a specific site generally dictates the type of node used. For example, in a data processing facility, it is desirable to use dual attachment stations for fault tolerance and network redundancy. In an office building, however, many single attachment stations might be connected to each concentrator in a "star" topology with typical cable lengths of less than 100 meters.

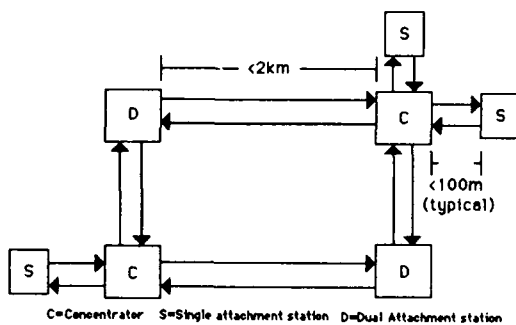


Figure 1 - Example of an FDDI Network

Table 1 highlights some of the significant FDDI standards under development by the various ANSI committees.<sup>1</sup> For some sub-layers, the effort has extended to the International Standards Organization (ISO) for final committee consensus. Other working groups are also in the process of defining transmission requirements which include network bridging to other transmission formats such as SONET and ISDN.

## Hard Polymer Clad "Fat Fiber"

This paper proposes the use of step-index "Fat Fiber" as a transmission medium in the FDDI horizontal cable plant. The Fat Fiber is composed of a Hard polymer-Cladding and a 200  $\mu$ m diameter pure Silica core (HCS®). The proprietary hard polymer cladding provides superior fiber strength as shown in the Weibull plot in Figure 2. The ultimate fiber breaking strength is typically around 800 kpsi. In this plot, fibers were tested according to TIA standard FOTP-28, using a 0.5 meter gage length and a 0.9 cm/s strain rate. As they are drawn, HCS fibers are online proof-tested to 200 kpsi as opposed to the 50 kpsi proof test typical for 62.5/125 graded index fibers. The static fatigue of the fiber is also improved because, the polymer cladding inhibits the growth of microcracks in the silica core due to stress corrosion by water molecules present at the fiber surface.<sup>2</sup>

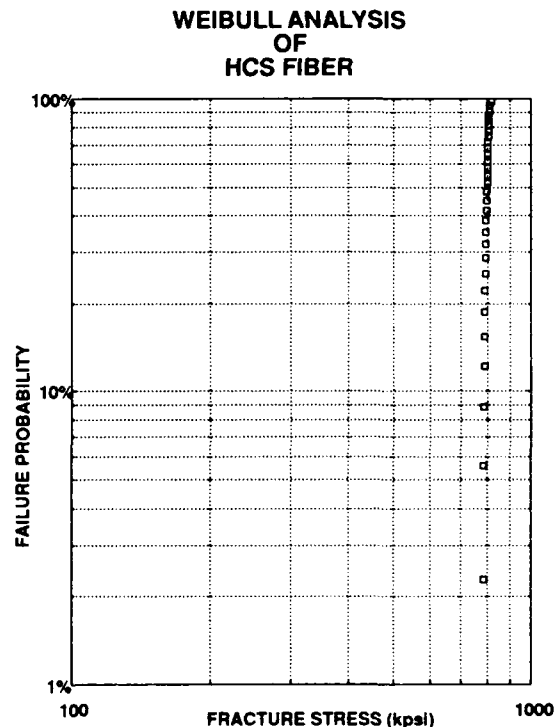


Figure 2

The HCS fiber core is composed of pure silica drawn from a low-water glass rod which typically contains less than or equal to 5 ppm of -OH concentration. This type of glass is used to maintain low infrared spectral absorption at 1300 nm. Figure 3 is a spectral attenuation plot for typical 200  $\mu\text{m}$  core HCS optical fiber. The fiber attenuation is approximately 30 dB/km at 1300 nm. This attenuation is sufficient for the 100 meter horizontal FDDI transmission length requirement. In fact, it is the fiber modal dispersion, not the attenuation, that restricts the maximum transmission distance to about 120 meters at FDDI data rates. Fortunately, the majority of point-to-point connection distances required within an office building are typically less than 100 meters.

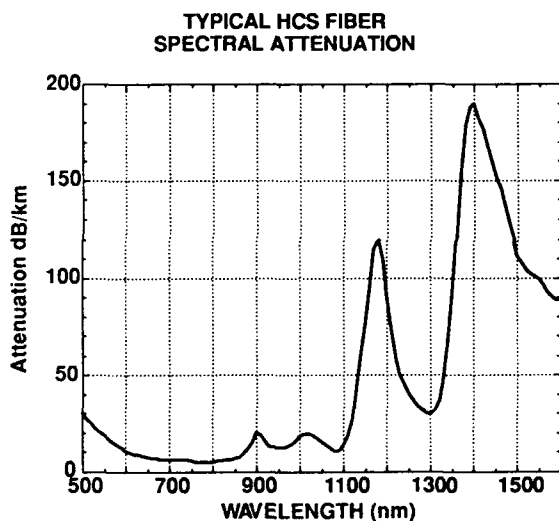


Figure 3

The bandwidth of an HCS fiber is predominantly limited by modal dispersion. Pulse spreading in the fiber is primarily caused by the time delay difference for the highest order mode and the lowest order mode to arrive at the transceiver detector. Also, the material dispersion in the fiber is essentially zero at the 1300 nm wavelength. Figure 4 shows a bandwidth versus distance plot for a typical HCS fiber.

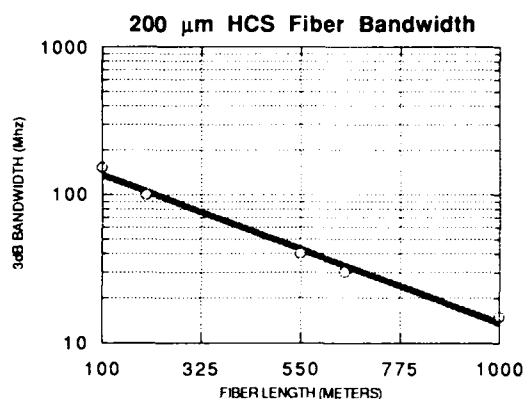


Figure 4

The HCS fiber has a measured bandwidth of about 150 Mhz for a 100 meter length using a 1300 nm surface emitting LED with a 0.28 injection NA.<sup>3</sup> This is sufficient to allow for the 100 Mbps FDDI data rate.

### HCS Cable Considerations

The high strength and static fatigue resistance of the HCS optical fiber allows special cable constructions to be considered. Table 3 shows a comparison between round duplex cables containing 62.5/125  $\mu\text{m}$  fibers and cables containing 200  $\mu\text{m}$  HCS fibers.<sup>4</sup> Duplex HCS cables have been manufactured without Kevlar® strength members while maintaining the sufficient cable tensile strengths shown. This type of cable has a smaller jacket diameter, reduced weight and improved flex/bend performance.

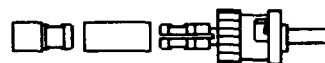
The elimination of Kevlar strength member tie-off at the connector and the ability to utilize simple crimp and cleave connectors, as discussed below, offers the possibility of economical mass production of duplex jumper cables for the FDDI plant. A machine has been constructed which will cleave both of the optical fibers in a duplex cable at once during the manufacturing process. As economies of scale evolve, the potential for fully automated cord set manufacture could become a reality for standard as well as coiled cable assemblies.

## **Crimp and Cleave Connectors**

One of the most significant advantages that an HCS fiber offers the system installer is the ability to apply low-cost crimp and cleave connectors without the need for epoxies and polishing in the field. The fiber's high strength and static fatigue resistance provide reliable and repeatable connections. The high core-to-clad ratio of the fiber also reduces the need for precision ferrules and high tolerance connector components. This allows for the manufacture of a low-cost connector as well as a reduction in transceiver costs. Field assembly simplicity means that crimp and cleave connectors can be installed on a cable in less than three minutes. This is about one-fourth the time it takes to glue and grind a typical epoxy/polish connector.

A metallic alloy sleeve is located inside the backshell of the crimp and cleave connector body shown in figure 5. This sleeve is designed with the proper mechanical creep and material flow properties. When the backshell is crimped, the sleeve will form around the surface of the fiber cladding, thus securing it in the ferrule assembly. (Fiber retention forces have been measured at 5 lb. nominal.) The ferrule assembly is then inserted in a cleave tool which imparts a specific tensile force sufficient to elongate the fiber prior to cleaving. A diamond cleave blade scribes the glass fiber, causing a controlled crack to propagate perpendicular to the fiber axis. The end of the cleaved fiber then retracts into the ferrule assembly, providing protection to its mirrored surface finish. Cleave angles for 200  $\mu\text{m}$  HCS fiber connectors are typically around 2.5 degrees with average losses of 1 dB per mated pair.

## **ST® Crimp and Cleave Connector**



### **Crimp and Cleave Attributes**

- Field installable in 3 minutes or less
- Cost-effective, substantially less than installed epoxy/polish
- High tensile strength - HCS® fiber permits crimping directly onto the hard cladding
- Static fatigue resistant
- Easy to assemble--no epoxy or other consumables required
- Reduced labor cost--no grinding or polishing
- Automated factory assembly also available

### **Cleaving Process**

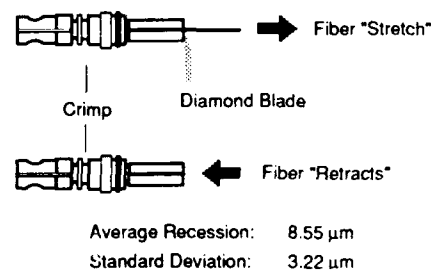


Figure 5

## **FDDI Fat-fiber Link Models**

A model of the cable plant is shown in figure 6. In this model, a duplex fiber optic jumper is connected from the desktop terminal equipment (such as a terminal or printer) to an FDDI duplex wall outlet plate. The terminal equipment contains a fiber optic transceiver specifically designed to couple the optical signal efficiently into the 200  $\mu\text{m}$  HCS fiber. Inside the wall outlet, a duplex cable is run through the wall and connected to a patch panel in a wiring closet. The patch panel allows the flexibility of reassigning the specific wall outlet plate locations when an office is reconfigured. A second duplex fiber optic jumper is connected from the patch panel to the optical transceiver at the concentrator node.



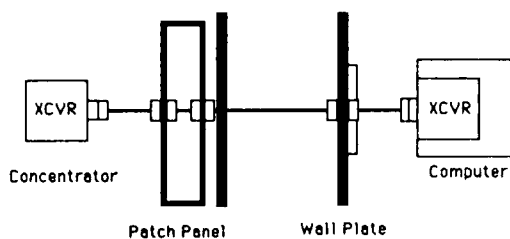


Figure 6 - FDDI Horizontal Wiring Model

The FDDI specification allows for interoperability between system components at the physical medium dependent layer. Graded index, 62.5/125  $\mu\text{m}$  fiber is chosen as the standard with allowance for 50/125, 85/125 and 100/140  $\mu\text{m}$  graded index fibers. The use of these fibers is outlined in Annex C of the ANSI PMD X3.166-1990 specification. When mixing of fiber media is necessary, connections from a fiber of larger core diameter to one of a smaller diameter may cause significant optical signal losses. It is important, therefore, for the system designer to consider all the losses encountered in a point-to-point link through the use of an optical loss budget.

Table 4 shows a proposed cost and power budget matrix for four simplex transmission media models used in the FDDI horizontal wiring model shown in Figure 6. Models A and B are for the use of single media and models C and D allow for mixing of the media from the concentrator to the computer. Model C, for example, proposes the use of 62.5/125  $\mu\text{m}$  fiber from the concentrator to the wall plate where a 200  $\mu\text{m}$  HCS jumper connects to the computer. Model D proposes using 200  $\mu\text{m}$  HCS from the transmitter at the concentrator to the wall plate where a 62.5/125  $\mu\text{m}$  jumper is used to connect to the optical receiver in the computer.

The assumptions used in preparation of the proposed models are listed at the bottom of the matrix. Each column provides a cost estimate for a particular system component as well as the component installation cost. These costs are estimated based on industry market studies.<sup>5</sup> Below the total cost in each column is a running tabulation of the optical link power at that component (in dBm units). This is listed from left to right, showing the coupled power at the transmitter in the concentrator to the received power at the computer node. The far right hand column shows the total component costs and the total received optical power. A factor for the cost per microwatt of received optical power is computed on each model at the bottom. The lowest  $\$/\mu\text{W}$  factor is about \$21 for model B which employs all 200  $\mu\text{m}$  HCS fiber in the link. This is followed by the mixed media model C using 62.5/125 fiber installed in the wall and a 200  $\mu\text{m}$  HCS jumper at the computer. A system using all 200  $\mu\text{m}$  HCS fiber is roughly half the cost per microwatt of the system using all 62.5/125  $\mu\text{m}$  fiber.

### Summary & Conclusions

Hard clad silica fat fiber has been proposed as an economical solution for short distance links in the horizontal FDDI wiring loop and is already included as a part of an IEC fiber optic standard. The high strength and stress corrosion properties of the fiber allow field installation of low-cost crimp and cleave connectors. The optical coupling provided by fat fiber relaxes the connector tolerances required at the transceiver and patch panel, thereby further reducing system costs. An analysis indicates the potential reduction of overall media component costs to half that of a 62.5/125 graded-index fiber system.

Fiber optic manufacturers are already producing optoelectronic devices for use with HCS fat fiber installed not only in office buildings, but also in the harsh environments of power plants and factory floors. Future developments for fat fiber in FDDI networks will depend on the economies of scale for optical transceivers and connectors which utilize the HCS advantages as well as the driving forces of the FDDI user community. A network using fat fiber from the concentrator to the desktop proposes to be the most viable solution to FDDI communication.

### **Acknowledgements**

Thanks are due to Dianne Grover for helping in the preparation of this document and to Sylvia Digby for help with the plots and figures.

HCS® is a registered trademark of Ensign-Bickford Optics Company  
Tefzel® is a registered trademark of E. I. DuPont de Nemours & Co  
ST® is a registered trademark of AT&T

### **References**

1. ANSI Standard; ANSI X3.166-1990 "Fibre Data Distributed Interface (FDDI) - Token Ring Physical Layer Medium Dependent (PMD).
2. B. J. Skutnik and R. E. Hille, "New Class of Step-Index Optical Fibers: Hard Clad Silica Fibers" CLEO 1983 p 166-167 May, 1983.
3. H. Nishimoto, Sumitomo Electric Industries, LTD. "Feasibility Study on FDDI 200  $\mu$ m Low Cost Fiber PMD," Presentation made to Low Cost Fiber - PMD Ad Hoc Working Group, Minneapolis, Minnesota, June 18, 1991.
4. W. B. Beck, Ensign-Bickford Optics Company, "200 Micron Fiber - Low Cost FDDI Models, Costs, Advantages," Presentation made to Low Cost Fiber - PMD Ad Hoc Working Group, St. Petersburg, Florida, April 23, 1991.
5. D. Krohn, 3M Specialty Fibers Group, Presentation made to Low Cost Fiber - PMD Ad Hoc Working Group, Boulder Colorado, August 20, 1991.



### **Author**

Rudolph A. Montgelas joined Ensign-Bickford Optics Company as Product Marketing Manager in March 1990. Previously, Rudy was New Product Development Manager for GTE Fiber Optic Products in Williamsport, PA. He graduated from Trinity College in Hartford, CT with a B.S. Engineering degree in 1975 and in 1980, received an M.S.E.E. degree from the University of Texas at Austin. Rudy has been involved with fiber optic component and system design since 1980. He is the published author of several papers and technical articles in fiber optics and has obtained two patents for fiber optic devices.

**Table 4 FDDI OPTICAL COST/POWER BUDGET MODELS**

Fiber Type:	62.5 $\mu$ m	62.5 $\mu$ m	62.5 $\mu$ m	Single Media - Model A		62.5 $\mu$ m	62.5 $\mu$ m	62.5 $\mu$ m	Totals
	Concentrator			62.5 $\mu$ m	62.5 $\mu$ m	Wall Plate		CPU	
	XCVR	Connector	50m cable	Connectors	50m cable	Connector	Jumper	XCVR	
Cost (\$)	\$150.00	\$15.00	\$60.00	\$25.00	\$60.00	\$15.00	\$50.00	\$150.00	\$525.00
Install Cost (\$)		\$10.00	\$75.00	\$14.00	\$75.00	\$10.00			\$184.00
Total cost (\$)	\$150.00	\$25.00	\$135.00	\$39.00	\$135.00	\$25.00	\$50.00	\$150.00	\$709.00
Power (dBm)	Coupled Power	-16.0	-16.0	-16.5	-16.6	-17.1	-17.6	-17.6	-17.6
								Cost/ $\mu$ W=	\$40.80
Fiber Type:	200 $\mu$ m	200 $\mu$ m	200 $\mu$ m	Single Media - Model B		200 $\mu$ m	200 $\mu$ m	200 $\mu$ m	Totals
	Concentrator			200 $\mu$ m	200 $\mu$ m	Wall Plate		CPU	
	XCVR	Connector	50m cable	Connectors	50m cable	Connector	Jumper	XCVR	
Cost (\$)	\$85.00	\$10.00	\$60.00	\$25.00	\$60.00	\$10.00	\$30.00	\$85.00	\$365.00
Install Cost (\$)		\$4.00	\$75.00	\$14.00	\$75.00	\$4.00			\$172.00
Total cost (\$)	\$85.00	\$14.00	\$135.00	\$39.00	\$135.00	\$14.00	\$30.00	\$85.00	\$537.00
Power (dBm)	Coupled Power	-10.0	-11.5	-12.5	-14.0	-15.0	-16.0	-16.0	-16.0
								Cost/ $\mu$ W=	\$21.38
Fiber Type:	62.5 $\mu$ m	62.5 $\mu$ m	62.5 $\mu$ m	Mixed Media - Model C		62.5 $\mu$ m	200 $\mu$ m	200 $\mu$ m	Totals
	Concentrator			62.5 $\mu$ m	62.5 $\mu$ m	Wall Plate		CPU	
	XCVR	Connector	50m cable	Connectors	50m cable	Connector	Jumper	XCVR	
Cost (\$)	\$150.00	\$15.00	\$60.00	\$25.00	\$60.00	\$15.00	\$30.00	\$85.00	\$440.00
Install Cost (\$)		\$10.00	\$75.00	\$14.00	\$75.00	\$10.00			\$184.00
Total cost (\$)	\$150.00	\$25.00	\$135.00	\$39.00	\$135.00	\$25.00	\$30.00	\$85.00	\$624.00
Power (dBm)	Coupled Power	-16.0	-16.0	-16.5	-16.5	-17.0	-17.5	-17.5	-17.5
								Cost/ $\mu$ W=	\$35.09
Fiber Type:	200 $\mu$ m	200 $\mu$ m	200 $\mu$ m	Mixed Media - Model D		62.5 $\mu$ m	62.5 $\mu$ m	62.5 $\mu$ m	Totals
	Concentrator			200 $\mu$ m	62.5 $\mu$ m	Wall Plate		CPU	
	XCVR	Connector	50m cable	Connectors	50m cable	Connector	Jumper	XCVR	
Cost (\$)	\$85.00	\$10.00	\$60.00	\$25.00	\$60.00	\$15.00	\$50.00	\$150.00	\$455.00
Install Cost (\$)		\$4.00	\$75.00	\$14.00	\$75.00	\$10.00			\$178.00
Total cost (\$)	\$85.00	\$14.00	\$135.00	\$39.00	\$135.00	\$25.00	\$50.00	\$150.00	\$633.00
Power (dBm)	Coupled Power	-10.0	-11.5	-21.5	-21.5	-22.0	-22.5	-22.5	-22.5
								Cost/ $\mu$ W=	\$112.57

**ASSUMPTIONS:**

62.5 $\mu$ m fiber=	0.52 dB/km @1300nm	Cost to install wallplate is the same for both fibers
200 $\mu$ m fiber=	30 dB/km @1300nm	Cable cost to install for both fiber types=
62.5 $\mu$ m connection loss=	0.5 dB	\$1.50
200 $\mu$ m connection loss=	1 dB	Cable cost for both fiber types
200 $\mu$ m to 62.5 $\mu$ m connection loss	10 dB	\$1.20
62.5 $\mu$ m to 200 $\mu$ m connection loss	0.4 dB	5 meter 62.5 $\mu$ m factory terminated jumper=
		\$50.00
		5 meter 200 $\mu$ m factory terminated jumper=
		\$30.00

**Table 1. ANSI FDDI 802.5 Token Ring Standards**

OSI Layer	Sub-Layer	Description	ANSI Standard (ISO Standard)
Network	SMT (Station Management Control)	Station Control Fault Isolation/Recovery	Future ISO/IEC Standard
Data Link	MAC (Media Access Control)	Addressing Data Checking/Framing	X3.139-1987
Physical	PHY (Physical Layer Protocol)	Data Encoding/Decoding Framing/ Clocking	X3.148-1988
Physical	PMD (Physical Medium Dependent)	Media Hardware: Cable Connectors, Xcvrs Jitter Specifications	X3.166-1990

**Table 2. Extensions to FDDI Standards Development**

Physical	SMF PMD (Singlemode Fiber)	Singlemode Hardware (<60km distance)	BSR- X3.184-19XX (DP-9314-4)
Data Link	HRC (Hybrid Ring Control)	Isochronous Data Transmission	BSR -X3.186 (DP-9314-5)
Physical	LCF (Low-cost Fiber)	Relaxed tolerance 62.5 200 $\mu$ m Hard-Clad Silica (<100 meters distance)	Future ISO/IEC Standard

**Table 3 CABLE COMPARISON**

Fiber Diameter ( $\mu$ m)	200/230/500	62.5/125/500/900
Cable Design	2 channel round	2 channel round
Jacket Diameter (mm)	3.0 $\pm$ 0.2	4.75 $\pm$ 0.25
Strength Member	none	Kevlar®
Tensile (N)	50	200
Break Strength (kg)	40	150
Minimum Bend Radius (mm)	15	50
Flex (cycles)	>10,000	5,000
Weight (kg/km)	7	18

Kevlar is a registered trademark of AT&amp;T

# Comparison of Twisted Wire Pair and Optical Fibers for FDDI

David A. Krohn

## 3M Specialty Optical Fibers

### ABSTRACT

While it is anticipated that the FDDI backbone will use 62.5/125 $\mu$ m graded-index optical fiber as the transmission medium, other portions of the network are under consideration with other media choices. The peripheral (horizontal) parts of the network will require 100 MHz bandwidth over only 100 meters. The broad use of 62.5/125 $\mu$ m graded-index fiber is currently too expensive in the high connector density peripheral network areas. Therefore, two logical choices arise: The first, copper twisted wire pair; and the second, 200/230 $\mu$ m step-index fiber.

This paper will outline FDDI media requirements. Twisted wire pair will be compared with 62.5/125 $\mu$ m graded index fiber and 200/230 $\mu$ m step-index fiber. The attenuation, bandwidth, and delivered power of the various media choices will be compared with FDDI needs. Also, the cost of cable, connectorization, and transceivers will be compared. *This analysis will provide the potential user with performance/cost trade-offs needed in system design.*

### INTRODUCTION

There is a growing need for high-speed data communications networks. The Fiber Distributed Data Interface (FDDI) will increase data speeds significantly above present data networks. While it is anticipated that the FDDI backbone will use 62.5/125 $\mu$ m graded-index optical fiber as the transmission medium, other portions of the network are under consideration with other media choices. The FDDI backbone will be required to function at 100 MHz over a 2 km distance. The horizontal (concentrator to workstation) portions of the network will require a bandwidth of 100 MHz over only 100 meters. In fact, the majority of the horizontal wiring applications will be 50 meters or less. Presently the broad use of 62.5/125 $\mu$ m fiber is limited because the cost of installing such a fiber system is high compared to conventional copper wire approaches.

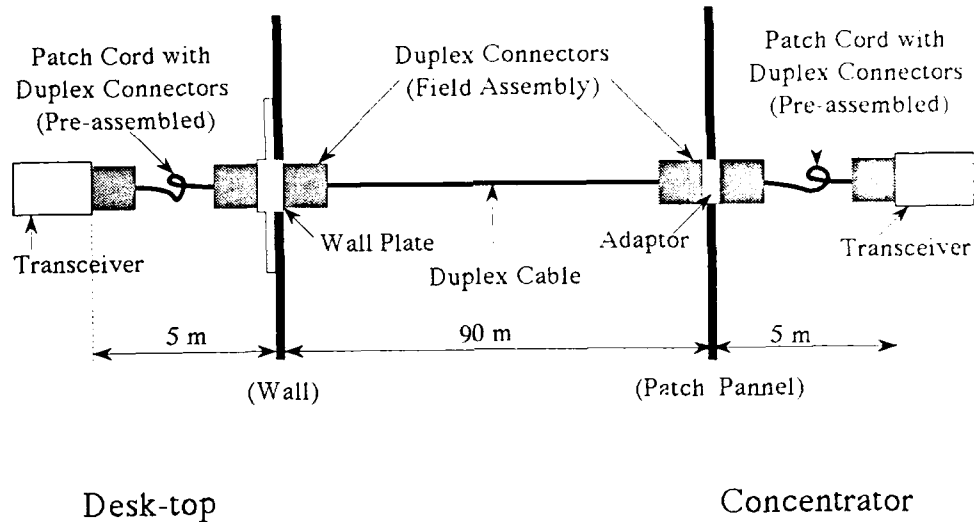
Two logical media alternatives for reducing cost arise: The first, copper twisted wire pair; and the second, 200/230 $\mu$ m step-index fiber. Twisted wire pair has some distinct advantages. The cost of cable, connectors, and connector installation is low if unshielded cable is used. Connector installation is straightforward with no special tools required. The cost of transceivers is low compared to those required for fiber. Also, there is a large installed base of unshielded twisted wire pair cable. The disadvantages of twisted wire pair copper cable are that bandwidth and attenuation limits transmission to a maximum of 100 meters. Unshielded copper twisted wire pair has the potential to be very noisy. Sophisticated transceiver designs will be required to eliminate the noise problem. The use of shielded twisted wire pair cable will minimize the noise, but increase cable cost as well as connectorization costs.

Step-index 200/230 $\mu$ m fiber is a low-cost fiber approach. The bandwidth and loss characteristics are adequate to function up to about 125 meters. Compared to 62.5/125 $\mu$ m fiber, large 200/230 $\mu$ m fiber is easier to terminate with a simple crimp-and-cleave technique. Epoxy and polishing steps usually associated with fiber termination are eliminated. The result is that large fibers provide a less costly, user-friendly termination scheme due to relaxed tolerances and the fact that they are easier to handle. Large-core 200/230 $\mu$ m fibers can deliver up to 800% more power than 62.5/125 $\mu$ m fibers with significant potential cost reduction in transceivers due to simplified electro-optic designs with greatly reduced alignment requirements.

### MEDIA COMPARISON (COST)

Figure 1 shows a model configuration of the horizontal wiring in an FDDI network. The typical system will use factory fabricated patch cords for workstation-to-wallplate and concentrator-to-patch panel interconnects. The cable link between the patch panel and wall will use field-installed connectors. A cost analysis is shown in Table 1. It is clear that 200/230 $\mu$ m fiber provides for a significant cost saving over 62.5/125 $\mu$ m fiber. The twisted wire pair

**Figure 1 - FDDI Model**



**TABLE 1 - Media Comparison Cost Analysis**

	62.5/125		200/230		Twisted Pair (Shielded)		Twisted Pair (Unshielded)	
	Unit	Sys.	Unit	Sys.	Unit	Sys.	Unit	Sys.
Transceivers (2) (1300nm)	\$150	\$300	\$75	\$150	\$15	\$30	\$25	\$50
Connectors (2 Duplex)	15	30	10	20	4.50	9	1	2
Patch Cord (2)	57	114	35	70	28	54	13	26
Coupler (1)	10	10	4	4	3	3	2	2
Wallplate (1)	24	24	24	24	10	10	10	10
Cable, 90 m	1.20/m	108	1.20/m	108	0.70/m	63	0.40/m	36
<b>Total Component Cost</b>		<b>\$586</b>		<b>\$376</b>		<b>\$169</b>		<b>\$126</b>
<b>Installation Cost</b>								
Connector Installation (4) (per end)	9.25	37	3.75	15	7.50	30	3.75	15
Wallplate Installation	20	20	20	20	20	20	20	20
Cable Installation	1.50/m	135	1.50/m	135	1.50/m	135	1.50/m	135
<b>Total Installation Cost</b>		<b>\$192</b>		<b>\$170</b>		<b>\$185</b>		<b>\$170</b>
<b>Total Cost</b>								
<b>Total Installed System</b>		<b>\$778</b>		<b>\$546</b>		<b>\$354</b>		<b>\$296</b>
<b>Relative System Cost</b>		<b>100%</b>		<b>70%</b>		<b>46%</b>		<b>38%</b>

approach is the least expensive media choice. However, it is estimated that fiber system implementation will drastically reduce costs in the future by as much as 30%, while copper cable installation, being a mature technology, will not drop further. As a result, fiber optic media based systems will become much more attractive from a cost standpoint. The 200/230 $\mu$ m fiber media approach will actually become cost competitive with shielded twisted wire pair.

Another often overlooked cost consideration is the distinction between an experienced installation crew that initially installs an FDDI network and less skilled maintenance personnel that might do system reconfiguration and maintenance. The user-friendly nature of putting connectors on 200/230 $\mu$ m fiber can make system reconfiguration costs drop to 50% of the value when 62.5/125 $\mu$ m fiber is the media.

#### MEDIA COMPARISON (PHYSICAL PROPERTIES)

Table 2 compares the physical properties of the various media under consideration. Twisted wire pair cable has attenuations which are significantly higher than fiber. Also, the bandwidth will restrict system links to 100 meters or less with little likelihood of future system expansion. Any copper system will be subject to radio frequency interference (RFI) and electromagnetic interference (EMI). This potential noise source is especially a problem in unshielded cables.

The fiber approach eliminates the RFI and EMI noise problems. The bandwidth of either the 62.5/125 $\mu$ m fiber or 200/230 $\mu$ m fiber will not limit current 100 MHz requirements at 100 meters. Obviously the very high bandwidth of 62.5/125 fiber will allow for significant system expansion.

The FDDI systems are required to work at an operating wavelength of 1300nm when fiber is the transmission medium. At the 100 meter requirement, the loss of the large fiber is about 1.6 dB, which does not represent a serious power budget limitation. The bandwidth limits the 200/230 $\mu$ m fiber to operating distances of about 125 meters when the light source is a surface emitting LED. Laser diode sources allow 500-meter operation. The 62.5/125 $\mu$ m fiber has adequate bandwidth and attenuation properties to function at 2 km and beyond.

The primary requirement for a user-friendly system is the ease with which a connector can be installed. The larger 200/230 $\mu$ m fiber with a significantly higher numerical aperture delivers nearly 800% more power than the 62.5/125 $\mu$ m fiber. The enhanced light coupling efficiency of the larger fiber allows tolerances of connectorization to be relaxed and the termination procedure simplified. The simplified crimp-and-cleave termination eliminates the epoxy application and cure cycles as well as polishing required for the smaller fiber. The crimp-and-cleave fiber connector approximates the simple termination of an unshielded twisted wire pair cable.

TABLE 2 - Media Comparison<sup>(2,3)</sup>

	62.5/125	200/230	Twisted Pair (Unshielded)	Twisted Pair (Shielded)
<b>Attenuation</b>				
850nm	3dB/km	5dB/km	>50dB/km	>50dB/km
1300nm	1dB/km	16dB/km		
<b>Numerical Aperture</b>	0.275	0.37	--	--
<b>Bandwidth</b>				
850nm	160-200 MHz-km	150 MHz(100m)	100 MHz(80m)	100 MHz(100m)
1300nm	200-1000 MHz-km	150-400 MHz(100m)		
<b>Source Width Fiber Window</b>	Open	1220-1340nm	--	--
<b>Delivered Power</b>	100%	773%	--	--
<b>Strength</b>				
Strength (<10m)	2.1 - 4.1 x 10 <sup>9</sup> nt/m <sup>2</sup>	4.8 - 5.5 x 10 <sup>9</sup> nt/m <sup>2</sup>		
Static Fatigue (n)	22	26	--	--
Min. Bend Dia.	12.7mm	12.7mm	--	--
<b>Microbending Loss</b>				
12.7mm Bend Dia.	0.5db	0dB	--	--
<b>Intermateability</b>				
to 62.5/125	-0.2dB	-11.5dB	--	--
to 200/230	-0.1dB	-0.2dB	--	--

The intermateability loss in Table 2 is the attenuation penalty associated with mixing media. There is sufficient power available that a mixed media interface can be accommodated; but to fully realize the advantages of large fiber, mixed media should be avoided in any particular media link.

The 200/230 $\mu$ m fiber, which is coated with a hard fluoropolymer material, has mechanical advantages over the 62.5/125 $\mu$ m fiber. The larger fiber is stronger, less susceptible to static fatigue and microbending loss. The result is the potential to use a simpler, less expensive cable construction.

### CONCLUSION

Full system performance out to 2 km can only be achieved with 62.5/125 $\mu$ m fiber. The high delivered power makes 200/230 $\mu$ m fiber easier to implement for applications less than 100 meters. The overall immunity of fiber optic systems to EMI and RFI should give superior system performance compared to copper twisted wire pair systems even when the copper cables are properly shielded. However, in the near term twisted wire pair media systems are significantly less expensive to install. In the longer-term, fiber will become more cost competitive. The large-core fiber media system will actually approach the cost of copper media systems, but with all the advantages of optical data transmission.

### REFERENCES

1. McClure, R.B., Feb. 1991, "Distributing FDDI's Power," *Lightwave*, pp. 32-42.
2. Nishimoto, H., Abo, E., Mishima, T., Tejika, Y., Nagese, H. and Akie, T., 1991, "High NA, Wide-Band, Hard-Clad PCF," *Sumitomo Electric Technical Review*, No. 31, pp. 64-69.
3. Krohn, D.A., Kuczma, A.S., Jr., Maklad, M.S., Laumer, J.W., and Babirad, S., 1990, "Technology-Enhanced Polymeric Clad Silica Fibers for Industrial Applications," *ISA Proceedings*, pp. 1633-1637.

### AUTHOR

David A. Krohn, general manager at 3M Specialty Optical Fibers, has published numerous papers and holds several patents relating to optical fibers. He received a PhD in metallurgy and science from Lehigh University, an MS in metallurgy from Case Western Reserve University, and a BS in ceramics from Rutgers University. Krohn is a member of several societies, including SPIE, ISA, and the American Ceramic Society. 3M Specialty Optical Fibers is located at 420 Frontage Road, West Haven, CT 06516-4190.



# 40TH INTERNATIONAL WIRE AND CABLE SYMPOSIUM (IWCS)

## SYMPOSIUM COMMITTEE

ELMER F. GODWIN  
(President/Director)  
GEF Associates  
3A Buttonwood Drive  
Shrewsbury, NJ 07702  
Office: (908) 389-0990  
Fax: (908) 389-0991  
Home: (908) 741-8864

IRVING KOLODNY  
(Director's Assistant)  
80-56 230th Street  
Bellerose Manor, NY 11427  
Tel & Fax: (718) 464-9197

JAMES J. PICKERING  
(Chairman)  
Neste Chemicals, Inc.  
303 George Street  
Suite 103  
New Brunswick, NJ 08901  
Tel: (908) 249-3900  
Fax: (908) 249-4884

Dr. Ken-ichi Aihara  
NTT American, Inc.  
One Landmark Square, Rm 700  
Stamford, CT 06901  
Tel: (203) 967-9379  
Fax: (203) 325-2316

Rene G. Freeman  
Union Carbide Chemicals and  
Plastic Company, Inc.  
2970 Clairmont Road  
Suite 500  
Atlanta, GA 30329  
Tel: (404) 320-3527  
Fax: (404) 320-3520

Manuel R. Santana  
AT&T Bell Laboratories  
2000 NE Expressway  
Norcross, GA 30071  
Tel: (404) 447-2754  
Fax: (404) 441-7154

Dr. Robert Baboian  
(Treasurer)  
Texas Instruments, Inc.  
34 Forest Street  
MS 10-13  
Attleboro, MA 02703  
Tel: (508) 699-1350  
Fax: (508) 699-3476

Xavier Mann  
Fitel General Corp.  
P. O. Box 486  
Carrollton, GA 30117  
Tel: (404) 830-6616  
Fax: (404) 836-8820

Frank Short  
B.I.C.C. Cables Limited  
Helsby, Warrington, Cheshire  
WA6 0DJ  
England  
Tel: 011-44-92872-2727 or 4363  
Fax: 011-44-92872-3005  
Telex: 628811 (BECLH)

David Fallowfield  
(Vice Chairman)  
c/o COM-LINK Ltd.  
59-61 Phahonyothin Soi 5  
Samsen Nai, Phayathal  
Bangkok 10400, Thailand  
Tel: 011-66-2-279-2507/2503  
-9920/9921  
Fax: 011-66-2-271-4635

Hans A. Mayer  
Olex Cables Division of  
Pacific Dunlop Ltd.  
207 Sunshine Road  
Tottenham, 3012  
Melbourne, Australia  
Tel: 011-61-3-316-2222  
Fax: 011-61-3-314-0383

Homer Vela  
(Secretary)  
AT&T Network Cable Systems  
505 North 51st Avenue  
P. O. Box 13369  
Phoenix, AZ 85002  
Tel: (602) 233-5552  
Fax: (602) 233-5069

Dave Fischer  
Superior Cable Corp.  
150 Interstate North Parkway  
Suite 300  
Atlanta, GA 30339  
Tel: (404) 953-8338  
Fax: (404) 980-2808/2812

Dieter S. Nordmann  
Kabelmetal Electro  
P. O. Box 260  
Kabelkamp 20  
D-3000 Hannover 1  
West Germany  
Tel: 011-49-511-676-2020  
Fax: 011-49-511-676-3226

## ADVISORY

Dr. Peter R. Bark  
Siecor Corporation  
P. O. Box 489  
489 Siecor Park  
Hickory, NC 28603  
Tel: (704) 323-6205  
Fax: (704) 323-6264

Michael A. DeLucia  
David Taylor Research Center  
Energy R&D Office, Code 2759  
Annapolis, MD 21402-5067  
Tel: (301) 267-3825  
Fax: (301) 267-2875

Leo Chattler  
DCM Industries, Inc.  
2930 Faber Street  
Union City, CA 94587  
Tel: (510) 429-9500  
Fax: (510) 429-1250

Marta Farago  
Northern Telecom Canada Ltd.  
P. O. Box 6122, Station A  
Montreal, Quebec H3C-3J4  
Canada  
Tel: (514) 639-2320 (Direct)  
Tel: (514) 639-2000, X2321 (Sec)  
Fax: (514) 634-9684

## CONSULTANTS

Dr. Reiner J. Gerdes  
Consultant—Telecommunications  
812 Oakdale Rd., N.E.  
Atlanta, GA 30307  
Tel & Fax: (404) 377-8608

Dr. Raymond E. Jaeger  
SpecTran Corporation  
50 Hall Road  
Sturbridge, MA 01566  
Tel: (508) 347-2261  
Fax: (508) 347-2747

# AUTHORS INDEX

Name	Page	Name	Page
Abiru, T. ....	806	de Vecchis, M. ....	444, 596
Ahn, W. ....	673	DeBoer, A. T. ....	673
Akiyama, M. ....	463	Dennis, S. M. ....	576
Akiyama, T. ....	155, 227	deVecchis, M. ....	31
Andreassen, J. S. ....	628	DeVito, A. ....	700
Araki, S. ....	126	Ding, L. ....	178
Arroyo, C. J. ....	326, 723	Dissado, L. A. ....	634
Asakawa, S. ....	78	Doble, I. ....	634
Asano, Y. ....	309	Drouet, D. ....	576
Ashida, S. ....	105	Eng, Jr., W. ....	86
Bakalidis, G. N. ....	733	Ericksson, M. ....	550
Bennett, Jr., J. G. ....	348	Esposito, F. ....	749
Bensink, J. J. ....	526	Fann, D-M. ....	482, 504
Berthelsen, G. ....	628	Fann, D. M. ....	511
Betten, E. ....	531	Farro, J. J. ....	693
Biazzi, R. ....	779	Ferguson, D. A. ....	576
Bidinger, A. ....	218	Ficke, W. H. ....	714
Billet, G. ....	319	Fickling, P. ....	550
Birkeland, T. ....	628	Fielding, A. ....	319
Bishop, J. ....	634	Fluevog, J. B. ....	707, 714, 723
Björk, A. ....	535	Franken, G. ....	521
Boirat, R. ....	596	Frantz, R. A. ....	134, 438, 693
Bolza, A. ....	612	Franz, P. ....	372
Bonicel, J.P. ....	31, 487	Friesen, H. W. ....	93
Boscher, D. ....	24	Frost, P. L. J. ....	499
Botelho, M. A. ....	413	Fudou, H. ....	738
Bowmer, T. N. ....	476	Fujibayashi, I. ....	172
Brückner, H. W. ....	521	Fujisaki, A. ....	738
Buckland, E. L. ....	55, 341	Fujita, I. ....	309
Cahall, T. K. ....	417	Gaillard, P. ....	444, 487
Camara, S. ....	540	Gautier, K. ....	565
Carpenter, Jr., R. B. ....	433	Gennaro, A. ....	316
Chan, H. K. C. ....	634	Gentry, S. P. ....	723
Chang, T-C. ....	482	Georgopoulos, C. J. ....	733
Chawla, C. P. ....	141	Giraud, P. F. ....	487
Chen, K-Y. ....	482, 504, 511	Glaesemann, G. S. ....	582, 819
Cheron, P. ....	24	Goblot, J-Y. ....	565
Chung, S-V. ....	178	Gouronnec, A. ....	653
Coden, M. ....	839	Griffioen, W. ....	673, 758
Consiglio, G. ....	766	Grimado, P. B. ....	438
Coover, D. R. ....	404	Groeger, J. H. ....	388
Cortines, C. G. ....	540	Groom, J. ....	766
Crico, S. ....	319, 779	Grosso, P. ....	800
Croft, P. V. ....	242	Haag, H. G. ....	206
Crosnier, J. J. ....	319	Hah, J. Y. ....	492
Cubukciyan, N. H. ....	316	Haibara, T. ....	296
Curtis, D. I. ....	587	Hamada, M. ....	309
D'Amico, J. N. ....	476	Hardy, I. ....	800
Darden, B. V. ....	707	Hatfield, B. ....	839
Davies, A. E. ....	634	Hayashi, S. ....	234
Davis, C. ....	433	Hendewerk, M. ....	397

Name	Page	Name	Page
Hirabayashi, K.	161, 155	Krohn, D. A.	861
Hirahara, T.	105	Kroushi, P. W.	361
Hiramatsu, H.	155	Kuwabara, M.	167
Hoffart, M.	206	Kuwata, Y.	38
Hög, G. F.	206	Kuyt, G.	815
Hopland, S.	742	Lang, G.	628
Hore, L. M.	251	Latoszynski, P.	766
Horima, H.	38	Le Comte, J.	444
Horng, Y. T.	511	Le Noane, G.	24
Hosoya, H.	463	Le Sergent, C.	800
Hosoya, T.	149	Leach, J.	319
Hsiao, C-M.	482	Lee, J. S.	448
Hsiao, J-M.	504	Lee, N. A.	561
Huber, J. C.	316, 848	Lee, Y. I.	453
Huotari, P.	383	LeFevre, B. G.	707
Ikegami, S.	167	Lenge, N.	556
Ishii, T.	38	Levy, A. C.	242
James, S. M.	576	Lin, Y-C.	504
Jamet, P.	24	Lincot, C.	319
Jenkins, A. C.	44	Liu, W. S.	714
Jenkins, P. D.	499	Lynen, W.	218
Jimbo, K.	291	Maeda, K.	679, 810
Jocteur, R.	596	Magnani, F.	612
Johansen, E.	766	Maltz, G.	186
Johansen, M.	531	Marsman, H.	815
Johnson, A. J.	643	Marugome, I.	620
Jun, K. I.	453	Mashikian, M. S.	388
Kado, M.	270	Mathis, D.	44
Kalomiris, V. E.	707	Matsuda, N.	260
Kanen, R. M.	643	Matsuda, Y.	149, 161
Kang, H. J.	448	Matsuhashi, S.	78, 172
Katagiri, T.	285	Matsumoto, H.	787
Katayose, H.	773	Matsumoto, M.	8, 296
Katherisan, K.	707	Matsuno, S.	38
Kathiresan, K.	714, 723	Medlen, N. J.	499
Katsuyama, Y.	285	Menze, B.	186
Kawada, Y.	155	Middel, H.	830
Kawanabe, T.	172	Missout, B.	653
Kawata, O.	602	Miyamoto, M.	333, 457
Kelly, T.	372	Mogi, A.	457
Kenny, R. D.	119	Moisan, M.	800
Kessel, S. L.	348	Mönchengladbach, J. v.	206
Key, P. L.	686	Montalti, F.	749
Kilmer, J. P.	693, 700	Montgelas, R. A.	853
Kim, Y. S.	492	Morita, Y.	260
Kim, Y. T.	453	Moriya, Y.	195
Kiss, L.	766	Morland, G.	469
Kloepper, S.	186	Nakagawa, Y.	105
Kobayashi, I.	234	Nakayama, M.	806
Kobayashi, K.	126	Nanni, F.	749
Kohtala, J.	550	Nassar, H.	16
Kokura, K.	167	Nelson, E. D.	277
Komaki, Y.	195	Neveux, Jr., P. E.	55, 341
Koon, D. N.	119	Ney, R.	218
Koyamada, Y.	285, 793	Nimura, H.	738
Krahn, F.	556	Nishimoto, M.	161

Name	Page
Noguchi, Y. ....	620
Nomura, Y. ....	291
Norimatsu, N. ....	620
Nudd, H. R. ....	66
Nyaas, K. ....	628
Occhini, E. ....	612
Oestreich, U. ....	16
Ohba, M. ....	602
Ohmori, T. ....	463
Ohnuma, H. ....	810
Ohshiro, S. ....	602
Ohtsuki, F. ....	793
Okagawa, S. ....	679, 810
Osaka, K. ....	309
Otake, A. ....	227
Parmar, D. S. ....	521
Paucke, W. J. ....	326
Pavy, D. ....	800
Plitz, I. M. ....	134
Prins, G. J. ....	758
Pryma, J. ....	424
Puchhammer, J. T. ....	316
Pycok, S. J. ....	663
Rampalli, S. ....	66
Ramsey, B. ....	839
Rees, D. ....	469
Reith, L. A. ....	517
Richter, S. ....	112
Rockosi, R. J. ....	357
Rogers, C. E. ....	348
Russell, J. N. ....	587
Ryoo, K. S. ....	448
Sakaguchi, T. ....	78
Sakamoto, K. ....	234
Sano, A. ....	457
Sato, K. ....	787
Sato, N. ....	365
Sato, Y. ....	126, 333, 365
Sawano, H. ....	333
Schauer, F. ....	545
Schick, G. ....	643
Schmid, S. R. ....	134
Schulte, J. ....	303
Schulte, J. ....	186, 319
Schweiger, G. ....	830
Segers, G. ....	673
Sherrets, L. R. ....	723
Sheu, J. J. ....	326
Shimizu, R. ....	270
Shimizu, S. ....	227
Sikora, E. S. R. ....	663
Smith, J. L. ....	428
Sommer, R. G. ....	206
Spenadel, L. ....	397
Stender, M. T. ....	316
Stensland, L. ....	535

Name	Page
Suga, K. ....	260
Sugimura, M. ....	234
Sumski, R. ....	410
Suzuki, H. ....	365
Szostak, T. ....	316
Szum, D. M. ....	141
Tachikura, M. ....	285
Takai, T. ....	260
Tamaki, Y. ....	773
Tanaka, T. ....	270
Tanji, H. ....	195
Tanskanen, J. ....	550
Tatat, O. ....	31
Tateda, M. ....	793
Taylor, D. L. ....	428
Tellefsen, K. A. ....	643
Teucher, F. ....	186
Tomia, S. ....	296
Tomita, S. ....	8
Tregoat, D. ....	800
Trombert, P. ....	24
Tsurusaki, K. ....	126
Ueda, K. ....	105
Uenoya, T. ....	8, 602, 787
van den Bos, A. L. ....	526
Varachi, Jr., J. P. ....	517, 686, 700
Vethanayagam, T. K. ....	428
Volotinen, T. ....	535
Vyas, M. K. R. ....	55
Wang, J. H. ....	511
Wang, S.-I. ....	504
Wauben, R. ....	815
Weckerle, G. ....	556
Wei, T. ....	826
Welch, S. C. ....	242
White, G. ....	469
Wieczorek, C. ....	700
Wieczorek, C. J. ....	643, 693
Wilson, C. G. ....	44
Wolfe, S. V. ....	634
Worthington, P. ....	587
Wright, J. V. ....	663
Yabuta, T. ....	8, 296
Yamamoto, H. ....	620
Yamamoto, S. ....	270
Yamamoto, T. ....	105
Yamashita, K. ....	793
Yamauchi, R. ....	806
Yamazaki, Y. ....	620
Yates, M. J. ....	663
Yin, H. B. ....	319
Yokoo, Y. ....	787
Yokosuka, H. ....	291, 773
Yu, P.-L. ....	482
Yuce, H. H. ....	517, 686, 693, 700, 826
Zako, H. ....	105



**IWCS**

# **International Wire & Cable Symposium**

**SPONSORED BY: IWCS, INC.  
EATONTOWN, NEW JERSEY**

**With Participation By:**

**U.S. Army Communications-Electronics  
Command  
(CECOM)**

**Fort Monmouth, New Jersey**

**41st International Wire & Cable Symposium**

**16, 17, 18 and 19 November 1992**

**Bally's Reno Hotel, Reno, Nevada**

Please provide a 300-500 word abstract (25 copies) of proposed technical or poster papers on such subjects as design, application, materials, and manufacturing of communications and electronics wire and cable of interest to the commercial and military electronics industries. Such offers should be submitted no later than 13 March 1992 to: IWCS, Inc., 174 Main Street, Eatontown, NJ 07724.

I. PAPER/POSTER TITLE: \_\_\_\_\_

AUTHOR(S): \_\_\_\_\_

CONTACT FOR CORRESPONDENCE: \_\_\_\_\_

COMPANY NAME: \_\_\_\_\_

ADDRESS AND TELEPHONE NUMBER: \_\_\_\_\_

\_\_\_\_\_  
\_\_\_\_\_

II. BACKGROUND (Why was work undertaken?):

III. PRIMARY CONCLUSION OR RESULT:

IV. DESCRIPTION OF THE NOVELTY AND HOW THIS WORK ADVANCES THEORY/TECHNOLOGY OR  
MARKETING STRATEGIES:

V. 300 TO 500 WORD COMPREHENSIVE ABSTRACT INCLUDING METHODOLOGY IN REACHING CON-  
CLUSIONS OR RESULTS:

Fold Here

Stamp

IWCS, Inc.  
Crystal Brook Professional Bldg.  
174 Main Street  
Eatontown, NJ 07724

Fold Here